ResearchOnline@JCU

This file is part of the following reference:

Prendergast, Kylie (2003) *Porphyry-related hydrothermal systems in the Estberg District, Papua, Indonesia.* PhD thesis, James Cook University.

Access to this file is available from:

http://eprints.jcu.edu.au/27155/

If you believe that this work constitutes a copyright infringement, please contact ResearchOnline@jcu.edu.au and quote **http://eprints.jcu.edu.au/27155/**

JAMES COOK UNIVERSITY AUSTRALIA

Porphyry-related hydrothermal systems in the Ertsberg District, Papua, Indonesia.

Thesis submitted by

Kylie Prendergast
(BSc HON 1)

In October 2003

For the Degree of Doctor of Philosophy in the School of Earth Sciences
James Cook University, Australia.

STATEMENT OF ACCESS

I, the undersigned author of this work, understand that James Cook University will make this thesis available for use within the University Library and, via the Australian Digital Theses network, for use elsewhere.

I understand that, as an unpublished work, a thesis has significant protection under the Copyright Act and;

I do not wish to place any further restriction on access to this work

Signature

Date 1/11/04

ELECTRONIC COPY

I, the undersigned, the author of this work, declare that the electronic copy of this thesis provided to the James Cook University Library, is an accurate copy of the print thesis submitted, within the limits of the technology available.

1/11/04

Signature Date

STATEMENT ON SOURCES

Declaration

I declare that this thesis is my own work and has not been submitted in any form for another degree or diploma at any university or other institution of tertiary education. Information derived from the published or unpublished work of others has been acknowledged in the text and a list of references is given.

(Signature) .....1/11/04 (Date)

Abstract

The Ertsberg district hosts multiple skarn and porphyry-related deposits comprising one of the largest Cu-Au resources in the world. The geological and geochronological framework suggests economically significant igneous and hydrothermal events in the district occurred as two distinct evolving episodes separated by less than 500,000 years. The igneous complexes (Grasberg Igneous Complex ca <3.33-3Ma and Ertsberg ca 3-2.67Ma) are respectively post-dated by early porphyry-style mineralisation and spatially related skarn Cu-Au mineralisation. Deep-intermediate high sulphidation style mineralisation occurred as a late development at both locations.

The West Grasberg estimated gold resource (ca. 700,000 ounces) overprints limestone breccias and banded clay maar sediments on the western margin of the Grasberg Igneous Complex (GIC). Volcanic-diatreme activity is interpreted to have facilitated banded clay subsidence after extensive porphyry-style potassic, magnetite and quartz alteration occurred in the GIC but prior to cessation of hydrothermal mineralisation. Native gold±pyrite occurrences are spatially associated with smectite-chlorite clay, and Au-As-Bi-Te bearing pyrite. Gold mineralisation may have occurred contemporaneously with high sulphidation Au-As-Bi associations in the Kucing Liar Cu-Au deposit which occurs at depth nearby.

Separate but near identical pyrite-Au-As-Zn-Bi-Te occurrences overprint earlier skarn Cu-Au at Wanagon Gold (ca. 2 million ounces gold) and Big Gossan. The Big Gossan occurrence is younger (<2.82±0.04Ma based on a new $^{40}Ar/^{39}Ar$ phlogopite date from the Big Gossan skarn). Adularia deposited in leached sandstone at the Wanagon Gold occurrence has a $^{40}Ar/^{39}Ar$ K-feldspar age of 3.62±0.05Ma. A published K-Ar date (3.81±0.06Ma) from the Wanagon Sill constrains formation of the overprinting skarn Cu-Au and late-stage Wanagon Gold occurrence to a period of ca. 0.2Ma. $\delta^{34}S$ of sulphide (-0.7 to 5.1‰) from skarn Cu-Au and overprinting pyrite-Au-As-Zn-Bi-Te occurrences at both deposits are interpreted as magmatic. Laser ablation analyses show pyrites deposited by copper-depositing hydrothermal fluids contain a maximum of 0.01ppm Au and 370ppm As whereas pyrite deposited by Au-As-Bi-Te-depositing fluids contains up to 57ppm Au and 20000ppm As. Textural relationships are consistent with late-stage gold being transported as both $AuHS^-$ and AuHS° complexes and respectively precipitated by sulphidation reactions and adsorption by pyrite surfaces. Fluid inclusion microthermometry indicates the pyrite-Au-As-Zn-Bi-Te forming fluids had salinities of ca. 9 wt% $NaCl_{equiv}$ and homogenisation temperatures of ca. 248°C. Despite the close spatial and temporal association with skarn Cu-Au, the occurrences are interpreted to represent incursion of a new fluid with a different composition.

78 $\delta^{18}O$ and $\delta^{13}C$ analyses of hydrothermal carbonates in the district suggest non-magmatic fluids were insignificant contributors except at Kucing Liar where calculated $\delta^{18}O$ fluid values from

carbonate associated with leaching, quartz and clay alteration are 2.2-4.8‰. $\delta^{18}O_{SMOW}$ values of secondary calcite (11.7‰ to 17.5‰) associated with a carbonate alteration and dissolution event in the Ertsberg East Skarn System were determined in situ by SIMS. Carbonate alteration selveges and vein infill from the Big Gossan skarn and mineralisation have magmatic $\delta^{18}O_{SMOW}$ and $\delta^{13}C_{PDB}$ values with $\delta^{18}O_{H2O}$ and $\delta^{13}C$ of ca. 5.9‰ and ca. -3.2‰ respectively. Analyses of texturally distinct dolomitisation of dolostone and limestone peripheral to the GIC define a mixing line from marine carbonate host rocks ($\delta^{18}O_{SMOW}$ =30.9‰ and $\delta^{13}C_{PDB}$ =1.2‰) to altered dolostone ($\delta^{18}O_{SMOW}$ =8.7‰ and $\delta^{13}C_{PDB}$ =-1.6‰). Fluids are considered to have been magmatic H_2O+CO_2.

The two key findings from this research include a) recognition of magmatic-dominated $\delta^{13}C$ and $\delta^{18}O$ compositions from hydrothermal carbonates and b) characterisation of two separate but near identical late stage pyrite-Au-As-Zn-Bi-Te occurrences. The depleted $\delta^{13}C$ values from skarns and mineralised vein carbonates are interpreted to represent contribution from magmatic carbon. The presence of magmatic CO_2 as a volatile component in intrusion-related deposits has significant genetic consequences as it is considered to promote early phase separation, which can lead to selective partitioning of ore body components (i.e. Cu, Au, As, Zn, S, Cl etc) between brine and vapour. The pyrite-Au-As-Zn-Bi-Te occurrences were formed from ca. 9 wt% $NaCl_{equiv}$ magmatic fluids that homogenised at temperatures of ca. 248°C. Such fluids were capable of transporting and depositing significant pyrite, Au, As and lesser Zn, Pb, Cu, Bi and Te. These fluids may represent the precursor to fluids documented in epithermal deposits that form at shallower levels with an additional significant meteoric component.

Acknowledgements

Thanks are due to PT Freeport Indonesia who generously facilitated and supported this research. Roger Taylor and Peter Pollard are recognised for their vision in initiating the project and, along with Gavin Clarke, for allowing access to a treasure trove of unpublished information. Patrick Williams is acknowledged for his outstanding supervisory role. Staff, post-doc and student members (especially Damien) of the School of Earth Sciences are thanked for providing ad hoc assistance throughout the project.

Personal thanks are due to some special friends for their love and support in different ways: Pooh & Mary; Marnie & Derek; Lucy & Andrew; Frana & John; Ilma & Richard; Warren & Joanna; Julie & Atay; Pat; Sya; Nicole; Margot; Chantell.

Most significantly, I am so grateful to Kay & Colin for letting me be here; Bruce for showing me how lucky I am; and my adorable near-perfect husband James Lally (who turned out to be an exceptional draftsperson).

Thesis Contents

Statement of access		i
Statement of sources declaration		ii
Abstract		iii to iv
Acknowledgements		v
List of Figures and Tables		vii to x
List of Appendicies		xi
Introduction		I-1 to 3
Section A	Diatreme volcanicity, hydrothermal gold mineralisation and surficial weathering developed on the western margin of the Grasberg Igneous Complex.	A-1 to 44
Section B	Genesis of pyrite-Au-As-Zn-Bi-Te zones associated with Cu-Au skarns: Evidence from Big Gossan and Wanagon Gold deposits, Ertsberg District, Papua, Indonesia.	B-1 to 38
Section C	Magmatic $\delta^{18}O_{SMOW}$ and $\delta^{13}C_{PDB}$ compositions in porphyry-related hydrothermal carbonates from the Ertsberg District, Papua, Indonesia.	C-1 to 36
Section D	New insights into the evolution of igneous and hydrothermal events in the Ertsberg District, Papua, Indonesia.	D-1 to 44
References		R-1 to 11

List of Figures and Tables

Introduction

Figure I-1. Ertsberg District location. I-1

Section A

Figure A-1. Ertsberg District location, regional geology, major deposits/prospects and location of West Grasberg area. A-2

Figure A-2. Photographs from the northern wall volcanics and West Grasberg. A-3

Figure A-3. GIC geology and location of West Grasberg (modified from Freeport Indonesia geological mapping). A-4

Figure A-4. Paragenesis and timing of igneous and hydrothermal events at Grasberg and Kucing Liar. A-7

Figure A-5. Local Geology at West Grasberg. A-8

Figure A-6. West Grasberg cross sections. A-9 to 16

Figure A-7. Photographs of hand specimens from drillcore at West Grasberg. A-21

Figure A-8. Photographs and reflected light photomicrographs of West Grasberg sulphide mineralogy. A-23

Figure A-9. Selected XRD traces of samples from West Grasberg. A-25

Figure A-10. 3D Isometric view (looking east) of the NNE-trending limestone breccia. A-26

Figure A-11. SEM backscatter image and energy dispersive X-ray spectra from pan concentrated sample of gold alloy contained in diaspore. A-31

Figure A-12. Bivariant pots of elements from West Grasberg samples (Appendix 4) of limestone breccia (oxidised and unoxidised), Dalam breccia, clay, marble breccia with skarn and samples of skarn and limestone breccia analysed by Brannon (1991). A-32

Figure A-13. Bivariant plots of LA-ICPMS trace element analyses from grains of pyrite and one grain of sphalerite. A-34

Figure A-14. Range in homogenisation temperatures and wt%$NaCl_{equiv}$ for fluid inclusions from sphalerite-galena-quartz-fluorite veins along NE-striking structures at West Grasberg (Kyle, 1993). A-38

Figure A-15. Possible contribution of invisible gold in euhedral pyrite to the West Grasberg gold resource. A-40

Figure A-16. Schematic cross section evolution of West Grasberg. A-42

Table A-1. Summary of XRD results from West Grasberg. A18 to 19

Table A-2. West Grasberg paragenesis for limestone breccias, marble, marble breccias, banded clay and non-banded clay. A-28

Table A-3. Correlation coefficients of Log10 normalised assay results from West Grasberg samples. A-31

Table A-4. Clay phases preferentially developed in different volcanic terrains. A-36

Table A-5. Summary of conditions of stability for allophane, and halloysite-kaolin phases. A-43

Section B

Figure B-1.	Ertsberg District location, regional geology (modified from Freeport Indonesia geological mapping) and major deposits/prospects (EESS: Ertsberg East Skarn System; DOM: Dom skarn).	B-2
Figure B-2.	Geology of Big Gossan and Wanagon Gold (modified from PT Freeport Indonesia Geological maps).	B-6
Figure B-3.	40Ar/39Ar age spectrum and isochron for A, B) Big Gossan skarn phlogopite and C, D) Wanagon Gold K-feldspar (Appendix 1, 12).	B-8
Figure B-4.	Parageneses of Big Gossan and Wanagon Gold.	B-10
Figure B-5.	Big Gossan photographs and photomicrographs.	B-13
Figure B-6.	Big Gossan and Wanagon Gold Stage 1 and Stage 2 native gold microprobe compositions (Appendix 5).	B-14
Figure B-7.	Geological cross section BGU26.	B-15
Figure B-8.	Wanagon Gold and Big Gossan hand specimens, polished section microphotographs and fluid inclusion samples.	B-17
Figure B-9.	Composite Wanagon Gold cross section looking NW.	B-19
Figure B-10.	Element correlations from Big Gossan (A-G; n= ca. 15,000 analyses) and Wanagon Gold (H-L; n= ca. 4,000 analyses) drillhole assay data.	B-20
Figure B-11.	BGU26-1 downhole drill log with assay results and pyrite content (PT Freeport Indonesia), geology and Cu:10000Au, Cu:Zn and Pb:Zn ratios.	B-21
Figure B-12.	Big Gossan cross section 27 and distribution of assay ratios and elements.	B-23
Figure B-13.	Big Gossan long section looking NE.	B-25
Figure B-14.	$\delta^{34}S_{CDT}$ from Big Gossan and Wanagon Gold Stage 1 and Stage 2 sulphides (A).	B-26
Figure B-15.	Histogram of Big Gossan and Wanagon Gold fluid inclusion freezing study results used to estimate salinity for Figure B 16 (cf. Bodnar, 1993).	B-26
Figure B-16.	Th-salinity diagram for Big Gossan and Wanagon Gold fluid inclusions.	B-27
Figure B-17.	Laser Ablation correlation plots of element relationships in sulphides from Big Gossan and Wanagon Gold.	B-29
Table B-1.	Comparison between Big Gossan, Wanagon Gold and other mineralisation styles.	B-36

Section C

Figure C-1.	Location of the Ertsberg district, stratigraphy and stratigraphic distribution of $\delta^{18}O$ and $\delta^{13}C$ samples.	C-3
Figure C-2.	Ertsberg district geology, location of intrusions and skarns (modified from PT Freeport Indonesia geological mapping) and location of drillholes sampled for isotope analyses.	C-5
Figure C-3.	Geology and sample locations for drillhole VZW53 on Mine Cross Section 13.	C-13
Figure C-4.	Photographs and photomicrographs from VZW53, GRS125, KLS3-1 and KLS1-1.	C-15
Figure C-5.	Location, geology and isotope sample locations of drillhole GRS125.	C-16
Figure C-6.	Summary paragenesis and $^{40}Ar/^{39}Ar$ dates for Kucing Liar skarn and overprinting mineralisation (Pollard and Taylor, 2003; B. New pers comm., 2003: Pollard et al., submitted).	C-17

Figure C-7.	Microprobe analyses of wt% Ca, Mg and Mn+Fe in carbonate.	C-17
Figure C-8.	Stratigraphy, sample location and conventional carbonate $\delta^{18}O_{SMOW}$ and $\delta^{13}C_{PDB}$ results from KLS1-1 and KLS3-1 (logging from New, unpublished).	C-19
Figure C-9.	Geology of the EESS.	C-20
Figure C-10.	Summary paragenesis for the EESS (modified from Mertig et al., 1994; Coutts et al., 1999; Friehauf et al., 2002 and this study).	C-21
Figure C-11.	Carbonate textures from the EESS, and Big Gossan.	C-22
Figure C-12.	Backscatter electron microprobe images of carbonate infill in the EESS carbonate breccia.	C-23
Figure C-13.	Big Gossan local geology at 2930RL elevation and location of isotope samples.	C-24
Figure C-14.	Summary paragenesis and $^{40}Ar/^{39}Ar$ date for Big Gossan (Section B).	C-24
Figure C-15.	$\delta^{18}O_{SMOW}$ and $\delta^{13}C_{PDB}$ isotope results from VZW53, GRS125, KLS1-1, KLS3-1 and EESS.	C-26
Figure C-16.	$\delta^{18}O_{SMOW}$ and $\delta^{13}C_{PDB}$ isotope results from Big Gossan.	C-28
Figure C-17.	Compilation and interpretation of $\delta^{18}O_{SMOW}$ and $\delta^{13}C_{PDB}$ carbonate isotope results from the Ertsberg district.	C-29
Figure C-18.	Calculated $\delta^{18}O_{FLUID}$ compositions for fluids at Big Gossan, Kucing Liar and DOM.	C-33
Table C-1.	Sample descriptions and isotopic results from the Ertsberg district.	C-8 to 9
Table C-2.	SIMS analytical parameters (K. Prince, pers comm. 2003).	C-10
Table C-3.	Calculations of $\delta^{18}O_{FLUID}$ for carbonate $\delta^{18}O$ samples in Figure C-18 using assumed fractionations of Golyshev et al., (1981).	C-33

Section D

Figure D-1.	New Guinea, major tectonic elements and location of the Ertsberg district and PT Freeport Indonesia deposits and prospects (1-9).	D-4
Figure D-2.	Stratigraphy and timing of tectonic and magmatic activity in Papua (modified from Quarles Van Ufford, 1996).	D-7
Figure D-3.	Ertsberg District regional geology and location of major deposits and prospects (modified from PT Freeport Indonesia maps).	D-9
Figure D-4.	Geochronology of igneous hydrothermal events in the Ertsberg District.	D-11
Figure D-5.	$\delta^{34}S_{CDT}$ results from the Ertsberg District.	D-16
Figure D-6.	Gold microprobe from deposits in the Ertsberg district and alluvial sources.	D-17
Figure D-7.	Calculated $\delta^{18}O_{FLUID}$ and δD_{FLUID} and silicate and oxide $\delta^{18}O_{VSMOW}$ results from Grasberg, Big Gossan, Kucing Liar and DOM.	D-19
Figure D-8.	Compilation and interpretation of $\delta^{18}O_{SMOW}$ and $\delta^{13}C_{PDB}$ carbonate isotope results from the Ertsberg district.	D-20
Figure D-9.	Grasberg and GIC fluid inclusion results from quartz.	D-21
Figure D-10.	Fluid Inclusions from Ertsberg district skarn and ore deposits.	D-23

Figure D-11.	Cu:10000Au and Cu:Ag ratios from major deposits and prospects in the Ertsberg District including Big Gossan and Wanagon Gold (Section B), DOM and the EESS.	D-24
Figure D-12.	Metal zoning in Big Gossan long section looking NE (modified from Section B).	D-26
Figure D-13.	Grasberg drillhole AM96-43-07 and variation in Cu:10000Au ratios with Cu-Au mineralogical context.	D-28
Figure D-14.	Range of Cu:10000Au ratios for porphyry-, HS-, skarn Cu-Au and pyrite-Au-As-Zn-Bi-Te mineralisation in the Ertsberg District, Cu:10000Au ratios from Grasberg brine and vapour fluid inclusions and resource-reserves for Ertsberg District deposits.	D-29
Figure D-15.	Laser ablation results from analysis of pyrite from West Grasberg (Section A), Big Gossan and Wanagon Gold (Section B).	D-30
Figure D-16.	Correlation between major igneous and hydrothermal events in the Ertsberg District.	D-31
Figure D-17.	Evolution of major igneous and hydrothermal events in the Ertsberg district.	D-34
Figure D-18.	Possible sources and mechanisms responsible for fluids, metals, and igneous components in the Ertsberg district.	D-37
Figure D-19.	Experimental data for the relationship between pressure, temperature and salinity.	D-41
Table D-1.	Ore reserves in the Ertsberg district as at 31st December, 2002 (Freeport McMoRan Copper & Gold Inc 2002 Annual Report).	D-3
Table D-2.	Recent models for the Cainozoic tectonic evolution of New Guinea and emplacement of Cu-Au bearing magmas in the Ertsberg District, Papua.	D-6

List of Appendicies

Appendix	Section	Description	Data
Appendix 1	All	Analytical techniques	Digital
Appendix 2a	All	Specimen list, JCU catalogue number, drillhole and depth; brief sample description and index of work completed	Digital
Appendix 2b	All	Freeport drillhole assay results and XYZ coordinates (Projection WGS84 / UTM zone 53)	Digital
Appendix 3	All	XRD results (West Grasberg printed as Table in Section A)	Digital
Appendix 4	A	Reassay sample descriptions and results	Digital
Appendix 5	A, B, C	Microprobe results (this study) carbonate, gold, sphalerite	Digital
Appendix 6	A, B, C	Drillhole database; Description of database codes; Detailed Geology logs (West Grasberg, VZW53, Big Gossan, Wanagon Gold, GRS125); Collar and survey data for all drillholes sampled in this study	Digital
Appendix 7	A, B, D	LA-ICPMS sample description, paragenesis, corrected results; LA-ICPMS results: Glass (NIST) standard RUN1-6; LA-ICPMS results: Nickel sulphide standard PGEARUN1-6	Digital
Appendix 8	B	Fluid inclusion results	Digital
Appendix 9	B	Sulphur isotope sample description and results	Digital
Appendix 10	B,C	Sample and polished section descriptions and local sample paragenesis (Big Gossan, Wanagon Gold, EESS, GRS125, West Grasberg)	Digital
Appendix 11	B	XRF of Wanagon Gold samples	Digital
Appendix 12	B	$^{40}Ar/^{39}Ar$ dating reports	Digital
Appendix 13	C	SIMS data processing	Digital

Introduction

Porphyry-related hydrothermal systems in the Ertsberg district, Papua, Indonesia.

Porphyry districts are the source of the majority of the world's copper and the Ertsberg porphyry district contains one of the largest gold and copper resources in the world. It is located in the mountainous Central Ranges of Papua (Figure A-1) on a collision boundary between the westwards-migrating Indo-Pacific plate and the north-moving Australian plate (Quarles Van Ufford, 1996; Sapiie, 1998; Sapiie et al., 1999; Quarles Van Ufford and Cloos, submitted). The Ertsberg district contains two main episodes of intrusive activity accompanied by a variety of porphyry-related hydrothermal systems including porphyry Cu-Au, skarn Cu-Au, deep-intermediate high-sulphidation Cu-Au and pyrite-Au-As-Zn-Bi-Te occurrences. The hydrothermal systems are hosted in Pliocene igneous and Cretaceous-Tertiary clastic and carbonate sedimentary rocks.

Previous work in the Ertsberg District has sought to constrain the stratigraphy, tectonics and igneous events (McMahon, 1994a, 1994a, b; Quarles Van Ufford, 1996; Weiland and Cloos, 1996; Sapiie, 1998; Sapiie et al., 1999; Housh and McMahon, 2000; McMahon, 2000a, b; Sapiie and Cloos, submitted; Quarles Van Ufford and Cloos, submitted; Sapiie and Cloos, in press) and describe the major mineralised deposits in the district (Katchan, 1982; McDonald and Arnold, 1994; Mertig et al., 1994; Mertig, 1995; Rubin, 1996; Malensek, 1997; Meinert et al., 1997; Rubin and Kyle, 1997; Coutts et al., 1999; Harrison, 1999; New, 1999; Friehauf et al., 2000; Friehauf, 2000; Gibbins, 2000; Gibbens, 2000;

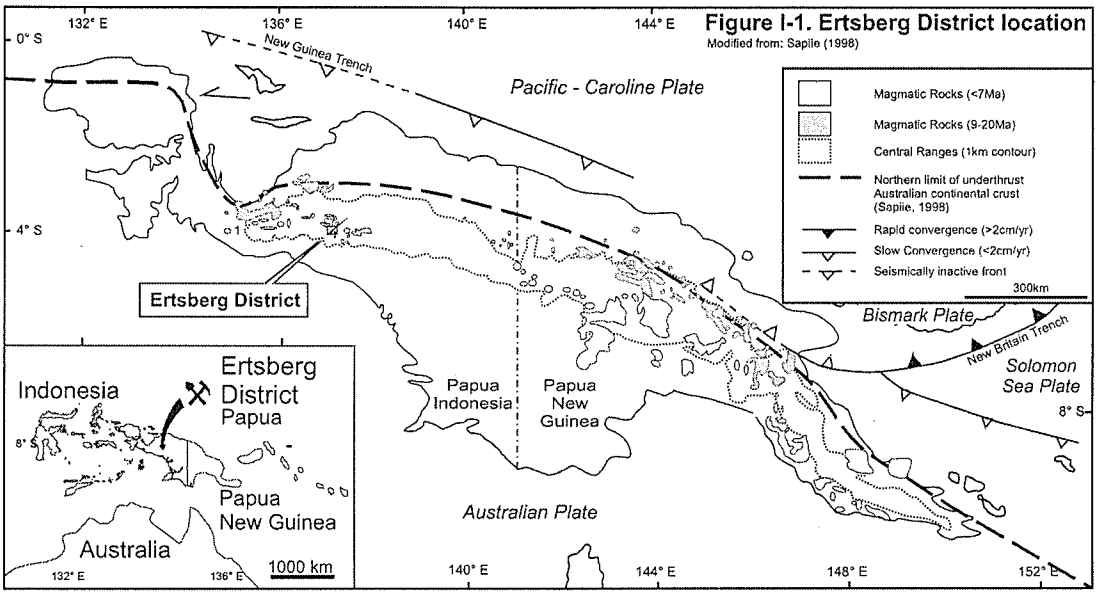

Figure I-1. Ertsberg District location
Modified from: Sapiie (1998)

Lambert, 2000; Clarke, 2002; Pollard and Taylor, 2002; Clarke, 2003; Pollard and Taylor, 2003). Other investigations have addressed the source of metals and fluids in the district (Kyle, 1993; James and Housh, 1995; Lambert, 2000; Mathur et al., 2000; Meinert et al., 2003; Mathur et al., submitted; Mathur, 2000) and mechanisms of transport for hydrothermal components in the Grasberg porphyry system (Heinrich et al., 1999; Ulrich et al., 1999; Williams et al., 2003; Fu et al., 2003a; Fu et al., 2003b). K-Ar (McDowell et al., 1996) and $^{40}Ar/^{39}Ar$ (Pollard et al., submitted) geochronology for igneous and hydrothermal activity in the district spans ca. 2 Ma.

Despite considerable advances, there are many questions regarding the transport mechanisms and sources of metals and components in porphyry districts. In the Erstberg District, two areas of knowledge notably missing from the previous work include firstly, the character of unexplained gold occurrences and their relationship to other mineralised deposits in the district, and secondly, the degree of interaction between the carbonate-dominated sedimentary host rocks, any pre-existing non-magmatic fluids and porphyry-related hydrothermal fluid. Although deep circulation and interaction between surface waters is traditionally implicated in porphyry-terrains (Taylor, 1997), more recently it has been demonstrated that primary magmatic fluids can be dominant (Harris and Golding, 2002; Meinert et al., 2003).

This PhD research project addresses these two areas and places the new results into context with the results from previous work. In doing so, the project has significantly increased understanding of the geological processes responsible for the metal endowment that establishes the Ertsberg District as one of the largest gold and copper producers in the world. These results are significant beyond the scope of the Ertsberg District as they are applicable to magmatic related hydrothermal systems worldwide.

This Thesis has been written as a series of four papers (Sections A-D) and each Section is cross-referenced as a separate paper accordingly. New results from the Ertsberg district include description of the relationship between gold mineralisation and late stage volcanic processes at West Grasberg (Section A), identification of distinct Au-rich hydrothermal events occurring at 3.62±0.05Ma and <2.82±0.04Ma (Section B) and characterisation of $\delta^{18}O$ and $\delta^{13}C$ compositions of carbonate alteration related to hydrothermal fluids in the district (Section C). Incorporation of new results and correlation of different tectonic, magmatic, structural and hydrothermal events in the Ertsberg district has resulted in a time-space synthesis portraying "the evolution of the Ertsberg district" (Section D).

Section A

Section A examines the relationship between gold and base-metal occurrences and late-stage volcanic-surficial processes operating in a diatreme environment at West Grasberg (on the Western margin of the Grasberg Igenous Complex which is host to the Grasberg porphyry system). It seeks to ascertain the origin and timing of gold mineralisation, which is spatially associated with the West Grasberg banded clay, through examination of the temporal and spatial relationships between the banded clay occurrence and structural and hydrothermal events. Techniques utilised in the investigation include detailed lithological and structural analysis of the geological setting in combination with mineralogical (petrography and XRD analysis) and geochemical (re-analysis of mineralised intervals, microprobe and LA-ICPMS) methods.

Section B

Previous work (Rae et al., 1994; Malensek, 1997; Meinert et al., 1997) has documented gold enrichment associated with pyrite-As-Zn-Bi-Te minerals present in two skarn Cu-Au deposits at a single stratigraphic position but separated by 2km of strike. This Section examines the nature of these gold occurrences through structural-stratigraphic analysis of the geological setting and metal zoning, a detailed paragenetic study, $^{40}Ar/^{39}Ar$ geochronology, mineral identification (petrography, XRD, microprobe), geochemical (microprobe and LA-ICPMS analysis, stable isotope) and fluid inclusion studies.

Section C

The objective of Section C is to establish the source/s of the hydrothermal fluids responsible for carbonate alteration in the district through a $\delta^{18}O$ and $\delta^{13}C$ stable isotope study. Samples are stratigraphically constrained, distributed on a district scale and paragenetically constrained with respect to the evolution of igneous and hydrothermal events in the Ertsberg district.

Section D

The new results have been placed into context with previous work to establish the evolution of igneous and hydrothermal events in the district. Consideration of the timing and character of igneous and hydrothermal features in combination with the tectonic setting leads to an appreciation of factors that were important for the significant metal inventory in the Ertsberg district.

Section A
Diatreme volcanicity, hydrothermal gold mineralisation and surficial weathering developed on the western margin of the Grasberg Igneous Complex.

Abstract

The West Grasberg estimated gold resource of 700,000 ounces occurs on the margin of the Grasberg Igneous Complex (GIC) in banded clay sediments exhibiting contorted layers and brecciated limestone. The banded clays are composed of 10 and 7Å halloysite-kaolin, consistent with formation under near neutral pH conditions at temperatures less than 100°C and is interpreted to have been formed in a surficial lacustrine environment. Subsidence into a void at the margin of the GIC may have been facilitated by volcanic-diatreme activity. The banded clay was incorporated after extensive porphyry-style potassic, magnetite and quartz alteration present in the GIC and prior to cessation of hydrothermal mineralisation.

Banded clay and surrounding recrystallised and brecciated limestone have locally been overprinted by base-metal and pyrite mineralisation. Deposition of bitumen was associated with at least one generation of pyrite. Native gold±pyrite occurrences were late and spatially associated with smectite-chlorite clay, diaspore and Au-As-Bi-Te bearing pyrite. Euhedral pyrite at West Grasberg contains 2-8 g/t Au (LA-ICPMS) and calculations indicate that almost 200,000 ounces of the limestone breccia gold resource (508,625 ounces) would be as invisible gold if 10% of the 8g/t euhedral pyrite were present. Gold mineralisation is tentatively correlated with unconstrained Au-As-Bi associations expressed in surface geochemistry associated with faults near West Grasberg and also documented at the Kucing Liar Cu-Au deposit which occurs at depth nearby.

Surface-related leaching and texture-destructive 10 and 7Å halloysite-kaolin clay alteration affected both banded clay and adjacent GIC and the alteration is interpreted to represent weathering in a high rainfall environment. The unstable amorphous aluminosilicate phase allophane, which is common in high rainfall, high leaching environments, is developed at depths greater than 50m below current surface.

The banded clay at West Grasberg is not an isolated occurrence as similar material also occurs on the eastern margin of the GIC. The combination of the banded clay occurrences and relatively unaltered tuffs, which occur on the northern margin of the GIC, suggest late stage volcanic processes operated in the Ertsberg district and that the GIC was exposed during the later part of its hydrothermal evolution.

Introduction

The Ertsberg district is located in the mountainous Central Ranges of West Papua (Figure A-1). Pliocene intrusive activity was accompanied by hydrothermal systems that formed one of the largest gold and copper resources in the world. The Grasberg Igneous Complex (GIC), host to the Grasberg porphyry Cu-Au deposit, is interpreted to have been emplaced at shallow depths into a cover of volcaniclastic rocks and (trachy)andesite flows and domes (McDonald and Arnold, 1994; Sapiie and Cloos, submitted). Remnants of the volcaniclastic cover were reported to contain surficial and aqueous volcanic textures (McDonald and Arnold, 1994; Sapiie and Cloos, submitted).

Banded and crystalline tuffs currently exposed by mining on the northern margin of the GIC (Figure A-2a, b) overly an unconformity on limestone and appear relatively unaltered (Margotomo et al., 2001). They may be analogous to the Tertiary Volcanic Sediments documented by Sapiie and Cloos (submitted). Banded clay is reported from the western and eastern margins of the GIC (Figure A-3) (Brannon, 1991; Kavalieris, 1994; Prendergast, 2001). The banded clay may have been derived from banded lacustrine sediments with tuffaceous component (Kavalieris, 1994). Kavalieris (2000) considered that the banded clay may have formed in a volcanic lake and that karst dissolution from acidic hot spring activity allowed the banded clay to slump into the margin of the GIC. As gold and base metals occur nearby it has been suggested that an epithermal mineralisation system existed at this time

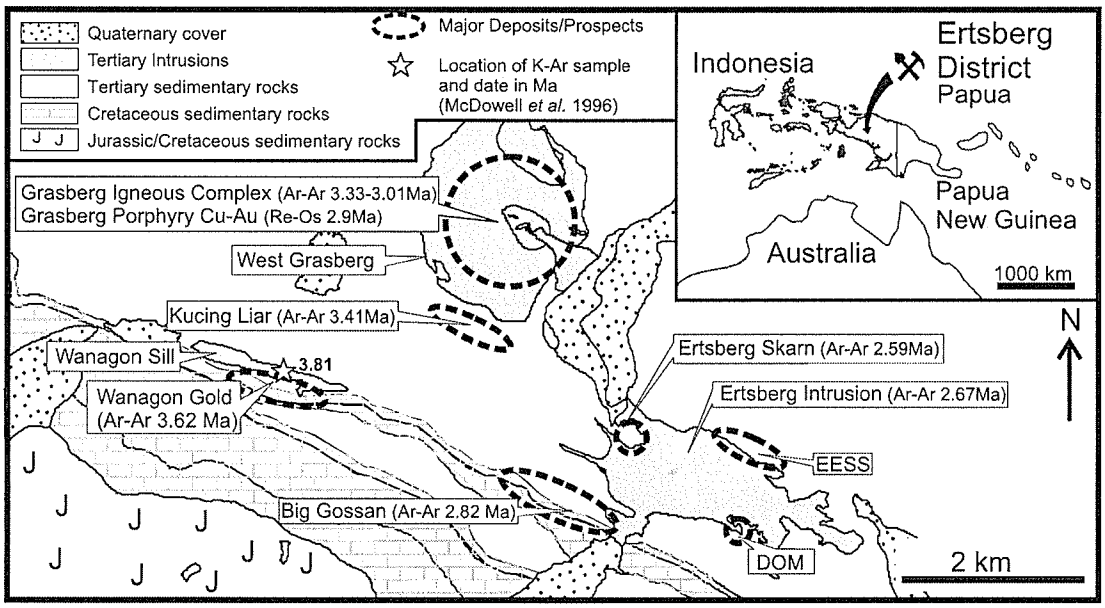

Figure A-1. Ertsberg District location, regional geology, major deposits/prospects and location of West Grasberg area. Modified from Freeport Indonesia geological mapping (EESS: Ertsberg East Skarn System; DOM: Dom skarn). Grasberg Igneous Complex biotite $^{40}Ar/^{39}Ar$ date range, Kucing Liar skarn phlogopite $^{40}Ar/^{39}Ar$ date, Ertsberg skarn phlogopite and Ertsberg Intrusion biotite $^{40}Ar/^{39}Ar$ dates from Pollard et al. (submitted). Grasberg porphyry Cu-Au Re-Os date from Mathur et al. (2000). Big Gossan skarn phlogopite $^{40}Ar/^{39}Ar$ date and Wanagon Gold K-feldspar $^{40}Ar/^{39}Ar$ date from Section B. Wanagon Sill biotite K-Ar date and sample location from McDowell et al. (1996).

Figure A-2. Photographs from the northern wall volcanics and West Grasberg. a) Outcrop of northern volcanic tuffs on unconformity on limestone adjacent to the GIC (photo courtesy of P. Pollard). b) Weakly altered banded and non-banded tuff. X = XRD analysis sites (Samples 4612-323 and 4612-325 in (Table A-1). c) West Grasberg Banded clay outcrop overlain by fluvioglacial sediments. d) (WGZ8, 90m) Banded clay with white alteration along fractures. e) (WGZ8, 104.7m) Banded and non-banded clay in drillcore (greyscale photo).

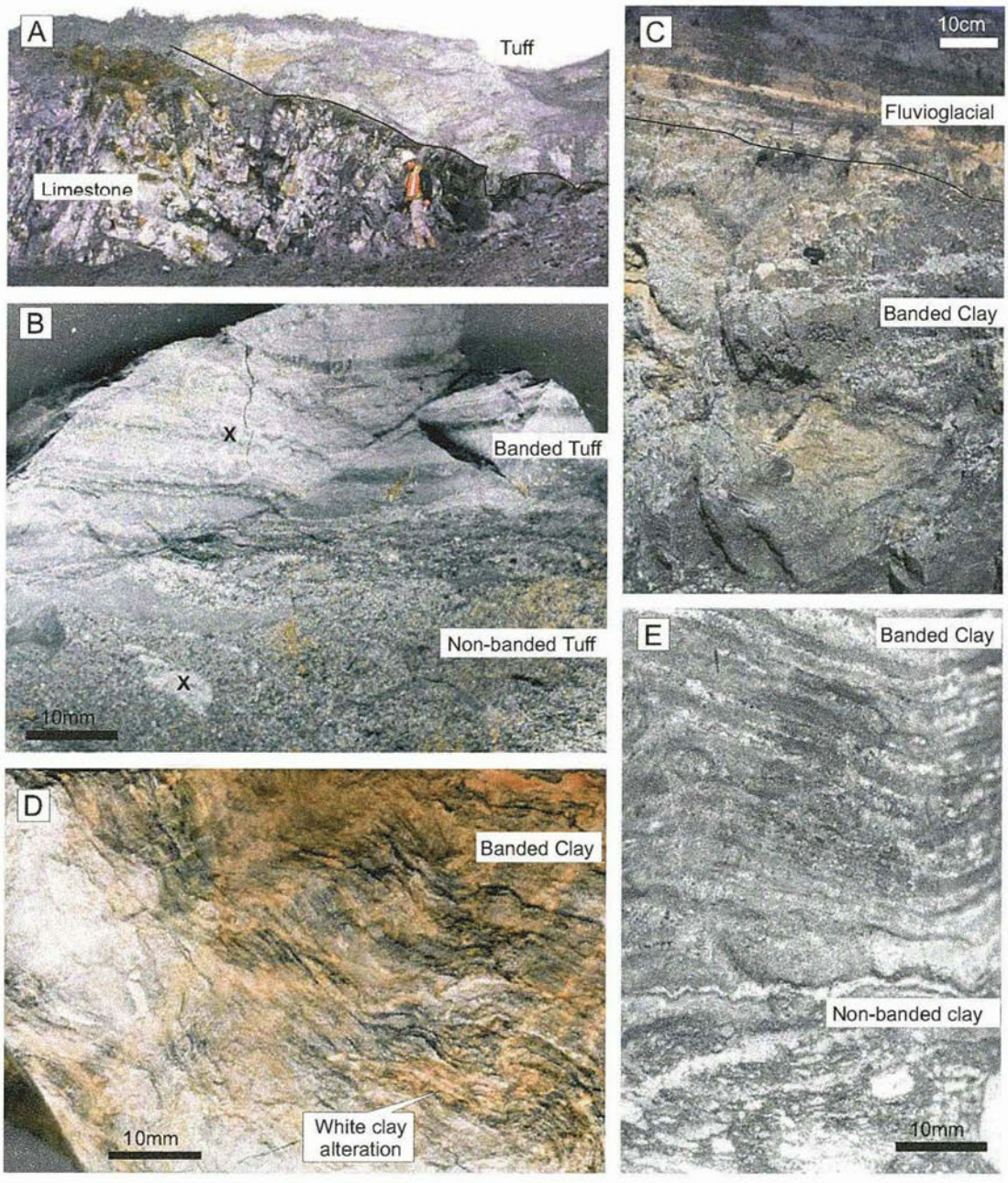

Figure A-3. GIC geology and location of West Grasberg (modified from Freeport Indonesia geological mapping). Banded clay intersected in drill hole P3850-28 at 48.7m (Kavalieris, 2000). The dominant clay phase in P3850-28 is 10Å halloysite (Table A-1).

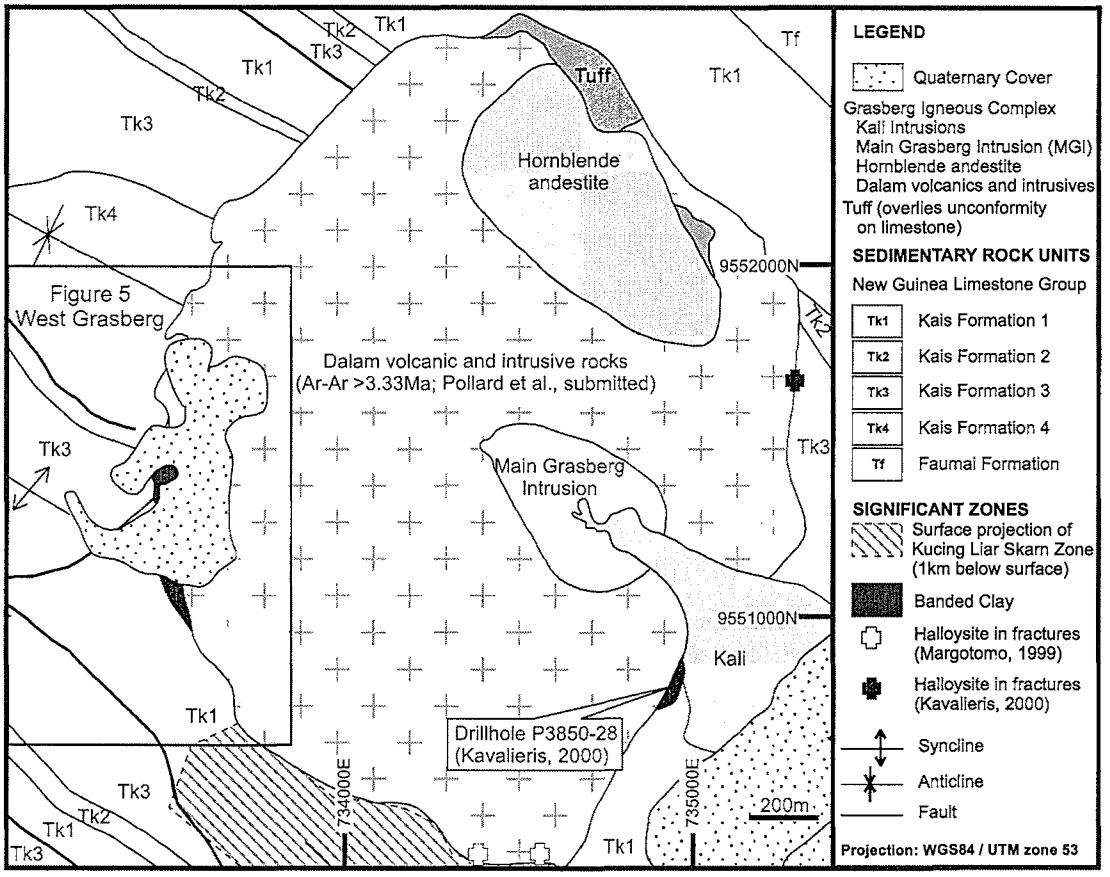

(Brannon, 1991). Sapiie and Cloos (submitted) consider that the banded clay is a relict of a once extensive field of boiling hot springs and formed by leaching of igneous wall rocks.

This investigation seeks to ascertain the origin and timing of the West Grasberg banded clay and associated mineralisation through an examination of the temporal and spatial relationships between the banded clay occurrence and structural and hydrothermal events. Techniques utilised in the investigation include detailed lithological and structural analysis of the geological setting in combination with mineral identification (petrography and XRD analysis) and geochemical (re-analysis of mineralised intervals, microprobe and LA-ICPMS) methods.

Previous work and history

Samples were collected in 1975 from the western New Guinea Limestone Group - GIC contact and the surrounding area was mapped and sampled in detail during February 1989 (Atwood, 1989a). Elevated Au (<10.4ppm), Ag (<0.23%), Cu (<9%), Pb (<69.5%), and Zn (<19%) were reported and a drill program comprising 4 fans of drillholes was proposed in 1989 to test the extent of mineralisation at West Grasberg (Atwood, 1989a).

Five drillholes for 1300m completed by August 1989 established that brecciated and altered rocks at West Grasberg dip at approximately 50 degrees to the east beneath the western margin of the GIC (Atwood, 1989a). Mapping and drilling reported an area of abundant clays, silica nodules, pyrite and distinctive metal associations (anomalous mercury, arsenic, antimony, lead, zinc, silver and gold) interpreted to belong to a shallow and possibly surficial hydrothermal system (Brannon, 1991). Atwood (1989a) observed that the distribution of West Grasberg mineralisation (Au±Zn-Pb) was not coincident with Grasberg copper mineralisation. In addition to the Au±Zn-Pb occurrences at the contact, gold-only mineralisation was intersected in limestone breccias west of the contact.

Further drilling (WGR6 - WGR22) completed by 1990 defined the extent of the resource at West Grasberg and acted as sterilisation drilling for the western waste dumps (Brannon, 1991). An inferred geologic resource of 10 million tonnes at 2.17 g/t gold (approximately 700,000 ounces of gold) was estimated from a combination of gold intercepts in the banded-clay zones and the limestone breccia zones (Brannon, 1991). Metallurgical testing of three "ore-types" was completed in late 1989 (Atwood, 1989b) with poor gold recovery results from cyanidation and roast-cyanidation. Flotation techniques and gravity separation were not tested (Brannon, 1991). In light of the poor recoveries (Atwood, 1989b), and failure to discover larger reserves (Brannon, 1991), the West Grasberg gold resource was deemed uneconomic and subsequently covered by the western waste dumps.

Geological Setting

The oldest rocks in the Ertsberg district are the clastic and carbonate sedimentary rocks of the Jurassic-Cretaceous Kembelangan Group and the Tertiary New Guinea Limestone Group (Figure 1: Dow et al., 1988). Quaternary alluvium occurs in valleys with glacial till and colluvium along slopes. Deformation in the district was initiated in Miocene times during arc-continent collision (Sapiie et al., 1999). The northern edge of the Australian continent entered a north-dipping subduction zone beneath the island of Papua producing a fold and thrust belt characterised by en echelon, kilometre-scale NW-trending folds with chevron and open symmetrical geometries. 20-9 Ma magmatic activity recognised elsewhere on the island is not present in the Ertsberg District. Westwards movement of the Pacific-Caroline plate with respect to the Australian plate at ca 4-2 Ma induced left-lateral, strike-slip faulting parallel to the upturned strata. In the Ertsberg district two major intrusive igneous complexes at Grasberg and Ertsberg (Figure A-1) and numerous smaller stocks, dykes and sills were emplaced at this time (McDowell et al., 1996; Pollard et al., submitted). Apatite fission track results indicate the intrusions were emplaced at <2km depth and had a rapid cooling history (Weiland and Cloos, 1996).

The GIC comprises early fragmented volcanic and igneous rocks of the Dalam breccia and

a series of nested intrusions (McDonald and Arnold, 1994; Pollard and Taylor, 2002; Sapiie and Cloos, submitted). The age of the GIC is constrained by structural relationships and $^{40}Ar/^{39}Ar$ data (Figure 4: Pollard and Taylor, 2002; Pollard et al., submitted). The GIC rocks are described as extensively altered and veined by multiple hydrothermal events (McDonald and Arnold, 1994; Pollard and Taylor, 2002; Sapiie and Cloos, submitted). The paragenetic timing and extent of separate alteration and veining events are documented by Pollard and Taylor (2002).

A biotite date of 3.07Ma (Pollard and Taylor, 2002; Pollard et al., submitted) from a premineralisation quartz-anhydrite-bearing vein constrains the maximum age of main Grasberg sulphide development (Figure A-4). Skarn developed in carbonate rocks at the eastern contact of the GIC has been dated by $^{40}Ar/^{39}Ar$ at 3.01±0.6Ma (Pollard et al., submitted). The Kucing Liar skarn and Cu-Au deposit (New, 1999) are hosted in sedimentary rocks adjacent to the GIC approximately 1km below the current exposed GIC surface (Figure A-3). The skarn, dated at 3.41±0.3 to 3.18±0.2Ma, was synchronous with the earliest GIC events (Figure 4: New, 1999; Pollard et al., submitted). Similar mineralisation styles are developed at Grasberg and Kucing Liar (Figure 4: Pollard and Taylor, 2003). Re-Os age of 2.9±0.3Ma for Grasberg main stage sulphides (Mathur et al., 2000) and 3.01±0.02Ma for molybdenite from Kucing Liar (Mathur et al., submitted) support a cogenetic relationship between the deposits.

West Grasberg Geology

Local Geology

Mapping in the West Grasberg area by Kavalieris (1992) shows that surface geological exposure is limited by alluvial cover (Figure A-5). West Grasberg geology is constrained from drillholes on 8 cross sections (Figure A-6a-h). The western contact of the GIC strikes roughly north (Figure A-5) and dips approximately 45 degrees to the east (Figure A-6c, f). The banded clay at West Grasberg has a sharp wedge shaped geometry at the western GIC contact (Brannon, 1991: this study). The banded clay is up to 65m wide at surface and pinches out at both ends of its six hundred meter strike and pinches out at depth (Brannon, 1991: this study). The Kais Formation of the New Guinea Limestone Group occurs below and to the west of the banded clay (Quarles Van Ufford, 1996). The Kais Formation limestone is altered to marble and brecciated near the GIC contact (Figure A-6b, c, e-h)

Kavalieris (1992) documented upright folds with NW trending fold axes in the Kais limestone (Figure A-5). A strong NE trend in limestone is identified by elongate zones (3-6m wide by 10m long) containing massive sphalerite, pyrite and pale green fluorite and fractures with karst patterns (Kavalieris, 1992). Brannon (1991) identified a NE striking gold-bearing breccia

Figure A-4. Paragenesis and timing of igneous and hydrothermal events at Grasberg and Kucing Liar. Incorporation of West Grasberg banded clay must have occurred at least subsequent to "P1" alteration of the adjacent Dalam volcanics and intrusives and may have occurred even later (i.e. after P2, P3, P4 alteration).

Description of annotations:

A) Kucing Liar Stage III chalcopyrite mineralisation may be coeval with Grasberg main stage sulphides (Pollard and Taylor, 2002; 2003: B. New pers comm., 2003).

B) Pb-Zn sulphides developed on the margins of the GIC may correlate with Pb-Zn sulphides developed at the GIC which appear late in the paragenesis at West Grasberg (Pollard and Taylor, 2002).

C) Leaching and deep to intermediate High Sulphidation occurrences at Kucing Liar and Grasberg are considered to be genetically related (Pollard and Taylor, 2003).

D) West Grasberg gold±pyrite occurrence is tentatively correlated with Kucing Liar and Grasberg deep to intermediate High Sulphidation sulphides.

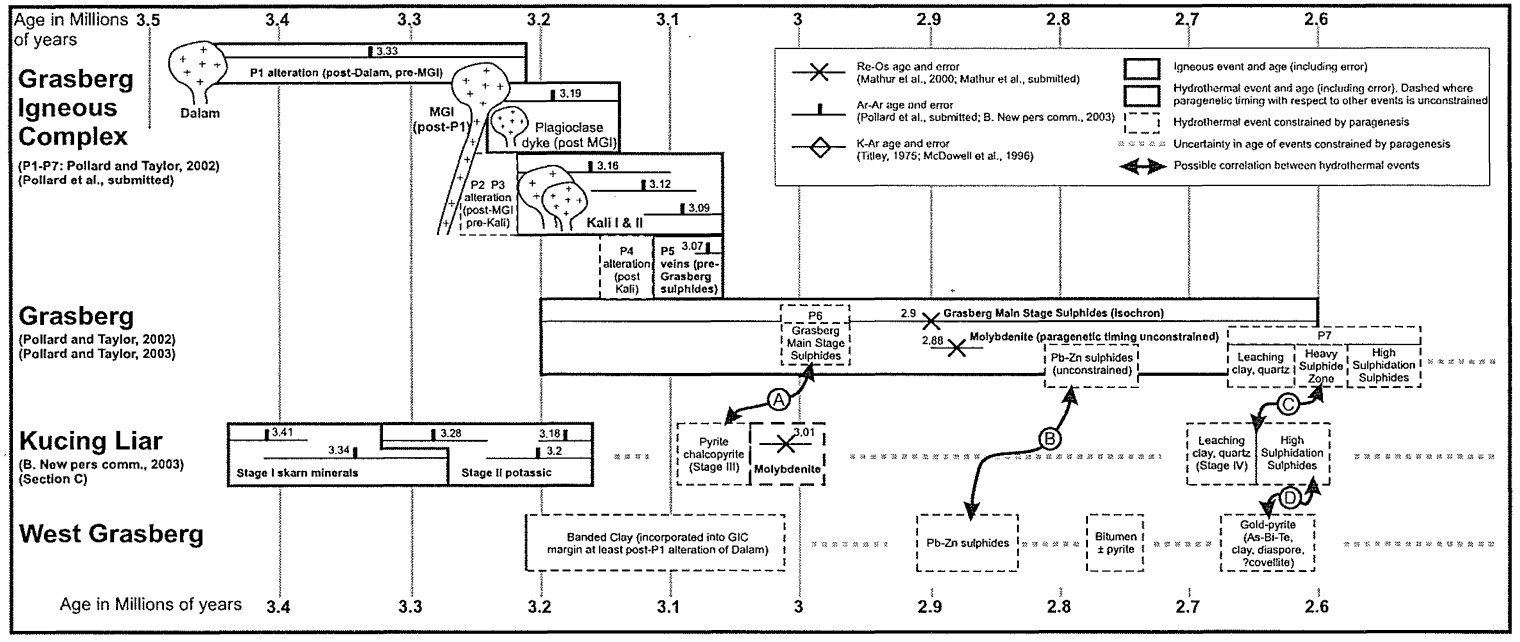

zone in the Kais limestone (Figure A-5). The NE structural influence is also reflected in a larger scale fault that offsets units of the Kais Formation (Figure A-5). A second gold-bearing limestone breccia zone strikes WNW (Figure A-5) and is interpreted to be concordant with bedding (Atwood, 1989a).

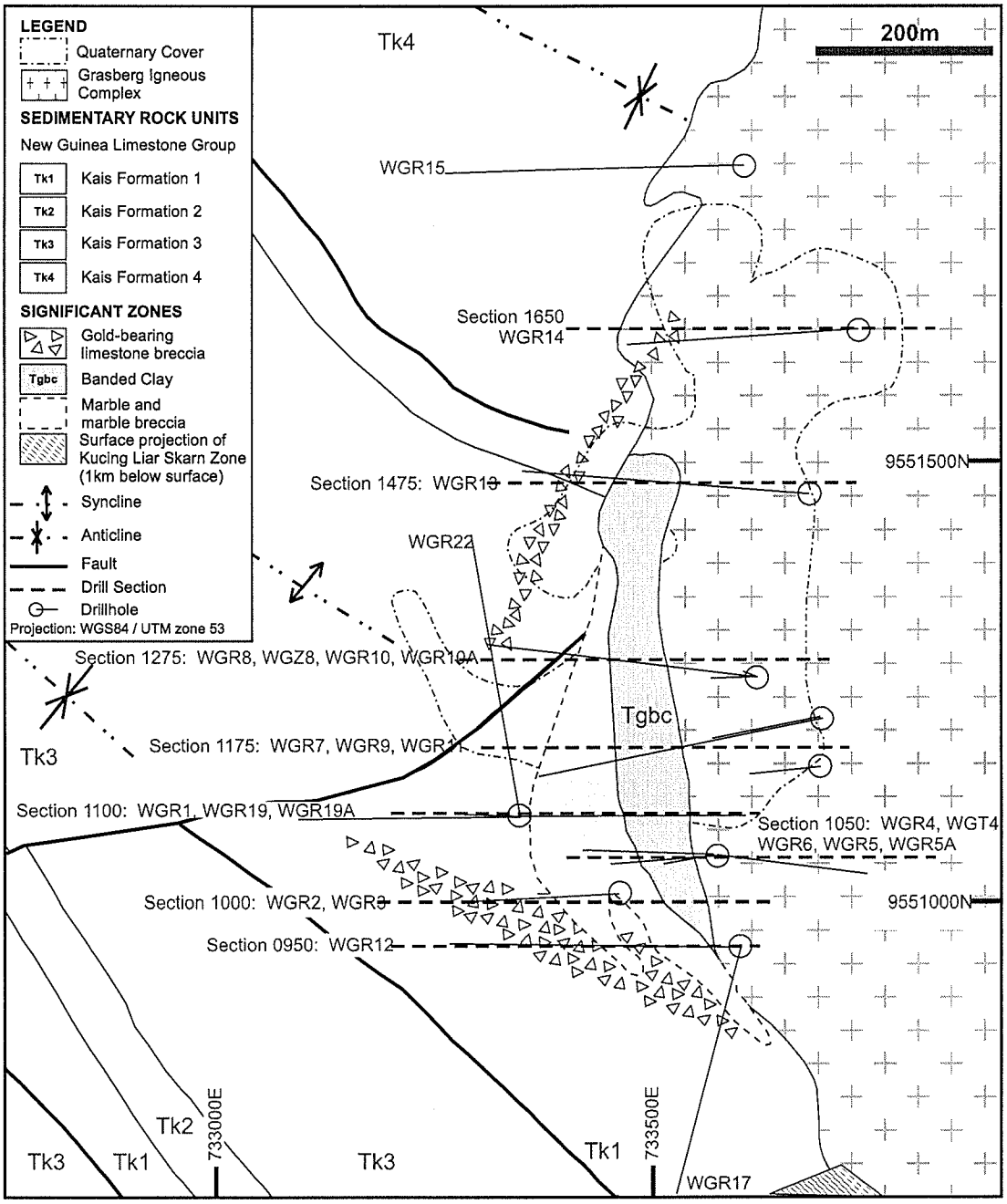

Figure A-5. Local Geology at West Grasberg. Modified from Freeport Indonesia geological mapping and this study. Location of main structural features, surface distribution of limestone breccias. Location of cross sections (Figure A-6a-h).

Figure A-6a. West Grasberg cross sections. Bedding trends and surface geology derived from Freeport Indonesia cross sections. West Grasberg drill logs in Appendix 6. Section 0950. BXI was intersected in WGR12 (97.25-103.45m) and offsection in WGR17; 367-400.6m. Significant intersections include: A) (162-375m, 1.31g/t Au) WNW gold-bearing limestone breccia zone. B) vuggy sphalerite-galena-fluorite veins (WGR12, 72m). C) (60-69m, 3.19g/t Au) Gold along the Dalam breccia and intrusive breccia contact. D) (39-45m, 1.64g/t Au) gold in banded clay. E) (30-39m, 0.59g/t Au and 1.54% Cu) Elevated Cu along the contact between banded clay and Dalam breccia.

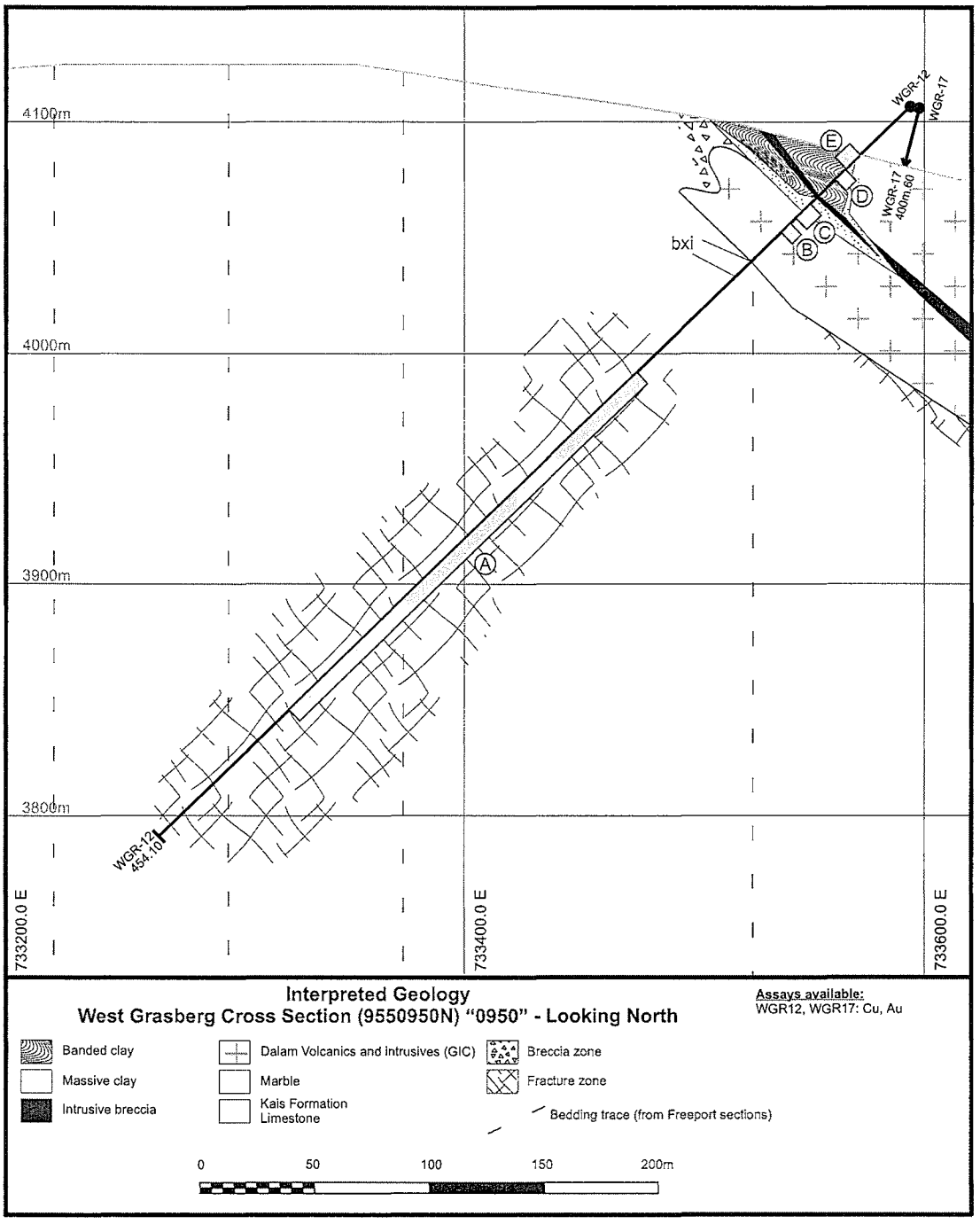

Figure A-6b. West Grasberg cross sections. Bedding trends and surface geology derived from Freeport Indonesia cross sections. West Grasberg drill logs in Appendix 6. Section 1000. Significant intersection: A) (135-282m, 1.86g/t Au) WNW gold-bearing limestone breccia zone.

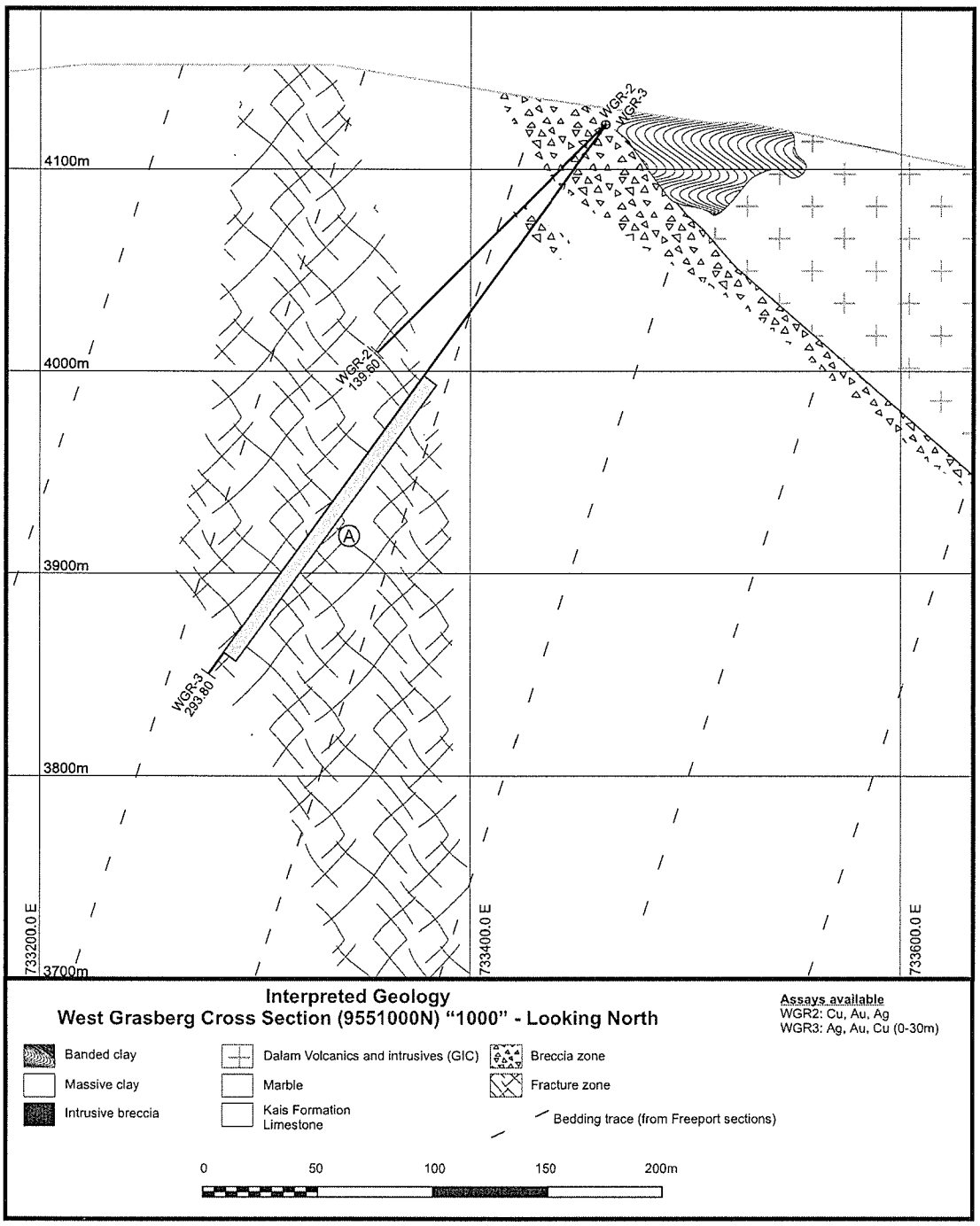

Figure A-6c. West Grasberg cross sections. Bedding trends and surface geology derived from Freeport Indonesia cross sections. West Grasberg drill logs in Appendix 6. Section 1050. Significant intersections include: A) (72-96m, 9.39g/t Au) Gold mineralisation developed in several rock types including marble (70-86m), limestone (86-88.4m), igneous with intense clay alteration (88.4-90m) and banded clay and sulphide rubble (90.4-97m). Cu to 2.56% (72-75m). B) (84-96m, 4.28g/t Au) Banded clay -limestone contact in WGT4. C) (207-210m, 73ppm Ag). Silver assays in WGR6 may correspond to Pb-Zn veins (logs and drillcore not observed). D) (45-57m, 2.34% Cu) Elevated Cu along the Dalam breccia and marble contact.

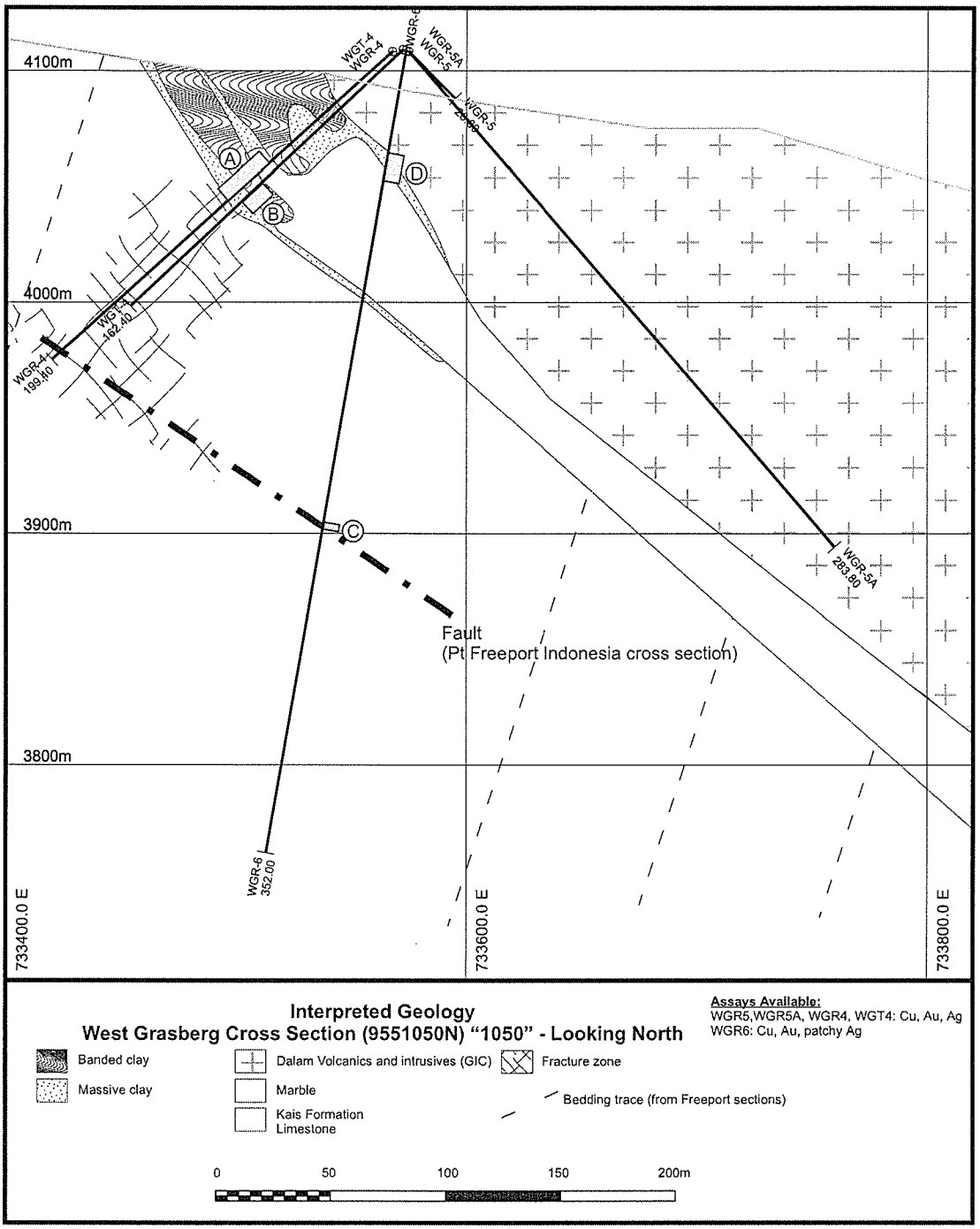

Figure A-6d. West Grasberg cross sections. Bedding trends and surface geology derived from Freeport Indonesia cross sections. West Grasberg drill logs in Appendix 6. Section 1100. Significant intersections include: A) (147-192m, 1.55g/t Au) Limestone breccia hosted gold does not correlate with other occurrences.

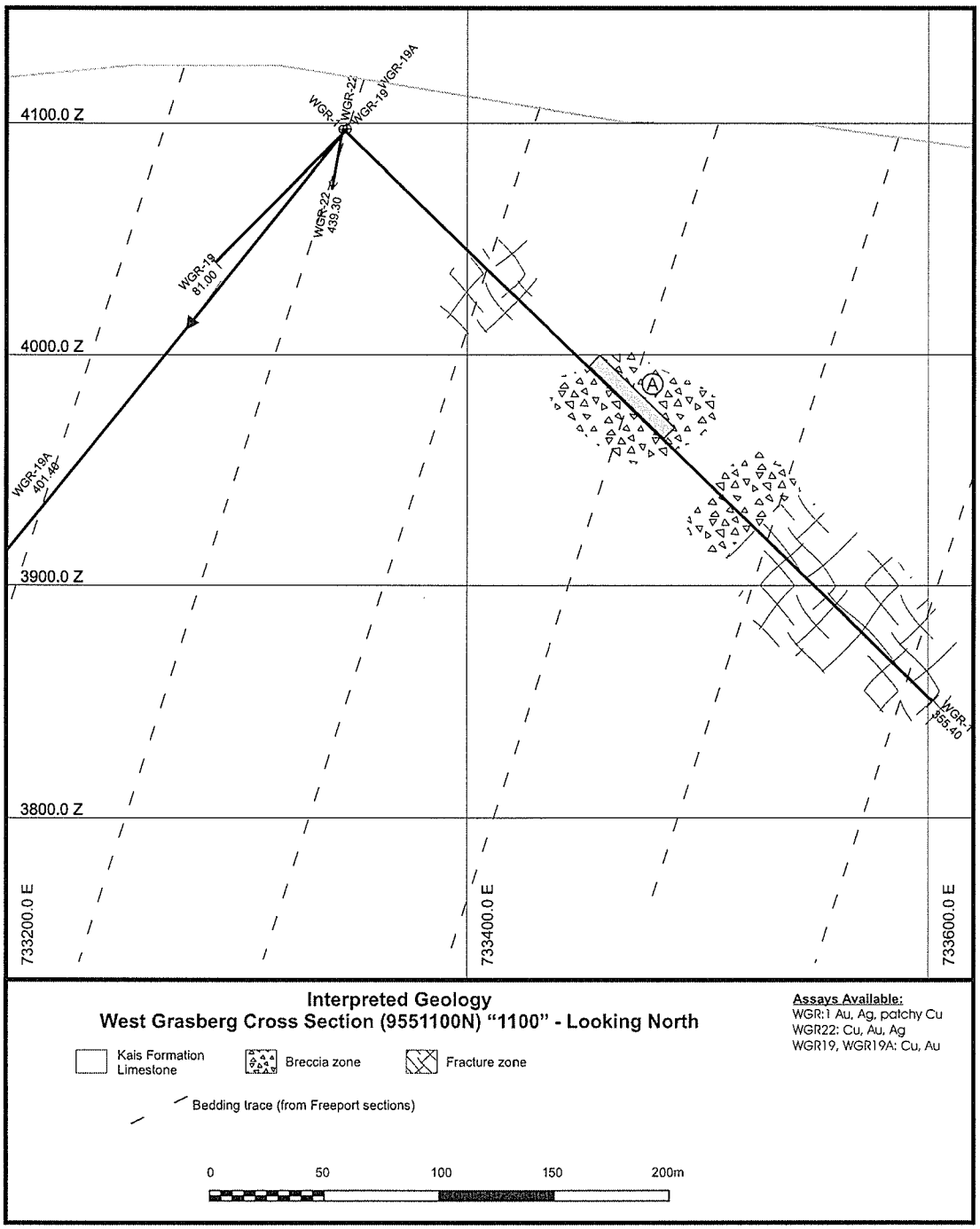

Figure A-6e. West Grasberg cross sections. Bedding trends and surface geology derived from Freeport Indonesia cross sections. West Grasberg drill logs in Appendix 6. Section 1175. Significant intersections include: A) (207-210m, 1.02g/t Au) Fractured marble. B) (150-183m, 1.32g/t Au) intrusive breccia and banded clay. C) (63-81m, 0.52% Cu and 0.37g/t Au) Dalam breccia with pyrite spot alteration. D) Crackle breccia with minor pyrite and no significant gold mineralisation (266.7-292m in WGR11). E) (150-153m, 17g/t Ag) Elevated silver assays in gritty breccia may correspond with the presence of galena fragments.

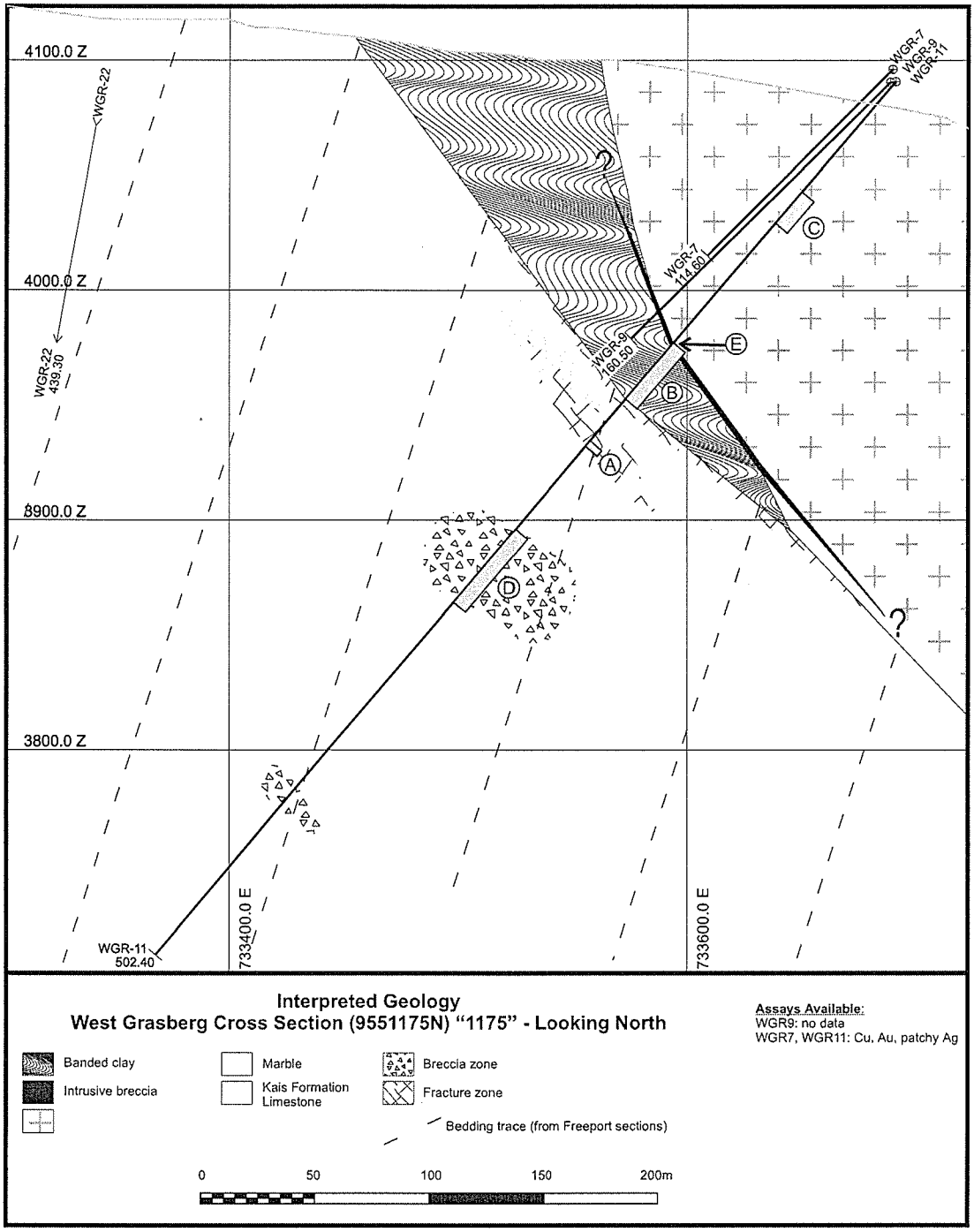

Figure A-6f. West Grasberg cross sections. Bedding trends and surface geology derived from Freeport Indonesia cross sections. West Grasberg drill logs in Appendix 6. Section 1275. Significant intersections include: A) (282-378m, 1.12g/t Au) NE gold-bearing limestone breccia zone. B) (75-78m, 2.34g/t Au) Elevated gold in intrusive breccia. C) Elevated Cu values to 1.12% occur in the intrusive breccia (72-75m). D) (120-192m, 0.96g/t Au) Gold in marble breccia.

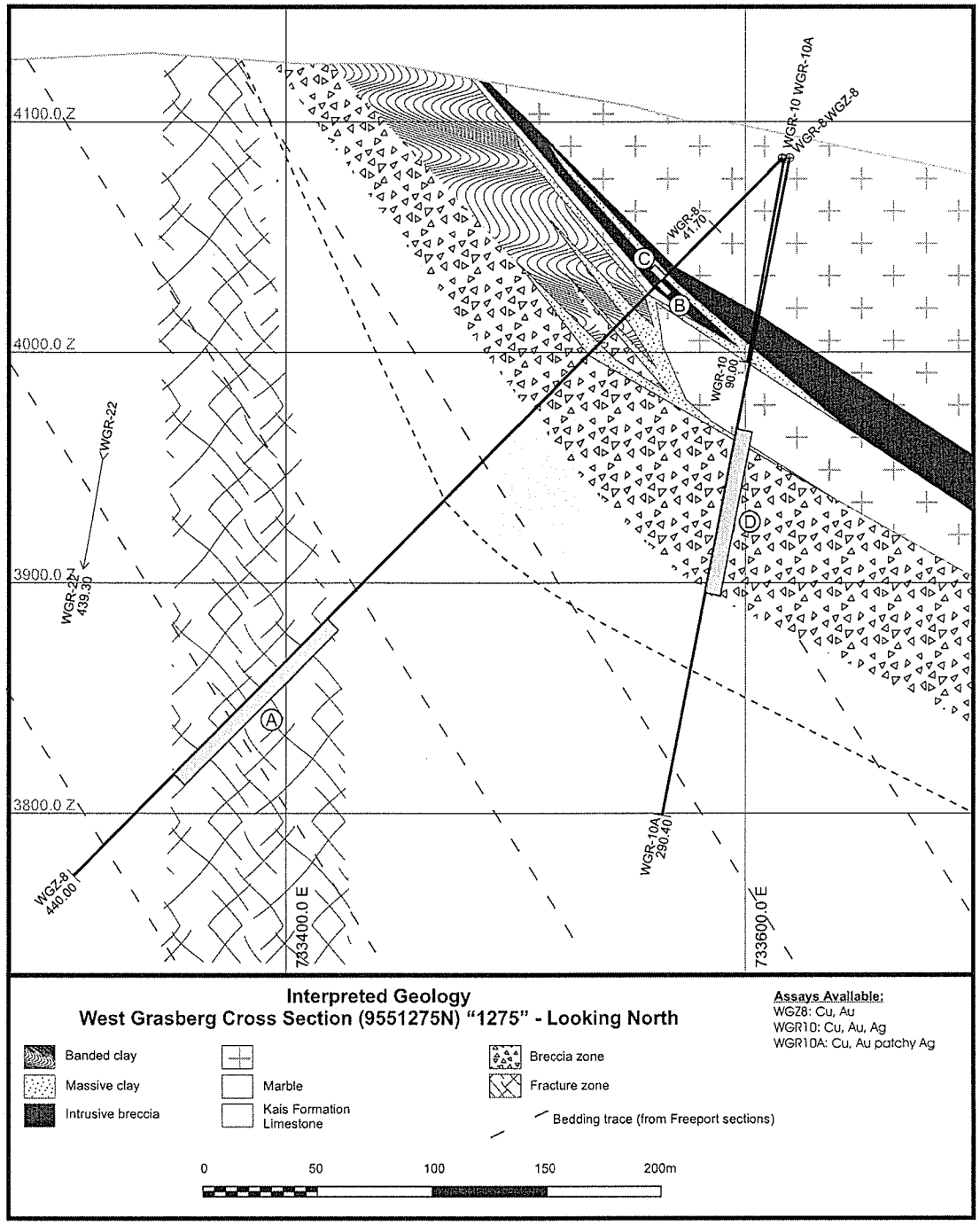

Figure A-6g. West Grasberg cross sections. Bedding trends and surface geology derived from Freeport Indonesia cross sections. West Grasberg drill logs in Appendix 6. Section 1475. BXI was intersected in WGR13 (263-304m). Significant intersections include: A) (162-165m, 0.78g/t Au and 171-174m, 0.61g/t Au) Minor gold in fractured marble. B) (198-261m, 1.15g/t Au) NE gold-bearing limestone breccia zone. C) (270-291m, 1.22g/t Au) Gold in BXI is coincident with black clay and pyrite alteration. D) 1-2m zone of massive sphalerite, pyrite and galena form as infill and alteration of marble at the contact with banded clay (Brannon, 1991).

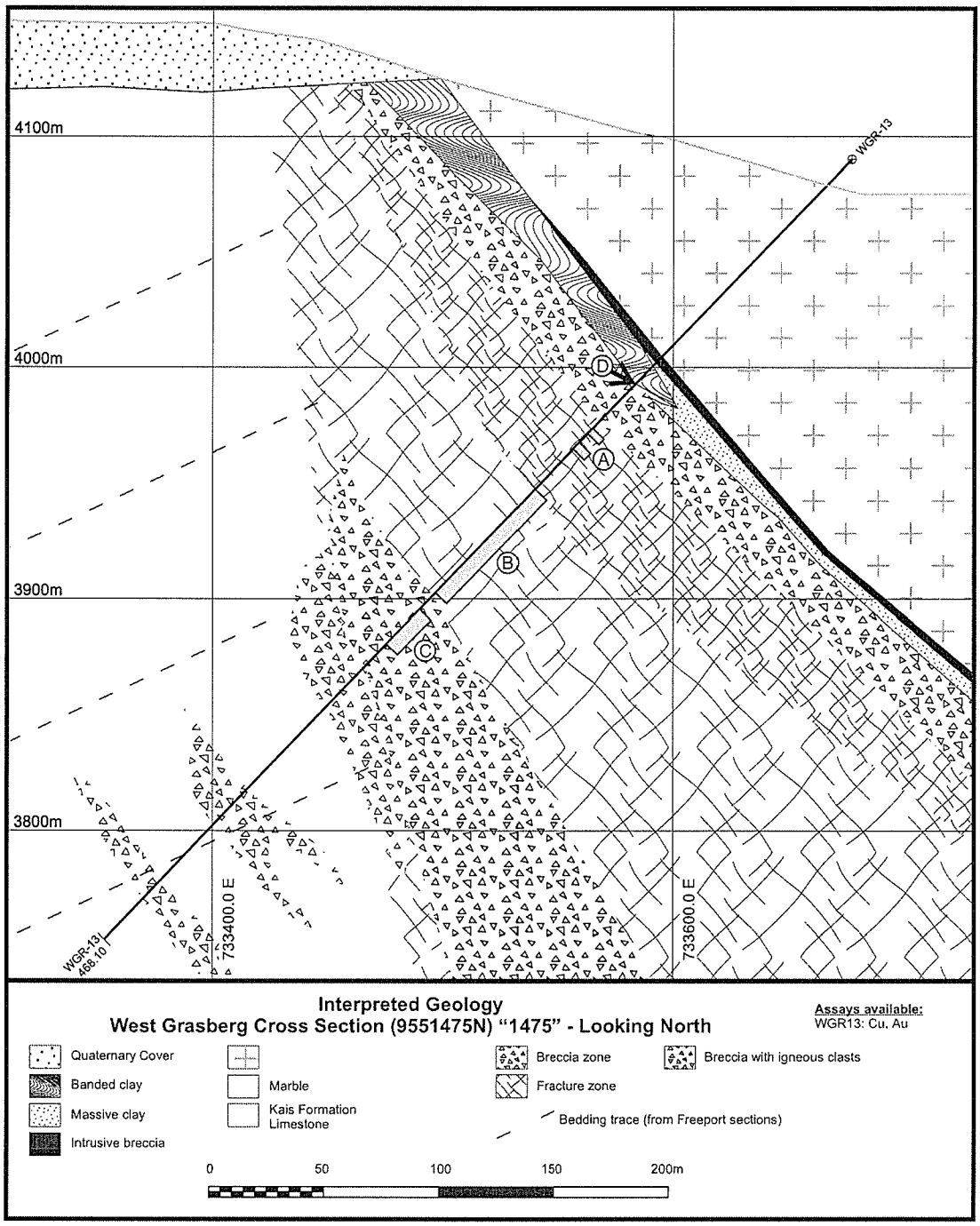

Figure A-6h. West Grasberg cross sections. Bedding trends and surface geology derived from Freeport Indonesia cross sections. West Grasberg drill logs in Appendix 6. Section 1650. Geology from PT Freeport Geological cross section. (drilllogs and core not viewed). A) (18-30m, 0.52g/t Au) Dalam breccia. B) (60-78m, 0.53g/t Au) Dalam breccia. C) (153-180m, 7.9g/t Au) Gold in fractured and skarn altered marble. D) (291-345m, 0.68g/t Au) Northern extent of NE gold-bearing limestone breccia zone.

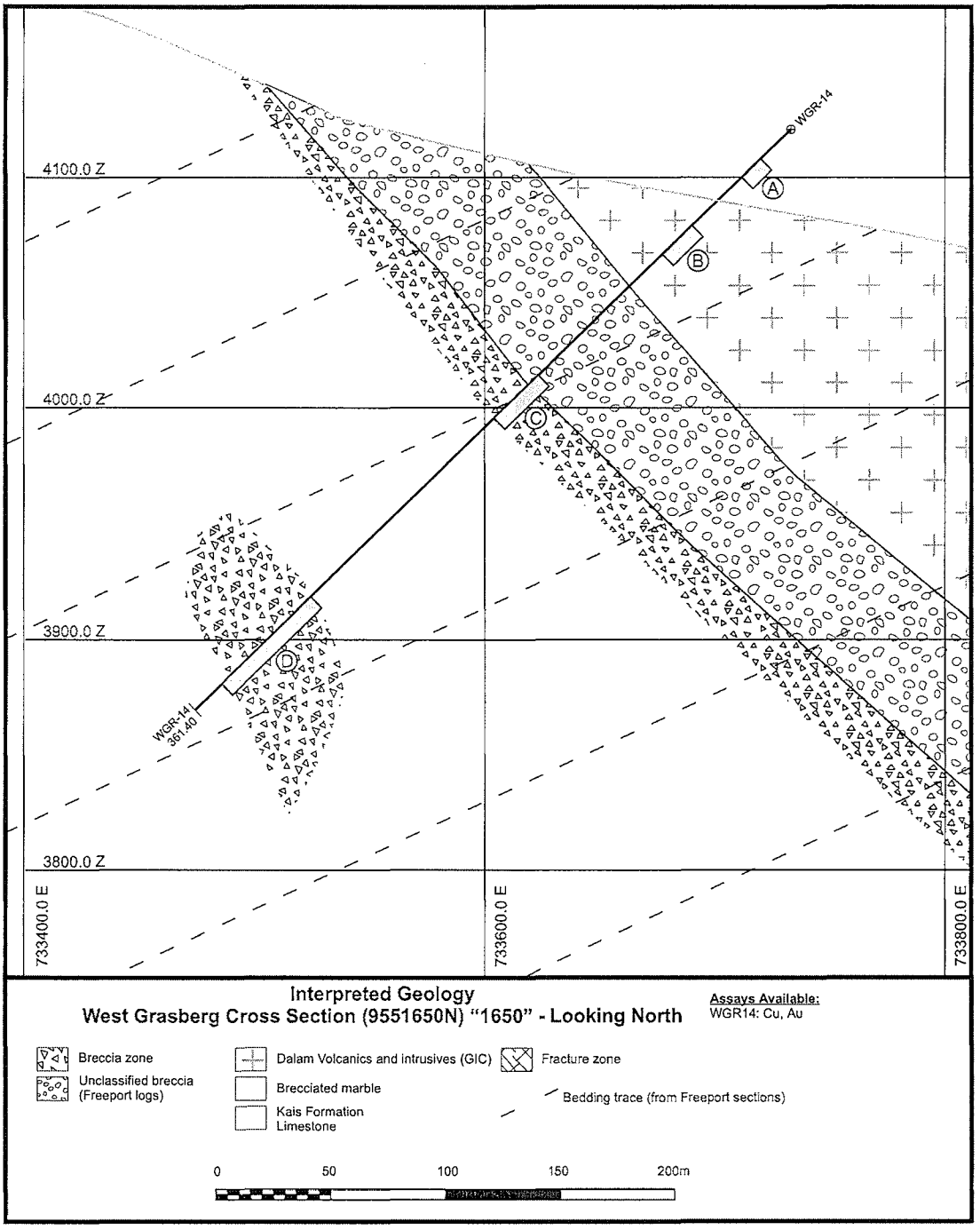

Rock Types

With the exception of the surface outcrop of fragmented banded clay, rock types from West Grasberg are described from drillcore samples.

Dalam breccia of the GIC

At its western contact, the GIC is comprised of Dalam volcanics and intrusives (described by McDonald and Arnold, 1994; Pollard and Taylor, 2002; Sapiie and Cloos, submitted), which appear as a matrix supported breccia with polymictic fragments of dominantly igneous composition. At West Grasberg, the fragments and matrix are intensely altered by magnetite, sericite, epidote, pyrite, at least two potassic assemblages, texture destructive illite and minor 10Å halloysite (Table A-1). Due to intense potassic and clay alteration, it is not certain that all the igneous-dominated material intersected in drillholes is Dalam breccia.

Intrusive breccia

This breccia dips approximately 40° to the east, varies in width from 1.5 to 22m and potentially extends for 700m strike at the margin of the GIC (Figure A-6a, e-g). Fragments are polymictic, highly rounded, generally less than 3cm in size and matrix supported (Figure A-7a, f). Compositionally, fragments and matrix are dominated by sulphides (chalcopyrite, pyrite, covellite, sphalerite and galena), with lesser epidote, igneous fragments and clay. The surface intersection and distribution of the intrusive breccia at depth are unknown although it appears to follow the GIC contact (Figure A-6f).

Banded clay

The banded-clay was interpreted by Brannon (1991) as a continuous zone up to 40m thick. However, outcrop and drillcore reveal that zones of massive non-banded clay also occurs and both clay types are highly fragmented and convoluted (Figure A-2c-e; Figure A-7b-e). Continuous zones of banded-clay are not more than 20cm wide in drillcore. Banded and non-banded clay are crosscut by the intrusive breccia, fractures filled with white clay and other zones of breccia (Figure A-2d; Figure A-7a-e). The zones of breccia observed in outcrop and drillcore contain fragments of black shale, banded clay and strongly altered fragments interpreted as igneous rock (Taylor, 2003). The banded clay surface outcrop is overlain by a thin soil horizon and further banded sediments with low angle crossbeds (Figure A-2c) considered to be fluvioglacial deposits by Cloos (pers comm. 2002).

Banded clay is characterised by grey and white clay bands (1-10mm thick). No difference between the composition of the white and grey bands was distinguished using the XRD technique. The dominant clay types in both the white and grey bands of the banded clay samples produce XRD peaks at 10Å and 7.2Å and are interpreted to be halloysite-kaolin (Table A-1; Figure A-9).

Table A-1. Summary of XRD results from West Grasberg.

X = major component; (x) minor component; ? = unclear or unable to confirm. Other minerals listed in brackets are minor components. Techniques are described fully in Appendix 1 and include XRD (XRD analysis of sample prepared by smear mount method); GLY (treating with ethylene glycol at 60°C for at least 8 hours); H400 (heat to 400°C for at least ½ hour); H500 (heat to 550°C for at least ½ hour), GADDS (non-destructive in situ XRD analysis of hand specimen samples).

AAC Sample#	Drillhole	Depth (m)	Lithology	Description of material analysed	10A halloysite	7A Halloysite-Kaolin	Kaolinite	Illite	Smectite-mica/illite	Smectite	Smectite-chlorite	Vermiculite	Chlorite	Other minerals	Technique	Comments
3752-12	WGZ8	117.0	Banded clay	Black-grey and white clay band	X	(x)									XRD,GLY,H400	
3752-13	WGZ8	117.0	Banded clay	White clay band	X	(x)									XRD,GLY,H400	
3752-43	WGZ8	90.0	Banded clay	White bleached - banded clay	X										XRD,GLY,H400	
3752-03	WGZ8	92.5	Clay	White and grey clay (not-banded)		X		(x)		?					XRD,GLY,H400,H500	14A area disordered and difficult to identify if smectite
3752-06	WGR12	43.3	Clay	White clay - no texture	(x)	X				(x)					XRD,GLY,H400	14A area disordered and difficult to identify
3752-15	WGZ8	69.5	Clay	white clay - no texture		X									XRD,GLY,H400	
3752-20	WGZ8	76.6	Clay	Grey and black and white mottled clay (not banded)	(x)	(x)								galena, pyrite, woodhouseite	XRD,GLY,H400	Example of grey colouration due to sulphides (3m assay interval = 234g/t Au)
3752-41	WGZ8	48.0	Dalam Diatreme	Intrusive breccia - white clay	X	(x)		(x)						K-feldspar	XRD,GLY,H400	
3752-42	WGZ8	39.0	Dalam Diatreme	Intrusive breccia - white clay				X				(x)		quartz, K-feldspar	XRD,GLY,H400	
3752-50	WGZ8	48.0	Dalam Diatreme	Intrusive breccia - white clay	?			?							GADDS	Unable to confirm if illite or halloysite from GADDS result alone
3752-51	WGZ8	48.0	Dalam Diatreme	Intrusive breccia - white clay	?			?						K-feldspar	GADDS	Unable to confirm if illite or halloysite from GADDS result alone
3752-18	WGR12	367.0	Limestone	Leached carbonate rock, friable material from leached zones										calcite	XRD,GLY,H400	
3752-21	WGR12	369.5	Limestone Breccia	Black on fracture and white alteration of limestone (crackle zone)	(x)				(x)					calcite, dolomite	XRD,GLY,H400	(3m assay interval = 188g/t Au)
3752-08	WGZ8	387.5	Limestone Breccia	White clay and minor pyrite fracture fill in dark grey limestone				X						calcite, pyrite	XRD,GLY,H400	(3m assay interval = 018g/t Au)
3752-04	WGZ8	370.0	Limestone Breccia	Clay and pyrite bearing matrix from limestone breccia. Breccia is fine grained with matrix supported rounded fragments of limestone (crackle zone)	(x)						(?)			quartz, calcite, K-feldspar, pyrite	XRD,GLY,H400,H500	Disordered and difficult to identify if smectite (3m assay interval = 08g/t Au)
3752-05	WGZ8	307.0	Limestone Breccia	Black slickenside material						X				pyrite, quartz, calcite	XRD,GLY,H400,H500	(3m assay interval = 005g/t Au)
4612-319	WGZ8	166.0	Limestone Breccia	Black-vitreous clay on fracture (crackle zone)	X							X			XRD,GLY,H400,H500	(3m assay interval = 28g/t Au)

AAC Sample#	Drillhole	Depth (m)	Lithology	Description of material analysed	10A halloysite	7A Halloysite-Kaolin	Kaolinite	Illite	Smectite-mica/illite	Smectite	Smectite-chlorite	Vermiculite	Chlorite	Other minerals	Technique	Comments
4612-327	WGR12	302.2	Limestone Breccia	Black carbonaceous? on fractures			(x)		X						XRD,GLY,H400,H500	(3m assay interval = 14g/t Au)
4612-329	WGR3	15.2	Limestone Breccia	Clay-black breccia matrix			X					X		pyrite, quartz, calcite	XRD,GLY,H400,H500	(3m assay interval = 037g/t Au)
4612-328	WGR12	168.6	Limestone Breccia	Clay-black breccia matrix		(x)					X	X			XRD,GLY,H400,H500	(3m assay interval = 534g/t Au)
4612-332	WGR12	177.0	Limestone Breccia	Clay-black breccia matrix		X	(x)				X			quartz, pyrite	XRD,GLY,H400,H500	(3m assay interval = 402g/t Au)
4612-333	WGR12	173.0	Limestone Breccia	Clay-black breccia matrix			(x)				X			quartz, pyrite, muscovite	XRD,GLY,H400,H500	(3m assay interval = 284g/t Au)
4612-334	WGR12	174.3	Limestone Breccia	Clay-black breccia matrix		(x)	X				X			quartz, pyrite	XRD,GLY,H400,H500	(3m assay interval = 308g/t Au)
4612-335	WGR12	294.6	Limestone Breccia	Clay-black breccia matrix		X			X					quartz, pyrite	XRD,GLY,H400,H500	(3m assay interval = 57g/t Au)
3752-19	WGZ8	316.0	Limestone Breccia	Clay-black breccia matrix		X				?		?	(x)	calcite, quartz (pyrite)	XRD,GLY,H400	14A area Disordered and difficult to identify if smectite or vermiculite (3m assay interval = 373g/t Au)
3752-01	WGR12	37.0	Translucent clay	Opaque green-grey material		X									XRD,GLY,H400,H500	
3752-14	WGZ8	69.5	Translucent clay	Grey translucent material		X		X							XRD,GLY,H400	
3752-44	WGR12	30.0	Translucent clay	Opaque green-grey material	X							X		Jarosite	XRD,GLY,H400	
3752-47	WGZ8	94.0	Translucent clay	Opaline material	X										XRD,GLY,H400	
3752-02	WGZ8	92.5	Sulphide in clay	Disseminated pyrite and white clay in white clay host	X			X		(?)		(?)	(?)	pyrite	XRD,GLY,H400,H500	14A area disordered and difficult to identify
3752-07	WGR12	43.3	Sulphide in clay	Hairline brown vein within unidentified clay host rock.	(x)	X							(x)	pyrite	XRD,GLY,H400	
3752-54	WGZ8	64.0	Sulphide fragment	Sphalerite fragment in gritty breccia. Calcite present with fragment	X									sphalerite, pyrite, chalcopyrite (galena)	GADDS	Sphalerite peaks overlap with pyrite Unclear if present
3752-57	WGZ8	77.0	Sulphide	Black hairline veinlets in bleached white clay rock										pyrite, ?sphalerite? (galena)	GADDS	Sphalerite peaks overlap with pyrite Unclear if present (3m assay interval = 234g/t Au)
3752-57b	WGZ8	77.0	Sulphide	Black hairline veinlets in bleached white clay rock										sphalerite (galena, chalcopyrite)	GADDS	(3m assay interval = 234g/t Au)
3752-57c	WGZ8	77.0	Sulphide	Black hairline veinlets in bleached white clay rock										pyrite, ?sphalerite? (galena)	GADDS	Sphalerite peaks overlap with pyrite Unclear if present (3m assay interval = 234g/t Au)
3752-40	WGZ8	63.2	Yellow-white infill	Yellow-white in fracture network (displacing sulphides)	X					(?)				pyrite, woodhouseite	XRD,GLY,H400	Disordered 15A peak difficult to identify
3752-45	WGZ8	94.0	Yellow-white infill	Yellow crystals	(x)	(x)				?				?allophane	XRD,GLY,H400	Disordered 15A peak difficult to identify
3752-46	WGZ8	94.0	Yellow-white infill	White clay with yellow crystals	X					?				allophane, alunite	XRD,GLY,H400	Disordered 15A peak difficult to identify
3752-48	WGZ8	118.0	Yellow-white infill	White clay with yellow crystals	X									allophane?	GADDS	
4612-323			Tuffaceous outcrop sample	Banded clay area of volcanic sample				X					(x)	K-feldspar, quartz (plagioclase)	XRD,GLY,H400,H500	Outcrop
4612-325			Tuffaceous outcrop sample	Very fine grained non-banded fragmental part of volcanic sample				X					(x)	K-feldspar, quartz (plagioclase)	XRD,GLY,H400,H500	Outcrop
3752-39	P3850-28	48.7	Clay	Analysis of white banded clay documented by Kavileris (1994)	X								X		XRD,GLY,H400	

Non-banded clay is mottled grey and white. Grey and black colouration in some samples is attributed to chlorite (sample 3752-03) and minor sulphides (sample 3752-20; pyrite and galena; Table A-1). Sporadic opaline silica nodules (up to 5cm) were reported from the clay with an increase in nodules in the higher-grade zones (Brannon, 1991). No silica nodules were observed during this study although translucent material with a nodule-like form was analysed by XRD from areas of non-banded clay and found to be dominantly composed of 10Å and 7Å halloysite with minor illite and smectite (Table A-1).

Marble and Marble Breccia.

Marble is observed in most drillholes, at the contact between the West Grasberg clay units and New Guinea Limestone. The marble is varyingly brecciated and mineralised and evidence of several episodes of brecciation is present locally (Figure A-7g-j). The marble breccia is mainly monomict with subangular to rounded fragments that range in size from sub-millimetre to 10cm. Other fragments recognised include sphalerite, galena (Figure A-7h), pyrite and chalcopyrite and rare igneous fragments. The matrix is generally composed of fine-grained grey-white marble. In places, the matrix is fractured and altered by dark-grey to black bitumen alteration accompanied by fine-grained pyrite (Figure A-8f). On Section 1275 in WGZ8, zones of competent marble <2m occurring between 1-4m zones of brecciated marble could be large fragments. Massive textureless mottled marble occurring between banded clay intersections may also be fragments (Figure A-6f).

The grey-white mottled marble breccia fragments on the northern sections (1475 & 1650) are angular fragment supported with minor matrix. A broad crackle zone extends into adjacent limestone. Minor black shale fragments are present and an overprinting arcuate fracture pattern contains abundant pyrite. The brecciated marble hosts yellow-green phlogopite as infill between angular fragments and alteration of pale matrix (Figure A-7j). Sulphides are

Figure A-7. Photographs of hand specimens from drillcore at West Grasberg. a) (WGZ8, 64.2m) White bleached banded clay crosscut by pyrite-rich intrusive breccia containing clasts of sphalerite. b) (WGZ8, 95m) Grey clay and clasts of pyrite crosscut by fractures containing white clay. c) (WGZ8, 94m) Non-banded fragmented grey and white clay crosscut by a zone of white clay and allophane. d) (WGZ8, 96.1m) Void in banded clay containing growth of allophane. e) (WGR12, 92.5m) Partly banded grey and white clay (3752-03 XRD result: smectite, 7Å halloysite and illite) crosscut by white clay and pyrite (3752-02 XRD result: illite, jarosite, and minor 10Å halloysite, chlorite and talc). f) (WGZ8, 64m) Intrusive breccia. Fragments of sphalerite (black) and pyrite. Matrix is dominated by fine-grained pyrite and clay. g) (WGR12, 100.4m) Two marble/limestone breccias (breccia 1 and 2) overprinted by very fine grained pyrite and black clay or bitumen. h) (WGZ8, 136m) Marble breccia with two generations of brecciation (breccia 1 and 2) and a galena fragment. Both breccia stages are overprinted by pyrite and black clay or bitumen. i) (WGR13, 201m) Marble-limestone breccia overprinted by pyrite and black bitumen. j) (WGR13, 153m) Marble breccia with phlogopite alteration of matrix. Minor epidote and pyrite also present. k) (WGR13, 309-312m) Crackle limestone breccia. Degree of black alteration and fracture fill increases with degree of fracturing. l) (WGZ8, 307m) Milled limestone breccia with rounded fragments and clay matrix (306-309m, 0.02% Cu and 0.05g/t Au).

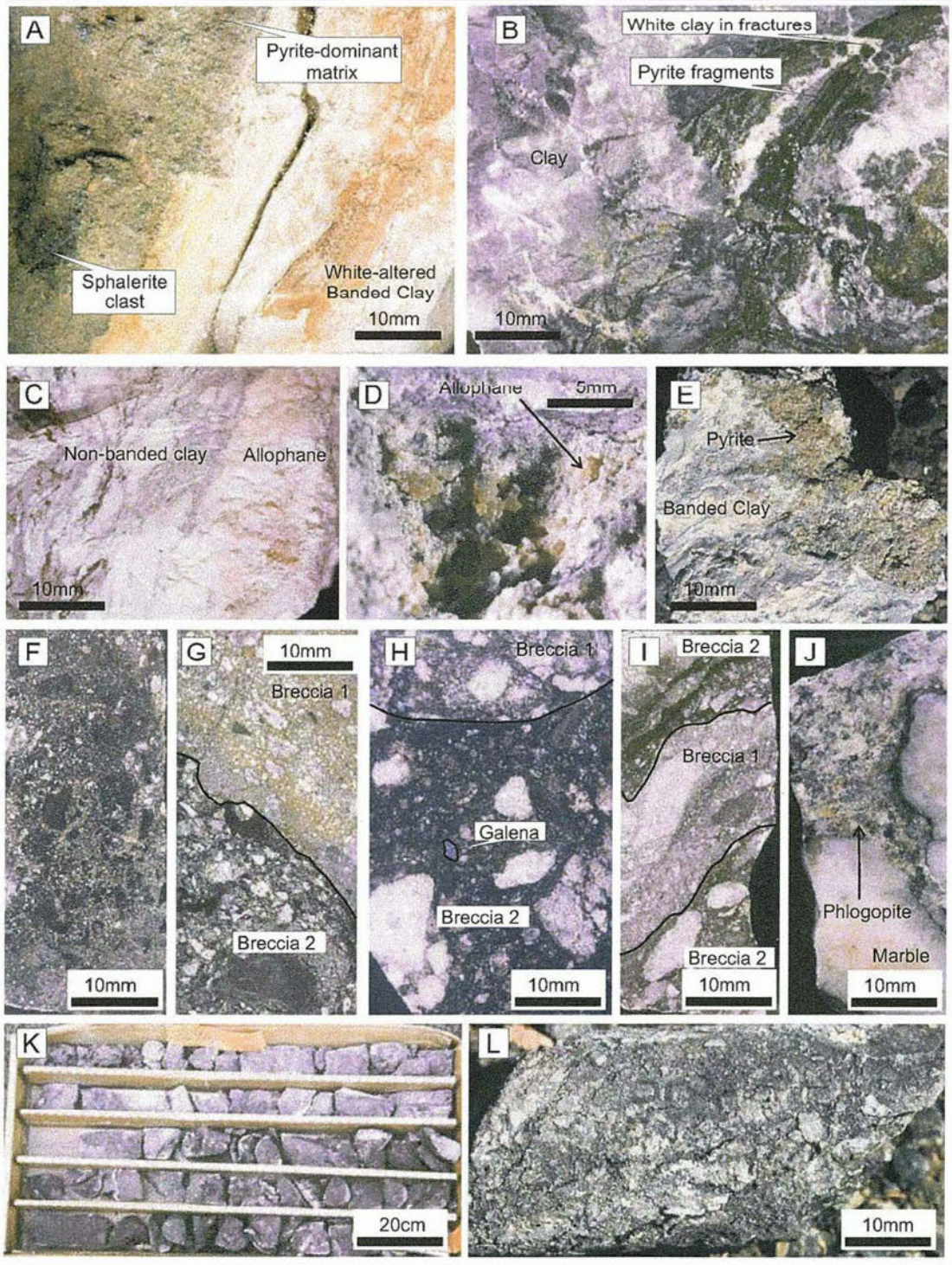
A
Pyrite-dominant matrix
Sphalerite clast
White-altered Banded Clay
10mm
B
White clay in fractures
Pyrite fragments
Clay
10mm
C
Non-banded clay
Allophane
10mm
D
Allophane
5mm
E
Pyrite
Banded Clay
10mm
F
10mm
G
10mm
Breccia 1
Breccia 2
H
Breccia 1
Galena
Breccia 2
10mm
I
Breccia 2
Breccia 1
Breccia 2
10mm
J
Phlogopite
Marble
10mm
K
20cm
L
10mm

present as alteration throughout the phlogopite-altered breccia matrix and as infill in fractures that crosscut the phlogopite. Fractures containing white clay crosscut unbroken marble (Figure A-6c).

New Guinea Limestone Group and brecciated limestone zones.

Several brecciated zones have been documented in mapping and intersected by drilling in the Kais Formation west of the GIC contact. Fragments are dominantly limestone although isolated occurrences of igneous (WGR13; 433-444m) or epidote fragments (WGR11, 260-263) are known. Two textural styles are represented in the breccias. The dominant style is fragment-supported with a crackle fracture pattern (Figure A-7k). The crackle breccias often contain minor pyrite but no significant gold mineralisation (Figure A-6e). Brannon (1991) reported carbonaceous material in the matrix. XRD results from this study identified vermiculite, smectite, mixed-layer illite-smectite, halloysite, kaolinite and pyrite (Table A-1). Illite was identified with pyrite on a fracture within the limestone crackle zone (Table A-1: 3752-08).

The second breccia style displays local evidence for extensive movement and/or milling of fragments and has a grey clay matrix (Figure A-7l). This milled breccia style is recognised in two main locations (Brannon, 1991) as steeply dipping tabular zones up to 40m wide (Figure A-5). One broad vertical zone strikes NNE (Figure A-5; Figure A-6f-h) and occurs parallel to a mapped northeast structure. The second strikes WNW (Figure A-5; Figure A-6a, b) parallel to regional bedding. The milled breccias occur in the centre of crackle breccia zones whereby the intensity of the crackle fracture breccias increase towards the milled breccias. XRD analysis identified smectite-chlorite clay (Figure A-9) in addition to pyrite, vermiculite, kaolinite, halloysite, smectite-micas, and minor chlorite (Table A-1).

Figure A-8. Photographs and reflected light photomicrographs of West Grasberg sulphide mineralogy (Ccp=chalcopyrite; Gn=galena; Py=pyrite; Sp=sphalerite; Tet= Tetrahedrite-tennantite). a) (WGR13, 162m) Banded massive sulphide (pyrite, sphalerite, galena, chalcopyrite) replacement of marble-limestone. b) (WGZ8, 77m) White clay with hairline black veinlets of pyrite, sphalerite and chalcopyrite (identified by XRD; Table 1). c) (WGR13, 173m) Reflected light photomicrograph of massive sulphide replacement in limestone. Sphalerite, chalcopyrite, and galena surround and fill fractures in euhedral pyrite. Galena appears late. d) (WGR13, 199.2m). Reflected light photomicrograph of massive sulphide replacement in limestone. Tetrahedrite-tennantite, galena and pyrite occur as infill in fractures in sphalerite. Sphalerite exhibits chalcopyrite disease. e) (WGR13, 199.2m) Reflected light photomicrograph of massive sulphide replacement in limestone. Fine-grained framboidal pyrite overprints earlier coarse pyrite and sphalerite (grey). f) (WGR13, 201m) Limestone and marble breccia (Figure A-7i) reflected light photomicrograph. Coarse grained Stage 1 pyrite is present in the breccia matrix. Fine-grained bitumen and a second generation of framboidal pyrite crosscut the breccia. g) (WGR13, 201m) Limestone and marble breccia (Figure A-7i) reflected light photomicrograph. Grey sphalerite is surrounded by fine-grained bitumen and a generation of fine-grained pyrite. h) (WGR13, 201m) Limestone and marble breccia (Figure A-7i) reflected light photomicrograph. Coarse-grained Stage 1 pyrite surrounded by a second stage of fine-grained pyrite. i) (WGR13, 201m) Limestone and marble breccia (Figure A-7i) reflected light photomicrograph. Fine-grained framboidal pyrite associated with bitumen in Figure A-8f.

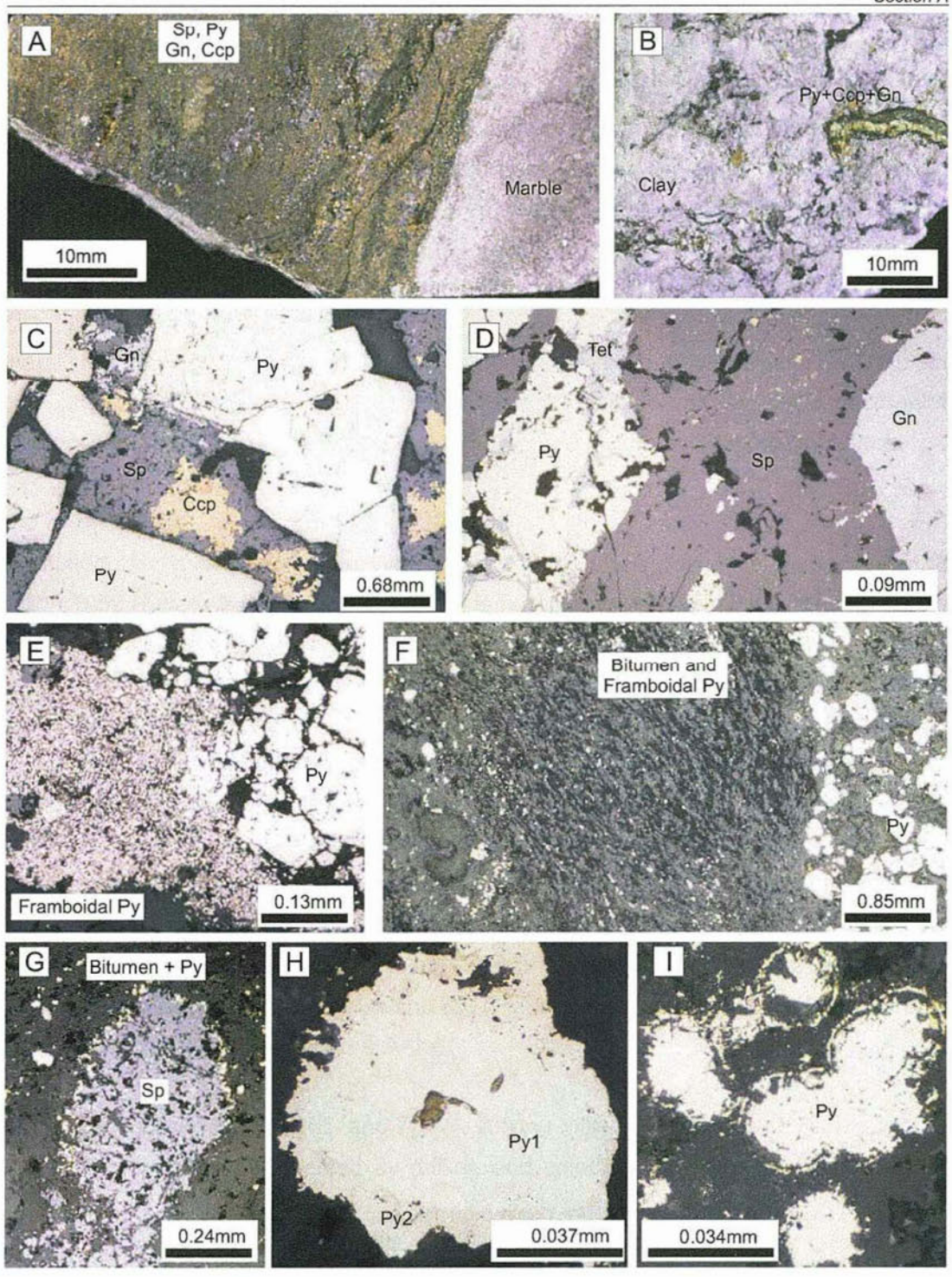
A
Sp, Py
Gn, Ccp
Marble
10mm
B
Py+Ccp+Gn
Clay
10mm
C
Gn
Py
Sp
Ccp
Py
0.68mm
D
Tet
Gn
Py
Sp
0.09mm
E
Py
Framboidal Py
0.13mm
F
Bitumen and
Framboidal Py
Py
0.85mm
G
Bitumen + Py
Sp
0.24mm
H
Py1
Py2
0.037mm
I
Py
0.034mm

BXI (breccia with igneous fragments) in limestone

Areas of breccia dominated by fragments of an igneous composition (BXI) hosted in Kais Formation were intersected in drillholes on Section 0950 and 1475. (Figure A-6a, g). The relationship between the occurrences is unconstrained. On Section 1475 the breccia contains variably altered igneous fragments. The matrix is not affected by K-feldspar alteration which is present in fragments, indicating fragments were altered before incorporation into the breccia. Rare limestone fragments are also present.

Distribution of mineralisation

Mineralisation constrained from drill core observation and drillhole assays (Cu, Au and incomplete Ag) includes gold only, copper only and lead-zinc-silver. The depth of complete oxidation is shallow as fresh sulphides occur in banded clay from 20m below surface.

Gold distribution

Gold distribution is not host rock dependent as elevated gold occurs in all rock types. On Section 1050 (Figure A-6c), gold (<12.9ppm) is hosted within a brecciated zone containing fragments of marble, limestone, altered igneous material and clay and sulphide rubble. On Section 1175 (Figure A-6e) gold is present in both the intrusive breccia and adjacent banded-clay. On Section 0950 gold occurs in banded clay (Figure A-6a). Elevated gold is documented from the intrusive breccia on Section 1275 (Figure A-6f). Only low levels of gold are recorded from isolated occurrences in the Dalam breccia (Figure A-6h). Gold mineralisation is only documented from the marble where it is fractured (Figure A-6e-h). Four gold occurrences are at lithological contacts namely a) on Section 1650 where gold mineralisation up to 21.33g/t is present at the contact between marble breccia and an unclassified breccia (Figure A-6h), b) at the contact between banded-clay and limestone (Figure A-6c), c) a broad zone along the contact between limestone breccia and BXI (Figure A-6g) and d) along the Dalam breccia and intrusive breccia contact (Figure A-6a).

Gold is concentrated in the NNE- and WNW- striking milled limestone breccias west of the GIC. Both zones were intersected by drilling and coincide with mapped breccia zones.

Figure A-9. Selected XRD traces of samples from West Grasberg. Refer to Appendix 1 for analytical technique. a) Dalam breccia (WGZ8, 48m; Sample ID 3752-41). b) Banded clay dark grey band (WGZ8, 117m; Sample ID 3752-12). 10Å halloysite and minor 7Å halloysite-kaolinite. 10Å halloysite expands slightly after glycolation and collapses to 7.2Å after heating. The 7.2Å clay could be either halloysite or kaolinite, however, given that the 7.2Å phase expands slightly after glycolation and then collapses after heating, it is interpreted as halloysite. c) Banded clay white band (WGZ8, 117m; Sample ID 3752-13). Same composition as Figure A-9b. d) White pervasive clay alteration is dominantly 10Å halloysite (WGZ8, 90m; Sample ID 3752-43). e) Yellow crystals with white clay (WGZ8, 94m; Sample ID 3752-46). Allophane displays a broad disordered peak at 15Å. Microprobe analysis confirmed a composition of Al and Si. f) Black matrix from limestone breccia (WGR12, 177m; Sample ID 4612-332). The 14Å peak could be smectite-chlorite or smectite. It expands slightly after GLY and then collapses to 10Å after H400. As the 10Å peak intensifies slightly after H500, it is likely chlorite is present.

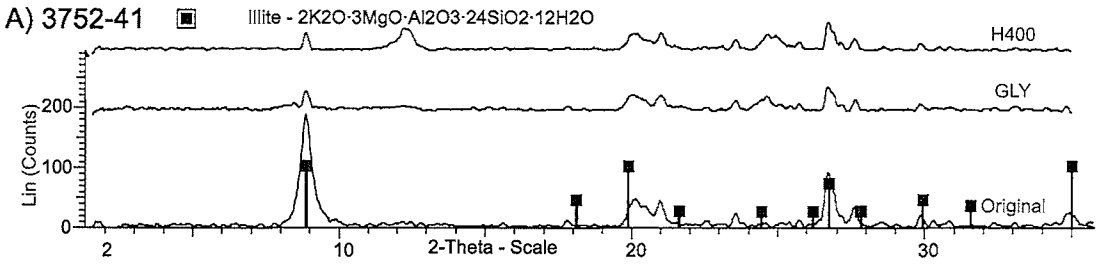
A) 3752-41
Illite - 2K2O·3MgO·Al2O3·24SiO2·12H2O
H400
GLY
Original
Lin (Counts)
2-Theta - Scale

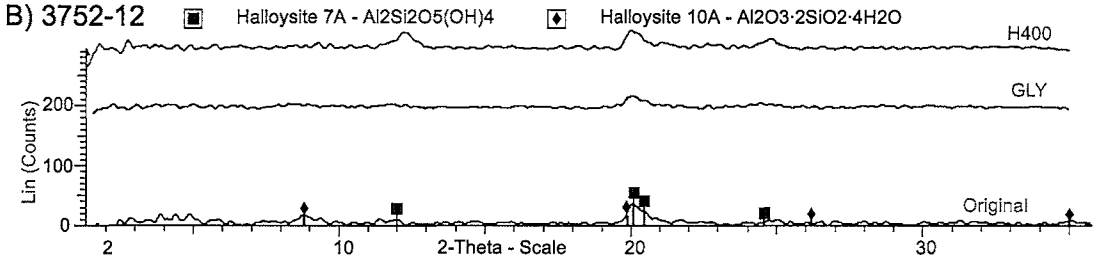
B) 3752-12
Halloysite 7A - Al2Si2O5(OH)4
Halloysite 10A - Al2O3·2SiO2·4H2O
H400
GLY
Original
Lin (Counts)
2-Theta - Scale

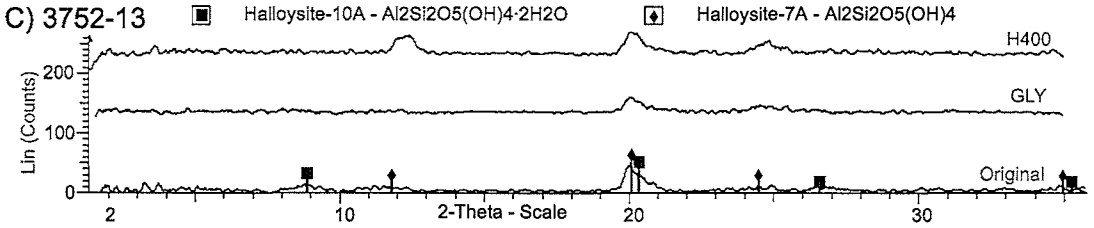
C) 3752-13
Halloysite-10A - Al2Si2O5(OH)4·2H2O
Halloysite-7A - Al2Si2O5(OH)4
H400
GLY
Original
Lin (Counts)
2-Theta - Scale

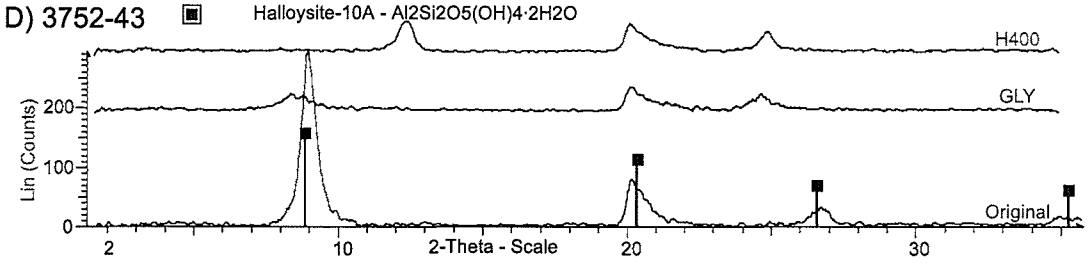
D) 3752-43
Halloysite-10A - Al2Si2O5(OH)4·2H2O
H400
GLY
Original
Lin (Counts)
2-Theta - Scale

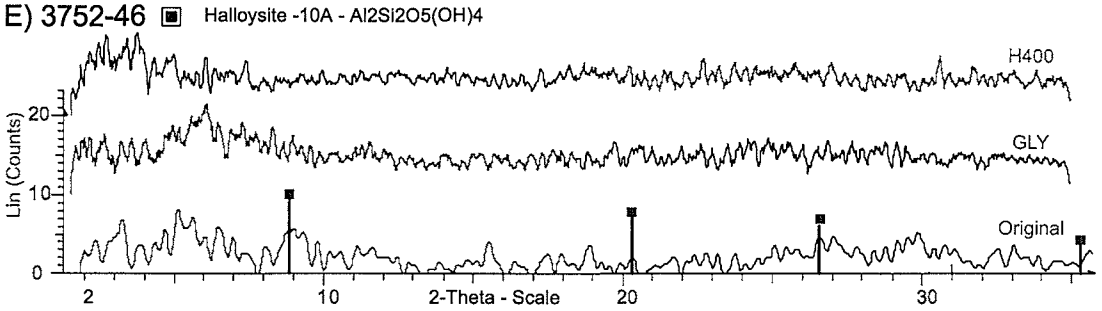
E) 3752-46
Halloysite -10A - Al2Si2O5(OH)4
H400
GLY
Original
Lin (Counts)
2-Theta - Scale

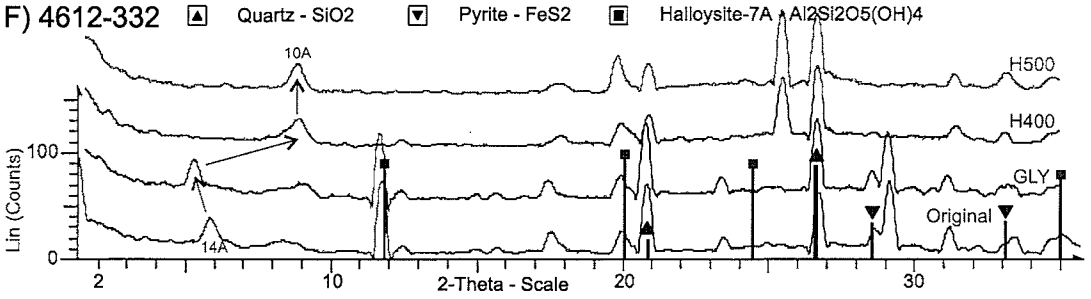
F) 4612-332
Quartz - SiO2
Pyrite - FeS2
Halloysite-7A - Al2Si2O5(OH)4
10A
14A
H500
H400
GLY
Original
Lin (Counts)
2-Theta - Scale

Comparison of mapped surface features and drillhole intercepts was used to determine the distribution and controls on gold mineralisation. The gold-enriched zone in the NNE-trending breccia body plunges SSW (Figure A-10). On Section 1475 (Figure A-6g), gold only occurs in the NNE limestone breccia where it is coincident with grey-clay and milled breccia zones. The adjacent BXI also contains variable gold concentrations up to 2.21g/t (263-304m) and coincident black-grey alteration (Figure A-6g). Gold enrichment in the WNW breccia zone (Figure A-6a, b) may be discontinuous along strike to the west where the projected breccia zone was not intersected by drillhole WGR19A (Figure A-5; Figure A-6d). On Section 1100, there are occurrences of gold in a separate limestone breccia body (Figure A-6d).

Lead-zinc-silver distribution

As there are no lead or zinc assays, distribution of lead-zinc-silver is constrained from drill core observation and corresponding silver assays. Zones of massive galena-sphalerite-pyrite up to several metres thick with sharp contacts have been recorded from the lithological contact between the banded clay and marble (Figure A-6g) and also within the banded clay (Brannon, 1991). On Section 0950, vuggy sphalerite-galena-fluorite veins occur in mottled grey marble (Figure A-6a). A number of outcrop occurrences of fluorite-sphalerite-galena veins were reported by Kavalieris (1992). Lead and zinc mineralisation is also present as

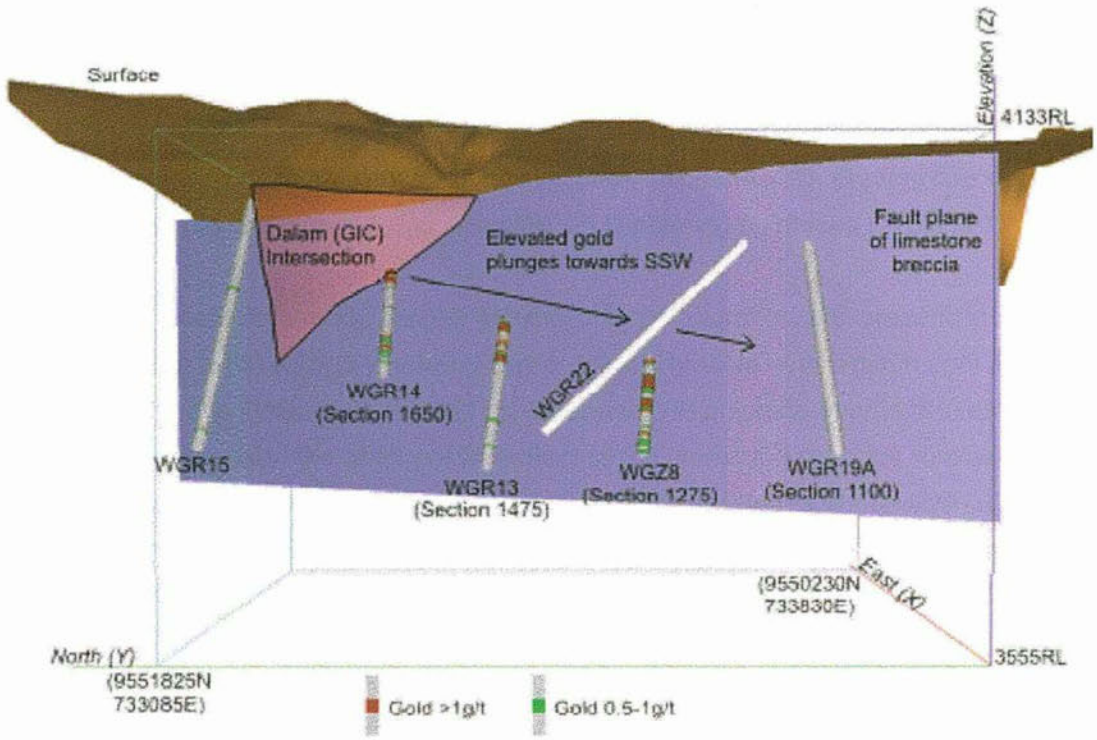

Figure A-10. 3D Isometric view (looking east) of the NNE-trending limestone breccia. Drillholes WGR22 and WGR19A do not intersect gold enriched zones suggesting that these may plunge towards the SSW. (Projection WGS84, UTM zone 53).

sphalerite and galena fragments within the intrusive breccia and have corresponding elevated silver assays (Figure A-6e). High silver values in limestone on Section 1050, (WGR6; no core or drilllogs viewed) could also correspond to base metal veins (Figure A-6c).

Copper distribution

Copper mineralisation in the Dalam breccia is not economically significant. Only one location at West Grasberg contains coincident elevated copper and gold and corresponds with an increase in spotty pyrite alteration in the Dalam breccia (Figure A-6e). Copper minerals in other locations are concentrated along lithological contacts including: a) the contact between Dalam breccia and banded-clay (Figure A-6a), and b) the Dalam breccia and marble contact on Section 1050 (Figure A-6c). Low levels of copper within the intrusive breccia (i.e. Figure A-6f) correspond to observed fragments of chalcopyrite and covellite. No significant copper is present on the northern Sections 1475, 1650 or 1875.

Paragenesis

The sequence of structural, hydrothermal and volcanic events at West Grasberg has been established from drillcore, outcrop and thin section examination (Table A-2). XRD analysis of clay compositions, re-assay of mineralised drillhole intervals and LA-ICPMS analysis of pyrite have been used to constrain the character of the hydrothermal events. Clay-bearing material from 39 samples was selectively analysed by XRD techniques (Table A-1) at the James Cook University Advanced Analytical Centre using a Siemens D5000 X-ray Diffractometer to provide information on the different paragenetic stages in the samples. Clay mineralogy was discriminated by treating with ethylene glycol and heating to 400°C and 500°C (Appendix 1). The Siemens General Area Detector Diffraction System (GADDS) was used for in situ routine mineral identification (Appendix 1). Supergene alunite and woodhouseite are present in 3 clay samples, all containing sulphides (Table A-1).

At least two potassic events, magnetite and chlorite alteration are present in the Dalam breccia and not in the adjacent banded clay or marble breccia. A late pyrite spot alteration is also present in the Dalam breccia and its relationship to sulphide events at West Grasberg is unclear. Additionally, the timing of formation of the limestone breccias relative to marble formation and phlogopite and epidote alteration in the marble is unconstrained. Although similar sulphide associations occur in different rock types, they cannot be conclusively correlated and are discussed separately.

Table A-2. West Grasberg paragenesis for limestone breccias, marble, marble breccias, banded clay and non-banded clay. ? = correlation between events in different rock types is unconstrained. * = Formation of intrusive breccia with respect to other sulphide events is unconstrained although intrusive breccia predates gold mineralisation. ** = Timing of gold in limestone breccias is unconstrained with respect to other sulphides.

		Limestone Breccia Matrix (Kais Formation)		Marble (Kais Formation)		Banded clay
Early	**Untimed and early events**	*Possible initial development of limestone breccias.* *Development of intrusive breccias*	?	*Formation of marble* *Brecciation of marble* *Sphalerite + galena mineralisation of marble (Stage 1?)* *Brecciation to create sphalerite+galena fragments* *Introduction of skarn sulphides to brecciated marble*	?	*Formation of banded and non-banded clay.* *Possible clay alteration or weathering in lake environment before incorporation into GIC* *Incorporation of banded clay into GIC margin*
	Sulphide events	Disseminated euhedral pyrite, sphaleite, minor galena and chalcopyrite occur in the breccia matrix and may represent more than one paragenetic stage. Disseminated fine grained framboidal pyrite ±covellite	?	(Stage 1) Pyrite, sphalerite, galena, chalcopyrite veinlets overprint skarn and marble breccia		(Stage 1) Hairline pyrite, sphalerite, galena, pyrite veinlets in clay.
			?	(Stage 2) Disseminated fine grained framboidal pyrite + secondary bitumen occur in channelways. Framboidal pyrite occurs as overgrowths on Stage 1 sphalerite and euhedral pyrite.	?	(?Stage 2) Pyrite + illite replacement of clay
?	**Structural event*			*Formation of intrusive breccia, incorporating sulphides from heavy sulphide zone.*		
?	****Stage 3 (native gold pyrite)**	Milled Breccia zones. Native gold in diaspore. Distinct XRD smectite-chlorite clay signature. Elevated gold assays coincident with abundant pyrite of unconstrained timing.	?	Native gold not observed. Elevated gold assays coincident with fine grained pyrite	?	Native gold observed by Brannon (1991)
	Structural event			*Development of fracture system in banded clay to host Stage 3*		
Late	**Late clay alteration and infill**			Halloysite and allophane		

Banded clay, marble and marble breccia

Stage 1 sulphides (pyrite, sphalerite, galena, chalcopyrite)

The earliest sulphide event produced an assemblage of pyrite, sphalerite, galena and minor chalcopyrite and is manifested as veinlets in banded and non-banded clay (Figure A-7b, Figure A-8b) and in the marble breccia. Massive sulphide replacement of limestone and marble (Figure A-8a), as well as sphalerite and galena fragments that occur in multiply brecciated marble breccia (Figure A-7h), may also have occurred in this stage.

Stage 1 sulphide minerals consistently occur together. Pyrite is present as infill and clearly predates sphalerite, chalcopyrite and galena in some samples (Figure A-8c). Evidence from other samples indicates that crystallisation of pyrite occurred throughout Stage 1. Qualitative microprobe examination indicates the sphalerite is manganese-bearing. In all samples examined, galena postdates sphalerite, forming as infill in fractures or along grain contacts (Figure A-8c, d). Minor tetrahedrite-tennantite is associated with galena (Figure A-8d). Bournonite and bornite have also been documented in association with galena from banded clay samples (Honea, 1990).

Stage 2 sulphides (fine grained pyrite/marcasite ± chalcopyrite ± galena) ± bitumen

A generation of fine-grained pyrite occurs in marble breccia (Figure A-8e-i), and may be coeval with fine-grained pyrite and associated illite that replaces banded clay (Table A-1; Figure A-7e). Minor galena and chalcopyrite inclusions occur within pyrite in marble breccia. In one occurrence, matrix alteration and network-fracture infill by bitumen is associated with fine-grained framboidal pyrite (Figure A-8f, i). The bitumen was too fine-grained for qualitative temperature estimates with a conventional microscope under oil-immersion.

Gold

Fine-grained pyrite, base metal and one gold grain were recorded from a sample (WGR12 60-63m) of banded-clay that was crushed and panned by Brannon (1991). Elevated gold assays are coincident with hairline fractures containing fine grained pyrite throughout the matrix of marble breccias. Thin section examination did not detect any bitumen and microprobe examination suggest the veinlets are comprised of very fine grained pyrite and minor clay.

Late-stage clay alteration and fracture-fill

White texture-destructive bleaching of the banded and mottled clay units and Dalam breccia decreases in intensity with depth. XRD analysis concurs with previous work (Kavalieris, 1994) in that the dominant clay mineral is 7Å halloysite-kaolinite with minor 10Å halloysite. Alteration in the banded clay created a porous bleached and leached clay rock with a lower density than the banded clay (Figure A-7a). Below the pervasive texture-destructive alteration,

fractures filled with infill of white clay and yellow crystals interpreted as allophane are developed (Figure A-7b-d). Analysis of mixtures of allophane and clay returned a poorly crystalline XRD trace (Figure A-9) with a broad 15Å peak (possibly allophane or disordered smectite) and halloysite peaks. Microprobe examination of the crystals revealed varying ratios of aluminium and silica which is consistent with the presence of a poorly crystalline amorphous aluminosilicate phase such as allophane. The fracture system is brittle and crosscuts all rock types at West Grasberg including the banded-clay, marble breccia and intrusive breccia and occurs along the GIC-banded clay contact. The allophane present with the white clay is generally observed deeper than 50m below current surface.

Limestone breccias

Euhedral pyrite, sphalerite, galena, chalcopyrite, framboidal pyrite ± covellite

Disseminated euhedral pyrite, sphalerite, galena, chalcopyrite and framboidal pyrite with covellite occur in the limestone breccias. The paragenetic sequence of sulphide minerals in the limestone breccias is unconstrained. It is also not possible to establish if the limestone breccia-hosted sulphides correlate with similar occurrences documented in the banded clay, marble and marble breccia (Table A-2). The presence of two generations of pyrite, framboidal and cubic, in limestone breccias was also noted by Honea (1990).

Gold

Native gold is rarely observed in polished section. Successful isolation of gold grains in thin section is impeded by a) the small sample size of a thin section when compared with a 3m composite assay zone and gold grades generally <3ppm gold, and b) the fragile nature of the milled limestone breccia zones which are poorly preserved during drilling and storage. Abundant fine-grained pyrite, and small grains of fine-grained, bright yellow gold were panned from a sample (WGR12 213-216m) of black shaly/clay matrix from a mineralised zone (Brannon, 1991). Honea (1990) described the gold in the limestone breccia samples to in-part corrode framboidal pyrite (suggesting a later deposition). XRD analysis of the clay gangue from gold-bearing milled limestone breccia zones identified distinct smectite-chlorite clay and minor 7Å halloysite and kaolinite (Table A-1; Figure A-9).

Microprobe analysis identified isolated gold-bearing alloys composed of Au-Cu-Zn-Ag in a pan concentrated sample from a gold-bearing limestone breccia with abundant clay (Figure A-11). Gold-alloy grains identified were hosted by an aluminosilicate with a Al:Si=5 ratio interpreted to be diaspore (Figure A-11). Other minerals identified in the sample by microprobe include, chalcopyrite, sphalerite, euhedral pyrite, framboidal pyrite with covellite, tetrahedrite-tennantite, and a Pb-Te phase (possibly altaite) containing minor gold.

Figure A-11. SEM backscatter image and energy dispersive X-ray spectra from pan concentrated sample of gold alloy contained in diaspore. WGR4, 89m: 9m composite interval 10g/tAu and 0.14%Cu. a) SEM backscatter image of gold-alloys hosted in Al-Si phase. b) Energy dispersive X-ray spectrum of gold alloy. c) Energy dispersive X-ray spectrum of Al-Si phase.

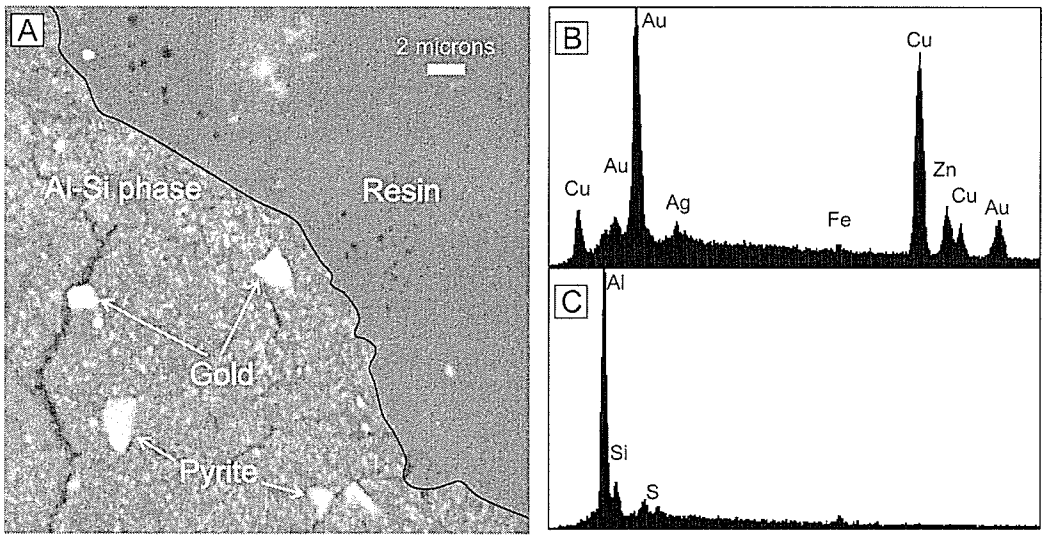

Metal associations

Re-analysis of 27 drillcore samples from West Grasberg and statistical analysis of the results was conducted to determine element associations. Element associations were derived from correlation analysis of log10 transformed data (Table A-3) and XY scatter plots (Figure A-12). Correlation analysis distinguished three groups of element association (Table A-3).

A strong correlation exists between Group 1 elements Zn-Pb-Ag-Se-Sb-Bi-As (Table A-3). V and Ni are strongly correlated with each other and most of the Group 1 elements. Copper

	Cu	*Au*	*Ag*	*Pb*	*Zn*	*Se*	*Co*	*Ni*	*Mo*	*As*	*Sb*	*Bi*	*V*
Cu	1.00												
Au	-0.37	1.00											
Ag	0.06	0.29	1.00										
Pb	-0.04	0.11	0.73	1.00									
Zn	-0.01	0.01	0.73	0.77	1.00								
Se	0.21	-0.09	0.52	0.35	0.69	1.00							
Co	0.55	-0.41	0.08	0.01	0.31	0.64	1.00						
Ni	-0.03	0.22	0.47	0.20	0.50	0.42	0.22	1.00					
Mo	0.40	-0.01	0.12	0.19	0.08	0.05	0.15	0.26	1.00				
As	-0.14	0.52	0.63	0.68	0.67	0.44	-0.05	0.39	0.58	1.00			
Sb	0.11	0.19	0.58	0.76	0.70	0.42	0.16	0.12	0.02	0.62	1.00		
Bi	0.27	0.21	0.74	0.50	0.77	0.74	0.36	0.53	-0.14	0.65	0.55	1.00	
V	0.33	0.04	0.52	0.36	0.58	0.55	0.54	0.80	0.29	0.43	0.32	0.64	1.00

>0.50 Group 1
0.55 Group 2
0.52 Group 3

Table A-3. Correlation coefficients of Log10 normalised assay results from West Grasberg samples. All West Grasberg results (Appendix 4) display a log-normal distribution and log10 transformation reduced skewness. At n=27 (number of samples), a correlation coefficient (r value) greater than 0.45 is statistically significant at the 99% confidence level (Rollinson, 1996). From the correlation coefficients, three different element groups are recognised: Group 1 (r>0.50) comprises Zn-Pb-Ag-Se-Sb-Bi-As (V and Ni correlate with one or more of the Group 1 elements); Group 2 (r=0.55) comprises Cu-Co; Group 3 (r=0.52) comprises Au-As. Below detection values = null.

Figure A-12. Bivariant pots of elements from West Grasberg samples (Appendix 4) of limestone breccia (oxidised and unoxidised), Dalam breccia, clay, marble breccia with skarn and samples of skarn and limestone breccia analysed by Brannon (1991).

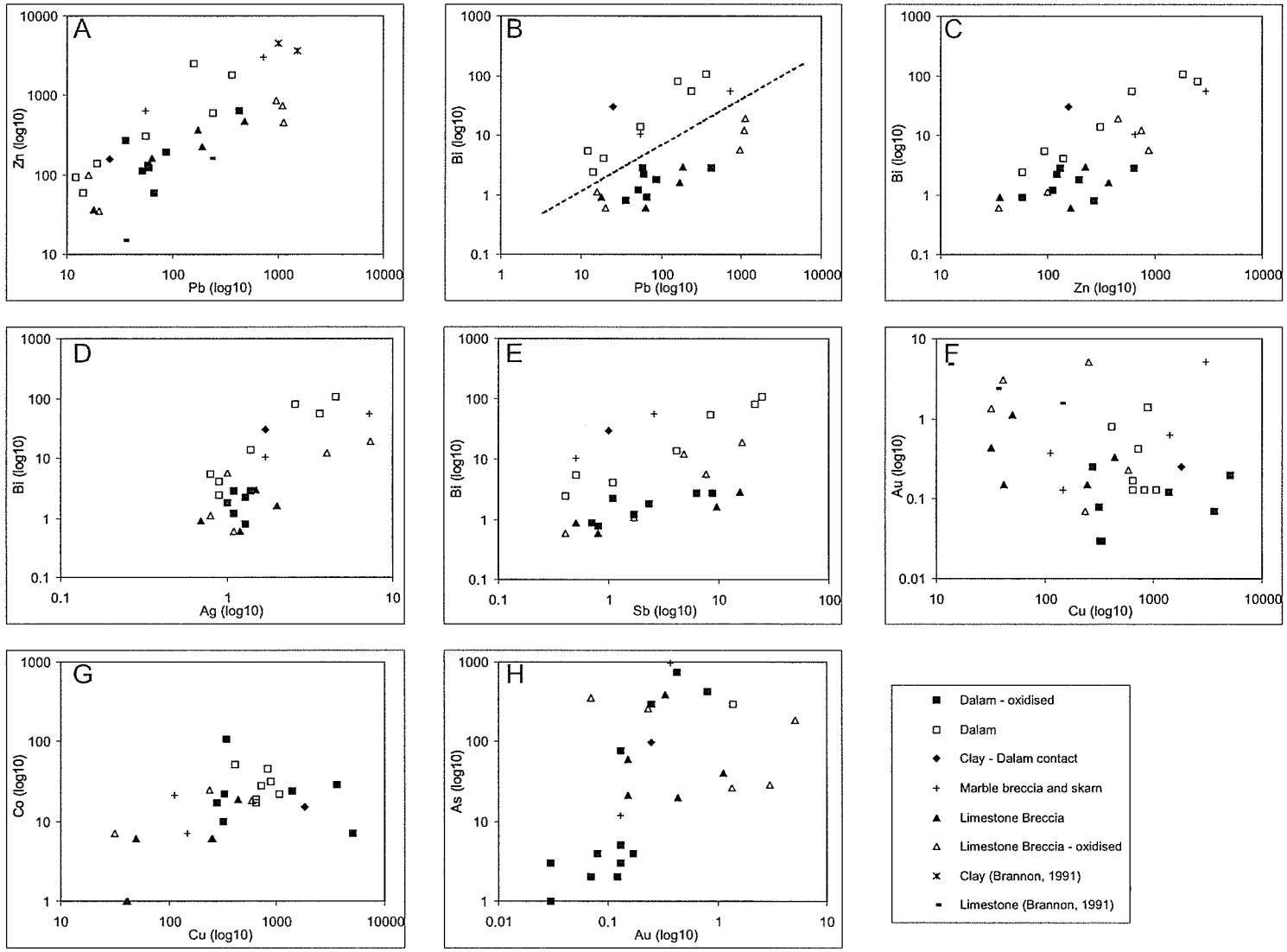

does not correlate with gold or any of the elements analysed except Co (Group 2; Table A-3; Figure A-12f, g). Au only correlates with As (Group 3: Table A-3), although the limestone breccia samples do not correlate as well as samples from other locations (Figure A-12h). Pb and Zn display a strong correlation in all samples (Figure A-12a). With respect to Bi, samples from the limestone breccias (oxidised and unoxidised) and oxidised Dalam breccia display elevated Pb, Zn, Ag and Sb (Figure A-12b-e). Samples from the limestone breccias (oxidised and unoxidised) generally contain elevated As (Figure A-12h).

LA-ICPMS analysis of limestone breccia pyrites

The preliminary element association study of gold in limestone breccia samples indicates it may be associated with arsenic but is not associated with any other metals. It is possible that a proportion of the West Grasberg gold is contained within some of the sulphide phases present. Au or As were not detected in euhedral or framboidal pyrite by microprobe (detection limit ca. 0.5wt%). Euhedral and framboidal pyrite and one sphalerite grain were analysed by LA-ICPMS from the gold-diaspore –bearing pan concentrate sample (Figure A-11; Figure A-13). Euhedral pyrite contains elevated Au, As, Bi and Te to Cu ratios with respect to the framboidal pyrite (Figure A-13a-e). West Grasberg pyrite display a consistent Au:As correlation (Figure A-13f). Euhedral pyrite displays distinct As:Te, As:Bi, Au:Te, Au:Bi and Bi:Te associations separate to framboidal pyrite (Figure A-13g-k).

Discussion

Significance of clays developed at West Grasberg

Kavalieris (1994) and Brannon (1991) both considered that the banded clay was possibly derived from fine tuffaceous ash through diatreme volcanicity with intercalated carbonaceous material, which may have been deposited in a glacial lake. Kavalieris (1994) reported rare clasts of lapillic tuff in the banded clay.

The distributions of clay minerals in West Grasberg must be considered in geological and paragenetic context. From the textures in the clay, it is evident that at least two clay forming events took place. The earliest and most problematic of these was the development of the

Figure A-13. Bivariant plots of LA-ICPMS trace element analyses from grains of pyrite and one grain of sphalerite. Analyses from a pan concentrate sample (WGR4, 89m; 87-96m, 10g/tAu) were obtained using a LA-ICPMS system in the Geochemical Analysis Unit, ARC National Key Centre GEMOC, Macquarie University. Analytical technique described in Appendix 1. For full results, 2 sigma errors and detection limits refer to Appendix 7. a) Cu:Au. Euhedral pyrite is elevated in Au:Cu with respect to framboidal pyrite. 2 sigma error bars from Appendix 7. f) Au:As. Big Gossan Stage 1 and Stage 2 pyrite analyses plotted for comparison (Section B; Appendix 7). West Grasberg pyrite analyses display Au:As correlation consistent with that observed from Big Gossan pyrite. j) Au:Bi. Big Gossan Stage 1 and Stage 2 pyrite analyses plotted for comparison (Section B; Appendix 7). West Grasberg euhedral pyrite compares well with Big Gossan Stage 2 pyrite. k) Bi:Te. Big Gossan Stage 1 and Stage 2 pyrite analyses plotted for comparison (Section B; Appendix 7).

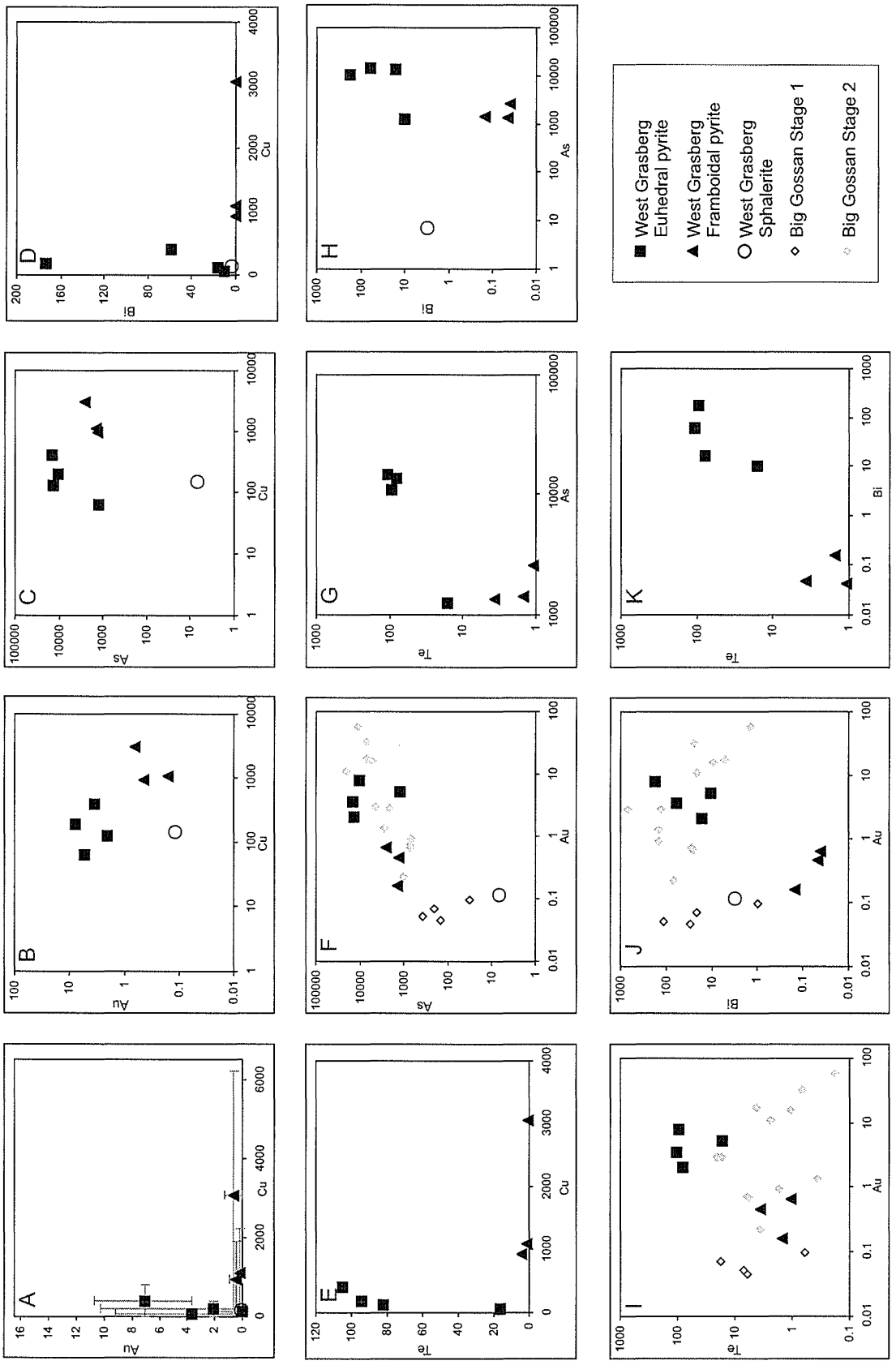
A
Au
Cu
B
Au
Cu
C
As
Cu
D
Bi
Cu
E
Te
Cu
F
As
Au
G
Te
As
H
Bi
As
I
Te
Au
J
Bi
Au
K
Te
Bi
West Grasberg Euhedral pyrite
West Grasberg Framboidal pyrite
West Grasberg Sphalerite
Big Gossan Stage 1
Big Gossan Stage 2

banded clay. The convoluted texture in the banded clay is interpreted as soft sediment deformation of a lake sediment. The occurrence of banded clay or maar sediments is common in volcanic-diatreme environments (Sillitoe, 1985; Baker et al., 1986; Corbett and Leach, 1998). Fine grained tuffaceous material would be altered to clay in the lake environment. The second generation of clay alteration at West Grasberg is texturally destructive and decreases in intensity with depth. It is interpreted to represent surface-related recent weathering.

The dominant clay phases in the banded clay are 10Å halloysite and 7Å halloysite-kaolin. Given that the 7Å phase expands slightly after glycolation and then collapses after heating, it is more likely to be halloysite than kaolinite (Kaylene Camuti, pers comm, 2001). However, examination of clay particles by transmission electron microscope would be required to accurately determine this. Kavalieris (1994) also documented halloysite in the West Grasberg clays from XRD analysis. Grey colouration of the bands could be due to the presence of sulphide or carbonaceous material although not present in significant enough quantities to be detected during XRD analysis. 7Å halloysite-kaolin is the dominant phase in non-banded mottled grey and white clay.

Halloysite is a common constituent of many volcanic soils (Takahashi et al., 1993) and a common weathering or low temperature hydrothermal alteration product of rocks with widely differing compositions (Hurst and Kunkle, 1985). Hydrated 10Å halloysite contains more water in its interlayers than 7Å halloysite and is confined to a narrow stability field governed by temperatures less than ca. 100°C and water pressures above liquid/vapour pressure (Hurst and Kunkle, 1985). If water pressure drops below L/V pressure, 10Å halloysite irreversibly dehydrates to 7Å halloysite (Hurst and Kunkle, 1985). Above ca. 110°C halloysite tends to transform to kaolinite at any water pressure (Hurst and Kunkle, 1985).

The widespread distribution of 10Å halloysite in the banded clay constrains temperatures of clay formation to less than ca. 100°C and water pressures to above liquid/vapour pressure. The GIC is dominantly andesitic, as would be the composition of any tuffaceous material associated with the GIC. Formation of halloysite from andesitic tuffaceous material is commonly observed in other locations (Table A-4: Takahashi et al., 1993; Cronin et al., 1996). From the information available in this study, neither parageneitc stage nor geological context constrains the distribution of 10Å or 7Å halloysite-kaolin.

Another distinctive component at West Grasberg is the amorphous aluminosilicate phase interpreted to be allophane. Allophane commonly, though not exclusively occurs as a major constituent of soil clays derived from volcanic material (Fey and LeRoux, 1975). It is an unstable solid and with time will transform toward more stable better-ordered forms such as

Table A-4. Clay phases preferentially developed in different volcanic terrains.

Host Rock	Clay types and interpreted controls	Location	Reference
Quartz trachyite and tephretic fragments in surface layer	Allophane, kaolinite, illite	San Martino, Italy	(Lorenzoni et al., 1995)
Quartz trachyte, below surface layer	Halloysite, illite	San Martino, Italy	(Lorenzoni et al., 1995)
Latitic volcanic rocks	Kaolinite, illite, HIV (poor in Al and Si)	My Cimino, Italy	(Lorenzoni et al., 1995)
Leucite (foidite) tephritic lava	Halloysite, amorphous imogolite/allophane (Al easily available from break-down of leucite favours formation of allophane: high Al:Si ratio)	Mt Fogliano, Italy	(Lorenzoni et al., 1995)
Rhyolite	Allophane-dominant (intense leaching environment: >2600mm precipitation)	North Island, New Zealand	(Parfitt and Wilison, 1985)
Rhyolite	Halloysite-dominant (moderate leaching environment: <1200mm precipitation)	North Island, New Zealand	(Parfitt and Wilison, 1985)
Andesite and minor rhyolite	Allophane and halloysite (formation governed by the presence of an xeric soil moisture regime: high leaching between November to February precipitation (1000mm) causes low Si-concentration and allophane formation and dehydration during the dry summer causes increased Si-concentration and halloysite and poorly crystalline kaolinite formation)	Northern California	(Takahashi et al., 1993)
Andesite ash	Allophane, halloysite, ferrihydrite (allophane and ferrihydrite formed initially in shallow ash deposits, later burrial by lahar and tephra favoured halloysite formation by increased Si-mobility and a perched water table)	Ruaphehu, New Zealand	(Cronin et al., 1996)

halloysite and kaolinite (Su and Harsh, 1998). At West Grasberg, allophane does display some depth association in that it is predominantly though not exclusively concentrated in fractures below the development of pervasive white alteration. The brittle fracture system containing late stage halloysite-kaolinite and allophane crosscuts all earlier mineralisation and breccias.

Based on compositional information and late stage paragenesis, the halloysite-kaolinite and allophane fracture fill are interpreted to be derived from downward-percolation of fluids that leached components from the banded-clay at surface. The concentration of soluble silica, which is closely governed by environmental factors, in particular rainfall, is considered to be the primary factor regulating preferential formation of halloysite versus allophane (Table A-4: Takahashi et al., 1993). In soil horizons, a pH >5 is required for the formation of allophane phases (Takahashi et al., 1993).

Formation of halloysite and allophane in a high rainfall, highly leached environment is consistent with observations made by Parfitt and Wilison (1985) from the North Island in New Zealand. Tropical rainy conditions currently inundate the Ertsberg District with approximately 3m/yr rainfall and Weiland and Cloos (1996) consider this may have been responsible for <2km of erosional unroofing(Weiland and Cloos, 1996). inferred that similar climatic conditions existed for millions of years as New Guinea has only moved approximately

200km northwards in the last 3Ma (Scotese et al., 1988).

Minor illite is present in samples interpreted to contain igneous fragments. The illite could be a product of hydrothermal alteration by one of the three widespread sericite-illite alteration events documented in the GIC (Pollard and Taylor, 2002). Alternatively, the formation of illite in addition to halloysite and kaolinite by weathering more alkali-rich igneous rock is entirely consistent with observations recorded from volcanic soil terranes by Lorenzoni et al. (1995) (Table A-4).

Correlation of events at West Grasberg, the GIC and Kucing Liar

The limestone breccias in the Tertiary Kais Formation west of the GIC contact display variable brecciation, of which the time of formation and reactivation are unknown. Two textural styles are present in the limestone breccias. The crackle-breccia zones share similarities with limestone breccias south of the GIC considered by Sapiie (1998) to have developed through a combination of tectonic and solution processes. Brecciated zones in the New Guinea Limestone Group adjacent to the GIC are numerous and display a spatial relationship with intrusive bodies (Kavalieris pers comm 2000). It is possible that the limestone breccias were formed during emplacement of the GIC and then reactivated during successive tectonic events. The second breccia style is characterised by milled breccia texture with well-rounded fragments supported by a matrix of grey clay. Gold mineralisation occurs with smectite-chlorite clay in this breccia style. The SW plunge of gold mineralisation in the NE-trending breccia suggests a structural control (Figure A-10). The plunge could be controlled either by movement direction in the structure or the intersection lineation between the breccia zones and bedding.

Several events preceded the incorporation of banded clay and development of sulphides at West Grasberg. The marble breccia contains evidence of phlogopite "skarn" alteration and infill. It is unclear from the relationships in drillcore if the marble breccia was: a) formed during the process that incorporated the banded clay into the GIC margin or b) present before the banded clay was incorporated. It is likely that the marble is related to intrusion of the GIC as a marble alteration halo (cf. Hefton et al., 1995). The timing of the skarn alteration/ infill in the marble breccia is also unconstrained with respect to formation of the banded clay as no fragments or veinlets of phlogopite skarn were observed in the banded clay zone.

All stages of mineralisation at West Grasberg were confined to structurally favourable locations including contacts between lithological units, and existing breccia or fractured rocks. Marble breccia, skarn and banded clay are post-dated by Stage 1 sphalerite and galena. Element associations suggest that a minor element assemblage of Ag-Se-Sb-Bi-As occurs with sphalerite and galena. Fluid inclusion measurements (Kyle, 1993; Figure A-14) from sphalerite-

Figure A-14. Range in homogenisation temperatures and wt%$NaCl_{equiv}$ for fluid inclusions from sphalerite-galena-quartz-fluorite veins along NE-striking structures at West Grasberg (Kyle, 1993).

Solid symbols indicate average compositions. Numbers in brackets = number of inclusions analysed. Type 1 inclusions are two phase liquid dominant + vapour. Type 3 inclusions are liquid dominant + vapour + halite solid. As boiling conditions are not apparent, a pressure correction needs to applied to these results (Kyle, 1993).

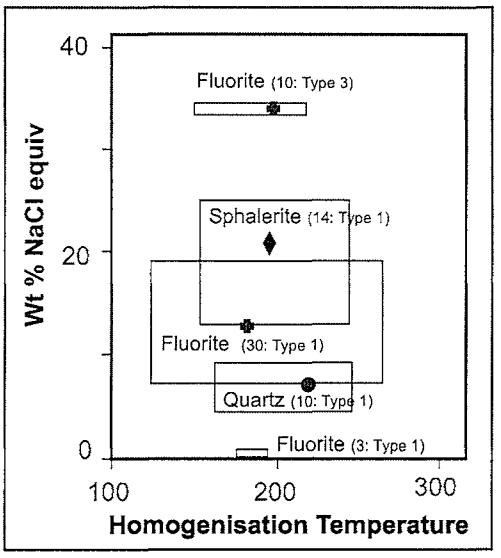

galena-quartz-fluorite veins along NE-striking structures at West Grasberg are considered to be sourced from saline fluids, possibly derived from fluids responsible for the Grasberg porphyry Cu-Au deposit (Kyle, 1993).

The main copper sulphide stage recognised at Grasberg is not observed at West Grasberg suggesting either a) the West Grasberg banded clay and breccias formed after these sulphide events or b) West Grasberg was distal from the locus of copper distribution. The latter interpretation is reasonable as Grasberg main stage chalcopyrite-bornite veins display a narrow distribution confined to the core of the GIC (Pollard and Taylor, 2002). Sphalerite and galena are known to crosscut the heavy sulphide pyrite and are interpreted to occur late in the Grasberg and Kucing Liar paragenesis (Pollard and Taylor, 2002: B. New pers comm., 2003). Stage 1 sulphides may correlate with other sphalerite and galena occurrences around the GIC (Figure A-4).

A sulphide association similar to that of Stage 1 also occurs in the intrusive breccia as fragments. A similar sulphide-bearing intrusive breccia also occurs parallel to the south contact of the GIC (Margotomo, 1999). The heavy sulphide zone which occurs extensively along the GIC contact (Pollard and Taylor, 2002) at depth below the sulphide-bearing intrusive breccias is the interpreted source for the abundant sulphide fragments.

Stage 2 is characterised by fine-grained pyrite ± marcasite ± chalcopyrite ± galena ± bitumen. Pyrite and illite are noted in the banded clay and along fractures in limestone. Framboidal pyrite and covellite occur in the limestone breccia and may correlate with paragenetically constrained framboidal pyrite-covellite textures documented in the nearby Grasberg and Kucing Liar deposits (R. Taylor pers comm.). The pyrite-covellite associations and Stage 2 sulphides in the banded clay, marble and marble breccias display strongest resemblance to package 7 of the GIC paragenesis (Figure A-4) which comprises covellite-pyrite-marcasite-

sericite±chalcopyrite (Pollard and Taylor, 2002). Package 7 assemblage also occurs at Kucing Liar and is interpreted as high sulphidation-style mineralisation by Pollard and Taylor (2003).

The extent of remobilised bitumen at West Grasberg is poorly understood as is its relationship, if any, to the distribution of sulphides and/or gold mineralisation. Units 1-3 of the Tertiary Kais Formation are variably carbonaceous (Quarles Van Ufford, 1996) and host the limestone breccias at West Grasberg. Fine-grained framboidal pyrite either postdates (utilising the same fluid pathways), or is coeval with hydrocarbon migration. A petrographic study of limestones flanking and overlying Kucing Liar and the GIC noted that the New Guinea Limestone Group is oil-prone and samples showed evidence in situ kerogen and migrated liquid and solid hydrocarbons (Hornibrook, 1998).

The distribution and character of samples with elevated gold suggest that gold mineralisation resulted from an event separate to Stage 1 and 2. Elevated gold occurs with fine grained pyrite and smectite-chlorite clay in the milled breccias and may also be associated with fine grained pyrite and clay in the marble breccias. The distribution of Stage 1 pyrite, sphalerite, chalcopyrite and galena and occurrences of Stage 2 associations which includes remobilised bitumen, do not appear coincident with elevated gold assays. Element associations also provide support that gold is independent of other elements analysed with the exception of arsenic. The precise timing of gold mineralisation is inconclusive although based on the distribution of drillhole gold assays it appears to overprint the intrusive breccia and adjacent rock types (Figure A-6e), suggesting gold was the latest hydrothermal event at West Grasberg.

At Big Gossan, pyrite with elevated Au is associated with native gold occurrences (Section B). LA-ICPMS analysis of West Grasberg pyrite from the limestone breccia are most consistent with gold being associated with a generation of euhedral pyrite rather than the framboidal pyrite ± covellite stage. 2-8g/t Au is present in euhedral pyrite as invisible gold (Figure A-13). Calculations indicate that 200,000 ounces of the limestone breccia gold resource (508,625 ounces) would be as invisible gold if 10% of the 8g/t euhedral pyrite were present (Figure A-15). Although the amount of euhedral pyrite in the West Grasberg limestone breccias has not been quantified, rare occurrences of native gold grains (Figure A-11) and the absence of massive pyrite zones suggests the resource contains significant native gold.

West Grasberg euhedral pyrite displays similar Au:As and Au:Bi correlations and higher Te levels than Big Gossan pyrite (Figure A-13f, i, j) that occurs with native gold, Bi sulphosalts and tellurides (Section B). The chemical or physical processes responsible for partitioning Au and As into pyrite were not isolated events in the Ertsberg district. The association of Au and As may reflect a Au-As bond (i.e. Cathelineau et al., 1989). The presence of arsenic in fluids creates reducing conditions that can enhance gold precipitation (Pokrovski et al., 2001).

Figure A-15. Possible contribution of invisible gold in euhedral pyrite to the West Grasberg gold resource.

Calculations for different percentages of pyrite based on maximum euhedral pyrite LA-ICPMS analysis of 8g/t (Figure A-13). Limestone breccia gold resource estimated by Brannon (1991).

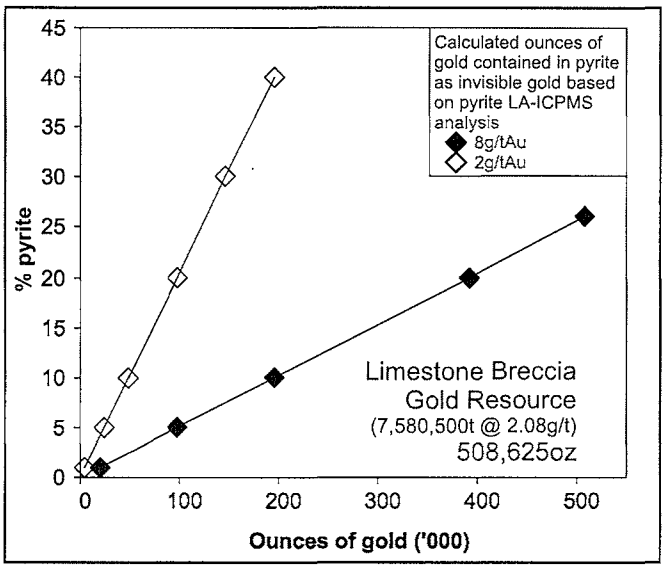

West Grasberg gold-only occurrences do not correlate with events documented in the GIC. If the diaspore is primary, it is consistent with advanced argillic conditions (Kingston-Morrison, 1997). A possible source for the gold-bearing fluids is the Kucing Liar deposit which a) has documented high sulphidation mineralisation, b) occurs spatially nearby at depth and c) contains Au-As-Bi associations which are geochemically expressed at surface from soil and rock samples in faults above the deposit and close to West Grasberg (Agnew, 1998). It is also possible that there could be more than one gold generation, or that gold may have been remobilised from a pre-existing deposit.

Evolution of the West Grasberg contact zone and implications for the GIC

West Grasberg contains a small area of brecciated rocks on the western margin of the much larger GIC. West Grasberg is significant as it preserves evidence of surficial volcanic features overprinted by tectonic, hydrothermal and clay events. The GIC was emplaced at depths of <2km (cf. Figure A-16a) and other studies advocate that it was exposed to surface during this time and a maar depression was present (McDonald and Arnold, 1994; Sapiie and Cloos, submitted). It is possible that active volcanicity was taking place on the surface above the GIC (Figure A-16a) and that the banded clay may have formed from lake sediments as documented in other diatreme-maar environments (Baker et al., 1986). Further occurrences of convoluted banded clay and fractures containing white clay and yellow crystals, which may be halloysite and allophane, have been documented from other locations (Figure A-3) at the GIC margin (Kavalieris, 2000; Sapiie and Cloos, submitted) indicating that some of the processes occurring at West Grasberg were not isolated events.

There is no evidence at West Grasberg of the multiple episodes of intense alteration documented in the adjacent GIC (Pollard and Taylor, 2002). However, fragments of igneous rock with potassic and clay alteration are present in brecciated areas of banded clay. This constrains incorporation of the banded clay into the GIC margin to after formation of the

documented porphyry-style alteration stages (Figure 4: Pollard and Taylor, 2002).

Two scenarios for incorporation of the banded clay into the margin of the GIC are considered here (Figure A-16b and c). Firstly, a void on the GIC margin may have been created by an episode of explosive diatreme activity (Figure A-16b) or karst dissolution (c.f. Kavalieris, 2000) although the acidic conditions postulated by Kavalieris (2000) are not supported by the pervasive clay mineralogy developed in the banded clay. A late stage diatreme event on the GIC margin could have been caused by a phreatomagmatic eruption (c.f. Baker et al., 1986) and contorted layers may have resulted when the banded clay slumped into the newly created void.

An alternative interpretation is that the banded clay was already present in the volcanic cover and was incorporated into the GIC margin through faulting (Figure A-16c) although the banded clay must still have been distal to the GIC porphyry-style hydrothermal alteration. The clay composition and distribution of banded clay on both western and eastern margins of the GIC is more consistent with a common process of incorporation, such as a late-stage diatreme volcanic event, that was not localised to West Grasberg. (Figure A-16b). The marginal breccia zone documented by Sapiie and Cloos (submitted) may be analogous to late-stage diatreme-breccia activity described at West Grasberg.

Unaltered tuffs overlying an unconformity on limestone adjacent to the GIC provide added local evidence of late-stage volcanic activity (Figure A-16b). Additionally it is unclear from McDonald and Arnold (1994) and Sapiie and Cloos (submitted) how the porphyry-related

Figure A-16. Schematic cross section evolution of West Grasberg. a) Emplacement of GIC to depths of <2km (Weiland and Cloos, 1996) into Cretaceous-Tertiary sedimentary rocks and interpreted volcanic cover (McDonald and Arnold, 1994). The GIC was affected by extensive alteration events (Pollard and Taylor, 2002). Present known vertical extent of GIC is approximately 2km and the GIC is open to depth. Possible scenario for formation of banded clay from tuffaceous material deposited in a lake above the GIC or banded clay may have been contained within the volcanic cover. b) Possible scenario for incorporation of banded clay lake sediment into margin of the GIC through diatreme activity. Depth of the GIC is unconstrained. Late stage crystal and banded tuff occurs on unconformity on northern margin of the GIC may also be representative of late-stage diatreme activity. c) Possible scenario for incorporation of banded clay into margin of the GIC through faulting. Depth of the GIC is poorly constrained. Banded clay must have been sufficiently removed from the GIC so it was not affected by extensive GIC alteration events (Pollard and Taylor, 2002). d) West Grasberg. Base metal mineralisation in limestone, marble, marble breccia and along the banded clay-GIC contact. Fragments of base metals in multiply brecciated marble breccias may be from this generation of mineralisation. Timing of the development of crackle breccia zones is unknown. e) West Grasberg. Formation of intrusive breccia. Sulphide clasts may have been derived from heavy sulphide zone that occurs along the GIC contact (Figure A-16F). Gold mineralisation overprints milled limestone breccia, marble breccia, banded clay and intrusive breccia. f) At surface the banded clay is characterised by an unconformity and overlain by crossbedded fine grained sediment, interpreted as glacial alluvium (Cloos, pers comm. 2003). Schematic location of the heavy sulphide zone and possible source for intrusive breccia sulphide fragments. g) West Grasberg, present day. White texture destructive halloysite alteration decreases in intensity from surface. White halloysite and yellow allophane are concentrated in fractures that crosscut all rock types at West Grasberg.

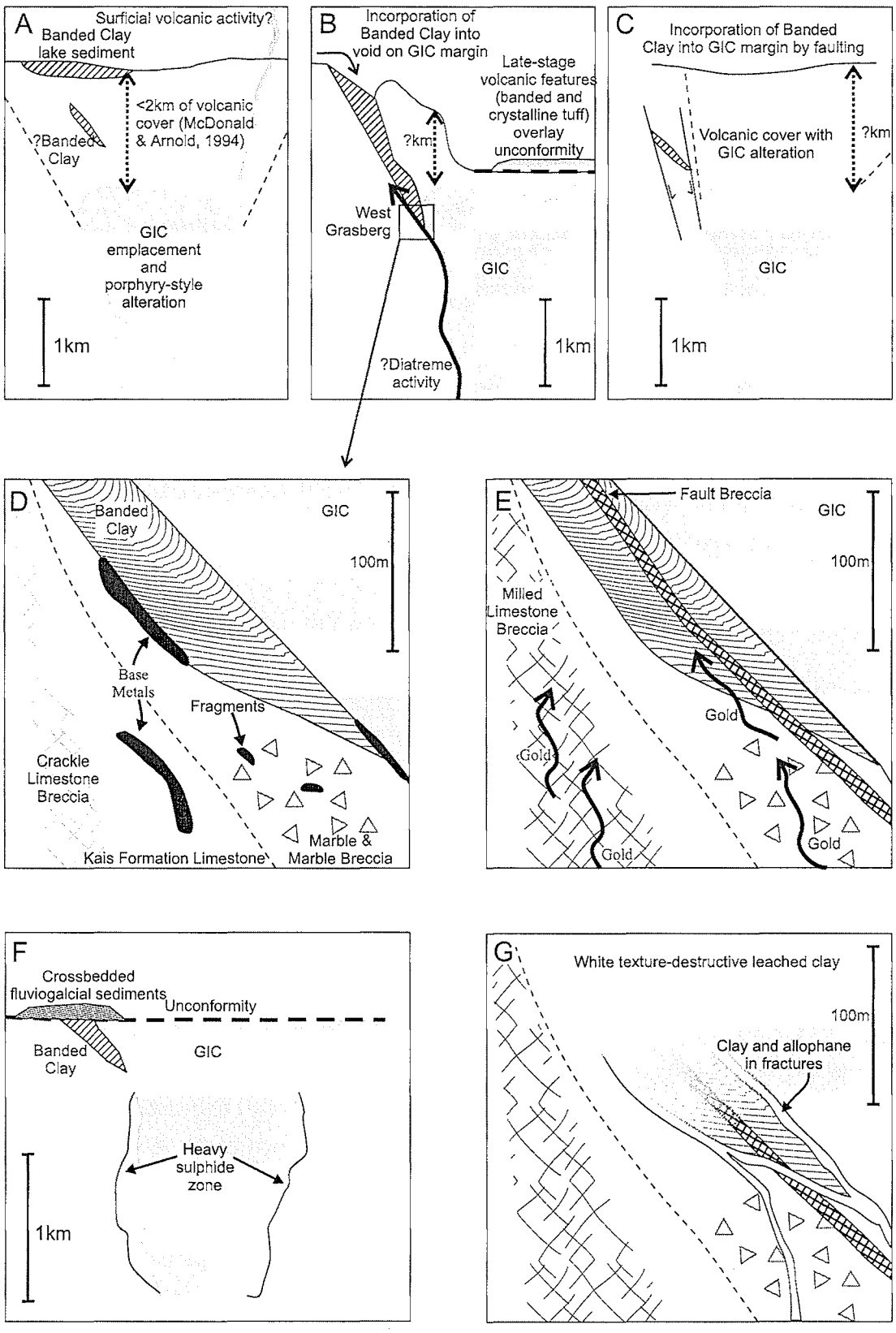
A
Surficial volcanic activity?
Banded Clay lake sediment
<2km of volcanic cover (McDonald & Arnold, 1994)
?Banded Clay
GIC emplacement and porphyry-style alteration
1km
B
Incorporation of Banded Clay into void on GIC margin
Late-stage volcanic features (banded and crystalline tuff) overlay unconformity
?km
West Grasberg
GIC
?Diatreme activity
1km
C
Incorporation of Banded Clay into GIC margin by faulting
Volcanic cover with GIC alteration
?km
GIC
1km
D
Banded Clay
GIC
100m
Base Metals
Fragments
Crackle Limestone Breccia
Kais Formation Limestone
Marble & Marble Breccia
E
Fault Breccia
GIC
100m
Milled Limestone Breccia
Gold
Gold
Gold
Gold
F
Crossbedded fluviogalcial sediments
Unconformity
Banded Clay
GIC
Heavy sulphide zone
1km
G
White texture-destructive leached clay
100m
Clay and allophane in fractures

Table A-5. Summary of conditions of stability for allophane, and halloysite-kaolin phases.

Conditions	Allophane	10 Å Halloysite	7 Å metahalloysite (or kaolinite)
pH (Takahashi et al., 1993) (Farmer et al., 1991)	pH >5	*Slightly higher pH than allophane	
Silica in solution (Singleton et al., 1989)	<= 10mg/L	>= 10mg/L	
Rainfall and degree of leaching (Parfitt and Wilison, 1985)	High rainfall and high leaching environment	more dehydrated environment, less leaching	
Water pressure relative to L/V pressure (Hurst and Kunkle, 1985)		Water pressure above L/V	Water pressure below L/V
Temperature (Hurst and Kunkle, 1985)		temperature < ~100 C	temperature > ~100 C
Summary of primary controls:	Unstable solid (Su and Harsh, 1998). Soluble silica concentration is the primary factor regulating formation of allophane and halloysite (Takahashi et al., 1993).	Hydrated halloysite has a narrow stability field governed by water pressures above L/V pressure and temperatures < ~100 C (Hurst and Kunkle, 1985)	Dehydration from 10Å halloysite is irreversible and occurs at water pressures below L/V pressure and temperatures < ~100 C. Kaolinite forms > ~110 C at any L/V pressure (Hurst and Kunkle, 1985).

alteration in the GIC is manifested in the volcanic cover considered to predate GIC intrusion. It is possible some of the volcanic features described by McDonald and Arnold (1994) are related to a late-stage episode of volcanicity responsible for the unaltered tuffs and banded clay.

The presence of cross-cutting pyrite along with base metal and gold suggests the banded clay had been incorporated prior to cessation of hydrothermal activity in the district (Figure A-16d, e). The proximity and occurrence of similar sulphide assemblages in both the limestone breccias and the marble and banded clay may indicate they were affected by the same hydrothermal events. Formation of an intrusive breccia containing abundant sulphide fragments in interpreted to have preceded gold mineralisation (Table A-2; Figure A-16e). The banded clay at West Grasberg provides evidence that volcanic and structural events on the margins of the GIC rendered the GIC open surface prior to cessation of hydrothermal activity.

Late-stage processes at West Grasberg include development of an unconformity which is overlain by crossbedded sediments interpreted to be fluvioglacial (Figure A-16f). The high rainfall environment facilitated surface-related leaching and alteration to clay (Figure A-16g). Downward percolation of water channelled clay into fractures developed at West Grasberg (Figure A-16g) and other GIC locations. Interplay between low-temperature processes controlled the aluminosilicate phases developed (Table A-5).

Conclusions

Incorporation of the banded clay into the GIC post-dated multiple potassic, magnetite and quartz porphyry-style alteration events. The banded clay was affected by at least two separate sulphide-depositing events, namely sphalerite-galena and pyrite-illite, similar to those occurring in the adjacent Grasberg and Kucing Liar Cu-Au deposits. Tuffs occurring on the northern margin of the GIC, which also appear unaffected by extensive GIC porphyry-style alteration, may be an additional example of late stage volcanic processes in the district.

Clay and sulphide distribution and paragenesis at West Grasberg is not consistent with a surficial epithermal environment. At least 3 different hydrothermal mineralisation events are recognised. Separate base-metal, pyrite and gold±pyrite events postdate the banded clay and adjacent brecciated and marbleised limestone. Gold occurrences are characterised by distinct smectite-chlorite clay, diaspore and a Au-As-Bi-Te bearing generation of pyrite. Diaspore-hosted gold and the presence of a pyrite-covellite association are both indicative of infiltration by fluids responsible for high sulphidation mineralisation which is documented nearby at 1km depth in Kucing Liar and also at Grasberg. The West Grasberg gold occurrences are tentatively correlated with the Kucing Liar deposit that occurs nearby at depth that contains unconstrained Au-As-Bi associations also expressed in surface geochemistry adjacent to West Grasberg.

The LA-ICPMS Au-As-Bi-Te composition of pyrite from the limestone breccias is similar to pyrite occurrences in late-stage pyrite-Au-As-Zn-Bi-Te mineralisation at Big Gossan (<2.82Ma) and Wanagon Gold (3.62Ma). Euhedral pyrite contains 2-8g/t Au. Rare occurrences of native gold grains and the absence of massive pyrite zones suggests the West Grasberg limestone breccia-hosted gold resource is not entirely as invisible gold. If 10% euhedral pyrite (at 8g/t Au) were present, 200,000 ounces of gold would be as invisible gold in pyrite.

Surface-related leaching and alteration in the banded clay and GIC is due to the high rainfall environment and is the primary control on the low temperature aluminosilicate phases developed. Downward percolation of low temperature near-neutral pH water channelled clay into fractures developed at West Grasberg and other GIC locations.

Acknowledgements

PT Freeport Indonesia is acknowledged for logistical and analytical funding and permission to publish this work. GEMCOM software generously provided a full version of its software as an educational license. Feedback from Freeport staff, particularly Clyde Leys is appreciated. Kaylene Camuti provided assistance with XRD interpretation and Peter Crosdale assisted with oil immersion microscopy. Thank you also to researchers from University of Arizona and University of Texas (particularly Mark Cloos), Peter Pollard and Roger Taylor for providing access to unpublished information. James Lally generously drafted a number of the diagrams.

Section B
Genesis of pyrite-Au-As-Zn-Bi-Te zones associated with Cu-Au skarns: Evidence from Big Gossan and Wanagon Gold deposits, Ertsberg District, Papua, Indonesia.

Abstract:

The Ertsberg district hosts multiple skarn and porphyry-related deposits comprising one of the largest Cu-Au resources in the world. Earlier skarn Cu-Au deposits are overprinted by distinct late-stage occurrences containing pyrite-sphalerite-arsenopyrite-native gold with localised Bi and Te minerals at Big Gossan and 2 km along strike to the NW at Wanagon Gold. The Big Gossan occurrence is younger than 2.82±0.04Ma based on a new $^{40}Ar/^{39}Ar$ date from the Big Gossan skarn and the Wanagon Gold occurrence has a $^{40}Ar/^{39}Ar$ K-feldspar age of 3.62±0.05Ma. A K-Ar date (3.81±0.06Ma) from the Wanagon Sill constrains formation of the overprinting skarn Cu-Au and late-stage Wanagon Gold occurrence to a period of ca. 0.2Ma. The Wanagon Gold occurrence contains an estimated resource of approximately 2 million ounces gold.

At Big Gossan, earlier skarn Cu-Au distributions display temperature zonation in cross and long section. The highest temperature core (defined by low Zn:Cu) plunges to the NW and is open at depth. Highest Cu grades and greatest development of the overprinting pyrite-Au-As-Zn-Bi-Te association occur to the NW coincident with NE-striking faults. Pyrite-Au-As-Zn-Bi-Te occurrences are also distributed in faults and fractures in the hanging wall of the Big Gossan skarn Cu-Au deposit. At Wanagon Gold, an event that leached skarn and sandstone preceded introduction of the pyrite-Au-As-Zn-Bi-Te occurrences. In the sandstone, the pyrite-Au-As-Zn-Bi-Te mineralisation was accompanied by a gangue of K-feldspar (adularia) and minor quartz. In carbonate rocks, neither the leaching nor K-feldspar are developed, and sulphides are accompanied by a gangue of quartz and dolomite.

$\delta^{34}S$ of sulphide from skarn Cu-Au and overprinting pyrite-Au-As-Zn-Bi-Te occurrences at both deposits range from -0.7 to 5.1‰. LA-ICPMS analyses show pyrites from the overprinting occurrences at both localities are distinct from those in the earlier skarn Cu-Au deposit and contain up to 60ppm Au, 2% As, 680ppm Bi and 40ppm Te. Minerals in the overprinting occurrences includes native gold, argentian tetrahedrite and tennantite, a silver-antimony-sulphide and Bi and Te -(Ag-Au) minerals including cosalite, bismuthinite, petzite, hessite, altaite and tetradymite. Native gold fineness (1000Au/Au+Ag) varies consistently with sulphide association. Lowest fineness native gold (737-863) occurs with Pb-minerals (galena and sulphosalts) and highest fineness native gold (904-974) occurs trapped within pyrite or in association with bismuthinite. Sulphidation reactions and

adsorption are interpreted to be the primary processes responsible for gold precipitation.

Fluid inclusions from sphalerite and quartz in the Big Gossan pyrite-Au-As-Zn-Bi-Te occurrence have an average salinity of 9 wt% $NaCl_{equiv}$ and average homogenisation temperature of 248°C. Stable isotopes from this ($\delta^{18}O_{FLUID}$ value of ca. 5.9‰) and other studies indicate the fluids were magmatic. A direct genetic relationship to earlier skarn Cu-Au is not clear. The pyrite-Au-As-Zn-Bi-Te occurrences are considered to represent deposits formed by incursion of a new fluid with a different composition. The pyrite-Au-As-Zn-Bi-Te fluids may represent the magmatic component in fluids recognised in low and high sulphidation epithermal deposits that typically develop at shallow levels and can contain significant contribution of non-magmatic (i.e. meteoric) water.

Introduction

The Ertsberg district is located in the mountainous Central Ranges of Papua (Figure B-1). Pliocene intrusive activity was accompanied by hydrothermal systems that affected igneous and clastic - carbonate sedimentary rocks and formed one of the largest gold and copper resources in the world. In addition to porphyry Cu-Au and numerous skarn Cu-Au systems, there are pyrite-gold-sphalerite-arsenopyrite occurrences with local Bi and Te minerals at Big Gossan and Wanagon Gold, which contain significant gold

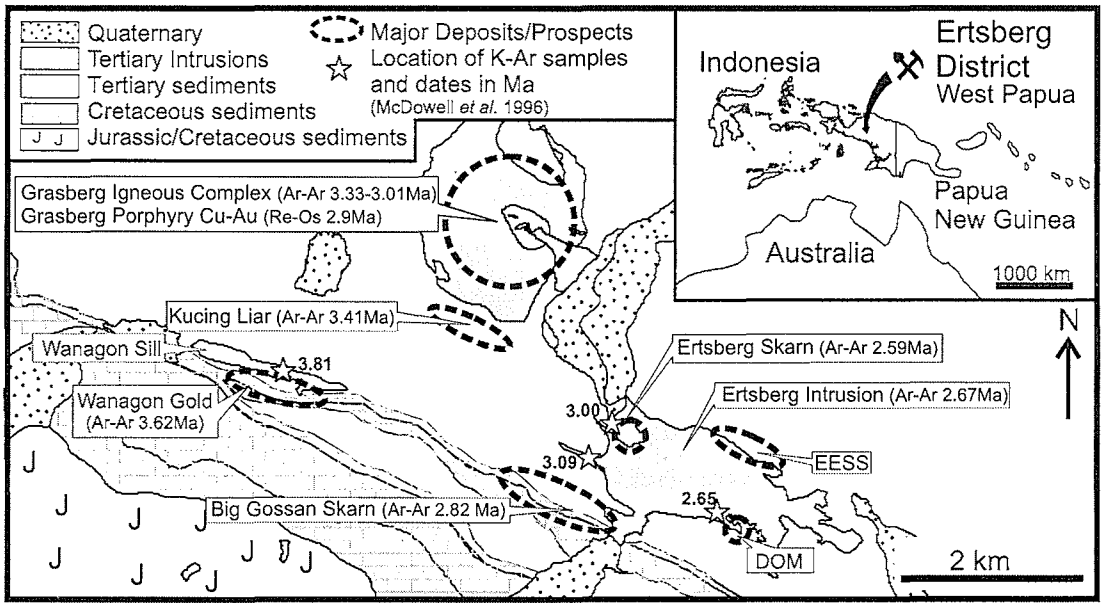

Figure B-1. Ertsberg District location, regional geology (modified from Freeport Indonesia geological mapping) and major deposits/prospects (EESS: Ertsberg East Skarn System; DOM: Dom skarn). Grasberg Igneous Complex biotite $^{40}Ar/^{39}Ar$ date range, Kucing Liar skarn phlogopite $^{40}Ar/^{39}Ar$ date, Ertsberg skarn phlogopite and Ertsberg Intrusion biotite $^{40}Ar/^{39}Ar$ dates from Pollard et al. (submitted). Grasberg porphyry Cu-Au Re-Os date from Mathur et al. (2000). Big Gossan skarn phlogopite and Wanagon Gold adularia $^{40}Ar/^{39}Ar$ dates from this study (Appendix 12). Wanagon Sill and Ertsberg Intrusion biotite K-Ar dates and sample locations from McDowell et al. (1996).

resources. The Wanagon Gold occurrence contains an estimated resource of approximately 2 million ounces gold and the full significance of the Big Gossan occurrence has not yet been estimated by Freeport Indonesia.

At Big Gossan, the occurrences have been previously interpreted as a component of outwards temperature zonation of the skarn Cu-Au system (Meinert et al., 1997). Meinert et al. (1997) recognised vertical and lateral metal zonation in the Big Gossan skarn whereby Mo increases with depth and Cu, Au, Ag, Pb, Zn, As, Co increase towards the top of the system and towards the western and eastern margins. Subsequently it was suggested that much of this zonation is a product of structurally controlled overprinting sulphide stages (Prendergast et al., 2001).

Wanagon Gold occurs 2 km along structural-stratigraphic strike to the NW of Big Gossan (Figure B-1). The pyrite-gold-sphalerite-arsenopyrite occurrences (with local Bi and Te minerals) are spatially associated with the Wanagon Sill, a skarn Cu-Au deposit and leached sandstone (Prendergast, 2002).

This investigation seeks to ascertain the nature of the pyrite-Au-As-Zn-Bi-Te occurrences at both locations through structural-stratigraphic analysis of the geological setting and metal zoning, a detailed paragenetic study and application of $^{40}Ar/^{39}Ar$ geochronology, mineralogical (petrography, XRD, microprobe), geochemical (microprobe and LA-ICPMS, stable isotope) and fluid inclusion studies.

Geological setting

The oldest rocks in the Ertsberg district are the clastic and carbonate sedimentary rocks of the Cretaceous Kembelangan Group and the Tertiary New Guinea Limestone Group (NGLG) (Dow et al., 1988; Quarles Van Ufford, 1996). Quaternary alluvium occurs in valleys with glacial till and colluvium along slopes.

Deformation in the district was initiated in Miocene times during arc-continent collision (Sapiie et al., 1999). The northern edge of the Australian continent entered a north-dipping subduction zone beneath the island of Papua producing a fold and thrust belt characterised by en echelon, kilometre-scale NW-trending folds with chevron and open symmetrical geometries. 20-9 Ma magmatic activity recognised elsewhere on the island is not present in the Ertsberg District. Westwards movement of the Pacific-Caroline plate with respect to the Australian plate at ca 4-2 Ma induced left-lateral, strike-slip faulting parallel to the upturned strata. In the Ertsberg district two major intrusive igneous complexes at Grasberg and Ertsberg and numerous smaller stocks, dykes and sills were emplaced at this time to depths of 2 km or less (McDowell et al., 1996; Weiland and Cloos, 1996; Pollard et al.,

submitted).

The Grasberg Igneous Complex (GIC) comprises a series of nested intrusions. Emplacement of the GIC and related hydrothermal events are constrained by paragenetic relationships and $^{40}Ar/^{39}Ar$ ages (Pollard and Taylor, 2002; Pollard et al., submitted). Pollard and Taylor (2002) interpret seven mineralogical packages (P1-P7) to represent discrete hydrothermal fluid events. A biotite date of 3.07Ma from a pre-mineralisation quartz-anhydrite-bearing vein constrains the maximum age of main Grasberg sulphide development. The Kucing Liar skarn and Cu-Au deposit is hosted in faulted sediments adjacent to the GIC (Figure B-1). Skarn formation, dated at 3.41±0.3Ma, was synchronous with the earliest GIC events (Pollard et al., submitted). A late-stage mixed copper sulphide assemblage (chalcopyrite, bornite, nukundamite, digenite-chalcocite, covellite and pyrite) is developed at both Kucing Liar and Grasberg and occurs as infill in cavities formed during a leaching event, which was extensive at Kucing Liar (New, pers comm.). At Grasberg, the mixed copper sulphide association postdates the main stage Grasberg chalcopyrite event (Pollard et al., submitted). Re-Os ages of 2.9±0.3Ma for Grasberg main stage sulphides (Mathur et al., 2000) and 3.01±0.02Ma for late-stage molybdenite from Kucing Liar (Mathur et al., submitted) support a cogenetic relationship between the deposits (New, pers comm.).

The Ertsberg Intrusion has been dated by $^{40}Ar/^{39}Ar$ and K-Ar methods at 2.65±0.12 to 3.1±0.12 (Titley, 1975; McDowell et al., 1996; Pollard et al., submitted). The youngest date is almost 500Ky younger than Grasberg and Kucing Liar mineralisation (Pollard et al., submitted). The variation in Ertsberg Intrusion K-Ar dates may reflect different cooling ages in a single pluton or the presence of secondary biotite (McDowell et al., 1996). Complexity of igneous phases in the Ertsberg intrusion are not constrained. McMahon (1994a) considered that mineral textures and trace element variation in the Ertsberg Intrusion were consistent with in-situ fractional variation. Pollard et al. (submitted) suggest that the distribution in dates may reflect separate intrusive events.

Several major skarn Cu-Au systems occur close to and postdate the Ertsberg Intrusion. These include Ertsberg (Katchan, 1982; Clarke, 2003), Big Gossan (Meinert et al., 1997; Taylor et al., 1999; Prendergast, 2002), DOM and the Ertsberg East Skarn System (EESS) (Mertig et al., 1994; Rubin, 1996; Coutts et al., 1999). Phlogopite from the Ertsberg skarn Cu-Au deposit has an $^{40}Ar/^{39}Ar$ age of 2.59±0.15Ma, indicating a close temporal relationship with the nearby Ertsberg intrusion based on the $^{40}Ar/^{39}Ar$ age (Pollard et al., submitted) and the 2.65±0.12Ma K-Ar age derived from an intrusive igneous rock adjacent to the skarn (McDowell et al., 1996). The DOM and the EESS are undated and Big Gossan has been dated in this study.

Local geology

In the Big Gossan and Wanagon Gold areas, the sedimentary rocks of the Kembelangan Group and NGLG strike WNW (Figure B-2a) and dip steeply NNE. The skarns at Big Gossan and Wanagon Gold are separated by 2 km of strike and both occur at the contact between lower NGLG Waripi Formation dolostone and upper Kembelangan Group Ekmai Formation shale and limestone (Figure B-2).

Big Gossan

The Big Gossan skarn and associated Cu-Au deposit (Figure B-2c) are concentrated in a breccia developed in the lower Waripi Formation near the Kembelangan Group contact (Taylor et al., 1999). The Ekmai shale varies from 3-5 metres in thickness and occurs along the entire strike length of the Big Gossan orebody. The Big Gossan ore zone has a maximum strike length of more than 1,100 metres, a width of 4-60 metres and a known vertical extent of over 700 metres. The Big Gossan resource remains open at depth and along the NW extension (Hefton et al., 1995). At the end of 2002, Big Gossan reserves were 33 million tonnes at 2.81% Cu, 1g/t Au and 16.85g/t Ag (Freeport McMoRan Copper & Gold Inc 2002 Annual Report).

Two texturally distinct zones of major bedding-parallel faulting are recognised underground at Big Gossan and predate the skarn and mineralisation (Taylor et al., 1999; Clarke, 2002). A zone of ductile style layer parallel shearing, resulting in fine anastomosing shear textures occurs within the Ekmai Formation around 30-40m south of the Kembelangan shale-limestone contact. The second structure is a fault breccia parallel to the centre of the mineralised skarn in the Waripi Formation. It is recognised in underground crosscuts and drill holes to the west and east of the skarn (Taylor et al., 1999; Clarke, 2002). It has a variable width of 1-6m and is characterised by calcitic-marble clasts with interstitial black clay and carbonaceous material. The breccia texture can be traced into the skarn where it is overprinted by pyroxene and garnet alteration (Taylor et al., 1999).

NE striking faults NW of the Big Gossan deposit appear to have caused minimal disruption of stratigraphy at the Big Gossan drift level (Figure B-2c). The precise relationship between the faults and northwestern part of the Cu-Au deposit is unclear as only minor Cu-Au

Figure B-2. Geology of Big Gossan and Wanagon Gold (modified from PT Freeport Indonesia Geological maps). a) Local surface geology at Big Gossan and Wanagon Gold. Wanagon drill holes were drilled from surface. Big Gossan drill sections were collared underground at the 2930 elevation level. b) Interpreted Wanagon Gold cross section (XX′ on Figure B-2a) displaying geology (adapted from PT Freeport Indonesia Geological section) and distribution of hydrothermal systems (as interpreted from marked drillhole extents). Wanagon skarn Cu-Au is open to depth. c) Big Gossan 2930 elevation level geological map (from underground mapping and drill holes) and location of underground drives and drill sections. Modified from PT Freeport Indonesia drawing and Taylor et al. (1999).

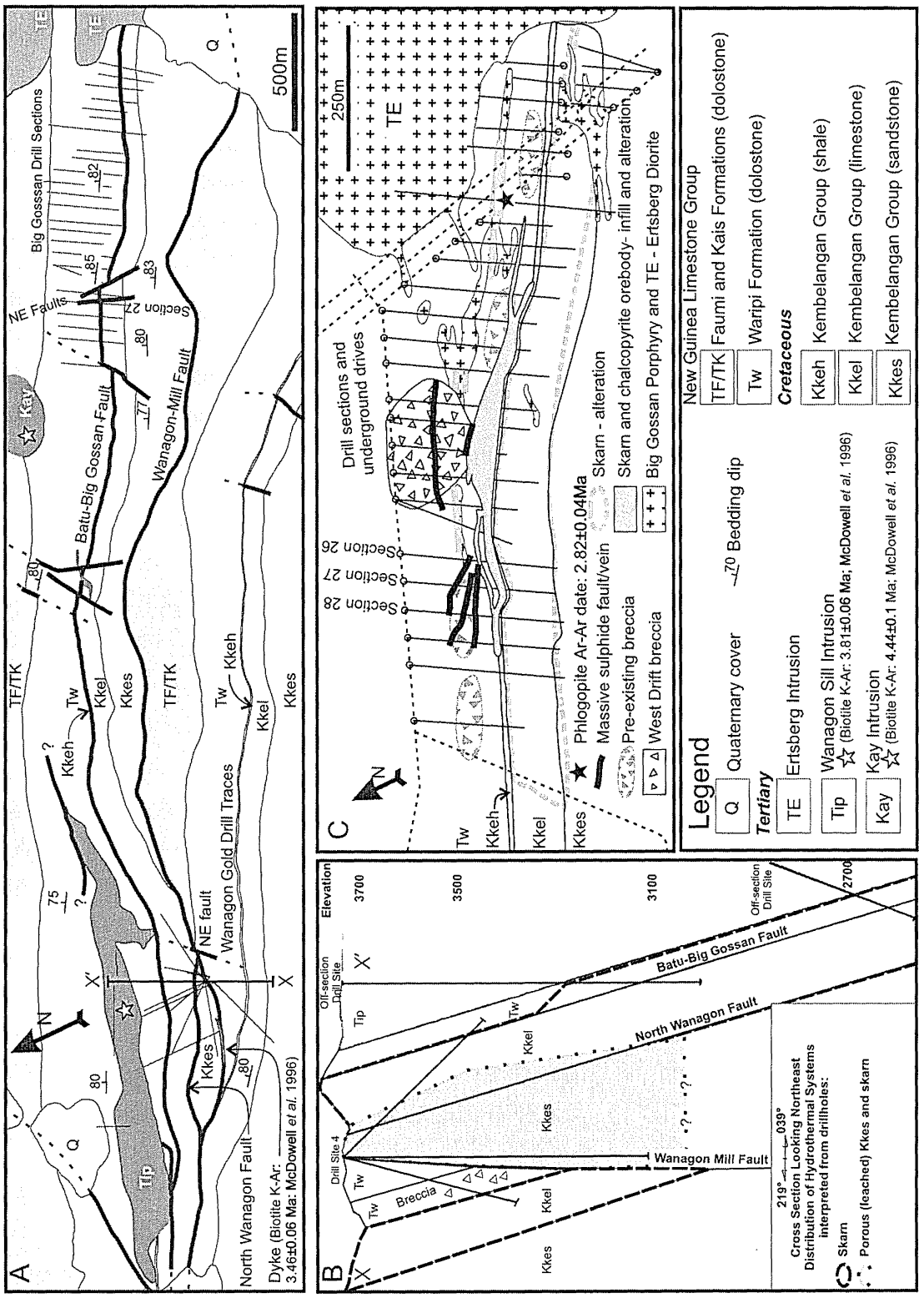
A
Big Gosssan Drill Sections
TE
Kay
NE Faults
Section 27
Batu-Big Gossan Fault
Wanagon-Mill Fault
TF/TK
Tw
Kkeh
Kkel
Kkes
Tip
Q
500m
NE fault
Wanagon Gold Drill Traces
North Wanagon Fault
Dyke (Biotite K-Ar: 3.46±0.06 Ma: McDowell et al. 1996)
B
Elevation
3700
3500
3100
2700
Off-section Drill Site
Drill Site 4
Breccia
Batu-Big Gossan Fault
North Wanagon Fault
Wanagon Mill Fault
219°
039°
Cross Section Looking Northeast
Distribution of Hydrothermal Systems interpreted from drillholes:
Skarn
Porous (leached) Kkes and skarn
C
250m
Drill sections and underground drives
Section 26
Section 27
Section 28
Phlogopite Ar-Ar date: 2.82±0.04Ma
Massive sulphide fault/vein
Pre-existing breccia
West Drift breccia
Skarn - alteration
Skarn and chalcopyrite orebody- infill and alteration
Big Gossan Porphyry and TE - Ertsberg Diorite
Legend
Q Quaternary cover
70 Bedding dip
Tertiary
TE Ertsberg Intrusion
Tip Wanagon Sill Intrusion (Biotite K-Ar: 3.81±0.06 Ma; McDowell et al. 1996)
Kay Kay Intrusion (Biotite K-Ar: 4.44±0.1 Ma; McDowell et al. 1996)
New Guinea Limestone Group
TF/TK Faumi and Kais Formations (dolostone)
Tw Waripi Formation (dolostone)
Cretaceous
Kkeh Kembelangan Group (shale)
Kkel Kembelangan Group (limestone)
Kkes Kembelangan Group (sandstone)

development extends past the interpreted location of the faults (approximately Section 28). A breccia body (upper breccia) has been intersected in drilling below the mapped surface fault traces. Angular sulphide clasts reported in the upper breccia (Freeport drill logs) indicate that at least one episode of movement postdates mineralisation.

The 200-250m diameter West Drift breccia pipe (hydrothermal breccia in Meinert et al., 1997) occurs in the Waripi Formation immediately NE of the Big Gossan skarn. It extends vertically down at least 600m and its NE contact dips steeply SW towards the skarn. It has not been documented in Freeport surface mapping 5-600 metres above level RL2930. The breccia is coincident with the widest part of the Big Gossan Cu-Au orebody (Figure B-2c).

Additional areas of brecciation recognised include "intrusive breccia" (Meinert et al., 1997) which refers to restricted zones of breccia in the Waripi Formation hanging wall which exhibit fragment rounding, high matrix content and mixed fragments (sedimentary and igneous). "Contact breccia" occurs adjacent to the contact with the Ertsberg Intrusion (Meinert et al., 1997). Both these breccia types predate the Big Gossan skarn alteration.

Distended bedding planes and dip-slip faults appear to have controlled emplacement of numerous sills and dykes at Big Gossan (Hefton et al., 1995; Taylor et al., 1999). Two texturally different types of intrusions (Meinert et al., 1997; Taylor et al., 1999) predate the Big Gossan skarn alteration (Taylor et al., 1999). One of these contains abundant mafic minerals (amphibole, biotite) and was classified by Rae et al. (1994) as quartz monzonite as it is visually identical to the monzonitic Ertsberg pluton to the east. The second, known locally as Big Gossan porphyry, is more leucocratic and contains prominent feldspar phenocrysts (Taylor et al., 1999).

A $^{40}Ar/^{39}Ar$ mica date from phlogopite in a calcite and anhydrite vein that crosscuts garnet skarn at Big Gossan is 2.82±0.04Ma (Figure B-3; Appendix 1). The date is older and not within error of $^{40}Ar/^{39}Ar$ 2.67±0.03Ma age for the Ertsberg Intrusion (Pollard et al., submitted) but within error of the K-Ar 3.09±0.25Ma age (McDowell et al., 1996) from an area of the Ertsberg Intrusion near to Big Gossan (Figure B-1).

Wanagon Gold

The Wanagon Gold prospect has a resource potential of 2 million ounces of gold (Sanusi, 1994). The surface geology and geological setting have been described by Sanusi (1994) and Malensek (1997). Bedding generally strikes NW and dips between 75° and 85° to the NE. NW-SE trending faults dominate the structure in the area (Figure B-2). Of the three recognised faults, namely the Batu-Big Gossan Fault, the North Wanagon Fault,

Figure B-3. $^{40}Ar/^{39}Ar$ age spectrum and isochron for A, B) Big Gossan skarn phlogopite and C, D) Wanagon Gold K-feldspar (Appendix 1, 12).

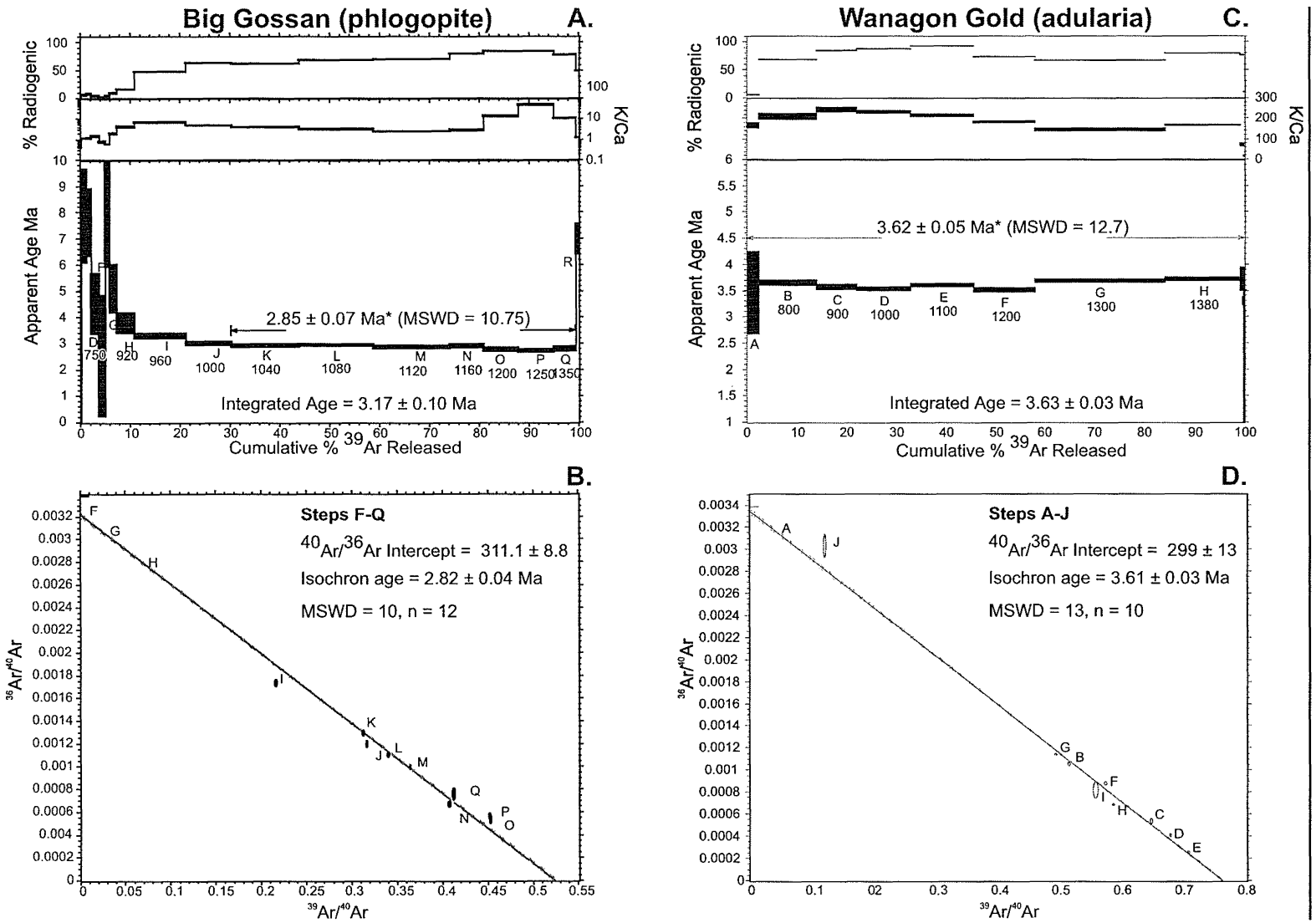

and the Wanagon-Mill Fault, only the latter crosscuts bedding. The Batu-Big Gossan fault is considered to lie on the contact between Kembelangan Group and Waripi Formation, parallel to stratigraphy and along strike from Big Gossan, although there is little evidence for significant movement (P. Warren pers comm.). This contact is a focus for skarn alteration and Cu-Au mineralisation. The North Wanagon Fault is located at the Kembelangan Group sandstone-limestone contact, has an unknown displacement, strikes 290° to 320° and dips 70° to 85° NE. The Wanagon-Mill fault crosscuts bedding and causes repetition of the Kembelangan Group and Waripi Formation (Figure B-2).

Major structural breaks and intersections appear to have controlled sill and dyke emplacement at the Wanagon Gold prospect. The igneous rocks are predominantly intermediate in composition (Sanusi, 1994). The main intrusive body, the Wanagon Sill, is a quartz-bearing diorite or monzodiorite porphyry (Honea, 1993a). McDowell (1996) determined its age using the K-Ar method at 3.81±0.06Ma. Smaller diorite dykes parallel to stratigraphy have been noted in mapping and drillcore (Sanusi, 1994). A NE-striking fault in the centre of the Wanagon Gold area is coincident with NE extension of the Wanagon Sill and elevated gold assays in surface and drillhole samples (P. Warren pers comm.).

The Waripi Formation in the footwall of the Wanagon Mill fault is brecciated and altered to marble. The marble clasts are surrounded by dark-grey and black calcitic matrix (Sanusi, 1994), which may have developed by pressure solution processes (cf. Logan, 1984), and are locally replaced by massive sulphides. Drilling and surface mapping suggest the breccia is concordant and coincident with a change in curvature of the Wanagon Mill fault from SW-dipping to NE-dipping with depth (P. Warren pers comm.).

Hydrothermal paragenesis

Big Gossan

The paragenesis of Big Gossan skarn and associated Cu-Au mineralisation (Figure B-4) has been described previously by Meinert et al. (1997) and Taylor et al. (1999). The development of the skarn was multi-staged with repeated refracturing and successive fluid influxes which resulted in overprinting paragenetic stages (Taylor et al., 1999). High fluid pressure is also postulated to have resulted in major dilational brecciation causing development of coarse grained infill skarn mineral textures and subsequent concentration of sulphide in dilatational sites .

A hydrous skarn event affected all stratigraphic units and overprinted the Big Gossan pyroxene and garnet skarn. An extensive crackle fracture system throughout the Waripi

Figure B-4. Parageneses of Big Gossan and Wanagon Gold.Compiled from this study and previous work (Allen, 1992b; Honea, 1993a, b, 1994; Rae et al., 1994; Honea, 1996a; Meinert et al., 1997; Taylor et al., 1999; Allen, 1992a). "Paragenetic sequence" refers to textural chronological order of formation and the term hydrothermal "association" does not imply equilibrium (Hemley and Hunt, 1992). Hydrothermal association: * timing unclear with respect to earlier stages; ** timing unclear with respect to later stages. Paragenetic sequence: a) b) c) is the observed sequence within hydrothermal association and ? indicates sequence not confirmed. Stratigraphic distribution: X major occurrence; (x) minor occurrence; ? Occurrence unknown. Stratigraphic abbreviations from Quarles Van Ufford (1996) and Dow et al. (1988).

WANAGON GOLD

Hydrothermal Association		Paragenetic Sequence	Stratigraphic Distribution (looking WNW) From S to N								
			Kkeh-Kkel	Tw (includes Breccia)	Wanagon Mill Fault	Kkes	North Wanagon Fault	Kkel-Kkeh	Batu- Big Gossan Fault	Tw	Tpiw
Skarn (anhydrous)	a)	pyroxene+garnet	X			X		X		X	(x)
	b)	?olivine, wollanstonite	?			?		(x)		(x)	?
Skarn (hydrous)	?	?amphibole	?			?		X		(x)	(x)
	?	epidote	X					X		(x)	(x)
*Oxide	?	magnetite	?			?		X		(x)	(x)
**Stage WG1 sulphides	a)	quartz	?					X		(x)	(x)
	b)	pyrite						X		(x)	(x)
	c)	chalcopyrite (sphalerite, galena, arsenopyrite, gold)						X		(x)	(x)
Leaching		leaching				X		(x)			
		kaolinite, smectite				X		(x)			
Stage WG2 Gold & Fe-Zn-As sulphides & local Bi & Te minerals		pyrite, sphalerite, galena, gold, (minor chalcopyrite) tetrahedrite, petzite, hessite, altaite, tetradymite, silver-antimony-sulphide, K-feldspar, quartz, calcite	?	X		X		(x)			
Late		calcite, Fe-oxides	?	X		X		X		X	?

BIG GOSSAN

Hydrothermal Association		Paragenetic Sequence	Kkel-Kkeh	Batu- Big Gossan Fault	Tw (skarn)	Tw (hanging wall)	Tw (West Drift Breccia)	Intrusions
Early	?	biotite, K-feldspar	X					
	?	marble	?		X	(x)		
Skarn (anhydrous)	a)	pale pyroxene (diopside), calcite, quartz	X		(x)			(x)
	b)	dark green pyroxene (diopside-hedenbergite), calcite, quartz	(x)		X			(x)
	c)	andradite garnet, calcite, quartz	(x)		X			(x)
Skarn (hydrous)	a)	carbonate, amphibole (actinolite and tremolite), phlogopite	(x)		X		X	(x)
	b)	carbonate, talc	(x)		X		X	(x)
Sulphate		anhydrite	(x)		X		X	?
Fe-oxide		magnetite	(x)		X	X	X	?
Stage BG1 Gold & Fe-Cu-Ag sulphides	a)	early coarse grained pyrite no gold	(x)		?		X	(?)
	?	pyrrhotite	(x)		(x)	(x)		(?)
	c)	chalcopyrite, hematite-magnetite, pyrrhotite, sphalerite, bornite, (galena), gold	(x)		X	(x)	(x)	(?)
	c)	chalcopyrite, gold, Fe-bearing sphalerite, galena, arsenopyrite, scheelite	(x)		X	(x)	(x)	(?)
Stage BG2 Gold & Fe-Zn-Pb-As sulphides & local Bi & Te minerals	a)	early coarse pyrite, gold (Type 1)	(x)		(x)		X	(?)
	b)	pyrite, sphalerite (Fe-bearing and Fe-poor), galena, chalcopyrite, gold, siderite, quartz	(x)		(x)	X	X	(?)
	b)	galena (dominant), sphalerite, chalcopyrite, gold (Type 2), siderite	(x)		(x)	X	X	(?)
	c)	cosalite, bismuthinite, tetradymite, argentian tetrahedrite and tennantite, gold (Type 3)	(x)		(x)	X	X	(?)
	d)	marcasite-arsenopyrite, ?gold	(x)		(x)	X	X	(?)
	?	*massive pyrite, gold (Type 4; Cu-Fe-Zn -bearing)				X		(?)
Late		epidote, chlorite, hematite, pyrite	(x)		(x)	(x)	(x)	(x)

Formation features alteration selvedges and vein fill of amphibole, talc and anhydrite. The absence of anhydrous skarn alteration in the West Drift breccia and the presence of rare anhydrous skarn fragments (Sugiri, 1999) suggests that the breccia developed after formation of the anhydrous skarn. The West Drift breccia does have extensively developed amphibole and talc. There is no evidence to suggest that the hydrous paragenesis in the West Drift breccia is distinct from that developed in the adjacent Big Gossan skarn. The earliest mineral in the hydrous event is amphibole. In the Big Gossan skarn, actinolite predominantly replaces pyroxene (Gonzalez, 1993; Taylor et al., 1999). Tremolite occurs as vugh fill in the skarn, (Gonzalez, 1993) and in fractures in the Waripi Formation and throughout the West Drift breccia.

The West Drift breccia has been described previously by Rae et al. (1994) and Sugiri (1999), who focused on the relationship between the breccia and the adjacent Big Gossan skarn and mineralisation. The abundance of amphibole, talc and anhydrite increase westwards where amphibole clasts are altered to talc and enclosed in younger, coarse-grained anhydrite. Rae et al. (1994) measured fluid inclusion homogenisation temperatures in anhydrite from the breccia (301-378°C) which are lower than those of inclusions from anhydrite in the skarn (375-405°C; (Meinert et al., 1997).

Magnetite veins crosscut amphibole and anhydrite in the West Drift breccia and postdate the Big Gossan anhydrous and hydrous skarn. Coarse-grained pyrite replaces magnetite in the West Drift breccia and post-magnetite pyrite is common in the adjacent skarn. Drill core assays indicate that significant levels of gold are not associated with this generation of pyrite (Figure B-5i). Most generations of calcite in the West Drift breccia appear to be late and associated with magnetite or pyrite. Rae et al. (1994) measured fluid inclusion homogenisation temperatures in late calcite from the breccia of 127-135°C.

Stage BG1 Cu-Au mineralisation

Stage BG1 Cu-Au mineralisation crosscuts the skarn and restricted zones in the Waripi Formation and West Drift breccia. Skarn and Stage BG1 Cu-Au were not observed in the upper breccia. Pyrrhotite occurs as corroded clasts enclosed by chalcopyrite and altered to pyrite and marcasite. Chalcopyrite is the dominant copper sulphide and occurs interstitial to earlier magnetite and pyrite. Homogeneous, dark coloured iron-bearing sphalerite occurs with chalcopyrite and exhibits chalcopyrite disease. Some adjacent chalcopyrite grains contain small star-shaped inclusions of sphalerite. Galena is less common and occurs in late stage veinlets. Late-stage arsenopyrite crystals occur locally and rare scheelite occurs on chalcopyrite grain-boundaries. Specular hematite, partly altered to magnetite, occurs with chalcopyrite although its distribution is not constrained. Rare Stage BG1 electrum occurs in pyrrhotite, chalcopyrite and on chalcopyrite grain boundaries and does not display

high fineness (Figure B-6). Non-sulphide gangue includes quartz and minor calcite.

Stage BG2 Pyrite-Au-As-Zn-Bi-Te occurrences

Stage BG2 sulphides are widely distributed along the skarn-Waripi Formation contact, within the upper breccia, in faults in the Waripi Formation (Figure B-7), along faults in the West Drift breccia and along the contact between the West Drift breccia and the Waripi Formation (Figure B-2c). The late-stage sulphide association exhibits a number of different textural styles but is characterised by consistent mineral associations and geochemistry. Pyrite is the dominant sulphide with decreasing amounts of sphalerite, chalcopyrite, galena and native gold. Sphalerite ranges from pale to dark (0.57 to 11.76 wt % Fe) and is locally zoned. The minor non-sulphide gangue includes ankerite and quartz.

Clasts of quartz containing chalcopyrite interpreted to belong to Stage BG1 occur entrained within a breccia matrix of massive Stage BG2 pyrite in a fault in the Waripi Formation, 30m NE of the skarn contact (Figure B-5a). This Stage BG2 massive pyrite intersection contains coincident elevated zinc, arsenic, lead and native gold (1.9%, 1380ppm, 1030ppm and 19.4ppm respectively). A similar relationship is observed within the Big Gossan skarn where clasts of skarn with pyrite and chalcopyrite mineralisation occur within massive Stage BG2 pyrite (Figure B-5f). Where Stage BG2 sulphides replace carbonate in the Waripi Formation, pyrite and sphalerite rod textures (cf. Thompson and Arehart, 1990) are developed. Pyrite rod-texture grainsize mimics original bedding grainsize variation. Centimetre-scale marble alteration halos are associated with sulphide veins and replacement in carbonate (Figure B-8b). A zone of banded veins containing quartz,

Figure B-5. Big Gossan photographs and photomicrographs. (Apy-arsenopyrite; Bm-bismuthinite; Ccp-chalcopyrite; Cbt-carbonate; Cct-calcite; Cub-cubanite; Dol-dolomite; Gn-galena; Py-pyrite; Qtz-quartz; Sd-siderite; Sp-sphalerite). Sample location in brackets is drillhole and depth. a) (BGU18-3, 212m) Big Gossan clast of quartz entrained within Stage BG2 massive pyrite. Polished section examination documented chalcopyrite (interpreted as Stage BG1) within the quartz clast. b) (BGU21-3, 24.6m). Banded carbonate and quartz with Stage BG2 pyrite. 3m assay interval contains 0.05% Cu, 2.31ppm Au, 430ppm Pb, 1160ppm Zn, 1250ppm As. c) (BGU21-3, 24.5m). Big Gossan native gold flake within banded and botryoidal quartz and carbonate (Stage BG2). Sphalerite and pyrite are also present. d) (BGU24-10, 305m) Big Gossan Stage BG2 sphalerite-galena-pyrite- gold-siderite vein crosscuts skarn-hosted Stage BG1 chalcopyrite-pyrite-magnetite. Stage BG1 and Stage BG2 pyrite in this sample have distinctly different LA-ICPMS geochemistry (Appendix 7). e) (BGU21-10, 12m) Big Gossan West Drift breccia matrix is altered by Stage BG2 pyrite-sphalerite-arsenopyrite-siderite. 2.8m assay interval contains 2.24ppm Au, 0.01% Cu, 2800ppm Zn, 1700ppm Pb, 2100ppm As (Appendix 2). f) (BGU19-3, 233.35m). Clast composed of skarn and Stage BG1 chalcopyrite and pyrite entrained within fine-grained Stage BG2 pyrite (Py2) 3m assay interval contains 9.5ppm Au, 1.09% Cu (Appendix 2). g) BGU28-5, 268m) Reflected light photomicrograph. Stage BG2 bismuthinite, native gold, cubanite and hematite occur along fractures in earlier Stage BG1 pyrite and quartz vein. Native gold also coats pyrite surfaces. h) (BGU21-2, 13.3m) Reflected light photomicrograph. Stage BG2 arsenopyrite replacement of sphalerite, chalcopyrite and galena. i) (BGU24-10-16) Big Gossan massive cubic pyrite in West Drift breccia (Stage BG1). Gold grades for 1m pyrite-rich intersection are 0.1ppm (Appendix 2). j) (BGU21-2, 13.3m) Reflected light photomicrograph. Stage BG2 native gold closely associated with galena with bismuthinite inclusion.

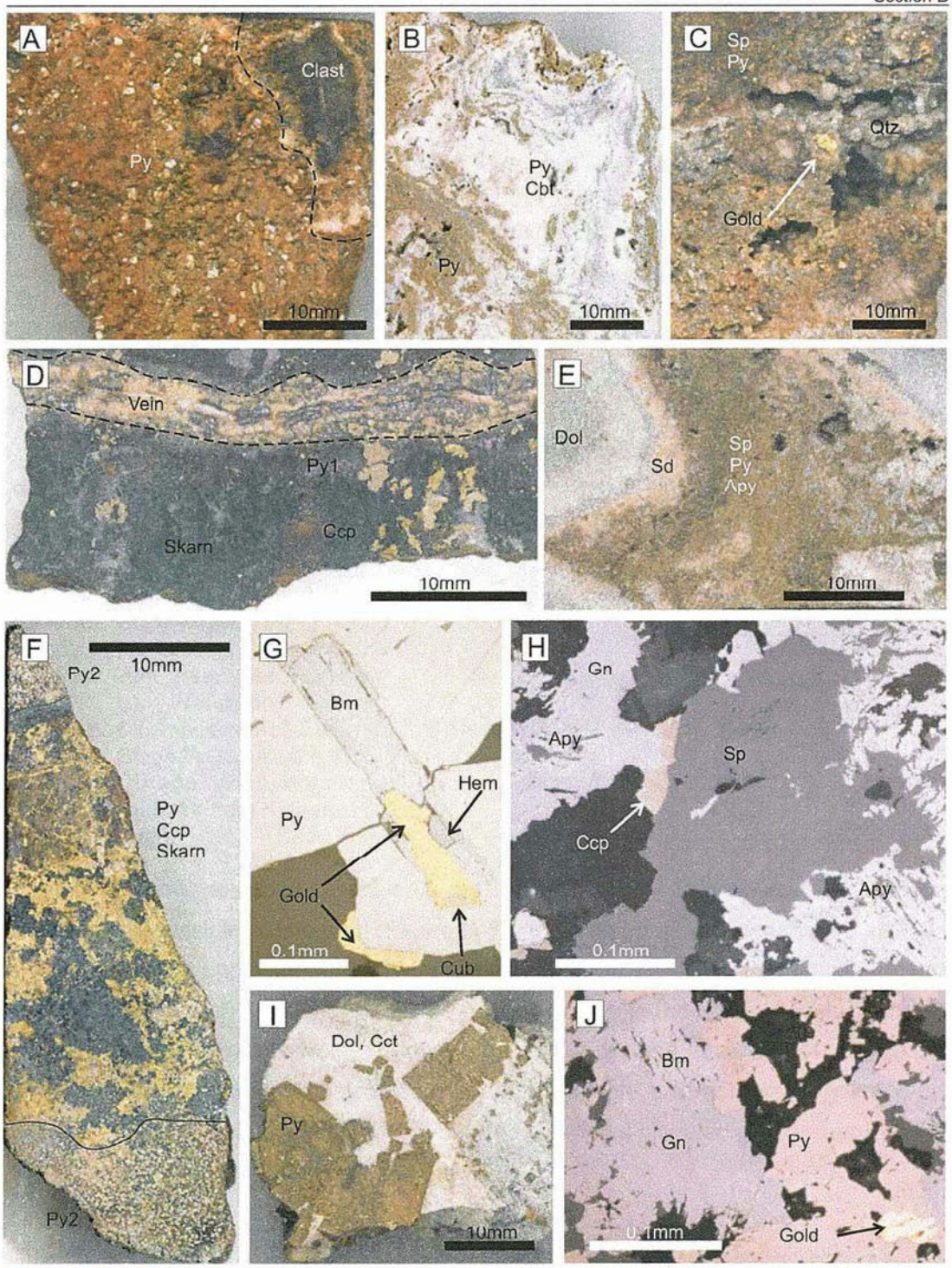
A
Clast
Py
10mm
B
Py
Cbt
Py
10mm
C
Sp
Py
Qtz
Gold
10mm
D
Vein
Py1
Ccp
Skarn
10mm
E
Dol
Sd
Sp
Py
Apy
10mm
F
10mm
Py2
Py
Ccp
Skarn
Py2
G
Bm
Hem
Py
Gold
0.1mm
Cub
H
Gn
Apy
Sp
Ccp
Apy
0.1mm
I
Dol, Cct
Py
10mm
J
Bm
Gn
Py
0.1mm
Gold

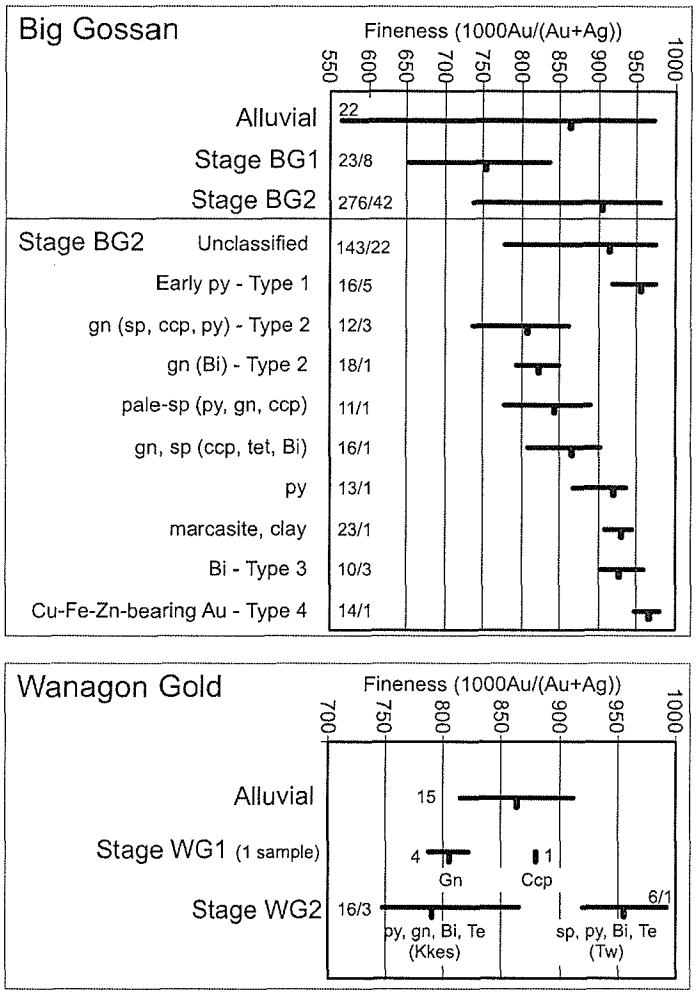

Figure B-6. Big Gossan and Wanagon Gold Stage 1 and Stage 2 native gold microprobe compositions (Appendix 5). Local alluvial native gold analyses (Allen and Palmer, 1992) plotted for comparison. Only probe analyses with totals between 98-102 were included. Fineness ranges are annotated with "number of grains analysed/number of samples". (Bi-Bi minerals; Ccp-chalcopyrite; Gn-galena; Py-pyrite; Sp-sphalerite; Te-Te minerals; Tet-tetrahedrite). a) Big Gossan native gold microprobe composition and examples of the composition of Stage BG2 native gold occurring with different sulphide assemblages. Big Gossan results include 15 Stage BG1 analyses from 2 drillcore samples (Rubin, 1996). Big Gossan Stage BG2 and "unclassified" results includes 86 analyses from 10 samples (Rae et al., 1994) and 12 analyses from 2 samples (Rubin, 1996). b) Wanagon Gold microprobe composition of Stage WG1 and Stage WG2 native gold. Wanagon Stage WG2 results include 4 analyses from 1 sample (Honea, 1996b).

carbonate, pyrite and minor sphalerite crosscuts the West Drift breccia and contains bonanza-style visible native gold (Figure B-5b, c). Banded quartz also occurs at higher elevations in the upper breccia. Rhythmically banded magnetite with sulphides (pyrite-sphalerite dominant) without appreciable gangue occurs in the upper breccia and in the Waripi Formation. Narrow veins of low-Fe sphalerite, galena, ankerite and native gold crosscut skarn containing chalcopyrite, pyrite, magnetite and hematite (Figure B-5d). Ankerite, pyrite, sphalerite and arsenopyrite with coincident elevated gold assays overprint the West Drift breccia matrix (Figure B-5e).

The earliest generation of Stage BG2 native gold at Big Gossan has high-fineness (Figure B-6; Type 1) and occurs as inclusions in early coarse-grained Stage BG2 pyrite. A second generation of Stage BG2 native gold is associated with sulphides interstitial to pyrite and

Figure B-7. Geological cross section BGU26. Modified from PT Freeport geological cross section and drill logging. Stage BG1 copper-gold mineralisation correlates with the distribution of the Big Gossan skarn. Stage BG2 occurs in faults in the Waripi Formation hanging wall and Kembelangan Limestone footwall and along the contact between the Big Gossan skarn and Waripi Formation hanging wall. Location of BGU26-1 (Figure B-11) is annotated. Cu:10000Au ratio for Stage 2 ore intervals are <0.2 and Stage 1 ore intervals are typically >1.88.

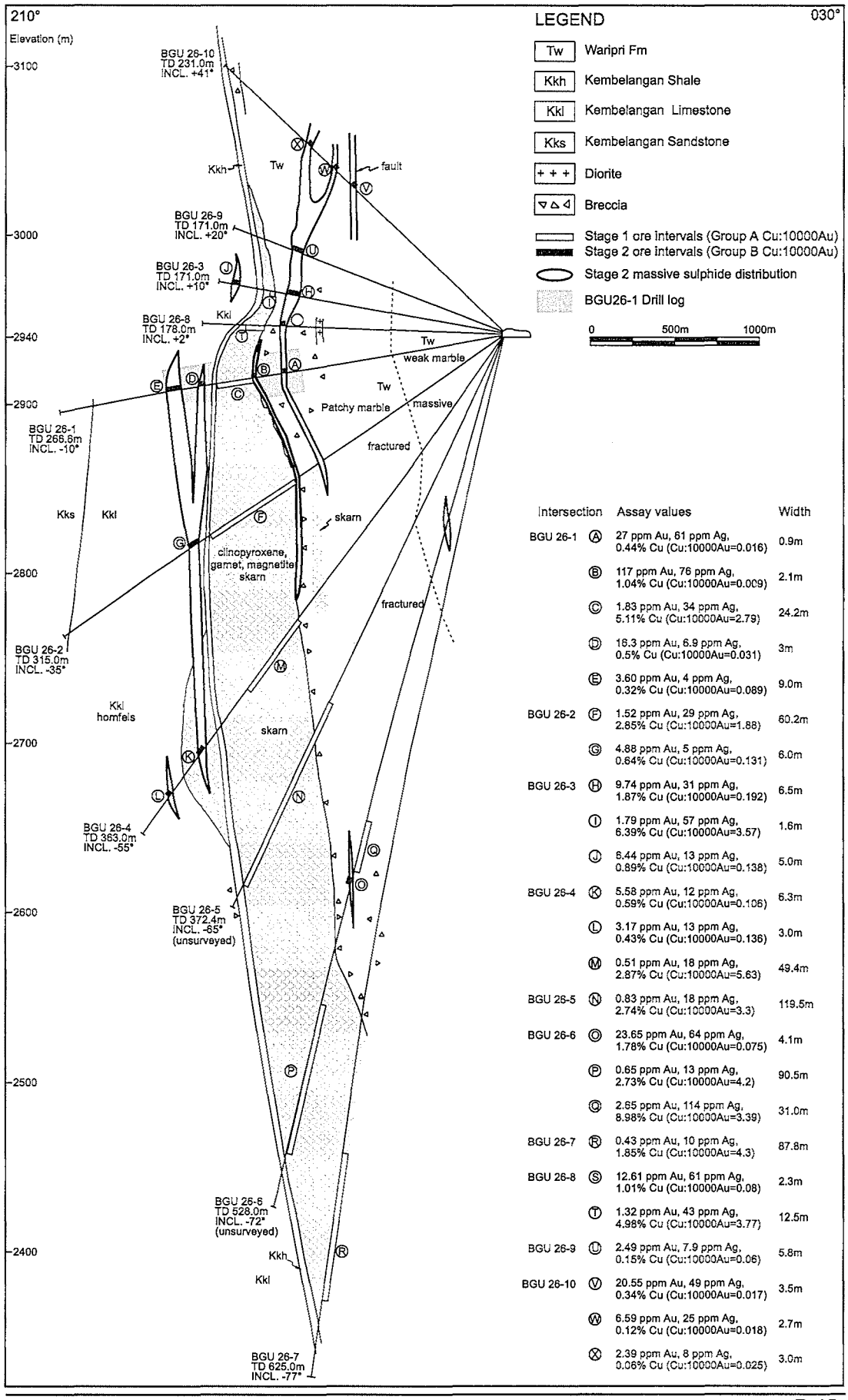

Intersection		Assay values	Width
BGU 26-1	Ⓐ	27 ppm Au, 61 ppm Ag, 0.44% Cu (Cu:10000Au=0.016)	0.9m
	Ⓑ	117 ppm Au, 76 ppm Ag, 1.04% Cu (Cu:10000Au=0.009)	2.1m
	Ⓒ	1.83 ppm Au, 34 ppm Ag, 5.11% Cu (Cu:10000Au=2.79)	24.2m
	Ⓓ	16.3 ppm Au, 6.9 ppm Ag, 0.5% Cu (Cu:10000Au=0.031)	3m
	Ⓔ	3.60 ppm Au, 4 ppm Ag, 0.32% Cu (Cu:10000Au=0.089)	9.0m
BGU 26-2	Ⓕ	1.52 ppm Au, 29 ppm Ag, 2.85% Cu (Cu:10000Au=1.88)	60.2m
	Ⓖ	4.88 ppm Au, 5 ppm Ag, 0.64% Cu (Cu:10000Au=0.131)	6.0m
BGU 26-3	Ⓗ	9.74 ppm Au, 31 ppm Ag, 1.87% Cu (Cu:10000Au=0.192)	6.5m
	Ⓘ	1.79 ppm Au, 57 ppm Ag, 6.39% Cu (Cu:10000Au=3.57)	1.6m
	Ⓙ	6.44 ppm Au, 13 ppm Ag, 0.89% Cu (Cu:10000Au=0.138)	5.0m
BGU 26-4	Ⓚ	5.58 ppm Au, 12 ppm Ag, 0.59% Cu (Cu:10000Au=0.106)	6.3m
	Ⓛ	3.17 ppm Au, 13 ppm Ag, 0.43% Cu (Cu:10000Au=0.136)	3.0m
	Ⓜ	0.51 ppm Au, 18 ppm Ag, 2.87% Cu (Cu:10000Au=5.63)	49.4m
BGU 26-5	Ⓝ	0.83 ppm Au, 18 ppm Ag, 2.74% Cu (Cu:10000Au=3.3)	119.5m
BGU 26-6	Ⓞ	23.65 ppm Au, 64 ppm Ag, 1.78% Cu (Cu:10000Au=0.075)	4.1m
	Ⓟ	0.65 ppm Au, 13 ppm Ag, 2.73% Cu (Cu:10000Au=4.2)	90.5m
	Ⓠ	2.65 ppm Au, 114 ppm Ag, 8.98% Cu (Cu:10000Au=3.39)	31.0m
BGU 26-7	Ⓡ	0.43 ppm Au, 10 ppm Ag, 1.85% Cu (Cu:10000Au=4.3)	87.8m
BGU 26-8	Ⓢ	12.61 ppm Au, 61 ppm Ag, 1.01% Cu (Cu:10000Au=0.08)	2.3m
	Ⓣ	1.32 ppm Au, 43 ppm Ag, 4.98% Cu (Cu:10000Au=3.77)	12.5m
BGU 26-9	Ⓤ	2.49 ppm Au, 7.9 ppm Ag, 0.15% Cu (Cu:10000Au=0.06)	5.8m
BGU 26-10	Ⓥ	20.55 ppm Au, 49 ppm Ag, 0.34% Cu (Cu:10000Au=0.017)	3.5m
	Ⓦ	6.59 ppm Au, 25 ppm Ag, 0.12% Cu (Cu:10000Au=0.018)	2.7m
	Ⓧ	2.39 ppm Au, 8 ppm Ag, 0.06% Cu (Cu:10000Au=0.025)	3.0m

display fineness variations with the associated sulphide mineralogy (Figure B-6). Where galena is dominant, lower fineness gold (Figure B-6; Type 2) commonly occurs within galena. Native gold in sphalerite-dominant samples is higher fineness than native gold associated with galena-dominated samples (Figure B-6).

Localised Bi and Te minerals include cosalite ($Bi_3Pb_2S_5$ with minor Ag), bismuthinite (Bi_2S_3), tetradymite ($Bi_{14}Te_{13}S_8$) and Ag-bearing tennantite-tetrahedrite solid solutions ($(CuAgFe)_{12}Sb_4S_{13}$ and $(CuAgFe)_{12}As_4S_{13}$) also occur (Rae et al., 1994: this study). Minor cubanite is associated with bismuthinite (Figure B-5g). Native gold associated with Bi and Te minerals has high fineness (Figure B-6; Type 3). Where native gold with bismuthinite overprints Stage BG1 mineralisation, abundant native gold grains occur in fractures and along pyrite grain edges (Figure B-5g). These relationships are not apparent at hand specimen scale. Arsenopyrite and marcasite are the youngest sulphides in the Stage 2 association. They enclose earlier cubic pyrite and replace sphalerite, chalcopyrite and galena (Figure B-5h). The relative timing of coarse native gold grains in these samples is unclear although it appears closely associated with galena containing bismuthinite inclusions (Figure B-5j). In the upper breccia, high fineness native gold containing trace Cu, Fe and Zn occurs in fractures in a temporally unconstrained generation of massive pyrite with minor interstitial sphalerite and chalcopyrite. (Figure B-6; Type 4).

Figure B-8. Wanagon Gold and Big Gossan hand specimens, polished section microphotographs and fluid inclusion samples. (Alt-altaite; Cct-calcite; Kfs-K-feldspar; Kkes-Kembelangan Group sandstone; Pe-petzite; Phl-phlogopite; Py-pyrite; Rexal-recrystallised marble; Sp-sphalerite; Td-tetradymite). a) (WAN4-3, 63.2m) Wanagon Gold leached Kembelangan Group sandstone with Stage WG2 pyrite and K-feldspar in vughs and veins. K-feldspar sampled for $^{40}Ar/^{39}Ar$ geochronology. b) (BGU18-3, 211m) Big Gossan marble and (fluid inclusion-bearing; Figure B-8l) recrystallised marble halo (0.5mm) directly adjacent to Stage BG2 pyrite-sphalerite-gold replacement. c) (WAN4-1, 58m) Transmitted light photomicrograph. Stage WG2 K-feldspar crystals morphology suggests adularia) within a matrix of transparent to dark sphalerite. d) (WAN4-6, 28m) Reflected light photomicrograph. Stage WG2 pyrite with inclusions of white altaite. Tetradymite (pale grey), native gold (yellow) and petzite (dark grey) occur with altaite. Nearby in the same pyrite grain, hessite in altaite and galena in altaite also occur (not pictured). e) (WAN4-3, 138.1m) Typical Kkel skarn sample (XRD results in Appendix 3). f) (WAN4-3, 130.5m) Leached Kkel skarn sample, minor clay and pyrite developed in vughs (XRD results in Appendix 3). g) (WAN4-4, 603m) Wanagon Gold leached and silicified sandstone used for fluid inclusion study. Fluid inclusions are contained in the grey silicified areas (Figure B-8k). Minor Stage WG2 pyrite in vughs. h) (BGU26-4, 275m) Big Gossan Stage BG2 sphalerite (fluid inclusion-bearing; Figure B-8m) and pyrite-galena vein crosscuts skarn. Pyrite has a distinct Stage BG2 Bi and Te signature (LA-ICPMS; Appendix 7). Skarn contains submicroscopic fluid inclusion-bearing quartz (Figure B-8j). i) (BGU17-4, 400m) Green phlogopite and calcite vein crosscuts Big Gossan skarn. Phlogopite dated by the $^{40}Ar/^{39}Ar$ technique at 3.62±0.05Ma (Appendix 1, 12). j) (BGU26-4, 275m) Submicroscopic fluid inclusion-bearing quartz within skarn (Figure B-8h) contains two-phase fluid inclusions on secondary trails. k) (WAN4-4, 603m) Two phase fluid inclusions (paragenesis uncertain) in silicified Wanagon Gold sandstone (Figure B-8g). l) (BGU18-3, 211m) Two-phase fluid inclusion in recrystallised marble associated with Stage BG2 sulphides (Figure B-8b). m) (BGU26-4, 275m) Two-phase fluid inclusions in clusters in sphalerite from Stage BG2 sulphide vein (Figure B-8h).

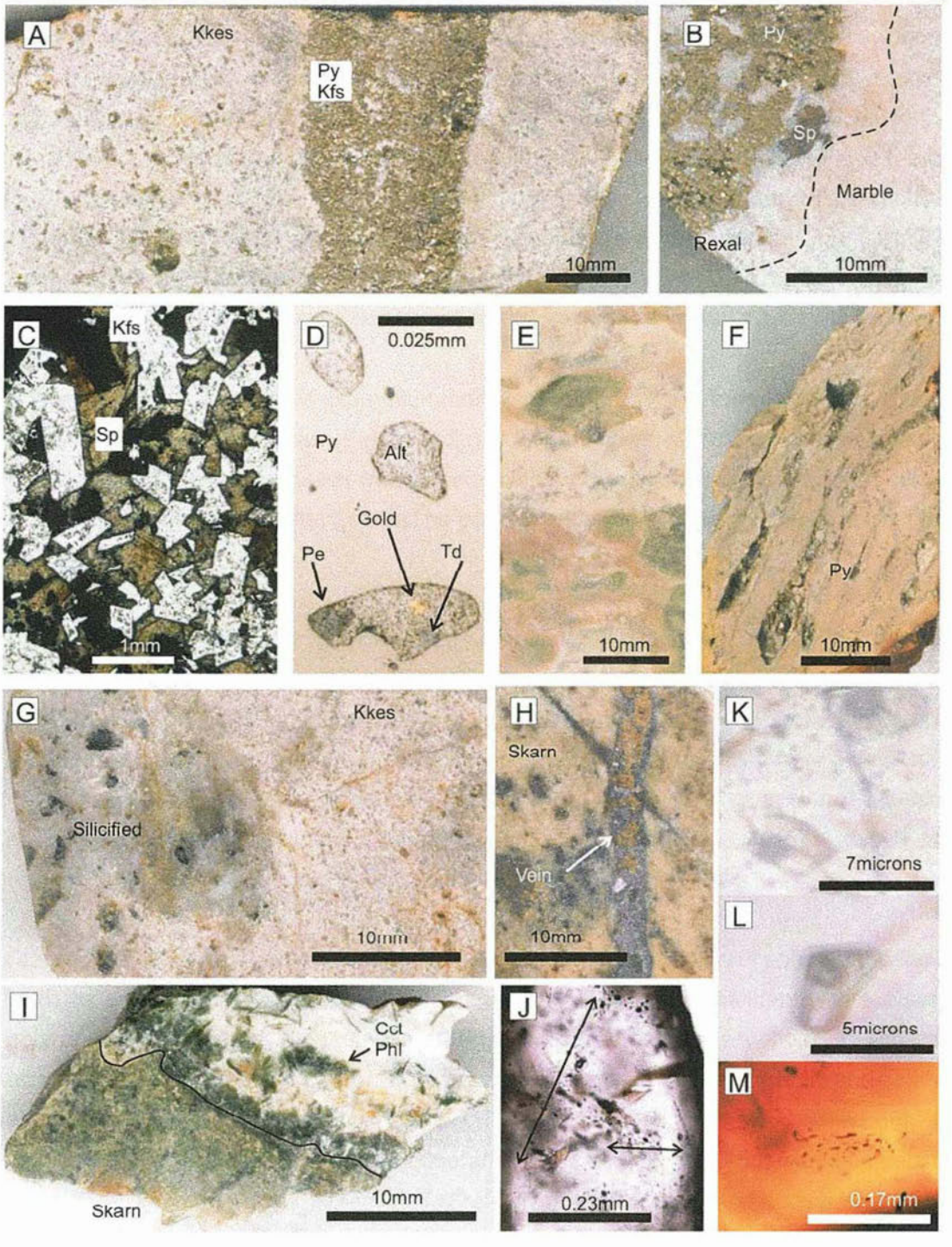
A
Kkes
Py
Kfs
10mm
B
Py
Sp
Marble
Rexal
10mm
C
Kfs
Sp
1mm
D
0.025mm
Py
Alt
Gold
Pe
Td
E
10mm
F
Py
10mm
G
Kkes
Silicified
10mm
H
Skarn
Vein
10mm
K
7microns
L
5microns
M
0.17mm
I
Cct
Phl
Skarn
10mm
J
0.23mm

Wanagon Gold

Surface sampling and limited drilling at the Wanagon Gold prospect has revealed evidence that there were several hydrothermal events, including two distinct phases of sulphide mineralisation (Figure B-4). Skarn alteration is pervasive in sedimentary rocks of the Kembelangan Group and Waripi Formation (Figure B-2b) and occurs as veins in the ca 3.81Ma Wanagon Sill (Honea, 1993a). Stage WG1 chalcopyrite-dominant sulphides overprint skarn at depth. Minor galena and sphalerite are also present. Overprinting relationships between Stage WG1 Cu-Au sulphides and Stage WG2 pyrite-Au-As-Zn-Bi-Te occurrences is unconstrained due to vertical distribution and limited availability of drilling.

A leaching event overprinted skarn alteration (Figure B-8e, f) and removed feldspar from the Kembelangan sandstone (Figure B-2b). XRD analyses of fresh and altered skarn show the development of clays (minor vermiculite, smectite and halloysite) in leached samples. Narrow alteration margins on fine-grained andesitic intrusive dykes are dominated by 7Å kaolinite.

Stage WG2 sulphides occur in the leached Kembelangan Group sandstone (Figure B-8a) and adjacent brecciated Waripi Formation (Figure B-2b). K-feldspar is texturally associated with Stage 2 sulphides in leach holes and veins in the Kembelangan Group sandstone (Figure B-8a, c). Petrographic morphology (Browne and Ellis, 1970; Dong and Morrison, 1995) indicates the feldspar is adularia (Figure B-8c). A $^{40}Ar/^{39}Ar$ date from K-feldspar associated with pyrite in leached sandstone is 3.62±0.05Ma (Figure B-3; Figure B-8a; Appendix 1).

Stage WG2 sulphides include abundant pyrite and rare occurrences of sphalerite-galena in vughs and veins in Kembelangan Group sandstone and are coincident with elevated gold and arsenic (Figure B-9). Honea (1996) considered that the secondary K-feldspar was introduced by the same event that introduced gold. Fine-grained sphalerite and galena are disseminated through the sandstone. In massive pyrite samples, native gold is associated with galena and Bi and Te minerals (Figure B-8; Figure B-5d) including petzite (Ag_3AuTe_2), hessite (Ag_2Te), altaite (PbTe), tetradymite ($Bi_{14}Te_{13}S_8$) and a silver-antimony-sulphide (Ag_3SbS_3) which could be either pyrargyrite or pyrostilpnite (Rae et al., 1994: this investigation).

Stage WG2 sulphides are accompanied by dolomite where they replace calcitic marble in brecciated Waripi Formation adjacent to the Kembelangan Group sandstone. K-feldspar is not evident and sulphides include dominant sphalerite (with chalcopyrite disease) and pyrite with lesser galena and minor chalcopyrite. These sulphides are crosscut by veinlets containing arsenical pyrite and tetrahedrite. Native gold is closely associated with

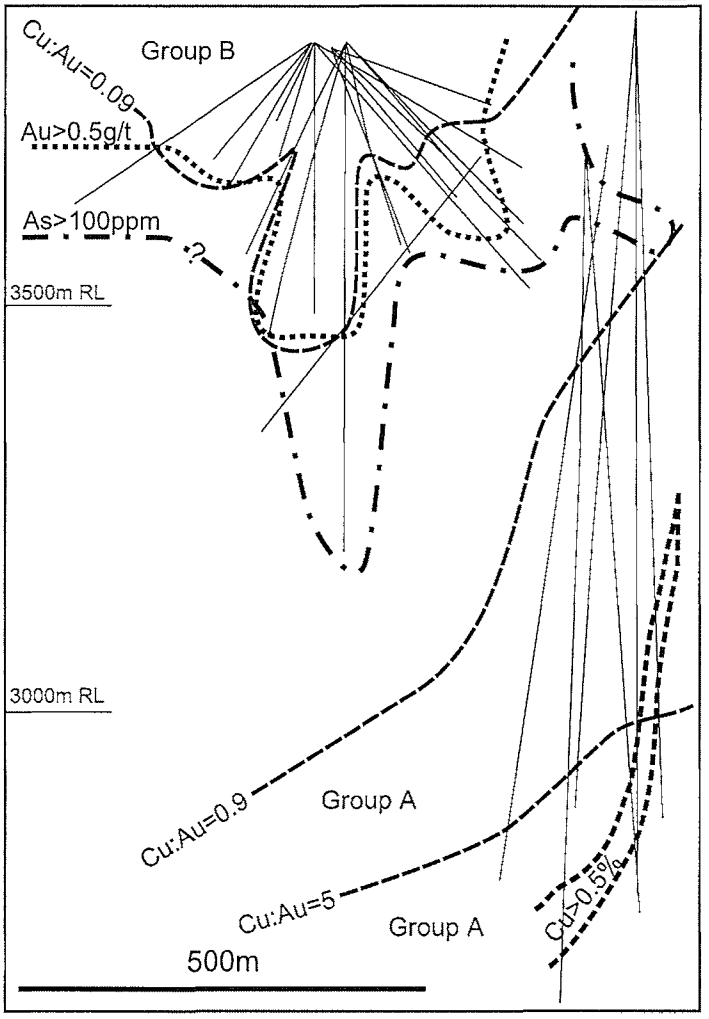

Figure B-9. Composite Wanagon Gold cross section looking NW. Drill holes and distribution of Cu:10000Au ratios and Cu>5%, As>100ppm, Au>0.5g/t contours. PT Freeport Indonesia assay data.

tetradymite and petzite, enclosed within sphalerite and pyrite and has a higher fineness than native gold hosted in the Kembelangan Group sandstone (Figure B-6).

Metal distributions from drillhole assays

Big Gossan assay correlation and distribution

Cu:10000Au assay ratios from Big Gossan are variable and have been divided into 3 groups (Figure B-10a, b). Group A is characterised by a ratio >0.9 and distinct Cu:Ag and Ag:10000Au relationships (Figure B-10c, d) indicating that Cu, Au and Ag are strongly associated in this group. The spatial distribution of Group A reflects that of Stage BG1 chalcopyrite (Figure B-11). Two key aspects of Stage BG1 metal zoning in Big Gossan Group A, firstly, that highest Cu grades are coincident with the lowest Pb:Zn ratios (Figure B-11, 10b); and secondly, that the highest Cu:10000Au ratios (>5; Figure B-12a) are coincident with the lowest Zn:Cu ratios (Figure B-12a, c). These ratios define areas of copper dominant mineralisation. A zone containing the lowest Zn:Cu ratios can be traced throughout the deposit in long section and plunges towards the NW (Figure B-13b). Cu>5% occurs in the NW of the deposit coincident with the location of the NE faults (Figure

Figure B-10. Element correlations from Big Gossan (A-G; n= ca. 15,000 analyses) and Wanagon Gold (H-L; n= ca. 4,000 analyses) drillhole assay data. a) Cu:10000Au. Group A >0.9 and Group B<0.09. Intermediate datapoints (Cu:10000Au = 0.09-0.9) represents overlap between the Groups. b) log Cu:10000Au. c) Cu:Ag. d) log Ag:Au. e) log Cu:Zn. f) log Cu:10000As. g) log 10000Ag:Pb. h) Cu:10000Au. i) log Cu:10000Ag. j) log Cu:Zn. k) log Cu:10000As. l) log Cu:Pb.

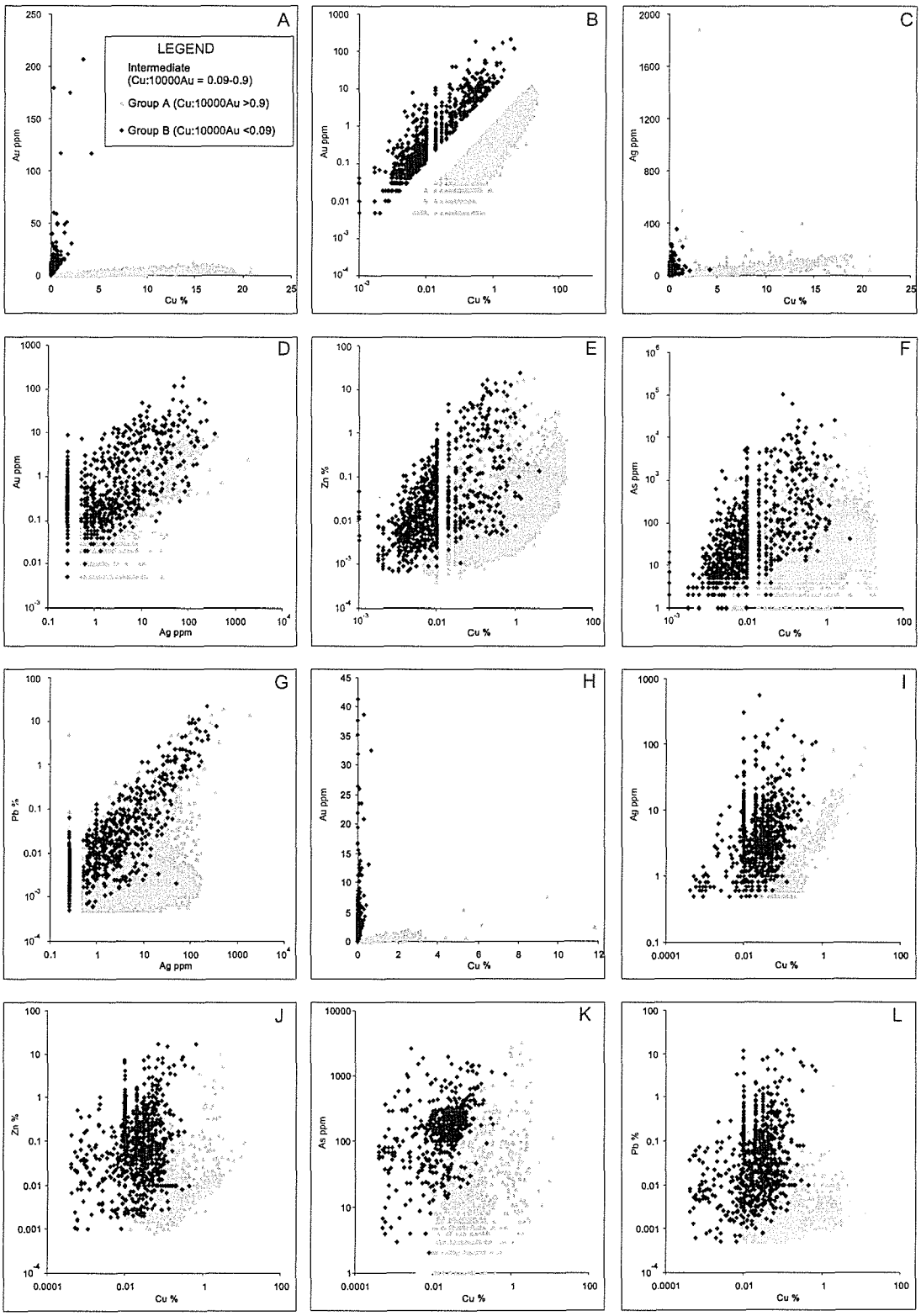

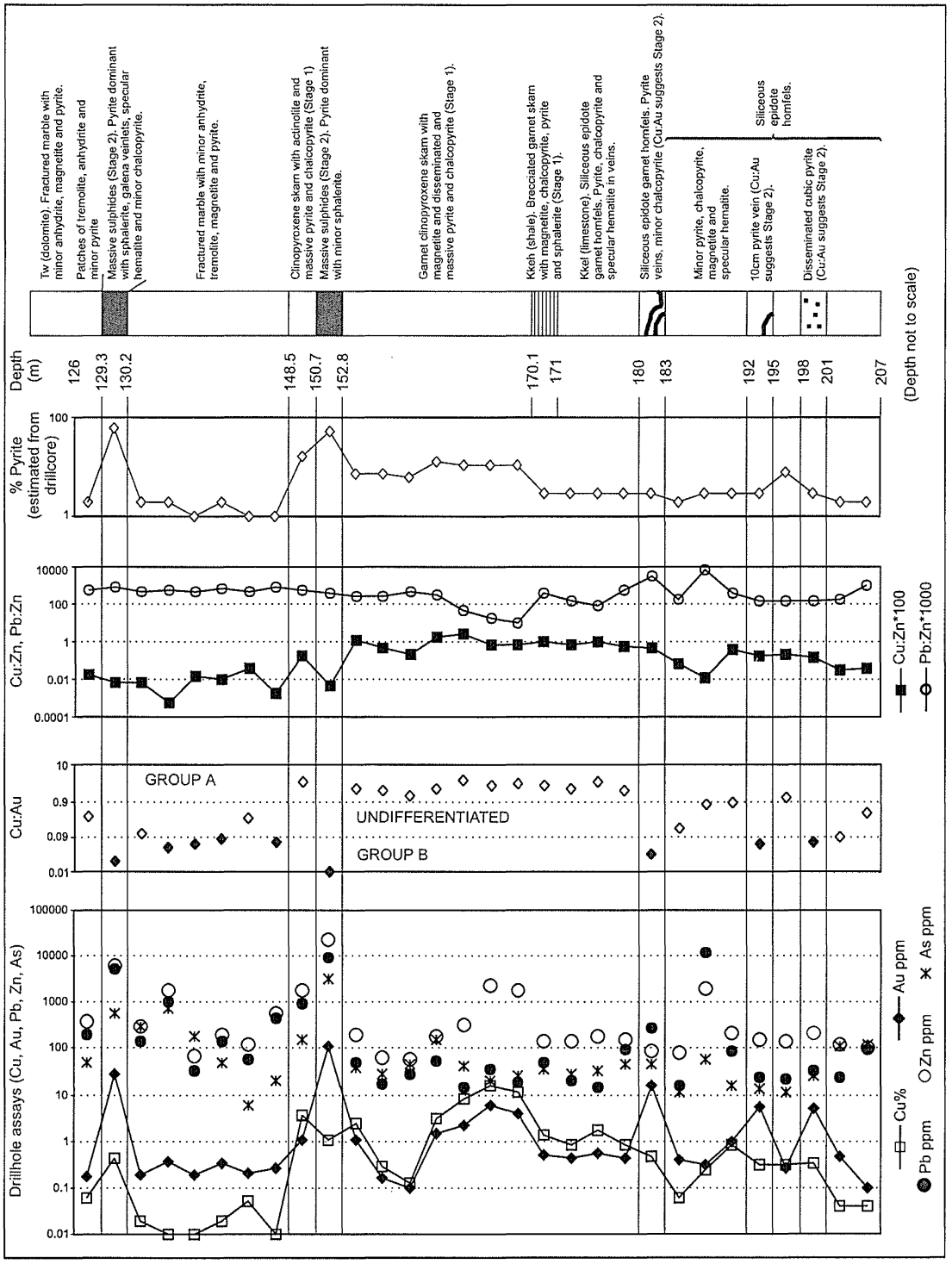

Figure B-11. B G U 2 6 - 1 downhole drill log with assay results and pyrite content (PT Freeport Indonesia), geology and Cu:10000Au, Cu:Zn and Pb:Zn ratios. Drillhole location annotated on Figure B-7.

B-13b).

Group B (Cu:10000Au ratio <0.09; Figure B-10a, b) assay intervals are comparable with the distribution of Stage BG2 sulphide occurrences (Figure B-11). Relative to Cu, Group B samples have higher Au, Zn, and As concentrations than Group A samples (Figure B-10b, e, f, g). Group B samples also contain higher Pb concentrations than Group A samples and Ag and Pb are strongly correlated (Figure B-10g). Group B has a distinct high-Au and low-Cu relationship but Au does not display a positive correlation with any analysed elements. This is consistent with the textural observation that native gold is dominantly associated with pyrite in the Stage BG2 paragenesis. Group B may display minor variation with elevation as Zn:Cu ratio increases towards surface (Figure B-12c). Overlap between Group A and Group B occurs at the NW end of the deposit (Figure B-13a) coincident with the location of the surface exposed NE striking faults.

Wanagon Gold assay data

Two distinct groups analogous to those at Big Gossan are represented in the Wanagon Gold Cu:10000Au assay data (Figure B-10h). Group A represents the deeper Stage WG1 Cu-Au-Ag skarn mineralisation (Figure B-10h, i) and Group B, which is analogous to Stage WG2, is developed in sandstone, carbonate breccia and faults truncating skarn at high elevations (Figure B-9). Group B clearly contains elevated Au, Ag, Zn, As and Pb with respect to Group A (Figure B-10h-l).

Sulphur isotope geochemistry

$\delta^{34}S_{CDT}$ was analysed in sulphides from Stage 1 and Stage 2 at Big Gossan and Wanagon Gold (Appendix 1, 9; Figure B-14). No obvious difference between Stage 1 and Stage 2 sulphides at either deposit is apparent although the dataset is limited to seven samples from Big Gossan and three samples from Wanagon Gold. The results range from -0.7 to 5.1‰ and are indistinguishable from sulphide values from other deposits in the district.

Fluid inclusion study

Big Gossan

Fluid inclusions large enough for thermometric study are sparse in quartz and carbonate associated with Stage BG2 sulphide veins at Big Gossan. Rare fluid inclusions are present in pale, transparent late-stage sphalerite. All fluid inclusions observed were liquid-rich,

Figure B-12. Big Gossan cross section 27 and distribution of assay ratios and elements. PT Freeport Indonesia assay data. a) Geology, drill holes and distribution of Group A (>0.9) and Group B (<0.09) Cu:10000Au ratios. b) Drill holes and distribution of Au>0.5g/t. Cu>1% is coincident with an area of Pb:Zn 0.1-0.2. Cu>5% is coincident with area of lowest Pb:Zn values (<0.1). c) Drill holes and distribution of Zn:Cu ratios. Modification of near-surface assay ratios by surface weathering and enrichment may account for distribution of Zn:Cu ratios.

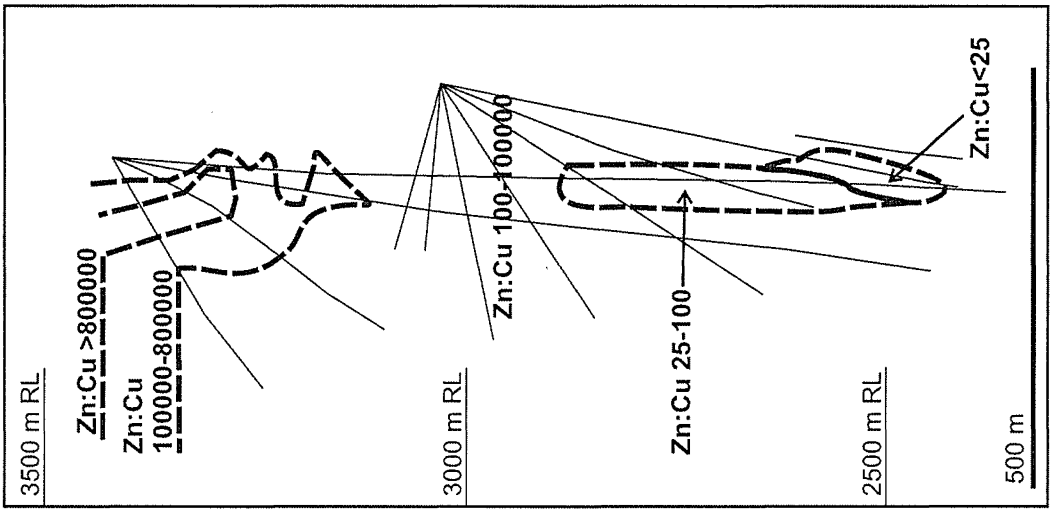
3500 m RL
Zn:Cu >800000
Zn:Cu
100000-800000
3000 m RL
Zn:Cu 100-100000
Zn:Cu 25-100
2500 m RL
Zn:Cu<25
500 m

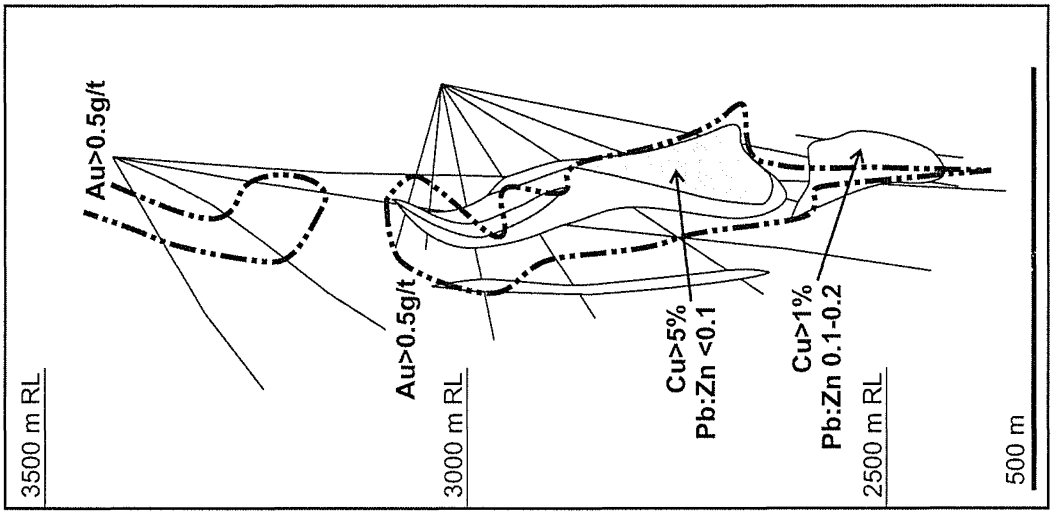
3500 m RL
Au>0.5g/t
Au>0.5g/t
3000 m RL
Cu>5%
Pb:Zn <0.1
Cu>1%
Pb:Zn 0.1-0.2
2500 m RL
500 m

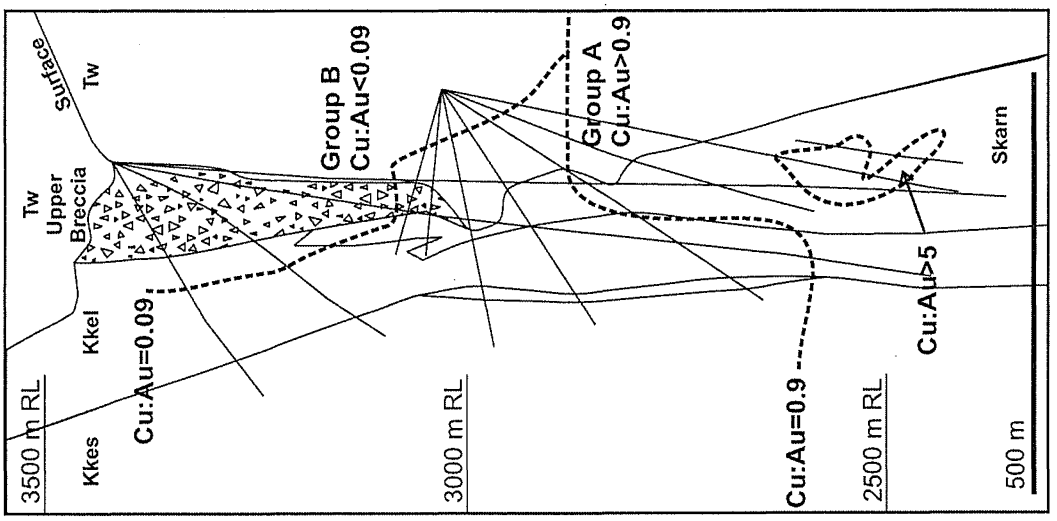
3500 m RL
Kkes
Kkel
Tw
Upper
Breccia
Tw
surface
Cu:Au=0.09
Group B
Cu:Au<0.09
3000 m RL
Group A
Cu:Au>0.9
Cu:Au=0.9
2500 m RL
Cu:Au>5
Skarn
500 m

liquid-vapour type. Salinity (wt% $NaCl_{equiv}$) was estimated from freezing results (Figure B-15; Appendix 1, 8)(Bodnar, 1993). Homogenisation temperatures were measured for 46 inclusions from 6 samples at Big Gossan (Figure B-16; Appendix 1, 8). All inclusions homogenised by vapour disappearance.

Inclusions occurring along secondary fractures in quartz grains in skarn (Figure B-8h,j ; Figure B-16 - quartz with skarn) have the highest salinity (3-26 wt% $NaCl_{equiv}$) and homogenisation temperatures (305-460°C) and are similar to inclusions identified in pyroxene by Meinert et al. (1997). Primary inclusions in sphalerite from a sphalerite-galena-pyrite vein that crosscuts the quartz and skarn sample (Figure B-5h,m) have significantly lower homogenisation temperatures (230-256°C) and a narrow salinity range (8-14 wt% $NaCl_{equiv}$). Quartz with a close hydrothermal infill relationship with Stage 2 sulphides from 4 other samples contains rare clusters of small inclusions. The salinity range (1-14 wt% $NaCl_{equiv}$) and homogenisation temperatures (160 to 300°C) are similar to those of the sphalerite-hosted inclusions. Stage BG2 inclusions from sphalerite and quartz have an average salinity of 9 wt% $NaCl_{equiv}$ and average homogenisation temperature of 248°C. Inclusions from a carbonate alteration halo around a Stage BG2 sphalerite-pyrite-native gold vein (Figure B-5b,l) have salinities of 16-22 wt% $NaCl_{equiv}$ and homogenisation temperatures of 283-325°C.

Where observed, the initial melting temperatures of ice in all except two samples range from -20 to -33°C which is consistent with a water-KCl-NaCl mixture (Brown, 1998). Two inclusions from quartz in the skarn had initial melting temperatures of -40°C implying additional cations (i.e. Fe^{2+}, Ca^{2+} or Mg^{2+}) may also be present (Brown, 1998).

Wanagon Gold

The leached Kembelangan Group sandstone at Wanagon Gold (Figure B-8g,k) contains abundant fluid inclusions where it is silicified. All fluid inclusions are liquid-rich, liquid-vapour type. Homogenisation temperatures were measured for 53 inclusions from 3 samples (Figure B-16; Appendix 1, 8). All inclusions appear to be secondary and are located on secondary trails in sandstone quartz grains. Hydrohalite was observed on cooling in three inclusions and dissolution temperatures of >0.1°C in two of these indicate that it is metastable (Roedder, 1984).

Figure B-13. Big Gossan long section looking NE. PT Freeport Indonesia assay data. a) Location of cross section 26 and 27 and distribution of drill holes and Cu:10000Au ratios as constrained from existing drilling. b) Distribution of Group A and B, Zn:Cu ratios and Cu>1% and Cu>5% contours as constrained from existing drilling.

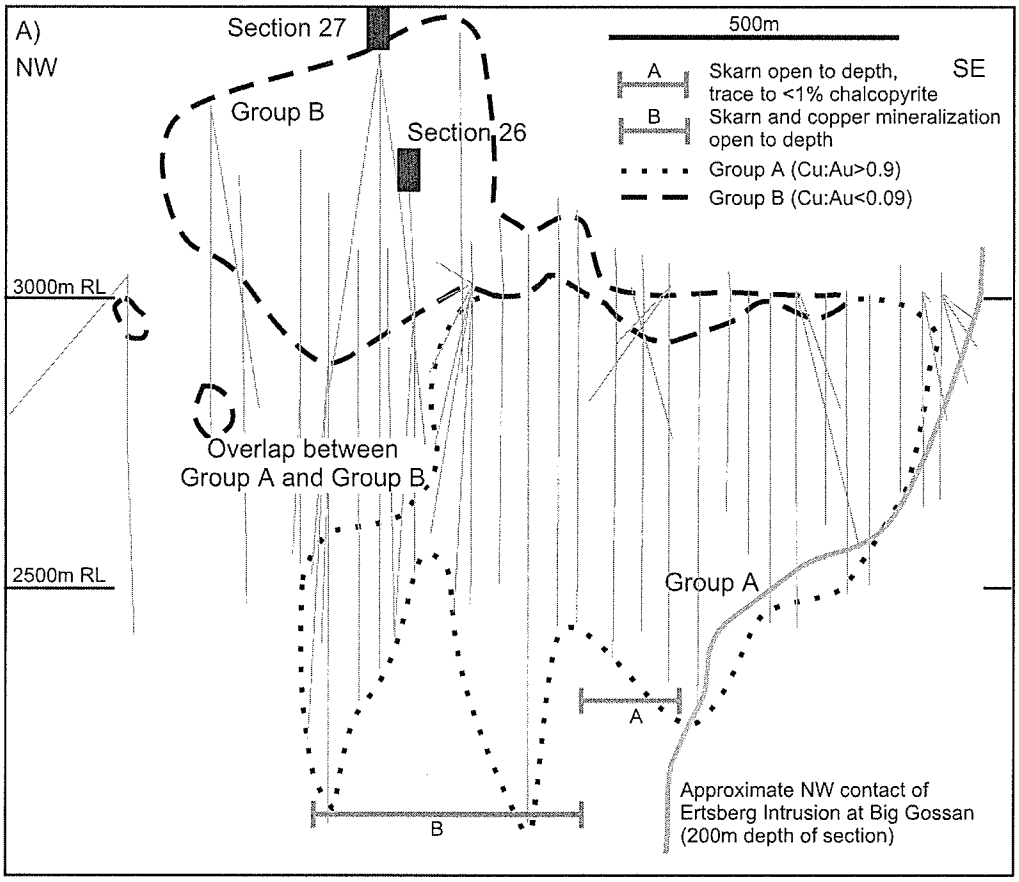
A)
NW
SE
Section 27
Section 26
Group B
500m
A
Skarn open to depth, trace to <1% chalcopyrite
B
Skarn and copper mineralization open to depth
Group A (Cu:Au>0.9)
Group B (Cu:Au<0.09)
3000m RL
2500m RL
Overlap between Group A and Group B
Group A
A
B
Approximate NW contact of Ertsberg Intrusion at Big Gossan (200m depth of section)

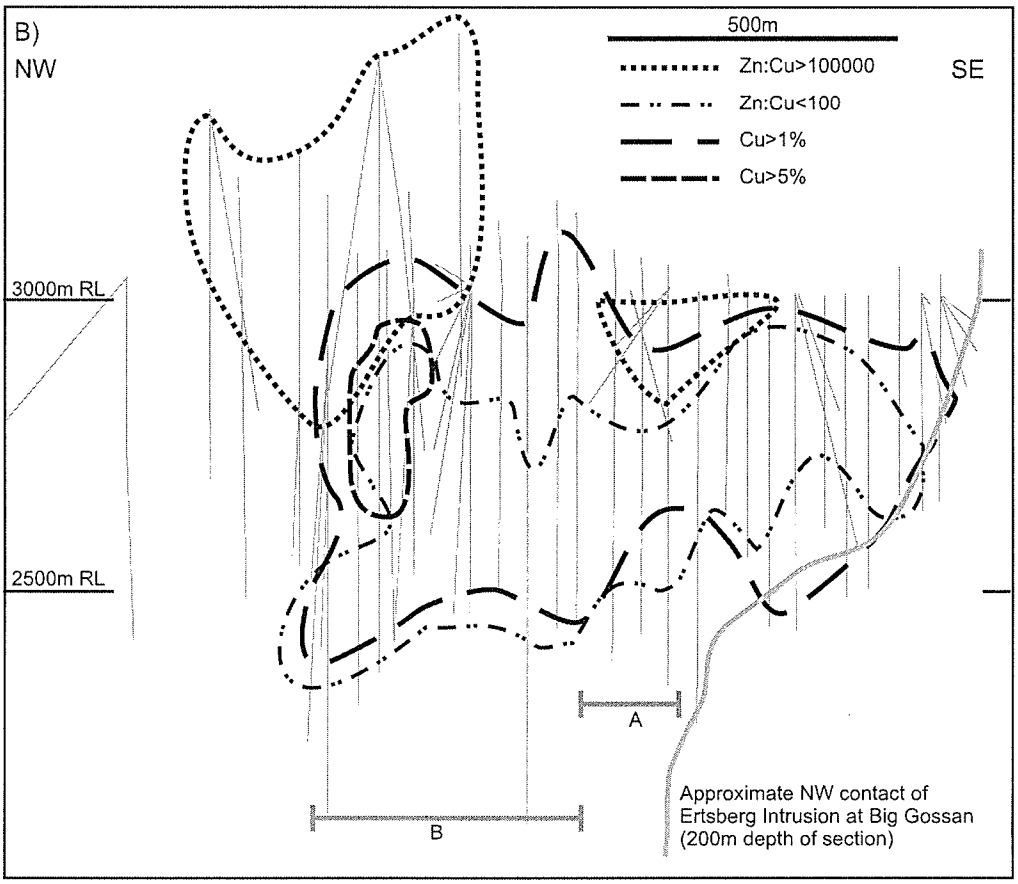
B)
NW
SE
500m
Zn:Cu>100000
Zn:Cu<100
Cu>1%
Cu>5%
3000m RL
2500m RL
A
B
Approximate NW contact of Ertsberg Intrusion at Big Gossan (200m depth of section)

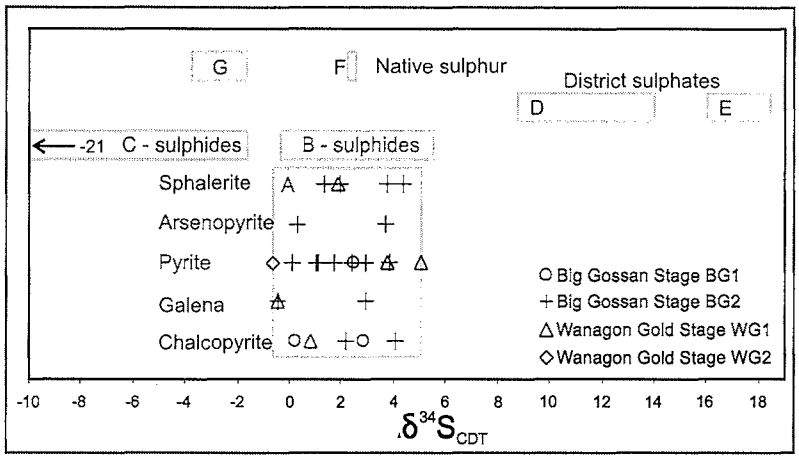

Figure B-14. $\delta^{34}S_{CDT}$ from Big Gossan and Wanagon Gold Stage 1 and Stage 2 sulphides (A). Stage 2 pyrite generally displays lower $\delta^{34}S_{CDT}$ than Stage 1 pyrite. The range of values from Big Gossan and Wanagon Gold (Appendix 9) is comparable to the range of sulphide values (B) from other deposits in the district: Kucing Liar (New, pers comm.), southwest Grasberg (Gibbins, 2000) and Grasberg, Ertsberg East Skarn System, DOM and distal veins (Kyle, 1992). Results from this study are not comparable with a second range of sulphide values (C) from Kucing Liar (New, pers comm.) and southwest Grasberg (Gibbins, 2000). (D) Hydrothermal sulphates from Kucing Liar (New, pers comm.), southwest Grasberg (Gibbins, 2000), EESS and other district locations and (E) sedimentary sulphates from unspecified locations in the district (Kyle, 1992; Kyle and Dworkin, 1995) Sulphur from (F) southwest Grasberg (Gibbins, 2000) and (G) Grasberg (Kyle, 1992).

Figure B-15. Histograms of Big Gossan and Wanagon Gold fluid inclusion freezing study results, and heating experiment results used for Figure B-16 (cf. Bodnar, 1993), (Appendix 8).

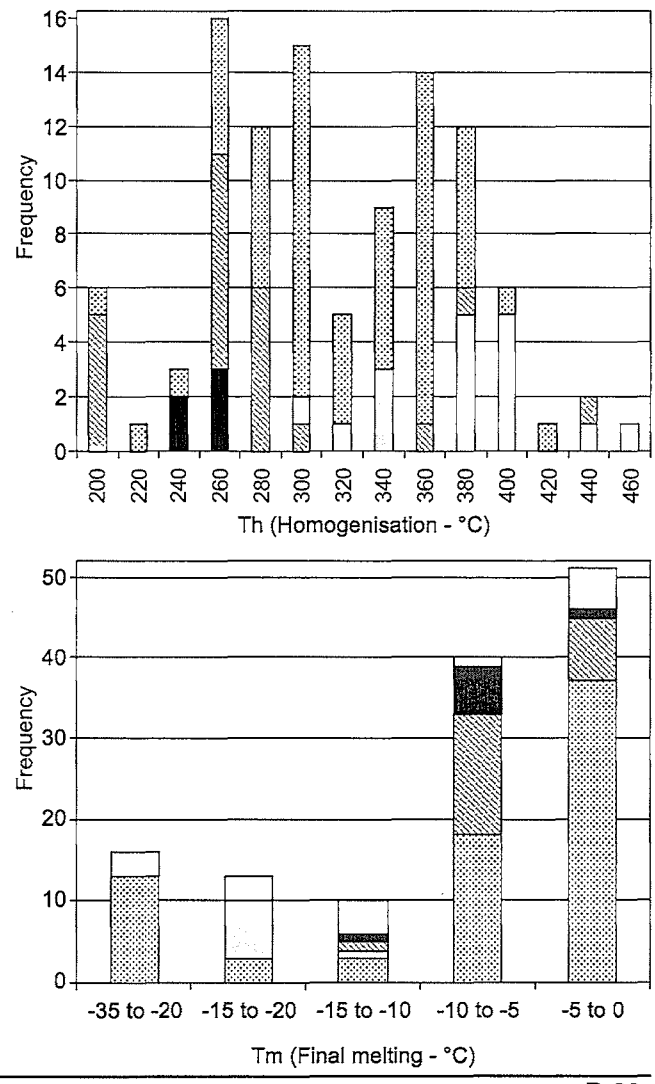

Figure B-16. Th-salinity diagram for Big Gossan and Wanagon Gold fluid inclusions. Salinity (wt%$NaCl_{equiv}$) was estimated using the equation from Bodnar (1993). Fluid inclusion data from Meinert et al. (1997) is plotted for comparison (1-4). Pyroxene fluid inclusions contain 1) liquid + vapour + halite + sylvite ± opaques (?hematite ± chalcopyrite) and 2) liquid + vapour + halite ± opaques. Salinity for sylvite-bearing inclusions is 1) wt%$NaCl_{equiv}$ or 1a) NaCl+KCl wt % from Meinert et al. (1997). 3) Anhydrite fluid inclusions are vapour-rich ± minor liquid-rich. 4) Early quartz with anhydrite contains vapour-rich ± liquid-rich and minimum homogenisation temperatures in quartz are 255°C. Big Gossan fluid inclusion measurements from Stage BG2 minerals in this study include: 5) sphalerite inclusions in a Stage BG2 vein that crosscuts 6) quartz associated with skarn (Figure B-5h); 7) quartz from four samples associated with Stage BG2 sulphides and 8) inclusions in a marble alteration halo around a pyrite-sphalerite vein. 9) Wanagon Gold fluid inclusion measurements from liquid +vapour inclusions in the Kembelangan Group sandstone. 10) Range from 21 measurements from unconstrained generation/s of Big Gossan quartz (Kyle, 1994). 11) Range from 7 measurements from unconstrained generation/s of Big Gossan sphalerite (Kyle, 1994).

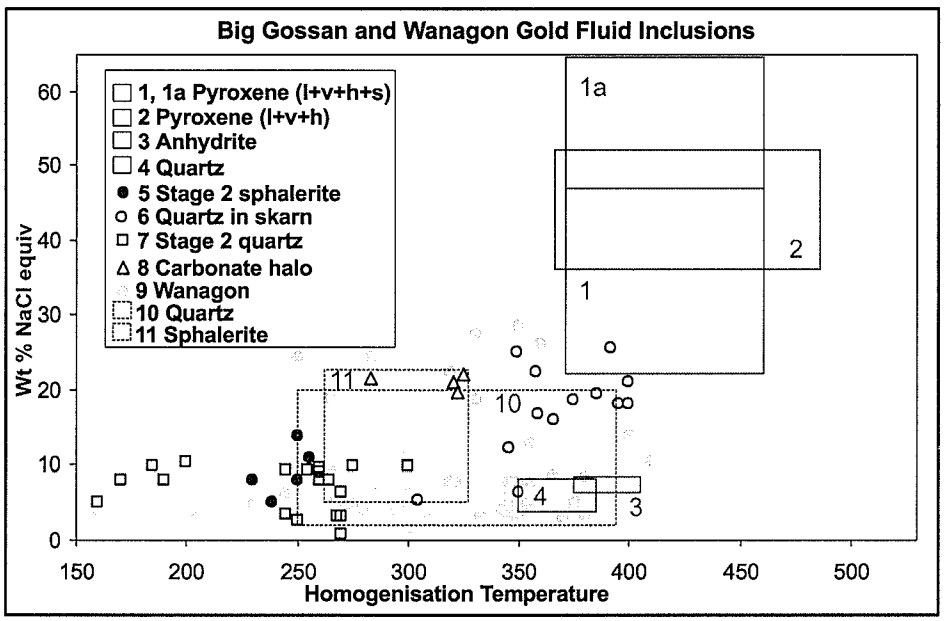

Salinity estimates indicate there are possibly two populations of fluid inclusions. A lower salinity group (<13 wt% $NaCl_{equiv}$) displays a wide range in homogenisation temperature (160-410°C) and is similar to Big Gossan anhydrite, quartz and Stage BG2 inclusions. The range in homogenisation temperatures may be due to fluid inclusion leakage (which will cause higher homogenisation temperatures) or simply result from cooling of the hydrothermal system. Alternatively, the range in data may represent the presence of more than one generation of fluid inclusion. Where observed, initial melting temperatures in the majority of inclusions display a tight range from -16 to -20°C implying water-NaCl mixtures (Brown, 1998). Seven inclusions had initial melting temperatures from -22 to -28°C which is consistent with a water-KCl-NaCl mixture (Brown, 1998).

The higher salinity group (19-29 wt% $NaCl_{equiv}$) displays homogenisation temperatures of 250-350°C. Initial melting temperatures are as low as -29°C but are predominantly -40 to -57°C implying that in addition to water-KCl-NaCl mixtures, additional cations (i.e. Fe^{2+},

Mg^{2+}, or Ca^{2+}) may also be present (Brown, 1998). This group have similar salinities to inclusions from carbonate, pyroxene, and quartz from skarn at Big Gossan.

Laser Ablation – ICPMS analysis of sulphides

Selected trace element contents were determined through LA-ICPMS analyses (Appendix 1; 7) from Big Gossan and Wanagon Gold sphalerite (Figure B-17a-b), chalcopyrite (Figure B-17c-e) and pyrite (Figure B-17f-k). All minerals analysed were inspected by microscope and microprobe for homogeneity.

Big Gossan

Sphalerite demonstrably from Stage BG1 was not analysed although there are two analyses of unknown stage and two analyses from the breccia that could be from this stage. Stage BG2 sphalerite displays a strongly positive Au:As correlation and variable Au:Cu (Figure B-17a, b). Stage BG1 chalcopyrite displays positive Au:Bi correlation and contains up to 20ppm Bi and between 0.05-0.1ppm Au (Figure B-17c). Stage 2 chalcopyrite displays less consistent correlation but generally contains lower Cu, higher As and similar gold contents (Figure B-17d, e).

Stage BG1 pyrite displays positive correlations of As:Bi and As:Te and a negative Au:As correlation (Figure B-17f, g, h). Cu content is variable but generally covaries with Au in Stage BG1 and BG2 pyrite (Figure B-17i). Stage BG2 pyrite displays positive Au:As correlations and contains higher As and Au than Stage BG1 pyrite (Figure B-17h). Two Stage BG2 populations are apparent in As or Au against Bi or Te correlations (Figure B-17f, g, j, k). Stage BG2(x) pyrite samples which are texturally associated with Bi or Te minerals as identified by microprobe analysis display distinct negative As or Au against Bi or Te correlations (Figure B-17f, g, j, k). The distinct Stage BG2(x) pyrite chemistry may represent a separate generation of pyrite within Stage BG2. Stage BG1 and BG2 chalcopyrites contain similar amounts of Bi (Figure B-17c) and pyrites from both stages contain similar amounts of Bi and Te (Figure B-17j, k).

Figure B-17. Laser Ablation correlation plots of element relationships in sulphides from Big Gossan and Wanagon Gold. All values are in ppm (raw data and full sample descriptions in Appendix 7). "Unclassified" samples and "breccia" samples from the West Drift Breccia were texturally ambiguous and could not be interpreted as Stage BG1 or Stage BG2. One of the unclassified Big Gossan chalcopyrite samples correlates with Stage BG1. At Big Gossan, the pyrite breccia samples and one unclassified sample correlates with Stage BG1. The remaining unclassified Big Gossan samples generally correlate with Stage BG2. Big Gossan pyrite Stage BG2(x) samples are characterised by distinct Au:Bi,Te and As:Bi,Te correlations. a) Sphalerite: Au:As. b) Sphalerite: Cu:Au. c) Chalcopyrite: Bi:Au. d) Chalcopyrite: Cu:As. e) Chalcopyrite: Cu:Au. f) Pyrite: As:Bi. g) Pyrite: As:Te. h) Pyrite: Au:As. i) Pyrite: Au:Cu. j) Pyrite: Au:Bi. k) Pyrite: Te:Au.

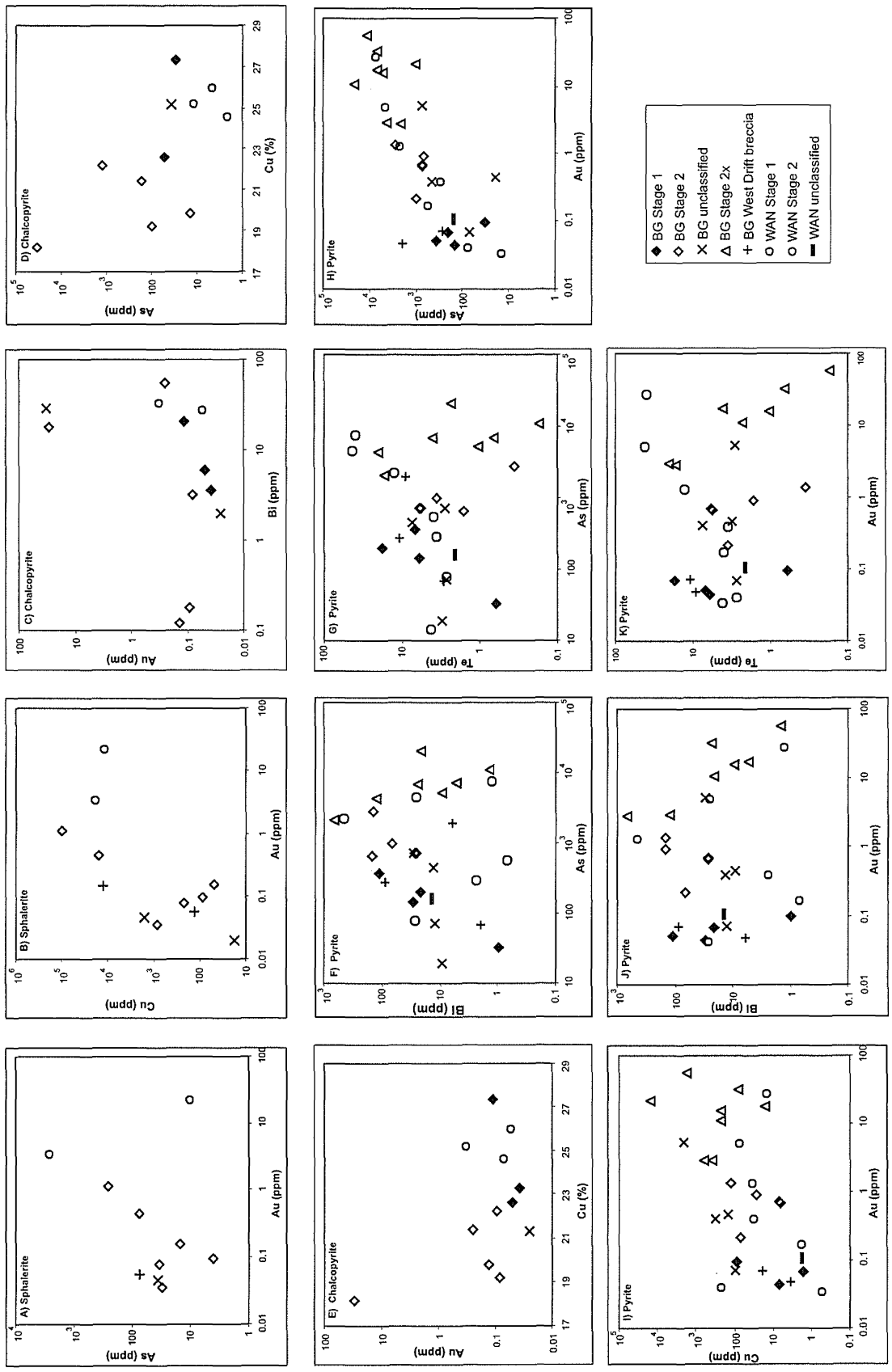
A) Sphalerite
As (ppm)
Au (ppm)
B) Sphalerite
Cu (ppm)
Au (ppm)
C) Chalcopyrite
Au (ppm)
Bi (ppm)
D) Chalcopyrite
As (ppm)
Cu (%)
E) Chalcopyrite
Au (ppm)
Cu (%)
F) Pyrite
Bi (ppm)
As (ppm)
G) Pyrite
Te (ppm)
As (ppm)
H) Pyrite
As (ppm)
Au (ppm)
I) Pyrite
Cu (ppm)
Au (ppm)
J) Pyrite
Bi (ppm)
Au (ppm)
K) Pyrite
Te (ppm)
Au (ppm)
BG Stage 1
BG Stage 2
BG unclassified
BG Stage 2x
BG West Drift breccia
WAN Stage 1
WAN Stage 2
WAN unclassified

Wanagon Gold

The compositions of Stage 2 sphalerite from Wanagon Gold and are similar to their equivalents from Big Gossan (Figure B-17a, b). The Stage WG1 sphalerite analysis has a high Au:As ratio (Figure B-17a). Stage WG1 chalcopyrite has a similar chemical signature to Stage BG1 (Figure B-17c, d, e). There are no Stage WG2 chalcopyrite analyses. The low As and Au contents of Stage WG1 pyrites are analogous to Stage BG1 pyrite (Figure B-17h). However Stage WG1 pyrite displays a distinct negative As:Bi correlation and a narrow range of Te values which differs from Stage BG1 (Figure B-17f, g). Stage WG2 pyrite element correlations are all directly comparable with those of Big Gossan Stage BG2(x) (Figure B-17f, g, j, k).

Discussion

The evolution of the skarn at Wanagon Gold is not discussed here and Big Gossan skarn evolution has been documented by Meinert et al. (1997).

Structural and stratigraphic setting

Big Gossan skarn and Stage BG1 Cu-Au overprinted a fault breccia near the base of the Waripi Formation. The Wanagon Gold skarn is predominantly hosted in the Kembelangan limestone and shale as pervasive alteration and does not display the dilational textures observed at Big Gossan. The absence of massive open-space infill textures in the skarn at Wanagon Gold may be a function of absence of pre-existing brecciated host material. In the explored portion of the Wanagon Gold system, depth or structural constraints may not have favoured development of dilational features although the deposit is still open to depth.

The absence of anhydrous skarn minerals and the presence of hydrous skarn minerals suggest that the West Drift breccia at Big Gossan developed in the Waripi Formation coincident with the onset of hydrous skarn. Stage BG1 sulphides overprint the earlier anhydrous skarn. This distribution suggests the structural regime operating during anhydrous skarn formation at Big Gossan influenced introduction of Stage BG1 fluids. The West Drift breccia was not a favoured conduit for Stage BG1 Cu-Au suggesting that the breccia was only minimally re-broken prior to or during Stage BG1.

Anhydrite at Big Gossan is a component of the hydrous mineral association postdating anhydrous skarn and immediately preceding Stage BG1 Cu-Au. From fluid inclusion boiling evidence in anhydrite and quartz, Meinert et al. (1997) estimated a pressure of 20 MPa which they interpreted to correspond to a paleodepth of 2 km under hydrostatic conditions. At the same depth under lithostatic conditions, which are considered likely for skarn formation, Meinert et al. (1997) estimated a pressure 50 MPa. Conditions at Wanagon

Gold are unconstrained.

Stage 2 occurrences in both deposits occupy partly different structural settings to the earlier skarn and Stage 1 Cu-Au. The NE striking faults that crosscut stratigraphy were important at both deposits for focusing Stage 2 fluids (Figure B-2a). At Big Gossan the NE striking faults coincide with the upper breccia and most extensive development of Stage BG2 products. They are also proximal to the NW limit of the Stage BG1 Cu-Au deposit and coincident with the >5%Cu contour, suggesting they were important structural conduits in Stage BG1.

The Kembelangan Group sandstone is an important host lithology at Wanagon Gold. Secondary porosity developed due to a leaching event that post-dated skarn and predated Stage WG2 occurrences. The mineralogy of leached sedimentary, skarn and igneous rocks suggests argillic conditions. There is an absence of advanced argillic or sulphate mineral phases (i.e. pyrophyllite, dickite, alunite) that would be indicative of acidic fluid conditions (cf. Hedenquist et al., 1994).

Stage 1 and Stage 2 mineralogy and metal zonation

The gangue paragenesis is different at Big Gossan and Wanagon Gold. K-feldspar, interpreted as adularia on textural evidence (Browne and Ellis, 1970; Dong and Morrison, 1995), is only developed in close association with Stage WG2 sulphides in silicate host rocks at Wanagon Gold. As adularia is not developed in the adjacent carbonate rocks, a local control has strongly influenced gangue mineralogy. Adularia is stable under near-neutral alkaline conditions with low Na^+/K^+ conditions and preferentially occurs within high fluid-flow permeable conditions (Browne, 1978). Rapid boiling where the CO_2 content of the fluid is high can result in precipitation of adularia due to fluid pH increase (Corbett and Leach, 1998). This is consistent with its development in the highly permeable leached Kembelangan Group sandstone. In the adjacent lower porosity Waripi Formation, Stage WG2 sulphides occur as carbonate replacement with dolomite and K-feldspar is notably absent. K-feldspar has not been observed in Stage BG2 occurrences at Big Gossan.

Big Gossan and Wanagon Gold Stage 1 Cu:10000Au ratios are similar to other skarn Cu-Au deposits in the district and are different to those of Stage 2 sulphides (Section D). The Stage 1 and 2 products can be differentiated in mine drill core assays and in LA-ICPMS analysis of single sulphide minerals. Chalcopyrite is the dominant Stage 1 sulphide and contains a maximum of 0.1ppm gold (Figure B-17e). The amount of Au dissolved in chalcopyrite is orders of magnitude less than that present in Stage 1 drillhole assay intervals indicating the majority of gold is present as native gold.

The distribution of highest temperatures in Stage BG1 Cu-Au is considered to be represented by the NW plunging core zone of lowest Zn:Cu ratios (Figure B-13b). This zone is not coincident with the known contact of the Ertsberg Intrusion and remains open to depth. Away from this central zone, high Cu grades correlate with lowest Pb:Zn ratios and have consistent Zn:Cu ratios. These areas display local outward Cu+Zn to Pb temperature zoning (Figure B-11). This is consistent with the observed close sphalerite and chalcopyrite textural association and late-stage nature of galena in Stage BG1.

Zonation in Stage 2 sulphides at both deposits is less obvious. At Big Gossan there is an increase in Zn:Cu ratios towards the surface in the upper breccia although this is likely to be a product of surface-related leaching due to weathering (Figure B-12). The lower Zn:Cu ratio on cross section BGU27 could be an expression of overlap of Stage BG2 on earlier Stage BG1 Cu-Au.

Rubin and Kyle (1997) concluded from a limited sample suite that native gold fineness from within the massive-sulphide gold zones at Big Gossan increased with elevation. This study established that native gold compositions display no systematic variation with respect to elevation. However, native gold fineness correlates with gold paragenesis which reflects the original fluid and mineral depositional conditions. Highest fineness native gold is encapsulated in Big Gossan Stage BG2 early pyrite or associated with bismuthinite. The lowest fineness native gold is associated with Pb-bearing minerals (i.e. galena and sulphosalts). Similar gold fineness correlations were observed at the Kidston carbonate base metal deposit, Queensland, Australia (Baker, 1987).

At both locations, the LA-ICPMS results indicate that Au and As are closely associated in Stage 2 sphalerite and pyrite and that Stage 2 pyrite contains elevated Au and As compared to Stage 1 pyrite. The majority of Stage 2 pyrites display distinct negative correlations of Au and As with Bi and Te, which are not present in Stage 1 pyrite. As native gold was not observed by microscope during conventional or electron studies, gold detected by LA-ICPMS analysis is interpreted to be contained within the mineral lattice. The consistent association of Au and As may reflect an Au-As bond (cf. Cathelineau et al., 1989). It has been demonstrated that Au distribution in arsenopyrite may be strongly heterogeneous (Cathelineau et al., 1989) and the heterogeneity of Au in pyrite and arsenical pyrite at Big Gossan and Wanagon Gold is unknown.

Big Gossan Stage BG1 and Stage BG2 fluid conditions and chemistry

Meinert et al. (1997; 2003) concluded from $\delta^{18}O$ and δD results at Big Gossan that the fluids responsible for anhydrous and hydrous skarn formation were dominantly magmatic

and typical of porphyry copper skarn systems. A magmatic origin for quartz intergrown with hydrous skarn is supported by a $\delta^{18}O$ value of +12.3‰ (Kyle, 1994). Kyle (1994) considered this generation of quartz could represent deposition of silica from a magmatic-derived fluid with an average $\delta^{18}O_{SMOW}$ value of ca. 7‰ and $\delta^{18}O_{H2O\text{-}quartz}$ of about +5‰ at 400°C. A late stage barren quartz vein has a $\delta^{18}O$ value of +14.7‰ (Kyle, 1994). Kyle (1994) documented fluid inclusion salinities from unconstrained generations of quartz and sphalerite (Figure B-16) that averaged 10 and 17 wt% $NaCl_{equiv}$ respectively and were interpreted to represent mixing with meteoric water.

$\delta^{13}C$ and $\delta^{18}O$ results from different generations of carbonate alteration and infill at Big Gossan reflect mixing between sedimentary host rocks and magmatic fluids with $\delta^{18}O_{FLUID}$ values of ca. 5.9‰ (Section C). Sr isotopes from Big Gossan anhydrite also provide evidence for involvement of sedimentary components (Kyle and Dworkin, 1995). Big Gossan anhydrite has $^{87}Sr/^{86}Sr$ values of 0.7699-0.70708 and $\delta^{34}S$ values of 12.5-13.2‰. The $\delta^{34}S$ values compare well with other district analyses of hydrothermal anhydrite (Kyle and Dworkin, 1995). The Sr values are interpreted to represent mixing between sedimentary and magmatic Sr sources, or a separate hydrothermal fluid whose composition is not reflected by the igneous rocks exposed in the district (Kyle and Dworkin, 1995).

Meinert et al. (1997; 2003) proposed that both the anhydrous and hydrous skarn could relate to influx of moderate salinity (6-8 wt% $NaCl_{equiv}$) brines (exolved from a cooling pluton) that followed different cooling paths. A component of meteoric water was not deemed necessary to explain the data. At lithostatic conditions of 50 MPa, the brine boiled and separated into a 50wt%$NaCl_{equiv}$ hypersaline liquid (and 0.7wt%$NaCl_{equiv}$ vapour) responsible for deposition of anhydrous skarn Meinert et al. (1997; 2003). At hydrostatic conditions of 20 MPa, a similar brine would boil at less than 400°C producing 70% liquid at 10wt% NaCl and 30% vapour with a salinity of 0.02 wt percent (Meinert et al., 1997; Meinert et al., 2003) capable of depositing hydrous skarn and Stage BG1 Cu-Au. Chalcopyrite daughter minerals in pyroxene-hosted fluid inclusions (Meinert et al., 1997) indicate copper was present in the early high temperature Big Gossan skarn fluids and support the interpretation for a common source for skarn and Stage BG1 mineralising fluids.

Big Gossan Stage BG2 fluids were NaCl-KCl brines of moderate salinity (average 9 wt% $NaCl_{equiv}$). Although inclusions at Wanagon Gold are paragenetically unconstrained, a similar population to Stage BG2 fluid inclusions suggests Stage WG2 fluids may have had slightly lower salinities. The Stage BG2 sphalerite and quartz fluid inclusions record lower temperature but similar estimated salinity to those from hydrous skarn (Rae et al.,

1994; Meinert et al., 1997). The covariation of salinity and homogenisation temperatures in the inclusions from Big Gossan quartz in skarn may define mixing between high temperature skarn fluids and lower temperature Stage BG2 sphalerite and quartz fluids.

The degree of influence from externally derived fluids (i.e. meteoric water) at Big Gossan is not clear from the fluid inclusion evidence alone. The depth of the deposit, stable isotope results and similarities between salinities from hydrous skarn (modelled by Meinert et al., 1997; Meinert et al., 2003 as dominantly derived from a magmatic brine) and Stage BG2 occurrences suggest that contribution of external fluids was not significant during development of skarn, Stage BG1 or Stage BG2.

The distributions of Zn:Cu and Pb:Zn ratios in Big Gossan Stage BG1 Cu-Au signify temperature zonation consistent with that observed in metal solubility experiments and other ore deposits (Hemley and Hunt, 1992) and are consistent with metal transport as chloride complexes (Hemley et al., 1992). Stage 2 fluids were capable of transporting and precipitating Fe, Au, As, Zn, Pb, Te, Bi and minor Cu. The telluride phases developed at Big Gossan and Wanagon Gold are consistent with those expected from the normal range of fS_2, fO_2 and fTe_2 in hydrothermal ore deposits (Afifi et al., 1988).

Gold transport in pyrite-stable fluids at temperatures <400°C is likely to be by bisulphide complexes (Seward, 1991; Gammons and Williams-Jones, 1997), primarily as AuHS in low sulphidation deposits (Cooke and Simmons, 2000). The elevated LA-ICPMS gold concentrations in Stage BG2 pyrite suggest that sulphidation reactions were important for inducing gold precipitation (Cooke and Simmons, 2000):

$$Au(HS)_2^- + [FeO] + H^+ \text{ --> } Au_{(s)} + FeS_{2(s)} + H_2O_{(l)} + 0.5H_{2(aq)}$$

Gold at Big Gossan is also commonly located on pyrite surfaces. Adsorption of gold onto pyrite surfaces is favoured by AuHS° and not $Au(HS)^-$ (Wilder and Seward, 2002). AuHS° speciation is often implicated in lower pH high sulphidation epithermal gold deposits (Seward and Barnes, 1997; Cooke and Simmons, 2000). Arsenic-bearing pyrite may be important for chemosorption whereby local dissolution of arsenic on the surface may reduce Au^{3+} to Au° (cf. Pokrovski et al., 2001).

Sphalerite and galena, which are closely associated with gold in Stage BG2, were probably transported as chloride complexes (Barnes, 1979; Seward and Barnes, 1997). Decreasing temperature (although no temperature zoning was observed in Stage BG2 base metals) and/or pH increase, through replacement of carbonate host rocks are effective mechanisms for depositing metals transported as chloride complexes (Hemley and Hunt,

1992; Seward and Barnes, 1997).

Genesis of pyrite Au-As-Zn-Bi-Te zones in porphyry-related skarn systems

The $^{40}Ar/^{39}Ar$ date of 3.62±0.05Ma for Stage WG2 K-feldspar at Wanagon Gold is ca. 200ky younger than the 3.81±0.06Ma K-Ar date for the Wanagon Sill. The skarn and by inference Stage WG1 Cu-Au mineralisation postdate the Wanagon Sill and were developed during this period, demonstrating a close temporal link between skarn and Stage WG1 Cu-Au and Stage WG2. It is not clear how much time elapsed between Stages BG1 and BG2 although there was clearly a change in structural conditions.

Big Gossan and Wanagon Gold Stage 1 and Stage 2 sulphides have similar sulphur sources interpreted as magmatic (cf. Ohmoto and Goldhaber, 1997). Evidence for a secondary sulphur source with low $\delta^{34}S_{CDT}$ is only observed at Kucing Liar and nearby at SW Grasberg (Gibbins, 2000: New, pers comm.). Pb isotopes from Big Gossan samples do suggest a minor contribution from sedimentary sources (Kyle et al., 1996) although sample paragenesis is unconstrained with respect to this study.

The Stage 2 geochemical association is also inherent to a range of other deposits (Table B-1). The overall characteristics of Big Gossan are most like those documented from epithermal carbonate-base metal deposits (cf. Corbett and Leach, 1998) although the large amounts of carbonate and quartz gangue formed by mixing of magmatic fluids with bicarbonate ground waters are absent. Leaching developed in the Wanagon Gold sandstone is suggestive of high sulphidation conditions however extensive alteration of the carbonate host rocks (cf. Fontbote and Bendezu, 1999; Bendezu et al., 2003) is not observed. The leaching is interpreted to have been formed by an event independent of overprinting Stage WG2 mineralisation, such as mixing of magmatic volatiles or vapour with groundwater (Hedenquist and Lowenstern, 1994).

The mechanism of collapse is often invoked to explain the overprint of base-metal-gold superimposed on earlier high temperature Cu-Au (cf. Corbett and Leach, 1998). An outwards temperature zonation is suggested in BGU26-1 (Figure B-11) from hotter skarn and Stage BG1 Cu-Au to cooler Stage BG2 sulphides. There are insufficient fluid inclusion or stable isotope constraint from the Stage BG1 and BG2 occurrences to dispel this model. However, given the unique geochemistry, zoning and structural setting of both Stages at Big Gossan it is unlikely that they resulted simply from at site zoning or collapse of a single magmatically derived hydrothermal fluid.

Alternatively, it is more likely that Stage BG2 mineralisation resulted from incursion of a completely separate hydrothermal fluid of similar salinity to Stage BG1 hydrous skarn

Table B-1. Comparison between Big Gossan, Wanagon Gold and other mineralisation styles.

Deposit Style	Associated Elements	Gangue or Associated Alteration	Fluid Inclusion Homogenisation Temperatures (°C)	Fluid Inclusion Salinity (wt% $NaCl_{equiv}$)	Fluid Sources (stable isotopes)
Pyrite-Au-As-Zn-Bi-Te (Big Gossan)	Au, As, Zn, Pb, Bi, Te	siderite, dolomite (quartz)	248 (average)	9 (average)	Magmatic (Meinert et al., 2003; Section C)
Pyrite-Au-As-Zn-Bi-Te (Wanagon Gold)	Au, As, Zn, Pb, Bi, Te	K-feldspar in leached sandstone; dolomite in marble	?160-410	?<13	
Quartz-sulphide gold copper systems i.e. Kidston (Baker, 1987; Corbett and Leach, 1998).	Au, Mo, Cu, As, Bi, Te	quartz, ankerite, calcite	120-300	2-10	Magmatic + meteoric
Epithermal carbonate-base metal deposits i.e. Porgera A veins (Richards and Kerrich, 1993; Corbett and Leach, 1998; Richards and Laudrum, 1998; Ronacher and Richards, 1999).	Zn, Pb, Au, Cu	abundant carbonates and quartz	211-365	7.2-15.2 (CO_2 -bearing)	Magmatic (mixed with CO_2 groundwaters)
Late-stage high-level epithermal quartz gold-silver systems i.e. Mt Kare D veins (Richards and Laudrum, 1998; Corbett and Leach, 1998).	Au, Ag, Bi, Te, As	quartz, adularia, roscoelite	163-203	7-8.4 (CO_2 -bearing)	
Oxidised gold skarn deposits i.e. Wabu (Sunyoto, 1999; Meinert, 2000). *Also similar to outward zoning in the gold-bearing skarn deposits in the middle and lower Yangtze River Valley (Zhao et al., 1999).*	Au, Zn, Cu, Bi, Te	iron rich -carbonates and -chlorite epidote	300-320	40-50	
Carbonate-hosted high sulphidation deposits i.e. Colquijirca district (Fontbote and Bendezu, 1999; Bendezu and Fontbote, 2002; Bendezu et al., 2003).	Cu, Zn, Pb, Ag, Au, Bi	alunite, dickite, kaolinite, siderite			
Gold deposits related to reduced intrusions (Thompson and Newberry, 2000; Baker, 2002)	Au, Bi, Te, As, Mo, Zn, Sn, Cu	quartz, K-feldspar, biotite, albite, micas, calcite, dolomite, tourmaline	>350	<10 to >40 (CO_2 -bearing)	Magmatic

conditions but with a different composition. Preliminary stable isotope studies suggest the fluids and sulphur were of magmatic origin. The fluid may have been derived from the same cooling or evolving pluton source postulated for the preceding skarn Cu-Au (Meinert et al., 1997; Meinert et al., 2003). A further scenario is that the gold and H_2S -rich fluids were derived from a condensed vapour formed during phase separation (Gammons and Williams-Jones, 1997; Heinrich, 2003).

The presence of two temporally distinct pyrite-Au-As-Zn-Bi-Te occurrences indicates that a common process occurred in the magmatic evolution of the Ertsberg District at different times. Quartz and sphalerite -hosted fluid inclusions from the Big Gossan pyrite-Au-As-Zn-Bi-Te occurrence have average homogenisation temperatures of 248°C and average salinities of 9 wt%$NaCl_{equiv}$. The pyrite-Au-As-Zn-Bi-Te fluids may represent the magmatic precursor to epithermal deposit styles that contain significant non-magmatic (i.e. meteoric) water (cf. Cooke and Simmons, 2000).

Conclusion

Two distinct metallogenic styles characterise the Big Gossan and Wanagon Gold skarn-bearing ore-systems. An association of pyrite-sphalerite-arsenopyrite-gold with localised Bi-Te minerals and sulphosalts (Stage 2) overprints the earlier skarn Cu-Au (Stage 1). Abundant native gold, sulphosalts and tellurides are texturally associated with Stage 2 minerals and pyrite has a distinct enriched Au-As composition (LA-ICPMS analysis). Textural relationships are consistent with gold being transported as both $AuHS^-$ and $AuHS^0$ complexes and precipitated by sulphidation reactions, adsorption and chemosorption.

A phlogopite $^{40}Ar/^{39}Ar$ date for the Big Gossan skarn of 2.82±0.04Ma is within error of some K-Ar dates for the nearby Ertsberg Intrusion and provides a maximum age for the Stage BG2 occurrence. At Wanagon Gold, a close temporal link of ca. 200ky between skarn Cu-Au (which overprints the 3.81±0.06Ma Wanagon Sill) and the pyrite-Au-As-Zn-Bi-Te occurrence (where there is a new 3.62±0.05Ma $^{40}Ar/^{39}Ar$ date for K-feldspar) has been demonstrated.

At Big Gossan, the unique chemistry, zoning and structural setting suggest that the pyrite-Au-As-Zn-Bi-Te occurrences are products of a separate hydrothermal event. The current research and theoretical models suggest the low salinity (ca. 9 wt% $NaCl_{equiv}$) magmatic fluid was derived directly by exsolution from an evolving magma chamber, or is the product of a condensed magmatic vapour. Pyrite-Au-As-Zn-Bi-Te occurrences do not readily conform to high or low sulphidation models although the likely manifestations of both these types in deep carbonate-dominated terrains where there has been minimal interaction with non-magmatic fluids is poorly constrained. The pyrite-Au-As-Zn-Bi-Te fluids

may represent the magmatic precursor to fluids recognised in low and high sulphidation epithermal deposits that typically develop at shallow levels and contain significant contribution of non-magmatic (i.e. meteoric) water.

Acknowledgements

PT Freeport Indonesia is acknowledged for logistical and analytical funding and permission to publish this work. An Australian Institute of Geologists Student Bursary awarded to the senior author provided valuable additional funding for LA-ICPMS analyses. The LA-ICPMS analyses in this paper are from contribution XXX from the ARC National Key Centre for Geochemical Evolution and Metallogeny of Continents (GEMOC). GEMCOM software generously provided a full version of its software at cost. James Lally drafted a number of the diagrams. Feedback regarding Big Gossan and Wanagon Gold from Freeport staff (Clyde Leys, Norris Beluz, Nur Widodo, Paul Warren and Steve Hughes) is appreciated. Thank you also to Peter Pollard, Roger Taylor and researchers from University of Arizona and University of Texas, for providing access to unpublished information.

Section C
Magmatic $\delta^{18}O_{SMOW}$ and $\delta^{13}C_{PDB}$ compositions in porphyry-related hydrothermal carbonates from the Ertsberg District, Papua, Indonesia.

Abstract

A $\delta^{18}O$ and $\delta^{13}C$ investigation (78 carbonate analyses) of carbonate alteration associated with several porphyry-related hydrothermal systems was conducted in the Ertsberg district. Stratigraphically and paragenetically constrained altered and mineralised wallrocks and vein infill associated with different hydrothermal and igneous events were compared with unaltered and unmineralised sedimentary host rocks.

Dolomitisation of dolostone and limestone peripheral to the Grasberg Igneous Complex is manifested as planar, inclusion-poor euhedral and subhedral grain textures, which differ from the dominantly non-planar, inclusion-rich dolomite grain textures observed in unaltered Waripi Formation. Isotope analyses define a mixing line from original host Waripi Formation dolostone ($\delta^{18}O_{SMOW}$ =30.9‰ and $\delta^{13}C_{PDB}$ =1.2‰), which conforms with marine carbonate values, to the most altered dolostone whose isotopic composition conforms with magmatic values ($\delta^{18}O_{SMOW}$ =8.7‰ and $\delta^{13}C_{PDB}$ =-1.6‰). The texturally and isotopically modified porous dolostones may record H_2O+CO_2 magmatic degassing.

The in situ SIMS technique was used to analyse generations of calcite and dolomite infill related to an episode of carbonate alteration associated with an alteration and dissolution event in the Ertsberg East Skarn System. $\delta^{18}O_{SMOW}$ values of secondary calcite range from 11.7‰ to 17.5‰ which is lower than the values from unaltered dolostone. A magmatic fluid that leached carbonate from the adjacent carbonate stratigraphy is considered to have caused the alteration. Some involvement of non-magmatic fluids is indicated during an episode of leaching, quartz and clay alteration at Kucing Liar where calculated $\delta^{18}O$ fluid values are approximately 2.2-4.8‰.

Analyses of carbonate alteration selvages and late-stage vein infill from the Big Gossan skarn have a narrow range of $\delta^{18}O_{SMOW}$ and $\delta^{13}C_{PDB}$. Calculated $\delta^{18}O_{H2O}$ during skarn formation at Big Gossan is ca. 5.9‰ and the $\delta^{13}C$ value of the fluid may have been ca. -3.2‰, which is consistent with a magmatic source.

New and published stable isotope data suggest that, with the exception of late-stage hydrothermal events at Kucing Liar, contribution of non-magmatic fluids to hydrothermal ore deposits in the Ertsberg District was insignificant. The depleted $\delta^{13}C$ values from skarns and mineralised vein carbonates are interpreted to represent contribution from

magmatic carbon.

Introduction

Porphyry deposits are the source of the majority of the world's copper and the Ertsberg district, located in the mountainous Central Ranges of Papua (Figure C-1), contains one of the largest gold and copper resources in the world. Intrusive activity and several porphyry-related hydrothermal systems are hosted in Cretaceous-Tertiary clastic and carbonate sedimentary rocks (Figure C-2). Carbonate-hosted hydrothermal systems include numerous Cu-Au skarns, deep-intermediate high sulphidation Cu-Au, and precious and base metal carbonate-replacement deposits (Section D). Sedimentary rocks of the Cretaceous Kembelangan Group and Tertiary New Guinea Limestone Group (Figure C-1) crop out in the Ertsberg district (Quarles Van Ufford, 1996). Of these, the limestone and dolostone accumulations in the lower New Guinea Limestone Group Waripi Formation are significant hosts to mineral deposits in the district. The Ertsberg district is an ideal setting to asses the degree of interaction between porphyry-related hydrothermal fluids and the carbonate host rocks.

Although deep circulation and interaction between surface waters is traditionally implicated in porphyry-terrains (Taylor, 1997), more recently it has been demonstrated that primary magmatic fluids can be dominant (Harris and Golding, 2002; Meinert et al., 2003). Limited previous stable isotope studies in the Ertsberg district suggest that meteoric fluids may not have been significant during formation of major porphyry and skarn Cu-Au deposits (Meinert et al., 1997; Harrison, 1999; Meinert et al., 2003: B. New pers comm., 2003). Mertig (1995) reported $\delta^{13}C_{PDB}$ and $\delta^{18}O_{SMOW}$ measurements from six hydrothermal ferroan dolomite samples directly adjacent to the DOM skarn and five dolomite samples of unaltered Waripi Formation from the Wanagon drainage (Figure C-2). New (pers comm., 2003) analysed $\delta^{13}C_{PDB}$ and $\delta^{18}O_{SMOW}$ from one calcite and one dolomite sample at Kucing Liar and one dolomite from drillhole KLS3-1 (Figure C-2).

$\delta^{13}C$ and $\delta^{18}O$ stable isotope studies of carbonate-hosted hydrothermal systems can provide valuable information on the sources and evolution of hydrothermal fluids. This investigation comprises a reconnaissance $\delta^{13}C$ and $\delta^{18}O$ isotope study of carbonates in porphyry-related hydrothermal systems in the Ertsberg district using conventional isotopic techniques and in situ Secondary Ion Mass Spectrometry (SIMS). Stratigraphically- and paragenetically- constrained altered and mineralised wallrocks and vein infill associated with different hydrothermal and igneous events in the district have been compared with unaltered and unmineralised sedimentary host rocks.

Figure C-1. Location of the Ertsberg district, stratigraphy and stratigraphic distribution of $\delta^{18}O$ and $\delta^{13}C$ samples. a) Location of the Ertsberg District, Papua. b) Stratigraphy and depositional facies of the New Guinea Limestone Group in the Ertsberg District (modified from Quarles Van Ufford, 1996). Stratigraphic distribution of $\delta^{18}O$ and $\delta^{13}C$ isotope samples (cf. Figure C-2) in the district. Dashed lines where stratigraphic position is uncertain.

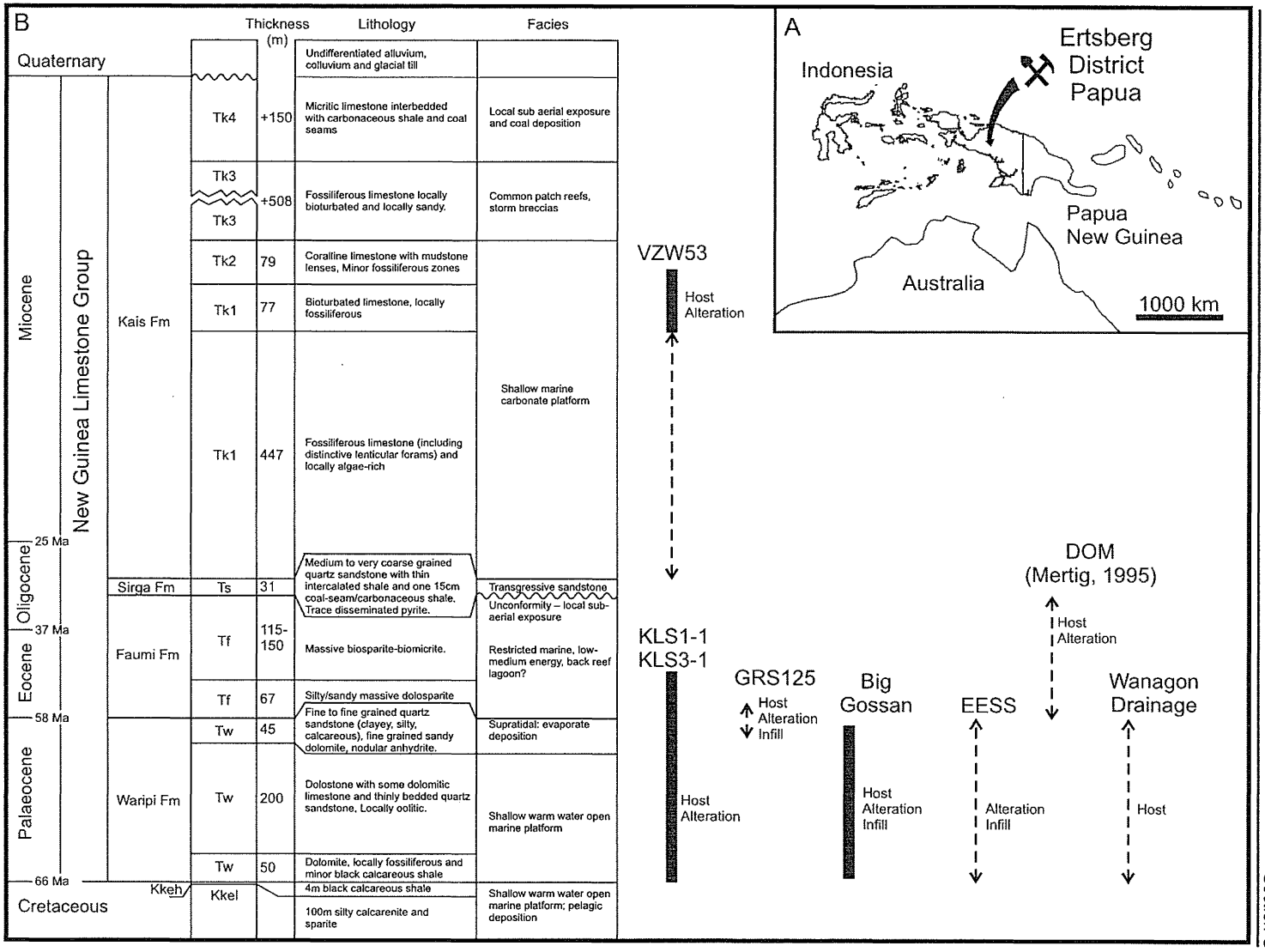

Geological setting

The oldest rocks in the Ertsberg District belong to the Cretaceous Kembelangan Group which consists of approximately 800m of siltstone, sandstone, sandy limestone, shale and limestone (Dow et al., 1988; Quarles Van Ufford, 1996) (Figure C-1). This is overlain by the Tertiary New Guinea Limestone Group composed of the Waripi, Faumi, Sirga and Kais Formations. The Waripi Formation (ca. 300m) comprises thinly bedded dolostone, siltstone and calcareous sandstone and significant anhydrite evaporites are also present. The Faumi Formation (ca. 200m) comprises fossiliferous limestone and dolostone. The Sirga Formation (ca. 30m) is a quartzose sandstone and the Kais Formation (>1000m) comprises limestone which is commonly sandy, shaley or fossiliferous. The sedimentary units in the Ertsberg District are interpreted to have been deposited as marine platform sediments in a passive margin setting (Quarles Van Ufford, 1996). Quaternary units in the district include alluvium in valleys, and till and colluvium along slopes.

Deformation of the passive margin was initiated in Miocene times during arc-continent collision when the northern edge of the Australian continent entered a north-dipping subduction zone beneath the Island of Papua (Sapiie et al., 1999). The passive margin sediments were deformed into a fold and thrust belt characterised by en echelon, kilometre-scale NW-trending folds with chevron and open symmetrical geometries (Figure 2: Sapiie et al., 1999).

Westwards movement of the Pacific-Caroline plate with respect to the Australian plate at ca. 4-2 Ma induced left-lateral, strike-slip faulting parallel to the upturned strata (Sapiie et al., 1999). In the Ertsberg district (Figure C-2) two major intrusive igneous complexes at Grasberg and Ertsberg and numerous smaller stocks, dykes and sills were emplaced at this time to depths of 2 km or less (McDowell et al., 1996; Weiland and Cloos, 1996; Pollard et al., submitted). The intrusive activity was accompanied by porphyry-related hydrothermal activity responsible for one of the largest Cu-Au resources in the world at 2.6 billion tonnes at 1.12% Cu and 1.02g/t Au (Freeport McMoRan Copper & Gold Inc 2002 Annual Report).

Figure C-2. Ertsberg district geology, location of intrusions and skarns (modified from PT Freeport Indonesia geological mapping) and location of drillholes sampled for isotope analyses. Isotope sample areas include DOM (Mertig, 1995); drillhole VZW53 and Section 13 (Figure C-3); Ertsberg East Skarn System Section 220E (Figure C-9); GRS125 (Figure C-5); Big Gossan (Figure C-13); drillholes KLS1-1 and KLS3-1 (Figure C-8). Estimated location (P. Warren pers comm., 2003) of "Wanagon drainage" Waripi Formation dolostone isotope samples reported by Mertig (1995). Approximate outline of Kucing Liar skarn projected from 1km below surface.

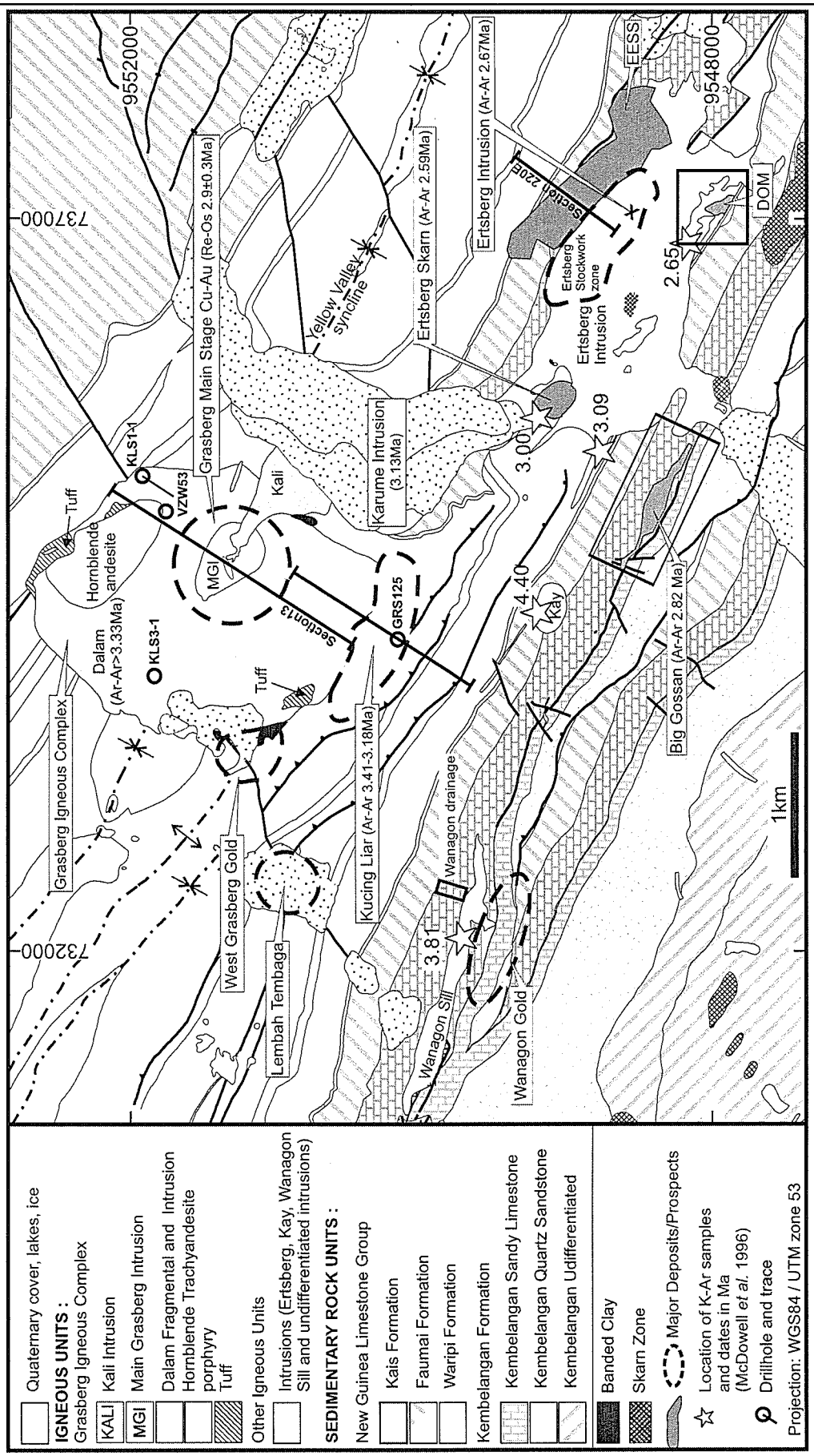
Quaternary cover, lakes, ice
IGNEOUS UNITS :
Grasberg Igneous Complex
KALI Kali Intrusion
MGI Main Grasberg Intrusion
Dalam Fragmental and Intrusion
Hornblende Trachyandesite
porphyry
Tuff
Other Igneous Units
Intrusions (Ertsberg, Kay, Wanagon
Sill and undifferentiated intrusions)
SEDIMENTARY ROCK UNITS :
New Guinea Limestone Group
Kais Formation
Faumai Formation
Waripi Formation
Kembelangan Formation
Kembelangan Sandy Limestone
Kembelangan Quartz Sandstone
Kembelangan Udifferentiated
Banded Clay
Skarn Zone
Major Deposits/Prospects
Location of K-Ar samples
and dates in Ma
(McDowell et al. 1996)
Drillhole and trace
Projection: WGS84 / UTM zone 53
Grasberg Igneous Complex
Dalam
(Ar-Ar>3.33Ma)
Hornblende
andesite
Tuff
KLS1-1
VZW53
KLS3-1
MGI
Kali
Grasberg Main Stage Cu-Au (Re-Os 2.9±0.3Ma)
Yellow Valley
syncline
Karume Intrusion
(3.13Ma)
Ertsberg Skarn (Ar-Ar 2.59Ma)
Ertsberg Intrusion (Ar-Ar 2.67Ma)
Section 220E
Ertsberg
Stockwork
zone
Ertsberg
Intrusion
EESS
DOM
2.65
3.09
3.00
4.40
Kay
Big Gossan (Ar-Ar 2.82 Ma)
Section13
GRS125
Kucing Liar (Ar-Ar 3.41-3.18Ma)
Wanagon drainage
3.81
Wanagon Sill
Wanagon Gold
West Grasberg Gold
Lembah Tembaga
Tuff
9552000
9548000
737000
732000
1km

Igneous geology and porphyry-related hydrothermal events

The GIC comprises early fragmented volcanic and igneous rocks of the Dalam phase and a series of nested intrusions (Figure C-2) (McDonald and Arnold, 1994; Pollard and Taylor, 2002; Sapiie and Cloos, submitted). Emplacement of the GIC and related hydrothermal events are constrained by paragenetic relationships and $^{40}Ar/^{39}Ar$ ages (Pollard and Taylor, 2002; Pollard et al., submitted). A biotite date of 3.07Ma from a premineralisation quartz-anhydrite-bearing vein provides a maximum age of main Grasberg sulphide development (Pollard and Taylor, 2002; Pollard et al., submitted). The Kucing Liar skarn (B. New pers comm., 2003) and Cu-Au deposit is hosted in faulted sediments adjacent to the GIC (Figure C-2). Skarn formation, dated at 3.41±0.3 to 3.18±0.2 Ma, was synchronous with the earliest GIC events (B. New pers comm., 2003: Pollard et al., submitted). Re-Os ages of 2.9±0.3Ma for Grasberg main stage sulphides (Mathur et al., 2000) and 3.01±0.02Ma for late-stage molybdenite from Kucing Liar (Mathur et al., submitted) support a cogenetic relationship between the deposits.

The Ertsberg Intrusion, dated at 2.67±0.3Ma by $^{40}Ar/^{39}Ar$, and overprinting hydrothermal products are considered almost 500ky younger than Grasberg and Kucing Liar mineralisation (Pollard et al., submitted). The $^{40}Ar/^{39}Ar$ age is within error of K-Ar biotite ages from the Ertsberg Intrusion, which range from 2.65±0.12 to 3.1±0.12Ma (McDowell et al., 1996; Titley, 1975). It is not clear whether the different Ertsberg Intrusion dates are different cooling ages in a single pluton (McDowell et al., 1996) or reflect different intrusive episodes (Pollard et al., submitted). Several major skarn Cu-Au systems occur close to, and postdate the Ertsberg Intrusion (Figure C-2). These include Ertsberg (Katchan, 1982; Clarke, 2003), Big Gossan (Section B: Meinert et al., 1997); DOM and the Ertsberg East Skarn System (EESS) (Mertig et al., 1994; Rubin, 1996; Coutts et al., 1999; Pollard and Taylor, 2003). Phlogopite from the Ertsberg skarn Cu-Au has an $^{40}Ar/^{39}Ar$ age of 2.59±0.15Ma. The Big Gossan skarn has an $^{40}Ar/^{39}Ar$ age of 2.82±0.04Ma (Section B), which is within error of K-Ar dates from the nearby Ertsberg Intrusion (McDowell et al., 1996).

Carbonate occurrences selected for this study include a) marble alteration and dolomitised rocks spatially-associated with the GIC and Kucing Liar, b) marble and veins related to the Big Gossan skarn and mineralisation and c) carbonate alteration associated with leaching events at Kucing Liar and the EESS (Figure C-2).

Methods

Carbonate identification

The paragenesis of the different carbonate events was determined from textural and mineralogical analysis at hand specimen, petrographic and electron microscope scales. Carbonate composition (Table C-1) was constrained by the following techniques:

a) Staining with a dilute hydrochloric acid solution containing alizarin red S and potassium ferricyanide (Hitzman, 1999) was used to identify carbonate component (dolomite, calcite, ferroan dolomite and ferroan calcite) in thin sections and hand specimens.
b) The James Cook University Siemens General Area Detector Diffraction System Diffractometer (GADDS) was used for routine non-destructive identification of in situ carbonate phases in hand specimens (Appendix 1).
c) Routine EDS analysis and backscatter electron imaging with the James Cook University Advanced Analytical Centre's JEOL 840A electron microprobe (EMPA; Appendix 1).
d) Samples analysed by the SIMS technique (discussed below) were also inspected for homogeneity by cathodoluminescence on James Cook University JEOL JSM-5410LV Scanning Electron Microscope.

Conventional isotope analysis technique

All samples were separated by hand under a binocular microscope and results are reported as $\delta^{13}C_{PDB}$ and $\delta^{18}O_{SMOW}$ (Table C-1). $\delta^{13}C$ and $\delta^{18}O$ analysis of 61 samples was conducted at Monash University Stable Isotope Laboratory (for details of the technique see Appendix 1). A sample of calcite selected for use as a standard was analysed at the University of Tasmania Central Science Laboratory.

SIMS technique and data reduction

A second suite of samples considered too fine-grained for hand separation were analysed in situ by Secondary Ion Mass Spectrometry (SIMS) at the Australian Nuclear Science and Technology Organisation (Table C-2). Carbonate samples were mounted in resin and gold coated prior to analysis (Table C-2).

The calcite standard utilised on all 4 days was a large hydrothermal calcite crystal from Mary Kathleen mine, Queensland, Australia (L. Marshall pers comm., 2003) and is known to be isotopically homogenous ($\delta^{13}C$ = -6.2‰ and $\delta^{18}O$ = 12.3‰; Table C-1). Dolomite from a Waripi Formation dolostone of known isotopic composition was used as a dolomite standard on days 1-3 (BGU24-11, 177m; $\delta^{13}C$ = 2.2‰ and $\delta^{18}O$ = 25.7‰). On day 4, a hydrothermally altered dolostone with a homogenous texture was used as a standard

Table C-1. Sample descriptions and isotopic results from the Ertsberg district. Big Gossan mineral Stages are displayed in Figure C-14. Description of carbonate identification and analytical techniques in text (Con1 = Monash stable isotope laboratory; Con2 = CSL Stable isotope laboratory). Strat = Stratigraphy, refer to Figure C-1 for full description. STD = conventional analysis of standards used to calibrate SIMS analyses. Sample numbers for SIMS analyses refer to raw data in Appendix 13.

Location	Description	Strat	Composition	Carbonate identification techniques	Isotope analytical technique	^{13}C PDB	^{18}O SMOW	Sample
Big Gossan Waripi Formation dolomite (West Drift Breccia)								
BGU24-11, 177m	Centre of grey breccia clast	Tw	Dolomite	Probe	Con1 (STD)	2.2	25.7	KP43
BGU21-03, 59m	Centre of grey breccia clast	Tw	Dolomite	GADDS/Stain	Con1	1.4	24.1	KP34
BGU21-1, 13m	Centre of grey breccia clast	Tw	Dolomite	Stain	Con1	1.6	24.9	KP29
BGU23-06, 66m	Centre of grey breccia clast	Tw	Dolomite	GADDS/Stain	Con1	1.1	22.4	KP31
BGU21-10, 12m	Centre of grey breccia clast	Tw	Dolomite	Probe	Con1	2.3	25.6	KP40
Big Gossan marble								
Underground sample F at 0m from skarn contact	Marble	Tw	Dolomite	Stain	Con1	0.6	18.8	KP04
Underground sample G at 10m from skarn contact	Marble	Tw	Dolomite	Stain	Con1	0.4	19.0	KP03
Underground sample D within marble alteration adjacent to Ertsberg Intrusion	Marble	Tw	Dolomite	Stain	Con1	0.3	20.2	KP06
Underground sample E within marble alteration adjacent to Ertsberg Intrusion	Marble	Tw	Dolomite	Stain	Con1	0.3	20.7	KP05
Big Gossan dolomite and calcite infill and alteration in skarn								
BGU18-3, 211.2m	Marble recrystallised near skarn (anhydrous-hydrous skarn)	Tw	Calcite	Stain	Con1	-4.9	8.9	KP65
BGU14-7, 590m	Calcite after pyroxene (anhydrous skarn)	Tw	Calcite	GADDS	Con1	-6.6	11.7	KP08
BGU17-7, 460m	Calcite infill with coarse pyroxene and garnet (anhydrous skarn)	Tw	Dolomite	GADDS	Con1	-1.6	8.2	KP26
BGU28-7, 185.4m	Garnet skarn sample. Calcite infill after brown dolomite (Stage ?)	Tw	Calcite	GADDS/Stain	Con1	-2.2	11.3	KP46
Big Gossan West Drift Breccia alteration								
BGU24-11, 177m	White alteration on edge of grey breccia clast (hydrous skarn)	Tw	Calcite	Probe	Con1	-4.7	9.3	KP42
BGU24-11, 177m	Calcite + tremolite alteration on dolostone clast (hydrous skarn)		Calcite	Probe	SIMS	-6.3	8.3	11030306, 7
BGU23-06, 66m	White alteration on edge of grey dolostone breccia clast (hydrous skarn)	Tw	Dolomite	GADDS/Stain	Con1	-3.9	9.8	KP30
BGU21-03, 59m	White alteration on edge of grey dolostone breccia clast (hydrous skarn)	Tw	Dolomite	GADDS/Stain	Con1	-4.8	8.8	KP33
Big Gossan dolomite and calcite infill in West Drift Breccia								
BGU21-01, 13m	Coarse calcite after dolomite infill (hydrous skarn)	Tw	Calcite	Stain	Con1	-4.0	9.7	KP27
BGU21-01, 13m	White dolomite infill (hydrous skarn)	Tw	Dolomite	GADDS/Stain	Con1	-4.9	10.2	KP28
BGU21-03, 59m	White dolomite infill (hydrous skarn)	Tw	Dolomite	GADDS/Stain	Con1	-4.6	9.1	KP45
BGU24-11, 177m	Calcite infill after tremolite (hydrous skarn)	Tw	Calcite	Probe	Con1	-3.3	7.6	KP41
BGU24-11, 177m	Calcite infill after tremolite (hydrous skarn)	Tw	Calcite	Probe	SIMS	-4.3	1.8	11030308, 9
BGU23-06, 66m	White dolomite infill (hydrous skarn)	Tw	Dolomite	GADDS/Stain	Con1	-3.9	8.7	KP32
Big Gossan - dolomite and calcite infill with sulphides								
BGU28-7, 185.4m	Brown dolomite, possibly with pyrite (Stage BG1) that crosscuts garnet skarn	Tw	Dolomite	GADDS/Stain	Con1	-2.1	10.7	KP35
Underground sample A	Calcite veins after garnet. Possibly with chalcopyrite, magmetite, coarse-pyrite assemblage (Stage BG1)	Tw	Calcite	Stain	Con1	-6.5	9.4	KP25
Underground sample B	Coarse grained pyrite, quartz, calcite, chalcopyrite (Stage BG1)	Tw	Calcite	Stain	Con1	-5.3	10.5	KP44
Underground sample C	Coarse grained pyrite infill (Stage BG1) with calcite infill	Tw	Calcite	Stain	Con1	-4.4	7.9	KP24
BGU21-10, 12m	Siderite infill with Stage BG2 sulphides	Tw	Siderite	Probe	Con1	-4.2	16.4	KP38
BGU21-10, 12m	White infill with sulphides on edge of grey dolostone breccia clast (Stage BG2?)	Tw	Siderite	Probe	Con1	-4.6	9.4	KP39
BGU18-3, 211.2m	Infill or rexallised crystals (Stage BG2). Average fluid inclusion homogenisation temperature 313 C (Section B).	Tw	Calcite	Stain	Con1	-5.3	9.3	KP64

Table C-1. continued

Location	Description	Strat	Composition	Carbonate identification techniques	Isotope analytical technique	^{13}C PDB	^{18}O SMOW	Sample
Ertsberg East Skarn System, carbonate metasomatism								
DOZ underground sample	Recrystallised Waripi Formation (sample KP07)	Tw	Calcite	GADDS/Stain	Con1	1.4	12.9	KP47
DOZB1-D	Carbonate alteration of EESS. Clear late infill	Tw	Calcite	Probe	SIMS	-3.6	13.5	18030305, 6
DOZB1-D	Carbonate alteration of EESS. Dolomite infill near magnetite	Tw	Dolomite and ankerite	Probe	SIMS	-2.4	11.7	18030304, 7
DOZ-B2-A	Carbonate alteration of EESS. Clear late infill	Tw	Calcite	Probe	SIMS	-6.3	11.7	12030306, 7
DOZ-B2-A	Carbonate alteration of EESS. Inclusion rich early calcite (host?)	Tw	Calcite	Probe	SIMS	-7.1	17.5	12030308, 9
GRS125 - Kucing Liar carbonate and silica alteration of carbonates								
GRS125, 590.7m	Limestone	Tw	Calcite	GADDS/Stain	Con1	-0.7	8.1	KP20
GRS125, 590.7m	Fine grained matrix	Tw	Calcite	Probe	SIMS	-3.2	6.9	18030318, 9
GRS125, 590.7m	Shell fragment	Tw	Calcite	Probe	SIMS	-3.7	6.4	18030316, 7
GRS125, 600m	White zones. Minor sulphide and grey contamination	Tw	Dolomite	GADDS/Probe	Con1	-2.2	6.3	KP18
GRS125, 595.6m	White dolomite crystals in vein	Tw	Dolomite	GADDS	Con1	-1.6	8.7	KP21
GRS125, 600m	Grey dolostone (altered)	Tw	Dolomite	GADDS	Con1	-1.6	8.7	KP19
GRS125, 602.7m	Grey dolostone (altered)	Tw	Dolomite	GADDS	Con1	-1.1	9.4	KP37
GRS125, 595.6m	White dolomite alteration associated with silica alteration of carbonate	Tw	Dolomite	GADDS/Stain	Con1	-1.1	7.9	KP22
GRS125, 610m	White silica and dolomite aleration. Minor pyrite and abundant quartz.	Tw	Dolomite	GADDS	Con1	-1.5	6.3	KP16
GRS125, 602.7m	White dolomite alteration	Tw	Dolomite	GADDS	Con1	-1.7	6.1	KP36
GRS125, 608.6m	Pale grey dolomite alterration. Minor sulphides and quartz.	Tw	Dolomite	GADDS	Con1	-1.6	6.1	KP23
GRS125, 600m	Pale grey alteration on late stage fractures	Tw	Siderite	Probe	Con1	-2.1	7.7	KP17
GIC - marble and dolomite								
VZW53, 330m	Brown dolomite alteration of grey limestone	TK1?	Dolomite	GADDS/Stain	Con1	-1.1	14.6	KP14
VZW53, 282m	White recrystallised marble	TK1?	Calcite	GADDS/Stain	Con1	0.1	9.1	KP10
VZW53, 188m	Pale recrystalised friable marble	TK1?	Calcite	GADDS/Stain	Con1	-2.6	12.2	KP12
VZW53, 173m	Coarse grained marble	TK1?	Calcite	GADDS/Stain	Con1	-0.4	9.9	KP13
VZW53, 188m	Dark grey limestone	TK1?	Calcite	GADDS/Stain	Con1	-3.4	12.1	KP11
VZW53, 282m	Dark grey limestone	TK1?	Calcite	GADDS/Stain	Con1	-0.2	10.8	KP09
VZW53, 330m	Grey limestone	TK1?	Calcite	GADDS/Stain	Con1	-3.6	13.6	KP15
KLS1-1 and KLS3-1 dolomite								
KLS1-1, 1345.3m	Dolostone	Tf	Dolomite	Stain	Con1	-1.1	9.7	KP48
KLS1-1, 1436.5m	Dolostone	Tf	Dolomite	Stain	Con1	-2.5	9.6	KP49
KLS1-1, 1447.4m	Quartz sandstone with dolomite matrix	Tw	Dolomite	Stain	Con1	0.5	18.7	KP50
KLS1-1, 1509.7m	Skarn altered quartz sandstone with dolomite matrix	Tw	Dolomite	Stain	Con1	0.2	16.1	KP51
KLS1-1, 1535.4m	Dolomite from homogeneous sample	Tw	Dolomite	Probe	SIMS	-0.5	6.2	18030312, 13
KLS1-1, 1535.4m	Dolomite from homogeneous sample	Tw	Dolomite	Probe	SIMS	-1.8	7.9	18030314, 15
KLS1-1, 1573m	Quartz sandstone with dolomite matrix	Tw	Dolomite	Stain	Con1	0.1	17.9	KP52
KLS1-1, 1605m	Equigranular dolomite rhombs with rare dolomite infill crystals in voids	Tw	Dolomite	Stain	Con1	-3.8	10.3	KP53
KLS1-1, 1796.7m	Skarn altered quartz sandstone with dolomite matrix	Tw	Dolomite	Stain	Con1	-4.7	7.8	KP54
KLS1-1, 1854.7m	Coarse relict peloidal texture retained by dolomite rhombs	Tw	Dolomite	Stain	Con1	-2.3	11.1	KP55
KLS3-1, 1485.7m	Dolostone	Tf	Dolomite	Stain	Con1	-0.7	13.2	KP56
KLS3-1, 1535.4m	Dolostone	Tf	Dolomite	Stain	Con1	-1.1	12.1	KP57
KLS3-1, 1556.3m	Quartz sandstone with dolomite matrix	Tw	Dolomite	Stain	Con1	0.0	18.1	KP58
KLS3-1, 1582.5m	Fine grained matrix with dolomite rhombs	Tw	Dolomite	Probe	SIMS	-1.2	9.4	18030322, 23
KLS3-1, 1582.5m	Shell fragment	Tw	Calcite	Probe	SIMS	-5.4	8.1	18030320, 21
KLS3-1, 1612.4m	Quartz sandstone with dolomite matrix	Tw	Dolomite	Stain	Con1	0.2	17.6	KP59
KLS3-1, 1623m	Texture retentive dolomite (peloidal)	Tw	Dolomite	Stain	Con1	-1.8	9.2	KP60
KLS3-1, 1744.8m	Texture retentive dolomite (peloidal)	Tw	Dolomite	Stain	Con1	-1.5	10.3	KP61
KLS3-1, 1855.8m	Very fine grained texture destructive dolomite	Tw	Dolomite	Stain	Con1 (STD)	-2.3	9.1	KP62
KLS3-1, 1983m	Calcite micrite-peloidal	Tw	Calcite	Probe	SIMS	-1.7	9.6	12030316, 17
KLS3-1, 1983m	Late stage spar infill in foram-shaped voids	Tw	Dolomite	Probe	SIMS	0.6	30.0	12030314, 15
KLS3-1, 1983m	Dolostone (alteration)	Tw	Dolomite	Probe	SIMS	1.2	12.2	12030318, 19
KLS3-1, 1983m	Late stage spar infill	Tw	Dolomite	Probe	SIMS	1.7	24.8	12030313, 12
Calcite Standard - Tribulation quarry, Mary Kathleen Fold Belt (L. Marshall pers comm, 2003)								
Single hydrothermal calcite crystal - 10cm (average analysis of 3 sample separates)			Calcite		Con2 (STD)	-6.2	12.4	
Single hydrothermal calcite crystal - 10cm (average analysis of 3 sample separates)			Calcite		Con2 (STD)	-6.1	12.2	

(KLS3-1, 1855.8m; $\delta^{13}C$ = -2.3‰ and $\delta^{18}O$ = 9.1‰).

Isotopic abundances are reported as a delta-value (δ) which is the isotopic ratio, $^{13}C/^{12}C$ or $^{18}O/^{16}O$, measured relative to an arbitrary standard, in this case PDB and SMOW respectively (Hoefs, 1980; Rollinson, 1996). To correct the SIMS measured isotope ratios obtained from unknown samples to the PDB and SMOW scales, the following formulae were used:

$$\delta^{13}C_{SIMS\text{-}PDB} = [((^{13}C/^{12}C)_{SIMS} / (^{13}C/^{12}C)_{PDB}) - 1] \times 1000$$
$$\delta^{18}O_{SIMS\text{-}SMOW} = [((^{18}O/^{16}O)_{SIMS} / (^{18}O/^{16}O)_{SMOW}) - 1] \times 1000$$

The $\delta^{13}C_{SIMS\text{-}PDB}$ and $\delta^{18}O_{SIMS\text{-}SMOW}$ data were corrected to separate calcite and dolomite standards of known composition through calculation of fractionation factors, $Cff_{standard}$ and $Off_{standard}$ (Paterson et al., 1997):

$$Cff_{standard} = \delta^{13}C_{SIMS\text{-}PDB} / \delta^{13}C_{known\text{-}standard\text{-}PDB}$$
$$Off_{standard} = \delta^{18}O_{SIMS\text{-}SMOW} / \delta^{18}O_{known\text{-}standard\text{-}SMOW}$$

ANSTO CAMECA ims 5f SIMS, Lucas Heights, Australia.	
Primary beam	$^{133}Cs^+$
Primary voltage	10keV
Primary current	~30nA
Focussed to a spot of	ca 30μm diameter
Secondary Ions	$^{16}O^-$ $^{18}O^-$ $^{12}C^-$ $^{13}C^-$
Sample voltage	-4150v
Field Aperture	750μm (O) and 400μm (C)
Contrast Aperture	400μm
Image Field	150μm
Mass Resolution	~5000 (to resolve $^{12}C^1H$ from ^{13}C and $H_2{}^{16}O^-$ from $^{18}O^-$)
Energy Window	60eV
Count Times	
^{16}O	1 sec
^{18}O	5 sec
^{12}C	1 sec
^{13}C	20 sec
3 blocks, 10 cycles per block. Isotopic ratios calculated by Cameca software with 1σ rejection.	

Table C-2. SIMS analytical parameters (K. Prince, pers comm. 2003). Analyses were corrected for dead time by the Cameca software. Gold coat of 10-15nm applied for charge compensation. Extreme Energy Filtering Technique.

Where:

$\delta^{13}C_{PDB} = \delta^{13}C_{SIMS\text{-}PDB}/Cff_{standard}$
$\delta^{18}O_{SMOW} = \delta^{18}O_{SIMS\text{-}SMOW}/Off_{standard}$

All SIMS $\delta^{13}C_{PDB}$ and $\delta^{18}O_{SMOW}$ results were corrected for instrumental drift that occurs over time (Fitzsimons et al., 2000). Fitzsimons et al. (2000) used a least squares regression to correct for instrumental drift. A linear regression between $ff_{standard}$ from calcite standard measurements throughout the day was used for this investigation.

Separate calcite and dolomite standards were measured to negate the matrix effect inherent in minerals of different composition (Eiler et al., 1997; Valley et al., 1997; Leshin et al., 1998; Riciputi and Greenwood, 1998). As the dolomite standard was measured less frequently, the calcite standard linear regression was applied to the dolomite standard measurements to establish $ff_{standard}$ linear regressions for dolomite analyses.

$\delta^{18}O$ and $\delta^{13}C$ internal and external precision

Data reduction (including reduction of internal precision) and calculation for drift corrections is dependent on the isotopic homogeneity of the standard material and in this study, the assumption that instrumental drift between standard measurements was linear. Due to the exploratory nature of the investigation, local dolomite samples were used as standards. Although chemically and texturally homogenous under microprobe, in both instances the isotopic homogeneity of the dolomite standards cannot be guaranteed.

For most elements, internal precisions (Fitzsimons et al., 2000) of ±0.5-1‰ may be expected for ion microprobe analyses (Hinton, 1995). Internal precision was highly variable for this study (Appendix 13) and ranged between 0.3-8‰ for $\delta^{13}C$ and 0.8-12.8‰ $\delta^{18}O$. Internal precision for the calcite standard varied between 0.7-3.7‰ for $\delta^{13}C$ and 0.8-4.5‰ $\delta^{18}O$ for this study. $\delta^{13}C$ external precision estimated from the reproducibility in consecutive analyses from the calcite standard in this investigation is ±0.8‰. A $\delta^{18}O$ external precision (reproducibility) of ±1.4‰ (1sigma) was established in a previous carbonate investigation at the ANSTO SIMS facility (Hazelton, 1997). A $d^{18}O_{SMOW}$ ion microprobe investigation by Reeder et al. (1997) on a synthetic calcite crystal demonstrated that although internal precision was slightly better than 1‰, reproducibility throughout the investigation (18 measurements) varied by 2.3‰. Internal precision reported from measurements of Mg-calcite and dolomite by Mojzsis et al. (1999) was <1.6‰ $d^{13}C$ and <1.3‰ $d^{18}O$. Internal precision from this study was higher than that documented in previous published studies.

Sample locations, geology and paragenesis

GIC marble

Marble has been recognised to extend for up to 100m around the GIC (Hefton et al., 1995) and is generally considered the product of contact metamorphic processes. Although it is not possible to constrain exactly what thermal or hydrothermal events were responsible for marble development, samples from VZW53 encompassing the least altered limestone and most altered marble were submitted for isotope analysis (Table C-1; Figure C-1; Figure C-3). The intrusive contact is characterised by strong silica, pyrite, magnetite and clay alteration (Figure C-3). At the contact (173m), marble is white, strongly crystallised and friable. Recrystallisation intensity decreases downhole away from the intrusive contact becoming mottled (188m) and at 282m marble is localised along discordant fractures (Figure C-4a). A narrow zone of discordant brown dolomitisation crosscuts grey limestone at 330m (Figure C-4b). A textural relationship between the brown dolomite alteration and white marble was not observed.

It is not clear where in the Kais stratigraphy the samples are located. Distinguishing features in the limestone are not apparent in marble. Distinct lenticular foraminifera characteristic of the Tk1 Kais Formation unit (Figure C-1) are not visible in the top 165m of marble altered limestone in VZW53 (PT Freeport Indonesia geological drilllog). Based on the thickness of Tk1 on Section 13 (Figure C-3), the samples are inferred to occur at the top of Tk1 unit (Figure C-1). However, karstified breccia and fractured zones (Figure C-3) may have reduced the stratigraphic thickness and the marble samples could be sourced from higher in the stratigraphy.

GRS125 - carbonate alteration associated with leaching and silicification at Kucing Liar

Silicified and leached Waripi Formation dolostone was intersected in drillhole GRS125 above the Kucing Liar skarn deposit (Figure C-5, Figure C-4c). Grey dolostone is altered to white dolomite and silica where leach holes occur (Figure C-4c). The leaching, silicification and dolomite alteration are interpreted to be components of the episode of leaching and silicification at Kucing Liar (Figure C-6; Stage IV) that immediately preceded

Figure C-3. Geology and sample locations for drillhole VZW53 on Mine Cross Section 13. a) Geology on Mine Cross Section 13 through the GIC (modified from PT Freeport Indonesia drawing) and projected location of drillhole VZW53 which is situated 70m SE of Section 13 (Figure C-2). January 2001 Grasberg pit outline. b) VZW53 downhole geology (from this study and PT Freeport Indonesia geological drilllog) and isotope sample locations.

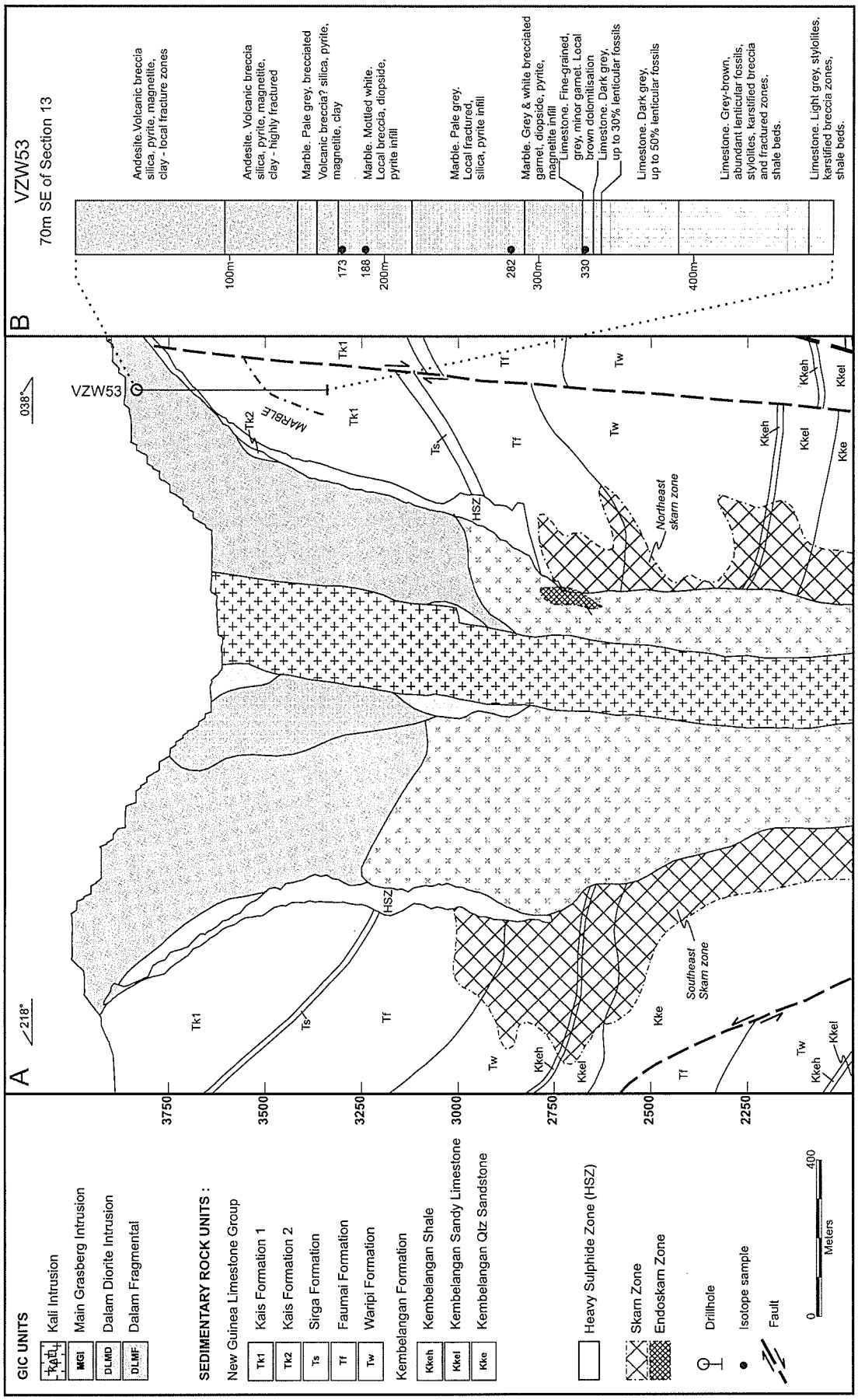
GIC UNITS
Kali Intrusion
Main Grasberg Intrusion
Dalam Diorite Intrusion
Dalam Fragmental
SEDIMENTARY ROCK UNITS :
New Guinea Limestone Group
Kais Formation 1
Kais Formation 2
Sirga Formation
Faumai Formation
Waripi Formation
Kembelangan Formation
Kembelangan Shale
Kembelangan Sandy Limestone
Kembelangan Qtz Sandstone
Heavy Sulphide Zone (HSZ)
Skarn Zone
Endoskarn Zone
Drillhole
Isotope sample
Fault
0
400
Meters
A
218°
038°
VZW53
MARBLE
HSZ
Northeast skarn zone
Southeast Skarn zone
3750
3500
3250
3000
2750
2500
2250
B
VZW53
70m SE of Section 13
Andesite. Volcanic breccia silica, pyrite, magnetite, clay - local fracture zones
Andesite. Volcanic breccia silica, pyrite, magnetite, clay - highly fractured
Marble. Pale grey, brecciated Volcanic breccia? silica, pyrite, magnetite, clay
Marble. Mottled white. Local breccia, diopside, pyrite infill
Marble. Pale grey. Local fractured, silica, pyrite infill
Marble. Grey & white brecciated garnet, diopside, pyrite, magnetite infill
Limestone. Fine-grained, grey, minor garnet. Local brown dolomitisation
Limestone. Dark grey, up to 30% lenticular fossils
Limestone. Dark grey, up to 50% lenticular fossils
Limestone. Grey-brown, abundant lenticular fossils, stylolites, karstified breccia and fractured zones, shale beds.
Limestone. Light grey, stylolites, karstified breccia zones, shale beds.
100m
173
188
200m
282
300m
330
400m

high sulphidation mineralisation (Pollard and Taylor, 2003; New, 1999).

The intensity of leaching, silicification and white alteration (Figure C-4c, d) increases towards sandstone units in the upper Waripi Formation (Figure C-1) which have undergone extensive brecciation (Figure C-5). Microprobe analysis indicate that altered white dolomite is chemically identical to grey unaltered dolostone (Figure C-7a). Samples from grey relatively unaltered Waripi Formation and white altered dolomite from leached and silicified areas were selected for isotope analysis (Figure C-5; Table C-1).

KLS1-1 and KLS3-1 stratigraphically constrained dolostone

Drill holes KLS1-1 (total depth 2199m) and KLS3-1 (total depth 2235m), completed in the course of district exploration, were used in a detailed definition of the limestone-dominated stratigraphy by New (1998). The drill holes are respectively located northeast (northern limb of Yellow Valley Syncline) and northwest (axis of Yellow Valley Syncline of the GIC (Figure C-2). Drillholes are collared in the GIC and contain locally significant dolomite and skarn alteration (New, 1998). Drillhole KLS3-1 is near vertical in the axis of the Yellow Valley syncline and the thicknesses of each stratigraphic unit intersected is considered near to true thicknesses (New, 1998) as they compare with estimates from district and regional studies (Quarles Van Ufford, 1996). The orientation of drillhole KLS1-1 is vertical for 400m, then angled at 60° towards the southwest to intersect a near-vertical fault, and reverts to vertical for the remainder of the hole (New, 1998). The section of KLS1-1 sampled in this study is oriented at 60° toward 213° (New, 1998). Neither drillhole intersected igneous bodies at depth.

Figure C-4. Photographs and photomicrographs from VZW53, GRS125, KLS3-1 and KLS1-1. Classification of carbonate textures from Sibley and Gregg (1987). "X" marks schematic context of sample area used for conventional isotope analyses. "S" marks schematic context of sample area analysed by SIMS. a) VZW53, 282m. Mottled grey Kais Formation (Tk) limestone with white calcitic marble alteration. White marble alteration also occurs on fractures. b) VZW53, 330m. Grey Kais Formation (Tk) limestone crosscut by discordant brown dolomite alteration. c) GRS125, 602.7m. Grey Waripi Formation (Tw) dolostone with patchy white alteration to silica and dolomite. Minor quartz infill in leach hole. No calcite is present (sample has been stained and inspected by microprobe). d) GRS125, 608.6m. Grey quartz surrounds clasts of white dolostone and silica. Sample located adjacent to contact with silicified and leached sandstone (Figure 8b). No calcite is present. e) KLS3-1, 1983m. Transmitted light photomicrograph. Planar euhedral to subhedral texture destructive dolomite replacement of micritic limestone (stained red). f) KLS3-1, 1983m. Transmitted light photomicrograph. Selective replacement of calcitic micrite and peloids (stained red) by inclusion-poor planar euhedral to subhedral dolomite. g) KLS3-1, 1623m. Transmitted light photomicrograph. Planar euhedral to subhedral texture-retentive dolomitisation by inclusion-poor dolomite. Can see original peloidal texture. Abundant porosity. No calcite is present (sample has been stained). h) KLS1-1, 1573m Transmitted light photomicrograph. Sandstone with abundant fine-grained non-planar inclusion-rich dolomite. No porosity is apparent. No calcite is present (sample has been stained).

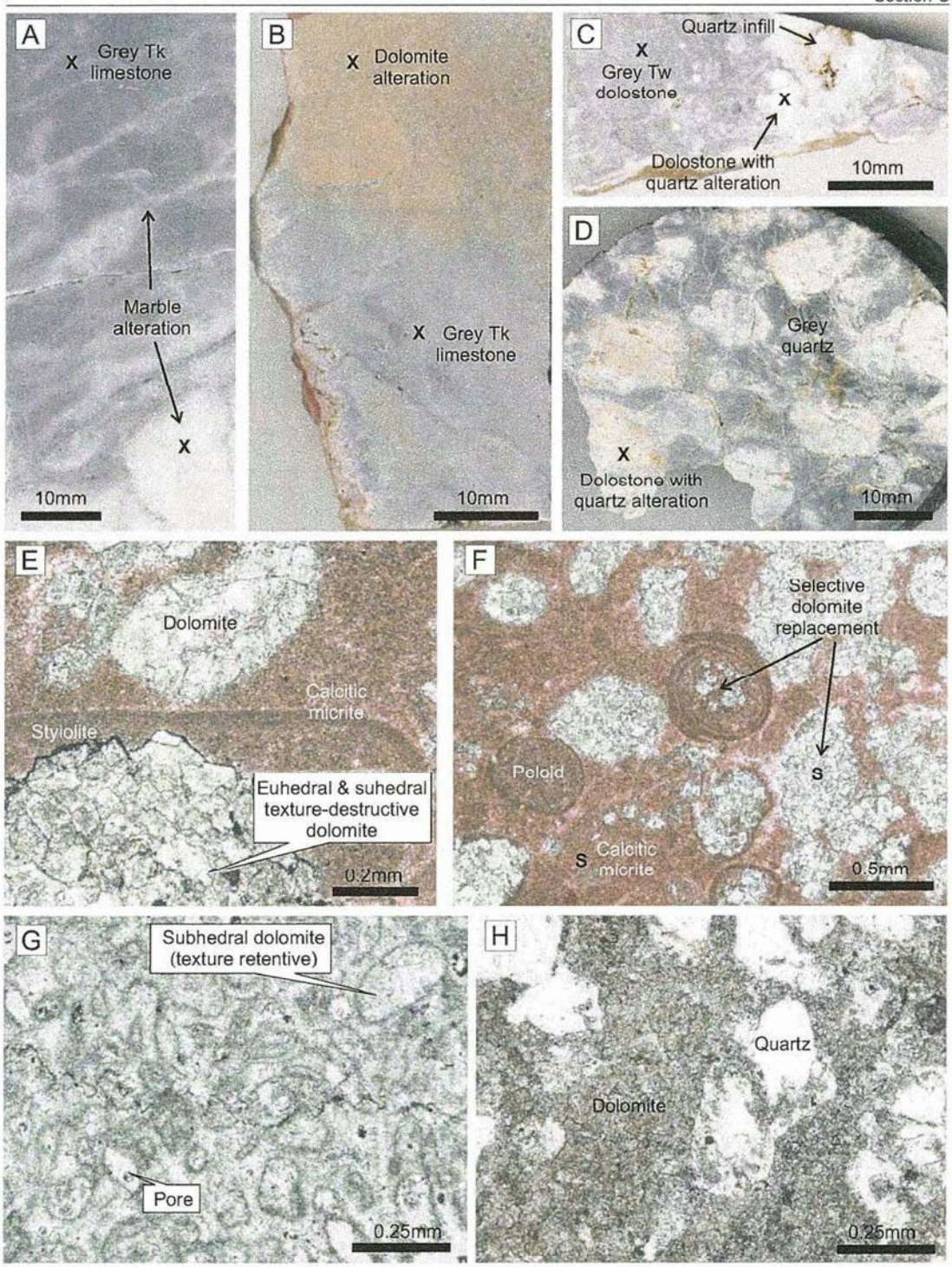
A
Grey Tk limestone
Marble alteration
10mm
B
Dolomite alteration
Grey Tk limestone
10mm
C
Quartz infill
Grey Tw dolostone
Dolostone with quartz alteration
10mm
D
Grey quartz
Dolostone with quartz alteration
10mm
E
Dolomite
Calcitic micrite
Stylolite
Euhedral & suhedral texture-destructive dolomite
0.2mm
F
Selective dolomite replacement
Peloid
S
Calcitic micrite
0.5mm
G
Subhedral dolomite (texture retentive)
Pore
0.25mm
H
Quartz
Dolomite
0.25mm

Figure C-5. Location, geology and isotope sample locations of drillhole GRS125. a) Geology and location of drillhole GRS125, Kucing Liar skarn and southern margin of GIC (modified from PT Freeport Indonesia drawing). Schematic stratigraphic location of sample KL38-05, 814.1m derived from nearby cross section KL32 (B. New pers comm., 2003). b) GRS125 downhole geology and isotope sample locations.

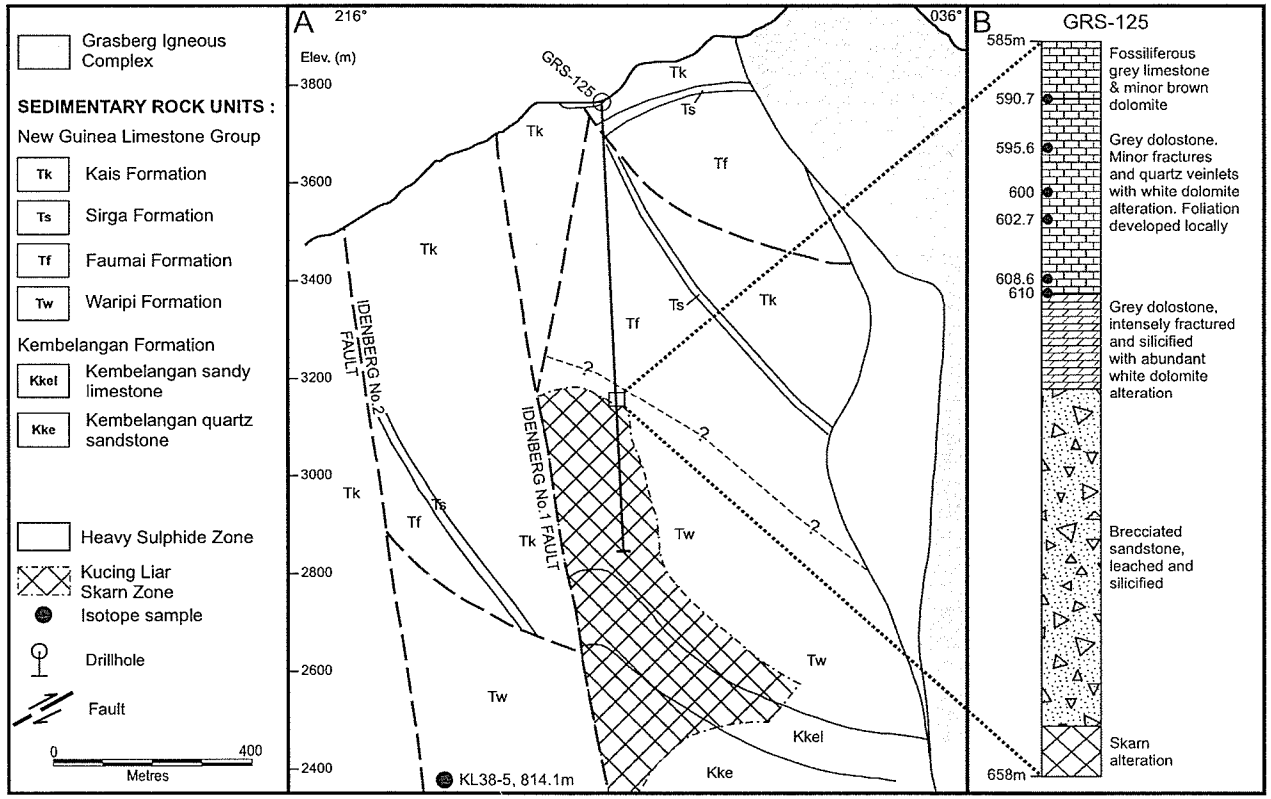

Figure C-6. Summary paragenesis and $^{40}Ar/^{39}Ar$ dates for Kucing Liar skarn and overprinting mineralisation (Pollard and Taylor, 2003; B. New pers comm., 2003: Pollard et al., submitted).

Stage I (3.41±0.03Ma)	Skarn - pyroxene, garnet, humite, forsterite, phlogopite (phlogopite age; Pollard et al., submitted)
Stage II (3.28±0.04Ma) (3.2±0.04Ma) (3.18±0.02Ma)	K-feldspar, biotite, phlogopite, quartz (phlogopite ages; B. New pers comm., 2003)
Stage III	Pyrite, chalcopyrite, magnetite, amphibole, anhydrite, crysotile
Stage IV (3.18±0.02Ma)	Leaching, muscovite, talc, quartz (muscovite age; B. New pers comm., 2003)
Stage V	High sulphidation sulphides (Pollard and Taylor, 2003). Pyrite, mixed Cu sulphides (chalcopyrite, covellite, enargite, nukundamite, chalcocite) native sulphur, and gold
Late	Sphalerite, galena

Figure C-7. Microprobe analyses of wt% Ca, Mg and Mn+Fe in carbonate. Raw data in Appendix 5. a) GRS125, 590.7, 600, 608.6m (Figure C-4c, d). b) BGU21-10, 21m (Figure C-11j). c) BGU24-11, 177m (Figure C-11i). d) DOZB1-D and DOZB2-A (Figure C-11b, c; Figure C-12a, b, c)

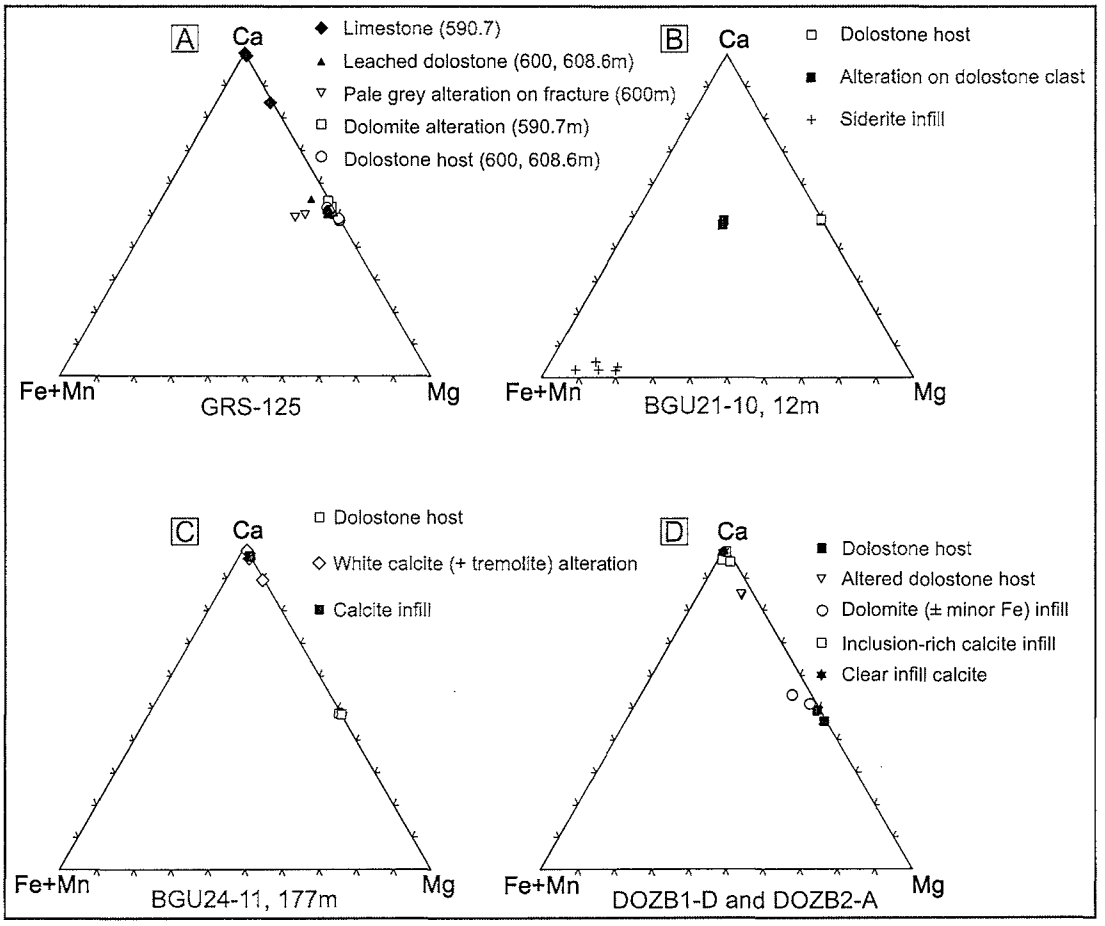

The stratigraphic sequences intersected by the drillholes can be broadly correlated on the basis of lithological packages (Figure C-8). Samples were selected from the Faumai Formation and Waripi Formation to establish variation in isotope composition: a) laterally, between similar lithological packages in the two drillholes, and b) vertically, down stratigraphy (Figure C-8; Table C-1).

The stratigraphic formations sampled are dominated by dolostone. Rare occurrences of micritic and peloidal limestone textures, which may represent original pre-dolomitisation limestone, have been selectively replaced by planar euhedral to subhedral, inclusion-poor dolomite (Figure C-4e, f). In the Waripi Formation, dolostone displays abundant secondary porosity and the planar euhedral to subhedral, inclusion-poor dolomite is interpreted as texture-retentive replacement (Figure C-4g). Dolomite in the sandstone samples is texturally different and characterised by fine-grained, inclusion-rich and non-planar textures (Figure C-4h). Minor fine-grained skarn (Figure C-8) was identified in thin sections in several samples (New, 1998).

Ertsberg East Skarn System carbonate alteration

The EESS is located on the northern margin of the Ertsberg Intrusion (Figure C-1; Figure C-9). The skarn is hosted in the Faumai and Waripi Formation at the contact with the Ertsberg Intrusion and has a vertical extent greater than 1 km (Figure C-9). Several episodes of intrusive activity and alteration and mineralisation are represented (Figure C-10). Leaching, brecciation and subsequent carbonate alteration affects all earlier skarn and mineralisation stages and caused recrystallisation and alteration of the adjacent Waripi Formation (carbonate breccia in Figure C-9; Figure C-10). Underground samples in the EESS contain leached dolomite and later infill of inclusion-rich calcite overgrown by inclusion-free calcite (Figure C-7d; Figure C-11a, b; Figure C-12a, b, c). The two generations of infill calcite evident in the underground samples are the dominant components of the carbonate alteration event. Calcite alteration is also manifested as alteration of breccia clasts composed of magnetite and dolomite (Figure C-11b; Figure C-12c). In some magnetite-bearing samples, an earlier generation of finely intergrown dolomite and ankerite predates the calcite infill (Figure C-7d; Figure C-11c; Figure C-12a, b).

A recrystallised calcite marble of the Waripi Formation, from the northern margin of the leaching, brecciation and carbonate alteration zone was analysed by conventional isotope

Figure C-8. Stratigraphy, sample location and conventional carbonate $\delta^{18}O_{SMOW}$ and $\delta^{13}C_{PDB}$ results from KLS1-1 and KLS3-1 (logging from New, pers comm., 2003). Results in Table C-1. KLS1-1 and KLS3-1 stratigraphy and composition modified from New (pers comm., 2003). General correlation between lithological packages. Sample KLS3-1, 1420.2m from New (pers comm., 2003).

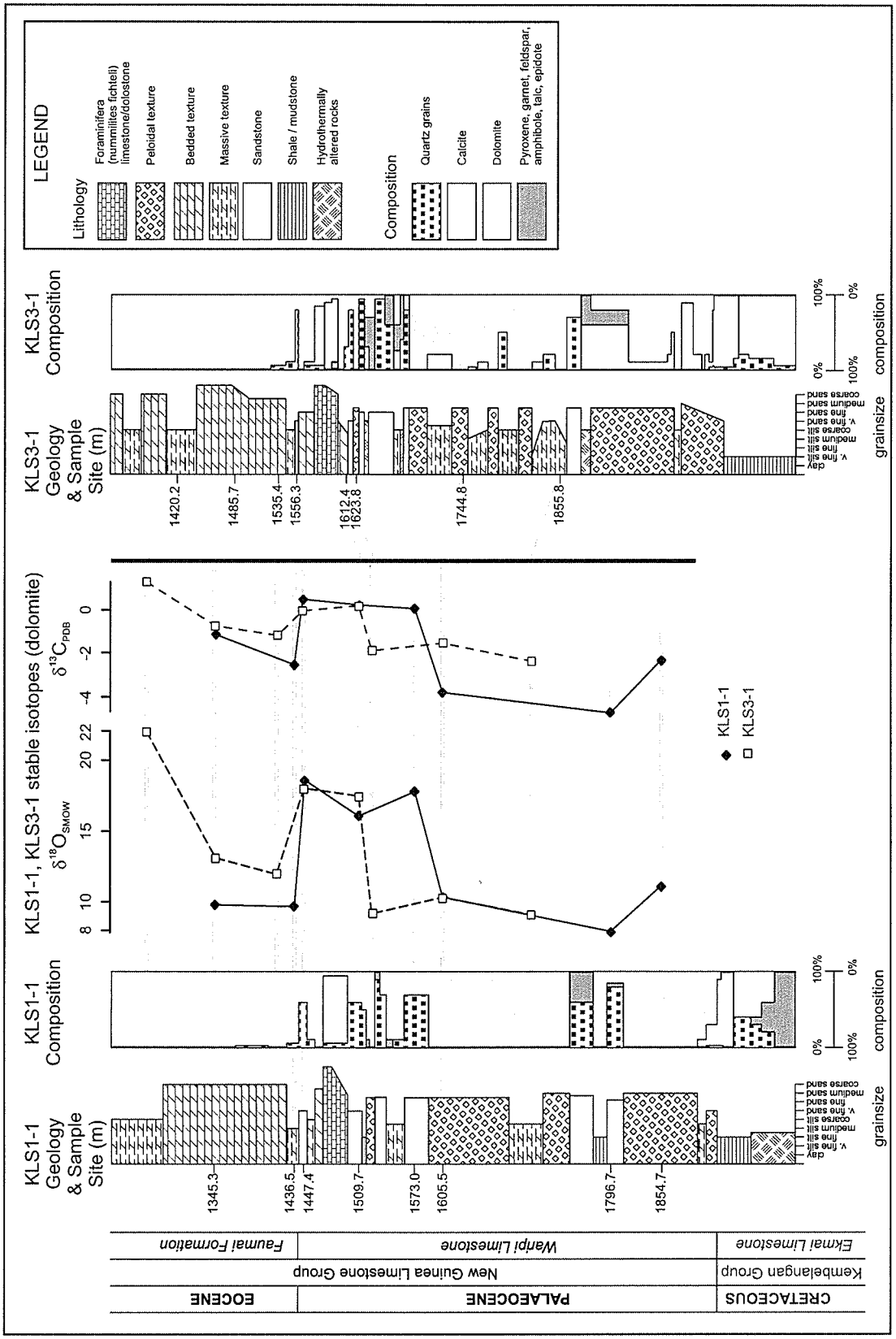
LEGEND
Lithology
Foraminifera (nummilites fichteli) limestone/dolostone
Peloidal texture
Bedded texture
Massive texture
Sandstone
Shale / mudstone
Hydrothermally altered rocks
Composition
Quartz grains
Calcite
Dolomite
Pyroxene, garnet, feldspar, amphibole, talc, epidote
KLS3-1 Composition
KLS3-1 Geology & Sample Site (m)
1420.2
1485.7
1535.4
1556.3
1612.4
1623.8
1744.8
1855.8
KLS1-1, KLS3-1 stable isotopes (dolomite)
δ18OSMOW
δ13CPDB
KLS1-1
KLS3-1
KLS1-1 Composition
KLS1-1 Geology & Sample Site (m)
1345.3
1436.5
1447.4
1509.7
1573.0
1605.5
1796.7
1854.7
grainsize
composition
0%
100%
CRETACEOUS
PALAEOCENE
EOCENE
Kembelangan Group
New Guinea Limestone Group
Ekmai Limestone
Waripi Limestone
Faumai Formation

Figure C-9. Geology of the EESS. a) Cross section 220E. b) Plan level 3050 (modified from PT Freeport Indonesia drawing). Location of the zone of leaching, brecciation and carbonate alteration of the EESS and adjacent Waripi Formation. Ore reserves as at December 31st 2000 (Freeport McMoRan Copper & Gold Inc 2000 Annual Report).

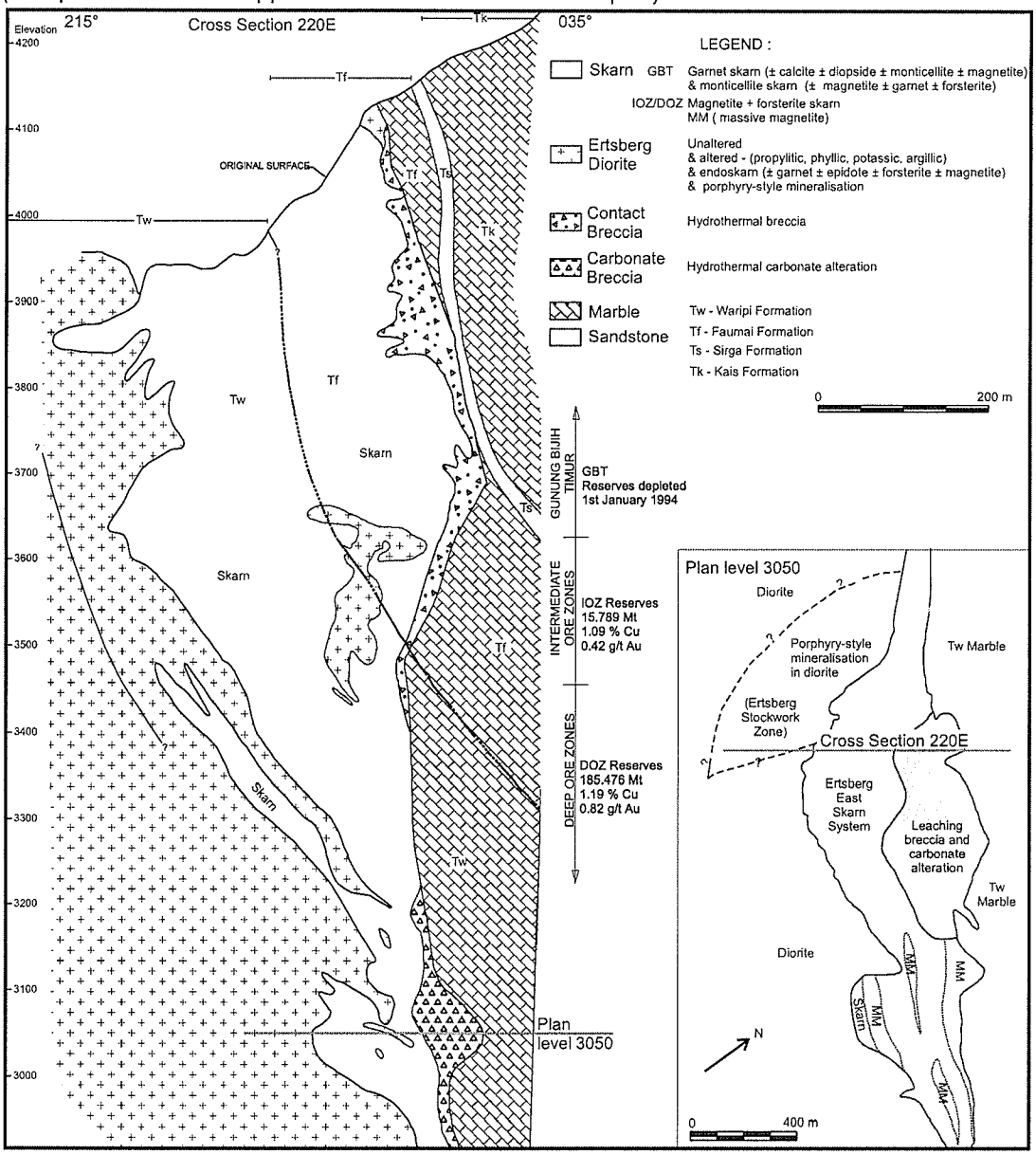

analytical techniques (Figure C-9; Table C-1). Late stage dolomite and calcite infill (Figure C-11b, c) were analysed with the high-resolution SIMS technique (Table C-1).

Big Gossan

The Big Gossan skarn occurs in the lower Waripi Formation near the Kembelangan Group contact (Figure C-13). Ore reserves at Big Gossan were 33 million tonnes at 2.81% Cu, 1g/t Au and 16.85g/t Ag at the end of 2002 (Freeport McMoRan Copper & Gold Inc 2002 Annual Report). At Big Gossan, the unaltered Waripi Formation is predominantly dolostone and is characterised by inclusion-rich dolomite with a non-planar anhedral texture (Figure C-11d). The dolostone is variably altered to marble adjacent to the Ertsberg Intrusion and

Figure C-10. Summary paragenesis for the EESS (modified from Mertig et al., 1994; Coutts et al., 1999; Friehauf et al., 2002 and this study).

	Igneous and hydrothermal events	Ertsberg Intrusion clinopyroxene-dominant and biotite= clinopyroxene equigranular phases (Friehauf et al., 2002)		Waripi Formation and Faumai Formation sediments
Early	Porphyry-style mineralisation	Feldspar-stable bornite+ biotite (Friehauf et al., 2002).		?
	Porphyry dykes	Of the 3 phases recognised, the phase most closely related spatially and temporally to mineralisation contains 40% plagioclase phenocrysts, 3-5% hornblende and 1% biotite in a sugary, aplitic groundmass		?
	Skarn	Garnet-bearing endoskarn alteration of Ertsberg Intrusion and Porphyry dykes.	? →	Skarn, anhydrous and hydrous (Mertig et al., 1994)
	Cu-Au Mineralisation	Early bornite and later pyrite, ±chalcopyrite (Friehauf et al., 2002)	→	Bornite, chalcopyrite, gold and minor pyrite (Mertig et al., 1994)
	High Sulphidation Style Mineralisation	?		Chalcopyrite, covellite ± digenite, idaite, chalcocite (Rubin and Kyle, 1997; Coutts et al., 1999; Pollard and Taylor, 2003)
	Leaching and carbonate alteration	?		Leaching and brecciation. Followed by abundant calcite (minor dolomite) alteration and infill (Coutts et al., 1999: this study)
Late	Mineralisation	?		Chalcopyrite, pyrite, galena (Coutts et al., 1999: this study)

Figure C-11. Carbonate textures from the EESS, and Big Gossan. Classification of carbonate textures from Sibley and Gregg (1987). "X" marks schematic context of sample area used for conventional isotope analyses. "S" marks schematic context of sample area analysed by SIMS. Scale bar 1cm unless specified. a) DOZB1-E (Sample from the EESS carbonate breccia; sample collected by Spera (2001). Transmitted light photomicrograph. Leaching has left relict dolomite rib textures in the Waripi Formation. b) DOZB2-A (Sample from the EESS carbonate breccia; sample collected by Spera (2001)) Sample offcut used for SIMS analysis. Transmitted light photomicrograph. Dolomite and magnetite clast (with calcite alteration) surrounded by inclusion-rich calcite. Late euhedral clear-calcite crystals grow into voids (voids are stained blue). c) DOZB1-D (EESS sample courtesy of Spera (2001); offcut used for SIMS analysis). Transmitted light photomicrograph. Magnetite grains surrounded by a brown dolomite (with minor ankerite) and banded inclusion-rich calcite. Late euhedral clear-calcite in voids. d) BGU 23-06, 104m. Transmitted light photomicrograph. Relatively unaltered non planar Waripi Formation dolostone at Big Gossan. e) BG Underground marble sample from near Ertsberg Intrusion (samples 13 and 14 on Figure C-13). Transmitted light photomicrograph. Where recrystallised, dolomite marble has less inclusions and is coarser grained than the Waripi Formation dolostone. f) BGU23-06, 66m. Grey dolostone clast with white dolomite alteration and white dolomite infill. Late calcite infill (stained red) and alteration of clasts and fragments of dolomite infill. g) BGU21-01, 13m. Grey dolostone clast and white dolomite infill. Late calcite infill (stained red). h) BGU21-03, 59m. Grey dolostone clast with white dolomite alteration and dolomite infill. i) BGU 24-11, 177m. Resin mounted block used for SIMS analyses. The dolostone clast in this sample was used for SIMS standard analyses and the sample off-cut used for conventional isotope analyses (Table C-1). Grey dolostone clast with white alteration margin of calcite and tremolite and green tremolite infill. A late vein contains calcite infill and minor magnetite (black). A sharp isotopic gradient is observed between the alteration margin ($\delta^{18}O_{SMOW}$ = 9.3‰ and $\delta^{13}C_{PDB}$ = -4.7‰) and grey dolostone ($\delta^{18}O_{SMOW}$ = 25.7‰ and $\delta^{13}C_{PDB}$ = 2.2‰) (Nabelek, 1991). j) BGU21-10, 12m. Resin mounted block used for SIMS analyses. Dolomite & siderite alteration margin on dolostone clast. Siderite and sulphide infill.

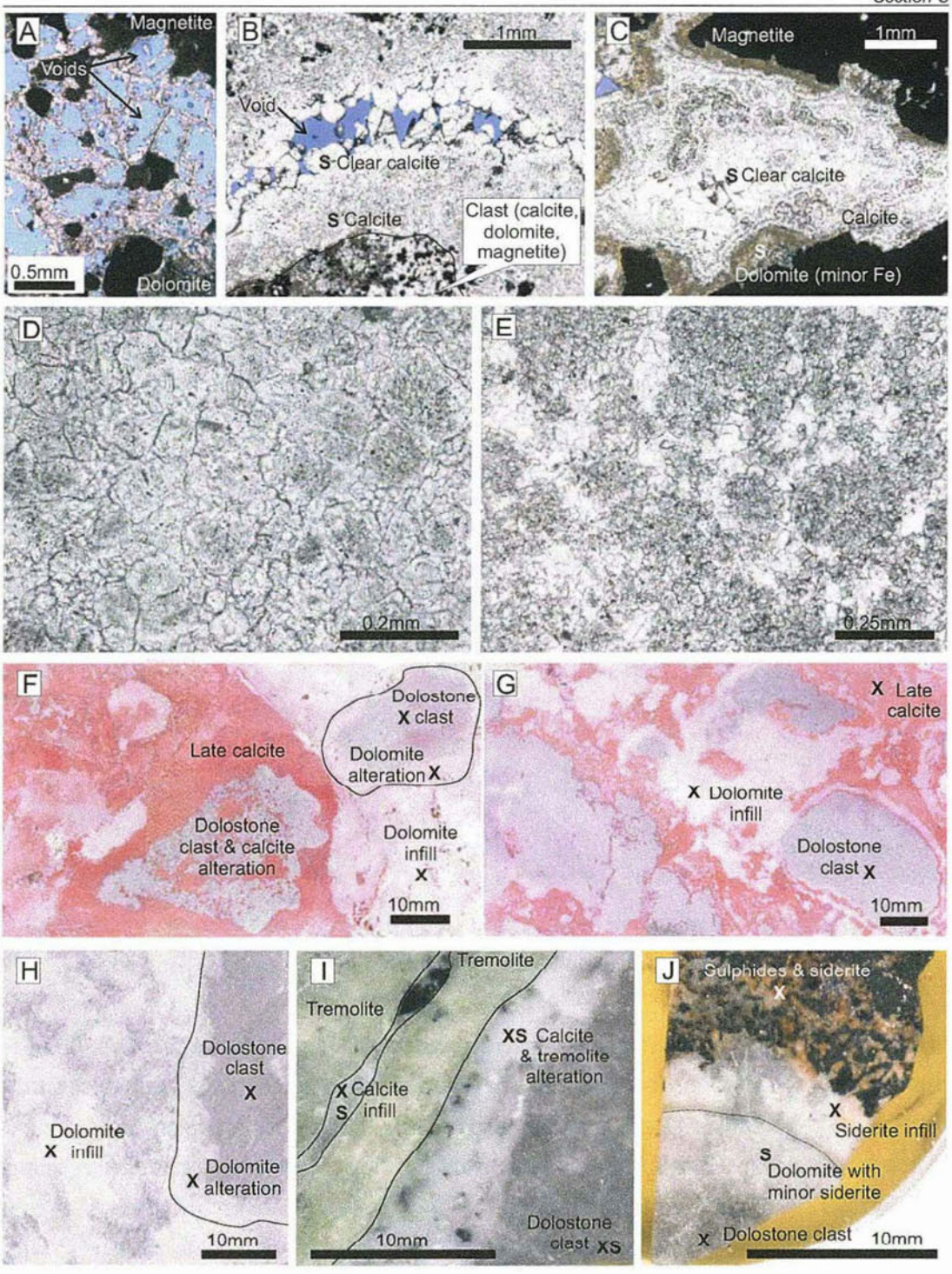
A
Magnetite
Voids
0.5mm
Dolomite
B
1mm
Void
S Clear calcite
S Calcite
Clast (calcite, dolomite, magnetite)
C
Magnetite
1mm
S Clear calcite
Calcite
S
Dolomite (minor Fe)
D
0.2mm
E
0.25mm
F
Dolostone X clast
Late calcite
Dolomite alteration X
Dolostone clast & calcite alteration
Dolomite infill X
10mm
G
X Late calcite
X Dolomite infill
Dolostone clast X
10mm
H
Dolostone clast X
Dolomite X infill
X Dolomite alteration
10mm
I
Tremolite
Tremolite
XS Calcite & tremolite alteration
X Calcite S infill
Dolostone clast XS
10mm
J
Sulphides & siderite
X
X Siderite infill
S Dolomite with minor siderite
X Dolostone clast
10mm

Figure C-12. Backscatter electron microprobe images of carbonate infill in the EESS carbonate breccia. a) DOZB1-D (Sample from the EESS carbonate breccia; sample collected by Spera (2001)) Offcut used for SIMS analysis. Magnetite grains surrounded by dolomite (containing minor Fe), dolomite (no Fe) and calcite. b) Banded dolomite (containing minor Fe), dolomite (no Fe) and inclusion-rich calcite from inset area in Figure C-12a. c) DOZB2-A (Sample from the EESS carbonate breccia; sample collected by Spera (2001)) Offcut used for SIMS analysis. Clast containing magnetite, rare dolomite and calcite alteration surrounded by calcite. Late euhedral calcite crystals grow into voids. Photomicrograph in Figure C-11b.

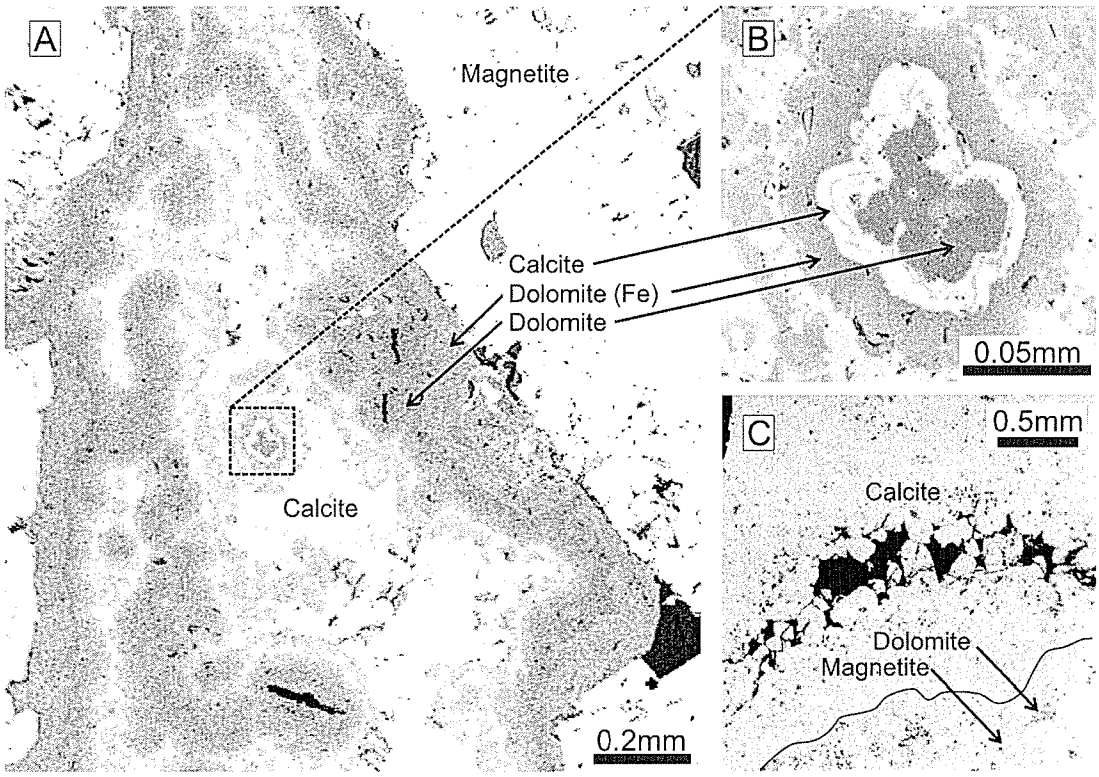

adjacent to the Big Gossan skarn (Figure C-11e). Marble occurs in the hanging wall of the Big Gossan skarn for tens to hundreds of metres (Meinert et al., 1997).

The 200-250m diameter West Drift breccia pipe occurs in the Waripi Formation immediately northeast of the Big Gossan skarn (Figure C-13). Due to the absence of anhydrous skarn alteration and the presence of hydrous skarn alteration, the West Drift breccia is considered to have formed at the onset of hydrous skarn alteration (Section B). Two generations of secondary carbonate (Stage 3; Figure C-14) occur throughout the West Drift breccia, namely an early dolomite alteration and infill and subsequent calcite infill (Figure C-11f, g, h). The two generations of sulphide mineralisation documented at Big Gossan, including early Cu-Au mineralisation (Stage BG1) and pyrite-sphalerite-arsenopyrite-native gold with localised Bi and Te minerals (Stage BG2), have minor calcite and siderite associated (Section B; Figure C-14).

Several generations of carbonate alteration and vein infill documented in the Big Gossan paragenesis (Figure C-14) were sampled for isotope analysis (Figure C-13; Table C-1)

Figure C-13. Big Gossan local geology at 2930RL elevation and location of isotope samples. Geology modified from PT Freeport Indonesia drawing (Projection: WGS84 / UTM zone 53). Drillhole carbonate isotope samples projected to 2930RL elevation. Underground samples 1 and 2 provided by Gavin Clarke (Taylor et al., 1999).

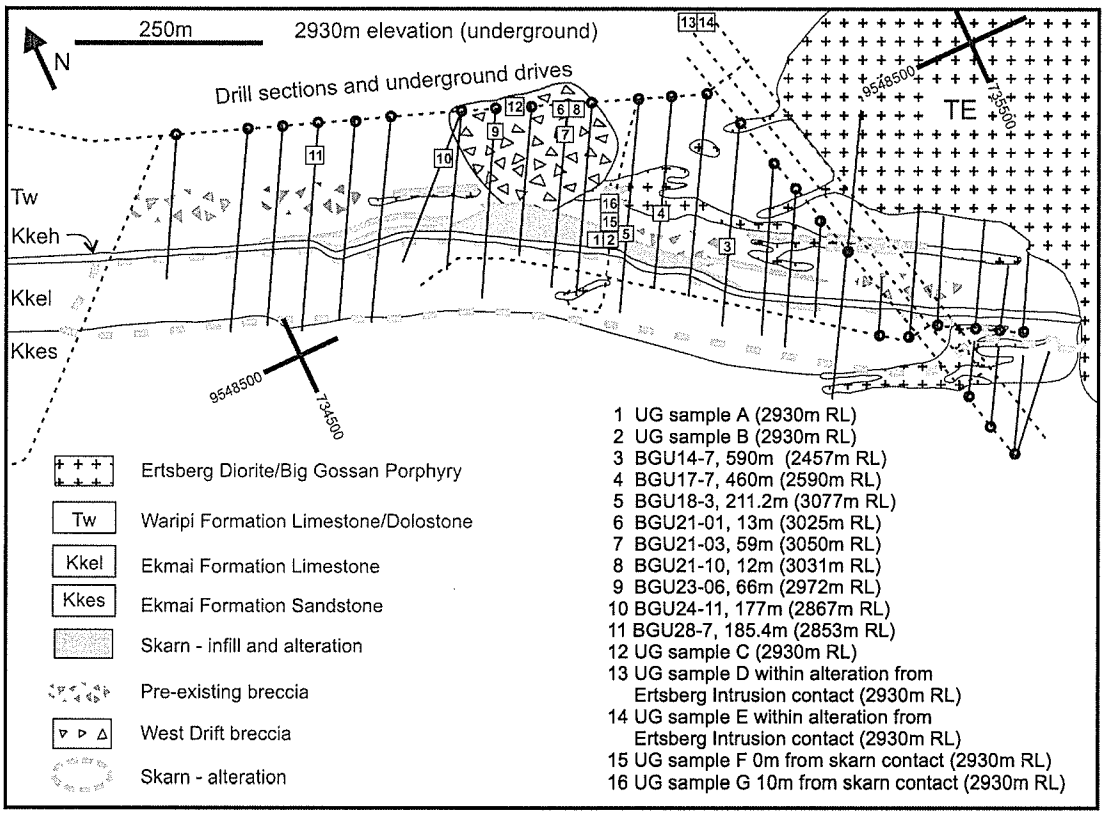

Figure C-14. Summary paragenesis and $^{40}Ar/^{39}Ar$ date for Big Gossan (Section B).

Hydrothermal Association	Minerals
Early	marble (adjacent to skarn, adjacent to Ertsberg Intruision)
Skarn (anhydrous)	pyroxene, garnet, calcite, quartz
Skarn (hydrous) 2.82±0.04Ma	calcite, dolomite, amphibole, phlogopite, talc, anhydrite, magnetite
Stage BG1 Gold & Fe-Cu-Ag sulphides	pyrite, pyrrhotite, chalcopyrite, hematite-magnetite, pyrrhotite, sphalerite, bornite, (galena), gold, arsenopyrite, scheelite, calcite
Stage BG2 Gold & Fe-Zn-Pb-As sulphides & local Bi & Te minerals	pyrite, sphalerite, galena, chalcopyrite, gold, siderite, quartz, cosalite, bismuthinite, tetradymite, argentian tetrahedrite and tennantite, arsenopyrite
Late	epidote, chlorite, hematite, pyrite

including:

a) Samples of least altered Waripi Formation dolostone from breccia clasts in the West Drift breccia (Figure C-11f, g, h, i, j).
b) Marble alteration of Waripi Formation sampled from near the Big Gossan skarn contact and marble alteration spatially associated with the Ertsberg Intrusion (Figure C-11e). Marble was sampled along the drift at <1m and 10m to the NE and laterally away from the Big Gossan skarn (Figure C-13). Marble samples display varying intensity of recrystallisation of original dolostone texture (Figure C-11e).
c) Dolomite and calcite alteration and vein infill in the West Drift Breccia interpreted to be components of the hydrous skarn event (Figure C-7c; Figure C-11f, g, h, i).
d) Dolomite and calcite vein infill and alteration in the Big Gossan skarn.
e) Vein infill associated with Stage 4 and Stage 5 sulphides in the Big Gossan skarn and West Drift breccia (Figure C-7b; Figure C-11j).

$\delta^{18}O_{SMOW}$ and $\delta^{13}C_{PDB}$ results

GIC marble (VZW53)

The least altered samples may represent the isotopic composition of the original Kais Formation limestone (Figure C-15a). The most altered marble sample and one sample of mottled limestone marble have slightly lower $\delta^{18}O_{SMOW}$ and $\delta^{13}C_{PDB}$ ca. 3‰ higher than the least altered samples (Figure C-15a). The discordant dolomite alteration displays $\delta^{18}O_{SMOW}$ and $\delta^{13}C_{PDB}$ values similar to those of dolomite in KLS1-1 and KLS3-1 (Figure C-15c).

Carbonate alteration associated with leaching and silicification at Kucing Liar (GRS125)

Unleached dolostone in GRS125 has similar $\delta^{18}O_{SMOW}$ and $\delta^{13}C_{PDB}$ to Waripi Formation samples from KLS1-1 and KLS3-1 (Figure C-15c). $\delta^{13}C_{PDB}$ displays minimal variation between grey unaltered and white altered (leached and silicified) dolostone (Figure C-15b). White altered dolomite on fractures has $\delta^{18}O_{SMOW}$ up to 3‰ less than unalteredd samples. Late-stage infill dolomite has $\delta^{18}O_{SMOW}$ and $\delta^{13}C_{PDB}$ similar to the host rock. Analyses of calcitic shell and matrix (GRS125, 590.7m) by SIMS are within error (internal precision) of the result from a conventional analysis (mixed shell and matrix) of the same sample (Figure C-15b).

Figure C-15. $\delta^{18}O_{SMOW}$ and $\delta^{13}C_{PDB}$ isotope results from VZW53, GRS125, KLS1-1, KLS3-1 and EESS. Samples were analysed by conventional techniques unless specified as "SIMS". SIMS uncertainties are internal precision (Appendix 13). Conventional uncertainties are ±0.1‰ $\delta^{13}C$ and $\delta^{18}O$ (Appendix 1). a) VZW53. b) GRS125. c) KLS1-1, KLS3-1 and VZW53 dolomite. d) EESS

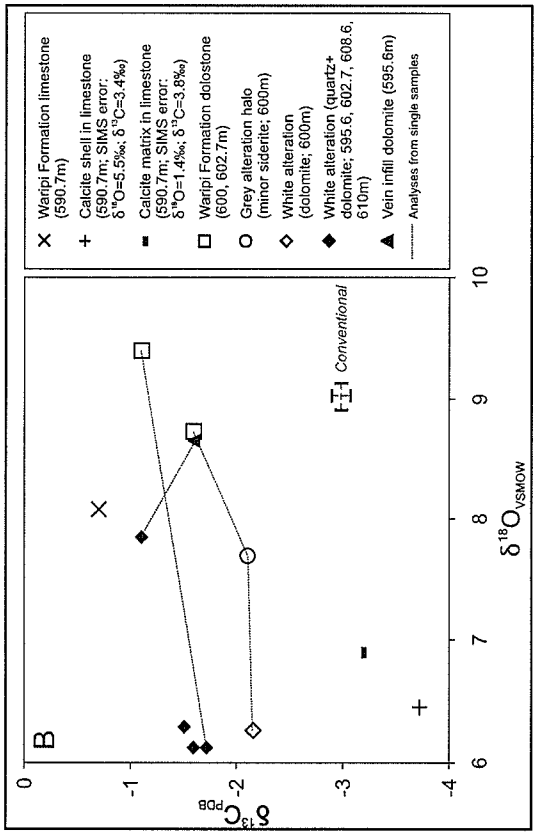
B
Conventional
Waripi Formation limestone (590.7m)
Calcite shell in limestone (590.7m; SIMS error: δ18O=5.5‰; δ13C=3.4‰)
Calcite matrix in limestone (590.7m; SIMS error: δ18O=1.4‰; δ13C=3.8‰)
Waripi Formation dolostone (600, 602.7m)
Grey alteration halo (minor siderite; 600m)
White alteration (dolomite; 600m)
White alteration (quartz+ dolomite; 595.6, 602.7, 608.6, 610m)
Vein infill dolomite (595.6m)
Analyses from single samples
δ13CPDB
δ18OVSMOW

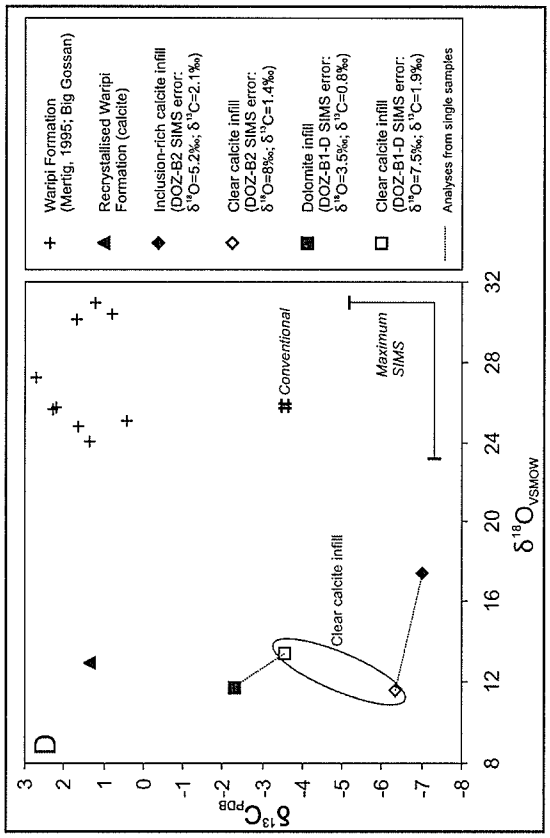
D
Conventional
Clear calcite infill
Maximum SIMS
Waripi Formation (Mertig, 1995; Big Gossan)
Recrystallised Waripi Formation (calcite)
Inclusion-rich calcite infill (DOZ-B2 SIMS error: δ18O=5.2‰; δ13C=2.1‰)
Clear calcite infill (DOZ-B2 SIMS error: δ18O=8‰; δ13C=1.4‰)
Dolomite infill (DOZ-B1-D SIMS error: δ18O=3.5‰; δ13C=0.8‰)
Clear calcite infill (DOZ-B1-D SIMS error: δ18O=7.5‰; δ13C=1.9‰)
Analyses from single samples
δ13CPDB
δ18OVSMOW

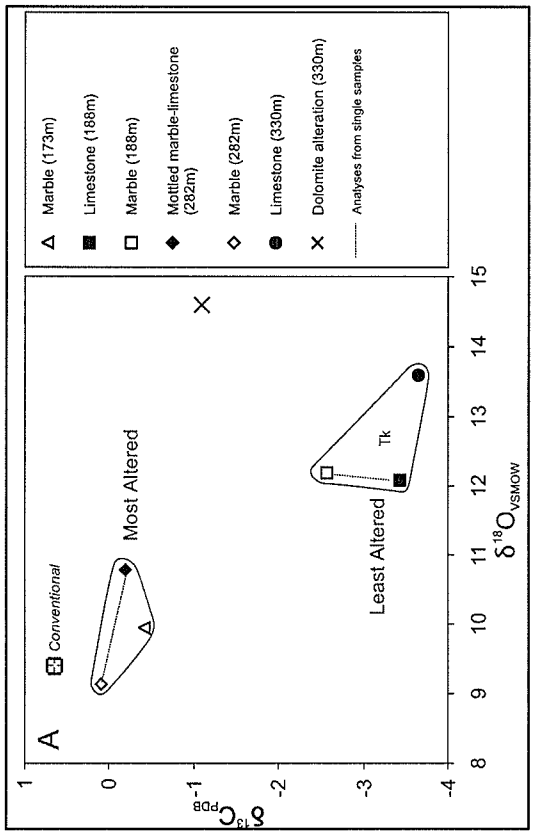
A
Conventional
Most Altered
Least Altered
Tk
Marble (173m)
Limestone (188m)
Marble (188m)
Mottled marble-limestone (282m)
Marble (282m)
Limestone (330m)
Dolomite alteration (330m)
Analyses from single samples
δ13CPDB
δ18OVSMOW

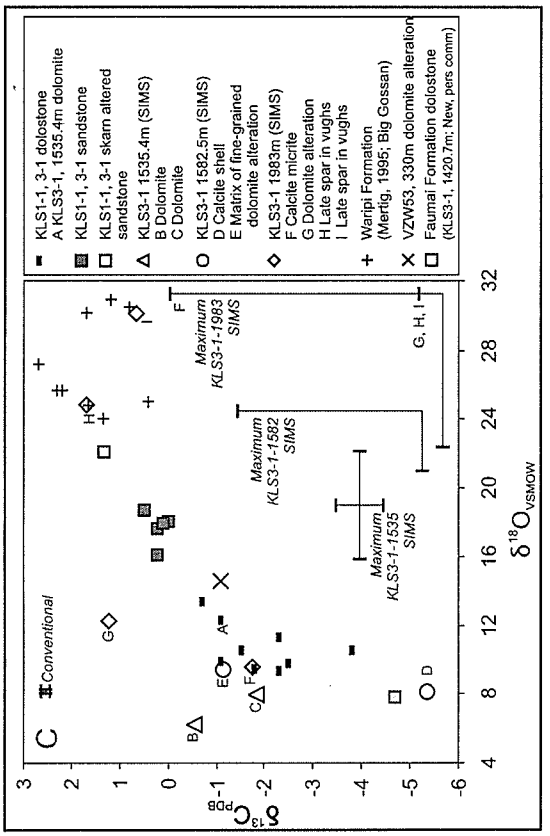
C
Conventional
Maximum KLS3-1-1983 SIMS
Maximum KLS3-1-1582 SIMS
Maximum KLS3-1-1535 SIMS
G, H, I
KLS1-1, 3-1 dolostone
A KLS3-1, 1535.4m dolomite
KLS1-1, 3-1 sandstone
KLS1-1, 3-1 skarn altered sandstone
KLS3-1 1535.4m (SIMS)
B Dolomite
C Dolomite
KLS3-1 1582.5m (SIMS)
D Calcite shell
E Matrix of fine-grained dolomite alteration
KLS3-1 1983m (SIMS)
F Calcite micrite
G Dolomite alteration
H Late spar in vughs
I Late spar in vughs
Waripi Formation (Mertig, 1995; Big Gossan)
VZW53, 330m dolomite alteration
Faumai Formation dolostone (KLS3-1, 1420.7m; New, pers comm)
δ13CPDB
δ18OVSMOW

KLS1-1 and KLS3-1

$\delta^{18}O_{SMOW}$ and $\delta^{13}C_{PDB}$ vary with elevation (Figure C-8), do not vary significantly between laterally equivalent lithological units in the two drillholes and lithology-specific variation is present (Figure C-15c). $\delta^{18}O_{SMOW}$ and $\delta^{13}C_{PDB}$ values from dolomite in sandstone in the Waripi Formation are higher than those from dolostone in the same drillholes (Figure C-15c). Samples from the Waripi Formation dolostone display a range of $\delta^{18}O_{SMOW}$ and $\delta^{13}C_{PDB}$ values different to those in dolostone analyses from the Wanagon drainage (Mertig, 1995) and Big Gossan (Figure C-15c). A Faumai Formation sample analysed by New (pers comm. 2003) is the shallowest stratigraphically and has $\delta^{18}O_{SMOW}$ and $\delta^{13}C_{PDB}$ values (Figure C-8; Figure C-15c) similar to less altered Faumai and Waripi Formation from DOM (Mertig, 1995) and Big Gossan. $\delta^{18}O_{SMOW}$ and $\delta^{13}C_{PDB}$ values of dolomite in a sandstone sample from the base of the Waripi Formation that contains skarn alteration (Figure C-8; Figure C-15c) are similar to those of Big Gossan skarn dolomite and calcite (Figure C-16).

SIMS analysis of calcitic micrite (KLS3-1, 1983m; Figure C-4f; Figure C-15c) returned $\delta^{18}O_{SMOW}$ and $\delta^{13}C_{PDB}$ values similar to KLS1-1 and KLS3-1 dolostone analyses although it has large internal precision. Dolomite alteration in the same sample (KLS3-1, 1983m; Figure C-4f; Figure C-15c) has higher $\delta^{13}C_{PDB}$ than KLS1-1 and KLS3-1 dolostone. Late dolomite spar (KLS3-1, 1983m) in porous dolostone has values similar to Waripi Formation at Wanagon drainage (Mertig, 1995) and Big Gossan (Figure C-15c).

SIMS analyses of dolomite from dolostone in KLS3-1, 1535.4m vary by ca. 1.3‰ $\delta^{13}C_{PDB}$, which is within external precision (±0.8‰), and 1.8‰ $\delta^{18}O_{SMOW}$ which is within internal precision documented in this study (Figure C-15c). The SIMS analyses differ from the conventional analysis by at least 0.6‰ $\delta^{13}C_{PDB}$ which is within error, and at least 4.2‰ $\delta^{18}O_{SMOW}$ which exceeds errors on both techniques (Figure C-15c). SIMS results from fine-grained dolomite matrix in a foraminiferal limestone-dolostone compare well with other KLS1-1 and KLS3-1 dolostone values (KLS3-1, 1582.5m; Figure C-15c). The SIMS $\delta^{18}O_{SMOW}$ value of the calcitic foraminifera shell is within error of the matrix dolomite although the $\delta^{13}C_{PDB}$ of the shell is lower than the matrix by 4.2‰ (Figure C-15c). All SIMS analyses have significantly lower values than dolostone from Wanagon drainage (Mertig, 1995) and Big Gossan (Figure C-15c) with the exception of late-stage dolomite spar (KLS3-1, 1983m).

EESS carbonate alteration

Recrystallised Waripi Formation calcite adjacent to the EESS has lower $\delta^{18}O_{SMOW}$ than least altered Waripi Formation dolostone (Figure C-15d). SIMS results from late stage dolomite and calcite alteration and infill within the EESS display a range of $\delta^{18}O_{SMOW}$ and

$\delta^{13}C_{PDB}$ values with lower $\delta^{18}O_{SMOW}$ and $\delta^{13}C_{PDB}$ than least altered Waripi Formation dolostone (Figure C-15d). $\delta^{18}O_{SMOW}$ and $\delta^{13}C_{PDB}$ values of late clear calcite infill from different samples (Figure C-11b, c) display variations of ca. <2.7‰ and are within error of each other.

Big Gossan

The least altered Big Gossan Waripi Formation dolostone samples (Figure C-16) have a similar isotopic composition to unaltered Waripi Formation samples analysed by Mertig (1995). Marble at Big Gossan has lower $\delta^{18}O_{SMOW}$ (ca. 4‰) values than the dolostone samples (Figure C-16). Different generations of hydrothermal calcite and dolomite alteration and vein infill from Big Gossan skarn and West Drift breccia display a narrow and significantly lower $\delta^{18}O_{SMOW}$ range and ca. 5‰ $\delta^{13}C_{PDB}$ range than unaltered Waripi Formation dolostone (Figure C-16). Siderite in a Stage 5 sulphide sample has a higher $\delta^{18}O_{SMOW}$ value (16.4‰; Figure C-11j; Figure C-16). SIMS analyses of the alteration margin from BGU24-11, 177m (Figure C-11i) are within SIMS error of the conventional analyses (<1.6‰ difference; Figure C-16). The SIMS $\delta^{18}O_{SMOW}$ value from late calcite infill is 5.8‰ lower than the conventional analysis (Figure C-16).

Interpretation and implications of $\delta^{18}O_{SMOW}$ and $\delta^{13}C_{PDB}$ results

Mertig (1995) reported $\delta^{18}O$ measurements from dolomite within the DOM skarn (-10.7 to -16‰) and unaltered Wanagon Waripi formation (-4.8 to 0.1‰) relative to SMOW. The values for unaltered Waripi Formation stratigraphy (Mertig, 1995) only correlate with the marine carbonate field (Veizer and Hoefs, 1976) and results from this study if they are treated as misreported PDB measurements and are converted to SMOW. The $\delta^{18}O$ measurements from DOM dolomite (Mertig, 1995) are also considered incorrectly reported and have been converted from PDB measurements to SMOW.

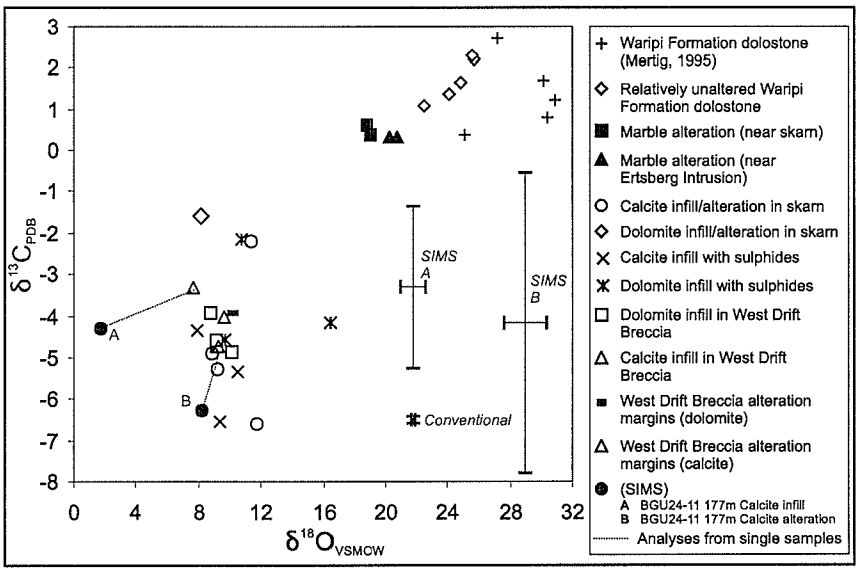

Figure C-16. $\delta^{18}O_{SMOW}$ and $\delta^{13}C_{PDB}$ isotope results from Big Gossan. Samples were analysed by conventional techniques unless specified as "SIMS". SIMS uncertainties are internal precision (Appendix 13). Conventional uncertainties are ±0.1‰ $\delta^{13}C$ and $\delta^{18}O$ (Appendix 1).

The advantage of the SIMS technique is its ability to produce in situ high-resolution isotopic analyses. Conventional analyses of the same samples are unable to demonstrate the isotopic variability in the sample and the result is a bulk analysis of mixed isotopic compositions. Subject to uncertainties, any differences between SIMS analyses in single samples demonstrate isotopic inhomogeneity. In texturally homogenous samples (i.e. KLS3-1, 1535.4m; Figure C-15c), further analyses would be required to establish the degree of isotopic inhomogeneity.

Unaltered host rocks in the Ertsberg district

Analyses from unaltered and least altered Waripi Formation dolostone from the district fit within the marine carbonate field (Veizer and Hoefs, 1976). During deposition of the New Guinea Limestone Group, three global carbon cycle aberrations (ca. 55, 34 and 23 Ma; Figure C-1), with amplitudes up to 3‰, are inferred from carbon isotope studies to have occurred (Zachos et al., 2001). The variation of local $\delta^{13}C$ values from Paleocene-Eocene Waripi and Faumai formations (Figure C-1; Figure C-17) are within the range of global $\delta^{13}C$ aberration (ca. 2.5‰) expected during this time (Zachos et al., 2001).

The least altered Faumai Formation dolostone sample from DOM (Mertig, 1995) is similar to a Faumai Formation sample from KLS3-1 (B. New pers comm., 2003) and marine carbonate values (Figure C-17). Calcitic micrite in KLS3-1, 1983m, limestone from the Kais Formation (VZW53) and limestone in the Waripi Formation (GRS125) have lower $\delta^{18}O_{SMOW}$ and $\delta^{13}C_{PDB}$ than the unaltered dolostones (Figure C-17). The isotopic variation in the carbonate stratigraphy of the New Guinea Limestone Group in the district has not been examined in detail. The $\delta^{18}O_{SMOW}$ values may represent stratigraphic variability although they are lower than typical Tertiary limestones (Veizer and Hoefs, 1976). Due to their proximity to the GIC and other hydrothermal systems, it is more likely that the limestone samples have been isotopically modified by one or more hydrothermal alteration events. The GRS125 and KLS3-1 limestone analyses have $\delta^{18}O_{SMOW}$ compositions most like the altered dolostone from KLS1-1 and KLS3-1 (Figure C-15b, c). Late stage dolomite spar infill in KLS3-1, 1983m has $\delta^{18}O_{SMOW}$ and $\delta^{13}C_{PDB}$ values that are within error as those of unaltered Waripi Formation dolostone. Late incursion of fluids equilibrated with un-altered stratigraphy may have deposited the spar.

Character of EESS carbonate alteration

In the EESS, the SIMS technique was used to differentiate between different generations of calcite and dolomite-ankerite infill (Figure C-11b, c). The $\delta^{18}O_{SMOW}$ values of the calcite and dolomite are within error of each other and cluster at lower $\delta^{18}O_{SMOW}$ than unaltered Waripi Formation (Figure C-15d). As the temperature of carbonate alteration is not known,

Figure C-17. Compilation and interpretation of $\delta^{18}O_{SMOW}$ and $\delta^{13}C_{PDB}$ carbonate isotope results from the Ertsberg district. Results from New (pers comm., 2003) and Mertig (1995) and this study. $\delta^{18}O_{SMOW}$ of primary magmatic water from Sheppard (1986). Magmatic $\delta^{13}C_{PDB}$ range ca. 0 to -10‰ (Ohmoto, 1986; Taylor, 1986). $\delta^{13}C$ variation up to ca. 2.5‰ in the New Guinea Limestone Group dolostones is not significant (Zachos et al., 2001). $\delta^{18}O_{SMOW}$ variation for H_2O-calcite and H_2O-dolomite fractionation at various temperatures from Golyshev (1981). Conventional uncertainties are ±0.1‰ $\delta^{13}C$ and $\delta^{18}O$ (Appendix 1).

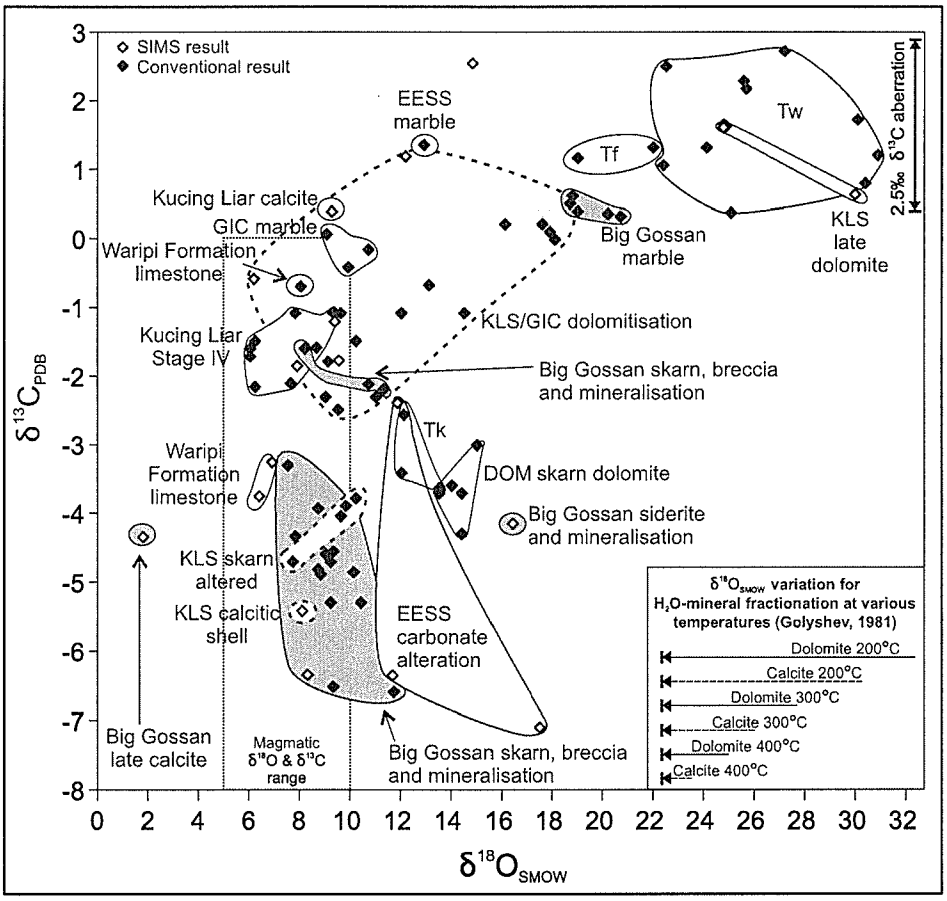

$\delta^{18}O_{FLUID}$ is unknown and it could have been higher than the magmatic water range (Figure C-17) and may have interacted with the host rocks. This is reasonable, as extensive leaching of carbonate in the skarn (Figure C-11a) and adjacent Waripi Formation dolostone could easily have contributed to the carbonate alteration.

Character of marble alteration adjacent to the GIC

Marble adjacent to the GIC displays a shift to higher $\delta^{13}C_{PDB}$ values from least altered (-3.2‰) to most altered (-0.2‰) samples (Table C-1). A shift to elevated $\delta^{13}C$ can result from hydrolysis of reduced carbon (Ohmoto and Rye, 1979). The Kais Formation is variably carbonaceous (Figure C-1) and CO_2 produced by hydrolysis reactions at temperatures between 350°C to 600°C would shift $\delta^{13}C$ to higher values than the graphite although values less than -10‰ are most likely (Ohmoto and Rye, 1979). However, a positive shift in carbonate $\delta^{13}C$ (and $\delta^{18}O$) may occur where the fluid contains both oxidised and reduced carbon species (S. Golding written comm., 2004). Marble alteration in VZW53 has $\delta^{13}C$ values of ca. 0‰, which are similar to those of the local unaltered marine carbonate

(Figure C-17). Dissolution of marine carbonate would have produced CO_2 with $\delta^{13}C$ values similar to those of the original carbonates (Ohmoto and Rye) and may have been responsible for the marble alteration present in VZW53.

Distribution and character of dolomitisation around the GIC

The $\delta^{18}O_{SMOW}$ and $\delta^{13}C_{PDB}$ results in association with textural evidence indicate that there is at least one generation of dolomite alteration related in space and time to the GIC. Dolomitisation in Kais Formation limestone (VZW53) occurs as discordant alteration. Texturally, dolomitisation in KLS1-1 and KLS3-1 is manifested as inclusion-poor planar euhedral and subhedral textures with variable porosity, which differs from the dominantly non-porous non-planar inclusion-rich dolomite observed in unaltered Waripi Formation (Figure C-4e, f, g; Figure C-11d). As the isotopic composition of the least-altered dolostone in GRS125 is similar to KLS1-1 and KLS3-1 dolostone (Figure C-17), GIC-related dolomitisation is also considered to be present at Kucing Liar. In GRS125, redolomitised Waripi Formation dolostone is overprinted by Kucing Liar Stage IV leaching and silicification implying the dolomitisation is older than ca. 3.18Ma (cf. Figure C-6).

The dolostone in GRS125, KLS3-1 and KLS1-1 is isotopically ($\delta^{18}O_{SMOW}$ and $\delta^{13}C_{PDB}$ are respectively ca. 17‰ and ca. 3‰ lower) and texturally distinct to that from the Waripi and Faumai Formations at Big Gossan, DOM and the Wanagon drainage (Figure C-1; Figure C-17). Its isotopic composition is confined to areas peripheral to the GIC and is not evident in a single sample of Waripi Formation dolostone from south of the Idenberg faults at Kucing Liar (Figure C-5; KL38-05, 814.1m) (B. New pers comm., 2003).

In KLS1-1 and KLS3-1, greater modification of isotopic ratios and development of secondary porosity is observed in dolostone as opposed to sandstone. Chemical changes in the dolostone such as dissolution of relict calcite may have favoured greater porosity development and greater isotopic modification in the dolostones. With the exception of the deepest KLS1-1 sample, $\delta^{13}C$ values in dolostone and sandstone respectively become lower downhole towards the Kembelangan limestone-Waripi Formation contact. This stratigraphic boundary is known to be a significant focus for hydrothermal flow throughout the district and is the host to many of the skarn deposits (Section D).

Results in KLS1-1 and KLS3-1 define a mixing line from original host Waripi Formation dolostone (Big Gossan and Wanagon drainage isotopic compositions) to the least altered dolostone in GRS125 (Figure C-17) interpreted to represent isotopic mixing between marine limestone and magmatic fluids. The absence of mineralogical modification for the majority of altered dolostone samples (Waripi and lower Faumai formations are also predominantly dolostone; Figure C-1) suggests the fluid/s responsible for dolomitisation

were predominantly $H_2O \pm CO_2$. Magma degassing commonly occurs in magmatic environments and large volumes of CO_2 can be released (Giggenbach, 1992; Lowenstern, 2001). The texturally and isotopically modified porous dolostones may record H_2O+CO_2 magmatic degassing.

$\delta^{18}O$ character of fluids in Kucing Liar Stage IV (leaching, quartz, clay)

For an assumed fractionation (Golyshev et al., 1981) between dolomite-water ($\Delta^{18}O$ = 3.9‰) at an estimated temperature of 350°C (derived from fluid inclusion analysis by B. New pers comm., 2003), $\delta^{18}O_{water}$ must have been 2.2-4.8‰ during Stage IV carbonate alteration (Figure C-6; $\delta^{18}O_{SMOW}$ = 6.1-8.7‰). This is within the range of 0-6‰ estimated by New (pers comm., 2003) for Stage IV $\delta^{18}O_{FLUID}$ (Figure C-18; Table C-3). As samples from GRS125 are distal to Kucing Liar (Figure C-5), Stage IV carbonate alteration may have occurred at a lower temperature than in the Kucing Liar skarn and ore body and $\delta^{18}O_{FLUID}$ values could actually have been lower (Figure C-18). Calculated Stage IV $\delta^{18}O_{FLUID}$ values for quartz and carbonate are lower than those expected for magmatic water (Sheppard, 1986) so it is likely that local meteoric water was present during Stage IV (Figure C-18).

$\delta^{18}O$ and $\delta^{13}C$ of fluids in Big Gossan and DOM skarns

Both calcite and dolomite alteration margins (typically 1-10cm on Waripi Formation dolostone) and infill in veins at Big Gossan fall within a narrow range of $\delta^{18}O_{SMOW}$ (Figure C-17). Isotopic gradients at Big Gossan can be sharp (i.e. BGU24-11, 177m; Figure C-11i; Figure C-16), approximately 1-2 centimetres, which demonstrates minimal infiltration by the fluids (cf. Nabelek, 1991).

For an assumed fractionation (Golyshev et al., 1981) between calcite-water ($\Delta^{18}O$ = 3.1-4.9‰) at the temperature of formation (283-325°C, average = 313°C; Section B fluid inclusion study: sample BGU18-3, 211m), the $\delta^{18}O_{water}$ at Big Gossan (Stage 2-3) must have been between ca. 4.5-6.9‰ (average = 5.9‰; Figure C-18; Table C-3). This is consistent with the 5-10‰ range for magmatic water (Sheppard, 1986) and comparable with the results from other Big Gossan studies (Figure C-18).

Dominantly closed system CO_2 degassing of a cooling magma can cause $\delta^{13}C$ variation of up to 6‰ (Taylor, 1986). The $\delta^{13}C$ range of ca. 5‰ in Big Gossan results is probably best explained by mixing between marine and magmatic carbon (Figure C-16). Assuming constant XCO_2 (calcite-CO_2 fractionation, $\Delta^{13}C$ = -1.8 to -2.3‰) at the temperature of formation (Ohmoto and Rye, 1979) for Big Gossan Stage 2 calcite (283-325°C, average = 313°C), the $\delta^{13}C$ value of the fluid must have been ca. -3.2‰ (Figure C-17).

Figure C-18. Calculated $\delta^{18}O_{FLUID}$ compositions for fluids at Big Gossan, Kucing Liar and DOM. Calculations are summarised in Table C-3. Three possible fluid compositions have been calculated for DOM dolomite, demonstrating that if the dolomite formed at temperatures less than 200°C, non-magmatic fluids would have been involved. Fluid inclusion measurements from Big Gossan recrystallised calcite with skarn (Table C-1) range from 283-325°C and average 313°C (Section B). Assumed fractionation between quartz-water, $\Delta^{18}O$ = 5‰ at 400°C for Big Gossan quartz (Kyle, 1994). Kucing Liar Stage IV carbonate alteration occurs distal to the Kucing Liar skarn where fluid inclusion homogenisation temperatures for Stage IV are 350°C (B. New pers comm., 2003). If Kucing Liar Stage IV carbonate alteration formed at or below 300°C, then $\delta^{18}O_{FLUID}$ values would have been lower. Magmatic water field from Sheppard (1986). Local water data from Harrison (1999).

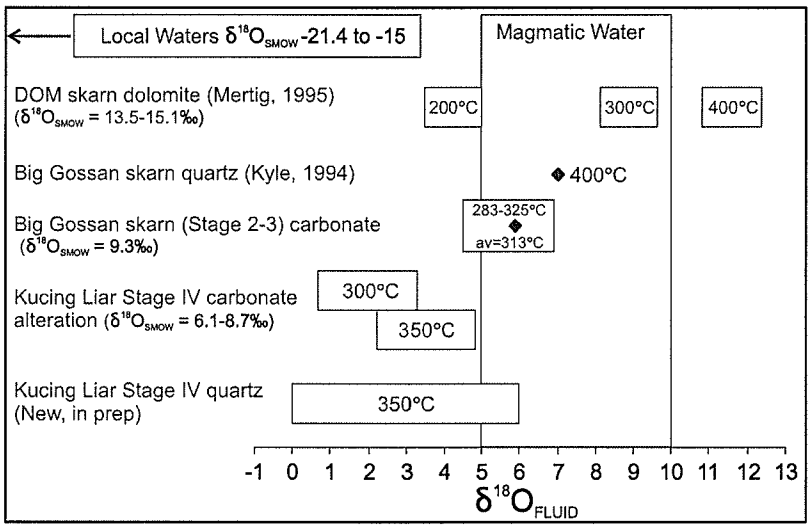

Table C-3. Calculations of $\delta^{18}O_{FLUID}$ for carbonate $\delta^{18}O$ samples in Figure C-18 using assumed fractionations of Golyshev et al., (1981).

Sample	$\delta^{18}O$	Temperature (C)	Calculated $\delta^{18}O_{FLUID}$
Kucing Liar Stage IV quartz (New, pers comm., 2003)	*minimum* 6.3	350	0
	maximum 11.3	350	6
Kucing Liar Stage IV carbonate alteration (Table C-1)	*minimum* 6.1	350	2.2
	maximum 8.7	350	4.8
	minimum 6.1	300	0.7
	maximum 8.7	300	3.3
Big Gossan skarn carbonate (Table C-1)	9.3	*average* 313	5.9
	9.3	*minimum* 283	6.9
	9.3	*maximum* 325	4.5
Big Gossan skarn quartz (Kyle, 1994)	12.3	400	7
DOM carbonate (Mertig, 1995)	*minimum* 13.5	200	3.5
	maximum 15.1	200	5.0
	minimum 13.5	300	8.1
	maximum 15.1	300	9.7
	minimum 13.5	400	10.8
	maximum 15.1	400	12.4

An analysis of siderite infill on the dolostone clast margin gave a $\delta^{18}O_{SMOW}$ value of 9.4‰ (Figure C-11j; Figure C-16; Table C-1). The siderite associated with Stage 2 sulphides, $\delta^{18}O_{SMOW}$ =16.4‰ (Figure C-11j; Figure C-16; Table C-1), may have been precipitated from a fluid that had partially equilibrated with host rocks. Alternatively, the $\delta^{18}O_{SMOW}$ =16.4‰ analysis may have been contaminated with H_2S or H_2O vapour. If not removed, H_2S (from reaction with traces of sulphide) or H_2O vapour impurity present in the CO_2 sample gas can result in more positive calculated $\delta^{13}C$ and, to a lesser extent, more positive $\delta^{18}O$ results (K. Harris, pers comm. 2003).

A single SIMS analysis of calcite vein infill at Big Gossan (BGU27-11, 177m; Figure C-11i) returned the lowest $\delta^{18}O$ value in the dataset which is also lower than the conventional result (Figure C-16; Figure C-17). The low $\delta^{18}O$ value may be indicative of late-stage incursion of meteoric water. The significance of this result cannot be confirmed without further analyses as similar low $\delta^{18}O$ values were not observed in any other Big Gossan samples.

The ferroan dolomite adjacent to the DOM skarn has a close association with the skarn minerals brucite, wollastonite and magnetite and was interpreted to be a product of hydrothermal alteration of Faumai Formation dolostone (Mertig, 1995). DOM hydrothermal dolomite contains liquid, vapour and halite-bearing fluid inclusions similar to those observed in early quartz and monticellite hosted inclusions from the adjacent skarn that homogenise at 291-629°C (Mertig, 1995). For an assumed fractionation (Golyshev et al., 1981) between dolomite-water ($\Delta^{18}O$ = 10.1‰ and 2.7‰ respectively) at possible temperatures of formation (200-400°C), the $\delta^{18}O_{water}$ in the DOM dolomite alteration ($\delta^{18}O_{SMOW}$ =13.5-15.1‰) may have been between ca. 3.5-12.4‰ (Figure C-18; Table C-3). If the dolomite formed at ca. 300°C the calculated $\delta^{18}O_{FLUID}$ is consistent with a magmatic source. Alternatively, if the dolomite was formed at higher temperatures (e.g. 400°C), then the calculated $\delta^{18}O_{FLUID}$ values suggest the Faumai Formation dolostone host influenced the hydrothermal dolomite $\delta^{18}O$ composition.

$\delta^{18}O_{SMOW}$ and $\delta^{13}C_{PDB}$ results from Big Gossan and possibly also from DOM correlate well with the magmatic field for O and C. A magmatic component has not always been recognised in $\delta^{18}O$ and $\delta^{13}C$ analyses falling within this field or displaying mixing between magmatic and sedimentary carbonate end members (Osaki, 1973; Shelton, 1983; Shikazono, 1989; Zeng, 1990). Magmatic $\delta^{18}O_{SMOW}$ and $\delta^{13}C_{PDB}$ values from this study compare well with studies of carbonate and skarns in contact metamorphic aureoles which are attributed alteration by magmatic O- and C- bearing fluids (cf. Valley, 1986; Nabelek, 1991) and other ore deposits where a magmatic source for carbon is postulated

(Richards and Kerrich, 1993; Torsten et al., 1993; Mulshaw et al., 1997; Callaghan, 2001; Maglambayan et al., 2001).

The presence of magmatic CO_2 in hydrothermal fluids has important genetic implications. CO_2 is considered to promote early phase separation within the magmatic volatile phase and in hydrothermal systems which can lead to selective partitioning of different ore-body components between brine and vapour (cf. Heinrich et al., 1999; Ulrich et al., 1999; Lowenstern, 2000, 2001; Ulrich et al., 2002). Magmatic CO_2 is common in fluid inclusions from intrusion-related gold systems (Jensen and Barton, 2000; Baker, 2002). CO_2 has been documented from ore-related fluid inclusions at Grasberg (Fu et al., 2003; Williams et al., 2003), Porgera and Mt Kare (Richards and Laudrum, 1998; Ronacher and Richards, 1999) and is also considered to contribute to the genesis of epithermal deposit styles (i.e. epithermal carbonate-base-metal styles: Richards and Kerrich, 1993; Corbett and Leach, 1998). The full extent of magmatic CO_2 contribution to porphyry-related hydrothermal systems is yet to be quantified.

Conclusions

Although SIMS internal precision from this study was higher and more variable than that documented in previous published studies, $\delta^{18}O$ and $\delta^{13}C$ results generally display clustering that compares well with conventional results. From this $\delta^{18}O$ and $\delta^{13}C$ investigation, it is concluded that hydrothermal carbonates in the Ertsberg district formed from magmatic fluids. Influence from local waters has only been recognised in analyses of carbonate affected by the high sulphidation related leaching event at Kucing Liar. Extensive carbonate infill and alteration in the EESS may have been derived by a fluid that leached carbonate from within the skarn and adjacent carbonate stratigraphy.

Isotopic mixing between magmatic fluids and the unaltered marine carbonate host rocks is evident in the dolomitisation halo surrounding the GIC and the marble from Big Gossan. The texturally and isotopically distinct dolomitisation halo may record H_2O+CO_2 magmatic degassing.

Depleted $\delta^{13}C$ values with respect to marine limestone values at Big Gossan and DOM are interpreted to represent the presence of magmatic carbon in the skarn and mineralising fluids. The presence of CO_2 as a volatile component in intrusion-related deposits has significant genetic consequences as it is considered to promote early phase separation, which can lead to selective partitioning of different ore-body components between brine and vapour.

Acknowledgements

PT Freeport Indonesia is acknowledged for logistical and analytical funding and permission to publish this work. An Australian Nuclear Science and Engineering Award (AINSE) enabled access to the SIMS facility at the Australian Nuclear Science and Technology Organisation (ANSTO) for the in situ C-O isotope investigation. Kathryn Prince and the SIMS team at ANSTO are thanked for technical advice and SIMS operation. Feedback from Freeport staff, particularly Clyde Leys and Paul Warren, is appreciated. Thank you also to Brian New, researchers from University of Arizona and University of Texas (Mark Cloos and Richard Kyle), Peter Pollard and Roger Taylor for providing access to unpublished information. James Lally generously drafted the majority of the diagrams.

Section D
New insights into the evolution of igneous and hydrothermal events in the Ertsberg District, Papua, Indonesia

Abstract

The Pliocene Ertsberg district in Papua, Indonesia is exceptional among porphyry districts. It has a huge high-grade Cu and Au metal inventory and is developed in a carbonate-rich sedimentary terrain. Mineralisation is considered to have occurred between <2km to potentially >4km below paleosurface. Mineralisation styles include porphyry Cu-Au, skarn Cu-Au, deep-intermediate high sulphidation Cu-Au and pyrite-Au-As-Zn-Bi-Te occurrences. Magmatic fluids were not directly sourced from the adjacent igneous bodies but rather derived by periodic tapping of deeper sources. No classic epithermal low or high sulphidation deposits are noted in the district although the fluids responsible for the pyrite-Au-As-Zn-Bi-Te occurrences documented in this investigation may represent a deeper, more saline magmatic precursor to fluids that occur in epithermal deposit styles.

The onset of westwards-movement of the Pacific Plate with respect to the Australian Plate at ca. 5 Ma was coincident with commencement of igneous, hydrothermal and volcanic activity in the district. Subducted Australian Archaean and Proterozoic continental crust beneath the Island of New Guinea contributed material to the Ertsberg District igneous bodies. The potential for two-stage melting processes to contribute to a large metal inventory is suggested in other southwest Pacific rim mineral-districts with similar tectonic settings. Magma chamber replenishment by influx of mafic magma may also have been important for introducing ore-body components and triggering emplacement of intrusions.

The geological and geochronological framework suggests that the economically-significant igneous and hydrothermal events in the district occurred as two distinct evolving episodes separated by less than 500,000 years. The igneous complexes (GIC ca <3.33-3Ma and Ertsberg ca 3-2.67Ma) are respectively post-dated by early porphyry-style mineralisation and spatially related skarn Cu-Au mineralisation. Deep-intermediate high sulphidation style mineralisation occurred as a late development at both locations.

New and published sulphur isotope data display a narrow range for all deposits, which is interpreted as magmatic, apart from a limited number of samples from one of the deep-intermediate high sulphidation occurrences. Radiogenic isotope results from previous investigations have lead to conflicting models for the source of metals in the district. Interpretation of Pb, Sr, Nd isotope results advocate the intrusions and ore deposits in the district display no evidence of significant interaction with the underlying exposed 12km of Precambrian-Miocene sedimentary stratigraphy. However the underlying sedimentary succession is considered to be a source for some of the metals in the district by either

leaching or assimilation from interpretation of Re-Os isotope results.

Banded clay sediments interpreted to be maar sediments incorporated into the margin of the Grasberg Igneous Complex (GIC) during a diatreme volcanic event prior to cessation of hydrothermal activity at Grasberg were documented in this study. Native gold±pyrite occurrences are spatially associated with smectite-chlorite clay, diaspore and Au-As-Bi-Te bearing pyrite. Gold mineralisation is correlated with unconstrained Au-As-Bi associations documented at the Kucing Liar high sulphidation Cu-Au deposit which occurs at depth nearby.

This investigation described separate but near identical pyrite-Au-As-Zn-Bi-Te occurrences at Big Gossan ($^{40}Ar/^{39}Ar$ < 2.82±0.04Ma) and Wanagon Gold ($^{40}Ar/^{39}Ar$ = 3.62±0.05Ma) that also attest to the phenomena of common magmatic-hydrothermal processes operating in the district at different times. A K-Ar date (3.81±0.06Ma) from the Wanagon Sill constrains formation of the overprinting skarn Cu-Au and late-stage Wanagon Gold occurrence to a period of ca. 0.2Ma.

Laser ablation analyses of pyrites from different ore systems demonstrate distinct chemical differences. Pyrites from copper-bearing hydrothermal events contain a maximum of 0.64ppm Au and 2500ppm As. Pyrite associated with Au-As-Bi-Te depositing hydrothermal fluids contains up to 57ppm Au and 20000ppm As. The pyrite chemistry reflects the chemistry of hydrothermal fluids from which it was precipitated.

A reconnaissance $\delta^{18}O$ and $\delta^{13}C$ investigation comprised 78 carbonate analyses and the results concur with previous work by suggesting non-magmatic fluids were not significant contributors to hydrothermal fluids in ore deposits in the district. $\delta^{13}C_{PDB}$ carbonate isotope results from this study display good correlation with the magmatic carbon field. The presence of magmatic CO_2 as a volatile component in intrusion-related deposits has significant genetic consequences as it is considered to promote early phase separation, which can lead to enrichment of ore body components in hydrothermal fluids and vapour through selective partitioning.

Introduction

The Ertsberg district is located in the mountainous central ranges of Papua, the easternmost province of Indonesia (Figure D-1). Multiple skarn and porphyry copper-gold deposits in the district have mineable reserves totalling 2.6 billion tonnes at 1.12% Cu and 1.02g/t Au (Table 1: Freeport McMoRan Copper & Gold Inc 2002 Annual Report).

Previous work in the Ertsberg District has sought to constrain the stratigraphy, tectonics

Table D-1. Ore reserves in the Ertsberg district as at 31st December, 2002 (Freeport McMoRan Copper & Gold Inc 2002 Annual Report).

By Deposit at Decmeber 31, 2002:	Tonnage (tonnes x 10^6)	Copper (%)	Gold (g/t)	Silver (g/t)
Developed and Producing				
Grasberg open pit	863	1.02	1.2	2.47
Deep Ore Zone	184	0.96	0.65	5.11
Intermediate Ore Reserves	2	1.14	0.15	9.45
Undeveloped				
Grasberg block cave	783	1.15	0.91	2.9
Kucing Liar	478	1.29	1.14	5.8
Ertsberg Stockwork Zone	121	0.54	0.9	1.64
Mill level zone	50	1.4	1.04	4.88
Big Gossan	**33**	**2.81**	**1**	**16.85**
DOM block cave	44	1.1	0.31	5.94
DOM open pit	27	1.8	0.43	9.6
Total Reserves	**2585**	**1.12**	**1.02**	**3.73**

and igneous events (McMahon, 1994a, b, c; Quarles Van Ufford, 1996; Weiland and Cloos, 1996; Sapiie, 1998; Sapiie et al., 1999; Housh and McMahon, 2000; McMahon, 2000a, b; Sapiie and Cloos, submitted; Quarles Van Ufford and Cloos, submitted; Sapiie and Cloos, in press) and describe the major mineralised deposits in the district (Katchan, 1982; McDonald and Arnold, 1994; Mertig et al., 1994; Mertig, 1995; Rubin, 1996; Malensek, 1997; Meinert et al., 1997; Rubin and Kyle, 1997; Coutts et al., 1999; Harrison, 1999; New, 1999; Friehauf et al., 2000; Friehauf, 2000; Gibbins, 2000, 2000b; Lambert, 2000; Clarke, 2002; Pollard and Taylor, 2002; Clarke, 2003; Pollard and Taylor, 2003). Other investigations have addressed the source of metals and fluids in the district (Kyle, 1993; James and Housh, 1995; Lambert, 2000; Mathur et al., 2000; Meinert et al., 2003; Mathur et al., submitted; Mathur, 2000) and mechanisms of transport for hydrothermal components in the Grasberg porphyry system (Heinrich et al., 1999; Ulrich et al., 1999; Williams et al., 2003; Fu et al., 2003a; Fu et al., 2003b). K-Ar (McDowell et al., 1996) and $^{40}Ar/^{39}Ar$ (Pollard et al., submitted) geochronology for igneous and hydrothermal activity in the district spans ca. 2 Ma.

Recent results from the Ertsberg district include description of late stage volcanic and hydrothermal processes at Grasberg (Section A), identification of distinct Au-rich

Figure D-1. New Guinea, major tectonic elements and location of the Ertsberg district and PT Freeport Indonesia deposits and prospects (1-9). Modified from PT Freeport Indonesia maps and Sapiie (1998). Wabu is described by Sunyoto (1999). Location, commodity and approximate age of deposits in New Guinea including Wafi (Tai-Loi and Andrew, 1990), Ok Tedi (Rush and Seegers, 1990), Morobe Goldfields (Sillitoe et al., 1984), Porgera (Richards and Kerrich, 1993), Yandera (Grant and Nielsen, 1975), Mt Kare (Richards and Laudrum, 1998) and Frieda River (Morrison et al., 1999). The Australian continental margin underlying New Guinea west of the Tasman Line is interpreted to consist of Precambrian basement (Plumb, 1979; Simons et al., 1999). Interpreted 4-2Ma convergence of the Pacific-Caroline Plate from Sapiie and Cloos (in press).

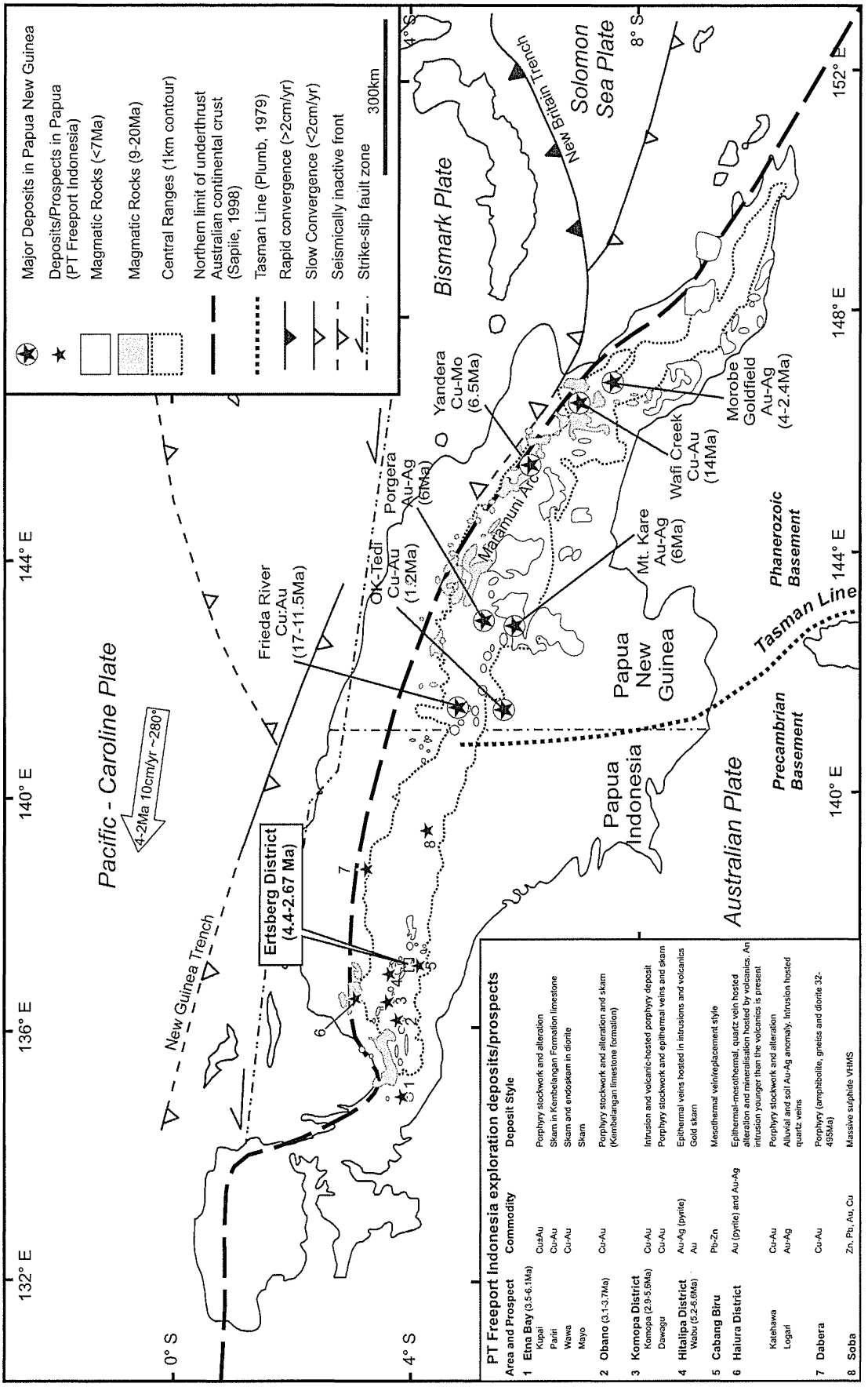
Major Deposits in Papua New Guinea
Deposits/Prospects in Papua (PT Freeport Indonesia)
Magmatic Rocks (<7Ma)
Magmatic Rocks (9-20Ma)
Central Ranges (1km contour)
Northern limit of underthrust Australian continental crust (Sapiie, 1998)
Tasman Line (Plumb, 1979)
Rapid convergence (>2cm/yr)
Slow Convergence (<2cm/yr)
Seismically inactive front
Strike-slip fault zone
300km
Pacific - Caroline Plate
4-2Ma 10cm/yr ~280°
New Guinea Trench
New Britain Trench
Bismark Plate
Solomon Sea Plate
Australian Plate
Papua New Guinea
Papua Indonesia
Tasman Line
Phanerozoic Basement
Precambrian Basement
Ertsberg District (4.4-2.67 Ma)
Frieda River Cu:Au (17-11.5Ma)
OK-Tedi Cu-Au (1.2Ma)
Porgera Au-Ag (6Ma)
Yandera Cu-Mo (6.5Ma)
Mt. Kare Au-Ag (6Ma)
Wafi Creek Cu-Au (14Ma)
Morobe Goldfield Au-Ag (4-2.4Ma)
Maramuni Arc
132° E
136° E
140° E
144° E
148° E
152° E
0° S
4° S
8° S
PT Freeport Indonesia exploration deposits/prospects
Area and Prospect | Commodity | Deposit Style
1 Etna Bay (3.5-6.1Ma) | | |
Kupai | Cu±Au | Porphyry stockwork and alteration
Pariri | Cu-Au | Skarn in Kembelangan Formation limestone
Wawa | Cu-Au | Skarn and endoskarn in diorite
Mayo | | Skarn
2 Obano (3.1-3.7Ma) | Cu-Au | Porphyry stockwork and alteration and skarn (Kembelangan limestone formation)
3 Komopa District | | |
Komopa (2.9-5.6Ma) | Cu-Au | Intrusion and volcanic-hosted porphyry deposit
Dawagu | Cu-Au | Porphyry stockwork and epithermal veins and skarn
4 Hitalipa District | | |
Wabu (5.2-6.6Ma) | Au-Ag (pyrite) | Epithermal veins hosted in intrusions and volcanics
| Au | Gold skarn
5 Cabang Biru | Pb-Zn | Mesothermal vein/replacement style
6 Halura District | Au (pyrite) and Au-Ag | Epithermal-mesothermal, quartz vein hosted alteration and mineralisation hosted by volcanics. An intrusion younger than the volcanics is present
Katehawa | Cu-Au | Porphyry stockwork and alteration
Logani | Au-Ag | Alluvial and soil Au-Ag anomaly. Intrusion hosted quartz veins
7 Dabera | Cu-Au | Porphyry (amphibolite, gneiss and diorite 32-495Ma)
8 Soba | Zn, Pb, Au, Cu | Massive sulphide VHMS

hydrothermal events occurring at 3.62±0.05Ma and <2.82±0.04Ma (Section B) and characterisation of $\delta^{18}O$ and $\delta^{13}C$ signatures of carbonate alteration in the district (Section C). Placing the recent results into context with previous work further constrains the evolution of igneous and hydrothermal events in the district. The geochemical character of igneous and hydrothermal features provides information about the sources of fluids and ore deposit components in the district. Considering the timing and character of igneous and hydrothermal features in combination with New Guinea tectonics will facilitate understanding of what factors were important for the significant metal inventory in the Ertsberg district.

New Guinea geological setting and metallogeny

The magmatic arcs of southeast Asia, including New Guinea (Figure D-1), contain some of the world's major gold deposits (Corbett and Leach, 1998; Sillitoe, 2000; Barley et al., 2002). Most gold deposits formed during intervals of tectonic plate reorganisation (25, 17 and 5Ma: Barley et al., 2002). The majority and largest deposits, including the Ertsberg District (Figure D-1), formed since 5Ma which was coincident with a change in relative plate motion between the Australian and Pacific Plates (Barley et al., 2002).

Differing models for Cainozoic tectonic development of the northern Australian-New Guinea margin and causes for emplacement of Cu-Au bearing magmas in the Ertsberg District, Papua (Table D-2; Figure D-1) have recently been discussed by Housh and McMahon (2000), Hall (2002), Hill et al., (2002) and Quarles van Ufford and Cloos (submitted). Hill et al., (2002) propose that magma emplacement occurred during compressional orogenesis in response to westwards subduction of the Soloman Sea Plate beneath eastern New Guinea. Local dilation and magma emplacement occurred in areas where uplift of the Central Ranges impinged on pre-existing NE lineaments (crustal fracture zones) and deep extensional faults which were being inverted (Hill et al., 2002).

Alternatively, others advocate that subduction of the Australian Plate beneath the Pacific Plate since Miocene times was responsible for creation of the Central Ranges fold belt (Quarles Van Ufford, 1996; Housh and McMahon, 2000; Quarles Van Ufford and Cloos, submitted). Quarles van Ufford and Cloos (submitted) consider that magma emplacement in the Ertsberg District occurred when strike-slip faulting was initiated at ca. 4Ma after active subduction of the Australian Plate beneath the Pacific Plate stalled (Figure D-1; Figure D-2; Table D-2). Arc polarity reversal leading to south-dipping subduction in the New Guinea Trench (Figure D-1) has been proposed as a cause for Pliocene Cu-Au related magmatism in New Guinea (cf. Barley et al., 2002). This mechanism is not favoured in recent analyses of tectonic timing (see discussion in Housh and McMahon, 2000) and tomographic images (Hall and Spakman, 2002).

Table D-2. Recent models for the Cainozoic tectonic evolution of New Guinea and emplacement of Cu-Au bearing magmas in the Ertsberg District, Papua.

Time (Ma)		Emplacement of Cu-Au bearing magmas considered to be related to stalling, lithospheric delamination and decompression melting of Australian Plate in a north dipping subduction (Figure 2: Quarles Van Ufford, 1996; Housh and McMahon, 2000)	Emplacement of Cu-Au bearing magmas considered to be related to orogenesis (uplift) which produced local dilation where intersections between pre-existing extensional faults and north-northeast trending fracture zones exist (Hill et al., 2002)	Emplacement of Cu-Au bearing magmas considered to be related to onset of dilation structures caused by strike-slip faulting (Sapiie and Cloos, accepted; Cloos and Sapiie, submitted; Quarles Van Ufford and Cloos, submitted; Sapiie and Cloos, submitted)
Present day	0		Convergence reduced and transpressional movement (westwards movement of pacific-Caroline Plate with respect to New Guinea) becomes dominant.	
	1			
Pliocene	2			Strike-slip faulting (westwards movement of Pacific-Caroline Plate with respect to New Guinea) coincident with onset of magmatism in the Ertsberg District
	3	Delamination, decompression melting of lithospheric mantle and upwelling of asthenospheric mantle coincident with <7Ma igneous activity	Ertsberg District magmatism (as orogenic belt development migrates southwards)	
	4			
Late	5		Rapid convergence between New Guinea and Caroline Plate cuased compression throughout new Guinea and building of an orogenic belt. Westward subduction of Solomon Sea plate wanes (Soloman Sea plate not considered to extend beneath New Guinea to Papua (see discussion in Hill et al, 2002)	Subduction of Australian Plate beneath New Guinea. Central Ranges (Figure 1) characterised by en echelon, kilometre-scale NW-trending folds with chevron and open symmetrical geometries (Sapiie et al., 1999)
Miocene	6			
	7	Subduction zone stalls due to buoyancy contrast in the Australian plate		
	8		Westwards movement of Caroline plate and westerly subduction of Solomon Sea plate beneath New Guinea (development of volcanic Maramuni Arc in eastern New Guinea, not extending into Papua).	
	9	North-dipping subduction of Australian Plate beneath New Guinea.		
Middle	10			
Miocene	12		Westwards Pacific plate convergence towards New Guinea plate and westerly subduction of Solomon Sea plate beneath New Guinea. Extension along northern New Guinea margin forms metamorphic core complexes	
Early Miocene	20			
	24		Collision (subduction) and then accretion between Australian Plate and New Guinea.	
Oligocene				

The Australian continental margin underlying New Guinea west of the Tasman Line (Figure D-1) is interpreted to consist of Precambrian basement (Plumb, 1979; Simons et al., 1999) similar to that underlying late Precambrian and Phanerozoic sedimentary rocks in northern Australia (Housh and McMahon, 2000). Two significant episodes of igneous activity (20-9Ma and <7Ma) are recognised in New Guinea (Figure D-1, Figure D-2). The isotopic characteristics of the <7Ma igneous rocks in Papua are unique in the Neogene

Figure D-2. Stratigraphy and timing of tectonic and magmatic activity in Papua (modified from Quarles Van Ufford, 1996). U-Pb zircon dates from Ertsberg district Dalam andesite (Housh and McMahon, 2000). Evolution of tectonic events modified from Quarles Van Ufford (1996), Housh and McMahon (2000) Quarles Van Ufford and Cloos (submitted). 9-20Ma North-dipping subduction zone of Australian crust beneath Pacific Crust and igneous activity. 7-8Ma Subduction zone stalls due to buoyancy contrast. 3-6Ma Delamination, decompression melting of lithospheric mantle and upwelling of asthenospheric mantle coincident with <7Ma igneous activity. At ca. 4Ma Pacific Plate (Figure D-1) began to move westwards with respect to Australian Plate (Sapiie et al., 1999). This was coincident with initiation of igneous and hydrothermal activity in the Ertsberg District. At 1Ma, possible south-dipping subduction of Pacific Plate.

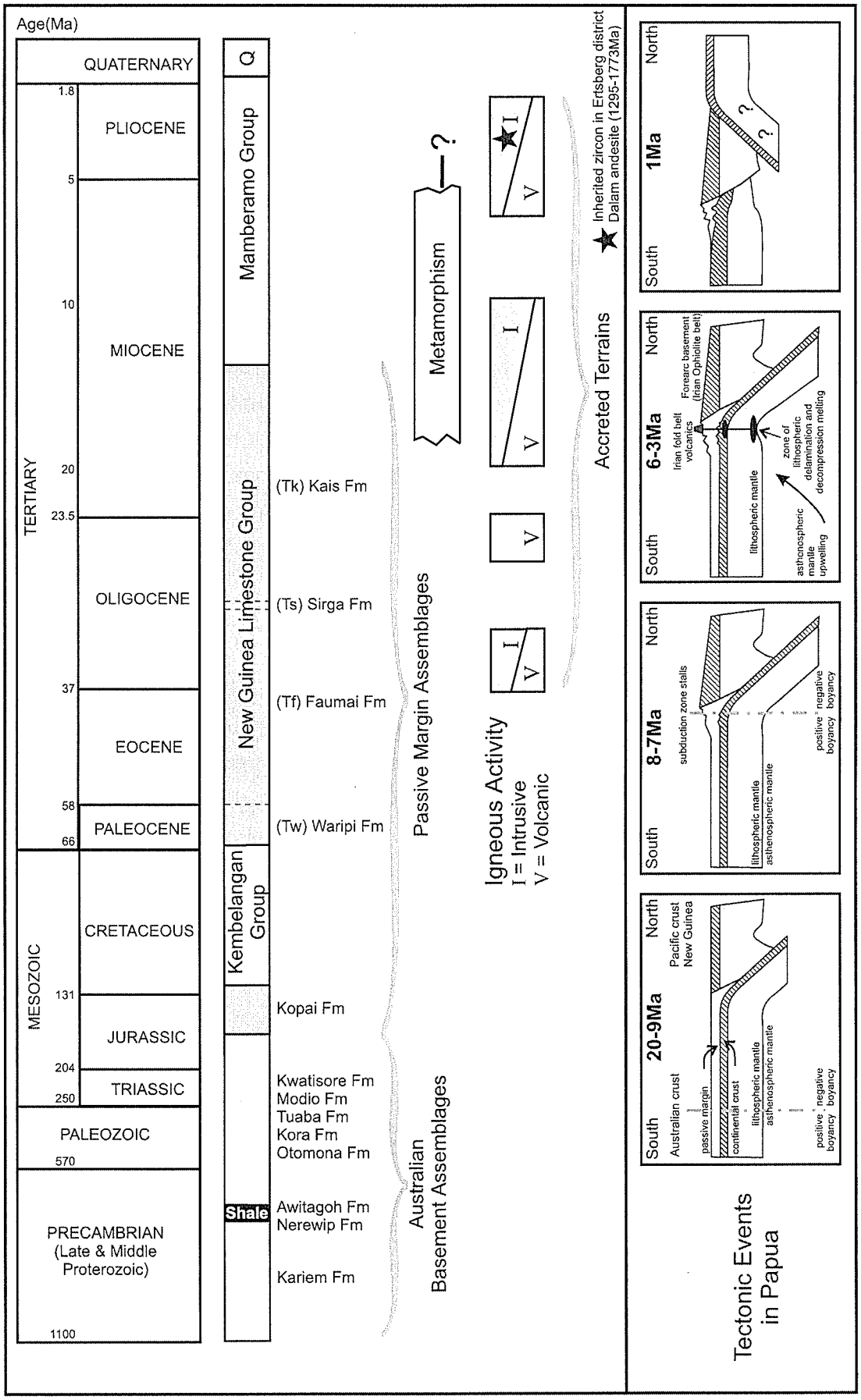
Age(Ma)
QUATERNARY
1.8
PLIOCENE
5
10
MIOCENE
20
23.5
OLIGOCENE
37
EOCENE
58
PALEOCENE
66
TERTIARY
CRETACEOUS
131
JURASSIC
204
TRIASSIC
250
MESOZOIC
PALEOZOIC
570
PRECAMBRIAN
(Late & Middle
Proterozoic)
1100
Q
Mamberamo Group
New Guinea Limestone Group
Kembelangan Group
Shale
(Tk) Kais Fm
(Ts) Sirga Fm
(Tf) Faumai Fm
(Tw) Waripi Fm
Kopai Fm
Kwatisore Fm
Modio Fm
Tuaba Fm
Kora Fm
Otomona Fm
Awitagoh Fm
Nerewip Fm
Kariem Fm
Australian
Basement Assemblages
Passive Margin Assemblages
Metamorphism
?
Igneous Activity
I = Intrusive
V = Volcanic
Accreted Terrains
Inherited zircon in Ertsberg district
Dalam andesite (1295-1773Ma)
South
North
20-9Ma
Australian crust
Pacific crust
New Guinea
passive margin
continental crust
lithospheric mantle
asthenospheric mantle
positive buoyancy
negative buoyancy
8-7Ma
subduction zone stalls
6-3Ma
Irian fold belt volcanics
Forearc basement (Irian Ophiolite belt)
zone of lithospheric delamination and decompression melting
asthenospheric mantle upwelling
1Ma
Tectonic Events
in Papua

magmatic province of New Guinea (Housh and McMahon, 2000). Models of radiogenic isotope signatures constrain the source to have consisted of 2-3% ancient enriched mantle and 98% depleted mantle with assimilation of either 10-17% Archaean or 35-75% Proterozoic Australian crust (Housh and McMahon, 2000). The presence of an ancient lithospheric mantle component in the <7Ma magmatic rocks is explained by the mechanism of collisional delamination (Figure D-2)(McMahon, 2000a). Incorporation of Precambrian material is suggested in the Ertsberg district Dalam andesite by the presence of inherited zircons with $^{207}Pb/^{206}Pb$ ages of 1295-1773Ma (Housh and McMahon, 2000).

Ertsberg district geological setting

The Ertsberg District lies within the Central Ranges (Figure D-1) which is composed predominantly of folded and faulted Mesozoic and Cenozoic passive margin strata (Sapiie et al., 1999). The oldest rocks in the Ertsberg district (Figure D-3) are the clastic and carbonate sedimentary rocks of the Cretaceous Kembelangan Group and the Tertiary New Guinea Limestone Group (Dow et al., 1988; Quarles Van Ufford, 1996). 20-9 Ma igneous activity recognised elsewhere in Papua is not present in the Ertsberg District. Igneous activity in the Ertsberg district occurred between 4.4–2.67 Ma at depths of 2 km or less (McDowell et al., 1996; Weiland and Cloos, 1996; Pollard et al., submitted).

Two economically significant igneous centres, the Grasberg Igneous Complex (GIC) and the Ertsberg Intrusion, along with numerous other smaller stocks, dykes and sills occur in the New Guinea Limestone Group (McDowell et al., 1996). $^{206}Pb/^{204}Pb$ and $^{87}Sr/^{86}Sr$ data indicate that there was insignificant contribution to the igneous suite by assimilation or hydrothermal circulation from the 12 km of Precambrian-Miocene sedimentary section (James, 2000a). Sr and Nd isotope results indicate there was at least 10% and as much as 75% input from the lower crust, which is the Precambrian crystalline basement interpreted to underlie the exposed sedimentary section (James, 2000a). Studies suggest intrusions in the district are derived from potassium-rich parental magmas (McMahon, 1994c, 2000a, b). The oldest dated intrusion in the district is the 4.4Ma Kay intrusion which occurs near the Big Gossan skarn (Figure D-3; Figure D-4). Other intrusions spatially associated with deposits or prospects include the Wanagon Sill, dated by K-Ar at 3.81±0.06 Ma (McDowell et al., 1996) and the undated Lembah Tembaga intrusion which is host to

Figure D-3. Ertsberg District regional geology and location of major deposits and prospects (modified from PT Freeport Indonesia maps). Sources of geochronological data: [1] $^{40}Ar/^{39}Ar$ ages this investigation (Section B); [2] $^{40}Ar/^{39}Ar$ ages and location of Ertsberg Intrusion sample from Pollard et al. (submitted); [3] $^{40}Ar/^{39}Ar$ ages from B. New (pers comm., 2003) [4] Re-Os isocron age from Mathur et al. (2000); [5] biotite K-Ar dates and sample locations from McDowell et al. (1996). Ertsberg East Skarn System (EESS) encompasses Gunung Bijih Timur, Intermediate Ore Zone and Deep Ore Zone. The Karume Intrusion extends further East under cover. The Ertsberg Intrusion extends further NW under cover.

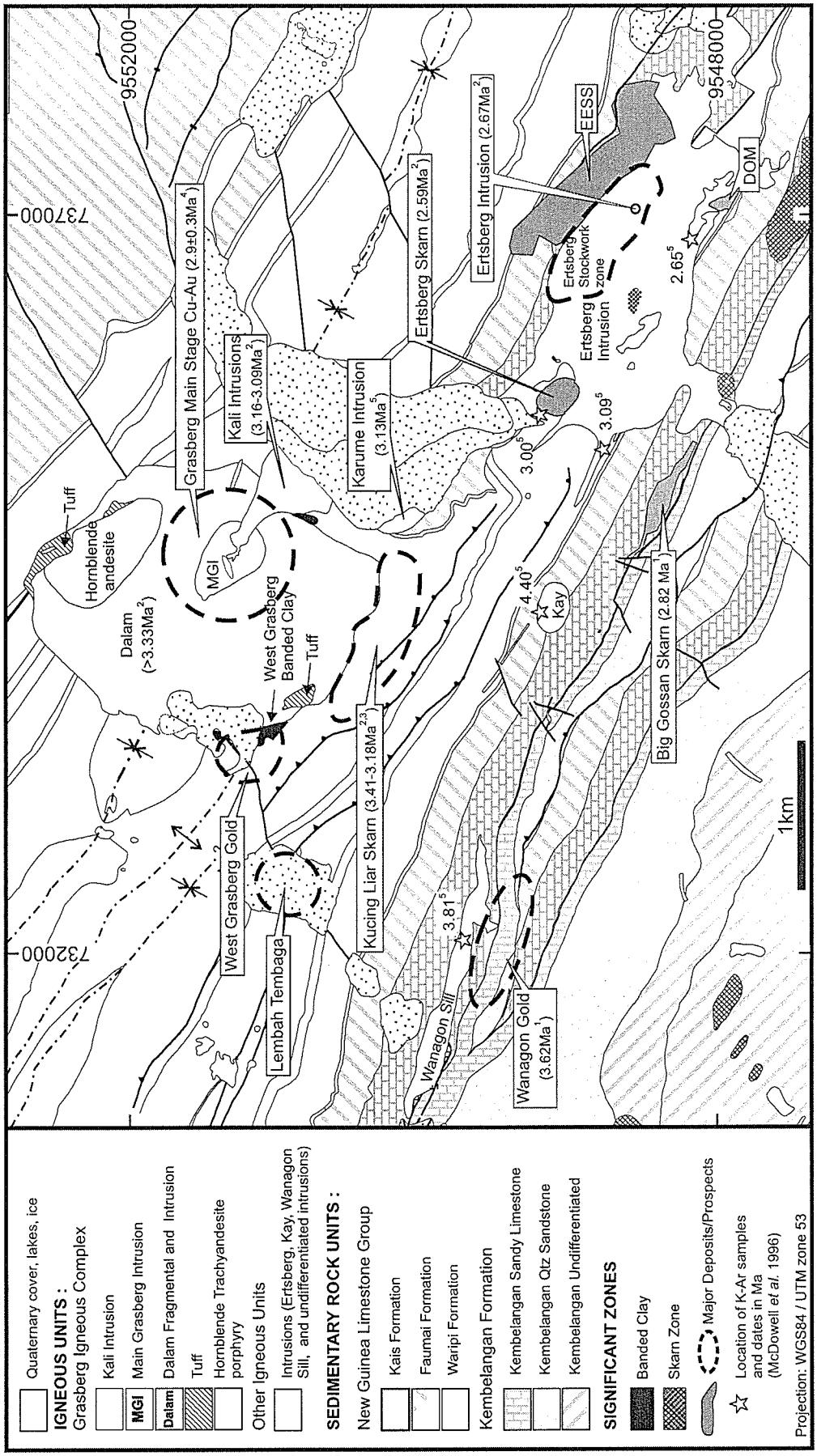
Quaternary cover, lakes, ice
IGNEOUS UNITS :
Grasberg Igneous Complex
Kali Intrusion
MGI Main Grasberg Intrusion
Dalam Dalam Fragmental and Intrusion
Tuff
Hornblende Trachyandesite porphyry
Other Igneous Units
Intrusions (Ertsberg, Kay, Wanagon Sill, and undifferentiated intrusions)
SEDIMENTARY ROCK UNITS :
New Guinea Limestone Group
Kais Formation
Faumai Formation
Waripi Formation
Kembelangan Formation
Kembelangan Sandy Limestone
Kembelangan Qtz Sandstone
Kembelangan Undifferentiated
SIGNIFICANT ZONES
Banded Clay
Skarn Zone
Major Deposits/Prospects
Location of K-Ar samples and dates in Ma (McDowell et al. 1996)
Projection: WGS84 / UTM zone 53
9552000
737000
732000
9548000
Grasberg Main Stage Cu-Au (2.9±0.3Ma[1])
Kali Intrusions (3.16-3.09Ma[2])
Karume Intrusion (3.13Ma[5])
Ertsberg Skarn (2.59Ma[2])
Ertsberg Intrusion (2.67Ma[2])
EESS
DOM
Ertsberg Stockwork zone
Ertsberg Intrusion
Tuff
Hornblende andesite
Dalam (>3.33Ma[2])
MGI
West Grasberg Banded Clay
Tuff
West Grasberg Gold
Lembah Tembaga
Kucing Liar Skarn (3.41-3.18Ma[2,3])
Wanagon Sill
Wanagon Gold (3.62Ma[1])
Kay
Big Gossan Skarn (2.82 Ma[1])
4.40[5]
3.81[5]
3.00[5]
3.09[5]
2.65[5]
1km

a porphyry-style deposit (Figure D-3; Figure D-4).

The GIC comprises early fragmented volcanic and igneous rocks of the Dalam phase and a series of nested intrusions interpreted to have been emplaced into volcanic cover (McDonald and Arnold, 1994; Pollard and Taylor, 2002; Sapiie and Cloos, submitted). GIC geochronology (Figure D-4) is consistent with observed overprinting relationships (Pollard and Taylor, 2002; Pollard et al., submitted). The GIC has been affected by multiple episodes of extensive porphyry-style alteration (Pollard and Taylor, 2002). Banded clay interpreted as surficial lacustrine sediments at West Grasberg and relatively unaltered tuff in the North Wall volcanics have not been affected by porphyry-style alteration although the banded clay does host sulphide mineralisation (Section A). The surficial features on the GIC margin suggest that late-stage volcanic processes operated after extensive porphyry-style alteration but prior to cessation of hydrothermal mineralisation (Section A).

The Ertsberg Intrusion has been dated by $^{40}Ar/^{39}Ar$ and K-Ar methods (Titley, 1975; McDowell et al., 1996; Pollard et al., submitted). The youngest date is almost 500Ky younger than Grasberg and Kucing Liar mineralisation (Pollard et al., 2001) (Figure D-4). The variation in Ertsberg Intrusion K-Ar dates may reflect different cooling ages in a single pluton or the presence of secondary biotite (McDowell et al., 1996). Complexity of igneous phases in the Ertsberg intrusion are not constrained. McMahon (1994a) considered that mineral textures and trace element variation in the Ertsberg Intrusion were consistent with in-situ fractional variation. Pollard et al. (submitted) suggest that the distribution in dates may reflect separate intrusive events. Friehauf et al. (2000) recently documented different phases of intrusion and crosscutting porphyry dykes. The oldest Ertsberg Intrusion dates are within error of the GIC Kali I, Kali II and Karume ages (Figure D-4). Younger Kali III intrusive phases have also been documented (Pollard and Taylor, 2002). The Karume intrusion is located between the GIC and Ertsberg Intrusions. Crosscutting relationships between the youngest GIC Kali intrusive phases, the Karume and the Ertsberg Intrusion have not been intersected by current mining activity.

The GIC is considered to be derived from a longer lived magma chamber cupola that was more evolved and hydrous than that which formed the Ertsberg Intrusion (McMahon, 1999). The GIC and Ertsberg Intrusion both display evidence of igneous evolution towards more mafic compositions (Pollard and Taylor, 2002; Pollard et al., submitted). Pollard et al. (submitted) suggested that replenishing the magma chamber, as evidenced by late mafic magma intrusions in the history of the GIC and also possibly the Ertsberg Intrusion, may have triggered emplacement of the shallow Ertsberg district intrusions and also introduced components into the ore deposits. Isotopic evidence also supports magma

Figure D-4. Geochronology of igneous hydrothermal events in the Ertsberg District. * Kucing Liar Stage 4 muscovite date considered erroneous (B. New pers comm., 2003). Apatite U-Th/He thermochronology (Sukarna et al., 2000) documents closure temperature for apatite (75°C). The ca. 0.5Ma difference between U-Th/He thermochronology and K-Ar geochronology (McDowell et al., 1996) is acceptable (N. Evans pers comm., 2002).

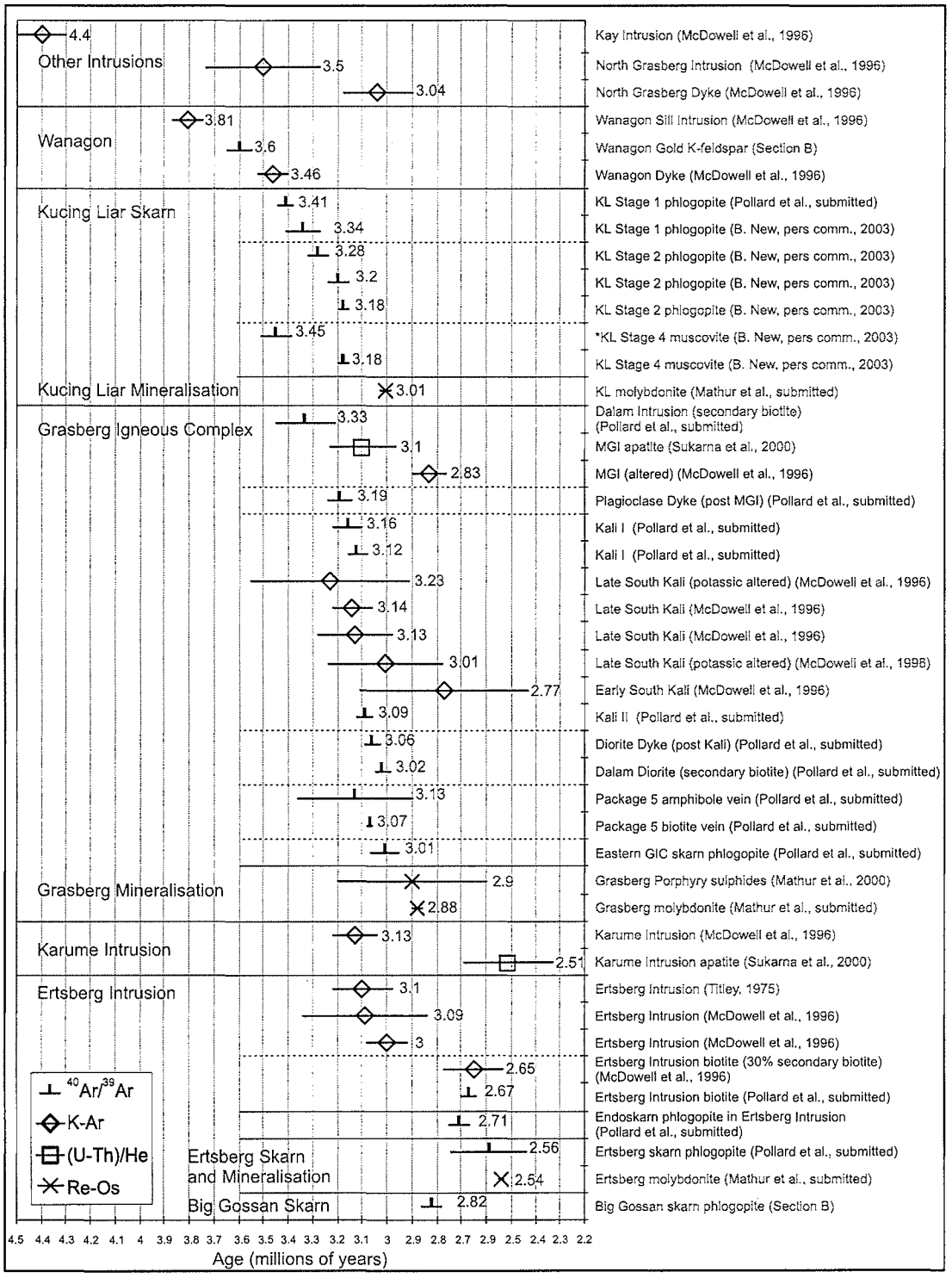

mixing late in the evolution of the GIC (James, 2000b; Sapiie and Cloos, submitted).

Apatite fission track thermochronology indicates that <2km of material was eroded from this part of the range since Pliocene times (Weiland and Cloos, 1996). Fission track data also indicate that unroofing of the central ranges was asymmetric, occurring between two and a half to five times faster on the southern slope than at the crest which is attributed to increased erosion on the slope due to orographically induced precipitation (Weiland and Cloos, 1996).

Ore deposits and hydrothermal events: distribution and geochronology

Porphyry-style Cu-Au mineralisation is documented at Grasberg, Lembah Tembaga and in the Ertsberg Stockwork (Figure D-3). Significant skarn Cu-Au deposits include Big Gossan, Ertsberg, the Ertsberg East Skarn System (EESS), DOM and Wanagon Gold. The Kucing Liar skarn may not be genetically related to the overprinting Cu-Au mineralisation (Pollard and Taylor, 2003). Deep-intermediate high sulphidation Cu-Au occurrences (HS) are documented at Grasberg, Kucing Liar, the EESS and Lembah Tembaga. Pyrite-Au-As-Zn-Bi-Te mineralisation is developed at Big Gossan and Wanagon Gold (Section B). Native gold±pyrite occurs in limestone breccias and banded clay at West Grasberg (Section A).

Grasberg, Kucing Liar and West Grasberg

Pollard and Taylor (2002) interpreted seven mineralogical packages (Package 1 - Package 7) to represent discrete hydrothermal fluid events that were intimately associated with emplacement of the GIC. The range in K-Ar and $^{40}Ar/^{39}Ar$ dates from the GIC overlap (Figure D-4) (Pollard et al., submitted) and crosscutting relationships between intrusive rocks and hydrothermal veining have been used to constrain different intrusion and hydrothermal events (Pollard and Taylor, 2002). Porphyry-style alteration (Package 1 - Package 4) overprints all intrusive phases and Grasberg main stage sulphide mineralisation did not occur until late in the paragenesis (Package 6) (Pollard and Taylor, 2002). An $^{40}Ar/^{39}Ar$ biotite date of 3.07±0.1 Ma (Figure D-4) from a pre-mineralisation quartz-anhydrite-bearing vein (Package 5) constrains the maximum age of Grasberg main stage sulphide development (Pollard et al., submitted) and is within error of a Re-Os isocron age of 2.9±0.3Ma for Grasberg main stage sulphides (Mathur et al., 2000) (Figure D-4).

The Kucing Liar skarn and Cu-Au deposit is hosted in faulted sedimentary rocks adjacent to the GIC (Figure D-3). Skarn formation, dated at 3.41±0.3Ma to 3.18±0.2Ma (Figure D-4; B. New pers comm., 2003), was synchronous with the earliest GIC events (Pollard et al., submitted). The sulphide phases developed at Kucing Liar are strikingly similar to

those adjacent at Grasberg and include a late stage HS occurrence (Package 7: Pollard and Taylor, 2002, 2003). A Re-Os age of 3.01±0.02Ma (Mathur et al., submitted) for late-stage molybdenite from Kucing Liar supports a cogenetic relationship between the deposits (Figure D-4; B. New pers comm., 2003).

The heavy sulphide zone is a distinct area of massive pyrite along the GIC margin (Lambert, 2000). The heavy sulphide zone was considered to precede Grasberg main stage sulphide development (Mathur et al., 2000; Gibbins, 2000; Pollard and Taylor, 2002) due to occurrences of overprinting chalcopyrite veins that were originally considered to belong to the Grasberg main sulphide stage. However, Pollard and Taylor (2003) have since suggested the heavy sulphide zone, chalcopyrite and other sulphides belong to the Package 7 HS occurrence and postdate Grasberg main stage sulphides (Pollard and Taylor, 2002).

Late-stage Pb and Zn sulphides at Grasberg and Kucing Liar (Pollard and Taylor, 2002: B. New pers comm., 2003) may be coeval with similar occurrences observed overprinting banded clay and in limestone at West Grabserg (Section A). Gold mineralisation at West Grasberg is characterised by diaspore-hosted gold-bearing alloys composed of Au-Cu-Zn-Ag (Section A). Gold mineralisation is also spatially associated with smectite-chlorite clay, Au-As bearing cubic pyrite and framboidal pyrite containing covellite inclusions (Section A). These features are tentatively correlated with unconstrained Au-As-Bi associations and framboidal pyrite-covellite occurrences documented in the Kucing Liar deposit, which occurs at depth nearby (Section A). The West Grasberg gold±pyrite occurrence also displays geochemical similarities to the pyrite-Au-As-Zn-Bi-Te occurrences in the district (Section A).

Wanagon Skarn Cu-Au

Skarn alteration is pervasively developed in carbonate sedimentary rocks of the Kembelangan Group and Waripi Formation and occurs as veins in the ca 3.81Ma Wanagon Sill (Section B). Chalcopyrite-dominant sulphides overprint skarn at depth (Section B). Minor galena and sphalerite are also present. At higher elevations, a pyrite-K-feldspar-Au-As-Zn-Bi-Te occurrence is developed in sandstone and carbonate sedimentary rocks (Section B).

Ertsberg Intrusion skarns and Cu-Au ore deposits

Skarn Cu-Au deposits around the Ertsberg Intrusion (Figure D-3) include Ertsberg (Katchan, 1982; Clarke, 2003), Big Gossan (Section B)(Meinert et al., 1997; Taylor et al., 1999; Clarke, 2002), DOM and the EESS (Mertig et al., 1994; Mertig, 1995; Rubin, 1996; Rubin and Kyle, 1998; Coutts et al., 1999; Friehauf et al., 2000). The majority are the

product of hydrothermal fluid events focused in structurally and lithologically favourable areas, commonly located at the contact of intrusive rocks and surrounding country rocks and/or along the Cretaceous Kembelangan limestone formation and Tertiary Waripi formation contact (Figure D-3). Both magnesium and calcic skarns are documented and skarn alteration affected igneous and sedimentary rocks.

Geochronological data are available for the Ertsberg and Big Gossan skarns. Phlogopite from the Ertsberg skarn has an $^{40}Ar/^{39}Ar$ age of 2.59±0.15Ma and phlogopite from the Big Gossan skarn has an $^{40}Ar/^{39}Ar$ age of 2.82±0.04Ma (Section B).The Big Gossan skarn postdates local igneous dykes and the $^{40}Ar/^{39}Ar$ age is within error of K-Ar dates from the nearby Ertsberg Intrusion (Section B; Figure D-3; Figure D-4). The Big Gossan skarn Cu-Au deposit is overprinted by an undated late-stage pyrite-Au-As-Zn-Bi-Te association (Section B). The DOM and the EESS skarns have not been dated although skarn alteration at the EESS is known to postdate the adjacent intrusion and Ertsberg stockwork (Friehauf et al., 2000) which has an $^{40}Ar/^{39}Ar$ age of 2.67±0.03Ma (Figure D-3; Figure D-4)(Pollard et al., submitted). A HS occurrence overprints skarn in the EESS (Rubin and Kyle, 1997; Coutts et al., 1999; Pollard and Taylor, 2003).

Ertsberg Stockwork (porphyry-style mineralisation)

Friehauf et al. (2000) documented a porphyry Cu-Au system distinct from the Grasberg deposit in the Ertsberg Intrusion. The timing of the mineralisation is constrained to be younger than the $^{40}Ar/^{39}Ar$ age (2.67±0.03Ma) for the Ertsberg Intrusion host (Figure D-3; Figure D-4)(Pollard et al., submitted). The porphyry-style mineralisation is characterised by hairline bornite-biotite veinlets which are cut by porphyryitic andesitic dykes. Garnet-bearing endoskarn and younger chalcopyrite and bornite veins (which may be analogous to skarn Cu-Au in the EESS) postdate both ages of intrusion. Friehauf (2000) interpreted a change in geological environment from a hot isotropic stress environment during early porphyry-style mineralisation to through-going fractures containing porphyry dykes and later skarn and Cu-Au sulphides.

High sulphidation (HS) occurrences

The HS occurrences in the district contain many features characteristic of deep to intermediate high sulphidation (Sillitoe, 1999; Hedenquist et al., 2000) including residual quartz, silicification, sericite, pyrite and high sulphidation-state sulphides (Pollard and Taylor, 2002, 2003). Advanced argillic phases such as alunite, dickite and barite that are characteristic of shallower high sulphidation deposits (Hedenquist et al., 2000) are notably absent. HS occurrences are observed at Grasberg, Kucing Liar (Gibbins, 2000; Lambert, 2000; Pollard and Taylor, 2002; 2003: B. New pers comm., 2003) the EESS (Katchan, 1982; Rubin and Kyle, 1997; Coutts et al., 1999) and Lembah Tembaga (Pollard and

Taylor, 2003). All occurrences post-date earlier skarn and porphyry-style mineralisation.

At Grasberg and Kucing Liar, the sulphide assemblage includes high sulphidation-state sulphides (chalcopyrite, bornite, nukundamite, digenite-chalcocite, covellite, enargite, and pyrite) and occurs as infill in cavities formed during a leaching event (Pollard and Taylor, 2002; 2003: B. New pers comm., 2003). Muscovite associated with Stage IV quartz leaching and illite clay development at Kucing Liar, has an $^{40}Ar/^{39}Ar$ age of 3.18±0.02Ma (Figure D-4 ; B. New pers comm., 2003), which places an upper age limit on the age of HS mineralisation at Kucing Liar.

The HS occurrence at Lembah Tembaga comprises an illite-muscovite-kaolinite alteration and minor covellite that overprints earlier porphyry and skarn Cu-Au mineralisation (Pollard and Taylor, 2003). In the EESS the HS occurrence overprints pre-exiting skarn Cu-Au (Rubin and Kyle, 1997; Coutts et al., 1999; Pollard and Taylor, 2003). Rare pyrophyllite has been documented at EESS (Pollard and Taylor, 2003). All mineralisation styles in the EESS are overprinted by texturally destructive carbonate alteration and late stage pyrite, galena and chalcopyrite (Section C)(Coutts et al., 1999).

Pyrite-Au-As-Zn-Bi-Te occurrences

Late-stage associations of pyrite-sphalerite-arsenopyrite-native gold with localised Bi and Te minerals overprint skarn Cu-Au at Big Gossan and also 2 km along strike to the NW at Wanagon Gold (Section B). At Big Gossan, the occurrences are considered younger than the Big Gossan skarn phlogopite age of 2.82±0.04Ma. The Big Gossan occurrences were previously interpreted as a component of outwards temperature zonation of a skarn Cu-Au system (Meinert et al., 1997). Recent work indicates that the pyrite-Au-As-Zn-Bi-Te occurrences are a separate overprinting sulphide stage (Section B).

The Wanagon Cu-Au skarn overprints the adjacent Wanagon Sill (ca. 3.81Ma). An event that leached the skarn and removed K-feldspar and plagioclase from sandstone preceded introduction of the pyrite-Au-As-Zn-Bi-Te occurrences. In the sandstone, late-stage sulphides were accompanied by a gangue of K-feldspar and minor quartz. The K-feldspar has a $^{40}Ar/^{39}Ar$ age of 3.62±0.05Ma (Section B). The carbonate rocks, display neither K-feldspar alteration nor leaching and late-stage sulphides are accompanied by a minor gangue of quartz and dolomite. A crosscutting relationship between Cu-Au mineralisation at depth and the pyrite-Au-As-Zn-Bi-Te occurrences which occur at higher elevations is not observed.

The mineral paragenesis of the Big Gossan and Wanagon Gold occurrences are almost identical. Native gold is associated with argentian tetrahedrite and tennantite, a silver-

antimony-sulphide and Bi and Te -(Ag-Au) minerals including cosalite, bismuthinite, petzite, hessite, altaite and tetradymite. A direct genetic relationship to earlier skarn Cu-Au is not clear. The occurrences could represent either a) a deposit style that evolved directly from earlier skarn Cu-Au fluids or b) a deposit formed by incursion of a new fluid with a different composition.

Evidence for source and character of fluids and ore components

Sulphur isotope geochemistry

Sulphur isotope compositions for most deposits in the district are indistinguishable and occupy a narrow range between -0.5-5.5‰ (Figure D-5) This suggests a common sulphur source for all Ertsberg District deposits which is probably igneous (c.f. Ohmoto and Goldhaber, 1997). Lower $\delta^{34}S$ occurs in sulphides at Kucing Liar and nearby at SW Grasberg (Gibbins, 2000: B. New pers comm., 2003). At SW Grasberg these values were interpreted as possibly being of sedimentary origin from biogenic sulphides (Gibbins, 2000).

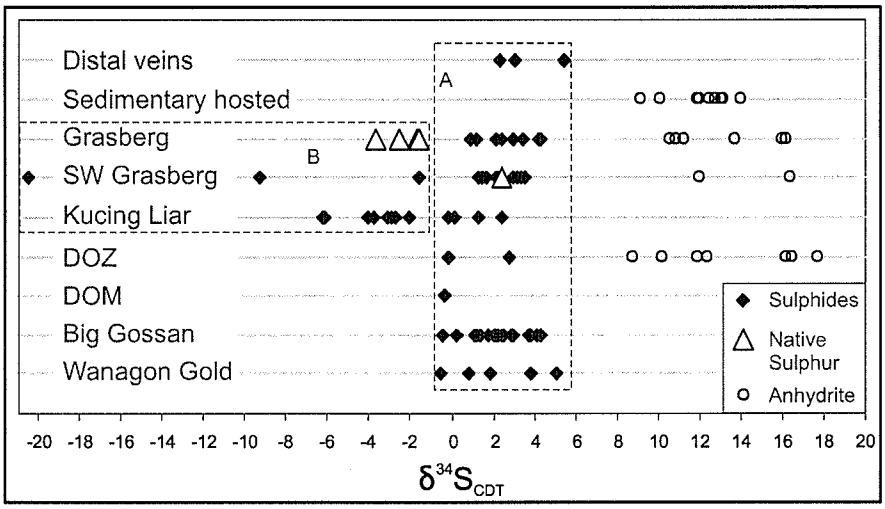

Figure D-5. $\delta^{34}S_{CDT}$ results from the Ertsberg District. The majority of sulphide $\delta^{34}S_{CDT}$ values from the Ertsberg District occupy a narrow range from -0.5 to 5.5‰ (A). Wanagon Gold and Big Gossan pyrite, sphalerite, chalcopyrite and galena from skarn Cu-Au mineralisation and late stage pyrite-Au-As-Zn-Bi-Te occurrences range from -0.7 to 5.1‰. (Section B). DOM chalcopyrite (Kyle, 1992). DOZ bornite, chalcopyrite, anhydrite and (Kyle, 1992). Grasberg native sulphur, anhydrite, chalcopyrite and pyrite (Kyle, 1992). Sedimentary hosted anhydrite from unspecified locations in the district (Kyle, 1992; Kyle and Dworkin, 1995). Distal sphalerite and galena veins (Kyle, 1992). Kucing Liar chalcopyrite, sphalerite, pyrite, covellite, galena (B. New pers comm., 2003). Of the Kucing Liar $\delta^{34}S_{CDT}$ results some pyrite, covellite and chalcopyrite display lower $\delta^{34}S_{CDT}$ (B). SW Grasberg native sulphur, anhydrite, pyrite, marcasite, enargite, covellite and chalcopyrite (Gibbins, 2000). Of the SW Grasberg samples, two of the covellite analyses have low values (-9.3‰ and -1.6‰) and the marcasite sample has a value of -21‰.

Gold microprobe analyses

Rubin and Kyle (1997) noted that gold compositions for all deposits occupy a wide range (Figure D-6). Pd-bearing gold is only documented at Grasberg (Rubin and Kyle, 1997). Depth, lateral distance, mineral assemblage or paragenetic relationship are considered to exert no control on gold fineness range in the EESS (Rubin and Kyle, 1997) although the results have not been considered in context with HS occurrences now recognised in the EESS (Coutts et al., 1999; Pollard and Taylor, 2003). Rubin and Kyle (1997) concluded from a limited sample suite that gold fineness from within the pyrite-Au-As-Zn-Bi-Te occurrences at Big Gossan increased with elevation. However, this investigation (Section B) established that gold fineness is not related to elevation but instead correlates with gold paragenesis which reflects the original fluid and mineral depositional conditions. Highest fineness gold is encapsulated in early pyrite or associated with bismuthinite. The lowest fineness gold is associated with Pb-bearing minerals (galena and sulphosalts).

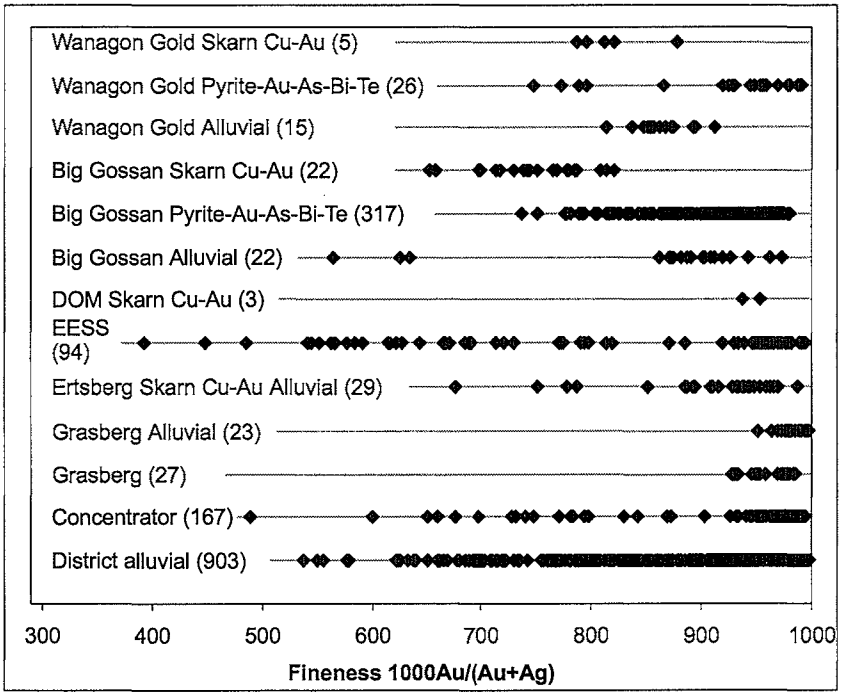

Figure D-6. Gold microprobe from deposits in the Ertsberg district and alluvial sources. Number of analyses in brackets. "Alluvial" results are analysis of alluvial gold grains sampled in drainages from those deposits. Wanagon skarn Cu:10000Au (Section B). Wanagon Gold Pyrite-Au-As-Zn-Bi-Te (Section B: Honea, 1996). Wanagon Gold alluvial (Allen and Palmer, 1992). Big Gossan skarn Cu:10000Au (Rae et al., 1994; Rubin, 1996). Big Gossan pyrite-Au-As-Zn-Bi-Te (Section B: Rae et al., 1994; Rubin, 1996). Big Gossan alluvial (Allen and Palmer, 1992). DOM skarn Cu:10000Au (Rubin, 1996). EESS (Rubin, 1996). Ertsberg and Grasberg alluvial (Allen and Palmer, 1992). Concentrator (Allen et al., 1994; Allen, 1993c; Allen and Palmer, 1992). Various alluvial gold (Allen and Palmer, 1992; Allen and Coote, 1993; Allen, 1993d, 1991).

Oxygen, hydrogen and carbon isotope geochemistry

The majority of silicate $\delta^{18}O$ and δD values from the district have magmatic signatures and no relationship to local meteoric water values (Figure D-7a, b). Meinert et al., (2003) concluded from $\delta^{18}O$ and δD results at Big Gossan that the fluids responsible for anhydrous and hydrous skarn formation were dominantly magmatic (Figure D-7a). Conventional and in situ Secondary Ion Mass Spectrometry (SIMS) techniques were utilised in a reconnaissance $\delta^{18}O$ and $\delta^{13}C$ investigation of a) marble and dolomitised rocks spatially-associated with the GIC and Kucing Liar, b) marble and veins related to the Big Gossan skarn, and c) carbonate alteration associated with leaching events at Kucing Liar and the EESS (Section C; Figure D-8). The $\delta^{18}O$ and $\delta^{13}C$ results from local studies at Kucing Lair (B. New pers comm., 2003) and DOM (Mertig, 1995) were also incorporated for comparison.

Magmatic signatures dominate the hydrothermal fluids in the Ertsberg district. Limited $\delta^{18}O_{FLUID}$ calculations indicate that influence from non-magmatic fluids (i.e. meteoric water) is only conclusively present in analyses from the Stage IV leaching, quartz and clay event at Kucing Liar (Section C; Figure D-8). Analyses from unaltered and least altered dolostones throughout the district compare well with marine carbonate values (Veizer and Hoefs, 1976). $\delta^{13}C$ variation in New Guinea Limestone Group values (Figure D-8) may not be significant as during deposition of the New Guinea Limestone Group, the presence of three global carbon cycle aberrations (ca. 55, 34 and 23 Ma) with amplitudes up to ca. 3‰, are inferred from carbon isotope studies (Zachos et al., 2001).

Influence from the isotopic signature of the local carbonate stratigraphy is evident in the dolomitisation halo surrounding the GIC and the marble from Big Gossan. Textural and isotopic results indicate that fluid/rock ratios at Big Gossan were high and resulted in complete modification of the host rock isotopic signature on alteration margins to values reflecting those of the invading magmatic fluid. $\delta^{18}O_{FLUID}$ calculations (ca. 5.9‰) for skarn-related calcite at Big Gossan are consistent with a dominantly magmatic origin (Section C).

The $\delta^{18}O_{SMOW}$ and $\delta^{13}C_{PDB}$ results in association with textural evidence indicate that there was at least one generation of dolomitisation peripheral to the GIC. Texturally, dolomitisation is manifested as low-inclusion bearing planar euhedral and subhedral textures, which differs from the dominantly non-planar inclusion-rich dolomite observed in unaltered dolostones (Section C). Isotopic compositions of the dolomitisation could be interpreted to represent mixing between marine limestone and magmatic fluids (Section C). Secondary carbonate in the EESS may have been derived by leaching carbonate in the skarn and adjacent carbonate stratigraphy (Section C; Figure D-8). As the temperatures of GIC

Figure D-7. Calculated $\delta^{18}O_{FLUID}$ and δD_{FLUID} and silicate and oxide $\delta^{18}O_{VSMOW}$ results from Grasberg, Big Gossan, Kucing Liar and DOM. $\delta^{18}O_{FLUID}$ and δD_{FLUID} calculations contained within respective references. Local water compositions measured include rainwater, lake water, melted glacial snow and ice and water from near the EESS (Harrison, 1999). Meteoric water line (Craig, 1961), magmatic fluid range (Campbell and Larson, 1998) and marine carbonate range (Veizer and Hoefs, 1976) included for comparison. Kucing Liar Stage IV quartz values have been recalculated using fluid inclusion homogenisation temperature information for each sample where available (B. New pers comm., 2003) and appropriate quartz-H_2O fractionations (Zheng, 1993). An arbitrary temperature of 350°C was used where no fluid inclusion evidence is available (B. New pers comm., 2003).

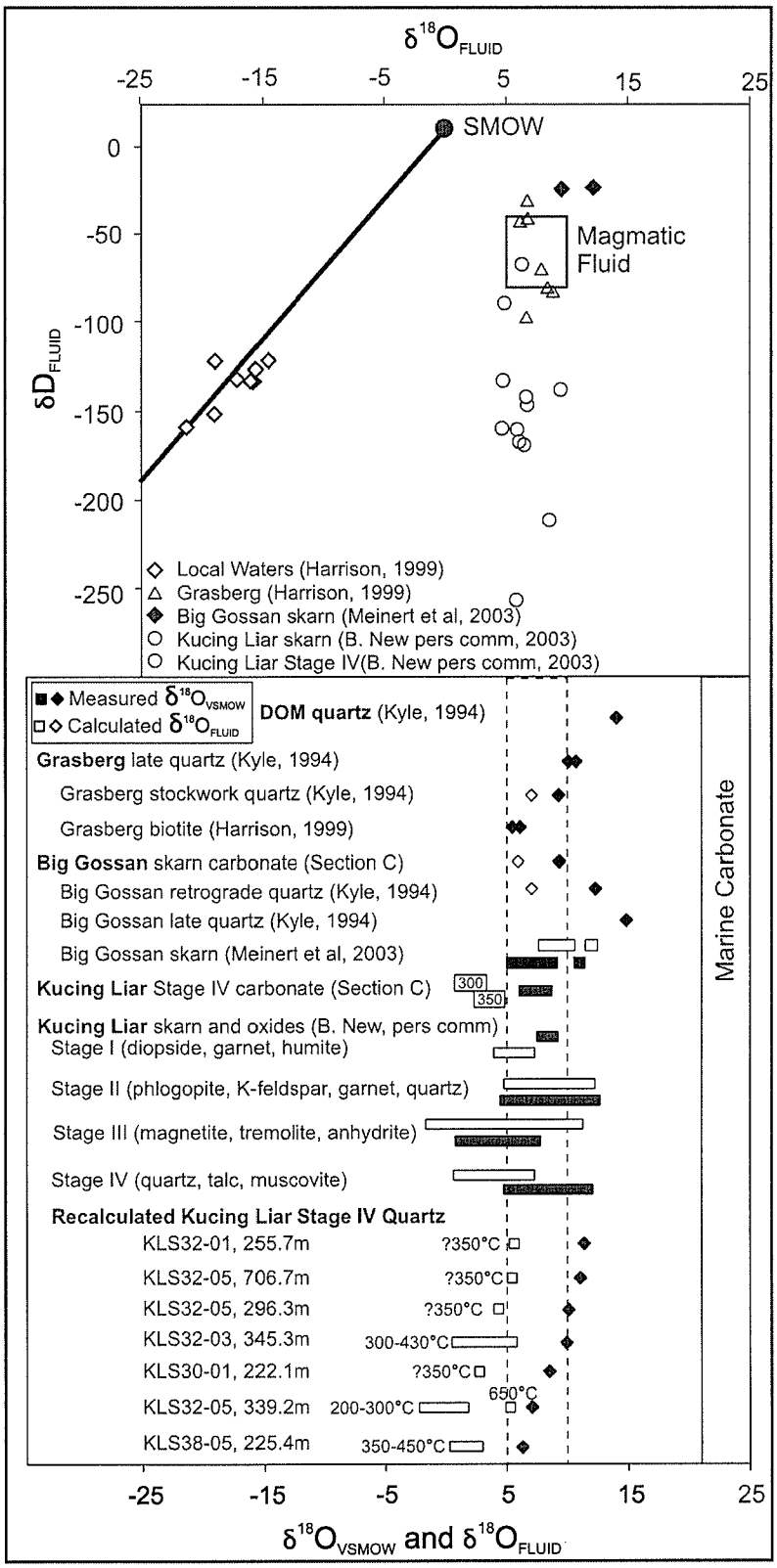

Figure D-8. Compilation and interpretation of $\delta^{18}O_{SMOW}$ and $\delta^{13}C_{PDB}$ carbonate isotope results from the Ertsberg district. Results from Mertig (1995), B. New (pers comm., 2003) and this investigation (Section C). $\delta^{18}O_{SMOW}$ of primary magmatic water from Sheppard (1986). Magmatic $\delta^{13}C_{PDB}$ range ca. 0 to -10 (Taylor, 1986). $\delta^{13}C$ variation up to ca. 2.5‰ in the New Guinea Limestone Group dolostones is not significant (Zachos et al., 2001). Possible range of corrections for $\delta^{18}O_{SMOW}$ to $\delta^{18}O_{FLUID}$ calculated for temperatures (200-400°C) from fractionation factors for H_2O and calcite/ dolomite (Golyshev et al., 1981). Even if Kucing Liar Stage IV carbonate alteration was formed at high temperatures (400°C), calculated $\delta^{18}O_{FLUID}$ values are below the magmatic range. DOM and EESS carbonates were formed from magmatic fluids if they formed at temperatures of ca. 300°C. SIMS uncertainties are ±0.75‰ $\delta^{13}C$ (this study) and ±1.4‰ $\delta^{18}O$ (Hazelton, 1997). Conventional uncertainties are ±0.09‰ $\delta^{13}C$ and ±0.11‰ $\delta^{18}O$ (Appendix 1).

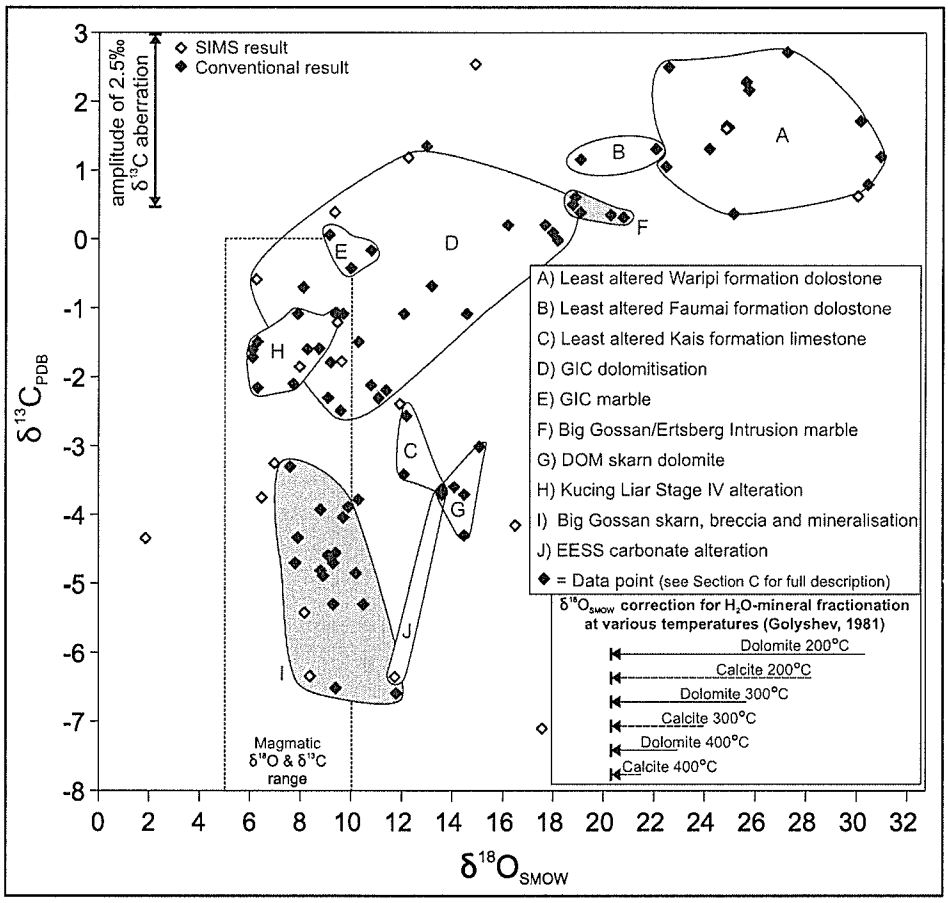

dolomitisation and EESS carbonate are unconstrained, $\delta^{18}O_{FLUID}$ could not be established.

Ore deposit radiogenic isotope geochemistry

Pb isotope ratios from the ores in the district overlap with those of associated igneous rocks (James, 2000a). Pb and Sr isotope analyses from ores and igneous suite are quiet different to those of the 12km of Precambrian-Miocene sedimentary section underlying the district (James, 2000a). Pb in pyrite, chalcopyrite and galena from the heavy sulphide zone was interpreted to be derived from an igneous source with no detectable influence from the country rocks (Lambert, 2000). In the EESS Pb isotope ratios are considered to indicate that ore-forming fluids were derived from a deeper source with less crustal contamination than the Ertsberg Intrusion (James and Housh, 1995).

Radiogenic $^{187}Os/^{188}Os$ values suggest a crustal-sedimentary source contribution for gold-bearing heavy sulphide zone (Mathur et al., 2000). The proposed geologic reservoir for mineralisation and radiogenic Os is metamorphosed black shale either incorporated into the melt by assimilation or accessed by fluids (Mathur et al., 2000). Re-Os isotope results (Mathur et al., submitted) suggest that the porphyry-style stockwork mineralisation at Grasberg and the Ertsberg stockwork developed independently and are not related to the same shallow (ca. 5km) intrusive stock. Results from Re-Os isotope analyses of the heavy sulphide zone, Kucing Liar and DOM mineralisation are also considered to display genetic links with the surrounding Mesozoic sedimentary rocks (Mathur et al., submitted).

Fluid inclusion constraints

Fluid inclusion studies have been conducted at Grasberg (Figure D-9), Wanagon Gold, West Grasberg and the major Cu-Au skarns Kucing Liar, Big Gossan, EESS and DOM (Figure D-10). The character of the skarns in the district is well-constrained and they display local variation in fluid inclusion homogenisation temperatures and estimated salinity. Fluid inclusions from Big Gossan anhydrous skarn minerals homogenise at temperatures more than 50°C below those documented at DOM (Figure D-10). Fluid inclusions were

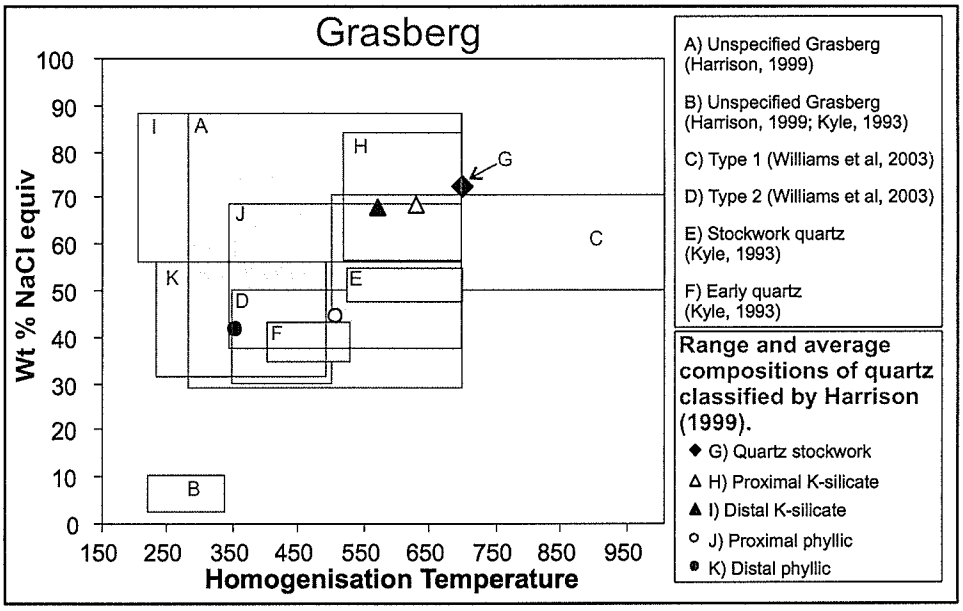

Figure D-9. Grasberg and GIC fluid inclusion results from quartz. Type 1 inclusions are liquid poor and multisolid-bearing; Type 2 inclusions are liquid-rich with halite and solids (Williams et al., 2003). For full descriptions and paragenesis see respective references. Some inclusions did not homogenisation at the upper limit of the instrument capability: A = 700°C (Harrison, 1999); C= 1000°C (Williams et al., 2003); E= 700°C (Kyle, 1993). Average composition of inclusions from quartz in distal locations displays lower salinity and temperature with respect to proximal quartz samples (Harrison, 1999). The quartz classifications of Harrison (1999) cannot be resolved within the paragenetic framework of Pollard and Taylor (2002). "Stockwork" quartz is texturally complicated and not all generations of quartz are related to Grasberg main stage sulphides (Penniston-Dorland, 2001; Pollard and Taylor, 2002: B. Fu pers comm., 2003).

not studied in Stage I anhydrous skarn at Kucing Liar (Figure D-10a) but measurements from quartz associated with Stage II potassic alteration revealed homogenisation temperatures >600°C (B. New pers comm., 2003).

At EESS and DOM the presence of lower salinity inclusions in late-stage quartz (Figure D-10d, e) was interpreted to represent mixing with less saline meteoric water (Kyle, 1993). However, inclusions with salinities <10 wt% $NaCl_{equiv}$ in retrograde minerals (quartz and anhydrite; Figure D-10b) at Big Gossan were interpreted to be magmatic fluids (Meinert et al., 1997; Meinert et al., 2003).

Fluid inclusions from late stage sphalerite and quartz in the Big Gossan pyrite-Au-As-Zn-Bi-Te occurrences (Figure D-10b) have an average salinity of 9 wt% $NaCl_{equiv}$ and average homogenisation temperature of 248°C. At Wanagon Gold, a population of fluid inclusions in sandstone that hosts pyrite-Au-As-Zn-Bi-Te have similar salinity and homogenisation temperatures to Big Gossan late-stage quartz and sphalerite. The results suggest fluids at Wanagon Gold may have had slightly lower salinities (Figure D-10c) which may represent mixing with lower salinity non-magmatic fluids (Section B).

Fluid inclusions from quartz associated with the leaching and HS occurrence (Stage IV and V) at Kucing Liar (B. New pers comm., 2003) display wide salinity and homogenisation temperature ranges (Figure D-10a). Fluids responsible for sphalerite-galena-quartz-fluorite veins at West Grasberg (Figure D-10f) are considered to be sourced from saline fluids, possibly derived from Grasberg (Kyle, 1993).

Cu:10000Au ratio variations

Skarn-hosted Cu-Au deposits throughout the district have characteristic Cu:10000Au ratios and similar and strong Cu:Ag associations (Figure D-11a, b). Cu:10000Au ratios in the EESS are complicated by the presence of at least 3 separate Cu-Au hydrothermal systems developed (Figure D-11a, c). Cu:10000Au ratios from intrusion-hosted porphyry-style mineralisation in the EESS displays significantly higher Au:Cu ratios than the mixed signature of skarn-hosted Cu-Au overprinted by HS-style Cu-Au mineralisation (Figure

Figure D-10. Fluid Inclusions from Ertsberg district skarn and ore deposits. Type 1 inclusions are liquid dominant + vapour; Type 3 inclusions are liquid + vapour + solid/s. For full descriptions and paragenesis see respective references. a) Kucing Liar Stage II quartz, Stage IV quartz and fluorite and Stage V quartz (B. New pers comm., 2003). Areas represent ranges or more than one value and points represent individual values. Some inclusions did not homogenise at the upper limit of the instrument capability: 600°C. Approximate distribution of Type 1 and Type 3 inclusions is marked. b) Big Gossan skarn and overprinting pyrite-Au-As-Zn-Bi-Te occurrence. c) Wanagon Gold fluid inclusions from leached and silicified sandstone hosting K-feldspar and pyrite-Au-As-Zn-Bi-Te occurrences. Two main populations are present. d) EESS. e) DOM skarn and late quartz. f) West Grasberg fluorite-sphalerite-galena veins in NE structures adjacent to the GIC.

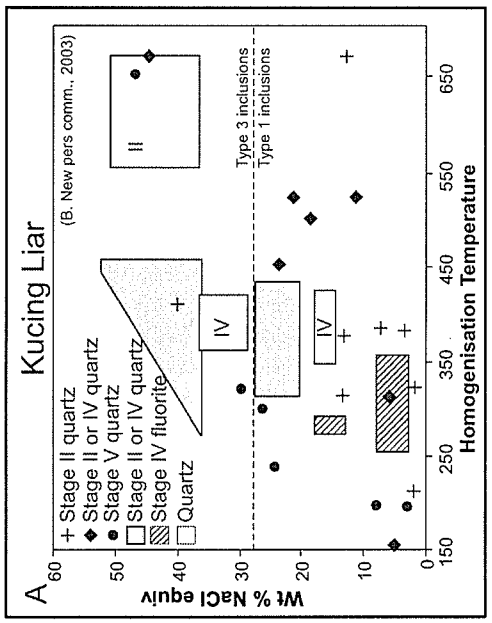
A
Kucing Liar
(B. New pers comm., 2003)
+ Stage II quartz
◆ Stage II or IV quartz
● Stage V quartz
Stage II or IV quartz
Stage IV fluorite
Quartz
II
IV
IV
Type 3 inclusions
Type 1 inclusions
Wt % NaCl equiv
Homogenisation Temperature

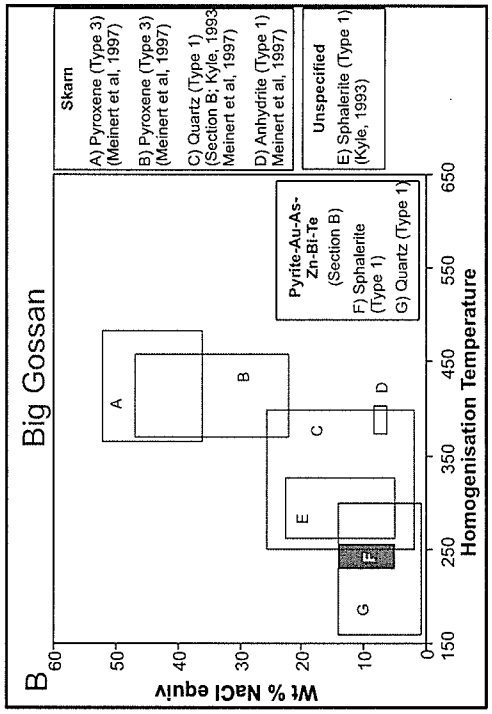
B
Big Gossan
Skarn
A) Pyroxene (Type 3) (Meinert et al, 1997)
B) Pyroxene (Type 3) (Meinert et al, 1997)
C) Quartz (Type 1) (Section B; Kyle, 1993 Meinert et al, 1997)
D) Anhydrite (Type 1) Meinert et al, 1997)
Unspecified
E) Sphalerite (Type 1) (Kyle, 1993)
Pyrite-Au-As-Zn-Bi-Te (Section B)
F) Sphalerite (Type 1)
G) Quartz (Type 1)
Wt % NaCl equiv
Homogenisation Temperature

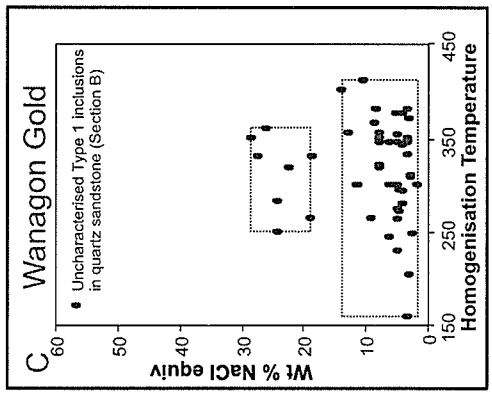
C
Wanagon Gold
Uncharacterised Type 1 inclusions in quartz sandstone (Section B)
Wt % NaCl equiv
Homogenisation Temperature

D
Ertsberg East Skarn System
(Rubin & Kyle, 1998)
A) Monticellite (Type 3)
B) Forsterite (Type 3)
C) Garnet (Type 3)
D) Early quartz (Type 3)
E) Early quartz (Type 3)
F) Late quartz (Type 1)
Wt % NaCl equiv
Homogenisation Temperature

E
DOM
(Mertig, 1995)
A) Monticellite (Type 3)
B) Early quartz (Type 3)
C) Early garnet (Type 1)
D) Intermediate garnet (Type 1)
E) Garnet (secondary Type 1)
F) Late quartz (Type 1)
G) Late quartz (secondary Type 1)
H) Calcite (Type 1)
Wt % NaCl equiv
Homogenisation Temperature

F
West Grasberg
(Kyle, 1993)
A) Fluorite (Type 3)
B) Sphalerite (Type 1)
C) Fluorite (Type 1)
D) Quartz (Type 1)
E) Fluorite (Type 1)
Wt % NaCl equiv
Homogenisation Temperature

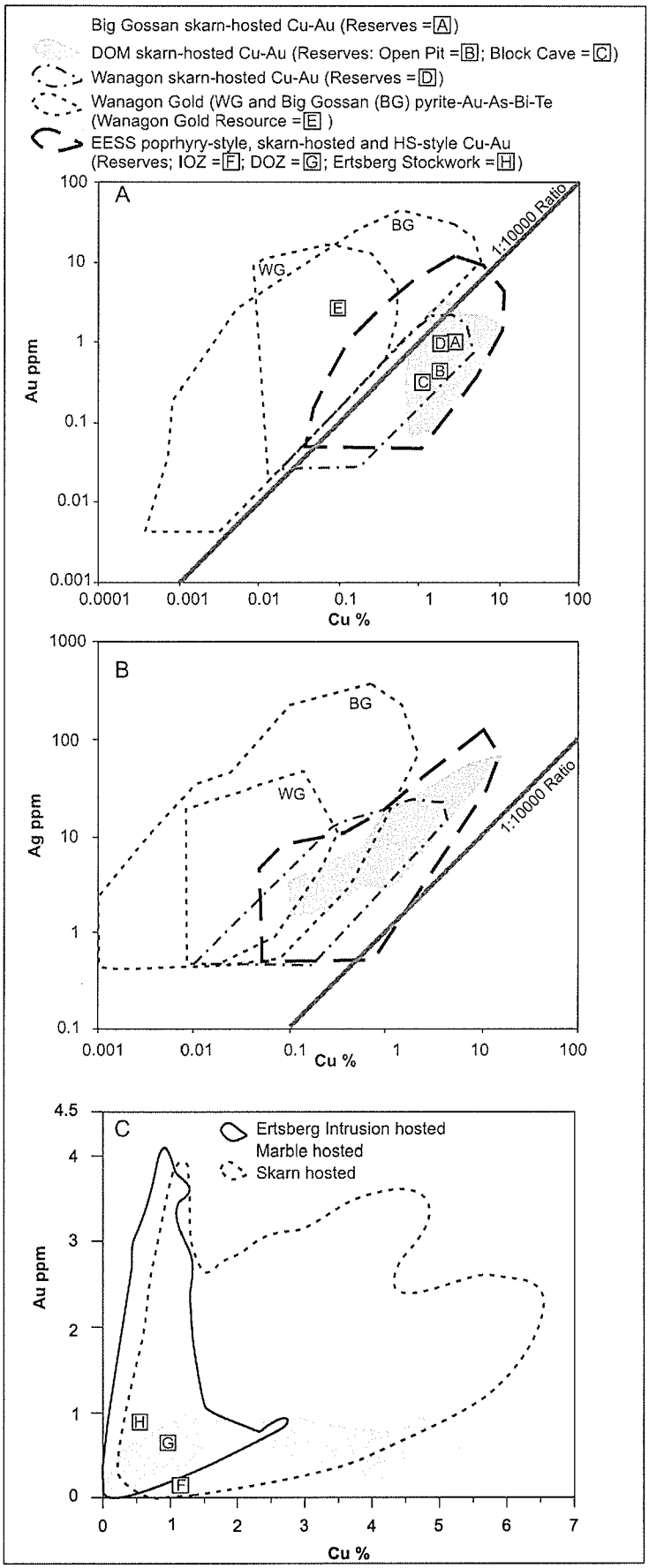

Figure D-11. Cu:10000Au and Cu:Ag ratios from major deposits and prospects in the Ertsberg District including Big Gossan and Wanagon Gold (Section B), DOM and the EESS. Reserves for EESS, DOM and Big Gossan skarn-hosted Cu-Au (Freeport McMoRan Copper & Gold Inc 2002 Annual Report) and possible geological resource for Wanagon Gold (Sanusi, 1994: an arbitrary grade of 0.1% Cu has been used) included for comparison. Wanagon skarn-hosted Cu-Au possible geological resource from Sanusi (1994). a,b) Ranges of Cu:10000Au and Cu:Ag ratios estimated from log-log plots of Pt Freeport drillhole assay data from each occurrence: Big Gossan (>15200 analyses), Wanagon Gold (>3600 analyses), Dom (>2500 analyses), EESS (>29500 analyses from representative drillholes). Strong Cu-Ag associations are present in each of the skarn-hosted Cu-Au deposits (Section B)(Mertig, 1995; Rubin, 1996). c) DOZ (deepest part of the EESS) Cu:10000Au ratios separated on the basis of host rock (graph modified from unpublished PT Freeport Indonesia report) correlate with what is understood of the 3 different styles of mineralisation developed (Rubin, 1996; Coutts et al., 1999; Pollard and Taylor, 2003). The intrusion-hosted high Au:Cu ratio is representative of the porphyry-style mineralisation and compares well with reserve figures for Ertsberg Stockwork [H] and distribution of Grasberg porphyry-style mineralisation (Figure D-13). Skarn hosted Cu:10000Au ratio for DOZ [G] Reserve figure is representative of more than one mineralisation style (skarn Cu-Au mineralisation and overprinting HS Cu-Au occurrences).

D-11c). Pyrite-Au-As-Zn-Bi-Te occurrences at Big Gossan and Wanagon Gold have higher Au:Cu and Ag:Cu ratios than the skarn Cu-Au deposits (Figure D-11a, b).

Metal zoning has only been definitively constrained with respect to paragenesis at Big Gossan where Cu:10000Au and Zn:Cu ratios display temperature zonation in cross and long section (Figure D-12; Section B). The highest temperature core (defined by low Zn:Cu) of the skarn-hosted Cu-Au mineralisation plunges to the NW and is open at depth (Figure D-12). Highest Cu grades occur to the NW coincident with NE-striking faults (Figure D-12).

Distinctly different Cu:10000Au ratios in the Grasberg porphyry-style Cu-Au and overprinting HS-style mineralisation (Figure D-13) have been constrained from the Section 13 mineral distributions of Pollard and Taylor (2002). Variation of Cu:10000Au with elevation in either porphyry-style or HS-style does not appear significant but cannot be accurately determined from the size of the dataset used (Figure D-13). Grasberg and Ertsberg Stockwork porphyry-style mineralisation have similar Cu:10000Au ratios (Figure D-13) that are higher than skarn-hosted Cu-Au mineralisation but not as elevated as those in the pyrite-Au-As-Zn-Bi-Te occurrences (Figure D-14).

Cu:10000Au ratios of resource and reserve figures from ore deposits in the district represent large samples and typically lie within the Cu:10000Au ratio ranges for the mineralisation style (Figure D-11, Figure D-13, Figure D-14). Exceptions include resources from Grasberg open pit and block cave, Kucing Liar, DOZ and IOZ which embody more than one mineralisation style that formed at different times (Figure D-11, Figure D-13, Figure D-14). The range of Cu:10000Au ratios present in Grasberg brine inclusions correlate with both the porphyry and HS Cu-Au mineralisation styles (Figure D-14). Grasberg vapour inclusions are less consistent although the Au-rich vapour inclusions show similar gold contents to pyrite-Au-As-Zn-Bi-Te mineralisation (Figure D-14).

Laser Ablation-ICPMS analyses of sulphides

Pyrite LA-ICPMS results from the Big Gossan and Wanagon Gold pyrite-Au-As-Zn-Bi-Te occurrences contain up to 60ppm Au, 2% As, 680ppm Bi and 40ppm Te and display distinct Bi and Te associations (Section B; Figure D-15). Pyrite associated with skarn Cu-Au mineralisation at Big Gossan and Wanagon Gold has lower As and Au contents (Figure D-15a). Two generations of pyrite were analysed from gold-bearing limestone breccias at

Figure D-12. Metal zoning in Big Gossan long section looking NE (modified from Section B). a) Distribution of drillholes Cu:10000Au ratios and skarn-hosted Cu-Au and pyrite-Au-As-Zn-Bi-Te occurrences as constrained from existing drilling. b) Distribution of Zn:Cu ratios and Cu>1% and Cu>5% contours as constrained from existing drilling. Orebody plunges towards the NW.

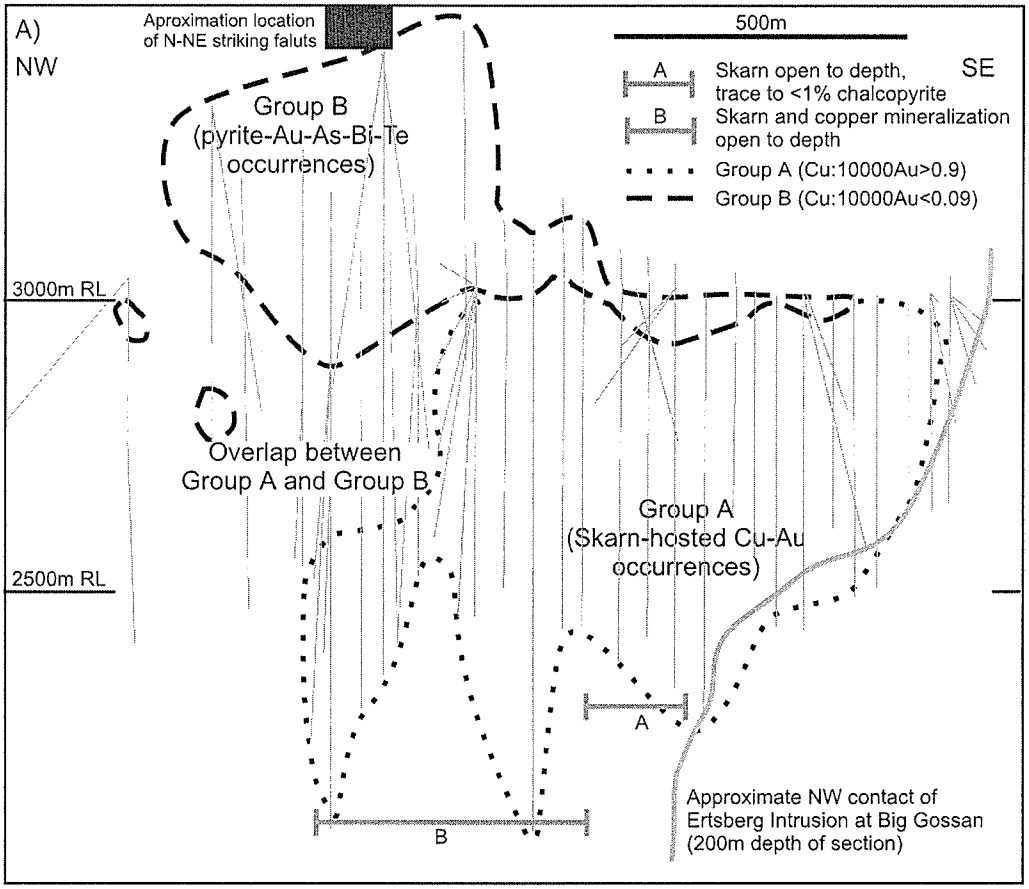
A)
NW
Aproximation location of N-NE striking faluts
500m
SE
A
Skarn open to depth, trace to <1% chalcopyrite
B
Skarn and copper mineralization open to depth
Group A (Cu:10000Au>0.9)
Group B (Cu:10000Au<0.09)
Group B (pyrite-Au-As-Bi-Te occurrences)
3000m RL
Overlap between Group A and Group B
Group A (Skarn-hosted Cu-Au occurrences)
2500m RL
A
B
Approximate NW contact of Ertsberg Intrusion at Big Gossan (200m depth of section)

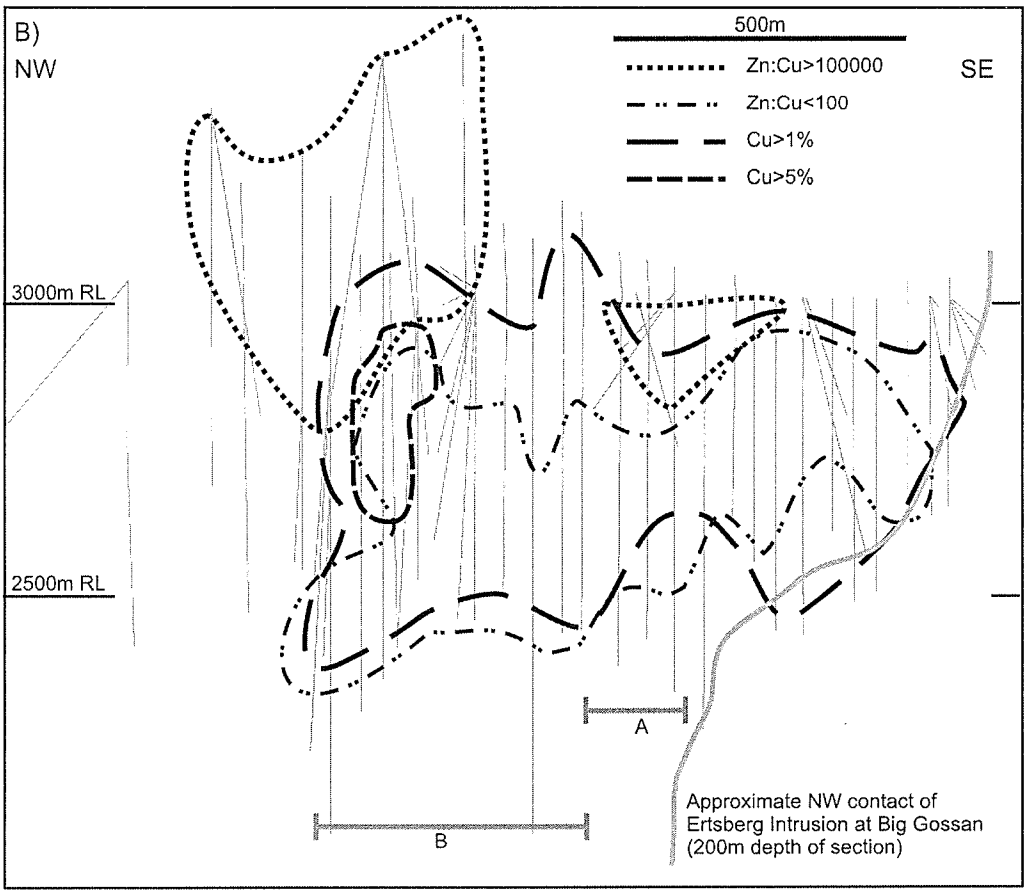
B)
NW
500m
SE
Zn:Cu>100000
Zn:Cu<100
Cu>1%
Cu>5%
3000m RL
2500m RL
A
B
Approximate NW contact of Ertsberg Intrusion at Big Gossan (200m depth of section)

West Grasberg (Section A). Framboidal pyrite associated with covellite (interpreted to be a component of the HS occurrence from nearby Grasberg and Kucing Liar) contains low levels of gold and elevated Cu contents (Figure D-15b). Euhedral pyrite in the same samples contains elevated Au and As and variable Bi and Te (Figure D-15a, c, d). Single pyrite analyses from the heavy sulphide zone and late-stage pyrite in the EESS both correlate well with pyrite samples from other copper-rich deposits (Figure D-15a, b, c, d). Two main styles of pyrite chemistry in Ertsberg district ore deposits have been identified from LA-ICPMS analysis. Pyrites from copper-rich hydrothermal events contain a maximum of 0.64ppm Au and 2500ppm As. Pyrites associated with Au-As-Bi-Te depositing hydrothermal fluids contain up to 57ppm Au and 2% As.

Discussion

Correlation of igneous and hydrothermal events in the Ertsberg district

Correlation of igneous and hydrothermal events in the Ertsberg district is constrained by geochronology and observed overprinting relationships (Figure D-16). Several points of uncertainty exist where limited geological and geochronological information contribute to difficulties in establishing time sequence:

I. *Further age constraint and radiogenic character of GIC and Ertsberg igneous events.* The full complexity of the Ertsberg intrusion is unknown and the geochronology suggests at least two phases of intrusion exist (Figure D-4). The older intrusive event could have been coeval with late-stage GIC intrusions and hydrothermal activity (Figure D-16). The evolution of igneous activity at the Ertsberg intrusion and GIC and the genetic implications for the magma chamber and generation of hydrothermal events in the district have not been fully investigated.

Figure D-13. Grasberg drillhole AM96-43-07 and variation in Cu:10000Au ratios with Cu-Au mineralogical context. Assay results from PT Freeport Indonesia. Drillhole geology and distribution of mineralogical phases courtesy of P. Pollard and R. Taylor (2003). Drillhole AM96-43-07 occurs below 3000m elevation (Pollard and Taylor, 2002). Package 6, which includes Grasberg main stage porphyry Cu-Au veins and is focussed near the Kali-MGI contact, displays a distinct Cu:10000Au ratio. Package 7, which includes the mixed Cu-sulphide assemblage and occurs predominately in leached and clay altered Dalam, is part of the HS assemblage (Pollard and Taylor, 2002, 2003) and displays higher Cu:10000Au ratios. Where Package 6 and Package 7 overlap, the Cu:10000Au ratio is mixed. Analyses from 4000-3500m elevation (drillhole assay results from PT Freeport Indonesia from drillholes GRS37-173, GRS37-171, GRS37-39, GRS37-161 and GRS37-33 (Pollard and Taylor, 2002)) display populations consistent with those observed in AM96-43-07. The range from Ertsberg Stockwork porphyry-style mineralisation (range estimated from 1003 analyses from representative drillholes TE03-01 to TE03-16; PT Freeport Indonesia assay data) is comparable with Grasberg main stage porphyry Cu-Au. The Cu:10000Au ratio for Ertsberg Stockwork reserves (Freeport McMoRan Copper & Gold Inc 2002 Annual Report) correlates with the estimated range. Cu:10000Au ratios for Grasberg open pit and block cave reserves (Freeport McMoRan Copper & Gold Inc 2002 Annual Report) are interpreted to represent a mix of Package 6 and Package 7 mineralisation.

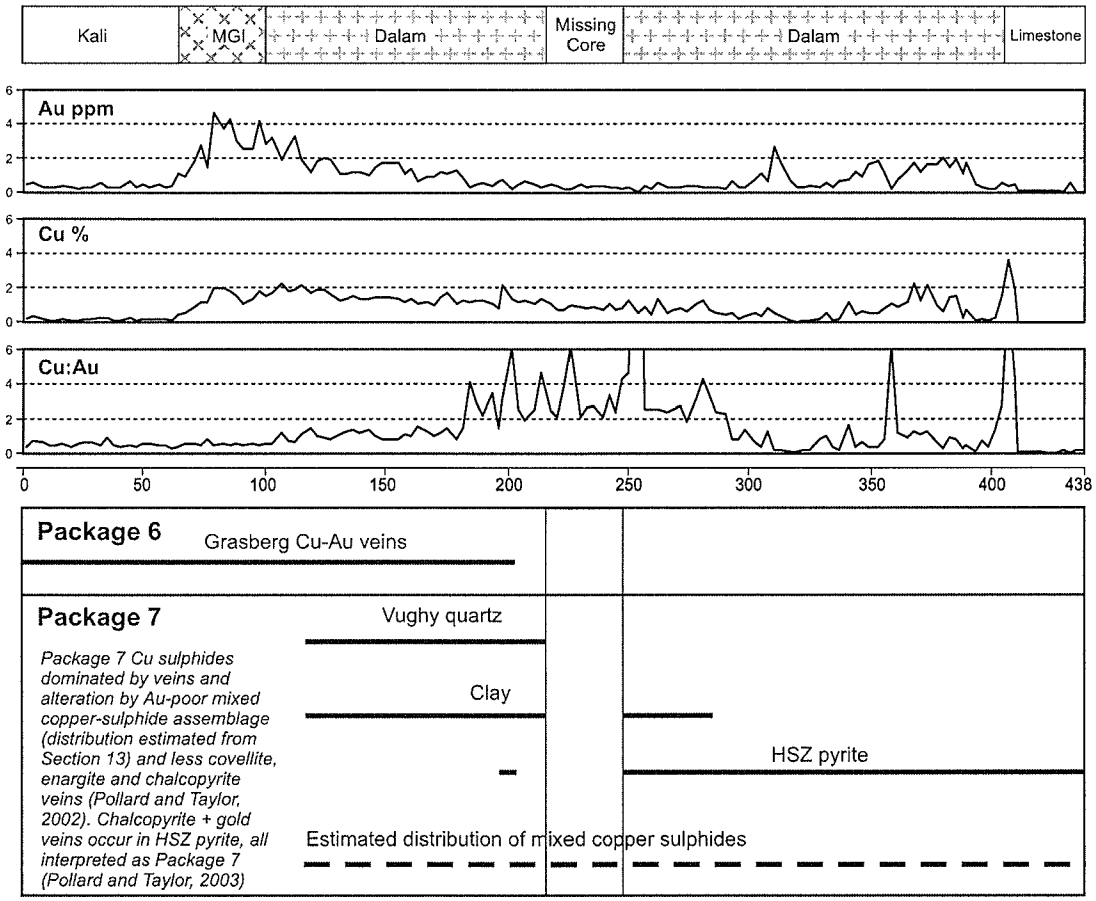

Arbitrary separation of Cu and Au assays

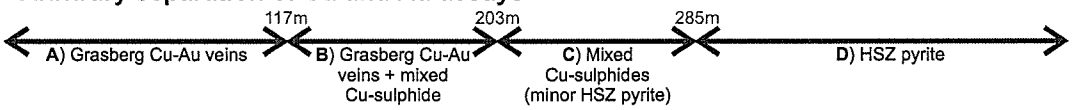

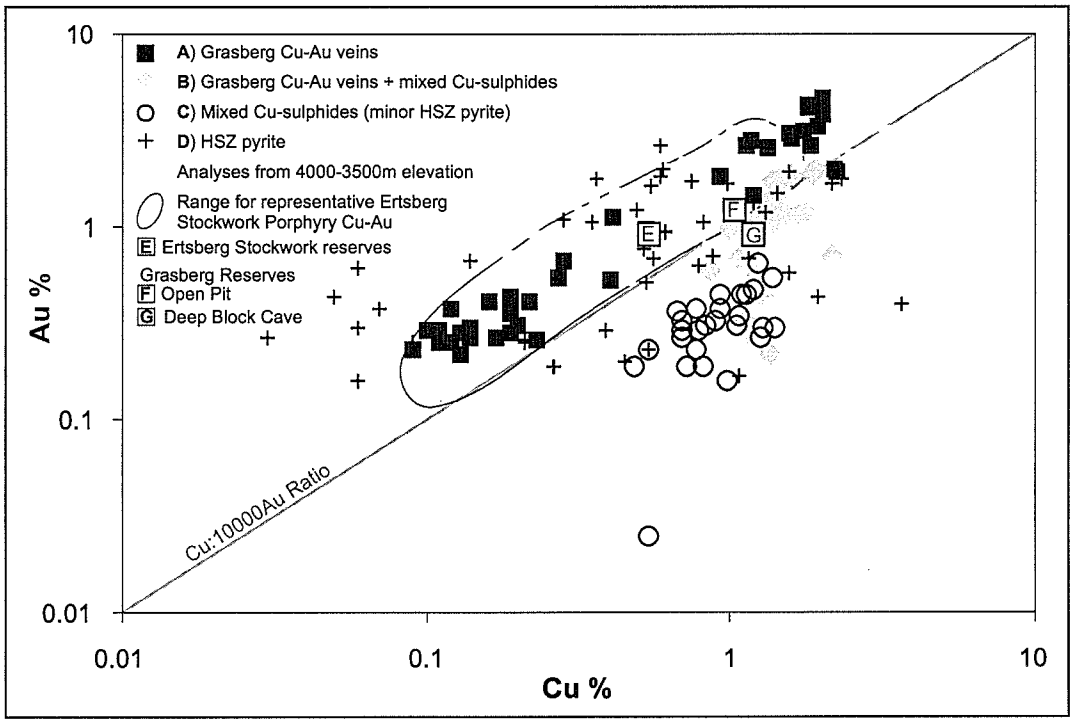

Figure D-14. Range of Cu:10000Au ratios for porphyry-, HS-, skarn Cu-Au and pyrite-Au-As-Zn-Bi-Te mineralisation in the Ertsberg District, Cu:10000Au ratios from Grasberg brine and vapour fluid inclusions and resource-reserves for Ertsberg District deposits. Range for Stockwork Porphyry and HS Cu:10000Au ratios derived from Figure D-13. Range for skarn and pyrite-Au-As-Zn-Bi-Te Cu:10000Au ratios derived from Figure D-11. Cu:10000Au ratios for Grasberg brine and vapour fluid inclusions from Ulrich et al. (1999). Reserves for Grasberg (open pit and block cave), EESS (DOZ=deep ore zone; IOZ=Intermediate ore zone; Ertsberg Stockwork zone), Kucing Liar, DOM (open pit and black cave) and Big Gossan skarn-hosted Cu-Au (Freeport McMoRan Copper & Gold Inc 2002 Annual Report). Possible geological resources for West Grasberg (Brannon, 1991) and Wanagon Gold (Sanusi, 1994) do not report Cu grades and an arbitrary grade of 0.1% Cu has been used. Wanagon skarn-hosted Cu-Au possible geological resource from Sanusi (1994). Ertsberg (Gunung Bijih) historical Reserve figure from Sunyoto (pers comm.).

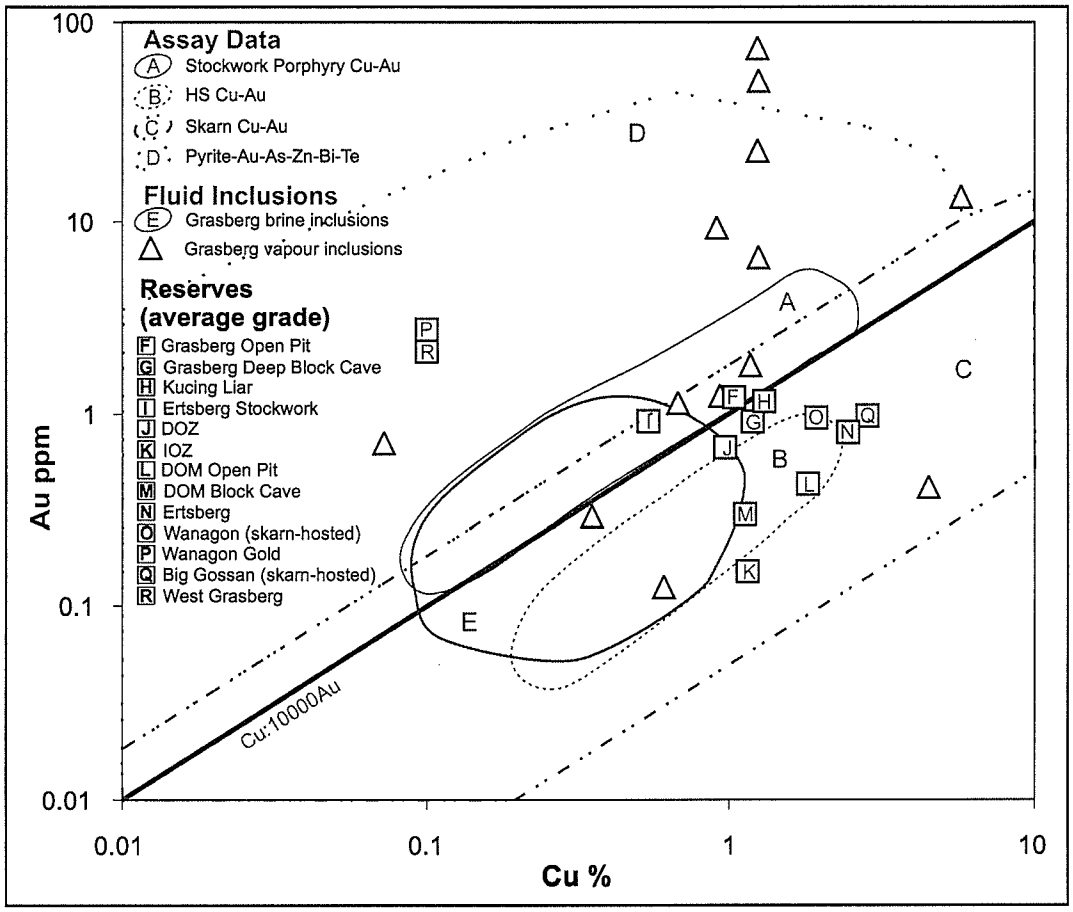

It is possible that some of the intrusive and hydrothermal events developed at the GIC and Ertsberg locations are related temporally and genetically.

II. *The late stage volcanic evolution of the GIC (Section A).* The banded clay at West Grasberg was not an isolated occurrence as banded clay occurrences are also documented on the eastern GIC margin (Section A). Weakly altered tuffs on the northern margin of the GIC and banded clay occurrences suggest late stage volcanic processes operated in the Ertsberg district and that the GIC was open to surface during the later part of its hydrothermal evolution. Neither the banded clay

Figure D-15. Laser ablation results from analysis of pyrite from West Grasberg (Section A), Big Gossan and Wanagon Gold (Section B). A single analysis was conducted on a representative pyrite sample from the heavy sulphide zone (sample A9431-1, 206m courtesy of P. Pollard and R. Taylor; Appendix 7). An analysis was also conducted on an underground late-stage pyrite sample that occurs in veins with minor galena and chalcopyrite and postdates the late-stage carbonate alteration and leaching that occurs in the EESS (Coutts et al., 1999). Full analysis details and sample descriptions in Appendix 1 and 7.

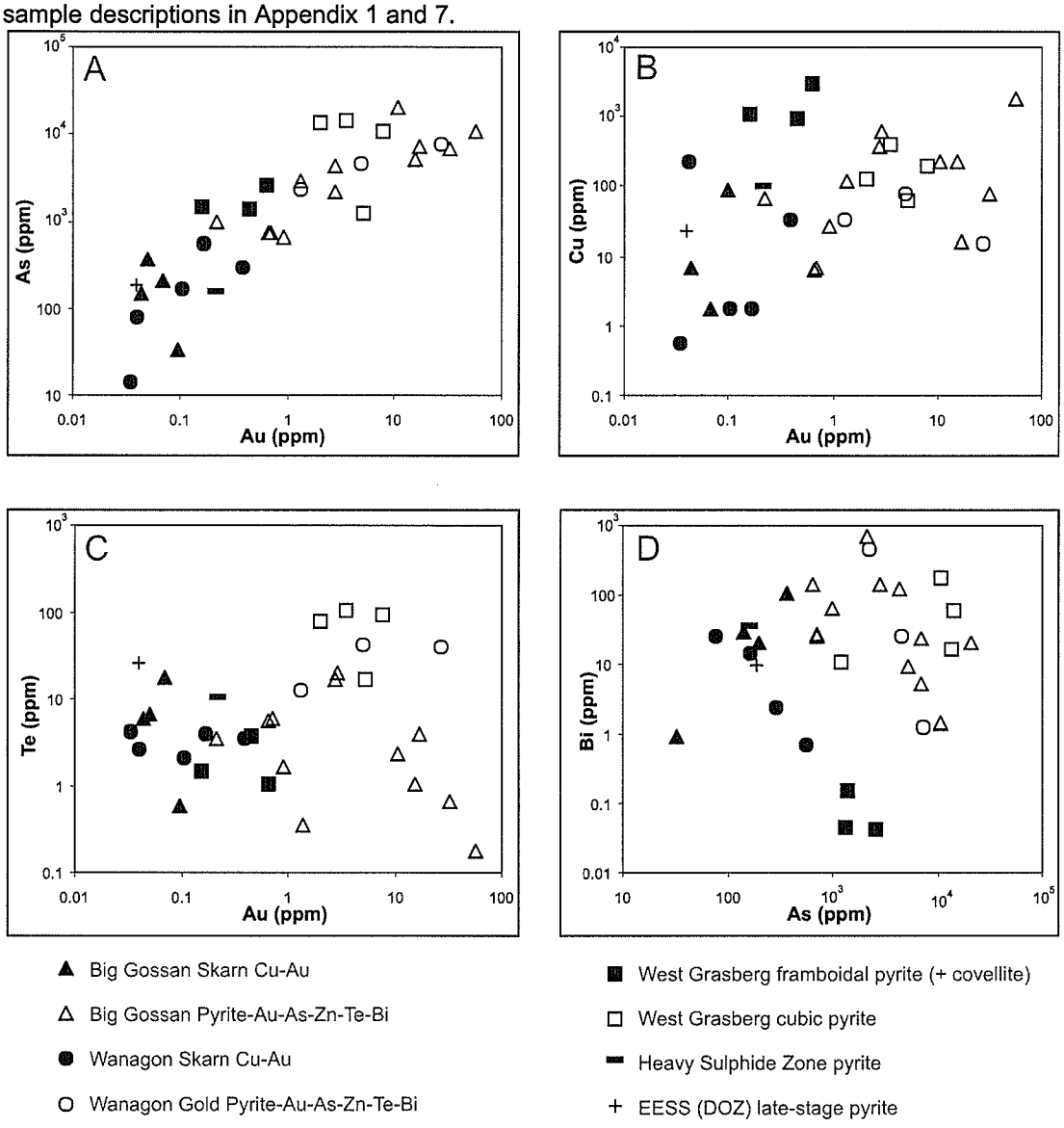

Figure D-16. Correlation between major igneous and hydrothermal events in the Ertsberg District. Description of annotations: A) Early high-temperature potassic alteration in Kucing Liar skarn (Stage I) may correlate with one or more episode of early porphyry-style potassic alteration developed at Grasberg (i.e. Package1 to 4) which has similar fluid inclusion homogenisation temperatures and salinities (Figure D-9; Figure D-10). B) Kucing Liar Stage III chalcopyrite mineralisation may have been coeval with Grasberg main stage sulphides. C) Pb-Zn sulphides developed on the margins of the GIC and appear late in the paragenesis, may correlate with Pb-Zn sulphides developed at West Grasberg (Section A: Pollard and Taylor, 2002). D) Leaching and HS occurrences at Kucing Liar and Grasberg are considered to be genetically related (Pollard and Taylor, 2003). E) West Grasberg gold-pyrite occurrence is tentatively correlated with Kucing Liar and Grasberg HS sulphides (Section A). F) Geochronology is not available to constrain the lower age limit of HS occurrences at Kucing Liar and Grasberg. The occurrence in the EESS (which is <2.67Ma old) may be genetically related to the Grasberg and Kucing Liar occurrences.

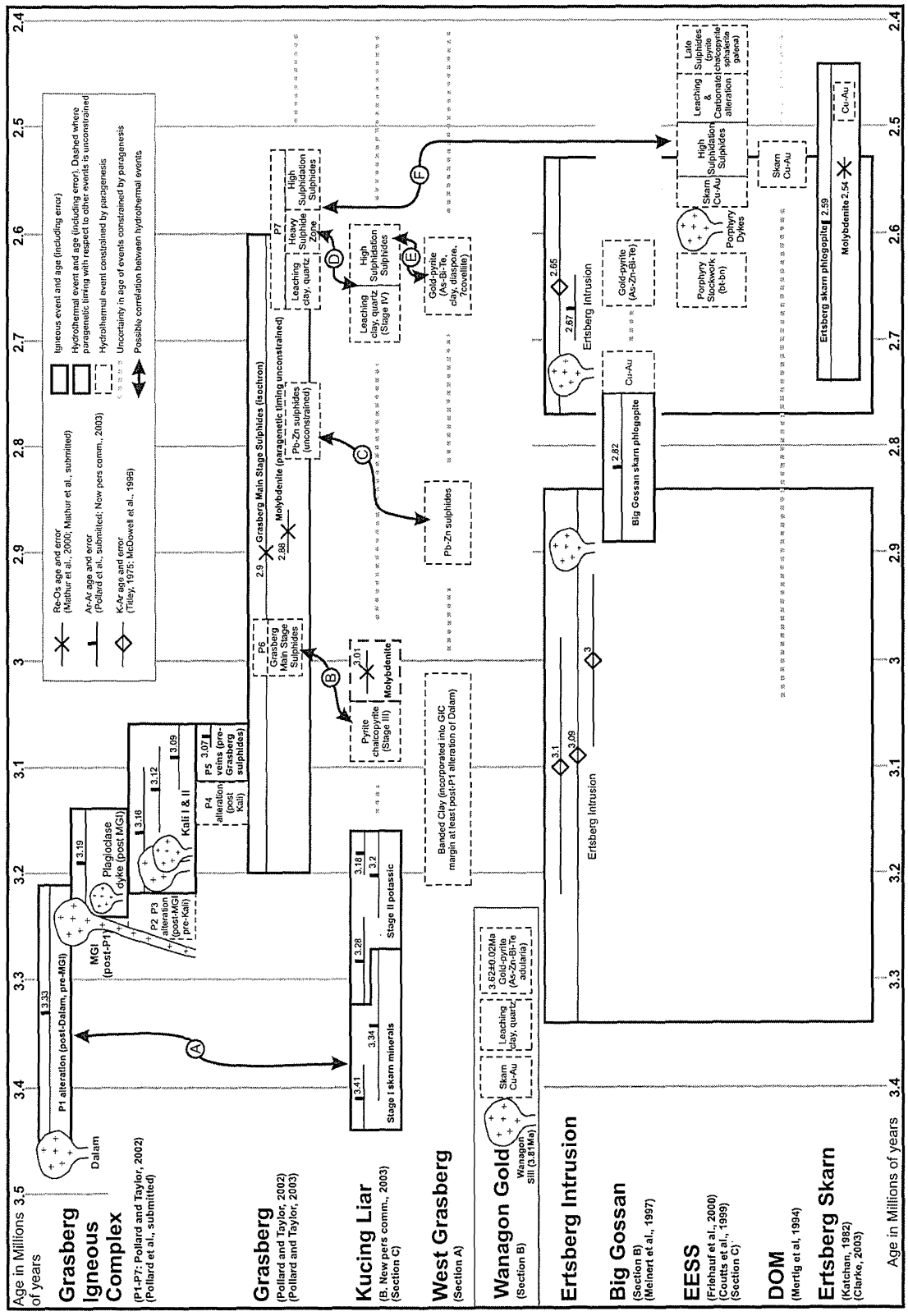
Age in Millions of years
Grasberg Igneous Complex
(P1-P7: Pollard and Taylor, 2002)
(Pollard et al., submitted)
Dalam
P1 alteration (post-Dalam, pre-MGI)
MGI (post-P1)
Plagiodase dyke (post MGI)
P2 P3 alteration (post-MGI pre-Kali)
Kali I & II
P4 alteration (post Kali)
P5 veins (pre-Grasberg sulphides)
Grasberg
(Pollard and Taylor, 2002)
(Pollard and Taylor, 2003)
P6 Grasberg Main Stage Sulphides
Grasberg Main Stage Sulphides (isotrhon)
Molybdenite (paragenetic timing unconstrained)
Pb-Zn sulphides (unconstrained)
P7
Leaching clay, quartz
Heavy Sulphide Zone
High Sulphidation Sulphides
Leaching clay, quartz (Stage IV)
High Sulphidation Sulphides
Gold-pyrite (As-Bi-Te, clay, diaspore, ?covellite)
Pb-Zn sulphides
Kucing Liar
(B. New pers comm., 2003)
(Section C)
Pyrite chalcopyrite (Stage III)
Molybdenite
Stage I skarn minerals
Stage II potassic
Banded Clay (incorporated into GIC margin at least post-P1 alteration of Dalam)
West Grasberg
(Section A)
Wanagon Gold
(Section B)
Wanagon Sill (3.81Ma)
Skarn Cu-Au
Leaching clay, quartz
3.6240.02Ma Gold-pyrite (As-Zn-Bi-Te adularia)
Ertsberg Intrusion
Big Gossan
(Section B)
(Meinert et al., 1997)
Big Gossan skarn phlogopite
Cu-Au
Gold-pyrite (As-Zn-Bi-Te)
EESS
(Friehauf et al., 2000)
(Coutts et al., 1999)
(Section C)
Porphyry Stockwork (Di-bn)
Porphyry Dykes
Skarn Cu-Au
High Sulphidation Sulphides
Late Sulphides (pyrite chalcopyrite sphalerite galena)
Leaching & Carbonate alteration
DOM
(Mertig et al, 1994)
Ertsberg Skarn
(Katchan, 1982)
(Clarke, 2003)
Ertsberg skarn phlogopite 2.59
Molybdenite 2.54
Re-Os age and error (Mathur et al., 2000; Mathur et al., submitted)
Ar-Ar age and error (Pollard et al., submitted; New pers comm., 2003)
K-Ar age and error (Tilley, 1975; McDowell et al., 1996)
Igneous event and age (including error)
Hydrothermal event and age (including error). Dashed where paragenetic timing with respect to other events is unconstrained
Hydrothermal event constrained by paragenesis
Uncertainty in age of events constrained by paragenesis
Possible correlation between hydrothermal events

or tuffs display evidence of extensive GIC porphyry-style alteration (Section A). Additionally McDonald and Arnold (1994) did not document the porphyry-style alteration (i.e. Pollard and Taylor, 2002) in the volcanic cover that they considered to predate GIC intrusions. It is possible some of the volcanic features described by McDonald and Arnold (1994) are related to a late-stage episode of volcanicity responsible for the tuffs and banded clay. Late-stage volcanic activity is common in porphyry environments (Sillitoe, 1997) and may have affected pressure gradients at the GIC.

III. *Correlation of sulphide events at Grasberg and Kucing Liar.* The close spatial relationship between the deposits and similarities in mineralogy and paragenesis of sulphide events suggests they are genetically related (Pollard and Taylor, 2002; 2003: B. New pers comm., 2003). Further geochronology is required to support these observations. As there is no lower age constraint for HS occurrences at Grasberg and Kucing Liar, their genetic relationship to the occurrence in the EESS is unconstrained (Figure D-16).

IV. *Skarn and sulphides at DOM and the EESS have not been dated.* An $^{40}Ar/^{39}Ar$ age of 2.67±0.3Ma for the Ertsberg intrusion near the EESS constrains the maximum age of the overprinting Ertsberg Stockwork, skarn Cu-Au and HS events although the absolute ages are unknown.

V. *Possible genetic relationships for pyrite-Au-As-Zn-Bi-Te occurrences developed at Big Gossan and Wanagon Gold (Section B).* Fluid inclusions from sphalerite and quartz at Big Gossan have an average salinity of 9 wt% $NaCl_{equiv}$ and average homogenisation temperature of 248°C. A direct genetic relationship to earlier skarn Cu-Au is not clear. Pyrite-Au-As-Zn-Bi-Te occurrences are considered to have formed by incursion of a new fluid with a different composition (Section B). Stable isotope geochemistry and further fluid inclusions studies might resolve the relationship between the occurrences and earlier skarn Cu-Au. The many similarities between the Big Gossan and Wanagon Gold occurrences, which are separated by ca. 0.8Ma, indicates that the process controlling their development was not isolated. The fluids responsible for the pyrite-Au-As-Zn-Bi-Te occurrences may represent a deeper, more saline, magmatic precursor to fluids documented from high and low sulphidation deposit styles that manifest at shallower levels and contain significant non-magmatic (i.e. meteoric) water (Corbett and Leach, 1998; Cooke and Simmons, 2000; Hedenquist et al., 2000). The mineralogy of the pyrite-Au-As-Zn-Bi-Te occurrences is similar to that found within a) the 5-6Ma Wabu gold-zinc skarn (Sunyoto, 1999; Meinert, 2000)(Figure D-1), and b)

Cordilleran base metal lode and replacement deposits (Bendezu et al., 2003).

Evolution of the Ertsberg district

The following proposed summary evolution of the Ertsberg district is derived from the new and published information outlined above (Figure D-17):

A) The Wanagon Sill (3.81Ma; Figure D-17a) is postdated by the Wanagon skarn Cu-Au that occurs nearby at depth. The skarn is postdated by the Wanagon Gold pyrite-Au-As-Zn-Bi-Te occurrence which occurred at 3.62Ma. Hydrothermal events at Wanagon Gold are the oldest documented in the district to date. The age of the earliest phase in the GIC, the Dalam phase (>3.33Ma) is within error of the Kucing Liar skarn (3.41-3.18Ma). The age of formation of the Karume intrusion (3.13Ma) is within error of the early Kali intrusions (3.16-3.09Ma). Extensive porphyry-style alteration affected the igneous rocks in the GIC and the same fluids may have been responsible for skarn alteration at Kucing Liar.

B) Incorporation of banded clay into the GIC margin could have been caused by a phreatomagmatic eruption that exposed parts of GIC open to surface during its evolution and would have affected pressure gradients (Section A; Figure D-17b). Timing of diatreme activity is poorly constrained but is considered to be younger than extensive porphyry-style alteration in the GIC and older than cessation of hydrothermal activity at Grasberg. One possibility is that volcanic activity was triggered by replenishment of the magma chamber by mafic magmas (cf. Edmonds et al., 2001; Hattori and Keith, 2001). Early Cu-Au mineralisation at Kucing Liar may correlate with Grasberg main stage sulphides. At least one phase of the Ertsberg Intrusion with unknown spatial extent was emplaced at ca. 3Ma within error of the age of late igneous activity in the GIC. The Big Gossan skarn formed at 2.82Ma (within error of igneous ages at the GIC and Ertsberg).

C) HS occurrences at Kucing Liar and Grasberg developed after formation of the Grasberg main stage sulphides (Figure D-17c). The heavy sulphide zone at Grasberg may also be part of the HS occurrence. The timing of the Lembah

Figure D-17. Evolution of major igneous and hydrothermal events in the Ertsberg district. Marked vertical scale is elevation. Vertical and lateral distribution of all deposits derived from PT Freeport Indonesia geology maps and cross sections. <2km of cover is considered to have been present during emplacement of intrusions (Weiland and Cloos, 1996). Approximate ages (Figure D-4) in millions of years in brackets. Topographic variation of current surface not displayed. The distribution of hydrothermal events moves from NW to SE with decreasing age. a) 3.81-3.08Ma. b) <3.08Ma. c) <2.9Ma. HS occurrences in the district. Timing is unconstrained. d) <2.67Ma.The DOM skarn occurs between 3800m elevation and surface (ca. 4300m). EESS occurs between 3000m elevation (extent of drilling) and surface (ca. 4100m).

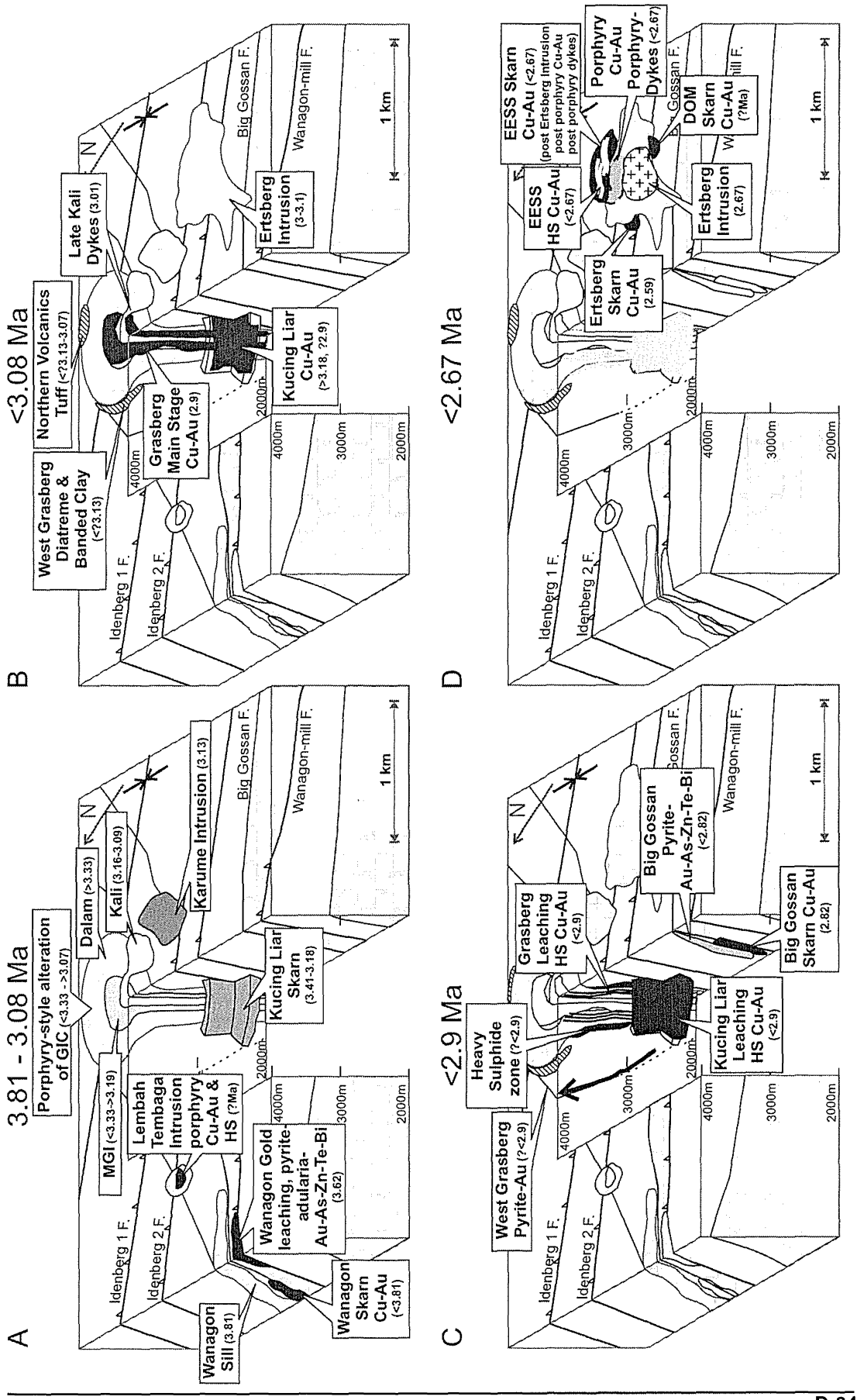
A
3.81 - 3.08 Ma
Porphyry-style alteration of GIC (<3.33 - >3.07)
Dalam (>3.33)
Kali (3.16-3.09)
Karume Intrusion (3.13)
MGI (<3.33->3.19)
Lembah Tembaga Intrusion porphyry Cu-Au & HS (?Ma)
Kucing Liar Skarn (3.41-3.18)
Wanagon Gold leaching, pyrite-adularia-Au-As-Zn-Te-Bi (3.62)
Wanagon Skarn Cu-Au (<3.81)
Wanagon Sill (3.81)
Idenberg 1 F.
Idenberg 2 F.
Big Gossan F.
Wanagon-mill F.
N
1 km
4000m
3000m
2000m
B
<3.08 Ma
West Grasberg Diatreme & Banded Clay (<?3.13)
Northern Volcanics Tuff (<?3.13-3.07)
Late Kali Dykes (3.01)
Grasberg Main Stage Cu-Au (2.9)
Kucing Liar Cu-Au (>3.18, ?2.9)
Ertsberg Intrusion (3-3.1)
C
<2.9 Ma
Heavy Sulphide zone (?<2.9)
West Grasberg Pyrite-Au (?<2.9)
Grasberg Leaching HS Cu-Au (<2.9)
Big Gossan Pyrite-Au-As-Zn-Te-Bi (<2.82)
Kucing Liar Leaching HS Cu-Au (<2.9)
Big Gossan Skarn Cu-Au (2.82)
D
<2.67 Ma
EESS Skarn Cu-Au (<2.67) (post Ertsberg intrusion post porphyry Cu-Au post porphyry dykes)
Porphyry Cu-Au Porphyry-Dykes (<2.67)
EESS HS Cu-Au (<2.67)
Ertsberg Skarn Cu-Au (2.59)
DOM Skarn Cu-Au (?Ma)
Ertsberg Intrusion (2.67)

Tembaga HS occurrence is unconstrained. Due to absence of geochronological constraint at Grasberg and Kucing Liar, an alternative interpretation is that the HS occurrences spatially-associated with the GIC, Ertsberg and Lembah Tembaga may represent a single late event in the history of the district that occurred after development of the EESS (Figure D-17d). The vertical distribution of HS occurrences is significant as they probably extended up to 4km below the paleosurface (Pollard and Taylor, 2003) and are not zoned with respect to the earlier skarn- and porphyry-style deposits (Pollard and Taylor, 2003). Pollard and Taylor (2003) suggested that the HS fluids were tapped from deeper evolving hydrothermal fluids and that HS mineralisation occurred separately to the porphyry systems. Evidence of non-magmatic fluid during Kucing Liar Stage IV leaching, silicification and clay event may indicate the presence of meteoric water. Gold±pyrite at West Grasberg is correlated with HS occurrences at Grasberg and Kucing Liar.

D) The pyrite-Au-As-Zn-Bi-Te occurrence at Big Gossan postdates the skarn Cu-Au (2.82Ma) (Figure D-17d). The Au-As-Bi-Te signature of the occurrences is also manifested at West Grasberg and a Au-As-Bi signature is reported from Kucing Liar although any genetic relationships are unconstrained. A younger phase of the Ertsberg intrusion (2.67Ma) from near the Ertsberg stockwork may be the same generation as that documented near DOM (2.65Ma; Figure D-3). The spatial distribution of the younger phase is unknown. Ertsberg stockwork porphyry Cu-Au and porphyry dykes are developed in the 2.67Ma generation of Ertsberg Intrusion (P. Pollard pers comm., 2003). Friehauf (2000) suggested early porphyry-style mineralisation formed deeper than Grasberg under a hot isotropic stress environment. The EESS postdates porphyry Cu-Au and porphyry dykes and the Ertsberg skarn is dated at 2.59Ma. The timing of the DOM skarn is unconstrained although if it is older than the 2.65Ma Ertsberg intrusion phase it could be coeval with the Ertsberg skarn and EESS (Figure D-3).

Character and sources of igneous and ore deposit components in the district

Both main igneous centres (GIC and Ertsberg) feature igneous rocks post-dated by early porphyry-style mineralisation, spatially related skarn Cu-Au mineralisation and late development of HS style mineralisation with comparable metal ratios in similar deposit types (Figure D-11;Figure D-13; Figure D-14). Two separate pyrite-Au-As-Zn-Bi-Te occurrences (Big Gossan and Wanagon Gold) exhibit similar metal associations and are temporally and spatially associated with older skarn Cu-Au systems.

LA-ICPMS pyrite-chemistry indicates common chemical processes operated in different deposits throughout the district. Variable pyrite chemistry probably reflects different fluid

conditions during deposition. Pyrite with elevated As and Au contents is associated with native gold ± bismuth sulphosalts and tellurides. Native and invisible gold is commonly associated with arsenian pyrite in mesothermal and epithermal deposits (Cathelineau et al., 1989; Cabri et al., 2000; Pokrovski et al., 2001). Textural relationships are consistent with late-stage gold being transported as both $AuHS^-$ and $AuHS^0$ complexes and respectively precipitated by sulphidation reactions and adsorption (Section B).

As hydrothermal fluids in the district are considered to have received insignificant contribution from meteoric sources (discussed below), the features observed in the district are indicative of common magmatic, hydrothermal and chemical processes operating at different times throughout the evolution of the district (Figure D-18).

Tectonics and possible sources for ore deposit components in the Ertsberg district

Several different sources for igneous components and metals have been proposed for the Ertsberg District and similar tectonic settings (Figure D-18). Although timing and longevity of active Australian Plate subduction beneath New Guinea remains unclear, the Proterozoic and or Archean Australian crust is known to have contributed to Ertsberg district magmas (Simons et al., 1999; Housh and McMahon, 2000; Hill et al., 2002; Quarles Van Ufford and Cloos, submitted) and may also have contributed metals. It is clear from evidence in the Ertsberg district that emplacement of magmas and related mineralisation was intimately related to dilational strike-slip faulting resulting from a change in Pacific

Figure D-18. Possible sources and mechanisms responsible for fluids, metals, and igneous components in the Ertsberg district. **I)** Sources for fluids, metals, and igneous components in the Ertsberg district. **II)** Evolution of porphyry and HS occurrences a) Porphyry alteration. Example: Grasberg uneconomic porphyry-style alteration: Package 1 to 4 (Pollard and Taylor, 2002). b) Porphyry Cu-Au. Example: Grasberg pre mineralisation anhydrite (Package 5) and Package 6 quartz and copper-gold mineralisation (Pollard and Taylor, 2002). Appearance of sulphur-bearing phases. c) HS leaching, clay and quartz development. Example: Grasberg Package 7 (Pollard and Taylor, 2002) and Kucing Liar (B. New pers comm., 2003). Possible fluid conditions from Kucing Liar Stage IV (Figure D-10). d) HS Cu-Au. Example: Grasberg Package 7 (Pollard and Taylor, 2002) and Kucing Liar (B. New pers comm., 2003). Possible fluid conditions for Cu-Au – bearing fluid from Kucing Liar Stage V (Figure D-10). **III)** Evolution of skarn Cu-Au and pyrite-Au-As-Zn-Bi-Te occurrences. e) Skarn alteration and magnetite. Phase separation models from Big Gossan (Meinert et al., 1997; Meinert et al., 2003). f) Skarn hosted Cu-Au mineralisation. Phase separation models from Big Gossan (Meinert et al., 1997; Meinert et al., 2003). g) Pyrite-Au-As-Zn-Bi-Te mineralisation. Example: Big Gossan and Wanagon Gold (Section B). Three possible magmatic hydrothermal fluid processes. See text for discussion. Sources of information: [1] (Housh and McMahon, 2000); [2] (James, 2000a); [3] (Mathur et al., 2000); [4] (Mathur et al., submitted); [5] (Soloman, 1990); [6] (McInnes et al., 2001; McInnes et al., 1999); [7] (Pollard et al., submitted); [8] (Meinert et al., 1997; Meinert et al., 2003); [9] (Quarles Van Ufford, 1996); [10] (Pollard and Taylor, 2002); [11] (James, 2000b); [12] (Sapiie, 1998), [13] (Heinrich et al., 1999; Ulrich et al., 1999); [14] (Heinrich, 2003); [15] (Shinohara, 1994; Burnham, 1997); [16] (Cline and Bodnar, 1991); [17] (Williams et al., 2003); [18] (Shinohara and Hedenquist, 1997); [19] (Edmonds et al., 2001); [20] (Bodnar et al., 1985); [21] (Lowenstern, 2000, 2001). Refer to figures, text and respective references for details regarding sulphur isotopes (Figure D-5), stable isotopes (Figure D-7; Figure D-8), fluid inclusion temperature and salinity results (Figure D-9; Figure D-10) and description of alteration-mineralisation styles.

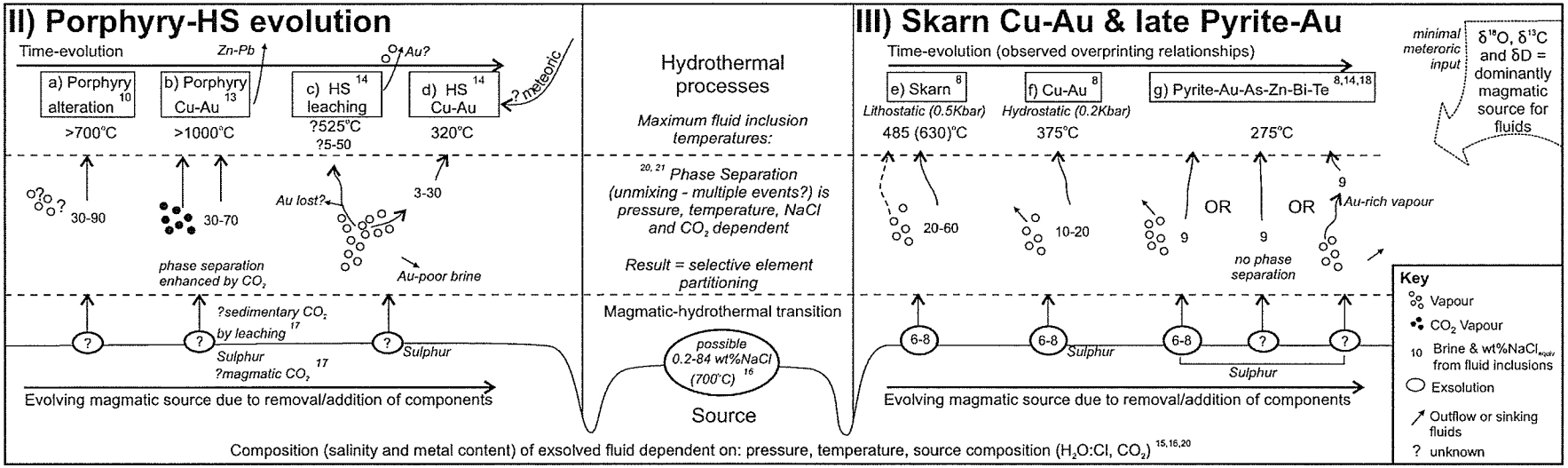
II) Porphyry-HS evolution
Time-evolution
Zn-Pb
Au?
a) Porphyry alteration 10
b) Porphyry Cu-Au 13
c) HS 14 leaching
d) HS 14 Cu-Au
? meteoric
>700°C
>1000°C
?525°C
?5-50
320°C
30-90
30-70
Au lost?
3-30
phase separation enhanced by CO2
Au-poor brine
?sedimentary CO2 by leaching 17
Sulphur
?magmatic CO2 17
Sulphur
Evolving magmatic source due to removal/addition of components
Hydrothermal processes
Maximum fluid inclusion temperatures:
20, 21 Phase Separation (unmixing - multiple events?) is pressure, temperature, NaCl and CO2 dependent
Result = selective element partitioning
Magmatic-hydrothermal transition
possible 0.2-84 wt%NaCl (700°C) 16
Source
III) Skarn Cu-Au & late Pyrite-Au
Time-evolution (observed overprinting relationships)
e) Skarn 8
f) Cu-Au 8
g) Pyrite-Au-As-Zn-Bi-Te 8,14,18
Lithostatic (0.5Kbar)
Hydrostatic (0.2Kbar)
485 (630)°C
375°C
275°C
minimal meteoric input
δ18O, δ13C and δD = dominantly magmatic source for fluids
20-60
10-20
9
OR
9
OR
9
Au-rich vapour
no phase separation
6-8
6-8
Sulphur
6-8
Sulphur
Evolving magmatic source due to removal/addition of components
Key
Vapour
CO2 Vapour
10 Brine & wt%NaCl equiv from fluid inclusions
Exsolution
Outflow or sinking fluids
? unknown
Composition (salinity and metal content) of exsolved fluid dependent on: pressure, temperature, source composition (H2O:Cl, CO2) 15,16,20

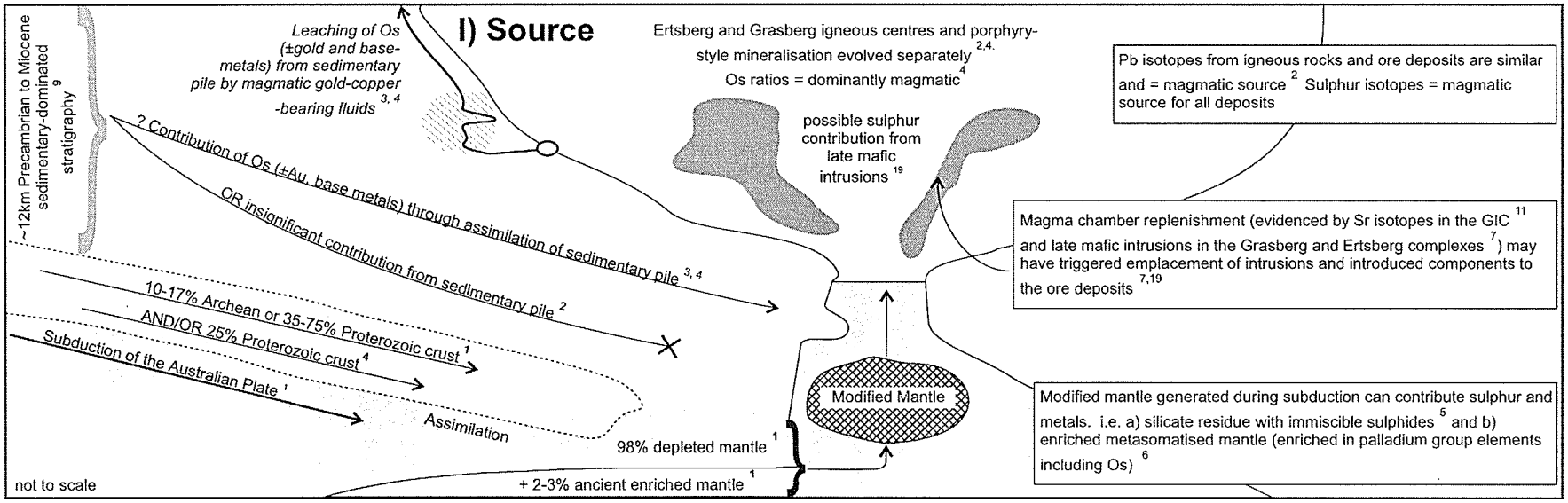
I) Source
~12km Precambrian to Miocene sedimentary-dominated stratigraphy 9
Leaching of Os (±gold and base-metals) from sedimentary pile by magmatic gold-copper -bearing fluids 3, 4
Ertsberg and Grasberg igneous centres and porphyry-style mineralisation evolved separately 2,4.
Os ratios = dominantly magmatic 4
possible sulphur contribution from late mafic intrusions 19
Pb isotopes from igneous rocks and ore deposits are similar and = magmatic source 2 Sulphur isotopes = magmatic source for all deposits
? Contribution of Os (±Au, base metals) through assimilation of sedimentary pile 3, 4
OR insignificant contribution from sedimentary pile 2
10-17% Archean or 35-75% Proterozoic crust 1
AND/OR 25% Proterozoic crust 4
Subduction of the Australian Plate 1
Assimilation
Magma chamber replenishment (evidenced by Sr isotopes in the GIC 11 and late mafic intrusions in the Grasberg and Ertsberg complexes 7) may have triggered emplacement of intrusions and introduced components to the ore deposits 7,19
Modified Mantle
98% depleted mantle 1
+ 2-3% ancient enriched mantle 1
Modified mantle generated during subduction can contribute sulphur and metals. i.e. a) silicate residue with immiscible sulphides 5 and b) enriched metasomatised mantle (enriched in palladium group elements including Os) 6
not to scale

Plate movement at ca. 5Ma (Barley et al., 2002). It is not clear whether the mechanism responsible for melting magmatic material was crustal thickening (Macpherson and Hall, 2002) during orogenesis (Hill et al., 2002), delamination due to stalled slab subduction (Housh and McMahon, 2000), or was otherwise related to the change in direction of Pacific Plate motion at ca. 5Ma. Nonetheless, the subduction setting has been identified as a significant feature in southwest Pacific and southeast Asia gold deposits (Sillitoe, 2000; Barley et al., 2002) where metal enrichment can be enhanced by processes such as two-stage melting and metasomatic alteration (Soloman, 1990; Sillitoe, 1997; McInnes et al., 2001; Macpherson and Hall, 2002).

Sulphur isotope ratios indicate a consistent magmatic sulphur source for all metal occurrences except in a limited number of samples from Kucing Liar and SW Grasberg (Figure D-5). It has been established in other locations that intrusion of mafic magma into andesitic or felsic magma chambers can trigger eruption and recharge sulphur contents (Edmonds et al., 2001; Hattori and Keith, 2001). A similar process may have occurred in the Ertsberg District (Figure D-18) where magma chamber replenishment and late mafic intrusions are observed (James, 2000b; Pollard and Taylor, 2003). The introduction of sulphur-bearing phases (i.e. anhydrite, sulphides or native sulphur) late in the paragenesis of porphyry, skarn and HS ore deposits may also be related to the timing of introduction of sulphur supplied by mafic-bearing intrusions (Figure D-18).

Interpretations of radiogenic isotope data from igneous rocks and ore deposits in the district are conflicting (Figure D-18). Pb, Nd and Sr isotope results suggest that there was insignificant contribution to the igneous suite or ore deposits in the district from the underlying exposed Precambrian-Miocene rocks (James, 2000a). However, Re-Os results have been used to propose a continental crustal source for some of the Os and by inference, other metals (Mathur et al., 2000; Mathur et al., submitted).

The source of Os is only an approximation of sources for base-metals and gold as it does not have exactly the same behaviour in hydrothermal fluids (Mathur et al., submitted). The Os (± ore metals) are considered to be derived either by leaching or assimilation of the sedimentary pile (Figure D-18)(Mathur et al., 2000; Mathur et al., submitted). Black shales, which contain larger concentrations of Re, Os and other metals compared to other sedimentary lithologies, may have been important (Mathur et al., 2000; Mathur et al., submitted) although no single lithological source has been identified in the exposed sedimentary pile. Other sources that may have contributed Os (± metals) include unexposed Australian basement assemblages and or partial melting of enriched metasomatised lower crust (Figure D-18)(McInnes et al., 1999).

Fluid sources in the Ertsberg district.

The hydrothermal features currently exposed in the Ertsberg district are considered to have formed at between <2-4km depth (Pollard and Taylor, 2003; Weiland and Cloos, 1996). The textural evidence indicates that ore-deposit fluids were sourced from deeper levels and not from the adjacent igneous bodies (Pollard and Taylor, pers comm. 2003). No evidence of classic epithermal low or high sulphidation deposits (Cooke and Simmons, 2000; Hedenquist et al., 2000) have been documented although they may have been present in the <2km of cover that has been removed from the district (Weiland and Cloos, 1996).

Although deep circulation and interaction between surface waters is traditionally implicated in porphyry-terrains (Taylor, 1997), more recently it has been demonstrated that primary magmatic fluids can be dominant (Harris and Golding, 2002; Meinert et al., 2003). Even though the stable isotope dataset for the district is not entirely representative of the ore-stage fluids, the evidence indicates that non-magmatic fluids (including local meteoric water) have not made a significant contribution to hydrothermal fluids in most deposits.

At high elevation, δD is sufficiently lower than that of the range for magmatic values to enable discrimination between magmatic and meteoric fluid sources (Taylor, 1997). Results from Kucing Liar, Grasberg and Big Gossan hydrous minerals display $\delta^{18}O_{FLUID}$ consistent with a magmatic origin and a wide range in δD (Figure D-7). The wide range of depleted δD values at Kucing Liar and Grasberg do not appear to display evidence of contribution from meteoric sources. However, although the δD and $\delta^{18}O_{FLUID}$ values for Stage IV muscovite and serpentine at Kucing Liar do not display evidence of a meteoric signature, calculated $\delta^{18}O_{FLUID}$ for Stave IV quartz, talc and muscovite do (Figure D-7).

$\delta^{18}O_{FLUID}$ calculations from $\delta^{18}O_{SMOW}$ and $\delta^{13}C_{PDB}$ analyses from the Ertsberg district (Section C; Figure D-8) are dependent on the availability of reliable information for the temperature of formation. From $\delta^{18}O_{FLUID}$ calculations, evidence for contribution of fluids from a meteoric source (lower $\delta^{18}O_{FLUID}$ values) has only been observed in silicate (B. New pers comm., 2003) and carbonate (Section C) stable isotope results from Kucing Liar (Figure D-7; Figure D-8). Although temperature is unconstrained for Stage IV carbonate alteration (Section C; Figure D-8), which occurs peripheral to Kucing Liar, calculated $\delta^{18}O_{FLUID}$ values (assuming a temperature of 300-400°C; B. New pers comm., 2003) are lower than magmatic values (Figure D-7). Recalculation of Kucing Liar quartz-H_2O fractionation (Zheng, 1993) for Stage IV samples from within Kucing Liar, utilising the full range of fluid inclusion evidence available (B. New pers comm., 2003) demonstrates that accurate assessment of the $\delta^{18}O$ values of the fluid is strongly dependent on temperature constraints of the fluid (Figure D-7). If quartz was precipitated at higher temperatures than an arbitrary

Phase separation, which promotes selective partitioning of components into vapour and brine, has been demonstrated to play a significant role in transportation of orebody components at Grasberg (Heinrich et al., 1999; Ulrich et al., 1999; Williams et al., 2003; Fu et al., 2003a; Fu et al., 2003b). Phase separation is governed by a combination of conditions including pressure, temperature, X_{NaCl} (Figure D-19) and CO_2 content (Bodnar et al., 1985; Lowenstern, 2000, 2001). The presence of the volatile CO_2 enhances immiscibility and induces the formation of CO_2-rich vapours and Cl-rich hydrosaline brine at crustal pressures (<5Kbar) (Lowenstern, 2000, 2001).

CO_2 recognised in Grasberg vapour inclusions is believed to indicate immiscibility at low pressures from magmatically derived fluids from a deep chamber (Fu et al., 2003a). Whether the CO_2 was derived by assimilation and/or fluid circulation involving the carbonate country rocks or from a deep-seated magmatic source is unclear (Figure D-18)(Williams et al., 2003). The role of CO_2 as a volatile in other hydrothermal fluids in the Ertsberg district is less constrained although $\delta^{18}O_{SMOW}$ and $\delta^{13}C_{PDB}$ carbonate isotope results from the Big Gossan and DOM skarns display values interpreted to represent a magmatic signature (Figure D-8; Section C).

Between 2-4km at the depth of district orebody formation, pressures correspond to 0.5-1kbar under lithostatic conditions and 0.2-0.4kbar under hydrostatic conditions. High salinity, high temperature fluids are considered responsible for formation of porphyry-style alteration at Grasberg (30-90 wt%$NaCl_{equiv}$, >700°C; Figure D-18). If significant CO_2 is not involved, at high temperature and salinity, phase separation will not take place (Figure D-19)(Bodnar et al., 1985). It is possible that some of the high temperature, high salinity fluids indicated by fluid inclusion studies represent fluid directly exsolved from the magma chamber that have not undergone phase separation (Figure D-19).

Following phase separation, S, Cu, As and Au can be selectively partitioned into the vapour phase (Heinrich, 2003). Modelling suggests the vapour can cool and condense into an aqueous liquid without further phase transition (cf. Heinrich, 2003). With downward retraction of isotherms, the vapour and condensate may have been responsible for producing the deep-intermediate HS leaching and Cu-Au mineralisation observed at Kucing Liar and Grasberg although minimal fluid contribution from meteoric sources is suggested from Kucing Liar stable isotopes (Figure D-18)(cf. Heinrich, 2003).

Lower salinity fluids (i.e. <10wt% $NaCl_{equiv}$) interpreted to have a dominantly magmatic origin from their calculated stable isotope compositions (Section C: Meinert et al., 2003)

350°C (B. New pers comm., 2003), $\delta^{18}O_{FLUID}$ values are more consistent with a magmatic source (Figure D-7).

Depending on the temperature of DOM skarn dolomite (estimated from fluid inclusion results from the adjacent skarn; Mertig, 1995), the $\delta^{18}O_{FLUID}$ calculations could be consistent with formation from magmatic fluids (Figure D-8; Section C). Carbonate and silicate stable isotope results from Big Gossan (Figure D-7; Figure D-8; Section C) are consistent with magmatic fluid sources. Ultimately, the role of external non-magmatic fluids in the district will only be resolved through further fluid inclusion and stable isotope investigations.

Character of magmatic hydrothermal fluids in the Ertsberg district

The character of exsolved magmatic fluids will be affected by the changing composition of the source magma chamber/s due to crystallisation, removal of components by exsolution or influx of new magma. Modelling indicates that salinity (wt.% NaCl) of the exsolved fluid can reach between <0.2 to saturation (i.e. 84 wt.% NaCl at 700°C)(Cline and Bodnar, 1991; Burnham, 1997). Factors that significantly influence the salinity and metal content of exsolved fluids (Figure D-18) include the H_2O:Cl ratios of the magma and the effects of pressure and temperature (Bodnar et al., 1985; Cline and Bodnar, 1991; Shinohara, 1994; Burnham, 1997).

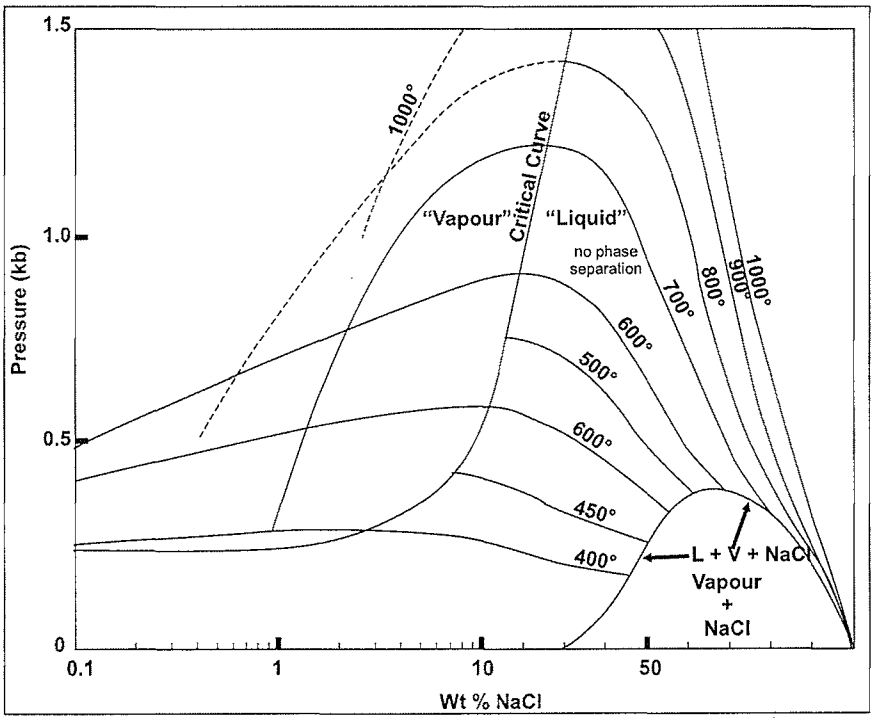

Figure D-19. Experimental data for the relationship between pressure, temperature and salinity. (modified from Sourirajan and Kennedy, 1962; Bodnar et al., 1985 and references therein). Assuming no CO_2 is present and lithostatic pressure for Grasberg porphyry alteration (0.5-1kbar), an exsolved fluid between 30-70 wt%NaCl will not separate into a low density, low salinity vapour and a high density, high salinity brine at 700°C.

are observed in two different and overprinting mineralisation styles at Big Gossan (Figure D-18). Meinert et al. (1997; 2003) considered that different episodes of phase separation of exsolved magmatic fluid (assuming an exsolved salinity of 6-8wt% NaCl) at Big Gossan accounted for the magmatic low salinity fluids (Figure D-18). This mechanism may also have produced the fluids responsible for pyrite-Au-As-Zn-Bi-Te mineralisation at Big Gossan (Section B).

Alternatively, at sufficiently low temperature gradients, phase separation may not occur (Figure D-18)(cf. Shinohara and Hedenquist, 1997). A further possible origin for the late-stage low salinity magmatic fluid responsible for pyrite-Au-As-Zn-Bi-Te mineralisation at Big Gossan and Wanagon Gold is a condensed gold-bearing vapour (Figure D-18)(cf. Heinrich, 2003).

With the exception of pyrite-Au-As-Zn-Bi-Te style mineralisation developed at Big Gossan and Wanagon Gold (Section B), and the presence of high concentrations of Zn and Pb in Grasberg fluid inclusions (Heinrich et al., 1999; Ulrich et al., 1999; Williams et al., 2003) no significant Zn or Pb-bearing deposits have been discovered in the district although they occur elsewhere in Papua (i.e. Cabung Biru and Wabu; Figure D-1). The Pb and Zn component in fluids at Grasberg, as suggested in fluid inclusion analyses (Heinrich et al., 1999; Ulrich et al., 1999; Williams et al., 2003; Fu et al., 2003a; Fu et al., 2003b), may have been deposited at higher elevations (and has been subsequently eroded) or dispersed into the water table (Figure D-18).

The mineral deposits developed in the Ertsberg district display affinities with gold deposits related to alkaline magmatism (Jensen and Barton, 2000). Characteristic features in the Ertsberg District include: Au-rich porphyry (i.e. Grasberg) and Au+Te-rich mineralisation (i.e. pyrite-Au-As-Zn-Bi-Te occurrences), voluminous K metasomatism (i.e. Grasberg porphyry alteration and adularia at Wanagon Gold), carbonation (i.e. Grasberg CO_2-bearing fluid inclusions and magmatic CO_2 in skarns) and poorly developed hydrolytic (acid) alteration (i.e. HS occurrences) (Jensen and Barton, 2000).

Conclusions

Compilation of previous work and new results has allowed partial synthesis of the evolution of the Ertsberg district. The compilation reveals temporal and spatial relationships between different deposit styles and suggests cyclical processes in the deeper chamber that sourced magmas and hydrothermal fluids. Similar hydrothermal systems developed at different times including a) the pyrite-Au-As-Zn-Bi-Te occurrences characterised in this investigation, and b) the separate GIC and Ertsberg igneous complexes which each feature igneous events post-dated by early porphyry-style mineralisation, spatially related skarn Cu-Au

mineralisation and late development of HS style mineralisation.

Sulphur isotope compositions from this and other studies in the district have a narrow range consistent with magmatic values. The source of the metals is less well constrained. The tectonic setting of the district above a subduction zone and emplacement of igneous and hydrothermal components coincident with a change in tectonic processes is analogous to other metal-rich porphyry-districts where two stage melting is considered to contribute to metal enrichment. Pb, Sr and Nd isotope studies imply insignificant interaction with the underlying 12km of Precambrian-Miocene sedimentary pile. 10-17% of Archaean or 35-75% of Proterozoic assimilant is assumed in assimilation-fractional crystallisation models. Re-Os isotopes suggest the underlying sedimentary pile could have been a source for some of the metals in the district by either leaching or assimilation although Os and other metals may also be concentrated by deep metasomatic mantle processes.

Fluids responsible for the ore-deposits in the district were sourced from deeper levels and not from the proximal intrusive igneous bodies. The deposits were formed between <2-4km and potentially deeper in a carbonate-dominated sedimentary terrain. Late stage diatreme and volcanic activity documented in this investigation on the GIC margin at West Grasberg, is similarly observed in other porphyry districts and may suggest shallower depths and hence lower pressure gradients in the evolution of the GIC and Grasberg.

Fluid inclusion studies from different deposits are inconclusive in respect to the source of fluids. New $\delta^{18}O$ and $\delta^{13}C$ data from carbonate alteration and infill complement other stable isotope studies and imply that external non-magmatic fluids may have had minimal influence on the genesis of ore deposits in the Ertsberg district. Lower $\delta^{13}C$ values in hydrothermal carbonates compared with the unaltered carbonate host rocks suggest magmatically derived CO_2 may have been present in hydrothermal fluids in the district. Influence from non-magmatic waters has been demonstrated in both new and previous results from the leaching, quartz and clay event at Kucing Liar.

No classic epithermal or significant Pb-Zn deposits are observed in the district. Late-stage pyrite-Au-As-Zn-Bi-Te occurrences may represent a deeper, more saline precursor to shallow high or low sulphidation deposit styles observed in other districts. Laser ablation analyses of pyrites from different ore systems directly reflect different fluid chemistry at time of deposition.

Acknowledgements

PT Freeport Indonesia is acknowledged for logistical and analytical support and permission to publish this work. An Australian Institute of Geologists Student Bursary provided valuable

additional funding for LA-ICPMS analyses. The LA-ICPMS analyses in this paper are from contribution XXXX from the ARC National Key Centre for Geochemical Evolution and Metallogeny of Continents (GEMOC). GEMCOM software generously provided a full version of its software at cost (educational license). Thank you also to Brian New, Mark Cloos, Peter Pollard, Roger Taylor, Ryan Mathur and Kurt Friehauf for providing feedback and access to unpublished information. James Lally is thanked for drafting a number of the diagrams.

References

Afifi, A. M., Kelly, W. C., and Essene, E. J., 1988, Phase relations among tellurides, sulphides, oxides: 1. Thermochemical data and calculated equilibria: Economic Geology, v. 83, p. 377-394.

Agnew, P., 1998, Freeport joint venture fault trace exploration in COW A: Stage 1 preliminary geochemistry and PIMA orientation results, Unpublished report (FP/97/19) for PT Freeport Indonesia.

Allen, J. M., 1991, Placer gold in the Otomona river, Irian Jaya, Indonesia: Physical Characteristics, Composition, Associated Minerals, Source Areas and Significance, Unpublished report (CMS390) for PT Freeport Indonesia.

Allen, J. M., 1992a, Petrology of 17 drill core samples from BG-1 with notes on gold detection, mineralogical zoning, thermal and PH_2O vectors and location of porphyry and skarn source region, Unpublished report (CMS448) for PT Freeport International.

Allen, J. M., 1992b, Skarn mineralogy, alteration, veining and mineralisation in drill core samples from holes BG 1-5, 1-6 and 1-7a, Big Gossan, Irian Jaya, Unpublished report (CMS489) for PT Freeport Indonesia.

Allen, J. M., 1993c, Gold from the Concentrator, Tembagapura Mill, Irian Jaya, Unpublished report (WOC 93-037) for PT Freeport Indonesia.

Allen, J. M., 1993d, Mineralogy and sources of alluvial gold and associated minerals from the Upper Otomona river between Waa and the Mill site, Unpublished report (CMS533) for PT Freeport Indonesia.

Allen, J. M., and Coote, A., 1993, Alluvial gold in three panconcentrates from the Minajewri river, Irian Jaya, Unpublished report (CMS525) for PT Freeport Indonesia.

Allen, J. M., and Palmer, K., 1992, Placer gold in the Otomona river and terraces, Irian Jaya: mineralogy, source areas and mining potential., Unpublished report (CMS474) for PT Freeport Indonesia.

Allen, J. M., Palmer, K., and Paterson, L., 1994, Gold in the concentrator, Tembagapura mill, Irian Jaya, Unpublished report (WOC 94-037) for PT Freeport Indonesia.

Atwood, G. W., 1989a, West Grasberg drilling program: update, Unpublished report for PT Freeport International.

Atwood, G. W., 1989b, West Grasberg metallurgical samples, with results from F11 74 lab attached, Unpublished report for PT Freeport International.

Baker, E. M., 1987, Geologic, petrographic and fluid inclusion study of breccia hosted gold mineralisation at Kidston, north Queensland: Unpub. PhD thesis, James Cook University of North Queensland, 409 p.

Baker, E. M., Kirwin, D. J., and Taylor, R. G., 1986, Hydrothermal breccia pipes, EGRU Contribution, 12. July, 1986.

Baker, T., 2002, Emplacement depth and carbon dioxide-rich fluid inclusions in intrusion-related gold deposits: Economic Geology, v. 97, p. 1111-1117.

Barley, M. E., Rak, P., and Wyman, D., 2002, Tectonic controls on magmatic-hydrothermal gold mineralisation in the magmatic arcs of SE Asia, *in* Blundell, D. J., Neubauer, F., and Von Quadt, A., eds., The timing and location of major ore deposits in an evolving orogen, Geological Society, London, Special Publications, 204, p. 39-47.

Barnes, H. L., 1979, Solubilities of ore minerals, *in* Barnes, H. L., ed., Geochemistry of hydrothermal ore deposits, John Wiley and Sons, Inc., p. 509-567.

Bendezu, R., and Fontbote, L., 2002, Late timing for high sulphidation Cordilleran base metal lode and replacement deposits in porphyry-related districts: the case of Colquijirca, central Peru: SGA News, v. 13, p. 1, 9-13.

Bendezu, R., Fontbote, L., and Cosca, M., 2003, Relative age of Cordilleran base metal lode and replacement deposits, and high sulphidation Au-(Ag) epithermal mineralisation in the Colquijirca mining district, Peru: Mineralium Deposita, v. 38, p. 683-694.

Bodnar, R. J., 1993, Revised equation and table for determining the freezing point depression of H_2O-NaCl solutions: Geochimica et Cosmochimica Acta, v. 57, p. 683-684.

Bodnar, R. J., Burnham, C. W., and Sterner, S. M., 1985, Synthetic fluid inclusions in natural quartz. III. Determination of phase equilibrium properties in the system H_2O-NaCl to 1000C and 1500 bars: Geochimica et Cosmochima Acta, v. 49, p. 1861-1873.

Brannon, C. A., 1991, West Grasberg project: summary report, Unpublished report for PT Freeport Indonesia, p. 12.

Brown, P. E., 1998, Fluid inclusion modelling for hydrothermal systems, *in* Richards, J. P., and Larson, P. B., eds., Techniques in hydrothermal ore deposits geology: Reviews in Economic geology, Volume 10, Society of Economic Geologists.

Browne, P. R. L., 1978, Hydrothermal alteration in active geothermal fields: Annual Reviews in Earth and Planetary Sciences, v. 6, p. 229-250.

Browne, P. R. L., and Ellis, A. J., 1970, The Ohaaki-Brodlands geothermal area, New Zealand: Mineralogy and related geochemistry: American Journal of Science, v. 269, p. 97-131.

Burnham, C. W., 1997, Magmas and hydrothermal fluids, *in* Barnes, H. L., ed., Geochemistry of hydrothermal ore deposits - 3rd edition, John Wiley & Sons, Inc. United States of America, p. 63-123.

Cabri, L. J., Newville, M., Gordon, R. A., Crozier, E. D., Sutton, S. R., McMahon, G., and Jiang, D.-T., 2000, Chemical speciation of gold in arsenopyrite: Canadian Mineralogist, v. 38, p. 1265-1281.

Callaghan, T., 2001, Geology and host-rock alteration of the Henty and Mount Julia Gold deposits, Western Tasmania: Economic Geology, v. 96, p. 1073-1088.

Campbell, A., and Larson, P., 1998, Introduction to stable isotope applications in hydrothermal systems, *in* Richards, J. P., and Larson, P. B., eds., Techniques in hydrothermal ore deposits geology: Reviews in Economic geology, Volume 10, Society of Economic Geologists, p. 173-193.

Cathelineau, M., Bioiron, M., Holliger, P., Marion, P., and Denis, M., 1989, Gold in arsenopyrites: Crystal chemistry, location and state, physical and chemical conditions of deposition: Economic Geology Monograph 6, p. 328–341.

Cathelineau, M., Bioiron, M., Holliger, P., Marion, P., and Denis, M., 1989, Gold in arsenopyrites: Crystal chemistry, location and state, physical and chemical conditions of deposition: Economic Geology Monograph 6, p. 328–341.

Clarke, G. W., 2002, Structural controls on skarn formation at the Big Gossan Cu-Au deposit, Grasberg District, West Papua: Deformation, Fluid Flow and Mineralisation (Rick Sibson Symposium), Extended symposium abstracts, EGRU Contribution 60, 2002, p. 11-18.

Clarke, G. W., 2002, Structural controls on skarn formation at the Big Gossan Cu-Au deposit, Grasberg District, West Papua: Deformation, Fluid Flow and Mineralisation (Rick Sibson Symposium), Extended symposium abstracts, EGRU Contribution 60, 2002, p. 11-18.

Clarke, G. W., 2003, Structural and hydrothermal features of the Gunung Bijih Cu skarn deposit, Ertsberg district, Irian Jaya: Magmas, fluids and porphyry-epithermal deposits, Extended symposium abstracts, Townsville, 4th March. EGRU Contribution 61, 2003, p. 66-73.

Cline, J. S., and Bodnar, R. J., 1991, Can economic porphyry copper mineralisation be generated by a typical calc-alkaline melt?: Journal of Geophysical Research, v. 96, p. 8113-8126.

Cooke, D. R., and Simmons, S. F., 2000, Characteristics and genesis of epithermal gold deposits, *in* Hagemann, S. G., and Brown, P. E., eds., Gold in 2000: Reviews in Economic Geology 13, Society of Economic Geologists., p. 221-244.

Corbett, G., and Leach, T. M., 1998, Southwest Pacific rim gold-copper systems: structure, alteration and mineralisation. Economic Geology: Special Publication 6., Society of Economic Geologists, 238 p.

Coutts, B. P., Susanto, H., Belluz, N., Flint, D., and Edwards, A., 1999, Geology of the Deep Ore Zone, Ertsberg East Skarn system, Irian Jaya: Pacrim '99, Bali, Indonesia, 1999, p. 539-547.

Craig, H., 1957, Isotopic standards for carbon and oxygen and corrective factors for mass spectrographic analysis of carbon dioxide: Geochimica et Cosmochima Acta, v. 12, p. 133-149.

Craig, H., 1961, Isotopic variations in meteoric waters: Science, v. 133, p. 1702-1703.

Cronin, S. J., Neall, V. E., and Palmer, A. S., 1996, Investigation of an aggrading paleosol developed into andesitic ring-plain deposits, Ruapehu volcano, New Zealand: Geoderma, v. 69, p. 119-135.

Dong, G., and Morrison, G. W., 1995, Adularia in epithermal veins, Queensland: morphology, structural state and origin: Mineralium Deposita, v. 30, p. 11-19.

Dow, D. B., Robinson, G. P., Hartono, U., and Tarman, N., 1988, Geology of Irian Jaya: Irian Jaya geological mapping project, Geological Research and Development centre, Indonesia, in

cooperation with the Bureau of Mineral Resources, Australia, on behalf of the Department of Mines and Energy, Indonesia, and the Australian Development Assistance Bureau, p. 298.

Edmonds, A., Pyle, D., and Oppenheimer, C., 2001, A model for degassing at the Soufriere Hills Volcano, Montserrat, West Indies, based on geochemical data: Earth and Planetary Science Letters, v. 186, p. 159-173.

Eiler, J. M., Graham, C., and Valley, J. W., 1997, SIMS analysis of oxygen isotopes: matrix efects in complex minerals and glasses: Chemical Geology, v. 138, p. 221-244.

Farmer, V. C., McHardy, W. J., Palmieri, P., Violante, A., and Violante, P., 1991, Synthetic allophanes formed in calcareous environments: nature, condition of formation, and transformations: Soil Science Society of America Journal, v. 55, p. 1162-1166.

Fey, M. V., and LeRoux, J., 1975, Quantitative determination of allophane in soil clays: Proceedings of the International Clay Conference, Wilmette, Illinois, USA, 1975.

Fitzsimons, C. W., Harte, B., and Clark, R. M., 2000, SIMS stable isotope measurement: counting statistics and analytical precision: Mineralogical Magazine, v. 64, p. 59-83.

Fontbote, L., and Bendezu, R., 1999, Carbonate hosted Zn-Pb San Gregorio deposit, Colquijirca district, central Peru, as part of a high sulphidation epithermal system, *in* Stanley, C. J., ed., Mineral deposits: processes to processing. 5th biennial SGA meeting and 10th quadrennial IAGOD symposium., Balkema Rotterdam Brookfield, p. 495-498.

Freeport McMoRan Copper & Gold Inc 2000 Annual Report.

Freeport McMoRan Copper & Gold Inc 2002 Annual Report.

Friehauf, K. C., 2000, Porphyry-style mineralisation in the Ertsberg diorite, Gunung Bijih (Grasberg) district, West Papua: Geological Society of America Abstracts with Programs. v 32, n 7, 2000, p. A-137.

Friehauf, K. C., Soebari, L., and Titley, S. R., 2000, Porphyry-style mineralization in the Ertsberg Diorite, Gunung Bijih (Ertsberg/Grasberg) District, Irian Jaya, Indonesia: Freeport - Institute of Technology Bandung Geological Symposium. Sheraton Hotel, Bandung, Indonesia. 26-28th September, 2000.

Fu, B., Baker, T., Margotomo, W., Mernagh, T. P., Pollard, P. J., Ryan, C. G., Ulrich, T., and Williams, P. J., 2003, Copper carried in CO2-bearing vapour? Microanalytical characterization of fluid inclusions from the Grasberg porphyry copper-gold deposit, Irian Jaya, Indonesia: Geochimica et Cosmochima Acta, v. 67, p. A105.

Fu, B., Williams, P. J., Oliver, N. H. S., Pollard, P. J., Baker, T., Margotomo, W., Xu, Z., Qui, J., Hu, W., and Ren, Q., 2003b, Fluid inclusions in Porphyry copper-gold deposits: examples from Grasberg, Indonesia and Shaxi, East China: Magmas, fluids and porphyry-epithermal deposits, Extended symposium abstracts, Townsville, 4th March. EGRU Contribution 61, 2003b, p. 38-46.

Gammons, C. H., and Williams-Jones, A. E., 1997, Chemical mobility of gold in the porphyry-epithermal environment: Economic Geology, v. 92, p. 45-59.

Gibbins, S. L., 2000, Alteration in the southwest wall rocks of the Grasberg Cu-Au porphyry deposit: Unpub. MSc thesis, The University of Arizona.

Gibbins, S. L., 2000b, Unusual advanced argillic alteration on the SW rim of the Grasberg Cu-Au porphyry deposit, Irian Jaya, Indonesia: Geological Society of America Abstracts with Programs. v 32, n 7, 2000, p. A-137.

Giggenbach, W. F., 1992, Magma degassing and mineral deposition in hydrothermal systems along convergent plate boundaries: Economic Geology, v. 87, p. 1927-1944.

Golyshev, S. I., Padalko, N. L., and Pechenkin, S. A., 1981, Fractionation of stable oxygen and carbon isotopes in carbonate systems: Geochemistry International, v. 18, p. 85-99.

Gonzalez, D. M., 1993, Preliminary paragenetic study of the Big Gossan copper skarn deposit, Ertsberg (Gunung Bijih) district, Irian Jaya, Indonesia, Unpublished report for PT Freeport International.

Grant, J. N., and Nielsen, R. L., 1975, Geology and geochronology of the Yandera porphyry copper deposit, Papua New Guinea: Economic Geology, v. 70, p. 1157-1174.

Hall, R., 2002, Cenozoic geological and plate tectonic evolution of SE asia and the SW Pacific: computer based reconstructions, model and animations: Journal of Asian Earth Sciences, v. 20, p. 353-431.

Hall, R., and Spakman, W., 2002, Subducted slabs beneath the eastern Indonesian-Tonga region: insights from tomography: Earth and Planetary Science Letters, v. 201, p. 321-336.

Harris, A. C., and Golding, S. D., 2002, New evidence of magmatic-fluid-related phyllic alteration: implications for the genesis of porphyry Cu deposits: Geology, v. 30, p. 335-338.

Harrison, J. S., 1999, Hydrothermal alteration and fluid evolution of the Gasberg Porphyry Cu-au deposit, Irian Jaya, Indonesia: Unpub. MSc thesis, University of Texas at Austin.

Hattori, K. H., and Keith, J. D., 2001, Contribution of mafic melt to porphyry copper mineralisation: exidence from Mount Pinatubo, Phillipines, and Bingham Canyon, Utah, USA: Mineralium Deposita, v. 36, p. 799-806.

Hazelton, B. M., 1997, Oxygen isotope ratios in marine carbonates as paleoclimatic indicators and their in situ, high spatial-resolution measurement by Secondary Ion Mass Spectronometry (SIMS): Unpub. Honours thesis, University of Wollongong, Sydney.

Hedenquist, J. F., and Lowenstern, J. B., 1994, The role of magmas in the formation of hydrothermal ore deposits: Nature, v. 370, p. 519-526.

Hedenquist, J. W., Arribas, A. R., and Gonzalez-Urien, E., 2000, Exploration for epithermal gold deposits, *in* Hagemann, S. G., and Brown, P. E., eds., Gold in 2000: Reviews in Economic Geology, 13, Society of Economic Geology., p. 245-277.

Hedenquist, J. W., Matsuhisa, Y., Izawa, E., White, N. C., Giggenbach, W. F., and Aoki, M., 1994, Geology, geochemistry and origin of high sulphidation Cu-Au mineralisation in the Nansatsu District, Japan: Economic Geology, v. 89, p. 1-30.

Hefton, K. K., MacDonald, G. D., Arnold, L. C., Schappert, A. L., and Ona, A., 1995, Copper-gold deposits of the Ertsberg (Gunung Bijih) Mining Dstrict, Irian Jaya, *in* Mayes, D., and Pollard, P., eds., Exploring the Tropics: Geology and Copper-Gold Deposits of the Ertsberg (Gunung Bijih) Mining Dstrict, Irian Jaya, Indonesia, EGRU Contribution, 53, p. 1-43.

Heinrich, C. A., 2003, Magmatic vapour condensation and the relation between porphyries and epithermal Au-(Cu-As) mineralisation: thermodynamic constraints, *in* Eliopoulos, D. G., ed., Mineral exploration and sustainable development: proceedings of the 7th biennial SGA meeting, Millpress, Netherlands, p. 279-282.

Heinrich, C. A., Gunther, D., Audetat, A., Ulrich, T., and Frischknecht, R., 1999, Metal fractionation between magmatic brine and vapour, determined by microanalysis of fluid inclusions: Geology, v. 27, p. 755-758.

Hemley, J. J., and Hunt, J. P., 1992, Hydrothermal ore-forming processes in the light of studies in rock-buffered systems: II. Some general geological applications: Economic Geology, v. 87, p. 23-43.

Hemley, J. J., Cygan, G. L., Fein, J. B., Robinson, G. R., and d'Angelo, W. M., 1992, Hydrothermal ore-forming processes in light of studies in rock buffered systems: 1. Iron-copper-zinc-lead-sulphide solubility relations: Economic Geology, v. 87.

Hill, K. C., Kendrick, R. D., Crowhurst, P. V., and Gow, P. A., 2002, Copper-gold mineralisation in New Guinea: tectonics, lineaments, thermochronology and structure: Australian Journal of Earth Sciences, v. 49, p. 737-752.

Hinton, R. W., 1995, Ion microprobe analysis in geology, *in* Potts, P. J., Bowles, J. F. W., Reed, S. J. B., and Cave, M. R., eds., Microprobe techniques in the Earth Sciences, Chapman and Hall, London.

Hitzman, M. W., 1999, Routine staining of drill core to determine carbonate mineralogy and distinguish carbonate alteration textures: Mineralium Deposita, v. 34, p. 794-798.

Hoefs, J., 1980, Stable isotope geochemistry, 2nd Edition, Springer-Verlag, Germany.

Honea, R. M., 1990, West Grasberg pan concentrates, Unpublished report for PT Freeport International.

Honea, R. M., 1993a, Petrography of BGU and WAN core, Unpublished report for PT Freeport International.

Honea, R. M., 1993b, Polished section data for Wanagon core suite, Unpublished report for PT Freeport International.

Honea, R. M., 1994, Polished section search for gold occurrence in Big Gossan core suite, Unpublished report for PT Freeport International.

Honea, R. M., 1996, Scanning electron microscope data for Wanagon hole 4-2, 234m (No. 2) Core, Unpublished report for PT Freeport International.

Honea, R. M., 1996a, Petrographic descriptions for Wanagon core suite, Unpublished report for PT Freeport International.

Honea, R. M., 1996b, Scanning electron microscope data for Wanagon hole 4-2, 234m (No. 2) Core, Unpublished report for PT Freeport International.

Hornibrook, M., 1998, Hydrocarbons and their Exploration Implications in the COW A area, Irian Jaya, Unpublished report for PT Freeport International.

Housh, T., and McMahon, T. P., 2000, Ancient isotopic characteristics of Neogene potassic magmatism in Western New Guinea (Irian Jaya, Indonesia). Lithos, v. 50, p. 217-239.

Hurst, V. J., and Kunkle, A. C., 1985, Dehydroxylation, rehydroxylation, and stability of kaolinite: Clays and Clay Minerals, v. 33, p. 1-14.

Huston, D. L., Power, M., Gemmell, J. B., and Large, R. R., 1995, Design, calibration and geological application of the first operational Australian laser ablation sulphur isotope microprobe: Australian Journal of Earth Sciences, v. 42, p. 549-555.

James, E. W., 2000a, Possible and impossible sources for magmas and metals: Pb, Sr and Nd isotopes of rocks and ores from the Ertsberg District.: Freeport - Institute of Technology Bandung Geological Symposium. Sheraton Hotel, Bandung, Indonesia. 26-28th September, 2000a.

James, E. W., 2000b, Rock/apatite Sr isotope disequilibrium, magma mixing, and rapid cooling in the Gunung Bijih (Ertsberg) mining district, Irian Jaya, Indonesia: Geological Society of America Abstracts with Programs. v 32, n 7, 2000b, p. A-51.

James, E. W., and Housh, T., 1995, Pb isotopic constaints on the sources of metals in the Gunung Bijih (Ertsberg) Mining district, Irian Jaya, Indonesia: Geological Society of America Abstracts with Programs. v 27, n 6, 1995, p. A65.

Jensen, E. P., and Barton, M. D., 2000, Gold deposits related to alkaline magmatism, *in* Hagemann, S. G., and Brown, P. E., eds., Gold in 2000: Reviews in Economic Geology, 13, Society of Economic Geology., p. 279-314.

Katchan, G., 1982, Mineralogy and geochemistry of the Ertsberg (Gunung Bijih) and Ertsberg East (Gunung Bijih Timor) skarns, Irian Jaya, Indonesia and Ok Tedi skarns, Papua New Guinea: Unpub. PhD thesis, University of Sydney.

Kavalieris, I., 1992, Notes on the 1:5000 West Grasberg Map Sheet, Unpublished report for PT Freeport Indonesia.

Kavalieris, I., 1994, The Grasberg superporphyry, CODES Key Centre, Masters of Economic Geology Short Course notes, University of Tasmania, (unpublished), p. 3.1-3.29.

Kavalieris, I., 2000, Alteration mapping glossary, Unpublished report for PT Freeport Indonesia.

Kingston-Morrison, 1997, Important hydrothermal minerals and their significance, Unpublished report. Kingston Morrison Limited - geothermal and mineral services division.

Kyle, J. R., 1992, Ore deposits research in the Ertsberg District, Unpublished report for PT Freeport International.

Kyle, J. R., 1993, Fluid Inclusion investigation of hydrothermal alteration and mineralisation in the Ertsberg District, Irian Jaya, Indonesia, Unpublished report for PT Freeport International.

Kyle, J. R., 1994, Ertsberg Project, Irian Jaya, Indonesia: Phase 1 ore studies review, Unpublished report for PT Freeport International.

Kyle, J. R., and Dworkin, S. I., 1995, Isotopic evidence for origin of Ertsberg district anhydrite, Unpublished report for PT Freeport Indonesia.

Kyle, J. R., and Dworkin, S. I., 1995, Isotopic evidence for origin of Ertsberg district anhydrite, Unpublished report for PT Freeport Indonesia.

Kyle, J. R., James, E. W., and Rubin, J. R., 1996, Magmatic-hydrothermal-epithermal transition in the Ertsberg (Gunung Bijih) district, Irian Jaya, Indonesia: Geological Society of America Abstracts with Programs. v 28, n 7, 1996.

Lambert, C. A., 2000, Subsurface meso-scale structural geology of the Kucing Liar and Amole Drifts and petrology of the heavy sulphide zone, south Grasberg Igneous complex, Irian Jaya, Indonesia: Unpub. MSc thesis, University of Texas at Austin.

Leshin, L. A., McKeegan, K. D., Carpenter, P. K., and Harvey, R. P., 1998, Oxygen isotopic constraints on the genesis of carbonates from Martian meteorite ALH84001: Geochimica et Cosmochima Acta, v. 62, p. 3-13.

Logan, B. W., 1984, Pressure responses (deformation) in carbonate sediments and rocks. Analysis and application, Canning Basin, *in* Purcell, P. G., ed., The Canning Basin, W.A, The Geological Society of Australia Incorporated, p. 235-251.

Lorenzoni, P., Mirabella, A., Bidini, D., and Lulli, L., 1995, Soil genesis on trachytic and leucititic lavas of Cimini volcanic complex (Latium, Italy): Geoderma, v. 68, p. 79-99.

Lowenstern, J. B., 2000, A review of the contrasting behaviour of two magmatic volatiles: chlorine and carbon dioxides: Journal of Geochemical Exploration, v. 69-71, p. 287-290.

Lowenstern, J. B., 2001, Carbon dioxide in magmas and implications for hydrothermal systems: Mineralium Deposita, v. 36, p. 490-502.

Macpherson, C. G., and Hall, R., 2002, Timing and tectonic controls in the evolving orogen of SE Asia and the western Pacific and some implications for ore generation, *in* Blundell, D. J., Neubauer, F., and Von Quadt, A., eds., The timing and location of major ore deposits in an evolving orogen, Geological Society, London, Special Publications, 204, p. 49-67.

Maglambayan, V. B., Daizo, I., Mizuta, T., Matsubaya, O., and Ishikawa, Y., 2001, Oxygen and carbon Isotope study of calcite and dolomite in the disseminated Au-Ag telluride bulawan deposit, Negros Island, Philippines: Resource Geology, v. 51, p. 107-116.

Malensek, G. A., 1997, Economic evaluation of the Wanagon Gold deposit, Irian Jaya, Indonesia: Unpub. MSc thesis, Colorado School of Mines.

Margotomo, W., 1999, South Contact mapping and sampling project, Unpublished report for PT Freeport Indonesia.

Margotomo, W., Sitohang, F., Judihanri, Perdana, A., Ginting, A., Coutts, B. P., Widodo, S., and Hyland, S., 2001, Geological Investigation of the North Wall area, Unpublished report for PT Freeport Indonesia. January 05 2001.

Mathur, R., 2000, Re-Os evidence for different sources of copper and gold in the Grasberg Cu-Au porphyry deposit, Irian Jaya: Geological Society of America Abstracts with Programs. v 32, n 7, 2000, p. A-137.

Mathur, R., Joaquin, R., Titley, S. R., Gibbins, S. L., and Margotomo, W., 2000, Different crustal sources for Au-rich and Au-poor ores of the Grasberg Cu-Au porphyry deposit: Earth and Planetary Science Letters, v. 183, p. 7-14.

Mathur, R., Titley, S. R., Ruiz, J., Gibbens, S. L., and Friehauf, K. C., A Re-Os study of ores and sedimentary rocks from the Ertsberg District, Irian Jaya, Indonesia: Economic Geology (in review).

McCrea, J. M., 1950, On the isotope chemistry of carbonates and a paleotemperature scale: Journal of Chemical Physics, v. 18, p. 849-857.

McDonald, G. D., and Arnold, L. C., 1994, Geological and geochemical zoning of the Grasberg Igneous Complex, Irian Jaya, Indonesia: Journal of Geochemical Exploration, v. 50, p. 143-178.

McDowell, F. W., McMahon, T. P., Warren, P. Q., and Cloos, M., 1996, Pliocene Cu-Au-bearing igneous intrusions of the Gunung Bijih (Ertsberg) district, Irian Jaya, Indonesia: K-Ar geochronology: Journal of Geology, v. 104, p. 327-340.

McInnes, B. I. A., Gregoire, M., Binns, R. A., Herzig, P. M., and Hannington, M. D., 2001, Hydrous metasomatism of oceanic sub-arc mantle, Lihir, Papua New Guinea: petrology and geochemistry of fluid metasomatised mantle wedge xenoliths: Earth and Planetary Science Letters, v. 188, p. 169-183.

McInnes, B. I. A., McBride, J. S., Evans, N. J., Lambert, D. D., and Andrew, A. S., 1999, Osmium isotope constraints on ore metal recycling in subduction zones: Science, v. 286, p. 512-516.

McMahon, T. P., 1994a, Pliocene intrusions in the Ertsberg (Gunung Bijih) mining district, Irian Jaya, Indonesia: Petrography, geochemistry and tectonic setting: Unpub. PhD thesis, University of Texas at Austin.

McMahon, T. P., 1994b, Pliocene intrusions in the Gunung Bijih (Ertsberg) mining district, Irian Jaya, Indonesia: major- and trace-element geochemistry: International Geology Review, v. 36, p. 925-946.

McMahon, T. P., 1994c, Pliocene intrusions in the Gunung Bijih (Ertsberg) mining district, Irian Jaya, Indonesia: petrography and mineral chemistry: International Geology Review, v. 36, p. 820-849.

McMahon, T. P., 1999, The Ertsberg Intrusion and the Grasberg Complex: contrasting styles of magmatic evolution and Cu-Au mineralisation in the Gunung Bijih (Ertsberg) mining district, Irian Jaya, Indonesia: Buletin Geologi, v. 31, p. 123-132.

McMahon, T. P., 2000a, Magmatism in an Arc-Continent collision zone: an example from Irian Jaya (western New Guinea), Indonesia: Buletin Geologi, v. 32, p. 1-22.

McMahon, T. P., 2000b, Origin of syn- to post-collisional magmatism in New Guinea: Buletin Geologi, v. 32, p. 89-104.

Meinert, L. D., 1989, Gold skarn deposits; geology and exploration criteria, The geology of gold deposits; the perspective in 1988, Economic Geology Monographs 6, p. 537-552.

Meinert, L. D., 2000, Gold in skarns related to epizonal intrusions, *in* Hagemann, S. G., and Brown, P. E., eds., Gold in 2000: Reviews in Economic Geology, 13, Society of Economic Geology., p. 347-376.

Meinert, L. D., Hedenquist, J. F., Satoh, H., and Matsuhisa, Y., 2003, Formation of anhydrous and hydrous skarn in Cu-Au ore deposits by magmatic fluids: Economic Geology, v. 98, p. 147-156.

Meinert, L. D., Hefton, K. K., Mayes, D., and Tasiran, I., 1997, Geology, zonation and fluid evolution of the Big Gossan Cu-Au skarn deposit, Ertsberg Mining District, Irian Jaya: Economic Geology, v. 92, p. 509-533.

Mertig, H. J., 1995, Geology and origin of the DOM copper skarn deposit, Ertsberg (Gunung Bijih) District, Irian Jaya, Indonesia: Unpub. PhD thesis, University of Texas.

Mertig, H. J., Rubin, J. N., and Kyle, J. R., 1994, Skarn Cu-Au orebodies of the Gunung Bijih (Ertsberg) district, Irian Jaya, Indonesia: Journal of Geochemical Exploration, v. 50, p. 179-202.

Mojzsis, S. J., Coath, C. D., Bunch, T., Blake, D., Treiman, A. H., and Amundsen, H. E. F., 1999, Carbonate "rosettes" in xenoliths from spitzbergen: SIMS analysis of O and C isotope ratios in a potential terrestrial analogue to martian meteorite: Abstracts of Papers Submitted to the Lunar and Planetary Science Conference 30 (1999) abstr. no. 2032.

Moore, D. M., and Reynolds, R. C., 1997, X-ray diffraction and identification and analysis of clay minerals, 2nd edition, Oxford University Press, New York, 378 p.

Morrison, G., Kary, G., and Handfield, R., 1999, Intrusion-alteration-mineralisation relationships in the Frieda River igneous complex, PNG: Enriched: PACRIM '99 congress proceedings. Australasian Institute of Mining and Metallurgy, 1999, p. 527-537.

Mulshaw, S. C., Puig, C., Spiro, B., and Buchanan, D. L., 1997, Genesis of epizonal Ag vein mineralisation at San Bartolome in central Equador: textural evidence, fluid inclusions and stable isotope geochemistry: Economic Geology, v. 92, p. 210-227.

Nabelek, P. I., 1991, Stable isotope monitors, *in* Kerrick, D. M., ed., Contact metamorphism. Reviews in mineralogy, Volume 26, Mineralogical Society of America, p. 395-435.

New, B. T. E., 1998, Correlation of district stratigraphy and alteration assemblages in the Kucing Liar deposit, Ertsberg Mine District, Irian Jaya, Indonesia, Unpublished report for PT Freeport Indonesia.

New, B. T. E., 1999, Kucing Liar, Irian Jaya: a sedimentary-hosted Cu-Au deposit, *in* Stanley, C. J., ed., Mineral deposits: processes to processing. 5th biennial SGA meeting and 10th quadrennial IAGOD symposium., Balkema Rotterdam, Brookfield, p. 1055-1058.

Ohmoto, H., 1986, Stable isotope geochemistry of ore deposits, *in* Valley, J. W., Taylor, H. P., and O'Neil, J. R., eds., Stable isotopes in high temperature geological processes. Reviews in mineralogy, Volume 16, Mineralogical Society of America, p. 491-559.

Ohmoto, H., and Goldhaber, M. B., 1997, Sulfur and carbon isotopes, *in* Barnes, H. L., ed., Geochemistry of hydrothermal ore deposits, John Wiley and Sons, USA, p. 517-611.

Ohmoto, H., and Rye, R. O., 1979, Isotopes of sulfur and carbon, *in* Barnes, H. L., ed., Geochemistry of hydrothermal ore deposits, John Wiley and Sons, Inc., p. 509-567.

Osaki, S., 1973, Carbon and oxygen isotopic composition of hydrothermal rhodochrisites from Oe, Inakuraishi and Jokoku mines, Hokkaido, Japan: Geochemical Journal, v. 6, p. 151-162.

Parfitt, R. L., and Wilison, A. D., 1985, Estimation of allophane and halloysite in three sequences of volcanic soils, New Zealand, *in* Caldas, E. F., and Yaalon, D. H., eds., Volcanic Sols, 7, Catena Suppl, p. 1-8.

Paterson, B. A., Riciputi, L. R., and McSween, H. Y., 1997, A comparison of sulfur isotope ratio measurement using two ion microprobe techniques and application to analysis of troilite in ordinary chrondrites: Geochimica et Cosmochimica Acta, v. 61, p. 601-609.

Penniston-Dorland, S. C., 2001, Illumination of vein quartz textures in a porphyry copper ore deposit using scanned cathodoluminescence: Grasberg Igneous Complex, Irian Jaya, Indonesia: American Mineralogist, v. 86, p. 652-666.

Plumb, K. A., 1979, The tectonic evolution of Australia: Earth Science Reviews, v. 14, p. 205-249.

Pokrovski, G. S., Kara, S., and Roux, J., 2001, Stability and solubility of arsenopyrite, FeAsS, in crustal fluids: Geochimica et Cosmochimica Acta, v. 66, p. 2361-2378.

Pollard, P. J., and Taylor, R. G., 2002, Paragenesis of the Grasberg Cu-Au deposit, Irian Jaya, Indonesia: results from logging section 13: Mineralium Deposita, v. 37, p. 117-136.

Pollard, P. J., and Taylor, R. G., 2003, High-sulphidation Cu-Au mineralisation in the Ertsberg district, Irian Jaya - implications for genetic models: Magmas, fluids and porphyry-epithermal deposits, Extended symposium abstracts, Townsville, 4th March. EGRU Contribution 61, 2003, p. 60-65.

Pollard, P. J., Taylor, R. G., and Peters, L., Age of intrusion, alteration and mineralization at the Grasberg Cu-Au deposit, Irian Jaya, Indonesia: Economic Geology (submitted).

Pollard, P. J., Taylor, R. G., and Widodo, S., 2001, Geochronology of intrusive rocks and Cu-Au mineralisation in the Ertsberg District, Irian Jaya, Indonesia: A hydrothermal odyssey, Extended Abstracts, Townsville 17-19 May 2001, 2001, p. 168-169.

Prendergast, K., 2001, Evolution of the West Grasberg breccia zone and gold-bearing limestone breccias; Ertsberg mining district, Irian Jaya, Indonesia: A hydrothermal odyssey, Extended Abstracts, Townsville 17-19 May 2001, 2001, p. 168-169.

Prendergast, K., 2002, Similarities between porphyry-related hydrothermal systems at Wanagon Gold and Big Gossan, Papua, Indonesia: Deformation, Fluid Flow and Mineralisation (Rick Sibson Symposium), Extended symposium abstracts, EGRU Contribution 60, 2002, p. 110-117.

Prendergast, K., Taylor, R. G., Clarke, G. W., and Pollard, P. J., 2001, Metal zonation and the timing of gold mineralisation associated with the Big Gossan Cu-Au deposit, Ertsberg District, Irian Jaya, Indonesia: Geological Society of America Abstracts with Programs. v 33, n 6, 2001, p. 358.

Quarles Van Ufford, A. I., 1996, Stratigraphy, structural geology and tectonics of a young forearc-continent collision, western Central Range, Irian Jaya (western New Guinea), Indonesia: Unpub. PhD thesis, University of Texas.

Quarles Van Ufford, A. I., and Cloos, M., Cenozoic tectonics of New Guinea: American Association of Petroleum Geologists Bulletin (submitted).

Rae, A. J., Allen, J. M., and Powell, N. G., 1994, Paragenesis, textural relations and chemistry of gold at the Big Gossan project, Gunung Bijih (Ertsberg) district, Irian Jaya, Indonesia, Unpublished report (JA63) for PT Freeport Indonesia.

Reeder, R. J., Valley, J. W., Graham, C. M., and Eiler, J. M., 1997, Ion microprobe study of oxygen isotopic compositions of structurally nonequivalent groth surfaces on synthetic calcite: Geochimica et Cosmochima Acta, v. 61, p. 5057-5063.

Richards, J. P., and Kerrich, R., 1993, The Porgera gold mine, Papua New Guinea: magmatic hydrothermal to epithermal evolution of an alkalic-type precious metal deposit: Economic Geology, v. 88.

Richards, J. P., and Laudrum, D., 1998, The Mt. Kare alkalic epithermal gold deposit, Papua New Guinea: Geological Society of America, 1998 annual meeting Abstracts with Programs - Geological Society of America 30, no. 7, 1998, p. 302.

Riciputi, L. R., and Greenwood, J. P., 1998, Analysis of sulfur and carbon isotope ratios in mixed matrices by secondary ion mass spectrometry: Implications for mass bias corrections: International Journal of Mass Spectrometry, v. 178, p. 65–71.

Robinson, B. W., and Kusakabe, M., 1975, Quantitative preparation of sulphur dioxide, for 34S/32S analyses, from sulphides by combustion with Cuprous Oxide: Analytical Chemistry, v. 47, p. 1179-1181.

Roedder, E., 1984, Fluid Inclusions, Reviews in mineralogy, v 12, Mineralogical Society of America.

Rollinson, H. R., 1996, Using geochemical data: evaluation, presentation, interpretation, Longman Group, UK, 352 p.

Ronacher, E., and Richards, J. P., 1999, Environments of ore deposition at the Porgera gold deposit, Papua New Guinea, *in* Stanley, C. J., ed., Mineral deposits: processes to processing. 5th biennial SGA meeting and 10th quadrennial IAGOD symposium., Balkema Rotterdam Brookfield, p. 95-98.

Rubin, J. R., 1996, Skarn formation and ore deposition at the Gunung Bijih Timur (Ertsberg) Complex, Irian Jaya, Indonesia: Unpub. PhD thesis, University of Texas.

Rubin, J. R., and Kyle, J. R., 1997, Precious metal mineralogy in porphyry- skarn- and replacement-type ore deposits of the Ertsberg (Gunung Bijih) district, Irian Jaya, Indonesia: Economic Geology, v. 92, p. 535-550.

Rubin, J. R., and Kyle, J. R., 1998, The Gunung Bijih Timur (Erstberg East) skarn complex, Irian Jaya, Indonesia: geology and genesis of a large, magnesian, Cu-Au skarn, *in* Lentz, D. R., ed., Mineralised intrusion-related skarn systems, Mineralogical Association of Canada

short course series. Short course volume 26. Quebec City, Quebec 1998, p. 245-288.
Rush, P. M., and Seegers, H. J., 1990, Ok Tedi copper-gold deposits: Australian Institute of Mining and Metallurgy Monograph 14, p. 1747-1754.
Sanusi, S., 1994, Wanagon prospect completion report, Unpublished internal report for PT Freeport Indonesia.
Sapiie, B., 1998, Strike-slip faulting and porphyry Cu-Au mineralisation in the Gunung Bijih (Ertsberg) Mining district, Irian Jaya, Indonesia: Unpub. PhD thesis, University of Texas.
Sapiie, B., and Cloos, M., Strike-slip faulting in the core of the Central Range of west New Guinea: Ertsberg mining district, Indonesia: Accepted for publication in Geological Society of America Bulletin.
Sapiie, B., Natawidjaya, D. H., and Cloos, M., 1999, Strike-slip tectonics of New Guinea: Transform motion between the Caroline and Australian plates: Proceedings of the Indonesian Association of Geologists: 28th Annual Convention, Jakata, Indonesia, 30 November - 1 December 1999., 1999.
Scotese, C. R., Gahagan, L. M., and Larson, R. L., 1988, Plate tetonic reconstructions of the Cretaceous and Cenozoic ocean basins: Tectonophysics, v. 155, p. 27-48.
Seward, T. M., 1991, The hydrothermal geochemistry of gold, *in* Forster, R. P., ed., Gold metallogeny and exploration, London, Blackie and Son, p. 37-62.
Seward, T. M., and Barnes, H. L., 1997, Metal transport in hydrothermal ore fluids, *in* Barnes, H. L., ed., Geochemistry of hydrothermal ore deposits - 3rd edition, John Wiley & Sons, Inc. United States of America, p. 435-486.
Shelton, K. L., 1983, Composition and origin of ore-forming fluids in a carbonate-hosted porphyry-copper and skarn deposit: a fluid inclusion and stable isotope study of Mines Gaspe, Quebec: Economic Geology, v. 78, p. 387-421.
Sheppard, S. M. F., 1986, Characterization and isotopic variations in natural waters, *in* Valley, J. W., Taylor, H. P., and O'Neil, J. R., eds., Stable isotopes in high temperature geological processes. Reviews in mineralogy, Volume 16, Mineralogical Society of America, p. 165-183.
Shikazono, N., 1989, Oxygen and carbon isotopic composition of carbonates from the Neogene epithermal vein-type deposits of Japan: implication for evolution of terrestrial geothermal activity.: Chemical Geology, v. 76, p. 239-247.
Shinohara, H., 1994, Exsolution of immiscible vapor and liquid phases from a crystallising silicate melt: implications for chlorine and metal transport: Geochimica et Cosmochima Acta, v. 58, p. 5215-5221.
Shinohara, H., and Hedenquist, J. F., 1997, Constraints on magma degassing beneath the Far Southeast porphyry Cu-Au deposit, Philippines: Journal of Petrology, v. 38, p. 1741-1752.
Sibley, D. F., and Gregg, J. M., 1987, Classification of dolomite rock textures: Journal of Sedimentary Petrology, v. 57, p. 967-975.
Sillitoe, R. H., 1985, Ore-related breccias in volcanoplutonic arcs: Economic Geology, v. 80, p. 1467-1514.
Sillitoe, R. H., 1997, Characteristics and controls of the largest porphyry copper-gold and epithermal gold deposits in the circum-Pacific region: Australian Journal of Earth Sciences, v. 44, p. 373-388.
Sillitoe, R. H., 1999, Styles of high sulphidation gold, silver and copper mineralisation in porphyry and epithermal environments: Pacrim '99, Bali, Indonesia, 1999, p. 29-44.
Sillitoe, R. H., 2000, Gold-rich porphyry deposits: descriptive and genetic models and their role in exploration and discovery, *in* Hagemann, S. G., and Brown, P. E., eds., Gold in 2000: Reviews in Economic Geology, 13, Society of Economic Geology., p. 315-345.
Sillitoe, R. H., Baker, E. M., and Brook, W. A., 1984, Gold deposits and hydrothermal eruption breccias associated with a maar volcano at Wau, Papua New Guinea: Economic Geology, v. 79, p. 638-655.
Simons, F. J., Zielhuis, A., and van der Hilst, R. D., 1999, The deep structure of the Australian continent from surface wave tomography: Lithos, v. 48, p. 17-43.
Singleton, P. L., McLeod, M., and Percival, H. J., 1989, Allophane and halloysite content and soil solution silica in soils from rhyolitic volcanic materials New Zealand: Australian Journal of Soil Research, v. 27, p. 66-77.
Soloman, M., 1990, Subduction, arc reversal, and the origin of porphyry copper-gold deposits in island arcs: Geology, v. 18, p. 630-633.

Sourirajan, S., and Kennedy, G. C., 1962, The system H2O-NaCl at elevated temperatures and pressures: American Journal of Science, v. 260, p. 115-141.

Spera, S. J., 2001, Petrographic descriptions of 18 rock samples from DOZ-halo, Unpublished report for PT Freeport Indonesia.

Starkey, H. C., Blackmoun, P. D., and Hauff, P. L., 1984, The routine mineralogical analysis of clay-bearing samples: U.S. Geological Survey Bulletin 1563, p. 32.

Su, C., and Harsh, J. B., 1998, Dissolution of allophane as a thermodynamically unstable solid in the presence of boehmite at elevated temperatures and equilibrium vapor pressures: Soil Science, v. 163, p. 299-312.

Sugiri, S. P., 1999, Big Gossan Breccia Project, Unpublished report for PT Freeport International.

Sukarna, D., McInnes, B., Evans, N., McSpadden, M., and McBride, J., 2000, U-Th/He thermochronology of the Main Grasberg and Karume Intrusions, Grasberg district, Irian Jaya: Freeport - Institute of Technology Bandung Geological Symposium. Sheraton Hotel, Bandung, Indonesia. 26-28th September, 2000.

Sunyoto, W., 1999, The nature and distribution of gold mineralisation in hole BO52-4 of the Wabu Skarn System, Irian Jaya: Unpub. M.Sc. thesis, James Cook University.

Swart, P. K., Burns, S. J., and Leder, J. J., 1991, Fractionation of the stable isotopes of oxygen and carbon in carbon dioxide during the reaction of calcite with phosphoric acid as a function of temperature and technique: Chemical Geology, v. 86, p. 89-96.

Tai-Loi, D., and Andrew, R. L., 1990, Wafi copper-gold deposit: Australian Institute of Mining and Metallurgy Monograph 22, p. 827-831.

Takahashi, T., Dahlgren, R., and van Susteren, P., 1993, Clay mineralogy and chemistry of soils formed in volcanic materials in the xeric moisture regime of northern California: Geoderma, v. 59, p. 131-150.

Taylor, B. E., 1986, Magmatic volatiles: isotopic variation of C, H, and S, *in* Valley, J. W., Taylor, H. P., and O'Neil, J. R., eds., Stable isotopes in high temperature geological processes. Reviews in mineralogy, Volume 16, Mineralogical Society of America, p. 185-225.

Taylor, H. P., 1997, Oxygen and hydrogen isotope relationships in hydrothermal mineral deposits, *in* Barnes, H. L., ed., Geochemistry of hydrothermal ore deposits - 3rd edition, John Wiley & Sons, Inc. United States of America, p. 229-302.

Taylor, R. G., 2003, Ore Textures Volume 5: Broken rocks, Breccia 2, Intrusive Breccia, James Cook University, Economic Geology Research Unit.

Taylor, R. G., Clarke, R. W., and Pollard, P. J., 1999, The Big Gossan copper-gold skarn system, Ertsberg district, Irian Jaya, Indonesia, Unpublished report for PT Freeport International.

Thompson, J. F. H., and Newberry, R. J., 2000, Gold deposits related to reduced granitic intrusions, *in* Hagemann, S. G., and Brown, P. E., eds., Gold in 2000: Reviews in Economic Geology, 13, Society of Economic Geology., p. 377-400.

Thompson, T. B., and Arehart, G. B., 1990, Geology and origin of ore deposits in the Leadville district, Colorado: Part 1. Geologic studies of orebodies and wallrocks: Economic Geology, v. Monograph 7, p. 130-155.

Titley, S. R., 1975, Geological characteristics and environment of some porphyry copper occurrences in the southwest Pacific: Economic Geology, v. 70, p. 499-514.

Torsten, W., Vennemann, J. L. M., Kesler, S. E., and O'Neil, J. R., 1993, Stable isotope evidence for magmatic fluids in the Pueblo Viejo epithermal acid sulphate Au-Ag deposit, Dominican Republic: Economic Geology, v. 88, p. 55-71.

Ulrich, T., Golding, S. D., Kamber, B. S., Zaw, K., and Taube, A., 2002, Different mineralisation styles in a volcanic-hosted ore deposit: the fluid and isotopic signatures of the Mt Morgan Au-Cu deposit, Australia.: Ore Geology Reviews., v. 22, p. 61-90.

Ulrich, T., Gunther, D., and Heinrich, C. A., 1999, Gold concentrations of magmatic brines and the metal budget of porphyry copper deposits: Nature, v. 399, p. 676-679.

Valley, J. W., 1986, Stable isotope geochemistry of metamorphic rocks, *in* Valley, J. W., Taylor, H. P., and O'Neil, J. R., eds., Stable isotopes in high temperature geological processes. Reviews in mineralogy, Volume 16, Mineralogical Society of America, p. 445-489.

Valley, J. W., Eiler, J. M., Graham, C. M., Gibson, E. K., Romaneck, C. S., and Stolper, E. M., 1997, Low temperature carbonate concretions in teh martian meteorite ALH84001: Evidence from stable isotopes and mineralogy: Science, v. 275, p. 1633-1638.

Van Achterbergh, E., Ryan, C. G., Jackson, S. E., and Griffin, W. L., 2001, Data reduction software for LA-ICPMS, *in* Sylvester, P., ed., Laser Ablation ICPMS in the Earth Sciences,

Mineralogical Association of Canada Short Course Vol 29, p. 239-243.

Veizer, J., and Hoefs, J., 1976, The nature of O^{18}/O^{16} and C^{13}/C^{12} secular trends in sedimentary carbonate rocks: Geochimica et Cosmochimica Acta, v. 40, p. 1387-1395.

Walters, L. J., Claypool, G. E., and Choquette, P. W., 1972, Reaction rates and d18O variation for the carbonate-phosphoric acid preparation method: Geochimica et Cosmochima Acta, v. 36, p. 129-140.

Weiland, R. J., and Cloos, M., 1996, Pliocene-Pleistocene asymmetric unroofing of the Irian fold belt, Irian Jaya, Indonesia: apatite fission-track thermochronology: Geological Society of America Bulletin, v. 108, p. 1438-1449.

Wilder, A. M., and Seward, T. M., 2002, The adsorption of gold(I) hydrosulphide complexes by iron sulphide surfaces: Geochimica et Cosmochimica Acta, v. 66, p. 383–402.

Williams, P. J., Fu, B., Pollard, P. J., Baker, T., Margotomo, W., Ryan, C. G., Van Achterbergh, E., Mernagh, T. P., Condliffe, E., and Yardley, B. W., 2003, Fluid inclusion geochemistry of the Grasberg Cu-Au porphyry: World class mineral deposits and earth evolution. Geological Society's flagship Fermor meeting. Applied Earth Sciences (Trans. Inst. Min. Metall. B), August 2003, v 112, 2003, p. B195-197.

Zachos, J., Pagani, M., Sloan, L., Thomas, E., and Billups, K., 2001, Trends, rhythms and aberrations in global climate 56 Ma to present: Science, v. 292, p. 686-693.

Zeng, Y. F., 1990, Carbon-oxygen isotopic covariation in hydrothermal calcite during degassing of CO_2: Mineralium Deposita, v. 25, p. 246-250.

Zhao, Y., Zhang, Y., and Bi, C., 1999, Geology of gold-bearing skarn deposits in the middle and lower Yangtze River Valley and adjacent regions: Ore Geology Reviews., v. 14, p. 227-249.

Zheng, Y. F., 1993, Calculation of oxygen isotope fractionation in anhydrous silicate minerals: Geochimica et Cosmochima Acta, v. 57, p. 1079-1091.

Appendix 1
Analytical techniques

PT Freeport Drillhole Assays

Section B

Big Gossan and Wanagon Gold drillhole assay data were obtained from PT Freeport Indonesia. Assay intervals are predominately three metres in length. All below detection values were removed. Distribution modelling was performed with GEMCOM software. Big Gossan drillholes with the "BG" and "BGU" prefix contained 15272 intervals containing both Cu and Au analyses. BGU drill sections are drilled from the RL2930 drift level and are considered to be below depth of weathering. BG drillholes are drilled from surface and intersect the upper breccia and Stage BG2 mineralisation. BG intervals within the zone of weathering but have not been not excluded from the database. Assay intervals within the zone of weathering are not excluded from the Wanagon Gold database (4046 intervals containing both Cu and Au analyses) as Stage WG2 mineralisation is only represented in shallow drillholes. Elements and units of measure used for correlation and distribution are Cu(%), Au(g/t), Ag(ppm), Zn(ppm), Pb (ppm), As (ppm). The distribution of Bi was incomplete.

Conventional Carbon and Oxygen Isotope analysis (Section C)

Monash University (cf. Ian Cartwright, 2003):

CO_2 was extracted from calcite by reaction of mixed carbonate-silicate powders with H_3PO_4 at 25°C for 12-18 hours in sealed vessels (McCrea, 1950). Internal calcite standard ISACC yielded $\delta^{13}C$ = -6.38±0.09‰ and $\delta^{18}O$ = 12.63±0.11‰ (n = 10). This standard was calibrated using IAEA-CO-1 and its long-term average $\delta^{13}C$ and $\delta^{18}O$ values are –6.37±0.06‰ and 12.68±0.13‰.

CSL, University of Tasmania (cf. Keith Harris, 2003):

The analysis method for the measurement of $\delta^{13}C$ w.rt.PDB and $\delta^{18}O$ w.r.t.PDB is an adaptation of the sealed vessel technique described in the early work of Mcrea (1950) and more recently by Swart et al. (1991). 3 ml. of 100%H_3PO_4 is aliquotted into the bottom of a lambda tube, with between 5-24 mg. of powdered carbonate-bearing sample in the arm of the vessel, and the whole is then evacuated to a vacuum of better than 10-4 mbars. The vessel is then placed in a controlled temperature water bath at 50 deg.C., and allowed to thermally equilibrate for an hour, before the acid is tipped into the sample position. Reaction is complete within 24 hr. for calcite, while reaction times of up to 72 hr. are required for dolomite and siderite; all times are of sufficient length to avoid isotopic fractionation as a result of partial reaction (Walters et al., 1972). After reaction, the CO_2 produced is frozen into a collection bottle with liquid nitrogen, passing first through a trap held at the freezing temperature of acetone (-78 deg.C.) to remove any water vapour present. All isotopic measurements are subsequently performed with a Micromass Optima dual inlet, triple collector, stable isotope mass spectrometer, using reference gas calibrated against the NBS-19 carbonate standard, and data corrected for the usual isobaric interferences at masses 45 and 46 (Craig, 1957), and to a temperature of 25 deg.C (Swart et al., 1991) for the oxygen results. Data are reported as $\delta^{13}C$ - and $\delta^{18}O$ -values for the CO_2 gas relative to PDB as defined by:

$$\delta^{18}O = [\ 18Rsample/18Rstandard - 1] \times 1000 \quad \text{(permil)}$$

where 18R is the isotopic $^{18}O/^{16}O$ ratio. Repeat analyses of the ANU-M1 calcite working standard ($\delta^{13}C$ =+1.32, $\delta^{18}O$ =-6.05) using the above methods show a reproducibility for both ratios to within +/-0.05 permil of the accepted values over a period of 3 years.

XRD (Appendix 3)

Samples were analysed by the James Cook University Advanced Analytical Centre's Siemens D5000 X-ray Diffractometer (Divergence slit = 1mm; Antiscatter slit=1mm; Secondary graphite monochronater slit = 0.2mm; Monochroneter slit = 0.6mm).

Samples were prepared for XRD analysis by the smear mount method (Moore and Reynolds, 1997). 2θ for the untreated XRD analysis was 1.3-65.3° (step size = 0.02; 2.4sec/step). Clay mineralogy was further discriminated (2θ=1.3-30°;step size = 0.02; 2.4sec/step) by additional analyses after treatment with a) GLY = treating with ethylene glycol at 60°C for at least 8 hours (Moore and Reynolds, 1997), b) H400 = heating to 400°C for at least ½ hour, c) H500 = heating to 550°C for at least ½ hour (Starkey et al., 1984).

The Siemens General Area Detector Diffraction System Micro-Diffractometer (GADDS = non-destructive in situ XRD analysis of hand specimen samples) was used for routine mineral identification. Analyses were conducted with the 800µm collimator. Count times ranged between 10-30 seconds (detailed in Appendix 3). Mineral/silicate 2θ scan range = 23-58° and Clay 2θ scan range = 10-45°.

XRD interpretation was performed with the "DIFFRAC^{plus} Evaluation Package (release 2002)" which utilised Powder Diffraction Files (release 2002) prepared by the International Centre for Diffraction Data (www.icdd.com).

Microprobe (Appendix 5)

Routine EDS analysis with the James Cook University Advanced Analytical Center's JEOL 840A electron microprobe (EMPA) is a high resolution SEM and a WD/ED Combined Electron Probe Microanalyser (EPMA). Each analysis was collected for a 40 second count. An internal standardisation procedure (ZAF corrected using MORAN scientific Software) was based on minerals with known stoichiomentry: Carbonate ("Astimex" calcite, dolomite and siderite standards); Sphalerite ("Astimex" and "RM Taylor" standards); Gold (Synthetic standards ranging from pure gold to pure silver with Au:Ag ratios of 80:20, 60:40, 40:60, 20:80).

Laser Ablation – ICPMS (Appendix 7)

GEMOC (Norman Pearson pers comm., 2003)

Trace element analyses of sulphides were obtained using a laser ablation ICPMS (LA-ICPMS) system in the Geochemical Analysis Unit, ARC National Key Centre GEMOC, Macquarie University. The system comprised a Merchantek LUV266 laser microprobe connected to an Agilent 7500s ICPMS. Laser operating conditions included a repetition rate of 5 Hz, output power of 50-60 mJ/pulse and a spot-size of 50 µm. Ablation was carried out in a mixture of He + Ar in a ratio of 30:70 percent. Raw counts were collected on the ICPMS in peak-hopping mode (dwell time 30 ms) and displayed in time-resolved format. This allowed each ablation to be monitored to identify heterogeneities due to fluid or mineral inclusions, and compositional variations with depth.

Trace element concentrations quantified using a synthetic nickel sulphide standard (PGE-A) as the external standard include: Te125-pge; Te128-pge; Cu65-pge; As75-pge; Bi209-pge; Se82-pge; S34-pge; Ni60-pge; Ni62-pge; Ir193-pge; Os189-pge; Os190-pge; Ru101-pge; Ru99-pge; Rh103-pge; Pt195-pge; Pd108-pge; Au197-pge. Sulphur was used as an internal standard. Sulphur concentrations for pyrite and chalcopyrite assumed stoichiometric compositions for these minerals, while those for sphalerite were obtained by electron microprobe analysis (Appendix 5).

Trace element concentrations quantified using a synthetic glass standard (NIST-500) as the external standard include: La139; Ce140; Nd146; Hf178; Au197; Ti49; Y89; Nb93; Mo95; W182; Ag107; As75; Bi209; Ca43; Cd111; Cu65; Fe57; Ga71; In115; Mn55; Pb208; Re185; Re187; Sb121; Se82; Si29; Sn118; Th232; U238; V51; Zn66; Zr90; Al27; Sc45; Cr53; Co59; Ni62; Ni60. Iron was used as an internal standard for pyrite and chalcopyrite (assumed stoichiometric compositions for these minerals), while zinc was used as an internal standard for sphalerite which was obtained by electron microprobe analysis (Appendix 5).

Data reduction used the GLITTER (www.es.mq.edu.au/gemoc/glitter) software package (Van Achterbergh et al., 2001).

Fluid Inclusions (Appendix 8)

A Linkam heating and cooling stage (www.linkam.co.uk) at James Cook University was used for all of the microthermometry measurements. The Linkam system consists of a TMS92 controller with a LNP2 pump and a THMSG600 stage, which is run by the Linksys software version 2.23. The stage was calibrated with “SYN FLINC” standards over a range of temperatures. For temperatures near or below 0°C, the accuracy of the stage is within ±0.5°C.

Sulphur Isotopes (Appendix 9)

CSL, University of Tasmania (cf. Keith Harris, 2003):

(1) Conventional Technique.

Sulphide mineral separates (8-25 milligrams, depending on sulphide species, purity and anticipated SO_2 yield) are ground with 150 milligrams of Cu_2O, cuprous oxide, in an agate mortar, then placed in a pre-ignited mullite ceramic boat. The Cu_2O serves as the oxidant for the subsequent ignition of the sulphide sample at 950 deg.C in vacuo (Robinson and Kusakabe, 1975). The use of excess Cu_2O in this method ensures the low pO_2 favourable for SO_2 production, and negligible SO_3 is produced. Contaminant gases are removed as follows: H_2O is frozen out at the freezing point of acetone (-95 deg.C), and CO_2 is then removed from the SO_2 at the freezing point of n-pentane (-131 deg.C). All isotopic compositions are defined as:

$$d^{34}S = [34R\ sample/^{34}R\ standard - 1] \times 1000 \quad \text{(in per mil)},$$

where 34R is the isotopic $^{34}S/^{32}S$ ratio. The standard is Canyon Diablo Troilite (CDT). Isotopic analysis of the extracted SO_2 is performed with a VG SIRA Series 2 triple-collector mass spectrometer, using reference gas SO_2 calibrated against NBS 123 Sphalerite (+17.1 per mil versus CDT), and using Broken Hill Galena (+3.4 per mil vs. CDT) and Rosebery Galena (+12.4 per mil vs. CDT) as working standards to establish a calibration curve. All isotopic data are reported in per mil relative to CDT, with analytical uncertainties better than +/- 0.3 per mil CDT for homogeneous mineral separates.

(2) Sulphur Isotopes by Laser Ablation.

The apparatus and method for sulphur isotope analysis by the in situ laser ablation of sulphide grains in polished thin sections is described fully in Huston et al. (1995). In particular, additive empirical correction factors which are determined by the comparison of results obtained by the conventional technique (see above) with raw $d^{34}S$ values measured from the SO_2 produced during the ablation, add an additional analytical uncertainty to the results obtained by this method. The latter is primarily due to minor, but real, isotopic inhomogeneities in the sulphide grains ablated for the calibration

experiments. Accordingly, analytical uncertainties of +/- 0.7 per mil CDT (1S.D.) apply to these results.

XRF (Appendix 11)

Samples were analysed by the James Cook University Advanced Analytical Centre's Siemens SRS3000 X-ray Fluorescence Spectrometer.

$^{40}Ar/^{39}Ar$ Geochronology (Appendix 12)

$^{40}Ar/^{39}Ar$ results:

Sample	Irradiation	mineral	analysis	# of steps	MSWD	Age	±2s	Comments
KP11	NM-162	muscovite	furnace step-heat	12	10	2.82	.04	isochron age
Prendergast adularia	NM-166	adularia	furnace step-heat	10	12.7	3.62	0.05	age spectrum

Instrumentation, analytical parameters and sample preparation and irradiation is fully detailed in Appendix 12.

SIMS analysis (Section C; Appendix 13)

(source: http://www.ansto.gov.au/ansto/environment1/capabilities/sims/howdoesitwork.htm)

SIMS is a destructive surface analytical technique. A primary ion bombards the surface, causing ions, atoms and molecules to be ejected ('sputtered') from the surface. The energy of the primary ions is of the order of 10 of keV, more than enough to eject atoms and molecules from the surface layers. The actual depth of interaction is usually a few nm.

As the beam moves ('rasters') across the surface it sputters a crater deeper into the sample. Continuous detection of this sputtering allows the SIMS to create a depth profile of the surface and underlying layers to a depth of 10 microns.

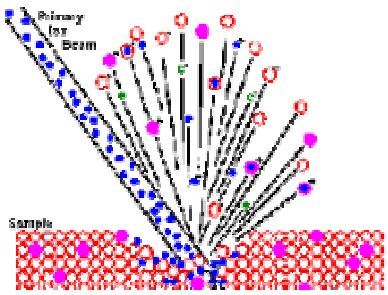

© Copyright Charles Evans & Associates

Main Steps of SIMS Analysis Process·

- Primary ions are produced by a cesium (1) source and are accelerated along the primary column (3-4) and focused onto the sample surface (5). ·
- Sputtered secondary ions pass through a secondary column (6-8), where they are collected and separated by charge (9).·
- The secondary ions are then collected and focussed through the mass spectrometer (13). ·
- The analysed ions are then directed into detectors, and a signal is measured. The electron multiplier (22) amplifies the incoming signal for each element to be large enough to be measured. ·

Schematic of Cameca ims 5f SIMS

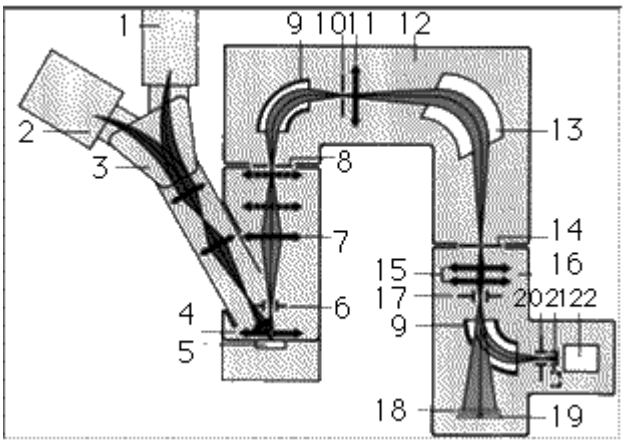

1. Cesium ion source	9. Electrostatic sector	17. Deflector
2. Duoplasmatron source	10. Energy slit	18. Channel-plate
3. Primary beam mass filter	11. Spectrometer lens	19. Fluorescent screen
4. Immersion lens	12. Spectrometer	20. Deflector
5. Specimen	13. Electromagnet	21. Remote controlled Faraday cup
6. Dynamic transfer system	14. Exit slit	22. Electron multiplier
7. Transfer optical system	15. Projection lens	
8. Entrance slit	16. Projection display & detection system	

Appendix 2a

Sample list

JCU catalogue number, drillhole and depth; brief sample description and index of work completed

Appendix 2b

Freeport drillhole assay results and XYZ coordinates (Projection WGS84 / UTM zone 53)

Notes to accompany Appendix 2A

Information	**Description**
JCU Number	James Cook University Catalogue Number
Sample_No	Sample Number (usually a combination of "Hole ID" and "Depth")
Location Hole ID	Location ID or Hole ID
Depth	Depth if sampled from drillhole
Description	Sample Description. More detailed description and/or paragenetic context in Appendix 10. Geological context available from summary drill hole logs in Appendix 6
Hand Specimen	Annotated if catalogued
Polished Section	Annotated with section number "KP", "BG", "JL" or source ("PM" = Phil Maguire manufactured section; "GC" = section courtesy of Gavin Clarke; "JCU" = JCU manufactured section)
Section offcut	Polished section offcut
Fluid Inclusion Section/ Chips	Annotated with sample number (Appendix 8)
GADDS Analyses	Annotated with sample number (Appendix 3)
XRD Analyses	Annotated with sample number (Appendix 3)
XRD Powders	Powdered duplicate sample available
XRF Analyses	Appendix 11
Micro probe Analysis	A=Gold analysis; C=Carbonate analysis; S=Sphalerite analysis (and sample number): Appendix 5
Sulphur Isotope Analysis & Sample	Annotated with sample number (Appendix 9)
Fluid Inclusion Analysis	Annotated with sample number where available (Appendix 8)
C-O Isotope Analysis	Conventional Analysis. Annotated with isotope sample number (Table 1; Section C)
C-O Isotope extra sample	Extra sample material - not separated
C-O Isotope powders	Extra sample material - powders
SIMS C-O Isotope Analysis	CO isotope analyses using the SIMS technique (Appendix 1, 13)
40Ar/ 39Ar Analysis	Appendix 12
LA-ICPMS Analysis & Section	Annotated with LA-ICPMS sample number (Appendix 7)
Re assay	Geochemical re-analysis of samples (Appendix 4)
Comments	General comments and location information (Projection WGS84 / UTM zone 53) where not available in Appendix 2B.
"Missing" denotes missing material	

Appendix 2a - List of Specimens

JCU Number	Sample_No	Location Hole ID	Depth	Description	Hand Specimen	Polished Section	Section offcut	Fluid Inclusion Section/ Chips	GADDS Analyses	XRD Analyses	XRD Powders	XRF Analyses	Re-Os Analysis	Micro probe Analysis
68974	31	GRS127	655.9	fine-grained pale grey limestone, moderate bleaching, small black specs (siltstone?)	X					3752-35	X			
68975	32	GRS127	660.9	broken/fracture fine-grained limestone. White, black and Iron-oxide on fracture	X					3752-36	X			
68976	42	GRS127	711.0	last limestone before silica-alteration - very bleached	X					3752-37	X			
68766	A94-31-1	A94-31-1	206.0	Massive pyrite from heavy sulphide zone, small crosscutting chalcopyrite veinlets			X							
68767	BG1-4A-229	BG01-04A	229.0	oxidised sulphide	X	(PM)	X							
68768	BG1-4A-256	BG01-04A	256.0	sandy and clay	X					3752-23	X			
68769	BG1-4A-330	BG01-04A	330.0	host and oxidised sulphide	X	(PM)	X							S
68770	BG1-4A-400	BG01-04A	400.0	oxidised sulphide	X	(PM)	X						?	A
68771	BG1-4A-423	BG01-04A	423.0	white clay alteration	X					3752-24	X			
68772	BG1-5-234	BG01-05	234.0	oxidised sulphide	X								?	
68773	BG1-5-238	BG01-05	238.0	oxidised sulphide	X	BG20	X						?	A
68774	BG1-5-256	BG01-05	256.0	oxidised sulphide	X	(PM)	X							A
68775	BG1-7-108	BG01-07	108.0	clay	X					3752-25	X			
68776	BG1-7-167	BG01-07	167.0	oxidised sulphide	X	(PM)	X							
68777	BG1-7-190	BG01-07	190.0	oxidised sulphide	X	(PM)	X							
68778	BGA	BGA		underground sample of west drift breccia. Anhydrite and talc	X		X	X						
68779	BGU07-6-221.2	BGU07-06	221.2	quartz crystal and sulphide and at other end, carbonate - host = silicified? Skarn	X				4612-214, 355					
68780	BGU07-6-268.8	BGU07-06	268.8	3 samples of brown dolomite? (also at 200m in 8-1) after chalcopyrite and white mineral alteration (calcite-rich) and 2nd white fibrous mineral (wollastonite?)	X								?	
68781	BGU07-6-342	BGU07-06	342.0	coarse pyrite		BG21	X							A
68784	BGU08-07-220.1	BGU08-07	220.1	pink hornfels rock	X				4612-199-203					
68782	BGU08-1-225	BGU08-01	225.0	coarse pyrite and chalcopyrite		BG23	X							A
68783	BGU08-5-190.1	BGU08-05	190.1	coarse pyrite		BG22	X							S-(BG22)
68785	BGU14-7-590b	BGU14-07	590.0	garnet and pyroxene for isotopes, carbonate with them	X				4612-345, 198					
68786	BGU17-07-400.4	BGU17-07	400.4	Big gossan phlogopite sample	X	(PM)	X							
68787	BGU17-07-460	BGU17-07	460.0	Coarse pyroxene and garnet with later infill carbonate	X				4612-352, 3					
68789	BGU18-03-192.5	BGU18-03	192.5	marble and limestone breccia - some marble clasts and some limestone clasts with alteration rims.	X				4612-220-3					
68790	BGU18-03-192.6	BGU18-03	192.6	marble and limestone breccia - some marble clasts and some limestone clasts with alteration rims.	X				4612-224, 5					
68791	BGU18-03-192.7	BGU18-03	192.7	marble and limestone breccia - some marble clasts and some limestone clasts with alteration rims.	X									
68792	BGU18-03-203	BGU18-03	203	white marble before skarn	X				4612-153, 4					

Appendix 2a - List of Specimens

JCU Number	Sample_No	Location Hole ID	Depth	Sulphur Isotope Analysis & Sample	Fluid Inclusion Analysis	C-O Isotope Analysis	C-O Isotope extra sample	C-O Isotope powders	SIMS C-O Isotope Analysis	40Ar/ 39Ar Analysis	LA-ICPMS Analysis & Section	Re assay	Comments
68974	31	GRS127	655.9										
68975	32	GRS127	660.9										
68976	42	GRS127	711.0										
68766	A94-31-1	A94-31-1	206.0								GIC		Courtesy of Pollard and Taylor: Location: Likely to be drillhole AM96-31-01 (collar = East 734702 North 9550572 Elev 3038 Azimuth 344 Dip -0.382 EOH 507.1)
68767	BG1-4A-229	BG01-04A	229.0										
68768	BG1-4A-256	BG01-04A	256.0										
68769	BG1-4A-330	BG01-04A	330.0	BG4a							BG34		LA-sulphur isotope analysis
68770	BG1-4A-400	BG01-04A	400.0										
68771	BG1-4A-423	BG01-04A	423.0										
68772	BG1-5-234	BG01-05	234.0										
68773	BG1-5-238	BG01-05	238.0										
68774	BG1-5-256	BG01-05	256.0								BG35		
68775	BG1-7-108	BG01-07	108.0										
68776	BG1-7-167	BG01-07	167.0										
68777	BG1-7-190	BG01-07	190.0										
68778	BGA	BGA											Location: near "UG sample C" (Section C)
68779	BGU07-6-221.2	BGU07-06	221.2										
68780	BGU07-6-268.8	BGU07-06	268.8										
68781	BGU07-6-342	BGU07-06	342.0										Called 324m in Gold probe
68784	BGU08-07-220.1	BGU08-07	220.1										
68782	BGU08-1-225	BGU08-01	225.0										
68783	BGU08-5-190.1	BGU08-05	190.1								JC22		
68785	BGU14-7-590b	BGU14-07	590.0			KP08	X	X					
68786	BGU17-07-400.4	BGU17-07	400.4							X			
68787	BGU17-07-460	BGU17-07	460.0			KP26	X	X					
68789	BGU18-03-192.5	BGU18-03	192.5										
68790	BGU18-03-192.6	BGU18-03	192.6										
68791	BGU18-03-192.7	BGU18-03	192.7			KP01	X	X					Mixed composition C-O isotope signal - result not used
68792	BGU18-03-203	BGU18-03	203										

Appendix 2a - List of Specimens

JCU Number	Sample_No	Location Hole ID	Depth	Description	Hand Specimen	Polished Section	Section offcut	Fluid Inclusion Section/ Chips	GADDS Analyses	XRD Analyses	XRD Powders	XRF Analyses	Re-Os Analysis	Micro probe Analysis
68793	BGU18-03-211.2	BGU18-03	211.2	host is carbonate - is recrystallised where sphalerite-pyrite-quartz replacement occurs	X	BG06	X	JC6	4612-301, 2					A, S-(BG06)
68794	BGU18-03-212	BGU18-03	212	massive pyrite and quartz with fragments of black material (host with chalcopyrite?)	X	BG19	X		4612-295-298					
68788	BGU18-03-32.5	BGU18-03	32.5	part of 3m zone of black alteration (biotite?) and calcite marble. This is overprinted by white-yellow marble and red alteration (garnet?)	X				4612-215-9					
68795	BGU19-03-184.7	BGU19-03	184.7	gold-rich massive sulphide zone (replacement?)	X	BG13	X	JC13						A, S-(BG13)
68796	BGU21-01-13	BGU21-01	13	carbonate breccia in simplest form. Limestone clasts with white alteration - yellow ? And later calcite.	X				4612-178-181; 339-341					
68798	BGU21-01-43	BGU21-01	43	green and purple alteration of breccia	X				4612-204-6					
68804	BGU21-03-24.5	BGU21-03	24.5	a flake of native gold in quartz and sulphide vein. Pyrite and sphalerite, ?As-rich. Carbonate as vugh rhomboids on late stage quartz. Occurs as replacement of pre-existing calcite alteration/breccia in grey limestone.	X				4612-317					
69129	BGU21-03-24.6	BGU21-03	24.6	banded quartz and carbonate	X									
68805	BGU21-03-51.3	BGU21-03	51.3	talc alteration of carbonate breccia	X				4612-159-161					
68806	BGU21-03-53.5	BGU21-03	53.5	talc alteration of breccia and anhydrite	X				4612-148-152					
68807	BGU21-03-59	BGU21-03	59	normal breccia	X				4612-182-183					
68808	BGU21-03-62	BGU21-03	62.0	green alteration of breccia	X				4612-155-158					
68817	BGU21-10-12	BGU21-10	12.0	Massive sphalerite, pyrite vuggy vein. Overprinting grey marble breccia with pale yellow matrix.	X	(PM)	X		4612-354					C
68818	BGU21-10-159	BGU21-10	159.0	black and white alteration of marble/skarn? Also have photo of core tray hornfels zone? From >70m	X				4612-147					
68819	BGU21-10-236.7	BGU21-10	236.7	skarn with chalcopyrite and minor pyrite, very distinctive coarse-grained chalcopyrite	X	BG08	X							A
68820	BGU21-10-251.4A	BGU21-10	251.4	Massive Sulphide vein (pyrite, magnetite) in rock with chlorite	X	(PM)	X							
68821	BGU21-10-251.4B	BGU21-10	251.4	Massive Sulphide vein (pyrite, magnetite) in rock with chlorite	X	(PM)	X							
68816	BGU21-10-7.5	BGU21-10	7.5	dull pyrite with quartz infill	X				4612-313-316					
68797	BGU21-1-20.4	BGU21-01	20.4	Only sulphide-rich sample from high grade Au zone	X	(PM)	X							
68800	BGU21-2-13.3A	BGU21-02	13.3	pyrite (vuggy) in limestone breccia	X	(PM)	X							A, S
68801	BGU21-2-13.3B	BGU21-02	13.3	pyrite (vuggy) in limestone breccia	X	(PM)	X	JL06						A
68802	BGU21-2-14	BGU21-02	14.0	limestone with magnetite and pyrite, chalcopyrite in breccia matrix. Nice alteration margin on grey limestone clast	X	(PM)	X							A
68809	BGU21-3-224.5	BGU21-03	224.5	skarn, coarse pyrite, chalcopyrite	X	BG04	X							

Appendix 2a - List of Specimens

JCU Number	Sample_No	Location Hole ID	Depth	Sulphur Isotope Analysis & Sample	Fluid Inclusion Analysis	C-O Isotope Analysis	C-O Isotope extra sample	C-O Isotope powders	SIMS C-O Isotope Analysis	40Ar/ 39Ar Analysis	LA-ICPMS Analysis & Section	Re assay	Comments
68793	BGU18-03-211.2	BGU18-03	211.2		BG06	KP64, KP65		X			BG06		
68794	BGU18-03-212	BGU18-03	212								BG19		
68788	BGU18-03-32.5	BGU18-03	32.5										
68795	BGU19-03-184.7	BGU19-03	184.7	BG13							BG13		LA-sulphur isotope analysis
68796	BGU21-01-13	BGU21-01	13		KP27, KP28, KP29		X	X					
68798	BGU21-01-43	BGU21-01	43										
68804	BGU21-03-24.5	BGU21-03	24.5										
69129	BGU21-03-24.6	BGU21-03	24.6										
68805	BGU21-03-51.3	BGU21-03	51.3										
68806	BGU21-03-53.5	BGU21-03	53.5										
68807	BGU21-03-59	BGU21-03	59		KP33, KP34, KP45		X	X					
68808	BGU21-03-62	BGU21-03	62.0										
68817	BGU21-10-12	BGU21-10	12.0		KP38, KP39, KP40		X	X	X				
68818	BGU21-10-159	BGU21-10	159.0										
68819	BGU21-10-236.7	BGU21-10	236.7										Called 236B in gold probe
68820	BGU21-10-251.4A	BGU21-10	251.4										
68821	BGU21-10-251.4B	BGU21-10	251.4										
68816	BGU21-10-7.5	BGU21-10	7.5										
68797	BGU21-1-20.4	BGU21-01	20.4										
68800	BGU21-2-13.3A	BGU21-02	13.3										
68801	BGU21-2-13.3B	BGU21-02	13.3	JL06							JL06		LA-sulphur isotope analysis
68802	BGU21-2-14	BGU21-02	14.0								BG30		
68809	BGU21-3-224.5	BGU21-03	224.5										

Appendix 2a - List of Specimens

JCU Number	Sample_No	Location Hole ID	Depth	Description	Hand Specimen	Polished Section	Section offcut	Fluid Inclusion Section/ Chips	GADDS Analyses	XRD Analyses	XRD Powders	XRF Analyses	Re-Os Analysis	Micro probe Analysis
68810	BGU21-3-225.1	BGU21-03	225.1	coarse pyrite, chalcopyrite, calcite and sphalerite infill. Sphalerite appears to vein chalcopyrite	X	(PM)	X							A
68811	BGU21-3-225.5	BGU21-03	225.5	coarse pyrite, chalcopyrite, calcite and sphalerite infill. Sphalerite appears to vein chalcopyrite	X	(PM)	X							
68812	BGU21-3-226.3	BGU21-03	226.3	coarse pyrite and sphalerite (minor chalcopyrite) vein in amphibole and dark green (clinopyroxene?) rock	X	(PM)	X	JL09						S
68813	BGU21-3-234.4	BGU21-03	234.4	finely bedded skarn rock with disseminated sulphide (high Ag)	X	(PM)	X							
68803	BGU21-3-24.3	BGU21-03	24.3	sphalerite, pyrite, magnetite and orange calcite vuggy vein	X	(PM)	X							
68814	BGU21-5-17.5	BGU21-05	17.5	marble breccia with cream matrix and magnetite and pyrite		(PM)	X	JL07						
68815	BGU21-5-22	BGU21-05	22.0	Marble with vuggy calcite, cubic pyrite and magnetite vein. Pyrite cubes in white breccia matrix	X		X	chips						
68823	BGU22-1-15.2	BGU22-01	15.2	magnetite, pyrite, sphalerite Massive Sulphide	X	(PM)	X							
68822	BGU22-1-8	BGU22-01	8.0	Massive Sulphide with vuggy pyrite, magnetite, sphalerite orange calcite	X	(PM)	X							
68828	BGU23-03-180	BGU23-03	180.0	sulphide (pyrite)	X	(PM)	X							
68835	BGU23-08-10	BGU23-08	10.0	carbonate with pyrite infill	X				4612-207-208					
68838	BGU23-08-86	BGU23-08	86.0	limestone with white alteration, then green tremolite, then fine-grained pyrite	X				4612-140-143					
68839	BGU23-08-87	BGU23-08	87.0	limestone with white alteration (a bit friable), pre-green mineral	X				4612-144-145					
68825	BGU23-2-46	BGU23-02	46.0	marble breccia, grey clasts and green-alteration matrix is breccia and infilled with pink anhydrite and grey-white calcite? Magnetite spots "vein" through pink anhydrite. One amphibole? Vugh on back of core. Magnetite vein and pale alteration in grey marble clast	X				4612-290-294					
68826	BGU23-2-48.6	BGU23-02	48.6	limestone breccia, grey clasts and pale-med green alteration/matrix. Possible minor translucent-grey calcite infill/matrix (relationship unclear)	X				4612-190-193					
68827	BGU23-2-64.8	BGU23-02	64.8	pale green matrix/alteration with magnetite, chlorite? (dark green clinopyroxene?) on fracture and veins, also pyrite	X	(PM)	X		3752-67-70					
68824	BGU23-2-9	BGU23-02	9.0	limestone breccia, grey clasts (one tending towards yellow-white) with pale green and cream matrix. This has been breccia and infilled with pink anhydrite and calcite (can see pale green clasts)	X				4612-171-177					

Appendix 2a - List of Specimens

JCU Number	Sample_No	Location Hole ID	Depth	Sulphur Isotope Analysis & Sample	Fluid Inclusion Analysis	C-O Isotope Analysis	C-O Isotope extra sample	C-O Isotope powders	SIMS C-O Isotope Analysis	40Ar/ 39Ar Analysis	LA-ICPMS Analysis & Section	Re assay	Comments
68810	BGU21-3-225.1	BGU21-03	225.1										
68811	BGU21-3-225.5	BGU21-03	225.5										
68812	BGU21-3-226.3	BGU21-03	226.3								JL09		
68813	BGU21-3-234.4	BGU21-03	234.4										
68803	BGU21-3-24.3	BGU21-03	24.3										
68814	BGU21-5-17.5	BGU21-05	17.5								JL07		
68815	BGU21-5-22	BGU21-05	22.0		BG25						BG31		Also called BGU27-5-22 in fluid inclusion analysis
68823	BGU22-1-15.2	BGU22-01	15.2										
68822	BGU22-1-8	BGU22-01	8.0										
68828	BGU23-03-180	BGU23-03	180.0										
68835	BGU23-08-10	BGU23-08	10.0										
68838	BGU23-08-86	BGU23-08	86.0										
68839	BGU23-08-87	BGU23-08	87.0										
68825	BGU23-2-46	BGU23-02	46.0										
68826	BGU23-2-48.6	BGU23-02	48.6										
68827	BGU23-2-64.8	BGU23-02	64.8										
68824	BGU23-2-9	BGU23-02	9.0										

Appendix 2a - List of Specimens

JCU Number	Sample_No	Location Hole ID	Depth	Description	Hand Specimen	Polished Section	Section offcut	Fluid Inclusion Section/ Chips	GADDS Analyses	XRD Analyses	XRD Powders	XRF Analyses	Re-Os Analysis	Micro probe Analysis
68829	BGU23-5-147.6	BGU23-05	147.6	Clay altered tremolite from zone with yellow garnets (147.5)	X					3752-26	X			
68833	BGU23-6-105.8	BGU23-06	105.8	pale silica and green alteration with anhydrite vein? Crosscut by epidote vein (white selvedge and internal black specs - magnetite?)	X				4612-210-213					
68834	BGU23-6-147.1	BGU23-06	147.1	2nd breccia? With magnetite-rich clast (or alteration?) and soft green clast (chlorite) and epidote, (and sulphide?) clast all with amphibole infill. Pale green material present	X				4612-194-196					
68830	BGU23-6-66	BGU23-06	66.0	limestone marble clasts breccia	X				4612-342-343					
68831	BGU23-6-80	BGU23-06	80.0	Massive Sulphide	X	(PM)	X							
68832	BGU23-6-80.5	BGU23-06	80.5	contact of marble with skarn/green minerals and sulphide vein - very sharp	X				3752-71-72					
68840	BGU23-8-144.2	BGU23-08	144.2	marble breccia with black matrix	X				4612-187-188					
68841	BGU23-8-212	BGU23-08	212.0	Vuggy sphalerite vein in skarn. Garnet present		(PM)	X							
68842	BGU23-8-212.6	BGU23-08	212.6	Vuggy sphalerite vein in skarn. Garnet present	X	(PM)	X							
68836	BGU23-8-25.5	BGU23-08	25.5	limestone breccia, pale yellow and white groundmass and magnetite spots	X				4612-184-186					
68837	BGU23-8-38.8	BGU23-08	38.8	breccia, pale green/grey limestone clasts (small white selvedge) and white/grey matrix with magnetite spots	X				4612-162-165					
69130	BGU24-10-16	BGU24-10	16	massive pyrite in breccia (no grade)	X									
68844	BGU24-10-305	BGU24-10	305.0	vein of sphalerite-galena-pyrite in chalcopyrite-bearing green skarn	X	BG05	X		4612-309, 310, 312					A, S-(BG05)
68845	BGU24-11-177	BGU24-11	177.0	symmetrical serpentine vein in limestone	X	(PM)			3752-58-61					C
68846	BGU24-11-343	BGU24-11	343.0	pyrite and dark veins (sphalerite?)		BG24	X							A, S-(BG24)
68847	BGU24-13-139	BGU24-13	139.0	sulphide (pyrite etc)	X	(PM)	X							
68848	BGU24-13-143.5	BGU24-13	143.5	sphalerite, pyrite and galena	X	(PM)	X							
68843	BGU24-8-255.2	BGU24-08	255.2	coarse pyrite, carbonate, minor chalcopyrite	X	BG17	X							
68850	BGU26-01-151.9	BGU26-01	151.9	Cubic pyrite - oxidised sulphide	X	(PM)	X							S
68851	BGU26-01-152.3	BGU26-01	152.3	Cubic pyrite - oxidised sulphide	X	(PM)	X						?	
68852	BGU26-01-165.2	BGU26-01	165.2	oxidised sulphide	X	(PM)	X						?	A
68854	BGU26-03-122.4	BGU26-03	122.4	crystal infill - sulphide-oxidised (impregnate)	X		X	chips						
68855	BGU26-04-215.6	BGU26-04	215.6	clay altered rocks in skarn	X					3752-27	X			
68856	BGU26-04-275.5	BGU26-04	275.5	sphalerite vein in skarn	X	(PM)	X	X						
68857	BGU26-04-298.2	BGU26-04	298.2	clay and pyrite vein in skarn	X					3752-28	X			
68858	BGU26-10-121.5	BGU26-10	121.5	banded massive sulphide	X	(PM)	X							S
68849	BGU26-1-151	BGU26-01	151.0	massive pyrite (high Au interval)	X	BG07	X							A
68853	BGU26-2-207	BGU26-02	207.0	coarse pyrite, hematite pseudomorphs, chalcopyrite	X	BG10 BG11	X							A
68862	BGU27-05-124	BGU27-05	124.0	oxidised sulphide	X	(PM)	X							
68863	BGU27-05-124.1	BGU27-05	124.1	oxidised sulphide	X	(PM)	X							
68859	BGU27-2-204.5	BGU27-02	204.5	chalcopyrite-rich, pyrite and carbonate	X	BG02	X							A

Appendix 2a - List of Specimens

JCU Number	Sample_No	Location Hole ID	Depth	Sulphur Isotope Analysis & Sample	Fluid Inclusion Analysis	C-O Isotope Analysis	C-O Isotope extra sample	C-O Isotope powders	SIMS C-O Isotope Analysis	40Ar/ 39Ar Analysis	LA-ICPMS Analysis & Section	Re assay	Comments
68829	BGU23-5-147.6	BGU23-05	147.6										
68833	BGU23-6-105.8	BGU23-06	105.8										
68834	BGU23-6-147.1	BGU23-06	147.1										
68830	BGU23-6-66	BGU23-06	66.0		KP30, KP31, KP32		X	X					
68831	BGU23-6-80	BGU23-06	80.0										
68832	BGU23-6-80.5	BGU23-06	80.5										
68840	BGU23-8-144.2	BGU23-08	144.2										
68841	BGU23-8-212	BGU23-08	212.0										
68842	BGU23-8-212.6	BGU23-08	212.6										
68836	BGU23-8-25.5	BGU23-08	25.5										
68837	BGU23-8-38.8	BGU23-08	38.8										
69130	BGU24-10-16	BGU24-10	16										
68844	BGU24-10-305	BGU24-10	305.0	BG05							BG05		LA-sulphur isotope analysis
68845	BGU24-11-177	BGU24-11	177.0		KP41, KP42, KP43			X	X				
68846	BGU24-11-343	BGU24-11	343.0	BG24							BG24		LA-sulphur isotope analysis
68847	BGU24-13-139	BGU24-13	139.0										
68848	BGU24-13-143.5	BGU24-13	143.5										
68843	BGU24-8-255.2	BGU24-08	255.2										
68850	BGU26-01-151.9	BGU26-01	151.9										
68851	BGU26-01-152.3	BGU26-01	152.3										
68852	BGU26-01-165.2	BGU26-01	165.2										
68854	BGU26-03-122.4	BGU26-03	122.4		BG27						BG32		
68855	BGU26-04-215.6	BGU26-04	215.6										
68856	BGU26-04-275.5	BGU26-04	275.5		BG26						BG33		Also called BGU26-4-327.5 in fluid inclusion analysis
68857	BGU26-04-298.2	BGU26-04	298.2										
68858	BGU26-10-121.5	BGU26-10	121.5										
68849	BGU26-1-151	BGU26-01	151.0										
68853	BGU26-2-207	BGU26-02	207.0										
68862	BGU27-05-124	BGU27-05	124.0										
68863	BGU27-05-124.1	BGU27-05	124.1										
68859	BGU27-2-204.5	BGU27-02	204.5										Also called BGU27-02-204 in Gold probe

Appendix 2a - List of Specimens

JCU Number	Sample_No	Location Hole ID	Depth	Description	Hand Specimen	Polished Section	Section offcut	Fluid Inclusion Section/ Chips	GADDS Analyses	XRD Analyses	XRD Powders	XRF Analyses	Re-Os Analysis	Micro probe Analysis
68861	BGU27-4-174	BGU27-04	174.0	pyrite chalcopyrite	X	BG12								
68864	BGU27-6-348.5	BGU27-06	348.5	sphalerite, pyrite	X	BG16	X							
68865	BGU27-6-349	BGU27-06	349.0	chalcopyrite, sphalerite, carbonate	X	BG18	X		4612-356-357					A, S-(BG18)
68866	BGU28-01-104	BGU28-01	104.0	2 pieces oxidised sulphide	X	(PM)	X							
68869	BGU28-07-185.4	BGU28-07	185.4	brown carbonate after sulphides and the late clear carbonate in vughs	X									
68870	BGU28-07-230	BGU28-07	230	sample courtesy of Roger Taylor - pyrrhotite with sphalerite vein and cu vein	X	(PM)	X							
68867	BGU28-5-267	BGU28-05	267.0	green rock, coarse pyrite, hematite pseudomorphs (magnetite).	X	BG03	X		4612-265-267					A
68868	BGU28-5-268	BGU28-05	268.0	green rock, coarse pyrite, hematite pseudomorphs (magnetite).	X	BG01	X							A
68871	BGU28-8-375	BGU28-08	375.0	massive pyrite - two textural types	X	BG14	X							
68872	BGU28-8-375-5	BGU28-08	375.5	massive pyrite - two textural types	X	BG09	X							
68873	BGU29-01-159	BGU29-01	159.0	sulphide - sphalerite - oxidised	X	(PM)	X							
68874	BGU29-02-242	BGU29-02	242.0	oxidised sulphide	X	(PM)	X							
68875	BGU29-07-130	BGU29-07	130.0	sand	X					3752-30	X			
68876	BGU29-07-197.5	BGU29-07	197.5	limestone with clay	X					3752-29	X			
68877	BGU30-03-180	BGU30-03	180.0	2 SECTIONS massive sulphide vein (pyrrhotite, pyrite, sphalerite, galena - possible order!)	X	(PM)								
68878	BGU30-03-180B	BGU30-03	180.0	2 SECTIONS massive sulphide vein (pyrrhotite, pyrite, sphalerite, galena - possible order!)	X	(PM)		JL10						S
68879	BGU30-04-137.9	BGU30-04	137.9	sulphides with quartz in talc-bearing rock	X		X	X						
68880	BGU30-04-138.9	BGU30-04	138.9	carbonate with talc and ?amphibole alteration and late stage pyrite, sphalerite	X				3752-64-66					
68881	BGU30-04-139.6	BGU30-04	139.6	carbonate with talc and ?amphibole alteration and late stage pyrite, sphalerite	X				3752-62-63					
68883	BGU30-06-173	BGU30-06	173.0	impregnate - oxidised sulphide	X	(PM)	X							
68884	BGU30-06-179	BGU30-06	179.0	oxidised sulphide	X	(PM)	X							A
68885	BGU30-08-186.5	BGU30-08	186.5	oxidised sulphide	X	(PM)	X							A
68882	BGU30-5-246	BGU30-05	246.0	massive pyrite	X	BG15	X		4612-311					A
68886	BG-underground	Big Gossan		West Drift breccia in west wall	X	KP01?	X							
68887	BG-underground	Big Gossan		at skarn contact - marble	X	KP02	X							
68888	BG-underground	Big Gossan		10m from corner "metamorphic marble"	X	KP03	X							
68889	BG-underground	Big Gossan		5m south wall "metamorphic marble"	X	KP05	X							
68890	BG-underground	Big Gossan		20m from skarn contact	X									
68891	BG-underground	Big Gossan		10m from skarn contact	X									
68892	BG-underground	Big Gossan		underground sample - coarse grained pyrite and quartz, carbonate crosscuts chalcopyrite and quartz.	X									

Appendix 2a - List of Specimens

JCU Number	Sample_No	Location Hole ID	Depth	Sulphur Isotope Analysis & Sample	Fluid Inclusion Analysis	C-O Isotope Analysis	C-O Isotope extra sample	C-O Isotope powders	SIMS C-O Isotope Analysis	40Ar/ 39Ar Analysis	LA-ICPMS Analysis & Section	Re assay	Comments
68861	BGU27-4-174	BGU27-04	174.0										
68864	BGU27-6-348.5	BGU27-06	348.5								BG36,37		
68865	BGU27-6-349	BGU27-06	349.0										
68866	BGU28-01-104	BGU28-01	104.0										
68869	BGU28-07-185.4	BGU28-07	185.4			KP35, KP46	X	No					
68870	BGU28-07-230	BGU28-07	230										
68867	BGU28-5-267	BGU28-05	267.0										
68868	BGU28-5-268	BGU28-05	268.0	BG01							BG01		LA-sulphur isotope analysis
68871	BGU28-8-375	BGU28-08	375.0	BG14							BG14		conventional S-isotope analysis. Also called 375.5
68872	BGU28-8-375-5	BGU28-08	375.5										
68873	BGU29-01-159	BGU29-01	159.0										
68874	BGU29-02-242	BGU29-02	242.0										
68875	BGU29-07-130	BGU29-07	130.0										
68876	BGU29-07-197.5	BGU29-07	197.5										
68877	BGU30-03-180	BGU30-03	180.0										
68878	BGU30-03-180B	BGU30-03	180.0		JL10						JL10		
68879	BGU30-04-137.9	BGU30-04	137.9		BG28						BG38		
68880	BGU30-04-138.9	BGU30-04	138.9										
68881	BGU30-04-139.6	BGU30-04	139.6										
68883	BGU30-06-173	BGU30-06	173.0										
68884	BGU30-06-179	BGU30-06	179.0										
68885	BGU30-08-186.5	BGU30-08	186.5										
68882	BGU30-5-246	BGU30-05	246.0										
68886	BG-underground	Big Gossan				KP07		X					Mixed composition C-O isotope signal - result not used: Location: near "UG sample C" (Section C)
68887	BG-underground	Big Gossan				KP04	X	X					Location: "UG sample 15" (Section C)
68888	BG-underground	Big Gossan				KP06		X					Location: "UG sample D" (Section C)
68889	BG-underground	Big Gossan				KP05	X	X					Location: "UG sample E" (Section C)
68890	BG-underground	Big Gossan				KP02		X					Mixed composition C-O isotope signal - result not used. Location: near "UG sample 16" (Section C)
68891	BG-underground	Big Gossan				KP03	X	X					Location: "UG sample 16" (Section C)
68892	BG-underground	Big Gossan				KP44	X	X					Location: "UG sample B" (Section C)

Appendix 2a - List of Specimens

JCU Number	Sample_No	Location Hole ID	Depth	Description	Hand Specimen	Polished Section	Section offcut	Fluid Inclusion Section/ Chips	GADDS Analyses	XRD Analyses	XRD Powders	XRF Analyses	Re-Os Analysis	Micro probe Analysis
68893	BG-underground	Big Gossan		carbonate after garnet, possible with chalcopyrite-magnetite/hematite (coarse-grained) pyrite assemblage.	Missing									
69070	BG-underground	Big Gossan		Underground rock. calcite and pyrite	X									
69126	Calcite standard	Calcite standard		Hydrothermal calcite crystal (10cm from larger crystal) from Mary Kathleen (Lucas Marshall, pers comm, 2003)	X		X							
68908	DOZ-B1-A	DOZ		Appendix 10	X	X								
68909	DOZ-B1-B	DOZ		Appendix 10	X	X								
68910	DOZ-B1-C	DOZ		Appendix 10	X	X								
68896	DOZ-B1-D	DOZ		Appendix 10	X	X	X							C
68911	DOZ-B1-E	DOZ		Appendix 10	X	X								
68912	DOZ-B1-F	DOZ		Appendix 10	X	X								
68913	DOZ-B1-G	DOZ		Appendix 10	X	X								
68897	DOZ-B2-A	DOZ		Appendix 10	X	X	X							C
68898	DOZ-B2-B	DOZ		Appendix 10	X	X								
68899	DOZ-B2-C	DOZ		Appendix 10	X	X								
68900	DOZ-B2-D	DOZ		Appendix 10	X	X								
68901	DOZ-B2-E	DOZ		Appendix 10	X	X								
68902	DOZ-B2-F	DOZ		Appendix 10	X	X								
68903	DOZ-B2-G	DOZ		Appendix 10	X	X								
68904	DOZ-B2-H	DOZ		Appendix 10	X	X								
68905	DOZ-B2-I	DOZ		Appendix 10	X	X								
68906	DOZ-B2-J	DOZ		Appendix 10	X	X								
68907	DOZ-B2-K	DOZ		Appendix 10	X	X								
68894	DOZ-underground	DOZ		Very leached carbonate from DOZ stop 1	X	KP06	X							
68895	DOZ-underground	DOZ		Recrystallised and friable carbonate from DOZ stop 1	X	KP07	X							
68916	GRS125-590.7	GRS125	590.7	carbonate host, calcite-rich. Stylolites seem to be defining a foliation.	X	(PM)	X	4612-66-71; 338						C
68917	GRS125-595.6	GRS125	595.6	Dark silica vein in carbonate host	X	(PM)	X	Section	4612-72-81; 346-348					

Appendix 2a - List of Specimens

JCU Number	Sample_No	Location Hole ID	Depth	Sulphur Isotope Analysis & Sample	Fluid Inclusion Analysis	C-O Isotope Analysis	C-O Isotope extra sample	C-O Isotope powders	SIMS C-O Isotope Analysis	40Ar/ 39Ar Analysis	LA-ICPMS Analysis & Section	Re assay	Comments
68893	BG-underground	Big Gossan				KP25	X	X					Location: "UG sample A" (Section C)
69070	BG-underground	Big Gossan				KP24	X	X					Location: "UG sample C" (Section C)
69126	Calcite standard	Calcite standard				KP63		X	X				Lucas Marshal pers comm, 2003
68908	DOZ-B1-A	DOZ											Unlocated samples courtesy of Stephen Spera (Spera, 2001) from EESS "Hydrothermal Carbonate Breccia" (Section C)
68909	DOZ-B1-B	DOZ											Unlocated samples courtesy of Stephen Spera (Spera, 2001) from EESS "Hydrothermal Carbonate Breccia" (Section C)
68910	DOZ-B1-C	DOZ											Unlocated samples courtesy of Stephen Spera (Spera, 2001) from EESS "Hydrothermal Carbonate Breccia" (Section C)
68896	DOZ-B1-D	DOZ							X				Unlocated samples courtesy of Stephen Spera (Spera, 2001) from EESS "Hydrothermal Carbonate Breccia" (Section C)
68911	DOZ-B1-E	DOZ											Unlocated samples courtesy of Stephen Spera (Spera, 2001) from EESS "Hydrothermal Carbonate Breccia" (Section C)
68912	DOZ-B1-F	DOZ											Unlocated samples courtesy of Stephen Spera (Spera, 2001) from EESS "Hydrothermal Carbonate Breccia" (Section C)
68913	DOZ-B1-G	DOZ											Unlocated samples courtesy of Stephen Spera (Spera, 2001) from EESS "Hydrothermal Carbonate Breccia" (Section C)
68897	DOZ-B2-A	DOZ							X				Unlocated samples courtesy of Stephen Spera (Spera, 2001) from EESS "Hydrothermal Carbonate Breccia" (Section C)
68898	DOZ-B2-B	DOZ											Unlocated samples courtesy of Stephen Spera (Spera, 2001) from EESS "Hydrothermal Carbonate Breccia" (Section C)
68899	DOZ-B2-C	DOZ											Unlocated samples courtesy of Stephen Spera (Spera, 2001) from EESS "Hydrothermal Carbonate Breccia" (Section C)
68900	DOZ-B2-D	DOZ											Unlocated samples courtesy of Stephen Spera (Spera, 2001) from EESS "Hydrothermal Carbonate Breccia" (Section C)
68901	DOZ-B2-E	DOZ											Unlocated samples courtesy of Stephen Spera (Spera, 2001) from EESS "Hydrothermal Carbonate Breccia" (Section C)
68902	DOZ-B2-F	DOZ											Unlocated samples courtesy of Stephen Spera (Spera, 2001) from EESS "Hydrothermal Carbonate Breccia" (Section C)
68903	DOZ-B2-G	DOZ											Unlocated samples courtesy of Stephen Spera (Spera, 2001) from EESS "Hydrothermal Carbonate Breccia" (Section C)
68904	DOZ-B2-H	DOZ											Unlocated samples courtesy of Stephen Spera (Spera, 2001) from EESS "Hydrothermal Carbonate Breccia" (Section C)
68905	DOZ-B2-I	DOZ											Unlocated samples courtesy of Stephen Spera (Spera, 2001) from EESS "Hydrothermal Carbonate Breccia" (Section C)
68906	DOZ-B2-J	DOZ											Unlocated samples courtesy of Stephen Spera (Spera, 2001) from EESS "Hydrothermal Carbonate Breccia" (Section C)
68907	DOZ-B2-K	DOZ											Unlocated samples courtesy of Stephen Spera (Spera, 2001) from EESS "Hydrothermal Carbonate Breccia" (Section C)
68894	DOZ-underground	DOZ											Location: X=737420 ; Y=9549050 ; Z=3120
68895	DOZ-underground	DOZ				KP47	X	X					Location: X=737420 ; Y=9549050 ; Z=3120
68916	GRS125-590.7	GRS125	590.7			KP20	X	X	X				
68917	GRS125-595.6	GRS125	595.6			KP21, KP22	X	X					

Appendix 2a - List of Specimens

JCU Number	Sample_No	Location Hole ID	Depth	Description	Hand Specimen	Polished Section	Section offcut	Fluid Inclusion Section/ Chips	GADDS Analyses	XRD Analyses	XRD Powders	XRF Analyses	Re-Os Analysis	Micro probe Analysis
68918	GRS125-599A	GRS125	599.0	Mottled calcite-rich host with white silica-rich zone (grey and white alteration)	X	(PM)	X							
68919	GRS125-599B	GRS125	599.0	Mottled calcite-rich host with white silica-rich zone (grey and white alteration)	X	(PM)	X		4612-89-95					
68920	GRS125-600	GRS125	600.0	Vuggy white vein. Can see grey and white material in vein (white around vughs)	X	(PM)	X	4612-82-88; 96-102						C
68921	GRS125-600.5	GRS125	600.5	vuggy silicified rock with sulphide and clay	X					3752-16	X			
68922	GRS125-601	GRS125	601.0	Grey carbonate with white vuggy silica veins. NB wherever vughs are white silica? veins seem to be	X	(PM)	X	4612-113-116						
68923	GRS125-601.4	GRS125	601.4	Crackle network. Vughs are in grey host. See Massive Sulphide to go around white.	X	(PM)	X							
68924	GRS125-602.7	GRS125	602.7	carbonate host with white vein.	X	(PM)	X	4612-105-107						
68925	GRS125-604	GRS125	604.0	Foliation present. Grey over white spot. Some leaching taking out white spot. Some extra white may also be present.	X	(PM)	X	4612-108-112						
68926	GRS125-608.6	GRS125	608.6	grey silica in carbonate rock	X	(PM)	X	4612-117-121; 336-337						C
68927	GRS125-610	GRS125	610.0	grey silica in carbonate rock	X	(PM)	X	4612-122-126						
68928	GRS125-611.3	GRS125	611.3	silica and carbonate and clay altered - can see grey silica	X					3752-33	X			
68929	GRS125-615	GRS125	615.0	clay altered carbonate. In fault zone	X					3752-32	X			
68930	GRS125-618	GRS125	618.0	limestone with black ?carbonaceous and Iron-oxide and sulphide in fracture	X									
68931	GRS125-620.6	GRS125	620.6	dark silica with dark sulphide	X	(PM)	X							
68932	GRS125-620.7	GRS125	620.7	pale vuggy silica with massive pyrite	X	(PM)	X							
68933	GRS125-621.5	GRS125	621.5	pale vuggy silica with massive pyrite and sulphides	X									
68934	GRS125-622.3	GRS125	622.3	dark silica with dark sulphide	X	(PM)	X							
68935	GRS125-623	GRS125	623.0	dark silica with dark sulphide	X	(PM)	X							
68936	GRS125-624.8	GRS125	624.8	silica vughs and base metals	X	(PM)	X							
68937	GRS125-626.2	GRS125	626.2	pale vuggy silica with dark sulphide -	X									
68938	GRS125-626.4	GRS125	626.4	pale vuggy silica with dark sulphide	X	(PM)	X							
68939	GRS125-629.8	GRS125	629.8	grey and white silica and abundant clay	X					3752-31	X			
68940	GRS125-630	GRS125	630.0	vuggy silicified rock with sulphide and clay	X					3752-17	X			
68941	GRS125-632	GRS125	632.0	2 pieces - slab - white vuggy clast and grey matrix	X	(PM)	X	4612-127-128						
68942	GRS125-653.5	GRS125	653.5	white vein/alteration in grey carbonate	X	(PM)	X	4612-129-133						
68943	GRS125-690.8	GRS125	690.8	Sphalerite and galena (up to 1cm width zones) infill and alteration of carbonate. Around pyrite crystals. Marble host.	X	(PM)	X							
68944	GRS125-692.8	GRS125	692.8	Veins in chalcopyrite rock… Disseminated pyrite infill in 1mm veinlets with dark material. Rare infill - cubes to 2mm.	X	Missing								
68945	GRS125-693.6	GRS125	693.6	Alteration and infill in zones up to 2cm. After chalcopyrite and sphalerite.	X	(PM)	X	4612-138-139						

Appendix 2a - List of Specimens

JCU Number	Sample_No	Location Hole ID	Depth	Sulphur Isotope Analysis & Sample	Fluid Inclusion Analysis	C-O Isotope Analysis	C-O Isotope extra sample	C-O Isotope powders	SIMS C-O Isotope Analysis	40Ar/ 39Ar Analysis	LA-ICPMS Analysis & Section	Re assay	Comments
68918	GRS125-599A	GRS125	599.0										
68919	GRS125-599B	GRS125	599.0										
68920	GRS125-600	GRS125	600.0		KP17, KP18, KP19			X	X				SIMS result not used - mixed signature
68921	GRS125-600.5	GRS125	600.5										
68922	GRS125-601	GRS125	601.0										
68923	GRS125-601.4	GRS125	601.4										
68924	GRS125-602.7	GRS125	602.7			KP36, KP37	X	X					
68925	GRS125-604	GRS125	604.0										
68926	GRS125-608.6	GRS125	608.6			KP23	X	X					
68927	GRS125-610	GRS125	610.0			KP16		X					
68928	GRS125-611.3	GRS125	611.3										
68929	GRS125-615	GRS125	615.0										
68930	GRS125-618	GRS125	618.0									X	
68931	GRS125-620.6	GRS125	620.6										
68932	GRS125-620.7	GRS125	620.7									X	
68933	GRS125-621.5	GRS125	621.5									X	
68934	GRS125-622.3	GRS125	622.3									X	
68935	GRS125-623	GRS125	623.0										
68936	GRS125-624.8	GRS125	624.8										
68937	GRS125-626.2	GRS125	626.2									X	
68938	GRS125-626.4	GRS125	626.4										
68939	GRS125-629.8	GRS125	629.8										
68940	GRS125-630	GRS125	630.0										
68941	GRS125-632	GRS125	632.0										
68942	GRS125-653.5	GRS125	653.5										
68943	GRS125-690.8	GRS125	690.8										
68944	GRS125-692.8	GRS125	692.8										
68945	GRS125-693.6	GRS125	693.6										

Appendix 2a - List of Specimens

JCU Number	Sample_No	Location Hole ID	Depth	Description	Hand Specimen	Polished Section	Section offcut	Fluid Inclusion Section/ Chips	GADDS Analyses	XRD Analyses	XRD Powders	XRF Analyses	Re-Os Analysis	Micro probe Analysis
68946	GRS125-696.2	GRS125	696.2	host (calcite and sulphide fragments (in one very broken location can also see galena fragments - 697.2)) clay?	X	(PM)	XX							
68947	GRS125-697.2	GRS125	697.2	host (calcite and sulphide fragments (in one very broken location can also see galena fragments - 697.2)) clay?	X	Missing	X							
68948	GRS125-700.7	GRS125	700.7	Fine grained massive pyrite alteration?	X	(PM)	X							
68949	GRS125-724.5	GRS125	724.5	Au and clay sample XRD-XRF	X	(PM)	X							
68950	GRS125-750.3	GRS125	750.3	infill in breccia matrix	X	(PM)	X							
68951	GRS125-751	GRS125	751.0	Sub mm to 2mm pyrite cube alteration.. Coarse pyrite veins crosscut. Also crosscut by clay filled fractures zone (with pyrite). Cut and broken by later calcite veins.	X	(PM)								
68952	GRS125-753	GRS125	753.0	Black clay gangue infill in fracture. possibly after sphalerite	X	(PM)	X							
68953	GRS125-759	GRS125	759.0	clay from within pale breccia (with sulphide clasts). black clay and sulphides zone overprints pale intrusive breccia. Photographed and clay samples	X					3752-34	X			
68954	GRS125-760.4	GRS125	760.4	Fragments of Pyrite 1 with siliceous grains in intrusive breccia. Possible fragment in Breccia (or may be infill on fracture)	X	(PM)	X							
68955	GRS125-761.5	GRS125	761.5	Massive alteration, 10cm zone . Possible blue mineral present	X	(PM)	X							
68956	GRS125-766.4	GRS125	766.4	Infill? Of pyrite crystals - sub-mm to 5mm (predominantly 1mm) , replacement also possible. Possible Fragments?	X	(PM)	X							
68957	GRS125-766.5	GRS125	766.5	banded blobs	X	(PM)	X							
68958	GRS125-766.8	GRS125	766.8	host (Granular silica host) Infill/alteration in bands (crystals predominantly 0.5mm)	X	(PM)	X							
68959	GRS125-776.85	GRS125	776.85	clay bearing and very soft	X	(PM)	X							
68960	GRS125-803.5	GRS125	803.5	pyrite and dark silica	X	(PM)	X							
68961	GRS125-836.6	GRS125	836.6	pyrite and dark silica and covellite	X	(PM)	X							
68962	GRS125-848.4	GRS125	848.4	Appendix 10	X	(PM)	X							
68963	GRS125-848.5	GRS125	848.5	silica, clay and sulphide		(PM)	X							
68964	GRS125-873.2	GRS125	873.2	Appendix 10	X	(PM)	X							
68965	GRS125-873.5	GRS125	873.5	Appendix 10	X	(PM)	X							
68966	GRS125-874.3	GRS125	874.3	silicification, vughs, clay alteration and sulphide	X	(PM)	X							
68967	GRS125-874.8	GRS125	874.8	Appendix 10	X	(PM)	X							
68968	GRS125-875	GRS125	875.0	Appendix 10	X	(PM)	X							
68969	GRS125-877.7	GRS125	877.7	silica, clay and sulphide		(PM)	X							
68970	GRS125-878	GRS125	878.0	silica, white and black clay and sulphide	X					3752-10	X			
68971	GRS125-878.5	GRS125	878.5	silica, clay and sulphide	X					3752-22	X			
68972	GRS125-899	GRS125	899.0	silica with vughs, pyrite and clay	X					3752-09				
68973	GRS125-917	GRS125	917.0	massive fine pyrite, coarse pyrite veins and covellite in fracture	X	(PM)	X							

JCU Number	Sample_No	Location Hole ID	Depth	Sulphur Isotope Analysis & Sample	Fluid Inclusion Analysis	C-O Isotope Analysis	C-O Isotope extra sample	C-O Isotope powders	SIMS C-O Isotope Analysis	40Ar/ 39Ar Analysis	LA-ICPMS Analysis & Section	Re assay	Comments
68946	GRS125-696.2	GRS125	696.2										
68947	GRS125-697.2	GRS125	697.2										
68948	GRS125-700.7	GRS125	700.7										
68949	GRS125-724.5	GRS125	724.5										
68950	GRS125-750.3	GRS125	750.3										
68951	GRS125-751	GRS125	751.0										
68952	GRS125-753	GRS125	753.0										
68953	GRS125-759	GRS125	759.0										
68954	GRS125-760.4	GRS125	760.4										
68955	GRS125-761.5	GRS125	761.5										
68956	GRS125-766.4	GRS125	766.4										
68957	GRS125-766.5	GRS125	766.5										
68958	GRS125-766.8	GRS125	766.8										
68959	GRS125-776.85	GRS125	776.85										
68960	GRS125-803.5	GRS125	803.5										
68961	GRS125-836.6	GRS125	836.6										
68962	GRS125-848.4	GRS125	848.4										
68963	GRS125-848.5	GRS125	848.5										
68964	GRS125-873.2	GRS125	873.2										
68965	GRS125-873.5	GRS125	873.5										
68966	GRS125-874.3	GRS125	874.3										
68967	GRS125-874.8	GRS125	874.8										
68968	GRS125-875	GRS125	875.0										
68969	GRS125-877.7	GRS125	877.7										
68970	GRS125-878	GRS125	878.0										
68971	GRS125-878.5	GRS125	878.5										
68972	GRS125-899	GRS125	899.0										
68973	GRS125-917	GRS125	917.0										

Appendix 2a - List of Specimens

JCU Number	Sample_No	Location Hole ID	Depth	Description	Hand Specimen	Polished Section	Section offcut	Fluid Inclusion Section/ Chips	GADDS Analyses	XRD Analyses	XRD Powders	XRF Analyses	Re-Os Analysis	Micro probe Analysis
68977	GRS127-887.2	GRS127	887.2	limestone with pyrite, clay and quartz in vugh	X	(PM)	X		4612-134-137					
68978	KLS1-1-1345.3	KLS1-1	1345.3	Dolostone	(Brian New, PhD thesis)									
68979	KLS1-1-1394.8	KLS1-1	1394.8	dolomite	(Brian New, PhD thesis)	X	X							
68980	KLS1-1-1436.5	KLS1-1	1436.5	Dolostone	(Brian New, PhD thesis)									
68981	KLS1-1-1447.4	KLS1-1	1447.4	Quartz sandstone with dolomite matrix	(Brian New, PhD thesis)									
68982	KLS1-1-1474	KLS1-1	1474	fossiliferous limestone	(Brian New, PhD thesis)	X								
68983	KLS1-1-1509.7	KLS1-1	1509.7	Skarn altered quartz sandstone with dolomite matrix	(Brian New, PhD thesis)									
68984	KLS1-1-1535.4	KLS1-1	1535.4	Dolomite from homogeneous sample	(Brian New, PhD thesis)									
68985	KLS1-1-1573	KLS1-1	1573	Quartz sandstone with dolomite matrix	(Brian New, PhD thesis)									
68986	KLS1-1-1605	KLS1-1	1605	Equi granular dolomite rhombs with rare dolomite infill crystals in voids	(Brian New, PhD thesis)									
68987	KLS1-1-1657	KLS1-1	1657	dolomite	(Brian New, PhD thesis)	X	X							
68988	KLS1-1-1705	KLS1-1	1705	dolomite, leached and minor sulphides	(Brian New, PhD thesis)	X	X							
68989	KLS1-1-1796.7	KLS1-1	1796.7	Skarn altered quartz sandstone with dolomite matrix	(Brian New, PhD thesis)									
68990	KLS1-1-1854.7	KLS1-1	1854.7	Coarse relict peloidal texture retained by dolomite rhombs	(Brian New, PhD thesis)									
68991	KLS3-1-1132	KLS3-1	1132	calcitic with fossils	(Brian New, PhD thesis)	X	X							
68992	KLS3-1-1485.7	KLS3-1	1485.7	Dolostone	(Brian New, PhD thesis)									
68993	KLS3-1-1535.4	KLS3-1	1535.4	Dolostone	(Brian New, PhD thesis)	X	X							
68994	KLS3-1-1556.3	KLS3-1	1556.3	Quartz sandstone with dolomite matrix	(Brian New, PhD thesis)									
68995	KLS3-1-1582.5	KLS3-1	1582.5	Shell-bearing, fine grained matrix with dolomite rhombs	(Brian New, PhD thesis)	X	X							
68996	KLS3-1-1612.4	KLS3-1	1612.4	Quartz sandstone with dolomite matrix	(Brian New, PhD thesis)									
68997	KLS3-1-1623	KLS3-1	1623	Texture retentive dolomite (peloidal)	(Brian New, PhD thesis)									
68998	KLS3-1-1719	KLS3-1	1719	dolomite and calcite- mixed	(Brian New, PhD thesis)	X	X							
68999	KLS3-1-1744.8	KLS3-1	1744.8	Texture retentive dolomite (peloidal)	(Brian New, PhD thesis)									
69000	KLS3-1-1855.8	KLS3-1	1855.8	Very fine grained texture destructive dolomite	(Brian New, PhD thesis)	X	X							
69001	KLS3-1-1983	KLS3-1	1983	Calcite micrite-peloidal with dolomite rhomb replacement and late stage spar fill	(Brian New, PhD thesis)	X	X							
69002	KLS3-1-2031	KLS3-1	2031	black Kkel with fossil fragments	(Brian New, PhD thesis)	X	X							
68914	KP04	DOZ		massive pyrite from DOZ stop 2	X	KP04	X							
68915	KP08	DOZ		leached and mineralised carbonate from DOZ stop 2	X	KP08	X							
69003	P3850-28-48.7	P3850-28	48.7	analysis of white banded clay documented by Kavalieris (2000)	X					3752-39	X			
69127	Tuff outcrop	Tuff outcrop		banded area of volcanic sample	X					4612-323	X			
69128	Tuff outcrop	Tuff outcrop		very fine grained non-banded fragmental part of tuffaceous outcrop	X					4612-325	X			

Appendix 2a - List of Specimens

JCU Number	Sample_No	Location Hole ID	Depth	Sulphur Isotope Analysis & Sample	Fluid Inclusion Analysis	C-O Isotope Analysis	C-O Isotope extra sample	C-O Isotope powders	SIMS C-O Isotope Analysis	40Ar/ 39Ar Analysis	LA-ICPMS Analysis & Section	Re assay	Comments
68977	GRS127-887.2	GRS127	887.2										
68978	KLS1-1-1345.3	KLS1-1	1345.3			KP48		X					Location: Brian New pers comm, 2003 and Section C
68979	KLS1-1-1394.8	KLS1-1	1394.8										Polished resin mounted sample (not used for SIMS analysis). Location: Brian New pers comm, 2003 and Section C
68980	KLS1-1-1436.5	KLS1-1	1436.5			KP49		X					Location: Brian New pers comm, 2003 and Section C
68981	KLS1-1-1447.4	KLS1-1	1447.4			KP50		X					Location: Brian New pers comm, 2003 and Section C
68982	KLS1-1-1474	KLS1-1	1474										Polished resin mounted sample (not used for SIMS analysis). Location: Brian New pers comm, 2003 and Section C
68983	KLS1-1-1509.7	KLS1-1	1509.7			KP51		X					Location: Brian New pers comm, 2003 and Section C
68984	KLS1-1-1535.4	KLS1-1	1535.4						X				Location: Brian New pers comm, 2003 and Section C
68985	KLS1-1-1573	KLS1-1	1573			KP52		X					Location: Brian New pers comm, 2003 and Section C
68986	KLS1-1-1605	KLS1-1	1605			KP53		X					Location: Brian New pers comm, 2003 and Section C
68987	KLS1-1-1657	KLS1-1	1657										Polished resin mounted sample (not used for SIMS analysis). Location: Brian New pers comm, 2003 and Section C
68988	KLS1-1-1705	KLS1-1	1705										Polished resin mounted sample (not used for SIMS analysis). Location: Brian New pers comm, 2003 and Section C
68989	KLS1-1-1796.7	KLS1-1	1796.7			KP54		X					Location: Brian New pers comm, 2003 and Section C
68990	KLS1-1-1854.7	KLS1-1	1854.7			KP55		X					Location: Brian New pers comm, 2003 and Section C
68991	KLS3-1-1132	KLS3-1	1132										Polished resin mounted sample (not used for SIMS analysis). Location: Brian New pers comm, 2003 and Section C
68992	KLS3-1-1485.7	KLS3-1	1485.7			KP56		X					Location: Brian New pers comm, 2003 and Section C
68993	KLS3-1-1535.4	KLS3-1	1535.4			KP57		X					Location: Brian New pers comm, 2003 and Section C
68994	KLS3-1-1556.3	KLS3-1	1556.3			KP58		X					Location: Brian New pers comm, 2003 and Section C
68995	KLS3-1-1582.5	KLS3-1	1582.5						X				Location: Brian New pers comm, 2003 and Section C
68996	KLS3-1-1612.4	KLS3-1	1612.4			KP59		X					Location: Brian New pers comm, 2003 and Section C
68997	KLS3-1-1623	KLS3-1	1623			KP60		X					Location: Brian New pers comm, 2003 and Section C
68998	KLS3-1-1719	KLS3-1	1719						X				SIMS result not used - mixed signature. Location: Brian New pers comm, 2003 and Section C
68999	KLS3-1-1744.8	KLS3-1	1744.8			KP61		X					Location: Brian New pers comm, 2003 and Section C
69000	KLS3-1-1855.8	KLS3-1	1855.8			KP62		X	X				Location: Brian New pers comm, 2003 and Section C
69001	KLS3-1-1983	KLS3-1	1983						X				Location: Brian New pers comm, 2003 and Section C
69002	KLS3-1-2031	KLS3-1	2031										Polished resin mounted sample (not used for SIMS analysis). Location: Brian New pers comm, 2003 and Section C
68914	KP04	DOZ									KP04		Location: X=737440 ; Y=9549020 ; Z=3120
68915	KP08	DOZ											Location: X=737440 ; Y=9549020 ; Z=3120
69003	P3850-28-48.7	P3850-28	48.7										Location: (Section A)
69127	Tuff outcrop	Tuff outcrop											Location: (Section A)
69128	Tuff outcrop	Tuff outcrop											Location: (Section A)

Appendix 2a - List of Specimens

JCU Number	Sample_No	Location Hole ID	Depth	Description	Hand Specimen	Polished Section	Section offcut	Fluid Inclusion Section/ Chips	GADDS Analyses	XRD Analyses	XRD Powders	XRF Analyses	Re-Os Analysis	Micro probe Analysis
69004	VZW53-173	VZW53	173.0	white coarse-grained marble	X				4612-245					
69005	VZW53-188	VZW53	188.0	dark limestone altered to white marble	X				4612-241-242					
69006	VZW53-192	VZW53	192.0	white fine-grained marble	X				4612-243-244					
69007	VZW53-277.7	VZW53	277.7	marble crosscut by fine veins of pale pink (harder than marble but still HCL+ at hand specimen scale)	X				4612-235-237					
69008	VZW53-279.5	VZW53	279.5	mottled grey limestone altered by marble and brown garnet?	X				4612-230-231					
69009	VZW53-281.5	VZW53	281.5	grey to dark banding or alteration crosscut by white marble alteration and recrystallisation - coarser	X				4612-232-234					
69010	VZW53-282	VZW53	282.0	mottled grey limestone altered by marble and brown garnet? - hairline fracture with garnet?	X				4612-238-240					
69011	VZW53-330	VZW53	330.0	brown altered limestone crosscut by alteration to limestone, also infill.	X				4612-226-229					
69012	WAN1-1-494.4	WAN1-1	494.4	Black calcareous rock with sulphide (highly oxidised)	X	(JCU)	X							
69013	WAN1-3-181	WAN1-3	181.0	Pyrite-rich vein in host	X	(JCU)	X							
69014	WAN1-3-759	WAN1-3	759.0	magnetite-rich rock (zone) with areas of medium green. This appears to be altered to pale green and overprinted by pyrite cubes and surrounding chalcopyrite. Can see pale green vein cutting magnetite.		(JCU)	X							
69015	WAN1-3-776	WAN1-3	776.0	green and ? Skarn? Alteration with overprinting magnetite vein with minor later sulphide-veins. This is post-dated by overprinting 1mm veins of soft opaque-white material (anhydrite/calcite?) which offset the sulphide veinlets	X	(JCU)	X							
69016	WAN2-2-852	WAN2-2	852.0	massive pyrite with chalcopyrite, Au, sphalerite, galena, late-marcasite? Veins. same paragenesis as WAN4-3-302 (KP11)		KP09	X	X						A, S-(KP09)
69018	WAN4-1-58A	WAN4-1	58.0	sphalerite vein, low angle to Core Axis, 1 cm wide	X	(PM)	X							
69019	WAN4-1-58B1	WAN4-1	58.0	sphalerite vein, low angle to Core Axis, 1 cm wide	X	(PM)	X							
69020	WAN4-1-58B2	WAN4-1	58.0	sphalerite vein, low angle to Core Axis, 1 cm wide	X	(PM)								
69021	WAN4-1-72.1	WAN4-1	72.1	silicified and leached sandstone with pyrite, quartz veinlet. Can see silicification of sandstone associated with quartz vein			XX	JL02						
69022	WAN4-2-234A	WAN4-2	234.0	sphalerite, pyrite and carbonate and Au with Telluride and Bi-S	X	(GC)								A, S-(W3)
69023	WAN4-2-234B	WAN4-2	234.0	sphalerite, pyrite and carbonate	X	(GC)								A

Appendix 2a - List of Specimens

JCU Number	Sample_No	Location Hole ID	Depth	Sulphur Isotope Analysis & Sample	Fluid Inclusion Analysis	C-O Isotope Analysis	C-O Isotope extra sample	C-O Isotope powders	SIMS C-O Isotope Analysis	40Ar/ 39Ar Analysis	LA-ICPMS Analysis & Section	Re assay	Comments
69004	VZW53-173	VZW53	173.0			KP13	X	X					Location: (Section C)
69005	VZW53-188	VZW53	188.0			KP11, KP12	X	X					Location: (Section C)
69006	VZW53-192	VZW53	192.0										Location: (Section C)
69007	VZW53-277.7	VZW53	277.7										Location: (Section C)
69008	VZW53-279.5	VZW53	279.5										Location: (Section C)
69009	VZW53-281.5	VZW53	281.5										Location: (Section C)
69010	VZW53-282	VZW53	282.0			KP09, KP10		X					Location: (Section C)
69011	VZW53-330	VZW53	330.0			KP14, KP15	X	X					Location: (Section C)
69012	WAN1-1-494.4	WAN1-1	494.4										
69013	WAN1-3-181	WAN1-3	181.0										
69014	WAN1-3-759	WAN1-3	759.0										
69015	WAN1-3-776	WAN1-3	776.0										
69016	WAN2-2-852	WAN2-2	852.0	KP09							JL19		LA-sulphur isotope analysis. NB offcut for this sample labled JL19
69018	WAN4-1-58A	WAN4-1	58.0										
69019	WAN4-1-58B1	WAN4-1	58.0										
69020	WAN4-1-58B2	WAN4-1	58.0										
69021	WAN4-1-72.1	WAN4-1	72.1								JL02		
69022	WAN4-2-234A	WAN4-2	234.0								WAN		Also called W3
69023	WAN4-2-234B	WAN4-2	234.0										

Appendix 2a - List of Specimens

JCU Number	Sample_No	Location Hole ID	Depth	Description	Hand Specimen	Polished Section	Section offcut	Fluid Inclusion Section/ Chips	GADDS Analyses	XRD Analyses	XRD Powders	XRF Analyses	Re-Os Analysis	Micro probe Analysis
69029	WAN4-2-245.2A	WAN4-2	245.2-247.9	carbonate host with pyrite, galena, sphalerite	X	(GC)	X							
69030	WAN4-2-245.2B	WAN4-2	245.2-247.9	carbonate host with pyrite, galena, sphalerite	X	(GC)								
69025	WAN4-2-300	WAN4-2	300.0	black veinlets in very fine-grained pale orange "hornfels" rock	X	(JCU)								
69026	WAN4-2-307	WAN4-2	307.0		X	(PM)	X							
69027	WAN4-2-314A	WAN4-2	314.0	1m breccia (?carbonaceous limestone?) within pale green zone (313-320)	X	(PM)	X							
69028	WAN4-2-314B	WAN4-2	314.0		X	(PM)	X							
69024	WAN4-236.5A	WAN4-2	236.5	sphalerite and pyrite with 50/50 carbonate and stannite		(GC)	X							S-(W2)
69017	WAN4-236.5B	WAN4-2	236.5	sphalerite and pyrite with 50/50 carbonate and stannite		(GC)	X							
69035	WAN4-3-103.6	WAN4-3	103.6	pyrite and vein	X	(GC)	X							
69036	WAN4-3-108.1	WAN4-3	108.1	pyrite, chlorite, sericite, chalcopyrite (and Au)	X	(GC)	X	JL04						
69131	WAN4-3-130.5	WAN4-3	130.5	silicified and leached Kkel skarn sample, minor clay (previously epidote?), pyrite forming in vughs	X					X				
69037	WAN4-3-134.5	WAN4-3	134.5	Calcrudite, slightly coarser grained than shale	X	(JCU)	X							
69132	WAN4-3-138.1	WAN4-3	138.1	green and white skarn, minor red/pink. More than one green stage	X					X				
69038	WAN4-3-193.5	WAN4-3	193.5	1cm pyrite vein in silicified quartzite	X	(JCU)	X							
69039	WAN4-3-256	WAN4-3	256.0	contact between skarn alteration and silica-alteration	X	(PM)	X							
69040	WAN4-3-288	WAN4-3	288.0	"hornfels" fine-grained. with black specs and pyrite	X	(JCU)	X							
69041	WAN4-3-302.5	WAN4-3	302.5	sphalerite vein, gold in early pyrite - same paragenesis as WAN2-2-852 JL09	X	KP11	X	KP11						A, S(KP11)
69042	WAN4-3-303.4	WAN4-3	303.4	pyrite, sericite, sphalerite	X	(GC)	X							
69043	WAN4-3-303.6A	WAN4-3	303.6	sphalerite, clay, pyrite	X	(GC)	X							
69044	WAN4-3-303.6B	WAN4-3	303.6	sphalerite, clay, pyrite	X	(GC)								
69031	WAN4-3-63	WAN4-3	63.0	striated pyrite infill in vugh in sandstone with adularia	X									
69032	WAN4-3-63.2	WAN4-3	63.2	silicified and leached sandstone with brown veinlets (K-feldspar?). And 2cm pyrite vein with K-spar	X								?	
69033	WAN4-3-80.5A	WAN4-3	80.5	vuggy	X	(GC)	X	JL03						
69034	WAN4-3-80.5B	WAN4-3	80.5	vuggy	X	(GC)								
69045	WAN4-4-60.3	WAN4-4	60.3	sandstone with zone of leaching and silica (and subsequent pyrite) bedding?? Pink or clay fracture offcuts	X		X	JL01						
69049	WAN4-5-171	WAN4-5	171.0	clay altered dyke	X					X		5445-06		
69050	WAN4-5-174	WAN4-5	174.0	intrusive dyke - predates silicification-leaching-pyrite alteration but is only altered on margins, fairly fresh in centre	X					X		5445-05		
69051	WAN4-5-174.5	WAN4-5	174.5	calcrudite	X	(PM)	X							

Appendix 2a - List of Specimens

JCU Number	Sample_No	Location Hole ID	Depth	Sulphur Isotope Analysis & Sample	Fluid Inclusion Analysis	C-O Isotope Analysis	C-O Isotope extra sample	C-O Isotope powders	SIMS C-O Isotope Analysis	40Ar/ 39Ar Analysis	LA-ICPMS Analysis & Section	Re assay	Comments
69029	WAN4-2-245.2A	WAN4-2	245.2-247.9										
69030	WAN4-2-245.2B	WAN4-2	245.2-247.9										
69025	WAN4-2-300	WAN4-2	300.0										
69026	WAN4-2-307	WAN4-2	307.0										
69027	WAN4-2-314A	WAN4-2	314.0										
69028	WAN4-2-314B	WAN4-2	314.0										
69024	WAN4-236.5A	WAN4-2	236.5										
69017	WAN4-236.5B	WAN4-2	236.5										
69035	WAN4-3-103.6	WAN4-3	103.6										
69036	WAN4-3-108.1	WAN4-3	108.1								JL04		
69131	WAN4-3-130.5	WAN4-3	130.5										
69037	WAN4-3-134.5	WAN4-3	134.5										
69132	WAN4-3-138.1	WAN4-3	138.1										
69038	WAN4-3-193.5	WAN4-3	193.5										
69039	WAN4-3-256	WAN4-3	256.0										
69040	WAN4-3-288	WAN4-3	288.0										
69041	WAN4-3-302.5	WAN4-3	302.5	KP11							KP11		LA-sulphur isotope analysis
69042	WAN4-3-303.4	WAN4-3	303.4										
69043	WAN4-3-303.6A	WAN4-3	303.6										
69044	WAN4-3-303.6B	WAN4-3	303.6										
69031	WAN4-3-63	WAN4-3	63.0										
69032	WAN4-3-63.2	WAN4-3	63.2							X			
69033	WAN4-3-80.5A	WAN4-3	80.5		JL03						JL03		
69034	WAN4-3-80.5B	WAN4-3	80.5										
69045	WAN4-4-60.3	WAN4-4	60.3		JL01						JL01		
69049	WAN4-5-171	WAN4-5	171.0										
69050	WAN4-5-174	WAN4-5	174.0										
69051	WAN4-5-174.5	WAN4-5	174.5										

Appendix 2a - List of Specimens

JCU Number	Sample_No	Location Hole ID	Depth	Description	Hand Specimen	Polished Section	Section offcut	Fluid Inclusion Section/ Chips	GADDS Analyses	XRD Analyses	XRD Powders	XRF Analyses	Re-Os Analysis	Micro probe Analysis
69052	WAN4-5-182	WAN4-5	182.0	Massive Sulphide with Bi and gold	X	(PM)	X							A
69053	WAN4-5-205	WAN4-5	205.0	Eg of skarn alteration in calcrudite	X	(JCU)	X							
69054	WAN4-5-211a	WAN4-5	211.0	silica alteration and massive pyrite (and cubic infill) veins	X	(JCU)	X							
69055	WAN4-5-211b	WAN4-5	211.0	silica alteration and massive pyrite (and cubic infill) veins	X	(JCU)	X							
69046	WAN4-5-50	WAN4-5	50.0	1cm pyrite vein in silica and vuggy quartzite, abundant disseminated pyrite and in vughs	X	(PM)	X							
69047	WAN4-5-50B	WAN4-5	50.0	1cm pyrite vein in silica and vuggy quartzite, abundant disseminated pyrite and in vughs	X	(PM)	X	JL05						
69048	WAN4-5-90.5	WAN4-5	90.5	2cm pyrite vein in silica, vuggy and sulphide quartzite (minor massive sulphide)	X	(JCU)	X							
69056	WAN4-6-28	WAN4-6	28.0	Massive pyrite with au and Telluride, Bi	X	KP10	X							A
69060	WGR12-168.6	WGR-12	168.6	limestone breccia - mill	X	(PM)	X			4612-328	X			
69061	WGR12-169.7	WGR-12	169.7	brecciated-fractured limestone rock with black ?carbonaceous matrix	X									
69062	WGR12-170.5	WGR-12	170.5	dark brown (altered?) limestone with hairline calcite fracture	X									
69063	WGR12-173	WGR-12	173.0	grey matrix in brown mill limestone breccia	X	(PM)				4612-333	X			
69134	WGR12-173.5	WGR12	173.5		X									
69064	WGR12-174.3	WGR-12	174.3	breccia with grey and yellow clay	X	(PM)				4612-334	X			
69135	WGR12-176	WGR12	176.0		X		X							
69065	WGR12-177	WGR-12	177.0	part of 20cm black and yellow clay zone with pyrite specs	X	(PM)				4612-332	X			
69066	WGR12-294.6	WGR-12	294.6	brecciated-fractured limestone rock with black ?carbonaceous matrix. Very broken	X					4612-335	X			
69057	WGR12-30	WGR-12	30.0	possible opaline silica?	X					3752-44	X			
69067	WGR12-302.2	WGR-12	302.2	Black infill and altered rock with overprinting calcite, quartz veins and vughs	X					4612-327	X			
69068	WGR12-367	WGR-12	367.0	pale limestone with black ?carbonaceous in fracture and white clay? Appears very leached	X					3752-18	X			
69069	WGR12-369.5	WGR-12	369.5	clay altered limestone	X					3752-21	X			
69058	WGR12-37	WGR-12	37.0	opaline material	X					3752-01	X			
69059	WGR12-43.3	WGR-12	43.3	brown vein cutting white clay	X	(PM)	X			3752-06, 7	XX			
69076	WGR13-118.5	WGR-13	118.5	vuggy breccia with sulphide in voids and red and Iron-oxide staining	X									
69077	WGR13-143	WGR-13	143.0	marble contact with sulphide-rich mill breccia breccia (skarn altered and foliated?) abundant disseminated sulphide	X	(PM)	X							
69078	WGR13-151.7	WGR-13	151.7	marble with veins of green and cream (with sulphide)	X									

Appendix 2a - List of Specimens

JCU Number	Sample_No	Location Hole ID	Depth	Sulphur Isotope Analysis & Sample	Fluid Inclusion Analysis	C-O Isotope Analysis	C-O Isotope extra sample	C-O Isotope powders	SIMS C-O Isotope Analysis	40Ar/ 39Ar Analysis	LA-ICPMS Analysis & Section	Re assay	Comments
69052	WAN4-5-182	WAN4-5	182.0										
69053	WAN4-5-205	WAN4-5	205.0										
69054	WAN4-5-211a	WAN4-5	211.0										
69055	WAN4-5-211b	WAN4-5	211.0										
69046	WAN4-5-50	WAN4-5	50.0										
69047	WAN4-5-50B	WAN4-5	50.0		JL05						JL05		
69048	WAN4-5-90.5	WAN4-5	90.5										
69056	WAN4-6-28	WAN4-6	28.0	KP10							KP10		conventional S-isotope analysis
69060	WGR12-168.6	WGR-12	168.6										
69061	WGR12-169.7	WGR-12	169.7									X	
69062	WGR12-170.5	WGR-12	170.5									X	
69063	WGR12-173	WGR-12	173.0										
69134	WGR12-173.5	WGR12	173.5										
69064	WGR12-174.3	WGR-12	174.3										
69135	WGR12-176	WGR12	176.0										
69065	WGR12-177	WGR-12	177.0										
69066	WGR12-294.6	WGR-12	294.6										
69057	WGR12-30	WGR-12	30.0										
69067	WGR12-302.2	WGR-12	302.2										
69068	WGR12-367	WGR-12	367.0									X	
69069	WGR12-369.5	WGR-12	369.5										
69058	WGR12-37	WGR-12	37.0										
69059	WGR12-43.3	WGR-12	43.3										
69076	WGR13-118.5	WGR-13	118.5									X	
69077	WGR13-143	WGR-13	143.0									X	
69078	WGR13-151.7	WGR-13	151.7									X	

Appendix 2a - List of Specimens

JCU Number	Sample_No	Location Hole ID	Depth	Description	Hand Specimen	Polished Section	Section offcut	Fluid Inclusion Section/ Chips	GADDS Analyses	XRD Analyses	XRD Powders	XRF Analyses	Re-Os Analysis	Micro probe Analysis
69079	WGR13-153	WGR-13	153.0	breccia with skarn? Alteration and sulphide in matrix - green alteration of clast	X	(PM)	X							
69080	WGR13-161.5	WGR-13	161.5	pyrite breccia with galena overprinting with calcite (slightly purple - fluorite?)	X	(PM)	X							
69081	WGR13-162	WGR-13	162.0	mottled pale grey limestone marble with sphalerite, galena veins	X	Missing	X							
69082	WGR13-169.5	WGR-13	169.5	black limestone and pale marble and black fracture	X	(PM)	X							
69083	WGR13-170	WGR-13	170.0	breccia, with marble clasts. Possible skarn minerals, minor black ?carbonaceous and sulphide	X	(PM)	X							
69084	WGR13-173	WGR-13	173.0	massive sulphide (also 172.5m)		(PM)	X							
69085	WGR13-173.8	WGR-13	173.8	massive sulphide	X	(PM)	X							
69086	WGR13-177.5	WGR-13	177.5	Polished Section SAMPLE = 177m. breccia, with marble clasts. Possible skarn minerals and sulphide	X	(PM)	X							
69087	WGR13-188	WGR-13	188.0	mottled pale-dark grey limestone marble. Pyrite vein along black fracture	X	Missing	X							
69088	WGR13-199.2A	WGR-13	199.2	Polished Section SAMPLE: 192A. limestone breccia (pale groundmass) and sulphide veins (galena, pyrite, sphalerite)		Missing	X							
69089	WGR13-199.2B	WGR-13	199.2	Polished Section SAMPLE: 192B. limestone breccia (pale groundmass) and sulphide veins (galena, pyrite, sphalerite)		(PM)	X							
69090	WGR13-201	WGR-13	201.0	limestone breccia with grey-dark matrix (?carbonaceous) and sulphide	X	(PM)	X							
69091	WGR13-215.5	WGR-13	215.5	(2 pieces). Black ?carbonaceous shale with pyrite front.. Also ?carbonaceous alteration?	X	(PM)	X							
69071	WGR13-32	WGR-13	32.0	spotty sulphide and black material in clay rock	X									
69072	WGR13-48	WGR-13	48.0	spotty sulphide and vughs in clay rock	X	X	X							
69073	WGR13-52	WGR-13	52.0	black sooty veins and pyrite in yellow and grey rock	X									
69074	WGR13-57.7	WGR-13	57.7	yellow stained clay with dark sulphide spots/veins (looks vuggy)	X									
69075	WGR13-60	WGR-13	60.0	yellow stained clay with dark sulphide spots/veins (looks vuggy). Pyrite in one vugh	X									
69092	WGR3-15.2	WGR-3	15.2	dark grey breccia and sulphides; analysis of oxidised ?carbonaceous material in limestone breccia	X					4612-329	X			
69093	WGR3-26.5	WGR-3	26.5	oxidised and white spots (after sulphides?) (swelling clay) breccia. Rare fragments, dark matrix	X									
69094	WGR3-54	WGR-3	54.0	oxidised ?carbonaceous material in limestone breccia	X									

Appendix 2a - List of Specimens

JCU Number	Sample_No	Location Hole ID	Depth	Sulphur Isotope Analysis & Sample	Fluid Inclusion Analysis	C-O Isotope Analysis	C-O Isotope extra sample	C-O Isotope powders	SIMS C-O Isotope Analysis	40Ar/ 39Ar Analysis	LA-ICPMS Analysis & Section	Re assay	Comments
69079	WGR13-153	WGR-13	153.0										
69080	WGR13-161.5	WGR-13	161.5										
69081	WGR13-162	WGR-13	162.0										
69082	WGR13-169.5	WGR-13	169.5										
69083	WGR13-170	WGR-13	170.0										
69084	WGR13-173	WGR-13	173.0										
69085	WGR13-173.8	WGR-13	173.8										
69086	WGR13-177.5	WGR-13	177.5										
69087	WGR13-188	WGR-13	188.0										
69088	WGR13-199.2A	WGR-13	199.2										
69089	WGR13-199.2B	WGR-13	199.2										
69090	WGR13-201	WGR-13	201.0										
69091	WGR13-215.5	WGR-13	215.5										
69071	WGR13-32	WGR-13	32.0									X	
69072	WGR13-48	WGR-13	48.0									X	
69073	WGR13-52	WGR-13	52.0									X	
69074	WGR13-57.7	WGR-13	57.7									X	
69075	WGR13-60	WGR-13	60.0									X	
69092	WGR3-15.2	WGR-3	15.2									X	
69093	WGR3-26.5	WGR-3	26.5									X	
69094	WGR3-54	WGR-3	54.0									X	

Appendix 2a - List of Specimens

JCU Number	Sample_No	Location Hole ID	Depth	Description	Hand Specimen	Polished Section	Section offcut	Fluid Inclusion Section/ Chips	GADDS Analyses	XRD Analyses	XRD Powders	XRF Analyses	Re-Os Analysis	Micro probe Analysis
69133	WGR4-89	WGR4	89.0	composite gold-bearing limestone breccia sample	X	3 blocks								A
69125	WGZ8-004	WGZ-8	94-95	late yellow-crystalline alteration	X					3752-45. 46, 47	XXX			
69113	WGZ8-005	WGZ-8	95.0	late yellow-crystalline alteration	X				3752-52					
69101	WGZ8-008	WGZ-8	48.0	clay alteration of intrusive breccia	X				3752-50-51	3752-41	X			
69100	WGZ8-010	WGZ-8	39.0	white and yellow	X					3752-42	X			
69106	WGZ8-014	WGZ-8	64.0	breccia with pyrite in networks	X	X	X		3752-54					
69110	WGZ8-015	WGZ-8	79.1		X				3752-56,b					
69114	WGZ8-117	WGZ-8	117.0	banded clay with breccia (sedimentary?) grey and white	X					3752-12, 13	XX			
69115	WGZ8-118	WGZ-8	118.0	EG of banded and other clasts with later white material in intrusive breccia	X				3752-48, 49					
69116	WGZ8-126	WGZ-8	126.0	limestone breccia, highly ferrugenised matrix (was groundmass black?)	X									
69117	WGZ8-148.3	WGZ-8	148.3	limestone breccia with marble clasts and ?carbonaceous matrix (white, bleached) disseminated pyrite	X	X	X							
69118	WGZ8-166	WGZ-8	166.0	limestone breccia	Missing					4612-319	X			
69119	WGZ8-210	WGZ-8	210.0	limestone breccia with ?carbonaceous matrix and minor Iron-oxide after sulphide?	X									
69095	WGZ8-23	WGZ-8	23.0	spotted white clay - spots may be magnetite, sulphide and greenish clay	X	(PM)	X							
69096	WGZ8-30.5	WGZ-8	30.5	Clay with spotted sulphide vughs? And black mineral (sooty), minor white vein, igneous host	X	(PM)	X							
69120	WGZ8-307	WGZ-8	307.0	mill breccia (recent fault also) and black matrix	X					3752-05	X			
69097	WGZ8-31.5	WGZ-8	31.5	breccia clasts. White matrix and sulphide replacing clasts	X									
69124	WGZ8-316	WGZ-8	316-318	composite of black gangue from Au-zone (black filled fracture in dark brown limestone)	X					3752-19	X			
69098	WGZ8-33.5	WGZ-8	33.5	white clay with vughs/spots with pyrite then black/grey sulphide mineral. Sulphides appear to be replacing clasts as spots	X									
69099	WGZ8-35	WGZ-8	35.0	vughs with sulphide and greenish clay and pyrite veins. White clay (silica?) host	X									
69121	WGZ8-370	WGZ-8	370.0	mill breccia, not black matrix - limestone fragments	X					3752-04	X			
69122	WGZ8-387.5	WGZ-8	387.5	mill breccia (brown limestone clasts) white clay alteration of matrix (and clasts?), minor coarse sulphide	X					3752-08	X			
69123	WGZ8-392	WGZ-8	392.0	20cm limestone breccia, pale grey matrix, abundant pyrite	X									
69102	WGZ8-60	WGZ-8	60.0	clay with sulphide spots (minor) and silicified and sulphur	X									

Appendix 2a - List of Specimens

JCU Number	Sample_No	Location Hole ID	Depth	Sulphur Isotope Analysis & Sample	Fluid Inclusion Analysis	C-O Isotope Analysis	C-O Isotope extra sample	C-O Isotope powders	SIMS C-O Isotope Analysis	40Ar/ 39Ar Analysis	LA-ICPMS Analysis & Section	Re assay	Comments
69133	WGR4-89	WGR4	89.0								WG3		
69125	WGZ8-004	WGZ-8	94-95										
69113	WGZ8-005	WGZ-8	95.0										
69101	WGZ8-008	WGZ-8	48.0										
69100	WGZ8-010	WGZ-8	39.0										
69106	WGZ8-014	WGZ-8	64.0										
69110	WGZ8-015	WGZ-8	79.1										
69114	WGZ8-117	WGZ-8	117.0										
69115	WGZ8-118	WGZ-8	118.0										
69116	WGZ8-126	WGZ-8	126.0									X	
69117	WGZ8-148.3	WGZ-8	148.3									X	
69118	WGZ8-166	WGZ-8	166.0										
69119	WGZ8-210	WGZ-8	210.0									X	
69095	WGZ8-23	WGZ-8	23.0									X	
69096	WGZ8-30.5	WGZ-8	30.5									X	
69120	WGZ8-307	WGZ-8	307.0										
69097	WGZ8-31.5	WGZ-8	31.5									X	
69124	WGZ8-316	WGZ-8	316-318										
69098	WGZ8-33.5	WGZ-8	33.5									X	
69099	WGZ8-35	WGZ-8	35.0									X	
69121	WGZ8-370	WGZ-8	370.0										
69122	WGZ8-387.5	WGZ-8	387.5									X	
69123	WGZ8-392	WGZ-8	392.0									X	
69102	WGZ8-60	WGZ-8	60.0									X	

Appendix 2a - List of Specimens

JCU Number	Sample_No	Location Hole ID	Depth	Description	Hand Specimen	Polished Section	Section offcut	Fluid Inclusion Section/ Chips	GADDS Analyses	XRD Analyses	XRD Powders	XRF Analyses	Re-Os Analysis	Micro probe Analysis
69103	WGZ8-61	WGZ-8	61.0	breccia appears silica with green/yellow fragments (skarn?) sulphides in vughs	X									
69104	WGZ8-63.2	WGZ-8	63.2	network of sulphide through clay and breccia by white-yellow	X					3752-40	X			
69105	WGZ8-63.5	WGZ-8	63.5	(mass chalcopyrite) clay with sulphide spots	X									
69107	WGZ8-69.5	WGZ-8	69.5	opaline, minor disseminated pyrite and later black fracture	X	(PM)	X			3752-14, 15	XX			
69108	WGZ8-76.6	WGZ-8	76.6	white clay with galena? Veinlets	X					3752-20	X			
69109	WGZ8-77	WGZ-8	77.0	white clay with black specs in veins	X				3752-57, b, c					
69111	WGZ8-91	WGZ-8	91.0	bleached white banded clay	X					3752-43	X			
69112	WGZ8-92.5	WGZ-8	92.5	banded clay with crosscutting massive pyrite	X	(PM)	X			3752-02, 3	XX			
68860	WGZ8-90	WGZ-8	90.0	bleached banded clay and white-yellow and grey and black fractures	X									
68799	WGZ8-018	WGZ-8	104.7	non-banded fragmented clay zone only 2.5 cm wide (banded on either side)	X									
69136	BGU19-03-233	BGU19-03	233.35	clast of skarn and cpy in massive fine grained pyrite	X									
69137	WGZ8-017	WGZ-8	64.2	intrusive breccia and white bleached banded clay contact	X									
69138	WGZ8-011	WGZ-8	96.1	allophane in void in clay	X									

Appendix 2a - List of Specimens

JCU Number	Sample_No	Location Hole ID	Depth	Sulphur Isotope Analysis & Sample	Fluid Inclusion Analysis	C-O Isotope Analysis	C-O Isotope extra sample	C-O Isotope powders	SIMS C-O Isotope Analysis	40Ar/ 39Ar Analysis	LA-ICPMS Analysis & Section	Re assay	Comments
69103	WGZ8-61	WGZ-8	61.0									X	
69104	WGZ8-63.2	WGZ-8	63.2										
69105	WGZ8-63.5	WGZ-8	63.5									X	
69107	WGZ8-69.5	WGZ-8	69.5										
69108	WGZ8-76.6	WGZ-8	76.6										
69109	WGZ8-77	WGZ-8	77.0										
69111	WGZ8-91	WGZ-8	91.0										
69112	WGZ8-92.5	WGZ-8	92.5										
68860	WGZ8-90	WGZ-8	90.0										
68799	WGZ8-018	WGZ-8	104.7										
69136	BGU19-03-233	BGU19-03	233.35										
69137	WGZ8-017	WGZ-8	64.2										
69138	WGZ8-011	WGZ-8	96.1										

Appendix 2b - Assay data and coordinates for drillhole samples used in this study (PT Freeport Indonesia)

JCU Number	Sample_No	Location Hole ID	Depth	Assay Interval FROM	Assay Interval TO	CU%	AU	AG	PB	ZN	MO	AS	BI	CO	SB	SE	CR	HG	Location X	Location Y	Location Z
68767	BG1-4A-229	BG01-04A	229	227.6	230.6	0.49	13.95	33	818	61111	-1	3881	108	68	2.3099999			0.78	734624	9548661	3195
68768	BG1-4A-256	BG01-04A	256	253.6	256.6	0.02	0.79	45	1657	1798	14	32	1	26	2.3			0.71	734622	9548657	3169
68769	BG1-4A-330	BG01-04A	330	329.5	331.1	0.29	7.27	20	1600	23953	4	5644	135	74	9.1999998			1.24	734617	9548647	3095
68770	BG1-4A-400	BG01-04A	400	398.5	400.7	2.06	26.84	55	2189	4081	-1	8033	645	146	12.6			-0.1	734613	9548640	3026
68771	BG1-4A-423	BG01-04A	423	420.7	423.7	0.00	0.65	-0.5	234	217	17	17	2	26	0.17			-0.1	734612	9548638	3003
68772	BG1-5-234	BG01-05	234	231.7	234.85	0.24	14.98	23	4039	13289	-1	1841	140		179			5.8099999	734593	9548681	3193
68773	BG1-5-238	BG01-05	238	237	239.35	0.32	38.799999	62	15714	67105	10	13000	194		424			5.25	734593	9548681	3188
68774	BG1-5-256	BG01-05	256	255.3	256.8	0.27	41.630001	22	7499	14079	4	3500	152		81.239998			2.76	734590	9548680	3170
68775	BG1-7-108	BG01-07	108	105.4	108.6	0.01	0.28	5	649	798	-1	222	-1		596			0.89	734646	9548672	3316
68776	BG1-7-167	BG01-07	167	165.9	169.1	0.57	15.1	133	22703	73077	5	1422	453		965			3.25	734649	9548662	3256
68777	BG1-7-190	BG01-07	190	187.5	190.8	0.07	0.81	43	20721	78846	-1	4933	-1		1135			6.02	734650	9548658	3235
68779	BGU07-6-221.2	BGU07-06	221	218.75	221.05	0.02	0.01	0.25	17	40	-2	14		3			37		735362	9548137	2802
68780	BGU07-6-268.8	BGU07-06	268	267.75	269.45	6.17	1.35	29.4	17	386	-2	110		54			52		735370	9548152	2756
68781	BGU07-6-342	BGU07-06	342	341.55	343.3	3.39	18.3	26.8	88	325	8	110		57			20		735382	9548173	2686
68782	BGU08-1-225	BGU08-01	225	223.2	225.4	10.50	8.25	95	21	12300	3	7		230			30		735449	9548151	2904
68783	BGU08-5-190.1	BGU08-05	190	189.5	190.35	0.51	7	21.5	5300	31300	2	1140		52			19		735444	9548143	3043
68784	BGU08-07-220.1	BGU08-07	220	199.9	243														735469	9548105	2870
68785	BGU14-7-590b	BGU14-07	590	588	591	0.02	0.005	0.25	19	35	12	17		5			25		735097	9548381	2457
68786	BGU17-07-400.4	BGU17-07	400	399.9	402	0.03	0.03	0.25	27	238	-2	11		10			29		735045	9548482	2646
68787	BGU17-07-460	BGU17-07	460	459	462	0.03	0.005	0.25	11	13	34	23		4			13		735034	9548463	2591
68788	BGU18-03-32.5	BGU18-03	32	30	33														735058	9548604	3030
68789	BGU18-03-192.5	BGU18-03	192	192	195														734980	9548469	3073
68790	BGU18-03-192.6	BGU18-03	192	192	195														734980	9548469	3073
68791	BGU18-03-192.7	BGU18-03	192	192	195														734980	9548469	3073
68792	BGU18-03-203	BGU18-03	203	201	204														734975	9548461	3075
68793	BGU18-03-211.2	BGU18-03	211	210.5	213.1	0.42	19.4	19.8	1030	18500	2	1380		86			27		734971	9548453	3078
68794	BGU18-03-212	BGU18-03	212	210.5	213.1	0.42	19.4	19.8	1030	18500	2	1380		86			27		734971	9548453	3078
68795	BGU19-03-184.7	BGU19-03	184	183.1	184.5	0.02	0.12	4.3	73	175	6	15		-2			13		734925	9548502	3088
69136	BGU19-03-233	BGU19-03	233.35	233.3	236.3	1.09	9.5	24.4	236	1240	41	70		147			96		734901	9548459	3104
68796	BGU21-01-13	BGU21-01	13	13	15	0.01	0.005	0.25	15	23	13	8		5			24		734971	9548652	3025
68797	BGU21-1-20.4	BGU21-01	20	18	21	0.68	23.2	29.5	450	4200	14	350		176			28		734969	9548647	3026
68798	BGU21-01-43	BGU21-01	43	42	45	0.00	0.005	0.25	6	146	-2	6		6			24		734957	9548626	3030
68799	BGU21-01-90	BGU21-01	90	89.5	91.5	0.06	0.02	0.25	9	224	-2	19		23			8		734934	9548586	3039
68800	BGU21-2-13.3A	BGU21-02	13	12	15	0.40	14.6	4.5	242	580	-2	240		6			29		734972	9548652	3028
68801	BGU21-2-13.3B	BGU21-02	13	12	15	0.40	14.6	4.5	242	580	-2	240		6			29		734972	9548652	3028
68802	BGU21-2-14	BGU21-02	14	12	15	0.40	14.6	4.5	242	580	-2	240		6			29		734972	9548652	3028
68803	BGU21-3-24.3	BGU21-03	24	24	27	0.05	2.31	3.3	430	1160	3	1250		11			28		734967	9548644	3036
68804	BGU21-03-24.5	BGU21-03	24	24	27	0.05	2.31	3.3	430	1160	3	1250		11			28		734967	9548644	3036
69129	BGU21-03-24.6	BGU21-03	24	24	27	0.05	2.31	3.3	430	1160	3	1250		11			28		734967	9548644	3036
68805	BGU21-03-51.3	BGU21-03	51	51	57	0.00	0.005	0.25	10	14	-2	9		5			37		734954	9548622	3049
68806	BGU21-03-53.5	BGU21-03	53	51	57	0.00	0.005	0.25	10	14	-2	9		5			37		734954	9548622	3049
68807	BGU21-03-59	BGU21-03	59	57	60	0.01	0.01	0.25	11	15	-2	6		6			29		734952	9548618	3051
68808	BGU21-03-62	BGU21-03	62	60	63	0.01	0.01	0.25	9	15	3	5		11			18		734951	9548616	3052
68809	BGU21-3-224.5	BGU21-03	224	221.4	224.3	2.76	8.25	27	119	17500	-2	76		98			30		734879	9548491	3125
68810	BGU21-3-225.1	BGU21-03	225	224.3	225.5	7.44	15	63	131	46500	-2	80		71			24		734879	9548490	3126
68811	BGU21-3-225.5	BGU21-03	225	224.3	225.5	7.44	15	63	131	46500	-2	80		71			24		734879	9548490	3126
68812	BGU21-3-226.3	BGU21-03	226	225.5	228.5	1.56	6.18	17.4	304	23900	-2	130		211			17		734878	9548488	3127
68813	BGU21-3-234.4	BGU21-03	234	231.4	234.6	0.11	2.54	6.3	810	11600	23	120		46			37		734875	9548484	3130
68814	BGU21-5-17.5	BGU21-05	17	15	18	0.02	9.11	0.25	23	159	-2	24		9			19		734971	9548650	3016
68815	BGU21-5-22	BGU21-05	22	19.4	22.6	0.29	10.2	3.2	50	2700	-2	64		9			19		734968	9548646	3015
68816	BGU21-10-7.5	BGU21-10	7	6	7.2	0.01	0.38	0.8	170	570	2	380		13			35		734976	9548659	3028
68817	BGU21-10-12	BGU21-10	12	10.4	13.2	0.01	2.24	4	1700	2800	3	2100		10			30		734973	9548655	3031
68818	BGU21-10-159	BGU21-10	159	159	162														734912	9548548	3115
68819	BGU21-10-236.7	BGU21-10	236	235.8	238	8.51	2.2	63	1150	4000	38	90		136			58		734881	9548494	3159
68820	BGU21-10-251.4A	BGU21-10	251	246.4	251.4	0.51	5.44	25.6	3250	31000	-2	1350		146			35		734876	9548485	3165
68821	BGU21-10-251.4B	BGU21-10	251	246.4	251.4	0.51	5.44	25.6	3250	31000	-2	1350		146			35		734876	9548485	3165
68822	BGU22-1-8	BGU22-01	8	6	9	0.05	12.9	2.5	92	216	9	550		170			20		734927	9548674	3023
68823	BGU22-1-15.2	BGU22-01	15	15	17.3	0.58	49	10.3	480	770	8	1240		70			35		734923	9548666	3021
68824	BGU23-2-9	BGU23-02	9	9	12	0.01	0.005	0.25	9	68	3	2		15			29		734879	9548687	3023
68825	BGU23-2-46	BGU23-02	46	45	48	0.00	0.005	0.25	6	23	4	4		6			23		734861	9548656	3020
68826	BGU23-2-48.6	BGU23-02	48	48	51	0.01	0.005	0.25	7	47	2	6		10			22		734859	9548654	3020
68827	BGU23-2-64.8	BGU23-02	64	60	64.8	0.07	0.02	0.25	18	40	2	15		59			22		734853	9548642	3019
68828	BGU23-03-180	BGU23-03	180	179	182	11.30	4.18	67	11	8750	3	26		610			30		734800	9548549	3090
68829	BGU23-5-147.6	BGU23-05	147	147	150	2.01	0.49	13	15	61	-2	140	3	64	0.7	14	36	-0.1	734819	9548584	2951
68830	BGU23-6-66	BGU23-06	66	66	69	0.03	0.02	0.25	23	33	4	1		18			13		734862	9548659	2971
68831	BGU23-6-80	BGU23-06	80	80	82	0.19	0.09	1.1	35	58	38	7		13			10		734858	9548652	2960

Appendix 2b - Assay data and coordinates for drillhole samples used in this study (PT Freeport Indonesia)

JCU Number	Sample_No	Location Hole ID	Depth	Assay Interval FROM	Assay Interval TO	CU%	AU	AG	PB	ZN	MO	AS	BI	CO	SB	SE	CR	HG	Location X	Location Y	Location Z
68832	BGU23-6-80.5	BGU23-06	80	80	82	0.19	0.09	1.1	35	58	38	7		13			10		734858	9548652	2960
68833	BGU23-6-105.8	BGU23-06	105	105	107	0.02	0.005	0.25	11	560	3	46		7			9		734850	9548638	2941
68834	BGU23-6-147.1	BGU23-06	147	146.5	148.4	0.15	0.05	1.3	23	140	12	11		38			13		734838	9548616	2908
68835	BGU23-08-10	BGU23-08	10	8.5	11.5	0.88	0.54	7.9	39	67	19	58		590			21		734879	9548688	3030
68836	BGU23-8-25.5	BGU23-08	25	23.5	26.5	0.04	0.08	0.25	20	28	20	31		30			15		734873	9548677	3037
68837	BGU23-8-38.8	BGU23-08	38	35.5	38.5	0.00	0.005	0.25	12	22	3	7		5			16		734868	9548668	3043
68838	BGU23-08-86	BGU23-08	86	83	86.5	0.01	0.005	0.25	11	24	3	8		5			21		734847	9548632	3067
68839	BGU23-08-87	BGU23-08	87	86.5	89.5	0.00	0.005	0.25	18	39	-2	6		3			14		734846	9548630	3069
68840	BGU23-8-144.2	BGU23-08	144	144	146.5	0.01	0.27	2.6	196	410	-2	45		2			40		734821	9548587	3098
68841	BGU23-8-212	BGU23-08	212	208.9	212.5	0.43	10.7	19.7	255	5000	18	79		34			54		734793	9548539	3132
68842	BGU23-8-212.6	BGU23-08	212	208.9	212.5	0.43	10.7	19.7	255	5000	18	79		34			54		734793	9548539	3132
68843	BGU24-8-255.2	BGU24-08	255	254	257	0.83	7.22	5.1	12	54	3	52		18			49		734679	9548573	2886
69130	BGU24-10-16	BGU24-10	16	15	18	0.04	0.1	0.25	9	29	16	16		37			25		734830	9548709	3013
68844	BGU24-10-305	BGU24-10	305	303	306	1.68	10	29.9	4800	7900	2	380		38			60		734706	9548597	2779
68845	BGU24-11-177	BGU24-11	177	177	180														734779	9548663	2866
68846	BGU24-11-343	BGU24-11	343	342	345	1.30	14.6	46	3450	5500	-2	100		16			36		734723	9548613	2719
68847	BGU24-13-139	BGU24-13	139	138.5	141	13.80	5.42	77.2	46	5100	-2	50		220			20		734775	9548601	3079
68848	BGU24-13-143.5	BGU24-13	143	141	143.1	1.57	0.61	11.7	322	1400	-2	34		92			35		734774	9548599	3080
68849	BGU26-1-151	BGU26-01	151	150.7	152.8	1.04	117	75.6	9300	22500	3	3200		12			33		734664	9548615	3005
68850	BGU26-01-151.9	BGU26-01	151	150.7	152.8	1.04	117	75.6	9300	22500	3	3200		12			33		734664	9548615	3005
68851	BGU26-01-152.3	BGU26-01	152	150.7	152.8	1.04	117	75.6	9300	22500	3	3200		12			33		734664	9548615	3005
68852	BGU26-01-165.2	BGU26-01	165	164.9	168	16.00	5.82	94.5	37	2250	17	21		298			55		734657	9548603	3003
68853	BGU26-2-207	BGU26-02	207	206.9	209	1.41	15.8	32.3	880	317	2	750	124	56	17.5	11.8	32	-0.1	734653	9548594	2913
68854	BGU26-03-122.4	BGU26-03	122	119.3	122.4	0.01	0.17	0.25	32	83	4	45		6			12		734679	9548640	3052
68855	BGU26-04-215.6	BGU26-04	215	214.3	217.3	2.60	0.55	13.6	20	110	2	60		52			18		734678	9548634	2855
68856	BGU26-04-275.5	BGU26-04	275	273	276	1.00	0.82	7.3	148	205	-2	100		49			37		734661	9548604	2807
68857	BGU26-04-298.2	BGU26-04	298	297	300	0.86	6.6	14.4	620	1280	349	170		75			59		734654	9548592	2788
68858	BGU26-10-121.5	BGU26-10	121	120.8	124.3	0.47	16.5	45.5	15400	2300	5	440		10			14		734695	9548667	3117
68859	BGU27-2-204.5	BGU27-02	204	204	207	2.61	23.5	40	378	335	54	220		141			43		734613	9548616	2918
68860	BGU27-4-172	BGU27-04	172	170.7	173.4	2.89	13.2	38	394	1300	14	33		65			31		734613	9548615	3046
68861	BGU27-4-174	BGU27-04	174	173.4	174.8	0.63	9.48	27.5	3580	13600	11	22		12			43		734612	9548614	3046
68862	BGU27-05-124	BGU27-05	124	114.3	124.8	0.72	7.2	42.3	21800	32000	5	2600		384			30		734641	9548664	3063
68863	BGU27-05-124.1	BGU27-05	124	114.3	124.8	0.72	7.2	42.3	21800	32000	5	2600		384			30		734641	9548664	3063
68864	BGU27-6-348.5	BGU27-06	348	348	351	9.18	12.2	220	3700	74000	12	790		9			25		734647	9548662	2701
68865	BGU27-6-349	BGU27-06	349	348	351	9.18	12.2	220	3700	74000	12	790		9			25		734647	9548662	2701
68866	BGU28-01-104	BGU28-01	104	102	108	1.97	4.78	92.6	5750	21000	2	7000		123			53		734598	9548695	3016
68867	BGU28-5-267	BGU28-05	267	267	268.7	1.05	19.2	9.3	25	76	53	72	162	66	1	6	112	-0.1	734577	9548652	2811
68868	BGU28-5-268	BGU28-05	268	267	268.7	1.05	19.2	9.3	25	76	53	72	162	66	1	6	112	-0.1	734577	9548652	2811
68869	BGU28-07-185.4	BGU28-07	185	184.2	186.4	0.49	0.16	5.7	58	208	2	300		48			30		734625	9548741	2853
68870	BGU28-07-230	BGU28-07	230	228.4	231	0.67	1.26	23.1	6200	9700	-2	1320		500			17		734620	9548732	2810
68871	BGU28-8-375	BGU28-08	375	374.2	376.5	2.28	5.76	83.9	6200	27400	2	2300		390			31		734643	9548770	2658
68872	BGU28-8-375-5	BGU28-08	375	374.2	376.5	2.28	5.76	83.9	6200	27400	2	2300		390			31		734643	9548770	2658
68873	BGU29-01-159	BGU29-01	159	158	160.5	0.17	17.9	77	46600	104000	-2	7400	60	61	111	17	23	1.39	734550	9548705	2918
68874	BGU29-02-242	BGU29-02	242	238.9	242.3	0.30	18.3	181	35000	136000	-2	16600	130	17	220	2	37	0.32	734554	9548720	2813
68875	BGU29-07-130	BGU29-07	130	126	167	0.06	0.38	31.7	620	8100	6	370		-2			14		734545	9548702	3130
68876	BGU29-07-197.5	BGU29-07	197	195	198	0.01	0.18	2.6	149	334	-2	10		-2			23		734526	9548668	3161
68877	BGU30-03-180	BGU30-03	180	179	181.1	0.75	19.5	81.7	16400	23200	-2	19900		204			36		734517	9548749	2874
68878	BGU30-03-180B	BGU30-03	180	179	181.1	0.75	19.5	81.7	16400	23200	-2	19900		204			36		734517	9548749	2874
68879	BGU30-04-137.9	BGU30-04	137	135	137.7														734536	9548783	2901
68880	BGU30-04-138.9	BGU30-04	138	137.7	138.45														734536	9548782	2899
68881	BGU30-04-139.6	BGU30-04	139	138.45	139.6														734536	9548782	2898
68882	BGU30-5-246	BGU30-05	246	245.6	246.6	1.63	50.8	71	8400	13600	-2	25500		76			18		734533	9548780	2789
68883	BGU30-06-173	BGU30-06	173	171.4	174.4	0.19	31.2	12.5	650	365	-2	210		220			34		734477	9548681	3108
68884	BGU30-06-179	BGU30-06	179	177	179.3	0.38	14.2	11.4	321	350	3	80		158			40		734474	9548677	3110
68885	BGU30-08-186.5	BGU30-08	186	170.5	186.2	0.00	0.07	0.25	24	50	2	28		-2			19		734506	9548729	3187
68916	GRS125-590.7	GRS-125	590	588	591	0.01	0.025												734149	9550186	3262
68917	GRS125-595.6	GRS-125	595	594	597	0.01	0.025												734149	9550187	3256
68918	GRS125-599A	GRS-125	599	597	600	0.01	0.025												734149	9550187	3253
68919	GRS125-599B	GRS-125	599	597	600	0.01	0.025												734149	9550187	3253
68920	GRS125-600	GRS-125	600	600	603	0.01	0.025												734149	9550187	3250
68921	GRS125-600.5	GRS-125	600	600	603	0.01	0.025												734149	9550187	3250
68922	GRS125-601	GRS-125	601	600	603	0.01	0.025												734149	9550187	3250
68923	GRS125-601.4	GRS-125	601	600	603	0.01	0.025												734149	9550187	3250
68924	GRS125-602.7	GRS-125	602	600	603	0.01	0.025												734149	9550187	3250
68925	GRS125-604	GRS-125	604	603	606	0.01	0.025												734149	9550187	3247
68926	GRS125-608.6	GRS-125	608	606	609	0.03	0.09												734149	9550187	3244

JCU Number	Sample_No	Location Hole ID	Depth	Assay Interval FROM	Assay Interval TO	CU%	AU	AG	PB	ZN	MO	AS	BI	CO	SB	SE	CR	HG	Location X	Location Y	Location Z
68927	GRS125-610	GRS-125	610	609	612	0.01	0.15												734149	9550187	3241
68928	GRS125-611.3	GRS-125	611	609	612	0.01	0.15												734149	9550187	3241
68929	GRS125-615	GRS-125	615	615	618	0.06	0.11												734149	9550188	3235
68930	GRS125-618	GRS-125	618	618	621	0.10	0.86												734149	9550188	3232
68931	GRS125-620.6	GRS-125	620	618	621	0.10	0.86												734149	9550188	3232
68932	GRS125-620.7	GRS-125	620	618	621	0.10	0.86												734149	9550188	3232
68933	GRS125-621.5	GRS-125	621	621	624	0.07	0.88												734150	9550188	3229
68934	GRS125-622.3	GRS-125	622	621	624	0.07	0.88												734150	9550188	3229
68935	GRS125-623	GRS-125	623	621	624	0.07	0.88												734150	9550188	3229
68936	GRS125-624.8	GRS-125	624	624	627	0.01	0.27												734150	9550188	3226
68937	GRS125-626.2	GRS-125	626	624	627	0.01	0.27												734150	9550188	3226
68938	GRS125-626.4	GRS-125	626	624	627	0.01	0.27												734150	9550188	3226
68939	GRS125-629.8	GRS-125	629	627	630	0.03	0.1												734150	9550188	3223
68940	GRS125-630	GRS-125	630	630	633	0.03	0.22												734150	9550188	3220
68941	GRS125-632	GRS-125	632	630	633	0.03	0.22												734150	9550188	3220
68942	GRS125-653.5	GRS-125	653	651	654	0.24	0.83												734150	9550189	3199
68943	GRS125-690.8	GRS-125	690	690	693	0.67	3.96												734152	9550190	3160
68944	GRS125-692.8	GRS-125	692	690	693	0.67	3.96												734152	9550190	3160
68945	GRS125-693.6	GRS-125	693	693	696	1.05	8.52												734152	9550191	3157
68946	GRS125-696.2	GRS-125	696	696	699	2.34	13.48												734152	9550191	3154
68947	GRS125-697.2	GRS-125	697	696	699	2.34	13.48												734152	9550191	3154
68948	GRS125-700.7	GRS-125	700	699	702	4.46	10.12	98											734152	9550191	3151
68949	GRS125-724.5	GRS-125	724	723	726	1.48	11.11												734153	9550192	3127
68950	GRS125-750.3	GRS-125	750	750	753	0.49	16.43	18											734153	9550193	3100
68951	GRS125-751	GRS-125	751	750	753	0.49	16.43	18											734153	9550193	3100
68952	GRS125-753	GRS-125	753	753	756	0.28	32.2												734153	9550193	3097
68953	GRS125-759	GRS-125	759	759	762	0.33	7.13												734154	9550193	3091
68954	GRS125-760.4	GRS-125	760	759	762	0.33	7.13												734154	9550193	3091
68955	GRS125-761.5	GRS-125	761	759	762	0.33	7.13												734154	9550193	3091
68956	GRS125-766.4	GRS-125	766	765	768	0.82	13.2												734154	9550193	3085
68957	GRS125-766.5	GRS-125	766	765	768	0.82	13.2												734154	9550193	3085
68958	GRS125-766.8	GRS-125	766	765	768	0.82	13.2												734154	9550193	3085
68959	GRS125-776.85	GRS-125	776	774	777	0.48	3.17												734154	9550194	3076
68960	GRS125-803.5	GRS-125	803	801	804	1.34	1.01												734155	9550195	3049
68961	GRS125-836.6	GRS-125	836	834	837	1.23	9.4												734156	9550196	3016
68962	GRS125-848.4	GRS-125	848	846	849	1.74	6												734156	9550196	3004
68963	GRS125-848.5	GRS-125	848	846	849	1.74	6												734156	9550196	3004
68964	GRS125-873.2	GRS-125	873	873	876	4.24	26.3												734157	9550198	2977
68965	GRS125-873.5	GRS-125	873	873	876	4.24	26.3												734157	9550198	2977
68966	GRS125-874.3	GRS-125	874	873	876	4.24	26.3												734157	9550198	2977
68967	GRS125-874.8	GRS-125	874	873	876	4.24	26.3												734157	9550198	2977
68968	GRS125-875	GRS-125	875	873	876	4.24	26.3												734157	9550198	2977
68969	GRS125-877.7	GRS-125	877	876	879	4.89	11.3												734157	9550198	2974
68970	GRS125-878	GRS-125	878	876	879	4.89	11.3												734157	9550198	2974
68971	GRS125-878.5	GRS-125	878	876	879	4.89	11.3												734157	9550198	2974
68972	GRS125-899	GRS-125	899	897	900	0.41	0.48												734158	9550198	2953
68973	GRS125-917	GRS-125	917	915	918	5.02	2.1												734158	9550199	2935
68974	31	GRS-127	655	654	657	0.01	0.64												734023	9550317	3209
68975	32	GRS-127	660	660	663	0.01	0.69												734024	9550318	3203
68976	42	GRS-127	711	711	714	0.43	0.85												734024	9550322	3152
68977	GRS127-887.2	GRS-127	887	885	888	1.25	1.34				13	160	389	27	8.6	166	120	-0.1	734015	9550329	2979
69012	WAN1-1-494.4	WAN1-1	494	491.9	494.4	1.81	1.2	16.9	34	6700	3	2200	10	69	7.4000001		31		732073	9549671	3373
69013	WAN1-3-181	WAN1-3	181																732106	9549702	3684
69014	WAN1-3-759	WAN1-3	759	758.1	760.7	0.73	0.53	4.4000001	20	93	7	5	1	89	0.3	6.1999998	18	-0.1	732167	9549679	3110
69015	WAN1-3-776	WAN1-3	776	776	778.9	1.07	0.38	7.0999999	50	89	18	64	1	13	-0.2	12	26	-0.1	732168	9549678	3092
69016	WAN2-2-852	WAN2-2	852	851.4	852.4	11.80	2.3599999	87.5	23	920	24	115	7	355	-0.2	60	50	-0.1	732029	9549751	2885
69018	WAN4-1-58A	WAN4-1	58	57.8	60.1	0.03	1.3200001	4.9000001	388	610	-2	100	-1	8	3.4000001	2.5999999	88	0.62	731915	9549391	3766
69019	WAN4-1-58B1	WAN4-1	58	57.8	60.1	0.03	1.3200001	4.9000001	388	610	-2	100	-1	8	3.4000001	2.5999999	88	0.62	731915	9549391	3766
69020	WAN4-1-58B2	WAN4-1	58	57.8	60.1	0.03	1.3200001	4.9000001	388	610	-2	100	-1	8	3.4000001	2.5999999	88	0.62	731915	9549391	3766
69021	WAN4-1-72.1	WAN4-1	72	70.9	72.7	0.03	1.53	3.8	530	2100	3	270	-1	5	3.2	2.5	83	0.11	731915	9549391	3753
69022	WAN4-2-234A	WAN4-2	234	232.9	236	0.66	32.5	109	40000	175000	12	1050	133	-2	105	27	38	0.6	731877	9549344	3598
69023	WAN4-2-234B	WAN4-2	234	232.9	236	0.66	32.5	109	40000	175000	12	1050	133	-2	105	27	38	0.6	731877	9549344	3598
69017	WAN4-236.5B	WAN4-2	236	236	237.6	0.14	13.8	42	24900	36800	4	350	4	-2	84	24	22	0.25	731877	9549343	3596
69024	WAN4-236.5A	WAN4-2	236	236	237.6	0.14	13.8	42	24900	36800	4	350	4	-2	84	24	22	0.25	731877	9549343	3596
69029	WAN4-2-245.2A	WAN4-2	245	241.9	245.2	0.01	0.65	1.8	790	1620	-2	110	-1	-2	14.9	1.4	21	-0.1	731876	9549342	3589
69030	WAN4-2-245.2B	WAN4-2	245	241.9	245.2	0.01	0.65	1.8	790	1620	-2	110	-1	-2	14.9	1.4	21	-0.1	731876	9549342	3589

Appendix 2b - Assay data and coordinates for drillhole samples used in this study (PT Freeport Indonesia)

JCU Number	Sample_No	Location Hole ID	Depth	Assay Interval FROM	Assay Interval TO	CU%	AU	AG	PB	ZN	MO	AS	BI	CO	SB	SE	CR	HG	Location X	Location Y	Location Z
69025	WAN4-2-300	WAN4-2	300	297.6	300.1	0.03	0.22	0.8	28	190	-2	140	3	14	5.5999999	5.9000001	99	-0.1	731867	9549332	3535
69026	WAN4-2-307	WAN4-2	307	306.8	310.4	0.02	0.45	1	75	2160	-2	21	8	17	1.5	4.4000001	80	-0.1	731866	9549330	3526
69027	WAN4-2-314A	WAN4-2	314	312.8	315.9	0.04	2.5	7.3000002	255	10400	3	275	12	7	22	12.7	61	0.35	731865	9549329	3520
69028	WAN4-2-314B	WAN4-2	314	312.8	315.9	0.04	2.5	7.3000002	255	10400	3	275	12	7	22	12.7	61	0.35	731865	9549329	3520
69031	WAN4-3-63	WAN4-3	63	61	64	0.03	1.08	5.8000002	510	1100	7	310	20	9	10.5	22	65	0.1	731913	9549441	3784
69032	WAN4-3-63.2	WAN4-3	63	61	64	0.03	1.08	5.8000002	510	1100	7	310	20	9	10.5	22	65	0.1	731913	9549441	3784
69033	WAN4-3-80.5A	WAN4-3	80	79	82	0.03	1.72	3	140	145	23	450	17	14	3.5	12.1	101	-0.1	731913	9549455	3773
69034	WAN4-3-80.5B	WAN4-3	80	79	82	0.03	1.72	3	140	145	23	450	17	14	3.5	12.1	101	-0.1	731913	9549455	3773
69035	WAN4-3-103.6	WAN4-3	103	102	105	0.09	3.6700001	2.9000001	62	74	6	510	126	18	1.7	47	123	-0.1	731913	9549473	3758
69036	WAN4-3-108.1	WAN4-3	108	105	108.2	0.12	12.1	3.5	56	66	7	360	154	15	1.3	43	135	-0.1	731913	9549475	3756
69131	WAN4-3-130.5	WAN4-3	130	127.6	131.2	0.06	3.6600001	6.5	343	2800	2	190	72	9	5.1999998	21	63	-0.1	731913	9549493	3742
69037	WAN4-3-134.5	WAN4-3	134	133	136	0.04	1.67	2.0999999	64	48	-2	110	33	5	4.5999999	12.5	92	-0.1	731913	9549497	3739
69132	WAN4-3-138.1	WAN4-3	138	136	139	0.01	0.91	-0.5	14	45	-2	21	2	3	0.7	3.0999999	67	-0.1	731913	9549499	3737
69038	WAN4-3-193.5	WAN4-3	193	192	196	0.03	5.2199998	3.7	410	161	24	130	4	20	2.5	11	75	-0.1	731913	9549543	3701
69039	WAN4-3-256	WAN4-3	256	256	259	0.03	0.5	-0.5	63	115	-2	180	2	4	2.3	1.8	98	0.32	731913	9549593	3661
69040	WAN4-3-288	WAN4-3	288	287.7	291.1	0.09	1.58	2.8	334	138	55	30	1	8	1.2	14.1	79	-0.1	731913	9549618	3642
69041	WAN4-3-302.5	WAN4-3	302	299.2	302.5	0.01	0.16	-0.5	176	224	-2	8	-1	-2	-0.2	4.4000001	15	-0.1	731913	9549627	3635
69042	WAN4-3-303.4	WAN4-3	303	302.5	303.6	0.34	4.2600002	58	51900	54000	73	180	25	7	33	990	36	0.1	731913	9549628	3633
69043	WAN4-3-303.6A	WAN4-3	303	302.5	303.6	0.34	4.2600002	58	51900	54000	73	180	25	7	33	990	36	0.1	731913	9549628	3633
69044	WAN4-3-303.6B	WAN4-3	303	302.5	303.6	0.34	4.2600002	58	51900	54000	73	180	25	7	33	990	36	0.1	731913	9549628	3633
69045	WAN4-4-603	WAN4-4	603	57.4	60.4	0.04	1.14	2.7	1720	1880	-2	200	3	3	10.4	4.3000002	80	0.16	731961	9549400	3787
69046	WAN4-5-50	WAN4-5	50	48.8	51.6	0.03	0.96	2.2	72	153	3	120	6	5	2.0999999	5.6999998	69	-0.1	731891	9549419	3791
69047	WAN4-5-50B	WAN4-5	50	48.8	51.6	0.03	0.96	2.2	72	153	3	120	6	5	2.0999999	5.6999998	69	-0.1	731891	9549419	3791
69048	WAN4-5-90.5	WAN4-5	90	89.3	92.3	0.07	0.84	4	263	510	4	230	24	53	59	9.6999998	120	0.1	731871	9549443	3764
69049	WAN4-5-171	WAN4-5	171	171	174.4	0.01	0.02	-0.5	10	77	-2	11	-1	13	-0.2	-0.5	14	-0.1	731831	9549490	3711
69050	WAN4-5-174	WAN4-5	174	171	174.4	0.01	0.02	-0.5	10	77	-2	11	-1	13	-0.2	-0.5	14	-0.1	731831	9549490	3711
69051	WAN4-5-174.5	WAN4-5	174	171	174.4	0.01	0.02	-0.5	10	77	-2	11	-1	13	-0.2	-0.5	14	-0.1	731831	9549490	3711
69052	WAN4-5-182	WAN4-5	182	181	184	0.08	3.53	4.3000002	210	250	14	480	8	9	66	6.6999998	90	4.6500001	731827	9549496	3705
69053	WAN4-5-205	WAN4-5	205	205	206.7	0.05	0.4	3.2	266	940	13	180	44	8	1	18.299999	72	-0.1	731815	9549510	3690
69054	WAN4-5-211a	WAN4-5	211	209.7	211.2	0.03	1.16	5.4000001	580	690	6	130	42	4	3.5	29	57	1.77	731812	9549513	3688
69055	WAN4-5-211b	WAN4-5	211	209.7	211.2	0.03	1.16	5.4000001	580	690	6	130	42	4	3.5	29	57	1.77	731812	9549513	3688
69056	WAN4-6-28	WAN4-6	28	27.5	28.7	0.02	16.799999	565	13700	4400	14	1970	194	5	34	5.8000002	56	0.25	731892	9549397	3806
69057	WGR12-30	WGR-12	30	30	33	1.02	0.4												733571	9550950	4085
69058	WGR12-37	WGR-12	37	36	39	2.03	0.6												733567	9550950	4081
69059	WGR12-43.3	WGR-12	43	42	45	2.37	1.92												733562	9550950	4076
69060	WGR12-168.6	WGR-12	168	168	171	0.01	5.34												733472	9550951	3989
69061	WGR12-169.7	WGR-12	169	168	171	0.01	5.34												733472	9550951	3989
69062	WGR12-170.5	WGR-12	170	168	171	0.01	5.34												733472	9550951	3989
69063	WGR12-173	WGR-12	173	171	174	0.01	2.84												733470	9550951	3987
69064	WGR12-174.3	WGR-12	174	174	177	0.01	3.08												733468	9550951	3985
69065	WGR12-177	WGR-12	177	177	180	0.01	4.02												733465	9550951	3983
69066	WGR12-294.6	WGR-12	294	294	297	0.01	5.7												733381	9550952	3901
69067	WGR12-302.2	WGR-12	302	300	303	0.01	1.4												733377	9550952	3897
69068	WGR12-367	WGR-12	367	366	369	0.02	0.98												733329	9550952	3851
69069	WGR12-369.5	WGR-12	369	369	372	0.02	1.88												733327	9550952	3849
69071	WGR13-32	WGR-13	32	30	33	0.17	0.05												733655	9551465	4067
69072	WGR13-48	WGR-13	48	48	51	0.03	0.01												733643	9551466	4054
69073	WGR13-52	WGR-13	52	51	54	0.04	0.09												733641	9551466	4052
69074	WGR13-57.7	WGR-13	57	57	60	0.20	0.03												733637	9551466	4048
69075	WGR13-60	WGR-13	60	60	63	0.19	0.06												733635	9551466	4046
69076	WGR13-118.5	WGR-13	118	117	120	0.15	0.19												733595	9551469	4005
69077	WGR13-143	WGR-13	143	141	144	0.02	0.13												733579	9551470	3988
69078	WGR13-151.7	WGR-13	151	150	153	0.01	0.39												733572	9551471	3981
69079	WGR13-153	WGR-13	153	153	156	0.30	0.23												733570	9551471	3979
69080	WGR13-161.5	WGR-13	161	159	162	0.09	0.33												733566	9551471	3975
69081	WGR13-162	WGR-13	162	162	165	0.01	0.78												733564	9551472	3972
69082	WGR13-169.5	WGR-13	169	168	171	0.15	0.04												733560	9551472	3968
69083	WGR13-170	WGR-13	170	168	171	0.15	0.04												733560	9551472	3968
69084	WGR13-173	WGR-13	173	171	174	0.13	0.61												733558	9551472	3966
69085	WGR13-173.8	WGR-13	173	171	174	0.13	0.61												733558	9551472	3966
69086	WGR13-177.5	WGR-13	177	177	180	0.01	0.08												733554	9551472	3962
69087	WGR13-188	WGR-13	188	186	189	0.02	0.11												733547	9551473	3955
69088	WGR13-199.2A	WGR-13	199	198	201	0.02	3.84												733539	9551473	3947
69089	WGR13-199.2B	WGR-13	199	198	201	0.02	3.84												733539	9551473	3947
69090	WGR13-201	WGR-13	201	201	204	0.03	0.62												733537	9551474	3944
69091	WGR13-215.5	WGR-13	215	213	216	0.03	1.11												733529	9551474	3936

Appendix 2b - Assay data and coordinates for drillhole samples used in this study (PT Freeport Indonesia)

JCU Number	Sample_No	Location Hole ID	Depth	Assay Interval FROM	Assay Interval TO	CU%	AU	AG	PB	ZN	MO	AS	BI	CO	SB	SE	CR	HG	Location X	Location Y	Location Z
69092	WGR3-15.2	WGR-3	15	15	18	0.02	0.37	1											733451	9551009	4086
69093	WGR3-26.5	WGR-3	26	24	27	0.01	0.77	1											733446	9551009	4078
69094	WGR3-54	WGR-3	54	54	57		0.98	1											733428	9551008	4054
69095	WGZ8-23	WGZ-8	23	21	24	0.15	1												733600	9551257	4068
69096	WGZ8-30.5	WGZ-8	30	30	33	0.07	0.16												733594	9551258	4062
69097	WGZ8-31.5	WGZ-8	31	30	33	0.07	0.16												733594	9551258	4062
69098	WGZ8-33.5	WGZ-8	33	33	36	0.10	0.1												733592	9551258	4060
69099	WGZ8-35	WGZ-8	35	33	36	0.10	0.1												733592	9551258	4060
69100	WGZ8-010	WGZ-8	39	36	42	0.04	0.14												733589	9551258	4056
69101	WGZ8-008	WGZ-8	48	48	51	0.11	0.66												733581	9551259	4049
69102	WGZ8-60	WGZ-8	60	60	63	0.09	0.42												733573	9551260	4040
69103	WGZ8-61	WGZ-8	61	60	63	0.09	0.42												733573	9551260	4040
69104	WGZ8-63.2	WGZ-8	63	63	66	0.19	0.5												733571	9551260	4038
69105	WGZ8-63.5	WGZ-8	63	63	66	0.19	0.5												733571	9551260	4038
69106	WGZ8-014	WGZ-8	64	63	66	0.19	0.5												733571	9551260	4038
69137	WGZ8-017	WGZ-8	64.2	63	66	0.19	0.5												733570	9551260	4038
69107	WGZ8-69.5	WGZ-8	69	69	72	0.30	0.4												733567	9551261	4034
69108	WGZ8-76.6	WGZ-8	76	75	78	0.09	2.34												733562	9551262	4030
69109	WGZ8-77	WGZ-8	77	75	78	0.09	2.34												733562	9551262	4030
69110	WGZ8-015	WGZ-8	79	78	81	0.01	0.38												733560	9551262	4028
68860	WGZ8-90	WGZ-8	90.0	90	93	0.09	0.27												733552	9551263	4019
69111	WGZ8-91	WGZ-8	91	90	93	0.09	0.27												733552	9551263	4019
69112	WGZ8-92.5	WGZ-8	92	90	93	0.09	0.27												733552	9551263	4019
69125	WGZ8-004	WGZ-8	94	93	96	0.03	1.1												733550	9551263	4017
69113	WGZ8-005	WGZ-8	95	93	96	0.03	1.1												733550	9551263	4017
69138	WGZ8-011	WGZ-8	96.1	96	99	0.03	0.23												733547	9551263	4015
68799	WGZ8-018	WGZ-8	104.7	102	105	0.01	0.18												733543	9551263	4010
69114	WGZ8-117	WGZ-8	117	117	120	0.01	0.1												733533	9551265	4000
69115	WGZ8-118	WGZ-8	118	117	120	0.01	0.1												733533	9551265	4000
69116	WGZ8-126	WGZ-8	126	126	132	0.07	0.08												733526	9551266	3993
69117	WGZ8-148.3	WGZ-8	148	147	150	0.01	0.16												733512	9551268	3979
69118	WGZ8-166	WGZ-8	166	165	168	0.02	0.28												733499	9551269	3966
69119	WGZ8-210	WGZ-8	210	210	213	0.01	0.48												733468	9551273	3934
69120	WGZ8-307	WGZ-8	307	306	309	0.02	0.05												733400	9551282	3867
69124	WGZ8-316	WGZ-8	316	315	318	0.01	3.73												733394	9551283	3860
69121	WGZ8-370	WGZ-8	370	369	372	0.06	0.8												733356	9551288	3822
69122	WGZ8-387.5	WGZ-8	387	387	390	0.01	0.18												733344	9551289	3809
69123	WGZ8-392	WGZ-8	392	390	393	0.01	0.3												733341	9551289	3807

Appendix 3

XRD results

(West Grasberg printed as a Table in Section A)

Appendix 3 - XRD results

AAC Sample#	Drillhole	Depth (m)	Sample material	Lithology	Description of material analysed	Technique	Dominant clay mineral	Other clay mineral	Minor clay minerals	Major minerals present	Minor minerals present	Comments
3752-24	BG1-4A	423.0	powder slide-smear		white cy alteration	XRD	smectite?			?		
3752-23	BG1-4A	256.0	powder slide-smear		sandy and cy	XRD	smectite (sharp peak)			dol, ccte, qtz?		
3752-25	BG1-7	108.0	powder slide-smear		clay	XRD	smectite (sharp peak)	talc				
4612-363	BGU rock sample - GAVIN		Hand specimen		Green Mica	GADDS				Phlogopite		
4612-345	BGU14-07	590.0	Hand specimen		possible calcite	GADDS				quartz and calcite?		NB XRD to check
4612-198	BGU14-7	590.0	hand specimen		green crystals - pyroxene	GADDS count 25s 0.8mm sample area (theta - 40-20) 06/09/02				pyroxene	calcite	
4612-352	BGU17-7	460.0	Hand specimen		white veins in pyroxene	GADDS				dolomite		
4612-353	BGU17-7	460.0	Hand specimen		white at edge in pyroxene	GADDS				dolomite		
4612-359	BGU17-7	404.8	Hand specimen		Green Mica	GADDS				Phlogopite		
4612-360	BGU17-7	404.8	Hand specimen		Green Mica	GADDS				Phlogopite		
4612-361	BGU17-7	404.4	Hand specimen		Green Mica	GADDS				Phlogopite		
4612-362	BGU17-7	404.4	Hand specimen		Green Mica	GADDS				Phlogopite		
4612-295	BGU18-3	212.0	hand specimen		calsts within massive pyrite	GADDS count 10s 0.8mm sample area (theta - 40-20) 11/09/02				quartz		
4612-296	BGU18-3	212.0	hand specimen		second area as above	GADDS count 10s 0.8mm sample area (theta - 40-20) 11/09/02				calcite	quartz?, chalcopyrite?	
4612-297	BGU18-3	212.0	hand specimen		clast with scratch	GADDS count 10s 0.8mm sample area (theta - 40-20) 11/09/02				quartz?		
4612-298	BGU18-3	212.0	hand specimen		cpy in unscratched clast	GADDS count 10s 0.8mm sample area (theta - 40-20) 11/09/02				calcite	pyrite?	
4612-301	BGU18-3	211.2	hand specimen		marble host (fine grained) to sulphide vein	GADDS count 20s 0.8mm sample area (theta - 40-20) 11/09/02				calcite, dolomite		
4612-302	BGU18-3	211.2	hand specimen		marble alteration (coarse) on pyrite vein selvege	GADDS count 20s 0.8mm sample area (theta - 40-20) 11/09/02				calcite		single crystal peak
4612-153	BGU18-3	203.0	hand specimen		green veinlet (narrow) in white calcite	GADDS count 25s 0.8mm sample area (theta - 40-20) 06/09/02				calcite, dolomite	?	
4612-154	BGU18-3	203.0	hand specimen		white clacite marble sample	GADDS count 25s 0.8mm sample area (theta - 40-20) 06/09/02				calcite, dolomite		
4612-224	BGU18-3	192.6	hand specimen		black limestone	GADDS count 25s 0.8mm sample area (theta - 40-20) 06/09/02				calcite		
4612-225	BGU18-3	192.6	hand specimen		white marble alteration on fractures	GADDS count 25s 0.8mm sample area (theta - 40-20) 06/09/02				dolomite, calcite		
4612-220	BGU18-3	192.5	hand specimen		grey clast in centre	GADDS count 25s 0.8mm sample area (theta - 40-20) 06/09/02				dolomite, calcite		
4612-221	BGU18-3	192.5	hand specimen		white rim on grey clast	GADDS count 25s 0.8mm sample area (theta - 40-20) 06/09/02				dolomite, calcite	orthoclase?	
4612-222	BGU18-3	192.5	hand specimen		white clast	GADDS count 25s 0.8mm sample area (theta - 40-20) 06/09/02				dolomite, calcite		
4612-223	BGU18-3	192.5	hand specimen		black solution veinlet	GADDS count 25s 0.8mm sample area (theta - 40-20) 06/09/02				dolomite, calcite	orthoclase, Quartz?	
4612-215	BGU18-3	32.5	hand specimen		pale brown alteration in white	GADDS count 25s 0.8mm sample area (theta - 40-20) 06/09/02				dolomite, calcite		
4612-216	BGU18-3	32.5	hand specimen		white adjacent to brown	GADDS count 25s 0.8mm sample area (theta - 40-20) 06/09/02				dolomite, calcite	orthoclase?	
4612-217	BGU18-3	32.5	hand specimen		pale brown near contact with black	GADDS count 25s 0.8mm sample area (theta - 40-20) 06/09/02				dolomite, calcite		
4612-218	BGU18-3	32.5	hand specimen		black area near brown contact	GADDS count 25s 0.8mm sample area (theta - 40-20) 06/09/02				dolomite, calcite		
4612-219	BGU18-3	32.5	hand specimen		white within brown-black	GADDS count 25s 0.8mm sample area (theta - 40-20) 06/09/02				dolomite, calcite	orthoclase?	
4612-204	BGU21-01	43.0	hand specimen		purple area at top	GADDS count 25s 0.8mm sample area (theta - 40-20) 06/09/02				dolomite	anhydrite, tremolite OR epidote	
4612-205	BGU21-01	43.0	hand specimen		green near white and vein	GADDS count 25s 0.8mm sample area (theta - 40-20) 06/09/02				dolomite	anhydrite, tremolite OR epidote	
4612-206	BGU21-01	43.0	hand specimen		white alteration zone	GADDS count 25s 0.8mm sample area (theta - 40-20) 06/09/02				dolomite	anhydrite, tremolite OR epidote	
4612-178	BGU21-01	13.0	hand specimen		small yellow fragments in matrix	GADDS count 25s 0.8mm sample area (theta - 40-20) 06/09/02				dolomite, calcite		
4612-179	BGU21-01	13.0	hand specimen		centre of dark grey clast (with alteration rims)	GADDS count 25s 0.8mm sample area (theta - 40-20) 06/09/02				dolomite		
4612-180	BGU21-01	13.0	hand specimen		yellow bit near edge of clast	GADDS count 25s 0.8mm sample area (theta - 40-20) 06/09/02				dolomite, calcite	cummingtonite/tremolite	
4612-181	BGU21-01	13.0	hand specimen		clear crystalls -last infill - calcite?	GADDS count 25s 0.8mm sample area (theta - 40-20) 06/09/02				dolomite		
4612-339	BGU21-01	13.0	Hand specimen		unstained carbonate in centre area - white coloured	GADDS				dolomite	minor quartz and calcite	
4612-340	BGU21-01	13.0	Hand specimen		unstained carbonate in centre area - white coloured - second example	GADDS				dolomite	minor calcite	
4612-341	BGU21-01	13.0	Hand specimen		unstained carbonate in centre area - clear	GADDS				dolomite		
4612-344	BGU21-03	15.3	Hand specimen		unstained slightly purple on staining carbonate	GADDS				dolomite		
4612-147	BGU21-10	159.0	hand specimen		black material on small flat piece	GADDS count 25s 0.8mm sample area (theta - 40-20) 06/09/02				calcite?		
4612-354	BGU21-10	12.0	Hand specimen		Brown carbonaate - Probe = Mn-Fe	GADDS				Siderite		

Appendix 3 - XRD results

AAC Sample#	Drillhole	Depth (m)	Sample material	Lithology	Description of material analysed	Technique	Dominant clay mineral	Other clay mineral	Minor clay minerals	Major minerals present	Minor minerals present	Comments
4612-313	BGU21-10	7.5	hand specimen		yellow alteration/infill	GADDS count 15s 0.8mm sample area (theta - 40-20) 11/09/02				dolomite	anhydrite, tremolite OR epidote	not all anhydrite peaks
4612-314	BGU21-10	7.5	hand specimen		clear white (last stage)	GADDS count 15s 0.8mm sample area (theta - 40-20) 11/09/02				dolomite		tall peak = crystal
4612-315	BGU21-10	7.5	hand specimen		clast - dark grey area	GADDS count 15s 0.8mm sample area (theta - 40-20) 11/09/02				dolomite		
4612-316	BGU21-10	7.5	hand specimen		clast - white area	GADDS count 15s 0.8mm sample area (theta - 40-20) 11/09/02				dolomite		
4612-155	BGU21-3	62.0	hand specimen		pale green on side	GADDS count 25s 0.8mm sample area (theta - 40-20) 06/09/02				cummingtonite/tremolite	calcite/dolomite	
4612-156	BGU21-3	62.0	hand specimen		second area of pale green on side	GADDS count 25s 0.8mm sample area (theta - 40-20) 06/09/02				cummingtonite/tremolite	calcite/dolomite	
4612-157	BGU21-3	62.0	hand specimen		dark green? Areas within pale green	GADDS count 25s 0.8mm sample area (theta - 40-20) 06/09/02				cummingtonite/tremolite	calcite/dolomite	
4612-158	BGU21-3	62.0	hand specimen		grey clast in centre	GADDS count 25s 0.8mm sample area (theta - 40-20) 06/09/02				dolomite		
4612-182	BGU21-3	59.0	hand specimen		grey clast in centre	GADDS count 25s 0.8mm sample area (theta - 40-20) 06/09/02				dolomite, calcite		
4612-183	BGU21-3	59.0	hand specimen		white at edge of clast	GADDS count 25s 0.8mm sample area (theta - 40-20) 06/09/02				dolomite, calcite		
4612-148	BGU21-3	53.5	hand specimen		anhydrite crystal	GADDS count 25s 0.8mm sample area (theta - 40-20) 06/09/02				anhydrite, gypsum, calcite		
4612-149	BGU21-3	53.5	hand specimen		white clay on carbonate host	GADDS count 25s 0.8mm sample area (theta - 40-20) 06/09/02				anhydrite, gypsum, calcite		
4612-150	BGU21-3	53.5	hand specimen		scond area of white clay? On carbonate host	GADDS count 25s 0.8mm sample area (theta - 40-20) 06/09/02				calcite	anhydrite, gypsum, muscovite?	
4612-151	BGU21-3	53.5	hand specimen		white carbonate (matrix)	GADDS count 25s 0.8mm sample area (theta - 40-20) 06/09/02				calcite	dolomite	
4612-152	BGU21-3	53.5	hand specimen		grey carbonate clast	GADDS count 25s 0.8mm sample area (theta - 40-20) 06/09/02				dolomite	calcite	
4612-159	BGU21-3	51.3	hand specimen		pale-green clay area	GADDS count 25s 0.8mm sample area (theta - 40-20) 06/09/02				tremolite + dolomite		
4612-160	BGU21-3	51.3	hand specimen		grey clast in centre	GADDS count 25s 0.8mm sample area (theta - 40-20) 06/09/02				caclite	tremolite + dolomite	
4612-161	BGU21-3	51.3	hand specimen		white matrix	GADDS count 25s 0.8mm sample area (theta - 40-20) 06/09/02				amphibole?	dolomite	
4612-317	BGU21-3	24.5	hand specimen		gold grain	GADDS count 15s 0.8mm sample area (theta - 40-20) 11/09/02				gold?		only one peak
4612-342	BGU23-06	66.0	Hand specimen		Unstained white carbonate	GADDS				dolomite		
4612-343	BGU23-06	66.0	Hand specimen		Unstained clear carbonate	GADDS				dolomite		
3752-69	BGU23-2	64.8	hand specimen		pale green zone	GADDS 12/02/2001, 30sec exposure				tremolite, calcite		
3752-70	BGU23-2	64.8	hand specimen		darker green areas	GADDS 12/02/2001, 30sec exposure				tremolite/amphibole	quartz, dolomite	
4612-190	BGU23-2	48.6	hand specimen		grey clast in centre	GADDS count 25s 0.8mm sample area (theta - 40-20) 06/09/02				dolomite, calcite		
4612-191	BGU23-2	48.6	hand specimen		white margin on edge of grey clast	GADDS count 25s 0.8mm sample area (theta - 40-20) 06/09/02				dolomite, cummingtonite?		
4612-192	BGU23-2	48.6	hand specimen		green in matrix	GADDS count 25s 0.8mm sample area (theta - 40-20) 06/09/02				dolomite, calcite	?chlorite	
4612-193	BGU23-2	48.6	hand specimen		green in matrix	GADDS count 25s 0.8mm sample area (theta - 40-20) 06/09/02				dolomite, calcite	?chlorite	
4612-290	BGU23-2	46.0	hand specimen		pale green (tremolite?)	GADDS count 20s 0.8mm sample area (theta - 40-20) 11/09/02				calcite, tremolite		
4612-291	BGU23-2	46.0	hand specimen		dark band on margin of green and host	GADDS count 20s 0.8mm sample area (theta - 40-20) 11/09/02				calcite	?magnetite, ?tremolite	
4612-292	BGU23-2	46.0	hand specimen		altered green-grey host near green vein	GADDS count 20s 0.8mm sample area (theta - 40-20) 11/09/02				calcite	dolomite?	
4612-293	BGU23-2	46.0	hand specimen		pale-white alteration host	GADDS count 20s 0.8mm sample area (theta - 40-20) 11/09/02				calcite, dolomite		
4612-294	BGU23-2	46.0	hand specimen		grey host	GADDS count 20s 0.8mm sample area (theta - 40-20) 11/09/02				calcite, dolomite		
4612-171	BGU23-2	9.0	hand specimen		centre of dark grey clast (with alteration rims)	GADDS count 25s 0.8mm sample area (theta - 40-20) 06/09/02				dolomite	quartz, kutnorhorite or orthoclase	
4612-172	BGU23-2	9.0	hand specimen		white alteration margin of dark grey clast	GADDS count 25s 0.8mm sample area (theta - 40-20) 06/09/02				dolomite, quartz	calcite, ?magnetite (unable to tell if present)	
4612-173	BGU23-2	9.0	hand specimen		small black pieces (magnetite?) of outer dark halo around clast	GADDS count 25s 0.8mm sample area (theta - 40-20) 06/09/02				dolomite, quartz	calcite, ?magnetite (unable to tell if present)	
4612-174	BGU23-2	9.0	hand specimen		pale matrix fill around clast- minor green?	GADDS count 25s 0.8mm sample area (theta - 40-20) 06/09/02				dolomite		
4612-175	BGU23-2	9.0	hand specimen		white clacite infill (last)	GADDS count 25s 0.8mm sample area (theta - 40-20) 06/09/02				calcite	dolomite	
4612-176	BGU23-2	9.0	hand specimen		clay-white soft infill	GADDS count 25s 0.8mm sample area (theta - 40-20) 06/09/02				anhydrite, calcite	dolomite	
4612-177	BGU23-2	9.0	hand specimen		back of sample - green-white material	GADDS count 25s 0.8mm sample area (theta - 40-20) 06/09/02				calcite, dolomite, brucite		
3752-26	BGU23-5	147.6	powder slide-smear	sk	yellow grts and clay alteration of tremolite	XRD	talc	7A halloysite?		?		
4612-194	BGU23-6	147.1	hand specimen		dark green clast at top	GADDS count 25s 0.8mm sample area (theta - 40-20) 06/09/02				calcite	biotite?	
4612-195	BGU23-6	147.1	hand specimen		dark red? Clast in middle	GADDS count 25s 0.8mm sample area (theta - 40-20) 06/09/02				calcite		
4612-196	BGU23-6	147.1	hand specimen		white alteration matrix material	GADDS count 25s 0.8mm sample area (theta - 40-20) 06/09/02				tremolite/cummingtonite		
4612-210	BGU23-6	105.8	hand specimen		dark green siliceous (host?)	GADDS count 25s 0.8mm sample area (theta - 40-20) 06/09/02				pyroxene, quartz, dolomite		

Appendix 3 - XRD results

AAC Sample#	Drillhole	Depth (m)	Sample material	Lithology	Description of material analysed	Technique	Dominant clay mineral	Other clay mineral	Minor clay minerals	Major minerals present	Minor minerals present	Comments
4612-211	BGU23-6	105.8	hand specimen		vein - anhydrite?	GADDS count 25s 0.8mm sample area (theta - 40-20) 06/09/02				calcite, tremolite, ?dolomite		
4612-212	BGU23-6	105.8	hand specimen		pale green coloured siliceous at top	GADDS count 25s 0.8mm sample area (theta - 40-20) 06/09/02				dolomite, calcite	?tremolite	
4612-213	BGU23-6	105.8	hand specimen		green epidote? Hairline vein	GADDS count 25s 0.8mm sample area (theta - 40-20) 06/09/02				dolomite, calcite	?tremolite	
3752-71	BGU23-6	80.5	hand specimen		darker green (uncut edge) - bad scan	GADDS 12/02/2001, 30sec exposure				diopside - bad scan		
3752-72	BGU23-6	80.5	hand specimen		Darker green cut edge	GADDS 12/02/2001, 30sec exposure				tremolite/amphibole		
4612-187	BGU23-8	144.2	hand specimen		black areas in unaltered limestone - limestone breccia?	GADDS count 25s 0.8mm sample area (theta - 40-20) 06/09/02				calcite		
4612-188	BGU23-8	144.2	hand specimen		pale limestone clasts	GADDS count 25s 0.8mm sample area (theta - 40-20) 06/09/02				calcite, brucite (Mg(OH)2)	? Minor kutnorhorite (Ca-Mn-Fe-MgCo3) and d=3.52 mineral	
4612-144	BGU23-8	87.0	hand specimen		Dark grey limestone	GADDS count 25s 0.8mm sample area (theta - 40-20) 06/09/02				dolomite		Have different peaks (structure?)
4612-145	BGU23-8	87.0	hand specimen		white alterationon edge	GADDS count 25s 0.8mm sample area (theta - 40-20) 06/09/02				dolomite		Have different peaks (structure?)
4612-140	BGU23-8	86.0	hand specimen		grey limestone - host	GADDS count 30s 0.8mm sample area (theta - 40-20) 06/09/02				dolomite	calcite	
4612-141	BGU23-8	86.0	hand specimen		white vein selvedge	GADDS count 20s 0.8mm sample area (theta - 40-20) 06/09/02				tremolite + dolomite	calcite	
4612-142	BGU23-8	86.0	hand specimen		pale green centre vein (1mm) - a bit narrow	GADDS count 30s 0.8mm sample area (theta - 40-20) 06/09/02				calcite	dolomite and tremolite	
4612-143	BGU23-8	86.0	hand specimen		green on back of sample	GADDS count 30s 0.8mm sample area (theta - 40-20) 06/09/02				calcite, dolomite	tremolite	
3752-67	BGU23-8	65.5	hand specimen		white clay (10s)	GADDS 12/02/2001, 10sec exposure				tremolite, talc		
3752-68	BGU23-8	65.5	hand specimen		white crystals in centre (10s)	GADDS 12/02/2001, 10sec exposure				pyrophyllite?		
4612-162	BGU23-8	38.8	hand specimen		grey clast in centre	GADDS count 25s 0.8mm sample area (theta - 40-20) 06/09/02				dolomite		
4612-163	BGU23-8	38.8	hand specimen		green clasts	GADDS count 25s 0.8mm sample area (theta - 40-20) 06/09/02				cummingtonite	calcite	
4612-164	BGU23-8	38.8	hand specimen		white-clear calcite?	GADDS count 25s 0.8mm sample area (theta - 40-20) 06/09/02				calcite		
4612-165	BGU23-8	38.8	hand specimen		pale alteration margin on clast	GADDS count 25s 0.8mm sample area (theta - 40-20) 06/09/02				dolomite	amphibole	
4612-184	BGU23-8	25.5	hand specimen		on back - small grey clast	GADDS count 25s 0.8mm sample area (theta - 40-20) 06/09/02				dolomite		
4612-185	BGU23-8	25.5	hand specimen		yellow alteration on edge of clast	GADDS count 25s 0.8mm sample area (theta - 40-20) 06/09/02				dolomite, calcite		
4612-186	BGU23-8	25.5	hand specimen		pale matrix/infill	GADDS count 25s 0.8mm sample area (theta - 40-20) 06/09/02				calcite, dolomite	Brucite?, pyrite	
4612-207	BGU23-8	10.0	hand specimen		grey limestone	GADDS count 25s 0.8mm sample area (theta - 40-20) 06/09/02				dolomite		
4612-208	BGU23-8	10.0	hand specimen		yellow-white alteration of limestone (associated with sulphides)	GADDS count 25s 0.8mm sample area (theta - 40-20) 06/09/02				dolomite		slightly different peaks
4612-309	BGU24-10	305.0	hand specimen		yellow infill in vein	GADDS count 10s 0.8mm sample area (theta - 40-20) 11/09/02				anhydrite?		
4612-310	BGU24-10	305.0	hand specimen		black sphalerite? In vein	GADDS count 10s 0.8mm sample area (theta - 40-20) 11/09/02				dolomite, pyroxene	sphalerite?	host?? - look at sample
4612-312	BGU24-10	305.0	hand specimen		green host rock	GADDS count 10s 0.8mm sample area (theta - 40-20) 11/09/02				calcite, pyroxene		CHECK sample - is this real???
3752-58	BGU24-11	177.0	hand specimen		grey carbonate 0.5cm from vein	GADDS 12/02/2001, 30sec exposure				talc?, dolomite, ?, minor tremolite		
3752-59	BGU24-11	177.0	hand specimen		white carbonate alteration rim	GADDS 12/02/2001, 30sec exposure				calcite, tremolite	mnr pyrophyllite?	
3752-60	BGU24-11	177.0	hand specimen		pale green zone	GADDS 12/02/2001, 30sec exposure				tremolite, calcite	mnr pyrophyllite?	
3752-61	BGU24-11	177.0	hand specimen		crystaline vein in centre	GADDS 12/02/2001, 30sec exposure				calcite		
3752-28	BGU26-04	298.2	powder slide-smear	?	cy and py vein in skarn	XRD	illite	?		qtz		
3752-27	BGU26-04	215.6	powder slide-smear	sk	cy altered rocks in skarn	XRD	talc	? D=8.4				
4612-356	BGU27-6	349.0	Hand specimen		Brown carbonate after cpy	GADDS				Quartz	dolomite	
4612-357	BGU27-6	349.0	Hand specimen		Brown carbonate after cpy	GADDS				quartz, dolomite	siderite	
4612-265	BGU28-5	267.0	hand specimen		medium green host rock	GADDS count 15s 0.8mm sample area (theta - 40-20) 11/09/02				pyroxene	tremolite? Calcite	
4612-266	BGU28-5	267.0	hand specimen		dark green mottles alteration	GADDS count 15s 0.8mm sample area (theta - 40-20) 11/09/02				pyroxene	calcite	
4612-267	BGU28-5	267.0	hand specimen		dark green infill - chlorite	GADDS count 15s 0.8mm sample area (theta - 40-20) 11/09/02				pyroxene	tremolite	
3752-29	BGU29-07	197.5	powder slide-smear	lmst	lmst with cy	XRD	chlorite	mnr halloysite		qtz, calcite, dolomite, pyrite		
3752-30	BGU29-07	130.0	powder slide-smear	sand	sandy clay	XRD	talc	montmorillonite	halloysite?	quartz, calcite, dolomite		
3752-62	BGU30-4	139.6	hand specimen		Grey material	GADDS 12/02/2001, 30sec exposure				dolomite, magnetite		
3752-63	BGU30-4	139.6	hand specimen		white alteration	GADDS 12/02/2001, 30sec exposure				tremolite	pyrophyllite	
3752-64	BGU30-4	138.9	hand specimen		area above #1	GADDS 12/02/2001, 30sec exposure				anhydrite, quartz, tremolite		
3752-65	BGU30-4	138.9	hand specimen		centre grey area	GADDS 12/02/2001, 30sec exposure				quartz, anhydrite	dolomite	
3752-65a	BGU30-4	138.9	hand specimen		centre grey area (10sec)	GADDS 12/02/2001, 10sec exposure				anhydrite, quartz		
3752-66	BGU30-4	138.9	hand specimen		lower pink area	GADDS 12/02/2001, 30sec exposure				quartz, anhydrite, tremolite		
4612-311	BGU30-5	246.2	hand specimen		white carbonate in vugh	GADDS count 5s 0.8mm sample area (theta - 40-20) 11/09/02				calcite	?anhydrite	

Appendix 3 - XRD results

AAC Sample#	Drillhole	Depth (m)	Sample material	Lithology	Description of material analysed	Technique	Dominant clay mineral	Other clay mineral	Minor clay minerals	Major minerals present	Minor minerals present	Comments
4612-214	BGU7-6	221.2	hand specimen		yellow crystals after sulphides (carbonate)	GADDS count 25s 0.8mm sample area (theta - 40-20) 06/09/02				calcite, tremolite, ?dolomite		
4612-355	BGU7-6	221.2	Hand specimen			GADDS				Calcite and Dolomite		
4612-199	BGU8-7	220.1	hand specimen		pale-white-cream area of hornnfels	GADDS count 25s 0.8mm sample area (theta - 40-20) 06/09/02				orthoclase		
4612-200	BGU8-7	220.1	hand specimen		pink area	GADDS count 25s 0.8mm sample area (theta - 40-20) 06/09/02				orthoclase		
4612-201	BGU8-7	220.1	hand specimen		pale-white-cream area of hornnfels	GADDS count 25s 0.8mm sample area (theta - 40-20) 06/09/02				orthoclase		
4612-202	BGU8-7	220.1	hand specimen		vein - creal crystals and sulphides	GADDS count 25s 0.8mm sample area (theta - 40-20) 06/09/02				orthoclase		
4612-203	BGU8-7	220.1	hand specimen		pink area	GADDS count 25s 0.8mm sample area (theta - 40-20) 06/09/02				orthoclase		
4612-358	DOZ stop 1		Hand specimen		white leached carbonate	GADDS				calcite and dolomite		
4612-089	GRS125	599b	polished thin section		clay and calcite	GADDS count 10s 0.5mm sample area (theta - 40-20) 27/03/02				calcite, quartz, dolomite		
4612-090	GRS125	599b	polished thin section		white carbonate	GADDS count 15s 0.5mm sample area (theta - 40-20) 27/03/02				dolomite, quartz	calcite	
4612-091	GRS125	599b	polished thin section		host	GADDS count 15s 0.5mm sample area (theta - 40-20) 27/03/02				calcite, quartz	dolomite, pyrite	
4612-092	GRS125	599b	polished thin section		calcite	GADDS count 10s 0.5mm sample area (theta - 40-20) 27/03/02				dolomite	quartz, calcite	
4612-093	GRS125	599b	polished thin section		vugh with clay	GADDS count 20s 0.5mm sample area (theta - 40-20) 27/03/02				dolomite, quartz	calcite	
4612-094	GRS125	599b	polished thin section		calcite in vugh	GADDS count 10s 0.5mm sample area (theta - 40-20) 27/03/02				quartz	calcite, dolomite	
4612-095	GRS125	599b	polished thin section		clay	GADDS count 20s 0.5mm sample area (theta - 40-20) 27/03/02				dolomite, quartz, pyrophyllite?, olivine?	calcite	
4612-082	GRS125	599a	polished thin section		paler carbonate	GADDS count 15s 0.5mm sample area (theta - 40-20) 27/03/02				calcite, quartz	dolomite	
4612-083	GRS125	599a	polished thin section		clay and fine grained carbonate	GADDS count 20s 0.5mm sample area (theta - 40-20) 27/03/02				quartz, calcite	dolomite	
4612-084	GRS125	599a	polished thin section		carbonate?	GADDS count 20s 0.5mm sample area (theta - 40-20) 27/03/02				quartz, calcite	dolomite	
4612-085	GRS125	599a	polished thin section		darker carbonate	GADDS count 15s 0.5mm sample area (theta - 40-20) 27/03/02				calcite	quartz, dolomite?	
4612-086	GRS125	599a	polished thin section		clay and calcite	GADDS count 20s 0.5mm sample area (theta - 40-20) 27/03/02				quartz, calcite	dolomite	
4612-087	GRS125	599a	polished thin section		crystals	GADDS count 20s 0.5mm sample area (theta - 40-20) 27/03/02				quartz	calcite	
4612-088	GRS125	599a	polished thin section		coarser calcite	GADDS count 10s 0.5mm sample area (theta - 40-20) 27/03/02				calcite	quartz	
3752-09	GRS125	899.0	powder slide-smear	silica	clay from vughs. Slightly oxidised	XRD	illite	smectite-mica	10A halloysite	quartz, pyrite		
3752-22	GRS125	878.5	powder slide-smear	silica	mnr white cy (mnr fe-ox) in su-rich altered rock.	XRD	illite	7A halloysite		quartz, pyrite		
3752-10	GRS125	878.0	powder slide-smear	silica	white clay from rock	XRD	illite	10A halloysite		quartz, pyrite		
3752-34	GRS125	759.0	powder slide-smear	bx	clay from within pale breccia (with sulphide clasts)	XRD	illite	halloysite -or- sepiolite		pyrite		
4612-138	GRS125	693.6	polished thin section		clay and sulphide	GADDS count 30s 0.5mm sample area (theta - 40-20) 27/03/02				phlogopite/talc?	Brucite?, pyrite	
4612-139	GRS125	693.6	polished thin section		clay	GADDS count 30s 0.5mm sample area (theta - 40-20) 27/03/02				phlogopite/talc?, Brucite		
4612-129	GRS125	653.5	polished thin section		fine grained carbonate	GADDS count 20s 0.5mm sample area (theta - 40-20) 27/03/02				dolomite		
4612-130	GRS125	653.5	polished thin section		medium grained carbonate	GADDS count 15s 0.5mm sample area (theta - 40-20) 27/03/02				dolomite		
4612-131	GRS125	653.5	polished thin section		fine-coarse grained carbonate	GADDS count 15s 0.5mm sample area (theta - 40-20) 27/03/02				dolomite	calcite	
4612-132	GRS125	653.5	polished thin section		fine grained carbonate	GADDS count 15s 0.5mm sample area (theta - 40-20) 27/03/02				dolomite		
4612-133	GRS125	653.5	polished thin section		fine grained carbonate	GADDS count 10s 0.5mm sample area (theta - 40-20) 27/03/02				dolomite		
4612-127	GRS125	632.0	polished thin section		paler clast	GADDS count 20s 0.5mm sample area (theta - 40-20) 27/03/02				quartz		
4612-128	GRS125	632.0	polished thin section		darker matrix	GADDS count 20s 0.5mm sample area (theta - 40-20) 27/03/02				quartz		
3752-17	GRS125	630.0	powder slide-smear	silica	vughy si-rock, white si near vughs - possibly cy present - and black stuff in vughs sampled	XRD	7 and 10A halloysite			quartz, pyrite		halloysite formed in core tray
3752-31	GRS125	629.8	powder slide-smear	silica	gy and white si of vugh - cy present?	XRD	halloysite (rare)?			quartz		
3752-32	GRS125	615.0	powder slide-smear	lmst	cy altered cbt. In fault zone	XRD	illite	halloysite -or- sepiolite				
3752-33	GRS125	611.3	powder slide-smear	silica	si and cbt and cy alt - can see gy si	XRD	illite			quartz		
4612-122	GRS125	610.0	polished thin section		quartz	GADDS count 15s 0.5mm sample area (theta - 40-20) 27/03/02				quartz		
4612-123	GRS125	610.0	polished thin section		quartz	GADDS count 15s 0.5mm sample area (theta - 40-20) 27/03/02				quartz		
4612-124	GRS125	610.0	polished thin section		clay and pyrite	GADDS count 20s 0.5mm sample area (theta - 40-20) 27/03/02				dolomite	kaolinite, pyrite, quartz	
4612-125	GRS125	610.0	polished thin section		clay and pyrite	GADDS count 20s 0.5mm sample area (theta - 40-20) 27/03/02				dolomite	kaolinite, pyrite	
4612-126	GRS125	610.0	polished thin section		fine grained calcite	GADDS count 15s 0.5mm sample area (theta - 40-20) 27/03/02				dolomite	quartz	
4612-117	GRS125	608.6	polished thin section		carbonate?	GADDS count 15s 0.5mm sample area (theta - 40-20) 27/03/02				dolomite	calcite	
4612-118	GRS125	608.6	polished thin section		quartz	GADDS count 15s 0.5mm sample area (theta - 40-20) 27/03/02				quartz		
4612-119	GRS125	608.6	polished thin section		quartz	GADDS count 15s 0.5mm sample area (theta - 40-20) 27/03/02				quartz	dolomite	
4612-120	GRS125	608.6	polished thin section		carbonate clast	GADDS count 15s 0.5mm sample area (theta - 40-20) 27/03/02				dolomite		
4612-121	GRS125	608.6	polished thin section		quartz	GADDS count 15s 0.5mm sample area (theta - 40-20) 27/03/02				quartz	dolomite	

Appendix 3 - XRD results

AAC Sample#	Drillhole	Depth (m)	Sample material	Lithology	Description of material analysed	Technique	Dominant clay mineral	Other clay mineral	Minor clay minerals	Major minerals present	Minor minerals present	Comments
4612-336	GRS125	608.6	Hand specimen		Dark grey alteration and matrix	GADDS				quartz	minor dolomite?	
4612-337	GRS125	608.6	Hand specimen		white clasts	GADDS				dolomite		
4612-108	GRS125	604.0	polished thin section		clay or host	GADDS count 20s 0.5mm sample area (theta - 40-20) 27/03/02				kaolinite/dickite	dolomite, aragonite?	
4612-109	GRS125	604.0	polished thin section		coarse grained carbonate	GADDS count 10s 0.5mm sample area (theta - 40-20) 27/03/02				dolomite	calcite	
4612-110	GRS125	604.0	polished thin section		clay	GADDS count 20s 0.5mm sample area (theta - 40-20) 27/03/02				dolomite, calcite	kaolinite/dickite	
4612-111	GRS125	604.0	polished thin section		carbonate?	GADDS count 10s 0.5mm sample area (theta - 40-20) 27/03/02				dolomite	quartz	
4612-112	GRS125	604.0	polished thin section		host	GADDS count 15s 0.5mm sample area (theta - 40-20) 27/03/02				dolomite, quartz		
4612-105	GRS125	602.7	polished thin section		host	GADDS count 15s 0.5mm sample area (theta - 40-20) 27/03/02				dolomite	calcite	
4612-106	GRS125	602.7	polished thin section		white carbonate	GADDS count 10s 0.5mm sample area (theta - 40-20) 27/03/02				dolomite	quartz	
4612-107	GRS125	602.7	polished thin section		quartz crystals	GADDS count 10s 0.5mm sample area (theta - 40-20) 27/03/02				dolomite, quartz		
4612-103	GRS125	601.4	polished thin section		white carbonate	GADDS count 10s 0.5mm sample area (theta - 40-20) 27/03/02				dolomite	quartz	
4612-104	GRS125	601.4	polished thin section		host	GADDS count 15s 0.5mm sample area (theta - 40-20) 27/03/02				dolomite	trace quartz	
4612-113	GRS125	601.0	polished thin section		calcite crystals	GADDS count 15s 0.5mm sample area (theta - 40-20) 27/03/02				dolomite	calcite	
4612-114	GRS125	601.0	polished thin section		calcite crystals	GADDS count 10s 0.5mm sample area (theta - 40-20) 27/03/02				dolomite	calcite	
4612-115	GRS125	601.0	polished thin section		brown-white carbonate	GADDS count 10s 0.5mm sample area (theta - 40-20) 27/03/02				dolomite		
4612-116	GRS125	601.0	polished thin section		host	GADDS count 15s 0.5mm sample area (theta - 40-20) 27/03/02				dolomite	calcite	
3752-16	GRS125	600.5	powder slide-smear	silica	vughy si-rock, white si near vughs - possibly cy present - sampled	XRD	7A halloysite			dolomite, quartz		halloysite formed in core tray
4612-096	GRS125	600.0	polished thin section		fine grained carbonate alteration halo	GADDS count 15s 0.5mm sample area (theta - 40-20) 27/03/02				dolomite	calcite, quartz	
4612-097	GRS125	600.0	polished thin section		infill and sulphide?	GADDS count 15s 0.5mm sample area (theta - 40-20) 27/03/02				dolomite	calcite, quartz	
4612-098	GRS125	600.0	polished thin section		fine grained clast	GADDS count 15s 0.5mm sample area (theta - 40-20) 27/03/02				dolomite	calcite, quartz	
4612-099	GRS125	600.0	polished thin section		fine grained clast	GADDS count 15s 0.5mm sample area (theta - 40-20) 27/03/02				dolomite	calcite, quartz	
4612-100	GRS125	600.0	polished thin section		crystals	GADDS count 10s 0.5mm sample area (theta - 40-20) 27/03/02				dolomite	calcite	
4612-101	GRS125	600.0	polished thin section		coarse grained carbonate	GADDS count 30s 0.5mm sample area (theta - 40-20) 27/03/02				dolomite		
4612-102	GRS125	600.0	polished thin section		dirtier limesone	GADDS count 10s 0.5mm sample area (theta - 40-20) 27/03/02				dolomite	calcite, quartz	
4612-072	GRS125	595.6	polished thin section		quartz?	GADDS count 10s 0.5mm sample area (theta - 40-20) 27/03/02				quartz		
4612-073	GRS125	595.6	polished thin section		quartz?	GADDS count 5s 0.5mm sample area (theta - 40-20) 27/03/02				quartz		
4612-074	GRS125	595.6	polished thin section		calcite	GADDS count 10s 0.5mm sample area (theta - 40-20) 27/03/02				dolomite		
4612-075	GRS125	595.6	polished thin section		host	GADDS count 10s 0.5mm sample area (theta - 40-20) 27/03/02				dolomite		
4612-076	GRS125	595.6	polished thin section		clearer	GADDS count 10s 0.5mm sample area (theta - 40-20) 27/03/02				dolomite		
4612-077	GRS125	595.6	polished thin section		darker area - fine grained quartz?	GADDS count 15s 0.5mm sample area (theta - 40-20) 27/03/02				quartz		
4612-078	GRS125	595.6	polished thin section		brown host	GADDS count 15s 0.5mm sample area (theta - 40-20) 27/03/02				dolomite	calcite	
4612-079	GRS125	595.6	polished thin section		host?	GADDS count 15s 0.5mm sample area (theta - 40-20) 27/03/02				dolomite	calcite	
4612-080	GRS125	595.6	polished thin section		host and minor white	GADDS count 10s 0.5mm sample area (theta - 40-20) 27/03/02				dolomite		
4612-081	GRS125	595.6	polished thin section		quartz	GADDS count 10s 0.5mm sample area (theta - 40-20) 27/03/02				quartz		
4612-346	GRS125	595.6	Hand specimen		brown area in altered carbonate	GADDS				quartz		
4612-347	GRS125	595.6	Hand specimen		pale white area in altered carbonate	GADDS				dolomite		
4612-348	GRS125	595.6	Hand specimen		white vein in pale carbonate	GADDS				dolomite		
4612-066	GRS125	590.7	polished thin section		coarse grained fossils	GADDS count 25s 0.5mm sample area (theta - 25-12) 27/03/02				calcite	dolomite?	
4612-067	GRS125	590.7	polished thin section		more fine grained - looks like a fossil	GADDS count 25s 0.5mm sample area (theta - 25-12) 27/03/02				calcite	dolomite	
4612-068	GRS125	590.7	polished thin section		coarse grained zone	GADDS count 25s 0.5mm sample area (theta - 25-12) 27/03/02				dolomite	calcite	
4612-069	GRS125	590.7	polished thin section		fine grained zone	GADDS count 20s 0.5mm sample area (theta - 25-12) 27/03/02				calcite	dolomite	
4612-070	GRS125	590.7	polished thin section		quartz in carbonate	GADDS count 15s 0.5mm sample area (theta - 25-12) 27/03/02				dolomite	calcite	
4612-071	GRS125	590.7	polished thin section		fine grained carbonate	GADDS count 15s 0.5mm sample area (theta - 25-12) 27/03/02				dolomite	calcite	
4612-338	GRS125	590.7	Hand specimen		carbonate host rock	GADDS				Mg-rich calcite		
4612-134	GRS127	887.2	polished thin section		fine grained carbonate	GADDS count 10s 0.5mm sample area (theta - 40-20) 27/03/02				dolomite		
4612-135	GRS127	887.2	polished thin section		white edges	GADDS count 20s 0.5mm sample area (theta - 40-20) 27/03/02				dolomite	quartz, calcite	
4612-136	GRS127	887.2	polished thin section		fine grained carbonate	GADDS count 15s 0.5mm sample area (theta - 40-20) 27/03/02				dolomite		
4612-137	GRS127	887.2	polished thin section		calcite in vein	GADDS count 15s 0.5mm sample area (theta - 40-20) 27/03/02				quartz	dolomite	
3752-37	GRS127	711.0	powder slide-smear	lmst	last lmst before si-alt - very bleached	XRD				dolomite		
3752-36	GRS127	660.9	powder slide-smear	lmst	brocken/fx fg lmst. White, black and feox on fx	XRD	illite?	vermiculite?		calcite, quartz, dolomite		
3752-35	GRS127	655.9	powder slide-smear	lmst	fg pale gy lmst, mod bleaching, small black specs (slst?)	XRD	kaolinite			calcite, quartz, dolomite		
3752-39	P3850-28	48.7	powder slide-smear	clay	Analysis of white banded clay documented by Kavileris (1994)	XRD,GLY,H400	10A halloysite	chlorite				
4612-226	VZW53	330.0	hand specimen		grey-white from top left of sample	GADDS count 25s 0.8mm sample area (theta - 40-20) 11/09/02				dolomite, calcite		

Appendix 3 - XRD results

AAC Sample#	Drillhole	Depth (m)	Sample material	Lithology	Description of material analysed	Technique	Dominant clay mineral	Other clay mineral	Minor clay minerals	Major minerals present	Minor minerals present	Comments
4612-227	VZW53	330.0	hand specimen		dark grey veinlets within grey-white	GADDS count 25s 0.8mm sample area (theta - 40-20) 11/09/02				dolomite, calcite		
4612-228	VZW53	330.0	hand specimen		pale yellow fine veinlets and lateration	GADDS count 25s 0.8mm sample area (theta - 40-20) 11/09/02				dolomite, calcite		
4612-229	VZW53	330.0	hand specimen		brown-grey near yellow	GADDS count 25s 0.8mm sample area (theta - 40-20) 11/09/02				dolomite, calcite		
4612-238	VZW53	282.0	hand specimen		white marble	GADDS count 25s 0.8mm sample area (theta - 40-20) 11/09/02				calcite		
4612-239	VZW53	282.0	hand specimen		grey limestone	GADDS count 25s 0.8mm sample area (theta - 40-20) 11/09/02				calcite		
4612-240	VZW53	282.0	hand specimen		black limestone	GADDS count 25s 0.8mm sample area (theta - 40-20) 11/09/02				calcite		
4612-232	VZW53	281.5	hand specimen		white marble vein in centre	GADDS count 25s 0.8mm sample area (theta - 40-20) 11/09/02				calcite		
4612-233	VZW53	281.5	hand specimen		dark black areas within mottled host limestone	GADDS count 25s 0.8mm sample area (theta - 40-20) 11/09/02				calcite		
4612-234	VZW53	281.5	hand specimen		brown-clear in host area	GADDS count 25s 0.8mm sample area (theta - 40-20) 11/09/02				calcite		
4612-230	VZW53	279.5	hand specimen		white marble at edge	GADDS count 25s 0.8mm sample area (theta - 40-20) 11/09/02				calcite		
4612-231	VZW53	279.5	hand specimen		black-grey mottles 2cm inwards	GADDS count 25s 0.8mm sample area (theta - 40-20) 11/09/02				calcite		
4612-235	VZW53	277.7	hand specimen		white marble - large zone	GADDS count 25s 0.8mm sample area (theta - 40-20) 11/09/02				calcite		
4612-236	VZW53	277.7	hand specimen		brown veinlets in marble	GADDS count 25s 0.8mm sample area (theta - 40-20) 11/09/02				calcite	garnet, ___?	
4612-237	VZW53	277.7	hand specimen		brown alteratered marble	GADDS count 25s 0.8mm sample area (theta - 40-20) 11/09/02				calcite	garnet	
4612-243	VZW53	192.0	hand specimen		uncut sample white	GADDS count 25s 0.8mm sample area (theta - 40-20) 11/09/02				calcite		
4612-244	VZW53	192.0	hand specimen		pale grey	GADDS count 25s 0.8mm sample area (theta - 40-20) 11/09/02				calcite		
4612-241	VZW53	188.0	hand specimen		dark grey limestone	GADDS count 25s 0.8mm sample area (theta - 40-20) 11/09/02				calcite		different peaks emphasised
4612-242	VZW53	188.0	hand specimen		white marble alteration on fractures	GADDS count 25s 0.8mm sample area (theta - 40-20) 11/09/02				calcite		
4612-245	VZW53	173.0	hand specimen		marble - coarse grained	GADDS count 25s 0.8mm sample area (theta - 40-20) 11/09/02				calcite		different peaks emphasised
X	WAN4-3	138.1	powder slide-smear		skarn	XRD,GLY,H400,H500	no clay					
X	WAN4-3	130.5	powder slide-smear		leached skarn	XRD,GLY,H400,H500	smectite, halloysite		vermiculite			
X	WAN4-5	171.0	powder slide-smear		clay altered dyke	XRD,GLY,H400,H500						
X	WAN4-5	174.0	powder slide-smear		intrusive dyke	XRD,GLY,H400,H500	7A halloysite					
3752-21	WGR12	369.5	powder slide-smear	Limestone Breccia	black on fracture and white alteration of limestone	XRD,GLY,H400			10A halloysite, illite-smectite mixed layer	calcite, dolomite		(3m assay interval = 1.88g/t Au).
3752-18	WGR12	367.0	powder slide-smear	Limestone	leached carbonate rock, friable material from leached zones	XRD,GLY,H400				calcite		
4612-327	WGR12	302.2	powder slide-smear	Limestone Breccia	Black carbonaceous on fractures	XRD,GLY,H400,H500	smectite-mica		kaolinite			(3m assay interval = 1.4g/t Au).
4612-335	WGR12	294.6	powder slide-smear	Limestone Breccia	Clay-black breccia matrix	XRD,GLY,H400,H500	smectite-mica	7A halloysite		quartz, pyrite		(3m assay interval = 5.7g/t Au).
4612-332	WGR12	177.0	powder slide-smear	Limestone Breccia	Clay-black breccia matrix	XRD,GLY,H400,H500	smectite-chlorite	7A halloysite	kaolinite	quartz, pyrite		(3m assay interval = 4.02g/t Au).
4612-334	WGR12	174.3	powder slide-smear	Limestone Breccia	Clay-black breccia matrix	XRD,GLY,H400,H500	smectite-chlorite	kaolinite	7A halloysite	quartz, pyrite		(3m assay interval = 3.08g/t Au).
4612-333	WGR12	173.0	powder slide-smear	Limestone Breccia	Clay-black breccia matrix	XRD,GLY,H400,H500	smectite-chlorite		kaolinite	quartz, pyrite, muscovite		(3m assay interval = 2.84g/t Au).
4612-328	WGR12	168.6	powder slide-smear	Limestone Breccia	Clay-black breccia matrix	XRD,GLY,H400,H500	smectite-chlorite	vermiculite	7A halloysite			(3m assay interval = 5.34g/t Au).
3752-06	WGR12	43.3	powder slide-smear	clay	white clay - no texture	XRD,GLY,H400	7A halloysite		10A halloysite, ?smectite			14A area disordered and difficult to identify
3752-07	WGR12	43.3	powder slide-smear	Sulphide in clay	Hairline brown vein within unidentified clay host rock.	XRD,GLY,H400	7A halloysite		10A halloysite, chlorite	pyrite		
3752-01	WGR12	37.0	powder slide-smear	opaline	opaque green-grey material	XRD,GLY,H400,H500	7A halloysite					
3752-44	WGR12	30.0	powder slide-smear	opaline	opaque green-grey material	XRD,GLY,H400	10A halloysite	vermiculite		Jarosite		
4612-329	WGR3	15.2	powder slide-smear	Limestone Breccia	Clay-black breccia matrix	XRD,GLY,H400,H500	vermiculite	kaolinite		pyrite, quartz, calcite	?4.42 peak	(3m assay interval = 0.37g/t Au).
3752-08	WGZ8	387.5	powder slide-smear	Limestone Breccia	White clay and minor pyrite fracture fill in dark grey limestone	XRD	illite			calcite, pyrite		(3m assay interval = 0.18g/t Au).
3752-04	WGZ8	370.0	powder slide-smear	Limestone Breccia	Clay and pyrite bearing matrix from limestone breccia. Breccia is fine grained with matrix supported rounded fragments of black, limestone (unclear if also igneous).	XRD,GLY,H400,H500			10A halloysite, disordered smectite?	quartz, calcite, K-feldspar, pyrite		(3m assay interval = 0.8g/t Au).
3752-19	WGZ8	316.0	powder slide-smear	Limestone Breccia	black gangue	XRD,GLY,H400	vermiculite/smectite	7A halloysite	chlorite	calcite, quartz	pyrite	14A area disordered and difficult to identify. (3m assay interval = 3.73g/t Au).
3752-05	WGZ8	307.0	powder slide-smear	Limestone Breccia	black clay-rich rock - slickenside material	XRD,GLY,H400,H500	smectite			pyrite, quartz, calcite		(3m assay interval = 0.05g/t Au).

Appendix 3 - XRD results

AAC Sample#	Drillhole	Depth (m)	Sample material	Lithology	Description of material analysed	Technique	Dominant clay mineral	Other clay mineral	Minor clay minerals	Major minerals present	Minor minerals present	Comments
4612-319	WGZ8	166.0	powder slide-smear	Limestone Breccia	black-vitreous clay on fracture	XRD,GLY,H400,H500	vermiculite	10A halloysite				(3m assay interval = .28g/t Au).
3752-48	WGZ8	118.0	Insitu	Yellow-white infill	White clay with yellow crystals	GADDS	10A halloysite		allophane?			
3752-49	WGZ8	118.0	Insitu	Yellow-white infill	yellow crystal: hardly any xrd trace	GADDS	allophane?					
3752-12	WGZ8	117.0	powder slide-smear	Banded clay	black-grey and white clay band	XRD,GLY,H400	10A halloysite		7A halloysite			
3752-13	WGZ8	117.0	powder slide-smear	Banded clay	white clay band	XRD,GLY,H400	10A halloysite		7A halloysite			
3752-52	WGZ8	95.0	Insitu	Yellow-white infill	patch of yellow-white crystals: hardly any trace	GADDS	10A halloysite					
3752-45	WGZ8	94.0	powder slide-smear	Yellow-white infill	Yellow crystals	XRD,GLY,H400	vermiculite/smectite		7 and 10A halloysite			Disordered and difficult to identify
3752-46	WGZ8	94.0	powder slide-smear	Yellow-white infill	White clay with yellow crystals	XRD,GLY,H400	vermiculite/smectite	10A halloysite	allophane, alunite			Disordered and difficult to identify
3752-47	WGZ8	94.0	powder slide-smear	opaline	opaline material	XRD,GLY,H400	10A halloysite					
3752-02	WGZ8	92.5	powder slide-smear	Sulphide in clay	disseminated pyrite and white clay in white clay host	XRD,GLY,H400,H500	illite	10A halloysite	chlorite/vermiculite/smectite	pyrite		14A area disordered and difficult to identify
3752-03	WGZ8	92.5	powder slide-smear	clay	white and grey clay (not-banded)	XRD,GLY,H400,H500	disordered smectite	7A halloysite	illite			14A area disordered and difficult to identify
3752-43	WGZ8	90.0	powder slide-smear	Banded clay	White bleached - banded clay	XRD,GLY,H400	10A halloysite					
3752-56	WGZ8	79.1	Insitu	Yellow-white infill	Yellow crystals and minor white clay: hardly any trace	GADDS	10A halloysite	allophane?				
3752-56b	WGZ8	79.1	Insitu	Yellow-white infill	Yellow crystals and minor white clay: hardly any trace	GADDS	allophane?					
3752-57	WGZ8	77.0	Insitu	Sulphide	Black hairline veinlets in bleached white clay rock	GADDS				pyrite, ?sphalerite?	galena	Sphalerite peaks overlap with pyrite. Unclear if present. (3m assay interval = 2.34g/t Au).
3752-57b	WGZ8	77.0	Insitu	Sulphide	Black hairline veinlets in bleached white clay rock	GADDS				sphalerite	galena, chalcopyrite	(3m assay interval = 2.34g/t Au).
3752-57c	WGZ8	77.0	Insitu	Sulphide	Black hairline veinlets in bleached white clay rock	GADDS				pyrite, ?sphalerite?	galena	Sphalerite peaks overlap with pyrite. Unclear if present. (3m assay interval = 2.34g/t Au).
3752-20	WGZ8	76.6	powder slide-smear	clay	Grey and black and white mottled clay (not banded)	XRD,GLY,H400			10A halloysite, 7A halloysite	galena, pyrite, woodhouseite		Example of grey colouration due to sulphides. (3m assay interval = 2.34g/t Au).
3752-14	WGZ8	69.5	powder slide-smear	opaline	grey translucent material	XRD,GLY,H400	7A halloysite	illite				
3752-15	WGZ8	69.5	powder slide-smear	clay	white clay - no texture	XRD,GLY,H400	7A halloysite					
3752-54	WGZ8	64.0	Insitu	Sulphide fragment	sphalerite fragment in gritty breccia. Calcite present with fragment	GADDS	10A halloysite			sphalerite, pyrite, chalcopyrite	galena	Sphalerite peaks overlap with pyrite. Unclear if present
3752-40	WGZ8	63.2	powder slide-smear	Yellow-white infill	Yellow-white in fracture network (displacing sulphides)	XRD,GLY,H400	10A halloysite		disordered smectite/vermiculite	pyrite, woodhouseite		Disordered and difficult to identify
3752-41	WGZ8	48.0	powder slide-smear	Dalam Diatreme	Intrusive breccia - white clay	XRD,GLY,H400	10A halloysite		illite, 7A halloysite	K-feldspar		
3752-50	WGZ8	48.0	Insitu	Dalam Diatreme	Intrusive breccia - white clay	GADDS	*10A halloysite OR illite					
3752-51	WGZ8	48.0	Insitu	Dalam Diatreme	Intrusive breccia - white clay	GADDS	*10A halloysite OR illite			K-feldspar		
3752-42	WGZ8	39.0	powder slide-smear	Dalam Diatreme	Intrusive breccia - white clay	XRD,GLY,H400	illite		vermiculite	quartz, K-feldspar		
4612-323	Tuff		powder slide-smear	Tuffaceous outcrop sample	banded clay area of volcanic sample	XRD,GLY,H400,H500	illite		chlorite	K-feldspar, quartz	plagioclase	Outcrop
4612-325	Tuff		powder slide-smear	Tuffaceous outcrop sample	vfg non-banded fragmental part of volcanic sample	XRD,GLY,H400,H500	illite		chlorite	K-feldspar, quartz	plagioclase	Outcrop

Appendix 4

Reassay sample descriptions and results

West Grasberg Re-assay Sample Descriptions

Hole	Depth (m)	Sample Number	Freeport Assay Number	Description	Code For Graphs
WGR13	118.5	WGR13-118.5	174464	Oxidised Dalam. Vughy breccia with fresh sulphides in voids and red and orange iron-oxide staining	Clay - Dalam contact
WGR3	26.5	WGR3-26.5	174468	Oxidised Dalam. Iron oxides and white sulphates (after sulphides?). Swelling clay with rare breccia fragments preserved.	Dalam - oxidised
WGR13	32.0	WGR13-32	174459	Oxidised Dalam. Spotty sulphides with associated black material (oxidised) in clay-dominated rock.	Dalam - oxidised
WGZ8	35.0	WGZ8-35	174474	Oxidised Dalam. Grey clay with sulphide spots	Dalam - oxidised
WGR13	48.0	WGR13-48	174460	Oxidised Dalam. Spotty sulphides and vughs in clay rock	Dalam - oxidised
WGR13	52.0	WGR13-52	174461	black sooty veins and pyrite in yellow (iron-oxides) and grey rock	Dalam - oxidised
WGR13	57.7	WGR13-57.7	174462	Oxidised Dalam. Yellow stained clay-rich rock with dark sulphide spots/veins (looks vughy)	Dalam - oxidised
WGR13	60.0	WGR13-60	174463	Oxidised Dalam. Yellow stained clay-rich rock with dark sulphide spots/veins (looks vughy)	Dalam - oxidised
WGZ8	60.0	WGZ8-60	174475	Dalam. Clay with minor sulphide spots. Sulphates present	Dalam
WGZ8	30.5	WGZ8-30.5	174471	Dalam. Clay-rich with sulphide spots	Dalam
WGZ8	23.0	WGZ8-23	174470	Dalam. Clay-rich with sulphide spots	Dalam
WGZ8	33.5	WGZ8-33.5	174473	Dalam. White clay with vughs/spots containing pyriterite then black-grey mineral (hematite?). Sulphides appear to be replacing clasts as spots	Dalam
WGZ8	31.5	WGZ8-31.5	174472	Dalam. Clay-rich with sulphide spots	Dalam
WGZ8	61.0	WGZ8-61	174476	Dalam. Clay-rich with minor sulphide spots	Dalam
WGZ8	63.5	WGZ8-63.5	174477	Dalam. Clay-rich with sulphide spots - abundant chalcopyriterite	Dalam
WGZ8	148.3	WGZ8-148.3	174479	Limestone breccia with black (carbonaceous) matrix and marble clasts	Limestone breccia
WGR12	169.7	WGR12-169.7	174456	Fractured and brecciated limestone rock with black (carbonaceous?) matrix	Limestone breccia
WGR12	367.0	WGR12-367	174458	pale limestone with black (carbonaceous?) material in fractures with minor white clay? Appears very leached	Limestone breccia
WGZ8	387.5	WGZ8-387.5	174482	Brecciated limestone with bleached white soft clasts. Dark to grey matrix	Limestone breccia
WGZ8	392.0	WGZ8-392	174481	limestone breccia with (carbonaceous?) black-grey matrix and sulphides	Limestone breccia
WGR3	15.2	WGR3-15.2	174467	Oxidised black (carbonaceous?) material in limestone breccia	Limestone breccia - oxidised
WGZ8	210.0	WGZ8-210	174480	limestone breccia with balck (carbonaceous?) matrix and minor iron-oxide after sulphides?	Limestone breccia - oxidised
WGR3	54.0	WGR3-54	174469	oxidised balck (carbonaceous?) material in limestone breccia	Limestone breccia - oxidised
WGZ8	126.0	WGZ8-126	174478	limestone breccia with oxidised matrix	Limestone breccia - oxidised
WGR12	170.5	WGR12-170.5	174457	dark brown (altered?) limestone with hairline calcite fractures	Limestone breccia - oxidised
WGR13	143.0	WGR13-143	174465	marble with breccia (skarn alteration and infill in matrix) and abundant disseminated sulphides	Marble breccia and skarn
WGR13	151.7	WGR13-151.7	174466	marble with veins of skarn (green and cream) with sulphides	Marble breccia and skarn
WGZ8	87-105	WGZ8-87-105	Brannon (1991)	Clay	Clay
WGR4	60-102	WGR4-60-102	Brannon (1991)	Clay	Clay
WGZ10	72-102	WGZ10-72-102	Brannon (1991)	Clay	Clay
WGZ8	309-345	WGZ8-309-345	Brannon (1991)	Limestone	limestone
WGR3	159-177	WGR3-159-177	Brannon (1991)	Limestone	limestone
WGR3	222-279	WGR3-222-279	Brannon (1991)	Limestone	limestone

Assays from West Grasberg Samples (Lab: Sucofindo)

	Assay Units:	ppm	ppm	ppm	ppm	ppm	ppm	ppm	ppm	ppm	ppm	ppm	ppm	ppm	ppm
	Detection Limit:	**0.01**	**5**	**0.5**	**5**	**5**	**1**	**1**	**5**	**2**	**1**	**0.1**	**0.5**	**0.2**	**5**
	Assay Method:	**1031**	**1001**	**1001**	**1001**	**1001**	**1040**	**1001**	**1001**	**1001**	**1040**	**1001**	**1040**	**1040**	**1001**
	Element:	**Au**	**Cu**	**Ag**	**Pb**	**Zn**	**Se**	**Co**	**Ni**	**Mo**	**As**	**Sb**	**Bi**	**Te**	**V**
Drillhole - depth /interval	**Freeport Sample Number /Source**														
WGR12-169.7	174456	1.12	50	0.7	18	36	1.96	6	21	-2	40	0.5	0.9	1	54
WGR12-170.5	174457	3.03	41	1.1	20	35	1.05	1	10	-2	29	0.4	0.6	1	54
WGR12-367	174458	0.43	32	1.2	64	162	6.27	-1	7	-2	20	0.8	0.6	1	38
WGR13-32	174459	0.20	5067	-0.5	67	58	1.52	7	-5	8	-1	0.7	0.9	-0.2	100
WGR13-48	174460	0.03	325	1.0	87	195	10.6	22	15	-2	1	2.3	1.8	-0.2	85
WGR13-52	174461	0.03	342	1.3	36	269	57.6	108	31	-2	3	0.8	0.8	-0.2	154
WGR13-57.7	174462	0.12	1400	1.4	58	131	10.2	24	10	-2	2	6.3	2.8	1	108
WGR13-60	174463	0.07	3618	1.3	60	123	4.7	29	9	-2	2	1.1	2.2	-0.2	77
WGR13-118.5	174464	0.25	1827	1.7	25	158	24.3	15	32	-2	98	1.0	29.7	1	169
WGR13-143	174465	0.37	112	7.2	734	3000	40.5	21	131	4	981	2.6	56.5	-0.2	569
WGR13-151.7	174466	0.13	147	1.7	55	648	22.1	7	21	-2	12	0.5	10.4	-0.2	69
WGR3-15.2	174467	0.23	590	1.0	958	878	10.08	18	8	4	264	7.7	5.6	1	100
WGR3-26.5	174468	0.25	279	1.1	425	638	8.94	17	21	4	292	8.7	2.8	1	169
WGR3-54	174469	1.35	32	0.8	16	100	2.7	7	12	-2	26	1.7	1.1	1	46
WGZ8-23	174470	0.17	649	0.8	12	93	9.16	19	5	-2	4	0.5	5.4	-0.2	54
WGZ8-30.5	174471	0.13	643	0.9	19	140	6.13	17	-5	2	5	1.1	4.1	-0.2	108
WGZ8-31.5	174472	0.13	833	0.9	14	58	9.72	45	5	2	3	0.4	2.4	-0.2	108
WGZ8-33.5	174473	0.13	1062	1.4	55	311	9.14	22	-5	-2	76	4.1	13.7	-0.2	92
WGZ8-35	174474	0.08	319	1.1	52	112	5.45	10	-5	2	4	1.7	1.2	-0.2	69
WGZ8-60	174475	1.38	890	3.6	239	608	615	32	36	4	293	8.3	54.4	-0.2	215
WGZ8-61	174476	0.80	413	2.6	159	2514	670	52	56	4	420	21.0	80.6	-0.2	331
WGZ8-63.5	174477	0.42	725	4.5	362	1803	625	28	13	2	741	24.7	107.2	-0.2	85
WGZ8-126	174478	0.07	238	4.0	1100	753	330	25	7	4	356	4.8	12.2	-0.2	85
WGZ8-148.3	174479	0.15	42	1.9	475	470	3.33	1	9	2	60	5.3	-0.5	-0.2	54
WGZ8-210	174480	5.13	254	7.3	1121	453	2.13	6	20	2	184	16.1	19.1	-0.2	115
WGZ8-392	174481	0.15	247	2.0	172	370	2.16	6	6	4	21	9.6	1.6	-0.2	52
WGZ8-387.5	174482	0.33	443	1.5	188	226	8.3	19	6	4	385	15.4	2.9	-0.2	85
WGZ8-87-105	(Brannon, 1991)	0.63	1430	11	1009	4487					118	10			
WGR4-60-102	(Brannon, 1991)	5.1	3065	3	1530	3639									
WGZ10-72-102	(Brannon, 1991)	1.42	528	96											
WGZ8-309-345	(Brannon, 1991)	1.57	141	4	35	15					11				
WGR3-159-177	(Brannon, 1991)	4.81	13			15									
WGR3-222-279	(Brannon, 1991)	2.42	36	2	230	160									

Appendix 5

Microprobe results (this study) carbonate, gold, sphalerite

Appendix 5 - Carbonate Microprobe

Sample	AAC-ID	Comments	FeO (wt%)	MnO (wt%)	MgO (wt%)	CaO (wt%)	Total	FeO +/-2 SIGMA	MnO +/-2 SIGMA	MgO +/-2 SIGMA	CaO +/-2 SIGMA	Fe (2 oxygens)	Mn (2 oxygens)	Mg (2 oxygens)	Ca (2 oxygens)	TOTAL (2 oxygens)	Fe m/M	Mn m/M	Mg m/M	Ca m/M	total m/M	Fe mol%	Mn mol%	Ca mol%	Mg mol%	wt% CO2 equ.	analysis total
BGU21-10-12	bg21-10-12-01	centre of clast	0	0.23	22.69	30.57	53.48	0	0.24	0.73	0.59	0.000	0.006	1.013	0.981	2	0.000	0.004	0.563	0.545	1.11	0.00	0.34	49.03	50.63	48.93	102.41
BGU21-10-12	bg21-10-12-02	clast - closer to edge	0	0.15	22.62	30.7	53.47	0	0.23	0.74	0.6	0.000	0.004	1.010	0.986	2	0.000	0.002	0.561	0.547	1.11	0.00	0.22	49.27	50.51	48.90	102.37
BGU21-10-12	bg21-10-12-03	Alteration margin - analysis of pale veinlets in dark	6.21	11.09	9.92	26.15	53.36	0.61	0.6	0.57	0.55	0.181	0.327	0.515	0.976	2	0.086	0.182	0.246	0.466	0.98	8.81	18.55	47.54	25.09	43.17	96.53
BGU21-10-12	bg21-10-12-05	Alteration margin - analysis of pale veinlets in dark	6.7	10.14	9.76	26.91	53.51	0.63	0.57	0.57	0.56	0.195	0.298	0.505	1.002	2	0.093	0.166	0.242	0.480	0.98	9.50	16.95	48.88	24.67	43.20	96.71
BGU21-10-12	bg21-10-12-06	infill crystals on margin of clast	28.95	20.15	7.11	1.23	57.44	1.07	0.75	0.54	0.2	0.910	0.642	0.398	0.050	2	0.403	0.331	0.176	0.022	0.93	43.24	35.48	2.35	18.93	41.02	98.46
BGU21-10-12	bg21-10-12-07	infill crystals on margin of clast	27.56	19.89	6.94	1.78	56.17	1.08	0.75	0.54	0.21	0.884	0.646	0.396	0.073	2	0.384	0.326	0.172	0.032	0.91	41.97	35.71	3.47	18.84	40.22	96.39
BGU21-10-12	bg21-10-12-08	dirty brown carbonate matrix?	27.58	25	2.84	1.3	56.71	1.06	0.83	0.46	0.2	0.925	0.849	0.170	0.056	2	0.384	0.410	0.070	0.023	0.89	43.24	46.21	2.61	7.94	39.07	95.78
BGU21-10-12	bg21-10-12-09	dirty brown carbonate matrix?	33.09	17.29	4.35	2.6	57.34	1.13	0.7	0.49	0.23	1.073	0.568	0.252	0.108	2	0.461	0.284	0.108	0.046	0.90	51.25	31.58	5.16	12.01	39.55	96.89
BGU21-10-12	bg21-10-12-10	dirty brown carbonate matrix?	23.9	26.13	5.12	1.39	56.54	1.01	0.84	0.5	0.2	0.780	0.864	0.298	0.058	2	0.333	0.429	0.127	0.025	0.91	36.42	46.95	2.71	13.91	40.19	96.73
BGU21-10-12	bg21-10-12-12	carbonate that hosts pyrite and apy	6.82	15.93	6.92	25.38	55.05	0.63	0.68	0.51	0.54	0.201	0.476	0.364	0.959	2	0.095	0.261	0.172	0.453	0.98	9.68	26.66	46.15	17.51	43.16	98.21
BGU24-11-177	bg24-11-177-01	carbonate host	0.39	0.12	22.59	29.67	52.79	0.29	0.23	0.74	0.59	0.010	0.003	1.022	0.965	2	0.005	0.002	0.560	0.529	1.10	0.49	0.18	48.23	51.09	48.28	101.07
BGU24-11-177	bg24-11-177-02	carbonate host closer to vein	0.12	0	23.07	29.83	53.03	0.28	0.19	0.74	0.59	0.003	0.000	1.035	0.962	2	0.002	0.000	0.572	0.532	1.11	0.15	0.00	48.10	51.75	48.68	101.71
BGU24-11-177	bg24-11-177-04	carbonate within alteration zone	0.21	0.11	4.03	49.09	53.43	0.33	0.27	0.45	0.75	0.006	0.003	0.204	1.787	2	0.003	0.002	0.100	0.875	0.98	0.30	0.18	89.32	10.20	43.13	96.56
BGU24-11-177	bg24-11-177-05	pale carbonate within alteration zone	0.21	0.33	1.33	54.28	56.16	0.31	0.26	0.39	0.79	0.006	0.009	0.066	1.919	2	0.003	0.005	0.033	0.968	1.01	0.29	0.54	95.90	3.27	44.42	100.58
BGU24-11-177	bg24-11-177-08	carbonate adjacent to dark fibrous blades (#07) in vein zone	0	0.23	0.51	56.15	56.89	0	0.28	0.35	0.8	0.000	0.006	0.025	1.969	2	0.000	0.004	0.013	1.001	1.02	0.00	0.37	98.39	1.24	44.79	101.68
BGU24-11-177	bg24-11-177-09	carbonate infill crystals in vein zne	0.21	0.08	1.28	56.11	57.68	0.33	0.26	0.36	0.8	0.006	0.002	0.061	1.931	2	0.003	0.001	0.032	1.001	1.04	0.28	0.13	96.53	3.06	45.62	103.30
BGU24-11-177	bg24-11-177-12	coarse carbonate crystal with FI	0.19	0.13	1.1	56.35	57.77	0.31	0.27	0.35	0.8	0.005	0.004	0.053	1.939	2	0.003	0.002	0.027	1.005	1.04	0.26	0.21	96.91	2.63	45.63	103.40
DOZ-B1-D	dzb1-01	clear infill crystals	0.72	0.42	0.97	54.87	56.98	0.36	0.29	0.36	0.82	0.020	0.012	0.047	1.921	2	0.010	0.007	0.024	0.978	1.02	0.98	0.68	95.98	2.36	44.86	101.84
DOZ-B1-D	dzb1-02	brown host??	0.47	0.01	23.71	28.38	52.57	0.32	0.19	0.77	0.6	0.012	0.000	1.069	0.920	2	0.007	0.000	0.588	0.506	1.10	0.59	0.01	45.96	53.43	48.46	101.03
DOZ-B1-D	dzb1-08	brown host near edge with magnetite - darker grey zone	0.6	0.17	21.31	29.2	51.27	0.32	0.23	0.74	0.6	0.016	0.004	0.997	0.983	2	0.008	0.003	0.529	0.521	1.06	0.79	0.26	49.10	49.85	46.68	97.95
DOZ-B1-D	dzb1-09	pale infill crystals	1.07	0.21	0.3	53.53	55.11	0.37	0.26	0.32	0.79	0.030	0.006	0.015	1.948	2	0.015	0.003	0.007	0.955	0.98	1.52	0.35	97.37	0.76	43.14	98.25
DOZ-B2-A	dzb2-02	inclusion-rich at edge of void	1.07	0.21	0.78	56.15	58.21	0.37	0.27	0.35	0.8	0.029	0.006	0.037	1.928	2	0.015	0.003	0.019	1.001	1.04	1.43	0.33	96.37	1.86	45.72	103.93
DOZ-B2-A	dzb2-03	brown - original carbonate?	1.59	0.53	4.8	48.06	54.98	0.4	0.27	0.46	0.75	0.044	0.015	0.237	1.704	2	0.022	0.009	0.119	0.857	1.01	2.20	0.86	85.11	11.83	44.32	99.30
DOZ-B2-A	dzb2-04	inclusion-rich at edge of void	0.66	0.33	0.46	55.81	57.25	0.35	0.27	0.34	0.8	0.018	0.009	0.022	1.951	2	0.009	0.005	0.011	0.995	1.02	0.90	0.53	97.45	1.12	44.94	102.19
DOZ-B2-A	dzb2-05	clear infill crystals in void	1.09	0.31	0	56.06	57.46	0.38	0.28	0	0.8	0.030	0.009	0.000	1.962	2	0.015	0.005	0.000	1.000	1.02	1.49	0.50	98.01	0.00	44.89	102.35
DOZ-B2-A	dzb2-06	inclusion-rich adjacent to brown carbonate	1.24	0.66	0.47	51.96	54.33	0.37	0.29	0.34	0.77	0.036	0.019	0.024	1.921	2	0.017	0.011	0.012	0.927	0.97	1.79	1.12	95.89	1.21	42.53	96.86
DOZ-B2-A	dzb2-07	brown - carbonate - slightly mottled pale and dark	1.81	0.43	4.55	48.53	55.32	0.4	0.26	0.45	0.74	0.050	0.012	0.224	1.714	2	0.025	0.007	0.113	0.865	1.01	2.49	0.70	85.64	11.17	44.47	99.79
DOZ-B2-A	dzb2-12	brown host?	0.45	0.09	0.4	56.56	57.5	0.34	0.26	0.34	0.8	0.012	0.002	0.019	1.966	2	0.006	0.001	0.010	1.009	1.03	0.61	0.14	98.28	0.97	45.17	102.67
DOZ-B2-A	dzb2-14	mottled host - paler zones - matrix? - silica also present	0.85	0.08	1.41	53.51	55.85	0.34	0.26	0.38	0.78	0.023	0.002	0.070	1.904	2	0.012	0.001	0.035	0.954	1.00	1.18	0.13	95.20	3.49	44.11	99.96
DOZ-B2-A	dzb2-16	clear infill crystals in void	0.18	0.61	0.22	53.21	54.22	0.33	0.27	0.35	0.77	0.005	0.018	0.012	1.965	2	0.003	0.010	0.005	0.949	0.97	0.26	1.04	98.14	0.56	42.55	96.77
DOZ-B2-A	dzb2-18	dark rims in brown carbonate (which has a calcite composition)	3.63	0.27	17.31	31.68	52.89	0.47	0.25	0.67	0.6	0.096	0.007	0.819	1.078	2	0.051	0.004	0.429	0.565	1.05	4.81	0.42	53.83	40.93	46.18	99.07
DOZ-B2-A	dzb2-189	dark colouration within brown host?	1.31	0.08	21.14	31.99	54.52	0.36	0.23	0.72	0.61	0.033	0.002	0.941	1.024	2	0.018	0.001	0.525	0.570	1.11	1.64	0.12	51.18	47.06	49.05	103.57
GRS125-590-7	125-590-01	fragment of carbonate	0	0.32	20.4	31.64	52.37	0	0.26	0.72	0.61	0.000	0.008	0.942	1.050	2	0.000	0.005	0.506	0.564	1.08	0.00	0.49	52.45	47.06	47.34	99.71
GRS125-590-7	125-590-02	fine grained brown carbonate adjacent to fragment	0	0.05	0.06	57.74	57.86	0	0.25	0.35	0.81	0.000	0.001	0.003	1.995	2	0.000	0.001	0.001	1.030	1.03	0.00	0.08	99.78	0.14	45.42	103.28
GRS125-590-7	125-590-03	shell fragment	0.02	0	0.38	56.56	56.95	0.31	0	0.34	0.81	0.000	0.000	0.018	1.981	2	0.000	0.000	0.009	1.009	1.02	0.03	0.00	99.05	0.93	44.81	101.76
GRS125-590-7	125-590-07	darker carbonate matrix	0	0.34	19.81	33.2	53.35	0	0.25	0.7	0.62	0.000	0.009	0.903	1.088	2	0.000	0.006	0.492	0.592	1.09	0.00	0.51	54.36	45.13	47.93	101.28
GRS125-590-7	125-590-09	shell? Fragment	0	0.44	6.19	49.81	56.44	0	0.28	0.49	0.75	0.000	0.012	0.293	1.695	2	0.000	0.007	0.154	0.888	1.05	0.00	0.69	84.67	14.64	46.17	102.61
GRS125-600	125-600-01	host away from alteration	0.05	0.26	22.53	29.62	52.46	0.29	0.25	0.74	0.59	0.001	0.007	1.024	0.968	2	0.001	0.004	0.559	0.528	1.09	0.06	0.39	48.36	51.18	48.07	100.53
GRS125-600	125-600-02	host closer to alteration	0.35	0.75	21.7	30.52	53.31	0.29	0.28	0.73	0.6	0.009	0.019	0.980	0.992	2	0.005	0.012	0.538	0.544	1.10	0.44	1.12	49.48	48.95	48.40	101.71
GRS125-600	125-600-03	Patchy paler carbonate - adjacent to fracture	0	1.22	20.19	31.89	53.31	0	0.3	0.71	0.61	0.000	0.032	0.922	1.046	2	0.000	0.020	0.501	0.569	1.09	0.00	1.84	52.19	45.97	47.95	101.26

Sample	AAC-ID	Comments	FeO (wt%)	MnO (wt%)	MgO (wt%)	CaO (wt%)	Total	FeO +/-2 SIGMA	MnO +/-2 SIGMA	MgO +/-2 SIGMA	CaO +/-2 SIGMA	Fe (2 oxygens)	Mn (2 oxygens)	Mg (2 oxygens)	Ca (2 oxygens)	TOTAL (2 oxygens)	Fe m/M	Mn m/M	Mg m/M	Ca m/M	total m/M	Fe mol%	Mn mol%	Ca mol%	Mg mol%	wt% CO2 equ.	analysis total
GRS125-600	125-600-04	alteration adjacent to fracture. Paler material (slightly more Mn) appears as veins and fx in darker carbonate	0.07	7.62	16.79	30.02	54.49	0.36	0.5	0.68	0.59	0.002	0.203	0.786	1.010	2	0.001	0.125	0.417	0.535	1.08	0.09	11.60	49.66	38.65	47.44	101.93
GRS125-600	125-600-05	fine grained alteration (paler)	0	5.5	17.35	29.78	52.62	0	0.45	0.67	0.59	0.000	0.149	0.828	1.022	2	0.000	0.090	0.430	0.531	1.05	0.00	8.58	50.49	40.93	46.29	98.91
GRS125-600	125-600-06	grey host away from fractures	0.25	0.11	22.95	30.8	54.11	0.3	0.24	0.74	0.6	0.006	0.003	1.013	0.978	2	0.003	0.002	0.569	0.549	1.12	0.31	0.16	48.87	50.66	49.46	103.57
GRS125-600	125-600-09	Crystal infill in void with minor clay	0	0.58	21.21	30.48	52.27	0	0.27	0.72	0.6	0.000	0.015	0.976	1.009	2	0.000	0.010	0.526	0.544	1.08	0.00	0.88	50.36	48.76	47.50	99.77
GRS125-600	125-600-10	Host away from fractures and infill	0	1.07	20.09	30.71	51.87	0	0.28	0.71	0.6	0.000	0.028	0.939	1.032	2	0.000	0.018	0.498	0.548	1.06	0.00	1.65	51.49	46.86	46.81	98.68
GRS125-608-6	125-608-02	carbonate in small fracture cutting quartz	0.15	1.25	20.4	31.65	53.45	0.31	0.3	0.7	0.61	0.004	0.032	0.928	1.036	2	0.002	0.021	0.506	0.564	1.09	0.19	1.88	51.63	46.30	48.11	101.56
GRS125-608-6	125-608-05	paler carbonate, with very minor silica contamination	0.04	1.63	20.26	31.45	53.38	0.3	0.31	0.71	0.6	0.001	0.042	0.925	1.032	2	0.001	0.027	0.503	0.561	1.09	0.05	2.45	51.41	46.08	48.01	101.39
GRS125-608-6	125-608-06	area containing texturally different carbonate - not visible under backscatter.	0.21	1.9	20.74	30.5	53.36	0.3	0.32	0.71	0.6	0.005	0.049	0.946	1.000	2	0.003	0.031	0.515	0.544	1.09	0.27	2.85	49.78	47.10	48.08	101.44
GRS125-608-6	125-608-07	area containing texturally different carbonate - not visible under backscatter.	0	1.15	20.17	30.96	52.29	0	0.29	0.7	0.6	0.000	0.030	0.936	1.033	2	0.000	0.019	0.500	0.552	1.07	0.00	1.76	51.53	46.71	47.15	99.44
GRS125-608-6	125-608-08	area containing texturally different carbonate (paler and darker in TS) - not visible under backscatter.	0.12	1.63	20.33	30.91	52.99	0.31	0.31	0.71	0.6	0.003	0.042	0.934	1.021	2	0.002	0.027	0.504	0.551	1.08	0.15	2.47	50.85	46.53	47.71	100.70
GRS125-608-6	125-608-09	area containing texturally different carbonate (possibly paler ?) - not visible under backscatter.	0.04	1.66	20.26	31.46	53.42	0.3	0.31	0.7	0.6	0.001	0.043	0.924	1.032	2	0.001	0.027	0.503	0.561	1.09	0.05	2.50	51.40	46.06	48.04	101.46
GRS125-608-6	125-608-10	area containing texturally different carbonate (paler and darker in TS) - not visible under backscatter.	0.1	1.17	20.34	30.3	51.91	0.3	0.29	0.7	0.59	0.003	0.031	0.949	1.017	2	0.001	0.019	0.505	0.540	1.07	0.13	1.80	50.71	47.36	46.90	98.81
GRS125-608-6	125-608-10b	area containing texturally different carbonate (paler and darker in TS) - not visible under backscatter.	0.13	1.64	20.15	31.13	53.06	0.3	0.3	0.7	0.6	0.003	0.043	0.926	1.028	2	0.002	0.027	0.500	0.555	1.08	0.17	2.48	51.22	46.13	47.70	100.76
GRS125-608-6	125-608-112	area containing texturally different carbonate (paler and darker in TS) - not visible under backscatter.	0.12	1.24	20.07	30.15	51.59	0.29	0.3	0.7	0.59	0.003	0.033	0.944	1.020	2	0.002	0.020	0.498	0.538	1.06	0.16	1.92	50.83	47.08	46.55	98.14
GRS125-608-6	125-608-13	area containing texturally different carbonate (paler and darker in TS) - not visible under backscatter.	0.09	1.72	20.73	31.53	54.07	0.29	0.31	0.71	0.6	0.002	0.044	0.933	1.021	2	0.001	0.028	0.514	0.562	1.11	0.11	2.55	50.83	46.50	48.68	102.75
GRS125-608-6	125-608-14	area containing texturally different carbonate (paler and darker in TS) - not visible under backscatter.	0	1.12	20.17	30.82	52.11	0	0.3	0.7	0.6	0.000	0.030	0.939	1.031	2	0.000	0.018	0.500	0.550	1.07	0.00	1.72	51.44	46.84	47.02	99.13
GRS125-608-6	608-125-16	carbonate in clay vein	0.13	3.16	17.33	32.2	52.82	0.31	0.36	0.67	0.61	0.003	0.085	0.818	1.093	2	0.002	0.052	0.430	0.574	1.06	0.17	4.90	54.28	40.65	46.56	99.38
GRS125-608-6	1st analysis	carbonate in quartz	0	1.16	20.88	31.05	53.1	0	0.29	0.71	0.6	0.000	0.030	0.952	1.018	2	0.000	0.019	0.518	0.554	1.09	0.00	1.75	50.76	47.49	48.01	101.11
Calibration: C:\MSEDS\USER\CARB15KV.wds																											
Date: 05/11/02																											
Time: 40 seconds																											
Settings: kV= 15, Angle = 40, B.C. = 10.																											

Appendix 5 - Gold Microprobe

Sample	AAC-ID	Date	Ag (wt%)	Au (wt%)	Cu (wt%)	Total	Ag +/-2 SIGMA	Au +/-2 SIGMA	Cu +/-2 SIGMA	Ag Atom%	Au Atom%	Cu Atom%	Fineness 1000Au/ (Au+Ag)	Sample Mineralogy (refer Appendix 10)	Comments
BG1-4A-400	kp010	19/04/02	3.83	94.64	0.08	98.54	0.91	4.47	0.47	6.86	92.91	0.23	961	upper-bx-py-sph-cpy	10 micron grain. Very low Ag
BG1-4A-400	kp011	19/04/02	3	97.72	0.73	101.45	0.88	4.48	0.5	5.19	92.65	2.15	970	upper-bx-py-sph-cpy	
BG1-4A-400	kp011c	19/04/02	1.99	97.75	0.51	100.24	1.61	8.13	0.95	3.53	94.94	1.53	980	upper-bx-py-sph-cpy	Minor Cu-Zn-Fe in trace
BG1-4A-400	kp011d	19/04/02	2.01	96.81	0.12	98.94	1.5	7.63	0.86	3.64	95.99	0.37	980	upper-bx-py-sph-cpy	Minor Cu-Zn-Fe in trace
BG1-4A-400	kp013	19/04/02	4.1	91.54	4.17	99.82	0.92	4.54	0.61	6.70	81.74	11.56	957	upper-bx-py-sph-cpy	
BG1-4A-400	kp014	19/04/02	3.99	92.54	4.56	101.09	0.93	4.58	0.61	6.40	81.19	12.41	959	upper-bx-py-sph-cpy	Fe-Cu-Zn with Au.
BG1-4A-400	kp015	19/04/02	5.04	88.55	5.27	98.86	2.03	10.12	1.4	8.07	77.60	14.33	946	upper-bx-py-sph-cpy	Fe-Cu-Zn with Au.
BG1-4A-400	kp016	19/04/02	4.18	96.29	0.41	100.88	0.91	4.41	0.48	7.26	91.52	1.22	958	upper-bx-py-sph-cpy	Photo. Less Cu-Zn-Fe present
BG1-4A-400	kp020	19/04/02	3.13	95.5	0	98.63	0.88	4.44	0	5.65	94.35	0	968	upper-bx-py-sph-cpy	top grain, minor iron
BG1-4A-400	kp020a	19/04/02	4.33	94.48	0.06	98.87	1.37	6.7	0.7	7.71	92.12	0.17	956	upper-bx-py-sph-cpy	
BG1-4A-400	kp021	19/04/02	3.27	95.36	0	98.63	1.19	5.88	0	5.89	94.11	0	967	upper-bx-py-sph-cpy	
BG1-4A-400	kp023a	19/04/02	3.51	95.64	0	99.15	1.62	7.7	0	6.28	93.72	0	965	upper-bx-py-sph-cpy	
BG1-4A-400	kp025a	19/04/02	3.32	98.21	0	101.53	1.71	8.63	0	5.82	94.18	0	967	upper-bx-py-sph-cpy	
BG1-4A-400	kp025b	19/04/02	2.25	98.3	0	100.55	1.12	5.75	0	4.02	95.98	0	978	upper-bx-py-sph-cpy	
BG1-5-238	1-5-238-01	13/01/03	8.12	91.95	0.65	100.72	1.08	4.35	0.5	13.64	84.50	1.85	919	cpy	Au in fracture in pyrite
BG1-5-256	kp001	19/04/02	10.88	89.01	0	99.89	1.26	4.87	0	18.26	81.74	0	891	sph-apy	
BG1-5-256	kp002	19/04/02	10.32	88.29	0	98.61	1.12	4.32	0	17.60	82.40	0	895	sph-apy	
BG1-5-256	kp003r	19/04/02	10.69	88.85	0	99.54	1.12	4.32	0	18.03	81.97	0	893	sph-apy	
BG1-5-256	kp004	19/04/02	11.22	89.84	0	101.07	1.15	4.33	0	18.59	81.41	0	889	sph-apy	
BG1-5-256	kp004r	19/04/02	13.3	86.2	0	99.5	1.19	4.34	0	22.00	78.00	0	866	sph-apy	
BG1-5-256	kp005	19/04/02	12.7	85.94	0	98.63	1.17	4.28	0	21.26	78.74	0	871	sph-apy	
BG1-5-256	kp005a	19/04/02	12.35	86.83	0	99.18	1.86	6.88	0	20.63	79.37	0	875	sph-apy	
BG1-5-256	kp006	19/04/02	11.01	87.07	0	98.08	1.1	4.33	0	18.77	81.23	0	888	sph-apy	
BG1-5-256	kp006a	19/04/02	10.19	87.87	0	98.07	1.12	4.37	0	17.49	82.51	0	896	sph-apy	
BG1-5-256	kp006b	19/04/02	10.01	90.06	0	100.07	1.11	4.35	0	16.89	83.11	0	900	sph-apy	
BG1-5-256	kp006b2	19/04/02	9.82	88.47	0	98.29	1.09	4.34	0	16.86	83.14	0	900	sph-apy	
BG1-5-256	kp006b3	19/04/02	13.45	87.51	0	100.96	1.14	4.3	0	21.93	78.07	0	867	sph-apy	
BG1-5-256	kp006b4	19/04/02	13.45	87.51	0	100.96	1.14	4.3	0	21.93	78.07	0	867	sph-apy	
BG1-5-256	kp007	19/04/02	14.19	85.32	0	99.51	1.21	4.24	0	23.31	76.69	0	857	sph-apy	Small grain (6 microns)
BG1-5-256	kp008	19/04/02	9.7	89.72	0	99.43	1.11	4.32	0	16.50	83.50	0	902	sph-apy	Au grain (20-30 microns long) with arsenopyrite crystals (chalcopyrite and pyrite host)
BG1-5-256	kp009	19/04/02	12.23	88.17	0.43	100.83	1.14	4.23	0.47	19.98	78.83	1.19	878	sph-apy	small Au grain. Very minor iron (contamination?) no Cu
BGU07-06-324	7-6-324-02	13/01/03	9.98	91.12	0	101.11	1.12	4.34	0	16.68	83.32	0	901	sph-cpy	large Au in fracture
BGU08-01-225	8-1-225-01	13/01/03	16.32	83.65	0	99.97	1.26	4.21	0	26.29	73.71	0	837	sph-cpy	Au grain in pyrrhotite. Lots of scheelite in rock
BGU18-03-211	KPBG06-02	14/12/02	5.16	93.69	0	98.85	0.98	4.47	0	9.15	90.85	0	948		Au with grey (Au-Fe-S??)
BGU18-03-211	KPBG06-04	14/12/02	20.99	78.69	0	99.68	1.37	4.2	0	32.77	67.23	0	789	Py-sph-gn	with galena
BGU18-03-211	KPBG06-05	14/12/02	25.84	72.27	0	98.11	1.45	4.1	0	39.52	60.48	0	737	Py-sph-gn	at pyrite edge
BGU18-03-211	KPBG06-08	14/12/02	18.28	83.55	0	101.83	1.33	4.26	0	28.56	71.44	0	820	Py-sph-gn	
BGU18-03-211	KPBG06-09	14/12/02	18.42	83.65	0	102.08	1.3	4.28	0	28.70	71.30	0	820	Py-sph-gn	Au in pyrite, also galena inclusion in other pyrites
BGU19-03-184.7	KPBG13-01	14/12/02	15.04	85.13	0	100.17	1.26	4.31	0	24.41	75.59	0	850	sph-cpy-py	host = pyrite, minor Arsenopyrite inclusion also
BGU19-03-184.7	KPBG13-02	14/12/02	15.12	84.49	0	99.61	1.22	4.26	0	24.65	75.35	0	848	sph-cpy-py	host = pyrite, minor Arsenopyrite inclusion also
BGU19-03-184.7	KPBG13-03	14/12/02	14.82	86.75	0	101.56	1.24	4.25	0	23.79	76.21	0	854	sph-cpy-py	host = pyrite, minor Arsenopyrite inclusion also
BGU19-03-184.7	KPBG13-06	14/12/02	15.38	87.38	0	102.76	1.26	4.32	0	24.34	75.66	0	850	sph-cpy-py	near chalcopyrite and low iron sphalerite and iron-Manganese carbonate (minor Ca)
BGU19-03-184.7	KPBG13-07	14/12/02	16.43	84.88	0.24	101.55	1.28	4.28	0.5	25.96	73.38	0.66	838	sph-cpy-py	at Chalcopyrite contact
BGU19-03-184.7	KPBG13-12	14/12/02	11.31	90.14	0	101.45	1.14	4.44	0	18.65	81.35	0	889	sph-cpy-py	long Au
BGU19-03-184.7	KPBG13-14	14/12/02	18.55	84.16	0	102.71	1.3	4.23	0	28.72	71.28	0	819	sph-cpy-py	Au
BGU19-03-184.7	KPBG13-15	14/12/02	11.44	90.62	0	102.06	1.15	4.46	0	18.75	81.25	0	888	sph-cpy-py	
BGU19-03-184.7	KPBG13-16	14/12/02	18.38	80.84	0	99.22	1.32	4.33	0	29.35	70.65	0	815	sph-cpy-py	pink = chalcopyrite; low iron sphalerite host
BGU19-03-184.7	KPBG13-17	14/12/02	18.62	83.23	0	101.85	1.32	4.3	0	29.02	70.98	0	817	sph-cpy-py	

Sample	AAC-ID	Date	Ag (wt%)	Au (wt%)	Cu (wt%)	Total	Ag +/-2 SIGMA	Au +/-2 SIGMA	Cu +/-2 SIGMA	Ag Atom%	Au Atom%	Cu Atom%	Fineness 1000Au/ (Au+Ag)	Sample Mineralogy (refer Appendix 10)	Comments
BGU19-03-184.7	KPBG13-18	14/12/02	22.65	78.9	0	101.56	1.4	4.21	0	34.42	65.58	0	777	sph-cpy-py	
BGU21-02-13.3A	21-2-13A-01	13/01/03	8.7	90.84	0	99.55	1.1	4.37	0	14.90	85.10	0	913	sph-gn-apy	
BGU21-02-13.3A	21-2-13A-03	13/01/03	12.87	88.36	0	101.23	1.22	4.24	0	21.03	78.97	0	873	sph-gn-apy	
BGU21-02-13.3A	21-2-13A-09	13/01/03	6.94	95	0	101.94	1.05	4.37	0	11.78	88.22	0	932	sph-gn-apy	large Au with grey (galena - no Bi) in void
BGU21-02-13.3A	21-2-13A-10	13/01/03	11.42	88.18	0	99.6	1.17	4.31	0	19.14	80.86	0	885	sph-gn-apy	large Au
BGU21-02-13.3B	21-2-13B-01	13/01/03	12.19	86.36	0	98.55	1.2	4.26	0	20.51	79.49	0	876	sph-gn-apy	large Au grain
BGU21-02-13.3B	21-2-13B-03	13/01/03	14.15	84.56	0.34	99.05	1.24	4.26	0.48	23.20	75.85	0.95	857	sph-gn-apy	10 micron grain in grey min - galena (bi-bearing).
BGU21-02-13.3B	21-2-13B-04	13/01/03	11.83	87.63	0	99.46	1.19	4.32	0	19.79	80.21	0	881	sph-gn-apy	Au with Galena (Bi-bearing)
BGU21-03-225	21-3-225-01	13/01/03	10.31	88.83	0	99.15	1.13	4.32	0	17.50	82.50	0	896	sph-cpy	Au in sphalerite near quartz-sphalerite contact. Sphalerite 1:3 Fe:Zn
BGU21-10-236B	21-10-236B-04	13/01/03	4	94.8	0	98.8	0.94	4.43	0	7.16	92.84	0	960	Bi	long in Bi-Te-S at pyrite contact
BGU21-2-14	kp066	29/04/02	2.58	98.52	0.74	101.84	0.9	4.47	0.5	4.47	93.35	2.18	974	cpy	gold in pyrite grain
BGU21-2-14	kp068	29/04/02	6.05	94.27	0	100.32	0.94	4.45	0	10.49	89.51	0	940	cpy	one of several grains
BGU21-2-14	kp069	29/04/02	5.02	94.28	0	99.3	0.95	4.38	0	8.86	91.14	0	949	cpy	one of several grains
BGU21-2-14	kp070	29/04/02	4.34	94.71	0.03	99.08	0.96	4.37	0.46	7.73	92.19	0.08	956	cpy	one of several grains
BGU21-2-14	kp071	29/04/02	8.84	92.53	0.21	101.58	1.05	4.34	0.48	14.78	84.63	0.59	913	cpy	Au at edge of void
BGU21-2-14	kp073	29/04/02	5.79	93.9	0	99.69	0.94	4.4	0	10.13	89.87	0	942	cpy	
BGU21-2-14	kp074	29/04/02	6.91	92.33	0	99.24	1.03	4.4	0	12.03	87.97	0	930	cpy	
BGU21-2-14	kp075	29/04/02	4.91	93.53	0	98.45	0.95	4.44	0	8.76	91.24	0	950	cpy	
BGU21-2-14	kp077b	29/04/02	7.88	91.22	0	99.1	1.05	4.34	0	13.63	86.37	0	920	cpy	lower grain of 3
BGU21-2-14	kp078	29/04/02	5.9	93.65	0	99.54	0.95	4.41	0	10.32	89.68	0	941	cpy	upper grain of 3
BGU21-2-14	kp079	29/04/02	5.98	95.47	0	101.46	0.98	4.39	0	10.28	89.72	0	941	cpy	middle grain of 3
BGU21-2-14	kp079a	29/04/02	6.66	94.42	0	101.08	0.99	4.41	0	11.42	88.58	0	934	cpy	middle grain of 3
BGU21-2-14	kp084	29/04/02	9.47	88.96	0.54	98.97	1.08	4.3	0.49	16.03	82.41	1.56	904	cpy	Au in chalcopyrite
BGU21-2-14	kp084a	29/04/02	9.34	89.86	0.43	99.63	1.07	4.33	0.5	15.77	83.00	1.23	906	cpy	Au in chalcopyrite
BGU24-10-305	KPBG05-05-5	14/12/02	20.87	79.12	0	99.99	1.35	4.22	0	32.52	67.48	0	791	sph-gn-cpy-py	unnamed grain in pyrite
BGU24-10-305	KPBG05-10a	14/12/02	17.12	84.92	0	102.04	1.28	4.31	0	26.93	73.07	0	832	sph-gn-cpy-py	Au in galena
BGU24-10-305	KPBG05-10b	14/12/02	17.14	84.5	0	101.64	1.28	4.3	0	27.05	72.95	0	831	sph-gn-cpy-py	Au at galena edge
BGU24-10-305	KPBG05-11	14/12/02	16.57	84.85	0	101.42	1.3	4.27	0	26.30	73.70	0	837	sph-gn-cpy-py	Au in host
BGU24-10-305	KPBG05-11b	14/12/02	19.47	79.58	0	99.05	1.33	4.26	0	30.90	69.10	0	803	sph-gn-cpy-py	large Au with minor galena attached
BGU24-10-305	KPBG05-11c	14/12/02	24.72	74.74	0	99.45	1.44	4.09	0	37.67	62.33	0	751	sph-gn-cpy-py	small Au grain
BGU24-10-305	KPBG05-11d	14/12/02	19.89	80.69	0	100.58	1.36	4.23	0	31.06	68.94	0	802	sph-gn-cpy-py	long Au on fracture in host
BGU24-11-343	KPBG24-01	14/12/02	18.2	83.9	0	102.11	1.28	4.33	0	28.40	71.60	0	822	mixed/Bi-Te	In quartz and Fe>S
BGU24-11-343	KPBG24-02	14/12/02	17.76	84.44	0	102.2	1.29	4.34	0	27.76	72.24	0	826	mixed/Bi-Te	in fracture in pyrite
BGU24-11-343	KPBG24-03	14/12/02	21.21	81.64	0	102.85	1.34	4.21	0	32.20	67.80	0	794	mixed/Bi-Te	at pyrite quartz contact
BGU24-11-343	KPBG24-04	14/12/02	16.34	83.83	0	100.17	1.28	4.28	0	26.27	73.73	0	837	mixed/Bi-Te	in pyrite edge fracture
BGU24-11-343	KPBG24-05	14/12/02	16.57	84.77	0	101.34	1.3	4.3	0	26.32	73.68	0	836	mixed/Bi-Te	Au at pyrite edge with Fe>S
BGU24-11-343	KPBG24-06a	14/12/02	6.83	94.19	0	101.02	1.02	4.44	0	11.71	88.29	0	932	low Ag	Several
BGU24-11-343	KPBG24-07	14/12/02	19.53	80.29	0	99.82	1.31	4.22	0	30.77	69.23	0	804	mixed/Bi-Te	Au
BGU24-11-343	KPBG24-09	14/12/02	15.1	85.55	0	100.65	1.26	4.28	0	24.40	75.60	0	850	mixed/Bi-Te	Au in galena
BGU24-11-343	KPBG24-10	14/12/02	16.58	84.3	0	100.88	1.27	4.31	0	26.44	73.56	0	836	mixed/Bi-Te	
BGU24-11-343	KPBG24-11	14/12/02	18.59	84.18	0	102.78	1.33	4.24	0	28.76	71.24	0	819	mixed/Bi-Te	
BGU24-11-343	KPBG24-14	14/12/02	18.06	82.93	0	100.98	1.29	4.23	0	28.47	71.53	0	821	mixed/Bi-Te	Au with galena
BGU24-11-343	KPBG24-17	14/12/02	16.71	85.17	0	101.89	1.28	4.26	0	26.40	73.60	0	836	mixed/Bi-Te	pyrrhotite with Au (iron:S; 2:5). Sphalerite host, no iron
BGU24-11-343	KPBG24-19	14/12/02	17.98	81.05	0	99.03	1.3	4.25	0	28.85	71.15	0	818	mixed/Bi-Te	Au on Fracture in pyrite
BGU24-11-343	KPBG24-21	14/12/02	6.6	93.62	0	100.22	1.05	4.45	0	11.41	88.59	0	934	low Ag	Au in pyrite
BGU24-11-343	KPBG24-23	14/12/02	20.64	78.5	0	99.14	1.35	4.21	0	32.45	67.55	0	792	mixed/Bi-Te	Au at pyrite-quartz contact
BGU24-11-343	KPBG24-26	14/12/02	18.38	80.98	0	99.37	1.32	4.2	0	29.32	70.68	0	815	mixed/Bi-Te	Au in pyrite - fracture shaped
BGU24-11-343	KPBG24-27	14/12/02	8.25	93.21	0.55	102.02	1.08	4.46	0.5	13.71	84.73	1.55	919	low Ag	blob in pyrite
BGU24-11-343	KPBG24-28	14/12/02	8.01	94.85	0	102.86	1.07	4.47	0	13.37	86.63	0	922	low Ag	

Sample	AAC-ID	Date	Ag (wt%)	Au (wt%)	Cu (wt%)	Total	Ag +/-2 SIGMA	Au +/-2 SIGMA	Cu +/-2 SIGMA	Ag Atom%	Au Atom%	Cu Atom%	Fineness 1000Au/ (Au+Ag)	Sample Mineralogy (refer Appendix 10)	Comments
BGU24-11-343	KPBG24-A4a	14/12/02	17.6	81	0	98.6	1.3	4.25	0	28.42	71.58	0	822	pale-sph-bi-tet etc	Au with altered Pb mineral and Chalcopyrite
BGU24-11-343	KPBG24-A4a	14/12/02	17.6	81	0	98.6	1.3	4.25	0	28.42	71.58	0	822	mixed/Bi-Te	Au with altered Pb mineral and Chalcopyrite
BGU24-11-343	KPBG24-A6a	14/12/02	4.88	94.7	0.05	99.64	0.95	4.42	0.48	8.60	91.26	0.14	951	low Ag	
BGU24-11-343	KPBG24-A6f	14/12/02	17.05	85.11	0.09	102.25	1.28	4.26	0.49	26.74	73.02	0.24	833	mixed/Bi-Te	
BGU24-11-343	KPBG24-A6g	14/12/02	18.7	82.04	0.16	100.91	1.31	4.24	0.49	29.29	70.29	0.42	814	mixed/Bi-Te	
BGU26-01-151	KPBG07-03	14/12/02	12.21	88.74	0.04	101	1.15	4.38	0.48	20.07	79.81	0.12	879	Cpy-mixed-apy	
BGU26-01-151	KPBG07-06	14/12/02	8.33	94.45	0.03	102.81	1.09	4.44	0.47	13.88	86.03	0.09	919	Cpy-mixed-apy	
BGU26-01-151	KPBG07-07	14/12/02	13.1	85.98	0	99.08	1.2	4.36	0	21.78	78.22	0	868	Cpy-mixed-apy	
BGU26-01-151	KPBG07-09	14/12/02	7.83	94.7	0	102.53	1.05	4.49	0	13.12	86.88	0	924	Cpy-mixed-apy	
BGU26-01-151	KPBG07-10	14/12/02	6.5	92.15	0	98.65	1.01	4.45	0	11.42	88.58	0	934	Cpy-mixed-apy	
BGU26-01-151	KPBG07-19	14/12/02	6.47	93.39	0	99.86	1.02	4.44	0	11.24	88.76	0	935	Cpy-mixed-apy	in pyrite
BGU26-01-151	KPBG07-20	14/12/02	7.19	94.43	0	101.62	1.02	4.45	0	12.22	87.78	0	929	Cpy-mixed-apy	
BGU26-01-151	KPBG07-22	14/12/02	8.47	90.55	0	99.02	1.1	4.39	0	14.59	85.41	0	914	Cpy-mixed-apy	within pyrite
BGU26-01-151	KPBG07-23	14/12/02	7.2	94.91	0	102.11	1.04	4.41	0.56	12.18	87.81	0.01	929	Cpy-mixed-apy	
BGU26-01-151	KPBG07-27	14/12/02	7.09	95.75	0.11	102.96	1.02	4.51	0.5	11.88	87.80	0.32	931	Cpy-mixed-apy	
BGU26-01-151	KPBG07-28	14/12/02	13.82	86.8	0.53	101.15	1.2	4.36	0.5	22.22	76.34	1.44	863	with gn	in galena
BGU26-01-151	KPBG07-32	14/12/02	6.82	93.78	0	100.59	1.03	4.44	0	11.73	88.27	0	932	Cpy-mixed-apy	Grey = sphalerite 3:5 (Fe:Zn)
BGU26-01-151	KPBG07-35	14/12/02	7.95	91.42	0	99.37	1.04	4.44	0	13.72	86.28	0	920	Cpy-mixed-apy	Au in pyrite
BGU26-01-151	KPBG07-35b	14/12/02	6.77	92.4	0	99.17	1.03	4.43	0	11.81	88.19	0	932	Cpy-mixed-apy	Au in pyrite
BGU26-02-207B	26-2-207B-01	13/01/03	3.3	95.47	0	98.77	0.91	4.41	0	5.94	94.06	0	967	low Ag	bigger Au in pyrite
BGU26-1-165.2	kp028	19/04/02	9.02	88.59	0.78	98.39	1.06	4.32	0.5	15.33	82.42	2.25	908	cpy	NB count averages 100 for first 20seconds. 10 micron grain at edge of chalcopyrite and Si-Ca-Mg-Fe mineral.
BGU27-02-204	KPBG02-01	14/12/02	6.12	93.61	0	99.72	1.01	4.43	0	10.67	89.33	0	939	low Ag	
BGU27-02-204	KPBG02-02	14/12/02	4.52	95.08	0	99.61	0.95	4.48	0	8.00	92.00	0	955	low Ag	minor Iron
BGU27-02-204	KPBG02-04	14/12/02	17.01	79.91	1.15	98.07	1.26	4.24	0.5	27.14	69.75	3.12	824	cpy - may be Bi	more Fe than Cu, with chalcopyrite
BGU27-02-204	KPBG02-06	14/12/02	2.79	95.22	1.02	99.03	0.92	4.48	0.53	4.93	92.02	3.05	972	low Ag	Au in pyrite, also galena inclision in other pyrites
BGU27-02-204	KPBG02-07	14/12/02	3.77	95.93	0	99.69	0.94	4.44	0	6.69	93.31	0	962	low Ag	larger grain
BGU27-02-204	KPBG02-08	14/12/02	2.61	95.7	0	98.31	0.88	4.43	0	4.76	95.24	0	973	low Ag	smaller with grey (all grey = galena)
BGU27-06-349	KPBG18-06	14/12/02	21.48	77.26	0	98.74	1.35	4.1	0	33.70	66.30	0	782	sph-cpy-apy	large grain in pyrite
BGU27-06-349	KPBG18-07b	14/12/02	22.63	79.09	0	101.72	1.42	4.15	0	34.34	65.66	0	778	sph-cpy-apy	long on in pyrite; grey in pyrite = Fe-bearing sphalerite
BGU27-06-349	KPBG18-07d	14/12/02	13.16	88.14	0	101.3	1.2	4.38	0	21.43	78.57	0	870	sph-cpy-apy	On right in photo 07c minor iron
BGU27-06-349	KPBG18-07f	14/12/02	14.53	86.08	0	100.61	1.24	4.33	0	23.58	76.42	0	856	sph-cpy-apy	On left 07c (pyrrhotite spot in pyrite - more iron)
BGU28-05-267	KPBG03-01	14/12/02	3.13	97.77	0	100.9	0.94	4.46	0	5.52	94.48	0	969	low Ag	Au in pyrite; grey = magnetite
BGU28-05-267	KPBG03-04	14/12/02	7.82	94.5	0	102.32	1.08	4.5	0	13.14	86.86	0	924	cpy - may be Bi	
BGU28-05-267	KPBG03-14	14/12/02	9.39	91.56	0	100.96	1.1	4.4	0	15.79	84.21	0	907	cpy - may be Bi	
BGU28-05-267	KPBG03-15	14/12/02	3.03	96.75	0	99.78	0.93	4.5	0	5.41	94.59	0	970	low Ag	
BGU28-05-267	KPBG03-16	14/12/02	3.52	94.66	0	98.18	0.93	4.51	0	6.37	93.63	0	964	low Ag	
BGU28-05-267	KPBG03-17	14/12/02	3.75	98.57	0	102.32	0.91	4.54	0	6.49	93.51	0	963	low Ag	Au in pyrite, other inclusion include sphalerite (grey)
BGU28-05-268	KPBG01-10	14/12/02	2.86	100	0	102.89	0.91	4.53	0	4.97	95.03	0	972	low Ag	Au in pyrite, can't see much Ag
BGU28-05-268	KPBG01-11	14/12/02	9.84	92.18	0	102.03	1.1	4.39	0	16.33	83.67	0	904	Cpy-mixed-?Bi	
BGU28-05-268	KPBG01-20	14/12/02	6.45	96.1	0	102.55	1.02	4.47	0	10.93	89.07	0	937	Cpy-mixed-?Bi	Au on pyrite contact
BGU28-05-268	KPBG01-36	14/12/02	7.51	91.67	0	99.18	1.06	4.5	0	13.02	86.98	0	924	Cpy-mixed-?Bi	More Ag in this Au
BGU28-05-268	KPBG01-53	14/12/02	7.62	90.49	0	98.11	1.07	4.41	0	13.34	86.66	0	922	Cpy-mixed-?Bi	Au in pyrite
BGU28-05-268	KPBG01-56	14/12/02	7.52	93.96	0	101.48	1.05	4.44	0	12.76	87.24	0	926	Cpy-mixed-?Bi	At pyrite edge
BGU28-05-268	KPBG01-62	14/12/02	6.3	96.52	0	102.82	1.05	4.55	0	10.66	89.34	0	939	Cpy-mixed-?Bi	Au grain, minor Ag in pyrite
BGU28-05-268	KPBG01-63	14/12/02	7.28	91.92	0	99.2	1.05	4.46	0	12.64	87.36	0	927	Cpy-mixed-?Bi	Au grain, minor Ag in pyrite
BGU30-05-246	KPBG15-02	14/12/02	13.31	87.49	0	100.8	1.19	4.37	0	21.76	78.24	0	868	sph-cpy-gn-apy-tet	Au on fracture in pyrite, some age
BGU30-05-246	KPBG15-03	14/12/02	15.08	87.85	0	102.93	1.24	4.31	0	23.88	76.12	0	853	sph-cpy-gn-apy-tet	
BGU30-05-246	KPBG15-06	14/12/02	12.38	89.56	0	101.94	1.19	4.42	0	20.17	79.83	0	879	sph-cpy-gn-apy-tet	Au with grey (Fe-Cu-As-S-Ag no Sb)
BGU30-05-246	KPBG15-06r	14/12/02	12.43	89.2	0	101.63	1.18	4.38	0	20.30	79.70	0	878	sph-cpy-gn-apy-tet	Au with grey (Fe-Cu-As-S-Ag no Sb)

Sample	AAC-ID	Date	Ag (wt%)	Au (wt%)	Cu (wt%)	Total	Ag +/-2 SIGMA	Au +/-2 SIGMA	Cu +/-2 SIGMA	Ag Atom%	Au Atom%	Cu Atom%	Fineness 1000Au/ (Au+Ag)	Sample Mineralogy (refer Appendix 10)	Comments
BGU30-05-246	KPBG15-07	14/12/02	14.65	86.97	0	101.62	1.22	4.31	0	23.55	76.45	0	856	sph-cpy-gn-apy-tet	Au with pyrite, other small Au in chalcopyrite
BGU30-05-246	KPBG15-08	14/12/02	15.59	86.73	0	102.32	1.23	4.32	0	24.73	75.27	0	848	sph-cpy-gn-apy-tet	Au at pyrite, Arsenopyrite contact
BGU30-05-246	KPBG15-09	14/12/02	13.91	88.33	0	102.24	1.22	4.34	0	22.35	77.65	0	864	sph-cpy-gn-apy-tet	Au at pyrite host contact
BGU30-05-246	KPBG15-17	14/12/02	15.85	85.83	0.17	101.84	1.24	4.29	0.49	25.11	74.44	0.45	844	sph-cpy-gn-apy-tet	Au at pyrite edge, dark grey = sphalerite; pale grey=galena
BGU30-05-246	KPBG15-18	14/12/02	19.11	79.97	0.82	99.9	1.32	4.29	0.49	29.74	68.09	2.17	807	sph-cpy-gn-apy-tet	Long Au grain, dark grey = sphalerite; pale grey=galena
BGU30-05-246	KPBG15-22	14/12/02	13.37	86.83	0.24	100.45	1.19	4.36	0.47	21.82	77.52	0.66	867	sph-cpy-gn-apy-tet	white nearby = galena
BGU30-05-246	KPBG15-23	14/12/02	14.14	88.43	0	102.56	1.21	4.4	0	22.61	77.39	0	862	sph-cpy-gn-apy-tet	(grey = tetrahedrite, no Sb, minor Ag)
BGU30-05-246	KPBG15-24	14/12/02	13.79	87.94	0	101.74	1.2	4.37	0	22.28	77.72	0	864	sph-cpy-gn-apy-tet	in pyrite
BGU30-05-246	KPBG15-26	14/12/02	12.6	85.94	0	98.53	1.19	4.37	0	21.13	78.87	0	872	sph-cpy-gn-apy-tet	
BGU30-05-246	KPBG15-27	14/12/02	13.07	87.96	0	101.03	1.19	4.35	0	21.36	78.64	0	871	sph-cpy-gn-apy-tet	grey=tetrahedrite+Sb, no Ag
BGU30-05-246	KPBG15-31	14/12/02	9.95	91.95	0	101.9	1.13	4.41	0	16.51	83.49	0	902	sph-cpy-gn-apy-tet	Au in pyrite
BGU30-05-246	KPBG15-33	14/12/02	12.18	89.95	0	102.13	1.18	4.37	0	19.84	80.16	0	881	sph-cpy-gn-apy-tet	Au in pyrite
BGU30-6-179	kp037a	29/04/02	5.79	93.49	0	99.28	0.97	4.43	0	10.17	89.83	0	942	cpy-po	150 micron long Au grain in vein
BGU30-6-179	kp039	29/04/02	12.09	88.05	0	100.13	1.14	4.33	0	20.06	79.94	0	879	other	Au grains on fracture in void with Al-Si mineral (clay?) and iron-Manganese mineral (carbonate)
BGU30-6-179	kp040	29/04/02	6.12	93.26	0	99.38	1.01	4.36	0	10.71	89.29	0	938	cpy-po	Au in void
BGU30-6-179	kp041	29/04/02	6.79	92.15	0	98.94	1	4.36	0	11.87	88.13	0	931	cpy-po	second grain, in fracture
BGU30-6-179	kp042	29/04/02	9.04	90.29	0	99.33	1.06	4.31	0	15.46	84.54	0	909	cpy-po	in fracture
BGU30-6-179	kp044	29/04/02	6.99	94.33	0	101.31	0.99	4.4	0	11.92	88.08	0	931	cpy-po	30 micron Au grain with pyrrhotite
BGU30-6-179	kp045	29/04/02	5.63	93.49	0	99.12	1.01	4.43	0	9.91	90.09	0	943	cpy-po	Au on edge of fracture with quartzand carbonate infill in pyrrhotite host. Image taken
BGU30-6-179	kp046	29/04/02	5.73	94.6	0	100.34	0.99	4.41	0	9.97	90.03	0	943	cpy-po	40 micron Au on fracture in pyrrhotite with carbonate
BGU30-6-179	kp047	29/04/02	6.5	96.31	0	102.8	0.99	4.37	0	10.98	89.02	0	937	cpy-po	60 micron Au in vein with carbonate and black (Al-Si-K, trace Fe) mineral. Image taken
BGU30-6-179	kp050	29/04/02	8.23	90.22	0	98.45	1.04	4.38	0	14.30	85.70	0	916	cpy-po	25 micron Au grain. One of multiple grains in a void with cracked Al-Si mineral (clay?), image KP053.
BGU30-6-179	kp051	29/04/02	7.78	90.64	0	98.42	1.01	4.38	0	13.56	86.44	0	921	cpy-po	10 micron Au grain. One of multiple grains in a void with cracked Al-Si mineral (clay?), image KP053.
BGU30-6-179	kp052	29/04/02	9.14	92.07	0	101.2	1.06	4.31	0	15.35	84.65	0	910	cpy-po	One of multiple grains in a void with cracked Al-Si mineral (clay?), image KP053.
BGU30-6-179	kp054	29/04/02	6.92	94.81	0	101.72	1.01	4.35	0	11.77	88.23	0	932	cpy-po	10 microns, one of 3 grains
BGU30-6-179	kp055	29/04/02	8.35	90.11	0	98.46	1.07	4.35	0	14.49	85.51	0	915	cpy-po	near void
BGU30-6-179	kp056	29/04/02	6.36	92.8	0	99.16	0.99	4.37	0	11.13	88.87	0	936	cpy-po	near void containing Al-Si high K mineral with inclusion of P-Ca mineral
BGU30-6-179	kp057a	29/04/02	8	90.27	0	98.27	1.01	4.38	0	13.94	86.06	0	919	cpy-po	elongate grain
BGU30-6-179	kp058	29/04/02	7.44	94.75	0	102.2	1.01	4.38	0	12.56	87.44	0	927	cpy-po	Au in pyrrhotite
BGU30-6-179	kp058b	29/04/02	6.86	91.43	0	98.29	1.02	4.36	0	12.05	87.95	0	930	cpy-po	Au in pyrrhotite
BGU30-6-179	kp059	29/04/02	6.68	92.03	0	98.71	0.99	4.38	0	11.71	88.29	0	932	cpy-po	several grains in cracks in pyrrhotite
BGU30-6-179	kp060	29/04/02	8.02	93.74	0	101.76	1.04	4.38	0	13.53	86.47	0	921	cpy-po	several grains in cracks in pyrrhotite
BGU30-6-179	kp061	29/04/02	7.39	93.59	0.02	101	1.01	4.38	0.46	12.60	87.34	0.06	927	cpy-po	several grains in cracks in pyrrhotite, no cu
BGU30-6-179	kp062	29/04/02	7.14	94.03	0	101.17	1.02	4.34	0	12.19	87.81	0	929	cpy-po	several grains in cracks in pyrrhotite
BGU30-6-179	kp063a	29/04/02	6.91	94.62	0	101.53	1	4.4	0	11.78	88.22	0	932	cpy-po	several grains in cracks in pyrrhotite
BGU30-6-179	kp064	29/04/02	7.39	91.27	0	98.65	1.03	4.35	0	12.88	87.12	0	925	cpy-po	several grains in cracks in pyrrhotite
BGU30-8-186-5	kp030	29/04/02	15.41	82.68	0	98.09	1	3.46	0	25.41	74.59	0	843	Au-apy-sph-cpy?	Au grain 10 microns within pyrite
BGU30-8-186-5	kp031a	29/04/02	12.51	90.23	0	102.74	1.18	4.33	0	20.22	79.78	0	878	Au-apy-sph-cpy?	35 micron pitted Au, low count at quartz-pyrite contact
BGU30-8-186-5	kp032	29/04/02	16.48	82.4	0	98.89	1.22	4.23	0	26.77	73.23	0	833	Au-apy-sph-cpy?	10 micron Au, several blebs in pyrite
BGU30-8-186-5	kp034	29/04/02	10.89	88.72	0	99.61	1.13	4.28	0	18.32	81.68	0	891	Au-apy-sph-cpy?	Au grain in quartz -image taken
BGU30-8-186-5	kp036	29/04/02	15.54	82.98	0	98.52	1.25	4.24	0	25.50	74.50	0	842	Au-apy-sph-cpy?	10 micron grain, one of several small grains in pyrite
WAN4-5-182	KPW182-01	14/12/02	7.42	90.37	0	97.78	0.89	3.78	0	13.05	86.95	0	924		Au in pyrite

Appendix 5 - Gold Microprobe

Sample	AAC-ID	Date	Ag (wt%)	Au (wt%)	Cu (wt%)	Total	Ag +/-2 SIGMA	Au +/-2 SIGMA	Cu +/-2 SIGMA	Ag Atom%	Au Atom%	Cu Atom%	Fineness 1000Au/ (Au+Ag)	Sample Mineralogy (refer Appendix 10)	Comments
WAN4-5-182	KPW182-02	14/12/02	7.14	91.67	0	98.81	1.06	4.4	0	12.46	87.54	0	928		grey inclusion = sphalerite (1:3; Fe:Zn)
WAN4-5-182	KPW182-05	14/12/02	1.94	97.34	0	99.27	0.85	4.48	0	3.51	96.49	0	980		Au, grey = galena
WAN4-5-182	KPW182-07	14/12/02	4.02	94.99	0	99.01	0.94	4.47	0	7.18	92.82	0	959		Au in pyrite
WAN4-5-182	KPW182-08	14/12/02	1.12	99.98	0	101.09	0.86	4.46	0	2.00	98.00	0	989		
WAN4-5-182	KPW182-10	14/12/02	0.83	96.42	0	97.25	0.86	4.51	0	1.56	98.44	0	991		
WAN4-5-182	KPW182-12	14/12/02	4.51	97.53	0	102.04	0.97	4.47	0	7.79	92.21	0	956		
WAN4-5-182	KPW182-13	14/12/02	3.12	98.92	0	102.04	0.94	4.52	0	5.44	94.56	0	969		
WAN4-5-182	KPW182-22	14/12/02	4.34	99.28	0	103.62	0.96	4.54	0	7.39	92.61	0	958		
WAN4-5-182	KPW182-23	14/12/02	5.48	92.93	0	98.41	0.98	4.43	0	9.73	90.27	0	944		Au grain with Bi-S-Fe attached
WAN4-5-182	KPW182-24	14/12/02	1.35	101	0	102.3	0.86	4.54	0	2.39	97.61	0	987		
WAN4-5-182	KPW182-25	14/12/02	2.06	97.92	0	99.98	0.88	4.53	0	3.71	96.29	0	979		
WAN4-2-234A	KPW3-01	14/12/02	6.43	85.4	1.99	93.82	1.05	4.27	0.55	11.37	82.66	5.97	930		Au (minor Te contamination) in grey (Au-Ag-Te; minor iron contamination?)
WAN4-2-234A	KPW3-02	14/12/02	4.44	87.72	0.03	92.19	0.95	4.35	0.46	8.46	91.44	0.10	952		Au + grey = sphalerite (white min = Bi-S-Te)
WAN4-2-234A	KPW3-03	14/12/02	4.42	97.22	0	101.64	0.97	4.47	0	7.68	92.32	0	957		Minor iron contamination (host?)
WAN4-2-234B	wan4-2-234B-04	13/01/03	4.59	92.58	0	97.17	0.94	4.39	0	8.31	91.69	0	953		
WAN4-6-28	kp10-3-1r	14/12/02	9.28	87.71	0	96.99	1.08	4.3	0	16.20	83.80	0	904		repeat of 3-1
WAN4-6-28	kp10-1-1	14/12/02	12.11	82.18	0	94.29	1.18	4.24	0	21.21	78.79	0	872		largest Au grain - minor iron
WAN4-6-28	kp10-1-2	14/12/02	13.34	86.26	0	99.6	1.24	4.26	0	22.03	77.97	0	866		2nd largest Au grain - minor iron
WAN4-6-28	kp10-1-3	14/12/02	14.24	82.07	0	96.31	1.22	4.3	0	24.07	75.93	0	852		Next to largest Au grain
WAN4-6-28	kp10-4-2	14/12/02	20.39	79.45	0	99.84	1.35	4.13	0	31.93	68.07	0	796		Au
WAN4-6-28	kp10-4-4	14/12/02	19.32	74.97	0	94.29	1.34	4.06	0	32.02	67.98	0	795		smaller one close to large one.
WAN4-6-28	kp10-4-1	14/12/02	21.77	80.94	0	102.71	1.4	4.19	0	32.95	67.05	0	788		large grain
WAN4-6-28	kp10-2-3	14/12/02	23.33	79.02	0	102.35	1.41	4.19	0	35.05	64.95	0	772		gold in centre, right side
WAN4-6-28	kp10-2-2	14/12/02	22.97	77.8	0	100.77	1.4	4.16	0	35.05	64.95	0	772		Au to right, attached to
WAN4-6-28	kp10-2-1	14/12/02	24.57	72.67	0	97.25	1.43	4.08	0	38.20	61.80	0	747		Au at left in pyrite
WAN4-6-28	kp10-4-5	14/12/02	26.98	68.61	0	95.58	1.47	3.9	0	41.81	58.19	0	718		repeat of far right Au grain
Calibration = C:\MSEDS\USER\AUCU20KV.wds															
Settings: kV= 20, Angle= 40, B.C.= 5. Time: 40 seconds															

Sample ID corresponds to Sample Number or Microprobe Analysis number (S=sphalerite) in (Appendix 2)									
File Creation Date & Time,#2003-03-07#,#11:19:33#									
c:\mseds\user\sulf15kv.wds			*07/03/03 11:19*	*Livetime = 40. Sec*		*kV= 15*	*Angle= 40*	*B.C.= 10.*	
ID = cu stnd 15kv 10na		*Fe*	*Co*	*Cu*	*S*	*As*	*Zn*	*Sb*	***TOTAL***
ELEMENT		*0.68*	*0.1*	*0*	*33.57*	*0*	*66.77*	*0.02*	***101.13***
+/-2 SIGMA		*0.32*	*0.35*	*0*	*0.59*	*0*	*2.36*	*0.47*	
ATOM%		*0.58154*	*0.08026*	*0*	*50.2799*	*0*	*49.0513*	*0.00685*	
c:\mseds\user\sulf15kv.wds			07/03/03 11:20	Livetime = 40. Sec		Angle= 40	B.C.= 10.		
ID = BG05-sph2		Fe	Co	Cu	S	As	Zn	Sb	**TOTAL**
ELEMENT		0.57	0.04	0	33.66	0	66.93	0	**101.2**
+/-2 SIGMA		0.32	0.35	0	0.59	0	2.34	0	
ATOM%		0.48858	0.03564	0	50.3627	0	49.1129	0	
C:\MSEDS\USER\SULF15KV.wds			07/03/03 14:07	Livetime = 40. Sec		Angle= 40	B.C.= 10.		
ID = BG22-sph3		Fe	Co	Cu	S	As	Zn	Sb	**TOTAL**
ELEMENT		10.11	0	0	33.53	0	58.28	0	**101.92**
+/-2 SIGMA		0.56	0	0	0.57	0	2.17	0	
ATOM%		8.54257	0	0	49.3725	0	42.0849	0	
ID = bgu21-3-226-sph2		Fe	Co	Cu	S	As	Zn	Sb	**TOTAL**
ELEMENT		6.22	0	0	33.11	0	58.62	0	**97.96**
+/-2 SIGMA		0.49	0	0	0.57	0	2.2	0	
ATOM%		5.46069	0	0	50.6039	0	43.9353	0	
C:\MSEDS\USER\SULF15KV.wds			07/03/03 14:55	Livetime = 40. Sec		Angle= 40	B.C.= 10.		
ID = bg1-4a-330-sph2		Fe	Co	Cu	S	As	Zn	Sb	**TOTAL**
ELEMENT		11.36	0	0	32.97	0	56.19	0	**100.52**
+/-2 SIGMA		0.61	0	0	0.58	0	2.14	0	
ATOM%		9.72851	0	0	49.1739	0	41.0975	0	
C:\MSEDS\USER\SULF15KV.wds			07/03/03 15:06	Livetime = 40. Sec		Angle= 40	B.C.= 10.		
ID = bgu30-3-180-sph1		Fe	Co	Cu	S	As	Zn	Sb	**TOTAL**
ELEMENT		10.57	0.06	0	33.22	0	57.22	0.36	**101.42**
+/-2 SIGMA		0.58	0.4	0	0.57	0	2.13	0.46	
ATOM%		8.99033	0.04604	0	49.234	0	41.5898	0.13972	
C:\MSEDS\USER\SULF15KV.wds			07/03/03 15:15	Livetime = 40. Sec		Angle= 40	B.C.= 10.		
ID = bg06-sph2		Fe	Co	Cu	S	As	Zn	Sb	**TOTAL**
ELEMENT		8.65	0	0.24	33.1	0	57.05	0.27	**99.3**
+/-2 SIGMA		0.55	0	0.57	0.57	0	2.16	0.45	
ATOM%		7.4973	0	0.1823	49.9728	0	42.2411	0.10635	
C:\MSEDS\USER\SULF15KV.wds			07/03/03 15:22	Livetime = 40. Sec		Angle= 40	B.C.= 10.		
ID = bg24-sph2		Fe	Co	Cu	S	As	Zn	Sb	**TOTAL**
ELEMENT		0.77	0	0.16	32.98	0	66.5	0	**100.41**
+/-2 SIGMA		0.31	0	0.59	0.57	0	2.31	0	
ATOM%		0.67247	0	0.12042	49.8818	0	49.3252	0	
C:\MSEDS\USER\SULF15KV.wds			07/03/03 15:42	Livetime = 40. Sec		Angle= 40	B.C.= 10.		
ID = W3-sph1		Fe	Co	Cu	S	As	Zn	Sb	**TOTAL**
ELEMENT		11.76	0	0	33.42	0	53.71	0.16	**99.05**
+/-2 SIGMA		0.59	0	0	0.57	0	2.12	0.46	
ATOM%		10.1469	0	0	50.2135	0	39.5751	0.06427	
C:\MSEDS\USER\SULF15KV.wds			07/03/03 15:51	Livetime = 40. Sec		Angle= 40	B.C.= 10.		
ID = bgu21-2-13-3a-sph4		Fe	Co	Cu	S	As	Zn	Sb	**TOTAL**
ELEMENT		8.65	0	1.96	33.2	0	56.56	0	**100.38**
+/-2 SIGMA		0.53	0	0.64	0.57	0	2.15	0	
ATOM%		7.42631	0	1.48061	49.6302	0	41.4628	0	
C:\MSEDS\USER\SULF15KV.wds			07/03/03 16:08	Livetime = 40. Sec		Angle= 40	B.C.= 10.		
ID = bg13-sph4		Fe	Co	Cu	S	As	Zn	Sb	**TOTAL**
ELEMENT		2.6	0.11	0	33.48	0	66.99	0	**103.18**
+/-2 SIGMA		0.38	0.37	0	0.58	0	2.29	0	
ATOM%		2.20049	0.08838	0	49.3158	0	48.3953	0	
C:\MSEDS\USER\SULF15KV.wds			07/03/03 16:25	Livetime = 40. Sec		Angle= 40	B.C.= 10.		
ID = kp11-sph2		Fe	Co	Cu	S	As	Zn	Sb	**TOTAL**
ELEMENT		3.31	0	0	33.42	0	63.71	0.23	**100.66**
+/-2 SIGMA		0.4	0	0	0.57	0	2.25	0.47	
ATOM%		2.84966	0	0	50.1634	0	46.8959	0.09094	

Appendix 6

Drill Log Sources

Description of database codes

Logs for drillholes from this study (Big Gossan, Wanagon Gold, GRS125, GRS127)

Detailed Geology logs (West Grasberg, VZW53)

Collar and survey data for all drillholes sampled in this study

Sources for Data and Drilllog Codes (Appendix 6)

Data Sources:

Area	Drillhole prefix	Sources for Drill Logs
Kucing Liar (Section C)	GRS	Drill logging from this study
Big Gossan (Section B)	BG and BGU	Derived from superb original PT Freeport hard copy drill logs. This Study: approximately 5 drillholes were relogged on each cross section against original logs. Logging was validated with 3D geological model created in GEMCOM.
Wanagon Gold (Section B)	WAN	Derived from original PT Freeport hard copy drill logs. This Study: All drillholes were relogged against original logs. Logging was validated with 3D geological model created in GEMCOM.
West Grasberg (Section A)	WGR and WGZ	This Study: Drillholes were relogged (some referral to original PT Freeport hard copy drill logs and cross sections). Logging was validated with 3D geological model created in GEMCOM.
GIC marble (Section C)	VZW53	Derived from original PT Freeport hard copy drill log. This Study: Drillhole was relogged against original log.

Data Column	Code	Description
Formation	Kk	Kembelangan (undifferentiated)
Formation	Kkeh	Kembelangan Shale
Formation	Kkel	Kembelangan Limestone
Formation	Kkes	Kembelangan Sandstone
Formation	Qa	Quaternary (undifferentiated)
Formation	Tf	Faumai Formation
Formation	Tgcb	Banded Clay
Formation	Tgdfa	Dalam volcanics and intrusives
Formation	Tipw	Wanagon Sill
Formation	Tk	Kais Formation
Formation	Tk1	Kais Formation (unit 1)
Formation	Tk2	Kais Formation (unit 2)
Formation	Tk3	Kais Formation (unit 3)
Formation	Ts	Sirga Formation
Formation	Tw	Waripi Formation
Formation	unk	unknown
Lithology	bc	Banded Clay
Lithology	bx	breccia
Lithology	bxh	breccia - hydrothermal
Lithology	bxi	breccia - intrusive
Lithology	bxu	breccia (undescribed)
Lithology	cly	clay
Lithology	cr	
Lithology	cs	
Lithology	cz	
Lithology	dia	Dalam volcanics and intrusives
Lithology	dio	diorite
Lithology	do	dolostone
Lithology	flt	fault
Lithology	gbx	breccia (intrusive with abundant sulphides)
Lithology	hf	hornfels
Lithology	ls-b	limestone black
Lithology	ls-bf	limestone buff
Lithology	ls-gy	limestone grey
Lithology	ls-ss	limestone sandy
Lithology	ls-st	limestone-sandstone
Lithology	mar	marble
Lithology	mbl	marble
Lithology	ms	massive sulphide
Lithology	mzp	monzodiorite porphyry
Lithology	qt	quartzite
Lithology	sh-cb	shale (carbonaceous)
Lithology	sk	skarn
Lithology	ss	sandstone
Lithology	unk	unknown
Protolith	bxa	breccia

Sources for Data and Drilllog Codes (Appendix 6)

Data Column	Code	Description
Protolith	bxh	hydrothermal breccia
Protolith	bxi	intrusive breccia
Protolith	cly	clay
Protolith	dio	diorite
Protolith	dol	dolomite
Protolith	do-ss	dolostone - sandy
Protolith	ls	limestone
Protolith	ls-ss	limestone - sandy
Protolith	ls-st	limestone
Protolith	mar	marble
Protolith	mzp	monzodiorite porphyry
Protolith	sh	shale
Protolith	sh-cb	shale (carbonaceous)
Protolith	ss	sandstone
Protolith	ss-ls	sandstone - limestone
Protolith	unk	unknown
Structure	bfx	fractures with black clay/carbonaceous fracture fill
Structure	bx	brecciated
Structure	fbx	fault breccia
Structure	flt	fault
Structure	fx	fractured
Structure	ms	massive sulphide
Structure	wf	weakly fractured
Structure infill	blk	black clay (possible carbonaceous)
Structure infill	cy	clay
Structure infill	fe	Iron-oxide
Structure infill	py	pyrite
Structure infill	sk	skarn
Structure infill	yw	white clay with yellow crystals (allophane - Section A)

Appendix 6 - Big Gossan, Wanagon Gold, GRS125, GRS127 Drilllogs (for samples in this study)

HOLE-ID	FROM (m)	TO (m)	FORMATION	PROTOLITH	LITHOLOGY	STRUCTURE
BG01-04	0	10.6	Qa	unk	unk	
BG01-04	10.6	19.4	Tw	ls-st	ca	wf
BG01-04	19.4	85.7	Tw	ls-ss	ca	bx
BG01-04	85.7	142	Tw	ls-ss	ca	wf
BG01-04A	111	141	Tw	ls-st	ca	
BG01-04A	141	151.8	Tw	ls-ss	ca	bx
BG01-04A	151.8	154	unk	dio	dio	wf
BG01-04A	154	212	Tw	dol	ca	bx
BG01-04A	212	220.3	Tw	ls-ss	ca	wf
BG01-04A	220.3	227.6	unk	dio	dio	wf
BG01-04A	227.6	256.6	unk	unk	ca	bx
BG01-04A	256.6	265.6	unk	unk	ca	bx
BG01-04A	265.6	329.5	Tw	ls-ss	ca	wf
BG01-04A	329.5	337.45	Tw	unk	ms	bx
BG01-04A	337.45	360.6	Tw	dol	ca	wf
BG01-04A	360.6	385.8	Kkel	ls-ss	sk	wf
BG01-04A	385.8	395.9	Kkel	ls-ss	ca	fx
BG01-04A	395.9	400.7	Kkel	ls-ss	ms	wf
BG01-04A	400.7	414.7	Kkel	ls-ss	ca	wf
BG01-04A	414.7	464.85	Kkel	ls-ss	ca	wf
BG01-04A	464.85	513.5	Kkel	ls-ss	sk	wf
BG01-04A	513.5	514.5	Kkel	ls-ss	ca	wf
BG01-04A	514.5	527.1	Kkel	ls-ss	sk	wf
BG01-04A	527.1	719.9	Kkel	ls-ss	hf	wf
BG01-04A	719.9	749.9	Kkel	ls-ss	hf	wf
BG01-04A	749.9	952.6	Kkes	ss	hf	wf
BG01-04A	952.6	957.9	Kkes	ss	hf	bx
BG01-04A	957.9	985.8	Kkes	ss	hf	wf
BG01-05	0	13.5	Qa	unk	unk	
BG01-05	13.5	54.1	Tw	ss-st	ss	wf
BG01-05	54.1	148.5	Tw	ls-ss	ca	bx
BG01-05	148.5	166.05	Tw	ss	ss	bx
BG01-05	166.05	169.2	unk	dio	dio	bx
BG01-05	169.2	258.8	Tw	ls-ss	ca	bx
BG01-05	258.8	293.2	Tw	ls-ss	ca	wf
BG01-05	293.2	312.6	Tw	ls-ss	ca	fx
BG01-05	312.6	329.3	Tw	ls-ss	ca	bx
BG01-05	329.3	337.95	unk	unk	sk	wf
BG01-05	337.95	383.9	Tw	ls-ss	ca	bx
BG01-05	383.9	448.9	Tw	ls	ca	fx
BG01-05	448.9	493.8	Kkel	unk	sk	ms
BG01-05	493.8	517	Kkel	ls-ss	sk	ms
BG01-05	517	630.5	Kkel	ls-ss	sk	ms
BG01-05	630.5	690.6	Kkel	ls-ss	hf	ms
BG01-05	690.6	794	Kkel	ls-ss	hf	ms
BG01-05	794	800	Kkel	ls-ss	hf	ms
BG01-07A	0	13.8	Qa	unk	unk	
BG01-07A	13.8	97.6	Tw	ls-st	ca	fx
BG01-07A	97.6	153	Tw	ls-ss	ca	bx
BG01-07A	153	254.2	Tw	ls-ss	ca	bx
BG01-07A	254.2	345.7	Tw	ls-ss	ca	fx
BG01-07A	345.7	353.6	Tw	ls-ss	sk	bx
BG01-07A	353.6	392.1	Tw	ls-ss	sk	
BG01-07A	392.1	428.3	Tw	ls-ss	sk	bx
BG01-07A	428.3	605	?Kkeh/Kkel	unk	sk	
BG01-07A	605	686	Kkel	ls-ss	hf	
BGU19-03	0	101.7	Tw	dol	ca	bx
BGU19-03	101.7	153.6	unk	dio	dio	bx
BGU19-03	153.6	182.2	Tw	dol	ca	bx
BGU19-03	182.2	201	unk	unk	sk	ms
BGU19-03	201	224.5	unk	unk	sk	ms
BGU19-03	224.5	227.3	Kkeh	sh	hf	ms
BGU19-03	227.3	250	Kkel	ls-ss	hf	ms
BGU21-01	0	75	Tw	dol	ca	bx
BGU21-01	75	94.7	Tw	dol	ca	fx
BGU21-01	94.7	115.9	unk	dio	dio	bx
BGU21-01	115.9	148.6	Tw	dol	ca	fx

Appendix 6 - Big Gossan, Wanagon Gold, GRS125, GRS127 Drilllogs (for samples in this study)

HOLE-ID	FROM (m)	TO (m)	FORMATION	PROTOLITH	LITHOLOGY	STRUCTURE
BGU21-01	148.6	188.1	Tw	dol	sk	wf
BGU21-01	188.1	192.5	Kkeh	sh	hf	wf
BGU21-01	192.5	205.5	Kkel	ls-ss	hf	wf
BGU21-02	0	83.4	Tw	dol	ca	bx
BGU21-02	83.4	96.4	Tw	dol	ca	fx
BGU21-02	96.4	125.2	unk	dio	dio	bx
BGU21-02	125.2	171.9	Tw	dol	ca	fx
BGU21-02	171.9	205.3	Tw	dol	sk	fx
BGU21-02	205.3	210	Kkeh	sh	hf	wf
BGU21-02	210	219	Kkel	ls-ss	sk	wf
BGU21-02	219	232.5	Kkel	ls-ss	hf	wf
BGU21-03	0	84	Tw	dol	ca	bx
BGU21-03	84	108	Tw	dol	ca	fx
BGU21-03	108	132.3	unk	dio	dio	bx
BGU21-03	132.3	163.8	Tw	dol	ca	wf
BGU21-03	163.8	202.2	Tw	dol	ca	wf
BGU21-03	202.2	231.4	Tw	dol	sk	fx
BGU21-03	231.4	236.3	Kkeh	sh	hf	wf
BGU21-03	236.3	251.1	Kkel	ls-ss	sk	wf
BGU21-05	0	93	Tw	dol	ca	bx
BGU21-05	93	96	unk	unk	sk	wf
BGU21-05	96	112.8	unk	dio	dio	bx
BGU21-05	112.8	132.8	Tw	dol	ca	wf
BGU21-05	132.8	150.2	Tw	unk	sk	fx
BGU21-05	150.2	190.7	unk	unk	sk	fx
BGU21-05	190.7	195.4	Kkeh	sh	hf	wf
BGU21-05	195.4	201	Kkel	ls-ss	sk	wf
BGU21-05	201	204	Kkel	ls-ss	hf	wf
BGU21-10	0	93	Tw	dol	ca	bx
BGU21-10	93	116	Tw	dol	ca	fx
BGU21-10	116	131	unk	dio	dio	bx
BGU21-10	131	189	Tw	dol	ca	fx
BGU21-10	189	225.5	Tw	dol	ca	ms
BGU21-10	225.5	246.4	unk	unk	sk	wf
BGU21-10	246.4	256	unk	unk	sk	wf
BGU21-10	256	262.3	Kkeh	sh	hf	wf
BGU21-10	262.3	268	Kkel	ls-ss	hf	wf
BGU22-01	0	113.1	Tw	dol	ca	bx
BGU22-01	113.1	172.5	Tw	unk	sk	fx
BGU22-01	172.5	177.3	Kkeh	sh	hf	wf
BGU22-01	177.3	186	Kkel	ls-ss	hf	wf
BGU22-01	186	195	Kkel	ls-ss	cr	wf
BGU23-02	0	77.4	Tw	dol	ca	bx
BGU23-02	77.4	88	unk	dio	dio	bx
BGU23-02	88	117.4	Tw	dol	ca	fx
BGU23-02	117.4	165.3	unk	unk	sk	ms
BGU23-02	165.3	169.6	Kkeh	sh	hf	ms
BGU23-02	169.6	178	Kkel	ls-ss	hf	ms
BGU23-03	0	77.1	Tw	dol	ca	bx
BGU23-03	77.1	86.2	Tw	dol	ca	fx
BGU23-03	86.2	104.1	unk	dio	dio	bx
BGU23-03	104.1	143.5	Tw	dol	ca	fx
BGU23-03	143.5	175.6	Tw	dol	ca	wf
BGU23-03	175.6	185.1	unk	unk	sk	wf
BGU23-03	185.1	190.1	Kkeh	sh	hf	wf
BGU23-03	190.1	200.5	Kkel	ls-ss	hf	wf
BGU23-05	0	103.3	Tw	dol	ca	bx
BGU23-05	103.3	178.3	unk	unk	sk	wf
BGU23-05	178.3	183	Kkeh	sh	hf	ms
BGU23-05	183	201	Kkel	ls-ss	sk	ms
BGU23-05	201	212	Kkel	ls-ss	hf	wf
BGU23-05	212	268.1	Kkel	ls-ss	hf	wf
BGU23-05	268.1	286	Kkes	ss	ss	wf
BGU23-06	0	136.6	Tw	dol	ca	bx
BGU23-06	136.6	146.5	unk	unk	sk	wf
BGU23-06	146.5	153.6	Tw	dol	ca	bx
BGU23-06	153.6	236.8	unk	unk	sk	wf

Appendix 6 - Big Gossan, Wanagon Gold, GRS125, GRS127 Drilllogs (for samples in this study)

HOLE-ID	FROM (m)	TO (m)	FORMATION	PROTOLITH	LITHOLOGY	STRUCTURE
BGU23-06	236.8	239.2	Kkeh	sh	hf	wf
BGU23-06	239.2	245.9	Tw	dol	sk	wf
BGU23-06	245.9	250.9	Kkeh	sh	hf	wf
BGU23-06	250.9	268.8	Kkel	ls-ss	sk	wf
BGU23-06	268.8	302.2	Kkel	ls-ss	hf	wf
BGU23-08	0	80	Tw	dol	ca	bx
BGU23-08	80	101.3	Tw	dol	ca	wf
BGU23-08	101.3	107.3	unk	dio	dio	bx
BGU23-08	107.3	140.5	Tw	dol	ca	wf
BGU23-08	140.5	144	unk	unk	sk	wf
BGU23-08	144	199.3	Tw	dol	ca	wf
BGU23-08	199.3	203.5	unk	unk	sk	wf
BGU23-08	203.5	208.9	Kkeh	sh	hf	wf
BGU23-08	208.9	220.5	Kkel	ls-ss	hf	ms
BGU24-08	0	22.4	Tw	dol	ca	bx
BGU24-08	22.4	125.5	Tw	dol	ca	fx?
BGU24-08	125.5	155.3	Tw	dol	ca	bx
BGU24-08	155.3	159.8	unk	dio	dio	wf
BGU24-08	159.8	192.2	Tw	dol	ca	bx
BGU24-08	192.2	244.9	unk	unk	sk	ms
BGU24-08	244.9	248.2	Kkeh	sh	hf	wf
BGU24-08	248.2	262.3	Kkel	ls-ss	sk	ms
BGU24-08	262.3	279	Kkel	ls-ss	hf	wf
BGU24-10	0	35.5	Tw	dol	ca	bx
BGU24-10	35.5	186	Tw	dol	ca	fx
BGU24-10	186	213	Tw	dol	ca	bx
BGU24-10	213	235.7	Tw	dol	ca	fx?
BGU24-10	235.7	251.9	unk	unk	sk	ms
BGU24-10	251.9	329	unk	unk	sk	ms
BGU24-10	329	337.2	Kkeh	sh	hf	wf
BGU24-10	337.2	348	Kkel	ls-ss	sk	wf
BGU24-10	348	351	Kkel	ls-ss	hf	ms
BGU24-11	0	41.8	Tw	dol	ca	bx
BGU24-11	41.8	162.2	Tw	dol	ca	fx
BGU24-11	162.2	259.8	Tw	dol	ca	bx
BGU24-11	259.8	266.4	unk	dio	dio	wf
BGU24-11	266.4	274.2	Tw	dol	ca	bx
BGU24-11	274.2	282	unk	unk	sk	ms
BGU24-11	282	384	unk	unk	sk	ms
BGU24-11	384	414.2	unk	unk	sk	ms
BGU24-11	414.2	417.8	Kkeh	sh	hf	wf
BGU24-11	417.8	451.5	Kkel	ls-ss	sk	ms
BGU24-11	451.5	483	Kkel	ls-ss	hf	wf
BGU24-13	0	21	Tw	dol	ca	bx
BGU24-13	21	48	Tw	dol	ca	fx
BGU24-13	48	89.9	Tw	dol	ca	bx?
BGU24-13	89.9	101.8	unk	dio	dio	wf
BGU24-13	101.8	125.9	Tw	dol	ca	wf
BGU24-13	125.9	153.7	unk	unk	sk	ms
BGU24-13	153.7	179.1	Tw	dol	ca	ms
BGU24-13	179.1	189.6	unk	unk	sk	ms
BGU24-13	189.6	195.2	Kkeh	sh	hf	wf
BGU24-13	195.2	204	Kkel	ls-ss	sk	ms
BGU26-01	0	59.7	Tw	dol	ca	wf
BGU26-01	59.7	90	Tw	dol	ca	bx
BGU26-01	90	148.3	Tw	dol	ca	fx
BGU26-01	148.3	170.1	unk	unk	sk	ms
BGU26-01	170.1	173	Kkeh	sh	hf	ms
BGU26-01	173	204	Kkel	ls-ss	sk	ms
BGU26-01	204	246.7	Kkel	ls-ss	hf	ms
BGU26-01	246.7	249	Kkes	ss	qt	ms
BGU26-01	249	251	unk	dio	dio	ms
BGU26-01	251	266.6	Kkes	ss	qt	ms
BGU26-02	0	73.5	Tw	dol	ca	wf
BGU26-02	73.5	132.7	Tw	dol	ca	fx
BGU26-02	132.7	148.8	Tw	dol	ca	bx
BGU26-02	148.8	171.9	unk	unk	sk	ms

Appendix 6 - Big Gossan, Wanagon Gold, GRS125, GRS127 Drilllogs (for samples in this study)

HOLE-ID	FROM (m)	TO (m)	FORMATION	PROTOLITH	LITHOLOGY	STRUCTURE
BGU26-02	171.9	210.8	unk	unk	sk	ms
BGU26-02	210.8	212.4	Kkeh	sh	hf	ms
BGU26-02	212.4	219	Kkel	ls-ss	sk	ms
BGU26-02	219	311.1	Kkel	ls-ss	hf	ms
BGU26-02	311.1	315	Kkes	ss	qt	ms
BGU26-03	0	63	Tw	dol	ca	wf
BGU26-03	63	136.9	Tw	dol	ca	fx
BGU26-03	136.9	142.2	unk	unk	sk	ms
BGU26-03	142.2	147.8	Kkeh	sh	hf	wf
BGU26-03	147.8	155.6	Kkel	ls-ss	sk	ms
BGU26-03	155.6	171	Kkel	ls-ss	hf	ms
BGU26-04	0	87	Tw	dol	ca	wf
BGU26-04	87	177	Tw	dol	ca	fx
BGU26-04	177	189	Tw	dol	sk	fx
BGU26-04	189	205.4	Tw	dol	ca	fx
BGU26-04	205.4	219.8	unk	unk	sk	ms
BGU26-04	219.8	280.8	unk	unk	sk	ms
BGU26-04	280.8	285	Kkeh	sh	hf	wf
BGU26-04	285	300	Kkel	ls-ss	sk	ms
BGU26-04	300	363	Kkel	ls-ss	hf	ms
BGU26-10	0	213.2	Tw	dol	ca	wf
BGU26-10	213.2	218.7	Tw	dol	ca	bx
BGU26-10	218.7	220.5	Tw	sl-ss	hf	ms
BGU26-10	220.5	227	Kkeh	sh	hf	ms
BGU26-10	227	231	Kkel	ls-ss	hf	ms
BGU27-02	0	69	Tw	dol	ca	wf
BGU27-02	69	122.6	Tw	dol	ca	wf
BGU27-02	122.6	139.8	Tw	dol	ca	bx
BGU27-02	139.8	191.7	unk	unk	sk	ms
BGU27-02	191.7	196	Kkeh	sh	hf	ms
BGU27-02	196	288	Kkel	ls-ss	hf	ms
BGU27-02	288	302.7	unk	ls-ss	sk	wf
BGU27-02	302.7	324	Kkes	ss	qt	wf
BGU27-04	0	69	Tw	dol	ca	wf
BGU27-04	69	96	Tw	dol	ca	fx?
BGU27-04	96	108.8	Tw	dol	ca	wf
BGU27-04	108.8	114.1	Tw	dol	sk	wf
BGU27-04	114.1	145.7	Tw	dol	ca	fx?
BGU27-04	145.7	174.8	unk	unk	sk	wf
BGU27-04	174.8	180.8	Kkeh	sh	hf	wf
BGU27-04	180.8	197.9	Kkel	ls-ss	sk	wf
BGU27-05	0	66	Tw	dol	ca	wf
BGU27-05	66	114.3	Tw	dol	ca	wf
BGU27-05	114.3	124.8	unk	unk	ms	
BGU27-05	124.8	131.5	Tw	dol	ca	wf
BGU27-05	131.5	152.6	Tw	dol	ms	wf
BGU27-05	152.6	160.5	unk	unk	sk	ms
BGU27-05	160.5	162.6	Kkeh	sh	hf	wf
BGU27-05	162.6	183.8	Kkel	ls-ss	sk	wf
BGU27-05	183.8	201	Kkel	ls-ss	hf	wf
BGU27-06	0	120.4	Tw	dol	ca	wf
BGU27-06	120.4	243.2	Tw	dol	ca	wf
BGU27-06	243.2	273.6	unk	unk	sk	ms
BGU27-06	273.6	290.7	Tw	dol	ca	wf
BGU27-06	290.7	402	unk	unk	sk	ms
BGU27-06	402	430.8	unk	unk	sk	bx
BGU27-06	430.8	440.6	Kkeh	sh	hf	wf
BGU27-06	440.6	468.5	Kkel	ls-ss	sk	wf
BGU28-01	0	151.7	Tw	dol	ca	wf
BGU28-01	151.7	162.9	unk	unk	sk	ms
BGU28-01	162.9	167.3	Kkeh	sh	hf	ms
BGU28-01	167.3	189	Kkel	ls-ss	sk	ms
BGU28-05	0	135.2	Tw	dol	ca	wf
BGU28-05	135.2	143.3	unk	unk	sk	wf
BGU28-05	143.3	159.5	Tw	dol	ca	wf
BGU28-05	159.5	167.4	unk	unk	sk	wf
BGU28-05	167.4	169.5	Tw	dol	ca	wf

Appendix 6 - Big Gossan, Wanagon Gold, GRS125, GRS127 Drilllogs (for samples in this study)

HOLE-ID	FROM (m)	TO (m)	FORMATION	PROTOLITH	LITHOLOGY	STRUCTURE
BGU28-05	169.5	172.9	unk	unk	sk	wf
BGU28-05	172.9	206.5	Tw	dol	ca	wf
BGU28-05	206.5	225.6	unk	unk	sk	ms
BGU28-05	225.6	261.1	unk	unk	sk	ms
BGU28-05	261.1	268.7	Kkeh	sh	hf	ms
BGU28-05	268.7	289.8	Kkel	ls-ss	sk	ms
BGU28-05	289.8	306.9	Kkel	ls-ss	sk	ms
BGU28-05	306.9	415.9	Kkel	ls-ss	hf	ms
BGU28-05	415.9	447.6	Kkel	ls-ss	sk	ms
BGU28-05	447.6	477	Kkes	ss	qt	ms
BGU28-07	0	184.2	Tw	dol	ca	wf
BGU28-07	184.2	195	unk	unk	sk	wf
BGU28-07	195	196.6	unk	unk	ms	
BGU28-07	196.6	221.8	Tw	dol	ca	wf
BGU28-07	221.8	238.1	unk	unk	sk	ms
BGU28-07	238.1	263.1	Tw	dol	ca	wf
BGU28-07	263.1	379.7	unk	unk	sk	wf
BGU28-07	379.7	381.9	Kkeh	sh	hf	ms
BGU28-07	381.9	422	Kkel	ls-ss	sk	ms
BGU28-07	422	436.4	Kkel	ls-ss	hf	ms
BGU28-07	436.4	471	Kkel	ls-ss	hf	ms
BGU28-08	0	360	Tw	dol	ca	wf
BGU28-08	360	369.9	unk	unk	sk	ms
BGU28-08	369.9	387.3	unk	unk	sk	wf
BGU28-08	387.3	409.2	Tw	dol	ca	ms
BGU28-08	409.2	470.6	Tw	dol	ca	bx
BGU28-08	470.6	630.3	unk	unk	sk	wf
BGU28-08	630.3	704.3	unk	unk	sk	wf
BGU28-08	704.3	723	Kkeh	sh	hf	wf
BGU29-01	0	122.6	Tw	dol	ca	wf
BGU29-01	122.6	200.1	Tw	dol	ca	wf
BGU29-01	200.1	206.3	unk	unk	sk	wf
BGU29-01	206.3	210	Kkeh	sh	hf	wf
BGU29-01	210	238.5	Kkel	ls-ss	sk	ms
BGU29-01	238.5	325.8	Kkel	ls-ss	hf	ms
BGU29-01	325.8	343.7	Kkel	ss-ls	hf	ms
BGU29-01	343.7	354	Kkes	ss	qt	ms
BGU29-02	0	184.8	Tw	dol	ca	wf
BGU29-02	184.8	238.9	Tw	dol	ca	wf
BGU29-02	238.9	254.2	unk	unk	sk	wf
BGU29-02	254.2	301.5	Tw	dol	ca	wf
BGU29-02	301.5	320.6	unk	unk	sk	ms
BGU29-02	320.6	330.4	Kkeh	sh	hf	ms
BGU29-02	330.4	357.5	Kkel	ls-ss	sk	ms
BGU29-02	357.5	520	Kkel	ls-ss	hf	ms
BGU29-02	520	539.7	Kkel	ls-ss	sk	ms
BGU29-02	539.7	555.4	Kkes	ss	qt	ms
BGU29-07	0	167	Tw	dol	ca	wf
BGU29-07	167	179	unk	unk	sk	ms
BGU29-07	179	206.5	Tw	dol	ca	ms
BGU29-07	206.5	213.5	unk	unk	sk	ms
BGU29-07	213.5	216.6	Kkeh	sh	hf	ms
BGU29-07	216.6	233.3	Kkel	ls-ss	hf	ms
BGU30-03	0	179.9	Tw	dol	ca	wf
BGU30-03	179.9	181.1	unk	unk	sk	ms
BGU30-03	181.1	205.45	Tw	dol	ca	wf
BGU30-03	205.45	254.7	Tw	dol	ca	bx?
BGU30-03	254.7	272.4	Tw	dol	ca	wf
BGU30-03	272.4	289.6	unk	unk	sk	wf
BGU30-03	289.6	299.5	Kkeh	sh	hf	wf
BGU30-03	299.5	346	Kkel	ls-ss	sk	wf
BGU30-04	0	360	Tw	dol	ca	wf
BGU30-04	360	392	Tw	dol	ca	fz?
BGU30-04	392	398.2	Tw	dol	ca	wf
BGU30-04	398.2	405.2	unk	unk	sk	ms
BGU30-04	405.2	415.6	Kkeh	sh	hf	wf
BGU30-04	415.6	457	Kkel	ls-ss	sk	wf

Appendix 6 - Big Gossan, Wanagon Gold, GRS125, GRS127 Drilllogs (for samples in this study)

HOLE-ID	FROM (m)	TO (m)	FORMATION	PROTOLITH	LITHOLOGY	STRUCTURE
BGU30-04	457	494	Kkel	ls-ss	hf	wf
BGU30-05	0	105.6	Tw	dol	ca	wf
BGU30-05	105.6	425.3	Tw	dol	ca	wf
BGU30-05	425.3	446	unk	unk	sk	ms
BGU30-05	446	491	Tw	dol	ca	wf
BGU30-06	0	110.6	Tw	dol	ca	wf
BGU30-06	110.6	144.3	Tw	dol	ca	wf
BGU30-06	144.3	156.5	unk	unk	sk	ms
BGU30-06	156.5	171.4	Tw	dol	ca	wf
BGU30-06	171.4	182.7	unk	unk	sk	ms
BGU30-06	182.7	189	Kkeh	sh	hf	ms
BGU30-06	189	195.6	Kkel	ls-ss	sk	ms
BGU30-06	195.6	250	Kkel	ls-ss	hf	ms
BGU30-08	0	88	Tw	dol	ca	wf
BGU30-08	88	260	Tw	dol	ca	wf
GRS-125	0	40	Tk	unk	unk	
GRS-125	40	74	Ts	unk	unk	
GRS-125	74	618	Tf	unk	unk	
GRS-125	618	635	Tw	unk	unk	
GRS-125	635	673	Tw	unk	unk	
GRS-125	673	799	Tw	unk	unk	
GRS-125	799	920.6	Tw	unk	unk	
GRS-127	0	135	Tk3	unk	unk	
GRS-127	135	368	Tk2	unk	unk	
GRS-127	368	400	Tk1	unk	unk	
GRS-127	400	713	Tf	unk	unk	
GRS-127	713	724	Tf	unk	unk	
GRS-127	724	875	Tf	unk	unk	
GRS-127	875	1097	Tw	unk	unk	
GRS-127	1097	1132.2	Tw	unk	unk	
GRS-127	1132.2	1180	Kkel	unk	unk	
GRS-127	1180	1186.5	Tgi	unk	unk	
GRS-127	1186.5	1224	Kkes	unk	unk	
GRS-127	1224	1300	Tw	unk	unk	
GRS-127	1300	1411	Kk	unk	unk	
WAN1-1	0	170	Tipw	mzp	mzp	
WAN1-1	170	171.15	Tipw	mzp	sk	
WAN1-1	171.15	191.05	Tipw	mzp	sk	
WAN1-1	191.05	196.9	Tipw	mzp	flt	flt
WAN1-1	196.9	198.4	Tipw	mzp	sk	
WAN1-1	198.4	283.7	Tw	do-ss	mar	fx
WAN1-1	283.7	427.5	Tipw	mzp	mzp	
WAN1-1	427.5	428.4	Tipw	mzp	flt	flt
WAN1-1	428.4	488.9	Tipw	mzp	mzp	
WAN1-1	488.9	505.3	Tw	do-ss	flt?	flt
WAN1-1	505.3	620.05	Tw	do-ss	mar	bx
WAN1-1	620.05	622.1	Tw	do-ss	sk	fx
WAN1-1	622.1	623.55	Tw	do-ss	mar	
WAN1-1	623.55	624.95	Tw	do-ss	sk	fx
WAN1-1	624.95	633.5	Tw	do-ss	mar	
WAN1-1	633.5	645.1	Kkeh	sh	hf	fx
WAN1-1	645.1	983.2	Kkel	ls-ss	hf	fx
WAN1-3	0	193.1	Tipw	mzp	mzp	
WAN1-3	193.1	219.4	Tipw	mzp	mzp	
WAN1-3	219.4	309.4	Tw	do-ss	mar	bx
WAN1-3	309.4	549.5	Tipw	mzp	mzp	
WAN1-3	549.5	558.2	Tw	do-ss	mar	bx
WAN1-3	558.2	593.4	Tipw	mzp	mzp	
WAN1-3	593.4	597.3	Tipw	mzp	sk	
WAN1-3	597.3	603.2	Tipw	mzp	mzp	
WAN1-3	603.2	614.3	Tipw	mzp	mzp	
WAN1-3	614.3	630.3	Tipw	mzp	sk	
WAN1-3	630.3	665.1	Tw	do-ss	sk	fx
WAN1-3	665.1	673.3	Tipw	mzp	mzp	
WAN1-3	673.3	684.6	Tipw	mzp	sk	
WAN1-3	684.6	740.2	Tipw	mzp	mzp	
WAN1-3	740.2	746.9	Tipw	mzp	sk	

Appendix 6 - Big Gossan, Wanagon Gold, GRS125, GRS127 Drilllogs (for samples in this study)

HOLE-ID	FROM (m)	TO (m)	FORMATION	PROTOLITH	LITHOLOGY	STRUCTURE
WAN1-3	746.9	819	Tw	do-ss	sk	fx
WAN1-3	819	833.7	Tipw	mzp	sk	
WAN1-3	833.7	842.4	Tipw	mzp	mzp	
WAN1-3	842.4	868.3	Kkeh	sh	hf	
WAN1-3	868.3	890.3	Tipw	mzp	mzp	
WAN1-3	890.3	900.2	Kkeh	sh	hf	
WAN1-3	900.2	999.7	Kkel	ls-ss	hf	fx
WAN2-2	0	283.9	Tipw	mzp	mzp	
WAN2-2	283.9	316.9	Tipw	mzp	sk	bx
WAN2-2	316.9	340.9	Tipw	mzp	sk	fx
WAN2-2	340.9	365.9	Tw	do-ss	bx	bx
WAN2-2	365.9	395.3	Tipw	mzp	mzp	
WAN2-2	395.3	398.3	Tipw	mzp	sk	fx
WAN2-2	398.3	550.8	Tipw	mzp	mzp	
WAN2-2	550.8	552.5	Tw	do-ss	bx	bx
WAN2-2	552.5	556.1	Tw	do-ss	sk	
WAN2-2	556.1	571.5	Tipw	mzp	mzp	
WAN2-2	571.5	572.9	Tw	do-ss	bx	bx
WAN2-2	572.9	593.2	Tipw	mzp	mzp	
WAN2-2	593.2	596.3	Tw	do-ss	bx	bx
WAN2-2	596.3	597.8	Tipw	mzp	mzp	
WAN2-2	597.8	611.8	Tw	do-ss	mar	fx
WAN2-2	611.8	623.1	Tipw	mzp	mzp	
WAN2-2	623.1	664.9	Tw	do-ss	mar	fx
WAN2-2	664.9	693.8	Tipw	mzp	mzp	
WAN2-2	693.8	695.2	Tipw	mzp	sk	fx
WAN2-2	695.2	699.8	Tipw	mzp	mzp	
WAN2-2	699.8	700.4	Tipw	mzp	sk	
WAN2-2	700.4	833.3	Tw	do-ss	mar	fx
WAN2-2	833.3	878.6	Tw	do-ss	sk	
WAN2-2	878.6	902	Kkeh	sh	hf	fx
WAN2-2	902	966.9	Kkel	ls-ss	hf	fx
WAN4-1	0	16.5	Tw	do-ss	do	
WAN4-1	16.5	22.7	Tw	do-ss	flt	flt
WAN4-1	22.7	623.3	Kkes	ss	ss	fx
WAN4-2	0	190.9	Tw	do-ss	do	fx
WAN4-2	190.9	288.1	Tw	do-ss	bx	bx
WAN4-2	288.1	312.8	Kkeh	sh	hf	fx
WAN4-2	312.8	365.7	Kkel	ls-ss	hf	fx
WAN4-3	0	4	unk	unk	unk	
WAN4-3	4	94.8	Kkes	ss	ss	fx
WAN4-3	94.8	284.7	Kkel	ls-ss	hf	fx
WAN4-3	284.7	293.2	Kkeh	sh	hf	fx
WAN4-3	293.2	352	Tw	do-ss	mbl	fx
WAN4-4	0	4	Tw	do-ss	do	fx
WAN4-4	4	7	Tw	do-ss	flt	flt
WAN4-4	7	424	Kkes	ss	ss	fx
WAN4-5	0	4	Tw	do-ss	do	fx
WAN4-5	4	8.5	Tw	do-ss	flt	flt
WAN4-5	8.5	171	Kkes	ss	ss	fx
WAN4-5	171	174.4	Tif	dio	dio	ms
WAN4-5	174.4	193	Kkes	ss	ss	fx
WAN4-5	193	412	Kkel	ls-ss	hf	fx
WAN4-6	0	15.5	Tw	do-ss	do	fx
WAN4-6	15.5	19	Tw	do-ss	flt	flt
WAN4-6	19	205.3	Kkes	ss	ss	fx
WAN4-6	205.3	220.7	Tif	dio	dio	ms
WAN4-6	220.7	401	Kkes	ss	ss	ms

PT Freeport Indonesia SUMMARY LOGGING
VZW – 53A: (Redrill VZW-53)

Coordinates	**:**		**Proposed : ?m**
Northing	**:**	**9551750**	
Easting	**:**	**735000**	
Bearing	**:**	**0º**	
Inclination	**:**	**- 90°**	
Elevation	**:**	**3835 meters**	**Logged and Summarized by RMS**

0 – 96.80 m	**Tgdva (?) Andesite,** light gray to gray, strongly sil-clay-py altered, mostly textures already destroyed, locally relict plagioclase; anhedral, altered to white clay; highly broken core, brittle and broken along sheeting fractures 0-15 and 30-45 to CA; highly clay/gouge at 26.0-29.50m, 60.0-73.50m and 85.30-93.80m possibly related to fault.
96.80 – 132.80m	**Tgdva (?) Andesite,** light gray to gray, gradually increasing silica alteration, locally breccia-volcanic (?) highly broken core.
132.80-144.00m	**Tgdva (?) Andesite,** breccia-volcanic ?, silica-pyrite-magnetite, highly broken core and highly clay.
144.00-156.50m	**Tk1 ? marble,** pale gray, break-up and infilled by silica-sulphides. Broken core**.**
156.50-170.20m	**Tgdva (?), breccia,** silicified –sulphides-epidote and few marble; highly broken Core and clayey.
170.20-217.80m	**Tk1? Marble,** breccia; infilled by diopside-pyrite. Massive Highly fractures at 210.8-213.75m and 214.3-216.30m.
217.80-290.80m	**Tk1? Marble,** pale gray, locally break –up and infilled by sil-pyrite. At depth gradually color to gray. Broken core at 217.80-228.80m273.0-244.10m and 248.0-261.00m.
290.80-328.20m	**Tk1? Marble-breccia,** gray, breccia infilled by greenish garnet-diopside-pyrite±magnetite.broken-highly fractures at 293.40-297.5, 308-312.40 and 321.30-323.30m.
328.20-335.30m	**Tk1? Limestone-marbelized,** gray, fine grained, minor greenish garnet
335.30-340.40m	**Tk1 Limestone,** dark gray, abundant lenticular fossil; up to 30%.
340.40-345.10m	**Tk1, Limestone,** karstified breccia, broken, loose.
345.10-390.20m	**Tk1, Limestone,** gray-dark gray, abundant lenticular fossil; up to50%, Karstified breccia at **361.70-362.90m and 364.10-367.30m**; broken and loose. Broken core at 355.50-357.00m, 361.70-362.90m and 363.80-367.30m.
390.20-474.10m	**Tk1, Limestone,** gray-brownish, abundant lenticular fossil and brownish-algae?; mod x-cut calcite vnlts; common stylolites; karstified breccia at **415.90-417.20m**; broken core with black clay/shale at : 411.50-417.20m; 438.5-441.2m and 452.3-454.4m; weakly fractured.
474.10-489.80m	**Tk1; Limestone;** lt-gray; moderately lenticular forams and brownish-algae?; mod x-cut calcite vnlts; common stylolites; karstified breccia at **415.90-417.20m**; broken core with black clay/shale at : 411.50-417.20m; 438.5-441.2m and 452.3-454.4m; weakly fractured.

West Grasberg Drillhole Geology

SECT	Hole_ID	From (m)	To (m)	Formation	Protolith	Lithology	Gross Structure	Structure Infill	Description
1100	WGR-1	0	79	Tk	ls	ls-bf			Brown limestone with fossils. Minor black and increasing intensity past 20m. 31-37 has burrow/fossils and mottled alteration. 50m recent slickenside. 63-69m has round coral fossils. 69-73m has burrows. 73-76 is a mill breccia with 20cm breccia and limestone fragments
1100	WGR-1	79	105	Tk	ls	ls-bf	bfx	blk	black fracture up to 5cm in pale-brown limestone (variable alteration)
1100	WGR-1	105	108	Tk	ls	ls-bf			black alteration
1100	WGR-1	108	121	Tk	ls	ls-bf			pale-brown limestone with fossils. calcite veins and rare black fracture
1100	WGR-1	110	119	Tk	ls	ls-gy			dark-grey limestone (also at 77.7m)
1100	WGR-1	121	187	Tk	ls	ls-bf			dark-pale brown limestone with black alteration fronts. intense network of 2-5mm calcite veins and minor (10cm) breccia with calcite. Abundant fossils
1100	WGR-1	136	187	Tk	ls	ls-bf	bx	blk	mill breccia. v-broken core. black ?carbonaceous groundmass. some v pale brown (30cm) zones
1100	WGR-1	187	226	Tk	ls	ls-bf			black-brown limestone. abundant coral/burrow-fossils. rare calcite veins. one area of sulphur
1100	WGR-1	226	227	Tk	ls	ls-bf	bx		mill breccia. pale groundmass
1100	WGR-1	227	236	Tk	ls	ls-gy			dark grey limestone
1100	WGR-1	236	241	Tk	ls	ls-bf	bx	blk	mill breccia. v-broken core. black ?carbonaceous groundmass. some v pale brown (30cm) zones
1100	WGR-1	241	355.4	Tk	ls	ls-gy	bfx	blk	very mottled black ?carbonaceous-rich limestone and several black fracture/faults in each tray. 248.5-249.5 and at 251-252 are black ?carbonaceous-rich fault/fracture parallel to 30 degrees to core axis.
1275	WGR-10	0	3	Tgdfa	bxi	dia			Iron-oxide and white alteration
1275	WGR-10	3	22	Tgdfa	bxi	dia			Strong white clay alteration
1275	WGR-10	22	57	Tgdfa	bxi	dia	bx		strong white clay and strong green spots
1275	WGR-10	57	66	Tgdfa	bxi	dia	bx		intense white clay
1275	WGR-10	66	68	Tgdfa	bxi	dia	bx		intense white clay. slightly greenish
1275	WGR-10	68	74	Unk	bxh	gbx	bx		Breccia with intense pyrite alteration and 1m of green chlorite? Alteration. Push up gritty breccia with clay?
1275	WGR-10	74	90	Unk	bxh	gbx	bx		EOH. Gritty breccia? Essentially sand. Massive pyrite with rare 2cm clay lumps (clasts?)
1175	WGR-11	0	10	Tgdfa	bxi	dia	bx		Igneous - weak Iron-oxide and clay alteration
1175	WGR-11	10	22	Tgdfa	bxi	dia	bx		strong white alteration of igneous
1175	WGR-11	22	63	Tgdfa	bxi	dia	bx		mod white; strong green spot alteration of igneous
1175	WGR-11	63	91	Tgdfa	bxi	dia	bx		mod white; strong green spot and pyrite spot alteration of igneous.
1175	WGR-11	91	96	Tgdfa	bxi	dia	bx		Strong white. strong green spot alteration of igneous
1175	WGR-11	96	120	Tgdfa	bxi	dia	bx		strong white. mod green. mod pyrite spot.
1175	WGR-11	120	130	Tgdfa	bxi	dia	bx		mod white. mod green. mod pyrite spot. Igneous
1175	WGR-11	130	134	Tgdfa	bxi	dia	bx	yw	Igneous fragments. White-yellow clay on fracture as infill - does not alter
1175	WGR-11	134	148	Tgdfa	bxi	dia	bx		mod white alteration
1175	WGR-11	148	150.5	Tgdfa	bxi	dia	bx	yw	Fragments of pyrite altered fine grained rock. Igneous fragments with anhydrite spots
1175	WGR-11	150.5	152	Unk	bxh	gbx	bx		Gritty breccia with pyrite alteration
1175	WGR-11	152	183	Tgcb	cly	bc	bx	yw	Banded clay. most continuous piece = 10cm. many white-yellow veins. Variably broken
1175	WGR-11	183	185	Tk	ls	mar	fx	py	Marble - crackle broken tectonic with fine-grained disseminated pyrite infill in crackle
1175	WGR-11	185	200	Tk	ls	mar			Marble - white-grey. mottled
1175	WGR-11	200	215.5	Tk	ls	ls-gy			limestone. dark grey
1175	WGR-11	215.5	219	Tk	ss-ls	ss-ls			Gritty sandstone. 20cm limestone breccia at 216
1175	WGR-11	219	224	Tk	ls	ls-bf			grey-brown limestone
1175	WGR-11	224	260	Tk	ls	ls-bf			fossiliferrous brown limestone. Variable content of fossils?. decreases at end
1175	WGR-11	260	263	Tk	ls	ls-bf	bx		Breccia. limestone fragments. 3cm to sub-mm. Pyrite in matrix. 3mm epidote clast
1175	WGR-11	263	266.7	Tk	ls	ls-bf			limestone with strong black content

SECT	Hole_ID	From (m)	To (m)	Formation	Protolith	Lithology	Gross Structure	Structure Infill	Description
1175	WGR-11	266.7	268.5	Tk	ls	ls-bf	bx	blk	Breccia limestone. very black matrix. disseminated pyrite
1175	WGR-11	268.5	290.4	Tk	ls	ls-bf	bfx	blk	limestone . dark grey-black with 10-20cm black fracture zones at 278.7. 280. 280.4. 290. Minor crackle calcite zones
1175	WGR-11	290.4	292	Tk	ls	ls-bf	bx		Breccia. limestone fragments and black alteration of grey matrix.
1175	WGR-11	292	298.9	Tk	ls	ls-gy			dark-grey - black limestone. Minor crackle calcite zones
1175	WGR-11	298.9	368.8	Tk	ls	ls-bf			missing
1175	WGR-11	368.8	406	Tk	ls	ls-bf			brown fossiliferrous limestone (long fossils!)
1175	WGR-11	406	407	Tk	ls	ls-bf			porous broken zone. limestone is leached
1175	WGR-11	407	412	Tk	ls	ls-bf			Brown limestone. variable fossil fragments and fossils. Variable black alteration.
1175	WGR-11	412	415	Tk	ls	ls-bf	bx	blk	Brown fragments in breccia and black alteration of matrix. Pyrite specs
1175	WGR-11	415	458	Tk	ls	ls-bf			Brown limestone. variable fossil fragments and fossils. Variable black alteration.
1175	WGR-11	458	502.4	Tk	ls	ls-bf			Brown limestone. appears more silty. Variable fossil fragments and fossils. Variable black alteration.
0950	WGR-12	0	18	Tgdfa	bxi	dia	bx		Intrusive mill breccia
0950	WGR-12	18	25	Tgdfa	bxi	dia	bx		Intrusive mill breccia. Intense white clay alteration
0950	WGR-12	25	30	Tgdfa	bxi	dia	bx		Intrusive mill breccia. Breccia generally very fine mill. dominantly 0.5cm clasts and matrix support. Clasts up to 3cm and dominantly limestone - pale-grey and textureless (also igneous). Intense white clay alteration. One 2 cm piece may be banded (green-grey coloured). 25-26m. possible interval of Silica/quartz? nodules - may be veins - can see crystals on one side of lump.
0950	WGR-12	30	31	Tgdfa	bxi	dia	bx		Zone of very rubbly brown clay and possible opaline material. Host appear to be strong-white potassic altered igneous rock
0950	WGR-12	31	32	Tgdfa	bxi	dia	bx	yw	altered igneous rock. minor epidote visible. Yellow-white veins and crystals on fracture
0950	WGR-12	32	33	Tgcb	cly	bc	bx	yw	Banded cy with variable re-break by white-yellow. Black fragments with later pyrite also present within massive ore breccia zones (increasingly white altered to 33m).
0950	WGR-12	33	33.5	Tgcb	cly	bc	bx		Banded clay protolith. White altered - intense - can see relict texture.
0950	WGR-12	33.5	35	Tgdfa	cly	cly	bx		Breccia. Clay rich fragments - protolith unsure. ferrugenised. mill breccia texture apparent in some fragments
0950	WGR-12	35	38	Tgdfa	bxi	dia			Breccia with igneous material (hard in places). strong Iron-oxide. mod white clay alteration and white-yellow infill? Also present. Grey-white clay. minor pieces of core and opaline (green) stuff. minor ?carbonaceous-rich layers. Disseminated pyrite
0950	WGR-12	38	42.3	Tgdfa	bxi	dia			Breccia with igneous material (hard in places). strong Iron-ox. intense white clay alteration and white-yellow infill? also present. White clay. minor ?carbonaceous-rich material with sulphide/s. Mill breccia texture
0950	WGR-12	42.3	55	Tgcb	cly	bc			Banded cy fragments. variably contorted with breccia zones of clay. White yellow veins (banded fragments max 15cm before broken zone).
0950	WGR-12	55	55.1	Unk	bxh	gbx			Rare fragment of gritty breccia
0950	WGR-12	55.1	56.7	Unk	bxh	gbx			Intrusive breccia. Very fine rubble. possible banded clay fragment. dominantly clay material (alteration). Minor black
0950	WGR-12	56.7	59.8	Unk	unk	unk			grey and yellow dirt. minor fragments (breccia) with leached grey and white clay veins? (later or causing?)
0950	WGR-12	59.8	64.9	Unk	unk	unk			Intense black and sulphidic (pyrite) "dirt". Rare 5cm pieces of very leached material (boxworks and residual silica)
0950	WGR-12	64.9	71.3	Tk	ls	mar			Recrystallised pale grey limestone
0950	WGR-12	71.3	72	Tk	ls	mar	fx	blk	Marbleised? Limestone. very mottled. Minor pyrite? Veins overprinting wavy fracture (black) also vughy veins with fluorite
0950	WGR-12	72	74	Tk	ls	mar			very broken core. At 72m is a vughy sphalerite vein (fill only) - host = limestone - pale and vughy (weathered/leached?)
0950	WGR-12	74	77.25	Tk	ls	ls-bf			grey fossiliferrous limestone. Minor black fracture. limestone gets darker towards 77.25
0950	WGR-12	77.25	83.5	Tk	ls	ls-bf			pale grey-brown limestone with fossils
0950	WGR-12	83.5	85	Tk	mar	mar	bx		Intrusive breccia with marble and minor ?carbonaceous fragments which are <2cm and ovoid to rounded (pyrite in matrix and replacing ?carbonaceous fragments).
0950	WGR-12	85	89.4	Tk	ls	ls-bf			Dark grey limestone. fine-grained fossiliferrous (same as interval above - just dark)
0950	WGR-12	89.4	95	Tgdfa	bxi	bxi	bx		Intrusive breccia. matrix support. Pale grey dominantly intrusive fragments. 2nd breccia has minor limestone and shale fragments. (Contact ~94.1m). Sulphide (py) in 2nd breccia matrix.
0950	WGR-12	95	97.25	Tk	ls	ls-bf			Limestone. pale grey. Increase in black towards contact with a breccia at 97.25m

SECT	Hole_ID	From (m)	To (m)	Formation	Protolith	Lithology	Gross Structure	Structure Infill	Description
0950	WGR-12	97.25	103.45	Tgdfa	bxi	bxi	bx		Breccia. dark grey INTRUSIVE. Clast of breccia with igneous fragments is within (100.5m). Also shale fragments within. Pyrite. some replacement along some layers very fine and foliation? Marble altered limestone with stylolites at 104.45
0950	WGR-12	103.45	109.3	Tk	ls	ls-bf			Very ?carbonaceous altered and minor black fracture brown limestone with abundant fossil/burrows and coral. Calcite flooding may post date black alteration. Recent fault and intense ?carbonaceous at end of tray
0950	WGR-12	113	116.35	Tk	ls	ls-bf			V ?carbonaceous-rich unit. pyrite/sulphide and ?carbonaceous gangue at 113.3m. At 114.5m is vein of honey sphalerite and galena and black mineral
0950	WGR-12	116.35	118	Tk	sh-cb	sh-cb			Black shale with coral (TK2)
0950	WGR-12	118	126.85	Tk	ls-st	ls-st			black limestone. shaley in part
0950	WGR-12	129.85	132.7	Tk	ls	ls-gy			Black ?carbonaceous-rich limestone. can see alteration of fossils/beds and alteration fronts (matrix preferable altered)
0950	WGR-12	132.7	136.55	Tk	ls-st	ls-st			black limestone. shaley in part
0950	WGR-12	136.55	140.4	Tk	ls	ls-b			fine grained ?carbonaceous altered brown limestone
0950	WGR-12	140.4	142.65	Tk	ls	ls-bf	bfx	blk	weakly ?carbonaceous altered fine to medium grained (granular sandstone texture) fossiliferrous limestone (grey)
0950	WGR-12	148.7	158	Tk	ls	ls-b	bfx	blk	Brown limestone. varying degrees of ?carbonaceous material in alteration/fracture and recent faults along minor mill breccia
0950	WGR-12	158	146.7	Tk	ls-st	ls-st			black limestone. shaley in part
0950	WGR-12	164.7	168	Tk	ls	ls-b	bfx	blk	Brown limestone becoming increasingly ?carbonaceous and black fracture towards 168m where it is breccia. Abundant white veins (calcite?). Possible example of black vein crosscutting black stuff
0950	WGR-12	168	170.7	Tk	ls	ls-b	bfx	blk	Black limestone. mill in places
0950	WGR-12	170.7	174	Tk	ls	ls-b	bfx	blk	Brown limestone. varying degrees of ?carbonaceous material in alteration/fracture. Grey in mill breccia
0950	WGR-12	174	177.3	Tk	ls	ls-b	bfx	blk	brown limestone. some grey and yellow and black clay/breccia zones
0950	WGR-12	177.3	180.1	Tk	ls	ls-b	bx	blk	predominantly mill breccia and highly fractured
0950	WGR-12	180.1	199.25	Tk	ls	ls-b	bfx	blk	Brown limestone with ?carbonaceous alteration and black fracture and calcite veins. Mill breccia in places
0950	WGR-12	206	209.6	Tk	ls	ls-b	bfx	blk	Brown limestone with ?carbonaceous alteration and black fracture and calcite veins. Mill breccia in places
0950	WGR-12	222	245	Tk	ls	ls-b	bfx	blk	Brown limestone with ?carbonaceous alteration and black fracture and intense calcite veins. Mill breccia in places
0950	WGR-12	245	246	Tk	bxa	flt	bfx	blk	highly broken black ?carbonaceous-rich zone
0950	WGR-12	246	255.3	Tk	ls	ls-b	bfx	blk	Brown limestone with ?carbonaceous alteration and black fracture and intense calcite veins. Mill breccia in places
0950	WGR-12	261.35	268	Tk	ls	ls-b	bfx	blk	Black. Brown ?carbonaceous limestone. various ?carbonaceous fault zones (up to 20cm) also calcite veins and black fracture
0950	WGR-12	270.7	273.75	Tk	ls	ls-b	bfx	blk	Brown limestone with ?carbonaceous alteration and black fracture and intense calcite veins. Mill breccia in places. Last 70cm limestone pale (weathered?)
0950	WGR-12	273.7	288.8	Tk	ls	ls-b	bfx	blk	Black. Brown ?carbonaceous limestone. various ?carbonaceous fault zones (up to 20cm) also calcite veins and black fracture. sulphide/s in places
0950	WGR-12	288.8	292.1	Tk	ls	ls-b			v mottled pale-med brown limestone. stylolite controlled mottles. Minor black ?carbonaceous zones and minor white vughy veins
0950	WGR-12	292.1	294.8	Tk	ls	ls-b	bfx	blk	brown limestone with sulphur on fracture. Weak-intense black fracture. minor mottling
0950	WGR-12	294.8	295.15	Tk	bxa	flt		blk	black and orange clay zone. highly fracture texture
0950	WGR-12	302.1	308.5	Tk	ls	ls-b			v ?carbonaceous-rich. minor brown limestone. quartz and calcite vughs and veins crosscut ?carbonaceous?
0950	WGR-12	316.1	327.7	Tk	ls	ls-b	bfx	blk	Brown limestone with ?carbonaceous alteration and black fracture and intense calcite veins. Mill breccia in places
0950	WGR-12	343	371.6	Tk	ls	ls-b	bfx	blk	pale brown limestone. black fracture. Leached at 367 and 369.5
0950	WGR-12	371.6	376.05	Tk	ls-ss	ls-ss	bfx	blk	Brown mottled med-grained (granular SST texture) limestone. Various black clay (10cm) zones and varying intensities of alteration.
0950	WGR-12	391	398.2	Tk	ls	ls-b			Variably leached limestone
0950	WGR-12	398.2	402.1	Tk	ls	ls-b	bfx	blk	brown limestone. minor breccia with black alteration
0950	WGR-12	411.5	414.6	Tk	ls	ls-b			Brown limestone with ?carbonaceous alteration. One sandstone grain sized layer and no ?carbonaceous-dominant zones
0950	WGR-12	420.65	430.15	Tk	ls	ls-b	bfx	blk	brown limestone. minor breccia with black alteration
0950	WGR-12	430.15	433.1	Tk	ls-ss	ls-ss	bfx	blk	More granular (fossiliferrous) limestone. Minor black fracture. Minor mill breccia with brown limestone and fossiliferous sandstone fragments. ?carbonaceous alteration of paler matrix
0950	WGR-12	442.45	446.8	Tk	ls	ls-bf	bfx	blk	1/2 tray ?carbonaceous-altered and fracture. And 2nd half fresh. Rock is pale brown granular (fossiliferrous) limestone

SECT	Hole_ID	From (m)	To (m)	Formation	Protolith	Lithology	Gross Structure	Structure Infill	Description
0950	WGR-12	446.8	454.1	Tk	ls	ls-bf			pale-brown fossiliferrous limestone
1475	WGR-13	0	103.7	Tgdfa	bxi	dia	bx		Bleached igneous rock. minor-intense sulphide-rich zones. Predominantly white alteration. Patchy zones slightly more potassic alteration of matrix.
1475	WGR-13	103.7	111.7	Unk	cly	cly	bx		very rubbly white altered core
1475	WGR-13	111.7	117.5	Tgdfa	bxi	dia	bx		pokachip like core
1475	WGR-13	117.5	119.3	Unk	cly	cly	bx		red coloured very soft rubble and fragments. Moderate sulphide and epidote fragments
1475	WGR-13	119.3	123	Unk	bxh	gbx	bx		Gritty breccia with sulphide. red colouration. 3cm sulphide fragment at 125.5. Minor epidote fragment
1475	WGR-13	123	125	Unk	cly	cly	bx		fragmented core
1475	WGR-13	125	132	Unk	cly	cly	bx		clayey rubble. orange stained
1475	WGR-13	132	135	Tgcb	cly	bc	bx		banded clay fragments <10cm and other broken material
1475	WGR-13	135	137	Tk	ls	mar			limestone (marble)
1475	WGR-13	137	143.5	Tk	ls	mar	bx	py	limestone (marble). With pyrite infill in breccia fragments
1475	WGR-13	143.5	145.5	Tk	ls	mar	bx		Marble breccia with minor black fragments. Possible foliation fabric and abundant pyrite.
1475	WGR-13	145.5	151	Tk	ls	mar			marble - grey to white mottled
1475	WGR-13	151	155.4	Tk	ls	mar	bx	sk	marble with yellow-green skarn (in fracture). Sulphides in pale matrix. (see log for details)
1475	WGR-13	155.4	155.6	Tk	ls	mar	bx	cy	breccia/fault with clay (grey and white but not banded) in between marble clasts. Fragments very deformed.
1475	WGR-13	155.6	181	Tk	ls	mar	fx	sk	white-grey marble. not breccia. minor veins with yellow mineral (refer to log for sulphide details)
1475	WGR-13	181	198	Tk	ls	mar	fx		
1475	WGR-13	198	202	Tk	ls	mar	bx	blk	
1475	WGR-13	202	235	Tk	ls	ls-gy	bfx	blk	
1475	WGR-13	235	240	Tk	ls	ls-bf	bfx	blk	
1475	WGR-13	240	262	Tk	ls	ls-bf	bfx	blk	Log missing 240-300. Unit is same as at 181-240m
1475	WGR-13	262	263	Tk	bxh	bxu	bx	blk	A ?carbonaceous and grey clay limestone breccia 262-263.
1475	WGR-13	263	304	Tgdfa	bxi	bxi			Breccia. Igneous. limestone clasts. Zone of dominantly igneous? clasts with rare limestone in the centre of interval. At the margins (262 and 301) is black-grey ?carbonaceous-rich breccia zone. Possible overprinting of ?carbonaceous.
1475	WGR-13	304	312	Tk	ls	ls-bf			
1475	WGR-13	312	314	Tk	ls	ls-bf	bx		
1475	WGR-13	314	323	Tk	ls	ls-bf			
1475	WGR-13	323	329	Tk	ls	ls-bf	bx	blk	
1475	WGR-13	329	342.5	Tk	ls	ls-bf			
1475	WGR-13	342.5	343	Tk	bxa	flt	flt	blk	Strongly fracture zone with poor recovery
1475	WGR-13	343	377	Tk	ls	ls-bf			
1475	WGR-13	377	385	Tk	ls	ls-bf	bx	blk	
1475	WGR-13	385	393	Tk	ls	ls-bf			
1475	WGR-13	393	398	Tk	ls	ls-bf	bx	blk	Very shaley with rip-up clasts? Suggests sedimentary
1475	WGR-13	398	433	Tk	ls	ls-bf			
1475	WGR-13	433	444	Tk	ls	ls-bf	bx	blk	Intense breccia. Also mention of fine grained. igneous rock in grey matrix?? Hydrochloric acid+
1475	WGR-13	444	468.1	Tk	ls	ls-bf			
1650	WGR-14	0	98	Tgdfa	bxi	dia	bx		
1650	WGR-14	98	105	Unk	bxa	flt			
1650	WGR-14	105	152	Unk	bxh	bxu			
1650	WGR-14	152	161	Unk	bxa	flt			
1650	WGR-14	161	179	Tk	ls	cs			

SECT	Hole_ID	From (m)	To (m)	Formation	Protolith	Lithology	Gross Structure	Structure Infill	Description
1650	WGR-14	179	361.4	Tk	ls	ls-bf			
0950	WGR-17	0	47	Tgdfa	bxh	bxu			Fault contact at 47m
0950	WGR-17	47	70	Tk	ls	mar	bx		
0950	WGR-17	70	89	Tk	ls	cs	bx		Calc silicate
0950	WGR-17	89	98	Tk	ls	mar	bx		
0950	WGR-17	98	128	Tk	ls	mar			
0950	WGR-17	128	150	Tk	ls	mar	bx		
0950	WGR-17	150	178	Tk	ls	mar	bx		Marbleised limestone
0950	WGR-17	178	189	Tk	cly	cly	bx		
0950	WGR-17	189	214	Tk	sh-cb	sh-cb			
0950	WGR-17	214	367	Tk	ls	ls-bf	bx		
0950	WGR-17	367	400.6	Tgdfa	bxi	bxi	bx		Intrusive breccia dike
1000	WGR-2	0	19	Tgcb	cly	cly			
1000	WGR-2	19	67	Tk	ls	mar	bx		
1000	WGR-2	67	139.6	Tk	ls	ls-bf			
1000	WGR-3	0	5	Unk	unk	unk			rubble/dirt
1000	WGR-3	5	12	Tk	ls	ls-gy	fx		grey limestone minor fractured/brecciated zones
1000	WGR-3	12	27	Tk	ls	ls-gy	fbx	blk	grey limestone with a number of breccia zones. I.e. 1m mill breccia at 15-16 (can see sulphide/s in matrix and not intensely ?carbonaceous). 26-27 breccia/rubble highly Iron-oxide and sulphides
1000	WGR-3	20	59	Tk	ls	mar	bx		
1000	WGR-3	27	53	Tk	ls	ls-gy			limestone. grey-black
1000	WGR-3	53	55	Tk	ls-st	ls-st	bx		black ?carbonaceous-rich breccia with coral fragments (sedimentary?)
1000	WGR-3	55	91	Tk	ls	ls-gy			black-grey limestone with fossils and calcite veins. fairly ?carbonaceous. At 63.5m sparry carbonate (replacement of fragments) and at 68m is a 20cm ?carbonaceous shear zone with minor white clay also present.
1000	WGR-3	59	293.8	Tk	ls	ls-bf			
1050	WGR-4	0	8.9	Tgdfa	bxi	dia	bx		Fragmental rock with epidote alteration. Abundant pyrite (ferrugenised) and strong white? Alteration. Appears silicified (or potassic?) - very hard
1050	WGR-4	8.9	34.1	Tgdfa	bxi	dia	bx		missing
1050	WGR-4	34.1	53	Tgdfa	bxi	bc/dia	bx		Intense white altered rubble. Can see both relict breccia and banded (50/50?) textures. Very poor recovery. i.e. 15m in 5m tray
1050	WGR-4	53	60	Unk	bxh	gbx			Gritty breccia. like sand - very unconsolidated
1050	WGR-4	60	70	Tgcb	cly	bc			Rare banded material amongst rubble. Increasing grey content of the clay breccia. texture clearly visible in the rubble
1050	WGR-4	70	86	Tk	ls	mar	bx	yw	F breccia with white (marble?) clasts and clay with a strong black content. Mineralisation (pyrite). Can see white-yellow stage. Black appears to be overprinting alteration
1050	WGR-4	86	88.4	Tk	ls	ls-gy	bfx		Limestone - strong black. Intense white calcite crackle and minor overprinting black stylolites. 20cm pyrite-bearing push-up zone at 87m
1050	WGR-4	88.4	90	Tgdfa	bxi	dia	bx	blk	Intense black clay alteration of matrix of Intrusive breccia. Fragments <1cm and dominantly intense clay alteration. Rare 2cm igneous fragments.
1050	WGR-4	90	90.4	Tk	ls	ls-gy	bx?		Limestone fragment? - dark grey-black
1050	WGR-4	90.4	97	Tk	cly	cly	bx		Intrusive breccia (intense clay-rubble). Fragments <2cm dominantly 0.5cm and clay. Minor black alteration of first 1-2m (very sulphide rich) and grey-orange coloured
1050	WGR-4	97	99	Tk	ls	ls-b			Limestone variably intensely leached and porous
1050	WGR-4	99	103	Tk	ls	ls-bf			Pale grey-brown. mottled limestone. Fossils and fragments clearly visible
1050	WGR-4	103	128	Tk	ls	ls-bf			Fossiliferrous grey to pale-brown limestone. mottled in places

SECT	Hole_ID	From (m)	To (m)	Formation	Protolith	Lithology	Gross Structure	Structure Infill	Description
1050	WGR-4	128	137.6	Tk	ls	ls-bf	bfx	blk	limestone becomes more ?carbonaceous (can see veins). Zone of burrow/fossils quite carbonaceous - Also black fracture. - alteration due to porous or composition?
1050	WGR-4	137.6	150	Tk	ls	ls-bf	bfx	blk	fine grained. minor fossiliferrous zones. Minor-mod black fracture and pale-med grey limestone. mottled. (missing core in centre of zone - 3m)
1050	WGR-4	150	154	Tk	ls	ls-bf	bfx	blk	black to dark grey limestone. very mottled freq black fracture and recent slickenside
1050	WGR-4	154	163	Tk	ls	ls-bf			dark grey-black limestone with burrow/fossils. Minor fine grained paler zone (repeat of 128-140?)
1050	WGR-4	163	193	Tk	ls	ls-bf	bfx	blk	Black limestone. minor slickenside. abundant ?carbonaceous veins and can see black alteration increasing towards faults (channelways
1050	WGR-4	193	199.4	Tk	bxa	flt	bx	blk	EOH. Mill breccia. medium grey clay groundmass. very Broken
1050	WGR-5A	0	283.8	Tgdfa	bxi	dia			
1050	WGR-6	0	44	Tgdfa	bxi	dia			
1050	WGR-6	44	53	Tgcb	cly	cly			
1050	WGR-6	53	106	Tk	ls	mar			
1050	WGR-6	106	201	Tk	ls	ls-bf			
1050	WGR-6	201	225	Tk	bxa	flt			Inferred on section
1050	WGR-6	225	352	Tk	ls	ls-bf			
1175	WGR-9	0	64	Tgdfa	bxi	dia			
1175	WGR-9	64	80	Tgdfa	bxi	dia	bx		
1175	WGR-9	80	90	Tgdfa	bxi	dia			
1175	WGR-9	90	95	Tgdfa	bxa	flt			
1175	WGR-9	95	115	Tgdfa	bxi	dia			
1175	WGR-9	115	130	Tgdfa	bxi	dia	bx		
1175	WGR-9	130	140	Tgdfa	bxa	flt			Gouge
1175	WGR-9	140	146	Tgdfa	bxh	bxu	bx		gouge with pyrite fragments
1175	WGR-9	146	158	Tgcb	cly	bc			Banded clay and silica zone
1175	WGR-9	158	160.5	Unk	bxa	bxu	bx	py	Mylonite - dark green-grey clasts with pyrite cement.
1050	WGT-4	0	21	Tgdfa	bxi	dia	bx		Very rubbly Intrusive breccia. likely igneous-dominated fragments. 19-21 is dominated by weathering of epidote (soft). Specular hem associated with Epidote. Epidote is veins/clasts? In/near igneous fragments
1050	WGT-4	21	39	Tgdfa	bxi	dia	bx		Intense white altered breccia. Can see relict green spot alteration and hem spots (after magnetite clasts?). Iron-oxide present. Likely igneous
1050	WGT-4	39	49	Tgcb	cly	bc			Intense white clay alteration. Relict banded texture. In most pieces. very likely broken texture also present
1050	WGT-4	49	50.5	Tgdfa	bxi	dia	bx		Intrusive breccia. Mill texture clear. Less white alteration suggesting different host? Strong mineralisation (indicated by Cu-SO4 and relict pyrite). Black clay alteration present. Some hard (Silica/quartz??) fragments. Cubic pyrite and black (silica/quartz?. ?carbonaceous?) occur on crackle fracture in harder fragments (comprised of white potassic alteration? but not Silica/quartz? or clay)
1050	WGT-4	50.5	69	Unk	cly	cly	bx	yw	Intense white alteration. 30/30/30 banded/breccia/unrecognised texture. 65-69m Fragments of possible white-yellow (I.e. the mythical opaline silica!)
1050	WGT-4	69	75	Unk	cly	cly	bx	yw	Intense white alteration. more grey present in clay. Majority of texture seems to be breccia. The "not" silica/quartz-nodules are present!
1050	WGT-4	75	96	Tgcb	cly	bc	bx	yw	Not banded. Intrusive breccia. rare 10cm banded zones. competent core. Can see yellow-white veins crosscut bands. 90-92m Increase in black stuff on later fractures. Shear fabric present (A white vein cross-cuts black filled fracture). At 91m. sphalerite and galena vein in cy
1050	WGT-4	96	97.4	Unk	unk	unk	bx	fe	very dark grey and Iron-oxide clay (sulphide/s-rich contact zone now easily broken dirt). Minor limestone fragment in the clay at contact
1050	WGT-4	97.4	126.5	Tk	ls	ls-bf			Fossiliferrous (abundant 2cm size) limestone. pale grey-brown. Minor darker areas. 96-105 areas of leaching (fossils?)
1050	WGT-4	126.5	162.4	Tk	ls-ss	ls-ss	bfx	blk	Coral (round to 1cm) and fossil shell? fragments (to 3cm long) in black limestone. Fossil content variable and only minor at 133-162.4. Core fairly massive and unbroken. Rare black fracture zones (i.e. 1 per m) at 150-162. 5cm sandstone gravel bed. 45 degrees to CA at 148m (other layers in this location have similar CA angle).

West Grasberg Drillhole Geology

SECT	Hole_ID	From (m)	To (m)	Formation	Protolith	Lithology	Gross Structure	Structure Infill	Description
1275	WGZ-8	0	21	Tgdfa	bxi	dia	bx		
1275	WGZ-8	21	27	Tgdfa	bxi	dia	bx		
1275	WGZ-8	27	36	Tgdfa	bxi	dia	bx		
1275	WGZ-8	36	43	Tgdfa	bxi	dia	bx		
1275	WGZ-8	43	48	Tgdfa	bxi	dia	bx		Fragments in clay matrix
1275	WGZ-8	48	58	Tgdfa	bxi	dia	bx		Hard diatreme chips
1275	WGZ-8	58	60	Tgdfa	bxi	dia	bx		Fragments in clay matrix
1275	WGZ-8	60	63.7	Tgdfa	bxi	dia	bx		Moderately broken
1275	WGZ-8	63.7	66.3	Tgcb	cly	bc	bx	py	Possible skarn fragments? Intense clay in unmineralised samples.
1275	WGZ-8	66.3	73	Unk	bxh	gbx	bx	py	Moderate relict fragments. Sphalerite fragments
1275	WGZ-8	73	79	Unk	bxh	gbx	bx		Rare relict fragments in clay matrix
1275	WGZ-8	79	79.5	Unk	bxh	gbx	bx	py	Heavy sulphide zone - massive pyrite. Possible grey (coverlite?) with pyrite.
1275	WGZ-8	79.5	85	Unk	cly	cly			minor bands present
1275	WGZ-8	85	91	Tgcb	cly	bc	fx	yw	Contorted with minor white veins present.
1275	WGZ-8	91	98.2	Tgcb	cly	bc	fx	yw	Strong white veins-infill. Clay host has a strong black content
1275	WGZ-8	98.2	104.7	Tgcb	cly	bc	fx	yw	Continuous zones of banded clay not more than 1m
1275	WGZ-8	104.7	108	Tk	ls	ls-gy			Massive textureless marble, grey to pale grey mottles
1275	WGZ-8	108	114	Tgcb	cly	bc	fx		Continuous zones of banded clay not more than 20cm, fairly broken.
1275	WGZ-8	114	116	Tgcb	cly	bc	fx		Continuous zones of banded clay not more than 10cm, fairly broken. Minor clay matrix. Minor limestone
1275	WGZ-8	116	120	Unk	bxh	bxh	bx		Polymictic. Clay, igneous? and other fragments. Sporadic zones of second breakup by ?carbonaceous and pyrite dominated material
1275	WGZ-8	120	126	Tk	ls	ls-gy			grey marble (mottled) possibly a clast
1275	WGZ-8	126	155.8	Tk	bxh	bxh	bx		Zones of competent marble (or large clasts) <2m between push-up zones of 1-4m. Clasts dominantly monolithic (marble) sub-angular to rounded size ranging from sub mm to 10cm (as can be observed in core). Matrix is fine-grained grey-white fragments with patchy pervasive pyrite alteration and dark-grey alteration. Sulphide clasts (sphalerite, galena; pyrite+chalcopyrite at 153m), Igneous clasts at 134m, orange crystalline (veins?) clasts. Preferential spotted pyrite alteration of some clasts (or pre-brecciation).
1275	WGZ-8	155.8	440	Tk	ls	ls-gy			Slightly bleached and with leached holes within.

HOLE-ID	DISTANCE	AZIMUTH	DIP
BG01-04A	0	208.91	-80
BG01-04A	110	208.91	-82
BG01-04A	150	208.91	-80.5
BG01-04A	216	208.91	-80.5
BG01-04A	247	208.91	-80.5
BG01-04A	387	208.91	-84
BG01-04A	469	208.91	-83
BG01-04A	490	208.91	-82.5
BG01-04A	559.5	208.91	-85
BG01-04A	600	208.91	-84
BG01-04A	658.8	208.91	-83
BG01-04A	700	208.91	-83
BG01-04A	769.8	208.91	-85
BG01-04A	900	208.91	-80.5
BG01-05	0	257.92	-73
BG01-05	75	257.92	-78.5
BG01-05	120	257.92	-78
BG01-05	153.2	257.92	-79
BG01-05	211	257.92	-80.5
BG01-05	261.7	257.92	-80.5
BG01-05	338.8	257.92	-78.5
BG01-05	373.3	257.92	-80
BG01-05	397.8	257.92	-77.5
BG01-05	459	257.92	-80
BG01-05	505	257.92	-80.5
BG01-05	562.4	257.92	-82
BG01-05	637.8	257.92	-82
BG01-05	652.8	257.92	-80.5
BG01-05	718.8	257.92	-78.5
BG01-05	767	257.92	-80.5
BG01-05	794	257.92	-82
BG01-07	0	166.91	-80
BG01-07	52.8	166.91	-77
BG01-07	114.1	166.91	-80.5
BG01-07	156.1	166.91	-79
BG01-07	207.1	166.91	-82
BGU07-06	0	29.92	-70
BGU07-06	50	29.92	-73.5
BGU07-06	100	29.92	-72
BGU07-06	150	29.92	-73
BGU07-06	200	29.92	-71
BGU07-06	250	29.92	-68.5
BGU07-06	300	29.92	-70
BGU07-06	365	29.92	-75
BGU08-01	0	29.92	-30.5
BGU08-01	50	29.92	-28.5
BGU08-01	100	29.92	-28
BGU08-01	150	29.92	-28
BGU08-01	200	29.92	-28
BGU08-01	250	29.92	-28
BGU08-01	285	29.92	-27
BGU08-05	0	29.92	9.5
BGU08-05	50	29.92	10
BGU08-05	100	29.92	9
BGU08-05	150	29.92	10
BGU08-05	200	29.92	9.5
BGU08-05	229.6	29.92	14
BGU08-07	0	42.92	-40
BGU08-07	50	42.92	-40.5
BGU08-07	100	42.92	-39
BGU08-07	150	42.92	-38.5

HOLE-ID	DISTANCE	AZIMUTH	DIP
BGU08-07	200	42.92	-38
BGU08-07	243	42.92	-36
BGU14-07	0	209.91	-70
BGU14-07	50	209.91	-71
BGU14-07	100	209.91	-70
BGU14-07	150	209.91	-70.5
BGU14-07	200	209.91	-72
BGU14-07	250	209.91	-71
BGU14-07	300	209.91	-69
BGU14-07	350	209.91	-70
BGU14-07	400	209.91	-70
BGU14-07	500	209.91	-74
BGU14-07	550	209.91	-72.5
BGU14-07	600	209.91	-74
BGU14-07	650	209.91	-73
BGU14-07	750	209.91	-71
BGU14-07	780	209.91	-71
BGU17-07	0	209.91	-66
BGU17-07	50	209.91	-67
BGU17-07	100	209.91	-66.5
BGU17-07	150	209.91	-68.5
BGU17-07	201	209.91	-68.5
BGU17-07	252	209.91	-68
BGU17-07	300	209.91	-68.5
BGU17-07	350	209.91	-70
BGU17-07	402	209.91	-67
BGU17-07	450	209.91	-69.5
BGU17-07	500	209.91	-65
BGU17-07	550	209.91	-66.5
BGU17-07	600	209.91	-68
BGU17-07	634	209.91	-84
BGU18-03	0	209.91	15
BGU18-03	50	209.91	15.5
BGU18-03	100	209.91	15
BGU18-03	150	209.91	15.5
BGU18-03	250	209.91	15
BGU19-03	0	209.91	20
BGU19-03	3	209.91	22
BGU19-03	50	209.91	22
BGU19-03	100	209.91	20.5
BGU19-03	150	209.91	19
BGU19-03	200	209.91	19
BGU19-03	250	209.91	19
BGU21-01	0	209.91	10
BGU21-01	50	209.91	10
BGU21-01	100.5	209.91	10
BGU21-01	150	209.91	9
BGU21-02	0	209.91	20
BGU21-02	51	209.91	20
BGU21-02	100.2	209.91	21.5
BGU21-02	150	209.91	21.5
BGU21-02	204	209.91	20
BGU21-02	232.5	209.91	20
BGU21-03	0	209.91	28
BGU21-03	50	209.91	27
BGU21-03	150	209.91	27
BGU21-03	200.9	209.91	27
BGU21-03	251.1	209.91	27.5
BGU21-05	0	209.91	-20
BGU21-05	100.8	209.91	-20
BGU21-05	150	209.91	-20

HOLE-ID	DISTANCE	AZIMUTH	DIP
BGU21-05	200	209.91	-20
BGU21-10	0	209.91	35
BGU21-10	3	209.91	34
BGU21-10	51	209.91	34
BGU21-10	102	209.91	35
BGU21-10	150	209.91	34
BGU21-10	201	209.91	35
BGU21-10	268	209.91	35
BGU22-01	0	209.91	-10
BGU22-01	51	209.91	-8.5
BGU22-01	195	209.91	-8.5
BGU23-02	0	209.91	-5
BGU23-02	3	209.91	-6
BGU23-02	50	209.91	-4.5
BGU23-02	100	209.91	-3
BGU23-02	150	209.91	-4
BGU23-02	178	209.91	-4
BGU23-03	0	209.91	20
BGU23-03	50	209.91	20
BGU23-03	100	209.91	20.5
BGU23-03	150	209.91	21
BGU23-03	200.5	209.91	20
BGU23-05	0	209.91	-30
BGU23-05	3	209.91	-29
BGU23-05	50	209.91	-29
BGU23-05	100	209.91	-29
BGU23-05	150	209.91	-30.5
BGU23-05	200	209.91	-30
BGU23-05	286	209.91	-30
BGU23-06	0	209.91	-50
BGU23-06	50	209.91	-50.5
BGU23-06	100	209.91	-51.5
BGU23-06	150	209.91	-51.5
BGU23-06	200	209.91	-51.5
BGU23-06	250	209.91	-50
BGU23-06	302.7	209.91	-50
BGU23-08	0	209.91	28
BGU23-08	50	209.91	30
BGU23-08	100	209.91	31
BGU23-08	150	209.91	31
BGU23-08	200	209.91	32
BGU24-08	0	227.91	-35
BGU24-08	50	227.91	-34
BGU24-08	100	227.91	-33
BGU24-08	150	227.91	-34
BGU24-08	200	227.91	-33
BGU24-08	250	227.91	-33
BGU24-10	0	227.91	-55
BGU24-10	50	227.91	-55
BGU24-10	102	227.91	-53.5
BGU24-10	150	227.91	-54.5
BGU24-10	201	227.91	-55
BGU24-10	252	227.91	-53
BGU24-10	300	227.91	-55
BGU24-10	351	227.91	-54.5
BGU24-11	0	227.91	-65
BGU24-11	3	227.91	-64.5
BGU24-11	50	227.91	-64
BGU24-11	100	227.91	-63.5
BGU24-11	150	227.91	-63.5
BGU24-11	201	227.91	-63

HOLE-ID	DISTANCE	AZIMUTH	DIP
BGU24-11	252	227.91	-63
BGU24-11	300	227.91	-63
BGU24-11	351	227.91	-63
BGU24-11	402	227.91	-63
BGU24-11	450	227.91	-63
BGU24-11	483	227.91	-63
BGU24-13	0	209.91	22
BGU26-01	0	209.91	-10
BGU26-01	50	209.91	-10
BGU26-01	100	209.91	-9
BGU26-01	150	209.91	-9
BGU26-01	200	209.91	-11
BGU26-01	250	209.91	-11
BGU26-02	0	209.91	-35
BGU26-02	50	209.91	-35
BGU26-02	100	209.91	-34
BGU26-02	150	209.91	-33
BGU26-02	200	209.91	-34
BGU26-02	300	209.91	-35
BGU26-02	315	209.91	-35
BGU26-03	0	209.91	10
BGU26-03	50	209.91	10
BGU26-03	100	209.91	10.5
BGU26-03	150	209.91	10.5
BGU26-03	171	209.91	9
BGU26-04	0	209.91	-55
BGU26-04	50	209.91	-55
BGU26-04	100	209.91	-53
BGU26-04	150	209.91	-53
BGU26-04	200	209.91	-54
BGU26-04	250	209.91	-54
BGU26-04	350	209.91	-55
BGU26-04	363	209.91	-55
BGU26-10	0	210.46	42
BGU26-10	3	210.41	42.55
BGU26-10	6	210.51	42.72
BGU26-10	9	210.65	42.73
BGU26-10	12	210.76	42.73
BGU26-10	15	210.76	42.75
BGU26-10	18	210.76	42.77
BGU26-10	21	210.8	42.79
BGU26-10	24	210.79	42.85
BGU26-10	27	210.74	42.93
BGU26-10	30	210.77	42.98
BGU26-10	33	210.76	42.99
BGU26-10	36	210.77	43.02
BGU26-10	39	210.84	43.02
BGU26-10	42	210.84	43.05
BGU26-10	45	210.9	43.13
BGU26-10	48	211.1	43.18
BGU26-10	51	211.26	43.18
BGU26-10	54	211.27	43.18
BGU26-10	57	211.38	43.12
BGU26-10	60	211.52	43.09
BGU26-10	63	211.57	43.09
BGU26-10	66	211.62	43.15
BGU26-10	69	211.82	43.21
BGU26-10	72	212.04	43.22
BGU26-10	75	212.05	43.13
BGU26-10	78	212.01	43.05
BGU26-10	81	212.09	43.02

HOLE-ID	DISTANCE	AZIMUTH	DIP
BGU26-10	84	212.15	43.02
BGU26-10	87	212.15	43.02
BGU26-10	90	212.13	43.04
BGU26-10	93	212.24	43.05
BGU26-10	96	212.35	43.09
BGU26-10	99	212.32	43.09
BGU26-10	102	212.37	43.09
BGU26-10	105	212.49	43.1
BGU26-10	108	212.54	43.05
BGU26-10	111	212.48	43.04
BGU26-10	114	212.43	43.07
BGU26-10	117	212.45	42.89
BGU26-10	120	212.38	42.69
BGU26-10	123	212.2	42.82
BGU26-10	126	212.15	42.81
BGU26-10	129	212.18	42.67
BGU26-10	132	212.21	42.68
BGU26-10	135	212.26	42.42
BGU26-10	138	212.48	42.33
BGU26-10	141	212.65	42.25
BGU26-10	144	212.71	42.28
BGU26-10	147	212.85	42.22
BGU26-10	150	212.9	42.16
BGU26-10	153	212.95	42.17
BGU26-10	156	213.16	42.19
BGU26-10	159	213.35	42.15
BGU26-10	162	213.29	42.05
BGU26-10	165	213.4	42.03
BGU26-10	168	213.46	42
BGU26-10	171	213.51	42.03
BGU26-10	174	213.6	42.1
BGU26-10	177	213.68	42.1
BGU26-10	180	213.65	42.14
BGU26-10	183	213.57	42.44
BGU26-10	186	213.51	42.85
BGU26-10	189	213.41	42.95
BGU26-10	192	213.38	42.98
BGU26-10	195	213.37	42.96
BGU26-10	198	213.46	42.98
BGU26-10	201	213.59	42.95
BGU26-10	204	213.6	42.91
BGU26-10	207	213.68	42.91
BGU26-10	210	213.93	42.9
BGU26-10	213	214.01	42.88
BGU26-10	216	214.1	42.86
BGU26-10	219	214.15	42.85
BGU26-10	222	214.24	42.85
BGU26-10	225	214.34	42.84
BGU26-10	228	214.4	42.82
BGU26-10	231	214.52	42.82
BGU27-02	0	209.91	-35
BGU27-02	51	209.91	-35
BGU27-02	101.5	209.91	-33
BGU27-02	150	209.91	-33
BGU27-02	201	209.91	-32
BGU27-02	251.6	209.91	-33
BGU27-02	300	209.91	-32.5
BGU27-02	324	209.91	-35
BGU27-02A	0	209.91	-25
BGU27-04	0	209.91	4.5
BGU27-04	50.2	209.91	5

HOLE-ID	DISTANCE	AZIMUTH	DIP
BGU27-04	102	209.91	5
BGU27-04	150	209.91	5
BGU27-04	197.9	209.91	5
BGU27-05	0	209.91	15
BGU27-05	51	209.91	15
BGU27-05	102	209.91	15.5
BGU27-05	150	209.91	16
BGU27-05	201	209.91	15
BGU27-06	0	209.91	-67
BGU27-06	3	209.74	-66.96
BGU27-06	6	209.73	-66.93
BGU27-06	9	209.52	-67.01
BGU27-06	12	209.65	-67.16
BGU27-06	15	209.57	-67.27
BGU27-06	18	209.8	-67.35
BGU27-06	21	210.07	-67.46
BGU27-06	24	210.24	-67.48
BGU27-06	27	210.41	-67.55
BGU27-06	30	210.01	-67.57
BGU27-06	33	209.52	-67.61
BGU27-06	36	209.15	-67.57
BGU27-06	39	209.05	-67.63
BGU27-06	42	208.9	-67.75
BGU27-06	45	208.7	-67.9
BGU27-06	48	208.51	-67.96
BGU27-06	51	208.54	-68.08
BGU27-06	54	208.45	-68.18
BGU27-06	57	208.43	-68.24
BGU27-06	60	208.16	-68.23
BGU27-06	63	208.13	-68.38
BGU27-06	66	208.13	-68.44
BGU27-06	69	208.15	-68.57
BGU27-06	72	208.16	-68.64
BGU27-06	75	208.15	-68.7
BGU27-06	78	207.95	-68.72
BGU27-06	81	207.98	-68.85
BGU27-06	84	208.02	-68.89
BGU27-06	87	208.04	-68.98
BGU27-06	90	208.24	-69.05
BGU27-06	93	208.24	-69.06
BGU27-06	96	208.15	-69.08
BGU27-06	99	208.13	-69.08
BGU27-06	102	207.82	-69.13
BGU27-06	105	207.51	-69.21
BGU27-06	108	207.41	-69.24
BGU27-06	111	207.43	-69.25
BGU27-06	114	207.45	-69.28
BGU27-06	117	207.52	-69.35
BGU27-06	120	207.54	-69.31
BGU27-06	123	207.68	-69.36
BGU27-06	126	207.71	-69.53
BGU27-06	129	207.6	-69.67
BGU27-06	132	207.38	-69.74
BGU27-06	135	207.46	-69.83
BGU27-06	138	207.68	-69.84
BGU27-06	141	207.6	-69.84
BGU27-06	144	207.46	-69.92
BGU27-06	147	207.38	-70.03
BGU27-06	150	207.21	-70.19
BGU27-06	153	207.26	-70.36
BGU27-06	156	207.27	-70.51

HOLE-ID	DISTANCE	AZIMUTH	DIP
BGU27-06	159	207.24	-70.57
BGU27-06	162	207.07	-70.64
BGU27-06	165	206.91	-70.73
BGU27-06	168	206.85	-70.85
BGU27-06	171	206.88	-70.98
BGU27-06	174	206.76	-71.09
BGU27-06	177	206.76	-71.1
BGU27-06	180	206.79	-71.12
BGU27-06	183	206.73	-71.16
BGU27-06	186	206.4	-71.25
BGU27-06	189	206.18	-71.35
BGU27-06	192	206.04	-71.46
BGU27-06	195	205.91	-71.57
BGU27-06	198	205.87	-71.68
BGU27-06	201	205.79	-71.76
BGU27-06	204	205.93	-71.8
BGU27-06	207	206.04	-71.78
BGU27-06	210	206.04	-71.79
BGU27-06	213	205.98	-71.82
BGU27-06	216	205.71	-71.78
BGU27-06	219	205.54	-71.82
BGU27-06	222	205.63	-71.94
BGU27-06	225	205.79	-72.02
BGU27-06	228	205.57	-72.1
BGU27-06	231	205.57	-72.11
BGU27-06	234	205.38	-72.21
BGU27-06	237	205.29	-72.34
BGU27-06	240	205.46	-72.43
BGU27-06	243	205.54	-72.46
BGU27-06	246	205.6	-72.46
BGU27-06	249	205.54	-72.56
BGU27-06	252	205.57	-72.65
BGU27-06	255	205.65	-72.79
BGU27-06	258	205.79	-72.89
BGU27-06	261	205.93	-72.94
BGU27-06	264	205.79	-72.94
BGU27-06	267	205.76	-72.96
BGU27-06	270	205.93	-73.02
BGU27-06	273	205.82	-73.1
BGU27-06	276	205.51	-73.13
BGU27-06	279	205.26	-73.14
BGU27-06	282	205.24	-73.22
BGU27-06	285	205.09	-73.22
BGU27-06	288	205.09	-73.24
BGU27-06	291	205.13	-73.25
BGU27-06	294	205.26	-73.26
BGU27-06	297	205.13	-73.28
BGU27-06	300	205.18	-73.33
BGU27-06	303	205.32	-73.36
BGU27-06	306	205.07	-73.43
BGU27-06	309	204.62	-73.5
BGU27-06	312	204.48	-73.58
BGU27-06	315	204.27	-73.64
BGU27-06	318	203.96	-73.68
BGU27-06	321	203.54	-73.7
BGU27-06	324	203.15	-73.67
BGU27-06	327	202.85	-73.67
BGU27-06	330	202.85	-73.7
BGU27-06	333	202.87	-73.8
BGU27-06	336	203.07	-73.86
BGU27-06	339	202.91	-73.93

HOLE-ID	DISTANCE	AZIMUTH	DIP
BGU27-06	342	202.63	-74.1
BGU27-06	345	202.57	-74.18
BGU27-06	348	202.7	-74.23
BGU27-06	351	203.13	-74.24
BGU27-06	354	203.43	-74.26
BGU27-06	357	203.46	-74.25
BGU27-06	360	203.54	-74.29
BGU27-06	363	203.18	-74.42
BGU27-06	366	202.9	-74.42
BGU27-06	369	202.85	-74.39
BGU27-06	372	202.43	-74.36
BGU27-06	375	201.95	-74.4
BGU27-06	378	201.65	-74.47
BGU27-06	381	201.51	-74.47
BGU27-06	384	201.54	-74.53
BGU27-06	387	201.88	-74.54
BGU27-06	390	201.88	-74.52
BGU27-06	393	202.18	-74.6
BGU27-06	396	202.2	-74.68
BGU27-06	399	201.82	-74.71
BGU27-06	402	201.62	-74.7
BGU27-06	405	201.77	-74.7
BGU27-06	408	201.68	-74.71
BGU27-06	411	201.73	-74.73
BGU27-06	414	201.91	-74.78
BGU27-06	417	202.01	-74.78
BGU27-06	420	201.62	-74.83
BGU27-06	423	201.13	-74.81
BGU27-06	426	200.82	-74.78
BGU27-06	429	200.38	-74.77
BGU27-06	432	200.01	-74.71
BGU27-06	435	199.7	-74.72
BGU27-06	438	199.51	-74.82
BGU27-06	441	199.27	-74.88
BGU27-06	444	199.23	-74.88
BGU27-06	447	199.18	-74.83
BGU27-06	450	198.73	-74.75
BGU27-06	453	198.68	-74.75
BGU27-06	456	198.62	-74.76
BGU27-06	459	198.57	-74.78
BGU27-06	462	198.51	-74.79
BGU27-06	465	198.43	-74.79
BGU27-06	468	198.4	-74.87
BGU27-06	468.5	198.3	-74.91
BGU28-01	0	209.91	-9
BGU28-01	50	209.91	-9
BGU28-01	100	209.91	-9
BGU28-01	150	209.91	-9
BGU28-01	189	209.91	-9
BGU28-05	0	209.91	-55
BGU28-05	50	209.91	-55
BGU28-05	100	209.91	-55
BGU28-05	200	209.91	-56
BGU28-05	250	209.91	-56
BGU28-05	300	209.91	-56
BGU28-05	350	209.91	-57
BGU28-05	410	209.91	-56
BGU28-05	477	209.91	-57
BGU28-07	0	209.91	-73
BGU28-07	3	209.62	-72.92
BGU28-07	6	209.63	-73

HOLE-ID	DISTANCE	AZIMUTH	DIP
BGU28-07	9	209.9	-72.98
BGU28-07	12	209.84	-72.89
BGU28-07	15	209.54	-72.89
BGU28-07	18	209.49	-72.99
BGU28-07	21	209.73	-73.11
BGU28-07	24	209.74	-73.15
BGU28-07	27	210.09	-73.11
BGU28-07	30	210.35	-73.09
BGU28-07	33	210.21	-73.11
BGU28-07	36	210.3	-73.12
BGU28-07	39	210.21	-73.2
BGU28-07	42	210.16	-73.29
BGU28-07	45	210.21	-73.32
BGU28-07	48	209.98	-73.35
BGU28-07	51	209.85	-73.42
BGU28-07	54	209.76	-73.48
BGU28-07	57	209.51	-73.44
BGU28-07	60	209.62	-73.41
BGU28-07	63	209.15	-73.51
BGU28-07	66	208.9	-73.53
BGU28-07	69	208.8	-73.57
BGU28-07	72	209.01	-73.64
BGU28-07	75	208.96	-73.63
BGU28-07	78	209.12	-73.63
BGU28-07	81	209.43	-73.69
BGU28-07	84	209.23	-73.7
BGU28-07	87	209.01	-73.78
BGU28-07	90	209.04	-73.89
BGU28-07	93	208.88	-74.05
BGU28-07	96	208.85	-74.16
BGU28-07	99	208.84	-74.31
BGU28-07	102	208.79	-74.48
BGU28-07	105	208.91	-74.6
BGU28-07	108	208.99	-74.7
BGU28-07	111	209.02	-74.84
BGU28-07	114	209.21	-74.99
BGU28-07	117	209.05	-75.09
BGU28-07	120	209.12	-75.12
BGU28-07	123	209.12	-75.15
BGU28-07	126	209.24	-75.23
BGU28-07	129	209.1	-75.3
BGU28-07	132	209.43	-75.4
BGU28-07	135	209.46	-75.43
BGU28-07	138	209.82	-75.52
BGU28-07	141	209.84	-75.63
BGU28-07	144	209.84	-75.73
BGU28-07	147	209.79	-75.8
BGU28-07	150	210.1	-75.83
BGU28-07	153	209.9	-75.82
BGU28-07	156	209.62	-75.81
BGU28-07	159	209.6	-75.8
BGU28-07	162	209.57	-75.78
BGU28-07	165	209.79	-75.81
BGU28-07	168	210.35	-75.81
BGU28-07	171	210.68	-75.9
BGU28-07	174	210.88	-75.97
BGU28-07	177	211.16	-75.97
BGU28-07	180	211.51	-76
BGU28-07	183	211.63	-76.04
BGU28-07	186	211.46	-76
BGU28-07	189	211.26	-75.97

HOLE-ID	DISTANCE	AZIMUTH	DIP
BGU28-07	192	211.49	-75.9
BGU28-07	195	211.6	-75.94
BGU28-07	198	211.82	-75.85
BGU28-07	201	211.9	-75.85
BGU28-07	204	211.57	-75.88
BGU28-07	207	211.55	-75.8
BGU28-07	210	211.01	-75.58
BGU28-07	213	210.79	-75.56
BGU28-07	216	210.74	-75.6
BGU28-07	219	210.96	-75.65
BGU28-07	222	211.21	-75.68
BGU28-07	225	211.24	-75.68
BGU28-07	228	211.07	-75.7
BGU28-07	231	210.96	-75.77
BGU28-07	234	210.99	-75.84
BGU28-07	237	211.38	-75.91
BGU28-07	240	211.62	-75.99
BGU28-07	243	211.4	-76.01
BGU28-07	246	211.21	-76
BGU28-07	249	211.38	-76.04
BGU28-07	252	211.32	-76.08
BGU28-07	255	211.38	-76.07
BGU28-07	258	211.12	-76.07
BGU28-07	261	210.93	-76.14
BGU28-07	264	210.79	-76.18
BGU28-07	267	210.8	-76.19
BGU28-07	270	210.66	-76.26
BGU28-07	273	211.16	-76.3
BGU28-07	276	211.24	-76.29
BGU28-07	279	211.45	-76.29
BGU28-07	282	211.49	-76.27
BGU28-07	285	211.68	-76.29
BGU28-07	288	211.41	-76.29
BGU28-07	291	211.38	-76.28
BGU28-07	294	211.24	-76.33
BGU28-07	297	211.23	-76.33
BGU28-07	300	211.26	-76.34
BGU28-07	303	211.01	-76.34
BGU28-07	306	210.38	-76.43
BGU28-07	309	209.76	-76.51
BGU28-07	312	209.27	-76.53
BGU28-07	315	209.1	-76.56
BGU28-07	318	208.9	-76.61
BGU28-07	321	208.85	-76.68
BGU28-07	324	208.6	-76.73
BGU28-07	327	208.54	-76.84
BGU28-07	330	208.15	-77.01
BGU28-07	333	207.73	-77.09
BGU28-07	336	207.41	-77.15
BGU28-07	339	207.57	-77.22
BGU28-07	342	207.21	-77.27
BGU28-07	345	206.85	-77.3
BGU28-07	348	206.96	-77.32
BGU28-07	351	207.27	-77.38
BGU28-07	354	207.41	-77.31
BGU28-07	357	207.51	-77.28
BGU28-07	360	207.57	-77.33
BGU28-07	363	207.4	-77.39
BGU28-07	366	207.18	-77.44
BGU28-07	369	207.15	-77.42
BGU28-07	372	207.05	-77.36

HOLE-ID	DISTANCE	AZIMUTH	DIP
BGU28-07	375	207.07	-77.36
BGU28-07	378	207.15	-77.34
BGU28-07	381	206.93	-77.4
BGU28-07	384	207.07	-77.42
BGU28-07	387	206.95	-77.47
BGU28-07	390	206.95	-77.52
BGU28-07	393	206.79	-77.56
BGU28-07	396	206.63	-77.59
BGU28-07	399	206.71	-77.54
BGU28-07	402	206.54	-77.53
BGU28-07	405	205.96	-77.38
BGU28-07	408	206.21	-77.42
BGU28-07	411	206.38	-77.44
BGU28-07	414	206.27	-77.49
BGU28-07	417	206.6	-77.52
BGU28-07	420	206.65	-77.49
BGU28-07	423	206.71	-77.41
BGU28-07	426	207.29	-77.36
BGU28-07	429	207.74	-77.32
BGU28-07	432	207.7	-77.21
BGU28-07	435	207.74	-77.18
BGU28-07	438	207.95	-77.14
BGU28-07	441	208.18	-77.17
BGU28-07	444	208.21	-77.14
BGU28-07	447	208.27	-77.09
BGU28-07	450	208.26	-77.05
BGU28-07	453	208.29	-77.02
BGU28-07	456	208.4	-76.99
BGU28-07	459	208.4	-76.94
BGU28-07	462	208.46	-76.89
BGU28-07	465	208.49	-76.87
BGU28-07	468	208.49	-76.82
BGU28-07	471	208.55	-76.81
BGU28-08	0	209.91	-82
BGU28-08	3	209.91	-82.01
BGU28-08	6	209.91	-82.12
BGU28-08	9	209.91	-82.22
BGU28-08	12	209.91	-82.29
BGU28-08	15	209.91	-82.33
BGU28-08	18	209.91	-82.34
BGU28-08	21	209.91	-82.39
BGU28-08	24	209.91	-82.47
BGU28-08	27	209.91	-82.55
BGU28-08	30	209.91	-82.58
BGU28-08	33	209.91	-82.58
BGU28-08	36	209.91	-82.6
BGU28-08	39	209.91	-82.58
BGU28-08	42	209.91	-82.64
BGU28-08	45	209.91	-82.69
BGU28-08	48	209.91	-82.67
BGU28-08	51	209.91	-82.69
BGU28-08	54	209.91	-82.71
BGU28-08	57	209.91	-82.76
BGU28-08	60	209.91	-82.81
BGU28-08	63	209.91	-82.79
BGU28-08	66	209.91	-83.15
BGU28-08	69	209.91	-84.41
BGU28-08	72	209.91	-84.95
BGU28-08	75	209.91	-84.93
BGU28-08	78	209.91	-84.94
BGU28-08	81	209.91	-85.04

HOLE-ID	DISTANCE	AZIMUTH	DIP
BGU28-08	84	209.91	-85.09
BGU28-08	87	209.91	-85.3
BGU28-08	90	209.91	-85.87
BGU28-08	93	209.91	-85.91
BGU28-08	96	209.91	-86.21
BGU28-08	99	209.91	-86.47
BGU28-08	102	209.91	-86.91
BGU28-08	105	209.91	-87.83
BGU28-08	108	209.91	-88.46
BGU28-08	111	209.91	-88.58
BGU28-08	114	209.91	-88.58
BGU28-08	117	209.91	-88.69
BGU28-08	120	209.91	-88.77
BGU28-08	123	209.91	-88.76
BGU28-08	126	209.91	-88.76
BGU28-08	129	209.91	-88.83
BGU28-08	132	209.91	-89.03
BGU28-08	135	209.91	-89.61
BGU28-08	138	209.91	-89.29
BGU28-08	141	209.91	-89.26
BGU28-08	144	209.91	-89.54
BGU28-08	147	209.91	-89.24
BGU28-08	150	209.91	-88.64
BGU28-08	153	209.91	-88.62
BGU28-08	156	209.91	-88.6
BGU28-08	159	209.91	-88.59
BGU28-08	162	209.91	-88.59
BGU28-08	165	209.91	-88.58
BGU28-08	168	209.91	-88.58
BGU28-08	171	209.91	-88.58
BGU28-08	174	209.91	-88.58
BGU28-08	177	209.91	-88.58
BGU28-08	180	209.91	-88.58
BGU28-08	183	209.91	-88.58
BGU28-08	186	209.91	-88.6
BGU28-08	189	209.91	-88.85
BGU28-08	192	209.91	-89.15
BGU28-08	195	209.91	-89.13
BGU28-08	198	209.91	-89.09
BGU28-08	201	209.91	-89.04
BGU28-08	204	209.91	-89.02
BGU28-08	207	209.91	-88.81
BGU28-08	210	209.91	-88.24
BGU28-08	213	209.91	-88.23
BGU28-08	216	209.91	-88.19
BGU28-08	219	209.91	-88.16
BGU28-08	222	209.91	-88.18
BGU28-08	225	209.91	-88.13
BGU28-08	228	209.91	-88.12
BGU28-08	231	209.91	-88.13
BGU28-08	234	209.91	-88.13
BGU28-08	237	209.91	-88.12
BGU28-08	240	209.91	-88.12
BGU28-08	243	209.91	-88.18
BGU28-08	246	209.91	-88.26
BGU28-08	249	209.91	-88.28
BGU28-08	252	209.91	-88.29
BGU28-08	255	209.91	-88.3
BGU28-08	258	209.91	-88.28
BGU28-08	261	209.91	-88.28
BGU28-08	264	209.91	-88.29

HOLE-ID	DISTANCE	AZIMUTH	DIP
BGU28-08	267	209.91	-88.34
BGU28-08	270	209.91	-88.39
BGU28-08	273	209.91	-88.47
BGU28-08	276	209.91	-88.56
BGU28-08	279	209.91	-88.61
BGU28-08	282	209.91	-88.6
BGU28-08	285	209.91	-88.76
BGU28-08	288	209.91	-89.1
BGU28-08	291	209.91	-89.69
BGU28-08	294	209.91	-89.69
BGU28-08	297	209.91	-89.62
BGU28-08	300	209.91	-89.67
BGU28-08	303	209.91	-89.33
BGU28-08	306	209.91	-89.04
BGU28-08	309	209.91	-89.59
BGU28-08	312	209.91	-89.47
BGU28-08	315	209.91	-89.31
BGU28-08	318	209.91	-89.26
BGU28-08	321	209.91	-89.24
BGU28-08	324	209.91	-89.24
BGU28-08	327	209.91	-89.27
BGU28-08	330	209.91	-89.33
BGU28-08	333	209.91	-89.41
BGU28-08	336	209.91	-89.51
BGU28-08	339	209.91	-89.59
BGU28-08	342	209.91	-89.63
BGU28-08	345	209.91	-89.64
BGU28-08	348	209.91	-89.68
BGU28-08	351	209.91	-89.69
BGU28-08	354	209.91	-89.69
BGU28-08	357	209.91	-89.32
BGU28-08	360	209.91	-89.78
BGU28-08	363	209.91	-89.76
BGU28-08	366	209.91	-89.63
BGU28-08	369	209.91	-89.36
BGU28-08	372	209.91	-89.39
BGU28-08	375	209.91	-89.28
BGU28-08	378	209.91	-88.93
BGU28-08	381	209.91	-88.47
BGU28-08	384	209.91	-88.2
BGU28-08	387	209.91	-86.96
BGU28-08	390	209.91	-85.77
BGU28-08	393	209.91	-85.19
BGU28-08	396	209.91	-85.23
BGU28-08	399	209.91	-85.08
BGU28-08	402	209.91	-84.57
BGU28-08	405	209.91	-84.59
BGU28-08	408	209.91	-84.67
BGU28-08	411	209.91	-84.75
BGU28-08	414	209.91	-84.61
BGU28-08	417	209.91	-84.06
BGU28-08	420	209.91	-84.06
BGU28-08	423	209.91	-84.17
BGU28-08	426	209.91	-84.25
BGU28-08	429	209.91	-84.29
BGU28-08	432	209.91	-84.22
BGU28-08	435	209.91	-84.05
BGU28-08	438	209.91	-83.81
BGU28-08	441	209.91	-83.83
BGU28-08	444	209.91	-83.89
BGU28-08	447	209.91	-83.98

HOLE-ID	DISTANCE	AZIMUTH	DIP
BGU28-08	450	209.91	-84.36
BGU28-08	453	209.91	-85.72
BGU28-08	456	209.91	-86.35
BGU28-08	459	209.91	-86.38
BGU28-08	462	209.91	-86.42
BGU28-08	465	209.91	-86.45
BGU28-08	468	209.91	-86.31
BGU28-08	471	209.91	-85.79
BGU28-08	474	209.91	-85.81
BGU28-08	477	209.91	-85.8
BGU28-08	480	209.91	-85.8
BGU28-08	483	209.91	-85.78
BGU28-08	486	209.91	-85.78
BGU28-08	489	209.91	-85.85
BGU28-08	492	209.91	-85.97
BGU28-08	495	209.91	-86.05
BGU28-08	498	209.91	-86.04
BGU28-08	501	209.91	-86.01
BGU28-08	504	209.91	-85.99
BGU28-08	507	209.91	-85.99
BGU28-08	510	209.91	-85.97
BGU28-08	513	209.91	-85.96
BGU28-08	516	209.91	-85.96
BGU28-08	519	209.91	-85.98
BGU28-08	522	209.91	-86.04
BGU28-08	525	209.91	-86.06
BGU28-08	528	209.91	-86.13
BGU28-08	531	209.91	-86.15
BGU28-08	534	209.91	-86.11
BGU28-08	537	209.91	-86.14
BGU28-08	540	209.91	-86.15
BGU28-08	543	209.91	-86.16
BGU28-08	546	209.91	-86.19
BGU28-08	549	209.91	-86.35
BGU28-08	552	209.91	-86.81
BGU28-08	555	209.91	-86.78
BGU28-08	558	209.91	-86.77
BGU28-08	561	209.91	-86.83
BGU28-08	564	209.91	-86.9
BGU28-08	567	209.91	-86.97
BGU28-08	570	209.91	-87.03
BGU28-08	573	209.91	-87.1
BGU28-08	576	209.91	-87.17
BGU28-08	579	209.91	-87.24
BGU28-08	582	209.91	-87.31
BGU28-08	585	209.91	-87.38
BGU28-08	588	209.91	-87.44
BGU28-08	591	209.91	-87.51
BGU28-08	594	209.91	-87.58
BGU28-08	597	209.91	-87.65
BGU28-08	600	209.91	-87.72
BGU28-08	603	209.91	-87.79
BGU28-08	606	209.91	-87.86
BGU28-08	609	209.91	-87.93
BGU28-08	612	209.91	-88
BGU28-08	615	209.91	-88.07
BGU28-08	618	209.91	-88.14
BGU28-08	621	209.91	-88.21
BGU28-08	624	209.91	-88.28
BGU28-08	627	209.91	-88.36
BGU28-08	630	209.91	-88.43

HOLE-ID	DISTANCE	AZIMUTH	DIP
BGU28-08	633	209.91	-88.5
BGU28-08	636	209.91	-88.57
BGU28-08	639	209.91	-88.64
BGU28-08	642	209.91	-88.72
BGU28-08	645	209.91	-88.79
BGU28-08	648	209.91	-88.86
BGU28-08	651	209.91	-88.93
BGU28-08	654	209.91	-89
BGU28-08	657	209.91	-89.08
BGU28-08	660	209.91	-89.15
BGU28-08	663	209.91	-89.22
BGU28-08	666	209.91	-89.29
BGU28-08	669	209.91	-89.37
BGU28-08	672	209.91	-89.44
BGU28-08	675	209.91	-89.51
BGU28-08	678	209.91	-89.58
BGU28-08	681	209.91	-89.65
BGU28-08	684	209.91	-89.72
BGU28-08	687	209.91	-89.79
BGU28-08	690	209.91	-89.86
BGU28-08	693	209.91	-89.93
BGU28-08	696	209.91	-89.93
BGU28-08	699	209.91	-89.93
BGU28-08	702	209.91	-89.93
BGU28-08	705	209.91	-89.95
BGU28-08	708	209.91	-89.98
BGU28-08	711	209.91	-90
BGU28-08	714	209.91	-89.97
BGU28-08	717	209.91	-89.93
BGU28-08	720	209.91	-89.9
BGU28-08	723	209.91	-89.89
BGU29-01	0	209.91	-45
BGU29-01	3	209.84	-45.12
BGU29-01	6	209.76	-45.15
BGU29-01	9	209.63	-45.22
BGU29-01	12	209.46	-45.44
BGU29-01	15	209.49	-45.62
BGU29-01	18	209.6	-45.71
BGU29-01	21	209.62	-45.76
BGU29-01	24	209.57	-45.76
BGU29-01	27	209.57	-45.8
BGU29-01	30	209.46	-46
BGU29-01	33	209.3	-46.04
BGU29-01	36	209.15	-45.88
BGU29-01	39	208.99	-45.84
BGU29-01	42	208.9	-45.95
BGU29-01	45	208.99	-46.19
BGU29-01	48	209.1	-46.47
BGU29-01	51	209.15	-46.59
BGU29-01	54	209.04	-46.48
BGU29-01	57	208.82	-46.69
BGU29-01	60	208.7	-47.01
BGU29-01	63	208.51	-46.82
BGU29-01	66	208.4	-46.48
BGU29-01	69	208.35	-46.46
BGU29-01	72	208.21	-46.64
BGU29-01	75	208.05	-46.98
BGU29-01	78	207.85	-47.19
BGU29-01	81	207.74	-47.21
BGU29-01	84	207.68	-47.39
BGU29-01	87	207.66	-47.66

HOLE-ID	DISTANCE	AZIMUTH	DIP
BGU29-01	90	207.62	-47.83
BGU29-01	93	207.6	-47.79
BGU29-01	96	207.51	-47.6
BGU29-01	99	207.35	-47.59
BGU29-01	102	207.16	-47.83
BGU29-01	105	207.12	-48.03
BGU29-01	108	207.18	-48.03
BGU29-01	111	207.26	-48
BGU29-01	114	207.21	-47.98
BGU29-01	117	207.21	-47.96
BGU29-01	120	207.21	-47.99
BGU29-01	123	207.23	-47.98
BGU29-01	126	207.4	-47.94
BGU29-01	129	207.49	-47.93
BGU29-01	132	207.52	-48.02
BGU29-01	135	207.51	-48.07
BGU29-01	138	207.6	-48.14
BGU29-01	141	207.7	-48.19
BGU29-01	144	207.98	-48.17
BGU29-01	147	208.12	-48.13
BGU29-01	150	208.07	-48.27
BGU29-01	153	207.99	-48.37
BGU29-01	156	207.87	-48.37
BGU29-01	159	207.85	-48.41
BGU29-01	162	207.76	-48.41
BGU29-01	165	207.74	-48.43
BGU29-01	168	207.82	-48.48
BGU29-01	171	207.77	-48.56
BGU29-01	174	207.77	-48.66
BGU29-01	177	207.79	-48.75
BGU29-01	180	207.8	-48.81
BGU29-01	183	207.91	-48.91
BGU29-01	186	208.01	-48.95
BGU29-01	189	208.1	-48.98
BGU29-01	192	208.15	-48.96
BGU29-01	195	208.15	-48.97
BGU29-01	198	208.24	-48.97
BGU29-01	201	208.38	-48.85
BGU29-01	204	208.54	-48.83
BGU29-01	207	208.79	-48.87
BGU29-01	210	209.01	-48.89
BGU29-01	213	209.15	-48.84
BGU29-01	216	209.21	-48.79
BGU29-01	219	209.18	-48.73
BGU29-01	222	209.26	-48.62
BGU29-01	225	209.37	-48.5
BGU29-01	228	209.54	-48.33
BGU29-01	231	209.68	-48.16
BGU29-01	234	209.82	-47.97
BGU29-01	237	209.95	-47.78
BGU29-01	240	210.07	-47.58
BGU29-01	243	210.18	-47.42
BGU29-01	246	210.24	-47.33
BGU29-01	249	210.35	-47.16
BGU29-01	252	210.4	-47.02
BGU29-01	255	210.55	-46.86
BGU29-01	258	210.73	-46.68
BGU29-01	261	210.82	-46.46
BGU29-01	264	210.93	-46.26
BGU29-01	267	210.96	-46.09
BGU29-01	270	211.09	-45.9

HOLE-ID	DISTANCE	AZIMUTH	DIP
BGU29-01	273	211.21	-45.75
BGU29-01	276	211.26	-45.56
BGU29-01	279	211.35	-45.33
BGU29-01	282	211.41	-45.1
BGU29-01	285	211.51	-44.89
BGU29-01	288	211.54	-44.69
BGU29-01	291	211.63	-44.48
BGU29-01	294	211.74	-44.29
BGU29-01	297	211.87	-44.1
BGU29-01	300	211.96	-43.92
BGU29-01	303	212.01	-43.75
BGU29-01	306	212.1	-43.54
BGU29-01	309	212.18	-43.33
BGU29-01	312	212.26	-43.11
BGU29-01	315	212.32	-42.89
BGU29-01	318	212.43	-42.67
BGU29-01	321	212.59	-42.45
BGU29-01	324	212.73	-42.24
BGU29-01	327	212.8	-42.03
BGU29-01	330	212.88	-41.81
BGU29-01	333	212.99	-41.58
BGU29-01	336	213.07	-41.36
BGU29-01	339	213.12	-41.14
BGU29-01	342	213.21	-40.93
BGU29-01	345	213.29	-40.72
BGU29-01	348	213.38	-40.49
BGU29-01	351	213.45	-40.27
BGU29-01	354	213.51	-40.22
BGU29-02	0	209.91	-65
BGU29-02	3	209.57	-65
BGU29-02	6	209.4	-65.02
BGU29-02	9	209.37	-65.01
BGU29-02	12	209.05	-65.01
BGU29-02	15	209.01	-65.16
BGU29-02	18	209.24	-65.27
BGU29-02	21	209.26	-65.38
BGU29-02	24	209.34	-65.45
BGU29-02	27	209.45	-65.58
BGU29-02	30	209.35	-65.61
BGU29-02	33	209.21	-65.73
BGU29-02	36	209.21	-65.88
BGU29-02	39	209.1	-66.08
BGU29-02	42	209.07	-66.1
BGU29-02	45	209.21	-66.22
BGU29-02	48	209.35	-66.3
BGU29-02	51	209.07	-66.17
BGU29-02	54	208.8	-66.16
BGU29-02	57	208.4	-66.25
BGU29-02	60	208.26	-66.29
BGU29-02	63	208.32	-66.3
BGU29-02	66	208.21	-66.39
BGU29-02	69	208.07	-66.48
BGU29-02	72	208.18	-66.59
BGU29-02	75	208.26	-66.61
BGU29-02	78	208.49	-66.68
BGU29-02	81	208.74	-66.72
BGU29-02	84	208.68	-66.69
BGU29-02	87	208.82	-66.75
BGU29-02	90	208.88	-66.78
BGU29-02	93	208.88	-66.78
BGU29-02	96	209.04	-66.79

HOLE-ID	DISTANCE	AZIMUTH	DIP
BGU29-02	99	209.18	-66.85
BGU29-02	102	209.26	-66.93
BGU29-02	105	209.18	-66.92
BGU29-02	108	209.21	-66.87
BGU29-02	111	209.37	-66.93
BGU29-02	114	209.49	-66.92
BGU29-02	117	209.43	-66.94
BGU29-02	120	209.73	-67.01
BGU29-02	123	209.9	-67.05
BGU29-02	126	209.99	-67.07
BGU29-02	129	210.26	-67.08
BGU29-02	132	210.32	-67.09
BGU29-02	135	210.38	-67.11
BGU29-02	138	210.49	-67.18
BGU29-02	141	210.66	-67.21
BGU29-02	144	210.45	-67.37
BGU29-02	147	210.46	-67.46
BGU29-02	150	210.46	-67.55
BGU29-02	153	210.48	-67.61
BGU29-02	156	210.65	-67.74
BGU29-02	159	210.6	-67.71
BGU29-02	162	210.79	-67.78
BGU29-02	165	211.04	-67.82
BGU29-02	168	211.32	-67.87
BGU29-02	171	211.46	-67.95
BGU29-02	174	211.51	-67.98
BGU29-02	177	211.66	-68
BGU29-02	180	211.93	-68.03
BGU29-02	183	212.15	-68.14
BGU29-02	186	212.37	-68.2
BGU29-02	189	212.37	-68.25
BGU29-02	192	212.4	-68.29
BGU29-02	195	212.76	-68.33
BGU29-02	198	212.79	-68.36
BGU29-02	201	213.15	-68.32
BGU29-02	204	213.32	-68.37
BGU29-02	207	213.6	-68.29
BGU29-02	210	213.76	-68.28
BGU29-02	213	214.16	-68.3
BGU29-02	216	214.48	-68.27
BGU29-02	219	214.63	-68.34
BGU29-02	222	214.63	-68.36
BGU29-02	225	214.79	-68.3
BGU29-02	228	215.02	-68.26
BGU29-02	231	215.34	-68.34
BGU29-02	234	215.63	-68.31
BGU29-02	237	215.8	-68.46
BGU29-02	240	215.96	-68.46
BGU29-02	243	216.2	-68.56
BGU29-02	246	216.38	-68.6
BGU29-02	249	216.84	-68.63
BGU29-02	252	217.07	-68.71
BGU29-02	255	217.21	-68.8
BGU29-02	258	217.62	-68.89
BGU29-02	261	217.74	-68.96
BGU29-02	264	217.85	-68.94
BGU29-02	267	218.18	-68.99
BGU29-02	270	218.34	-68.9
BGU29-02	273	218.32	-68.87
BGU29-02	276	218.51	-68.83
BGU29-02	279	218.59	-68.85

HOLE-ID	DISTANCE	AZIMUTH	DIP
BGU29-02	282	218.91	-68.92
BGU29-02	285	218.96	-68.96
BGU29-02	288	218.9	-68.95
BGU29-02	291	219.26	-68.95
BGU29-02	294	219.18	-68.97
BGU29-02	297	219.01	-69.03
BGU29-02	300	218.84	-68.97
BGU29-02	303	218.79	-68.86
BGU29-02	306	218.84	-68.78
BGU29-02	309	218.82	-68.77
BGU29-02	312	218.88	-68.74
BGU29-02	315	218.9	-68.75
BGU29-02	318	219.35	-68.74
BGU29-02	321	219.49	-68.74
BGU29-02	324	219.52	-68.71
BGU29-02	327	219.76	-68.7
BGU29-02	330	219.9	-68.74
BGU29-02	333	219.68	-68.7
BGU29-02	336	219.79	-68.64
BGU29-02	339	219.99	-68.59
BGU29-02	342	220.27	-68.47
BGU29-02	345	220.48	-68.33
BGU29-02	348	220.54	-68.17
BGU29-02	351	220.9	-68.09
BGU29-02	354	220.98	-67.97
BGU29-02	357	221.1	-67.87
BGU29-02	360	221.15	-67.77
BGU29-02	363	221.21	-67.64
BGU29-02	366	221.32	-67.52
BGU29-02	369	221.38	-67.42
BGU29-02	372	221.46	-67.31
BGU29-02	375	221.57	-67.21
BGU29-02	378	221.62	-67.11
BGU29-02	381	221.71	-66.97
BGU29-02	384	221.79	-66.86
BGU29-02	387	221.84	-66.76
BGU29-02	390	221.91	-66.64
BGU29-02	393	222.04	-66.54
BGU29-02	396	222.12	-66.43
BGU29-02	399	222.18	-66.32
BGU29-02	402	222.26	-66.2
BGU29-02	405	222.35	-66.09
BGU29-02	408	222.38	-65.99
BGU29-02	411	222.46	-65.88
BGU29-02	414	222.6	-65.76
BGU29-02	417	222.68	-65.65
BGU29-02	420	222.68	-65.53
BGU29-02	423	222.79	-65.43
BGU29-02	426	222.93	-65.32
BGU29-02	429	222.93	-65.2
BGU29-02	432	223.04	-65.1
BGU29-02	435	223.13	-64.98
BGU29-02	438	223.18	-64.87
BGU29-02	441	223.27	-64.77
BGU29-02	444	223.35	-64.66
BGU29-02	447	223.41	-64.54
BGU29-02	450	223.48	-64.42
BGU29-02	453	223.54	-64.33
BGU29-02	456	223.68	-64.22
BGU29-02	459	223.74	-64.1
BGU29-02	462	223.8	-63.99

HOLE-ID	DISTANCE	AZIMUTH	DIP
BGU29-02	465	223.87	-63.87
BGU29-02	468	223.9	-63.77
BGU29-02	471	224.02	-63.65
BGU29-02	474	224.12	-63.55
BGU29-02	477	224.18	-63.43
BGU29-02	480	224.24	-63.32
BGU29-02	483	224.32	-63.21
BGU29-02	486	224.41	-63.11
BGU29-02	489	224.48	-62.99
BGU29-02	492	224.54	-62.87
BGU29-02	495	224.62	-62.77
BGU29-02	498	224.71	-62.66
BGU29-02	501	224.77	-62.55
BGU29-02	504	224.82	-62.43
BGU29-02	507	224.91	-62.32
BGU29-02	510	224.99	-62.22
BGU29-02	513	225.09	-62.11
BGU29-02	516	225.13	-61.99
BGU29-02	519	225.2	-61.88
BGU29-02	522	225.3	-61.76
BGU29-02	525	225.35	-61.66
BGU29-02	528	225.45	-61.56
BGU29-02	531	225.52	-61.43
BGU29-02	534	225.57	-61.33
BGU29-02	537	225.65	-61.23
BGU29-02	540	225.74	-61.09
BGU29-02	543	225.82	-60.99
BGU29-02	546	225.9	-60.88
BGU29-02	549	225.96	-60.77
BGU29-02	552	226.01	-60.65
BGU29-02	555	226.29	-60.6
BGU29-02	555.4	226.77	-60.61
BGU29-07	0	209.91	40.12
BGU29-07	3	210.1	40.22
BGU29-07	6	210.1	40.34
BGU29-07	9	210.02	40.11
BGU29-07	12	210.04	39.87
BGU29-07	15	210.15	39.89
BGU29-07	18	210.15	40.03
BGU29-07	21	210.05	40.01
BGU29-07	24	210.09	39.81
BGU29-07	27	210.26	39.59
BGU29-07	30	210.41	39.61
BGU29-07	33	210.21	39.78
BGU29-07	36	209.9	39.72
BGU29-07	39	209.74	39.48
BGU29-07	42	209.66	39.26
BGU29-07	45	209.55	39.12
BGU29-07	48	209.54	39.08
BGU29-07	51	209.84	39.24
BGU29-07	54	210.04	39.42
BGU29-07	57	209.82	39.64
BGU29-07	60	209.71	39.76
BGU29-07	63	209.82	39.66
BGU29-07	66	210.02	39.44
BGU29-07	69	210.15	39.21
BGU29-07	72	210.21	39.15
BGU29-07	75	209.98	39.4
BGU29-07	78	209.35	39.74
BGU29-07	81	209.21	39.31
BGU29-07	84	209.87	38.39

HOLE-ID	DISTANCE	AZIMUTH	DIP
BGU29-07	87	209.82	38.44
BGU29-07	90	209.49	38.99
BGU29-07	93	209.35	39.27
BGU29-07	96	209.37	39.2
BGU29-07	99	209.48	39.02
BGU29-07	102	209.62	38.93
BGU29-07	105	209.73	38.88
BGU29-07	108	209.79	38.83
BGU29-07	111	209.85	38.74
BGU29-07	114	209.88	38.64
BGU29-07	117	209.8	38.52
BGU29-07	120	209.74	38.4
BGU29-07	123	209.76	38.21
BGU29-07	126	209.82	38.08
BGU29-07	129	209.76	37.97
BGU29-07	132	209.59	37.89
BGU29-07	135	209.4	37.83
BGU29-07	138	209.35	37.74
BGU29-07	141	209.48	37.65
BGU29-07	144	209.62	37.6
BGU29-07	147	209.68	37.61
BGU29-07	150	209.59	37.68
BGU29-07	153	209.55	37.7
BGU29-07	156	209.59	37.81
BGU29-07	159	209.54	38.2
BGU29-07	162	209.48	38.21
BGU29-07	165	209.46	38.15
BGU29-07	168	209.45	38.03
BGU29-07	171	209.4	37.96
BGU29-07	174	209.29	37.91
BGU29-07	177	209.26	37.84
BGU29-07	180	209.24	37.79
BGU29-07	183	209.2	37.73
BGU29-07	186	209.13	37.67
BGU29-07	189	209.12	37.62
BGU29-07	192	209.1	37.56
BGU29-07	195	209.02	37.49
BGU29-07	198	209.01	37.43
BGU29-07	201	208.96	37.38
BGU29-07	204	208.9	37.32
BGU29-07	207	208.88	37.26
BGU29-07	210	208.85	37.2
BGU29-07	213	208.82	37.14
BGU29-07	216	208.76	37.07
BGU29-07	219	208.73	37.02
BGU29-07	222	208.71	36.97
BGU29-07	225	208.68	36.91
BGU29-07	228	208.62	36.85
BGU29-07	231	208.6	36.78
BGU29-07	233.3	208.6	36.77
BGU30-03	0	209.91	-63
BGU30-03	3	209.88	-63.07
BGU30-03	6	209.71	-63.12
BGU30-03	9	209.66	-63.19
BGU30-03	12	209.48	-63.23
BGU30-03	15	209.29	-63.38
BGU30-03	18	209.24	-63.4
BGU30-03	21	209.1	-63.41
BGU30-03	24	208.95	-63.37
BGU30-03	27	208.96	-63.38
BGU30-03	30	209.02	-63.42

HOLE-ID	DISTANCE	AZIMUTH	DIP
BGU30-03	33	208.9	-63.39
BGU30-03	36	208.91	-63.38
BGU30-03	39	208.68	-63.51
BGU30-03	42	208.76	-63.54
BGU30-03	45	208.74	-63.51
BGU30-03	48	208.55	-63.52
BGU30-03	51	208.23	-63.6
BGU30-03	54	208.12	-63.6
BGU30-03	57	208.04	-63.5
BGU30-03	60	208.15	-63.46
BGU30-03	63	208.3	-63.45
BGU30-03	66	208.38	-63.42
BGU30-03	69	208.43	-63.41
BGU30-03	72	208.29	-63.45
BGU30-03	75	208.35	-63.45
BGU30-03	78	208.55	-63.45
BGU30-03	81	208.55	-63.45
BGU30-03	84	208.45	-63.51
BGU30-03	87	208.43	-63.57
BGU30-03	90	208.35	-63.63
BGU30-03	93	208.4	-63.69
BGU30-03	96	208.45	-63.74
BGU30-03	99	208.4	-63.85
BGU30-03	102	208.46	-63.89
BGU30-03	105	208.62	-63.89
BGU30-03	108	208.76	-63.9
BGU30-03	111	208.91	-63.99
BGU30-03	114	209.02	-64.01
BGU30-03	117	208.93	-64
BGU30-03	120	209.12	-64.01
BGU30-03	123	209.23	-64.03
BGU30-03	126	209.24	-64.06
BGU30-03	129	209.4	-64.1
BGU30-03	132	209.49	-64.14
BGU30-03	135	209.51	-64.15
BGU30-03	138	209.62	-64.17
BGU30-03	141	209.76	-64.18
BGU30-03	144	209.93	-64.15
BGU30-03	147	209.99	-64.11
BGU30-03	150	209.99	-64.12
BGU30-03	153	209.99	-64.13
BGU30-03	156	209.98	-64.15
BGU30-03	159	209.93	-64.17
BGU30-03	162	210.07	-64.15
BGU30-03	165	210.21	-64.15
BGU30-03	168	210.29	-64.19
BGU30-03	171	210.35	-64.22
BGU30-03	174	210.41	-64.27
BGU30-03	177	210.49	-64.29
BGU30-03	180	210.6	-64.28
BGU30-03	183	210.66	-64.28
BGU30-03	186	210.68	-64.23
BGU30-03	189	210.6	-64.21
BGU30-03	192	210.49	-64.21
BGU30-03	195	210.68	-64.22
BGU30-03	198	210.76	-64.29
BGU30-03	201	210.79	-64.32
BGU30-03	204	210.9	-64.33
BGU30-03	207	211.01	-64.37
BGU30-03	210	210.93	-64.41
BGU30-03	213	210.93	-64.42

HOLE-ID	DISTANCE	AZIMUTH	DIP
BGU30-03	216	210.96	-64.47
BGU30-03	219	211.04	-64.48
BGU30-03	222	211.04	-64.48
BGU30-03	225	211.21	-64.49
BGU30-03	228	211.34	-64.48
BGU30-03	231	211.51	-64.48
BGU30-03	234	211.59	-64.47
BGU30-03	237	211.82	-64.46
BGU30-03	240	211.93	-64.46
BGU30-03	243	212.04	-64.43
BGU30-03	246	212.23	-64.38
BGU30-03	249	212.27	-64.21
BGU30-03	252	212.24	-63.74
BGU30-03	255	212.48	-63.72
BGU30-03	258	212.45	-63.75
BGU30-03	261	212.26	-63.8
BGU30-03	264	212.27	-63.82
BGU30-03	267	212.15	-63.82
BGU30-03	270	212.1	-63.87
BGU30-03	273	212.24	-63.82
BGU30-03	276	212.38	-63.75
BGU30-03	279	212.41	-63.69
BGU30-03	282	212.49	-63.69
BGU30-03	285	212.51	-63.69
BGU30-03	288	212.57	-63.66
BGU30-03	291	212.79	-63.64
BGU30-03	294	212.93	-63.58
BGU30-03	297	213.1	-63.53
BGU30-03	300	213.24	-63.45
BGU30-03	303	213.43	-63.39
BGU30-03	306	213.37	-63.35
BGU30-03	309	213.62	-63.29
BGU30-03	312	213.73	-63.2
BGU30-03	315	213.73	-63.13
BGU30-03	318	213.9	-63.12
BGU30-03	321	214.1	-63.11
BGU30-03	324	214.16	-63.07
BGU30-03	327	214.24	-63.02
BGU30-03	330	214.32	-62.97
BGU30-03	333	214.37	-62.92
BGU30-03	336	214.38	-62.87
BGU30-03	339	214.49	-62.83
BGU30-03	342	214.57	-62.78
BGU30-03	345	214.62	-62.71
BGU30-03	346	214.76	-62.71
BGU30-04	0	209.91	-72
BGU30-04	3	210.02	-72.08
BGU30-04	6	210.1	-72.13
BGU30-04	9	210.05	-72.21
BGU30-04	12	209.93	-72.28
BGU30-04	15	209.76	-72.3
BGU30-04	18	209.68	-72.24
BGU30-04	21	209.38	-72.24
BGU30-04	24	209.34	-72.19
BGU30-04	27	209.12	-72.16
BGU30-04	30	209.18	-72.12
BGU30-04	33	208.99	-72.14
BGU30-04	36	208.74	-72.08
BGU30-04	39	208.62	-72.1
BGU30-04	42	208.45	-72.12
BGU30-04	45	208.34	-72.22

HOLE-ID	DISTANCE	AZIMUTH	DIP
BGU30-04	48	207.76	-72.26
BGU30-04	51	207.51	-72.29
BGU30-04	54	207.15	-72.35
BGU30-04	57	207.18	-72.4
BGU30-04	60	207.1	-72.42
BGU30-04	63	207.04	-72.46
BGU30-04	66	207.18	-72.41
BGU30-04	69	207.26	-72.33
BGU30-04	72	207.2	-72.31
BGU30-04	75	207.29	-72.3
BGU30-04	78	207.18	-72.31
BGU30-04	81	206.82	-72.28
BGU30-04	84	206.76	-72.31
BGU30-04	87	206.85	-72.3
BGU30-04	90	206.43	-72.36
BGU30-04	93	206.23	-72.33
BGU30-04	96	206.24	-72.31
BGU30-04	99	206.52	-72.39
BGU30-04	102	206.37	-72.44
BGU30-04	105	206.43	-72.48
BGU30-04	108	206.55	-72.51
BGU30-04	111	206.82	-72.42
BGU30-04	114	206.99	-72.35
BGU30-04	117	207.16	-72.34
BGU30-04	120	207.26	-72.35
BGU30-04	123	207.54	-72.36
BGU30-04	126	207.93	-72.32
BGU30-04	129	208.46	-72.35
BGU30-04	132	208.9	-72.35
BGU30-04	135	209.07	-72.34
BGU30-04	138	209.48	-72.34
BGU30-04	141	209.52	-72.35
BGU30-04	144	209.84	-72.39
BGU30-04	147	210.13	-72.41
BGU30-04	150	210.1	-72.44
BGU30-04	153	210.3	-72.46
BGU30-04	156	210.46	-72.58
BGU30-04	159	210.6	-72.63
BGU30-04	162	210.49	-72.7
BGU30-04	165	210.48	-72.8
BGU30-04	168	210.46	-72.9
BGU30-04	171	210.76	-72.92
BGU30-04	174	210.87	-72.98
BGU30-04	177	210.54	-72.88
BGU30-04	180	210.26	-72.84
BGU30-04	183	210.15	-72.78
BGU30-04	186	210.26	-72.75
BGU30-04	189	210.52	-72.74
BGU30-04	192	210.66	-72.73
BGU30-04	195	210.71	-72.7
BGU30-04	198	210.6	-72.75
BGU30-04	201	210.51	-72.82
BGU30-04	204	210.6	-72.83
BGU30-04	207	210.65	-72.84
BGU30-04	210	210.59	-72.87
BGU30-04	213	210.6	-72.93
BGU30-04	216	210.77	-72.91
BGU30-04	219	210.9	-72.87
BGU30-04	222	210.9	-72.89
BGU30-04	225	211.01	-72.9
BGU30-04	228	211.09	-72.87

HOLE-ID	DISTANCE	AZIMUTH	DIP
BGU30-04	231	211.24	-72.83
BGU30-04	234	211.65	-72.85
BGU30-04	237	211.93	-72.89
BGU30-04	240	212.12	-72.93
BGU30-04	243	212.45	-72.88
BGU30-04	246	212.66	-72.86
BGU30-04	249	212.62	-72.93
BGU30-04	252	212.55	-73
BGU30-04	255	212.55	-73.06
BGU30-04	258	212.41	-73.1
BGU30-04	261	212.62	-73.09
BGU30-04	264	212.54	-73.17
BGU30-04	267	212.41	-73.19
BGU30-04	270	212.38	-73.19
BGU30-04	273	212.57	-73.18
BGU30-04	276	212.62	-73.18
BGU30-04	279	212.68	-73.29
BGU30-04	282	212.65	-73.4
BGU30-04	285	212.74	-73.42
BGU30-04	288	213.15	-73.45
BGU30-04	291	213.79	-73.41
BGU30-04	294	214.12	-73.34
BGU30-04	297	214.45	-73.33
BGU30-04	300	214.76	-73.3
BGU30-04	303	215.21	-73.29
BGU30-04	306	215.54	-73.28
BGU30-04	309	216.24	-73.25
BGU30-04	312	217.07	-73.22
BGU30-04	315	217.87	-73.25
BGU30-04	318	218.62	-73.36
BGU30-04	321	219.4	-73.54
BGU30-04	324	219.88	-73.68
BGU30-04	327	220.18	-73.78
BGU30-04	330	220.21	-73.87
BGU30-04	333	220.38	-73.97
BGU30-04	336	220.52	-74.07
BGU30-04	339	220.93	-74.09
BGU30-04	342	221.2	-74.09
BGU30-04	345	221.49	-74.09
BGU30-04	348	221.59	-74.03
BGU30-04	351	221.54	-74.04
BGU30-04	354	221.68	-74.05
BGU30-04	357	222.18	-74.01
BGU30-04	360	222.57	-73.7
BGU30-04	363	222.34	-73.34
BGU30-04	366	222.24	-73.15
BGU30-04	369	222.34	-73.14
BGU30-04	372	222.71	-73.29
BGU30-04	375	222.85	-73.45
BGU30-04	378	222.41	-73.49
BGU30-04	381	222.12	-73.54
BGU30-04	384	221.8	-73.58
BGU30-04	387	221.54	-73.59
BGU30-04	390	221.21	-73.64
BGU30-04	393	221.21	-73.8
BGU30-04	396	221.4	-73.79
BGU30-04	399	221.29	-73.67
BGU30-04	402	221.3	-73.59
BGU30-04	405	221.49	-73.53
BGU30-04	408	221.62	-73.46
BGU30-04	411	221.38	-73.33

HOLE-ID	DISTANCE	AZIMUTH	DIP
BGU30-04	414	221.38	-73.2
BGU30-04	417	221.4	-73.1
BGU30-04	420	221.27	-73.01
BGU30-04	423	221.4	-72.89
BGU30-04	426	221.4	-72.79
BGU30-04	429	221.41	-72.68
BGU30-04	432	221.35	-72.54
BGU30-04	435	221.38	-72.43
BGU30-04	438	221.35	-72.33
BGU30-04	441	221.34	-72.21
BGU30-04	444	221.35	-72.1
BGU30-04	447	221.32	-72
BGU30-04	450	221.3	-71.87
BGU30-04	453	221.24	-71.76
BGU30-04	456	221.26	-71.65
BGU30-04	459	221.29	-71.54
BGU30-04	462	221.23	-71.42
BGU30-04	465	221.24	-71.31
BGU30-04	468	221.26	-71.2
BGU30-04	471	221.21	-71.06
BGU30-04	474	221.2	-70.96
BGU30-04	477	221.18	-70.86
BGU30-04	480	221.24	-70.74
BGU30-04	483	221.18	-70.63
BGU30-04	486	221.12	-70.51
BGU30-04	489	221.21	-70.4
BGU30-04	492	221.15	-70.28
BGU30-04	494	220.96	-70.25
BGU30-04A	0	209.91	-68
BGU30-05	0	209.91	-78
BGU30-05	50	209.91	-76
BGU30-05	101.5	209.91	-79
BGU30-05	150	209.91	-77.5
BGU30-05	200	209.91	-83
BGU30-05	252	209.91	-84.5
BGU30-05	300	209.91	-80
BGU30-05	350	209.91	-79
BGU30-05	402	209.91	-80
BGU30-06	0	209.91	25
BGU30-06	50	209.91	25
BGU30-06	100	209.91	23
BGU30-06	150	209.91	23
BGU30-06	200	209.91	20
BGU30-06	250	209.91	18
BGU30-08	0	209.91	55
BGU30-08A	0	209.91	55
GRS-125	0	37.3	-87.2
GRS-127	0	40.6	-85.3
WAN1-1	0	200	-85.05
WAN1-1	683	200	-85.5
WAN1-1	783	200	-85.5
WAN1-1	883	200	-85.5
WAN1-1	983	200	-86
WAN1-3	0	111	-83.5
WAN1-3	136.8	111	-83.5
WAN1-3	236.8	111	-83.5
WAN1-3	336.8	111	-83.5
WAN1-3	436.8	111	-83.5
WAN1-3	536.8	111	-83.5
WAN1-3	636.8	111	-83.5
WAN1-3	736.8	111	-84

HOLE-ID	DISTANCE	AZIMUTH	DIP
WAN1-3	836.8	111	-84
WAN1-3	936.8	111	-84
WAN1-3	999.7	111	-84
WAN2-2	0	115	-73
WAN2-2	166	115	-73
WAN2-2	266	115	-73
WAN2-2	366	115	-73
WAN2-2	466	115	-73
WAN2-2	566	115	-72
WAN2-2	666	115	-72
WAN2-2	766	115	-72
WAN2-2	866	115	-73
WAN2-2	966	115	-73
WAN4-1	0	0	-90
WAN4-1	100	0	-90
WAN4-1	200	0	-90
WAN4-1	250	0	-90
WAN4-1	300	0	-90
WAN4-1	350	0	-90
WAN4-1	400	0	-90
WAN4-1	450	0	-90
WAN4-1	500	0	-90
WAN4-1	550	0	-89
WAN4-1	623.3	0	-89
WAN4-2	0	219	-75
WAN4-2	50	219	-75
WAN4-2	100	219	-75
WAN4-2	150	219	-75
WAN4-2	200	219	-75
WAN4-2	250	219	-76
WAN4-2	300	219	-77
WAN4-2	365.7	219	-77
WAN4-3	0	0	-40
WAN4-3	50	0	-40
WAN4-3	100	0	-39
WAN4-3	150	0	-39
WAN4-3	200	0	-39
WAN4-3	250	0	-39
WAN4-3	300	0	-38
WAN4-3	352	0	-38
WAN4-4	0	82	-40
WAN4-4	50	82	-40
WAN4-4	100	82	-40
WAN4-4	150	82	-39
WAN4-4	200	82	-39
WAN4-4	250	82	-39
WAN4-4	300	82	-39
WAN4-4	350	82	-39
WAN4-4	400	82	-38
WAN4-4	424	82	-38
WAN4-5	0	320	-44
WAN4-5	50	320	-40
WAN4-5	100	320	-42
WAN4-5	150	320	-40
WAN4-5	200	320	-38
WAN4-5	250	320	-34
WAN4-5	300	320	-32
WAN4-5	350	320	-32
WAN4-5	412	320	-32
WAN4-6	0	285	-40
WAN4-6	50	285	-40.5

HOLE-ID	DISTANCE	AZIMUTH	DIP
WAN4-6	100	285	-40
WAN4-6	150	285	-40.5
WAN4-6	200	285	-40.5
WAN4-6	250	285	-40.5
WAN4-6	300	285	-39
WAN4-6	350	285	-39.5
WAN4-6	401	285	-40
WGR-12	0	270.5	-44
WGR-12	50	270.5	-44
WGR-12	100	270.5	-44
WGR-12	150	270.5	-44
WGR-12	200	270.5	-44
WGR-12	250	270.5	-44
WGR-12	300	270.5	-44
WGR-12	350	270.5	-44
WGR-12	400	270.5	-44
WGR-12	454.05	270.5	-44
WGR-13	0	274.3	-46
WGR-13	50	274.3	-46
WGR-13	100	274.3	-46
WGR-13	150	274.3	-46
WGR-13	200	274.3	-46
WGR-13	250	274.3	-46
WGR-13	300	274.3	-46
WGR-13	350	274.3	-46
WGR-13	400	274.3	-46
WGR-3	0	267.1	-54
WGR-3	22.75	267.1	-54
WGR-3	47.75	267.1	-54
WGR-3	72.75	267.1	-54
WGR-3	97.75	267.1	-54
WGR-3	122.75	267.1	-54
WGR-3	147.75	267.1	-54
WGR-3	172.75	267.1	-54
WGR-3	197.75	267.1	-54
WGR-3	223.75	267.1	-54
WGR-4	0	272.2	-42
WGR-4	50.4	272.2	-42
WGR-4	100.4	272.2	-42
WGR-4	150.4	272.2	-42
WGR-4	199.4	272.2	-42
WGZ-8	0	277.2	-45
WGZ-8	440	277.2	-45

Appendix 7

LA-ICPMS sample description, paragenesis, corrected results

LA-ICPMS results: Glass (NIST) standard RUN1-6

LA-ICPMS results: Nickel sulphide standard PGEARUN1-6

Appendix 7 - LA-ICPMS sample index, interpretation, recalculation

Run	Deposit	Mineral	Sample	Desc	Stage	Sample Number	Comments
Run2-12	BG	Chalcopyrite	BG30-CPY	cpy-1?	?	BGU21-02-14	
Run5-28	BG	Chalcopyrite-corrected	BG37-PY	cpy-?	?	BGU27-06-348	adjust (*) NIST by FeO standard = 304317.3/465531.7 =(0.653698); adjust (*) PGEA by SO standard = 349436.8/534495.6 =(0.653769)
Run5-18	BG	Chalcopyrite	BG14-CPY	cpy1	1	BGU28-08-375	
Run5-7	BG	Chalcopyrite	BG01-PY2	CPY-1	1	BGU28-05-268	
Run5-17	BG	Chalcopyrite	BG05-SP2	cpy-1	1	BGU24-10-305	
Run5-6	BG	Chalcopyrite	BG01-CPY	CPY-1	1	BGU28-05-268	
Run5-25	BG	Chalcopyrite	BG35-CPY	cpy-2	2	BG1-5-256	
Run1-11	BG	Chalcopyrite	JC22-CPY	cpy-?	2	BGU08-05-190	
Run5-22	BG	Chalcopyrite	BG34-CPY	cpy-2	2	BG1-4A-330	
Run3-8	BG	Chalcopyrite	JL10-CPY	cpy-2?	2	BGU30-03-180	
Run1-7	BG	Chalcopyrite	BG24-CPY	cpy-2?	2	BGU24-11-343	
Run5-16	BG	Pyrite	BG05-PY1	py-1	1	BGU24-10-305	
Run4-9	BG	Pyrite	BG32-PY	cg py (1?)	?	BGU26-03-122.4	2nd pgearun4 file
Run5-23	BG	Pyrite	BG34-PY2	py-cg-early	1	BG1-4A-330	
Run1-12	BG	Pyrite	BG14-PY	py-1?-ass	1	BGU28-08-375	
Run5-15	BG	Pyrite	BG19-PY	PY-?2	2	BGU18-03-212	
Run3-6	BG	Pyrite	JL10-PY1	py-2?ass-rep	2	BGU30-03-180	
Run2-25	BG	Pyrite	JL10-PY1	py-1?ass	2	BGU30-03-180	
Run5-8	BG	Pyrite	BG13-PY	PY-2	?2	BGU19-03-184.7	
Run3-10	BG	Pyrite	BG05-PY	py-2	2	BGU24-10-305	
Run4-10	BG	Pyrite	BG32-PY2	fg py (2?)	2-bi-te	BGU26-03-122.4	2nd pgearun4 file. Bi-Te minerals present in sample
Run5-24	BG	Pyrite	BG35-PY	py-2	2-bi-te	BG1-5-256	Bi-Te minerals present in sample
Run5-20	BG	Pyrite	BG34-PY	late-py-marc	2-bi-te	BG1-4A-330	Bi-Te minerals present in sample
Run2-17	BG	Pyrite	BG06-PY	py-2	2-bi-te	BGU18-03-211.2	Bi-Te minerals present in sample
Run1-9	BG	Pyrite	JC22-PY	py-?	2-bi-te	BGU08-05-190	Bi-Te minerals present in sample
Run2-14	BG	Pyrite	JL06-PY2	py-bx	2-bi-te	BGU21-02-13.3	Bi-Te minerals present in sample
Run5-14	BG	Pyrite	BG33-PY	PY-2	2-bi-te	BGU26-4-275F	Bi-Te minerals present in sample
Run4-15	BG	Pyrite	BG01-PY	PY-?2-Bi	2-con	BGU28-05-268	2nd pgearun4 file. Bi-Te minerals present in sample
Run5-27	BG	Pyrite	BG36-PY	Py-?1 (?Au)	?	BGU27-06-348	
Run5-29	BG	Pyrite	BG37-PY2	Py-?1 (?Au)	?	BGU27-06-348	
Run2-13	BG	Pyrite	BG30-PY	py-1?	?	BGU21-02-14	
Run1-6	BG	Pyrite	BG24-PY	py-(compat 1?	?	BGU24-11-343	
Run1-13	BG	Pyrite	JL09-PY	py-bx	bx	BGU21-3-226.3	
Run4-14	BG	Pyrite	JL07-PY	py-bx	bx	BGU21-5-17.5	2nd pgearun4 file
Run4-7	BG	Pyrite	BG31-CPY	PY-BX	bx	BGU21-5-22	2nd pgearun4 file
Run5-31	BG	Sphalerite	BG38-SPH	sph-(no assay	?	BGU30-04-137.9	Used Microprobe sphalerite for FeO and SO = same as JL06 (bgu21-2-13-3a-sph4; Appendix 5)
Run5-30	BG	Sphalerite	BG37-SPH	sph-?1 (?Au)	?	BGU27-06-348	Used Microprobe sphalerite for FeO and SO = same as JL06 (bgu21-2-13-3a-sph4; Appendix 5)
Run3-7	BG	Sphalerite	JL10-SPH	sph-2?	2	BGU30-03-180	checked Zn and S values (used sphalerite Microprobe result: bgu30-3-180-sph1; Appendix 5)
Run3-11	BG	Sphalerite	BG05-SPH	sph-2	2	BGU24-10-305	checked Zn and S values (used sphalerite Microprobe result: BG05-sph2; Appendix 5)
Run5-10	BG	Sphalerite	BG13-SP2	SPH-2	2	BGU19-03-184.7	checked Zn and S values (used sphalerite Microprobe result: bg13-sph4; Appendix 5)
Run2-16	BG	Sphalerite	BG06-SPH	sph-2	2	BGU18-03-211.2	checked Zn and S values (used sphalerite Microprobe result: bg06-sph2; Appendix 5)
Run1-16	BG	Sphalerite	BG24-SP2	sph-2 (24)	2	BGU24-11-343	checked Zn and S values (used sphalerite Microprobe result: bg24-sph2; Appendix 5)
Run1-15	BG	Sphalerite	BG24-SPH	sph-2 (24)	2	BGU24-11-343	checked Zn and S values (used sphalerite Microprobe result: bg24-sph2; Appendix 5)
Run5-13	BG	Sphalerite	BG33-SPH	SPH-2	2	BGU26-4-275F	Used Microprobe sphalerite for FeO and SO = same as JL06 (bgu21-2-13-3a-sph4; Appendix 5)
Run1-10	BG	Sphalerite	JC22-SPH	sph-2-SE	2	BGU08-05-190	checked Zn and S values (used sphalerite Microprobe result: BG22-sph3; Appendix 5)
Run5-26	BG	Sphalerite	BG35-SPH	sph-2 upper	2	BG1-5-256	Used Microprobe sphalerite for FeO and SO = same as JL06 (bgu21-2-13-3a-sph4; Appendix 5)
Run5-21	BG	Sphalerite	BG34-SPH	sph-2 upper	2	BG1-4A-330	checked Zn and S values (used sphalerite Microprobe result:BG1-4a-330-sph2; Appendix 5)
Run1-14	BG	Sphalerite	JL09-SPH	sph-bx	bx	BGU21-3-226.3	checked Zn and S values (used sphalerite Microprobe result: bgu21-3-226-sph2; Appendix 5)
Run2-15	BG	Sphalerite	JL06-SPH	sph-bx	bx	BGU21-02-13.3	checked Zn and S values (used sphalerite Microprobe result: bgu21-2-13-3a-sph4; Appendix 5)
Run5-19	WAN	Pyrite	KP10-PY		2	wan4-6-28	
Run4-6	WAN	Pyrite	JL05=JL01-PY		2	WAN4-5-50	2nd pgearun4 file
Run4-13	WAN	Pyrite	JL02-PY		2	WAN4-1-72.1	2nd pgearun4 file

Appendix 7 - LA-ICPMS sample index, interpretation, recalculation

Run	Deposit	Mineral	Sample	Desc	Stage	Sample Number	Comments
Run2-9	WAN	Pyrite	KP11-PY	su	1	WAN4-3-302.5	
Run5-11	WAN	Pyrite	JL04-PY		1	WAN4-3-108.8	
Run4-8	WAN	Pyrite	JL01-PY1		1	WAN4-4-603	2nd pgearun4 file
Run3-12	WAN	Pyrite	JL19-PY		1	WAN2-2-852	
Run4-12	WAN	Pyrite	JL03-PY		?	WAN4-3-80.5	2nd pgearun4 file
Run3-9	WAN	Sphalerite	WAN-SPH	sph	2	WAN24-2-234	checked Zn and S values (used sphalerite Microprobe result: W3-sph1)
Run2-11	WAN	Sphalerite	KP11-SPH	sph	1	WAN4-3-302.5	checked Zn and S values (used sphalerite Microprobe result: kp11-sph2)
Run2-10	WAN	Chalcopyrite	KP11-CPY	cpy	1	WAN4-3-302.5	
Run3-13	WAN	Chalcopyrite	JL19-CPY	cpy	1	WAN2-2-852	
Run5-12	WAN	Chalcopyrite	JL04-CPY	cpy	1	WAN4-3-108.8	
Run2-8	GIC	Pyrite	MS-PY	py		A94-31-1	
Run2-7	GIC	Chalcopyrite	MS-CPY	cpy		A94-31-1	
Run4-11	DOZ	Pyrite	KP04-PY	py		KP04	2nd pgearun4 file
Run6-15	WGR	Pyrite	WG3-PY7	py	C-1	WGR4-89	
Run6-14	WGR	Pyrite	WG3-PY6	py	C-3	WGR4-89	
Run6-9	WGR	Pyrite	WG3-PY2	py	C-3	WGR4-89	
Run6-8	WGR	Pyrite	WG3-PY	py	C-3	WGR4-89	
Run6-16	WGR	Pyrite	WG3-PY8	py	F-1	WGR4-89	
Run6-13	WGR	Pyrite	WG3-PY5	py	F-3	WGR4-89	
Run6-12	WGR	Pyrite	WG3-PY4	py	F-3	WGR4-89	
Run6-10	WGR	Sphalerite	WG3-SU1	sph	WGR	WGR4-89	Used Microprobe sphalerite for FeO and SO = same as JL10 (bgu30-3-180-sph1)

Corrected Analysis

correct from pyrite to chalcopyrite - NB error and detection limits in original file are invalid

adjust (*) GLASS by FeO standard = 304317.3/465531.7 =(0.653698); adjust (*) PGEA by SO standard = 349436.8/534495.6 =(0.653769)

all values in ppm

			PGEA	PGEA	PGEA	PGEA	PGEA
Run	**Sample**	**sample#**	**Te125**	**Te128**	**Cu65**	**As75**	**Bi209**
Run5-28	BG37-PY	BGU27-06-348	0.46417599	0.340613649	213523		1.96784469
PGEA	PGEA	PGEA	PGEA	PGEA	PGEA	PGEA	PGEA
Se82	**S34**	**Ni60**	**Ni62**	**Ir193**	**Os189**	**Os190**	**Ru101**
40.23948	349436.81	477.7809229	2.85697053	0	0	0.008237489	0.186977934
PGEA	PGEA	PGEA	PGEA	PGEA	Glass	Glass	Glass
Ru99	**Rh103**	**Pt195**	**Pd108**	**Au197**	**La139**	**Ce140**	**Nd146**
0.47006	22.849227	0.016997994	5.5570365	0.025235483	0.0537	0.03608413	0.012224153
Glass	Glass	Glass	Glass	Glass	Glass	Glass	Glass
Hf178	**Au197**	**Ti49**	**Y89**	**Nb93**	**Mo95**	**W182**	**Ag107**
0.142506	0.0333386	37.914484	0.380452236	0.004510516	0.4524	0.026801618	1043.498117
Glass	Glass	Glass	Glass	Glass	Glass	Glass	Glass
As75	**Bi209**	**Ca43**	**Cd111**	**Cu65**	**Fe57**	**Ga71**	**In115**
0	2.2029623	486.1944245	385.2896012	363513.0447	304317	25.87990382	9.06679126
Glass	Glass	Glass	Glass	Glass	Glass	Glass	Glass
Mn55	**Pb208**	**Re185**	**Re187**	**Sb121**	**Se82**	**Si29**	**Sn118**
2908.093	70.540551	0	0	2.30755394	30.9	20765.10919	16.23785832
Glass	Glass	Glass	Glass	Glass	Glass	Glass	Glass
Th232	**U238**	**V51**	**Zn66**	**Zr90**	**Al27**	**Sc45**	**Cr53**
0.277168	1.5165794	215.2366035	68550.38069	5.34071266	12165	1.26817412	117.672177
Glass	Glass	Glass					
Co59	**Ni62**	**Ni60**					
0.438631	2.6866988	441.2003911					

GLITTER4.0: Laser Ablation Analysis Results

G:\KYLIE\MAR13\RUN1
Fri Mar 14 17:11:52 2003

All values are reported in ppm

GLITTER!: Trace Element Concentrations MDL filtered.

	Run1-1	Run1-2	Run1-3	Run1-4	Run1-5	Run1-6	Run1-7	Discarded Run1-8	Run1-9	Run1-10	Run1-11	Run1-12	Run1-13	Run1-14	Run1-15	Run1-16	Run1-17	Run1-18	Run1-19	Run1-20	Run1-21
Element	STD610-1	STD610-2	BCR2G-1	PGEA-1	PGEA-2	BG24-PY	BG24-CPY	JL06-PY	JC22-PY	JC22-SPH	JC22-CPY	BG14-PY	JL09-PY	JL09-SPH	BG24-SPH	BG24-SP2	STD610-3	STD610-4	PGEA-3	PGEA-4	PGEA-5
Al27	10396.89	9883.86	48238.78	<0.00002	<*****	29.84	172.98	5.1	19.25	<0.61	0.9	119.39	1.8	10.41	203.29	47.26	9727.78	10663.39	<0.00031	<0.00035	<0.00096
Si29	348536.72	327274.47	151349.58	0.0351	<****	2324.01	9067.82	142.1	307.94	557.23	559.54	6264.41	147.09	412.94	17766.85	2954.51	322064.53	357519.16	0.16	<0.078	0.5
S34	<-NaN	<-NaN	<-NaN	<-NaN	<-NaN	<-NaN	<-NaN	<-NaN	<-NaN	<-NaN	<-NaN	<-NaN	<-NaN	<-NaN	<-NaN	<-NaN	<-NaN	<-NaN	<-NaN	<-NaN	<-NaN
Ca43	86332.28	79859.61	32661.78	<0.00230	0.15	155.91	1161.81	16.09	388.74	308.54	622.92	405.65	<18.18	901.38	1132.58	280.59	79615.38	86054.51	<0.050	<0.054	<0.145
Sc45	458.57	445.54	19.7	<0.00000	0.00022	0.057	0.142	0.109	0.296	<0.052	0.079	<0.050	<0.034	<0.032	0.148	0.029	437.17	472.29	<0.00009	<0.00010	<0.00027
Ti49	506.64	461.95	8656.21	<0.00004	******	4.94	10.51	2.31	154.53	0.52	9.69	19.04	1.33	20.61	4.78	4.24	460.07	506.29	0.0027	<0.00077	<0.0021
V51	457.28	437.32	235.15	<0.00000	0.00011	0.533	2.27	0.0704	4.27	0.141	0.07	0.834	0.051	0.132	2.89	1.436	428.99	472.5	<0.00006	<0.00007	<0.00019
Cr53	391.99	386.17	4.24	<0.00010	0.009	3.45	10.29	1.79	4.02	<1.11	<1.32	8.93	<0.75	<0.68	11.52	1.86	372.12	418.74	<0.00173	<0.00204	<0.0055
Mn55	445.62	431.67	978.6	<0.00001	0.0008	29.36	318.7	1.89	3.74	954.17	992.52	59.82	0.387	1667.27	1201.65	586.86	422.1	462.68	<0.00023	<0.00026	<0.00073
Fe57	453.1	453.1	55500	0.00777	0.008	465531.56	304317.28	465531.59	465531.59	55793.82	304317.28	465531.63	465531.59	33872.68	23655.59	7763.26	453.1	453.1	<0.0096	<0.0107	<0.030
Co59	401.59	381.17	22.42	0.00001	<*******	94.82	2.65	51	404.14	76.68	0.448	1.318	10	43.54	6.59	14.55	376.59	408.8	0.00009	0.00009	0.00026
Ni60	433.82	405.75	12.6	10.63	<****	114.54	3.48	5.75	5.2	0.226	0.236	2.03	<0.082	<0.089	8.28	2.21	403.39	436.24	413.06	264.22	658.39
Ni62	426.62	408.31	8.81	10.57	<****	119.07	4.53	5.94	5.16	<0.67	<0.84	3.04	<0.44	0.75	6.18	1.72	405.16	431.03	427.51	252.71	630.96
Cu65	451.01	423.84	11.23	0.00663	<****	112.91	473469.28	382.72	20.12	3194.23	383891.25	110.34	1.72	10115.53	119247.88	10966.11	420.98	454.26	0.23	0.161	0.39
Zn66	428.91	430.11	79.97	<0.00003	******	424.6	18291	9924.66	112.09	582767	11336.88	93.53	21.43	586141.19	664968.19	586141.19	417.06	448	0.0018	<0.00161	0.0049
Ga71	450.85	421.49	12.24	<0.00000	0.00011	0.287	4.22	0.205	0.09	1.226	0.824	0.078	0.025	0.219	62.09	31.03	417.57	456.34	<0.00006	<0.00007	<0.00021
As75	346.47	305.75	<1.39	0.00218	<****	53.39	230.47	18483.55	5366.93	2.88	1357.71	24.24	47.36	<1.29	192.62	33.45	310.22	330.77	0.082	0.055	0.14
Se82	110.19	114.04	<8.48	0.00229	<****	18.3	<4.11	<1.44	26.05	4.18	10.52	<2.94	35.64	13.83	<3.59	<1.39	99.73	133.39	0.066	0.053	0.13
Y89	499.61	485.12	20.27	0	*******	0.0201	3.57	0.0048	0.473	0.0506	0.0228	3.24	<0.0057	0.0051	2.47	2.53	472.12	524.71	<0.00001	<0.00001	<0.00003
Zr90	496.01	487	111.85	<0.00000	0.00001	0.071	8.01	<0.0084	3.67	0.278	0.066	18.53	0.0164	0.0228	4.66	3.46	473.31	520.86	0.00002	<0.00003	<0.00007
Nb93	519.99	507.81	7.77	<0.00000	*******	0.0115	0.522	0.0042	0.507	<0.0084	<0.0092	0.0315	<0.0053	0.0087	0.0246	<0.0042	496.34	540.05	<0.00001	<0.00001	<0.00003
Mo95	404.45	391.67	123.06	<0.00001	0.00009	3.66	24.81	0.081	0.22	0.127	<0.089	0.307	<0.036	0.107	25.46	5.41	383.7	418.59	0.045	<0.00009	<0.00028
Ru99	<-NaN	<-NaN	<-NaN	<-NaN	<-NaN	<-NaN	<-NaN	<-NaN	<-NaN	<-NaN	<-NaN	<-NaN	<-NaN	<-NaN	<-NaN	<-NaN	<-NaN	<-NaN	<-NaN	<-NaN	<-NaN
Ru101	<-NaN	<-NaN	<-NaN	<-NaN	<-NaN	<-NaN	<-NaN	<-NaN	<-NaN	<-NaN	<-NaN	<-NaN	<-NaN	<-NaN	<-NaN	<-NaN	<-NaN	<-NaN	<-NaN	<-NaN	<-NaN
Rh103	<-NaN	<-NaN	<-NaN	<-NaN	<-NaN	<-NaN	<-NaN	<-NaN	<-NaN	<-NaN	<-NaN	<-NaN	<-NaN	<-NaN	<-NaN	<-NaN	<-NaN	<-NaN	<-NaN	<-NaN	<-NaN
Ag107	241.64	238.28	0.243	0.0056	<****	1.94	72.85	20.17	0.684	16.7	402.8	10.52	<0.036	12.16	115.65	31.27	233.27	249.31	0.17	0.135	0.34
Pd108	<-NaN	<-NaN	<-NaN	<-NaN	<-NaN	<-NaN	<-NaN	<-NaN	<-NaN	<-NaN	<-NaN	<-NaN	<-NaN	<-NaN	<-NaN	<-NaN	<-NaN	<-NaN	<-NaN	<-NaN	<-NaN
Cd111	274.83	253.64	<1.12	0.00112	<****	2.57	99.89	68.04	1.1	2370.13	62.77	<0.40	<0.32	1641.34	1745	2063.24	258.25	265.14	0.035	0.031	0.065
In115	449.86	434.41	0.075	<0.00000	0.00008	0.216	38.48	0.0215	<0.0098	0.232	3.14	0.0589	<0.0074	7.64	5.96	1.942	428.72	458.88	<0.00002	<0.00002	<0.00006
Sn118	395.04	387.43	1.56	0.00005	<******	3.44	12.96	0.195	0.3	57.56	21.95	0.98	<0.071	0.23	18.32	6.4	376.87	414.06	0.00093	0.00088	0.0023
Sb121	389.02	388.3	0.445	0.00002	<******	2.38	14.37	170.8	16.76	0.67	22	2.67	0.501	0.269	29.37	40.31	376.82	407.66	0.00065	0.00093	0.002
Te125	<-NaN	<-NaN	<-NaN	<-NaN	<-NaN	<-NaN	<-NaN	<-NaN	<-NaN	<-NaN	<-NaN	<-NaN	<-NaN	<-NaN	<-NaN	<-NaN	<-NaN	<-NaN	<-NaN	<-NaN	<-NaN
Te128	<-NaN	<-NaN	<-NaN	<-NaN	<-NaN	<-NaN	<-NaN	<-NaN	<-NaN	<-NaN	<-NaN	<-NaN	<-NaN	<-NaN	<-NaN	<-NaN	<-NaN	<-NaN	<-NaN	<-NaN	<-NaN
La139	448.37	435.75	15.05	<0.00000	0.00001	0.0413	1.175	0.0364	0.0291	0.0585	0.0205	0.0869	<0.0052	<0.0037	0.15	0.0572	423.05	474.01	<0.00001	<0.00001	<0.00003
Ce140	461.29	438.28	31.9	<0.00000	*******	0.127	1.95	0.0054	0.0907	0.0644	0.135	0.122	0.0149	<0.0047	1.284	0.95	430.98	475.3	<0.00001	<0.00001	<0.00002
Nd146	461.78	449.76	17.92	<0.00000	*******	<0.036	0.442	0.11	0.122	0.231	<0.044	<0.039	<0.0210	<0.0260	0.838	0.131	442.51	473.34	0.00008	<0.00009	<0.00015
Hf178	467.21	453.17	2.88	<0.00000	*******	<0.032	0.136	<0.0140	0.091	<0.0219	<0.032	0.042	<0.0206	<0.0159	0.258	0.0445	442.18	488.03	<0.00004	<0.00004	<0.00013
W182	440.3	431.42	0.252	<0.00000	0.00022	0.297	0.431	0.144	1.72	0.268	2.77	0.141	0.059	<0.028	0.637	0.129	421.85	456.51	<0.00006	<0.00009	<0.00019
Re185	49.69	50.1	<0.077	<0.00000	*******	<0.025	<0.029	<0.0136	<0.0215	<0.0257	<0.028	<0.0233	<0.0211	<0.0204	<0.034	<0.0097	48.53	52.05	<0.00004	<0.00005	<0.00013
Re187	52.38	48.67	<0.049	0.00004	<******	<0.0138	<0.0187	<0.0073	<0.0124	<0.0146	<0.0148	<0.0132	0.0106	<0.0119	<0.0222	<0.0054	48.36	52.82	0.00111	0.00064	0.0019
Os189	<-NaN	<-NaN	<-NaN	<-NaN	<-NaN	<-NaN	<-NaN	<-NaN	<-NaN	<-NaN	<-NaN	<-NaN	<-NaN	<-NaN	<-NaN	<-NaN	<-NaN	<-NaN	<-NaN	<-NaN	<-NaN
Os190	<-NaN	<-NaN	<-NaN	<-NaN	<-NaN	<-NaN	<-NaN	<-NaN	<-NaN	<-NaN	<-NaN	<-NaN	<-NaN	<-NaN	<-NaN	<-NaN	<-NaN	<-NaN	<-NaN	<-NaN	<-NaN
Ir193	<-NaN	<-NaN	<-NaN	<-NaN	<-NaN	<-NaN	<-NaN	<-NaN	<-NaN	<-NaN	<-NaN	<-NaN	<-NaN	<-NaN	<-NaN	<-NaN	<-NaN	<-NaN	<-NaN	<-NaN	<-NaN
Pt195	<-NaN	<-NaN	<-NaN	<-NaN	<-NaN	<-NaN	<-NaN	<-NaN	<-NaN	<-NaN	<-NaN	<-NaN	<-NaN	<-NaN	<-NaN	<-NaN	<-NaN	<-NaN	<-NaN	<-NaN	<-NaN
Au197	24.12	22.24	<0.097	0.00499	<****	0.066	0.425	28.08	16.84	<0.027	0.126	0.091	<0.026	0.091	1.034	0.237	22.16	24.18	0.18	0.122	0.28
Pb208	430.78	412.81	5.84	0.00063	<*****	66.99	1424.04	1824.7	218.92	83.41	106.82	126.24	14.34	57.41	1083.56	934.48	411.41	431.69	0.016	0.0149	0.033
Bi209	386.31	367.54	<0.080	0.00367	<****	8.73	71.46	18.2	3.73	0.645	0.178	0.665	1.301	8.68	23.08	15	363.06	392.81	0.107	0.093	0.22

Element	STD610-1	STD610-2	BCR2G-1	PGEA-1	PGEA-2	BG24-PY	BG24-CPY	JL06-PY	JC22-PY	JC22-SPH	JC22-CPY	BG14-PY	JL09-PY	JL09-SPH	BG24-SPH	BG24-SP2	STD610-3	STD610-4	PGEA-3	PGEA-4	PGEA-5
Th232	495.69	473.55	3.52	<0.00000	*******	0.532	0.077	<0.0049	0.0272	<0.0101	<0.0157	0.0444	<0.0058	0.0099	0.0222	0.0113	466.29	507.89	<0.00002	0.00009	<0.00007
U238	511.95	475.36	0.983	<0.00000	*******	0.729	5.84	<0.0059	0.153	0.0329	<0.0178	0.172	<0.0089	<0.0070	3.61	0.827	472.65	513.85	<0.00002	<0.00002	0.0009
ThO248	<-NaN	<-NaN	<-NaN	<-NaN	<-NaN	<-NaN	<-NaN	<-NaN	<-NaN	<-NaN	<-NaN	<-NaN	<-NaN	<-NaN	<-NaN	<-NaN	<-NaN	<-NaN	<-NaN	<-NaN	<-NaN
GLITTER!: 1 sigma error.																					
Element	STD610-1	STD610-2	BCR2G-1	PGEA-1	PGEA-2	BG24-PY	BG24-CPY	JL06-PY	JC22-PY	JC22-SPH	JC22-CPY	BG14-PY	JL09-PY	JL09-SPH	BG24-SPH	BG24-SP2	STD610-3	STD610-4	PGEA-3	PGEA-4	PGEA-5
Al27	717.63	659.19	2783.85	0.00001	0.015	1.83	10.84	0.33	1.29	0.69	0.11	8.84	0.15	0.58	11.61	2.79	939.91	1073.07	0.00015	0.00015	0.0008
Si29	28517.85	26168.08	11022.44	0.0032	2.47	178.64	711.17	13.73	28.34	35.9	53.19	573.05	17.83	29.46	1227.36	211.98	37130.41	42833.23	0.11	0.032	0.75
S34	<0.00	<0.00	<0.00	<0.00	<0.00	<0.00	<0.00	<0.00	<0.00	<0.00	<0.00	<0.00	<0.00	<0.00	<0.00	<0.00	<0.00	<0.00	<0.00	<0.00	<0.00
Ca43	6170.1	5532.39	1985.55	0.00097	0.32	16.13	83.49	5.89	30.73	24.14	52.23	36.12	7.81	67.53	89.14	23.53	8243.98	9288.44	0.027	0.023	0.074
Sc45	28.11	26.12	0.96	0	0.00049	0.019	0.033	0.013	0.025	0.02	0.024	0.019	0.014	0.013	0.027	0.0096	35.11	39.53	0.00004	0.00004	0.00026
Ti49	40.53	36.06	602.68	0.00002	0.0014	0.44	0.92	0.22	12.75	0.19	0.95	1.82	0.2	1.75	0.51	0.41	55.1	63.14	0.0018	0.00033	0.003
V51	30.94	28.54	13.17	0	0.00026	0.038	0.15	0.0089	0.28	0.018	0.02	0.065	0.011	0.014	0.16	0.082	40.89	46.92	0.00005	0.00003	0.00009
Cr53	28.15	26.82	1.3	0.00004	0.018	0.46	0.95	0.24	0.44	0.42	0.51	0.83	0.3	0.27	0.79	0.22	37.92	44.4	0.00087	0.00084	0.0031
Mn55	29.01	27.03	51.62	0	0.0016	1.64	18.19	0.12	0.23	37.97	64.45	4.03	0.048	72.66	53.68	26.88	37.59	42.93	0.00016	0.00015	0.00093
Fe57	28.62	26.17	1757.94	0.00042	0.023	14722.28	9624.87	14721.88	14722.16	2883.09	9624.5	14722.29	14722.23	1995.41	1442.54	490.1	28.03	29.48	0.007	0.0063	0.016
Co59	26.51	24.21	1.23	0	0.00091	5.38	0.16	3.06	25.05	3.71	0.037	0.096	0.72	2.39	0.38	0.85	34.17	38.62	0.00006	0.00006	0.00039
Ni60	29.85	26.94	0.8	0.69	1811.56	6.9	0.26	0.38	0.36	0.057	0.068	0.17	0.036	0.036	0.58	0.16	38.68	43.53	264.18	153.26	973.85
Ni62	27.45	25.14	1.14	0.6	1687.08	6.07	0.59	0.41	0.44	0.28	0.33	0.38	0.18	0.19	0.6	0.2	32.34	35.73	272.19	145.71	932.36
Cu65	30.92	28.03	1.01	0.00043	1.08	6.72	28783.02	23.96	1.33	168.76	26499.73	7.91	0.23	608.89	7423.13	705.94	39.42	44.25	0.15	0.093	0.57
Zn66	30.96	30.03	5.02	0.00001	0.0029	25.95	1127.88	620.26	7.17	18429.01	744.84	6.33	1.53	18535.66	21028.53	18535.55	35.45	39.22	0.0014	0.00075	0.0074
Ga71	31.79	28.75	0.76	0	0.00025	0.029	0.29	0.02	0.015	0.082	0.074	0.019	0.011	0.022	4.24	2.19	42.26	48.11	0.00003	0.00003	0.0002
As75	40.99	35.84	0.56	0.00026	0.38	6.23	27.29	2229.63	661.77	0.86	175.84	3.34	6.52	0.52	26.16	4.79	49.4	54.35	0.054	0.033	0.21
Se82	21.28	21.19	3.42	0.00041	0.42	3.45	1.73	0.57	5.11	1.34	2.61	1.14	7.94	2.68	1.38	0.54	26.97	36.72	0.046	0.034	0.2
Y89	33.59	31.44	1.13	0	0.00007	0.0042	0.22	0.0018	0.033	0.0055	0.0046	0.24	0.0025	0.0022	0.12	0.12	44.71	51.77	0.00001	0.00001	0.00002
Zr90	31.63	29.79	5.72	0	0.00004	0.011	0.45	0.0033	0.22	0.019	0.012	1.21	0.005	0.0052	0.19	0.14	40.95	46.94	0.00002	0.00001	0.00006
Nb93	31.92	29.79	0.39	0	0.00003	0.0032	0.033	0.0018	0.031	0.0029	0.0039	0.0047	0.0023	0.0023	0.0056	0.0018	40.1	45.44	0.00001	0.00001	0.00001
Mo95	25.55	23.71	6.2	0	0.00027	0.21	1.37	0.015	0.03	0.029	0.033	0.038	0.016	0.021	1.14	0.25	32.44	36.85	0.029	0.00004	0.00016
Ru99	<0.00	<0.00	<0.00	<0.00	<0.00	<0.00	<0.00	<0.00	<0.00	<0.00	<0.00	<0.00	<0.00	<0.00	<0.00	<0.00	<0.00	<0.00	<0.00	<0.00	<0.00
Ru101	<0.00	<0.00	<0.00	<0.00	<0.00	<0.00	<0.00	<0.00	<0.00	<0.00	<0.00	<0.00	<0.00	<0.00	<0.00	<0.00	<0.00	<0.00	<0.00	<0.00	<0.00
Rh103	<0.00	<0.00	<0.00	<0.00	<0.00	<0.00	<0.00	<0.00	<0.00	<0.00	<0.00	<0.00	<0.00	<0.00	<0.00	<0.00	<0.00	<0.00	<0.00	<0.00	<0.00
Ag107	14.45	13.59	0.063	0.00031	0.97	0.11	3.52	1	0.049	0.57	21.24	0.59	0.016	0.43	3.92	1.07	17.19	19.12	0.11	0.078	0.51
Pd108	<0.00	<0.00	<0.00	<0.00	<0.00	<0.00	<0.00	<0.00	<0.00	<0.00	<0.00	<0.00	<0.00	<0.00	<0.00	<0.00	<0.00	<0.00	<0.00	<0.00	<0.00
Cd111	19.92	17.84	0.46	0.00009	0.19	0.28	6.4	4.4	0.17	162.74	4.48	0.16	0.12	131.03	144.87	178	24.48	26.1	0.023	0.018	0.096
In115	26.84	24.69	0.017	0	0.00017	0.015	1.88	0.0034	0.0041	0.015	0.18	0.008	0.0034	0.34	0.27	0.091	32.51	36.22	0.00001	0.00001	0.00003
Sn118	25.19	23.69	0.17	0.00001	0.0061	0.2	0.74	0.028	0.044	2.08	1.38	0.087	0.03	0.035	0.74	0.26	32.35	37	0.00061	0.00052	0.0034
Sb121	24.43	23.34	0.086	0	0.0042	0.14	0.78	9.07	0.93	0.047	1.28	0.18	0.045	0.027	0.96	1.27	29.42	33.06	0.00043	0.00054	0.0029
Te125	<0.00	<0.00	<0.00	<0.00	<0.00	<0.00	<0.00	<0.00	<0.00	<0.00	<0.00	<0.00	<0.00	<0.00	<0.00	<0.00	<0.00	<0.00	<0.00	<0.00	<0.00
Te128	<0.00	<0.00	<0.00	<0.00	<0.00	<0.00	<0.00	<0.00	<0.00	<0.00	<0.00	<0.00	<0.00	<0.00	<0.00	<0.00	<0.00	<0.00	<0.00	<0.00	<0.00
La139	30.85	28.94	0.87	0	0.00004	0.0052	0.079	0.0038	0.0042	0.0063	0.0051	0.009	0.0022	0.0015	0.012	0.0044	41.5	48.43	0.00001	0.00001	0.00002
Ce140	31.29	28.64	1.8	0	0.00006	0.011	0.13	0.0021	0.0085	0.0068	0.013	0.012	0.003	0.0022	0.079	0.059	41.26	47.37	0.00001	0.00001	0.00002
Nd146	26.97	24.97	0.86	0	0.00055	0.016	0.049	0.015	0.019	0.029	0.019	0.016	0.0083	0.0095	0.063	0.014	32.26	35.93	0.00006	0.00004	0.00014
Hf178	30.56	28.48	0.2	0	0.00017	0.012	0.021	0.0056	0.015	0.0095	0.013	0.014	0.0084	0.0056	0.028	0.0072	39.68	45.59	0.00002	0.00002	0.00006
W182	26.6	24.86	0.057	0	0.00047	0.031	0.047	0.016	0.11	0.029	0.18	0.022	0.017	0.011	0.05	0.013	32.66	36.78	0.00003	0.00004	0.00008
Re185	2.97	2.84	0.028	0	0.00024	0.01	0.011	0.0049	0.0078	0.0098	0.011	0.0089	0.008	0.0073	0.012	0.0036	3.5	3.9	0.00002	0.00002	0.00006
Re187	3.78	3.4	0.018	0	0.0055	0.0052	0.0077	0.0029	0.0045	0.0053	0.0067	0.0048	0.0042	0.0042	0.0077	0.002	4.97	5.64	0.00071	0.00037	0.0028
Os189	<0.00	<0.00	<0.00	<0.00	<0.00	<0.00	<0.00	<0.00	<0.00	<0.00	<0.00	<0.00	<0.00	<0.00	<0.00	<0.00	<0.00	<0.00	<0.00	<0.00	<0.00
Os190	<0.00	<0.00	<0.00	<0.00	<0.00	<0.00	<0.00	<0.00	<0.00	<0.00	<0.00	<0.00	<0.00	<0.00	<0.00	<0.00	<0.00	<0.00	<0.00	<0.00	<0.00
Ir193	<0.00	<0.00	<0.00	<0.00	<0.00	<0.00	<0.00	<0.00	<0.00	<0.00	<0.00	<0.00	<0.00	<0.00	<0.00	<0.00	<0.00	<0.00	<0.00	<0.00	<0.00
Pt195	<0.00	<0.00	<0.00	<0.00	<0.00	<0.00	<0.00	<0.00	<0.00	<0.00	<0.00	<0.00	<0.00	<0.00	<0.00	<0.00	<0.00	<0.00	<0.00	<0.00	<0.00
Au197	2.07	1.86	0.041	0.00039	0.82	0.019	0.053	2.21	1.37	0.012	0.024	0.018	0.011	0.016	0.093	0.024	2.53	2.85	0.11	0.071	0.42
Pb208	25.6	23.36	0.33	0.00004	0.099	3.13	67.37	88.09	10.83	3.74	5.57	6.75	0.8	2.87	55.43	49.2	29.74	32.44	0.01	0.0086	0.049
Bi209	25.76	23.62	0.032	0.00023	0.6	0.51	4.22	1.11	0.24	0.041	0.023	0.053	0.1	0.47	1.27	0.85	32.98	37.17	0.068	0.054	0.32
Th232	32.56	29.93	0.21	0	0.00006	0.036	0.012	0.0022	0.0048	0.0045	0.0058	0.0077	0.0029	0.0038	0.008	0.0025	42	47.65	0.00001	0.00006	0.00004
U238	36.46	32.77	0.076	0	0.00004	0.052	0.39	0.0023	0.015	0.008	0.0067	0.018	0.0037	0.0031	0.27	0.065	48.49	54.92	0.00002	0.00001	0.0014
ThO248	<0.00	<0.00	<0.00	<0.00	<0.00	<0.00	<0.00	<0.00	<0.00	<0.00	<0.00	<0.00	<0.00	<0.00	<0.00	<0.00	<0.00	<0.00	<0.00	<0.00	<0.00

Element	STD610-1	STD610-2	BCR2G-1	PGEA-1	PGEA-2	BG24-PY	BG24-CPY	JL06-PY	JC22-PY	JC22-SPH	JC22-CPY	BG14-PY	JL09-PY	JL09-SPH	BG24-SPH	BG24-SP2	STD610-3	STD610-4	PGEA-3	PGEA-4	PGEA-5
GLITTER!: Minimum detection limits (99% confidence).																					
Element	STD610-1	STD610-2	BCR2G-1	PGEA-1	PGEA-2	BG24-PY	BG24-CPY	JL06-PY	JC22-PY	JC22-SPH	JC22-CPY	BG14-PY	JL09-PY	JL09-SPH	BG24-SPH	BG24-SP2	STD610-3	STD610-4	PGEA-3	PGEA-4	PGEA-5
Al27	1.33	1.16	0.548	0.00002	<0.00000	0.181	0.266	0.0905	0.138	0.606	0.224	0.169	0.124	0.109	0.221	0.0821	1.08	1.21	0.00031	0.00035	0.00096
Si29	297.55	245.92	118.62	0.00364	<0.00000	38.28	56.86	18.7	30.49	39.61	48.38	38.26	27.15	24.39	47.24	17.32	238.55	258.77	0.0666	0.0779	0.207
S34	<0.00	<0.00	<0.00	<0.00	<0.00	<0.00	<0.00	<0.00	<0.00	<0.00	<0.00	<0.00	<0.00	<0.00	<0.00	<0.00	<0.00	<0.00	<0.00	<0.00	<0.00
Ca43	198.43	173.68	75.97	0.0023	<0.00000	26.47	46.53	14	20.97	25.45	34.68	29.22	18.18	16.71	32.53	13.21	157	196.51	0.0496	0.0545	0.145
Sc45	0.382	0.33	0.147	0	<0.00000	0.0469	0.0746	0.0259	0.0407	0.0524	0.0579	0.0499	0.034	0.0316	0.0617	0.024	0.311	0.344	0.00009	0.0001	0.00027
Ti49	3.04	2.6	0.956	0.00004	<0.00000	0.351	0.495	0.155	0.325	0.446	0.506	0.378	0.297	0.225	0.459	0.192	2.31	2.41	0.0007	0.00077	0.00209
V51	0.279	0.223	0.107	0	<0.00000	0.0354	0.0506	0.016	0.0294	0.0371	0.0468	0.0374	0.024	0.0243	0.0476	0.0169	0.222	0.267	0.00006	0.00007	0.00019
Cr53	7.78	6.86	3.21	0.0001	<0.00000	0.982	1.51	0.504	0.81	1.11	1.32	1.04	0.75	0.677	1.3	0.484	6.41	6.98	0.00173	0.00204	0.0055
Mn55	0.847	0.718	0.336	0.00001	<0.00000	0.108	0.16	0.0544	0.0922	0.127	0.159	0.128	0.0932	0.0862	0.163	0.0622	0.829	0.939	0.00023	0.00026	0.00073
Fe57	35.37	28.71	13.96	0.00044	<0.00000	4.71	6.84	2.23	4.05	5.43	6.73	5.32	3.69	3.46	7.06	2.61	34.01	37.64	0.00959	0.0107	0.03
Co59	0.172	0.169	0.0717	0	<0.00000	0.0205	0.0358	0.0128	0.0189	0.026	0.0303	0.0197	0.0179	0.0156	0.0302	0.011	0.161	0.184	0.00004	0.00005	0.00012
Ni60	0.942	0.862	0.367	0.00001	<0.00000	0.115	0.177	0.0593	0.0956	0.129	0.153	0.142	0.0825	0.0887	0.171	0.0584	0.683	0.797	0.00023	0.00111	0.0007
Ni62	5.06	3.76	1.94	0.00006	<0.00000	0.655	0.981	0.261	0.488	0.669	0.843	0.631	0.445	0.364	0.893	0.351	3.64	4.92	0.00106	0.00283	0.00373
Cu65	4.39	3.87	1.8	0.00006	<0.00000	0.563	0.875	0.296	0.489	0.68	0.807	0.642	0.444	0.407	0.791	0.299	3.86	4.14	0.001	0.00112	0.00304
Zn66	2.26	2.02	0.91	0.00003	<0.00000	0.311	0.438	0.175	0.243	0.304	1.99	0.442	0.29	0.225	0.662	0.972	8.67	7.6	0.00162	0.00161	0.00405
Ga71	0.238	0.202	0.0939	0	<0.00000	0.03	0.0462	0.0171	0.0247	0.0333	0.0449	0.0385	0.0219	0.017	0.0437	0.0167	0.174	0.282	0.00006	0.00007	0.00021
As75	3.12	2.99	1.39	0.00004	<0.00000	0.446	0.74	0.249	1.33	2.08	2.62	2.09	1.45	1.29	2.47	0.887	11.94	12.93	0.00326	0.00384	0.0102
Se82	22.45	18.57	8.48	0.00028	<0.00000	2.91	4.11	1.44	2.36	2.9	3.51	2.94	2.15	1.85	3.59	1.39	17.46	18.93	0.00531	0.00572	0.0159
Y89	0.061	0.0425	0.021	0	<0.00000	0.00759	0.0114	0.00379	0.00649	0.0062	0.00715	0.00785	0.00572	0.00456	0.00765	0.00284	0.0471	0.0661	0.00001	0.00001	0.00003
Zr90	0.11	0.0827	0.0288	0	<0.00000	0.0195	0.0184	0.00841	0.0126	0.0164	0.0196	0.0132	0.00906	0.00885	0.0159	0.00624	0.0833	0.104	0.00002	0.00003	0.00007
Nb93	0.0531	0.0483	0.0176	0	<0.00000	0.00579	0.0118	0.00392	0.00613	0.00838	0.00918	0.00643	0.00532	0.0038	0.0108	0.00415	0.0544	0.0407	0.00001	0.00001	0.00003
Mo95	0.374	0.344	0.152	0.00001	<0.00000	0.0499	0.0984	0.0274	0.0457	0.0595	0.0892	0.0528	0.0361	0.0374	0.0674	0.025	0.254	0.391	0.00008	0.00009	0.00028
Ru99	<0.00	<0.00	<0.00	<0.00	<0.00	<0.00	<0.00	<0.00	<0.00	<0.00	<0.00	<0.00	<0.00	<0.00	<0.00	<0.00	<0.00	<0.00	<0.00	<0.00	<0.00
Ru101	<0.00	<0.00	<0.00	<0.00	<0.00	<0.00	<0.00	<0.00	<0.00	<0.00	<0.00	<0.00	<0.00	<0.00	<0.00	<0.00	<0.00	<0.00	<0.00	<0.00	<0.00
Rh103	<0.00	<0.00	<0.00	<0.00	<0.00	<0.00	<0.00	<0.00	<0.00	<0.00	<0.00	<0.00	<0.00	<0.00	<0.00	<0.00	<0.00	<0.00	<0.00	<0.00	<0.00
Ag107	0.271	0.248	0.127	0	<0.00000	0.0434	0.0592	0.0197	0.0328	0.0401	0.0586	0.034	0.036	0.025	0.0575	0.0214	0.226	0.309	0.00006	0.00007	0.00023
Pd108	<0.00	<0.00	<0.00	<0.00	<0.00	<0.00	<0.00	<0.00	<0.00	<0.00	<0.00	<0.00	<0.00	<0.00	<0.00	<0.00	<0.00	<0.00	<0.00	<0.00	<0.00
Cd111	2.93	2.3	1.12	0.00003	<0.00000	0.389	0.522	0.188	0.26	0.351	0.454	0.398	0.318	0.221	0.57	0.235	3.03	2.86	0.00076	0.00093	0.0024
In115	0.0612	0.0848	0.0304	0	<0.00000	0.00665	0.0166	0.00503	0.0098	0.0071	0.0115	0.0118	0.00743	0.00687	0.0115	0.00323	0.0608	0.0802	0.00002	0.00002	0.00006
Sn118	0.888	0.74	0.315	0.00001	<0.00000	0.101	0.15	0.0543	0.0876	0.109	0.127	0.114	0.0715	0.0695	0.137	0.0491	0.634	0.772	0.00019	0.0002	0.00055
Sb121	0.297	0.3	0.157	0	<0.00000	0.0454	0.0727	0.0218	0.0274	0.0428	0.0621	0.0469	0.03	0.0322	0.0625	0.029	0.39	0.437	0.00009	0.00012	0.00034
Te125	<0.00	<0.00	<0.00	<0.00	<0.00	<0.00	<0.00	<0.00	<0.00	<0.00	<0.00	<0.00	<0.00	<0.00	<0.00	<0.00	<0.00	<0.00	<0.00	<0.00	<0.00
Te128	<0.00	<0.00	<0.00	<0.00	<0.00	<0.00	<0.00	<0.00	<0.00	<0.00	<0.00	<0.00	<0.00	<0.00	<0.00	<0.00	<0.00	<0.00	<0.00	<0.00	<0.00
La139	0.0387	0.0377	0.014	0	<0.00000	0.00517	0.00882	0.00271	0.00536	0.00779	0.00942	0.00583	0.0052	0.00369	0.00605	0.00194	0.0348	0.0563	0.00001	0.00001	0.00003
Ce140	0.0633	0.0475	0.0209	0	<0.00000	0.00485	0.0116	0.00433	0.00593	0.00727	0.00418	0.0082	0.0036	0.00471	0.00831	0.00329	0.0441	0.0557	0.00001	0.00001	0.00002
Nd146	0.211	0.257	0.108	0	<0.00000	0.0356	0.0443	0.0208	0.0272	0.038	0.0435	0.0387	0.021	0.026	0.0522	0.0173	0.255	0.215	0.00004	0.00009	0.00015
Hf178	0.259	0.161	0.0932	0	<0.00000	0.032	<0.00000	0.014	0.0238	0.0219	0.0319	0.0283	0.0206	0.0159	0.0269	0.00994	0.159	0.17	0.00004	0.00004	0.00013
W182	0.329	0.232	0.0976	0	<0.00000	0.0321	0.0432	0.0203	0.0278	0.0343	0.0417	0.0329	0.0328	0.0278	0.0446	0.0146	0.22	0.286	0.00006	0.00009	0.00019
Re185	0.172	0.163	0.077	0	<0.00000	0.0252	0.029	0.0136	0.0215	0.0257	0.0278	0.0233	0.0211	0.0204	0.0344	0.00971	0.13	0.129	0.00004	0.00005	0.00013
Re187	0.0697	0.081	0.0488	0	<0.00000	0.0138	0.0187	0.00729	0.0124	0.0146	0.0148	0.0132	0.00761	0.0119	0.0222	0.00538	0.0999	0.0548	0.00002	0.00003	0.00006
Os189	<0.00	<0.00	<0.00	<0.00	<0.00	<0.00	<0.00	<0.00	<0.00	<0.00	<0.00	<0.00	<0.00	<0.00	<0.00	<0.00	<0.00	<0.00	<0.00	<0.00	<0.00
Os190	<0.00	<0.00	<0.00	<0.00	<0.00	<0.00	<0.00	<0.00	<0.00	<0.00	<0.00	<0.00	<0.00	<0.00	<0.00	<0.00	<0.00	<0.00	<0.00	<0.00	<0.00
Ir193	<0.00	<0.00	<0.00	<0.00	<0.00	<0.00	<0.00	<0.00	<0.00	<0.00	<0.00	<0.00	<0.00	<0.00	<0.00	<0.00	<0.00	<0.00	<0.00	<0.00	<0.00
Pt195	<0.00	<0.00	<0.00	<0.00	<0.00	<0.00	<0.00	<0.00	<0.00	<0.00	<0.00	<0.00	<0.00	<0.00	<0.00	<0.00	<0.00	<0.00	<0.00	<0.00	<0.00
Au197	0.28	0.139	0.0968	0	<0.00000	0.0388	0.0484	0.0151	0.0366	0.0266	0.0306	0.0229	0.0263	0.0192	0.0386	0.0132	0.215	0.219	0.00006	0.00006	0.0002
Pb208	0.281	0.279	0.151	0	<0.00000	0.0415	0.0599	0.0253	0.038	0.0485	0.0611	0.0413	0.0258	0.0274	0.0566	0.0244	0.292	0.3	0.00008	0.00007	0.00024
Bi209	0.156	0.142	0.0799	0	<0.00000	0.0254	0.0402	0.0102	0.0148	0.0275	0.0347	0.0253	0.0213	0.0187	0.0415	0.0121	0.296	0.208	0.00006	0.00006	0.00015
Th232	0.0753	0.0525	0.0307	0	<0.00000	0.0115	0.0175	0.00487	0.00546	0.0101	0.0157	0.0119	0.0058	0.00719	0.0169	0.00379	0.0794	0.103	0.00002	0.00002	0.00007
U238	0.0829	0.0755	0.0356	0	<0.00000	0.00984	0.0215	0.00592	0.011	0.016	0.0178	0.0128	0.0089	0.00697	0.0149	0.00581	0.0929	0.0921	0.00002	0.00002	0.00008
ThO248	<0.00	<0.00	<0.00	<0.00	<0.00	<0.00	<0.00	<0.00	<0.00	<0.00	<0.00	<0.00	<0.00	<0.00	<0.00	<0.00	<0.00	<0.00	<0.00	<0.00	<0.00
GLITTER!: Trace element concentrations normalised to chondrite.																					
Element	STD610-1	STD610-2	BCR2G-1	PGEA-1	PGEA-2	BG24-PY	BG24-CPY	JL06-PY	JC22-PY	JC22-SPH	JC22-CPY	BG14-PY	JL09-PY	JL09-SPH	BG24-SPH	BG24-SP2	STD610-3	STD610-4	PGEA-3	PGEA-4	PGEA-5

Run1

Element	STD610-1	STD610-2	BCR2G-1	PGEA-1	PGEA-2	BG24-PY	BG24-CPY	JL06-PY	JC22-PY	JC22-SPH	JC22-CPY	BG14-PY	JL09-PY	JL09-SPH	BG24-SPH	BG24-SP2	STD610-3	STD610-4	PGEA-3	PGEA-4	PGEA-5
Al27	0.806	0.766	3.74	0	0	0.00231	0.01341	0.0004	0.00149	0	0.00007	0.00926	0.00014	0.00081	0.01576	0.00366	0.754	0.827	0	0	0
Si29	2.18	2.05	0.946	0	0	0.0145	0.0567	0.00089	0.00192	0.00348	0.0035	0.0392	0.00092	0.00258	0.111	0.0185	2.01	2.23	0	0	0
S34	<****	<****	<****	<****	<****	<****	<****	<****	<****	<****	<****	<****	<****	<****	<****	<****	<****	<****	<****	<****	<****
Ca43	6.39	5.92	2.42	0	0.00001	0.0115	0.0861	0.00119	0.0288	0.0229	0.0461	0.03	0	0.0668	0.0839	0.0208	5.9	6.37	0	0	0
Sc45	53.07	51.57	2.28	0	0.00003	0.0066	0.0165	0.0126	0.0343	0	0.0091	0	0	0	0.0171	0.0034	50.6	54.66	0	0	0
Ti49	0.775	0.706	13.24	0	*******	0.00755	0.0161	0.00353	0.236	0.0008	0.0148	0.0291	0.00203	0.0315	0.00731	0.00648	0.703	0.774	0	0	0
V51	5.38	5.14	2.77	0	0	0.00627	0.0268	0.00083	0.0503	0.00166	0.00082	0.00981	0.0006	0.00156	0.0339	0.01689	5.05	5.56	0	0	0
Cr53	0.0986	0.0971	0.00107	0	0	0.00087	0.00259	0.00045	0.00101	0	0	0.00225	0	0	0.0029	0.00047	0.0936	0.105	0	0	0
Mn55	0.1516	0.1468	0.333	0	0	0.00999	0.1084	0.00064	0.00127	0.325	0.338	0.0203	0.00013	0.567	0.409	0.1996	0.144	0.157	0	0	0
Fe57	0.00163	0.00163	0.1996	0	0	1.675	1.095	1.675	1.675	0.201	1.095	1.675	1.675	0.1218	0.0851	0.0279	0.00163	0.00163	0	0	0
Co59	0.526	0.499	0.0293	0	0	0.1241	0.00347	0.0667	0.529	0.1004	0.00059	0.00173	0.01309	0.057	0.00862	0.019	0.493	0.535	0	0	0
Ni60	0.0263	0.0246	0.00076	0.00064	0	0.00694	0.00021	0.00035	0.00031	0.00001	0.00001	0.00012	0	0	0.0005	0.00013	0.0244	0.0264	0.025	0.016	0.04
Ni62	0.0259	0.0247	0.00053	0.00064	0	0.00722	0.00027	0.00036	0.00031	0	0	0.00018	0	0.00005	0.00037	0.0001	0.0246	0.0261	0.026	0.0153	0.038
Cu65	2.68	2.52	0.0668	0.00004	0	0.672	2818.27	2.28	0.1197	19.01	2285.07	0.657	0.0102	60.21	709.81	65.27	2.51	2.7	0.0014	0.00096	0.0023
Zn66	0.928	0.931	0.173	0	*******	0.919	39.59	21.48	0.243	1261.4	24.54	0.202	0.0464	1268.7	1439.33	1268.7	0.903	0.97	0	0	0.00001
Ga71	29.66	27.73	0.805	0	0.00001	0.0189	0.277	0.0135	0.0059	0.0806	0.0542	0.0051	0.00168	0.0144	4.09	2.04	27.47	30.02	0	0	0
As75	120.72	106.53	0	0.00076	0	18.6	80.3	6440.26	1870.01	1	473.07	8.45	16.5	0	67.11	11.65	108.09	115.25	0.029	0.019	0.05
Se82	4.04	4.18	0	0.00008	0	0.67	0	0	0.95	0.153	0.385	0	1.31	0.506	0	0	3.65	4.89	0.0024	0.0019	0.0048
Y89	222.05	215.61	9.01	0	*******	0.0089	1.588	0.00214	0.21	0.0225	0.0101	1.44	0	0.00225	1.097	1.123	209.83	233.2	0	0	0
Zr90	89.53	87.91	20.19	0	0	0.0128	1.445	0	0.663	0.0503	0.0119	3.35	0.00297	0.00411	0.842	0.625	85.44	94.02	0	0	0
Nb93	1386.65	1354.16	20.72	0	*******	0.0306	1.391	0.0112	1.352	0	0	0.084	0	0.0233	0.066	0	1323.56	1440.14	0	0	0
Mo95	293.08	283.82	89.17	0	0.00007	2.66	17.98	0.059	0.16	0.092	0	0.222	0	0.077	18.45	3.92	278.04	303.33	0.033	0	0
Ru99	<****	<****	<****	<****	<****	<****	<****	<****	<****	<****	<****	<****	<****	<****	<****	<****	<****	<****	<****	<****	<****
Ru101	<****	<****	<****	<****	<****	<****	<****	<****	<****	<****	<****	<****	<****	<****	<****	<****	<****	<****	<****	<****	<****
Rh103	<****	<****	<****	<****	<****	<****	<****	<****	<****	<****	<****	<****	<****	<****	<****	<****	<****	<****	<****	<****	<****
Ag107	732.23	722.06	0.74	0.01698	0	5.89	220.75	61.11	2.07	50.62	1220.61	31.88	0	36.85	350.45	94.75	706.87	755.5	0.5	0.41	1.04
Pd108	<****	<****	<****	<****	<****	<****	<****	<****	<****	<****	<****	<****	<****	<****	<****	<****	<****	<****	<****	<****	<****
Cd111	272.1	251.12	0	0.00111	0	2.55	98.9	67.36	1.09	2346.66	62.15	0	0	1625.09	1727.73	2042.81	255.7	262.52	0.035	0.03	0.064
In115	3845	3712.87	0.64	0	0.0007	1.84	328.86	0.184	0	1.99	26.87	0.504	0	65.3	50.98	16.6	3664.26	3922.03	0	0	0
Sn118	156.76	153.74	0.617	0.00002	0	1.366	5.14	0.078	0.119	22.84	8.71	0.389	0	0.091	7.27	2.54	149.55	164.31	0.00037	0.00035	0.0009
Sb121	1669.61	1666.53	1.91	0.00011	0	10.2	61.69	733.05	71.92	2.88	94.42	11.47	2.15	1.15	126.06	172.98	1617.27	1749.63	0.0028	0.004	0.009
Te125	<****	<****	<****	<****	<****	<****	<****	<****	<****	<****	<****	<****	<****	<****	<****	<****	<****	<****	<****	<****	<****
Te128	<****	<****	<****	<****	<****	<****	<****	<****	<****	<****	<****	<****	<****	<****	<****	<****	<****	<****	<****	<****	<****
La139	1221.71	1187.34	41.01	0	0.00004	0.113	3.2	0.099	0.079	0.159	0.056	0.237	0	0	0.409	0.156	1152.74	1291.58	0	0	0
Ce140	482.02	457.97	33.33	0	*******	0.133	2.04	0.0056	0.0948	0.0673	0.141	0.128	0.0155	0	1.342	0.993	450.34	496.65	0	0	0
Nd146	649.48	632.57	25.21	0	*******	0	0.622	0.155	0.172	0.325	0	0	0	0	1.178	0.184	622.38	665.74	0.00011	0	0
Hf178	2610.1	2531.7	16.08	0	*******	0	0.76	0	0.508	0	0	0.235	0	0	1.44	0.248	2470.29	2726.41	0	0	0
W182	4947.16	4847.46	2.83	0	0.0025	3.34	4.84	1.62	19.31	3.02	31.17	1.59	0.67	0	7.15	1.45	4739.89	5129.28	0	0	0
Re185	903.5	910.98	0	0	******	0	0	0	0	0	0	0	0	0	0	0	882.4	946.39	0	0	0
Re187	952.33	884.92	0	0.0007	0	0	0	0	0	0	0	0	0.192	0	0	0	879.21	960.43	0.02	0.0116	0.035
Os189	<****	<****	<****	<****	<****	<****	<****	<****	<****	<****	<****	<****	<****	<****	<****	<****	<****	<****	<****	<****	<****
Os190	<****	<****	<****	<****	<****	<****	<****	<****	<****	<****	<****	<****	<****	<****	<****	<****	<****	<****	<****	<****	<****
Ir193	<****	<****	<****	<****	<****	<****	<****	<****	<****	<****	<****	<****	<****	<****	<****	<****	<****	<****	<****	<****	<****
Pt195	<****	<****	<****	<****	<****	<****	<****	<****	<****	<****	<****	<****	<****	<****	<****	<****	<****	<****	<****	<****	<****
Au197	110.66	102	0	0.0229	0	0.305	1.95	128.79	77.23	0	0.58	0.417	0	0.419	4.75	1.09	101.66	110.92	0.82	0.56	1.3
Pb208	118.02	113.1	1.6	0.00017	0	18.35	390.15	499.92	59.98	22.85	29.27	34.59	3.93	15.73	296.87	256.02	112.71	118.27	0.0043	0.0041	0.009
Bi209	2313.26	2200.86	0	0.022	0	52.29	427.88	108.96	22.31	3.86	1.06	3.98	7.79	52	138.19	89.83	2174.03	2352.14	0.64	0.56	1.3
Th232	11663.18	11142.35	82.89	0	******	12.53	1.82	0	0.64	0	0	1.05	0	0.234	0.52	0.266	10971.43	11950.25	0	0.0022	0
U238	41963.09	38963.59	80.56	0	******	59.78	478.82	0	12.5	2.7	0	14.08	0	0	296.04	67.81	38741.95	42118.91	0	0	0.08
ThO248	<****	<****	<****	<****	<****	<****	<****	<****	<****	<****	<****	<****	<****	<****	<****	<****	<****	<****	<****	<****	<****

GLITTER4.0: Laser Ablation Analysis Results

G:\KYLIE\MAR13\RUN2
Fri Mar 14 17:17:46 2003

All values are reported in ppm

GLITTER!: Trace Element Concentrations MDL filtered.

Element	STD610-1	STD610-2	BCR2G-1	PGEA-1	PGEA-2	PGEA-3	MS-CPY	MS-PY	KP11-PY	KP11-CPY	KP11-SPH	BG30-CPY	BG30-PY	JL06-PY2	JL06-SPH	BG06-SPH	BG06-PY	STD610-3	STD610-4	STD610-5	STD610-6	PGEA-4	PGEA-5	BCR2G-2	JL10-PY1
Al27	10465.31	9459.85	45424.45	<0.00010	0.017	0.00089	948.92	1156.45	<0.092	54.6	61.3	5.4	13.96	13.73	5.1	14.24	66.24	10385.35	7234.39	6672.51	10023.64	0.00057	<0.00050	43733.31	67.44
Si29	351052.59	317450.53	151012.59	0.18	0.34	0.093	5011.11	3694.95	66.32	1545.83	418.17	899.89	536.12	317.29	93.26	245.53	411.32	336203.91	285031.88	238000.36	323451.19	0.093	0.83	147658.48	350
S34	<0.00	<0.00	<0.00	<0.00	<0.00	<0.00	<0.00	<0.00	<0.00	<0.00	<0.00	<0.00	<0.00	<0.00	<0.00	<0.00	<0.00	<0.00	<0.00	<0.00	<0.00	<0.00	<0.00	<0.00	<0.00
Ca43	82886.04	76332.33	30591.24	<0.021	<0.053	<0.0190	521.66	<30.46	178.06	1244.44	340.9	370	805.16	<15.01	<7.66	499.36	872.47	86273.24	63459.9	59232.19	83317.05	0.0139	<0.090	30458.37	32.16
Sc45	453.98	408.16	18.16	0.00029	<0.00008	<0.00003	0.288	0.302	<0.030	0.036	0.043	<0.053	<0.0211	0.0173	<0.0103	<0.0123	<0.0184	465.22	309.45	305.64	450.59	0.00015	<0.00015	18.82	0.0319
Ti49	443.5	402.71	7332.22	0.00019	0.00074	0.00029	40.98	26.76	3.11	4.58	12.45	1.52	2.87	1.96	0.616	0.86	9.31	459.82	348.93	306.6	439.97	<0.00013	<0.0022	7322.23	14.84
V51	443.7	409.93	229.53	<0.00002	<0.00006	<0.00002	34.73	59.92	<0.0239	0.12	1.172	0.298	3	0.0464	0.0079	0.032	0.351	465.03	372.9	333.59	455.14	<0.00002	<0.00012	244.08	0.626
Cr53	411.52	382.96	6.29	<0.00111	<0.0032	<0.00109	7.34	7.49	<1.12	<1.41	5.79	<1.95	<0.85	<0.68	<0.38	1.32	0.76	420.94	364.86	317.25	408.64	<0.00069	<0.0054	6.67	3.89
Mn55	455.92	418.45	929.56	<0.00009	<0.00026	<0.00009	17.02	57.14	<0.105	24.51	1007.19	32.59	155.18	1.164	46.45	1206.53	97.97	445.83	396.74	345.11	427.72	<0.00007	<0.0006	915.86	11.47
Fe57	457.1	457.1	55500.02	0.0078	<0.0102	0.0078	304317.31	465531.63	465531.66	304317.31	22546.01	304317.31	465531.63	465531.63	6734.8	24111.27	465531.63	457.1	457.1	457.1	457.1	0.0078	<0.020	55500.02	465531.63
Co59	430.5	375.15	24.36	0.00012	0.00013	0.00005	0.205	49.57	19.88	0.0221	0.232	13.3	555.7	55.37	0.0425	16.53	5.46	422.35	398.02	330.2	411.27	0.00004	0.0004	23.01	277.22
Ni60	470.52	421.11	6.86	279.03	277.31	142.07	1.336	11.32	0.369	0.118	<0.30	0.411	4.27	1.358	0.146	0.279	0.813	459.33	446.55	334.19	441.94	93.2	899.14	8.85	1.87
Ni62	463.27	420.87	6.38	245.11	274.53	140.3	1.29	10	<0.42	3.43	<0.34	<0.75	5	71.81	<0.133	0.35	0.49	458.16	452.28	372.12	443.18	94.66	862.65	12.53	0.54
Cu65	465.61	415.54	11.95	0.126	0.163	0.081	452935.41	134.28	0.63	445068.16	9200.38	479861.44	2334.72	89.42	78.79	31.03	279.76	447.27	466.03	377.61	419.31	0.0539	0.48	20.58	7.94
Zn66	472.71	440.45	100.59	0.00079	0.147	0.00054	129.22	40.19	1.84	4690.34	637068.69	4204.46	2665.76	5.15	565572.44	570472.25	12799.01	421.64	676.06	552.6	518.75	0.0512	<0.0021	150.84	33.9
Ga71	463.74	413.85	12.16	<0.00002	<0.00006	<0.00002	3.21	2.95	0.0177	0.232	11.29	0.079	0.415	0.1053	1.76	1.87	0.163	448.56	410.01	360.44	441.35	<0.00001	<0.00014	13.23	0.059
As75	337.3	306.25	<3.67	0.039	0.056	0.0278	3.1	122.05	10.42	2.35	4.78	43.04	537.59	5006.54	28.35	5.97	4158.42	321	316.39	258.91	315.81	0.0169	0.19	<3.82	540.14
Se82	126.01	105.78	<4.30	0.044	0.059	0.0293	16.25	2.04	59.91	181.17	6.93	30.14	3.77	1.43	<0.53	3.83	1.05	113.42	95.93	81.22	101.29	0.0204	0.2	<3.64	11.03
Y89	454.03	414.43	16.86	<0.00000	0.00001	<0.00000	0.88	0.249	<0.0039	0.0125	0.182	0.0697	0.0938	0.0037	<0.00154	0.236	0.533	477.45	318.56	300.69	464.82	<0.00000	<0.00004	18.41	0.0614
Zr90	447.71	401.68	91.17	0.00001	<0.00002	<0.00001	4.76	2.18	<0.0113	0.041	3.27	0.095	0.0224	0.282	<0.0037	0.194	1.183	466.82	300.58	296.36	458.3	<0.00001	<0.00010	99.96	2.8
Nb93	431.34	385.59	5.88	<0.00000	<0.00001	<0.00000	0.0748	0.0456	0.0051	<0.0048	0.0287	<0.0080	0.0317	0.0107	0.00149	<0.00188	<0.0034	444.7	322	299.67	430.79	0.00009	<0.00003	6.43	0.0591
Mo95	395.69	349.05	117.78	<0.00003	<0.00006	0.00098	0.052	0.054	<0.036	89.93	5.64	<0.063	0.372	0.206	0.111	0.154	0.509	394.72	320.86	294.63	382.58	<0.00003	<0.00024	130.29	1.6
Ru99	<0.00	<0.00	<0.00	<0.00	<0.00	<0.00	<0.00	<0.00	<0.00	<0.00	<0.00	<0.00	<0.00	<0.00	<0.00	<0.00	<0.00	<0.00	<0.00	<0.00	<0.00	<0.00	<0.00	<0.00	<0.00
Ru101	<-NaN	<-NaN	<-NaN	<-NaN	<-NaN	<-NaN	<-NaN	<-NaN	<-NaN	<-NaN	<-NaN	<-NaN	<-NaN	<-NaN	<-NaN	<-NaN	<-NaN	<-NaN	<-NaN	<-NaN	<-NaN	<-NaN	<-NaN	<-NaN	<-NaN
Rh103	<0.00	<0.00	<0.00	<0.00	<0.00	<0.00	<0.00	<0.00	<0.00	<0.00	<0.00	<0.00	<0.00	<0.00	<0.00	<0.00	<0.00	<0.00	<0.00	<0.00	<0.00	<0.00	<0.00	<0.00	<0.00
Ag107	272.64	236.5	0.204	0.082	0.155	0.075	1.97	0.642	0.107	10.94	53.8	81.13	16.27	3.86	4.38	3.54	8.45	255.33	261.66	210.07	226.06	0.0486	0.44	0.363	1.6
Pd108	<0.00	<0.00	<0.00	<0.00	<0.00	<0.00	<0.00	<0.00	<0.00	<0.00	<0.00	<0.00	<0.00	<0.00	<0.00	<0.00	<0.00	<0.00	<0.00	<0.00	<0.00	<0.00	<0.00	<0.00	<0.00
Cd111	282.79	251.08	0.53	0.0198	0.035	0.0161	0.712	0.353	<0.177	28.38	1607.85	22.45	9.28	0.163	1762.74	1700.53	41.13	266.57	320.03	241.17	252.76	0.0112	0.1	<0.67	<0.181
In115	466.17	413.39	0.065	<0.00001	0.00002	<0.00001	5.13	0.0144	<0.0088	1.106	0.344	25.81	8.06	0.0146	0.00279	2.38	0.459	452.7	460.6	348.24	448.68	<0.00001	0.00006	0.0616	0.0055
Sn118	422.91	376.21	1.35	0.00055	0.00102	0.00053	282.53	2.62	<0.097	0.997	0.423	16.06	2.32	<0.061	0.164	0.731	5.03	408.43	376.07	327.23	394.67	0.0008	0.0026	1.4	0.134
Sb121	398.32	348.1	0.308	0.00047	0.00113	0.00063	8.33	0.908	0.053	1.17	1.04	2.35	18.78	32.84	17.53	2.44	8.84	380.2	374.12	306.13	367.16	0.00035	0.0042	0.387	16.97
Te125	<0.00	<0.00	<0.00	<0.00	<0.00	<0.00	<0.00	<0.00	<0.00	<0.00	<0.00	<0.00	<0.00	<0.00	<0.00	<0.00	<0.00	<0.00	<0.00	<0.00	<0.00	<0.00	<0.00	<0.00	<0.00
Te128	<0.00	<0.00	<0.00	<0.00	<0.00	<0.00	<0.00	<0.00	<0.00	<0.00	<0.00	<0.00	<0.00	<0.00	<0.00	<0.00	<0.00	<0.00	<0.00	<0.00	<0.00	<0.00	<0.00	<0.00	<0.00
La139	474.72	420.82	14.18	0.00001	<0.00001	<0.00000	1.64	0.273	<0.0034	0.0198	0.1006	<0.0091	0.0227	0.0173	<0.00185	0.0322	0.232	478.9	313.95	308.44	471.48	<0.00000	<0.00004	15.4	0.0048
Ce140	461.49	418.33	30.57	0.00001	0.00002	<0.00001	1.434	0.196	0.006	0.0172	0.211	0.0299	0.0674	0.0104	0.0582	0.0352	1.26	464.14	364.07	336.82	457.17	<0.00000	<0.00003	31.48	0.0094
Nd146	448.15	397.72	15.45	<0.00002	<0.00007	0.00001	0.692	<0.028	<0.0230	<0.031	0.127	<0.040	<0.0192	0.0168	<0.0054	<0.0092	<0.0172	448.55	312.49	290.1	442.77	<0.00002	<0.00009	16.65	<0.0220
Hf178	434.08	391.2	2.31	<0.00001	<0.00004	<0.00002	0.0432	<0.0091	<0.0139	<0.0188	0.081	0.0166	<0.0136	<0.0083	<0.0065	0.0266	0.041	431.07	288.16	285.21	424.9	<0.00001	<0.00010	2.65	0.06
W182	466.82	419.78	0.76	0.00002	<0.00008	<0.00002	7.77	9.25	<0.0220	0.115	0.534	7.2	0.336	<0.0152	0.0061	0.0159	0.0377	452.01	392.2	335.92	453.89	<0.00002	<0.00012	0.269	0.355
Re185	111.7	97.57	<0.078	<0.00002	<0.00003	<0.00003	<0.0208	<0.0197	<0.0189	<0.036	0.048	<0.050	<0.0120	<0.0113	<0.0114	<0.0083	0.0104	105.72	90.47	76.71	104.36	<0.00001	<0.00005	<0.060	<0.0238
Re187	110.93	100.01	<0.047	0.00191	0.0021	0.00105	<0.0125	<0.0137	<0.0093	<0.022	0.055	<0.0229	<0.0135	<0.0079	<0.0054	<0.0093	<0.0128	106.63	97.73	79.83	101.94	0.0006	0.006	<0.039	<0.0143
Os189	<-NaN	<-NaN	<-NaN	<-NaN	<-NaN	<-NaN	<-NaN	<-NaN	<-NaN	<-NaN	<-NaN	<-NaN	<-NaN	<-NaN	<-NaN	<-NaN	<-NaN	<-NaN	<-NaN	<-NaN	<-NaN	<-NaN	<-NaN	<-NaN	<-NaN
Os190	<-NaN	<-NaN	<-NaN	<-NaN	<-NaN	<-NaN	<-NaN	<-NaN	<-NaN	<-NaN	<-NaN	<-NaN	<-NaN	<-NaN	<-NaN	<-NaN	<-NaN	<-NaN	<-NaN	<-NaN	<-NaN	<-NaN	<-NaN	<-NaN	<-NaN
Ir193	<-NaN	<-NaN	<-NaN	<-NaN	<-NaN	<-NaN	<-NaN	<-NaN	<-NaN	<-NaN	<-NaN	<-NaN	<-NaN	<-NaN	<-NaN	<-NaN	<-NaN	<-NaN	<-NaN	<-NaN	<-NaN	<-NaN	<-NaN	<-NaN	<-NaN
Pt195	<0.00	<0.00	<0.00	<0.00	<0.00	<0.00	<0.00	<0.00	<0.00	<0.00	<0.00	<0.00	<0.00	<0.00	<0.00	<0.00	<0.00	<0.00	<0.00	<0.00	<0.00	<0.00	<0.00	<0.00	<0.00
Au197	25.63	22.43	0.072	0.107	0.123	0.061	0.189	0.212	0.0309	0.097	13.86	<0.033	4.77	28.53	0.0261	0.08	15.32	23.18	23.63	18.95	21.34	0.0391	0.38	0.086	0.649
Pb208	469.71	415.59	6.09	0.0084	0.0167	0.0079	23.38	20.73	0.538	19.49	54.36	71.41	814.94	817.86	4.96	9.24	517.74	413.34	444.36	357.4	398.99	0.00566	0.046	6.07	98.83
Bi209	418.75	366.65	<0.063	0.054	0.099	0.048	18.5	26.57	<0.0181	<0.025	<0.0171	7.54	20.01	16.07	0.0141	0.086	7.06	355.45	324.61	285.43	342.69	0.0291	0.28	<0.047	18.8
Th232	482.38	432.91	3.1	<0.00000	0.00003	<0.00000	0.234	<0.0054	<0.0047	<0.0058	0.321	0.0125	0.0467	0.0063	<0.0025	<0.00256	0.005	456.75	312.01	297.97	448.88	<0.00000	<0.00003	3.29	0.043
U238	490.27	444.74	1.033	<0.00001	<0.00002	<0.00000	1.725	0.0486	0.0219	0.0137	2.64	0.0099	0.235	<0.0038	0.00129	<0.0019	0.0545	459.15	378.64	349.9	453.57	<0.00000	<0.00004	0.984	0.191
ThO248	<-NaN	<-NaN	<-NaN	<-NaN	<-NaN	<-NaN	<-NaN	<-NaN	<-NaN	<-NaN	<-NaN	<-NaN	<-NaN	<-NaN	<-NaN	<-NaN	<-NaN	<-NaN	<-NaN	<-NaN	<-NaN	<-NaN	<-NaN	<-NaN	<-NaN

GLITTER!: 1 sigma error.

Element	STD610-1	STD610-2	BCR2G-1	PGEA-1	PGEA-2	PGEA-3	MS-CPY	MS-PY	KP11-PY	KP11-CPY	KP11-SPH	BG30-CPY	BG30-PY	JL06-PY2	JL06-SPH	BG06-SPH	BG06-PY	STD610-3	STD610-4	STD610-5	STD610-6	PGEA-4	PGEA-5	BCR2G-2	JL10-PY1
Al27	617.28	544.84	2306.05	0.00009	0.0085	0.00019	48.17	58.71	0.036	2.79	5.09	0.3	0.72	0.7	0.42	1.18	3.37	591.97	385.47	356.14	564.74	0.00008	0.00029	2220.16	3.43
Si29	22147.73	19616.28	8379.16	0.066	0.17	0.025	278.5	205.79	13.9	88.69	41.59	55.87	32.59	19.45	10.09	24.32	24.45	20588.99	16472.9	13774.99	19609.39	0.015	1.29	8192.88	22.91
S34	<0.00	<0.00	<0.00	<0.00	<0.00	<0.00	<0.00	<0.00	<0.00	<0.00	<0.00	<0.00	<0.00	<0.00	<0.00	<0.00	<0.00	<0.00	<0.00	<0.00	<0.00	<0.00	<0.00	<0.00	<0.00
Ca43	5277.24	4762.31	1716.1	0.015	0.026	0.0085	31.94	11.88	15.27	76.45	28.88	29.82	49.58	5.77	2.97	39.54	50.43	5329.04	3700.84	3459.43	5095.41	0.0046	0.075	1708.06	7.19
Sc45	30.69	27.1	1.11	0.0001	0.00004	0.00001	0.023	0.025	0.011	0.017	0.011	0.021	0.0099	0.0068	0.0041	0.005	0.0071	30.64	19.39	19.18	29.42	0.00002	0.00009	1.15	0.0096
Ti49	29.62	26.43	429.68	0.00016	0.00043	0.00012	2.45	1.63	0.24	0.4	1.12	0.24	0.25	0.15	0.073	0.1	0.58	29.79	21.41	18.85	28.24	0.00006	0.0064	429.08	0.94

Element	STD610-1	STD610-2	BCR2G-1	PGEA-1	PGEA-2	PGEA-3	MS-CPY	MS-PY	KP11-PY	KP11-CPY	KP11-SPH	BG30-CPY	BG30-PY	JL06-PY2	JL06-SPH	BG06-SPH	BG06-PY	STD610-3	STD610-4	STD610-5	STD610-6	PGEA-4	PGEA-5	BCR2G-2	JL10-PY1
V51	29.45	26.71	13.58	0.00002	0.00003	0.00001	2.06	3.55	0.0087	0.017	0.084	0.029	0.18	0.0065	0.003	0.006	0.023	30.04	22.87	20.49	29.14	0.00001	0.00015	14.44	0.042
Cr53	23.58	21.36	1.38	0.00095	0.0012	0.00049	0.54	0.6	0.42	0.63	0.65	0.78	0.39	0.25	0.15	0.24	0.26	23.01	18.36	16.03	22.05	0.00026	0.0045	0.98	0.41
Mn55	24.22	21.58	40.66	0.00007	0.0001	0.00004	0.75	2.5	0.04	1.09	92.89	1.44	6.79	0.059	4.28	111.27	4.29	22.69	18.51	16.14	21.45	0.00003	0.001	40.05	0.51
Fe57	24.21	22.77	1756.78	0.0037	0.0055	0.0023	9623.97	14722.16	14722.05	9625.02	2037.2	9624.79	14722.45	14721.77	608.55	2178.57	14721.82	22.13	17.85	17.96	21.42	0.0014	0.017	1756.65	14722.29
Co59	29.26	25.05	1.49	0.00005	0.00007	0.00001	0.016	3.02	1.21	0.0087	0.022	0.82	33.85	3.37	0.005	1.33	0.34	27.98	25.1	20.85	27.01	0.00001	0.00063	1.41	16.89
Ni60	27.73	24.24	0.41	94.8	139.2	29.87	0.09	0.59	0.048	0.05	0.23	0.077	0.25	0.082	0.021	0.036	0.057	26.12	23.68	17.77	24.84	12.35	1395	0.5	0.12
Ni62	27.17	24.16	0.72	83.18	137.72	29.41	0.18	0.64	0.18	0.46	0.14	0.33	0.43	3.5	0.053	0.084	0.1	25.7	23.27	19.25	24.54	12.44	1338.31	0.98	0.18
Cu65	28.59	24.97	0.73	0.043	0.082	0.017	24075.01	7.16	0.11	23657.33	979.28	25506.63	124.13	4.76	8.39	3.31	14.88	26.58	25.97	21.09	24.66	0.0072	0.75	1.16	0.46
Zn66	47.37	43.79	9.64	0.00037	0.075	0.00016	12.31	3.86	0.21	445.83	20146.06	399.65	253.39	0.51	17885.04	18040.03	1216.39	41.83	65.3	53.41	51.1	0.008	0.0013	14.41	3.27
Ga71	26.83	23.36	0.62	0.00001	0.00002	0.00001	0.17	0.16	0.007	0.03	0.93	0.018	0.033	0.0098	0.15	0.16	0.014	25.03	21.3	18.76	24.33	0	0.0002	0.68	0.012
As75	28.59	25.66	1.38	0.014	0.029	0.0061	0.48	9.56	0.95	0.73	0.61	3.51	42	390.81	2.61	0.62	324.61	26.81	25.37	20.84	26.23	0.0025	0.3	1.51	42.19
Se82	12.52	10.56	1.6	0.015	0.03	0.0065	1.51	0.64	5.13	15.4	1.18	2.9	0.7	0.38	0.21	0.65	0.39	11	8.66	7.44	9.99	0.0031	0.32	1.4	1.16
Y89	32.15	28.86	1.09	0	0.00001	0	0.058	0.019	0.0015	0.0038	0.015	0.0084	0.0092	0.0015	0.00069	0.018	0.036	33.01	21.06	19.9	31.89	0	0.00006	1.18	0.0065
Zr90	33.97	30.04	6.36	0.00001	0.00001	0	0.33	0.16	0.0047	0.0087	0.23	0.015	0.0053	0.022	0.0017	0.016	0.085	34.69	21.49	21.21	33.83	0	0.00026	6.97	0.2
Nb93	30.78	27.07	0.39	0	0	0	0.0066	0.0052	0.0018	0.0026	0.0037	0.0032	0.0046	0.0016	0.00057	0.00079	0.0014	31	21.48	20.01	29.8	0.00001	0.00002	0.42	0.0062
Mo95	26.44	22.91	7.03	0.00002	0.00004	0.00022	0.013	0.017	0.013	5.38	0.47	0.027	0.04	0.021	0.013	0.019	0.039	25.66	19.8	18.21	24.65	0.00001	0.00016	7.77	0.11
Ru99	<0.00	<0.00	<0.00	<0.00	<0.00	<0.00	<0.00	<0.00	<0.00	<0.00	<0.00	<0.00	<0.00	<0.00	<0.00	<0.00	<0.00	<0.00	<0.00	<0.00	<0.00	<0.00	<0.00	<0.00	<0.00
Ru101	<0.00	<0.00	<0.00	<0.00	<0.00	<0.00	<0.00	<0.00	<0.00	<0.00	<0.00	<0.00	<0.00	<0.00	<0.00	<0.00	<0.00	<0.00	<0.00	<0.00	<0.00	<0.00	<0.00	<0.00	<0.00
Rh103	<0.00	<0.00	<0.00	<0.00	<0.00	<0.00	<0.00	<0.00	<0.00	<0.00	<0.00	<0.00	<0.00	<0.00	<0.00	<0.00	<0.00	<0.00	<0.00	<0.00	<0.00	<0.00	<0.00	<0.00	<0.00
Ag107	21.5	18.42	0.043	0.028	0.078	0.016	0.15	0.056	0.016	0.82	7.24	5.91	1.2	0.29	0.59	0.48	0.62	19.75	19.51	15.68	17.38	0.0069	0.68	0.046	0.13
Pd108	<0.00	<0.00	<0.00	<0.00	<0.00	<0.00	<0.00	<0.00	<0.00	<0.00	<0.00	<0.00	<0.00	<0.00	<0.00	<0.00	<0.00	<0.00	<0.00	<0.00	<0.00	<0.00	<0.00	<0.00	<0.00
Cd111	18.43	16.08	0.17	0.0068	0.017	0.0034	0.1	0.089	0.072	1.76	179.44	1.41	0.63	0.054	196.69	189.76	2.33	16.79	18.79	14.24	15.77	0.0015	0.15	0.25	0.074
In115	28.44	24.67	0.011	0	0.00001	0	0.28	0.004	0.0031	0.068	0.029	1.38	0.43	0.0022	0.0009	0.18	0.027	26.75	25.56	19.35	26.22	0	0.0001	0.0097	0.0027
Sn118	24.55	21.31	0.13	0.00021	0.00053	0.00012	13.97	0.15	0.037	0.095	0.058	0.83	0.14	0.024	0.022	0.073	0.26	22.86	19.6	17.08	21.82	0.00011	0.004	0.13	0.037
Sb121	25.08	21.47	0.069	0.00018	0.00057	0.00014	0.47	0.064	0.022	0.092	0.1	0.16	1.05	1.82	1.62	0.23	0.49	23.22	21.52	17.64	22.19	0.00005	0.0065	0.072	0.95
Te125	<0.00	<0.00	<0.00	<0.00	<0.00	<0.00	<0.00	<0.00	<0.00	<0.00	<0.00	<0.00	<0.00	<0.00	<0.00	<0.00	<0.00	<0.00	<0.00	<0.00	<0.00	<0.00	<0.00	<0.00	<0.00
Te128	<0.00	<0.00	<0.00	<0.00	<0.00	<0.00	<0.00	<0.00	<0.00	<0.00	<0.00	<0.00	<0.00	<0.00	<0.00	<0.00	<0.00	<0.00	<0.00	<0.00	<0.00	<0.00	<0.00	<0.00	<0.00
La139	33.27	29	0.9	0.00001	0	0	0.11	0.02	0.0014	0.0048	0.0093	0.004	0.0041	0.0024	0.0008	0.0035	0.016	32.76	20.51	20.17	31.99	0	0.00006	0.98	0.0021
Ce140	28.2	25	1.63	0.00001	0.00001	0	0.079	0.014	0.0018	0.0045	0.018	0.0055	0.007	0.0018	0.005	0.0038	0.069	27.47	20.24	18.76	26.76	0	0.00002	1.68	0.0026
Nd146	30.3	26.41	0.96	0.00001	0.00003	0.00001	0.053	0.011	0.0097	0.013	0.019	0.017	0.0094	0.0061	0.0022	0.0044	0.0068	29.53	19.56	18.19	28.89	0.00001	0.00011	1.03	0.0082
Hf178	26.04	22.93	0.14	0.00001	0.00001	0.00001	0.0076	0.0048	0.0053	0.0093	0.012	0.0075	0.0062	0.0033	0.0028	0.0057	0.0065	25	15.65	15.52	24.36	0	0.00011	0.16	0.01
W182	26.9	23.6	0.068	0.00002	0.00004	0.00001	0.39	0.47	0.0079	0.023	0.05	0.38	0.033	0.0061	0.0028	0.0046	0.0076	25.1	20.25	17.38	24.89	0.00001	0.00011	0.039	0.033
Re185	7.01	6.01	0.027	0.00001	0.00002	0.00001	0.0081	0.0081	0.0086	0.016	0.014	0.02	0.0079	0.0051	0.0042	0.0042	0.0052	6.42	5.15	4.38	6.27	0.00001	0.00006	0.024	0.0097
Re187	6.39	5.63	0.017	0.00066	0.0011	0.00022	0.0047	0.0053	0.0047	0.011	0.01	0.0097	0.0059	0.003	0.0023	0.0038	0.0044	5.91	5.02	4.11	5.58	0.00008	0.0094	0.015	0.0067
Os189	<0.00	<0.00	<0.00	<0.00	<0.00	<0.00	<0.00	<0.00	<0.00	<0.00	<0.00	<0.00	<0.00	<0.00	<0.00	<0.00	<0.00	<0.00	<0.00	<0.00	<0.00	<0.00	<0.00	<0.00	<0.00
Os190	<0.00	<0.00	<0.00	<0.00	<0.00	<0.00	<0.00	<0.00	<0.00	<0.00	<0.00	<0.00	<0.00	<0.00	<0.00	<0.00	<0.00	<0.00	<0.00	<0.00	<0.00	<0.00	<0.00	<0.00	<0.00
Ir193	<0.00	<0.00	<0.00	<0.00	<0.00	<0.00	<0.00	<0.00	<0.00	<0.00	<0.00	<0.00	<0.00	<0.00	<0.00	<0.00	<0.00	<0.00	<0.00	<0.00	<0.00	<0.00	<0.00	<0.00	<0.00
Pt195	<0.00	<0.00	<0.00	<0.00	<0.00	<0.00	<0.00	<0.00	<0.00	<0.00	<0.00	<0.00	<0.00	<0.00	<0.00	<0.00	<0.00	<0.00	<0.00	<0.00	<0.00	<0.00	<0.00	<0.00	<0.00
Au197	2.01	1.74	0.026	0.037	0.062	0.013	0.02	0.023	0.0081	0.021	1.89	0.015	0.34	1.99	0.0055	0.014	1.07	1.77	1.72	1.38	1.62	0.0055	0.59	0.02	0.055
Pb208	30.39	26.37	0.37	0.0029	0.0084	0.0017	1.34	1.19	0.04	1.14	6.41	4.1	46.58	46.74	0.59	1.09	29.59	25.99	26.43	21.29	24.85	0.00077	0.072	0.37	5.66
Bi209	30.31	26.13	0.024	0.018	0.05	0.01	1.22	1.75	0.007	0.01	0.0069	0.5	1.32	1.06	0.0038	0.013	0.47	25.16	22.01	19.37	24.07	0.004	0.44	0.018	1.24
Th232	26.09	22.76	0.15	0	0.00002	0	0.014	0.0023	0.002	0.0033	0.031	0.0033	0.0059	0.0017	0.001	0.00096	0.0018	23.71	14.91	14.27	22.97	0	0.00002	0.16	0.0055
U238	25.42	22.36	0.054	0	0.00001	0	0.077	0.0052	0.0039	0.0047	0.24	0.0041	0.015	0.0013	0.00058	0.001	0.0044	22.76	17.13	15.86	22.14	0	0.00007	0.051	0.013
ThO248	<0.00	<0.00	<0.00	<0.00	<0.00	<0.00	<0.00	<0.00	<0.00	<0.00	<0.00	<0.00	<0.00	<0.00	<0.00	<0.00	<0.00	<0.00	<0.00	<0.00	<0.00	<0.00	<0.00	<0.00	<0.00

GLITTER!: Minimum detection limits (99% confidence).

Element	STD610-1	STD610-2	BCR2G-1	PGEA-1	PGEA-2	PGEA-3	MS-CPY	MS-PY	KP11-PY	KP11-CPY	KP11-SPH	BG30-CPY	BG30-PY	JL06-PY2	JL06-SPH	BG06-SPH	BG06-PY	STD610-3	STD610-4	STD610-5	STD610-6	PGEA-4	PGEA-5	BCR2G-2	JL10-PY1
Al27	0.801	0.66	0.304	0.0001	0.00026	0.00008	0.0754	0.093	0.0919	0.115	0.0756	0.166	0.0706	0.0562	0.0307	0.0422	0.0575	0.569	0.283	0.304	0.588	0.00006	0.0005	0.21	0.0784
Si29	268.49	226.82	102.9	0.0334	0.0985	0.0342	30.36	36.55	35.13	44.37	29.72	59.89	27.57	21.07	12.12	16.02	21.81	207.15	98.73	112.8	203.61	0.0222	0.179	77.01	27.84
S34	<0.00000	<0.00000	<0.00000	<0.00000	<0.00000	<0.00000	<0.00000	<0.00000	<0.00000	<0.00000	<0.00000	<0.00000	<0.00000	<0.00000	<0.00000	<0.00000	<0.00000	<0.00000	<0.00000	<0.00000	<0.00000	<0.00000	<0.00000	<0.00000	<0.00000
Ca43	199.51	146.56	65.61	0.0212	0.053	0.019	16.4	30.46	24.6	29.19	18.91	39.41	21.53	15.01	7.66	8.19	10.76	117.6	51.35	59.82	104.05	0.0107	0.0899	35.81	14.68
Sc45	0.242	0.181	0.0795	0.00003	0.00008	0.00003	0.0255	0.0304	0.0297	0.0356	0.025	0.0526	0.0211	0.0172	0.0103	0.0123	0.0184	0.173	0.0799	0.0869	0.172	0.00002	0.00015	0.0603	0.0204
Ti49	0.929	1.28	0.498	0.00016	0.0005	0.0002	0.148	0.177	0.212	0.238	0.161	0.434	0.152	0.129	0.0763	0.081	0.104	1.24	0.534	0.6	1.22	0.00013	0.00216	0.39	0.147
V51	0.143	0.144	0.0676	0.00002	0.00006	0.00002	0.0182	0.0194	0.0239	0.0245	0.0199	0.0429	0.0176	0.0133	0.00712	0.0118	0.0147	0.121	0.0736	0.0712	0.128	0.00002	0.00012	0.0511	0.0185
Cr53	9.25	7.73	3.53	0.00111	0.00319	0.00109	0.977	1.17	1.12	1.41	0.946	1.95	0.852	0.679	0.377	0.493	0.676	6.58	3.09	3.49	6.38	0.00069	0.00538	2.36	0.817
Mn55	0.706	0.61	0.28	0.00009	0.00026	0.00009	0.0821	0.103	0.105	0.135	0.0877	0.188	0.0841	0.0665	0.0385	0.0506	0.0677	0.676	0.33	0.357	0.649	0.00007	0.00058	0.245	0.0895
Fe57	26.28	21.72	9.98	0.00333	0.0102	0.00343	3.16	3.84	3.84	4.76	3.13	6.86	3.1	2.53	1.32	1.91	2.49	23.14	11.03	12.42	21.5	0.00243	0.0203	8.73	3.02
Co59	0.124	0.1	0.0401	0.00001	0.00004	0.00002	0.0103	0.0139	0.0172	0.0151	0.0129	0.0308	0.0111	0.0116	0.00564	0.00724	0.0108	0.0932	0.0585	0.0614	0.1	0.00001	0.00009	0.0325	0.0137
Ni60	0.55	0.482	0.255	0.00007	0.00039	0.00008	0.0797	0.0781	0.089	0.0971	0.302	0.149	0.0624	0.0515	0.0302	0.0401	0.0537	0.538	0.259	0.301	0.567	0.00005	0.0383	0.231	0.0764
Ni62	2.08	2.75	1.15	0.00031	0.00089	0.00025	0.285	0.324	0.421	0.555	0.344	0.747	0.286	0.228	0.133	0.131	0.193	2.77	1.07	1.34	2.57	0.0003	0.104	1.05	0.357
Cu65	1.72	1.54	0.644	0.00044	0.00081	0.00023	0.199	0.268	0.251	0.35	0.251	0.457	0.215	0.159	0.0992	0.119	0.159	1.53	0.747	0.781	1.51	0.00017	0.00166	0.554	0.208
Zn66	1.35	1.29	0.485	0.00021	0.00067	0.00019	0.16	0.168	0.17	0.241	0.162	1.4	0.237	0.175	0.0841	0.311	0.834	7.67	2.89	1.33	2.14	0.00024	0.00208	0.742	0.242
Ga71	0.107	0.116	0.058	0.00002	0.00006	0.00002	0.0134	0.0108	0.0146	0.0305	0.0142	0.0293	0.0153	0.00947	0.00691	0.00751	0.0128	0.0977	0.0471	0.0693	0.0913	0.00001	0.00014	0.0385	0.0191
As75	9.19	7.79	3.67	0.00115	0.00339	0.00116	1.05	1.25	1.23	1.56	1.02	2.18	0.975	0.765	0.507	0.675	0.969	10.17	4.92	5.63	10.27	0.00112	0.00881	3.82	1.35
Se82	10.66	9.25	4.3	0.00138	0.00402	0.00144	1.25	1.53	1.55	1.83	1.29	2.77	1.26	0.911	0.533	0.675	0.985	9.35	4.67	4.91	9.82	0.00107	0.00801	3.64	1.32
Y89	0.0341	0.0305	0.0145	0	0.00001	0	0.00258	0.00659	0.00393	0.00486	0.00416	0.00681	0.00576	0.00349	0.00154	0.00205	0.00322	0.0307	0.0157	0.0177	0.0245	0	0.00004	0.0121	0.00382
Zr90	0.0751	0.0363	0.0245	0.00001	0.00002	0.00001	0.00502	0.0107	0.0113	0.00732	0.0106	0.0187	0.00528	0.00409	0.00374	0.00424	0.00586	0.0597	0.0269	0.0256	0.0673	0.00001	0.0001	0.0204	0.00802

Element	STD610-1	STD610-2	BCR2G-1	PGEA-1	PGEA-2	PGEA-3	MS-CPY	MS-PY	KP11-PY	KP11-CPY	KP11-SPH	BG30-CPY	BG30-PY	JL06-PY2	JL06-SPH	BG06-SPH	BG06-PY	STD610-3	STD610-4	STD610-5	STD610-6	PGEA-4	PGEA-5	BCR2G-2	JL10-PY1
Nb93	0.0255	0.0185	0.0144	0	0.00001	0	0.00148	0.00478	0.00348	0.00481	0.00252	0.00798	0.00355	0.0018	0.001	0.00188	0.00338	0.0215	0.0179	0.0165	0.0217	0	0.00003	0.0127	0.00267
Mo95	0.296	0.212	0.114	0.00003	0.00006	0.00003	0.0217	0.0325	0.0361	0.0428	0.029	0.0626	0.0267	0.0242	0.011	0.0173	0.0244	0.144	0.0931	0.14	0.234	0.00003	0.00024	0.0718	0.0245
Ru99	<0.00000	<0.00000	<0.00000	<0.00000	<0.00000	<0.00000	<0.00000	<0.00000	<0.00000	<0.00000	<0.00000	<0.00000	<0.00000	<0.00000	<0.00000	<0.00000	<0.00000	<0.00000	<0.00000	<0.00000	<0.00000	<0.00000	<0.00000	<0.00000	<0.00000
Ru101	<0.00	<0.00	<0.00	<0.00	<0.00	<0.00	<0.00	<0.00	<0.00	<0.00	<0.00	<0.00	<0.00	<0.00	<0.00	<0.00	<0.00	<0.00	<0.00	<0.00	<0.00	<0.00	<0.00	<0.00	<0.00
Rh103	<0.00000	<0.00000	<0.00000	<0.00000	<0.00000	<0.00000	<0.00000	<0.00000	<0.00000	<0.00000	<0.00000	<0.00000	<0.00000	<0.00000	<0.00000	<0.00000	<0.00000	<0.00000	<0.00000	<0.00000	<0.00000	<0.00000	<0.00000	<0.00000	<0.00000
Ag107	0.147	0.138	0.0856	0.00003	0.00005	0.00002	0.0217	0.0256	0.0235	0.0329	0.0214	0.0369	0.0198	0.0113	0.00812	0.0113	0.0146	0.158	0.0897	0.0788	0.153	0.00001	0.00083	0.0519	0.0167
Pd108	<0.00000	<0.00000	<0.00000	<0.00000	<0.00000	<0.00000	<0.00000	<0.00000	<0.00000	<0.00000	<0.00000	<0.00000	<0.00000	<0.00000	<0.00000	<0.00000	<0.00000	<0.00000	<0.00000	<0.00000	<0.00000	<0.00000	<0.00000	<0.00000	<0.00000
Cd111	1.3	0.94	0.334	0.0002	0.00052	0.0002	0.137	0.168	0.177	0.253	0.161	0.354	0.177	0.122	0.0722	0.106	0.241	1.38	0.589	0.82	1.15	0.00011	0.00129	0.669	0.181
In115	0.0414	0.0347	0.0165	0.00001	0.00002	0.00001	0.00644	0.00744	0.00875	0.00542	0.0052	0.0132	0.00586	0.00262	0.00146	0.00354	0.00492	0.0383	0.0151	0.0147	0.0386	0.00001	0.00004	0.0123	0.00502
Sn118	0.673	0.594	0.249	0.00008	0.00027	0.00008	0.0825	0.101	0.0968	0.127	0.0907	0.176	0.0822	0.0612	0.0347	0.0481	0.0614	0.545	0.268	0.315	0.579	0.00006	0.0005	0.235	0.079
Sb121	0.218	0.258	0.156	0.00004	0.0001	0.00004	0.0399	0.043	0.0527	0.0529	0.0355	0.0994	0.0434	0.0347	0.0208	0.0238	0.0313	0.311	0.195	0.194	0.317	0.00004	0.00037	0.157	0.0374
Te125	<0.00000	<0.00000	<0.00000	<0.00000	<0.00000	<0.00000	<0.00000	<0.00000	<0.00000	<0.00000	<0.00000	<0.00000	<0.00000	<0.00000	<0.00000	<0.00000	<0.00000	<0.00000	<0.00000	<0.00000	<0.00000	<0.00000	<0.00000	<0.00000	<0.00000
Te128	<0.00000	<0.00000	<0.00000	<0.00000	<0.00000	<0.00000	<0.00000	<0.00000	<0.00000	<0.00000	<0.00000	<0.00000	<0.00000	<0.00000	<0.00000	<0.00000	<0.00000	<0.00000	<0.00000	<0.00000	<0.00000	<0.00000	<0.00000	<0.00000	<0.00000
La139	0.0145	0.0171	0.0153	0	0.00001	0	0.00237	0.00356	0.00342	0.00546	0.0033	0.00906	0.00374	0.00335	0.00185	0.00195	0.00256	0.0211	0.0195	0.0175	0.0246	0	0.00004	0.0118	0.00351
Ce140	0.0379	0.0268	0.0114	0	0.00001	0.00001	0.00332	0.00498	0.00276	0.00541	0.00284	0.00678	0.00302	0.00287	0.00145	0.00245	0.00179	<0.00000	0.0143	0.00926	0.0298	0	0.00003	0.0117	0.00388
Nd146	0.0972	0.182	0.0776	0.00002	0.00007	0.00001	0.0195	0.0276	0.023	0.0307	0.0207	0.0398	0.0192	0.0126	0.00537	0.00923	0.0172	0.1	0.0624	0.0628	0.101	0.00002	0.00009	0.0646	0.022
Hf178	<0.00000	0.0852	0.0574	0.00001	0.00004	0.00002	0.00913	0.00913	0.0139	0.0188	0.0104	0.0108	0.0136	0.00832	0.00653	0.00824	0.009	0.0939	0.0453	0.0416	0.0948	0.00001	0.0001	0.0214	0.0078
W182	0.114	0.123	0.0526	0.00002	0.00008	0.00002	0.0187	0.0209	0.022	0.0193	0.0199	0.0382	0.0184	0.0152	0.00516	0.00561	0.0117	0.0786	0.0464	0.0852	0.125	0.00002	0.00012	0.0536	0.0226
Re185	0.24	0.116	0.0783	0.00002	0.00003	0.00003	0.0208	0.0197	0.0189	0.0358	0.0241	0.0502	0.012	0.0113	0.0114	0.00832	0.01	0.0955	0.0651	0.0897	0.136	0.00001	0.00005	0.0595	0.0238
Re187	0.145	0.0809	0.0473	0.00001	0.00002	0.00001	0.0125	0.0137	0.00932	0.0216	0.00967	0.0229	0.0135	0.0079	0.00542	0.00931	0.0128	0.0407	0.0393	0.0494	0.116	0.00001	0.00016	0.0393	0.0143
Os189	<0.00	<0.00	<0.00	<0.00	<0.00	<0.00	<0.00	<0.00	<0.00	<0.00	<0.00	<0.00	<0.00	<0.00	<0.00	<0.00	<0.00	<0.00	<0.00	<0.00	<0.00	<0.00	<0.00	<0.00	<0.00
Os190	<0.00	<0.00	<0.00	<0.00	<0.00	<0.00	<0.00	<0.00	<0.00	<0.00	<0.00	<0.00	<0.00	<0.00	<0.00	<0.00	<0.00	<0.00	<0.00	<0.00	<0.00	<0.00	<0.00	<0.00	<0.00
Ir193	<0.00	<0.00	<0.00	<0.00	<0.00	<0.00	<0.00	<0.00	<0.00	<0.00	<0.00	<0.00	<0.00	<0.00	<0.00	<0.00	<0.00	<0.00	<0.00	<0.00	<0.00	<0.00	<0.00	<0.00	<0.00
Pt195	<0.00000	<0.00000	<0.00000	<0.00000	<0.00000	<0.00000	<0.00000	<0.00000	<0.00000	<0.00000	<0.00000	<0.00000	<0.00000	<0.00000	<0.00000	<0.00000	<0.00000	<0.00000	<0.00000	<0.00000	<0.00000	<0.00000	<0.00000	<0.00000	<0.00000
Au197	0.193	0.132	0.0563	0.00002	0.00006	0.00002	0.0116	0.02	0.0136	0.0238	0.0115	0.0334	0.0139	0.00999	0.00685	0.00744	0.00882	0.094	0.0672	0.0456	0.112	0.00001	0.00087	0.0287	0.00855
Pb208	0.176	0.17	0.0888	0.00002	0.00006	0.00002	0.0182	0.0214	0.0248	0.0297	0.0168	0.0322	0.0185	0.0153	0.00632	0.00971	0.0161	0.158	0.0639	0.0656	0.122	0.00002	0.00042	0.05	0.022
Bi209	0.152	0.119	0.0634	0.00002	0.00005	0.00002	0.016	0.0186	0.0181	0.0248	0.0171	0.0356	0.0136	0.0128	0.00749	0.00837	0.0114	0.11	0.0645	0.0732	0.118	0.00001	0.00053	0.0466	0.0174
Th232	0.0485	0.0406	0.0168	0	0.00001	0	0.00444	0.00544	0.00467	0.00578	0.00443	<0.00000	0.00361	0.00313	0.00248	0.00256	0.00371	0.0289	0.0251	0.0192	0.0386	0	0.00003	0.0151	0.00508
U238	0.0222	0.0348	0.0166	0.00001	0.00002	0	0.00545	0.00445	0.00677	0.00701	0.00363	0.00743	0.0037	0.00385	0.00102	0.00192	0.0034	<0.00000	0.0156	0.0215	0.0327	0	0.00004	0.0138	0.00466
ThO248	<0.00	<0.00	<0.00	<0.00	<0.00	<0.00	<0.00	<0.00	<0.00	<0.00	<0.00	<0.00	<0.00	<0.00	<0.00	<0.00	<0.00	<0.00	<0.00	<0.00	<0.00	<0.00	<0.00	<0.00	<0.00

GLITTER!: Trace element concentrations normalised to chondrite.

Element	STD610-1	STD610-2	BCR2G-1	PGEA-1	PGEA-2	PGEA-3	MS-CPY	MS-PY	KP11-PY	KP11-CPY	KP11-SPH	BG30-CPY	BG30-PY	JL06-PY2	JL06-SPH	BG06-SPH	BG06-PY	STD610-3	STD610-4	STD610-5	STD610-6	PGEA-4	PGEA-5	BCR2G-2	JL10-PY1
Al27	0.811	0.733	3.52	0	0	0	0.0736	0.0896	0	0.00423	0.00475	0.00042	0.00108	0.00106	0.0004	0.0011	0.00514	0.805	0.561	0.517	0.777	0	0	3.39	0.00523
Si29	2.19	1.98	0.944	0	0	0	0.0313	0.0231	0.00041	0.00966	0.00261	0.00562	0.00335	0.00198	0.00058	0.00153	0.00257	2.1	1.78	1.488	2.02	0	0.00001	0.923	0.00219
S34	<****	<****	<****	<****	<****	<****	<****	<****	<****	<****	<****	<****	<****	<****	<****	<****	<****	<****	<****	<****	<****	<****	<****	<****	<****
Ca43	6.14	5.65	2.27	0	0	0	0.0386	0	0.0132	0.0922	0.0253	0.0274	0.0596	0	0	0.037	0.0646	6.39	4.7	4.39	6.17	0	0	2.26	0.00238
Sc45	52.54	47.24	2.1	0.00003	0	0	0.0333	0.0349	0	0.0042	0.005	0	0	0.002	0	0	0	53.85	35.82	35.38	52.15	0.00002	0	2.18	0.0037
Ti49	0.678	0.616	11.21	0	0	0	0.0627	0.0409	0.00476	0.007	0.019	0.00232	0.00439	0.003	0.00094	0.00132	0.01424	0.703	0.534	0.469	0.673	0	0	11.2	0.0227
V51	5.22	4.82	2.7	0	0	0	0.409	0.705	0	0.00141	0.01379	0.00351	0.0353	0.00055	0.00009	0.00038	0.00413	5.47	4.39	3.92	5.35	0	0	2.87	0.00737
Cr53	0.1035	0.0963	0.00158	0	0	0	0.00185	0.00188	0	0	0.00146	0	0	0	0	0.00033	0.00019	0.1059	0.0918	0.0798	0.1028	0	0	0.00168	0.00098
Mn55	0.1551	0.1423	0.316	0	0	0	0.00579	0.01944	0	0.00834	0.343	0.01108	0.0528	0.0004	0.0158	0.41	0.0333	0.1516	0.1349	0.1174	0.1455	0	0	0.312	0.0039
Fe57	0.00164	0.00164	0.1996	0	0	0	1.095	1.675	1.675	1.095	0.0811	1.095	1.675	1.675	0.0242	0.0867	1.675	0.00164	0.00164	0.00164	0.00164	0	0	0.1996	1.675
Co59	0.563	0.491	0.0319	0	0	0	0.00027	0.0649	0.026	0.00003	0.0003	0.0174	0.727	0.0725	0.00006	0.0216	0.00714	0.553	0.521	0.432	0.538	0	0	0.0301	0.363
Ni60	0.0285	0.0255	0.00042	0.0169	0.0168	0.0086	0.00008	0.00069	0.00002	0.00001	0	0.00002	0.00026	0.00008	0.00001	0.00002	0.00005	0.0278	0.0271	0.0203	0.0268	0.00565	0.054	0.00054	0.00011
Ni62	0.0281	0.0255	0.00039	0.0149	0.0166	0.0085	0.00008	0.00061	0	0.00021	0	0	0.0003	0.00435	0	0.00002	0.00003	0.0278	0.0274	0.0226	0.0269	0.00574	0.052	0.00076	0.00003
Cu65	2.77	2.47	0.0712	0.00075	0.00097	0.00048	2696.04	0.799	0.00376	2649.22	54.76	2856.32	13.9	0.532	0.469	0.185	1.665	2.66	2.77	2.25	2.5	0.00032	0.0029	0.1225	0.0472
Zn66	1.02	0.953	0.218	0	0.00032	0	0.28	0.087	0.00397	10.15	1378.94	9.1	5.77	0.0111	1224.18	1234.79	27.7	0.913	1.46	1.2	1.12	0.00011	0	0.326	0.0734
Ga71	30.51	27.23	0.8	0	0	0	0.211	0.194	0.00116	0.0152	0.742	0.0052	0.0273	0.00693	0.1161	0.123	0.01072	29.51	26.97	23.71	29.04	0	0	0.871	0.00389
As75	117.53	106.71	0	0.0136	0.0196	0.0097	1.08	42.53	3.63	0.82	1.66	15	187.32	1744.44	9.88	2.08	1448.93	111.85	110.24	90.21	110.04	0.00591	0.07	0	188.2
Se82	4.62	3.87	0	0.00161	0.0022	0.00107	0.595	0.075	2.19	6.64	0.254	1.1	0.138	0.052	0	0.14	0.039	4.15	3.51	2.98	3.71	0.00075	0.007	0	0.404
Y89	201.79	184.19	7.5	0	0	0	0.391	0.1109	0	0.0056	0.0807	0.031	0.0417	0.00167	0	0.1049	0.237	212.2	141.58	133.64	206.59	0	0	8.18	0.0273
Zr90	80.81	72.51	16.46	0	0	0	0.859	0.393	0	0.0074	0.59	0.0171	0.00404	0.0509	0	0.035	0.214	84.26	54.26	53.49	82.73	0	0	18.04	0.505
Nb93	1150.25	1028.24	15.67	0	0	0	0.199	0.122	0.0136	0	0.0765	0	0.085	0.0285	0.004	0	0	1185.85	858.68	799.13	1148.78	0.00023	0	17.15	0.158
Mo95	286.73	252.94	85.35	0	0	0.00071	0.0375	0.039	0	65.16	4.09	0	0.269	0.149	0.0804	0.111	0.369	286.03	232.51	213.5	277.23	0	0	94.41	1.158
Ru99	0	0	0	0	0	0	0	0	0	0	0	0	0	0	0	0	0	0	0	0	0	0	0	0	0
Ru101	<****	<****	<****	<****	<****	<****	<****	<****	<****	<****	<****	<****	<****	<****	<****	<****	<****	<****	<****	<****	<****	<****	<****	<****	<****
Rh103	0	0	0	0	0	0	0	0	0	0	0	0	0	0	0	0	0	0	0	0	0	0	0	0	0
Ag107	826.18	716.68	0.62	0.249	0.47	0.228	5.97	1.94	0.324	33.16	163.03	245.84	49.31	11.7	13.28	10.74	25.6	773.73	792.92	636.59	685.02	0.147	1.32	1.1	4.85
Pd108	0	0	0	0	0	0	0	0	0	0	0	0	0	0	0	0	0	0	0	0	0	0	0	0	0
Cd111	279.99	248.6	0.52	0.0196	0.034	0.0159	0.705	0.35	0	28.1	1591.93	22.23	9.18	0.162	1745.29	1683.69	40.72	263.93	316.86	238.78	250.25	0.0111	0.1	0	0
In115	3984.34	3533.23	0.553	0	0.00014	0	43.83	0.123	0	9.45	2.94	220.58	68.85	0.125	0.0239	20.37	3.92	3869.25	3936.78	2976.39	3834.88	0	0.00052	0.526	0.047
Sn118	167.82	149.29	0.535	0.00022	0.00041	0.00021	112.11	1.042	0	0.396	0.168	6.37	0.919	0	0.0652	0.29	2	162.08	149.23	129.85	156.61	0.00032	0.001	0.556	0.053
Sb121	1709.53	1493.98	1.32	0.00201	0.0049	0.00272	35.73	3.9	0.227	5.02	4.46	10.09	80.61	140.94	75.23	10.46	37.92	1631.78	1605.65	1313.86	1575.81	0.00149	0.018	1.66	72.83
Te125	0	0	0	0	0	0	0	0	0	0	0	0	0	0	0	0	0	0	0	0	0	0	0	0	0
Te128	0	0	0	0	0	0	0	0	0	0	0	0	0	0	0	0	0	0	0	0	0	0	0	0	0
La139	1293.52	1146.64	38.64	0.00002	0	0	4.47	0.744	0	0.054	0.274	0	0.062	0.047	0	0.0877	0.633	1304.89	855.45	840.42	1284.7	0	0	41.95	0.0131

RUN2

Element	STD610-1	STD610-2	BCR2G-1	PGEA-1	PGEA-2	PGEA-3	MS-CPY	MS-PY	KP11-PY	KP11-CPY	KP11-SPH	BG30-CPY	BG30-PY	JL06-PY2	JL06-SPH	BG06-SPH	BG06-PY	STD610-3	STD610-4	STD610-5	STD610-6	PGEA-4	PGEA-5	BCR2G-2	JL10-PY1
Ce140	482.22	437.13	31.94	0.00001	0.00003	0	1.498	0.205	0.0063	0.0179	0.221	0.0312	0.0704	0.0109	0.0608	0.0368	1.316	484.99	380.43	351.95	477.71	0	0	32.9	0.0098
Nd146	630.31	559.39	21.73	0	0	0.00002	0.973	0	0	0	0.179	0	0	0.0236	0	0	0	630.87	439.51	408.02	622.75	0	0	23.42	0
Hf178	2425.03	2185.46	12.89	0	0	0	0.241	0	0	0	0.453	0.093	0	0	0	0.149	0.229	2408.22	1609.8	1593.37	2373.77	0	0	14.82	0.333
W182	5245.11	4716.58	8.54	0.00026	0	0	87.35	103.91	0	1.3	6	80.89	3.78	0	0.068	0.178	0.424	5078.8	4406.76	3774.34	5099.88	0	0	3.02	3.99
Re185	2030.98	1773.98	0	0	0	0	0	0	0	0	0.87	0	0	0	0	0	0.19	1922.21	1644.83	1394.77	1897.51	0	0	0	0
Re187	2016.86	1818.38	0	0.035	0.038	0.019	0	0	0	0	1	0	0	0	0	0	0	1938.79	1776.91	1451.46	1853.5	0.0109	0.11	0	0
Os189	<****	<****	<****	<****	<****	<****	<****	<****	<****	<****	<****	<****	<****	<****	<****	<****	<****	<****	<****	<****	<****	<****	<****	<****	<****
Os190	<****	<****	<****	<****	<****	<****	<****	<****	<****	<****	<****	<****	<****	<****	<****	<****	<****	<****	<****	<****	<****	<****	<****	<****	<****
Ir193	<****	<****	<****	<****	<****	<****	<****	<****	<****	<****	<****	<****	<****	<****	<****	<****	<****	<****	<****	<****	<****	<****	<****	<****	<****
Pt195	0	0	0	0	0	0	0	0	0	0	0	0	0	0	0	0	0	0	0	0	0	0	0	0	0
Au197	117.56	102.87	0.33	0.49	0.56	0.28	0.868	0.97	0.142	0.444	63.57	0	21.9	130.89	0.12	0.366	70.3	106.35	108.4	86.92	97.88	0.18	1.74	0.394	2.98
Pb208	128.69	113.86	1.67	0.00229	0.0046	0.00215	6.4	5.68	0.147	5.34	14.89	19.57	223.27	224.07	1.36	2.53	141.85	113.24	121.74	97.92	109.31	0.00155	0.013	1.66	27.08
Bi209	2507.5	2195.53	0	0.32	0.59	0.288	110.76	159.09	0	0	0	45.17	119.8	96.24	0.085	0.515	42.25	2128.44	1943.78	1709.15	2052.04	0.174	1.7	0	112.58
Th232	11350.12	10186.05	72.93	0	0.00065	0	5.51	0	0	0	7.54	0.293	1.1	0.148	0	0	0.117	10747.01	7341.45	7011.05	10561.99	0	0	77.42	1.01
U238	40185.77	36453.93	84.67	0	0	0	141.4	3.98	1.79	1.12	216.33	0.81	19.25	0	0.105	0	4.46	37635.28	31036.08	28680.17	37178.18	0	0	80.69	15.64
ThO248	<****	<****	<****	<****	<****	<****	<****	<****	<****	<****	<****	<****	<****	<****	<****	<****	<****	<****	<****	<****	<****	<****	<****	<****	<****

GLITTER4.0: Laser Ablation Analysis Results

G:\KYLIE\MAR13\RUN3
Fri Mar 14 17:46:27 2003

All values are reported in ppm

GLITTER!: Trace Element Concentrations MDL filtered.

	Run3-1	Run3-2	Run3-3	Run3-4	Run3-5	Run3-6	Run3-7	Run3-8	Run3-9	Run3-10	Run3-11	Run3-12	Run3-13	Discarded Run3-14	Run3-15	Run3-16	Run3-17	Run3-18
Element	STD610-3	STD610-6	PGEA-4	PGEA-5	BCR2G-2	JL10-PY1	JL10-SPH	JL10-CPY	WAN-SPH	BG05-PY	BG05-SPH	JL19-PY	JL19-CPY	JL19-SPH	STD610-7	STD610-8	PGEA-6	PGEA-7
Al27	10303.06	9862.73	0.00057	<0.00049	43216.33	66.39	4.83	10.63	6.45	200.99	18.39	8.74	75.42	633698.56	10413.92	9770.57	<0.00001	<0.00035
Si29	336638.09	321470.97	0.093	0.83	147357.36	358.79	138.3	457.42	137.4	1010.11	1285.18	298.22	876.03	5293911.5	341906.22	322487.53	0.01	<0.13
S34	<0.00	<0.00	<0.00	<0.00	<0.00	<0.00	<0.00	<0.00	<0.00	<0.00	<0.00	<0.00	<0.00	<0.00	<0.00	<0.00	<0.00	<0.00
Ca43	83939.55	80878.59	0.0136	<0.088	29702.29	31.91	44.74	2379.03	270.55	1233.12	518.54	62.51	427.15	**********	85239.23	79847.05	<0.00165	<0.054
Sc45	453.79	436.6	0.00014	<0.00015	18.26	0.032	<0.033	<0.126	<0.0062	<0.0150	0.08	<0.0220	<0.040	2403.27	457.21	430.48	<0.00000	<0.00011
Ti49	445.45	423.36	<0.00013	<0.0021	7066.88	15.76	0.86	11.45	12.77	4.94	1.07	1.17	1.77	73463.12	455.45	425.41	0.00019	0.0021
V51	453.46	439.33	<0.00002	<0.00012	237.4	0.629	<0.029	<0.093	0.404	1.047	0.716	<0.0189	0.995	1488198.75	455.73	430.98	<0.00000	<0.00009
Cr53	408.49	391.85	<0.00067	<0.0052	6.46	3.87	<1.21	<4.52	0.398	<0.57	<1.18	<0.80	<1.39	10567.12	429.5	401.15	<0.00013	<0.0037
Mn55	439.5	417.76	<0.00007	<0.00057	900.25	10.56	623.78	52.95	580.43	254.2	1417.3	5	97.74	7988161	454.98	430.98	<0.00001	<0.00042
Fe57	457.1	457.1	0.0078	<0.020	55500.01	465531.59	47852.3	304317.28	39509.25	465531.59	5775.29	465531.59	304317.28	**********	457.1	457.1	0.00777	<0.0147
Co59	410.05	394.71	0.00004	0.00039	22.25	241.36	20.44	0.437	0.258	229.23	2.87	146.31	0.928	396.08	422.69	400.8	0.00001	0.00036
Ni60	451.24	433.43	91.64	884.07	8.71	2.03	<0.103	1.93	0.272	48.61	2.45	0.341	1.95	7718.87	473.07	434.3	15.73	627.6
Ni62	451.31	436.52	93.16	848.96	12.33	<0.35	2.22	6.15	0.285	48.04	1.56	0.78	1.39	6346.23	476.51	430.11	15.71	656.69
Cu65	449.48	418.08	0.0541	0.49	20.66	7.39	772.73	490045.88	11746.18	152.91	195.57	258.4	428704.44	125866.07	436.31	427.45	0.00892	0.38
Zn66	396.81	486.75	0.0481	<0.0019	141.59	18.25	572172.06	3297.72	537073.5	415.9	669266.88	57.82	31000.72	559872.44	465.07	492.32	0.00006	0.04
Ga71	443.3	426.98	<0.00001	<0.00014	12.99	0.059	2.5	13.16	2.28	0.492	53.94	0.0179	2.34	12668.73	468.55	429.56	<0.00000	<0.00010
As75	330.54	322.97	0.0175	0.2	<3.95	520.79	17.44	22.4	1043.3	2260.51	18.36	54.6	4.82	43039	307.2	314.92	0.00308	0.12
Se82	113.85	98.41	0.0202	0.2	<3.61	10.54	<1.85	<6.93	6.37	1.36	<1.80	6.02	<2.38	<3816.04	115.32	110.03	0.00361	0.16
Y89	458.6	443.07	<0.00000	<0.00004	17.64	0.0456	<0.0044	<0.0168	0.946	0.0171	0.302	0.424	0.801	15597.48	467.92	441.4	<0.00000	<0.00002
Zr90	447.44	435.77	<0.00001	<0.00009	95.4	1.507	0.175	<0.036	0.699	0.275	0.724	0.37	1.127	3210.35	454.1	431.73	<0.00000	<0.00003
Nb93	426.7	410.55	0.00008	<0.00003	6.16	0.0628	<0.0039	0.033	0.1022	0.0569	<0.0044	<0.0027	0.0179	1330.13	437.57	412.94	<0.00000	0.00002
Mo95	381.43	369.06	<0.00003	<0.00023	125.93	1.648	0.15	1.98	0.625	0.081	0.631	<0.0247	24.54	2612.7	393.87	371.26	<0.00000	<0.00011
Ru99	<0.00	<0.00	<0.00	<0.00	<0.00	<0.00	<0.00	<0.00	<0.00	<0.00	<0.00	<0.00	<0.00	<0.00	<0.00	<0.00	<0.00	<0.00
Ru101	<0.00	<0.00	<0.00	<0.00	<0.00	<0.00	<0.00	<0.00	<0.00	<0.00	<0.00	<0.00	<0.00	<0.00	<0.00	<0.00	<0.00	<0.00
Rh103	<0.00	<0.00	<0.00	<0.00	<0.00	<0.00	<0.00	<0.00	<0.00	<0.00	<0.00	<0.00	<0.00	<0.00	<0.00	<0.00	<0.00	<0.00
Ag107	252.16	219.83	0.0478	0.43	0.357	1.4	10.12	929.2	85.33	40.84	9.92	2.75	134.84	17207.39	260.99	242.66	0.00821	0.36
Pd108	<0.00	<0.00	<0.00	<0.00	<0.00	<0.00	<0.00	<0.00	<0.00	<0.00	<0.00	<0.00	<0.00	<0.00	<0.00	<0.00	<0.00	<0.00
Cd111	272.62	255.54	0.0114	0.1	<0.68	<0.183	2242.42	16.99	1409.06	2.94	1768.81	0.339	159.65	4756.22	269.49	251.14	0.00192	0.08
In115	452.8	425.45	<0.00000	0.00006	0.0613	0.0067	1.88	0.493	0.111	0.886	0.325	0.0834	8.12	206.64	461.57	437.77	<0.00000	<0.00003
Sn118	397.17	379.28	0.00077	0.0025	1.36	0.116	27.09	54.04	1.202	0.22	2.23	0.151	8.09	44646.92	412.16	401.02	0.00011	0.002
Sb121	379.02	362.87	0.00034	0.0042	0.384	15.72	4.9	4.32	257	20.37	28.82	0.486	7.37	13118.8	380.28	361.46	0.00006	0.0031
Te125	<0.00	<0.00	<0.00	<0.00	<0.00	<0.00	<0.00	<0.00	<0.00	<0.00	<0.00	<0.00	<0.00	<0.00	<0.00	<0.00	<0.00	<0.00
Te128	<0.00	<0.00	<0.00	<0.00	<0.00	<0.00	<0.00	<0.00	<0.00	<0.00	<0.00	<0.00	<0.00	<0.00	<0.00	<0.00	<0.00	<0.00
La139	467.73	456.75	<0.00000	<0.00004	14.97	0.0056	<0.0074	<0.0172	0.00548	0.0253	0.0416	<0.0044	0.0145	705.47	469.4	446.99	<0.00000	<0.00002
Ce140	453.82	444.07	<0.00000	<0.00003	30.69	0.0109	<0.0054	<0.0191	0.0341	0.736	0.0833	0.0423	0.367	1790.11	463.31	439.42	<0.00000	0.00013
Nd146	437.68	430.11	<0.00002	<0.00009	16.23	<0.0214	<0.024	<0.116	0.0158	0.0433	<0.026	<0.0167	0.084	803.85	447.94	419.65	<0.00000	<0.00008
Hf178	423.35	414.84	<0.00001	<0.00009	2.6	0.0458	<0.0172	<0.094	0.0173	<0.0060	<0.0176	<0.0149	0.095	47.79	426.46	412.01	0	0.00007
W182	449.43	448.36	<0.00002	<0.00011	0.267	0.374	0.038	0.11	2.24	7.53	0.052	0.0288	0.521	1994286.13	456.13	435.73	<0.00000	<0.00007
Re185	107.06	104.29	<0.00001	<0.00005	<0.060	<0.0238	<0.033	<0.130	<0.0074	<0.0125	<0.039	<0.0200	1.024	45.75	107.23	100.12	<0.00000	<0.00010

RUN3

Element	STD610-3	STD610-6	PGEA-4	PGEA-5	BCR2G-2	JL10-PY1	JL10-SPH	JL10-CPY	WAN-SPH	BG05-PY	BG05-SPH	JL19-PY	JL19-CPY	JL19-SPH	STD610-7	STD610-8	PGEA-6	PGEA-7
Re187	106.48	101.04	0.0006	0.006	<0.039	<0.0142	<0.0186	<0.083	<0.0033	<0.0092	<0.0155	<0.0170	1.539	<47.17	107.35	102.36	0.0001	0.004
Os189	<-NaN	<-NaN	<-NaN	<-NaN	<-NaN	<-NaN	<-NaN	<-NaN	<-NaN	<-NaN	<-NaN	<-NaN	<-NaN	<-NaN	<-NaN	<-NaN	<-NaN	<-NaN
Os190	<-NaN	<-NaN	<-NaN	<-NaN	<-NaN	<-NaN	<-NaN	<-NaN	<-NaN	<-NaN	<-NaN	<-NaN	<-NaN	<-NaN	<-NaN	<-NaN	<-NaN	<-NaN
Ir193	<-NaN	<-NaN	<-NaN	<-NaN	<-NaN	<-NaN	<-NaN	<-NaN	<-NaN	<-NaN	<-NaN	<-NaN	<-NaN	<-NaN	<-NaN	<-NaN	<-NaN	<-NaN
Pt195	<0.00	<0.00	<0.00	<0.00	<0.00	<0.00	<0.00	<0.00	<0.00	<0.00	<0.00	<0.00	<0.00	<0.00	<0.00	<0.00	<0.00	<0.00
Au197	24.1	21.95	0.0407	0.39	0.089	0.627	0.026	0.271	1.86	1.427	0.057	0.0375	0.068	537.27	23.53	21.69	0.00693	0.28
Pb208	424.93	408.46	0.00582	0.048	6.24	95.73	73.17	166.42	63.96	4597.06	3892.03	39.2	10529.06	137576.53	403.58	418.25	0.00093	0.036
Bi209	372.52	356.52	0.0304	0.3	<0.049	17.94	0.192	0.18	2.39	110.24	0.07	17.86	27.99	1288.08	363.22	349.38	0.0053	0.21
Th232	474.36	463.94	<0.00000	<0.00003	3.41	0.0284	0.0209	<0.024	0.00361	<0.0034	<0.0081	<0.0048	0.142	164.94	446.93	436.73	<0.00000	<0.00003
U238	477.82	468.27	<0.00000	<0.00004	1.021	0.186	0.0295	0.045	0.0431	0.0234	<0.0075	0.0154	12.6	2957.65	458.42	442.4	<0.00000	<0.00002
ThO248	<-NaN	<-NaN	<-NaN	<-NaN	<-NaN	<-NaN	<-NaN	<-NaN	<-NaN	<-NaN	<-NaN	<-NaN	<-NaN	<-NaN	<-NaN	<-NaN	<-NaN	<-NaN
GLITTER!: 1 sigma error.																		
Element	STD610-3	STD610-6	PGEA-4	PGEA-5	BCR2G-2	JL10-PY1	JL10-SPH	JL10-CPY	WAN-SPH	BG05-PY	BG05-SPH	JL19-PY	JL19-CPY	JL19-SPH	STD610-7	STD610-8	PGEA-6	PGEA-7
Al27	520.6	490.05	0.00008	0.00029	1854	2.86	0.36	0.55	0.47	8.63	1.34	0.38	3.25	46323.38	519.17	474.18	0	0.00017
Si29	19577.14	18460.26	0.015	1.29	7613.53	22.38	20.3	72.69	10.35	53.09	94.24	18.34	49.93	389499.53	19683.07	18197.02	0.0015	0.11
S34	<0.00	<0.00	<0.00	<0.00	<0.00	<0.00	<0.00	<0.00	<0.00	<0.00	<0.00	<0.00	<0.00	<0.00	<0.00	<0.00	<0.00	<0.00
Ca43	4123.27	3902.28	0.0045	0.073	1224.6	7.19	10.27	127.44	20.79	54.05	41.65	6.46	26.34	829243.25	4127.22	3755.77	0.00062	0.042
Sc45	21.95	20.74	0.00002	0.00009	0.75	0.0096	0.014	0.056	0.0023	0.0069	0.014	0.0083	0.018	199.08	21.8	19.92	0	0.00006
Ti49	22.97	21.48	0.00005	0.0062	303.81	0.78	0.17	1.05	1.08	0.28	0.16	0.13	0.23	6497.86	23.17	21.05	0.00002	0.002
V51	21.49	20.43	0.00001	0.00015	9.29	0.032	0.013	0.044	0.029	0.046	0.055	0.0072	0.051	106421.02	21.27	19.5	0	0.00004
Cr53	21.58	20.38	0.00025	0.0044	0.95	0.41	0.54	1.99	0.09	0.25	0.45	0.3	0.61	1630.13	22.36	20.34	0.00005	0.0024
Mn55	22.33	20.87	0.00003	0.00099	38.85	0.46	46	2.34	42.79	10.97	104.49	0.22	4.23	593283.81	22.81	21.04	0	0.0003
Fe57	22.52	21.72	0.0014	0.017	1756.65	14722.42	3349.7	9629.38	2765.42	14722.11	404.4	14721.88	9624.99	**********	21.88	20.6	0.00047	0.0099
Co59	19.84	18.75	0.00001	0.00061	0.91	9.72	1.46	0.058	0.019	9.23	0.21	5.89	0.051	54.03	20.15	18.55	0	0.00033
Ni60	24.44	23.13	12.02	1371.52	0.47	0.13	0.048	0.27	0.025	2.3	0.22	0.038	0.15	739.02	25.32	22.7	0.93	565.94
Ni62	26.43	25.22	12.33	1317.14	0.98	0.17	0.43	1.26	0.049	2.55	0.27	0.14	0.34	1170.27	27.55	24.34	0.97	592.28
Cu65	22.33	20.41	0.007	0.75	0.94	0.36	56.84	20316.44	863.52	6.37	14.39	10.73	17770.81	9455.3	21.4	20.35	0.00049	0.35
Zn66	41.1	50.05	0.0076	0.0012	14.13	1.86	18094.06	327.81	16983.79	41.34	21164.26	5.77	3079.24	19072.86	47.87	50.33	0.00002	0.036
Ga71	23.79	22.57	0	0.00019	0.63	0.013	0.21	0.7	0.18	0.032	4.27	0.0067	0.13	1058.03	24.84	22.23	0	0.00008
As75	27.67	26.88	0.0026	0.31	1.56	40.63	1.71	3.94	84.35	176.22	1.74	4.31	1.18	4322.96	25.63	25.92	0.00028	0.1
Se82	9.82	8.72	0.0029	0.31	1.39	1.03	0.86	3.16	0.73	0.41	0.71	0.68	1.01	2073.75	9.81	9.15	0.0003	0.14
Y89	21.62	20.49	0	0.00005	0.69	0.005	0.0025	0.0084	0.067	0.0027	0.024	0.019	0.039	1130.4	21.72	19.86	0	0.00001
Zr90	20.35	19.41	0	0.00025	3.52	0.066	0.02	0.014	0.049	0.016	0.054	0.018	0.057	254.67	20.31	18.67	0	0.00003
Nb93	20.32	19.19	0.00001	0.00002	0.25	0.0058	0.0019	0.011	0.0077	0.0048	0.0018	0.0012	0.0047	110.66	20.53	18.79	0	0.00002
Mo95	18.22	17.3	0.00001	0.00015	4.99	0.092	0.033	0.2	0.049	0.015	0.059	0.0095	1.01	276.53	18.53	16.93	0	0.00005
Ru99	<0.00	<0.00	<0.00	<0.00	<0.00	<0.00	<0.00	<0.00	<0.00	<0.00	<0.00	<0.00	<0.00	<0.00	<0.00	<0.00	<0.00	<0.00
Ru101	<0.00	<0.00	<0.00	<0.00	<0.00	<0.00	<0.00	<0.00	<0.00	<0.00	<0.00	<0.00	<0.00	<0.00	<0.00	<0.00	<0.00	<0.00
Rh103	<0.00	<0.00	<0.00	<0.00	<0.00	<0.00	<0.00	<0.00	<0.00	<0.00	<0.00	<0.00	<0.00	<0.00	<0.00	<0.00	<0.00	<0.00
Ag107	19.41	16.8	0.0068	0.67	0.045	0.11	1.04	66.94	8.67	2.95	1.01	0.2	9.72	1801.86	19.97	18.36	0.00066	0.32
Pd108	<0.00	<0.00	<0.00	<0.00	<0.00	<0.00	<0.00	<0.00	<0.00	<0.00	<0.00	<0.00	<0.00	<0.00	<0.00	<0.00	<0.00	<0.00
Cd111	16.26	15.06	0.0015	0.15	0.25	0.079	208.31	1.5	130.84	0.23	164.28	0.073	8.38	777.32	15.92	14.52	0.00013	0.072
In115	23.03	21.28	0	0.0001	0.0094	0.003	0.15	0.049	0.0088	0.043	0.027	0.0065	0.36	31.84	23.16	21.39	0	0.00001
Sn118	20.12	18.89	0.00011	0.0039	0.12	0.036	1.99	2.45	0.089	0.03	0.18	0.03	0.39	3339.84	20.59	19.5	0.00001	0.0018
Sb121	18.71	17.59	0.00005	0.0065	0.07	0.67	0.38	0.31	18.83	0.86	2.12	0.036	0.34	1043.12	18.5	17.09	0.00001	0.0028
Te125	<0.00	<0.00	<0.00	<0.00	<0.00	<0.00	<0.00	<0.00	<0.00	<0.00	<0.00	<0.00	<0.00	<0.00	<0.00	<0.00	<0.00	<0.00
Te128	<0.00	<0.00	<0.00	<0.00	<0.00	<0.00	<0.00	<0.00	<0.00	<0.00	<0.00	<0.00	<0.00	<0.00	<0.00	<0.00	<0.00	<0.00
La139	21.4	20.47	0	0.00006	0.57	0.0022	0.0032	0.0097	0.00081	0.0033	0.0049	0.0018	0.0046	65.44	21.12	19.46	0	0.00001

RUN3

Element	STD610-3	STD610-6	PGEA-4	PGEA-5	BCR2G-2	JL10-PY1	JL10-SPH	JL10-CPY	WAN-SPH	BG05-PY	BG05-SPH	JL19-PY	JL19-CPY	JL19-SPH	STD610-7	STD610-8	PGEA-6	PGEA-7
Ce140	20.66	19.8	0	0.00002	1.14	0.0028	0.0026	0.0086	0.0028	0.031	0.0081	0.0036	0.022	141.9	20.75	19.03	0	0.00012
Nd146	20.91	20.16	0.00001	0.00011	0.68	0.0084	0.01	0.052	0.0034	0.0096	0.011	0.0065	0.022	121.49	21.08	19.15	0	0.00007
Hf178	18.3	17.52	0	0.00011	0.12	0.0091	0.0074	0.035	0.0024	0.0028	0.0075	0.0052	0.018	31.1	18.09	16.83	0	0.00008
W182	20.26	19.78	0.00001	0.00011	0.038	0.033	0.014	0.049	0.16	0.29	0.014	0.0087	0.05	138297.89	20.21	18.65	0	0.00003
Re185	5.69	5.46	0.00001	0.00006	0.024	0.0096	0.014	0.057	0.0029	0.0069	0.014	0.0077	0.083	32.1	5.63	5.12	0	0.00005
Re187	5.33	4.97	0.00008	0.0093	0.015	0.007	0.0098	0.039	0.0013	0.0042	0.0064	0.0057	0.091	29.52	5.3	4.91	0.00001	0.0036
Os189	<0.00	<0.00	<0.00	<0.00	<0.00	<0.00	<0.00	<0.00	<0.00	<0.00	<0.00	<0.00	<0.00	<0.00	<0.00	<0.00	<0.00	<0.00
Os190	<0.00	<0.00	<0.00	<0.00	<0.00	<0.00	<0.00	<0.00	<0.00	<0.00	<0.00	<0.00	<0.00	<0.00	<0.00	<0.00	<0.00	<0.00
Ir193	<0.00	<0.00	<0.00	<0.00	<0.00	<0.00	<0.00	<0.00	<0.00	<0.00	<0.00	<0.00	<0.00	<0.00	<0.00	<0.00	<0.00	<0.00
Pt195	<0.00	<0.00	<0.00	<0.00	<0.00	<0.00	<0.00	<0.00	<0.00	<0.00	<0.00	<0.00	<0.00	<0.00	<0.00	<0.00	<0.00	<0.00
Au197	1.61	1.45	0.0055	0.61	0.02	0.05	0.014	0.07	0.19	0.093	0.014	0.0091	0.017	93.35	1.56	1.41	0.00048	0.26
Pb208	19.58	18.44	0.00075	0.074	0.27	3.59	4.43	6.34	3.85	171.62	234.4	1.47	393.09	8459.61	18.31	18.34	0.00005	0.032
Bi209	17.82	16.74	0.0039	0.46	0.019	0.72	0.023	0.053	0.17	4.37	0.012	0.71	1.12	121.32	17.12	15.97	0.00028	0.19
Th232	24.64	23.72	0	0.00002	0.16	0.0049	0.0058	0.013	0.00086	0.0016	0.0032	0.0019	0.014	27.77	22.92	21.83	0	0.00001
U238	24.13	23.25	0	0.00007	0.053	0.013	0.0064	0.017	0.0036	0.0035	0.0032	0.0025	0.55	232.33	22.84	21.45	0	0.00001
ThO248	<0.00	<0.00	<0.00	<0.00	<0.00	<0.00	<0.00	<0.00	<0.00	<0.00	<0.00	<0.00	<0.00	<0.00	<0.00	<0.00	<0.00	<0.00
GLITTER!: Minimum detection limits (99% confidence).																		
Element	STD610-3	STD610-6	PGEA-4	PGEA-5	BCR2G-2	JL10-PY1	JL10-SPH	JL10-CPY	WAN-SPH	BG05-PY	BG05-SPH	JL19-PY	JL19-CPY	JL19-SPH	STD610-7	STD610-8	PGEA-6	PGEA-7
Al27	0.567	0.584	0.00006	0.00049	0.208	0.0772	0.107	0.391	0.019	0.0518	0.114	0.0702	0.134	201.89	0.5	0.509	0.00001	0.00035
Si29	208.63	204.33	0.0221	0.178	76.86	27.68	39.2	152.55	7.34	17.91	39.13	25.7	44.93	78608.18	186.19	165.16	0.00364	0.129
S34	<0.00000	<0.00000	<0.00000	<0.00000	<0.00000	<0.00000	<0.00000	<0.00000	<0.00000	<0.00000	<0.00000	<0.00000	<0.00000	<0.00000	<0.00000	<0.00000	<0.00000	<0.00000
Ca43	115.74	102.03	0.0105	0.0877	34.92	14.26	18.42	73.15	4.09	11.01	20.3	12.96	24.47	48268.4	109.27	83.42	0.00165	0.0542
Sc45	0.17	0.168	0.00002	0.00015	0.0585	0.0197	0.0334	0.126	0.00619	0.015	0.0308	0.022	0.0398	63.28	0.156	0.147	0	0.00011
Ti49	1.21	1.19	0.00013	0.00208	0.377	0.141	0.241	0.994	0.039	0.104	0.27	0.239	0.324	434.63	1.18	0.862	0.00002	0.00073
V51	0.119	0.125	0.00002	0.00012	0.0497	0.0179	0.0295	0.0931	0.00472	0.0136	0.027	0.0189	0.0299	46.99	0.119	0.123	0	0.00009
Cr53	6.43	6.21	0.00067	0.00521	2.28	0.788	1.21	4.52	0.217	0.566	1.18	0.802	1.39	2300.59	5.68	5.1	0.00013	0.00367
Mn55	0.671	0.642	0.00007	0.00057	0.241	0.0877	0.126	0.487	0.0241	0.0609	0.128	0.0926	0.157	261.36	0.644	0.556	0.00001	0.00042
Fe57	23.35	21.62	0.00243	0.0203	8.73	3.01	4.34	17.29	0.819	2.15	4.38	3.6	5.36	9080.86	20.91	18.28	0.00068	0.0147
Co59	0.0909	0.0972	0.00001	0.00008	0.0314	0.0132	0.0209	0.0757	0.00371	0.00832	0.0177	0.0159	0.0248	39.07	0.0805	0.133	0	0.00007
Ni60	0.533	0.561	0.00005	0.0376	0.227	0.0748	0.103	0.364	0.0172	0.104	0.0965	0.0674	0.141	196.12	0.733	0.446	0.00006	0.00155
Ni62	2.76	2.54	0.0003	0.102	1.03	0.35	0.574	1.85	0.0767	0.252	0.452	0.26	0.589	930.64	1.79	2.07	0.00006	0.00384
Cu65	1.55	1.53	0.00017	0.00167	0.556	0.208	0.292	1.09	0.0789	0.158	0.297	0.195	0.351	629.95	2.93	1.29	0.00003	0.00095
Zn66	7.27	2.02	0.00023	0.00195	0.696	0.227	0.32	1.73	0.0901	0.869	0.477	0.506	0.76	993.06	2.23	2.19	0.00004	0.00137
Ga71	0.0968	0.0901	0.00001	0.00014	0.0378	0.0187	0.0281	0.083	0.0046	0.0106	0.0269	0.0151	0.0276	47.7	0.135	0.124	0	0.0001
As75	10.59	10.65	0.00116	0.00908	3.95	1.39	2.01	7.74	0.369	1.09	2.3	1.48	2.55	4277.34	10.14	9.03	0.0002	0.00691
Se82	9.35	9.8	0.00106	0.00794	3.61	1.3	1.85	6.93	0.338	0.866	1.8	1.29	2.38	3816.04	8.7	7.9	0.00017	0.00606
Y89	0.0297	0.0236	0	0.00004	0.0116	0.00365	0.00437	0.0168	0.00138	0.00288	0.00979	0.00307	0.00648	9.69	0.0288	0.0411	0	0.00002
Zr90	0.0575	0.0646	0.00001	0.00009	0.0194	0.00763	0.0136	0.0357	0.00165	0.00588	0.00946	0.00753	0.0125	27.41	0.0528	0.065	0	0.00003
Nb93	0.0208	0.0209	0	0.00003	0.0122	0.00255	0.00387	0.0129	0.00119	0.00285	0.00442	0.00272	0.00715	12	0.0156	0.0371	0	0.00002
Mo95	0.14	0.228	0.00003	0.00023	0.0694	0.0236	0.0436	0.127	0.00602	0.0182	0.0292	0.0247	0.0433	84.55	0.172	0.167	0	0.00011
Ru99	<0.00000	<0.00000	<0.00000	<0.00000	<0.00000	<0.00000	<0.00000	<0.00000	<0.00000	<0.00000	<0.00000	<0.00000	<0.00000	<0.00000	<0.00000	<0.00000	<0.00000	<0.00000
Ru101	<0.00000	<0.00000	<0.00000	<0.00000	<0.00000	<0.00000	<0.00000	<0.00000	<0.00000	<0.00000	<0.00000	<0.00000	<0.00000	<0.00000	<0.00000	<0.00000	<0.00000	<0.00000
Rh103	<0.00000	<0.00000	<0.00000	<0.00000	<0.00000	<0.00000	<0.00000	<0.00000	<0.00000	<0.00000	<0.00000	<0.00000	<0.00000	<0.00000	<0.00000	<0.00000	<0.00000	<0.00000
Ag107	0.157	0.152	0.00001	0.00082	0.051	0.0163	0.0216	0.143	0.0039	0.0144	0.0276	0.0171	0.038	68.28	0.0844	0.135	0	0.0001
Pd108	<0.00000	<0.00000	<0.00000	<0.00000	<0.00000	<0.00000	<0.00000	<0.00000	<0.00000	<0.00000	<0.00000	<0.00000	<0.00000	<0.00000	<0.00000	<0.00000	<0.00000	<0.00000
Cd111	1.41	1.17	0.00011	0.0013	0.678	0.183	0.239	0.926	0.0386	0.138	0.286	0.146	0.345	486.73	1.28	1.03	0.00003	0.0007
In115	0.0385	0.0273	0	0.00004	0.0123	0.00498	0.00775	0.0195	0.00114	0.00321	0.00423	0.00544	0.0108	13.44	0.0828	0.0355	0	0.00003

RUN3

Element	STD610-3	STD610-6	PGEA-4	PGEA-5	BCR2G-2	JL10-PY1	JL10-SPH	JL10-CPY	WAN-SPH	BG05-PY	BG05-SPH	JL19-PY	JL19-CPY	JL19-SPH	STD610-7	STD610-8	PGEA-6	PGEA-7
Sn118	0.532	0.564	0.00006	0.00049	0.227	0.0761	0.116	0.425	0.0212	0.0513	0.106	0.072	0.126	211.83	0.517	0.453	0.00001	0.00036
Sb121	0.311	0.317	0.00004	0.00037	0.156	0.037	0.0641	0.273	0.0134	0.0363	0.0754	0.0547	0.0917	159.85	0.33	0.343	0.00001	0.0003
Te125	<0.00000	<0.00000	<0.00000	<0.00000	<0.00000	<0.00000	<0.00000	<0.00000	<0.00000	<0.00000	<0.00000	<0.00000	<0.00000	<0.00000	<0.00000	<0.00000	<0.00000	<0.00000
Te128	<0.00000	<0.00000	<0.00000	<0.00000	<0.00000	<0.00000	<0.00000	<0.00000	<0.00000	<0.00000	<0.00000	<0.00000	<0.00000	<0.00000	<0.00000	<0.00000	<0.00000	<0.00000
La139	0.0207	0.0241	0	0.00004	0.0114	0.0034	0.00738	0.0172	0.00106	0.00289	0.00322	0.00443	0.00738	7.22	<0.00000	0.0382	0	0.00002
Ce140	<0.00000	0.0293	0	0.00003	0.0114	0.00377	0.00541	0.0191	0.00106	0.00266	0.00505	0.00269	0.00579	10.13	0.0309	0.0414	0	0.00003
Nd146	0.0987	0.0993	0.00002	0.00009	0.063	0.0214	0.0237	0.116	0.00619	0.0104	0.0265	0.0167	0.0278	59.44	0.156	0.121	0	0.00008
Hf178	0.0929	0.0934	0.00001	0.00009	0.0209	0.00761	0.0172	0.0943	0.00275	0.00601	0.0176	0.0149	0.0219	43.71	0.0986	0.0743	0	0.00005
W182	0.0787	0.125	0.00002	0.00011	0.0532	0.0223	0.0179	0.0691	0.00532	0.0102	0.0258	0.0178	0.0364	51.06	0.128	0.16	0	0.00007
Re185	0.0966	0.137	0.00001	0.00005	0.0597	0.0238	0.0334	0.13	0.00739	0.0125	0.0387	0.02	0.0421	33.45	0.168	0.144	0	0.0001
Re187	0.041	0.117	0.00001	0.00016	0.0392	0.0142	0.0186	0.0831	0.00331	0.00918	0.0155	0.017	0.0236	47.17	0.0939	0.0866	0	0.00004
Os189	<0.00	<0.00	<0.00	<0.00	<0.00	<0.00	<0.00	<0.00	<0.00	<0.00	<0.00	<0.00	<0.00	<0.00	<0.00	<0.00	<0.00	<0.00
Os190	<0.00	<0.00	<0.00	<0.00	<0.00	<0.00	<0.00	<0.00	<0.00	<0.00	<0.00	<0.00	<0.00	<0.00	<0.00	<0.00	<0.00	<0.00
Ir193	<0.00	<0.00	<0.00	<0.00	<0.00	<0.00	<0.00	<0.00	<0.00	<0.00	<0.00	<0.00	<0.00	<0.00	<0.00	<0.00	<0.00	<0.00
Pt195	<0.00000	<0.00000	<0.00000	<0.00000	<0.00000	<0.00000	<0.00000	<0.00000	<0.00000	<0.00000	<0.00000	<0.00000	<0.00000	<0.00000	<0.00000	<0.00000	<0.00000	<0.00000
Au197	0.0988	0.118	0.00001	0.0009	0.0299	0.00887	0.0258	0.0951	0.0039	0.0114	0.0264	0.0183	0.0215	37.47	0.0856	0.0865	0	0.00008
Pb208	0.164	0.126	0.00002	0.00043	0.0514	0.0226	0.0266	0.286	0.0432	0.0199	0.0527	0.0345	0.256	814.91	1.56	0.227	0	0.00018
Bi209	0.116	0.124	0.00001	0.00056	0.0487	0.0181	0.0244	0.0993	0.00436	0.0116	0.0238	0.0152	0.0272	51.22	0.134	0.124	0	0.00008
Th232	0.0302	0.0401	0	0.00003	0.0156	0.00525	0.00795	0.0242	0.00165	0.00338	0.00812	0.00484	0.0057	16.64	0.0392	0.0566	0	0.00003
U238	<0.00000	0.0341	0	0.00004	0.0143	0.00481	0.00774	0.0263	0.00071	0.00335	0.00745	0.00362	0.00675	15.27	0.0339	0.0367	0	0.00002
ThO248	<0.00	<0.00	<0.00	<0.00	<0.00	<0.00	<0.00	<0.00	<0.00	<0.00	<0.00	<0.00	<0.00	<0.00	<0.00	<0.00	<0.00	<0.00
GLITTER!: Trace element concentrations normalised to chondrite.																		
Element	STD610-3	STD610-6	PGEA-4	PGEA-5	BCR2G-2	JL10-PY1	JL10-SPH	JL10-CPY	WAN-SPH	BG05-PY	BG05-SPH	JL19-PY	JL19-CPY	JL19-SPH	STD610-7	STD610-8	PGEA-6	PGEA-7
Al27	0.799	0.765	0	0	3.35	0.00515	0.00037	0.00082	0.0005	0.01558	0.00143	0.00068	0.00585	49.12	0.807	0.757	0	0
Si29	2.1	2.01	0	0.00001	0.921	0.00224	0.00086	0.00286	0.00086	0.00631	0.00803	0.00186	0.00548	33.09	2.14	2.02	0	0
S34	<****	<****	<****	<****	<****	<****	<****	<****	<****	<****	<****	<****	<****	<****	<****	<****	<****	<****
Ca43	6.22	5.99	0	0	2.2	0.00236	0.00331	0.1762	0.02	0.0913	0.0384	0.00463	0.0316	795.55	6.31	5.91	0	0
Sc45	52.52	50.53	0.00002	0	2.114	0.0037	0	0	0	0	0.0092	0	0	278.16	52.92	49.82	0	0
Ti49	0.681	0.647	0	0	10.81	0.0241	0.00131	0.0175	0.0195	0.00756	0.00163	0.00179	0.00271	112.33	0.696	0.65	0	0
V51	5.33	5.17	0	0	2.79	0.0074	0	0	0.00475	0.01232	0.00842	0	0.01171	17508.22	5.36	5.07	0	0
Cr53	0.1028	0.0986	0	0	0.00162	0.00097	0	0	0.0001	0	0	0	0	2.66	0.108	0.1009	0	0
Mn55	0.1495	0.1421	0	0	0.306	0.00359	0.212	0.01801	0.197	0.0865	0.482	0.0017	0.0332	2717.06	0.1548	0.1466	0	0
Fe57	0.00164	0.00164	0	0	0.1996	1.675	0.172	1.095	0.1421	1.675	0.0208	1.675	1.095	1937.32	0.00164	0.00164	0	0
Co59	0.537	0.517	0	0	0.0291	0.316	0.0268	0.00057	0.00034	0.3	0.00375	0.1915	0.00121	0.518	0.553	0.525	0	0
Ni60	0.0273	0.0263	0.00555	0.054	0.00053	0.00012	0	0.00012	0.00002	0.00295	0.00015	0.00002	0.00012	0.468	0.0287	0.0263	0.00095	0.038
Ni62	0.0274	0.0265	0.00565	0.051	0.00075	0	0.00013	0.00037	0.00002	0.00291	0.00009	0.00005	0.00008	0.385	0.0289	0.0261	0.00095	0.04
Cu65	2.68	2.49	0.00032	0.0029	0.123	0.044	4.6	2916.94	69.92	0.91	1.164	1.538	2551.81	749.2	2.6	2.54	0.00005	0.0023
Zn66	0.859	1.05	0.0001	0	0.306	0.0395	1238.47	7.14	1162.5	0.9	1448.63	0.125	67.1	1211.85	1.01	1.07	0	0.00009
Ga71	29.16	28.09	0	0	0.855	0.00389	0.164	0.866	0.15	0.0324	3.55	0.00118	0.1542	833.47	30.83	28.26	0	0
As75	115.17	112.53	0.00609	0.07	0	181.46	6.08	7.81	363.52	787.64	6.4	19.03	1.68	14996.17	107.04	109.73	0.00107	0.04
Se82	4.17	3.6	0.00074	0.007	0	0.386	0	0	0.233	0.05	0	0.221	0	0	4.22	4.03	0.00013	0.0059
Y89	203.82	196.92	0	0	7.84	0.0203	0	0	0.42	0.0076	0.134	0.1883	0.356	6932.21	207.96	196.18	0	0
Zr90	80.77	78.66	0	0	17.22	0.272	0.0315	0	0.1262	0.0497	0.1307	0.0668	0.203	579.48	81.97	77.93	0	0
Nb93	1137.86	1094.81	0.00022	0	16.42	0.168	0	0.088	0.272	0.152	0	0	0.048	3547.01	1166.84	1101.16	0	0.00005
Mo95	276.4	267.44	0	0	91.25	1.194	0.109	1.43	0.453	0.059	0.457	0	17.78	1893.26	285.42	269.03	0	0
Ru99	0	0	0	0	0	0	0	0	0	0	0	0	0	0	0	0	0	0
Ru101	0	0	0	0	0	0	0	0	0	0	0	0	0	0	0	0	0	0

RUN3

Element	STD610-3	STD610-6	PGEA-4	PGEA-5	BCR2G-2	JL10-PY1	JL10-SPH	JL10-CPY	WAN-SPH	BG05-PY	BG05-SPH	JL19-PY	JL19-CPY	JL19-SPH	STD610-7	STD610-8	PGEA-6	PGEA-7
Rh103	0	0	0	0	0	0	0	0	0	0	0	0	0	0	0	0	0	0
Ag107	764.12	666.15	0.145	1.3	1.08	4.25	30.67	2815.74	258.58	123.76	30.06	8.35	408.62	52143.61	790.87	735.33	0.0249	1.09
Pd108	0	0	0	0	0	0	0	0	0	0	0	0	0	0	0	0	0	0
Cd111	269.92	253.01	0.0113	0.1	0	0	2220.21	16.82	1395.11	2.91	1751.29	0.336	158.07	4709.13	266.83	248.66	0.0019	0.079
In115	3870.1	3636.36	0	0.00052	0.524	0.058	16.05	4.21	0.949	7.57	2.78	0.713	69.36	1766.16	3945.03	3741.63	0	0
Sn118	157.61	150.51	0.00031	0.001	0.538	0.046	10.75	21.45	0.477	0.087	0.885	0.06	3.21	17717.03	163.56	159.14	0.00005	0.00079
Sb121	1626.7	1557.38	0.00148	0.018	1.65	67.45	21.02	18.56	1103	87.44	123.71	2.09	31.63	56303.87	1632.09	1551.31	0.00025	0.013
Te125	0	0	0	0	0	0	0	0	0	0	0	0	0	0	0	0	0	0
Te128	0	0	0	0	0	0	0	0	0	0	0	0	0	0	0	0	0	0
La139	1274.48	1244.54	0	0	40.78	0.0154	0	0	0.0149	0.0688	0.113	0	0.039	1922.26	1279.02	1217.95	0	0
Ce140	474.21	464.02	0	0	32.07	0.0113	0	0	0.0357	0.769	0.0871	0.0442	0.384	1870.54	484.12	459.16	0	0.00013
Nd146	615.59	604.93	0	0	22.83	0	0	0	0.0222	0.061	0	0	0.118	1130.6	630.01	590.22	0	0
Hf178	2365.07	2317.55	0	0	14.52	0.256	0	0	0.097	0	0	0	0.53	266.99	2382.48	2301.76	0.00002	0.00042
W182	5049.82	5037.75	0	0	3	4.21	0.43	1.23	25.16	84.63	0.58	0.323	5.85	**********	5125	4895.8	0	0
Re185	1946.52	1896.13	0	0	0	0	0	0	0	0	0	0	18.63	831.86	1949.64	1820.42	0	0
Re187	1936.01	1837.1	0.0109	0.11	0	0	0	0	0	0	0	0	27.99	0	1951.73	1861.01	0.00174	0.072
Os189	<****	<****	<****	<****	<****	<****	<****	<****	<****	<****	<****	<****	<****	<****	<****	<****	<****	<****
Os190	<****	<****	<****	<****	<****	<****	<****	<****	<****	<****	<****	<****	<****	<****	<****	<****	<****	<****
Ir193	<****	<****	<****	<****	<****	<****	<****	<****	<****	<****	<****	<****	<****	<****	<****	<****	<****	<****
Pt195	0	0	0	0	0	0	0	0	0	0	0	0	0	0	0	0	0	0
Au197	110.55	100.67	0.187	1.81	0.41	2.87	0.12	1.25	8.51	6.55	0.259	0.172	0.312	2464.52	107.96	99.5	0.0318	1.3
Pb208	116.42	111.91	0.00159	0.013	1.711	26.23	20.05	45.59	17.52	1259.47	1066.31	10.74	2884.67	37692.2	110.57	114.59	0.00025	0.0097
Bi209	2230.63	2134.86	0.182	1.77	0	107.41	1.15	1.08	14.29	660.15	0.417	106.94	167.58	7713.05	2174.98	2092.11	0.0317	1.28
Th232	11161.44	10916.28	0	0	80.15	0.67	0.49	0	0.085	0	0	0	3.35	3880.99	10515.91	10276.01	0	0
U238	39165.26	38383.11	0	0	83.67	15.21	2.42	3.67	3.54	1.92	0	1.26	1032.96	242430.34	37575.52	36261.91	0	0
ThO248	<****	<****	<****	<****	<****	<****	<****	<****	<****	<****	<****	<****	<****	<****	<****	<****	<****	<****

GLITTER4.0: Laser Ablation Analysis Results

G:\KYLIE\MAR13\RUN4
Fri Mar 14 18:35:14 2003

All values are reported in ppm

GLITTER!: Trace Element Concentrations MDL filtered.

	Run4-1	Run4-2	Run4-3	Run4-4	Run4-5	Run4-6	Run4-7	Run4-8	Run4-9	Run4-10	Run4-11	Run4-12	Run4-13	Run4-14	Run4-15	Run4-16	Run4-17	Run4-18	Run4-19
Element	STD610-1	STD610-2	BCR2G-1	PGEA-1	PGEA-2	JL01-PY	BG31-CPY	JL01-PY1	BG32-PY	BG32-PY2	KP04-PY	JL03-PY	JL02-PY	JL07-PY	BG01-PY	STD610-3	STD610-4	PGEA-3	PGEA-4
Al27	10458.34	10644.79	45839.6	0.001	0.00116	9.39	5.43	1790.86	20.17	3.61	18.01	1.91	72.04	59.52	135.58	9642.26	10738.05	<0.00010	0.00006
Si29	337768	342738.19	152533.88	0.0221	0.121	198.38	170.17	2302.76	1411.31	110.63	1614.02	97.37	520.12	1697.66	2773.94	319657.91	343082.91	0.54	0.0165
S34	<0.00	<0.00	<0.00	<0.00	<0.00	<0.00	<0.00	<0.00	<0.00	<0.00	<0.00	<0.00	<0.00	<0.00	<0.00	<0.00	<0.00	<0.00	<0.00
Ca43	83885.39	86771.67	30046.35	0.0053	<0.034	60.57	281.06	2662.21	514	58.65	74.2	37.68	247.34	149.2	949.34	79246.35	87244.31	<0.0233	<0.0047
Sc45	461.22	474.86	18.74	<0.00000	<0.00005	<0.0204	<0.0136	0.338	<0.0124	<0.0066	0.0285	<0.0192	0.1197	0.383	0.0675	424.52	472.8	<0.00004	<0.00001
Ti49	440.54	457.44	7429.59	0.00004	0.00039	28.69	1.92	519.52	48.89	1.333	4.71	1.38	90.15	26.13	26.79	420.28	468.68	0.00043	0.00015
V51	425.03	442	234.23	0	<0.00004	0.137	0.0629	8.38	1.116	0.0415	0.499	0.0176	2.106	13.05	0.828	447.2	443.85	<0.00003	<0.00001
Cr53	388.61	405.6	6.19	<0.00017	<0.00188	<0.85	0.91	4.44	1.57	<0.28	3.65	<0.84	3.51	6.3	3.7	410.81	407.24	<0.00152	<0.00030
Mn55	434.29	438.27	928.85	0.00008	<0.00021	8.56	0.607	27.23	46.13	21.37	25.54	0.444	20.72	27.62	72.14	431.45	434.58	<0.00018	0.00004
Fe57	457.1	457.1	55500.01	0.00777	0.0078	465531.66	465531.66	465531.66	465531.66	465531.66	465531.66	465531.66	465531.66	465531.63	465531.63	457.1	457.1	0.0078	0.00777
Co59	390.64	402.03	23.6	0.00002	0.00008	2.357	0.375	12.32	40	719.84	1.408	37.05	0.739	1.777	55.04	410.49	407.08	0.00007	0.00001
Ni60	434.28	448.59	7.78	27.78	251.02	301.85	3.03	780	1.322	1.101	2.26	24.28	1.869	0.346	22.58	447.42	440.28	193.52	46.82
Ni62	440.99	450.57	8.22	28.18	254.95	296.14	2.15	767.43	0.75	1.07	4.57	21.75	2.46	6.34	17.99	441.14	451.09	196.61	47.15
Cu65	414.55	427.91	11.74	0.01645	0.145	37.48	4.58	40.46	8.64	434.09	29.32	1.86	18.17	24.12	26993.04	439.34	424.46	0.111	0.0271
Zn66	416.39	442.48	126.78	0.00833	0.0098	5.68	12.79	43.88	33.83	2389.98	52.45	71.03	28.36	13.37	499.54	494.73	438.99	0.00065	0.00054
Ga71	427.63	439.21	13.1	<0.00000	<0.00004	0.0319	0.0159	0.701	0.0755	0.0437	0.122	<0.0141	0.495	0.911	1.114	444.27	430.91	<0.00003	<0.00000
As75	310.55	333.23	<4.45	0.00599	0.054	1700.79	1774.82	254.59	126.95	1657.75	159.83	117.19	6294.62	244.63	1160.21	318.33	311.12	0.041	0.00987
Se82	111.32	117.61	<3.97	0.00691	0.061	8.48	<0.92	59.54	9.84	14.34	65.19	9.21	8.3	4.93	150.22	105.69	112.51	0.049	0.01097
Y89	474.36	487.39	18.17	<0.00000	<0.00001	0.0949	<0.0024	1.62	0.0932	0.00379	0.019	0.0051	0.53	0.0663	0.959	430.57	495.46	<0.00001	<0.00000
Zr90	462.01	476.12	98.83	0	0.00002	0.195	0.0378	3.03	0.515	0.0058	1.113	0.0108	3.17	0.159	1.9	421.45	482.59	<0.00001	<0.00000
Nb93	426.11	441.97	6.23	<0.00000	<0.00001	0.0535	<0.0022	0.672	0.095	0.00098	0.0039	0.0026	0.247	0.0426	0.0176	407.57	445.77	<0.00001	<0.00000
Mo95	368.41	380.4	129.56	<0.00000	<0.00005	0.042	2.71	3.42	0.217	2.815	83.94	0.091	0.743	1.311	5.49	377.43	381.2	<0.00003	<0.00001
Ru99	<0.00	<0.00	<0.00	<0.00	<0.00	<0.00	<0.00	<0.00	<0.00	<0.00	<0.00	<0.00	<0.00	<0.00	<0.00	<0.00	<0.00	<0.00	<0.00
Ru101	<-NaN	<-NaN	<-NaN	<-NaN	<-NaN	<-NaN	<-NaN	<-NaN	<-NaN	<-NaN	<-NaN	<-NaN	<-NaN	<-NaN	<-NaN	<-NaN	<-NaN	<-NaN	<-NaN
Rh103	<0.00	<0.00	<0.00	<0.00	<0.00	<0.00	<0.00	<0.00	<0.00	<0.00	<0.00	<0.00	<0.00	<0.00	<0.00	<0.00	<0.00	<0.00	<0.00
Ag107	243.46	247.45	0.381	0.01622	0.145	43.12	0.156	4.65	0.678	43.95	0.742	1.886	18.74	1.223	49.97	237.98	235.22	0.111	0.0266
Pd108	<0.00	<0.00	<0.00	<0.00	<0.00	<0.00	<0.00	<0.00	<0.00	<0.00	<0.00	<0.00	<0.00	<0.00	<0.00	<0.00	<0.00	<0.00	<0.00
Cd111	262.74	274.58	<0.59	0.00346	0.0306	0.7	<0.090	0.148	0.077	8.53	5.56	0.76	2.31	<0.112	7.86	268.84	232.84	0.0244	0.00594
In115	426.43	446.72	0.118	0	<0.00001	<0.0062	0.0066	0.0121	0.0054	0.257	0.009	<0.0042	0.0117	0.066	0.599	449.37	432.06	<0.00001	<0.00000
Sn118	383.83	388.21	2.15	0.00009	0.00077	<0.085	<0.057	0.314	0.36	0.217	0.355	<0.074	0.209	<0.057	1.036	404.06	394.4	0.00057	0.0002
Sb121	366.62	391.22	0.383	0.00009	0.00156	0.881	0.129	4.66	0.784	17.58	2.17	0.731	2.067	0.831	221.47	366.23	364.2	0.00074	0.00013
Te125	<0.00	<0.00	<0.00	<0.00	<0.00	<0.00	<0.00	<0.00	<0.00	<0.00	<0.00	<0.00	<0.00	<0.00	<0.00	<0.00	<0.00	<0.00	<0.00
Te128	<0.00	<0.00	<0.00	<0.00	<0.00	<0.00	<0.00	<0.00	<0.00	<0.00	<0.00	<0.00	<0.00	<0.00	<0.00	<0.00	<0.00	<0.00	<0.00
La139	485.3	492.44	14.95	<0.00000	0.00001	0.124	0.0138	1.67	0.0034	0.00313	0.0235	<0.0033	0.1254	0.0283	0.1334	438.73	493.68	<0.00001	0
Ce140	458.05	467.04	30.08	0	<0.00001	0.0215	0.0024	3.68	0.0201	0.00216	0.1286	<0.0031	0.314	0.0308	0.437	436.34	469.06	<0.00001	<0.00000
Nd146	456.29	469.65	16.37	<0.00000	<0.00002	0.0183	<0.0112	1.94	<0.0091	<0.0070	<0.0192	<0.0151	0.45	0.0202	0.084	412.72	464.24	<0.00003	0.00001
Hf178	452.37	471.63	2.65	<0.00000	<0.00002	<0.0098	<0.0057	0.118	0.024	<0.0028	0.0225	<0.0099	0.108	0.0076	0.0443	397.42	453.96	<0.00003	<0.00000
W182	446.38	462.47	0.29	<0.00000	<0.00004	0.082	<0.0097	6.43	0.231	0.0163	1.16	0.0272	0.157	0.269	0.0734	440.98	446.93	<0.00004	<0.00001
Re185	105.24	108.68	0.053	<0.00000	<0.00003	<0.0087	0.0281	0.0187	<0.0107	<0.0082	<0.027	<0.0153	<0.0074	0.0115	<0.0082	101.93	104.88	<0.00004	<0.00000
Re187	102.43	105.59	<0.029	0.0002	0.00153	<0.01	0.0223	0.0274	<0.0082	<0.0024	0.1	<0.0103	<0.0050	<0.0085	<0.0062	103.98	102.85	0.00122	0.0003
Os189	<-NaN	<-NaN	<-NaN	<-NaN	<-NaN	<-NaN	<-NaN	<-NaN	<-NaN	<-NaN	<-NaN	<-NaN	<-NaN	<-NaN	<-NaN	<-NaN	<-NaN	<-NaN	<-NaN
Os190	<-NaN	<-NaN	<-NaN	<-NaN	<-NaN	<-NaN	<-NaN	<-NaN	<-NaN	<-NaN	<-NaN	<-NaN	<-NaN	<-NaN	<-NaN	<-NaN	<-NaN	<-NaN	<-NaN

RUN4

Element	STD610-1	STD610-2	BCR2G-1	PGEA-1	PGEA-2	JL01-PY	BG31-CPY	JL01-PY1	BG32-PY	BG32-PY2	KP04-PY	JL03-PY	JL02-PY	JL07-PY	BG01-PY	STD610-3	STD610-4	PGEA-3	PGEA-4
Ir193	<0.00	<0.00	<0.00	<0.00	<0.00	<0.00	<0.00	<0.00	<0.00	<0.00	<0.00	<0.00	<0.00	<0.00	<0.00	<0.00	<0.00	<0.00	<0.00
Pt195	<0.00	<0.00	<0.00	<0.00	<0.00	<0.00	<0.00	<0.00	<0.00	<0.00	<0.00	<0.00	<0.00	<0.00	<0.00	<0.00	<0.00	<0.00	<0.00
Au197	22.89	23.52	<0.068	0.01249	0.112	1.157	0.0495	0.392	0.0453	2.56	0.0388	0.088	26.21	0.072	28.95	22.56	21.44	0.083	0.0199
Pb208	425.2	452.57	21.37	0.00175	0.0155	1638.59	5.61	399.02	22.86	565.83	45.58	71.56	42.9	22.72	47428.7	413.14	389.6	0.0115	0.00276
Bi209	385.01	406.04	0.666	0.01124	0.097	340.47	5.47	2.07	25.13	530.28	8.69	10.14	1.073	77.07	658153.13	349.66	345.34	0.071	0.0175
Th232	507.29	526.85	3.41	<0.00000	<0.00001	0.0082	<0.0039	0.796	0.0239	0.00331	0.0045	<0.0036	0.148	0.0131	0.0451	427.25	481.9	<0.00001	0
U238	485.78	504.26	0.981	0	<0.00001	0.0443	<0.0027	0.151	0.0537	0.0473	0.0095	<0.0026	0.1427	0.0917	10	443.06	460.66	<0.00001	<0.00000
ThO248	<-NaN	<-NaN	<-NaN	<-NaN	<-NaN	<-NaN	<-NaN	<-NaN	<-NaN	<-NaN	<-NaN	<-NaN	<-NaN	<-NaN	<-NaN	<-NaN	<-NaN	<-NaN	<-NaN
GLITTER!: 1 sigma error.																			
Element	STD610-1	STD610-2	BCR2G-1	PGEA-1	PGEA-2	JL01-PY	BG31-CPY	JL01-PY1	BG32-PY	BG32-PY2	KP04-PY	JL03-PY	JL02-PY	JL07-PY	BG01-PY	STD610-3	STD610-4	PGEA-3	PGEA-4
Al27	652.95	670.17	2660.04	0.00007	0.00037	0.55	0.32	103.91	1.18	0.21	1.05	0.12	4.18	3.46	7.87	583.46	668.85	0.00004	0.00001
Si29	20736.62	21224.66	8680.99	0.0028	0.046	17.67	13.65	131.79	80.76	7.52	92.96	14.8	30.39	97.47	158.14	18999.17	21012.33	0.14	0.0044
S34	<0.00	<0.00	<0.00	<0.00	<0.00	<0.00	<0.00	<0.00	<0.00	<0.00	<0.00	<0.00	<0.00	<0.00	<0.00	<0.00	<0.00	<0.00	<0.00
Ca43	4750.31	4966.67	1555.34	0.0012	0.015	9.48	17.76	139.6	28.11	4.35	8.44	8.1	14.33	11.61	50.36	4314.26	4927.67	0.0088	0.0018
Sc45	29.04	30.15	1.11	0	0.00002	0.0089	0.0058	0.024	0.0049	0.0026	0.0087	0.0086	0.0097	0.027	0.007	25.92	29.71	0.00001	0
Ti49	25.64	26.95	390.45	0.00001	0.00019	1.6	0.16	27.34	2.6	0.09	0.31	0.16	4.77	1.45	1.44	23.47	27.22	0.00017	0.00003
V51	18.34	19.41	8.54	0	0.00002	0.013	0.0073	0.31	0.043	0.0034	0.024	0.0079	0.079	0.48	0.033	18.02	19.06	0.00001	0
Cr53	17.51	18.62	1.09	0.00006	0.0007	0.37	0.26	0.38	0.21	0.11	0.38	0.37	0.23	0.4	0.25	17.2	18.27	0.00058	0.00011
Mn55	17.17	17.69	29.76	0.00001	0.00008	0.29	0.038	0.88	1.48	0.69	0.83	0.049	0.67	0.89	2.31	15.7	17.08	0.00007	0.00001
Fe57	20.76	21.41	1756.78	0.00045	0.0034	14722.45	14722.06	14721.98	14721.75	14721.62	14722.08	14722.56	14721.74	14722.25	14721.75	18.22	20.57	0.0027	0.00064
Co59	17.06	17.87	0.89	0	0.00003	0.098	0.02	0.46	1.48	26.63	0.059	1.38	0.031	0.074	2.04	16.77	17.7	0.00002	0
Ni60	18.24	19.22	0.35	1.35	78.58	10.51	0.13	27.06	0.062	0.048	0.11	0.9	0.081	0.04	0.8	17.42	18.42	47.53	2.99
Ni62	19.19	20.18	0.72	1.35	79.79	10.36	0.2	26.15	0.1	0.091	0.32	1.06	0.16	0.42	0.72	17.53	19.66	48.27	2.99
Cu65	19.49	20.45	0.56	0.00087	0.046	1.56	0.21	1.67	0.37	17.62	1.22	0.13	0.75	1.01	1094.86	19.46	19.89	0.027	0.0018
Zn66	36.12	38.58	10.62	0.00075	0.0032	0.52	1.09	3.68	2.83	198.79	4.39	5.96	2.37	1.15	41.56	42.13	38.04	0.0002	0.00006
Ga71	17.99	18.83	0.49	0	0.00002	0.0083	0.0051	0.035	0.0074	0.0043	0.014	0.0057	0.023	0.046	0.046	17.37	18.04	0.00001	0
As75	25.04	26.99	1.84	0.00051	0.017	129.26	134.87	19.37	9.66	125.96	12.18	8.96	478.27	18.62	88.16	25.04	25.11	0.011	0.00095
Se82	7.76	8.33	1.51	0.00046	0.019	0.8	0.4	3.34	0.65	0.82	3.65	0.88	0.56	0.56	8.16	6.75	7.9	0.012	0.00087
Y89	33.5	34.65	1.22	0	0	0.0092	0.0011	0.11	0.0073	0.00075	0.0028	0.0021	0.036	0.0067	0.065	29.67	34.93	0	0
Zr90	31.93	33.14	6.45	0	0.00001	0.018	0.0057	0.2	0.036	0.0013	0.077	0.0035	0.21	0.015	0.13	28.39	33.29	0	0
Nb93	22.73	23.85	0.31	0	0	0.0057	0.0011	0.035	0.006	0.00049	0.0015	0.0016	0.013	0.0046	0.0019	20.82	23.71	0	0
Mo95	14.82	15.63	4.28	0	0.00002	0.014	0.11	0.13	0.016	0.1	2.76	0.019	0.035	0.068	0.19	13.97	15.26	0.00001	0
Ru99	<0.00	<0.00	<0.00	<0.00	<0.00	<0.00	<0.00	<0.00	<0.00	<0.00	<0.00	<0.00	<0.00	<0.00	<0.00	<0.00	<0.00	<0.00	<0.00
Ru101	<0.00	<0.00	<0.00	<0.00	<0.00	<0.00	<0.00	<0.00	<0.00	<0.00	<0.00	<0.00	<0.00	<0.00	<0.00	<0.00	<0.00	<0.00	<0.00
Rh103	<0.00	<0.00	<0.00	<0.00	<0.00	<0.00	<0.00	<0.00	<0.00	<0.00	<0.00	<0.00	<0.00	<0.00	<0.00	<0.00	<0.00	<0.00	<0.00
Ag107	10.59	10.97	0.04	0.00081	0.046	1.6	0.016	0.18	0.032	1.61	0.041	0.093	0.69	0.062	1.83	9.66	10.2	0.027	0.0017
Pd108	<0.00	<0.00	<0.00	<0.00	<0.00	<0.00	<0.00	<0.00	<0.00	<0.00	<0.00	<0.00	<0.00	<0.00	<0.00	<0.00	<0.00	<0.00	<0.00
Cd111	19.94	21.02	0.22	0.00028	0.0098	0.12	0.046	0.066	0.034	0.62	0.45	0.14	0.19	0.051	0.59	19.85	17.72	0.0062	0.00054
In115	19.02	20.26	0.013	0	0	0.003	0.0022	0.0027	0.0017	0.011	0.0032	0.0018	0.0018	0.0065	0.025	18.81	19.19	0	0
Sn118	16.87	17.37	0.15	0.00001	0.00025	0.038	0.025	0.037	0.027	0.016	0.042	0.034	0.022	0.026	0.05	16.6	17.26	0.00015	0.00002
Sb121	16.97	18.39	0.065	0.00001	0.0005	0.057	0.019	0.2	0.04	0.71	0.1	0.058	0.091	0.053	8.84	15.95	16.79	0.00019	0.00001
Te125	<0.00	<0.00	<0.00	<0.00	<0.00	<0.00	<0.00	<0.00	<0.00	<0.00	<0.00	<0.00	<0.00	<0.00	<0.00	<0.00	<0.00	<0.00	<0.00
Te128	<0.00	<0.00	<0.00	<0.00	<0.00	<0.00	<0.00	<0.00	<0.00	<0.00	<0.00	<0.00	<0.00	<0.00	<0.00	<0.00	<0.00	<0.00	<0.00
La139	32.34	33.06	0.94	0	0	0.011	0.0026	0.11	0.001	0.00064	0.0037	0.0017	0.009	0.0039	0.0096	28.45	32.84	0	0
Ce140	22.77	23.52	1.33	0	0	0.0037	0.0011	0.16	0.0021	0.00071	0.0086	0.0018	0.015	0.0039	0.021	20.62	23.23	0	0
Nd146	31.1	32.25	1.08	0	0.00001	0.0087	0.0043	0.13	0.0043	0.0028	0.0092	0.0069	0.034	0.01	0.01	27.38	31.58	0.00001	0
Hf178	35.76	37.49	0.22	0	0.00001	0.0048	0.0026	0.014	0.0044	0.0013	0.0057	0.0054	0.011	0.0042	0.0059	30.81	35.84	0.00001	0
W182	18.61	19.66	0.037	0	0.00001	0.015	0.0053	0.24	0.015	0.0034	0.057	0.0094	0.012	0.025	0.0089	17.05	18.55	0.00002	0
Re185	4.94	5.2	0.015	0	0.00002	0.0054	0.009	0.0089	0.0045	0.003	0.01	0.0063	0.0037	0.0071	0.0035	4.48	4.91	0.00001	0
Re187	4.3	4.53	0.012	0.00001	0.00048	<0.00	0.0058	0.0065	0.0033	0.0012	0.011	0.0044	0.0024	0.0046	0.0025	4.03	4.3	0.0003	0.00002

RUN4

Element	STD610-1	STD610-2	BCR2G-1	PGEA-1	PGEA-2	JL01-PY	BG31-CPY	JL01-PY1	BG32-PY	BG32-PY2	KP04-PY	JL03-PY	JL02-PY	JL07-PY	BG01-PY	STD610-3	STD610-4	PGEA-3	PGEA-4
Os189	<0.00	<0.00	<0.00	<0.00	<0.00	<0.00	<0.00	<0.00	<0.00	<0.00	<0.00	<0.00	<0.00	<0.00	<0.00	<0.00	<0.00	<0.00	<0.00
Os190	<0.00	<0.00	<0.00	<0.00	<0.00	<0.00	<0.00	<0.00	<0.00	<0.00	<0.00	<0.00	<0.00	<0.00	<0.00	<0.00	<0.00	<0.00	<0.00
Ir193	<0.00	<0.00	<0.00	<0.00	<0.00	<0.00	<0.00	<0.00	<0.00	<0.00	<0.00	<0.00	<0.00	<0.00	<0.00	<0.00	<0.00	<0.00	<0.00
Pt195	<0.00	<0.00	<0.00	<0.00	<0.00	<0.00	<0.00	<0.00	<0.00	<0.00	<0.00	<0.00	<0.00	<0.00	<0.00	<0.00	<0.00	<0.00	<0.00
Au197	1.26	1.32	0.029	0.00072	0.035	0.07	0.0095	0.027	0.0064	0.12	0.0086	0.015	1.23	0.012	1.36	1.17	1.19	0.021	0.0014
Pb208	24.32	26.15	1.14	0.00011	0.0049	85.54	0.3	20.83	1.2	29.53	2.39	3.75	2.24	1.2	2475.34	22.74	22.23	0.0029	0.00021
Bi209	25.29	26.88	0.056	0.00079	0.031	20.93	0.34	0.13	1.55	32.58	0.54	0.63	0.068	4.74	40437.08	22.32	22.64	0.018	0.0014
Th232	44.72	46.65	0.3	0	0	0.0033	0.0016	0.07	0.0031	0.00097	0.0021	0.0022	0.014	0.0034	0.0051	37.09	42.44	0	0
U238	28.89	30.27	0.062	0	0	0.0058	0.0013	0.011	0.0045	0.0035	0.0028	0.0015	0.0094	0.0084	0.55	25.45	27.33	0	0
ThO248	<0.00	<0.00	<0.00	<0.00	<0.00	<0.00	<0.00	<0.00	<0.00	<0.00	<0.00	<0.00	<0.00	<0.00	<0.00	<0.00	<0.00	<0.00	<0.00
GLITTER!: Minimum detection limits (99% confidence).																			
Element	STD610-1	STD610-2	BCR2G-1	PGEA-1	PGEA-2	JL01-PY	BG31-CPY	JL01-PY1	BG32-PY	BG32-PY2	KP04-PY	JL03-PY	JL02-PY	JL07-PY	BG01-PY	STD610-3	STD610-4	PGEA-3	PGEA-4
Al27	0.364	0.527	0.177	0.00001	0.00012	0.0522	0.0358	0.0477	0.163	0.0182	0.0529	0.052	0.025	0.0373	0.0264	0.218	0.407	0.0001	0.00002
Si29	191.71	191.48	98.52	0.00628	0.0704	30.3	21.79	29.5	18.16	10.09	30.95	30.36	15.71	21.8	17.23	138.88	178.57	0.0553	0.0111
S34	<0.00000	<0.00000	<0.00000	<0.00000	<0.00000	<0.00000	<0.00000	<0.00000	<0.00000	<0.00000	<0.00000	<0.00000	<0.00000	<0.00000	<0.00000	<0.00000	<0.00000	<0.00000	<0.00000
Ca43	102.7	93.36	47.15	0.00271	0.0342	16.97	13	17.64	10.45	5.49	15.16	14.94	7.6	11.08	7.86	62.45	79.14	0.0233	0.00471
Sc45	0.123	0.159	0.0634	0	0.00005	0.0204	0.0136	0.019	0.0124	0.00664	0.0198	0.0192	0.0111	0.0145	0.0112	0.0941	0.115	0.00004	0.00001
Ti49	0.957	1.01	0.49	0.00003	0.00034	0.141	0.0833	0.136	0.0959	0.0441	0.179	0.166	0.0855	0.117	0.102	0.762	1.09	0.00032	0.00005
V51	0.11	0.127	0.0588	0	0.00004	0.0183	0.0114	0.0151	0.00939	0.00506	0.0158	0.016	0.00829	0.0125	0.00846	0.0791	0.109	0.00003	0.00001
Cr53	5.07	4.93	2.73	0.00017	0.00188	0.854	0.579	0.807	0.495	0.278	0.847	0.844	0.426	0.593	0.469	3.72	4.75	0.00152	0.0003
Mn55	0.58	0.559	0.298	0.00002	0.00021	0.092	0.066	0.09	0.0551	0.0317	0.0963	0.0964	0.049	0.0697	0.0539	0.471	0.574	0.00018	0.00004
Fe57	17.7	16.96	8.9	0.00057	0.00637	2.71	1.93	2.66	2.07	1.07	2.96	6.65	1.67	3.59	1.73	12.29	15.17	0.00484	0.00096
Co59	0.07	0.0862	0.0344	0	0.00002	0.0129	0.00985	0.0118	0.00834	0.00461	0.012	0.0157	0.0063	0.00957	0.00779	0.0584	0.0716	0.00002	0
Ni60	0.353	0.409	0.215	0.00001	0.00166	0.0857	0.0436	0.0624	0.0407	0.0187	0.0666	0.0683	0.0386	0.0502	0.0317	0.307	0.562	0.00012	0.00032
Ni62	1.56	1.88	0.948	0.00005	0.00453	0.299	0.156	0.217	0.157	0.106	0.249	0.322	0.0926	0.182	0.173	1.26	2.49	0.00044	0.00087
Cu65	0.796	0.749	0.401	0.00002	0.00025	0.116	0.086	0.115	0.0694	0.0406	0.141	0.118	0.0553	0.088	0.0735	0.506	0.622	0.00021	0.00004
Zn66	0.8	0.725	0.368	0.00003	0.00025	0.146	0.0986	0.102	0.0811	0.0441	0.162	0.132	0.0767	0.101	0.0804	0.489	0.669	0.00022	0.00004
Ga71	0.0955	0.124	0.0162	0	0.00004	0.00988	0.00746	0.00926	0.008	0.00402	0.0192	0.0141	0.00541	0.00823	0.0117	0.0716	0.101	0.00003	0
As75	8.95	8.65	4.45	0.00027	0.00297	1.27	0.928	1.3	0.798	0.442	1.42	1.42	0.74	1.16	0.932	7.32	9.53	0.00304	0.00061
Se82	7.69	7.73	3.97	0.00025	0.0028	1.22	0.925	1.26	0.768	0.416	1.23	1.33	0.646	0.939	0.718	5.67	7.67	0.00234	0.00046
Y89	0.019	0.0701	0.0117	0	0.00001	0.00358	0.00242	0.00274	0.00219	0.00097	0.00201	0.00296	0.0016	0.00243	0.0021	0.0128	0.0333	0.00001	0
Zr90	0.0235	0.0695	0.0132	0	<0.00000	0.00638	0.00545	0.00708	0.00349	0.0019	0.00786	0.00289	0.00343	0.00368	0.00309	0.0353	0.0514	0.00001	0
Nb93	0.0169	0.0617	0.00824	0	0.00001	0.00324	0.00219	0.00384	0.00198	0.00096	0.00244	0.00254	0.00159	0.00264	0.00157	0.0155	0.0412	0.00001	0
Mo95	0.131	0.159	0.0683	0	0.00005	0.0225	0.0115	0.0239	0.0137	0.00399	0.0203	0.0211	0.0125	0.0155	0.0122	0.111	0.16	0.00003	0.00001
Ru99	<0.00000	<0.00000	<0.00000	<0.00000	<0.00000	<0.00000	<0.00000	<0.00000	<0.00000	<0.00000	<0.00000	<0.00000	<0.00000	<0.00000	<0.00000	<0.00000	<0.00000	<0.00000	<0.00000
Ru101	<0.00	<0.00	<0.00	<0.00	<0.00	<0.00	<0.00	<0.00	<0.00	<0.00	<0.00	<0.00	<0.00	<0.00	<0.00	<0.00	<0.00	<0.00	<0.00
Rh103	<0.00000	<0.00000	<0.00000	<0.00000	<0.00000	<0.00000	<0.00000	<0.00000	<0.00000	<0.00000	<0.00000	<0.00000	<0.00000	<0.00000	<0.00000	<0.00000	<0.00000	<0.00000	<0.00000
Ag107	0.118	0.148	0.04	0	0.00004	0.0183	0.0136	0.0151	0.00912	0.00784	0.0214	0.0204	0.00844	0.0111	0.0104	0.0921	0.104	0.00004	0.00001
Pd108	<0.00000	<0.00000	<0.00000	<0.00000	<0.00000	<0.00000	<0.00000	<0.00000	<0.00000	<0.00000	<0.00000	<0.00000	<0.00000	<0.00000	<0.00000	<0.00000	<0.00000	<0.00000	<0.00000
Cd111	0.993	0.75	0.589	0.00004	0.00034	0.127	0.0899	0.146	0.0737	0.0499	0.156	0.172	0.059	0.112	0.0754	0.723	0.943	0.00025	0.00004
In115	0.0339	0.0719	0.0151	0	0.00001	0.00617	0.0034	0.00431	0.00356	0.00168	0.00633	0.00417	0.00225	0.00306	0.00273	0.0201	0.0524	0.00001	0
Sn118	0.513	0.542	0.247	0.00002	0.00019	0.085	0.0566	0.0776	0.0472	0.025	0.0862	0.0743	0.0415	0.0565	0.0463	0.368	0.452	0.00014	0.00003
Sb121	0.281	0.331	0.14	0.00001	0.00011	0.0381	0.0304	0.0377	0.0255	0.0204	0.0686	0.068	0.0396	0.0452	0.0325	0.24	0.383	0.0001	0.00002
Te125	<0.00000	<0.00000	<0.00000	<0.00000	<0.00000	<0.00000	<0.00000	<0.00000	<0.00000	<0.00000	<0.00000	<0.00000	<0.00000	<0.00000	<0.00000	<0.00000	<0.00000	<0.00000	<0.00000
Te128	<0.00000	<0.00000	<0.00000	<0.00000	<0.00000	<0.00000	<0.00000	<0.00000	<0.00000	<0.00000	<0.00000	<0.00000	<0.00000	<0.00000	<0.00000	<0.00000	<0.00000	<0.00000	<0.00000
La139	<0.00000	0.0601	0.00915	0	0.00001	0.00455	0.00287	0.00399	0.00171	0.00054	0.00496	0.00326	0.00137	0.00208	0.00231	0.0186	0.0494	0.00001	0
Ce140	0.0202	0.0607	0.0102	0	0.00001	0.00347	0.00148	0.00356	0.0019	0.00136	0.00337	0.00314	0.00107	0.00258	0.00145	0.00676	0.033	0.00001	0
Nd146	0.0751	0.124	0.0345	0	0.00002	0.0129	0.0112	0.0121	0.00911	0.007	0.0192	0.0151	0.00632	0.0175	0.00699	0.0563	0.127	0.00003	0
Hf178	0.0856	0.123	0.0278	0	0.00002	0.00979	0.00572	0.0121	0.00519	0.00282	0.00674	0.00991	0.00588	0.00631	0.00265	0.0524	0.0924	0.00003	0
W182	0.0935	0.17	0.0408	0	0.00004	0.0161	0.00969	0.015	0.00439	0.00477	0.0156	0.0103	0.00703	0.016	0.011	0.094	0.0914	0.00004	0.00001

RUN4

Element	STD610-1	STD610-2	BCR2G-1	PGEA-1	PGEA-2	JL01-PY	BG31-CPY	JL01-PY1	BG32-PY	BG32-PY2	KP04-PY	JL03-PY	JL02-PY	JL07-PY	BG01-PY	STD610-3	STD610-4	PGEA-3	PGEA-4
Re185	0.125	0.0516	<0.00000	0	0.00003	0.00874	0.0132	0.0183	0.0107	0.00822	0.0269	0.0153	0.00742	0.0113	0.00821	0.0935	0.111	0.00004	0
Re187	0.0594	0.0851	0.029	0	0.00003	0.0135	0.00769	0.0107	0.00825	0.0024	0.00859	0.0103	0.00499	0.00848	0.00618	0.0545	0.0918	0.00003	0
Os189	<0.00	<0.00	<0.00	<0.00	<0.00	<0.00	<0.00	<0.00	<0.00	<0.00	<0.00	<0.00	<0.00	<0.00	<0.00	<0.00	<0.00	<0.00	<0.00
Os190	<0.00	<0.00	<0.00	<0.00	<0.00	<0.00	<0.00	<0.00	<0.00	<0.00	<0.00	<0.00	<0.00	<0.00	<0.00	<0.00	<0.00	<0.00	<0.00
Ir193	<0.00000	<0.00000	<0.00000	<0.00000	<0.00000	<0.00000	<0.00000	<0.00000	<0.00000	<0.00000	<0.00000	<0.00000	<0.00000	<0.00000	<0.00000	<0.00000	<0.00000	<0.00000	<0.00000
Pt195	<0.00000	<0.00000	<0.00000	<0.00000	<0.00000	<0.00000	<0.00000	<0.00000	<0.00000	<0.00000	<0.00000	<0.00000	<0.00000	<0.00000	<0.00000	<0.00000	<0.00000	<0.00000	<0.00000
Au197	0.148	0.147	0.0682	0	0.00005	0.0136	0.013	0.0147	0.00832	0.00452	0.0132	0.0159	0.00861	0.0143	0.00952	0.0686	0.0447	0.00003	0.00001
Pb208	0.203	0.179	0.081	0.00001	0.00005	0.0204	0.0142	0.0178	0.0129	0.00802	0.0211	0.0199	0.0103	0.0136	0.0118	0.286	0.144	0.00004	0.00001
Bi209	0.112	0.144	0.0613	0	0.00005	0.0191	0.013	0.019	0.0103	0.00634	0.0188	0.0164	0.00861	0.0131	0.0105	0.29	0.283	0.00007	0.00001
Th232	0.0266	0.0703	0.0116	0	0.00001	0.0054	0.0039	0.00331	0.00177	0.00166	0.00397	0.00358	0.00347	0.0043	0.00313	0.0236	0.0465	0.00001	0
U238	0.0234	0.0751	0.0118	0	0.00001	0.00403	0.00272	0.00413	0.00348	0.0006	0.00526	0.00258	0.00249	0.00424	0.00169	0.0208	0.0522	0.00001	0
ThO248	<0.00	<0.00	<0.00	<0.00	<0.00	<0.00	<0.00	<0.00	<0.00	<0.00	<0.00	<0.00	<0.00	<0.00	<0.00	<0.00	<0.00	<0.00	<0.00
GLITTER!: Trace element concentrations normalised to chondrite.																			
Element	STD610-1	STD610-2	BCR2G-1	PGEA-1	PGEA-2	JL01-PY	BG31-CPY	JL01-PY1	BG32-PY	BG32-PY2	KP04-PY	JL03-PY	JL02-PY	JL07-PY	BG01-PY	STD610-3	STD610-4	PGEA-3	PGEA-4
Al27	0.811	0.825	3.55	0	0	0.00073	0.00042	0.1388	0.00156	0.00028	0.0014	0.00015	0.00558	0.00461	0.01051	0.747	0.832	0	0
Si29	2.11	2.14	0.953	0	0	0.00124	0.00106	0.01439	0.00882	0.00069	0.01009	0.00061	0.00325	0.01061	0.01734	2	2.14	0	0
S34	<****	<****	<****	<****	<****	<****	<****	<****	<****	<****	<****	<****	<****	<****	<****	<****	<****	<****	<****
Ca43	6.21	6.43	2.23	0	0	0.00449	0.0208	0.197	0.0381	0.00434	0.0055	0.00279	0.0183	0.01105	0.0703	5.87	6.46	0	0
Sc45	53.38	54.96	2.17	0	0	0	0	0.0391	0	0	0.0033	0	0.0139	0.0444	0.00781	49.13	54.72	0	0
Ti49	0.674	0.699	11.36	0	0	0.0439	0.00293	0.794	0.0748	0.00204	0.0072	0.00211	0.1378	0.04	0.041	0.643	0.717	0	0
V51	5	5.2	2.76	0	0	0.00161	0.00074	0.0986	0.01313	0.00049	0.00587	0.00021	0.02478	0.1536	0.00974	5.26	5.22	0	0
Cr53	0.0978	0.102	0.00156	0	0	0	0.00023	0.00112	0.0004	0	0.00092	0	0.00088	0.00158	0.00093	0.1033	0.1024	0	0
Mn55	0.1477	0.1491	0.316	0	0	0.00291	0.00021	0.00926	0.01569	0.00727	0.00869	0.00015	0.00705	0.00939	0.02454	0.1468	0.1478	0	0
Fe57	0.00164	0.00164	0.1996	0	0	1.675	1.675	1.675	1.675	1.675	1.675	1.675	1.675	1.675	1.675	0.00164	0.00164	0	0
Co59	0.511	0.526	0.0309	0	0	0.00309	0.00049	0.01613	0.0524	0.942	0.00184	0.0485	0.00097	0.00233	0.072	0.537	0.533	0	0
Ni60	0.0263	0.0272	0.00047	0.00168	0.0152	0.01829	0.00018	0.0473	0.00008	0.00007	0.00014	0.00147	0.00011	0.00002	0.00137	0.0271	0.0267	0.0117	0.00284
Ni62	0.0267	0.0273	0.0005	0.00171	0.0155	0.01795	0.00013	0.0465	0.00005	0.00006	0.00028	0.00132	0.00015	0.00038	0.00109	0.0267	0.0273	0.0119	0.00286
Cu65	2.47	2.55	0.0699	0.0001	0.00087	0.2231	0.0273	0.2408	0.0514	2.58	0.1745	0.01105	0.1081	0.1436	160.67	2.62	2.53	0.00066	0.00016
Zn66	0.901	0.958	0.274	0.00002	0.00002	0.0123	0.0277	0.095	0.0732	5.17	0.1135	0.154	0.0614	0.0289	1.081	1.071	0.95	0	0
Ga71	28.13	28.9	0.862	0	0	0.0021	0.00104	0.0461	0.00497	0.00288	0.00805	0	0.0326	0.0599	0.0733	29.23	28.35	0	0
As75	108.2	116.11	0	0.00209	0.0189	592.61	618.4	88.71	44.23	577.61	55.69	40.83	2193.25	85.24	404.26	110.92	108.4	0.0143	0.00344
Se82	4.08	4.31	0	0.00025	0.00224	0.311	0	2.18	0.361	0.525	2.39	0.337	0.304	0.18	5.5	3.87	4.12	0.00178	0.0004
Y89	210.83	216.62	8.07	0	0	0.0422	0	0.718	0.0414	0.00169	0.0084	0.00228	0.236	0.0294	0.426	191.36	220.2	0	0
Zr90	83.4	85.94	17.84	0	0	0.0352	0.0068	0.548	0.0929	0.00104	0.201	0.00194	0.573	0.0286	0.343	76.07	87.11	0	0
Nb93	1136.3	1178.59	16.62	0	0	0.143	0	1.793	0.253	0.0026	0.0104	0.0069	0.659	0.113	0.0469	1086.86	1188.72	0	0
Mo95	266.96	275.65	93.88	0	0	0.03	1.966	2.476	0.157	2.04	60.83	0.066	0.539	0.95	3.98	273.5	276.23	0	0
Ru99	0	0	0	0	0	0	0	0	0	0	0	0	0	0	0	0	0	0	0
Ru101	<****	<****	<****	<****	<****	<****	<****	<****	<****	<****	<****	<****	<****	<****	<****	<****	<****	<****	<****
Rh103	0	0	0	0	0	0	0	0	0	0	0	0	0	0	0	0	0	0	0
Ag107	737.77	749.85	1.15	0.0492	0.44	130.66	0.471	14.08	2.055	133.17	2.25	5.72	56.79	3.7	151.42	721.15	712.78	0.337	0.0807
Pd108	0	0	0	0	0	0	0	0	0	0	0	0	0	0	0	0	0	0	0
Cd111	260.14	271.86	0	0.00343	0.0303	0.7	0	0.146	0.076	8.45	5.5	0.75	2.29	0	7.78	266.18	230.53	0.0241	0.00588
In115	3644.72	3818.13	1.01	0.00001	0	0	0.056	0.104	0.046	2.194	0.077	0	0.1	0.564	5.12	3840.8	3692.85	0	0
Sn118	152.31	154.05	0.853	0.00004	0.0003	0	0	0.125	0.143	0.086	0.141	0	0.0828	0	0.411	160.34	156.51	0.00023	0.00008
Sb121	1573.46	1679.07	1.65	0.0004	0.0067	3.78	0.552	19.99	3.37	75.47	9.3	3.14	8.87	3.57	950.51	1571.82	1563.08	0.00316	0.00055
Te125	0	0	0	0	0	0	0	0	0	0	0	0	0	0	0	0	0	0	0
Te128	0	0	0	0	0	0	0	0	0	0	0	0	0	0	0	0	0	0	0
La139	1322.34	1341.81	40.72	0	0.00002	0.339	0.0377	4.56	0.0093	0.0085	0.064	0	0.342	0.077	0.363	1195.46	1345.17	0	0
Ce140	478.63	488.02	31.43	0	0	0.0224	0.0025	3.85	0.021	0.00226	0.1343	0	0.328	0.0321	0.457	455.95	490.14	0	0
Nd146	641.75	660.55	23.02	0	0	0.026	0	2.72	0	0	0	0	0.633	0.028	0.118	580.48	652.94	0	0.00001

RUN4

Element	STD610-1	STD610-2	BCR2G-1	PGEA-1	PGEA-2	JL01-PY	BG31-CPY	JL01-PY1	BG32-PY	BG32-PY2	KP04-PY	JL03-PY	JL02-PY	JL07-PY	BG01-PY	STD610-3	STD610-4	PGEA-3	PGEA-4
Hf178	2527.18	2634.79	14.82	0	0	0	0	0.658	0.134	0	0.126	0	0.605	0.043	0.247	2220.24	2536.11	0	0
W182	5015.49	5196.3	3.26	0	0	0.92	0	72.22	2.59	0.184	13.04	0.31	1.76	3.02	0.825	4954.78	5021.73	0	0
Re185	1913.47	1975.96	0.96	0	0	0	0.51	0.34	0	0	0	0	0	0.21	0	1853.2	1906.82	0	0
Re187	1862.34	1919.9	0	0.00364	0.0277	0	0.41	0.5	0	0	1.82	0	0	0	0	1890.51	1870.02	0.0222	0.00544
Os189	<****	<****	<****	<****	<****	<****	<****	<****	<****	<****	<****	<****	<****	<****	<****	<****	<****	<****	<****
Os190	<****	<****	<****	<****	<****	<****	<****	<****	<****	<****	<****	<****	<****	<****	<****	<****	<****	<****	<****
Ir193	0	0	0	0	0	0	0	0	0	0	0	0	0	0	0	0	0	0	0
Pt195	0	0	0	0	0	0	0	0	0	0	0	0	0	0	0	0	0	0	0
Au197	105	107.88	0	0.0573	0.52	5.31	0.227	1.8	0.208	11.73	0.178	0.404	120.21	0.331	132.81	103.48	98.36	0.381	0.0914
Pb208	116.49	123.99	5.86	0.00048	0.0042	448.93	1.538	109.32	6.26	155.02	12.49	19.61	11.75	6.22	12994.17	113.19	106.74	0.00314	0.00076
Bi209	2305.48	2431.41	3.99	0.0673	0.58	2038.74	32.75	12.42	150.5	3175.34	52.02	60.73	6.42	461.49	3941036.75	2093.79	2067.91	0.42	0.1048
Th232	11936.13	12396.37	80.35	0	0	0.192	0	18.73	0.561	0.078	0.106	0	3.49	0.308	1.06	10052.85	11338.76	0	0.00004
U238	39818.36	41332.41	80.44	0.0002	0	3.63	0	12.37	4.41	3.88	0.78	0	11.7	7.52	819.82	36316.56	37759.19	0	0
ThO248	<****	<****	<****	<****	<****	<****	<****	<****	<****	<****	<****	<****	<****	<****	<****	<****	<****	<****	<****

GLITTER4.0: Laser Ablation Analysis Results

G:\KYLIE\MAR13\RUN5
Fri Mar 14 20:57:05 2003

All values are reported in ppm

GLITTER!: Trace Element Concentrations MDL filtered.	Run5-1	Run5-2	Run5-3	Run5-4	Run5-5	Run5-6	Run5-7	Run5-8	Discarded Run5-9	Run5-10	Run5-11	Run5-12	Run5-13	Run5-14	Run5-15	Run5-16	Run5-17	Run5-18	Run5-19	Run5-20
Element	STD610-3	STD610-4	PGEA-3	PGEA-4	BCR2G-1	BG01-CPY	BG01-PY2	BG13-PY	BG13-SPH	BG13-SP2	JL04-PY	JL04-CPY	BG33-SPH	BG33-PY	BG19-PY	BG05-PY1	BG05-SP2	BG14-CPY	KP10-PY	BG34-PY
Al27	9693.99	10917.89	<0.00010	0.00006	48194.66	137.6	856.13	9.81	5731.98	18.69	2.51	7963.87	1.52	1.417	671.73	0.09	278.25	87.31	116	182.39
Si29	329831.03	358841.34	0.56	0.0173	164227.83	1493.06	4638.35	525.77	2278480	236.25	248.31	40451.54	127.77	<22.69	4351.43	56.3	19328.46	2981.26	2534.85	735.73
S34	<0.00	<0.00	<0.00	<0.00	<0.00	<0.00	<0.00	<0.00	<0.00	<0.00	<0.00	<0.00	<0.00	<0.00	<0.00	<0.00	<0.00	<0.00	<0.00	<0.00
Ca43	81495.34	90647.91	<0.0232	<0.0049	32155.55	717.29	721.29	64.63	11339.83	<18.48	26.26	51091.01	149.98	13.54	250.79	<13.21	24714.64	977.55	48.55	429
Sc45	441.5	498.81	<0.00004	<0.00001	20.21	<0.066	0.167	<0.0160	6.16	<0.0233	<0.0183	3.61	<0.0092	<0.0157	0.0604	<0.0184	0.057	0.211	0.0982	0.0254
Ti49	458.01	517.03	0.00045	0.00017	8506.38	28.41	26.67	68.62	173.55	32.87	3.83	4660.22	1.03	1.53	6.89	1.48	11.3	22.13	3.69	84.23
V51	451.67	454.08	<0.00003	<0.00001	245.85	2.05	5.68	0.467	2.11	0.118	0.172	60.87	<0.0087	0.0165	0.622	<0.0141	2.44	6.94	1.38	1.828
Cr53	382.82	386.88	<0.00137	<0.00028	7.11	8.77	4.81	3.9	<13.07	<0.88	<0.71	57.53	<0.34	<0.57	4.68	<0.66	<1.10	8.21	2.76	5.2
Mn55	425.23	432.7	<0.00017	0.00004	931.54	33.95	76.77	17.47	6989	1038.42	1.425	1146.98	564.31	0.636	68.24	0.137	754.7	311.56	22.1	396.41
Fe57	453.1	453.1	0.0078	0.00777	55500.02	304317.34	304317.34	465531.69	**********	13455.45	465531.72	304317.34	18613.34	465531.69	465531.69	465531.72	304317.34	304317.34	465531.69	465531.72
Co59	380.9	381.61	0.00006	0.00001	21.86	0.522	1.388	0.755	0.85	0.174	0.151	0.398	0.0927	0.0491	344.5	13.51	31.73	7.28	2.46	2.51
Ni60	404.56	402.8	169.95	42.57	7.59	3.89	4.29	1.241	16.99	0.325	0.526	2.1	0.155	0.052	3.82	10.81	7.01	3.71	3.22	0.188
Ni62	397.78	410.41	172.95	42.88	7.8	2.48	<1.79	2.58	19.51	<0.28	0.58	0.84	9.34	2.78	3.18	10.76	4.84	4.23	2.31	0.449
Cu65	427.1	417.68	0.105	0.0266	11.35	490674.25	489736.94	32.86	186.59	72.46	1.88	394099.22	23.15	2085.69	76.23	1.94	380821.53	454397.81	90.95	252.11
Zn66	478.81	380.56	0.00064	0.00052	81.16	3251.27	1987.95	50.21	669868.81	669868.81	8.01	1692.35	565572.38	226.62	2310.24	16.34	4360.72	5184.12	937.91	33.84
Ga71	419.74	413.59	<0.00003	<0.00000	12.75	0.399	1.39	0.364	5.26	3.85	0.0217	4.13	9.53	0.419	0.273	<0.0097	0.53	0.701	0.17	0.134
As75	312.94	314.72	0.0391	0.0098	<3.93	<5.02	<6.33	531.62	2035.08	2.32	389.98	11.84	<0.69	8503.68	713.06	151.23	55.55	32.34	3508.13	14783.45
Se82	106.86	116.65	0.049	0.0113	<3.14	4.82	<5.55	4.39	29.11	<1.55	86.53	169.58	<0.58	<1.00	31.01	52.24	49.64	38.56	15.73	6.89
Y89	465.48	541.15	<0.00001	<0.00000	20.56	1.201	0.169	0.0661	1.51	0.9	0.0087	7.79	0.0028	<0.00234	0.176	0.0165	0.227	2.37	0.314	0.466
Zr90	463.94	535.65	<0.00001	<0.00000	114.19	3.97	1.32	0.307	4.67	1.54	0.0335	38.12	<0.0036	0.0051	0.385	<0.0071	0.117	1.66	3.1	0.648
Nb93	484.85	539.82	<0.00001	<0.00000	7.7	0.157	0.841	0.0059	1.84	0.0128	0.0136	10.36	<0.00211	<0.0034	0.0956	<0.0042	0.0423	0.0139	0.246	0.244
Mo95	386.02	395.78	<0.00003	<0.00001	134.06	0.704	0.94	1.523	96.04	0.277	<0.0194	0.331	0.078	0.0225	0.577	0.717	0.232	0.823	1.336	0.629
Ru99	<0.00	<0.00	<0.00	<0.00	<0.00	<0.00	<0.00	<0.00	<0.00	<0.00	<0.00	<0.00	<0.00	<0.00	<0.00	<0.00	<0.00	<0.00	<0.00	<0.00
Ru101	<-NaN	<-NaN	<-NaN	<-NaN	<-NaN	<-NaN	<-NaN	<-NaN	<-NaN	<-NaN	<-NaN	<-NaN	<-NaN	<-NaN	<-NaN	<-NaN	<-NaN	<-NaN	<-NaN	<-NaN
Rh103	<0.00	<0.00	<0.00	<0.00	<0.00	<0.00	<0.00	<0.00	<0.00	<0.00	<0.00	<0.00	<0.00	<0.00	<0.00	<0.00	<0.00	<0.00	<0.00	<0.00
Ag107	213.73	222.3	0.099	0.0243	0.228	27.7	53.99	10.52	130.81	2.91	0.529	35.3	2.55	23.65	5.27	0.701	532.28	347.98	34.52	119.7
Pd108	<0.00	<0.00	<0.00	<0.00	<0.00	<0.00	<0.00	<0.00	<0.00	<0.00	<0.00	<0.00	<0.00	<0.00	<0.00	<0.00	<0.00	<0.00	<0.00	<0.00
Cd111	263.62	235.86	0.0233	0.00588	<0.34	12.45	28.24	0.441	41.07	1965.79	<0.133	12.35	1823.51	3.66	6.4	<0.134	43.52	31.5	6.13	0.336
In115	413.17	410.43	<0.00001	<0.00000	0.0676	11.43	9.79	<0.0040	0.8	0.15	<0.0043	8.6	0.492	0.116	0.0531	<0.0046	2.59	9.15	0.308	0.0355
Sn118	372.2	369.55	0.00052	0.00018	1.12	3.65	1.62	0.241	4.15	34.79	0.08	8.65	0.561	0.114	1.547	0.077	3.69	8.51	1.137	0.3
Sb121	352.54	365.45	0.00067	0.00012	0.671	2.31	6.14	1.61	155.54	1.99	0.382	2.1	0.611	22.14	12.65	0.76	16.31	6.47	5.44	549.57
Te125	<0.00	<0.00	<0.00	<0.00	<0.00	<0.00	<0.00	<0.00	<0.00	<0.00	<0.00	<0.00	<0.00	<0.00	<0.00	<0.00	<0.00	<0.00	<0.00	<0.00
Te128	<0.00	<0.00	<0.00	<0.00	<0.00	<0.00	<0.00	<0.00	<0.00	<0.00	<0.00	<0.00	<0.00	<0.00	<0.00	<0.00	<0.00	<0.00	<0.00	<0.00
La139	415.86	475.71	<0.00001	0	14.97	0.469	2.57	0.682	23.89	0.94	0.0278	2.55	<0.00186	<0.0073	0.167	0.01	0.0677	0.0858	0.0371	0.0533
Ce140	424.59	462.4	<0.00001	<0.00000	30.71	0.694	2.11	1.759	141.02	243.01	0.0113	12.4	0.0107	<0.0027	0.7	<0.0022	0.173	0.281	0.1627	0.424
Nd146	427.18	487.88	<0.00003	0.00001	17.64	0.467	0.128	4.3	3.88	0.743	<0.0131	11.86	<0.0079	<0.0114	0.0338	<0.0131	0.099	0.0433	0.023	0.0442
Hf178	433.86	504.08	<0.00003	<0.00000	3.09	<0.031	<0.050	<0.0075	0.209	0.116	<0.0091	1.49	<0.0070	<0.0097	0.0169	<0.0144	<0.0178	0.057	0.125	0.0147
W182	426.52	440.69	<0.00004	<0.00001	0.217	0.184	2.28	0.0306	3.28	0.0219	<0.0145	13.87	0.0113	<0.0115	0.111	<0.0145	16.38	0.249	0.122	14.43
Re185	47.85	50.16	<0.00002	<0.00000	<0.0275	<0.036	<0.054	<0.0074	<0.174	<0.0090	<0.0078	<0.0121	<0.0049	<0.0068	<0.0083	<0.0078	<0.0061	<0.0113	<0.0041	<0.0054
Re187	49.37	50.02	0.00057	0.00014	<0.0138	<0.0141	<0.0228	<0.0039	<0.084	<0.0061	<0.0046	<0.0085	0.00188	<0.0040	<0.0052	<0.0051	<0.0063	<0.0067	<0.00213	<0.0032
Os189	<-NaN	<-NaN	<-NaN	<-NaN	<-NaN	<-NaN	<-NaN	<-NaN	<-NaN	<-NaN	<-NaN	<-NaN	<-NaN	<-NaN	<-NaN	<-NaN	<-NaN	<-NaN	<-NaN	<-NaN
Os190	<-NaN	<-NaN	<-NaN	<-NaN	<-NaN	<-NaN	<-NaN	<-NaN	<-NaN	<-NaN	<-NaN	<-NaN	<-NaN	<-NaN	<-NaN	<-NaN	<-NaN	<-NaN	<-NaN	<-NaN
Ir193	<0.00	<0.00	<0.00	<0.00	<0.00	<0.00	<0.00	<0.00	<0.00	<0.00	<0.00	<0.00	<0.00	<0.00	<0.00	<0.00	<0.00	<0.00	<0.00	<0.00
Pt195	<0.00	<0.00	<0.00	<0.00	<0.00	<0.00	<0.00	<0.00	<0.00	<0.00	<0.00	<0.00	<0.00	<0.00	<0.00	<0.00	<0.00	<0.00	<0.00	<0.00
Au197	22.55	22.2	0.081	0.0202	0.091	0.063	<0.070	0.882	17.37	0.063	0.139	0.371	<0.0093	52.52	0.189	0.061	0.064	0.147	4.56	9.24
Pb208	400.25	391.68	0.0108	0.00271	6.88	66.52	1096.86	270.57	12408.06	21.9	6.79	46.4	1.88	438.15	852.4	53.87	151.44	2094.09	1669.49	685.66
Bi209	346.59	359.53	0.069	0.0176	0.114	4.91	4.28	118.96	191.88	1.68	0.486	34.35	0.277	1.131	47.29	15.98	6.66	22.49	19.41	15.24
Th232	486.32	555.41	<0.00001	0	3.86	0.0222	0.048	<0.0037	0.407	0.0218	0.0054	1.33	<0.0030	<0.0042	0.0111	<0.0059	0.088	0.0596	0.0243	0.0691
U238	501	525.85	<0.00001	<0.00000	1.131	0.282	2.84	0.0193	5.22	<0.0096	<0.0046	1.75	<0.00223	<0.0050	0.687	0.0032	0.154	14.31	0.1007	0.217
ThO248	<-NaN	<-NaN	<-NaN	<-NaN	<-NaN	<-NaN	<-NaN	<-NaN	<-NaN	<-NaN	<-NaN	<-NaN	<-NaN	<-NaN	<-NaN	<-NaN	<-NaN	<-NaN	<-NaN	<-NaN

RUN5

Element	STD610-3	STD610-4	PGEA-3	PGEA-4	BCR2G-1	BG01-CPY	BG01-PY2	BG13-PY	BG13-SPH	BG13-SP2	JL04-PY	JL04-CPY	BG33-SPH	BG33-PY	BG19-PY	BG05-PY1	BG05-SP2	BG14-CPY	KP10-PY	BG34-PY
GLITTER!: 1 sigma error.																				
Element	STD610-3	STD610-4	PGEA-3	PGEA-4	BCR2G-1	BG01-CPY	BG01-PY2	BG13-PY	BG13-SPH	BG13-SP2	JL04-PY	JL04-CPY	BG33-SPH	BG33-PY	BG19-PY	BG05-PY1	BG05-SP2	BG14-CPY	KP10-PY	BG34-PY
Al27	607.62	691.25	0.00004	0.00001	2899.67	8.3	51.53	0.59	613.13	2	0.16	479.12	0.16	0.09	40.41	0.023	16.75	5.26	6.98	10.98
Si29	23182.83	25424.92	0.14	0.0046	11176.7	110.25	321.07	37.01	227360.39	27.83	20.84	2753.36	13.92	8.79	296.43	12.6	1316.06	203.57	172.72	50.68
S34	<0.00	<0.00	<0.00	<0.00	<0.00	<0.00	<0.00	<0.00	<0.00	<0.00	<0.00	<0.00	<0.00	<0.00	<0.00	<0.00	<0.00	<0.00	<0.00	<0.00
Ca43	5331.5	5986.33	0.0089	0.0018	2027.27	55.16	59.15	6.45	1210.22	7.13	6.19	3218.87	16.29	4.36	17.79	5.7	1559.83	64	5.25	28.51
Sc45	30.87	35.16	0.00001	0	1.37	0.027	0.039	0.0059	0.72	0.0093	0.008	0.25	0.0036	0.006	0.0084	0.0081	0.016	0.019	0.0089	0.0053
Ti49	29.3	33.43	0.00018	0.00003	518.65	1.93	1.91	4.22	20.91	3.86	0.3	284.2	0.14	0.14	0.47	0.17	0.83	1.41	0.25	5.17
V51	23.18	23.66	0.00001	0	11.86	0.11	0.29	0.025	0.25	0.014	0.014	2.94	0.0035	0.0061	0.033	0.0066	0.13	0.34	0.068	0.091
Cr53	18.09	18.66	0.00053	0.00011	0.81	1.07	1.31	0.29	5.51	0.34	0.29	2.64	0.13	0.22	0.33	0.29	0.5	0.51	0.2	0.3
Mn55	19.5	20.22	0.00006	0.00001	39.41	1.46	3.27	0.74	639.22	94.97	0.075	48.51	51.61	0.041	2.89	0.038	31.93	13.18	0.94	16.77
Fe57	18.23	19.11	0.0026	0.00064	1756.44	9625.52	9626.45	14721.79	756611.88	999	14722.13	9624.98	1381.79	14721.85	14721.89	14722.28	9624.95	9624.02	14721.71	14721.82
Co59	17.86	18.22	0.00002	0	0.96	0.039	0.084	0.036	0.14	0.019	0.012	0.029	0.0095	0.0057	14.95	0.59	1.39	0.32	0.11	0.11
Ni60	20.32	20.57	40.89	3.03	0.4	0.25	0.29	0.077	1.82	0.046	0.049	0.14	0.024	0.021	0.19	0.53	0.38	0.2	0.16	0.021
Ni62	20.62	21.71	41.62	3.06	0.62	0.46	0.79	0.2	3.49	0.12	0.13	0.25	0.98	0.24	0.24	0.68	0.63	0.34	0.17	0.085
Cu65	20.18	20.11	0.025	0.0018	0.56	21399.58	21359.28	1.45	15.96	6.1	0.12	17187.43	1.95	90.97	3.34	0.12	16608.36	19816.61	3.98	11.01
Zn66	43.19	34.54	0.00019	0.00006	7.22	286.94	175.52	4.45	21186.1	21183.27	0.75	149.38	17885.03	20.04	203.85	1.48	384.8	457.41	82.76	3
Ga71	21.1	21.13	0.00001	0	0.62	0.041	0.1	0.022	0.58	0.35	0.0065	0.22	0.86	0.026	0.019	0.0053	0.043	0.042	0.012	0.011
As75	25.87	26.26	0.0098	0.00097	1.49	2.02	2.57	42.55	199.89	0.74	31.23	1.35	0.27	680.35	57.06	12.14	4.61	2.7	280.67	1182.75
Se82	8.06	9.02	0.012	0.001	1.22	1.76	2.26	0.49	10.18	0.61	5.89	11.55	0.23	0.39	2.17	3.63	3.62	2.72	1.12	0.59
Y89	32.98	38.64	0	0	1.42	0.09	0.02	0.0058	0.21	0.11	0.0021	0.54	0.0011	0.00096	0.014	0.0032	0.02	0.17	0.023	0.033
Zr90	32.85	38.23	0	0	7.84	0.29	0.11	0.024	0.61	0.19	0.0057	2.62	0.0017	0.0023	0.03	0.003	0.016	0.12	0.21	0.047
Nb93	30.81	34.64	0	0	0.48	0.017	0.063	0.0016	0.24	0.0033	0.0026	0.64	0.00078	0.0013	0.0077	0.0016	0.0071	0.0027	0.016	0.017
Mo95	18.89	19.7	0.00001	0	6.13	0.075	0.1	0.08	9.38	0.036	0.0086	0.042	0.011	0.0076	0.038	0.053	0.036	0.054	0.069	0.039
Ru99	<0.00	<0.00	<0.00	<0.00	<0.00	<0.00	<0.00	<0.00	<0.00	<0.00	<0.00	<0.00	<0.00	<0.00	<0.00	<0.00	<0.00	<0.00	<0.00	<0.00
Ru101	<0.00	<0.00	<0.00	<0.00	<0.00	<0.00	<0.00	<0.00	<0.00	<0.00	<0.00	<0.00	<0.00	<0.00	<0.00	<0.00	<0.00	<0.00	<0.00	<0.00
Rh103	<0.00	<0.00	<0.00	<0.00	<0.00	<0.00	<0.00	<0.00	<0.00	<0.00	<0.00	<0.00	<0.00	<0.00	<0.00	<0.00	<0.00	<0.00	<0.00	<0.00
Ag107	27.06	28.22	0.026	0.0033	0.041	3.49	6.78	1.32	22.22	0.5	0.071	4.43	0.43	2.97	0.66	0.094	66.7	43.6	4.33	15
Pd108	<0.00	<0.00	<0.00	<0.00	<0.00	<0.00	<0.00	<0.00	<0.00	<0.00	<0.00	<0.00	<0.00	<0.00	<0.00	<0.00	<0.00	<0.00	<0.00	<0.00
Cd111	17.65	16.02	0.0057	0.0005	0.14	0.99	2.07	0.065	3.91	132.2	0.053	0.93	122.59	0.28	0.45	0.055	2.91	2.06	0.42	0.055
In115	31.25	31.26	0	0	0.0095	0.85	0.73	0.0017	0.13	0.019	0.0018	0.64	0.057	0.01	0.0056	0.0025	0.2	0.68	0.024	0.004
Sn118	21.83	21.93	0.00014	0.00002	0.11	0.25	0.18	0.029	0.74	3.51	0.03	0.51	0.06	0.025	0.096	0.029	0.23	0.49	0.07	0.027
Sb121	34.93	36.36	0.00018	0.00002	0.09	0.25	0.63	0.16	22.56	0.29	0.05	0.22	0.091	2.16	1.24	0.086	1.6	0.64	0.53	53.54
Te125	<0.00	<0.00	<0.00	<0.00	<0.00	<0.00	<0.00	<0.00	<0.00	<0.00	<0.00	<0.00	<0.00	<0.00	<0.00	<0.00	<0.00	<0.00	<0.00	<0.00
Te128	<0.00	<0.00	<0.00	<0.00	<0.00	<0.00	<0.00	<0.00	<0.00	<0.00	<0.00	<0.00	<0.00	<0.00	<0.00	<0.00	<0.00	<0.00	<0.00	<0.00
La139	27.95	32.25	0	0	0.98	0.038	0.18	0.046	2.83	0.11	0.0036	0.17	0.00076	0.0025	0.012	0.0024	0.0085	0.0077	0.0034	0.0047
Ce140	22.94	25.33	0	0	1.57	0.044	0.12	0.092	15.14	26.03	0.0024	0.64	0.0018	0.0012	0.038	0.0012	0.014	0.017	0.0096	0.023
Nd146	28.12	32.41	0.00001	0	1.14	0.056	0.043	0.28	0.6	0.097	0.0069	0.78	0.0032	0.0055	0.0079	0.0053	0.021	0.0098	0.0059	0.0078
Hf178	30.98	36.28	0.00001	0	0.23	0.014	0.019	0.0033	0.1	0.019	0.0041	0.12	0.0024	0.0032	0.0052	0.0049	0.0087	0.0099	0.012	0.0042
W182	19.55	20.59	0.00001	0	0.033	0.03	0.16	0.0081	0.44	0.0091	0.0065	0.62	0.0035	0.0042	0.012	0.0066	0.73	0.022	0.011	0.62
Re185	2.49	2.66	0.00001	0	0.01	0.013	0.022	0.003	0.066	0.0034	0.0035	0.0042	0.0019	0.0025	0.0032	0.003	0.0043	0.0041	0.0018	0.0025
Re187	2.15	2.23	0.00014	0.00001	0.0057	0.007	0.0089	0.0017	0.04	0.0024	0.002	0.0044	0.00087	0.0016	0.002	0.002	0.0036	0.0026	0.00097	0.0015
Os189	<0.00	<0.00	<0.00	<0.00	<0.00	<0.00	<0.00	<0.00	<0.00	<0.00	<0.00	<0.00	<0.00	<0.00	<0.00	<0.00	<0.00	<0.00	<0.00	<0.00
Os190	<0.00	<0.00	<0.00	<0.00	<0.00	<0.00	<0.00	<0.00	<0.00	<0.00	<0.00	<0.00	<0.00	<0.00	<0.00	<0.00	<0.00	<0.00	<0.00	<0.00
Ir193	<0.00	<0.00	<0.00	<0.00	<0.00	<0.00	<0.00	<0.00	<0.00	<0.00	<0.00	<0.00	<0.00	<0.00	<0.00	<0.00	<0.00	<0.00	<0.00	<0.00
Pt195	<0.00	<0.00	<0.00	<0.00	<0.00	<0.00	<0.00	<0.00	<0.00	<0.00	<0.00	<0.00	<0.00	<0.00	<0.00	<0.00	<0.00	<0.00	<0.00	<0.00
Au197	1.1	1.11	0.02	0.0014	0.018	0.017	0.031	0.045	1.56	0.012	0.016	0.036	0.0032	2.28	0.015	0.012	0.015	0.016	0.2	0.41
Pb208	25.94	25.63	0.0026	0.00022	0.45	4.17	68.36	16.86	1258.91	2.23	0.43	2.91	0.19	27.3	53.1	3.37	9.45	130.44	103.99	42.71
Bi209	25.98	27.15	0.017	0.0016	0.036	0.37	0.33	8.67	23.72	0.21	0.041	2.51	0.035	0.088	3.45	1.17	0.49	1.64	1.42	1.11
Th232	35.95	41.36	0	0	0.28	0.0074	0.017	0.0016	0.082	0.0047	0.0019	0.1	0.0013	0.0017	0.0024	0.0022	0.012	0.0068	0.0031	0.0068
U238	28.42	30.2	0	0	0.069	0.025	0.17	0.0033	0.49	0.0037	0.0019	0.1	0.00094	0.002	0.04	0.0015	0.015	0.77	0.007	0.014
ThO248	<0.00	<0.00	<0.00	<0.00	<0.00	<0.00	<0.00	<0.00	<0.00	<0.00	<0.00	<0.00	<0.00	<0.00	<0.00	<0.00	<0.00	<0.00	<0.00	<0.00
GLITTER!: Minimum detection limits (99% confidence).																				
Element	STD610-3	STD610-4	PGEA-3	PGEA-4	BCR2G-1	BG01-CPY	BG01-PY2	BG13-PY	BG13-SPH	BG13-SP2	JL04-PY	JL04-CPY	BG33-SPH	BG33-PY	BG19-PY	BG05-PY1	BG05-SP2	BG14-CPY	KP10-PY	BG34-PY
Al27	0.223	0.385	0.0001	0.00002	2.03	0.19	0.208	0.0384	0.927	0.0658	0.0499	0.0678	0.0317	0.0403	0.0385	0.0465	0.0782	0.0866	0.0283	0.0265

RUN5

Element	STD610-3	STD610-4	PGEA-3	PGEA-4	BCR2G-1	BG01-CPY	BG01-PY2	BG13-PY	BG13-SPH	BG13-SP2	JL04-PY	JL04-CPY	BG33-SPH	BG33-PY	BG19-PY	BG05-PY1	BG05-SP2	BG14-CPY	KP10-PY	BG34-PY
Si29	145.3	173.07	0.0555	0.0116	83.59	103.67	128.19	23.69	540.45	37.8	28.32	40.57	13.99	22.69	23.11	27.31	45.43	34.48	15.73	16.45
S34	<0.00000	<0.00000	<0.00000	<0.00000	<0.00000	<0.00000	<0.00000	<0.00000	<0.00000	<0.00000	<0.00000	<0.00000	<0.00000	<0.00000	<0.00000	<0.00000	<0.00000	<0.00000	<0.00000	<0.00000
Ca43	64.87	76.16	0.0232	0.00489	49.74	48.03	55.59	10.21	283.24	18.48	12.61	18.05	6.36	10.23	10.46	13.21	19.9	17.12	8.88	7.96
Sc45	0.0992	0.112	0.00004	0.00001	0.0646	0.0658	0.0809	0.016	0.367	0.0233	0.0183	0.0268	0.00919	0.0157	0.0151	0.0184	0.0311	0.0231	0.00992	0.0105
Ti49	0.844	1.11	0.00034	0.00006	2.82	0.452	0.77	0.0951	3.05	0.261	0.171	0.252	0.106	0.146	0.156	0.171	0.255	0.237	0.0907	0.0956
V51	0.0809	0.103	0.00003	0.00001	0.125	0.0564	0.0759	0.0136	0.269	0.0203	0.0164	0.0228	0.00868	0.0147	0.0126	0.0141	0.0248	0.0196	0.00795	0.00865
Cr53	3.5	4.14	0.00137	0.00028	1.87	2.41	3.12	0.574	13.07	0.881	0.713	1.01	0.341	0.568	0.58	0.658	1.1	0.847	0.385	0.407
Mn55	0.47	0.53	0.00017	0.00004	0.342	0.315	0.382	0.0716	1.62	0.118	0.0858	0.126	0.0435	0.0725	0.0714	0.0838	0.141	0.108	0.0483	0.049
Fe57	12.29	14.06	0.00466	0.00096	14.94	8.32	13.04	2.05	62.99	4.76	2.43	3.99	1.2	2.2	2.44	3.52	4.4	3.07	1.32	1.38
Co59	0.0547	0.0621	0.00002	0	0.0464	0.0335	0.0407	0.00849	0.197	0.0134	0.00919	0.0169	0.00525	0.00878	0.00845	0.0105	0.0144	0.0109	0.00587	0.00548
Ni60	0.279	0.473	0.00011	0.00029	0.14	0.151	0.194	0.09	0.908	0.0599	0.0624	0.073	0.0422	0.0507	0.0448	0.0515	0.078	0.062	0.0727	0.0264
Ni62	1.15	2.1	0.00038	0.0008	0.465	0.771	1.79	0.209	3.96	0.276	0.195	0.409	0.112	0.324	0.175	0.243	0.978	0.321	0.149	0.133
Cu65	0.495	0.564	0.00019	0.00004	0.294	0.356	3	0.103	2.22	0.139	0.106	0.155	0.145	0.0873	0.0877	0.104	0.232	0.462	0.0635	0.0646
Zn66	0.473	0.572	0.00021	0.00004	0.343	0.393	0.55	0.102	1.93	3.05	0.364	0.367	0.103	2.49	0.28	0.207	0.629	0.235	0.096	0.0988
Ga71	0.0684	0.0898	0.00003	0	0.058	0.0313	0.0518	0.00992	0.268	0.0145	0.0105	0.0151	0.00516	0.0109	0.0112	0.00972	0.0208	0.0148	0.00745	0.00556
As75	7.26	8.77	0.0029	0.0006	3.93	5.02	6.33	1.14	26.74	1.84	1.37	2.01	0.692	1.11	1.2	1.45	2.36	1.83	0.789	0.873
Se82	5.86	7.34	0.00233	0.00048	3.14	4.27	5.55	0.959	22.4	1.55	1.23	1.76	0.583	0.998	0.993	1.17	1.98	1.49	0.687	0.696
Y89	0.014	0.0338	0.00001	0	0.0386	0.013	0.00938	0.0022	0.0396	0.00205	0.00232	0.00466	0.00219	0.00234	0.00269	0.00329	0.0047	0.00354	0.00239	0.00188
Zr90	0.0394	0.0532	0.00001	0	0.0938	0.0279	0.0264	0.0062	0.125	0.00999	0.00534	0.011	0.00356	0.00465	0.00479	0.00708	0.0105	0.00706	0.00318	0.00335
Nb93	0.0187	0.0462	0.00001	0	0.0206	0.0116	0.0162	0.00311	0.075	0.00501	0.00254	0.00456	0.00211	0.00339	0.00263	0.00416	0.0068	0.00336	0.00196	0.00206
Mo95	0.115	0.154	0.00003	0.00001	0.177	0.0649	0.0813	0.0121	0.301	0.022	0.0194	0.028	0.00784	0.0143	0.0132	0.0195	0.0315	0.0257	<0.00000	0.0122
Ru99	<0.00000	<0.00000	<0.00000	<0.00000	<0.00000	<0.00000	<0.00000	<0.00000	<0.00000	<0.00000	<0.00000	<0.00000	<0.00000	<0.00000	<0.00000	<0.00000	<0.00000	<0.00000	<0.00000	<0.00000
Ru101	<0.00	<0.00	<0.00	<0.00	<0.00	<0.00	<0.00	<0.00	<0.00	<0.00	<0.00	<0.00	<0.00	<0.00	<0.00	<0.00	<0.00	<0.00	<0.00	<0.00
Rh103	<0.00000	<0.00000	<0.00000	<0.00000	<0.00000	<0.00000	<0.00000	<0.00000	<0.00000	<0.00000	<0.00000	<0.00000	<0.00000	<0.00000	<0.00000	<0.00000	<0.00000	<0.00000	<0.00000	<0.00000
Ag107	0.0841	0.088	0.00003	0.00001	0.0482	0.0582	0.0515	0.0117	0.292	0.0159	0.0132	0.0192	0.00717	0.0128	0.0145	0.0175	0.0163	0.0246	0.0092	0.00717
Pd108	<0.00000	<0.00000	<0.00000	<0.00000	<0.00000	<0.00000	<0.00000	<0.00000	<0.00000	<0.00000	<0.00000	<0.00000	<0.00000	<0.00000	<0.00000	<0.00000	<0.00000	<0.00000	<0.00000	<0.00000
Cd111	0.716	0.865	0.00024	0.00004	0.345	0.543	0.547	0.0998	2.57	0.194	0.133	0.179	0.0598	0.23	0.112	0.134	0.254	0.139	0.0595	0.0754
In115	0.0188	0.0455	0.00001	0	0.00966	0.0111	0.0212	0.00405	0.12	0.00488	0.00427	0.00355	0.00194	0.00315	0.0029	0.00458	0.00633	0.00641	0.00289	0.00268
Sn118	0.343	0.39	0.00013	0.00003	0.183	0.239	0.295	0.0585	1.28	0.0852	0.0667	0.0991	0.032	0.058	0.0537	0.0613	0.0929	0.0786	0.0365	0.038
Sb121	0.235	0.346	0.0001	0.00002	0.122	0.146	0.244	0.0383	1.09	0.085	0.0569	0.0859	0.0283	0.0541	0.0517	0.0578	0.114	0.0869	0.0281	0.0341
Te125	<0.00000	<0.00000	<0.00000	<0.00000	<0.00000	<0.00000	<0.00000	<0.00000	<0.00000	<0.00000	<0.00000	<0.00000	<0.00000	<0.00000	<0.00000	<0.00000	<0.00000	<0.00000	<0.00000	<0.00000
Te128	<0.00000	<0.00000	<0.00000	<0.00000	<0.00000	<0.00000	<0.00000	<0.00000	<0.00000	<0.00000	<0.00000	<0.00000	<0.00000	<0.00000	<0.00000	<0.00000	<0.00000	<0.00000	<0.00000	<0.00000
La139	0.0178	0.0439	0.00001	0	0.0212	0.0114	0.0157	0.00274	0.0541	0.00343	0.00224	0.00402	0.00186	0.00731	0.00164	0.00259	0.00453	0.00382	0.00133	0.00182
Ce140	0.00666	0.0301	0.00001	0	0.0442	0.0143	0.00894	0.00171	0.0702	0.0123	0.00338	0.00344	0.00183	0.00273	0.00162	0.00222	0.00501	0.00447	0.00241	0.00179
Nd146	0.059	0.123	0.00003	0	0.0704	<0.00000	0.0723	0.0138	0.304	0.0281	0.0131	0.0176	0.00792	0.0114	0.0117	0.0131	0.0162	0.0122	0.0103	0.00821
Hf178	0.058	0.0949	0.00003	0	0.0384	0.0311	0.0503	0.00745	0.164	0.012	0.00908	0.0158	0.00698	0.0097	0.00911	0.0144	0.0178	0.012	0.00605	0.00638
W182	0.0924	0.0832	0.00004	0.00001	0.053	<0.00000	0.0506	0.0168	0.242	0.0177	0.0145	0.0205	0.00545	0.0115	0.00918	0.0145	0.0207	0.0156	0.00787	0.00982
Re185	0.0445	0.049	0.00002	0	0.0275	0.0364	0.0545	0.00738	0.174	0.009	0.00778	0.0121	0.0049	0.00679	0.00826	0.00781	0.0061	0.0113	0.00415	0.00536
Re187	0.0263	0.0411	0.00001	0	0.0138	0.0141	0.0228	0.00391	0.0838	0.00613	0.00461	0.00849	0.00154	0.00402	0.00523	0.00507	0.00626	0.00668	0.00213	0.00317
Os189	<0.00	<0.00	<0.00	<0.00	<0.00	<0.00	<0.00	<0.00	<0.00	<0.00	<0.00	<0.00	<0.00	<0.00	<0.00	<0.00	<0.00	<0.00	<0.00	<0.00
Os190	<0.00	<0.00	<0.00	<0.00	<0.00	<0.00	<0.00	<0.00	<0.00	<0.00	<0.00	<0.00	<0.00	<0.00	<0.00	<0.00	<0.00	<0.00	<0.00	<0.00
Ir193	<0.00000	<0.00000	<0.00000	<0.00000	<0.00000	<0.00000	<0.00000	<0.00000	<0.00000	<0.00000	<0.00000	<0.00000	<0.00000	<0.00000	<0.00000	<0.00000	<0.00000	<0.00000	<0.00000	<0.00000
Pt195	<0.00000	<0.00000	<0.00000	<0.00000	<0.00000	<0.00000	<0.00000	<0.00000	<0.00000	<0.00000	<0.00000	<0.00000	<0.00000	<0.00000	<0.00000	<0.00000	<0.00000	<0.00000	<0.00000	<0.00000
Au197	0.0697	0.0421	0.00003	0.00001	0.0245	0.0187	0.0702	0.00896	0.165	0.017	0.0164	0.0147	0.00927	0.0101	0.0104	0.0157	0.0166	0.0198	0.00488	0.00785
Pb208	0.281	0.131	0.00004	0.00001	0.0708	0.0745	0.0829	0.0148	0.331	0.0336	0.0188	0.0277	0.00565	0.0119	0.015	0.0137	0.0355	0.0268	0.0106	0.0872
Bi209	0.292	0.264	0.00007	0.00001	0.0862	0.0944	0.121	0.0211	0.535	0.0311	0.0239	0.0343	0.0123	0.0585	0.0182	0.0202	0.0331	0.0263	0.0108	0.0119
Th232	0.0272	0.0496	0.00001	0	0.0257	0.011	0.0323	0.00373	0.0808	0.0066	0.00197	0.0081	0.00298	0.0042	0.00306	0.00592	0.0069	0.0026	0.00287	0.00303
U238	0.0237	0.0553	0.00001	0	0.0178	0.0118	0.0225	0.00632	0.0606	0.00957	0.00455	0.00535	0.00223	0.00498	0.00437	0.00173	0.00427	0.00455	0.00251	0.00216
ThO248	<0.00	<0.00	<0.00	<0.00	<0.00	<0.00	<0.00	<0.00	<0.00	<0.00	<0.00	<0.00	<0.00	<0.00	<0.00	<0.00	<0.00	<0.00	<0.00	<0.00
GLITTER!: Trace element concentrations normalised to chondrite.																				
Element	STD610-3	STD610-4	PGEA-3	PGEA-4	BCR2G-1	BG01-CPY	BG01-PY2	BG13-PY	BG13-SPH	BG13-SP2	JL04-PY	JL04-CPY	BG33-SPH	BG33-PY	BG19-PY	BG05-PY1	BG05-SP2	BG14-CPY	KP10-PY	BG34-PY
Al27	0.751	0.846	0	0	3.74	0.01067	0.0664	0.00076	0.444	0.00145	0.00019	0.617	0.00012	0.00011	0.0521	0.00001	0.0216	0.00677	0.00899	0.01414
Si29	2.06	2.24	0	0	1.026	0.00933	0.029	0.00329	14.24	0.00148	0.00155	0.253	0.0008	0	0.0272	0.00035	0.1208	0.0186	0.0158	0.0046
S34	<****	<****	<****	<****	<****	<****	<****	<****	<****	<****	<****	<****	<****	<****	<****	<****	<****	<****	<****	<****
Ca43	6.04	6.71	0	0	2.38	0.0531	0.0534	0.00479	0.84	0	0.00194	3.78	0.0111	0.001	0.0186	0	1.83	0.0724	0.0036	0.0318
Sc45	51.1	57.73	0	0	2.34	0	0.0193	0	0.713	0	0	0.417	0	0	0.00699	0	0.0065	0.0244	0.0114	0.00294

RUN5

Element	STD610-3	STD610-4	PGEA-3	PGEA-4	BCR2G-1	BG01-CPY	BG01-PY2	BG13-PY	BG13-SPH	BG13-SP2	JL04-PY	JL04-CPY	BG33-SPH	BG33-PY	BG19-PY	BG05-PY1	BG05-SP2	BG14-CPY	KP10-PY	BG34-PY
Ti49	0.7	0.791	0	0	13.01	0.0434	0.0408	0.1049	0.265	0.0503	0.00585	7.13	0.00158	0.00234	0.01054	0.00226	0.0173	0.0338	0.00564	0.1288
V51	5.31	5.34	0	0	2.89	0.0241	0.0668	0.0055	0.0248	0.00139	0.00202	0.716	0	0.00019	0.00732	0	0.0287	0.0816	0.01623	0.0215
Cr53	0.0963	0.0973	0	0	0.00179	0.00221	0.00121	0.00098	0	0	0	0.01447	0	0	0.00118	0	0	0.00207	0.0007	0.00131
Mn55	0.1446	0.1472	0	0	0.317	0.01155	0.0261	0.00594	2.38	0.353	0.00048	0.39	0.192	0.00022	0.02321	0.00005	0.257	0.106	0.00752	0.1348
Fe57	0.00163	0.00163	0	0	0.1996	1.095	1.095	1.675	36.66	0.0484	1.675	1.095	0.067	1.675	1.675	1.675	1.095	1.095	1.675	1.675
Co59	0.499	0.499	0	0	0.0286	0.00068	0.00182	0.00099	0.00111	0.00023	0.0002	0.00052	0.00012	0.00006	0.451	0.01768	0.0415	0.00952	0.00322	0.00328
Ni60	0.0245	0.0244	0.0103	0.00258	0.00046	0.00024	0.00026	0.00008	0.00103	0.00002	0.00003	0.00013	0.00001	0	0.00023	0.00066	0.00042	0.00022	0.0002	0.00001
Ni62	0.0241	0.0249	0.0105	0.0026	0.00047	0.00015	0	0.00016	0.00118	0	0.00004	0.00005	0.00057	0.00017	0.00019	0.00065	0.00029	0.00026	0.00014	0.00003
Cu65	2.54	2.49	0.00063	0.00016	0.0676	2920.68	2915.1	0.1956	1.111	0.431	0.0112	2345.83	0.138	12.41	0.454	0.01153	2266.79	2704.75	0.541	1.501
Zn66	1.036	0.824	0	0	0.176	7.04	4.3	0.1087	1449.93	1449.93	0.0173	3.66	1224.18	0.491	5	0.0354	9.44	11.22	2.03	0.0733
Ga71	27.61	27.21	0	0	0.839	0.0262	0.0912	0.024	0.346	0.254	0.00143	0.272	0.627	0.0276	0.018	0	0.0348	0.0461	0.01117	0.0088
As75	109.04	109.66	0.0136	0.00341	0	0	0	185.23	709.09	0.81	135.88	4.13	0	2962.95	248.45	52.69	19.36	11.27	1222.34	5151.03
Se82	3.91	4.27	0.00178	0.00042	0	0.177	0	0.161	1.07	0	3.17	6.21	0	0	1.136	1.91	1.82	1.413	0.576	0.252
Y89	206.88	240.51	0	0	9.14	0.534	0.0753	0.0294	0.672	0.398	0.00385	3.46	0.00126	0	0.0784	0.0073	0.1011	1.055	0.139	0.207
Zr90	83.74	96.69	0	0	20.61	0.716	0.238	0.0554	0.84	0.277	0.006	6.88	0	0.00092	0.0694	0	0.0212	0.299	0.559	0.117
Nb93	1292.92	1439.52	0	0	20.53	0.418	2.24	0.0157	4.91	0.0341	0.0363	27.63	0	0	0.255	0	0.113	0.0371	0.655	0.65
Mo95	279.72	286.79	0	0	97.14	0.51	0.684	1.104	69.59	0.201	0	0.24	0.0563	0.0163	0.418	0.519	0.168	0.596	0.968	0.456
Ru99	0	0	0	0	0	0	0	0	0	0	0	0	0	0	0	0	0	0	0	0
Ru101	<****	<****	<****	<****	<****	<****	<****	<****	<****	<****	<****	<****	<****	<****	<****	<****	<****	<****	<****	<****
Rh103	0	0	0	0	0	0	0	0	0	0	0	0	0	0	0	0	0	0	0	0
Ag107	647.67	673.65	0.299	0.074	0.69	83.95	163.59	31.88	396.38	8.83	1.6	106.96	7.74	71.68	15.98	2.12	1612.96	1054.49	104.61	362.72
Pd108	0	0	0	0	0	0	0	0	0	0	0	0	0	0	0	0	0	0	0	0
Cd111	261.01	233.52	0.0231	0.00582	0	12.32	27.96	0.436	40.66	1946.33	0	12.22	1805.46	3.62	6.33	0	43.09	31.19	6.07	0.333
In115	3531.35	3507.92	0	0	0.578	97.73	83.68	0	6.82	1.28	0	73.46	4.21	0.994	0.454	0	22.17	78.24	2.64	0.304
Sn118	147.7	146.64	0.00021	0.00007	0.444	1.45	0.644	0.096	1.65	13.81	0.032	3.43	0.222	0.045	0.614	0.031	1.464	3.38	0.451	0.119
Sb121	1513.05	1568.47	0.00288	0.00053	2.88	9.9	26.35	6.91	667.56	8.55	1.64	8.99	2.62	95.02	54.28	3.26	69.98	27.78	23.35	2358.66
Te125	0	0	0	0	0	0	0	0	0	0	0	0	0	0	0	0	0	0	0	0
Te128	0	0	0	0	0	0	0	0	0	0	0	0	0	0	0	0	0	0	0	0
La139	1133.13	1296.21	0	0	40.79	1.28	7.02	1.86	65.09	2.55	0.0758	6.94	0	0	0.455	0.0272	0.184	0.234	0.1011	0.145
Ce140	443.66	483.18	0	0	32.08	0.726	2.21	1.838	147.36	253.92	0.0118	12.96	0.0112	0	0.732	0	0.181	0.293	0.17	0.443
Nd146	600.81	686.18	0	0.00001	24.81	0.657	0.18	6.05	5.46	1.04	0	16.68	0	0	0.048	0	0.14	0.061	0.0323	0.062
Hf178	2423.78	2816.08	0	0	17.26	0	0	0	1.16	0.65	0	8.32	0	0	0.094	0	0	0.318	0.699	0.082
W182	4792.38	4951.62	0	0	2.44	2.07	25.62	0.344	36.86	0.25	0	155.84	0.127	0	1.25	0	184.06	2.79	1.37	162.09
Re185	869.94	911.93	0	0	0	0	0	0	0	0	0	0	0	0	0	0	0	0	0	0
Re187	897.59	909.37	0.0104	0.00263	0	0	0	0	0	0	0	0	0.034	0	0	0	0	0	0	0
Os189	<****	<****	<****	<****	<****	<****	<****	<****	<****	<****	<****	<****	<****	<****	<****	<****	<****	<****	<****	<****
Os190	<****	<****	<****	<****	<****	<****	<****	<****	<****	<****	<****	<****	<****	<****	<****	<****	<****	<****	<****	<****
Ir193	0	0	0	0	0	0	0	0	0	0	0	0	0	0	0	0	0	0	0	0
Pt195	0	0	0	0	0	0	0	0	0	0	0	0	0	0	0	0	0	0	0	0
Au197	103.46	101.84	0.373	0.0928	0.418	0.287	0	4.05	79.66	0.291	0.638	1.7	0	240.91	0.866	0.281	0.294	0.673	20.9	42.39
Pb208	109.66	107.31	0.00297	0.00074	1.88	18.23	300.51	74.13	3399.47	6	1.86	12.71	0.515	120.04	233.53	14.76	41.49	573.72	457.39	187.85
Bi209	2075.41	2152.89	0.41	0.1056	0.68	29.38	25.6	712.34	1148.96	10.05	2.91	205.68	1.66	6.77	283.16	95.67	39.86	134.67	116.21	91.27
Th232	11442.86	13068.38	0	0.00005	90.9	0.52	1.14	0	9.57	0.51	0.127	31.2	0	0	0.261	0	2.06	1.4	0.571	1.63
U238	41065.49	43102.16	0	0	92.71	23.08	232.55	1.58	427.5	0	0	143.51	0	0	56.3	0.26	12.61	1172.57	8.25	17.81
ThO248	<****	<****	<****	<****	<****	<****	<****	<****	<****	<****	<****	<****	<****	<****	<****	<****	<****	<****	<****	<****

GLITTER4.0: Laser Ablation Ar																
G:\KYLIE\MAR13\RUN5																
Fri Mar 14 20:57:05 2003																
All values are reported in ppm																
								Modified								
GLITTER!: Trace Element Concentrations MDL filtered.	Run5-21	Run5-22	Run5-23	Run5-24	Run5-25	Run5-26	Run5-27	Run5-28	Run5-29	Run5-30	Run5-31	Run5-32	Run5-33	Run5-34	Run5-35	Run5-36
Element	BG34-SPH	BG34-CPY	BG34-PY2	BG35-PY	BG35-CPY	BG35-SPH	BG36-PY	BG37-PY	BG37-PY2	BG37-SPH	BG38-SPH	STD610-5	STD610-6	PGEA-5	PGEA-6	BCR2G-2
Al27	27.41	0.81	0.909	33.74	1307.32	0.235	9.12	18608.75	52.53	44.17	33.82	10929.28	9809.61	0.00441	<0.00018	46233.75
Si29	241.09	358.58	65.87	4025.44	3253.92	281.98	468.29	31765.6	1845.91	639.22	198.2	363137.41	322421.28	0.49	<0.043	154069.42
S34	<0.00	<0.00	<0.00	<0.00	<0.00	<0.00	<0.00	<0.00	<0.00	<0.00	<0.00	<0.00	<0.00	<0.00	<0.00	<0.00
Ca43	67.91	165.27	100.25	469.23	515.76	<18.01	219.97	743.76	175.56	68.94	119.62	88437.85	78485.84	0.228	<0.0233	30991.51
Sc45	<0.021	<0.0143	<0.0186	0.0902	0.252	0.0264	<0.0193	1.94	<0.0204	<0.0117	<0.0102	498.54	432.26	0.00065	<0.00003	19.73
Ti49	12.55	3.48	2.03	7.29	6.12	1.21	2.03	58	9.49	1.69	6.49	518.68	463.34	0.00543	<0.00036	8340.36
V51	0.298	0.0411	0.0216	0.313	7.92	0.0186	0.367	329.26	0.957	1.02	0.274	473.04	428.89	<0.00013	0.00003	248.21
Cr53	<0.78	<0.53	<0.68	2.92	8.29	<0.72	<0.68	180.01	0.83	1.26	1.6	415.16	382	<0.0060	<0.00105	7.5
Mn55	1383.77	375.4	4.69	926.58	33036.82	109.48	298.98	4448.68	166.68	1043.97	146.55	464.02	434.83	0.00082	<0.00013	908.39
Fe57	50950.53	304317.34	465531.69	465531.72	304317.34	21524.14	465531.69	465531.69	465531.72	44665.95	10563.54	453.1	453.1	0.078	0.0078	55500.02
Co59	22.22	0.205	39.38	275.69	0.187	0.486	0.773	0.671	6.31	1.098	<0.0068	415.19	385.31	0.00037	0.00014	22.09
Ni60	0.515	0.828	0.227	3.19	0.171	0.068	9.07	674.93	656.84	1.11	0.081	446.65	415.4	970.07	193.21	7.29
Ni62	<0.26	<0.166	0.53	2.82	0.157	<0.35	7.44	4.11	641.11	1.44	<0.127	442.16	417.81	985.42	198.28	6.15
Cu65	77.51	297166.56	<0.88	673.96	278398.09	382.01	165.21	556087.13	338.7	1069.02	11.52	457.89	433.31	0.653	0.12	11.85
Zn66	561879.31	29546.4	<0.90	725.08	14809.73	565572.38	3337.48	104865.52	10861.03	565572.38	565572.38	418.24	445.98	0.326	0.00268	84.45
Ga71	0.641	0.368	<0.0142	0.106	2.35	71.54	0.0323	39.59	0.436	1.37	4.62	461.72	434.62	<0.00011	<0.00002	12.9
As75	4.33	97.53	259.64	3180.75	33546.34	32.05	14.3	<2.34	325.39	16.19	<1.20	345.21	313.19	0.216	0.0449	<5.02
Se82	4.51	4.65	6.48	19.04	11.73	<1.24	44.86	47.27	33.33	4.33	0.99	123.92	109.22	0.28	0.057	<3.31
Y89	0.0051	0.0142	<0.0029	0.132	0.975	0.242	0.0608	0.582	0.117	0.37	0.0067	546.27	479.16	0.00008	<0.00000	22
Zr90	0.085	0.122	0.0378	0.186	0.441	0.0298	4.52	8.17	0.0436	0.182	0.0356	548.82	480.52	<0.00007	0.00001	119.01
Nb93	0.0055	0.0032	<0.0028	0.0132	0.0055	<0.0031	<0.0032	0.0069	0.0115	<0.0022	<0.0019	567.53	506.41	<0.00003	<0.00001	8.03
Mo95	0.302	0.078	0.042	0.184	43.36	0.552	36.66	0.692	0.153	0.24	0.37	427.62	391.92	0.00029	<0.00015	144.55
Ru99	<0.00	<0.00	<0.00	<0.00	<0.00	<0.00	<0.00	<0.00	<0.00	<0.00	<0.00	<0.00	<0.00	<0.00	<0.00	<0.00
Ru101	<-NaN	<-NaN	<-NaN	<-NaN	<-NaN	<-NaN	<-NaN	<-NaN	<-NaN	<-NaN	<-NaN	<-NaN	<-NaN	<-NaN	<-NaN	<-NaN
Rh103	<0.00	<0.00	<0.00	<0.00	<0.00	<0.00	<0.00	<0.00	<0.00	<0.00	<0.00	<0.00	<0.00	<0.00	<0.00	<0.00
Ag107	3.02	297.87	3.55	17.89	471.21	6.98	1.85	1596.3	5.48	12.55	2.92	286.18	271.23	0.59	0.114	0.171
Pd108	<0.00	<0.00	<0.00	<0.00	<0.00	<0.00	<0.00	<0.00	<0.00	<0.00	<0.00	<0.00	<0.00	<0.00	<0.00	<0.00
Cd111	1745.94	150.03	<0.177	5.69	54.54	2328.16	18.67	589.4	67.77	2525.59	2033.41	271.45	268.94	0.142	0.0265	<0.37
In115	6.24	3.66	<0.0052	0.368	9.72	<0.0041	0.975	13.87	2.53	17.64	0.008	487.12	461.81	<0.00006	<0.00001	0.062
Sn118	0.2	1.97	<0.062	0.818	1.96	0.198	0.483	24.84	0.657	1.95	0.624	414.6	403.69	0.00361	0.00063	1.12
Sb121	0.46	22.3	0.52	3.71	379.53	314.04	10.91	3.53	6.17	2.04	1.21	435.55	424.42	0.00364	0.00086	0.555
Te125	<0.00	<0.00	<0.00	<0.00	<0.00	<0.00	<0.00	<0.00	<0.00	<0.00	<0.00	<0.00	<0.00	<0.00	<0.00	<0.00
Te128	<0.00	<0.00	<0.00	<0.00	<0.00	<0.00	<0.00	<0.00	<0.00	<0.00	<0.00	<0.00	<0.00	<0.00	<0.00	<0.00
La139	<0.0036	0.0071	<0.0028	0.0207	0.1246	0.0026	0.0186	0.0822	0.0157	0.0443	<0.00186	487.84	433.64	<0.00002	<0.00001	15.61
Ce140	0.0065	0.0189	<0.0024	1.07	0.463	<0.0033	0.0553	0.0552	0.0697	0.096	<0.00182	479.69	444.1	<0.00003	0.00001	31.67
Nd146	0.054	<0.0085	<0.0173	0.0125	0.39	<0.0168	<0.0157	0.0187	<0.0191	<0.0115	<0.0093	499.23	449.89	<0.00011	<0.00002	18.67
Hf178	<0.0171	<0.0084	<0.0130	<0.0065	<0.0054	<0.0126	0.138	0.218	0.0289	0.0148	<0.0096	511.88	448.54	<0.00006	<0.00002	3.24
W182	0.104	0.0413	<0.0143	0.182	1.769	<0.0149	0.0171	0.041	0.063	0.28	0.0294	461.63	427.89	<0.00013	<0.00003	0.295
Re185	0.0105	<0.0079	<0.0092	<0.0050	0.005	<0.0101	0.0161	<0.0094	<0.0086	<0.0056	<0.0058	53.8	49.78	<0.00009	<0.00001	<0.0200
Re187	<0.0065	<0.0052	<0.0055	0.1548	<0.0031	<0.0047	0.0118	<0.0051	<0.0079	<0.0039	<0.0041	52.64	49.17	0.003	0.0006	0.0161
Os189	<-NaN	<-NaN	<-NaN	<-NaN	<-NaN	<-NaN	<-NaN	<-NaN	<-NaN	<-NaN	<-NaN	<-NaN	<-NaN	<-NaN	<-NaN	<-NaN
Os190	<-NaN	<-NaN	<-NaN	<-NaN	<-NaN	<-NaN	<-NaN	<-NaN	<-NaN	<-NaN	<-NaN	<-NaN	<-NaN	<-NaN	<-NaN	<-NaN
Ir193	<0.00	<0.00	<0.00	<0.00	<0.00	<0.00	<0.00	<0.00	<0.00	<0.00	<0.00	<0.00	<0.00	<0.00	<0.00	<0.00
Pt195	<0.00	<0.00	<0.00	<0.00	<0.00	<0.00	<0.00	<0.00	<0.00	<0.00	<0.00	<0.00	<0.00	<0.00	<0.00	<0.00
Au197	<0.0179	0.099	0.043	2.5	34.94	<0.0166	0.407	0.051	0.339	0.0241	0.0099	23.51	23.15	0.453	0.088	0.078
Pb208	11.13	26.74	114.56	1082.91	235.94	91.36	656.05	107.91	978.29	30.71	3.79	450.79	435.76	0.0613	0.0126	6.4
Bi209	3.16	3.22	77.75	91.34	18.14	0.101	6.85	3.37	9.49	1.08	0.246	414.95	390.15	0.385	0.075	0.226
Th232	0.0085	<0.0056	<0.0056	0.0349	0.182	<0.0046	0.0334	0.424	<0.0065	0.0074	0.0047	515.15	457.15	<0.00004	<0.00001	3.7
U238	0.0185	<0.0037	<0.0032	0.0303	46.93	0.0253	0.365	2.32	0.0199	0.109	0.0428	503.82	467.09	<0.00005	<0.00001	1.082
ThO248	<-NaN	<-NaN	<-NaN	<-NaN	<-NaN	<-NaN	<-NaN	<-NaN	<-NaN	<-NaN	<-NaN	<-NaN	<-NaN	<-NaN	<-NaN	<-NaN

Element	BG34-SPH	BG34-CPY	BG34-PY2	BG35-PY	BG35-CPY	BG35-SPH	BG36-PY	BG37-PY	BG37-PY2	BG37-SPH	BG38-SPH	STD610-5	STD610-6	PGEA-5	PGEA-6	BCR2G-2
GLITTER!: 1 sigma error.																
Element	BG34-SPH	BG34-CPY	BG34-PY2	BG35-PY	BG35-CPY	BG35-SPH	BG36-PY	BG37-PY	BG37-PY2	BG37-SPH	BG38-SPH	STD610-5	STD610-6	PGEA-5	PGEA-6	BCR2G-2
Al27	2.94	0.055	0.067	2.03	78.65	0.036	0.55	1119.5	3.17	4.73	3.62	687.93	608.58	0.00056	0.00037	2781.76
Si29	28.62	26.11	13.2	274.12	221.58	30.81	33.79	2161.85	126.35	64.26	21.2	25609.22	22477.83	0.1	0.037	10485.72
S34	<0.00	<0.00	<0.00	<0.00	<0.00	<0.00	<0.00	<0.00	<0.00	<0.00	<0.00	<0.00	<0.00	<0.00	<0.00	<0.00
Ca43	11.46	12.55	11.7	30.74	33.45	7.5	16.88	49.41	14.72	9.07	14.24	5807.94	5085.22	0.05	0.0093	1955.17
Sc45	0.011	0.006	0.0085	0.0085	0.019	0.0093	0.0079	0.13	0.0082	0.0052	0.0048	34.98	29.97	0.00011	0.00001	1.34
Ti49	1.53	0.26	0.21	0.47	0.4	0.19	0.19	3.6	0.64	0.23	0.79	33.31	29.31	0.00096	0.00015	508.57
V51	0.03	0.0061	0.0074	0.017	0.38	0.0076	0.022	15.87	0.051	0.087	0.025	24.43	21.68	0.00005	0.00001	11.97
Cr53	0.38	0.22	0.3	0.21	0.4	0.3	0.27	7.83	0.29	0.21	0.24	19.76	17.68	0.0022	0.00042	0.84
Mn55	126.55	15.88	0.21	39.18	1396.96	10.02	12.65	188.12	7.05	95.48	13.4	21.44	19.55	0.00029	0.00005	38.43
Fe57	3782.52	9623.86	14722.49	14721.73	9623.64	1597.98	14722.01	14722.05	14722.05	3315.81	784.3	18.6	17.31	0.011	0.0021	1756.76
Co59	1.97	0.013	1.72	11.97	0.01	0.046	0.039	0.034	0.28	0.099	0.0033	19.61	17.73	0.00006	0.00003	0.97
Ni60	0.071	0.055	0.036	0.16	0.017	0.025	0.44	31.62	30.78	0.11	0.021	22.58	20.51	107.6	37.41	0.4
Ni62	0.12	0.08	0.13	0.2	0.055	0.13	0.47	0.33	30.42	0.2	0.068	23.04	21.2	109.48	38.42	0.58
Cu65	6.53	12959.59	0.67	29.4	12141	32.08	7.23	24251.19	14.82	89.73	0.98	21.8	20.09	0.072	0.023	0.59
Zn66	17768.47	2606.83	0.65	63.99	1306.64	17885.14	294.48	9252.07	958.27	17885.08	17885.11	37.84	40.02	0.044	0.00059	7.52
Ga71	0.068	0.024	0.0057	0.0088	0.11	6.46	0.0088	1.87	0.029	0.13	0.42	23.36	21.5	0.00005	0.00001	0.63
As75	1.04	7.84	20.82	254.48	2683.86	3.31	1.45	0.93	26.07	1.67	0.55	28.74	25.77	0.028	0.0093	2.02
Se82	0.89	0.53	0.78	1.34	0.84	0.53	3.11	3.28	2.36	0.63	0.34	9.29	8.02	0.034	0.011	1.3
Y89	0.0023	0.0026	0.0018	0.01	0.068	0.03	0.0059	0.042	0.01	0.045	0.0017	38.83	33.67	0.00002	0	1.52
Zr90	0.015	0.012	0.0076	0.015	0.032	0.0069	0.31	0.56	0.007	0.024	0.0069	38.98	33.75	0.00003	0.00001	8.17
Nb93	0.0025	0.0014	0.0014	0.0018	0.0012	0.0013	0.0014	0.0025	0.0024	0.0012	0.0011	36.21	31.86	0.00001	0	0.5
Mo95	0.044	0.012	0.015	0.016	1.98	0.064	1.68	0.047	0.019	0.029	0.044	21.07	18.84	0.00008	0.00012	6.62
Ru99	<0.00	<0.00	<0.00	<0.00	<0.00	<0.00	<0.00	<0.00	<0.00	<0.00	<0.00	<0.00	<0.00	<0.00	<0.00	<0.00
Ru101	<0.00	<0.00	<0.00	<0.00	<0.00	<0.00	<0.00	<0.00	<0.00	<0.00	<0.00	<0.00	<0.00	<0.00	<0.00	<0.00
Rh103	<0.00	<0.00	<0.00	<0.00	<0.00	<0.00	<0.00	<0.00	<0.00	<0.00	<0.00	<0.00	<0.00	<0.00	<0.00	<0.00
Ag107	0.52	37.32	0.45	2.24	59.04	1.19	0.24	200.01	0.69	2.13	0.5	36.26	34.25	0.095	0.026	0.035
Pd108	<0.00	<0.00	<0.00	<0.00	<0.00	<0.00	<0.00	<0.00	<0.00	<0.00	<0.00	<0.00	<0.00	<0.00	<0.00	<0.00
Cd111	117.47	9.59	0.082	0.39	3.5	156.56	1.25	37.56	4.37	169.81	136.74	18.25	17.8	0.017	0.0053	0.15
In115	0.72	0.27	0.0021	0.028	0.72	0.002	0.074	1.02	0.19	2.03	0.0027	36.95	34.68	0.00002	0	0.01
Sn118	0.045	0.12	0.03	0.053	0.11	0.037	0.043	1.4	0.054	0.2	0.07	24.43	23.38	0.00048	0.00013	0.11
Sb121	0.081	2.18	0.065	0.36	36.98	45.36	1.07	0.35	0.61	0.3	0.18	43.22	41.87	0.00056	0.00019	0.092
Te125	<0.00	<0.00	<0.00	<0.00	<0.00	<0.00	<0.00	<0.00	<0.00	<0.00	<0.00	<0.00	<0.00	<0.00	<0.00	<0.00
Te128	<0.00	<0.00	<0.00	<0.00	<0.00	<0.00	<0.00	<0.00	<0.00	<0.00	<0.00	<0.00	<0.00	<0.00	<0.00	<0.00
La139	0.002	0.0018	0.0013	0.0023	0.009	0.0013	0.0027	0.0075	0.0027	0.0062	0.00099	32.9	28.88	0.00001	0	1.02
Ce140	0.0023	0.0025	0.0015	0.056	0.025	0.0016	0.0049	0.005	0.0058	0.011	0.00092	26.07	23.66	0.00001	0	1.62
Nd146	0.016	0.0047	0.0069	0.0048	0.029	0.0075	0.0071	0.0061	0.0072	0.0055	0.0057	32.98	29.33	0.00005	0.00001	1.21
Hf178	0.006	0.0041	0.0053	0.003	0.0026	0.0056	0.015	0.022	0.0065	0.0051	0.004	36.67	31.77	0.00003	0.00001	0.24
W182	0.021	0.0085	0.005	0.014	0.081	0.006	0.0077	0.011	0.011	0.031	0.0077	21.32	19.22	0.00005	0.00001	0.036
Re185	0.0059	0.0032	0.0043	0.002	0.0018	0.0037	0.0046	0.0037	0.0037	0.0022	0.0024	2.82	2.55	0.00003	0.00001	0.0099
Re187	0.0026	0.002	0.0023	0.0087	0.0015	0.0018	0.0033	0.0021	0.0027	0.0015	0.0023	2.31	2.09	0.00034	0.00012	0.0065
Os189	<0.00	<0.00	<0.00	<0.00	<0.00	<0.00	<0.00	<0.00	<0.00	<0.00	<0.00	<0.00	<0.00	<0.00	<0.00	<0.00
Os190	<0.00	<0.00	<0.00	<0.00	<0.00	<0.00	<0.00	<0.00	<0.00	<0.00	<0.00	<0.00	<0.00	<0.00	<0.00	<0.00
Ir193	<0.00	<0.00	<0.00	<0.00	<0.00	<0.00	<0.00	<0.00	<0.00	<0.00	<0.00	<0.00	<0.00	<0.00	<0.00	<0.00
Pt195	<0.00	<0.00	<0.00	<0.00	<0.00	<0.00	<0.00	<0.00	<0.00	<0.00	<0.00	<0.00	<0.00	<0.00	<0.00	<0.00
Au197	0.01	0.011	0.01	0.11	1.52	0.0065	0.027	0.0088	0.025	0.0058	0.005	1.16	1.1	0.05	0.017	0.018
Pb208	1.14	1.67	7.15	67.45	14.7	9.27	40.87	6.73	60.94	3.12	0.39	29.33	27.96	0.0073	0.0025	0.42
Bi209	0.39	0.24	5.67	6.65	1.32	0.017	0.5	0.25	0.7	0.14	0.033	31.2	29.04	0.048	0.015	0.031
Th232	0.0036	0.002	0.0026	0.004	0.014	0.002	0.005	0.033	0.0024	0.0022	0.0023	38.2	33.55	0.00002	0	0.27
U238	0.0045	0.0015	0.002	0.0031	2.53	0.0043	0.023	0.13	0.0037	0.011	0.0058	28.73	26.17	0.00002	0	0.067
ThO248	<0.00	<0.00	<0.00	<0.00	<0.00	<0.00	<0.00	<0.00	<0.00	<0.00	<0.00	<0.00	<0.00	<0.00	<0.00	<0.00
GLITTER!: Minimum detection limits (99% confidence).																
Element	BG34-SPH	BG34-CPY	BG34-PY2	BG35-PY	BG35-CPY	BG35-SPH	BG36-PY	BG37-PY	BG37-PY2	BG37-SPH	BG38-SPH	STD610-5	STD610-6	PGEA-5	PGEA-6	BCR2G-2
Al27	0.0515	0.0358	0.0453	0.0247	0.0213	0.0518	0.0463	0.0481	0.19	0.0276	0.0334	0.939	0.507	0.0005	0.00018	0.13

RUN5

Element	BG34-SPH	BG34-CPY	BG34-PY2	BG35-PY	BG35-CPY	BG35-SPH	BG36-PY	BG37-PY	BG37-PY2	BG37-SPH	BG38-SPH	STD610-5	STD610-6	PGEA-5	PGEA-6	BCR2G-2
Si29	31.39	21.37	27.16	15.26	11.81	28.36	26.72	28.97	27.7	15.16	15.69	141.91	108.72	0.225	0.0429	68.89
S34	<0.00000	<0.00000	<0.00000	<0.00000	<0.00000	<0.00000	<0.00000	<0.00000	<0.00000	<0.00000	<0.00000	<0.00000	<0.00000	<0.00000	<0.00000	<0.00000
Ca43	13.83	9.25	15.83	7.76	6.12	18.01	15.6	17.57	17.27	9.34	8.72	80.72	64.13	0.103	0.0233	33.31
Sc45	0.0211	0.0143	0.0186	0.0103	0.0073	0.019	0.0193	0.0216	0.0204	0.0117	0.0102	0.0785	0.116	0.00017	0.00003	0.0509
Ti49	0.191	0.166	0.165	0.0826	0.0901	0.174	0.187	0.16	0.183	0.108	0.123	0.783	0.775	0.0015	0.00036	0.499
V51	0.0142	0.0112	0.0139	0.00864	0.00664	0.016	0.0165	0.0153	0.0233	0.00853	0.00944	0.0949	0.0904	0.00013	0.00003	0.0471
Cr53	0.776	0.528	0.68	0.375	0.294	0.716	0.684	0.747	0.708	0.386	0.398	3.59	2.79	0.00602	0.00105	1.8
Mn55	0.0971	0.0744	0.0854	0.047	0.103	0.117	0.0862	0.0895	0.14	0.0492	0.0536	0.442	0.363	0.00073	0.00013	0.226
Fe57	5.24	2.33	3.75	1.41	2.64	2.65	2.68	3.71	6.37	2.14	1.64	13.19	9.45	0.0197	0.00353	6.01
Co59	0.0135	0.0113	0.00863	0.00535	0.00389	0.0116	0.0208	0.0128	0.0127	0.00588	0.00683	0.0655	0.0824	0.00008	0.00002	0.0264
Ni60	0.0555	0.0409	0.0464	0.0291	0.0214	0.0482	0.0504	0.0583	0.0474	0.0379	0.033	0.252	0.244	0.00034	0.00198	0.157
Ni62	0.26	0.166	0.127	0.137	0.111	0.346	0.21	0.337	0.235	0.151	0.127	1.27	0.79	0.0024	0.0051	0.477
Cu65	0.116	0.0811	0.877	0.126	0.0759	0.494	0.116	0.139	2.21	0.0888	0.071	0.616	0.512	0.0009	0.00017	0.263
Zn66	0.188	2.51	0.9	0.38	0.117	0.211	2.04	0.249	1.76	0.432	1.12	3.01	1.22	0.00207	0.00034	0.577
Ga71	0.0088	0.0103	0.0142	0.00564	0.00579	0.0115	0.0175	0.0145	0.0152	0.0059	0.00784	0.0639	0.118	0.00011	0.00002	0.0376
As75	1.97	1.36	1.73	0.99	0.777	2.38	2.22	2.34	2.2	1.17	1.2	10.64	8.17	0.0168	0.00301	5.02
Se82	1.34	0.937	1.22	0.669	0.509	1.24	1.22	1.3	1.2	0.706	0.667	6.28	5.12	0.00982	0.00179	3.31
Y89	0.00264	0.00364	0.0029	0.0022	0.0017	0.00315	0.00204	0.00362	0.00469	0.00221	0.00086	0.025	0.0649	0.00004	0	0.0102
Zr90	0.00859	0.0057	0.00765	0.0038	0.00505	0.00795	0.00952	0.00658	0.00934	0.00407	0.00568	0.0406	0.0956	0.00007	0.00001	0.023
Nb93	0.00289	0.00271	0.00275	0.00148	0.00164	0.00308	0.00315	0.00486	0.00281	0.00223	0.00188	0.0177	0.0705	0.00003	0.00001	0.0073
Mo95	0.0201	0.0111	0.0225	0.0154	0.00822	0.0227	0.0158	0.0162	0.0182	0.011	0.0153	0.105	0.182	0.00014	0.00015	0.0422
Ru99	<0.00000	<0.00000	<0.00000	<0.00000	<0.00000	<0.00000	<0.00000	<0.00000	<0.00000	<0.00000	<0.00000	<0.00000	<0.00000	<0.00000	<0.00000	<0.00000
Ru101	<0.00	<0.00	<0.00	<0.00	<0.00	<0.00	<0.00	<0.00	<0.00	<0.00	<0.00	<0.00	<0.00	<0.00	<0.00	<0.00
Rh103	<0.00000	<0.00000	<0.00000	<0.00000	<0.00000	<0.00000	<0.00000	<0.00000	<0.00000	<0.00000	<0.00000	<0.00000	<0.00000	<0.00000	<0.00000	<0.00000
Ag107	0.0176	0.0105	0.0285	0.00857	0.011	0.0184	0.0142	0.0178	0.093	0.00917	0.00668	0.0868	0.108	0.00022	0.00005	0.0443
Pd108	<0.00000	<0.00000	<0.00000	<0.00000	<0.00000	<0.00000	<0.00000	<0.00000	<0.00000	<0.00000	<0.00000	<0.00000	<0.00000	<0.00000	<0.00000	<0.00000
Cd111	0.177	0.196	0.177	0.0548	0.066	0.125	0.224	0.132	0.239	0.079	0.196	0.821	0.648	0.00116	0.00021	0.37
In115	0.00575	0.00365	0.00525	0.00572	0.00181	0.00412	0.00347	0.00563	0.00669	0.00222	0.00397	0.0358	0.0647	0.00006	0.00001	0.0123
Sn118	0.0706	0.0501	0.0623	0.0404	0.0273	0.0624	0.0614	0.0687	0.0707	0.0384	0.0387	0.341	0.271	0.00049	0.0001	0.164
Sb121	0.0674	0.0455	0.0562	0.03	0.0274	0.0585	0.0882	0.0831	0.0889	0.0497	0.0491	0.39	0.332	0.00048	0.0001	0.156
Te125	<0.00000	<0.00000	<0.00000	<0.00000	<0.00000	<0.00000	<0.00000	<0.00000	<0.00000	<0.00000	<0.00000	<0.00000	<0.00000	<0.00000	<0.00000	<0.00000
Te128	<0.00000	<0.00000	<0.00000	<0.00000	<0.00000	<0.00000	<0.00000	<0.00000	<0.00000	<0.00000	<0.00000	<0.00000	<0.00000	<0.00000	<0.00000	<0.00000
La139	0.00361	0.00309	0.0028	0.00184	0.00173	0.00193	0.00197	0.00494	0.0032	0.0018	0.00186	0.0121	0.0666	0.00002	0.00001	0.00982
Ce140	0.00204	0.00273	0.0024	0.00166	0.00171	0.00327	0.00238	0.00244	0.00245	0.00137	0.00182	0.0168	0.0614	0.00003	0	0.0082
Nd146	0.0148	0.00853	0.0173	0.00931	0.00618	0.0168	0.0157	0.00721	0.0191	0.0115	0.00933	0.093	0.167	0.00011	0.00002	0.0375
Hf178	0.0171	0.00839	0.013	0.00647	0.00543	0.0126	0.00976	0.0123	0.00711	0.00746	0.00963	0.0423	0.142	0.00006	0.00002	0.0291
W182	0.0186	0.0126	0.0143	0.0109	0.00612	0.0149	0.0156	0.0195	0.0131	0.0036	0.00742	0.0711	0.135	0.00013	0.00003	0.0294
Re185	0.00866	0.00788	0.00924	0.00496	0.00294	0.0101	0.00748	0.00941	0.00861	0.0056	0.00577	0.0592	0.0553	0.00009	0.00001	0.02
Re187	0.00645	0.00516	0.00547	0.00318	0.00315	0.00472	0.00587	0.00509	0.00791	0.00395	0.00407	0.0272	0.0351	0.00005	0.00001	0.0118
Os189	<0.00	<0.00	<0.00	<0.00	<0.00	<0.00	<0.00	<0.00	<0.00	<0.00	<0.00	<0.00	<0.00	<0.00	<0.00	<0.00
Os190	<0.00	<0.00	<0.00	<0.00	<0.00	<0.00	<0.00	<0.00	<0.00	<0.00	<0.00	<0.00	<0.00	<0.00	<0.00	<0.00
Ir193	<0.00000	<0.00000	<0.00000	<0.00000	<0.00000	<0.00000	<0.00000	<0.00000	<0.00000	<0.00000	<0.00000	<0.00000	<0.00000	<0.00000	<0.00000	<0.00000
Pt195	<0.00000	<0.00000	<0.00000	<0.00000	<0.00000	<0.00000	<0.00000	<0.00000	<0.00000	<0.00000	<0.00000	<0.00000	<0.00000	<0.00000	<0.00000	<0.00000
Au197	0.0179	0.00943	0.0114	0.00727	0.00748	0.0166	0.0114	0.0104	0.0148	0.00694	0.00826	0.0623	0.0724	0.00014	0.00005	0.0235
Pb208	0.0289	0.0146	0.0175	0.00665	0.0921	0.0199	0.018	0.0224	0.0179	0.0137	0.0115	0.0987	0.137	0.00017	0.00004	0.048
Bi209	0.034	0.0152	0.0211	0.0106	0.0401	0.0209	0.0182	0.0193	0.017	0.0112	0.0109	0.107	0.103	0.00016	0.00004	0.0477
Th232	0.0044	0.00556	0.00564	0.00362	0.00263	0.00455	0.0056	0.00575	0.00654	0.00295	0.00372	0.0318	0.0824	0.00004	0.00001	0.0179
U238	0.0033	0.00367	0.00323	0.00245	0.00218	0.00305	0.00453	0.006	0.00539	0.00255	0.00372	0.0245	0.0694	0.00005	0.00001	0.0148
ThO248	<0.00	<0.00	<0.00	<0.00	<0.00	<0.00	<0.00	<0.00	<0.00	<0.00	<0.00	<0.00	<0.00	<0.00	<0.00	<0.00
GLITTER!: Trace element concentrations normalised to chondrite.																
Element	BG34-SPH	BG34-CPY	BG34-PY2	BG35-PY	BG35-CPY	BG35-SPH	BG36-PY	BG37-PY	BG37-PY2	BG37-SPH	BG38-SPH	STD610-5	STD610-6	PGEA-5	PGEA-6	BCR2G-2
Al27	0.00212	0.00006	0.00007	0.00262	0.1013	0.00002	0.00071	1.443	0.00407	0.00342	0.00262	0.847	0.76	0	0	3.58
Si29	0.00151	0.00224	0.00041	0.0252	0.0203	0.00176	0.00293	0.199	0.01154	0.004	0.00124	2.27	2.02	0	0	0.963
S34	<****	<****	<****	<****	<****	<****	<****	<****	<****	<****	<****	<****	<****	<****	<****	<****
Ca43	0.00503	0.01224	0.00743	0.0348	0.0382	0	0.0163	0.0551	0.013	0.00511	0.0089	6.55	5.81	0.00002	0	2.3
Sc45	0	0	0	0.01044	0.0292	0.0031	0	0.224	0	0	0	57.7	50.03	0.00007	0	2.28

RUN5

Element	BG34-SPH	BG34-CPY	BG34-PY2	BG35-PY	BG35-CPY	BG35-SPH	BG36-PY	BG37-PY	BG37-PY2	BG37-SPH	BG38-SPH	STD610-5	STD610-6	PGEA-5	PGEA-6	BCR2G-2
Ti49	0.0192	0.00531	0.00311	0.01115	0.00935	0.00185	0.00311	0.0887	0.01452	0.00259	0.0099	0.793	0.708	0.00001	0	12.75
V51	0.0035	0.00048	0.00025	0.00368	0.0932	0.00022	0.00432	3.87	0.01126	0.012	0.00322	5.57	5.05	0	0	2.92
Cr53	0	0	0	0.00073	0.00208	0	0	0.0453	0.00021	0.00032	0.0004	0.1044	0.0961	0	0	0.00189
Mn55	0.471	0.1277	0.0016	0.315	11.24	0.0372	0.1017	1.513	0.0567	0.355	0.0498	0.1578	0.1479	0	0	0.309
Fe57	0.183	1.095	1.675	1.675	1.095	0.0774	1.675	1.675	1.675	0.161	0.038	0.00163	0.00163	0	0	0.1996
Co59	0.0291	0.00027	0.0515	0.361	0.00024	0.00064	0.00101	0.00088	0.00826	0.00144	0	0.543	0.504	0	0	0.0289
Ni60	0.00003	0.00005	0.00001	0.00019	0.00001	0	0.00055	0.0409	0.0398	0.00007	0	0.0271	0.0252	0.0588	0.0117	0.00044
Ni62	0	0	0.00003	0.00017	0.00001	0	0.00045	0.00025	0.0389	0.00009	0	0.0268	0.0253	0.0597	0.012	0.00037
Cu65	0.461	1768.85	0	4.01	1657.13	2.27	0.983	3310.04	2.016	6.36	0.0685	2.73	2.58	0.00389	0.00071	0.0706
Zn66	1216.19	63.95	0	1.57	32.06	1224.18	7.22	226.98	23.51	1224.18	1224.18	0.905	0.965	0.0007	0.00001	0.183
Ga71	0.0422	0.0242	0	0.00698	0.1545	4.71	0.00212	2.6	0.0287	0.0899	0.304	30.38	28.59	0	0	0.849
As75	1.51	33.98	90.47	1108.28	11688.62	11.17	4.98	0	113.38	5.64	0	120.28	109.12	0.0752	0.0157	0
Se82	0.165	0.17	0.237	0.697	0.43	0	1.64	1.73	1.221	0.159	0.036	4.54	4	0.0103	0.00209	0
Y89	0.0023	0.0063	0	0.0587	0.433	0.107	0.027	0.259	0.0519	0.164	0.00296	242.79	212.96	0.00004	0	9.78
Zr90	0.0154	0.0221	0.0068	0.0335	0.0795	0.0054	0.817	1.47	0.0079	0.0328	0.0064	99.06	86.74	0	0	21.48
Nb93	0.0148	0.0084	0	0.0352	0.0148	0	0	0.0185	0.0306	0	0	1513.41	1350.42	0	0	21.41
Mo95	0.219	0.0564	0.031	0.134	31.42	0.4	26.57	0.501	0.111	0.174	0.268	309.87	284	0.00021	0	104.75
Ru99	0	0	0	0	0	0	0	0	0	0	0	0	0	0	0	0
Ru101	<****	<****	<****	<****	<****	<****	<****	<****	<****	<****	<****	<****	<****	<****	<****	<****
Rh103	0	0	0	0	0	0	0	0	0	0	0	0	0	0	0	0
Ag107	9.16	902.64	10.77	54.21	1427.9	21.17	5.6	4837.26	16.62	38.04	8.85	867.2	821.9	1.79	0.346	0.52
Pd108	0	0	0	0	0	0	0	0	0	0	0	0	0	0	0	0
Cd111	1728.65	148.54	0	5.63	54	2305.11	18.49	583.57	67.1	2500.59	2013.27	268.76	266.27	0.141	0.0263	0
In115	53.31	31.32	0	3.14	83.04	0	8.34	118.51	21.61	150.76	0.069	4163.42	3947.13	0	0	0.532
Sn118	0.079	0.783	0	0.325	0.778	0.079	0.192	9.86	0.261	0.774	0.248	164.52	160.19	0.00143	0.00025	0.446
Sb121	1.97	95.71	2.23	15.93	1628.89	1347.83	46.83	15.14	26.49	8.74	5.19	1869.32	1821.56	0.0156	0.00369	2.38
Te125	0	0	0	0	0	0	0	0	0	0	0	0	0	0	0	0
Te128	0	0	0	0	0	0	0	0	0	0	0	0	0	0	0	0
La139	0	0.0193	0	0.0565	0.339	0.007	0.0507	0.224	0.0428	0.121	0	1329.27	1181.59	0	0	42.54
Ce140	0.0068	0.0197	0	1.118	0.484	0	0.0578	0.0577	0.0729	0.1	0	501.24	464.05	0	0.00001	33.09
Nd146	0.076	0	0	0.0175	0.548	0	0	0.0263	0	0	0	702.15	632.75	0	0	26.25
Hf178	0	0	0	0	0	0	0.773	1.22	0.161	0.083	0	2859.69	2505.84	0	0	18.08
W182	1.17	0.465	0	2.04	19.87	0	0.192	0.47	0.71	3.15	0.33	5186.9	4807.72	0	0	3.31
Re185	0.19	0	0	0	0.091	0	0.292	0	0	0	0	978.09	905.08	0	0	0
Re187	0	0	0	2.82	0	0	0.215	0	0	0	0	957.06	894.06	0.0546	0.0108	0.29
Os189	<****	<****	<****	<****	<****	<****	<****	<****	<****	<****	<****	<****	<****	<****	<****	<****
Os190	<****	<****	<****	<****	<****	<****	<****	<****	<****	<****	<****	<****	<****	<****	<****	<****
Ir193	0	0	0	0	0	0	0	0	0	0	0	0	0	0	0	0
Pt195	0	0	0	0	0	0	0	0	0	0	0	0	0	0	0	0
Au197	0	0.456	0.197	11.47	160.29	0	1.87	0.234	1.55	0.111	0.046	107.83	106.17	2.08	0.406	0.356
Pb208	3.05	7.33	31.39	296.69	64.64	25.03	179.74	29.56	268.02	8.41	1.04	123.5	119.39	0.0168	0.00345	1.75
Bi209	18.93	19.29	465.56	546.93	108.63	0.6	40.99	20.19	56.86	6.49	1.47	2484.72	2336.25	2.31	0.448	1.35
Th232	0.2	0	0	0.821	4.27	0	0.79	9.97	0	0.174	0.112	12121.08	10756.47	0	0	87.16
U238	1.51	0	0	2.49	3846.74	2.07	29.96	190.53	1.63	8.97	3.51	41297.07	38285.91	0	0	88.69
ThO248	<****	<****	<****	<****	<****	<****	<****	<****	<****	<****	<****	<****	<****	<****	<****	<****

GLITTER4.0: Laser Ablation Analysis Results

G:\KYLIE\MAR14\RUN1 (really Run 6)
Fri Mar 14 19:44:52 2003

All values are reported in ppm

GLITTER!: Trace Element Concentrations MDL filtered.

	Run6-1	Run6-2	Run6-3	Run6-4	Run6-5	Run6-6	Run6-7	Run6-8	Run6-9	Run6-10	Discarded Run6-11	Run6-12	Run6-13	Run6-14	Run6-15	Run6-16	Run6-17	Run6-18	Run6-19	Run6-20	Run6-21	Run6-22
Element	STD610-1	STD610-2	BCRG-1	PGEA-1	PGEA-2	PGEA-3	PGEA-4	WG3-PY	WG3-PY2	WG3-SU1	WG3-PY3	WG3-PY4	WG3-PY5	WG3-PY6	WG3-PY7	WG3-PY8	STD610-3	STD610-4	BCRG-2	PGEA-5	PGEA-6	PGEA-7
Al27	10035.74	10613.06	44040.86	0.00165	0.00662	<0.00026	0.00081	707.09	2947.4	0.977	3006.39	8.95	71.07	2079.29	107.89	233.13	12667.72	9948.34	42481.82	<0.00004	0.0158	0.00014
Si29	336221.78	350056.53	148295.88	0.0445	0.078	0.26	0.0209	1365.78	4839.17	107.24	6866.77	61.52	389.97	4793.76	595.72	1251.63	428463.56	324579.19	141996.5	0.157	<0.089	0.0059
S34	<0.00	<0.00	<0.00	<0.00	<0.00	<0.00	<0.00	<0.00	<0.00	<0.00	<0.00	<0.00	<0.00	<0.00	<0.00	<0.00	<0.00	<0.00	<0.00	<0.00	<0.00	<0.00
Ca43	83394.59	88113.35	30356.11	<0.0070	<0.0064	<0.085	<0.0032	54.82	1359.16	<12.51	636.12	53.53	94.33	2274.99	286.46	150.7	105047.71	80947.26	29465.86	<0.0110	<0.035	0.00203
Sc45	448.24	466.84	18.33	<0.00001	<0.00001	<0.00011	<0.00000	0.0307	0.694	<0.0188	0.2338	0.0053	0.0076	1.839	0.0471	0.0291	564.7	437.09	17.72	<0.00002	<0.00006	<0.00000
Ti49	424.96	445.94	7107.81	0.00079	0.00056	<0.0011	0.00008	4.73	318.17	6.77	27.22	1.796	2.35	783.29	18.71	12.58	547.99	435.99	7095.59	0.00074	0.00088	0.00011
V51	439.59	464.73	234.5	0.00002	0.0001	<0.00010	0	3.38	31.54	0.29	26	4.11	2.94	14.82	4.26	5.8	585.99	440.44	236.31	<0.00002	0.0019	<0.00000
Cr53	403.68	428.08	9.11	<0.00038	<0.00043	<0.0044	<0.00016	5.12	47.31	<0.74	14.65	0.821	1.09	1.78	0.56	2.31	535.97	403.79	8.64	<0.00066	<0.0023	<0.00012
Mn55	429.7	453.99	918.06	<0.00006	0.00014	<0.0006	<0.00002	16.26	14.54	519.68	1386.72	1335.97	1428.94	59.17	16.95	1197.1	576.14	432.68	915.71	0.00214	<0.00031	<0.00002
Fe57	457.1	457.1	55500.02	0.0078	0.0078	<0.021	0.00777	465531.66	465531.66	1581.6	465531.66	465531.72	465531.66	465531.69	465531.69	465531.69	457.1	457.1	55500.02	0.0078	<0.0091	0.00777
Co59	398.11	412.61	23.06	0.00006	0.0001	0.00042	0.00001	0.633	48.3	0.384	969.78	1662.88	1521.81	274.59	199.9	2348.15	549.79	406.55	22.77	0.00015	0.00019	0.00001
Ni60	439.99	448.17	14.41	180.82	301.39	848.23	29.2	1.507	41.74	0.946	144.95	242.25	157.75	79.61	81.55	265.74	590.38	444.73	30.6	405.88	401.4	31.27
Ni62	437.52	455.23	15.18	184.86	310.4	865.2	29.56	1.57	43.35	0.79	140.12	242.45	157.55	80.07	79.89	267.37	600.06	445.02	184.54	422.98	392.69	32.22
Cu65	431.83	457.48	56.14	0.1	0.183	0.55	0.01792	90.31	560.47	112.14	14481.77	1331.79	1606.25	235.25	175.36	3951.72	584.3	427.72	14.3	0.266	0.24	0.0194
Zn66	434.09	438.34	130.74	0.00197	0.00201	0.0077	0.00418	33.44	1624.89	572172.13	4515.5	115.39	278.8	63.72	30.19	1871.39	622.76	467.69	387.14	0.00169	0.071	0.00798
Ga71	425.3	440.65	13.16	0.00001	<0.00000	<0.00010	<0.00000	0.144	1.4	0.941	0.697	0.0085	0.0366	0.553	0.148	0.1299	596.78	442.41	12.92	<0.00001	0.00011	0
As75	304.9	318.98	<3.55	0.0316	0.0562	0.17	0.00561	980.29	11296.96	2.95	1280.22	1071.35	1150.86	7311.97	10231.18	1837.84	427.03	323.41	<4.35	0.116	0.07	0.00586
Se82	106.01	123.38	<3.53	0.036	0.0659	0.2	0.00709	205.69	55.65	3.73	11.53	23.67	5.1	74.71	241.08	1.44	150.05	108.71	<3.28	0.104	0.094	0.00765
Y89	443.96	466.02	17.18	<0.00000	0	<0.00003	<0.00000	0.0663	1.478	0.0125	3.041	0.0566	0.0599	0.836	0.0159	0.292	577.69	450.38	17.76	0	<0.00001	<0.00000
Zr90	429.57	457.58	91.76	0.00003	<0.00000	<0.00004	<0.00000	0.0429	28.91	<0.0079	1.148	0.1068	0.0705	38.64	0.0352	0.532	569.04	441.85	96.03	0.00013	0.00004	0
Nb93	407.81	424.52	6.13	<0.00000	0.00001	<0.00002	<0.00000	0.0063	0.747	0.1207	0.1665	0.017	0.0083	2.417	0.0745	0.0266	546.92	422.98	6.56	<0.00000	<0.00001	0
Mo95	361.54	379.29	121	<0.00001	0.00011	<0.00011	0.00001	0.368	2.56	0.324	66.5	41.07	24.96	0.088	0.629	23.99	495.95	382.36	125.12	0.00005	<0.00006	0.00001
Ru99	<0.00	<0.00	<0.00	<0.00	<0.00	<0.00	<0.00	<0.00	<0.00	<0.00	<0.00	<0.00	<0.00	<0.00	<0.00	<0.00	<0.00	<0.00	<0.00	<0.00	<0.00	<0.00
Ru101	<-NaN	<-NaN	<-NaN	<-NaN	<-NaN	<-NaN	<-NaN	<-NaN	<-NaN	<-NaN	<-NaN	<-NaN	<-NaN	<-NaN	<-NaN	<-NaN	<-NaN	<-NaN	<-NaN	<-NaN	<-NaN	<-NaN
Rh103	<0.00	<0.00	<0.00	<0.00	<0.00	<0.00	<0.00	<0.00	<0.00	<0.00	<0.00	<0.00	<0.00	<0.00	<0.00	<0.00	<0.00	<0.00	<0.00	<0.00	<0.00	<0.00
Ag107	231.09	239.76	0.78	0.073	0.14	0.44	0.0146	0.947	7.69	2.179	36.64	0.0369	0.0204	1.849	1.389	0.1294	329.69	242.44	0.865	0.201	0.21	0.01739
Pd108	<0.00	<0.00	<0.00	<0.00	<0.00	<0.00	<0.00	<0.00	<0.00	<0.00	<0.00	<0.00	<0.00	<0.00	<0.00	<0.00	<0.00	<0.00	<0.00	<0.00	<0.00	<0.00
Cd111	243.86	245.83	0.32	0.016	0.0336	0.087	0.00269	0.189	21.74	1313.08	43.49	0.108	0.474	0.655	0.586	9.82	353.04	267.9	<0.32	0.064	0.039	0.00341
In115	423.55	438.39	0.092	<0.00000	<0.00000	0.00052	0	0.007	1.643	53.79	0.0435	0.00422	0.0021	0.33	0.0277	0.00488	595.61	448.6	0.25	0.00001	<0.00002	0
Sn118	378.95	419.16	1.63	0.00049	0.00081	0.0028	0.0001	0.138	4.45	45.46	0.863	0.0318	0.03	0.927	0.312	0.0483	524.1	400.98	1.53	0.00135	0.0015	0.00009
Sb121	354.98	355.03	0.709	0.00025	0.00048	0.0021	0.00007	64.12	318.55	0.419	41.54	1.046	4.09	62.13	17.86	11.35	502.17	375.37	0.741	0.00071	0.00123	0.00012
Te125	<0.00	<0.00	<0.00	<0.00	<0.00	<0.00	<0.00	<0.00	<0.00	<0.00	<0.00	<0.00	<0.00	<0.00	<0.00	<0.00	<0.00	<0.00	<0.00	<0.00	<0.00	<0.00
Te128	<0.00	<0.00	<0.00	<0.00	<0.00	<0.00	<0.00	<0.00	<0.00	<0.00	<0.00	<0.00	<0.00	<0.00	<0.00	<0.00	<0.00	<0.00	<0.00	<0.00	<0.00	<0.00
La139	448.48	464.69	14.42	<0.00000	0	<0.00001	0	0.0294	2.267	<0.0030	5.49	0.0143	0.312	0.55	0.0466	0.621	580.84	459.69	14.72	<0.00000	<0.00001	<0.00000
Ce140	436.49	453.79	29.35	<0.00000	0.00009	<0.00001	<0.00000	0.0542	3.94	0.0128	6.76	0.037	0.494	0.999	0.0679	1.285	573.79	451.14	30.14	0	<0.00001	0
Nd146	431.67	462.68	15.35	<0.00001	0.00002	<0.00012	<0.00000	0.0255	1.219	0.148	3.61	0.0264	0.1274	0.68	0.0221	0.617	552.01	428.14	15.81	0.00002	<0.00005	0.00001
Hf178	410.97	429.18	2.5	<0.00000	<0.00001	<0.00004	<0.00000	<0.0078	0.658	<0.0089	0.0274	<0.00231	0.0031	1.159	<0.0066	0.0125	528.23	418.85	2.43	<0.00001	<0.00004	<0.00000
W182	441.05	458.38	0.271	0.00001	<0.00001	<0.00014	0.00002	1.041	1.417	0.0256	52.21	91.91	20.14	0.188	0.104	2.936	579.23	445.46	0.26	<0.00002	<0.00006	<0.00000
Re185	101.31	105.03	<0.038	<0.00001	<0.00001	0.00008	0.00001	<0.0238	0.0326	<0.0164	0.284	0.574	0.602	<0.0104	0.114	0.274	136.54	104.4	<0.047	<0.00002	<0.00009	<0.00000
Re187	101.15	107.45	<0.027	0.00137	0.00162	0.0072	0.0002	<0.0105	0.0263	<0.0161	0.29	0.6	0.57	<0.0047	0.166	0.285	137.25	104.24	0.026	0.00278	0.0026	0.00022
Os189	<-NaN	<-NaN	<-NaN	<-NaN	<-NaN	<-NaN	<-NaN	<-NaN	<-NaN	<-NaN	<-NaN	<-NaN	<-NaN	<-NaN	<-NaN	<-NaN	<-NaN	<-NaN	<-NaN	<-NaN	<-NaN	<-NaN
Os190	<-NaN	<-NaN	<-NaN	<-NaN	<-NaN	<-NaN	<-NaN	<-NaN	<-NaN	<-NaN	<-NaN	<-NaN	<-NaN	<-NaN	<-NaN	<-NaN	<-NaN	<-NaN	<-NaN	<-NaN	<-NaN	<-NaN
Ir193	<0.00	<0.00	<0.00	<0.00	<0.00	<0.00	<0.00	<0.00	<0.00	<0.00	<0.00	<0.00	<0.00	<0.00	<0.00	<0.00	<0.00	<0.00	<0.00	<0.00	<0.00	<0.00
Pt195	<0.00	<0.00	<0.00	<0.00	<0.00	<0.00	<0.00	<0.00	<0.00	<0.00	<0.00	<0.00	<0.00	<0.00	<0.00	<0.00	<0.00	<0.00	<0.00	<0.00	<0.00	<0.00
Au197	22.86	23.85	0.141	0.0783	0.132	0.36	0.01206	5.46	3.63	0.066	297.49	0.466	0.17	7.06	2.065	0.605	30.13	22.29	0.282	0.164	0.165	0.01356
Pb208	418.07	431.4	26.53	0.00862	0.0154	0.044	0.00166	658.16	2438.54	20.67	26387.41	69.93	170.33	971.15	534.26	909.2	547.17	410.42	11.48	0.026	0.022	0.00185
Bi209	355.17	374.33	1.165	0.0497	0.093	0.28	0.00939	8.19	46.06	1.31	0.559	0.0363	0.1227	117.42	12.18	0.029	466.52	357.08	0.2	0.156	0.131	0.0107
Th232	491.49	513.31	3.36	<0.00000	<0.00000	<0.00003	<0.00000	0.0117	0.548	0.0041	2.22	0.0544	0.0204	0.313	0.0111	0.159	558.45	439.15	3.1	0.00001	<0.00001	<0.00000
U238	487.43	500.68	1.55	<0.00000	<0.00000	<0.00002	<0.00000	0.944	15.25	<0.0078	3.46	0.421	0.223	1.302	0.0289	1.935	574.93	447.62	1.447	<0.00000	<0.00001	<0.00000
ThO248	<-NaN	<-NaN	<-NaN	<-NaN	<-NaN	<-NaN	<-NaN	<-NaN	<-NaN	<-NaN	<-NaN	<-NaN	<-NaN	<-NaN	<-NaN	<-NaN	<-NaN	<-NaN	<-NaN	<-NaN	<-NaN	<-NaN

RUN6

Element	STD610-1	STD610-2	BCRG-1	PGEA-1	PGEA-2	PGEA-3	PGEA-4	WG3-PY	WG3-PY2	WG3-SU1	WG3-PY3	WG3-PY4	WG3-PY5	WG3-PY6	WG3-PY7	WG3-PY8	STD610-3	STD610-4	BCRG-2	PGEA-5	PGEA-6	PGEA-7
GLITTER!: 1 sigma error.																						
Element	STD610-1	STD610-2	BCRG-1	PGEA-1	PGEA-2	PGEA-3	PGEA-4	WG3-PY	WG3-PY2	WG3-SU1	WG3-PY3	WG3-PY4	WG3-PY5	WG3-PY6	WG3-PY7	WG3-PY8	STD610-3	STD610-4	BCRG-2	PGEA-5	PGEA-6	PGEA-7
Al27	449.35	529.8	1606.59	0.00019	0.00088	0.00018	0.00005	25.79	107.49	0.056	109.64	0.33	2.6	75.83	3.94	8.5	602.28	410.54	1549.72	0.00002	0.0089	0.00001
Si29	18929.05	21169.39	7408.45	0.009	0.014	0.28	0.0028	68.83	241.97	13.33	343.04	3.92	19.97	239.62	30.92	62.64	25075.91	17381.54	7093.79	0.031	0.055	0.0018
S34	<0.00	<0.00	<0.00	<0.00	<0.00	<0.00	<0.00	<0.00	<0.00	<0.00	<0.00	<0.00	<0.00	<0.00	<0.00	<0.00	<0.00	<0.00	<0.00	<0.00	<0.00	<0.00
Ca43	3866.85	4544.66	1163.12	0.0028	0.0032	0.033	0.0012	5.18	53.97	5.02	24.95	2.83	5	88.1	13.6	6.5	5145.84	3470.39	1129.32	0.005	0.018	0.00075
Sc45	19.87	23.15	0.67	0	0	0.00009	0	0.0062	0.028	0.007	0.0095	0.0015	0.0028	0.068	0.0064	0.0026	26.6	17.81	0.65	0.00001	0.00003	0
Ti49	18.62	22.38	238.51	0.00011	0.00011	0.001	0.00002	0.21	10.72	0.34	0.93	0.078	0.11	26.29	0.7	0.44	25.38	17.25	238.1	0.00017	0.00058	0.00001
V51	18.78	22.38	7.95	0	0.00002	0.00004	0	0.12	1.07	0.018	0.88	0.14	0.1	0.5	0.15	0.2	26.72	17.18	8.01	0.00001	0.0011	0
Cr53	17.81	21.46	0.73	0.00016	0.00019	0.0017	0.00006	0.27	1.66	0.28	0.52	0.068	0.11	0.14	0.19	0.11	25	16.18	0.76	0.00031	0.0015	0.00004
Mn55	18.4	21.9	31.16	0.00002	0.00003	0.001	0.00001	0.56	0.5	23.21	47.03	45.31	48.47	2.01	0.58	40.6	26.32	16.91	31.08	0.00039	0.00014	0.00001
Fe57	22.15	26.35	1756.4	0.0012	0.0014	0.011	0.00051	14721.74	14721.83	68.82	14721.54	14721.53	14721.65	14721.69	14721.9	14721.54	24.45	19.1	1756.42	0.0019	0.0062	0.00041
Co59	16.93	19.81	0.79	0.00001	0.00002	0.00043	0	0.025	1.62	0.02	32.52	55.77	51.04	9.21	6.71	78.75	24.96	15.76	0.78	0.00003	0.00011	0
Ni60	18.59	21.54	0.53	20.07	39.69	874.26	1.53	0.065	1.39	0.06	4.75	7.94	5.18	2.62	2.69	8.71	26.6	17.03	1.07	72.06	225.18	1.38
Ni62	19.92	24.16	0.86	20.57	40.95	891.77	1.56	0.13	1.59	0.14	4.75	8.18	5.37	2.78	2.84	9.02	28.51	18.1	6.62	75.16	220.31	1.44
Cu65	19.79	23.44	2.15	0.011	0.024	0.57	0.00099	3.37	20.86	5.64	538.63	49.54	59.75	8.76	6.54	146.98	28.29	18.05	0.59	0.047	0.13	0.00093
Zn66	26.89	29.15	7.33	0.00025	0.0003	0.0079	0.00029	1.88	89.97	18093.81	249.94	6.4	15.45	3.55	1.71	103.59	39.68	27.63	21.53	0.00035	0.04	0.00051
Ga71	18.74	21.79	0.49	0	0	0.00004	0	0.011	0.058	0.044	0.027	0.0015	0.0042	0.025	0.013	0.007	27.93	17.87	0.48	0	0.00007	0
As75	24.26	26.56	1.34	0.0041	0.0083	0.17	0.00049	72.42	834.42	0.65	94.56	79.13	85.01	540.08	755.7	135.75	34.62	25.06	1.7	0.022	0.04	0.00048
Se82	7.8	10	1.32	0.0043	0.0092	0.2	0.0005	11.01	3.04	0.65	0.65	1.29	0.36	4.03	12.92	0.16	10.56	7.18	1.3	0.019	0.053	0.00049
Y89	18.5	21.99	0.57	0	0	0.00002	0	0.0037	0.051	0.0022	0.1	0.0025	0.0032	0.029	0.0021	0.01	25.77	17.05	0.59	0	0.00001	0
Zr90	18.56	22.24	3.17	0.00001	0	0.00003	0	0.0044	1	0.0027	0.041	0.0049	0.0046	1.33	0.0045	0.02	26.19	17.45	3.32	0.00003	0.00003	0
Nb93	17.59	20.59	0.22	0	0	0.00001	0	0.0011	0.028	0.0069	0.0065	0.0011	0.001	0.085	0.0047	0.0015	25.15	16.69	0.23	0	0.00001	0
Mo95	17.01	19.84	4.73	0	0.00002	0.00011	0	0.023	0.11	0.025	2.58	1.6	0.98	0.0094	0.037	0.93	24.59	16.65	4.89	0.00002	0.00003	0
Ru99	<0.00	<0.00	<0.00	<0.00	<0.00	<0.00	<0.00	<0.00	<0.00	<0.00	<0.00	<0.00	<0.00	<0.00	<0.00	<0.00	<0.00	<0.00	<0.00	<0.00	<0.00	<0.00
Ru101	<0.00	<0.00	<0.00	<0.00	<0.00	<0.00	<0.00	<0.00	<0.00	<0.00	<0.00	<0.00	<0.00	<0.00	<0.00	<0.00	<0.00	<0.00	<0.00	<0.00	<0.00	<0.00
Rh103	<0.00	<0.00	<0.00	<0.00	<0.00	<0.00	<0.00	<0.00	<0.00	<0.00	<0.00	<0.00	<0.00	<0.00	<0.00	<0.00	<0.00	<0.00	<0.00	<0.00	<0.00	<0.00
Ag107	10.79	12.47	0.053	0.0082	0.019	0.45	0.00082	0.043	0.3	0.087	1.41	0.0037	0.0036	0.077	0.063	0.0074	16.23	10.46	0.057	0.036	0.12	0.00084
Pd108	<0.00	<0.00	<0.00	<0.00	<0.00	<0.00	<0.00	<0.00	<0.00	<0.00	<0.00	<0.00	<0.00	<0.00	<0.00	<0.00	<0.00	<0.00	<0.00	<0.00	<0.00	<0.00
Cd111	15.7	17.17	0.12	0.0019	0.0047	0.09	0.0002	0.04	1.28	42.02	2.48	0.019	0.048	0.063	0.075	0.57	23.2	16.36	0.13	0.012	0.022	0.00023
In115	20.1	22.98	0.01	0	0	0.00054	0	0.0017	0.068	1.72	0.0026	0.00069	0.0009	0.015	0.0032	0.00085	29.82	19.8	0.018	0	0.00001	0
Sn118	18.7	22.74	0.12	0.00006	0.00012	0.0029	0.00001	0.024	0.2	1.72	0.04	0.0074	0.012	0.047	0.031	0.0088	27.14	18.46	0.11	0.00025	0.00086	0.00001
Sb121	17.8	19.54	0.061	0.00003	0.00007	0.0022	0.00001	2.74	13.57	0.031	1.77	0.047	0.18	2.65	0.77	0.49	26.39	17.61	0.061	0.00014	0.0007	0.00001
Te125	<0.00	<0.00	<0.00	<0.00	<0.00	<0.00	<0.00	<0.00	<0.00	<0.00	<0.00	<0.00	<0.00	<0.00	<0.00	<0.00	<0.00	<0.00	<0.00	<0.00	<0.00	<0.00
Te128	<0.00	<0.00	<0.00	<0.00	<0.00	<0.00	<0.00	<0.00	<0.00	<0.00	<0.00	<0.00	<0.00	<0.00	<0.00	<0.00	<0.00	<0.00	<0.00	<0.00	<0.00	<0.00
La139	18.75	21.99	0.48	0	0	0.00001	0	0.0024	0.077	0.0013	0.18	0.0011	0.012	0.02	0.0037	0.021	25.99	17.47	0.49	0	0.00001	0
Ce140	18.61	21.81	1	0	0.00001	0.00001	0	0.0034	0.14	0.0022	0.23	0.0019	0.018	0.036	0.0047	0.044	26.12	17.55	1.03	0	0.00001	0
Nd146	19.1	22.99	0.58	0	0.00001	0.00007	0	0.0065	0.055	0.017	0.13	0.003	0.0095	0.031	0.0064	0.026	25.93	17.37	0.6	0.00001	0.00003	0
Hf178	17.12	20.31	0.11	0	0	0.00003	0	0.0029	0.029	0.0035	0.0026	0.00094	0.0015	0.043	0.0026	0.0017	23.55	15.82	0.1	0	0.00002	0
W182	18.4	21.75	0.032	0	0.00001	0.0001	0	0.043	0.058	0.0082	1.69	2.97	0.66	0.013	0.012	0.099	25.84	16.84	0.034	0.00001	0.00003	0
Re185	4.6	5.43	0.018	0	0	0.0001	0	0.0079	0.0067	0.0064	0.014	0.024	0.029	0.0036	0.013	0.014	6.52	4.31	0.02	0.00001	0.00005	0
Re187	4.62	5.53	0.012	0.00016	0.00022	0.0074	0.00001	0.0044	0.005	0.0056	0.013	0.024	0.026	0.0018	0.013	0.013	6.61	4.36	0.011	0.0005	0.0015	0.00001
Os189	<0.00	<0.00	<0.00	<0.00	<0.00	<0.00	<0.00	<0.00	<0.00	<0.00	<0.00	<0.00	<0.00	<0.00	<0.00	<0.00	<0.00	<0.00	<0.00	<0.00	<0.00	<0.00
Os190	<0.00	<0.00	<0.00	<0.00	<0.00	<0.00	<0.00	<0.00	<0.00	<0.00	<0.00	<0.00	<0.00	<0.00	<0.00	<0.00	<0.00	<0.00	<0.00	<0.00	<0.00	<0.00
Ir193	<0.00	<0.00	<0.00	<0.00	<0.00	<0.00	<0.00	<0.00	<0.00	<0.00	<0.00	<0.00	<0.00	<0.00	<0.00	<0.00	<0.00	<0.00	<0.00	<0.00	<0.00	<0.00
Pt195	<0.00	<0.00	<0.00	<0.00	<0.00	<0.00	<0.00	<0.00	<0.00	<0.00	<0.00	<0.00	<0.00	<0.00	<0.00	<0.00	<0.00	<0.00	<0.00	<0.00	<0.00	<0.00
Au197	1.22	1.45	0.021	0.009	0.018	0.37	0.00071	0.24	0.16	0.01	12.6	0.022	0.011	0.3	0.097	0.028	1.65	1.09	0.03	0.029	0.093	0.0007
Pb208	18.29	21.23	0.96	0.00097	0.002	0.046	0.00009	23	85.19	1.05	921.7	2.45	5.96	33.93	18.67	31.76	25.46	16.44	0.43	0.0046	0.012	0.00009
Bi209	15.31	18.17	0.056	0.0055	0.012	0.28	0.0005	0.28	1.58	0.064	0.021	0.0026	0.0068	4.02	0.42	0.0026	21.43	14.07	0.022	0.028	0.074	0.00049
Th232	32.27	35.58	0.21	0	0	0.00003	0	0.0023	0.035	0.0019	0.13	0.0039	0.0022	0.02	0.0021	0.01	37.74	27.8	0.19	0	0.00001	0
U238	27.54	30.39	0.085	0	0	0.00001	0	0.049	0.77	0.0032	0.17	0.022	0.012	0.067	0.0034	0.098	33.75	24.05	0.08	0	0	0
ThO248	<0.00	<0.00	<0.00	<0.00	<0.00	<0.00	<0.00	<0.00	<0.00	<0.00	<0.00	<0.00	<0.00	<0.00	<0.00	<0.00	<0.00	<0.00	<0.00	<0.00	<0.00	<0.00
GLITTER!: Minimum detection limits (99% confidence).																						
Element	STD610-1	STD610-2	BCRG-1	PGEA-1	PGEA-2	PGEA-3	PGEA-4	WG3-PY	WG3-PY2	WG3-SU1	WG3-PY3	WG3-PY4	WG3-PY5	WG3-PY6	WG3-PY7	WG3-PY8	STD610-3	STD610-4	BCRG-2	PGEA-5	PGEA-6	PGEA-7
Al27	0.247	0.357	0.104	0.00002	0.00003	0.00026	0.00001	0.032	0.0188	0.0451	0.0098	0.00918	0.0147	0.0194	0.0264	0.0105	0.27	0.298	0.103	0.00004	0.00014	0.00001
Si29	177.11	162.55	75.62	0.0182	0.0187	0.199	0.00689	21.67	13.94	31.12	7.19	6.05	9.29	13	18.81	7.05	179.41	141.81	64.51	0.0254	0.0886	0.00477
S34	<0.00000	<0.00000	<0.00000	<0.00000	<0.00000	<0.00000	<0.00000	<0.00000	<0.00000	<0.00000	<0.00000	<0.00000	<0.00000	<0.00000	<0.00000	<0.00000	<0.00000	<0.00000	<0.00000	<0.00000	<0.00000	<0.00000

RUN6

Element	STD610-1	STD610-2	BCRG-1	PGEA-1	PGEA-2	PGEA-3	PGEA-4	WG3-PY	WG3-PY2	WG3-SU1	WG3-PY3	WG3-PY4	WG3-PY5	WG3-PY6	WG3-PY7	WG3-PY8	STD610-3	STD610-4	BCRG-2	PGEA-5	PGEA-6	PGEA-7
Ca43	70.01	56.91	30.98	0.00696	0.00644	0.0846	0.00319	10.78	6.49	12.51	2.79	2.85	4.1	5.35	7.94	2.67	78.66	59.16	27.11	0.011	0.0353	0.00189
Sc45	0.102	0.107	0.041	0.00001	0.00001	0.00011	0	0.0154	0.00809	0.0188	0.00398	0.00361	0.0063	0.00776	0.0125	0.00475	0.12	0.1	0.0379	0.00002	0.00006	0
Ti49	0.824	0.799	0.237	0.00008	0.0001	0.00109	0.00004	0.121	0.0594	0.182	0.0453	0.0482	0.0692	0.0984	0.112	0.0434	1.23	0.852	0.337	0.00014	0.00049	0.00003
V51	0.0994	0.0899	0.0354	0.00001	0.00001	0.0001	0	0.0113	0.00704	0.0159	0.00434	0.00289	0.00509	0.00672	0.0109	0.00389	0.0948	0.0921	0.0399	0.00002	0.00005	0
Cr53	3.76	3.47	1.61	0.00038	0.00043	0.00441	0.00016	0.495	0.33	0.741	0.17	0.144	0.221	0.298	0.473	0.175	4.52	3.61	1.67	0.00066	0.00231	0.00012
Mn55	0.539	0.504	0.241	0.00006	0.00006	0.00064	0.00002	0.069	0.0463	0.1	0.0241	0.0201	0.0361	0.0434	0.0639	0.0234	0.627	0.493	0.226	0.00009	0.00031	0.00002
Fe57	18.83	16.66	8.17	0.00188	0.00201	0.0207	0.00077	2.18	1.42	9.37	0.759	0.852	2.62	2.38	1.95	1.54	26.46	14.68	6.59	0.00268	0.00909	0.0005
Co59	0.0648	0.0715	0.0303	0	0.00001	0.00006	0	0.00788	0.00589	0.0104	0.0028	0.004	0.0203	0.0141	0.00616	0.00488	0.156	0.065	0.0247	0.00001	0.00004	0
Ni60	0.252	0.263	0.122	0.00003	0.00044	0.00057	0.00001	0.0395	0.0234	0.0522	0.0139	0.00538	0.0262	0.0186	0.0353	0.0105	0.336	0.246	0.118	0.00003	0.00018	0.00001
Ni62	1.48	1.46	0.576	0.00012	0.00123	0.00166	0.00006	0.164	0.128	0.246	0.0575	0.0451	0.0927	0.102	0.149	0.0384	4.93	1.51	0.595	0.00024	0.00097	0.00004
Cu65	0.512	0.441	0.188	0.00005	0.00006	0.00058	0.00002	0.0622	0.0423	0.0928	0.0218	0.0474	0.0514	0.0415	0.0611	0.0199	0.625	0.404	0.184	0.00008	0.00028	0.00001
Zn66	0.978	0.987	0.398	0.00011	0.00011	0.00128	0.00004	0.13	0.0888	0.193	0.404	0.116	0.141	0.164	0.17	0.0616	1.53	1.18	0.491	0.00021	0.00068	0.00004
Ga71	0.06	0.0788	0.0448	0.00001	0	0.0001	0	0.0118	0.00827	0.011	0.00286	0.00202	0.00412	0.00857	0.0118	0.00342	0.103	0.076	0.0272	0.00001	0.00003	0
As75	8.14	7.54	3.55	0.00085	0.00089	0.00931	0.00033	1.01	0.67	1.68	0.394	0.346	0.543	0.778	1.13	0.461	12.05	9.72	4.35	0.0017	0.00589	0.00031
Se82	8	7.09	3.53	0.00083	0.00092	0.009	0.00032	1.02	0.668	1.53	0.342	0.293	0.46	0.61	0.897	0.346	8.73	7.09	3.28	0.00126	0.0043	0.00023
Y89	0.025	0.0417	0.00718	0	0	0.00003	0	0.00164	0.0018	0.00343	0.00072	0.00069	0.00106	0.0018	0.0022	<0.00000	0.0192	0.0263	0.00617	<0.00000	0.00001	0
Zr90	0.0231	0.0578	0.0199	0	0	0.00004	0	0.00642	0.00216	0.00795	0.00142	0.00055	0.00225	0.00125	0.00546	0.00099	0.0476	0.0457	0.0135	0	0.00002	0
Nb93	0.0146	0.0382	0.00627	0	0	0.00002	0	0.00165	0.00158	0.00218	0.00086	0.00049	0.00098	0.00091	0.00222	0.00063	0.0212	0.0293	0.00539	0	0.00001	0
Mo95	0.0718	0.106	0.031	0.00001	0.00001	0.00011	0	0.00706	0.0103	0.0186	0.00395	0.00454	0.0121	0.0103	0.012	0.00437	0.128	0.0858	0.0461	0.00001	0.00006	0
Ru99	<0.00000	<0.00000	<0.00000	<0.00000	<0.00000	<0.00000	<0.00000	<0.00000	<0.00000	<0.00000	<0.00000	<0.00000	<0.00000	<0.00000	<0.00000	<0.00000	<0.00000	<0.00000	<0.00000	<0.00000	<0.00000	<0.00000
Ru101	<0.00	<0.00	<0.00	<0.00	<0.00	<0.00	<0.00	<0.00	<0.00	<0.00	<0.00	<0.00	<0.00	<0.00	<0.00	<0.00	<0.00	<0.00	<0.00	<0.00	<0.00	<0.00
Rh103	<0.00000	<0.00000	<0.00000	<0.00000	<0.00000	<0.00000	<0.00000	<0.00000	<0.00000	<0.00000	<0.00000	<0.00000	<0.00000	<0.00000	<0.00000	<0.00000	<0.00000	<0.00000	<0.00000	<0.00000	<0.00000	<0.00000
Ag107	0.0835	0.0895	0.0329	0.00001	0.00001	0.0001	0	0.0116	0.0069	0.0108	0.00351	0.00515	0.00469	0.00736	0.00698	0.00208	0.0497	0.0864	0.0334	0.00002	0.00005	0
Pd108	<0.00000	<0.00000	<0.00000	<0.00000	<0.00000	<0.00000	<0.00000	<0.00000	<0.00000	<0.00000	<0.00000	<0.00000	<0.00000	<0.00000	<0.00000	<0.00000	<0.00000	<0.00000	<0.00000	<0.00000	<0.00000	<0.00000
Cd111	0.749	0.594	0.258	0.00009	0.00007	0.00076	0.00003	0.077	0.0647	0.16	0.0393	0.0324	0.0407	0.0622	0.0925	0.0292	1.04	0.54	0.324	0.00012	0.00061	0.00003
In115	0.0303	0.0459	0.0119	0	0	0.00004	0	0.00344	0.00284	0.00453	0.00144	0.00093	0.0017	0.0025	0.00253	0.00141	0.0361	0.0533	0.0102	0.00001	0.00002	0
Sn118	0.484	0.44	0.205	0.00005	0.00005	0.00054	0.00002	0.0605	0.0419	0.0894	0.021	0.0174	0.0266	0.0369	0.0546	0.0205	0.547	0.409	0.186	0.00007	0.00024	0.00001
Sb121	0.149	0.225	0.0897	0.00002	0.00003	0.00022	0.00001	0.0275	0.0159	0.0484	0.0126	0.0102	0.0167	0.0221	0.0238	0.00924	0.247	0.275	0.0795	0.00004	0.00013	0.00001
Te125	<0.00000	<0.00000	<0.00000	<0.00000	<0.00000	<0.00000	<0.00000	<0.00000	<0.00000	<0.00000	<0.00000	<0.00000	<0.00000	<0.00000	<0.00000	<0.00000	<0.00000	<0.00000	<0.00000	<0.00000	<0.00000	<0.00000
Te128	<0.00000	<0.00000	<0.00000	<0.00000	<0.00000	<0.00000	<0.00000	<0.00000	<0.00000	<0.00000	<0.00000	<0.00000	<0.00000	<0.00000	<0.00000	<0.00000	<0.00000	<0.00000	<0.00000	<0.00000	<0.00000	<0.00000
La139	0.0162	0.037	0.00901	0	0	0.00001	0	0.0013	0.00124	0.00298	0.00081	0.00077	<0.00000	0.00143	0.00191	0.00107	0.00964	0.037	0.00774	0	0.00001	0
Ce140	0.0244	0.0439	0.00975	0	0	0.00001	0	0.00128	0.00173	0.00294	0.00072	0.00044	0.00127	0.00141	0.00289	0.00089	0.019	0.0366	0.00684	0	0.00001	0
Nd146	0.0614	0.119	0.0324	0.00001	0.00001	0.00012	0	0.0135	0.00879	0.0196	0.00337	0.00293	0.00391	0.00331	0.0103	0.00374	0.11	0.104	0.0278	0.00001	0.00005	0
Hf178	0.0484	0.0586	0.0241	0	0.00001	0.00004	0	0.00778	0.00524	0.00892	0.00266	0.00231	0.00252	0.00523	0.00661	0.0012	0.0763	0.0579	0.0232	0.00001	0.00004	0
W182	0.0745	0.145	0.0371	0	0.00001	0.00014	0	0.0134	0.00871	0.0158	0.0041	0.00325	0.0118	0.00805	0.0144	0.00454	0.0768	0.0962	0.0478	0.00002	0.00006	0
Re185	0.0893	0.108	0.0385	0.00001	0.00001	0.00008	0	0.0238	0.00683	0.0164	0.00347	0.00522	0.00536	0.0104	0.0106	0.00628	0.0921	0.115	0.0468	0.00002	0.00009	0
Re187	0.0758	0.0735	0.0267	0	0.00001	0.00008	0	0.0105	0.00626	0.0161	0.00269	0.00234	0.0036	0.00473	0.00731	0.00267	0.0553	0.037	0.0198	0.00001	0.00004	0
Os189	<0.00	<0.00	<0.00	<0.00	<0.00	<0.00	<0.00	<0.00	<0.00	<0.00	<0.00	<0.00	<0.00	<0.00	<0.00	<0.00	<0.00	<0.00	<0.00	<0.00	<0.00	<0.00
Os190	<0.00	<0.00	<0.00	<0.00	<0.00	<0.00	<0.00	<0.00	<0.00	<0.00	<0.00	<0.00	<0.00	<0.00	<0.00	<0.00	<0.00	<0.00	<0.00	<0.00	<0.00	<0.00
Ir193	<0.00000	<0.00000	<0.00000	<0.00000	<0.00000	<0.00000	<0.00000	<0.00000	<0.00000	<0.00000	<0.00000	<0.00000	<0.00000	<0.00000	<0.00000	<0.00000	<0.00000	<0.00000	<0.00000	<0.00000	<0.00000	<0.00000
Pt195	<0.00000	<0.00000	<0.00000	<0.00000	<0.00000	<0.00000	<0.00000	<0.00000	<0.00000	<0.00000	<0.00000	<0.00000	<0.00000	<0.00000	<0.00000	<0.00000	<0.00000	<0.00000	<0.00000	<0.00000	<0.00000	<0.00000
Au197	0.0961	0.0381	0.0254	0	0.00001	0.00007	0	0.00818	0.0052	0.014	0.00264	0.00344	0.00353	0.00734	0.012	0.00358	0.0927	0.076	0.0281	0.00001	0.00003	0
Pb208	0.0956	0.101	0.0476	0.00001	0.00001	0.00013	0	0.0172	0.00944	0.0403	0.00619	0.0301	0.014	0.0172	0.0168	0.0161	0.192	0.126	0.0541	0.00002	0.00006	0
Bi209	0.106	0.109	0.0472	0.00001	0.00001	0.00012	0	0.0137	0.00914	0.0179	0.00402	0.00341	0.00491	0.0228	0.0119	0.00446	0.115	0.0934	0.0397	0.00002	0.00005	0
Th232	0.0208	0.053	0.0104	0	0	0.00003	0	0.00443	0.00159	0.00388	0.00105	0.00107	0.00165	0.00243	0.00201	0.00104	0.0464	0.038	0.0141	0	0.00001	0
U238	0.0195	0.0489	0.0119	0	0	0.00002	0	0.00444	0.00211	0.00785	0.00088	0.00114	0.00176	0.00211	0.00298	0.00119	0.026	0.0405	0.0111	0	0.00001	0
ThO248	<0.00	<0.00	<0.00	<0.00	<0.00	<0.00	<0.00	<0.00	<0.00	<0.00	<0.00	<0.00	<0.00	<0.00	<0.00	<0.00	<0.00	<0.00	<0.00	<0.00	<0.00	<0.00

GLITTER!: Trace element concentrations normalised to chondrite.

Element	STD610-1	STD610-2	BCRG-1	PGEA-1	PGEA-2	PGEA-3	PGEA-4	WG3-PY	WG3-PY2	WG3-SU1	WG3-PY3	WG3-PY4	WG3-PY5	WG3-PY6	WG3-PY7	WG3-PY8	STD610-3	STD610-4	BCRG-2	PGEA-5	PGEA-6	PGEA-7
Al27	0.778	0.823	3.41	0	0	0	0	0.0548	0.2285	0.00008	0.2331	0.00069	0.00551	0.1612	0.00836	0.01807	0.982	0.771	3.29	0	0	0
Si29	2.1	2.19	0.927	0	0	0	0	0.00854	0.0302	0.00067	0.0429	0.00038	0.00244	0.03	0.00372	0.00782	2.68	2.03	0.887	0	0	0
S34	<****	<****	<****	<****	<****	<****	<****	<****	<****	<****	<****	<****	<****	<****	<****	<****	<****	<****	<****	<****	<****	<****
Ca43	6.18	6.53	2.249	0	0	0	0	0.00406	0.1007	0	0.0471	0.00397	0.00699	0.1685	0.0212	0.01116	7.78	6	2.183	0	0	0
Sc45	51.88	54.03	2.122	0	0	0	0	0.00356	0.0803	0	0.0271	0.00061	0.00088	0.2129	0.00545	0.00337	65.36	50.59	2.051	0	0	0
Ti49	0.65	0.682	10.87	0	0	0	0	0.00723	0.486	0.01035	0.0416	0.00275	0.00359	1.198	0.0286	0.01924	0.838	0.667	10.85	0	0	0
V51	5.17	5.47	2.759	0	0	0	0	0.0398	0.371	0.00341	0.306	0.0484	0.0346	0.1744	0.0501	0.0683	6.89	5.18	2.78	0	0.00002	0
Cr53	0.1016	0.1077	0.00229	0	0	0	0	0.00129	0.0119	0	0.00369	0.00021	0.00027	0.00045	0.00014	0.00058	0.1348	0.1016	0.00217	0	0	0
Mn55	0.1462	0.1544	0.312	0	0	0	0	0.00553	0.00494	0.1768	0.472	0.454	0.486	0.02013	0.00577	0.407	0.196	0.1472	0.311	0	0	0

RUN6

Element	STD610-1	STD610-2	BCRG-1	PGEA-1	PGEA-2	PGEA-3	PGEA-4	WG3-PY	WG3-PY2	WG3-SU1	WG3-PY3	WG3-PY4	WG3-PY5	WG3-PY6	WG3-PY7	WG3-PY8	STD610-3	STD610-4	BCRG-2	PGEA-5	PGEA-6	PGEA-7
Fe57	0.00164	0.00164	0.1996	0	0	0	0	1.675	1.675	0.00569	1.675	1.675	1.675	1.675	1.675	1.675	0.00164	0.00164	0.1996	0	0	0
Co59	0.521	0.54	0.0302	0	0	0	0	0.00083	0.0632	0.0005	1.269	2.177	1.992	0.359	0.2617	3.07	0.72	0.532	0.0298	0	0	0
Ni60	0.0267	0.0272	0.00087	0.011	0.0183	0.051	0.00177	0.00009	0.00253	0.00006	0.00878	0.01468	0.00956	0.00482	0.00494	0.01611	0.0358	0.027	0.00185	0.0246	0.024	0.0019
Ni62	0.0265	0.0276	0.00092	0.0112	0.0188	0.052	0.00179	0.0001	0.00263	0.00005	0.00849	0.01469	0.00955	0.00485	0.00484	0.0162	0.0364	0.027	0.01118	0.0256	0.024	0.00195
Cu65	2.57	2.72	0.334	0.0006	0.00109	0.0033	0.00011	0.538	3.34	0.668	86.2	7.93	9.56	1.4	1.044	23.52	3.48	2.55	0.0851	0.00158	0.00141	0.00012
Zn66	0.94	0.949	0.283	0	0	0.00002	0.00001	0.0724	3.52	1238.47	9.77	0.25	0.603	0.1379	0.0654	4.05	1.348	1.012	0.838	0	0.00015	0.00002
Ga71	27.98	28.99	0.866	0	0	0	0	0.00948	0.0921	0.0619	0.0459	0.00056	0.00241	0.0364	0.00973	0.00855	39.26	29.11	0.85	0	0.00001	0
As75	106.24	111.14	0	0.011	0.0196	0.058	0.00195	341.56	3936.22	1.03	446.07	373.29	401	2547.72	3564.87	640.36	148.79	112.69	0	0.0403	0.025	0.00204
Se82	3.88	4.52	0	0.00132	0.00241	0.0072	0.00026	7.53	2.04	0.137	0.422	0.867	0.187	2.74	8.83	0.0528	5.5	3.98	0	0.00382	0.0034	0.00028
Y89	197.31	207.12	7.63	0	0	0	0	0.0294	0.657	0.00556	1.351	0.0251	0.0266	0.372	0.00705	0.1297	256.75	200.17	7.89	0	0	0
Zr90	77.54	82.6	16.56	0.00001	0	0	0	0.00775	5.22	0	0.2072	0.01927	0.01272	6.97	0.00636	0.096	102.72	79.76	17.33	0.00002	0.00001	0
Nb93	1087.5	1132.05	16.34	0	0.00002	0	0	0.0168	1.992	0.322	0.444	0.0454	0.0221	6.44	0.199	0.0708	1458.45	1127.94	17.5	0	0	0.00001
Mo95	261.99	274.85	87.68	0	0.00008	0	0.00001	0.267	1.857	0.235	48.19	29.76	18.09	0.0638	0.456	17.38	359.39	277.08	90.66	0.00003	0	0.00001
Ru99	0	0	0	0	0	0	0	0	0	0	0	0	0	0	0	0	0	0	0	0	0	0
Ru101	<****	<****	<****	<****	<****	<****	<****	<****	<****	<****	<****	<****	<****	<****	<****	<****	<****	<****	<****	<****	<****	<****
Rh103	0	0	0	0	0	0	0	0	0	0	0	0	0	0	0	0	0	0	0	0	0	0
Ag107	700.26	726.53	2.36	0.221	0.424	1.32	0.0442	2.87	23.3	6.6	111.03	0.112	0.062	5.6	4.21	0.392	999.05	734.66	2.62	0.61	0.65	0.0527
Pd108	0	0	0	0	0	0	0	0	0	0	0	0	0	0	0	0	0	0	0	0	0	0
Cd111	241.45	243.4	0.32	0.0159	0.0332	0.086	0.00266	0.187	21.52	1300.08	43.06	0.107	0.469	0.649	0.58	9.72	349.54	265.25	0	0.064	0.039	0.00338
In115	3620.12	3746.96	0.789	0	0	0.0045	0.00003	0.06	14.05	459.72	0.372	0.036	0.0179	2.82	0.237	0.0417	5090.67	3834.17	2.13	0.00011	0	0.00001
Sn118	150.38	166.34	0.645	0.00019	0.00032	0.0011	0.00004	0.0548	1.765	18.04	0.342	0.0126	0.0119	0.368	0.124	0.0192	207.98	159.12	0.607	0.00054	0.00059	0.00004
Sb121	1523.52	1523.73	3.04	0.00109	0.00206	0.0091	0.00031	275.19	1367.19	1.8	178.28	4.49	17.57	266.67	76.63	48.71	2155.25	1611.04	3.18	0.00306	0.0053	0.00052
Te125	0	0	0	0	0	0	0	0	0	0	0	0	0	0	0	0	0	0	0	0	0	0
Te128	0	0	0	0	0	0	0	0	0	0	0	0	0	0	0	0	0	0	0	0	0	0
La139	1222.02	1266.18	39.28	0	0.00001	0	0	0.0801	6.18	0	14.97	0.0391	0.85	1.499	0.1269	1.692	1582.68	1252.56	40.12	0	0	0
Ce140	456.1	474.18	30.66	0	0.00009	0	0	0.0566	4.11	0.0134	7.06	0.0387	0.516	1.044	0.071	1.343	599.57	471.41	31.49	0.00001	0	0
Nd146	607.13	650.74	21.59	0	0.00002	0	0	0.0358	1.715	0.208	5.08	0.0372	0.179	0.956	0.0311	0.868	776.38	602.17	22.24	0.00003	0	0.00001
Hf178	2295.93	2397.66	13.96	0	0	0	0	0	3.68	0	0.153	0	0.0173	6.47	0	0.0698	2950.98	2339.96	13.57	0	0	0
W182	4955.56	5150.38	3.04	0.00007	0	0	0.00019	11.69	15.92	0.288	586.63	1032.73	226.24	2.11	1.17	32.98	6508.21	5005.19	2.92	0	0	0
Re185	1842.02	1909.64	0	0	0	0.0015	0.00013	0	0.59	0	5.17	10.44	10.95	0	2.08	4.99	2482.58	1898.17	0	0	0	0
Re187	1839.18	1953.57	0	0.025	0.0294	0.13	0.00362	0	0.478	0	5.27	10.91	10.36	0	3.01	5.18	2495.38	1895.35	0.48	0.0505	0.047	0.00401
Os189	<****	<****	<****	<****	<****	<****	<****	<****	<****	<****	<****	<****	<****	<****	<****	<****	<****	<****	<****	<****	<****	<****
Os190	<****	<****	<****	<****	<****	<****	<****	<****	<****	<****	<****	<****	<****	<****	<****	<****	<****	<****	<****	<****	<****	<****
Ir193	0	0	0	0	0	0	0	0	0	0	0	0	0	0	0	0	0	0	0	0	0	0
Pt195	0	0	0	0	0	0	0	0	0	0	0	0	0	0	0	0	0	0	0	0	0	0
Au197	104.87	109.39	0.647	0.359	0.604	1.66	0.0553	25.05	16.67	0.301	1364.65	2.14	0.781	32.37	9.47	2.78	138.23	102.26	1.29	0.75	0.76	0.0622
Pb208	114.54	118.19	7.27	0.00236	0.00422	0.012	0.00045	180.32	668.09	5.66	7229.43	19.16	46.67	266.07	146.37	249.09	149.91	112.44	3.14	0.0071	0.0061	0.00051
Bi209	2126.77	2241.48	6.97	0.298	0.556	1.65	0.0563	49.01	275.78	7.84	3.35	0.217	0.735	703.09	72.92	0.174	2793.54	2138.18	1.2	0.93	0.79	0.0641
Th232	11564.49	12077.77	79.1	0	0	0	0	0.276	12.9	0.097	52.22	1.281	0.481	7.35	0.261	3.74	13139.95	10332.83	72.86	0.00017	0	0
U238	39953.54	41039.23	127.06	0	0	0	0	77.37	1250.32	0	283.7	34.53	18.27	106.71	2.37	158.62	47125.72	36690.37	118.59	0	0	0
ThO248	<****	<****	<****	<****	<****	<****	<****	<****	<****	<****	<****	<****	<****	<****	<****	<****	<****	<****	<****	<****	<****	<****

GLITTER4.0: Laser Ablation Analysis Results

G:\KYLIE\MAR13\PGEARUN1
Fri Mar 14 16:50:07 2003

All values are reported in ppm

GLITTER!: Trace Element Concentrations MDL filtered.

	Run1-1	Run1-2	Run1-3	Run1-4	Run1-5	Run1-6	Run1-7	Discarded Run1-8	Run1-9	Run1-10	Run1-11	Run1-12	Run1-13	Run1-14	Run1-15	Run1-16	Run1-17	Run1-18	Run1-19	Run1-20	Run1-21
Element	STD610-1	STD610-2	BCR2G-1	PGEA-1	PGEA-2	BG24-PY	BG24-CPY	JL06-PY	JC22-PY	JC22-SPH	JC22-CPY	BG14-PY	JL09-PY	JL09-SPH	BG24-SPH	BG24-SP2	STD610-3	STD610-4	PGEA-3	PGEA-4	PGEA-5
Al27	<-NaN	<-NaN	<-NaN	<-NaN	<-NaN	<-NaN	<-NaN	<-NaN	<-NaN	<-NaN	<-NaN	<-NaN	<-NaN	<-NaN	<-NaN	<-NaN	<-NaN	<-NaN	<-NaN	<-NaN	<-NaN
Si29	<-NaN	<-NaN	<-NaN	<-NaN	<-NaN	<-NaN	<-NaN	<-NaN	<-NaN	<-NaN	<-NaN	<-NaN	<-NaN	<-NaN	<-NaN	<-NaN	<-NaN	<-NaN	<-NaN	<-NaN	<-NaN
S34	0.00667	0.00667	0.00667	278000.03	278000.03	534495.63	349436.88	534495.63	534495.63	335271.28	349436.91	534495.63	534495.69	331071.81	329772.25	329772.22	0.00667	0.00667	0.00667	278000.09	278000.09
Ca43	<-NaN	<-NaN	<-NaN	<-NaN	<-NaN	<-NaN	<-NaN	<-NaN	<-NaN	<-NaN	<-NaN	<-NaN	<-NaN	<-NaN	<-NaN	<-NaN	<-NaN	<-NaN	<-NaN	<-NaN	<-NaN
Sc45	<-NaN	<-NaN	<-NaN	<-NaN	<-NaN	<-NaN	<-NaN	<-NaN	<-NaN	<-NaN	<-NaN	<-NaN	<-NaN	<-NaN	<-NaN	<-NaN	<-NaN	<-NaN	<-NaN	<-NaN	<-NaN
Ti49	<-NaN	<-NaN	<-NaN	<-NaN	<-NaN	<-NaN	<-NaN	<-NaN	<-NaN	<-NaN	<-NaN	<-NaN	<-NaN	<-NaN	<-NaN	<-NaN	<-NaN	<-NaN	<-NaN	<-NaN	<-NaN
V51	<-NaN	<-NaN	<-NaN	<-NaN	<-NaN	<-NaN	<-NaN	<-NaN	<-NaN	<-NaN	<-NaN	<-NaN	<-NaN	<-NaN	<-NaN	<-NaN	<-NaN	<-NaN	<-NaN	<-NaN	<-NaN
Cr53	<-NaN	<-NaN	<-NaN	<-NaN	<-NaN	<-NaN	<-NaN	<-NaN	<-NaN	<-NaN	<-NaN	<-NaN	<-NaN	<-NaN	<-NaN	<-NaN	<-NaN	<-NaN	<-NaN	<-NaN	<-NaN
Mn55	<-NaN	<-NaN	<-NaN	<-NaN	<-NaN	<-NaN	<-NaN	<-NaN	<-NaN	<-NaN	<-NaN	<-NaN	<-NaN	<-NaN	<-NaN	<-NaN	<-NaN	<-NaN	<-NaN	<-NaN	<-NaN
Fe57	<-NaN	<-NaN	<-NaN	<-NaN	<-NaN	<-NaN	<-NaN	<-NaN	<-NaN	<-NaN	<-NaN	<-NaN	<-NaN	<-NaN	<-NaN	<-NaN	<-NaN	<-NaN	<-NaN	<-NaN	<-NaN
Co59	<-NaN	<-NaN	<-NaN	<-NaN	<-NaN	<-NaN	<-NaN	<-NaN	<-NaN	<-NaN	<-NaN	<-NaN	<-NaN	<-NaN	<-NaN	<-NaN	<-NaN	<-NaN	<-NaN	<-NaN	<-NaN
Ni60	0.0002	0.0002	0.00002	720617.56	705431.69	169.08	2.82	9.25	7.5	0.45	0.243	3	<0.131	<0.197	12.32	5.63	0.00013	0.00013	0.01839	727689.19	709421
Ni62	0.0002	0.00021	0.00001	742771.5	681516.25	182.42	3.82	9.93	7.74	<1.39	<0.91	4.68	<0.73	1.72	9.54	4.55	0.00013	0.00013	0.0199	726897.38	710333.88
Cu65	0.00011	0.00012	0.00001	249.44	233.27	92.73	214127.19	343.84	16.23	3573.58	222263.14	91.79	1.53	12629.63	100167.19	15825.46	0.00008	0.00008	0.00001	253.01	238.12
Zn66	<-NaN	<-NaN	<-NaN	<-NaN	<-NaN	<-NaN	<-NaN	<-NaN	<-NaN	<-NaN	<-NaN	<-NaN	<-NaN	<-NaN	<-NaN	<-NaN	<-NaN	<-NaN	<-NaN	<-NaN	<-NaN
Ga71	<-NaN	<-NaN	<-NaN	<-NaN	<-NaN	<-NaN	<-NaN	<-NaN	<-NaN	<-NaN	<-NaN	<-NaN	<-NaN	<-NaN	<-NaN	<-NaN	<-NaN	<-NaN	<-NaN	<-NaN	<-NaN
As75	0.00015	0.00014	<0.00000	135.96	134.75	72.21	170.96	27127.29	7044.19	5.23	1268.74	32.42	67.64	<2.55	256.01	76.01	0.00009	0.00009	0	135.38	135.77
Se82	0.00008	0.00009	<0.00002	238.93	251.34	42.07	<5.23	<3.65	59.66	13.47	17.47	<7.04	92.01	51.06	<8.97	<6.00	0.00005	0.00007	0	249.21	240.34
Y89	<-NaN	<-NaN	<-NaN	<-NaN	<-NaN	<-NaN	<-NaN	<-NaN	<-NaN	<-NaN	<-NaN	<-NaN	<-NaN	<-NaN	<-NaN	<-NaN	<-NaN	<-NaN	<-NaN	<-NaN	<-NaN
Zr90	<-NaN	<-NaN	<-NaN	<-NaN	<-NaN	<-NaN	<-NaN	<-NaN	<-NaN	<-NaN	<-NaN	<-NaN	<-NaN	<-NaN	<-NaN	<-NaN	<-NaN	<-NaN	<-NaN	<-NaN	<-NaN
Nb93	<-NaN	<-NaN	<-NaN	<-NaN	<-NaN	<-NaN	<-NaN	<-NaN	<-NaN	<-NaN	<-NaN	<-NaN	<-NaN	<-NaN	<-NaN	<-NaN	<-NaN	<-NaN	<-NaN	<-NaN	<-NaN
Mo95	<-NaN	<-NaN	<-NaN	<-NaN	<-NaN	<-NaN	<-NaN	<-NaN	<-NaN	<-NaN	<-NaN	<-NaN	<-NaN	<-NaN	<-NaN	<-NaN	<-NaN	<-NaN	<-NaN	<-NaN	<-NaN
Ru99	<0.00000	<0.00000	<0.00000	233.35	221.83	<0.103	0.226	<0.048	0.12	<0.126	0.303	<0.118	<0.075	<0.092	0.12	<0.074	<0.00000	<0.00000	0.00001	238.52	224.78
Ru101	<0.00000	<0.00000	<0.00000	228.1	230.66	<0.058	0.085	<0.045	<0.060	<0.077	0.125	<0.077	<0.047	<0.066	0.082	<0.035	<0.00000	<0.00000	0.00001	230.24	228.47
Rh103	0	0	<0.00000	243.09	242.86	<0.087	10.33	<0.053	<0.082	0.231	11	<0.113	<0.085	0.628	4.01	0.713	0	0	0.00001	251.12	239.62
Ag107	<-NaN	<-NaN	<-NaN	<-NaN	<-NaN	<-NaN	<-NaN	<-NaN	<-NaN	<-NaN	<-NaN	<-NaN	<-NaN	<-NaN	<-NaN	<-NaN	<-NaN	<-NaN	<-NaN	<-NaN	<-NaN
Pd108	0	0	<0.00000	260.8	251.61	0.1	0.826	1.15	0.065	51.78	0.663	<0.059	<0.052	43.42	30.34	57.42	0	0	0.00001	278.07	249.63
Cd111	<-NaN	<-NaN	<-NaN	<-NaN	<-NaN	<-NaN	<-NaN	<-NaN	<-NaN	<-NaN	<-NaN	<-NaN	<-NaN	<-NaN	<-NaN	<-NaN	<-NaN	<-NaN	<-NaN	<-NaN	<-NaN
In115	<-NaN	<-NaN	<-NaN	<-NaN	<-NaN	<-NaN	<-NaN	<-NaN	<-NaN	<-NaN	<-NaN	<-NaN	<-NaN	<-NaN	<-NaN	<-NaN	<-NaN	<-NaN	<-NaN	<-NaN	<-NaN
Sn118	<-NaN	<-NaN	<-NaN	<-NaN	<-NaN	<-NaN	<-NaN	<-NaN	<-NaN	<-NaN	<-NaN	<-NaN	<-NaN	<-NaN	<-NaN	<-NaN	<-NaN	<-NaN	<-NaN	<-NaN	<-NaN
Sb121	<-NaN	<-NaN	<-NaN	<-NaN	<-NaN	<-NaN	<-NaN	<-NaN	<-NaN	<-NaN	<-NaN	<-NaN	<-NaN	<-NaN	<-NaN	<-NaN	<-NaN	<-NaN	<-NaN	<-NaN	<-NaN
Te125	0.00014	0.00015	<0.00000	236.09	249.04	2.7	0.8	0.52	4.09	<1.12	<0.52	0.6	2.85	<0.60	1.24	0.67	0.00009	0.00009	0	262.8	232.34
Te128	0.00014	0.00014	<0.00000	248.93	230.38	2.86	<0.65	0.72	3.34	<1.05	<0.68	<0.80	3.21	0.75	1.06	<0.64	0.00009	0.00009	0	248.18	238.03
La139	<-NaN	<-NaN	<-NaN	<-NaN	<-NaN	<-NaN	<-NaN	<-NaN	<-NaN	<-NaN	<-NaN	<-NaN	<-NaN	<-NaN	<-NaN	<-NaN	<-NaN	<-NaN	<-NaN	<-NaN	<-NaN
Ce140	<-NaN	<-NaN	<-NaN	<-NaN	<-NaN	<-NaN	<-NaN	<-NaN	<-NaN	<-NaN	<-NaN	<-NaN	<-NaN	<-NaN	<-NaN	<-NaN	<-NaN	<-NaN	<-NaN	<-NaN	<-NaN
Nd146	<-NaN	<-NaN	<-NaN	<-NaN	<-NaN	<-NaN	<-NaN	<-NaN	<-NaN	<-NaN	<-NaN	<-NaN	<-NaN	<-NaN	<-NaN	<-NaN	<-NaN	<-NaN	<-NaN	<-NaN	<-NaN
Hf178	<-NaN	<-NaN	<-NaN	<-NaN	<-NaN	<-NaN	<-NaN	<-NaN	<-NaN	<-NaN	<-NaN	<-NaN	<-NaN	<-NaN	<-NaN	<-NaN	<-NaN	<-NaN	<-NaN	<-NaN	<-NaN
W182	<-NaN	<-NaN	<-NaN	<-NaN	<-NaN	<-NaN	<-NaN	<-NaN	<-NaN	<-NaN	<-NaN	<-NaN	<-NaN	<-NaN	<-NaN	<-NaN	<-NaN	<-NaN	<-NaN	<-NaN	<-NaN
Re185	<-NaN	<-NaN	<-NaN	<-NaN	<-NaN	<-NaN	<-NaN	<-NaN	<-NaN	<-NaN	<-NaN	<-NaN	<-NaN	<-NaN	<-NaN	<-NaN	<-NaN	<-NaN	<-NaN	<-NaN	<-NaN
Re187	<-NaN	<-NaN	<-NaN	<-NaN	<-NaN	<-NaN	<-NaN	<-NaN	<-NaN	<-NaN	<-NaN	<-NaN	<-NaN	<-NaN	<-NaN	<-NaN	<-NaN	<-NaN	<-NaN	<-NaN	<-NaN
Os189	<0.00000	<0.00000	<0.00000	197.7	189.66	<0.140	<0.113	<0.087	<0.129	<0.237	<0.136	<0.210	<0.117	<0.115	<0.187	<0.137	<0.00000	<0.00000	0	189.31	197.1
Os190	<0.00000	<0.00000	<0.00000	202.4	183.66	<0.071	<0.069	<0.043	<0.048	<0.123	<0.082	<0.077	<0.070	<0.097	<0.110	<0.097	<0.00000	<0.00000	0.00001	191.06	196.14
Ir193	0	<0.00000	<0.00000	106.59	106.69	<0.0186	<0.0201	<0.0111	<0.0139	<0.037	<0.0252	<0.0265	<0.0162	<0.0211	<0.030	<0.0201	<0.00000	<0.00000	0	108.41	105.84
Pt195	0	0	<0.00000	206.52	201.66	<0.067	<0.056	<0.041	<0.066	0.122	<0.061	<0.082	<0.058	<0.098	<0.111	<0.058	0	0	0.00001	206.44	203.85
Au197	0.00001	0.00001	<0.00000	238.66	225.76	0.07	0.246	32.3	17.42	<0.038	0.094	0.097	<0.030	0.148	1.12	0.443	0.00001	0.00001	0.00001	249.53	227.48
Pb208	<-NaN	<-NaN	<-NaN	<-NaN	<-NaN	<-NaN	<-NaN	<-NaN	<-NaN	<-NaN	<-NaN	<-NaN	<-NaN	<-NaN	<-NaN	<-NaN	<-NaN	<-NaN	<-NaN	<-NaN	<-NaN
Bi209	0.00017	0.00018	<0.00000	241.53	225.86	12.52	56.34	28.47	5.23	1.25	0.179	0.96	2.01	18.75	33.49	37.36	0.00011	0.00011	0	250.67	229.35

Element	STD610-1	STD610-2	BCR2G-1	PGEA-1	PGEA-2	BG24-PY	BG24-CPY	JL06-PY	JC22-PY	JC22-SPH	JC22-CPY	BG14-PY	JL09-PY	JL09-SPH	BG24-SPH	BG24-SP2	STD610-3	STD610-4	PGEA-3	PGEA-4	PGEA-5
Th232	<-NaN	<-NaN	<-NaN	<-NaN	<-NaN	<-NaN	<-NaN	<-NaN	<-NaN	<-NaN	<-NaN	<-NaN	<-NaN	<-NaN	<-NaN	<-NaN	<-NaN	<-NaN	<-NaN	<-NaN	<-NaN
U238	<-NaN	<-NaN	<-NaN	<-NaN	<-NaN	<-NaN	<-NaN	<-NaN	<-NaN	<-NaN	<-NaN	<-NaN	<-NaN	<-NaN	<-NaN	<-NaN	<-NaN	<-NaN	<-NaN	<-NaN	<-NaN
ThO248	<-NaN	<-NaN	<-NaN	<-NaN	<-NaN	<-NaN	<-NaN	<-NaN	<-NaN	<-NaN	<-NaN	<-NaN	<-NaN	<-NaN	<-NaN	<-NaN	<-NaN	<-NaN	<-NaN	<-NaN	<-NaN
GLITTER!: 1 sigma error.																					
Element	STD610-1	STD610-2	BCR2G-1	PGEA-1	PGEA-2	BG24-PY	BG24-CPY	JL06-PY	JC22-PY	JC22-SPH	JC22-CPY	BG14-PY	JL09-PY	JL09-SPH	BG24-SPH	BG24-SP2	STD610-3	STD610-4	PGEA-3	PGEA-4	PGEA-5
Al27	<0.00	<0.00	<0.00	<0.00	<0.00	<0.00	<0.00	<0.00	<0.00	<0.00	<0.00	<0.00	<0.00	<0.00	<0.00	<0.00	<0.00	<0.00	<0.00	<0.00	<0.00
Si29	<0.00	<0.00	<0.00	<0.00	<0.00	<0.00	<0.00	<0.00	<0.00	<0.00	<0.00	<0.00	<0.00	<0.00	<0.00	<0.00	<0.00	<0.00	<0.00	<0.00	<0.00
S34	0.00029	0.00029	0.00033	8859.51	8876.15	16913.9	11061.26	16909.13	16912.07	10619.57	11060.88	16913.86	16913.8	10484.44	10444.64	10438.15	0.00027	0.00027	0.00021	8859.56	8841.25
Ca43	<0.00	<0.00	<0.00	<0.00	<0.00	<0.00	<0.00	<0.00	<0.00	<0.00	<0.00	<0.00	<0.00	<0.00	<0.00	<0.00	<0.00	<0.00	<0.00	<0.00	<0.00
Sc45	<0.00	<0.00	<0.00	<0.00	<0.00	<0.00	<0.00	<0.00	<0.00	<0.00	<0.00	<0.00	<0.00	<0.00	<0.00	<0.00	<0.00	<0.00	<0.00	<0.00	<0.00
Ti49	<0.00	<0.00	<0.00	<0.00	<0.00	<0.00	<0.00	<0.00	<0.00	<0.00	<0.00	<0.00	<0.00	<0.00	<0.00	<0.00	<0.00	<0.00	<0.00	<0.00	<0.00
V51	<0.00	<0.00	<0.00	<0.00	<0.00	<0.00	<0.00	<0.00	<0.00	<0.00	<0.00	<0.00	<0.00	<0.00	<0.00	<0.00	<0.00	<0.00	<0.00	<0.00	<0.00
Cr53	<0.00	<0.00	<0.00	<0.00	<0.00	<0.00	<0.00	<0.00	<0.00	<0.00	<0.00	<0.00	<0.00	<0.00	<0.00	<0.00	<0.00	<0.00	<0.00	<0.00	<0.00
Mn55	<0.00	<0.00	<0.00	<0.00	<0.00	<0.00	<0.00	<0.00	<0.00	<0.00	<0.00	<0.00	<0.00	<0.00	<0.00	<0.00	<0.00	<0.00	<0.00	<0.00	<0.00
Fe57	<0.00	<0.00	<0.00	<0.00	<0.00	<0.00	<0.00	<0.00	<0.00	<0.00	<0.00	<0.00	<0.00	<0.00	<0.00	<0.00	<0.00	<0.00	<0.00	<0.00	<0.00
Co59	<0.00	<0.00	<0.00	<0.00	<0.00	<0.00	<0.00	<0.00	<0.00	<0.00	<0.00	<0.00	<0.00	<0.00	<0.00	<0.00	<0.00	<0.00	<0.00	<0.00	<0.00
Ni60	0.00001	0.00001	0	27510.06	27082.6	6.56	0.16	0.39	0.34	0.11	0.069	0.18	0.057	0.079	0.6	0.29	0.00001	0.00001	0.00085	34105.72	33846.34
Ni62	0.00001	0.00001	0	47420.99	43958.51	12.13	0.52	0.8	0.74	0.59	0.35	0.62	0.3	0.44	1.11	0.61	0.00001	0.00001	0.0018	66138.88	66405.59
Cu65	0.00001	0.00001	0	18.18	17.24	6.91	16192.82	26.52	1.3	288.16	18368.69	7.8	0.22	1131.8	9236.46	1502.27	0.00001	0.00001	0	27.12	26.28
Zn66	<0.00	<0.00	<0.00	<0.00	<0.00	<0.00	<0.00	<0.00	<0.00	<0.00	<0.00	<0.00	<0.00	<0.00	<0.00	<0.00	<0.00	<0.00	<0.00	<0.00	<0.00
Ga71	<0.00	<0.00	<0.00	<0.00	<0.00	<0.00	<0.00	<0.00	<0.00	<0.00	<0.00	<0.00	<0.00	<0.00	<0.00	<0.00	<0.00	<0.00	<0.00	<0.00	<0.00
As75	0.00001	0.00001	0	4.92	5.06	2.37	5.44	848.58	221.33	1.48	40.34	1.56	2.42	1.03	8.57	2.69	0	0	0	6.39	6.24
Se82	0.00001	0.00001	0.00001	19.27	20.69	3.76	2.13	1.44	4.34	3.82	2.66	2.7	6.62	4.72	3.45	2.27	0.00001	0.00001	0	23.85	23.4
Y89	<0.00	<0.00	<0.00	<0.00	<0.00	<0.00	<0.00	<0.00	<0.00	<0.00	<0.00	<0.00	<0.00	<0.00	<0.00	<0.00	<0.00	<0.00	<0.00	<0.00	<0.00
Zr90	<0.00	<0.00	<0.00	<0.00	<0.00	<0.00	<0.00	<0.00	<0.00	<0.00	<0.00	<0.00	<0.00	<0.00	<0.00	<0.00	<0.00	<0.00	<0.00	<0.00	<0.00
Nb93	<0.00	<0.00	<0.00	<0.00	<0.00	<0.00	<0.00	<0.00	<0.00	<0.00	<0.00	<0.00	<0.00	<0.00	<0.00	<0.00	<0.00	<0.00	<0.00	<0.00	<0.00
Mo95	<0.00	<0.00	<0.00	<0.00	<0.00	<0.00	<0.00	<0.00	<0.00	<0.00	<0.00	<0.00	<0.00	<0.00	<0.00	<0.00	<0.00	<0.00	<0.00	<0.00	<0.00
Ru99	0	0	0	15.53	15	0.038	0.051	0.021	0.034	0.055	0.057	0.045	0.03	0.039	0.052	0.033	0	0	0	22.73	22
Ru101	0	0	0	7.54	7.72	0.023	0.03	0.016	0.023	0.033	0.034	0.03	0.02	0.026	0.03	0.015	0	0	0	7.97	7.87
Rh103	0	0	0	11.83	11.93	0.034	0.52	0.021	0.031	0.064	0.59	0.043	0.034	0.063	0.25	0.06	0	0	0	16.39	16.01
Ag107	<0.00	<0.00	<0.00	<0.00	<0.00	<0.00	<0.00	<0.00	<0.00	<0.00	<0.00	<0.00	<0.00	<0.00	<0.00	<0.00	<0.00	<0.00	<0.00	<0.00	<0.00
Pd108	0	0	0	25.04	24.48	0.03	0.095	0.12	0.023	5.56	0.086	0.024	0.02	5.2	3.75	7.29	0	0	0	39.86	36.86
Cd111	<0.00	<0.00	<0.00	<0.00	<0.00	<0.00	<0.00	<0.00	<0.00	<0.00	<0.00	<0.00	<0.00	<0.00	<0.00	<0.00	<0.00	<0.00	<0.00	<0.00	<0.00
In115	<0.00	<0.00	<0.00	<0.00	<0.00	<0.00	<0.00	<0.00	<0.00	<0.00	<0.00	<0.00	<0.00	<0.00	<0.00	<0.00	<0.00	<0.00	<0.00	<0.00	<0.00
Sn118	<0.00	<0.00	<0.00	<0.00	<0.00	<0.00	<0.00	<0.00	<0.00	<0.00	<0.00	<0.00	<0.00	<0.00	<0.00	<0.00	<0.00	<0.00	<0.00	<0.00	<0.00
Sb121	<0.00	<0.00	<0.00	<0.00	<0.00	<0.00	<0.00	<0.00	<0.00	<0.00	<0.00	<0.00	<0.00	<0.00	<0.00	<0.00	<0.00	<0.00	<0.00	<0.00	<0.00
Te125	0.00002	0.00002	0	27.27	29.29	0.51	0.25	0.2	0.62	0.4	0.23	0.24	0.56	0.25	0.47	0.24	0.00001	0.00002	0	44.93	40.87
Te128	0.00001	0.00001	0	16.92	15.95	0.38	0.26	0.18	0.37	0.4	0.27	0.3	0.38	0.3	0.39	0.25	0.00001	0.00001	0	24.23	23.87
La139	<0.00	<0.00	<0.00	<0.00	<0.00	<0.00	<0.00	<0.00	<0.00	<0.00	<0.00	<0.00	<0.00	<0.00	<0.00	<0.00	<0.00	<0.00	<0.00	<0.00	<0.00
Ce140	<0.00	<0.00	<0.00	<0.00	<0.00	<0.00	<0.00	<0.00	<0.00	<0.00	<0.00	<0.00	<0.00	<0.00	<0.00	<0.00	<0.00	<0.00	<0.00	<0.00	<0.00
Nd146	<0.00	<0.00	<0.00	<0.00	<0.00	<0.00	<0.00	<0.00	<0.00	<0.00	<0.00	<0.00	<0.00	<0.00	<0.00	<0.00	<0.00	<0.00	<0.00	<0.00	<0.00
Hf178	<0.00	<0.00	<0.00	<0.00	<0.00	<0.00	<0.00	<0.00	<0.00	<0.00	<0.00	<0.00	<0.00	<0.00	<0.00	<0.00	<0.00	<0.00	<0.00	<0.00	<0.00
W182	<0.00	<0.00	<0.00	<0.00	<0.00	<0.00	<0.00	<0.00	<0.00	<0.00	<0.00	<0.00	<0.00	<0.00	<0.00	<0.00	<0.00	<0.00	<0.00	<0.00	<0.00
Re185	<0.00	<0.00	<0.00	<0.00	<0.00	<0.00	<0.00	<0.00	<0.00	<0.00	<0.00	<0.00	<0.00	<0.00	<0.00	<0.00	<0.00	<0.00	<0.00	<0.00	<0.00
Re187	<0.00	<0.00	<0.00	<0.00	<0.00	<0.00	<0.00	<0.00	<0.00	<0.00	<0.00	<0.00	<0.00	<0.00	<0.00	<0.00	<0.00	<0.00	<0.00	<0.00	<0.00
Os189	0	0	0	10.67	10.51	0.051	0.05	0.03	0.047	0.081	0.051	0.078	0.042	0.056	0.077	0.048	0	0	0	16.16	17.4
Os190	0	0	0	14.34	13.29	0.031	0.028	0.017	0.02	0.051	0.03	0.031	0.027	0.034	0.048	0.036	0	0	0	21.66	23.03
Ir193	0	0	0	3.95	4	0.0077	0.0082	0.0045	0.0055	0.013	0.0092	0.0096	0.0067	0.0092	0.012	0.0077	0	0	0	4.78	4.73
Pt195	0	0	0	7.55	7.49	0.025	0.022	0.016	0.025	0.038	0.025	0.032	0.024	0.037	0.041	0.023	0	0	0	8.77	8.73
Au197	0	0	0	21.17	20.3	0.021	0.033	3.06	1.69	0.018	0.018	0.02	0.012	0.028	0.14	0.059	0	0	0	33.03	31.02
Pb208	<0.00	<0.00	<0.00	<0.00	<0.00	<0.00	<0.00	<0.00	<0.00	<0.00	<0.00	<0.00	<0.00	<0.00	<0.00	<0.00	<0.00	<0.00	<0.00	<0.00	<0.00
Bi209	0.00002	0.00002	0	21.54	20.44	1.16	5.28	2.73	0.52	0.14	0.027	0.11	0.23	2.13	3.91	4.5	0.00001	0.00001	0	34.32	32.42
Th232	<0.00	<0.00	<0.00	<0.00	<0.00	<0.00	<0.00	<0.00	<0.00	<0.00	<0.00	<0.00	<0.00	<0.00	<0.00	<0.00	<0.00	<0.00	<0.00	<0.00	<0.00
U238	<0.00	<0.00	<0.00	<0.00	<0.00	<0.00	<0.00	<0.00	<0.00	<0.00	<0.00	<0.00	<0.00	<0.00	<0.00	<0.00	<0.00	<0.00	<0.00	<0.00	<0.00
ThO248	<0.00	<0.00	<0.00	<0.00	<0.00	<0.00	<0.00	<0.00	<0.00	<0.00	<0.00	<0.00	<0.00	<0.00	<0.00	<0.00	<0.00	<0.00	<0.00	<0.00	<0.00

Element	STD610-1	STD610-2	BCR2G-1	PGEA-1	PGEA-2	BG24-PY	BG24-CPY	JL06-PY	JC22-PY	JC22-SPH	JC22-CPY	BG14-PY	JL09-PY	JL09-SPH	BG24-SPH	BG24-SP2	STD610-3	STD610-4	PGEA-3	PGEA-4	PGEA-5
GLITTER!: Minimum detection limits (99% confidence).																					
Element	STD610-1	STD610-2	BCR2G-1	PGEA-1	PGEA-2	BG24-PY	BG24-CPY	JL06-PY	JC22-PY	JC22-SPH	JC22-CPY	BG14-PY	JL09-PY	JL09-SPH	BG24-SPH	BG24-SP2	STD610-3	STD610-4	PGEA-3	PGEA-4	PGEA-5
Al27	<0.00	<0.00	<0.00	<0.00	<0.00	<0.00	<0.00	<0.00	<0.00	<0.00	<0.00	<0.00	<0.00	<0.00	<0.00	<0.00	<0.00	<0.00	<0.00	<0.00	<0.00
Si29	<0.00	<0.00	<0.00	<0.00	<0.00	<0.00	<0.00	<0.00	<0.00	<0.00	<0.00	<0.00	<0.00	<0.00	<0.00	<0.00	<0.00	<0.00	<0.00	<0.00	<0.00
S34	0.00029	0.00026	0.00041	547.53	562.37	127.94	113.5	74.79	129.85	235.45	165.89	173.12	131.58	178.04	212.7	161.28	0.00025	0.00024	0.00001	764.67	643.69
Ca43	<0.00	<0.00	<0.00	<0.00	<0.00	<0.00	<0.00	<0.00	<0.00	<0.00	<0.00	<0.00	<0.00	<0.00	<0.00	<0.00	<0.00	<0.00	<0.00	<0.00	<0.00
Sc45	<0.00	<0.00	<0.00	<0.00	<0.00	<0.00	<0.00	<0.00	<0.00	<0.00	<0.00	<0.00	<0.00	<0.00	<0.00	<0.00	<0.00	<0.00	<0.00	<0.00	<0.00
Ti49	<0.00	<0.00	<0.00	<0.00	<0.00	<0.00	<0.00	<0.00	<0.00	<0.00	<0.00	<0.00	<0.00	<0.00	<0.00	<0.00	<0.00	<0.00	<0.00	<0.00	<0.00
V51	<0.00	<0.00	<0.00	<0.00	<0.00	<0.00	<0.00	<0.00	<0.00	<0.00	<0.00	<0.00	<0.00	<0.00	<0.00	<0.00	<0.00	<0.00	<0.00	<0.00	<0.00
Cr53	<0.00	<0.00	<0.00	<0.00	<0.00	<0.00	<0.00	<0.00	<0.00	<0.00	<0.00	<0.00	<0.00	<0.00	<0.00	<0.00	<0.00	<0.00	<0.00	<0.00	<0.00
Mn55	<0.00	<0.00	<0.00	<0.00	<0.00	<0.00	<0.00	<0.00	<0.00	<0.00	<0.00	<0.00	<0.00	<0.00	<0.00	<0.00	<0.00	<0.00	<0.00	<0.00	<0.00
Fe57	<0.00	<0.00	<0.00	<0.00	<0.00	<0.00	<0.00	<0.00	<0.00	<0.00	<0.00	<0.00	<0.00	<0.00	<0.00	<0.00	<0.00	<0.00	<0.00	<0.00	<0.00
Co59	<0.00	<0.00	<0.00	<0.00	<0.00	<0.00	<0.00	<0.00	<0.00	<0.00	<0.00	<0.00	<0.00	<0.00	<0.00	<0.00	<0.00	<0.00	<0.00	<0.00	<0.00
Ni60	0	0	0	0.85	0.734	0.169	0.144	0.0955	0.138	0.258	0.158	0.21	0.131	0.197	0.254	0.149	0	0	0	3.06	0.75
Ni62	0	0	0	4.54	4.68	1	0.827	0.436	0.732	1.39	0.905	0.972	0.734	0.836	1.38	0.93	0	0	0	8.13	4.2
Cu65	0	0	0	2.17	2.01	0.463	0.396	0.266	0.395	0.761	0.467	0.534	0.396	0.509	0.665	0.432	0	0	0	1.76	1.87
Zn66	<0.00	<0.00	<0.00	<0.00	<0.00	<0.00	<0.00	<0.00	<0.00	<0.00	<0.00	<0.00	<0.00	<0.00	<0.00	<0.00	<0.00	<0.00	<0.00	<0.00	<0.00
Ga71	<0.00	<0.00	<0.00	<0.00	<0.00	<0.00	<0.00	<0.00	<0.00	<0.00	<0.00	<0.00	<0.00	<0.00	<0.00	<0.00	<0.00	<0.00	<0.00	<0.00	<0.00
As75	0	0	0	2.74	2.91	0.603	0.549	0.366	1.74	3.78	2.45	2.79	2.07	2.55	3.28	2.02	0	0	0	9.38	9.7
Se82	0.00002	0.00001	0.00002	29.49	28.76	6.69	5.23	3.65	5.41	9.35	5.83	7.04	5.56	6.83	8.97	6	0.00001	0.00001	0	26.87	29.37
Y89	<0.00	<0.00	<0.00	<0.00	<0.00	<0.00	<0.00	<0.00	<0.00	<0.00	<0.00	<0.00	<0.00	<0.00	<0.00	<0.00	<0.00	<0.00	<0.00	<0.00	<0.00
Zr90	<0.00	<0.00	<0.00	<0.00	<0.00	<0.00	<0.00	<0.00	<0.00	<0.00	<0.00	<0.00	<0.00	<0.00	<0.00	<0.00	<0.00	<0.00	<0.00	<0.00	<0.00
Nb93	<0.00	<0.00	<0.00	<0.00	<0.00	<0.00	<0.00	<0.00	<0.00	<0.00	<0.00	<0.00	<0.00	<0.00	<0.00	<0.00	<0.00	<0.00	<0.00	<0.00	<0.00
Mo95	<0.00	<0.00	<0.00	<0.00	<0.00	<0.00	<0.00	<0.00	<0.00	<0.00	<0.00	<0.00	<0.00	<0.00	<0.00	<0.00	<0.00	<0.00	<0.00	<0.00	<0.00
Ru99	0	0	0	0.38	0.421	0.103	0.086	0.0484	0.0587	0.126	0.0893	0.118	0.075	0.092	0.108	0.0739	0	0	0	0.412	0.437
Ru101	0	0	0	0.361	0.305	0.058	0.0593	0.0446	0.06	0.0767	0.0675	0.0773	0.0467	0.0661	0.0546	0.0347	0	0	0	0.255	0.312
Rh103	0	0	0	0.397	0.395	0.087	0.0778	0.0532	0.0817	0.159	0.104	0.113	0.0853	0.114	0.147	0.0958	0	0	0	0.386	0.42
Ag107	<0.00	<0.00	<0.00	<0.00	<0.00	<0.00	<0.00	<0.00	<0.00	<0.00	<0.00	<0.00	<0.00	<0.00	<0.00	<0.00	<0.00	<0.00	<0.00	<0.00	<0.00
Pd108	0	0	0	0.243	0.233	0.0606	0.0359	0.0299	0.0487	0.0856	0.0617	0.0594	0.0519	0.0667	0.0607	0.0457	0	0	0	0.214	0.199
Cd111	<0.00	<0.00	<0.00	<0.00	<0.00	<0.00	<0.00	<0.00	<0.00	<0.00	<0.00	<0.00	<0.00	<0.00	<0.00	<0.00	<0.00	<0.00	<0.00	<0.00	<0.00
In115	<0.00	<0.00	<0.00	<0.00	<0.00	<0.00	<0.00	<0.00	<0.00	<0.00	<0.00	<0.00	<0.00	<0.00	<0.00	<0.00	<0.00	<0.00	<0.00	<0.00	<0.00
Sn118	<0.00	<0.00	<0.00	<0.00	<0.00	<0.00	<0.00	<0.00	<0.00	<0.00	<0.00	<0.00	<0.00	<0.00	<0.00	<0.00	<0.00	<0.00	<0.00	<0.00	<0.00
Sb121	<0.00	<0.00	<0.00	<0.00	<0.00	<0.00	<0.00	<0.00	<0.00	<0.00	<0.00	<0.00	<0.00	<0.00	<0.00	<0.00	<0.00	<0.00	<0.00	<0.00	<0.00
Te125	0	0	0	2.96	3.01	0.639	0.414	0.387	0.242	1.12	0.522	0.444	0.575	0.602	0.908	0.448	0	0	0	2.06	2.29
Te128	0	0	0	3.43	3.41	0.741	0.647	0.404	0.614	1.05	0.683	0.798	0.589	0.692	0.953	0.638	0	0	0	2.72	3.13
La139	<0.00	<0.00	<0.00	<0.00	<0.00	<0.00	<0.00	<0.00	<0.00	<0.00	<0.00	<0.00	<0.00	<0.00	<0.00	<0.00	<0.00	<0.00	<0.00	<0.00	<0.00
Ce140	<0.00	<0.00	<0.00	<0.00	<0.00	<0.00	<0.00	<0.00	<0.00	<0.00	<0.00	<0.00	<0.00	<0.00	<0.00	<0.00	<0.00	<0.00	<0.00	<0.00	<0.00
Nd146	<0.00	<0.00	<0.00	<0.00	<0.00	<0.00	<0.00	<0.00	<0.00	<0.00	<0.00	<0.00	<0.00	<0.00	<0.00	<0.00	<0.00	<0.00	<0.00	<0.00	<0.00
Hf178	<0.00	<0.00	<0.00	<0.00	<0.00	<0.00	<0.00	<0.00	<0.00	<0.00	<0.00	<0.00	<0.00	<0.00	<0.00	<0.00	<0.00	<0.00	<0.00	<0.00	<0.00
W182	<0.00	<0.00	<0.00	<0.00	<0.00	<0.00	<0.00	<0.00	<0.00	<0.00	<0.00	<0.00	<0.00	<0.00	<0.00	<0.00	<0.00	<0.00	<0.00	<0.00	<0.00
Re185	<0.00	<0.00	<0.00	<0.00	<0.00	<0.00	<0.00	<0.00	<0.00	<0.00	<0.00	<0.00	<0.00	<0.00	<0.00	<0.00	<0.00	<0.00	<0.00	<0.00	<0.00
Re187	<0.00	<0.00	<0.00	<0.00	<0.00	<0.00	<0.00	<0.00	<0.00	<0.00	<0.00	<0.00	<0.00	<0.00	<0.00	<0.00	<0.00	<0.00	<0.00	<0.00	<0.00
Os189	0	0	0	0.448	0.595	0.14	0.113	0.0868	0.129	0.237	0.136	0.21	0.117	0.115	0.187	0.137	0	0	0	0.617	0.834
Os190	0	0	0	0.375	0.33	0.0708	0.0693	0.0434	0.0475	0.123	0.0821	0.0772	0.0702	0.097	0.11	0.0966	0	0	0	0.355	0.397
Ir193	0	0	0	0.0817	0.0906	0.0186	0.0201	0.0111	0.0139	0.037	0.0252	0.0265	0.0162	0.0211	0.0301	0.0201	0	0	0	0.0731	0.0759
Pt195	0	0	0	0.385	0.303	0.0665	0.056	0.0409	0.0658	0.0688	0.0614	0.0818	0.0579	0.0976	0.111	0.0577	0	0	0	0.338	0.375
Au197	0	0	0	0.126	0.144	0.0407	0.028	0.0174	0.0378	0.0383	0.0228	0.0245	0.0303	0.031	0.0419	0.0247	0	0	0	0.129	0.158
Pb208	<0.00	<0.00	<0.00	<0.00	<0.00	<0.00	<0.00	<0.00	<0.00	<0.00	<0.00	<0.00	<0.00	<0.00	<0.00	<0.00	<0.00	<0.00	<0.00	<0.00	<0.00
Bi209	0	0	0	0.17	0.148	0.0364	0.0317	0.016	0.0208	0.0534	0.0349	0.0364	0.0329	0.0405	0.0602	0.0302	0	0	0	0.171	0.163
Th232	<0.00	<0.00	<0.00	<0.00	<0.00	<0.00	<0.00	<0.00	<0.00	<0.00	<0.00	<0.00	<0.00	<0.00	<0.00	<0.00	<0.00	<0.00	<0.00	<0.00	<0.00
U238	<0.00	<0.00	<0.00	<0.00	<0.00	<0.00	<0.00	<0.00	<0.00	<0.00	<0.00	<0.00	<0.00	<0.00	<0.00	<0.00	<0.00	<0.00	<0.00	<0.00	<0.00
ThO248	<0.00	<0.00	<0.00	<0.00	<0.00	<0.00	<0.00	<0.00	<0.00	<0.00	<0.00	<0.00	<0.00	<0.00	<0.00	<0.00	<0.00	<0.00	<0.00	<0.00	<0.00
GLITTER!: Trace element concentrations normalised to chondrite.																					
Element	STD610-1	STD610-2	BCR2G-1	PGEA-1	PGEA-2	BG24-PY	BG24-CPY	JL06-PY	JC22-PY	JC22-SPH	JC22-CPY	BG14-PY	JL09-PY	JL09-SPH	BG24-SPH	BG24-SP2	STD610-3	STD610-4	PGEA-3	PGEA-4	PGEA-5

Element	STD610-1	STD610-2	BCR2G-1	PGEA-1	PGEA-2	BG24-PY	BG24-CPY	JL06-PY	JC22-PY	JC22-SPH	JC22-CPY	BG14-PY	JL09-PY	JL09-SPH	BG24-SPH	BG24-SP2	STD610-3	STD610-4	PGEA-3	PGEA-4	PGEA-5
Al27	<****	<****	<****	<****	<****	<****	<****	<****	<****	<****	<****	<****	<****	<****	<****	<****	<****	<****	<****	<****	<****
Si29	<****	<****	<****	<****	<****	<****	<****	<****	<****	<****	<****	<****	<****	<****	<****	<****	<****	<****	<****	<****	<****
S34	Inf	Inf	Inf	Inf	Inf	Inf	Inf	Inf	Inf	Inf	Inf	Inf	Inf	Inf	Inf	Inf	Inf	Inf	Inf	Inf	Inf
Ca43	<****	<****	<****	<****	<****	<****	<****	<****	<****	<****	<****	<****	<****	<****	<****	<****	<****	<****	<****	<****	<****
Sc45	<****	<****	<****	<****	<****	<****	<****	<****	<****	<****	<****	<****	<****	<****	<****	<****	<****	<****	<****	<****	<****
Ti49	<****	<****	<****	<****	<****	<****	<****	<****	<****	<****	<****	<****	<****	<****	<****	<****	<****	<****	<****	<****	<****
V51	<****	<****	<****	<****	<****	<****	<****	<****	<****	<****	<****	<****	<****	<****	<****	<****	<****	<****	<****	<****	<****
Cr53	<****	<****	<****	<****	<****	<****	<****	<****	<****	<****	<****	<****	<****	<****	<****	<****	<****	<****	<****	<****	<****
Mn55	<****	<****	<****	<****	<****	<****	<****	<****	<****	<****	<****	<****	<****	<****	<****	<****	<****	<****	<****	<****	<****
Fe57	<****	<****	<****	<****	<****	<****	<****	<****	<****	<****	<****	<****	<****	<****	<****	<****	<****	<****	<****	<****	<****
Co59	<****	<****	<****	<****	<****	<****	<****	<****	<****	<****	<****	<****	<****	<****	<****	<****	<****	<****	<****	<****	<****
Ni60	0	0	0	43.67	42.75	0.01025	0.00017	0.00056	0.00045	0.00003	0.00001	0.00018	0	0	0.00075	0.00034	0	0	0	44.1	43
Ni62	0	0	0	45.02	41.3	0.01106	0.00023	0.0006	0.00047	0	0	0.00028	0	0.0001	0.00058	0.00028	0	0	0	44.05	43.05
Cu65	0	0	0	1.48	1.39	0.552	1274.57	2.05	0.0966	21.27	1322.99	0.546	0.0091	75.18	596.23	94.2	0	0	0	1.51	1.42
Zn66	<****	<****	<****	<****	<****	<****	<****	<****	<****	<****	<****	<****	<****	<****	<****	<****	<****	<****	<****	<****	<****
Ga71	<****	<****	<****	<****	<****	<****	<****	<****	<****	<****	<****	<****	<****	<****	<****	<****	<****	<****	<****	<****	<****
As75	0.00005	0.00005	0	47.37	46.95	25.16	59.57	9452.02	2454.42	1.82	442.07	11.3	23.57	0	89.2	26.48	0.00003	0.00003	0	47.17	47.31
Se82	0	0	0	8.75	9.21	1.54	0	0	2.19	0.49	0.64	0	3.37	1.87	0	0	0	0	0	9.13	8.8
Y89	<****	<****	<****	<****	<****	<****	<****	<****	<****	<****	<****	<****	<****	<****	<****	<****	<****	<****	<****	<****	<****
Zr90	<****	<****	<****	<****	<****	<****	<****	<****	<****	<****	<****	<****	<****	<****	<****	<****	<****	<****	<****	<****	<****
Nb93	<****	<****	<****	<****	<****	<****	<****	<****	<****	<****	<****	<****	<****	<****	<****	<****	<****	<****	<****	<****	<****
Mo95	<****	<****	<****	<****	<****	<****	<****	<****	<****	<****	<****	<****	<****	<****	<****	<****	<****	<****	<****	<****	<****
Ru99	0	0	0	217.88	207.12	0	0.211	0	0.112	0	0.283	0	0	0	0.112	0	0	0	0.00001	222.71	209.88
Ru101	0	0	0	212.98	215.37	0	0.079	0	0	0	0.116	0	0	0	0.076	0	0	0	0.00001	214.98	213.33
Rh103	0	0	0	1209.39	1208.28	0	51.38	0	0	1.15	54.74	0	0	3.13	19.96	3.55	0	0	0.00003	1249.35	1192.14
Ag107	<****	<****	<****	<****	<****	<****	<****	<****	<****	<****	<****	<****	<****	<****	<****	<****	<****	<****	<****	<****	<****
Pd108	0	0	0	311.96	300.96	0.12	0.99	1.37	0.077	61.94	0.79	0	0	51.93	36.3	68.69	0	0	0.00001	332.62	298.6
Cd111	<****	<****	<****	<****	<****	<****	<****	<****	<****	<****	<****	<****	<****	<****	<****	<****	<****	<****	<****	<****	<****
In115	<****	<****	<****	<****	<****	<****	<****	<****	<****	<****	<****	<****	<****	<****	<****	<****	<****	<****	<****	<****	<****
Sn118	<****	<****	<****	<****	<****	<****	<****	<****	<****	<****	<****	<****	<****	<****	<****	<****	<****	<****	<****	<****	<****
Sb121	<****	<****	<****	<****	<****	<****	<****	<****	<****	<****	<****	<****	<****	<****	<****	<****	<****	<****	<****	<****	<****
Te125	0.00004	0.00004	0	69.03	72.82	0.79	0.233	0.153	1.2	0	0	0.176	0.83	0	0.36	0.196	0.00003	0.00003	0	76.84	67.94
Te128	0.00004	0.00004	0	72.79	67.36	0.84	0	0.21	0.98	0	0	0	0.94	0.221	0.31	0	0.00003	0.00003	0	72.57	69.6
La139	<****	<****	<****	<****	<****	<****	<****	<****	<****	<****	<****	<****	<****	<****	<****	<****	<****	<****	<****	<****	<****
Ce140	<****	<****	<****	<****	<****	<****	<****	<****	<****	<****	<****	<****	<****	<****	<****	<****	<****	<****	<****	<****	<****
Nd146	<****	<****	<****	<****	<****	<****	<****	<****	<****	<****	<****	<****	<****	<****	<****	<****	<****	<****	<****	<****	<****
Hf178	<****	<****	<****	<****	<****	<****	<****	<****	<****	<****	<****	<****	<****	<****	<****	<****	<****	<****	<****	<****	<****
W182	<****	<****	<****	<****	<****	<****	<****	<****	<****	<****	<****	<****	<****	<****	<****	<****	<****	<****	<****	<****	<****
Re185	<****	<****	<****	<****	<****	<****	<****	<****	<****	<****	<****	<****	<****	<****	<****	<****	<****	<****	<****	<****	<****
Re187	<****	<****	<****	<****	<****	<****	<****	<****	<****	<****	<****	<****	<****	<****	<****	<****	<****	<****	<****	<****	<****
Os189	0	0	0	188.47	180.8	0	0	0	0	0	0	0	0	0	0	0	0	0	0	180.47	187.9
Os190	0	0	0	192.95	175.08	0	0	0	0	0	0	0	0	0	0	0	0	0	0.00001	182.14	186.98
Ir193	0	0	0	150.12	150.27	0	0	0	0	0	0	0	0	0	0	0	0	0	0	152.69	149.07
Pt195	0	0	0	144.42	141.02	0	0	0	0	0.085	0	0	0	0	0	0	0	0	0	144.37	142.55
Au197	0.00004	0.00004	0	1094.79	1035.62	0.32	1.13	148.18	79.9	0	0.431	0.447	0	0.68	5.16	2.03	0.00002	0.00002	0.00003	1144.64	1043.47
Pb208	<****	<****	<****	<****	<****	<****	<****	<****	<****	<****	<****	<****	<****	<****	<****	<****	<****	<****	<****	<****	<****
Bi209	0.00102	0.00105	0	1446.3	1352.46	74.97	337.39	170.45	31.3	7.5	1.07	5.74	12.02	112.29	200.53	223.72	0.00067	0.00067	0.00003	1501.05	1373.34
Th232	<****	<****	<****	<****	<****	<****	<****	<****	<****	<****	<****	<****	<****	<****	<****	<****	<****	<****	<****	<****	<****
U238	<****	<****	<****	<****	<****	<****	<****	<****	<****	<****	<****	<****	<****	<****	<****	<****	<****	<****	<****	<****	<****
ThO248	<****	<****	<****	<****	<****	<****	<****	<****	<****	<****	<****	<****	<****	<****	<****	<****	<****	<****	<****	<****	<****

GLITTER4.0: Laser Ablation Analysis Results

G:\KYLIE\MAR13\PGEARUN2
Fri Mar 14 17:44:59 2003

All values are reported in ppm

GLITTER!: Trace Element Concentrations MDL filtered.

Element	STD610-1	STD610-2	BCR2G-1	PGEA-1	PGEA-2	PGEA-3	MS-CPY	MS-PY	KP11-PY	KP11-CPY	KP11-SPH	BG30-CPY	BG30-PY	JL06-PY2	JL06-SPH	BG06-SPH	BG06-PY	STD610-3	STD610-4	STD610-5	STD610-6	PGEA-4	PGEA-5	BCR2G-2	JL10-PY1
Al27	<0.00	<0.00	<0.00	<0.00	<0.00	<0.00	<0.00	<0.00	<0.00	<0.00	<0.00	<0.00	<0.00	<0.00	<0.00	<0.00	<0.00	<0.00	<0.00	<0.00	<0.00	<0.00	<0.00	<0.00	<0.00
Si29	<0.00	<0.00	<0.00	<0.00	<0.00	<0.00	<0.00	<0.00	<0.00	<0.00	<0.00	<0.00	<0.00	<0.00	<0.00	<0.00	<0.00	<0.00	<0.00	<0.00	<0.00	<0.00	<0.00	<0.00	<0.00
S34	277999.75	277999.75	47632.28	277999.75	278000	278000	349436.88	534495.56	534495.56	349436.84	334173.16	349436.84	534495.56	534495.56	331971.66	330957.63	534495.56	277999.75	392.3	392.3	0.667	278000	278000	47632.28	534495.56
Ca43	<0.00	<0.00	<0.00	<0.00	<0.00	<0.00	<0.00	<0.00	<0.00	<0.00	<0.00	<0.00	<0.00	<0.00	<0.00	<0.00	<0.00	<0.00	<0.00	<0.00	<0.00	<0.00	<0.00	<0.00	<0.00
Sc45	<-NaN	<-NaN	<-NaN	<-NaN	<-NaN	<-NaN	<-NaN	<-NaN	<-NaN	<-NaN	<-NaN	<-NaN	<-NaN	<-NaN	<-NaN	<-NaN	<-NaN	<-NaN	<-NaN	<-NaN	<-NaN	<-NaN	<-NaN	<-NaN	<-NaN
Ti49	<-NaN	<-NaN	<-NaN	<-NaN	<-NaN	<-NaN	<-NaN	<-NaN	<-NaN	<-NaN	<-NaN	<-NaN	<-NaN	<-NaN	<-NaN	<-NaN	<-NaN	<-NaN	<-NaN	<-NaN	<-NaN	<-NaN	<-NaN	<-NaN	<-NaN
V51	<-NaN	<-NaN	<-NaN	<-NaN	<-NaN	<-NaN	<-NaN	<-NaN	<-NaN	<-NaN	<-NaN	<-NaN	<-NaN	<-NaN	<-NaN	<-NaN	<-NaN	<-NaN	<-NaN	<-NaN	<-NaN	<-NaN	<-NaN	<-NaN	<-NaN
Cr53	<-NaN	<-NaN	<-NaN	<-NaN	<-NaN	<-NaN	<-NaN	<-NaN	<-NaN	<-NaN	<-NaN	<-NaN	<-NaN	<-NaN	<-NaN	<-NaN	<-NaN	<-NaN	<-NaN	<-NaN	<-NaN	<-NaN	<-NaN	<-NaN	<-NaN
Mn55	<-NaN	<-NaN	<-NaN	<-NaN	<-NaN	<-NaN	<-NaN	<-NaN	<-NaN	<-NaN	<-NaN	<-NaN	<-NaN	<-NaN	<-NaN	<-NaN	<-NaN	<-NaN	<-NaN	<-NaN	<-NaN	<-NaN	<-NaN	<-NaN	<-NaN
Fe57	<0.00	<0.00	<0.00	<0.00	<0.00	<0.00	<0.00	<0.00	<0.00	<0.00	<0.00	<0.00	<0.00	<0.00	<0.00	<0.00	<0.00	<0.00	<0.00	<0.00	<0.00	<0.00	<0.00	<0.00	<0.00
Co59	<0.00	<0.00	<0.00	<0.00	<0.00	<0.00	<0.00	<0.00	<0.00	<0.00	<0.00	<0.00	<0.00	<0.00	<0.00	<0.00	<0.00	<0.00	<0.00	<0.00	<0.00	<0.00	<0.00	<0.00	<0.00
Ni60	8733.41	8004.8	40.52	733551.19	693480.56	732904.69	1.297	15.08	0.533	0.11	<0.65	0.362	6.11	2.004	0.409	0.727	1.083	3602.74	13.49	7.14	0.00882	718399	714146.44	37.31	2.66
Ni62	8532.37	7938.47	37.37	663565.56	681208.88	725538.63	1.25	13.22	<0.60	3.17	<0.74	<0.65	7.1	105.18	<0.38	0.91	0.64	3565.76	13.56	7.89	0.00877	720768.44	725390.06	52.38	0.76
Cu65	5132.5	4691.12	41.93	220.57	242.26	244.58	261005.34	106.21	0.542	246350.88	11590.44	251508.16	1985.28	78.39	130.17	47.44	221.23	2083.42	8.36	4.79	0.00497	241.35	243.39	51.51	6.71
Zn66	<0.00	<0.00	<0.00	<0.00	<0.00	<0.00	<0.00	<0.00	<0.00	<0.00	<0.00	<0.00	<0.00	<0.00	<0.00	<0.00	<0.00	<0.00	<0.00	<0.00	<0.00	<0.00	<0.00	<0.00	<0.00
Ga71	<-NaN	<-NaN	<-NaN	<-NaN	<-NaN	<-NaN	<-NaN	<-NaN	<-NaN	<-NaN	<-NaN	<-NaN	<-NaN	<-NaN	<-NaN	<-NaN	<-NaN	<-NaN	<-NaN	<-NaN	<-NaN	<-NaN	<-NaN	<-NaN	<-NaN
As75	5920.27	5505.06	<20.52	114.07	133.16	135.44	2.84	153.72	14.23	2.07	9.95	35.92	727.88	6988.37	77.39	15.08	5236.22	2380.87	9.04	5.23	0.00596	125.16	139.22	<15.24	727.3
Se82	3671.74	3156.8	<39.87	221.46	232.69	241.87	24.75	4.26	135.84	265.09	23.78	41.76	8.47	3.32	<2.40	15.95	2.2	1396.57	4.55	2.72	0.00317	240.78	249.92	<24.10	24.65
Y89	<-NaN	<-NaN	<-NaN	<-NaN	<-NaN	<-NaN	<-NaN	<-NaN	<-NaN	<-NaN	<-NaN	<-NaN	<-NaN	<-NaN	<-NaN	<-NaN	<-NaN	<-NaN	<-NaN	<-NaN	<-NaN	<-NaN	<-NaN	<-NaN	<-NaN
Zr90	<-NaN	<-NaN	<-NaN	<-NaN	<-NaN	<-NaN	<-NaN	<-NaN	<-NaN	<-NaN	<-NaN	<-NaN	<-NaN	<-NaN	<-NaN	<-NaN	<-NaN	<-NaN	<-NaN	<-NaN	<-NaN	<-NaN	<-NaN	<-NaN	<-NaN
Nb93	<-NaN	<-NaN	<-NaN	<-NaN	<-NaN	<-NaN	<-NaN	<-NaN	<-NaN	<-NaN	<-NaN	<-NaN	<-NaN	<-NaN	<-NaN	<-NaN	<-NaN	<-NaN	<-NaN	<-NaN	<-NaN	<-NaN	<-NaN	<-NaN	<-NaN
Mo95	<-NaN	<-NaN	<-NaN	<-NaN	<-NaN	<-NaN	<-NaN	<-NaN	<-NaN	<-NaN	<-NaN	<-NaN	<-NaN	<-NaN	<-NaN	<-NaN	<-NaN	<-NaN	<-NaN	<-NaN	<-NaN	<-NaN	<-NaN	<-NaN	<-NaN
Ru99	5.98	<5.79	0.42	209.02	227.28	241.51	0.587	0.046	<0.038	0.585	<0.068	0.603	0.46	0.052	<0.043	<0.043	<0.032	<2.23	0.0062	<0.0050	<0.00000	240.47	217.1	0.56	0.122
Ru101	<5.14	2.25	0.267	207.81	224.82	244.44	0.306	<0.032	<0.033	0.216	<0.054	0.289	<0.036	<0.0205	<0.0218	<0.046	<0.028	<1.12	<0.0024	<0.00234	<0.00000	232.49	220.88	<0.237	0.027
Rh103	34.9	29.3	<0.46	219.31	239.4	260.85	26.43	<0.039	<0.040	25.51	1.287	24.67	0.257	<0.029	0.034	<0.035	0.044	13.22	0.0486	0.0273	0.00003	258.39	229.13	<0.31	<0.041
Ag107	<0.00	<0.00	<0.00	<0.00	<0.00	<0.00	<0.00	<0.00	<0.00	<0.00	<0.00	<0.00	<0.00	<0.00	<0.00	<0.00	<0.00	<0.00	<0.00	<0.00	<0.00	<0.00	<0.00	<0.00	<0.00
Pd108	66.99	66.7	0.53	253.57	249.94	262.92	<0.0135	<0.030	<0.029	0.4	59.53	0.234	0.187	<0.0229	80.59	71.05	0.919	29.96	0.1185	0.0714	0.00007	265.43	254.79	<0.28	<0.025
Cd111	<0.00	<0.00	<0.00	<0.00	<0.00	<0.00	<0.00	<0.00	<0.00	<0.00	<0.00	<0.00	<0.00	<0.00	<0.00	<0.00	<0.00	<0.00	<0.00	<0.00	<0.00	<0.00	<0.00	<0.00	<0.00
In115	<0.00	<0.00	<0.00	<0.00	<0.00	<0.00	<0.00	<0.00	<0.00	<0.00	<0.00	<0.00	<0.00	<0.00	<0.00	<0.00	<0.00	<0.00	<0.00	<0.00	<0.00	<0.00	<0.00	<0.00	<0.00
Sn118	<0.00	<0.00	<0.00	<0.00	<0.00	<0.00	<0.00	<0.00	<0.00	<0.00	<0.00	<0.00	<0.00	<0.00	<0.00	<0.00	<0.00	<0.00	<0.00	<0.00	<0.00	<0.00	<0.00	<0.00	<0.00
Sb121	<0.00	<0.00	<0.00	<0.00	<0.00	<0.00	<0.00	<0.00	<0.00	<0.00	<0.00	<0.00	<0.00	<0.00	<0.00	<0.00	<0.00	<0.00	<0.00	<0.00	<0.00	<0.00	<0.00	<0.00	<0.00
Te125	5782.98	5172.88	<2.81	187.11	235.23	246.35	1	10.57	4.21	12.85	51.97	1.61	2.82	0.66	<0.206	<0.21	1.06	2379.33	7.96	5	0.00565	248.84	237.53	<2.69	5.85
Te128	5794.88	5212.59	<4.77	190.96	242.55	258.07	0.85	10.07	4.53	13.14	52.47	1.01	2.78	0.55	<0.28	<0.32	1.22	2350.13	8.18	5.22	0.00569	241.47	232.25	<2.81	5.68
La139	<-NaN	<-NaN	<-NaN	<-NaN	<-NaN	<-NaN	<-NaN	<-NaN	<-NaN	<-NaN	<-NaN	<-NaN	<-NaN	<-NaN	<-NaN	<-NaN	<-NaN	<-NaN	<-NaN	<-NaN	<-NaN	<-NaN	<-NaN	<-NaN	<-NaN
Ce140	<-NaN	<-NaN	<-NaN	<-NaN	<-NaN	<-NaN	<-NaN	<-NaN	<-NaN	<-NaN	<-NaN	<-NaN	<-NaN	<-NaN	<-NaN	<-NaN	<-NaN	<-NaN	<-NaN	<-NaN	<-NaN	<-NaN	<-NaN	<-NaN	<-NaN
Nd146	<-NaN	<-NaN	<-NaN	<-NaN	<-NaN	<-NaN	<-NaN	<-NaN	<-NaN	<-NaN	<-NaN	<-NaN	<-NaN	<-NaN	<-NaN	<-NaN	<-NaN	<-NaN	<-NaN	<-NaN	<-NaN	<-NaN	<-NaN	<-NaN	<-NaN
Hf178	<-NaN	<-NaN	<-NaN	<-NaN	<-NaN	<-NaN	<-NaN	<-NaN	<-NaN	<-NaN	<-NaN	<-NaN	<-NaN	<-NaN	<-NaN	<-NaN	<-NaN	<-NaN	<-NaN	<-NaN	<-NaN	<-NaN	<-NaN	<-NaN	<-NaN
W182	<-NaN	<-NaN	<-NaN	<-NaN	<-NaN	<-NaN	<-NaN	<-NaN	<-NaN	<-NaN	<-NaN	<-NaN	<-NaN	<-NaN	<-NaN	<-NaN	<-NaN	<-NaN	<-NaN	<-NaN	<-NaN	<-NaN	<-NaN	<-NaN	<-NaN
Re185	<-NaN	<-NaN	<-NaN	<-NaN	<-NaN	<-NaN	<-NaN	<-NaN	<-NaN	<-NaN	<-NaN	<-NaN	<-NaN	<-NaN	<-NaN	<-NaN	<-NaN	<-NaN	<-NaN	<-NaN	<-NaN	<-NaN	<-NaN	<-NaN	<-NaN
Re187	<0.00	<0.00	<0.00	<0.00	<0.00	<0.00	<0.00	<0.00	<0.00	<0.00	<0.00	<0.00	<0.00	<0.00	<0.00	<0.00	<0.00	<0.00	<0.00	<0.00	<0.00	<0.00	<0.00	<0.00	<0.00
Os189	<6.67	<5.72	<0.42	257.66	222.03	221.48	<0.049	<0.059	<0.079	<0.063	<0.077	<0.092	<0.061	<0.043	<0.046	<0.075	<0.042	<2.91	<0.0031	<0.0043	<0.00001	185.25	177.09	<0.56	<0.088
Os190	<3.77	<3.23	<0.53	243.48	220.19	214.59	0.0169	<0.038	<0.049	<0.032	<0.050	<0.047	<0.038	<0.032	<0.0261	<0.04	<0.029	0.83	<0.0028	<0.0028	<0.00000	179.78	183.41	<0.28	<0.035
Ir193	<1.17	<1.07	0.08	108.69	107.08	115.1	<0.0060	0.0115	0.0069	0.0064	<0.0117	<0.0111	<0.0072	<0.0064	<0.0068	<0.0106	<0.0040	<0.31	0.00084	<0.00057	<0.00000	107.41	101.56	0.113	<0.0092
Pt195	50.63	62.98	<0.38	198.27	212.8	217.56	<0.0270	<0.030	<0.045	<0.028	<0.044	<0.044	<0.021	<0.0167	<0.0145	<0.028	<0.0163	22.51	0.0851	0.0586	0.00006	207.38	192.43	<0.25	<0.020
Au197	364.46	326.62	0.33	234.49	235.82	240.79	0.141	0.216	0.0342	0.069	22.74	<0.023	5.24	32.27	0.0562	0.159	15.63	139.33	0.547	0.31	0.00033	231.46	230.42	0.277	0.708
Pb208	<0.00	<0.00	<0.00	<0.00	<0.00	<0.00	<0.00	<0.00	<0.00	<0.00	<0.00	<0.00	<0.00	<0.00	<0.00	<0.00	<0.00	<0.00	<0.00	<0.00	<0.00	<0.00	<0.00	<0.00	<0.00
Bi209	7805.16	6998.98	<0.38	193.49	247.57	250.42	18.02	35.53	<0.026	<0.0232	<0.036	6.69	28.77	23.82	0.039	0.22	9.43	2799.65	9.85	6.12	0.00687	225.47	228.72	<0.197	26.88
Th232	<-NaN	<-NaN	<-NaN	<-NaN	<-NaN	<-NaN	<-NaN	<-NaN	<-NaN	<-NaN	<-NaN	<-NaN	<-NaN	<-NaN	<-NaN	<-NaN	<-NaN	<-NaN	<-NaN	<-NaN	<-NaN	<-NaN	<-NaN	<-NaN	<-NaN
U238	<-NaN	<-NaN	<-NaN	<-NaN	<-NaN	<-NaN	<-NaN	<-NaN	<-NaN	<-NaN	<-NaN	<-NaN	<-NaN	<-NaN	<-NaN	<-NaN	<-NaN	<-NaN	<-NaN	<-NaN	<-NaN	<-NaN	<-NaN	<-NaN	<-NaN
ThO248	<-NaN	<-NaN	<-NaN	<-NaN	<-NaN	<-NaN	<-NaN	<-NaN	<-NaN	<-NaN	<-NaN	<-NaN	<-NaN	<-NaN	<-NaN	<-NaN	<-NaN	<-NaN	<-NaN	<-NaN	<-NaN	<-NaN	<-NaN	<-NaN	<-NaN

GLITTER!: 1 sigma error.

Element	STD610-1	STD610-2	BCR2G-1	PGEA-1	PGEA-2	PGEA-3	MS-CPY	MS-PY	KP11-PY	KP11-CPY	KP11-SPH	BG30-CPY	BG30-PY	JL06-PY2	JL06-SPH	BG06-SPH	BG06-PY	STD610-3	STD610-4	STD610-5	STD610-6	PGEA-4	PGEA-5	BCR2G-2	JL10-PY1
Al27	<0.00	<0.00	<0.00	<0.00	<0.00	<0.00	<0.00	<0.00	<0.00	<0.00	<0.00	<0.00	<0.00	<0.00	<0.00	<0.00	<0.00	<0.00	<0.00	<0.00	<0.00	<0.00	<0.00	<0.00	<0.00
Si29	<0.00	<0.00	<0.00	<0.00	<0.00	<0.00	<0.00	<0.00	<0.00	<0.00	<0.00	<0.00	<0.00	<0.00	<0.00	<0.00	<0.00	<0.00	<0.00	<0.00	<0.00	<0.00	<0.00	<0.00	<0.00
S34	11119.88	10872.32	1725.94	8818.25	8824.14	8819.51	11053.96	16908.71	16908.28	11060.12	10577.26	11058.57	16911.8	16905.72	10502.49	10472.88	16905.85	9494.88	14.04	13.29	0.022	8820.71	8813.92	1623.49	16910.31
Ca43	<0.00	<0.00	<0.00	<0.00	<0.00	<0.00	<0.00	<0.00	<0.00	<0.00	<0.00	<0.00	<0.00	<0.00	<0.00	<0.00	<0.00	<0.00	<0.00	<0.00	<0.00	<0.00	<0.00	<0.00	<0.00
Sc45	<0.00	<0.00	<0.00	<0.00	<0.00	<0.00	<0.00	<0.00	<0.00	<0.00	<0.00	<0.00	<0.00	<0.00	<0.00	<0.00	<0.00	<0.00	<0.00	<0.00	<0.00	<0.00	<0.00	<0.00	<0.00
Ti49	<0.00	<0.00	<0.00	<0.00	<0.00	<0.00	<0.00	<0.00	<0.00	<0.00	<0.00	<0.00	<0.00	<0.00	<0.00	<0.00	<0.00	<0.00	<0.00	<0.00	<0.00	<0.00	<0.00	<0.00	<0.00
V51	<0.00	<0.00	<0.00	<0.00	<0.00	<0.00	<0.00	<0.00	<0.00	<0.00	<0.00	<0.00	<0.00	<0.00	<0.00	<0.00	<0.00	<0.00	<0.00	<0.00	<0.00	<0.00	<0.00	<0.00	<0.00
Cr53	<0.00	<0.00	<0.00	<0.00	<0.00	<0.00	<0.00	<0.00	<0.00	<0.00	<0.00	<0.00	<0.00	<0.00	<0.00	<0.00	<0.00	<0.00	<0.00	<0.00	<0.00	<0.00	<0.00	<0.00	<0.00

Element	STD610-1	STD610-2	BCR2G-1	PGEA-1	PGEA-2	PGEA-3	MS-CPY	MS-PY	KP11-PY	KP11-CPY	KP11-SPH	BG30-CPY	BG30-PY	JL06-PY2	JL06-SPH	BG06-SPH	BG06-PY	STD610-3	STD610-4	STD610-5	STD610-6	PGEA-4	PGEA-5	BCR2G-2	JL10-PY1
Mn55	<0.00	<0.00	<0.00	<0.00	<0.00	<0.00	<0.00	<0.00	<0.00	<0.00	<0.00	<0.00	<0.00	<0.00	<0.00	<0.00	<0.00	<0.00	<0.00	<0.00	<0.00	<0.00	<0.00	<0.00	<0.00
Fe57	<0.00	<0.00	<0.00	<0.00	<0.00	<0.00	<0.00	<0.00	<0.00	<0.00	<0.00	<0.00	<0.00	<0.00	<0.00	<0.00	<0.00	<0.00	<0.00	<0.00	<0.00	<0.00	<0.00	<0.00	<0.00
Co59	<0.00	<0.00	<0.00	<0.00	<0.00	<0.00	<0.00	<0.00	<0.00	<0.00	<0.00	<0.00	<0.00	<0.00	<0.00	<0.00	<0.00	<0.00	<0.00	<0.00	<0.00	<0.00	<0.00	<0.00	<0.00
Ni60	345.11	312.99	1.98	25671.06	24275.45	25649.93	0.074	0.57	0.066	0.047	0.27	0.066	0.28	0.096	0.047	0.071	0.065	131.66	0.5	0.26	0.00032	25143.68	24986.9	1.66	0.15
Ni62	390.15	361.39	4.12	25851.16	26544.52	28266.78	0.17	0.77	0.25	0.42	0.3	0.29	0.59	4.25	0.15	0.21	0.13	151.71	0.57	0.33	0.00037	28082.23	28254.86	3.85	0.26
Cu65	182.71	164.85	1.86	6.86	7.54	7.58	7934.23	3.26	0.089	7491.04	352.49	7647.28	60.41	2.4	3.98	1.48	6.74	67.22	0.28	0.15	0.00016	7.49	7.52	1.91	0.25
Zn66	<0.00	<0.00	<0.00	<0.00	<0.00	<0.00	<0.00	<0.00	<0.00	<0.00	<0.00	<0.00	<0.00	<0.00	<0.00	<0.00	<0.00	<0.00	<0.00	<0.00	<0.00	<0.00	<0.00	<0.00	<0.00
Ga71	<0.00	<0.00	<0.00	<0.00	<0.00	<0.00	<0.00	<0.00	<0.00	<0.00	<0.00	<0.00	<0.00	<0.00	<0.00	<0.00	<0.00	<0.00	<0.00	<0.00	<0.00	<0.00	<0.00	<0.00	<0.00
As75	297.44	274.33	7.65	5.82	6.91	6.71	0.4	7.01	0.94	0.63	0.99	1.83	32.9	315.19	3.56	1.01	236.17	114.8	0.43	0.25	0.00029	6.62	6.77	5.83	32.87
Se82	224.68	198.58	14.81	10.97	12.13	11.81	1.38	1.3	5.77	10.93	2.22	2.55	1.44	0.84	0.95	1.48	0.81	80.06	0.23	0.14	0.00019	11.86	11.32	9.25	1.82
Y89	<0.00	<0.00	<0.00	<0.00	<0.00	<0.00	<0.00	<0.00	<0.00	<0.00	<0.00	<0.00	<0.00	<0.00	<0.00	<0.00	<0.00	<0.00	<0.00	<0.00	<0.00	<0.00	<0.00	<0.00	<0.00
Zr90	<0.00	<0.00	<0.00	<0.00	<0.00	<0.00	<0.00	<0.00	<0.00	<0.00	<0.00	<0.00	<0.00	<0.00	<0.00	<0.00	<0.00	<0.00	<0.00	<0.00	<0.00	<0.00	<0.00	<0.00	<0.00
Nb93	<0.00	<0.00	<0.00	<0.00	<0.00	<0.00	<0.00	<0.00	<0.00	<0.00	<0.00	<0.00	<0.00	<0.00	<0.00	<0.00	<0.00	<0.00	<0.00	<0.00	<0.00	<0.00	<0.00	<0.00	<0.00
Mo95	<0.00	<0.00	<0.00	<0.00	<0.00	<0.00	<0.00	<0.00	<0.00	<0.00	<0.00	<0.00	<0.00	<0.00	<0.00	<0.00	<0.00	<0.00	<0.00	<0.00	<0.00	<0.00	<0.00	<0.00	<0.00
Ru99	2.46	2.62	0.14	11.8	12.84	13.61	0.054	0.023	0.017	0.076	0.028	0.075	0.064	0.015	0.017	0.02	0.012	0.98	0.002	0.002	0	13.56	12.22	0.15	0.035
Ru101	1.7	1.08	0.096	10.36	11.22	12.17	0.03	0.012	0.014	0.036	0.021	0.041	0.019	0.0085	0.01	0.019	0.011	0.48	0.001	0.00081	0	11.59	10.99	0.099	0.015
Rh103	3.08	2.74	0.17	14.11	15.4	16.78	1.7	0.015	0.015	1.65	0.093	1.59	0.027	0.011	0.012	0.015	0.011	1.17	0.0037	0.0022	0	16.62	14.73	0.12	0.016
Ag107	<0.00	<0.00	<0.00	<0.00	<0.00	<0.00	<0.00	<0.00	<0.00	<0.00	<0.00	<0.00	<0.00	<0.00	<0.00	<0.00	<0.00	<0.00	<0.00	<0.00	<0.00	<0.00	<0.00	<0.00	<0.00
Pd108	4.89	4.75	0.11	9.66	9.54	10.02	0.0061	0.011	0.011	0.04	2.28	0.03	0.027	0.009	3.05	2.7	0.048	1.88	0.0063	0.0039	0	10.11	9.69	0.11	0.012
Cd111	<0.00	<0.00	<0.00	<0.00	<0.00	<0.00	<0.00	<0.00	<0.00	<0.00	<0.00	<0.00	<0.00	<0.00	<0.00	<0.00	<0.00	<0.00	<0.00	<0.00	<0.00	<0.00	<0.00	<0.00	<0.00
In115	<0.00	<0.00	<0.00	<0.00	<0.00	<0.00	<0.00	<0.00	<0.00	<0.00	<0.00	<0.00	<0.00	<0.00	<0.00	<0.00	<0.00	<0.00	<0.00	<0.00	<0.00	<0.00	<0.00	<0.00	<0.00
Sn118	<0.00	<0.00	<0.00	<0.00	<0.00	<0.00	<0.00	<0.00	<0.00	<0.00	<0.00	<0.00	<0.00	<0.00	<0.00	<0.00	<0.00	<0.00	<0.00	<0.00	<0.00	<0.00	<0.00	<0.00	<0.00
Sb121	<0.00	<0.00	<0.00	<0.00	<0.00	<0.00	<0.00	<0.00	<0.00	<0.00	<0.00	<0.00	<0.00	<0.00	<0.00	<0.00	<0.00	<0.00	<0.00	<0.00	<0.00	<0.00	<0.00	<0.00	<0.00
Te125	262.12	234.44	1.16	7.94	9.9	10.23	0.12	0.6	0.33	0.78	2.29	0.22	0.31	0.11	0.086	0.1	0.13	99.9	0.33	0.21	0.00024	10.34	9.74	0.94	0.44
Te128	307.62	275.32	1.78	9.61	12.19	12.93	0.11	0.56	0.3	0.72	2.66	0.2	0.23	0.11	0.11	0.14	0.12	119.48	0.42	0.26	0.00029	12.11	11.62	1.06	0.36
La139	<0.00	<0.00	<0.00	<0.00	<0.00	<0.00	<0.00	<0.00	<0.00	<0.00	<0.00	<0.00	<0.00	<0.00	<0.00	<0.00	<0.00	<0.00	<0.00	<0.00	<0.00	<0.00	<0.00	<0.00	<0.00
Ce140	<0.00	<0.00	<0.00	<0.00	<0.00	<0.00	<0.00	<0.00	<0.00	<0.00	<0.00	<0.00	<0.00	<0.00	<0.00	<0.00	<0.00	<0.00	<0.00	<0.00	<0.00	<0.00	<0.00	<0.00	<0.00
Nd146	<0.00	<0.00	<0.00	<0.00	<0.00	<0.00	<0.00	<0.00	<0.00	<0.00	<0.00	<0.00	<0.00	<0.00	<0.00	<0.00	<0.00	<0.00	<0.00	<0.00	<0.00	<0.00	<0.00	<0.00	<0.00
Hf178	<0.00	<0.00	<0.00	<0.00	<0.00	<0.00	<0.00	<0.00	<0.00	<0.00	<0.00	<0.00	<0.00	<0.00	<0.00	<0.00	<0.00	<0.00	<0.00	<0.00	<0.00	<0.00	<0.00	<0.00	<0.00
W182	<0.00	<0.00	<0.00	<0.00	<0.00	<0.00	<0.00	<0.00	<0.00	<0.00	<0.00	<0.00	<0.00	<0.00	<0.00	<0.00	<0.00	<0.00	<0.00	<0.00	<0.00	<0.00	<0.00	<0.00	<0.00
Re185	<0.00	<0.00	<0.00	<0.00	<0.00	<0.00	<0.00	<0.00	<0.00	<0.00	<0.00	<0.00	<0.00	<0.00	<0.00	<0.00	<0.00	<0.00	<0.00	<0.00	<0.00	<0.00	<0.00	<0.00	<0.00
Re187	<0.00	<0.00	<0.00	<0.00	<0.00	<0.00	<0.00	<0.00	<0.00	<0.00	<0.00	<0.00	<0.00	<0.00	<0.00	<0.00	<0.00	<0.00	<0.00	<0.00	<0.00	<0.00	<0.00	<0.00	<0.00
Os189	3.05	2.5	0.2	27.57	23.79	23.72	0.019	0.024	0.029	0.032	0.035	0.035	0.032	0.019	0.023	0.032	0.017	1.14	0.0015	0.0017	0	19.86	18.97	0.23	0.031
Os190	1.59	1.46	0.19	22.5	20.37	19.84	0.0075	0.015	0.018	0.015	0.02	0.019	0.015	0.012	0.0097	<0.00	0.012	0.41	0.0011	0.001	0	16.64	16.96	0.13	0.014
Ir193	0.49	0.47	0.033	6.03	5.94	6.38	0.0021	0.0036	0.0034	0.0037	0.0058	0.0046	0.003	0.0026	0.0028	0.0039	0.002	0.14	0.00023	0.00024	0	5.96	5.63	0.031	0.0033
Pt195	5.17	5.84	0.17	11.72	12.59	12.86	0.0095	0.011	0.015	0.013	0.018	0.018	0.01	0.0074	0.0065	0.012	0.0066	2.05	0.0066	0.0045	0.00001	12.27	11.37	0.1	0.011
Au197	15.87	14.2	0.12	8.25	8.3	8.47	0.012	0.02	0.0087	0.014	0.82	0.01	0.21	1.13	0.0094	0.017	0.55	5.59	0.021	0.012	0.00001	8.15	8.09	0.061	0.042
Pb208	<0.00	<0.00	<0.00	<0.00	<0.00	<0.00	<0.00	<0.00	<0.00	<0.00	<0.00	<0.00	<0.00	<0.00	<0.00	<0.00	<0.00	<0.00	<0.00	<0.00	<0.00	<0.00	<0.00	<0.00	<0.00
Bi209	445.1	397.01	0.14	10.53	13.47	13.62	0.98	1.93	0.01	0.0097	0.014	0.37	1.57	1.3	0.0095	0.02	0.52	154.21	0.55	0.34	0.00038	12.26	12.43	0.078	1.47
Th232	<0.00	<0.00	<0.00	<0.00	<0.00	<0.00	<0.00	<0.00	<0.00	<0.00	<0.00	<0.00	<0.00	<0.00	<0.00	<0.00	<0.00	<0.00	<0.00	<0.00	<0.00	<0.00	<0.00	<0.00	<0.00
U238	<0.00	<0.00	<0.00	<0.00	<0.00	<0.00	<0.00	<0.00	<0.00	<0.00	<0.00	<0.00	<0.00	<0.00	<0.00	<0.00	<0.00	<0.00	<0.00	<0.00	<0.00	<0.00	<0.00	<0.00	<0.00
ThO248	<0.00	<0.00	<0.00	<0.00	<0.00	<0.00	<0.00	<0.00	<0.00	<0.00	<0.00	<0.00	<0.00	<0.00	<0.00	<0.00	<0.00	<0.00	<0.00	<0.00	<0.00	<0.00	<0.00	<0.00	<0.00

GLITTER!: Minimum detection limits (99% confidence).

Element	STD610-1	STD610-2	BCR2G-1	PGEA-1	PGEA-2	PGEA-3	MS-CPY	MS-PY	KP11-PY	KP11-CPY	KP11-SPH	BG30-CPY	BG30-PY	JL06-PY2	JL06-SPH	BG06-SPH	BG06-PY	STD610-3	STD610-4	STD610-5	STD610-6	PGEA-4	PGEA-5	BCR2G-2	JL10-PY1
Al27	<0.00000	<0.00000	<0.00000	<0.00000	<0.00000	<0.00000	<0.00000	<0.00000	<0.00000	<0.00000	<0.00000	<0.00000	<0.00000	<0.00000	<0.00000	<0.00000	<0.00000	<0.00000	<0.00000	<0.00000	<0.00000	<0.00000	<0.00000	<0.00000	<0.00000
Si29	<0.00000	<0.00000	<0.00000	<0.00000	<0.00000	<0.00000	<0.00000	<0.00000	<0.00000	<0.00000	<0.00000	<0.00000	<0.00000	<0.00000	<0.00000	<0.00000	<0.00000	<0.00000	<0.00000	<0.00000	<0.00000	<0.00000	<0.00000	<0.00000	<0.00000
S34	10620.32	9552.75	1365.14	415.2	573.33	429.57	68.09	128.48	145.53	118.17	201.87	177.94	124.01	110.03	122.09	137.48	107.06	5581.59	10.01	7.09	0.0116	471.7	328.76	914.74	112.16
Ca43	<0.00000	<0.00000	<0.00000	<0.00000	<0.00000	<0.00000	<0.00000	<0.00000	<0.00000	<0.00000	<0.00000	<0.00000	<0.00000	<0.00000	<0.00000	<0.00000	<0.00000	<0.00000	<0.00000	<0.00000	<0.00000	<0.00000	<0.00000	<0.00000	<0.00000
Sc45	<0.00	<0.00	<0.00	<0.00	<0.00	<0.00	<0.00	<0.00	<0.00	<0.00	<0.00	<0.00	<0.00	<0.00	<0.00	<0.00	<0.00	<0.00	<0.00	<0.00	<0.00	<0.00	<0.00	<0.00	<0.00
Ti49	<0.00	<0.00	<0.00	<0.00	<0.00	<0.00	<0.00	<0.00	<0.00	<0.00	<0.00	<0.00	<0.00	<0.00	<0.00	<0.00	<0.00	<0.00	<0.00	<0.00	<0.00	<0.00	<0.00	<0.00	<0.00
V51	<0.00	<0.00	<0.00	<0.00	<0.00	<0.00	<0.00	<0.00	<0.00	<0.00	<0.00	<0.00	<0.00	<0.00	<0.00	<0.00	<0.00	<0.00	<0.00	<0.00	<0.00	<0.00	<0.00	<0.00	<0.00
Cr53	<0.00	<0.00	<0.00	<0.00	<0.00	<0.00	<0.00	<0.00	<0.00	<0.00	<0.00	<0.00	<0.00	<0.00	<0.00	<0.00	<0.00	<0.00	<0.00	<0.00	<0.00	<0.00	<0.00	<0.00	<0.00
Mn55	<0.00	<0.00	<0.00	<0.00	<0.00	<0.00	<0.00	<0.00	<0.00	<0.00	<0.00	<0.00	<0.00	<0.00	<0.00	<0.00	<0.00	<0.00	<0.00	<0.00	<0.00	<0.00	<0.00	<0.00	<0.00
Fe57	<0.00000	<0.00000	<0.00000	<0.00000	<0.00000	<0.00000	<0.00000	<0.00000	<0.00000	<0.00000	<0.00000	<0.00000	<0.00000	<0.00000	<0.00000	<0.00000	<0.00000	<0.00000	<0.00000	<0.00000	<0.00000	<0.00000	<0.00000	<0.00000	<0.00000
Co59	<0.00000	<0.00000	<0.00000	<0.00000	<0.00000	<0.00000	<0.00000	<0.00000	<0.00000	<0.00000	<0.00000	<0.00000	<0.00000	<0.00000	<0.00000	<0.00000	<0.00000	<0.00000	<0.00000	<0.00000	<0.00000	<0.00000	<0.00000	<0.00000	<0.00000
Ni60	10.21	9.16	1.5	0.376	0.981	0.424	0.0773	0.104	0.129	0.0905	0.646	0.132	0.0893	0.0761	0.0847	0.104	0.0715	4.22	0.00783	0.00644	0.00001	0.386	22.65	0.972	0.109
Ni62	38.33	51.96	6.71	1.67	2.2	1.32	0.275	0.428	0.603	0.514	0.74	0.654	0.407	0.334	0.375	0.343	0.255	21.59	0.0321	0.0285	0.00005	2.23	61.06	4.38	0.504
Cu65	18.93	17.41	2.26	1.43	1.2	0.726	0.115	0.212	0.215	0.194	0.317	0.24	0.183	0.139	0.164	0.183	0.126	7.11	0.0134	0.0099	0.00002	0.741	0.585	1.39	0.176
Zn66	<0.00000	<0.00000	<0.00000	<0.00000	<0.00000	<0.00000	<0.00000	<0.00000	<0.00000	<0.00000	<0.00000	<0.00000	<0.00000	<0.00000	<0.00000	<0.00000	<0.00000	<0.00000	<0.00000	<0.00000	<0.00000	<0.00000	<0.00000	<0.00000	<0.00000
Ga71	<0.00	<0.00	<0.00	<0.00	<0.00	<0.00	<0.00	<0.00	<0.00	<0.00	<0.00	<0.00	<0.00	<0.00	<0.00	<0.00	<0.00	<0.00	<0.00	<0.00	<0.00	<0.00	<0.00	<0.00	<0.00
As75	161.26	140.05	20.52	5.97	8.02	5.92	0.964	1.57	1.68	1.38	2.13	1.82	1.32	1.07	1.39	1.71	1.22	75.44	0.141	0.114	0.00019	7.93	4.93	15.24	1.82
Se82	310.68	275.99	39.87	11.83	15.8	12.24	1.91	3.19	3.5	2.68	4.42	3.83	2.84	2.11	2.4	2.81	2.06	115.08	0.221	0.165	0.00031	12.58	7.44	24.1	2.95
Y89	<0.00	<0.00	<0.00	<0.00	<0.00	<0.00	<0.00	<0.00	<0.00	<0.00	<0.00	<0.00	<0.00	<0.00	<0.00	<0.00	<0.00	<0.00	<0.00	<0.00	<0.00	<0.00	<0.00	<0.00	<0.00
Zr90	<0.00	<0.00	<0.00	<0.00	<0.00	<0.00	<0.00	<0.00	<0.00	<0.00	<0.00	<0.00	<0.00	<0.00	<0.00	<0.00	<0.00	<0.00	<0.00	<0.00	<0.00	<0.00	<0.00	<0.00	<0.00
Nb93	<0.00	<0.00	<0.00	<0.00	<0.00	<0.00	<0.00	<0.00	<0.00	<0.00	<0.00	<0.00	<0.00	<0.00	<0.00	<0.00	<0.00	<0.00	<0.00	<0.00	<0.00	<0.00	<0.00	<0.00	<0.00
Mo95	<0.00	<0.00	<0.00	<0.00	<0.00	<0.00	<0.00	<0.00	<0.00	<0.00	<0.00	<0.00	<0.00	<0.00	<0.00	<0.00	<0.00	<0.00	<0.00	<0.00	<0.00	<0.00	<0.00	<0.00	<0.00
Ru99	4.42	5.79	<0.00000	0.21	0.189	0.22	0.0345	0.045	0.0383	0.0529	0.0679	0.0759	0.0359	0.0235	0.0432	0.0435	0.0324	2.23	0.00337	0.00502	0	0.24	0.602	0.192	0.053
Ru101	5.14	1.56	<0.00000	0.134	0.213	0.186	0.0246	0.0321	0.0334	0.0218	0.0541	0.0409	0.0362	0.0205	0.0218	0.0465	0.0282	1.12	0.0024	0.00234	0	0.156	0.512	0.237	0.0239

Element	STD610-1	STD610-2	BCR2G-1	PGEA-1	PGEA-2	PGEA-3	MS-CPY	MS-PY	KP11-PY	KP11-CPY	KP11-SPH	BG30-CPY	BG30-PY	JL06-PY2	JL06-SPH	BG06-SPH	BG06-PY	STD610-3	STD610-4	STD610-5	STD610-6	PGEA-4	PGEA-5	BCR2G-2	JL10-PY1
Rh103	3.32	3.3	0.46	0.134	0.187	0.115	0.0206	0.0391	0.0397	0.0344	0.0573	0.048	0.0318	0.0286	0.0278	0.0355	0.0255	1.51	0.00298	0.00244	0	0.167	0.278	0.308	0.0409
Ag107	<0.00000	<0.00000	<0.00000	<0.00000	<0.00000	<0.00000	<0.00000	<0.00000	<0.00000	<0.00000	<0.00000	<0.00000	<0.00000	<0.00000	<0.00000	<0.00000	<0.00000	<0.00000	<0.00000	<0.00000	<0.00000	<0.00000	<0.00000	<0.00000	<0.00000
Pd108	3.52	2.7	<0.00000	0.123	0.0823	0.114	0.0135	0.03	0.0289	0.0267	0.0491	0.0396	0.0256	0.0229	0.0255	0.0284	0.0245	0.971	0.0018	0.00165	0	0.113	0.468	0.278	0.0253
Cd111	<0.00000	<0.00000	<0.00000	<0.00000	<0.00000	<0.00000	<0.00000	<0.00000	<0.00000	<0.00000	<0.00000	<0.00000	<0.00000	<0.00000	<0.00000	<0.00000	<0.00000	<0.00000	<0.00000	<0.00000	<0.00000	<0.00000	<0.00000	<0.00000	<0.00000
In115	<0.00000	<0.00000	<0.00000	<0.00000	<0.00000	<0.00000	<0.00000	<0.00000	<0.00000	<0.00000	<0.00000	<0.00000	<0.00000	<0.00000	<0.00000	<0.00000	<0.00000	<0.00000	<0.00000	<0.00000	<0.00000	<0.00000	<0.00000	<0.00000	<0.00000
Sn118	<0.00000	<0.00000	<0.00000	<0.00000	<0.00000	<0.00000	<0.00000	<0.00000	<0.00000	<0.00000	<0.00000	<0.00000	<0.00000	<0.00000	<0.00000	<0.00000	<0.00000	<0.00000	<0.00000	<0.00000	<0.00000	<0.00000	<0.00000	<0.00000	<0.00000
Sb121	<0.00000	<0.00000	<0.00000	<0.00000	<0.00000	<0.00000	<0.00000	<0.00000	<0.00000	<0.00000	<0.00000	<0.00000	<0.00000	<0.00000	<0.00000	<0.00000	<0.00000	<0.00000	<0.00000	<0.00000	<0.00000	<0.00000	<0.00000	<0.00000	<0.00000
Te125	9.9	30.61	2.81	0.814	1.47	0.765	0.104	0.267	0.315	0.291	0.323	0.193	0.242	0.17	0.206	0.207	0.154	7.05	0.0217	0.0116	0.00002	1.01	1.39	2.69	0.244
Te128	36.12	34.45	4.77	1.42	1.86	1.45	0.239	0.382	0.411	0.328	0.524	0.446	0.319	0.258	0.281	0.324	0.235	13.43	0.0255	0.0201	0.00004	1.4	1.11	2.81	0.34
La139	<0.00	<0.00	<0.00	<0.00	<0.00	<0.00	<0.00	<0.00	<0.00	<0.00	<0.00	<0.00	<0.00	<0.00	<0.00	<0.00	<0.00	<0.00	<0.00	<0.00	<0.00	<0.00	<0.00	<0.00	<0.00
Ce140	<0.00	<0.00	<0.00	<0.00	<0.00	<0.00	<0.00	<0.00	<0.00	<0.00	<0.00	<0.00	<0.00	<0.00	<0.00	<0.00	<0.00	<0.00	<0.00	<0.00	<0.00	<0.00	<0.00	<0.00	<0.00
Nd146	<0.00	<0.00	<0.00	<0.00	<0.00	<0.00	<0.00	<0.00	<0.00	<0.00	<0.00	<0.00	<0.00	<0.00	<0.00	<0.00	<0.00	<0.00	<0.00	<0.00	<0.00	<0.00	<0.00	<0.00	<0.00
Hf178	<0.00	<0.00	<0.00	<0.00	<0.00	<0.00	<0.00	<0.00	<0.00	<0.00	<0.00	<0.00	<0.00	<0.00	<0.00	<0.00	<0.00	<0.00	<0.00	<0.00	<0.00	<0.00	<0.00	<0.00	<0.00
W182	<0.00	<0.00	<0.00	<0.00	<0.00	<0.00	<0.00	<0.00	<0.00	<0.00	<0.00	<0.00	<0.00	<0.00	<0.00	<0.00	<0.00	<0.00	<0.00	<0.00	<0.00	<0.00	<0.00	<0.00	<0.00
Re185	<0.00	<0.00	<0.00	<0.00	<0.00	<0.00	<0.00	<0.00	<0.00	<0.00	<0.00	<0.00	<0.00	<0.00	<0.00	<0.00	<0.00	<0.00	<0.00	<0.00	<0.00	<0.00	<0.00	<0.00	<0.00
Re187	<0.00000	<0.00000	<0.00000	<0.00000	<0.00000	<0.00000	<0.00000	<0.00000	<0.00000	<0.00000	<0.00000	<0.00000	<0.00000	<0.00000	<0.00000	<0.00000	<0.00000	<0.00000	<0.00000	<0.00000	<0.00000	<0.00000	<0.00000	<0.00000	<0.00000
Os189	6.67	5.72	0.423	0.274	0.493	0.386	0.0495	0.0588	0.0791	0.0632	0.0769	0.0919	0.0606	0.0433	0.0461	0.0752	0.0423	2.91	0.00312	0.00429	0.00001	0.286	0.941	0.562	0.0876
Os190	3.77	3.23	0.535	0.183	0.171	0.126	0.0114	0.0384	0.049	0.0319	0.0501	0.0474	0.0375	0.0324	0.0261	0.0393	0.0293	0.671	0.00278	0.0028	0	0.228	0.73	0.284	0.035
Ir193	1.17	1.07	0.0559	0.0324	0.023	0.024	0.00596	0.00448	0.00661	0.00528	0.0117	0.0111	0.00716	0.0064	0.00682	0.0106	0.00395	0.314	<0.00000	0.00057	0	0.0338	0.23	0.047	0.00915
Pt195	4.2	3.37	0.377	0.122	0.174	0.152	0.027	0.0303	0.0446	0.0281	0.0442	0.0442	0.0209	0.0167	0.0145	0.0283	0.0163	1.59	0.0022	0.00207	0	0.114	0.532	0.251	0.0195
Au197	2.75	1.92	0.255	0.069	0.123	0.0725	0.00859	0.0204	0.0151	0.017	0.0189	0.0226	0.0153	0.0113	0.0147	0.0148	0.009	0.565	0.00156	0.00075	0	0.0817	0.393	0.0927	0.00933
Pb208	<0.00000	<0.00000	<0.00000	<0.00000	<0.00000	<0.00000	<0.00000	<0.00000	<0.00000	<0.00000	<0.00000	<0.00000	<0.00000	<0.00000	<0.00000	<0.00000	<0.00000	<0.00000	<0.00000	<0.00000	<0.00000	<0.00000	<0.00000	<0.00000	<0.00000
Bi209	2.84	2.27	0.376	0.091	0.12	0.0982	0.0156	0.0248	0.0263	0.0232	0.0361	0.0316	0.0196	0.019	0.0207	0.0214	0.0152	0.869	0.00196	0.00157	0	0.102	0.317	0.197	0.0249
Th232	<0.00	<0.00	<0.00	<0.00	<0.00	<0.00	<0.00	<0.00	<0.00	<0.00	<0.00	<0.00	<0.00	<0.00	<0.00	<0.00	<0.00	<0.00	<0.00	<0.00	<0.00	<0.00	<0.00	<0.00	<0.00
U238	<0.00	<0.00	<0.00	<0.00	<0.00	<0.00	<0.00	<0.00	<0.00	<0.00	<0.00	<0.00	<0.00	<0.00	<0.00	<0.00	<0.00	<0.00	<0.00	<0.00	<0.00	<0.00	<0.00	<0.00	<0.00
ThO248	<0.00	<0.00	<0.00	<0.00	<0.00	<0.00	<0.00	<0.00	<0.00	<0.00	<0.00	<0.00	<0.00	<0.00	<0.00	<0.00	<0.00	<0.00	<0.00	<0.00	<0.00	<0.00	<0.00	<0.00	<0.00

GLITTER!: Trace element concentrations normalised to chondrite.

Element	STD610-1	STD610-2	BCR2G-1	PGEA-1	PGEA-2	PGEA-3	MS-CPY	MS-PY	KP11-PY	KP11-CPY	KP11-SPH	BG30-CPY	BG30-PY	JL06-PY2	JL06-SPH	BG06-SPH	BG06-PY	STD610-3	STD610-4	STD610-5	STD610-6	PGEA-4	PGEA-5	BCR2G-2	JL10-PY1
Al27	0	0	0	0	0	0	0	0	0	0	0	0	0	0	0	0	0	0	0	0	0	0	0	0	0
Si29	0	0	0	0	0	0	0	0	0	0	0	0	0	0	0	0	0	0	0	0	0	0	0	0	0
S34	Inf	Inf	Inf	Inf	Inf	Inf	Inf	Inf	Inf	Inf	Inf	Inf	Inf	Inf	Inf	Inf	Inf	Inf	Inf	Inf	Inf	Inf	Inf	Inf	Inf
Ca43	0	0	0	0	0	0	0	0	0	0	0	0	0	0	0	0	0	0	0	0	0	0	0	0	0
Sc45	<****	<****	<****	<****	<****	<****	<****	<****	<****	<****	<****	<****	<****	<****	<****	<****	<****	<****	<****	<****	<****	<****	<****	<****	<****
Ti49	<****	<****	<****	<****	<****	<****	<****	<****	<****	<****	<****	<****	<****	<****	<****	<****	<****	<****	<****	<****	<****	<****	<****	<****	<****
V51	<****	<****	<****	<****	<****	<****	<****	<****	<****	<****	<****	<****	<****	<****	<****	<****	<****	<****	<****	<****	<****	<****	<****	<****	<****
Cr53	<****	<****	<****	<****	<****	<****	<****	<****	<****	<****	<****	<****	<****	<****	<****	<****	<****	<****	<****	<****	<****	<****	<****	<****	<****
Mn55	<****	<****	<****	<****	<****	<****	<****	<****	<****	<****	<****	<****	<****	<****	<****	<****	<****	<****	<****	<****	<****	<****	<****	<****	<****
Fe57	0	0	0	0	0	0	0	0	0	0	0	0	0	0	0	0	0	0	0	0	0	0	0	0	0
Co59	0	0	0	0	0	0	0	0	0	0	0	0	0	0	0	0	0	0	0	0	0	0	0	0	0
Ni60	0.529	0.485	0.00246	44.46	42.03	44.42	0.00008	0.00091	0.00003	0.00001	0	0.00002	0.00037	0.00012	0.00002	0.00004	0.00007	0.2183	0.00082	0.00043	0	43.54	43.28	0.00226	0.00016
Ni62	0.517	0.481	0.00226	40.22	41.29	43.97	0.00008	0.0008	0	0.00019	0	0	0.00043	0.00637	0	0.00006	0.00004	0.2161	0.00082	0.00048	0	43.68	43.96	0.00317	0.00005
Cu65	30.55	27.92	0.25	1.313	1.442	1.456	1553.6	0.632	0.00322	1466.37	68.99	1497.07	11.82	0.467	0.775	0.2824	1.317	12.4	0.0498	0.02851	0.00003	1.437	1.449	0.307	0.0399
Zn66	0	0	0	0	0	0	0	0	0	0	0	0	0	0	0	0	0	0	0	0	0	0	0	0	0
Ga71	<****	<****	<****	<****	<****	<****	<****	<****	<****	<****	<****	<****	<****	<****	<****	<****	<****	<****	<****	<****	<****	<****	<****	<****	<****
As75	2062.81	1918.14	0	39.75	46.4	47.19	0.99	53.56	4.96	0.72	3.47	12.52	253.62	2434.97	26.97	5.26	1824.47	829.57	3.15	1.822	0.00208	43.61	48.51	0	253.42
Se82	134.5	115.63	0	8.11	8.52	8.86	0.907	0.156	4.98	9.71	0.871	1.53	0.31	0.121	0	0.584	0.081	51.16	0.1666	0.0998	0.00012	8.82	9.15	0	0.903
Y89	<****	<****	<****	<****	<****	<****	<****	<****	<****	<****	<****	<****	<****	<****	<****	<****	<****	<****	<****	<****	<****	<****	<****	<****	<****
Zr90	<****	<****	<****	<****	<****	<****	<****	<****	<****	<****	<****	<****	<****	<****	<****	<****	<****	<****	<****	<****	<****	<****	<****	<****	<****
Nb93	<****	<****	<****	<****	<****	<****	<****	<****	<****	<****	<****	<****	<****	<****	<****	<****	<****	<****	<****	<****	<****	<****	<****	<****	<****
Mo95	<****	<****	<****	<****	<****	<****	<****	<****	<****	<****	<****	<****	<****	<****	<****	<****	<****	<****	<****	<****	<****	<****	<****	<****	<****
Ru99	5.59	0	0.39	195.17	212.21	225.5	0.548	0.043	0	0.546	0	0.563	0.429	0.049	0	0	0	0	0.0058	0	0	224.53	202.71	0.52	0.114
Ru101	0	2.1	0.25	194.03	209.91	228.24	0.286	0	0	0.201	0	0.27	0	0	0	0	0	0	0	0	0	217.07	206.24	0	0.026
Rh103	173.64	145.76	0	1091.07	1191.05	1297.75	131.49	0	0	126.93	6.4	122.73	1.28	0	0.169	0	0.217	65.79	0.242	0.136	0.00016	1285.54	1139.95	0	0
Ag107	0	0	0	0	0	0	0	0	0	0	0	0	0	0	0	0	0	0	0	0	0	0	0	0	0
Pd108	80.13	79.78	0.64	303.31	298.97	314.5	0	0	0	0.478	71.21	0.28	0.223	0	96.4	84.99	1.099	35.84	0.1417	0.0854	0.00008	317.5	304.77	0	0
Cd111	0	0	0	0	0	0	0	0	0	0	0	0	0	0	0	0	0	0	0	0	0	0	0	0	0
In115	0	0	0	0	0	0	0	0	0	0	0	0	0	0	0	0	0	0	0	0	0	0	0	0	0
Sn118	0	0	0	0	0	0	0	0	0	0	0	0	0	0	0	0	0	0	0	0	0	0	0	0	0
Sb121	0	0	0	0	0	0	0	0	0	0	0	0	0	0	0	0	0	0	0	0	0	0	0	0	0
Te125	1690.93	1512.54	0	54.71	68.78	72.03	0.291	3.09	1.23	3.76	15.19	0.471	0.825	0.192	0	0	0.311	695.71	2.329	1.462	0.00165	72.76	69.45	0	1.71
Te128	1694.41	1524.15	0	55.84	70.92	75.46	0.249	2.94	1.324	3.84	15.34	0.294	0.814	0.161	0	0	0.356	687.17	2.39	1.526	0.00167	70.61	67.91	0	1.66
La139	<****	<****	<****	<****	<****	<****	<****	<****	<****	<****	<****	<****	<****	<****	<****	<****	<****	<****	<****	<****	<****	<****	<****	<****	<****
Ce140	<****	<****	<****	<****	<****	<****	<****	<****	<****	<****	<****	<****	<****	<****	<****	<****	<****	<****	<****	<****	<****	<****	<****	<****	<****
Nd146	<****	<****	<****	<****	<****	<****	<****	<****	<****	<****	<****	<****	<****	<****	<****	<****	<****	<****	<****	<****	<****	<****	<****	<****	<****
Hf178	<****	<****	<****	<****	<****	<****	<****	<****	<****	<****	<****	<****	<****	<****	<****	<****	<****	<****	<****	<****	<****	<****	<****	<****	<****
W182	<****	<****	<****	<****	<****	<****	<****	<****	<****	<****	<****	<****	<****	<****	<****	<****	<****	<****	<****	<****	<****	<****	<****	<****	<****
Re185	<****	<****	<****	<****	<****	<****	<****	<****	<****	<****	<****	<****	<****	<****	<****	<****	<****	<****	<****	<****	<****	<****	<****	<****	<****
Re187	0	0	0	0	0	0	0	0	0	0	0	0	0	0	0	0	0	0	0	0	0	0	0	0	0

Element	STD610-1	STD610-2	BCR2G-1	PGEA-1	PGEA-2	PGEA-3	MS-CPY	MS-PY	KP11-PY	KP11-CPY	KP11-SPH	BG30-CPY	BG30-PY	JL06-PY2	JL06-SPH	BG06-SPH	BG06-PY	STD610-3	STD610-4	STD610-5	STD610-6	PGEA-4	PGEA-5	BCR2G-2	JL10-PY1
Os189	0	0	0	245.63	211.66	211.14	0	0	0	0	0	0	0	0	0	0	0	0	0	0	0	176.59	168.82	0	0
Os190	0	0	0	232.11	209.9	204.57	0.0161	0	0	0	0	0	0	0	0	0	0	0.79	0	0	0	171.39	174.84	0	0
Ir193	0	0	0.113	153.09	150.81	162.11	0	0.0163	0.0097	0.009	0	0	0	0	0	0	0	0	0.00118	0	0	151.28	143.05	0.159	0
Pt195	35.4	44.04	0	138.65	148.81	152.14	0	0	0	0	0	0	0	0	0	0	0	15.74	0.0595	0.041	0.00004	145.02	134.57	0	0
Au197	1671.83	1498.24	1.5	1075.65	1081.74	1104.52	0.646	0.993	0.157	0.317	104.31	0	24.02	148.03	0.258	0.73	71.72	639.11	2.509	1.422	0.0015	1061.74	1056.95	1.27	3.25
Pb208	0	0	0	0	0	0	0	0	0	0	0	0	0	0	0	0	0	0	0	0	0	0	0	0	0
Bi209	46737.49	41910.07	0	1158.62	1482.45	1499.51	107.93	212.77	0	0	0	40.03	172.25	142.65	0.234	1.32	56.5	16764.4	58.96	36.66	0.0411	1350.15	1369.56	0	160.97
Th232	<****	<****	<****	<****	<****	<****	<****	<****	<****	<****	<****	<****	<****	<****	<****	<****	<****	<****	<****	<****	<****	<****	<****	<****	<****
U238	<****	<****	<****	<****	<****	<****	<****	<****	<****	<****	<****	<****	<****	<****	<****	<****	<****	<****	<****	<****	<****	<****	<****	<****	<****
ThO248	<****	<****	<****	<****	<****	<****	<****	<****	<****	<****	<****	<****	<****	<****	<****	<****	<****	<****	<****	<****	<****	<****	<****	<****	<****

GLITTER4.0: Laser Ablation Analysis Results

G:\KYLIE\MAR13\PGEARUN3
Fri Mar 14 18:02:57 2003

All values are reported in ppm

GLITTER!: Trace Element Concentrations MDL filtered.

														Discarded				
	Run3-1	Run3-2	Run3-3	Run3-4	Run3-5	Run3-6	Run3-7	Run3-8	Run3-9	Run3-10	Run3-11	Run3-12	Run3-13	Run3-14	Run3-15	Run3-16	Run3-17	Run3-18
Element	STD610-3	STD610-6	PGEA-4	PGEA-5	BCR2G-2	JL10-PY1	JL10-SPH	JL10-CPY	WAN-SPH	BG05-PY	BG05-SPH	JL19-PY	JL19-CPY	JL19-SPH	STD610-7	STD610-8	PGEA-6	PGEA-7
Al27	<-NaN	<-NaN	<-NaN	<-NaN	<-NaN	<-NaN	<-NaN	<-NaN	<-NaN	<-NaN	<-NaN	<-NaN	<-NaN	<-NaN	<-NaN	<-NaN	<-NaN	<-NaN
Si29	<0.00	<0.00	<0.00	<0.00	<0.00	<0.00	<0.00	<0.00	<0.00	<0.00	<0.00	<0.00	<0.00	<0.00	<0.00	<0.00	<0.00	<0.00
S34	388.87	388.87	277999.97	277999.97	47632.27	534495.5	332171.75	349436.81	334173.09	534495.5	336568.06	534495.5	349436.81	343172.56	388.87	388.87	277999.94	277999.94
Ca43	<0.00	<0.00	<0.00	<0.00	<0.00	<0.00	<0.00	<0.00	<0.00	<0.00	<0.00	<0.00	<0.00	<0.00	<0.00	<0.00	<0.00	<0.00
Sc45	<-NaN	<-NaN	<-NaN	<-NaN	<-NaN	<-NaN	<-NaN	<-NaN	<-NaN	<-NaN	<-NaN	<-NaN	<-NaN	<-NaN	<-NaN	<-NaN	<-NaN	<-NaN
Ti49	<0.00	<0.00	<0.00	<0.00	<0.00	<0.00	<0.00	<0.00	<0.00	<0.00	<0.00	<0.00	<0.00	<0.00	<0.00	<0.00	<0.00	<0.00
V51	<-NaN	<-NaN	<-NaN	<-NaN	<-NaN	<-NaN	<-NaN	<-NaN	<-NaN	<-NaN	<-NaN	<-NaN	<-NaN	<-NaN	<-NaN	<-NaN	<-NaN	<-NaN
Cr53	<-NaN	<-NaN	<-NaN	<-NaN	<-NaN	<-NaN	<-NaN	<-NaN	<-NaN	<-NaN	<-NaN	<-NaN	<-NaN	<-NaN	<-NaN	<-NaN	<-NaN	<-NaN
Mn55	<-NaN	<-NaN	<-NaN	<-NaN	<-NaN	<-NaN	<-NaN	<-NaN	<-NaN	<-NaN	<-NaN	<-NaN	<-NaN	<-NaN	<-NaN	<-NaN	<-NaN	<-NaN
Fe57	<-NaN	<-NaN	<-NaN	<-NaN	<-NaN	<-NaN	<-NaN	<-NaN	<-NaN	<-NaN	<-NaN	<-NaN	<-NaN	<-NaN	<-NaN	<-NaN	<-NaN	<-NaN
Co59	<0.00	<0.00	<0.00	<0.00	<0.00	<0.00	<0.00	<0.00	<0.00	<0.00	<0.00	<0.00	<0.00	<0.00	<0.00	<0.00	<0.00	<0.00
Ni60	4.95	5.06	707750.88	713229.5	37.25	2.94	<0.191	1.29	0.708	62.62	4.68	0.505	1.96	98.68	5.66	6.37	724834.5	710627.5
Ni62	4.89	5.03	712002.5	711907.31	52.11	<0.50	4.12	4.08	0.74	61.14	2.97	1.14	1.39	80.9	5.64	6.23	712719.63	724972.88
Cu65	2.964	2.935	240.85	239.06	53.2	6.45	863.92	198181.89	18340.87	118.52	223.77	230.41	259982.94	965.75	3.14	3.77	243.98	246.4
Zn66	<0.00	<0.00	<0.00	<0.00	<0.00	<0.00	<0.00	<0.00	<0.00	<0.00	<0.00	<0.00	<0.00	<0.00	<0.00	<0.00	<0.00	<0.00
Ga71	<-NaN	<-NaN	<-NaN	<-NaN	<-NaN	<-NaN	<-NaN	<-NaN	<-NaN	<-NaN	<-NaN	<-NaN	<-NaN	<-NaN	<-NaN	<-NaN	<-NaN	<-NaN
As75	3.49	3.63	131.35	150.37	<16.24	726.94	31.56	14.49	2636.93	2801.92	34.01	77.85	4.67	534.55	3.54	4.45	134.62	130.64
Se82	1.91	1.76	233.91	252.22	<23.68	23.44	<5.36	<7.13	25.77	2.69	<5.34	13.67	<3.67	<75.88	2.12	2.47	249.63	244.06
Y89	<-NaN	<-NaN	<-NaN	<-NaN	<-NaN	<-NaN	<-NaN	<-NaN	<-NaN	<-NaN	<-NaN	<-NaN	<-NaN	<-NaN	<-NaN	<-NaN	<-NaN	<-NaN
Zr90	<0.00	<0.00	<0.00	<0.00	<0.00	<0.00	<0.00	<0.00	<0.00	<0.00	<0.00	<0.00	<0.00	<0.00	<0.00	<0.00	<0.00	<0.00
Nb93	<-NaN	<-NaN	<-NaN	<-NaN	<-NaN	<-NaN	<-NaN	<-NaN	<-NaN	<-NaN	<-NaN	<-NaN	<-NaN	<-NaN	<-NaN	<-NaN	<-NaN	<-NaN
Mo95	<-NaN	<-NaN	<-NaN	<-NaN	<-NaN	<-NaN	<-NaN	<-NaN	<-NaN	<-NaN	<-NaN	<-NaN	<-NaN	<-NaN	<-NaN	<-NaN	<-NaN	<-NaN
Ru99	<0.0030	<0.0026	228.78	224.96	0.54	0.095	<0.101	0.38	0.045	0.116	<0.080	<0.057	0.568	<1.30	<0.0028	<0.0032	228.04	233.79
Ru101	<0.00151	<0.00187	222.42	233.16	<0.230	0.032	<0.055	0.234	0.0282	<0.0133	<0.071	<0.0218	0.217	<0.79	<0.00218	<0.00209	234.76	227.06
Rh103	0.0179	0.0179	246.73	232.74	<0.30	<0.040	0.078	18.82	1.708	0.085	<0.071	0.035	22.49	2.38	0.0221	0.0211	244.11	243.82
Ag107	<0.00	<0.00	<0.00	<0.00	<0.00	<0.00	<0.00	<0.00	<0.00	<0.00	<0.00	<0.00	<0.00	<0.00	<0.00	<0.00	<0.00	<0.00
Pd108	0.0405	0.0369	254.91	258.71	<0.27	<0.025	59.37	0.147	60.67	0.044	55.57	<0.033	2.19	<0.65	0.0446	0.052	258.34	260.78
Cd111	<0.00	<0.00	<0.00	<0.00	<0.00	<0.00	<0.00	<0.00	<0.00	<0.00	<0.00	<0.00	<0.00	<0.00	<0.00	<0.00	<0.00	<0.00
In115	<-NaN	<-NaN	<-NaN	<-NaN	<-NaN	<-NaN	<-NaN	<-NaN	<-NaN	<-NaN	<-NaN	<-NaN	<-NaN	<-NaN	<-NaN	<-NaN	<-NaN	<-NaN
Sn118	<0.00	<0.00	<0.00	<0.00	<0.00	<0.00	<0.00	<0.00	<0.00	<0.00	<0.00	<0.00	<0.00	<0.00	<0.00	<0.00	<0.00	<0.00
Sb121	<0.00	<0.00	<0.00	<0.00	<0.00	<0.00	<0.00	<0.00	<0.00	<0.00	<0.00	<0.00	<0.00	<0.00	<0.00	<0.00	<0.00	<0.00
Te125	3.28	3.23	241.31	246.35	<2.68	5.67	<0.44	<0.64	155.62	0.355	<0.43	2.68	<0.29	4.52	3.64	4.25	247.62	230.35
Te128	3.26	3.28	238.68	245.71	<2.84	5.67	<0.62	<0.86	155.99	<0.201	<0.66	2.7	<0.40	19.27	3.57	4.09	241.66	242.82
La139	<-NaN	<-NaN	<-NaN	<-NaN	<-NaN	<-NaN	<-NaN	<-NaN	<-NaN	<-NaN	<-NaN	<-NaN	<-NaN	<-NaN	<-NaN	<-NaN	<-NaN	<-NaN
Ce140	<-NaN	<-NaN	<-NaN	<-NaN	<-NaN	<-NaN	<-NaN	<-NaN	<-NaN	<-NaN	<-NaN	<-NaN	<-NaN	<-NaN	<-NaN	<-NaN	<-NaN	<-NaN
Nd146	<-NaN	<-NaN	<-NaN	<-NaN	<-NaN	<-NaN	<-NaN	<-NaN	<-NaN	<-NaN	<-NaN	<-NaN	<-NaN	<-NaN	<-NaN	<-NaN	<-NaN	<-NaN
Hf178	<-NaN	<-NaN	<-NaN	<-NaN	<-NaN	<-NaN	<-NaN	<-NaN	<-NaN	<-NaN	<-NaN	<-NaN	<-NaN	<-NaN	<-NaN	<-NaN	<-NaN	<-NaN
W182	<-NaN	<-NaN	<-NaN	<-NaN	<-NaN	<-NaN	<-NaN	<-NaN	<-NaN	<-NaN	<-NaN	<-NaN	<-NaN	<-NaN	<-NaN	<-NaN	<-NaN	<-NaN

Element	STD610-3	STD610-6	PGEA-4	PGEA-5	BCR2G-2	JL10-PY1	JL10-SPH	JL10-CPY	WAN-SPH	BG05-PY	BG05-SPH	JL19-PY	JL19-CPY	JL19-SPH	STD610-7	STD610-8	PGEA-6	PGEA-7
Re185	<0.00	<0.00	<0.00	<0.00	<0.00	<0.00	<0.00	<0.00	<0.00	<0.00	<0.00	<0.00	<0.00	<0.00	<0.00	<0.00	<0.00	<0.00
Re187	<0.00	<0.00	<0.00	<0.00	<0.00	<0.00	<0.00	<0.00	<0.00	<0.00	<0.00	<0.00	<0.00	<0.00	<0.00	<0.00	<0.00	<0.00
Os189	<0.0043	<0.0050	190.75	209.63	<0.60	<0.093	<0.175	<0.256	<0.045	<0.042	<0.100	<0.069	<0.111	<1.88	<0.0044	<0.0059	195.53	189.96
Os190	0.00133	<0.00281	187.99	214.26	<0.30	<0.037	<0.099	<0.131	0.0178	<0.0213	<0.080	<0.035	<0.044	<0.99	<0.0031	<0.0024	199.71	186.09
Ir193	<0.00043	<0.00070	104.87	109.69	0.112	<0.0091	<0.0181	<0.0234	<0.0053	<0.0052	<0.0160	0.0105	<0.0115	<0.176	<0.00065	<0.00066	108.07	105.45
Pt195	0.0315	0.0346	205.21	206.41	<0.25	<0.020	<0.058	<0.099	<0.0144	<0.023	<0.055	<0.046	<0.045	<0.53	0.0468	0.0416	206.58	200.2
Au197	0.1946	0.1886	231.61	239.66	0.281	0.67	0.036	0.134	3.57	1.354	0.08	0.0409	0.051	5.08	0.2076	0.2344	234.6	233.35
Pb208	<0.00	<0.00	<0.00	<0.00	<0.00	<0.00	<0.00	<0.00	<0.00	<0.00	<0.00	<0.00	<0.00	<0.00	<0.00	<0.00	<0.00	<0.00
Bi209	4.05	4.13	233.71	242.15	<0.207	25.82	0.354	0.12	6.14	140.91	0.131	26.26	27.99	16.29	4.32	5.09	237.43	231.95
Th232	<0.00	<0.00	<0.00	<0.00	<0.00	<0.00	<0.00	<0.00	<0.00	<0.00	<0.00	<0.00	<0.00	<0.00	<0.00	<0.00	<0.00	<0.00
U238	<-NaN	<-NaN	<-NaN	<-NaN	<-NaN	<-NaN	<-NaN	<-NaN	<-NaN	<-NaN	<-NaN	<-NaN	<-NaN	<-NaN	<-NaN	<-NaN	<-NaN	<-NaN
ThO248	<-NaN	<-NaN	<-NaN	<-NaN	<-NaN	<-NaN	<-NaN	<-NaN	<-NaN	<-NaN	<-NaN	<-NaN	<-NaN	<-NaN	<-NaN	<-NaN	<-NaN	<-NaN
GLITTER!: 1 sigma error.																		
Element	STD610-3	STD610-6	PGEA-4	PGEA-5	BCR2G-2	JL10-PY1	JL10-SPH	JL10-CPY	WAN-SPH	BG05-PY	BG05-SPH	JL19-PY	JL19-CPY	JL19-SPH	STD610-7	STD610-8	PGEA-6	PGEA-7
Al27	<0.00	<0.00	<0.00	<0.00	<0.00	<0.00	<0.00	<0.00	<0.00	<0.00	<0.00	<0.00	<0.00	<0.00	<0.00	<0.00	<0.00	<0.00
Si29	<0.00	<0.00	<0.00	<0.00	<0.00	<0.00	<0.00	<0.00	<0.00	<0.00	<0.00	<0.00	<0.00	<0.00	<0.00	<0.00	<0.00	<0.00
S34	13.31	13.13	8823.22	8840.52	1623.49	16911.5	10523.03	11077.25	10569.75	16907.95	10652.94	16906.75	11060.8	11587.88	13.2	13.34	8819.69	8827.64
Ca43	<0.00	<0.00	<0.00	<0.00	<0.00	<0.00	<0.00	<0.00	<0.00	<0.00	<0.00	<0.00	<0.00	<0.00	<0.00	<0.00	<0.00	<0.00
Sc45	<0.00	<0.00	<0.00	<0.00	<0.00	<0.00	<0.00	<0.00	<0.00	<0.00	<0.00	<0.00	<0.00	<0.00	<0.00	<0.00	<0.00	<0.00
Ti49	<0.00	<0.00	<0.00	<0.00	<0.00	<0.00	<0.00	<0.00	<0.00	<0.00	<0.00	<0.00	<0.00	<0.00	<0.00	<0.00	<0.00	<0.00
V51	<0.00	<0.00	<0.00	<0.00	<0.00	<0.00	<0.00	<0.00	<0.00	<0.00	<0.00	<0.00	<0.00	<0.00	<0.00	<0.00	<0.00	<0.00
Cr53	<0.00	<0.00	<0.00	<0.00	<0.00	<0.00	<0.00	<0.00	<0.00	<0.00	<0.00	<0.00	<0.00	<0.00	<0.00	<0.00	<0.00	<0.00
Mn55	<0.00	<0.00	<0.00	<0.00	<0.00	<0.00	<0.00	<0.00	<0.00	<0.00	<0.00	<0.00	<0.00	<0.00	<0.00	<0.00	<0.00	<0.00
Fe57	<0.00	<0.00	<0.00	<0.00	<0.00	<0.00	<0.00	<0.00	<0.00	<0.00	<0.00	<0.00	<0.00	<0.00	<0.00	<0.00	<0.00	<0.00
Co59	<0.00	<0.00	<0.00	<0.00	<0.00	<0.00	<0.00	<0.00	<0.00	<0.00	<0.00	<0.00	<0.00	<0.00	<0.00	<0.00	<0.00	<0.00
Ni60	0.17	0.17	22498.85	22695.31	1.57	0.16	0.09	0.17	0.04	2.03	0.22	0.053	0.13	5.92	0.19	0.21	23037.3	22595.97
Ni62	0.17	0.18	22027.46	22048.17	3.63	0.24	0.7	0.82	0.11	2.19	0.45	0.2	0.34	13.13	0.2	0.22	22044.8	22434.84
Cu65	0.099	0.098	7.79	7.83	2.02	0.26	27.49	6286.05	581.1	3.79	7.14	7.32	8240.06	33.9	0.11	0.13	7.87	7.99
Zn66	<0.00	<0.00	<0.00	<0.00	<0.00	<0.00	<0.00	<0.00	<0.00	<0.00	<0.00	<0.00	<0.00	<0.00	<0.00	<0.00	<0.00	<0.00
Ga71	<0.00	<0.00	<0.00	<0.00	<0.00	<0.00	<0.00	<0.00	<0.00	<0.00	<0.00	<0.00	<0.00	<0.00	<0.00	<0.00	<0.00	<0.00
As75	0.22	0.23	8.83	10.07	6.3	44.23	2.59	2.44	160.21	170.26	2.66	4.82	1.12	45.46	0.22	0.28	9.01	8.84
Se82	0.11	0.11	12.21	13.64	9.09	1.86	2.45	3.25	1.29	0.8	2.06	1.33	1.55	41.22	0.12	0.14	12.53	12.73
Y89	<0.00	<0.00	<0.00	<0.00	<0.00	<0.00	<0.00	<0.00	<0.00	<0.00	<0.00	<0.00	<0.00	<0.00	<0.00	<0.00	<0.00	<0.00
Zr90	<0.00	<0.00	<0.00	<0.00	<0.00	<0.00	<0.00	<0.00	<0.00	<0.00	<0.00	<0.00	<0.00	<0.00	<0.00	<0.00	<0.00	<0.00
Nb93	<0.00	<0.00	<0.00	<0.00	<0.00	<0.00	<0.00	<0.00	<0.00	<0.00	<0.00	<0.00	<0.00	<0.00	<0.00	<0.00	<0.00	<0.00
Mo95	<0.00	<0.00	<0.00	<0.00	<0.00	<0.00	<0.00	<0.00	<0.00	<0.00	<0.00	<0.00	<0.00	<0.00	<0.00	<0.00	<0.00	<0.00
Ru99	0.0013	0.0012	7.68	7.74	0.15	0.033	0.046	0.099	0.012	0.025	0.033	0.025	0.07	0.51	0.0014	0.0014	7.62	7.89
Ru101	0.00067	0.00075	8.62	9.14	0.096	0.016	0.028	0.065	0.0064	0.0082	0.025	0.0098	0.04	0.24	0.00091	0.00088	9.06	8.82
Rh103	0.0013	0.0013	8.62	8.16	0.12	0.016	0.033	0.69	0.063	0.012	0.028	0.014	0.8	0.57	0.0014	0.0015	8.52	8.52
Ag107	<0.00	<0.00	<0.00	<0.00	<0.00	<0.00	<0.00	<0.00	<0.00	<0.00	<0.00	<0.00	<0.00	<0.00	<0.00	<0.00	<0.00	<0.00
Pd108	0.0024	0.0024	8.09	8.3	0.11	0.012	1.94	0.045	1.9	0.012	1.77	0.012	0.11	0.44	0.0026	0.003	8.18	8.3
Cd111	<0.00	<0.00	<0.00	<0.00	<0.00	<0.00	<0.00	<0.00	<0.00	<0.00	<0.00	<0.00	<0.00	<0.00	<0.00	<0.00	<0.00	<0.00
In115	<0.00	<0.00	<0.00	<0.00	<0.00	<0.00	<0.00	<0.00	<0.00	<0.00	<0.00	<0.00	<0.00	<0.00	<0.00	<0.00	<0.00	<0.00
Sn118	<0.00	<0.00	<0.00	<0.00	<0.00	<0.00	<0.00	<0.00	<0.00	<0.00	<0.00	<0.00	<0.00	<0.00	<0.00	<0.00	<0.00	<0.00
Sb121	<0.00	<0.00	<0.00	<0.00	<0.00	<0.00	<0.00	<0.00	<0.00	<0.00	<0.00	<0.00	<0.00	<0.00	<0.00	<0.00	<0.00	<0.00
Te125	0.15	0.15	10.87	11.6	0.93	0.46	0.19	0.25	6.48	0.084	0.18	0.24	0.14	3.38	0.16	0.19	11.02	10.55

Element	STD610-3	STD610-6	PGEA-4	PGEA-5	BCR2G-2	JL10-PY1	JL10-SPH	JL10-CPY	WAN-SPH	BG05-PY	BG05-SPH	JL19-PY	JL19-CPY	JL19-SPH	STD610-7	STD610-8	PGEA-6	PGEA-7
Te128	0.11	0.11	7.79	8.18	1.06	0.29	0.28	0.39	4.91	0.091	0.24	0.17	0.17	5.04	0.12	0.14	7.85	7.96
La139	<0.00	<0.00	<0.00	<0.00	<0.00	<0.00	<0.00	<0.00	<0.00	<0.00	<0.00	<0.00	<0.00	<0.00	<0.00	<0.00	<0.00	<0.00
Ce140	<0.00	<0.00	<0.00	<0.00	<0.00	<0.00	<0.00	<0.00	<0.00	<0.00	<0.00	<0.00	<0.00	<0.00	<0.00	<0.00	<0.00	<0.00
Nd146	<0.00	<0.00	<0.00	<0.00	<0.00	<0.00	<0.00	<0.00	<0.00	<0.00	<0.00	<0.00	<0.00	<0.00	<0.00	<0.00	<0.00	<0.00
Hf178	<0.00	<0.00	<0.00	<0.00	<0.00	<0.00	<0.00	<0.00	<0.00	<0.00	<0.00	<0.00	<0.00	<0.00	<0.00	<0.00	<0.00	<0.00
W182	<0.00	<0.00	<0.00	<0.00	<0.00	<0.00	<0.00	<0.00	<0.00	<0.00	<0.00	<0.00	<0.00	<0.00	<0.00	<0.00	<0.00	<0.00
Re185	<0.00	<0.00	<0.00	<0.00	<0.00	<0.00	<0.00	<0.00	<0.00	<0.00	<0.00	<0.00	<0.00	<0.00	<0.00	<0.00	<0.00	<0.00
Re187	<0.00	<0.00	<0.00	<0.00	<0.00	<0.00	<0.00	<0.00	<0.00	<0.00	<0.00	<0.00	<0.00	<0.00	<0.00	<0.00	<0.00	<0.00
Os189	0.0017	0.0017	8.3	9.29	0.24	0.033	0.07	0.098	0.017	0.016	0.045	0.027	0.041	1.25	0.002	0.0021	8.46	8.32
Os190	0.00063	0.00099	10.32	11.83	0.14	0.016	0.042	0.056	0.0081	0.0087	0.032	0.013	0.022	0.54	0.0012	0.001	10.93	10.23
Ir193	0.0002	0.00026	3.63	3.83	0.03	0.0035	0.0082	0.0091	0.002	0.002	0.0063	0.0028	0.0051	0.096	0.00028	0.00028	3.74	3.66
Pt195	0.0025	0.0026	6.86	7.01	0.11	0.012	0.025	0.037	0.006	0.011	0.022	0.016	0.018	0.37	0.0031	0.003	6.88	6.72
Au197	0.0073	0.0071	7.43	7.75	0.062	0.042	0.02	0.034	0.12	0.059	0.019	0.0097	0.013	0.73	0.0078	0.0088	7.51	7.5
Pb208	<0.00	<0.00	<0.00	<0.00	<0.00	<0.00	<0.00	<0.00	<0.00	<0.00	<0.00	<0.00	<0.00	<0.00	<0.00	<0.00	<0.00	<0.00
Bi209	0.14	0.14	7.75	8.07	0.081	0.87	0.037	0.036	0.21	4.64	0.021	0.87	0.94	1.16	0.15	0.17	7.86	7.7
Th232	<0.00	<0.00	<0.00	<0.00	<0.00	<0.00	<0.00	<0.00	<0.00	<0.00	<0.00	<0.00	<0.00	<0.00	<0.00	<0.00	<0.00	<0.00
U238	<0.00	<0.00	<0.00	<0.00	<0.00	<0.00	<0.00	<0.00	<0.00	<0.00	<0.00	<0.00	<0.00	<0.00	<0.00	<0.00	<0.00	<0.00
ThO248	<0.00	<0.00	<0.00	<0.00	<0.00	<0.00	<0.00	<0.00	<0.00	<0.00	<0.00	<0.00	<0.00	<0.00	<0.00	<0.00	<0.00	<0.00
GLITTER!: Minimum detection limits (99% confidence).																		
Element	STD610-3	STD610-6	PGEA-4	PGEA-5	BCR2G-2	JL10-PY1	JL10-SPH	JL10-CPY	WAN-SPH	BG05-PY	BG05-SPH	JL19-PY	JL19-CPY	JL19-SPH	STD610-7	STD610-8	PGEA-6	PGEA-7
Al27	<0.00	<0.00	<0.00	<0.00	<0.00	<0.00	<0.00	<0.00	<0.00	<0.00	<0.00	<0.00	<0.00	<0.00	<0.00	<0.00	<0.00	<0.00
Si29	<0.00000	<0.00000	<0.00000	<0.00000	<0.00000	<0.00000	<0.00000	<0.00000	<0.00000	<0.00000	<0.00000	<0.00000	<0.00000	<0.00000	<0.00000	<0.00000	<0.00000	<0.00000
S34	7.75	6.75	474.15	455.59	914.74	112.15	235.9	342.52	62.01	82.33	281	131.19	170.64	3451.94	6.85	7.67	501.94	472.71
Ca43	<0.00000	<0.00000	<0.00000	<0.00000	<0.00000	<0.00000	<0.00000	<0.00000	<0.00000	<0.00000	<0.00000	<0.00000	<0.00000	<0.00000	<0.00000	<0.00000	<0.00000	<0.00000
Sc45	<0.00	<0.00	<0.00	<0.00	<0.00	<0.00	<0.00	<0.00	<0.00	<0.00	<0.00	<0.00	<0.00	<0.00	<0.00	<0.00	<0.00	<0.00
Ti49	<0.00000	<0.00000	<0.00000	<0.00000	<0.00000	<0.00000	<0.00000	<0.00000	<0.00000	<0.00000	<0.00000	<0.00000	<0.00000	<0.00000	<0.00000	<0.00000	<0.00000	<0.00000
V51	<0.00	<0.00	<0.00	<0.00	<0.00	<0.00	<0.00	<0.00	<0.00	<0.00	<0.00	<0.00	<0.00	<0.00	<0.00	<0.00	<0.00	<0.00
Cr53	<0.00	<0.00	<0.00	<0.00	<0.00	<0.00	<0.00	<0.00	<0.00	<0.00	<0.00	<0.00	<0.00	<0.00	<0.00	<0.00	<0.00	<0.00
Mn55	<0.00	<0.00	<0.00	<0.00	<0.00	<0.00	<0.00	<0.00	<0.00	<0.00	<0.00	<0.00	<0.00	<0.00	<0.00	<0.00	<0.00	<0.00
Fe57	<0.00	<0.00	<0.00	<0.00	<0.00	<0.00	<0.00	<0.00	<0.00	<0.00	<0.00	<0.00	<0.00	<0.00	<0.00	<0.00	<0.00	<0.00
Co59	<0.00000	<0.00000	<0.00000	<0.00000	<0.00000	<0.00000	<0.00000	<0.00000	<0.00000	<0.00000	<0.00000	<0.00000	<0.00000	<0.00000	<0.00000	<0.00000	<0.00000	<0.00000
Ni60	0.00585	0.00654	0.387	0.468	0.971	0.109	0.191	0.245	0.0447	0.134	0.184	0.0998	0.142	2.51	0.00877	0.00654	2.99	1.9
Ni62	0.0298	0.0293	2.23	2.14	4.36	0.501	1.07	1.23	0.199	0.321	0.859	0.381	0.586	11.86	0.0211	0.0299	2.58	4.66
Cu65	0.0102	0.0107	0.769	0.67	1.43	0.182	0.327	0.44	0.123	0.122	0.34	0.174	0.213	4.83	0.0211	0.0114	0.76	0.699
Zn66	<0.00000	<0.00000	<0.00000	<0.00000	<0.00000	<0.00000	<0.00000	<0.00000	<0.00000	<0.00000	<0.00000	<0.00000	<0.00000	<0.00000	<0.00000	<0.00000	<0.00000	<0.00000
Ga71	<0.00	<0.00	<0.00	<0.00	<0.00	<0.00	<0.00	<0.00	<0.00	<0.00	<0.00	<0.00	<0.00	<0.00	<0.00	<0.00	<0.00	<0.00
As75	0.112	0.12	8.49	7.81	16.24	1.94	3.64	5	0.933	1.35	4.26	2.11	2.47	53.13	0.117	0.128	8.9	8.16
Se82	0.157	0.175	12.42	10.78	23.68	2.9	5.36	7.13	1.37	1.71	5.34	2.92	3.67	75.88	0.16	0.178	12.03	11.4
Y89	<0.00	<0.00	<0.00	<0.00	<0.00	<0.00	<0.00	<0.00	<0.00	<0.00	<0.00	<0.00	<0.00	<0.00	<0.00	<0.00	<0.00	<0.00
Zr90	<0.00000	<0.00000	<0.00000	<0.00000	<0.00000	<0.00000	<0.00000	<0.00000	<0.00000	<0.00000	<0.00000	<0.00000	<0.00000	<0.00000	<0.00000	<0.00000	<0.00000	<0.00000
Nb93	<0.00	<0.00	<0.00	<0.00	<0.00	<0.00	<0.00	<0.00	<0.00	<0.00	<0.00	<0.00	<0.00	<0.00	<0.00	<0.00	<0.00	<0.00
Mo95	<0.00	<0.00	<0.00	<0.00	<0.00	<0.00	<0.00	<0.00	<0.00	<0.00	<0.00	<0.00	<0.00	<0.00	<0.00	<0.00	<0.00	<0.00
Ru99	0.00297	0.00259	0.231	0.184	0.185	0.0509	0.101	0.119	0.0209	0.0291	0.08	0.0568	0.0486	1.3	0.00281	0.00318	0.166	0.183
Ru101	0.00151	0.00187	0.152	0.145	0.23	0.0232	0.0551	0.0767	0.0075	0.0133	0.0705	0.0218	0.0463	0.791	0.00218	0.00209	0.138	0.144
Rh103	0.00203	0.00219	0.163	0.145	0.299	0.0397	0.0693	0.0923	0.0164	0.022	0.0713	0.0349	0.0452	0.854	0.00192	0.00235	0.16	0.144
Ag107	<0.00000	<0.00000	<0.00000	<0.00000	<0.00000	<0.00000	<0.00000	<0.00000	<0.00000	<0.00000	<0.00000	<0.00000	<0.00000	<0.00000	<0.00000	<0.00000	<0.00000	<0.00000

Element	STD610-3	STD610-6	PGEA-4	PGEA-5	BCR2G-2	JL10-PY1	JL10-SPH	JL10-CPY	WAN-SPH	BG05-PY	BG05-SPH	JL19-PY	JL19-CPY	JL19-SPH	STD610-7	STD610-8	PGEA-6	PGEA-7
Pd108	0.00131	0.00191	0.111	0.109	0.271	0.0247	0.048	0.0668	0.0113	0.0191	0.0501	0.0329	0.0444	0.654	0.00114	0.00162	0.12	0.12
Cd111	<0.00000	<0.00000	<0.00000	<0.00000	<0.00000	<0.00000	<0.00000	<0.00000	<0.00000	<0.00000	<0.00000	<0.00000	<0.00000	<0.00000	<0.00000	<0.00000	<0.00000	<0.00000
In115	<0.00	<0.00	<0.00	<0.00	<0.00	<0.00	<0.00	<0.00	<0.00	<0.00	<0.00	<0.00	<0.00	<0.00	<0.00	<0.00	<0.00	<0.00
Sn118	<0.00000	<0.00000	<0.00000	<0.00000	<0.00000	<0.00000	<0.00000	<0.00000	<0.00000	<0.00000	<0.00000	<0.00000	<0.00000	<0.00000	<0.00000	<0.00000	<0.00000	<0.00000
Sb121	<0.00000	<0.00000	<0.00000	<0.00000	<0.00000	<0.00000	<0.00000	<0.00000	<0.00000	<0.00000	<0.00000	<0.00000	<0.00000	<0.00000	<0.00000	<0.00000	<0.00000	<0.00000
Te125	0.00975	0.0128	1.01	1.1	2.68	0.242	0.436	0.643	0.111	0.0741	0.426	0.286	0.293	4.42	0.0146	0.0156	1.22	1.23
Te128	0.0188	0.0207	1.42	1.4	2.84	0.343	0.618	0.859	0.161	0.201	0.661	0.317	0.395	8.24	0.0185	0.0205	1.47	1.37
La139	<0.00	<0.00	<0.00	<0.00	<0.00	<0.00	<0.00	<0.00	<0.00	<0.00	<0.00	<0.00	<0.00	<0.00	<0.00	<0.00	<0.00	<0.00
Ce140	<0.00	<0.00	<0.00	<0.00	<0.00	<0.00	<0.00	<0.00	<0.00	<0.00	<0.00	<0.00	<0.00	<0.00	<0.00	<0.00	<0.00	<0.00
Nd146	<0.00	<0.00	<0.00	<0.00	<0.00	<0.00	<0.00	<0.00	<0.00	<0.00	<0.00	<0.00	<0.00	<0.00	<0.00	<0.00	<0.00	<0.00
Hf178	<0.00	<0.00	<0.00	<0.00	<0.00	<0.00	<0.00	<0.00	<0.00	<0.00	<0.00	<0.00	<0.00	<0.00	<0.00	<0.00	<0.00	<0.00
W182	<0.00	<0.00	<0.00	<0.00	<0.00	<0.00	<0.00	<0.00	<0.00	<0.00	<0.00	<0.00	<0.00	<0.00	<0.00	<0.00	<0.00	<0.00
Re185	<0.00000	<0.00000	<0.00000	<0.00000	<0.00000	<0.00000	<0.00000	<0.00000	<0.00000	<0.00000	<0.00000	<0.00000	<0.00000	<0.00000	<0.00000	<0.00000	<0.00000	<0.00000
Re187	<0.00000	<0.00000	<0.00000	<0.00000	<0.00000	<0.00000	<0.00000	<0.00000	<0.00000	<0.00000	<0.00000	<0.00000	<0.00000	<0.00000	<0.00000	<0.00000	<0.00000	<0.00000
Os189	0.00429	0.00496	0.306	0.291	0.597	0.0931	0.175	0.256	0.0453	0.0421	0.1	0.0694	0.111	1.88	0.00439	0.00593	0.367	0.265
Os190	0.00099	0.00281	0.245	0.117	0.302	0.0373	0.0991	0.131	0.0171	0.0213	0.0803	0.0351	0.0445	0.986	0.00312	0.00237	0.192	0.164
Ir193	0.00043	0.0007	0.0338	0.0416	0.0468	0.00912	0.0181	0.0234	0.00528	0.00522	0.016	0.00384	0.0115	0.176	0.00065	0.00066	0.0343	0.0359
Pt195	0.00224	0.00196	0.117	0.143	0.255	0.0199	0.0579	0.0987	0.0144	0.0227	0.0552	0.0459	0.045	0.526	0.001	0.00226	0.132	0.113
Au197	0.0008	0.00101	0.0834	0.0684	0.0942	0.00947	0.0356	0.0471	0.00752	0.0108	0.0372	0.02	0.016	0.355	0.00076	0.00093	0.0746	0.0681
Pb208	<0.00000	<0.00000	<0.00000	<0.00000	<0.00000	<0.00000	<0.00000	<0.00000	<0.00000	<0.00000	<0.00000	<0.00000	<0.00000	<0.00000	<0.00000	<0.00000	<0.00000	<0.00000
Bi209	0.00127	0.00143	0.107	0.0896	0.207	0.0261	0.045	0.0662	0.0112	0.0148	0.0448	0.0224	0.0272	0.648	0.00159	0.0018	0.102	0.0961
Th232	<0.00000	<0.00000	<0.00000	<0.00000	<0.00000	<0.00000	<0.00000	<0.00000	<0.00000	<0.00000	<0.00000	<0.00000	<0.00000	<0.00000	<0.00000	<0.00000	<0.00000	<0.00000
U238	<0.00	<0.00	<0.00	<0.00	<0.00	<0.00	<0.00	<0.00	<0.00	<0.00	<0.00	<0.00	<0.00	<0.00	<0.00	<0.00	<0.00	<0.00
ThO248	<0.00	<0.00	<0.00	<0.00	<0.00	<0.00	<0.00	<0.00	<0.00	<0.00	<0.00	<0.00	<0.00	<0.00	<0.00	<0.00	<0.00	<0.00
GLITTER!: Trace element concentrations normalised to chondrite.																		
Element	STD610-3	STD610-6	PGEA-4	PGEA-5	BCR2G-2	JL10-PY1	JL10-SPH	JL10-CPY	WAN-SPH	BG05-PY	BG05-SPH	JL19-PY	JL19-CPY	JL19-SPH	STD610-7	STD610-8	PGEA-6	PGEA-7
Al27	<****	<****	<****	<****	<****	<****	<****	<****	<****	<****	<****	<****	<****	<****	<****	<****	<****	<****
Si29	0	0	0	0	0	0	0	0	0	0	0	0	0	0	0	0	0	0
S34	Inf	Inf	Inf	Inf	Inf	Inf	Inf	Inf	Inf	Inf	Inf	Inf	Inf	Inf	Inf	Inf	Inf	Inf
Ca43	0	0	0	0	0	0	0	0	0	0	0	0	0	0	0	0	0	0
Sc45	<****	<****	<****	<****	<****	<****	<****	<****	<****	<****	<****	<****	<****	<****	<****	<****	<****	<****
Ti49	0	0	0	0	0	0	0	0	0	0	0	0	0	0	0	0	0	0
V51	<****	<****	<****	<****	<****	<****	<****	<****	<****	<****	<****	<****	<****	<****	<****	<****	<****	<****
Cr53	<****	<****	<****	<****	<****	<****	<****	<****	<****	<****	<****	<****	<****	<****	<****	<****	<****	<****
Mn55	<****	<****	<****	<****	<****	<****	<****	<****	<****	<****	<****	<****	<****	<****	<****	<****	<****	<****
Fe57	<****	<****	<****	<****	<****	<****	<****	<****	<****	<****	<****	<****	<****	<****	<****	<****	<****	<****
Co59	0	0	0	0	0	0	0	0	0	0	0	0	0	0	0	0	0	0
Ni60	0.0003	0.00031	42.89	43.23	0.00226	0.00018	0	0.00008	0.00004	0.0038	0.00028	0.00003	0.00012	0.00598	0.00034	0.00039	43.93	43.07
Ni62	0.0003	0.0003	43.15	43.15	0.00316	0	0.00025	0.00025	0.00004	0.00371	0.00018	0.00007	0.00008	0.0049	0.00034	0.00038	43.2	43.94
Cu65	0.01765	0.01747	1.434	1.423	0.317	0.0384	5.14	1179.65	109.17	0.706	1.332	1.371	1547.52	5.75	0.01871	0.02247	1.452	1.467
Zn66	0	0	0	0	0	0	0	0	0	0	0	0	0	0	0	0	0	0
Ga71	<****	<****	<****	<****	<****	<****	<****	<****	<****	<****	<****	<****	<****	<****	<****	<****	<****	<****
As75	1.215	1.263	45.77	52.39	0	253.29	11	5.05	918.79	976.28	11.85	27.13	1.63	186.25	1.233	1.549	46.9	45.52
Se82	0.0701	0.0645	8.57	9.24	0	0.859	0	0	0.944	0.099	0	0.501	0	0	0.0775	0.0906	9.14	8.94
Y89	<****	<****	<****	<****	<****	<****	<****	<****	<****	<****	<****	<****	<****	<****	<****	<****	<****	<****
Zr90	0	0	0	0	0	0	0	0	0	0	0	0	0	0	0	0	0	0

PGEARUN3

Element	STD610-3	STD610-6	PGEA-4	PGEA-5	BCR2G-2	JL10-PY1	JL10-SPH	JL10-CPY	WAN-SPH	BG05-PY	BG05-SPH	JL19-PY	JL19-CPY	JL19-SPH	STD610-7	STD610-8	PGEA-6	PGEA-7
Nb93	<****	<****	<****	<****	<****	<****	<****	<****	<****	<****	<****	<****	<****	<****	<****	<****	<****	<****
Mo95	<****	<****	<****	<****	<****	<****	<****	<****	<****	<****	<****	<****	<****	<****	<****	<****	<****	<****
Ru99	0	0	213.62	210.05	0.5	0.088	0	0.355	0.042	0.109	0	0	0.531	0	0	0	212.92	218.29
Ru101	0	0	207.67	217.71	0	0.03	0	0.219	0.0264	0	0	0	0.202	0	0	0	219.2	212
Rh103	0.0889	0.0889	1227.53	1157.89	0	0	0.39	93.65	8.5	0.421	0	0.176	111.88	11.85	0.1098	0.105	1214.45	1213.03
Ag107	0	0	0	0	0	0	0	0	0	0	0	0	0	0	0	0	0	0
Pd108	0.0484	0.0442	304.91	309.46	0	0	71.02	0.175	72.57	0.053	66.47	0	2.63	0	0.0534	0.0621	309.02	311.94
Cd111	0	0	0	0	0	0	0	0	0	0	0	0	0	0	0	0	0	0
In115	<****	<****	<****	<****	<****	<****	<****	<****	<****	<****	<****	<****	<****	<****	<****	<****	<****	<****
Sn118	0	0	0	0	0	0	0	0	0	0	0	0	0	0	0	0	0	0
Sb121	0	0	0	0	0	0	0	0	0	0	0	0	0	0	0	0	0	0
Te125	0.96	0.946	70.56	72.03	0	1.66	0	0	45.5	0.104	0	0.784	0	1.32	1.066	1.241	72.4	67.36
Te128	0.955	0.958	69.79	71.85	0	1.657	0	0	45.61	0	0	0.788	0	5.63	1.043	1.195	70.66	71
La139	<****	<****	<****	<****	<****	<****	<****	<****	<****	<****	<****	<****	<****	<****	<****	<****	<****	<****
Ce140	<****	<****	<****	<****	<****	<****	<****	<****	<****	<****	<****	<****	<****	<****	<****	<****	<****	<****
Nd146	<****	<****	<****	<****	<****	<****	<****	<****	<****	<****	<****	<****	<****	<****	<****	<****	<****	<****
Hf178	<****	<****	<****	<****	<****	<****	<****	<****	<****	<****	<****	<****	<****	<****	<****	<****	<****	<****
W182	<****	<****	<****	<****	<****	<****	<****	<****	<****	<****	<****	<****	<****	<****	<****	<****	<****	<****
Re185	0	0	0	0	0	0	0	0	0	0	0	0	0	0	0	0	0	0
Re187	0	0	0	0	0	0	0	0	0	0	0	0	0	0	0	0	0	0
Os189	0	0	181.84	199.84	0	0	0	0	0	0	0	0	0	0	0	0	186.39	181.08
Os190	0.00127	0	179.21	204.25	0	0	0	0	0.017	0	0	0	0	0	0	0	190.38	177.4
Ir193	0	0	147.7	154.49	0.158	0	0	0	0	0	0	0.0148	0	0	0	0	152.21	148.52
Pt195	0.022	0.0242	143.5	144.34	0	0	0	0	0	0	0	0	0	0	0.0327	0.0291	144.46	140
Au197	0.892	0.865	1062.45	1099.36	1.29	3.07	0.165	0.62	16.39	6.21	0.366	0.188	0.232	23.32	0.952	1.075	1076.17	1070.4
Pb208	0	0	0	0	0	0	0	0	0	0	0	0	0	0	0	0	0	0
Bi209	24.26	24.71	1399.43	1450.01	0	154.61	2.12	0.72	36.76	843.8	0.79	157.24	167.58	97.54	25.84	30.46	1421.76	1388.94
Th232	0	0	0	0	0	0	0	0	0	0	0	0	0	0	0	0	0	0
U238	<****	<****	<****	<****	<****	<****	<****	<****	<****	<****	<****	<****	<****	<****	<****	<****	<****	<****
ThO248	<****	<****	<****	<****	<****	<****	<****	<****	<****	<****	<****	<****	<****	<****	<****	<****	<****	<****

GLITTER4.0: Laser Ablation Analysis Results

G:\KYLIE\MAR13\PGEARUN4
Fri Mar 21 16:05:08 2003

All values are reported in ppm

GLITTER!: Trace Element Concentrations MDL filtered.

	Run4-1	Run4-2	Run4-3	Run4-4	Run4-5	Run4-6	Run4-7	Run4-8	Run4-9	Run4-10	Run4-11	Run4-12	Run4-13	Run4-14	Run4-15	Run4-16	Run4-17	Run4-18	Run4-19
Element	STD610-1	STD610-2	BCR2G-1	PGEA-1	PGEA-2	JL01-PY	BG31-CPY	JL01-PY1	BG32-PY	BG32-PY2	KP04-PY	JL03-PY	JL02-PY	JL07-PY	BG01-PY	STD610-3	STD610-4	PGEA-3	PGEA-4
Al27	<-NaN	<-NaN	<-NaN	<-NaN	<-NaN	<-NaN	<-NaN	<-NaN	<-NaN	<-NaN	<-NaN	<-NaN	<-NaN	<-NaN	<-NaN	<-NaN	<-NaN	<-NaN	<-NaN
Si29	<0.00	<0.00	<0.00	<0.00	<0.00	<0.00	<0.00	<0.00	<0.00	<0.00	<0.00	<0.00	<0.00	<0.00	<0.00	<0.00	<0.00	<0.00	<0.00
S34	392.3	392.3	47632.29	278000.03	278000.03	534495.63	534495.63	534495.56	534495.56	534495.63	534495.63	534495.63	534495.56	534495.63	534495.63	392.3	392.3	278000.03	278000.03
Ca43	<-NaN	<-NaN	<-NaN	<-NaN	<-NaN	<-NaN	<-NaN	<-NaN	<-NaN	<-NaN	<-NaN	<-NaN	<-NaN	<-NaN	<-NaN	<-NaN	<-NaN	<-NaN	<-NaN
Sc45	<-NaN	<-NaN	<-NaN	<-NaN	<-NaN	<-NaN	<-NaN	<-NaN	<-NaN	<-NaN	<-NaN	<-NaN	<-NaN	<-NaN	<-NaN	<-NaN	<-NaN	<-NaN	<-NaN
Ti49	<0.00	<0.00	<0.00	<0.00	<0.00	<0.00	<0.00	<0.00	<0.00	<0.00	<0.00	<0.00	<0.00	<0.00	<0.00	<0.00	<0.00	<0.00	<0.00
V51	<-NaN	<-NaN	<-NaN	<-NaN	<-NaN	<-NaN	<-NaN	<-NaN	<-NaN	<-NaN	<-NaN	<-NaN	<-NaN	<-NaN	<-NaN	<-NaN	<-NaN	<-NaN	<-NaN
Cr53	<-NaN	<-NaN	<-NaN	<-NaN	<-NaN	<-NaN	<-NaN	<-NaN	<-NaN	<-NaN	<-NaN	<-NaN	<-NaN	<-NaN	<-NaN	<-NaN	<-NaN	<-NaN	<-NaN
Mn55	<-NaN	<-NaN	<-NaN	<-NaN	<-NaN	<-NaN	<-NaN	<-NaN	<-NaN	<-NaN	<-NaN	<-NaN	<-NaN	<-NaN	<-NaN	<-NaN	<-NaN	<-NaN	<-NaN
Fe57	<0.00	<0.00	<0.00	<0.00	<0.00	<0.00	<0.00	<0.00	<0.00	<0.00	<0.00	<0.00	<0.00	<0.00	<0.00	<0.00	<0.00	<0.00	<0.00
Co59	<0.00	<0.00	<0.00	<0.00	<0.00	<0.00	<0.00	<0.00	<0.00	<0.00	<0.00	<0.00	<0.00	<0.00	<0.00	<0.00	<0.00	<0.00	<0.00
Ni60	12.68	13.14	55.14	755562.5	762060.06	462.25	3.9	1046.29	1.75	1.63	3.07	38.76	2.57	0.461	22.74	5.52	4.65	667818.31	696862.81
Ni62	12.72	13.03	57.56	757155.88	764445.75	447.91	2.74	1016.74	0.98	1.57	6.14	34.29	3.34	8.35	17.89	5.38	4.7	670122.69	693039
Cu65	7.06	7.31	48.55	260.97	257.49	33.47	3.44	31.65	6.67	375.37	23.26	1.73	14.56	18.75	15850.62	3.16	2.61	222.5	235.66
Zn66	<0.00	<0.00	<0.00	<0.00	<0.00	<0.00	<0.00	<0.00	<0.00	<0.00	<0.00	<0.00	<0.00	<0.00	<0.00	<0.00	<0.00	<0.00	<0.00
Ga71	<-NaN	<-NaN	<-NaN	<-NaN	<-NaN	<-NaN	<-NaN	<-NaN	<-NaN	<-NaN	<-NaN	<-NaN	<-NaN	<-NaN	<-NaN	<-NaN	<-NaN	<-NaN	<-NaN
As75	7.83	8.42	<27.23	140.52	142.41	2247.52	1973.74	294.69	144.98	2120.95	187.64	161.41	7463.7	281.35	1008	3.39	2.83	122.28	126.76
Se82	4.54	4.81	<39.23	262.08	259.11	18.11	<1.66	111.43	18.17	29.67	123.73	20.5	15.91	9.16	211.02	1.82	1.66	233.79	227.78
Y89	<-NaN	<-NaN	<-NaN	<-NaN	<-NaN	<-NaN	<-NaN	<-NaN	<-NaN	<-NaN	<-NaN	<-NaN	<-NaN	<-NaN	<-NaN	<-NaN	<-NaN	<-NaN	<-NaN
Zr90	<-NaN	<-NaN	<-NaN	<-NaN	<-NaN	<-NaN	<-NaN	<-NaN	<-NaN	<-NaN	<-NaN	<-NaN	<-NaN	<-NaN	<-NaN	<-NaN	<-NaN	<-NaN	<-NaN
Nb93	<-NaN	<-NaN	<-NaN	<-NaN	<-NaN	<-NaN	<-NaN	<-NaN	<-NaN	<-NaN	<-NaN	<-NaN	<-NaN	<-NaN	<-NaN	<-NaN	<-NaN	<-NaN	<-NaN
Mo95	<-NaN	<-NaN	<-NaN	<-NaN	<-NaN	<-NaN	<-NaN	<-NaN	<-NaN	<-NaN	<-NaN	<-NaN	<-NaN	<-NaN	<-NaN	<-NaN	<-NaN	<-NaN	<-NaN
Ru99	0.0065	<0.0068	<0.84	238.6	242.84	<0.060	<0.022	<0.032	<0.029	0.485	<0.048	<0.034	0.018	<0.039	0.063	0.0024	<0.0022	216.31	222.03
Ru101	<0.0040	<0.0031	<0.65	238.16	238.34	<0.023	<0.0158	<0.026	<0.0120	<0.0103	<0.031	<0.042	<0.0122	<0.0147	0.0124	<0.00098	<0.00189	217.13	223.99
Rh103	0.0443	0.0503	<0.255	253.68	257.16	0.039	<0.0095	0.0178	<0.0097	0.0687	0.227	<0.0174	<0.0083	<0.0101	2.3	0.0206	0.0177	229.84	236.23
Ag107	<0.00	<0.00	<0.00	<0.00	<0.00	<0.00	<0.00	<0.00	<0.00	<0.00	<0.00	<0.00	<0.00	<0.00	<0.00	<0.00	<0.00	<0.00	<0.00
Pd108	0.1085	0.1188	<0.38	261.45	271.91	<0.030	<0.0162	<0.0185	<0.0093	0.234	0.212	<0.030	<0.0089	<0.0160	0.0541	0.042	0.0326	243.4	256.65
Cd111	<0.00	<0.00	<0.00	<0.00	<0.00	<0.00	<0.00	<0.00	<0.00	<0.00	<0.00	<0.00	<0.00	<0.00	<0.00	<0.00	<0.00	<0.00	<0.00
In115	<-NaN	<-NaN	<-NaN	<-NaN	<-NaN	<-NaN	<-NaN	<-NaN	<-NaN	<-NaN	<-NaN	<-NaN	<-NaN	<-NaN	<-NaN	<-NaN	<-NaN	<-NaN	<-NaN
Sn118	<0.00	<0.00	<0.00	<0.00	<0.00	<0.00	<0.00	<0.00	<0.00	<0.00	<0.00	<0.00	<0.00	<0.00	<0.00	<0.00	<0.00	<0.00	<0.00
Sb121	<0.00	<0.00	<0.00	<0.00	<0.00	<0.00	<0.00	<0.00	<0.00	<0.00	<0.00	<0.00	<0.00	<0.00	<0.00	<0.00	<0.00	<0.00	<0.00
Te125	7.46	8.01	<3.11	260.93	246.24	12.76	9.16	3.57	6.02	16.83	27.26	2.11	39	10.91	305.06	3.18	2.69	216.67	241.98
Te128	7.64	8.16	<4.55	260.4	250.36	13.42	9.81	3.07	5.61	17.58	28.29	2.27	40	9.93	305.62	3.17	2.76	220.88	235.81
La139	<-NaN	<-NaN	<-NaN	<-NaN	<-NaN	<-NaN	<-NaN	<-NaN	<-NaN	<-NaN	<-NaN	<-NaN	<-NaN	<-NaN	<-NaN	<-NaN	<-NaN	<-NaN	<-NaN
Ce140	<-NaN	<-NaN	<-NaN	<-NaN	<-NaN	<-NaN	<-NaN	<-NaN	<-NaN	<-NaN	<-NaN	<-NaN	<-NaN	<-NaN	<-NaN	<-NaN	<-NaN	<-NaN	<-NaN
Nd146	<-NaN	<-NaN	<-NaN	<-NaN	<-NaN	<-NaN	<-NaN	<-NaN	<-NaN	<-NaN	<-NaN	<-NaN	<-NaN	<-NaN	<-NaN	<-NaN	<-NaN	<-NaN	<-NaN
Hf178	<-NaN	<-NaN	<-NaN	<-NaN	<-NaN	<-NaN	<-NaN	<-NaN	<-NaN	<-NaN	<-NaN	<-NaN	<-NaN	<-NaN	<-NaN	<-NaN	<-NaN	<-NaN	<-NaN
W182	<0.00	<0.00	<0.00	<0.00	<0.00	<0.00	<0.00	<0.00	<0.00	<0.00	<0.00	<0.00	<0.00	<0.00	<0.00	<0.00	<0.00	<0.00	<0.00
Re185	<-NaN	<-NaN	<-NaN	<-NaN	<-NaN	<-NaN	<-NaN	<-NaN	<-NaN	<-NaN	<-NaN	<-NaN	<-NaN	<-NaN	<-NaN	<-NaN	<-NaN	<-NaN	<-NaN
Re187	<0.00	<0.00	<0.00	<0.00	<0.00	<0.00	<0.00	<0.00	<0.00	<0.00	<0.00	<0.00	<0.00	<0.00	<0.00	<0.00	<0.00	<0.00	<0.00
Os189	<0.0102	0.0047	<1.24	237.9	191.74	<0.050	<0.033	<0.041	<0.031	<0.0186	<0.050	<0.075	<0.038	<0.050	<0.031	<0.0032	<0.00197	159.72	201.62
Os190	<0.0050	0.0047	<0.45	242.03	191.54	<0.034	<0.0193	<0.028	<0.0156	<0.0134	<0.033	0.043	<0.0150	<0.029	<0.0121	<0.00169	0.00155	160.84	198.56

Element	STD610-1	STD610-2	BCR2G-1	PGEA-1	PGEA-2	JL01-PY	BG31-CPY	JL01-PY1	BG32-PY	BG32-PY2	KP04-PY	JL03-PY	JL02-PY	JL07-PY	BG01-PY	STD610-3	STD610-4	PGEA-3	PGEA-4
Ir193	0.001	<0.00097	<0.142	118.71	112.35	<0.0086	0.0024	0.0049	<0.0045	<0.00123	<0.0099	<0.0081	<0.0024	<0.0025	<0.0033	<0.00033	<0.00034	95.74	103.16
Pt195	0.0828	0.0955	<0.49	221.76	221.83	<0.033	<0.0250	<0.027	<0.0186	<0.0142	<0.028	<0.031	<0.0143	<0.0172	<0.0095	0.0353	0.0323	187.32	195.24
Au197	0.501	0.516	<0.36	254.44	255.55	1.33	0.0478	0.394	0.0449	2.84	0.0396	0.105	26.98	0.072	21.84	0.209	0.17	214.52	222.09
Pb208	<0.00	<0.00	<0.00	<0.00	<0.00	<0.00	<0.00	<0.00	<0.00	<0.00	<0.00	<0.00	<0.00	<0.00	<0.00	<0.00	<0.00	<0.00	<0.00
Bi209	9.72	10.28	4.08	264.27	255.4	450.59	6.09	2.4	28.75	679.46	10.21	13.99	1.27	88.77	572663.69	3.73	3.15	210.29	225.08
Th232	<0.00	<0.00	<0.00	<0.00	<0.00	<0.00	<0.00	<0.00	<0.00	<0.00	<0.00	<0.00	<0.00	<0.00	<0.00	<0.00	<0.00	<0.00	<0.00
U238	<-NaN	<-NaN	<-NaN	<-NaN	<-NaN	<-NaN	<-NaN	<-NaN	<-NaN	<-NaN	<-NaN	<-NaN	<-NaN	<-NaN	<-NaN	<-NaN	<-NaN	<-NaN	<-NaN
ThO248	<-NaN	<-NaN	<-NaN	<-NaN	<-NaN	<-NaN	<-NaN	<-NaN	<-NaN	<-NaN	<-NaN	<-NaN	<-NaN	<-NaN	<-NaN	<-NaN	<-NaN	<-NaN	<-NaN
GLITTER!: 1 sigma error.																			
Element	STD610-1	STD610-2	BCR2G-1	PGEA-1	PGEA-2	JL01-PY	BG31-CPY	JL01-PY1	BG32-PY	BG32-PY2	KP04-PY	JL03-PY	JL02-PY	JL07-PY	BG01-PY	STD610-3	STD610-4	PGEA-3	PGEA-4
Al27	<0.00	<0.00	<0.00	<0.00	<0.00	<0.00	<0.00	<0.00	<0.00	<0.00	<0.00	<0.00	<0.00	<0.00	<0.00	<0.00	<0.00	<0.00	<0.00
Si29	<0.00	<0.00	<0.00	<0.00	<0.00	<0.00	<0.00	<0.00	<0.00	<0.00	<0.00	<0.00	<0.00	<0.00	<0.00	<0.00	<0.00	<0.00	<0.00
S34	15.3	15.7	1829.03	8810.34	8815.15	16911.88	16907.32	16906.96	16905.03	16904.17	16907.91	16913.54	16905.04	16909.06	16904.34	12.89	13.12	8815.95	8811
Ca43	<0.00	<0.00	<0.00	<0.00	<0.00	<0.00	<0.00	<0.00	<0.00	<0.00	<0.00	<0.00	<0.00	<0.00	<0.00	<0.00	<0.00	<0.00	<0.00
Sc45	<0.00	<0.00	<0.00	<0.00	<0.00	<0.00	<0.00	<0.00	<0.00	<0.00	<0.00	<0.00	<0.00	<0.00	<0.00	<0.00	<0.00	<0.00	<0.00
Ti49	<0.00	<0.00	<0.00	<0.00	<0.00	<0.00	<0.00	<0.00	<0.00	<0.00	<0.00	<0.00	<0.00	<0.00	<0.00	<0.00	<0.00	<0.00	<0.00
V51	<0.00	<0.00	<0.00	<0.00	<0.00	<0.00	<0.00	<0.00	<0.00	<0.00	<0.00	<0.00	<0.00	<0.00	<0.00	<0.00	<0.00	<0.00	<0.00
Cr53	<0.00	<0.00	<0.00	<0.00	<0.00	<0.00	<0.00	<0.00	<0.00	<0.00	<0.00	<0.00	<0.00	<0.00	<0.00	<0.00	<0.00	<0.00	<0.00
Mn55	<0.00	<0.00	<0.00	<0.00	<0.00	<0.00	<0.00	<0.00	<0.00	<0.00	<0.00	<0.00	<0.00	<0.00	<0.00	<0.00	<0.00	<0.00	<0.00
Fe57	<0.00	<0.00	<0.00	<0.00	<0.00	<0.00	<0.00	<0.00	<0.00	<0.00	<0.00	<0.00	<0.00	<0.00	<0.00	<0.00	<0.00	<0.00	<0.00
Co59	<0.00	<0.00	<0.00	<0.00	<0.00	<0.00	<0.00	<0.00	<0.00	<0.00	<0.00	<0.00	<0.00	<0.00	<0.00	<0.00	<0.00	<0.00	<0.00
Ni60	0.8	0.84	3.82	46145.22	46545.49	28.27	0.26	63.91	0.12	0.11	0.21	2.42	0.17	0.058	1.4	0.34	0.29	40789.86	42560.63
Ni62	0.84	0.86	5.95	46928.9	47384.21	28.04	0.3	63.14	0.14	0.16	0.54	2.45	0.28	0.7	1.17	0.34	0.3	41538.17	42955.36
Cu65	0.51	0.53	3.71	18.37	18.13	2.37	0.26	2.23	0.48	26.36	1.65	0.15	1.03	1.33	1113.08	0.22	0.19	15.68	16.59
Zn66	<0.00	<0.00	<0.00	<0.00	<0.00	<0.00	<0.00	<0.00	<0.00	<0.00	<0.00	<0.00	<0.00	<0.00	<0.00	<0.00	<0.00	<0.00	<0.00
Ga71	<0.00	<0.00	<0.00	<0.00	<0.00	<0.00	<0.00	<0.00	<0.00	<0.00	<0.00	<0.00	<0.00	<0.00	<0.00	<0.00	<0.00	<0.00	<0.00
As75	0.54	0.58	10.99	9.52	9.79	146.16	128.33	19.19	9.44	137.88	12.24	10.58	485.19	18.33	65.54	0.22	0.19	8.75	8.82
Se82	0.37	0.4	14.92	19.35	19.41	1.91	0.72	8.07	1.47	2.18	8.96	2.18	1.3	1.13	15	0.14	0.13	17.64	16.98
Y89	<0.00	<0.00	<0.00	<0.00	<0.00	<0.00	<0.00	<0.00	<0.00	<0.00	<0.00	<0.00	<0.00	<0.00	<0.00	<0.00	<0.00	<0.00	<0.00
Zr90	<0.00	<0.00	<0.00	<0.00	<0.00	<0.00	<0.00	<0.00	<0.00	<0.00	<0.00	<0.00	<0.00	<0.00	<0.00	<0.00	<0.00	<0.00	<0.00
Nb93	<0.00	<0.00	<0.00	<0.00	<0.00	<0.00	<0.00	<0.00	<0.00	<0.00	<0.00	<0.00	<0.00	<0.00	<0.00	<0.00	<0.00	<0.00	<0.00
Mo95	<0.00	<0.00	<0.00	<0.00	<0.00	<0.00	<0.00	<0.00	<0.00	<0.00	<0.00	<0.00	<0.00	<0.00	<0.00	<0.00	<0.00	<0.00	<0.00
Ru99	0.0028	0.0031	0.35	13.23	13.49	0.023	0.011	0.015	0.013	0.038	0.019	0.021	0.0083	0.018	0.012	0.0011	0.001	12.03	12.32
Ru101	0.0015	0.0013	0.23	11.75	11.77	0.013	0.0061	0.01	0.0053	0.0041	0.013	0.015	0.0049	0.0091	0.0058	0.00046	0.00068	10.74	11.05
Rh103	0.0032	0.0037	0.096	13.77	13.97	0.011	0.0042	0.0057	0.0036	0.0057	0.018	0.0073	0.0035	0.0049	0.13	0.0013	0.0012	12.48	12.83
Ag107	<0.00	<0.00	<0.00	<0.00	<0.00	<0.00	<0.00	<0.00	<0.00	<0.00	<0.00	<0.00	<0.00	<0.00	<0.00	<0.00	<0.00	<0.00	<0.00
Pd108	0.0075	0.0084	0.15	12.34	12.84	0.014	0.007	0.0082	0.0045	0.017	0.023	0.013	0.0041	0.0076	0.0076	0.0026	0.0024	11.5	12.11
Cd111	<0.00	<0.00	<0.00	<0.00	<0.00	<0.00	<0.00	<0.00	<0.00	<0.00	<0.00	<0.00	<0.00	<0.00	<0.00	<0.00	<0.00	<0.00	<0.00
In115	<0.00	<0.00	<0.00	<0.00	<0.00	<0.00	<0.00	<0.00	<0.00	<0.00	<0.00	<0.00	<0.00	<0.00	<0.00	<0.00	<0.00	<0.00	<0.00
Sn118	<0.00	<0.00	<0.00	<0.00	<0.00	<0.00	<0.00	<0.00	<0.00	<0.00	<0.00	<0.00	<0.00	<0.00	<0.00	<0.00	<0.00	<0.00	<0.00
Sb121	<0.00	<0.00	<0.00	<0.00	<0.00	<0.00	<0.00	<0.00	<0.00	<0.00	<0.00	<0.00	<0.00	<0.00	<0.00	<0.00	<0.00	<0.00	<0.00
Te125	0.56	0.61	1.37	19.09	18.09	1.08	0.74	0.33	0.48	1.25	2.06	0.3	2.86	0.9	22.02	0.23	0.2	15.97	17.72
Te128	0.54	0.58	1.71	17.74	17.08	0.96	0.69	0.25	0.4	1.2	1.95	0.24	2.73	0.71	20.75	0.22	0.19	15.08	16.07
La139	<0.00	<0.00	<0.00	<0.00	<0.00	<0.00	<0.00	<0.00	<0.00	<0.00	<0.00	<0.00	<0.00	<0.00	<0.00	<0.00	<0.00	<0.00	<0.00
Ce140	<0.00	<0.00	<0.00	<0.00	<0.00	<0.00	<0.00	<0.00	<0.00	<0.00	<0.00	<0.00	<0.00	<0.00	<0.00	<0.00	<0.00	<0.00	<0.00
Nd146	<0.00	<0.00	<0.00	<0.00	<0.00	<0.00	<0.00	<0.00	<0.00	<0.00	<0.00	<0.00	<0.00	<0.00	<0.00	<0.00	<0.00	<0.00	<0.00
Hf178	<0.00	<0.00	<0.00	<0.00	<0.00	<0.00	<0.00	<0.00	<0.00	<0.00	<0.00	<0.00	<0.00	<0.00	<0.00	<0.00	<0.00	<0.00	<0.00
W182	<0.00	<0.00	<0.00	<0.00	<0.00	<0.00	<0.00	<0.00	<0.00	<0.00	<0.00	<0.00	<0.00	<0.00	<0.00	<0.00	<0.00	<0.00	<0.00
Re185	<0.00	<0.00	<0.00	<0.00	<0.00	<0.00	<0.00	<0.00	<0.00	<0.00	<0.00	<0.00	<0.00	<0.00	<0.00	<0.00	<0.00	<0.00	<0.00
Re187	<0.00	<0.00	<0.00	<0.00	<0.00	<0.00	<0.00	<0.00	<0.00	<0.00	<0.00	<0.00	<0.00	<0.00	<0.00	<0.00	<0.00	<0.00	<0.00

Element	STD610-1	STD610-2	BCR2G-1	PGEA-1	PGEA-2	JL01-PY	BG31-CPY	JL01-PY1	BG32-PY	BG32-PY2	KP04-PY	JL03-PY	JL02-PY	JL07-PY	BG01-PY	STD610-3	STD610-4	PGEA-3	PGEA-4
Os189	0.0037	0.0029	0.45	34.38	27.73	0.024	0.015	0.017	0.012	0.0072	0.024	0.033	0.014	0.018	0.012	0.0012	0.00096	23.11	29.15
Os190	0.002	0.0022	0.18	35.46	28.07	0.016	0.0099	0.011	0.0069	0.0053	0.013	0.021	0.0055	0.013	0.0052	0.00061	0.00067	23.58	29.09
Ir193	0.00031	0.00042	0.057	10.24	9.69	0.0039	0.0016	0.0024	0.0017	0.00066	0.0034	0.0042	0.001	0.0014	0.0012	0.00015	0.00016	8.26	8.9
Pt195	0.0086	0.0099	0.17	17.65	17.67	0.013	0.0089	0.01	0.007	0.005	0.011	0.016	0.0064	0.0084	0.0039	0.0033	0.0033	14.93	15.55
Au197	0.043	0.045	0.15	20.98	21.08	0.12	0.0097	0.038	0.007	0.24	0.0092	0.02	2.23	0.013	1.8	0.017	0.014	17.7	18.31
Pb208	<0.00	<0.00	<0.00	<0.00	<0.00	<0.00	<0.00	<0.00	<0.00	<0.00	<0.00	<0.00	<0.00	<0.00	<0.00	<0.00	<0.00	<0.00	<0.00
Bi209	0.95	1	0.46	25.35	24.5	43.2	0.59	0.23	2.76	65.14	0.98	1.35	0.12	8.51	54899.78	0.36	0.3	20.18	21.59
Th232	<0.00	<0.00	<0.00	<0.00	<0.00	<0.00	<0.00	<0.00	<0.00	<0.00	<0.00	<0.00	<0.00	<0.00	<0.00	<0.00	<0.00	<0.00	<0.00
U238	<0.00	<0.00	<0.00	<0.00	<0.00	<0.00	<0.00	<0.00	<0.00	<0.00	<0.00	<0.00	<0.00	<0.00	<0.00	<0.00	<0.00	<0.00	<0.00
ThO248	<0.00	<0.00	<0.00	<0.00	<0.00	<0.00	<0.00	<0.00	<0.00	<0.00	<0.00	<0.00	<0.00	<0.00	<0.00	<0.00	<0.00	<0.00	<0.00
GLITTER!: Minimum detection limits (99% confidence).																			
Element	STD610-1	STD610-2	BCR2G-1	PGEA-1	PGEA-2	JL01-PY	BG31-CPY	JL01-PY1	BG32-PY	BG32-PY2	KP04-PY	JL03-PY	JL02-PY	JL07-PY	BG01-PY	STD610-3	STD610-4	PGEA-3	PGEA-4
Al27	<0.00	<0.00	<0.00	<0.00	<0.00	<0.00	<0.00	<0.00	<0.00	<0.00	<0.00	<0.00	<0.00	<0.00	<0.00	<0.00	<0.00	<0.00	<0.00
Si29	<0.00000	<0.00000	<0.00000	<0.00000	<0.00000	<0.00000	<0.00000	<0.00000	<0.00000	<0.00000	<0.00000	<0.00000	<0.00000	<0.00000	<0.00000	<0.00000	<0.00000	<0.00000	<0.00000
S34	13.91	14.2	1739.2	424.38	534.27	114.57	75.28	113.04	68.43	52.93	146.28	178.09	78.89	93.74	54.89	4.96	5.65	540.69	480.62
Ca43	<0.00	<0.00	<0.00	<0.00	<0.00	<0.00	<0.00	<0.00	<0.00	<0.00	<0.00	<0.00	<0.00	<0.00	<0.00	<0.00	<0.00	<0.00	<0.00
Sc45	<0.00	<0.00	<0.00	<0.00	<0.00	<0.00	<0.00	<0.00	<0.00	<0.00	<0.00	<0.00	<0.00	<0.00	<0.00	<0.00	<0.00	<0.00	<0.00
Ti49	<0.00000	<0.00000	<0.00000	<0.00000	<0.00000	<0.00000	<0.00000	<0.00000	<0.00000	<0.00000	<0.00000	<0.00000	<0.00000	<0.00000	<0.00000	<0.00000	<0.00000	<0.00000	<0.00000
V51	<0.00	<0.00	<0.00	<0.00	<0.00	<0.00	<0.00	<0.00	<0.00	<0.00	<0.00	<0.00	<0.00	<0.00	<0.00	<0.00	<0.00	<0.00	<0.00
Cr53	<0.00	<0.00	<0.00	<0.00	<0.00	<0.00	<0.00	<0.00	<0.00	<0.00	<0.00	<0.00	<0.00	<0.00	<0.00	<0.00	<0.00	<0.00	<0.00
Mn55	<0.00	<0.00	<0.00	<0.00	<0.00	<0.00	<0.00	<0.00	<0.00	<0.00	<0.00	<0.00	<0.00	<0.00	<0.00	<0.00	<0.00	<0.00	<0.00
Fe57	<0.00000	<0.00000	<0.00000	<0.00000	<0.00000	<0.00000	<0.00000	<0.00000	<0.00000	<0.00000	<0.00000	<0.00000	<0.00000	<0.00000	<0.00000	<0.00000	<0.00000	<0.00000	<0.00000
Co59	<0.00000	<0.00000	<0.00000	<0.00000	<0.00000	<0.00000	<0.00000	<0.00000	<0.00000	<0.00000	<0.00000	<0.00000	<0.00000	<0.00000	<0.00000	<0.00000	<0.00000	<0.00000	<0.00000
Ni60	0.0103	0.012	1.53	0.288	5.02	0.131	0.0562	0.0837	0.0539	0.0277	0.0906	0.109	0.053	0.067	0.0319	0.00378	0.00593	0.419	4.77
Ni62	0.0449	0.0544	6.63	1.41	13.6	0.452	0.199	0.288	0.205	0.155	0.335	0.508	0.126	0.239	0.172	0.0154	0.0259	1.48	12.85
Cu65	0.0136	0.0128	1.66	0.387	0.447	0.103	0.0646	0.0903	0.0536	0.0351	0.112	0.11	0.0443	0.0684	0.0432	0.00364	0.00383	0.416	0.359
Zn66	<0.00000	<0.00000	<0.00000	<0.00000	<0.00000	<0.00000	<0.00000	<0.00000	<0.00000	<0.00000	<0.00000	<0.00000	<0.00000	<0.00000	<0.00000	<0.00000	<0.00000	<0.00000	<0.00000
Ga71	<0.00	<0.00	<0.00	<0.00	<0.00	<0.00	<0.00	<0.00	<0.00	<0.00	<0.00	<0.00	<0.00	<0.00	<0.00	<0.00	<0.00	<0.00	<0.00
As75	0.226	0.219	27.23	6.36	7.77	1.68	1.03	1.5	0.911	0.566	1.66	1.95	0.877	1.33	0.81	0.0779	0.0868	9.05	7.79
Se82	0.313	0.316	39.23	9.61	11.88	2.61	1.66	2.37	1.42	0.86	2.33	2.96	1.24	1.75	1.01	0.0975	0.113	11.29	9.63
Y89	<0.00	<0.00	<0.00	<0.00	<0.00	<0.00	<0.00	<0.00	<0.00	<0.00	<0.00	<0.00	<0.00	<0.00	<0.00	<0.00	<0.00	<0.00	<0.00
Zr90	<0.00	<0.00	<0.00	<0.00	<0.00	<0.00	<0.00	<0.00	<0.00	<0.00	<0.00	<0.00	<0.00	<0.00	<0.00	<0.00	<0.00	<0.00	<0.00
Nb93	<0.00	<0.00	<0.00	<0.00	<0.00	<0.00	<0.00	<0.00	<0.00	<0.00	<0.00	<0.00	<0.00	<0.00	<0.00	<0.00	<0.00	<0.00	<0.00
Mo95	<0.00	<0.00	<0.00	<0.00	<0.00	<0.00	<0.00	<0.00	<0.00	<0.00	<0.00	<0.00	<0.00	<0.00	<0.00	<0.00	<0.00	<0.00	<0.00
Ru99	0.00502	0.00675	0.841	0.218	0.252	0.0598	0.0222	0.0321	0.0293	0.0103	0.0479	0.0337	0.0141	0.0388	0.014	0.00239	0.00217	0.235	0.192
Ru101	0.00399	0.00314	0.646	0.102	<0.00000	0.0227	0.0158	0.0264	0.012	0.0103	0.0311	0.0415	0.0122	0.0147	0.0115	0.00098	0.00189	0.0963	0.167
Rh103	0.00203	0.00159	0.255	0.0567	0.0736	0.0191	0.00955	0.0125	0.00968	0.00589	0.0156	0.0174	0.0083	0.0101	0.00747	0.00065	0.00061	0.0725	0.081
Ag107	<0.00000	<0.00000	<0.00000	<0.00000	<0.00000	<0.00000	<0.00000	<0.00000	<0.00000	<0.00000	<0.00000	<0.00000	<0.00000	<0.00000	<0.00000	<0.00000	<0.00000	<0.00000	<0.00000
Pd108	0.00297	0.00198	0.376	0.0639	0.145	0.0303	0.0162	0.0185	0.00925	0.0065	0.0151	0.0301	0.00888	0.016	0.00953	0.00079	0.00112	0.0741	0.111
Cd111	<0.00000	<0.00000	<0.00000	<0.00000	<0.00000	<0.00000	<0.00000	<0.00000	<0.00000	<0.00000	<0.00000	<0.00000	<0.00000	<0.00000	<0.00000	<0.00000	<0.00000	<0.00000	<0.00000
In115	<0.00	<0.00	<0.00	<0.00	<0.00	<0.00	<0.00	<0.00	<0.00	<0.00	<0.00	<0.00	<0.00	<0.00	<0.00	<0.00	<0.00	<0.00	<0.00
Sn118	<0.00000	<0.00000	<0.00000	<0.00000	<0.00000	<0.00000	<0.00000	<0.00000	<0.00000	<0.00000	<0.00000	<0.00000	<0.00000	<0.00000	<0.00000	<0.00000	<0.00000	<0.00000	<0.00000
Sb121	<0.00000	<0.00000	<0.00000	<0.00000	<0.00000	<0.00000	<0.00000	<0.00000	<0.00000	<0.00000	<0.00000	<0.00000	<0.00000	<0.00000	<0.00000	<0.00000	<0.00000	<0.00000	<0.00000
Te125	0.0272	0.0214	3.11	0.693	0.705	0.173	0.132	<0.00000	0.0819	0.0827	0.177	0.245	0.108	0.0502	0.0781	0.00668	0.00804	0.869	0.659
Te128	0.0374	0.0388	4.55	1.15	1.36	0.311	0.188	0.27	0.163	0.0976	0.28	0.31	0.152	0.191	0.118	0.0114	0.0128	1.34	1.14
La139	<0.00	<0.00	<0.00	<0.00	<0.00	<0.00	<0.00	<0.00	<0.00	<0.00	<0.00	<0.00	<0.00	<0.00	<0.00	<0.00	<0.00	<0.00	<0.00
Ce140	<0.00	<0.00	<0.00	<0.00	<0.00	<0.00	<0.00	<0.00	<0.00	<0.00	<0.00	<0.00	<0.00	<0.00	<0.00	<0.00	<0.00	<0.00	<0.00
Nd146	<0.00	<0.00	<0.00	<0.00	<0.00	<0.00	<0.00	<0.00	<0.00	<0.00	<0.00	<0.00	<0.00	<0.00	<0.00	<0.00	<0.00	<0.00	<0.00
Hf178	<0.00	<0.00	<0.00	<0.00	<0.00	<0.00	<0.00	<0.00	<0.00	<0.00	<0.00	<0.00	<0.00	<0.00	<0.00	<0.00	<0.00	<0.00	<0.00
W182	<0.00000	<0.00000	<0.00000	<0.00000	<0.00000	<0.00000	<0.00000	<0.00000	<0.00000	<0.00000	<0.00000	<0.00000	<0.00000	<0.00000	<0.00000	<0.00000	<0.00000	<0.00000	<0.00000

Element	STD610-1	STD610-2	BCR2G-1	PGEA-1	PGEA-2	JL01-PY	BG31-CPY	JL01-PY1	BG32-PY	BG32-PY2	KP04-PY	JL03-PY	JL02-PY	JL07-PY	BG01-PY	STD610-3	STD610-4	PGEA-3	PGEA-4
Re185	<0.00	<0.00	<0.00	<0.00	<0.00	<0.00	<0.00	<0.00	<0.00	<0.00	<0.00	<0.00	<0.00	<0.00	<0.00	<0.00	<0.00	<0.00	<0.00
Re187	<0.00000	<0.00000	<0.00000	<0.00000	<0.00000	<0.00000	<0.00000	<0.00000	<0.00000	<0.00000	<0.00000	<0.00000	<0.00000	<0.00000	<0.00000	<0.00000	<0.00000	<0.00000	<0.00000
Os189	0.0102	0.00463	1.24	0.299	0.264	0.0502	0.0329	0.0412	0.0306	0.0186	0.0501	0.0748	0.0382	0.0497	0.031	0.00322	0.00197	0.213	0.201
Os190	0.005	0.00333	0.448	0.164	0.219	0.034	0.0193	0.0279	0.0156	0.0134	0.0329	0.0254	0.015	0.0292	0.0121	0.00169	0.00094	0.191	0.145
Ir193	<0.00000	0.00097	0.142	0.0313	0.0389	0.00856	0.00217	0.00445	0.00452	0.00123	0.00993	0.00808	0.00238	0.00248	0.00334	0.00033	0.00034	0.0397	0.0399
Pt195	0.00417	0.0015	0.494	0.128	0.135	0.0325	0.025	0.0267	0.0186	0.0142	0.0281	0.0313	0.0143	0.0172	0.00946	0.00093	0.00138	0.138	0.138
Au197	0.00325	0.00322	0.362	0.0698	0.123	0.0156	0.0125	0.0148	0.00825	0.00502	0.0135	0.019	0.00886	0.0143	0.00718	0.00063	0.00035	0.0764	0.0663
Pb208	<0.00000	<0.00000	<0.00000	<0.00000	<0.00000	<0.00000	<0.00000	<0.00000	<0.00000	<0.00000	<0.00000	<0.00000	<0.00000	<0.00000	<0.00000	<0.00000	<0.00000	<0.00000	<0.00000
Bi209	0.00284	0.00364	0.375	0.086	0.126	0.0253	0.0145	0.0221	0.0118	0.00813	0.0221	0.0226	0.0102	0.0151	0.0091	0.00309	0.00258	0.219	0.185
Th232	<0.00000	<0.00000	<0.00000	<0.00000	<0.00000	<0.00000	<0.00000	<0.00000	<0.00000	<0.00000	<0.00000	<0.00000	<0.00000	<0.00000	<0.00000	<0.00000	<0.00000	<0.00000	<0.00000
U238	<0.00	<0.00	<0.00	<0.00	<0.00	<0.00	<0.00	<0.00	<0.00	<0.00	<0.00	<0.00	<0.00	<0.00	<0.00	<0.00	<0.00	<0.00	<0.00
ThO248	<0.00	<0.00	<0.00	<0.00	<0.00	<0.00	<0.00	<0.00	<0.00	<0.00	<0.00	<0.00	<0.00	<0.00	<0.00	<0.00	<0.00	<0.00	<0.00
GLITTER!: Trace element concentrations normalised to chondrite.																			
Element	STD610-1	STD610-2	BCR2G-1	PGEA-1	PGEA-2	JL01-PY	BG31-CPY	JL01-PY1	BG32-PY	BG32-PY2	KP04-PY	JL03-PY	JL02-PY	JL07-PY	BG01-PY	STD610-3	STD610-4	PGEA-3	PGEA-4
Al27	<****	<****	<****	<****	<****	<****	<****	<****	<****	<****	<****	<****	<****	<****	<****	<****	<****	<****	<****
Si29	0	0	0	0	0	0	0	0	0	0	0	0	0	0	0	0	0	0	0
S34	Inf	Inf	Inf	Inf	Inf	Inf	Inf	Inf	Inf	Inf	Inf	Inf	Inf	Inf	Inf	Inf	Inf	Inf	Inf
Ca43	<****	<****	<****	<****	<****	<****	<****	<****	<****	<****	<****	<****	<****	<****	<****	<****	<****	<****	<****
Sc45	<****	<****	<****	<****	<****	<****	<****	<****	<****	<****	<****	<****	<****	<****	<****	<****	<****	<****	<****
Ti49	0	0	0	0	0	0	0	0	0	0	0	0	0	0	0	0	0	0	0
V51	<****	<****	<****	<****	<****	<****	<****	<****	<****	<****	<****	<****	<****	<****	<****	<****	<****	<****	<****
Cr53	<****	<****	<****	<****	<****	<****	<****	<****	<****	<****	<****	<****	<****	<****	<****	<****	<****	<****	<****
Mn55	<****	<****	<****	<****	<****	<****	<****	<****	<****	<****	<****	<****	<****	<****	<****	<****	<****	<****	<****
Fe57	0	0	0	0	0	0	0	0	0	0	0	0	0	0	0	0	0	0	0
Co59	0	0	0	0	0	0	0	0	0	0	0	0	0	0	0	0	0	0	0
Ni60	0.00077	0.0008	0.00334	45.79	46.19	0.028	0.00024	0.0634	0.00011	0.0001	0.00019	0.00235	0.00016	0.00003	0.00138	0.00033	0.00028	40.47	42.23
Ni62	0.00077	0.00079	0.00349	45.89	46.33	0.0271	0.00017	0.0616	0.00006	0.00009	0.00037	0.00208	0.0002	0.00051	0.00108	0.00033	0.00028	40.61	42
Cu65	0.042	0.0435	0.289	1.55	1.53	0.199	0.0205	0.188	0.0397	2.23	0.1385	0.01028	0.0867	0.1116	94.35	0.0188	0.0156	1.324	1.403
Zn66	0	0	0	0	0	0	0	0	0	0	0	0	0	0	0	0	0	0	0
Ga71	<****	<****	<****	<****	<****	<****	<****	<****	<****	<****	<****	<****	<****	<****	<****	<****	<****	<****	<****
As75	2.73	2.93	0	48.96	49.62	783.11	687.71	102.68	50.52	739.01	65.38	56.24	2600.59	98.03	351.22	1.181	0.987	42.61	44.17
Se82	0.166	0.176	0	9.6	9.49	0.664	0	4.08	0.666	1.087	4.53	0.751	0.583	0.336	7.73	0.0666	0.0607	8.56	8.34
Y89	<****	<****	<****	<****	<****	<****	<****	<****	<****	<****	<****	<****	<****	<****	<****	<****	<****	<****	<****
Zr90	<****	<****	<****	<****	<****	<****	<****	<****	<****	<****	<****	<****	<****	<****	<****	<****	<****	<****	<****
Nb93	<****	<****	<****	<****	<****	<****	<****	<****	<****	<****	<****	<****	<****	<****	<****	<****	<****	<****	<****
Mo95	<****	<****	<****	<****	<****	<****	<****	<****	<****	<****	<****	<****	<****	<****	<****	<****	<****	<****	<****
Ru99	0.0061	0	0	222.78	226.75	0	0	0	0	0.453	0	0	0.0169	0	0.058	0.0023	0	201.97	207.31
Ru101	0	0	0	222.37	222.54	0	0	0	0	0	0	0	0	0	0.0116	0	0	202.73	209.14
Rh103	0.22	0.25	0	1262.11	1279.4	0.193	0	0.088	0	0.342	1.13	0	0	0	11.45	0.1023	0.0878	1143.47	1175.27
Ag107	0	0	0	0	0	0	0	0	0	0	0	0	0	0	0	0	0	0	0
Pd108	0.1298	0.142	0	312.74	325.25	0	0	0	0	0.279	0.254	0	0	0	0.0647	0.0502	0.039	291.15	306.99
Cd111	0	0	0	0	0	0	0	0	0	0	0	0	0	0	0	0	0	0	0
In115	<****	<****	<****	<****	<****	<****	<****	<****	<****	<****	<****	<****	<****	<****	<****	<****	<****	<****	<****
Sn118	0	0	0	0	0	0	0	0	0	0	0	0	0	0	0	0	0	0	0
Sb121	0	0	0	0	0	0	0	0	0	0	0	0	0	0	0	0	0	0	0
Te125	2.18	2.34	0	76.3	72	3.73	2.68	1.045	1.76	4.92	7.97	0.616	11.4	3.19	89.2	0.929	0.788	63.35	70.76
Te128	2.23	2.39	0	76.14	73.21	3.92	2.87	0.898	1.64	5.14	8.27	0.664	11.7	2.9	89.36	0.928	0.806	64.58	68.95
La139	<****	<****	<****	<****	<****	<****	<****	<****	<****	<****	<****	<****	<****	<****	<****	<****	<****	<****	<****
Ce140	<****	<****	<****	<****	<****	<****	<****	<****	<****	<****	<****	<****	<****	<****	<****	<****	<****	<****	<****
Nd146	<****	<****	<****	<****	<****	<****	<****	<****	<****	<****	<****	<****	<****	<****	<****	<****	<****	<****	<****

PGEARUN4_2

Element	STD610-1	STD610-2	BCR2G-1	PGEA-1	PGEA-2	JL01-PY	BG31-CPY	JL01-PY1	BG32-PY	BG32-PY2	KP04-PY	JL03-PY	JL02-PY	JL07-PY	BG01-PY	STD610-3	STD610-4	PGEA-3	PGEA-4
Hf178	<****	<****	<****	<****	<****	<****	<****	<****	<****	<****	<****	<****	<****	<****	<****	<****	<****	<****	<****
W182	0	0	0	0	0	0	0	0	0	0	0	0	0	0	0	0	0	0	0
Re185	<****	<****	<****	<****	<****	<****	<****	<****	<****	<****	<****	<****	<****	<****	<****	<****	<****	<****	<****
Re187	0	0	0	0	0	0	0	0	0	0	0	0	0	0	0	0	0	0	0
Os189	0	0.0045	0	226.78	182.79	0	0	0	0	0	0	0	0	0	0	0	0	152.26	192.2
Os190	0	0.0045	0	230.72	182.59	0	0	0	0	0	0	0.041	0	0	0	0	0.00147	153.33	189.29
Ir193	0.0014	0	0	167.2	158.24	0	0.0034	0.0069	0	0	0	0	0	0	0	0	0	134.84	145.3
Pt195	0.0579	0.0668	0	155.08	155.12	0	0	0	0	0	0	0	0	0	0	0.0247	0.0226	130.99	136.53
Au197	2.3	2.37	0	1167.13	1172.25	6.09	0.219	1.81	0.206	13.03	0.182	0.483	123.74	0.331	100.17	0.957	0.778	984.02	1018.76
Pb208	0	0	0	0	0	0	0	0	0	0	0	0	0	0	0	0	0	0	0
Bi209	58.19	61.54	24.44	1582.48	1529.36	2698.13	36.47	14.39	172.13	4068.65	61.16	83.77	7.63	531.57	3429124	22.33	18.86	1259.22	1347.78
Th232	0	0	0	0	0	0	0	0	0	0	0	0	0	0	0	0	0	0	0
U238	<****	<****	<****	<****	<****	<****	<****	<****	<****	<****	<****	<****	<****	<****	<****	<****	<****	<****	<****
ThO248	<****	<****	<****	<****	<****	<****	<****	<****	<****	<****	<****	<****	<****	<****	<****	<****	<****	<****	<****

GLITTER4.0: Laser Ablation Analysis Results

G:\KYLIE\MAR13\PGEARUN5
Fri Mar 14 21:09:45 2003

All values are reported in ppm

GLITTER!: Trace Element Concentrations MDL filtered.	Run5-1	Run5-2	Run5-3	Run5-4	Run5-5	Run5-6	Run5-7	Run5-8	Discarded Run5-9	Run5-10	Run5-11	Run5-12	Run5-13	Run5-14	Run5-15	Run5-16	Run5-17	Run5-18	Run5-19
Element	STD610-3	STD610-4	PGEA-3	PGEA-4	BCR2G-1	BG01-CPY	BG01-PY2	BG13-PY	BG13-SPH	BG13-SP2	JL04-PY	JL04-CPY	BG33-SPH	BG33-PY	BG19-PY	BG05-PY1	BG05-SP2	BG14-CPY	KP10-PY
Al27	<-NaN	<-NaN	<-NaN	<-NaN	<-NaN	<-NaN	<-NaN	<-NaN	<-NaN	<-NaN	<-NaN	<-NaN	<-NaN	<-NaN	<-NaN	<-NaN	<-NaN	<-NaN	<-NaN
Si29	<-NaN	<-NaN	<-NaN	<-NaN	<-NaN	<-NaN	<-NaN	<-NaN	<-NaN	<-NaN	<-NaN	<-NaN	<-NaN	<-NaN	<-NaN	<-NaN	<-NaN	<-NaN	<-NaN
S34	388.87	388.87	278000	278000	47632.28	349436.84	349436.84	534495.56	334773.56	334773.56	534495.56	349436.84	331971.69	534495.56	534495.56	534495.56	349436.84	349436.88	534495.56
Ca43	<-NaN	<-NaN	<-NaN	<-NaN	<-NaN	<-NaN	<-NaN	<-NaN	<-NaN	<-NaN	<-NaN	<-NaN	<-NaN	<-NaN	<-NaN	<-NaN	<-NaN	<-NaN	<-NaN
Sc45	<-NaN	<-NaN	<-NaN	<-NaN	<-NaN	<-NaN	<-NaN	<-NaN	<-NaN	<-NaN	<-NaN	<-NaN	<-NaN	<-NaN	<-NaN	<-NaN	<-NaN	<-NaN	<-NaN
Ti49	<0.00	<0.00	<0.00	<0.00	<0.00	<0.00	<0.00	<0.00	<0.00	<0.00	<0.00	<0.00	<0.00	<0.00	<0.00	<0.00	<0.00	<0.00	<0.00
V51	<0.00	<0.00	<0.00	<0.00	<0.00	<0.00	<0.00	<0.00	<0.00	<0.00	<0.00	<0.00	<0.00	<0.00	<0.00	<0.00	<0.00	<0.00	<0.00
Cr53	<0.00	<0.00	<0.00	<0.00	<0.00	<0.00	<0.00	<0.00	<0.00	<0.00	<0.00	<0.00	<0.00	<0.00	<0.00	<0.00	<0.00	<0.00	<0.00
Mn55	<-NaN	<-NaN	<-NaN	<-NaN	<-NaN	<-NaN	<-NaN	<-NaN	<-NaN	<-NaN	<-NaN	<-NaN	<-NaN	<-NaN	<-NaN	<-NaN	<-NaN	<-NaN	<-NaN
Fe57	<0.00	<0.00	<0.00	<0.00	<0.00	<0.00	<0.00	<0.00	<0.00	<0.00	<0.00	<0.00	<0.00	<0.00	<0.00	<0.00	<0.00	<0.00	<0.00
Co59	<0.00	<0.00	<0.00	<0.00	<0.00	<0.00	<0.00	<0.00	<0.00	<0.00	<0.00	<0.00	<0.00	<0.00	<0.00	<0.00	<0.00	<0.00	<0.00
Ni60	5.6	5.27	693134.94	714791.25	38.86	3.4	3.64	1.87	0.672	0.707	0.912	2.48	0.447	0.08	6.37	17.39	7.69	4.12	5.06
Ni62	5.42	5.28	693531.75	707825.63	39.25	2.13	<1.50	3.82	0.76	<0.59	0.99	0.98	26.58	4.24	5.21	17.02	5.22	4.61	3.56
Cu65	3.21	2.96	232.54	242.28	31.54	232872.59	225361.69	26.85	4.02	85.98	1.77	252367.81	36.37	1757.47	68.96	1.69	226498.09	273345.97	77.44
Zn66	<0.00	<0.00	<0.00	<0.00	<0.00	<0.00	<0.00	<0.00	<0.00	<0.00	<0.00	<0.00	<0.00	<0.00	<0.00	<0.00	<0.00	<0.00	<0.00
Ga71	<-NaN	<-NaN	<-NaN	<-NaN	<-NaN	<-NaN	<-NaN	<-NaN	<-NaN	<-NaN	<-NaN	<-NaN	<-NaN	<-NaN	<-NaN	<-NaN	<-NaN	<-NaN	<-NaN
As75	3.6	3.42	132.41	135.41	<16.72	<3.65	<4.46	665.23	66.6	4.18	561.36	11.61	<1.65	10974	987.92	202.13	50.6	29.8	4574.38
Se82	1.78	1.83	238.9	230	<19.37	5.07	<5.66	7.95	1.39	<4.05	180.33	240.77	<2.02	<1.87	62.2	101.08	65.46	51.43	29.69
Y89	<-NaN	<-NaN	<-NaN	<-NaN	<-NaN	<-NaN	<-NaN	<-NaN	<-NaN	<-NaN	<-NaN	<-NaN	<-NaN	<-NaN	<-NaN	<-NaN	<-NaN	<-NaN	<-NaN
Zr90	<-NaN	<-NaN	<-NaN	<-NaN	<-NaN	<-NaN	<-NaN	<-NaN	<-NaN	<-NaN	<-NaN	<-NaN	<-NaN	<-NaN	<-NaN	<-NaN	<-NaN	<-NaN	<-NaN
Nb93	<0.00	<0.00	<0.00	<0.00	<0.00	<0.00	<0.00	<0.00	<0.00	<0.00	<0.00	<0.00	<0.00	<0.00	<0.00	<0.00	<0.00	<0.00	<0.00
Mo95	<-NaN	<-NaN	<-NaN	<-NaN	<-NaN	<-NaN	<-NaN	<-NaN	<-NaN	<-NaN	<-NaN	<-NaN	<-NaN	<-NaN	<-NaN	<-NaN	<-NaN	<-NaN	<-NaN
Ru99	<0.0024	<0.0022	218.84	222.23	0.349	0.612	0.418	<0.038	<0.026	<0.079	<0.033	0.526	<0.041	<0.033	0.255	<0.050	0.635	0.704	<0.025
Ru101	<0.00098	<0.00193	221.35	223.59	<0.207	0.237	0.206	<0.0158	0.0128	<0.062	<0.030	0.294	<0.0239	<0.0183	<0.0261	<0.031	0.265	0.319	<0.0163
Rh103	0.0204	0.0198	233.82	236.16	<0.132	24.11	24.16	0.0682	<0.0076	0.368	0.113	28.23	<0.0145	0.263	0.0198	<0.0152	24.89	30.52	0.0592
Ag107	<0.00	<0.00	<0.00	<0.00	<0.00	<0.00	<0.00	<0.00	<0.00	<0.00	<0.00	<0.00	<0.00	<0.00	<0.00	<0.00	<0.00	<0.00	<0.00
Pd108	0.0402	0.037	245.2	254.28	<0.210	0.112	0.362	<0.0139	0.525	72.79	<0.024	0.165	84.83	0.03	0.063	<0.0192	0.611	0.505	0.216
Cd111	<0.00	<0.00	<0.00	<0.00	<0.00	<0.00	<0.00	<0.00	<0.00	<0.00	<0.00	<0.00	<0.00	<0.00	<0.00	<0.00	<0.00	<0.00	<0.00
In115	<-NaN	<-NaN	<-NaN	<-NaN	<-NaN	<-NaN	<-NaN	<-NaN	<-NaN	<-NaN	<-NaN	<-NaN	<-NaN	<-NaN	<-NaN	<-NaN	<-NaN	<-NaN	<-NaN
Sn118	<0.00	<0.00	<0.00	<0.00	<0.00	<0.00	<0.00	<0.00	<0.00	<0.00	<0.00	<0.00	<0.00	<0.00	<0.00	<0.00	<0.00	<0.00	<0.00
Sb121	<0.00	<0.00	<0.00	<0.00	<0.00	<0.00	<0.00	<0.00	<0.00	<0.00	<0.00	<0.00	<0.00	<0.00	<0.00	<0.00	<0.00	<0.00	<0.00
Te125	3.26	3.16	226.1	248.17	1.76	<0.43	0.56	1.64	0.418	<0.33	3.9	3.87	0.209	0.175	3.55	17.48	0.53	2.59	42.33
Te128	3.2	3.14	229.65	239.94	<2.22	<0.53	<0.64	1.44	<0.122	1.06	4.01	2.66	<0.238	<0.203	3.68	17.1	0.75	1.84	41.45
La139	<-NaN	<-NaN	<-NaN	<-NaN	<-NaN	<-NaN	<-NaN	<-NaN	<-NaN	<-NaN	<-NaN	<-NaN	<-NaN	<-NaN	<-NaN	<-NaN	<-NaN	<-NaN	<-NaN
Ce140	<-NaN	<-NaN	<-NaN	<-NaN	<-NaN	<-NaN	<-NaN	<-NaN	<-NaN	<-NaN	<-NaN	<-NaN	<-NaN	<-NaN	<-NaN	<-NaN	<-NaN	<-NaN	<-NaN
Nd146	<0.00	<0.00	<0.00	<0.00	<0.00	<0.00	<0.00	<0.00	<0.00	<0.00	<0.00	<0.00	<0.00	<0.00	<0.00	<0.00	<0.00	<0.00	<0.00
Hf178	<-NaN	<-NaN	<-NaN	<-NaN	<-NaN	<-NaN	<-NaN	<-NaN	<-NaN	<-NaN	<-NaN	<-NaN	<-NaN	<-NaN	<-NaN	<-NaN	<-NaN	<-NaN	<-NaN
W182	<-NaN	<-NaN	<-NaN	<-NaN	<-NaN	<-NaN	<-NaN	<-NaN	<-NaN	<-NaN	<-NaN	<-NaN	<-NaN	<-NaN	<-NaN	<-NaN	<-NaN	<-NaN	<-NaN
Re185	<-NaN	<-NaN	<-NaN	<-NaN	<-NaN	<-NaN	<-NaN	<-NaN	<-NaN	<-NaN	<-NaN	<-NaN	<-NaN	<-NaN	<-NaN	<-NaN	<-NaN	<-NaN	<-NaN
Re187	<0.00	<0.00	<0.00	<0.00	<0.00	<0.00	<0.00	<0.00	<0.00	<0.00	<0.00	<0.00	<0.00	<0.00	<0.00	<0.00	<0.00	<0.00	<0.00
Os189	<0.0035	<0.00218	177.11	215.12	<0.70	<0.140	<0.157	<0.058	<0.028	<0.122	<0.070	<0.069	<0.047	<0.051	<0.056	<0.055	<0.059	<0.059	<0.032
Os190	<0.00188	0.00158	180.84	217.17	<0.34	<0.045	<0.086	<0.029	<0.0181	<0.060	<0.028	<0.029	<0.028	<0.028	<0.024	<0.044	<0.035	<0.027	<0.0243
Ir193	<0.00035	<0.00036	102.51	107.9	0.084	<0.0117	<0.0184	<0.0056	0.0022	<0.0168	<0.0076	<0.0095	<0.0099	<0.0075	<0.0065	0.0058	<0.0075	<0.0057	<0.0037
Pt195	0.036	0.0377	198.98	204.05	0.184	<0.052	<0.089	<0.0254	<0.0133	<0.049	<0.0165	<0.0247	<0.0231	<0.0204	<0.028	<0.019	<0.022	<0.030	<0.0154
Au197	0.2184	0.203	231.81	236.96	0.326	0.038	<0.042	0.929	0.486	0.098	0.169	0.306	<0.0189	57.04	0.22	0.069	0.049	0.114	5
Pb208	<0.00	<0.00	<0.00	<0.00	<0.00	<0.00	<0.00	<0.00	<0.00	<0.00	<0.00	<0.00	<0.00	<0.00	<0.00	<0.00	<0.00	<0.00	<0.00
Bi209	3.96	3.88	231.78	242.9	0.48	3.54	2.99	147.9	6.14	2.95	0.696	33.47	0.646	1.45	65.09	21.22	6.02	20.59	25.14
Th232	<-NaN	<-NaN	<-NaN	<-NaN	<-NaN	<-NaN	<-NaN	<-NaN	<-NaN	<-NaN	<-NaN	<-NaN	<-NaN	<-NaN	<-NaN	<-NaN	<-NaN	<-NaN	<-NaN
U238	<-NaN	<-NaN	<-NaN	<-NaN	<-NaN	<-NaN	<-NaN	<-NaN	<-NaN	<-NaN	<-NaN	<-NaN	<-NaN	<-NaN	<-NaN	<-NaN	<-NaN	<-NaN	<-NaN
ThO248	<-NaN	<-NaN	<-NaN	<-NaN	<-NaN	<-NaN	<-NaN	<-NaN	<-NaN	<-NaN	<-NaN	<-NaN	<-NaN	<-NaN	<-NaN	<-NaN	<-NaN	<-NaN	<-NaN

Element	STD610-3	STD610-4	PGEA-3	PGEA-4	BCR2G-1	BG01-CPY	BG01-PY2	BG13-PY	BG13-SPH	BG13-SP2	JL04-PY	JL04-CPY	BG33-SPH	BG33-PY	BG19-PY	BG05-PY1	BG05-SP2	BG14-CPY	KP10-PY
GLITTER!: 1 sigma error.																			
Element	STD610-3	STD610-4	PGEA-3	PGEA-4	BCR2G-1	BG01-CPY	BG01-PY2	BG13-PY	BG13-SPH	BG13-SP2	JL04-PY	JL04-CPY	BG33-SPH	BG33-PY	BG19-PY	BG05-PY1	BG05-SP2	BG14-CPY	KP10-PY
Al27	<0.00	<0.00	<0.00	<0.00	<0.00	<0.00	<0.00	<0.00	<0.00	<0.00	<0.00	<0.00	<0.00	<0.00	<0.00	<0.00	<0.00	<0.00	<0.00
Si29	<0.00	<0.00	<0.00	<0.00	<0.00	<0.00	<0.00	<0.00	<0.00	<0.00	<0.00	<0.00	<0.00	<0.00	<0.00	<0.00	<0.00	<0.00	<0.00
S34	12.79	12.92	8816.84	8813.47	1619.22	11060.58	11065	16905.35	10589.42	10595.75	16908.98	11060.54	10502.16	16905.96	16906.56	16909.79	11059.64	11054.17	16904.81
Ca43	<0.00	<0.00	<0.00	<0.00	<0.00	<0.00	<0.00	<0.00	<0.00	<0.00	<0.00	<0.00	<0.00	<0.00	<0.00	<0.00	<0.00	<0.00	<0.00
Sc45	<0.00	<0.00	<0.00	<0.00	<0.00	<0.00	<0.00	<0.00	<0.00	<0.00	<0.00	<0.00	<0.00	<0.00	<0.00	<0.00	<0.00	<0.00	<0.00
Ti49	<0.00	<0.00	<0.00	<0.00	<0.00	<0.00	<0.00	<0.00	<0.00	<0.00	<0.00	<0.00	<0.00	<0.00	<0.00	<0.00	<0.00	<0.00	<0.00
V51	<0.00	<0.00	<0.00	<0.00	<0.00	<0.00	<0.00	<0.00	<0.00	<0.00	<0.00	<0.00	<0.00	<0.00	<0.00	<0.00	<0.00	<0.00	<0.00
Cr53	<0.00	<0.00	<0.00	<0.00	<0.00	<0.00	<0.00	<0.00	<0.00	<0.00	<0.00	<0.00	<0.00	<0.00	<0.00	<0.00	<0.00	<0.00	<0.00
Mn55	<0.00	<0.00	<0.00	<0.00	<0.00	<0.00	<0.00	<0.00	<0.00	<0.00	<0.00	<0.00	<0.00	<0.00	<0.00	<0.00	<0.00	<0.00	<0.00
Fe57	<0.00	<0.00	<0.00	<0.00	<0.00	<0.00	<0.00	<0.00	<0.00	<0.00	<0.00	<0.00	<0.00	<0.00	<0.00	<0.00	<0.00	<0.00	<0.00
Co59	<0.00	<0.00	<0.00	<0.00	<0.00	<0.00	<0.00	<0.00	<0.00	<0.00	<0.00	<0.00	<0.00	<0.00	<0.00	<0.00	<0.00	<0.00	<0.00
Ni60	0.2	0.19	24017.25	24763.66	1.68	0.19	0.22	0.1	0.043	0.08	0.08	0.15	0.059	0.033	0.25	0.66	0.34	0.17	0.2
Ni62	0.21	0.21	24953.49	25463.85	2.91	0.39	0.66	0.28	0.12	0.26	0.21	0.29	1.16	0.35	0.36	0.94	0.66	0.34	0.24
Cu65	0.13	0.12	9.06	9.42	1.43	8971.5	8683.33	1.05	0.17	3.35	0.1	9722.54	1.42	67.71	2.68	0.1	8725.67	10528.66	2.99
Zn66	<0.00	<0.00	<0.00	<0.00	<0.00	<0.00	<0.00	<0.00	<0.00	<0.00	<0.00	<0.00	<0.00	<0.00	<0.00	<0.00	<0.00	<0.00	<0.00
Ga71	<0.00	<0.00	<0.00	<0.00	<0.00	<0.00	<0.00	<0.00	<0.00	<0.00	<0.00	<0.00	<0.00	<0.00	<0.00	<0.00	<0.00	<0.00	<0.00
As75	0.14	0.13	6.26	6.1	6.35	1.44	1.8	24.27	2.48	1.29	20.53	1.03	0.64	399.85	36.04	7.49	2.15	1.3	166.68
Se82	0.1	0.11	13.2	12.53	7.5	1.84	2.31	0.82	0.46	1.58	9.09	12.16	0.8	0.72	3.29	5.31	3.73	2.76	1.63
Y89	<0.00	<0.00	<0.00	<0.00	<0.00	<0.00	<0.00	<0.00	<0.00	<0.00	<0.00	<0.00	<0.00	<0.00	<0.00	<0.00	<0.00	<0.00	<0.00
Zr90	<0.00	<0.00	<0.00	<0.00	<0.00	<0.00	<0.00	<0.00	<0.00	<0.00	<0.00	<0.00	<0.00	<0.00	<0.00	<0.00	<0.00	<0.00	<0.00
Nb93	<0.00	<0.00	<0.00	<0.00	<0.00	<0.00	<0.00	<0.00	<0.00	<0.00	<0.00	<0.00	<0.00	<0.00	<0.00	<0.00	<0.00	<0.00	<0.00
Mo95	<0.00	<0.00	<0.00	<0.00	<0.00	<0.00	<0.00	<0.00	<0.00	<0.00	<0.00	<0.00	<0.00	<0.00	<0.00	<0.00	<0.00	<0.00	<0.00
Ru99	0.0011	0.001	10.12	10.26	0.098	0.08	0.077	0.013	0.011	0.03	0.018	0.069	0.016	0.013	0.032	0.02	0.073	0.057	0.01
Ru101	0.00044	0.00069	8.91	8.98	0.098	0.042	0.051	0.0074	0.0057	0.022	0.013	0.044	0.0091	0.0087	0.0084	0.012	0.038	0.029	0.0063
Rh103	0.0011	0.0011	10.17	10.27	0.049	1.06	1.06	0.0072	0.0035	0.026	0.012	1.24	0.0057	0.016	0.0061	0.0065	1.09	1.33	0.0054
Ag107	<0.00	<0.00	<0.00	<0.00	<0.00	<0.00	<0.00	<0.00	<0.00	<0.00	<0.00	<0.00	<0.00	<0.00	<0.00	<0.00	<0.00	<0.00	<0.00
Pd108	0.0024	0.0024	10.86	11.25	0.088	0.032	0.049	0.006	0.032	3.23	0.011	0.028	3.74	0.011	0.013	0.008	0.051	0.034	0.017
Cd111	<0.00	<0.00	<0.00	<0.00	<0.00	<0.00	<0.00	<0.00	<0.00	<0.00	<0.00	<0.00	<0.00	<0.00	<0.00	<0.00	<0.00	<0.00	<0.00
In115	<0.00	<0.00	<0.00	<0.00	<0.00	<0.00	<0.00	<0.00	<0.00	<0.00	<0.00	<0.00	<0.00	<0.00	<0.00	<0.00	<0.00	<0.00	<0.00
Sn118	<0.00	<0.00	<0.00	<0.00	<0.00	<0.00	<0.00	<0.00	<0.00	<0.00	<0.00	<0.00	<0.00	<0.00	<0.00	<0.00	<0.00	<0.00	<0.00
Sb121	<0.00	<0.00	<0.00	<0.00	<0.00	<0.00	<0.00	<0.00	<0.00	<0.00	<0.00	<0.00	<0.00	<0.00	<0.00	<0.00	<0.00	<0.00	<0.00
Te125	0.15	0.15	10.77	11.69	0.66	0.18	0.22	0.14	0.075	0.14	0.33	0.37	0.093	0.062	0.27	0.98	0.13	0.21	1.98
Te128	0.13	0.13	9.52	9.91	0.85	0.21	0.26	0.11	0.051	0.21	0.24	0.21	0.091	0.08	0.2	0.76	0.14	0.13	1.71
La139	<0.00	<0.00	<0.00	<0.00	<0.00	<0.00	<0.00	<0.00	<0.00	<0.00	<0.00	<0.00	<0.00	<0.00	<0.00	<0.00	<0.00	<0.00	<0.00
Ce140	<0.00	<0.00	<0.00	<0.00	<0.00	<0.00	<0.00	<0.00	<0.00	<0.00	<0.00	<0.00	<0.00	<0.00	<0.00	<0.00	<0.00	<0.00	<0.00
Nd146	<0.00	<0.00	<0.00	<0.00	<0.00	<0.00	<0.00	<0.00	<0.00	<0.00	<0.00	<0.00	<0.00	<0.00	<0.00	<0.00	<0.00	<0.00	<0.00
Hf178	<0.00	<0.00	<0.00	<0.00	<0.00	<0.00	<0.00	<0.00	<0.00	<0.00	<0.00	<0.00	<0.00	<0.00	<0.00	<0.00	<0.00	<0.00	<0.00
W182	<0.00	<0.00	<0.00	<0.00	<0.00	<0.00	<0.00	<0.00	<0.00	<0.00	<0.00	<0.00	<0.00	<0.00	<0.00	<0.00	<0.00	<0.00	<0.00
Re185	<0.00	<0.00	<0.00	<0.00	<0.00	<0.00	<0.00	<0.00	<0.00	<0.00	<0.00	<0.00	<0.00	<0.00	<0.00	<0.00	<0.00	<0.00	<0.00
Re187	<0.00	<0.00	<0.00	<0.00	<0.00	<0.00	<0.00	<0.00	<0.00	<0.00	<0.00	<0.00	<0.00	<0.00	<0.00	<0.00	<0.00	<0.00	<0.00
Os189	0.0013	0.001	15.3	18.54	0.25	0.047	0.056	0.02	0.011	0.05	0.026	0.026	0.018	0.019	0.021	0.023	0.024	0.023	0.013
Os190	0.00068	0.00065	13.84	16.59	0.13	0.024	0.036	0.011	0.0062	0.022	0.014	0.019	0.012	0.011	0.011	0.017	0.016	0.012	0.0083
Ir193	0.00016	0.00016	3.84	4.03	0.033	0.0046	0.0065	0.0021	0.0011	0.0062	0.0026	0.0035	0.0035	0.0028	0.0025	0.0034	0.0036	0.0023	0.0015
Pt195	0.0022	0.0025	6.92	7.07	0.078	0.021	0.033	0.009	0.0058	0.02	0.0084	0.0099	0.009	0.0071	0.011	0.01	0.012	0.01	0.0066
Au197	0.0077	0.0074	7.42	7.58	0.062	0.01	0.018	0.039	0.024	0.017	0.019	0.028	0.0066	1.82	0.017	0.013	0.012	0.012	0.17
Pb208	<0.00	<0.00	<0.00	<0.00	<0.00	<0.00	<0.00	<0.00	<0.00	<0.00	<0.00	<0.00	<0.00	<0.00	<0.00	<0.00	<0.00	<0.00	<0.00
Bi209	0.14	0.14	8.07	8.45	0.15	0.14	0.13	5.12	0.22	0.12	0.037	1.18	0.031	0.064	2.26	0.75	0.23	0.72	0.87
Th232	<0.00	<0.00	<0.00	<0.00	<0.00	<0.00	<0.00	<0.00	<0.00	<0.00	<0.00	<0.00	<0.00	<0.00	<0.00	<0.00	<0.00	<0.00	<0.00
U238	<0.00	<0.00	<0.00	<0.00	<0.00	<0.00	<0.00	<0.00	<0.00	<0.00	<0.00	<0.00	<0.00	<0.00	<0.00	<0.00	<0.00	<0.00	<0.00
ThO248	<0.00	<0.00	<0.00	<0.00	<0.00	<0.00	<0.00	<0.00	<0.00	<0.00	<0.00	<0.00	<0.00	<0.00	<0.00	<0.00	<0.00	<0.00	<0.00
GLITTER!: Minimum detection limits (99% confidence).																			
Element	STD610-3	STD610-4	PGEA-3	PGEA-4	BCR2G-1	BG01-CPY	BG01-PY2	BG13-PY	BG13-SPH	BG13-SP2	JL04-PY	JL04-CPY	BG33-SPH	BG33-PY	BG19-PY	BG05-PY1	BG05-SP2	BG14-CPY	KP10-PY
Al27	<0.00	<0.00	<0.00	<0.00	<0.00	<0.00	<0.00	<0.00	<0.00	<0.00	<0.00	<0.00	<0.00	<0.00	<0.00	<0.00	<0.00	<0.00	<0.00
Si29	<0.00	<0.00	<0.00	<0.00	<0.00	<0.00	<0.00	<0.00	<0.00	<0.00	<0.00	<0.00	<0.00	<0.00	<0.00	<0.00	<0.00	<0.00	<0.00
S34	4.9	5.7	539.84	493.23	919.1	197.45	279.7	80.71	66.25	289.75	134.68	145.06	115.99	111.05	117.72	128.03	138.86	113.59	62.28
Ca43	<0.00	<0.00	<0.00	<0.00	<0.00	<0.00	<0.00	<0.00	<0.00	<0.00	<0.00	<0.00	<0.00	<0.00	<0.00	<0.00	<0.00	<0.00	<0.00

Element	STD610-3	STD610-4	PGEA-3	PGEA-4	BCR2G-1	BG01-CPY	BG01-PY2	BG13-PY	BG13-SPH	BG13-SP2	JL04-PY	JL04-CPY	BG33-SPH	BG33-PY	BG19-PY	BG05-PY1	BG05-SP2	BG14-CPY	KP10-PY
Sc45	<0.00	<0.00	<0.00	<0.00	<0.00	<0.00	<0.00	<0.00	<0.00	<0.00	<0.00	<0.00	<0.00	<0.00	<0.00	<0.00	<0.00	<0.00	<0.00
Ti49	<0.00000	<0.00000	<0.00000	<0.00000	<0.00000	<0.00000	<0.00000	<0.00000	<0.00000	<0.00000	<0.00000	<0.00000	<0.00000	<0.00000	<0.00000	<0.00000	<0.00000	<0.00000	<0.00000
V51	<0.00000	<0.00000	<0.00000	<0.00000	<0.00000	<0.00000	<0.00000	<0.00000	<0.00000	<0.00000	<0.00000	<0.00000	<0.00000	<0.00000	<0.00000	<0.00000	<0.00000	<0.00000	<0.00000
Cr53	<0.00000	<0.00000	<0.00000	<0.00000	<0.00000	<0.00000	<0.00000	<0.00000	<0.00000	<0.00000	<0.00000	<0.00000	<0.00000	<0.00000	<0.00000	<0.00000	<0.00000	<0.00000	<0.00000
Mn55	<0.00	<0.00	<0.00	<0.00	<0.00	<0.00	<0.00	<0.00	<0.00	<0.00	<0.00	<0.00	<0.00	<0.00	<0.00	<0.00	<0.00	<0.00	<0.00
Fe57	<0.00000	<0.00000	<0.00000	<0.00000	<0.00000	<0.00000	<0.00000	<0.00000	<0.00000	<0.00000	<0.00000	<0.00000	<0.00000	<0.00000	<0.00000	<0.00000	<0.00000	<0.00000	<0.00000
Co59	<0.00000	<0.00000	<0.00000	<0.00000	<0.00000	<0.00000	<0.00000	<0.00000	<0.00000	<0.00000	<0.00000	<0.00000	<0.00000	<0.00000	<0.00000	<0.00000	<0.00000	<0.00000	<0.00000
Ni60	0.00386	0.00619	0.433	5.07	0.719	0.132	0.165	0.136	0.0359	0.13	0.108	0.0861	0.122	0.0787	0.0747	0.0829	0.0855	0.0688	0.114
Ni62	0.0156	0.0269	1.53	13.58	2.34	0.663	1.5	0.309	0.155	0.594	0.332	0.475	0.319	0.495	0.287	0.385	1.05	0.35	0.229
Cu65	0.00372	0.004	0.43	0.382	0.816	0.169	1.38	0.0839	0.0478	0.165	0.0994	0.0992	0.228	0.0735	0.0793	0.0911	0.138	0.278	0.0541
Zn66	<0.00000	<0.00000	<0.00000	<0.00000	<0.00000	<0.00000	<0.00000	<0.00000	<0.00000	<0.00000	<0.00000	<0.00000	<0.00000	<0.00000	<0.00000	<0.00000	<0.00000	<0.00000	<0.00000
Ga71	<0.00	<0.00	<0.00	<0.00	<0.00	<0.00	<0.00	<0.00	<0.00	<0.00	<0.00	<0.00	<0.00	<0.00	<0.00	<0.00	<0.00	<0.00	<0.00
As75	0.0836	0.0953	9.82	8.69	16.72	3.65	4.46	1.43	0.875	3.31	1.98	1.97	1.65	1.43	1.66	1.93	2.15	1.68	1.03
Se82	0.0976	0.115	11.42	10.02	19.37	4.5	5.66	1.74	1.07	4.05	2.56	2.5	2.02	1.87	1.99	2.26	2.61	1.98	1.3
Y89	<0.00	<0.00	<0.00	<0.00	<0.00	<0.00	<0.00	<0.00	<0.00	<0.00	<0.00	<0.00	<0.00	<0.00	<0.00	<0.00	<0.00	<0.00	<0.00
Zr90	<0.00	<0.00	<0.00	<0.00	<0.00	<0.00	<0.00	<0.00	<0.00	<0.00	<0.00	<0.00	<0.00	<0.00	<0.00	<0.00	<0.00	<0.00	<0.00
Nb93	<0.00000	<0.00000	<0.00000	<0.00000	<0.00000	<0.00000	<0.00000	<0.00000	<0.00000	<0.00000	<0.00000	<0.00000	<0.00000	<0.00000	<0.00000	<0.00000	<0.00000	<0.00000	<0.00000
Mo95	<0.00	<0.00	<0.00	<0.00	<0.00	<0.00	<0.00	<0.00	<0.00	<0.00	<0.00	<0.00	<0.00	<0.00	<0.00	<0.00	<0.00	<0.00	<0.00
Ru99	0.00237	0.00221	0.236	0.199	<0.00000	0.0847	0.092	0.0383	0.0265	0.0795	0.0329	0.0348	0.0411	0.0332	0.0284	0.05	0.0364	0.0359	0.0251
Ru101	0.00098	0.00193	0.0972	0.174	0.207	0.054	0.0804	0.0158	0.00891	0.0621	0.0303	0.0351	0.0239	0.0183	0.0261	0.0309	0.0212	0.0162	0.0163
Rh103	0.00065	0.00062	0.0733	0.0841	0.132	0.0303	0.0337	0.0121	0.00762	0.027	0.0166	0.0156	0.0145	0.0133	0.0135	0.0152	0.0186	0.0158	0.00658
Ag107	<0.00000	<0.00000	<0.00000	<0.00000	<0.00000	<0.00000	<0.00000	<0.00000	<0.00000	<0.00000	<0.00000	<0.00000	<0.00000	<0.00000	<0.00000	<0.00000	<0.00000	<0.00000	<0.00000
Pd108	0.00078	0.00113	0.074	0.114	0.21	0.0628	0.0577	0.0139	0.0104	0.0446	0.0238	0.0282	0.0197	0.0246	0.023	0.0192	0.0209	0.0201	0.0128
Cd111	<0.00000	<0.00000	<0.00000	<0.00000	<0.00000	<0.00000	<0.00000	<0.00000	<0.00000	<0.00000	<0.00000	<0.00000	<0.00000	<0.00000	<0.00000	<0.00000	<0.00000	<0.00000	<0.00000
In115	<0.00	<0.00	<0.00	<0.00	<0.00	<0.00	<0.00	<0.00	<0.00	<0.00	<0.00	<0.00	<0.00	<0.00	<0.00	<0.00	<0.00	<0.00	<0.00
Sn118	<0.00000	<0.00000	<0.00000	<0.00000	<0.00000	<0.00000	<0.00000	<0.00000	<0.00000	<0.00000	<0.00000	<0.00000	<0.00000	<0.00000	<0.00000	<0.00000	<0.00000	<0.00000	<0.00000
Sb121	<0.00000	<0.00000	<0.00000	<0.00000	<0.00000	<0.00000	<0.00000	<0.00000	<0.00000	<0.00000	<0.00000	<0.00000	<0.00000	<0.00000	<0.00000	<0.00000	<0.00000	<0.00000	<0.00000
Te125	0.00688	0.00848	0.905	0.706	1.33	0.425	0.4	0.0962	0.113	0.334	0.224	0.16	0.206	0.118	0.193	0.154	0.149	0.161	0.0891
Te128	0.0116	0.0134	1.38	1.21	2.22	0.531	0.636	0.214	0.122	0.495	0.285	0.299	0.238	0.203	0.228	0.267	0.286	0.234	0.145
La139	<0.00	<0.00	<0.00	<0.00	<0.00	<0.00	<0.00	<0.00	<0.00	<0.00	<0.00	<0.00	<0.00	<0.00	<0.00	<0.00	<0.00	<0.00	<0.00
Ce140	<0.00	<0.00	<0.00	<0.00	<0.00	<0.00	<0.00	<0.00	<0.00	<0.00	<0.00	<0.00	<0.00	<0.00	<0.00	<0.00	<0.00	<0.00	<0.00
Nd146	<0.00000	<0.00000	<0.00000	<0.00000	<0.00000	<0.00000	<0.00000	<0.00000	<0.00000	<0.00000	<0.00000	<0.00000	<0.00000	<0.00000	<0.00000	<0.00000	<0.00000	<0.00000	<0.00000
Hf178	<0.00	<0.00	<0.00	<0.00	<0.00	<0.00	<0.00	<0.00	<0.00	<0.00	<0.00	<0.00	<0.00	<0.00	<0.00	<0.00	<0.00	<0.00	<0.00
W182	<0.00	<0.00	<0.00	<0.00	<0.00	<0.00	<0.00	<0.00	<0.00	<0.00	<0.00	<0.00	<0.00	<0.00	<0.00	<0.00	<0.00	<0.00	<0.00
Re185	<0.00	<0.00	<0.00	<0.00	<0.00	<0.00	<0.00	<0.00	<0.00	<0.00	<0.00	<0.00	<0.00	<0.00	<0.00	<0.00	<0.00	<0.00	<0.00
Re187	<0.00000	<0.00000	<0.00000	<0.00000	<0.00000	<0.00000	<0.00000	<0.00000	<0.00000	<0.00000	<0.00000	<0.00000	<0.00000	<0.00000	<0.00000	<0.00000	<0.00000	<0.00000	<0.00000
Os189	0.0035	0.00218	0.233	0.227	0.703	0.14	0.157	0.0578	0.0276	0.122	0.0702	0.0688	0.0469	0.0508	0.0561	0.0552	0.0588	0.0594	0.032
Os190	0.00188	0.00107	0.214	0.167	0.345	0.0449	0.0862	0.0293	0.0181	0.0596	0.0276	0.0292	0.0281	0.0278	0.0238	0.0445	0.0353	0.0269	0.0243
Ir193	0.00035	0.00036	0.0422	0.0435	0.067	0.0117	0.0184	0.00558	0.00158	0.0168	0.00758	0.0095	0.00994	0.00749	0.00654	0.00547	0.00752	0.00574	0.00366
Pt195	0.00097	0.00147	0.145	0.15	0.146	0.0521	0.0894	0.0254	0.0133	0.0489	0.0165	0.0247	0.0231	0.0204	0.0285	0.0188	0.0224	0.0296	0.0154
Au197	0.00067	0.00038	0.0822	0.0734	0.0876	0.0114	0.0416	0.00943	0.00462	0.0263	0.0198	0.0121	0.0189	0.011	0.0121	0.0177	0.0127	0.0153	0.00535
Pb208	<0.00000	<0.00000	<0.00000	<0.00000	<0.00000	<0.00000	<0.00000	<0.00000	<0.00000	<0.00000	<0.00000	<0.00000	<0.00000	<0.00000	<0.00000	<0.00000	<0.00000	<0.00000	<0.00000
Bi209	0.00334	0.00285	0.239	0.207	0.364	0.0682	0.0844	0.0263	0.0171	0.0548	0.0341	0.0334	0.0287	0.075	0.0251	0.0269	0.0299	0.0241	0.014
Th232	<0.00	<0.00	<0.00	<0.00	<0.00	<0.00	<0.00	<0.00	<0.00	<0.00	<0.00	<0.00	<0.00	<0.00	<0.00	<0.00	<0.00	<0.00	<0.00
U238	<0.00	<0.00	<0.00	<0.00	<0.00	<0.00	<0.00	<0.00	<0.00	<0.00	<0.00	<0.00	<0.00	<0.00	<0.00	<0.00	<0.00	<0.00	<0.00
ThO248	<0.00	<0.00	<0.00	<0.00	<0.00	<0.00	<0.00	<0.00	<0.00	<0.00	<0.00	<0.00	<0.00	<0.00	<0.00	<0.00	<0.00	<0.00	<0.00
GLITTER!: Trace element concentrations normalised to chondrite.																			
Element	STD610-3	STD610-4	PGEA-3	PGEA-4	BCR2G-1	BG01-CPY	BG01-PY2	BG13-PY	BG13-SPH	BG13-SP2	JL04-PY	JL04-CPY	BG33-SPH	BG33-PY	BG19-PY	BG05-PY1	BG05-SP2	BG14-CPY	KP10-PY
Al27	<****	<****	<****	<****	<****	<****	<****	<****	<****	<****	<****	<****	<****	<****	<****	<****	<****	<****	<****
Si29	<****	<****	<****	<****	<****	<****	<****	<****	<****	<****	<****	<****	<****	<****	<****	<****	<****	<****	<****
S34	Inf	Inf	Inf	Inf	Inf	Inf	Inf	Inf	Inf	Inf	Inf	Inf	Inf	Inf	Inf	Inf	Inf	Inf	Inf
Ca43	<****	<****	<****	<****	<****	<****	<****	<****	<****	<****	<****	<****	<****	<****	<****	<****	<****	<****	<****
Sc45	<****	<****	<****	<****	<****	<****	<****	<****	<****	<****	<****	<****	<****	<****	<****	<****	<****	<****	<****
Ti49	0	0	0	0	0	0	0	0	0	0	0	0	0	0	0	0	0	0	0
V51	0	0	0	0	0	0	0	0	0	0	0	0	0	0	0	0	0	0	0
Cr53	0	0	0	0	0	0	0	0	0	0	0	0	0	0	0	0	0	0	0
Mn55	<****	<****	<****	<****	<****	<****	<****	<****	<****	<****	<****	<****	<****	<****	<****	<****	<****	<****	<****

PGEARUN5

Element	STD610-3	STD610-4	PGEA-3	PGEA-4	BCR2G-1	BG01-CPY	BG01-PY2	BG13-PY	BG13-SPH	BG13-SP2	JL04-PY	JL04-CPY	BG33-SPH	BG33-PY	BG19-PY	BG05-PY1	BG05-SP2	BG14-CPY	KP10-PY
Fe57	0	0	0	0	0	0	0	0	0	0	0	0	0	0	0	0	0	0	0
Co59	0	0	0	0	0	0	0	0	0	0	0	0	0	0	0	0	0	0	0
Ni60	0.00034	0.00032	42.01	43.32	0.00236	0.00021	0.00022	0.00011	0.00004	0.00004	0.00006	0.00015	0.00003	0	0.00039	0.00105	0.00047	0.00025	0.00031
Ni62	0.00033	0.00032	42.03	42.9	0.00238	0.00013	0	0.00023	0.00005	0	0.00006	0.00006	0.00161	0.00026	0.00032	0.00103	0.00032	0.00028	0.00022
Cu65	0.0191	0.01764	1.384	1.442	0.1877	1386.15	1341.44	0.1598	0.0239	0.512	0.01053	1502.19	0.2165	10.46	0.41	0.01007	1348.2	1627.06	0.461
Zn66	0	0	0	0	0	0	0	0	0	0	0	0	0	0	0	0	0	0	0
Ga71	<****	<****	<****	<****	<****	<****	<****	<****	<****	<****	<****	<****	<****	<****	<****	<****	<****	<****	<****
As75	1.255	1.191	46.14	47.18	0	0	0	231.79	23.21	1.46	195.6	4.05	0	3823.69	344.22	70.43	17.63	10.38	1593.86
Se82	0.0652	0.0672	8.75	8.42	0	0.186	0	0.291	0.051	0	6.61	8.82	0	0	2.28	3.7	2.4	1.88	1.087
Y89	<****	<****	<****	<****	<****	<****	<****	<****	<****	<****	<****	<****	<****	<****	<****	<****	<****	<****	<****
Zr90	<****	<****	<****	<****	<****	<****	<****	<****	<****	<****	<****	<****	<****	<****	<****	<****	<****	<****	<****
Nb93	0	0	0	0	0	0	0	0	0	0	0	0	0	0	0	0	0	0	0
Mo95	<****	<****	<****	<****	<****	<****	<****	<****	<****	<****	<****	<****	<****	<****	<****	<****	<****	<****	<****
Ru99	0	0	204.33	207.5	0.326	0.571	0.391	0	0	0	0	0.491	0	0	0.238	0	0.593	0.657	0
Ru101	0	0	206.68	208.77	0	0.221	0.193	0	0.0119	0	0	0.275	0	0	0	0	0.248	0.298	0
Rh103	0.1015	0.0986	1163.29	1174.94	0	119.94	120.18	0.339	0	1.83	0.562	140.45	0	1.307	0.098	0	123.84	151.82	0.294
Ag107	0	0	0	0	0	0	0	0	0	0	0	0	0	0	0	0	0	0	0
Pd108	0.0481	0.0443	293.3	304.16	0	0.134	0.433	0	0.628	87.07	0	0.198	101.47	0.036	0.075	0	0.731	0.604	0.258
Cd111	0	0	0	0	0	0	0	0	0	0	0	0	0	0	0	0	0	0	0
In115	<****	<****	<****	<****	<****	<****	<****	<****	<****	<****	<****	<****	<****	<****	<****	<****	<****	<****	<****
Sn118	0	0	0	0	0	0	0	0	0	0	0	0	0	0	0	0	0	0	0
Sb121	0	0	0	0	0	0	0	0	0	0	0	0	0	0	0	0	0	0	0
Te125	0.952	0.925	66.11	72.56	0.51	0	0.164	0.48	0.122	0	1.139	1.13	0.061	0.051	1.038	5.11	0.155	0.757	12.38
Te128	0.937	0.918	67.15	70.16	0	0	0	0.422	0	0.309	1.173	0.777	0	0	1.075	5	0.218	0.538	12.12
La139	<****	<****	<****	<****	<****	<****	<****	<****	<****	<****	<****	<****	<****	<****	<****	<****	<****	<****	<****
Ce140	<****	<****	<****	<****	<****	<****	<****	<****	<****	<****	<****	<****	<****	<****	<****	<****	<****	<****	<****
Nd146	0	0	0	0	0	0	0	0	0	0	0	0	0	0	0	0	0	0	0
Hf178	<****	<****	<****	<****	<****	<****	<****	<****	<****	<****	<****	<****	<****	<****	<****	<****	<****	<****	<****
W182	<****	<****	<****	<****	<****	<****	<****	<****	<****	<****	<****	<****	<****	<****	<****	<****	<****	<****	<****
Re185	<****	<****	<****	<****	<****	<****	<****	<****	<****	<****	<****	<****	<****	<****	<****	<****	<****	<****	<****
Re187	0	0	0	0	0	0	0	0	0	0	0	0	0	0	0	0	0	0	0
Os189	0	0	168.83	205.07	0	0	0	0	0	0	0	0	0	0	0	0	0	0	0
Os190	0	0.00151	172.39	207.03	0	0	0	0	0	0	0	0	0	0	0	0	0	0	0
Ir193	0	0	144.38	151.97	0.118	0	0	0	0.0031	0	0	0	0	0	0	0.0082	0	0	0
Pt195	0.0252	0.0264	139.15	142.69	0.129	0	0	0	0	0	0	0	0	0	0	0	0	0	0
Au197	1.002	0.931	1063.33	1086.97	1.5	0.175	0	4.26	2.23	0.448	0.773	1.4	0	261.64	1.01	0.316	0.226	0.522	22.94
Pb208	0	0	0	0	0	0	0	0	0	0	0	0	0	0	0	0	0	0	0
Bi209	23.73	23.24	1387.93	1454.5	2.88	21.22	17.93	885.62	36.74	17.69	4.17	200.41	3.87	8.69	389.78	127.05	36.07	123.27	150.55
Th232	<****	<****	<****	<****	<****	<****	<****	<****	<****	<****	<****	<****	<****	<****	<****	<****	<****	<****	<****
U238	<****	<****	<****	<****	<****	<****	<****	<****	<****	<****	<****	<****	<****	<****	<****	<****	<****	<****	<****
ThO248	<****	<****	<****	<****	<****	<****	<****	<****	<****	<****	<****	<****	<****	<****	<****	<****	<****	<****	<****

GLITTER4.0: Laser Ablation Analys

G:\KYLIE\MAR13\PGEARUN5
Fri Mar 14 21:09:45 2003

All values are reported in ppm

GLITTER!: Trace Element Concentrations MDL filtered.	Run5-20	Run5-21	Run5-22	Run5-23	Run5-24	Run5-25	Run5-26	Run5-27	Modified Run5-28	Run5-29	Run5-30	Run5-31	Run5-32	Run5-33	Run5-34	Run5-35	Run5-36
Element	BG34-PY	BG34-SPH	BG34-CPY	BG34-PY2	BG35-PY	BG35-CPY	BG35-SPH	BG36-PY	BG37-PY	BG37-PY2	BG37-SPH	BG38-SPH	STD610-5	STD610-6	PGEA-5	PGEA-6	BCR2G-2
Al27	<-NaN	<-NaN	<-NaN	<-NaN	<-NaN	<-NaN	<-NaN	<-NaN	<-NaN	<-NaN	<-NaN	<-NaN	<-NaN	<-NaN	<-NaN	<-NaN	<-NaN
Si29	<-NaN	<-NaN	<-NaN	<-NaN	<-NaN	<-NaN	<-NaN	<-NaN	<-NaN	<-NaN	<-NaN	<-NaN	<-NaN	<-NaN	<-NaN	<-NaN	<-NaN
S34	534495.56	329670.09	349436.84	534495.56	534495.56	349436.84	331971.66	534495.56	534495.56	534495.56	331971.66	331971.66	388.87	388.87	278000	278000	47632.28
Ca43	<-NaN	<-NaN	<-NaN	<-NaN	<-NaN	<-NaN	<-NaN	<-NaN	<-NaN	<-NaN	<-NaN	<-NaN	<-NaN	<-NaN	<-NaN	<-NaN	<-NaN
Sc45	<-NaN	<-NaN	<-NaN	<-NaN	<-NaN	<-NaN	<-NaN	<-NaN	<-NaN	<-NaN	<-NaN	<-NaN	<-NaN	<-NaN	<-NaN	<-NaN	<-NaN
Ti49	<0.00	<0.00	<0.00	<0.00	<0.00	<0.00	<0.00	<0.00	<0.00	<0.00	<0.00	<0.00	<0.00	<0.00	<0.00	<0.00	<0.00
V51	<0.00	<0.00	<0.00	<0.00	<0.00	<0.00	<0.00	<0.00	<0.00	<0.00	<0.00	<0.00	<0.00	<0.00	<0.00	<0.00	<0.00
Cr53	<0.00	<0.00	<0.00	<0.00	<0.00	<0.00	<0.00	<0.00	<0.00	<0.00	<0.00	<0.00	<0.00	<0.00	<0.00	<0.00	<0.00
Mn55	<-NaN	<-NaN	<-NaN	<-NaN	<-NaN	<-NaN	<-NaN	<-NaN	<-NaN	<-NaN	<-NaN	<-NaN	<-NaN	<-NaN	<-NaN	<-NaN	<-NaN
Fe57	<0.00	<0.00	<0.00	<0.00	<0.00	<0.00	<0.00	<0.00	<0.00	<0.00	<0.00	<0.00	<0.00	<0.00	<0.00	<0.00	<0.00
Co59	<0.00	<0.00	<0.00	<0.00	<0.00	<0.00	<0.00	<0.00	<0.00	<0.00	<0.00	<0.00	<0.00	<0.00	<0.00	<0.00	<0.00
Ni60	0.315	1.27	0.989	0.39	5.28	0.205	0.176	14.7	730.81	1106.44	2.98	0.232	6.41	7.92	718712.56	730374.5	27.67
Ni62	0.74	<0.63	<0.195	0.89	4.59	0.185	<0.88	11.86	4.37	1061.8	3.79	<0.36	6.24	7.83	721054.63	734884	22.95
Cu65	229.67	103.87	192535.53	<0.82	604.75	181591.45	539.43	145.23	326603.31	309.47	1559.03	18.03	3.56	4.48	248.94	244.15	24.42
Zn66	<0.00	<0.00	<0.00	<0.00	<0.00	<0.00	<0.00	<0.00	<0.00	<0.00	<0.00	<0.00	<0.00	<0.00	<0.00	<0.00	<0.00
Ga71	<-NaN	<-NaN	<-NaN	<-NaN	<-NaN	<-NaN	<-NaN	<-NaN	<-NaN	<-NaN	<-NaN	<-NaN	<-NaN	<-NaN	<-NaN	<-NaN	<-NaN
As75	20626.04	8.82	96.78	370.1	4371.14	33511.53	68.73	19.25	<2.10	455.32	35.86	<2.86	4.11	4.96	134.37	140.39	<15.84
Se82	13.92	13.35	6.68	13.38	37.88	16.97	<3.85	87.43	61.55	67.51	13.96	3.44	2.14	2.5	249.58	253.93	<15.10
Y89	<-NaN	<-NaN	<-NaN	<-NaN	<-NaN	<-NaN	<-NaN	<-NaN	<-NaN	<-NaN	<-NaN	<-NaN	<-NaN	<-NaN	<-NaN	<-NaN	<-NaN
Zr90	<-NaN	<-NaN	<-NaN	<-NaN	<-NaN	<-NaN	<-NaN	<-NaN	<-NaN	<-NaN	<-NaN	<-NaN	<-NaN	<-NaN	<-NaN	<-NaN	<-NaN
Nb93	<0.00	<0.00	<0.00	<0.00	<0.00	<0.00	<0.00	<0.00	<0.00	<0.00	<0.00	<0.00	<0.00	<0.00	<0.00	<0.00	<0.00
Mo95	<-NaN	<-NaN	<-NaN	<-NaN	<-NaN	<-NaN	<-NaN	<-NaN	<-NaN	<-NaN	<-NaN	<-NaN	<-NaN	<-NaN	<-NaN	<-NaN	<-NaN
Ru99	<0.0258	0.087	0.48	<0.054	0.199	0.435	<0.071	<0.038	0.719	<0.029	<0.044	<0.044	0.00281	<0.0023	237.13	234.58	<0.38
Ru101	<0.0165	<0.064	0.231	<0.041	<0.0199	0.201	<0.062	<0.027	0.286	<0.025	0.026	<0.0141	<0.00085	0.00149	234.27	234.64	<0.241
Rh103	0.0443	0.039	21.66	<0.0196	0.0778	20.24	0.077	0.0524	34.95	0.084	0.129	<0.0186	0.0244	0.0292	251.08	248.94	<0.115
Ag107	<0.00	<0.00	<0.00	<0.00	<0.00	<0.00	<0.00	<0.00	<0.00	<0.00	<0.00	<0.00	<0.00	<0.00	<0.00	<0.00	<0.00
Pd108	<0.0178	71.32	2.47	<0.026	0.124	1.015	92.59	0.619	8.5	1.224	102.34	93.12	0.0501	0.0701	267.7	259.05	<0.140
Cd111	<0.00	<0.00	<0.00	<0.00	<0.00	<0.00	<0.00	<0.00	<0.00	<0.00	<0.00	<0.00	<0.00	<0.00	<0.00	<0.00	<0.00
In115	<-NaN	<-NaN	<-NaN	<-NaN	<-NaN	<-NaN	<-NaN	<-NaN	<-NaN	<-NaN	<-NaN	<-NaN	<-NaN	<-NaN	<-NaN	<-NaN	<-NaN
Sn118	<0.00	<0.00	<0.00	<0.00	<0.00	<0.00	<0.00	<0.00	<0.00	<0.00	<0.00	<0.00	<0.00	<0.00	<0.00	<0.00	<0.00
Sb121	<0.00	<0.00	<0.00	<0.00	<0.00	<0.00	<0.00	<0.00	<0.00	<0.00	<0.00	<0.00	<0.00	<0.00	<0.00	<0.00	<0.00
Te125	2.34	0.46	0.32	6.83	20	0.361	<0.31	3.09	0.71	7.39	0.29	<0.26	3.93	4.88	245.34	243.14	<0.85
Te128	2.36	0.79	0.344	6.39	19.29	0.435	<0.45	2.67	0.521	7.86	<0.25	0.38	3.94	4.87	244.5	249.29	3.11
La139	<-NaN	<-NaN	<-NaN	<-NaN	<-NaN	<-NaN	<-NaN	<-NaN	<-NaN	<-NaN	<-NaN	<-NaN	<-NaN	<-NaN	<-NaN	<-NaN	<-NaN
Ce140	<-NaN	<-NaN	<-NaN	<-NaN	<-NaN	<-NaN	<-NaN	<-NaN	<-NaN	<-NaN	<-NaN	<-NaN	<-NaN	<-NaN	<-NaN	<-NaN	<-NaN
Nd146	<0.00	<0.00	<0.00	<0.00	<0.00	<0.00	<0.00	<0.00	<0.00	<0.00	<0.00	<0.00	<0.00	<0.00	<0.00	<0.00	<0.00
Hf178	<-NaN	<-NaN	<-NaN	<-NaN	<-NaN	<-NaN	<-NaN	<-NaN	<-NaN	<-NaN	<-NaN	<-NaN	<-NaN	<-NaN	<-NaN	<-NaN	<-NaN
W182	<-NaN	<-NaN	<-NaN	<-NaN	<-NaN	<-NaN	<-NaN	<-NaN	<-NaN	<-NaN	<-NaN	<-NaN	<-NaN	<-NaN	<-NaN	<-NaN	<-NaN
Re185	<-NaN	<-NaN	<-NaN	<-NaN	<-NaN	<-NaN	<-NaN	<-NaN	<-NaN	<-NaN	<-NaN	<-NaN	<-NaN	<-NaN	<-NaN	<-NaN	<-NaN
Re187	<0.00	<0.00	<0.00	<0.00	<0.00	<0.00	<0.00	<0.00	<0.00	<0.00	<0.00	<0.00	<0.00	<0.00	<0.00	<0.00	<0.00
Os189	<0.028	<0.118	<0.034	<0.070	<0.036	<0.0174	<0.100	<0.053	<0.045	<0.070	<0.066	0.062	<0.0035	<0.0030	204.86	179.57	<0.41
Os190	<0.0137	<0.056	<0.0165	<0.038	<0.0198	<0.0114	<0.065	0.036	0.0126	<0.048	<0.078	<0.050	<0.00224	<0.00197	198.68	181.85	<0.28
Ir193	<0.0051	<0.0107	<0.0043	<0.0115	<0.0042	<0.00315	<0.0128	<0.0090	<0.0052	<0.0063	<0.0090	<0.0070	<0.00040	0.00052	108.73	106.05	0.084
Pt195	<0.0159	<0.055	<0.0149	<0.025	0.0119	0.0068	<0.040	<0.031	0.026	<0.042	<0.027	<0.040	0.0402	0.0497	208.22	204.92	<0.180
Au197	10.85	<0.031	0.0831	0.051	2.89	29.38	<0.030	0.461	0.0386	0.399	0.046	0.02	0.2358	0.308	235.13	230.96	0.206
Pb208	<0.00	<0.00	<0.00	<0.00	<0.00	<0.00	<0.00	<0.00	<0.00	<0.00	<0.00	<0.00	<0.00	<0.00	<0.00	<0.00	<0.00
Bi209	21.13	6.29	3.18	110.11	124.71	18.01	0.211	9.16	3.01	13.2	2.345	0.571	4.91	6.14	234.83	232.87	0.709
Th232	<-NaN	<-NaN	<-NaN	<-NaN	<-NaN	<-NaN	<-NaN	<-NaN	<-NaN	<-NaN	<-NaN	<-NaN	<-NaN	<-NaN	<-NaN	<-NaN	<-NaN
U238	<-NaN	<-NaN	<-NaN	<-NaN	<-NaN	<-NaN	<-NaN	<-NaN	<-NaN	<-NaN	<-NaN	<-NaN	<-NaN	<-NaN	<-NaN	<-NaN	<-NaN
ThO248	<-NaN	<-NaN	<-NaN	<-NaN	<-NaN	<-NaN	<-NaN	<-NaN	<-NaN	<-NaN	<-NaN	<-NaN	<-NaN	<-NaN	<-NaN	<-NaN	<-NaN

Element	BG34-PY	BG34-SPH	BG34-CPY	BG34-PY2	BG35-PY	BG35-CPY	BG35-SPH	BG36-PY	BG37-PY	BG37-PY2	BG37-SPH	BG38-SPH	STD610-5	STD610-6	PGEA-5	PGEA-6	BCR2G-2
GLITTER!: 1 sigma error.																	
Element	BG34-PY	BG34-SPH	BG34-CPY	BG34-PY2	BG35-PY	BG35-CPY	BG35-SPH	BG36-PY	BG37-PY	BG37-PY2	BG37-SPH	BG38-SPH	STD610-5	STD610-6	PGEA-5	PGEA-6	BCR2G-2
Al27	<0.00	<0.00	<0.00	<0.00	<0.00	<0.00	<0.00	<0.00	<0.00	<0.00	<0.00	<0.00	<0.00	<0.00	<0.00	<0.00	<0.00
Si29	<0.00	<0.00	<0.00	<0.00	<0.00	<0.00	<0.00	<0.00	<0.00	<0.00	<0.00	<0.00	<0.00	<0.00	<0.00	<0.00	<0.00
S34	16905.9	10443.6	11053.41	16912.28	16905.11	11051.95	10509.96	16907.55	16906.02	16908.21	10505.38	10508.08	12.98	13	8809.41	8814.01	1585.08
Ca43	<0.00	<0.00	<0.00	<0.00	<0.00	<0.00	<0.00	<0.00	<0.00	<0.00	<0.00	<0.00	<0.00	<0.00	<0.00	<0.00	<0.00
Sc45	<0.00	<0.00	<0.00	<0.00	<0.00	<0.00	<0.00	<0.00	<0.00	<0.00	<0.00	<0.00	<0.00	<0.00	<0.00	<0.00	<0.00
Ti49	<0.00	<0.00	<0.00	<0.00	<0.00	<0.00	<0.00	<0.00	<0.00	<0.00	<0.00	<0.00	<0.00	<0.00	<0.00	<0.00	<0.00
V51	<0.00	<0.00	<0.00	<0.00	<0.00	<0.00	<0.00	<0.00	<0.00	<0.00	<0.00	<0.00	<0.00	<0.00	<0.00	<0.00	<0.00
Cr53	<0.00	<0.00	<0.00	<0.00	<0.00	<0.00	<0.00	<0.00	<0.00	<0.00	<0.00	<0.00	<0.00	<0.00	<0.00	<0.00	<0.00
Mn55	<0.00	<0.00	<0.00	<0.00	<0.00	<0.00	<0.00	<0.00	<0.00	<0.00	<0.00	<0.00	<0.00	<0.00	<0.00	<0.00	<0.00
Fe57	<0.00	<0.00	<0.00	<0.00	<0.00	<0.00	<0.00	<0.00	<0.00	<0.00	<0.00	<0.00	<0.00	<0.00	<0.00	<0.00	<0.00
Co59	<0.00	<0.00	<0.00	<0.00	<0.00	<0.00	<0.00	<0.00	<0.00	<0.00	<0.00	<0.00	<0.00	<0.00	<0.00	<0.00	<0.00
Ni60	0.033	0.14	0.058	0.061	0.21	0.019	0.063	0.55	25.32	38.34	0.16	0.057	0.23	0.28	24894.68	25304.19	1.25
Ni62	0.14	0.3	0.093	0.21	0.29	0.065	0.33	0.66	0.33	38.47	0.39	0.19	0.24	0.3	25934.92	26437.91	2.05
Cu65	8.86	4.08	7415.85	0.57	23.3	6994.01	20.83	5.62	12579.42	11.97	60.09	0.74	0.14	0.18	9.66	9.5	1.12
Zn66	<0.00	<0.00	<0.00	<0.00	<0.00	<0.00	<0.00	<0.00	<0.00	<0.00	<0.00	<0.00	<0.00	<0.00	<0.00	<0.00	<0.00
Ga71	<0.00	<0.00	<0.00	<0.00	<0.00	<0.00	<0.00	<0.00	<0.00	<0.00	<0.00	<0.00	<0.00	<0.00	<0.00	<0.00	<0.00
As75	751.5	1.96	3.6	13.63	159.28	1220.91	3.39	1.4	0.84	16.69	1.77	1.3	0.16	0.19	6.39	6.58	6.3
Se82	1	2.22	0.7	1.5	2.02	0.94	1.66	4.56	3.21	3.64	1.35	1.13	0.12	0.14	13.17	13.55	5.91
Y89	<0.00	<0.00	<0.00	<0.00	<0.00	<0.00	<0.00	<0.00	<0.00	<0.00	<0.00	<0.00	<0.00	<0.00	<0.00	<0.00	<0.00
Zr90	<0.00	<0.00	<0.00	<0.00	<0.00	<0.00	<0.00	<0.00	<0.00	<0.00	<0.00	<0.00	<0.00	<0.00	<0.00	<0.00	<0.00
Nb93	<0.00	<0.00	<0.00	<0.00	<0.00	<0.00	<0.00	<0.00	<0.00	<0.00	<0.00	<0.00	<0.00	<0.00	<0.00	<0.00	<0.00
Mo95	<0.00	<0.00	<0.00	<0.00	<0.00	<0.00	<0.00	<0.00	<0.00	<0.00	<0.00	<0.00	<0.00	<0.00	<0.00	<0.00	<0.00
Ru99	0.0092	0.042	0.041	0.024	0.024	0.031	0.033	0.014	0.058	0.015	0.018	0.02	0.00096	0.0011	10.91	10.82	0.15
Ru101	0.0074	0.025	0.022	0.015	0.0073	0.016	0.024	0.012	0.029	0.013	0.013	0.0085	0.00046	0.00061	9.38	9.43	0.095
Rh103	0.006	0.016	0.94	0.0081	0.0069	0.88	0.015	0.0092	1.52	0.012	0.013	0.0089	0.0014	0.0016	10.91	10.83	0.045
Ag107	<0.00	<0.00	<0.00	<0.00	<0.00	<0.00	<0.00	<0.00	<0.00	<0.00	<0.00	<0.00	<0.00	<0.00	<0.00	<0.00	<0.00
Pd108	0.0061	3.2	0.12	0.012	0.013	0.051	4.11	0.043	0.39	0.073	4.52	4.13	0.003	0.0039	11.82	11.46	0.064
Cd111	<0.00	<0.00	<0.00	<0.00	<0.00	<0.00	<0.00	<0.00	<0.00	<0.00	<0.00	<0.00	<0.00	<0.00	<0.00	<0.00	<0.00
In115	<0.00	<0.00	<0.00	<0.00	<0.00	<0.00	<0.00	<0.00	<0.00	<0.00	<0.00	<0.00	<0.00	<0.00	<0.00	<0.00	<0.00
Sn118	<0.00	<0.00	<0.00	<0.00	<0.00	<0.00	<0.00	<0.00	<0.00	<0.00	<0.00	<0.00	<0.00	<0.00	<0.00	<0.00	<0.00
Sb121	<0.00	<0.00	<0.00	<0.00	<0.00	<0.00	<0.00	<0.00	<0.00	<0.00	<0.00	<0.00	<0.00	<0.00	<0.00	<0.00	<0.00
Te125	0.18	0.18	0.07	0.53	0.98	0.048	0.16	0.26	0.1	0.48	0.11	0.11	0.19	0.23	11.47	11.49	0.43
Te128	0.13	0.23	0.069	0.35	0.81	0.044	0.19	0.17	0.085	0.37	0.11	0.13	0.16	0.2	10.07	10.3	0.7
La139	<0.00	<0.00	<0.00	<0.00	<0.00	<0.00	<0.00	<0.00	<0.00	<0.00	<0.00	<0.00	<0.00	<0.00	<0.00	<0.00	<0.00
Ce140	<0.00	<0.00	<0.00	<0.00	<0.00	<0.00	<0.00	<0.00	<0.00	<0.00	<0.00	<0.00	<0.00	<0.00	<0.00	<0.00	<0.00
Nd146	<0.00	<0.00	<0.00	<0.00	<0.00	<0.00	<0.00	<0.00	<0.00	<0.00	<0.00	<0.00	<0.00	<0.00	<0.00	<0.00	<0.00
Hf178	<0.00	<0.00	<0.00	<0.00	<0.00	<0.00	<0.00	<0.00	<0.00	<0.00	<0.00	<0.00	<0.00	<0.00	<0.00	<0.00	<0.00
W182	<0.00	<0.00	<0.00	<0.00	<0.00	<0.00	<0.00	<0.00	<0.00	<0.00	<0.00	<0.00	<0.00	<0.00	<0.00	<0.00	<0.00
Re185	<0.00	<0.00	<0.00	<0.00	<0.00	<0.00	<0.00	<0.00	<0.00	<0.00	<0.00	<0.00	<0.00	<0.00	<0.00	<0.00	<0.00
Re187	<0.00	<0.00	<0.00	<0.00	<0.00	<0.00	<0.00	<0.00	<0.00	<0.00	<0.00	<0.00	<0.00	<0.00	<0.00	<0.00	<0.00
Os189	0.012	0.057	0.011	0.028	0.015	0.0062	0.041	0.022	0.019	0.024	0.025	0.028	0.0014	0.0011	17.64	15.5	0.17
Os190	0.0069	0.029	0.0067	0.017	0.0084	0.005	0.027	0.013	0.007	0.019	0.027	0.021	0.00081	0.00081	15.17	13.91	0.11
Ir193	0.0019	0.0056	0.0015	0.0049	0.0017	0.00097	0.0059	0.0036	0.0022	0.0029	0.0036	0.0034	0.00018	0.00019	4.06	3.97	0.023
Pt195	0.0067	0.022	0.0066	0.013	0.0059	0.0036	0.018	0.011	0.0087	0.015	0.012	0.018	0.0025	0.0029	7.19	7.11	0.085
Au197	0.36	0.017	0.0087	0.012	0.1	0.94	0.012	0.028	0.0066	0.027	0.01	0.01	0.0084	0.011	7.51	7.39	0.047
Pb208	<0.00	<0.00	<0.00	<0.00	<0.00	<0.00	<0.00	<0.00	<0.00	<0.00	<0.00	<0.00	<0.00	<0.00	<0.00	<0.00	<0.00
Bi209	0.74	0.25	0.12	3.83	4.32	0.63	0.027	0.33	0.11	0.47	0.094	0.036	0.17	0.22	8.16	8.1	0.086
Th232	<0.00	<0.00	<0.00	<0.00	<0.00	<0.00	<0.00	<0.00	<0.00	<0.00	<0.00	<0.00	<0.00	<0.00	<0.00	<0.00	<0.00
U238	<0.00	<0.00	<0.00	<0.00	<0.00	<0.00	<0.00	<0.00	<0.00	<0.00	<0.00	<0.00	<0.00	<0.00	<0.00	<0.00	<0.00
ThO248	<0.00	<0.00	<0.00	<0.00	<0.00	<0.00	<0.00	<0.00	<0.00	<0.00	<0.00	<0.00	<0.00	<0.00	<0.00	<0.00	<0.00
GLITTER!: Minimum detection limits (99% confidence).																	
Element	BG34-PY	BG34-SPH	BG34-CPY	BG34-PY2	BG35-PY	BG35-CPY	BG35-SPH	BG36-PY	BG37-PY	BG37-PY2	BG37-SPH	BG38-SPH	STD610-5	STD610-6	PGEA-5	PGEA-6	BCR2G-2
Al27	<0.00	<0.00	<0.00	<0.00	<0.00	<0.00	<0.00	<0.00	<0.00	<0.00	<0.00	<0.00	<0.00	<0.00	<0.00	<0.00	<0.00
Si29	<0.00	<0.00	<0.00	<0.00	<0.00	<0.00	<0.00	<0.00	<0.00	<0.00	<0.00	<0.00	<0.00	<0.00	<0.00	<0.00	<0.00
S34	76.12	245.71	82.5	153.48	82.41	55.57	254.85	152.69	104.77	177.99	144.91	148.93	6.12	6.26	461.42	442.09	669.66
Ca43	<0.00	<0.00	<0.00	<0.00	<0.00	<0.00	<0.00	<0.00	<0.00	<0.00	<0.00	<0.00	<0.00	<0.00	<0.00	<0.00	<0.00

Element	BG34-PY	BG34-SPH	BG34-CPY	BG34-PY2	BG35-PY	BG35-CPY	BG35-SPH	BG36-PY	BG37-PY	BG37-PY2	BG37-SPH	BG38-SPH	STD610-5	STD610-6	PGEA-5	PGEA-6	BCR2G-2
Sc45	<0.00	<0.00	<0.00	<0.00	<0.00	<0.00	<0.00	<0.00	<0.00	<0.00	<0.00	<0.00	<0.00	<0.00	<0.00	<0.00	<0.00
Ti49	<0.00000	<0.00000	<0.00000	<0.00000	<0.00000	<0.00000	<0.00000	<0.00000	<0.00000	<0.00000	<0.00000	<0.00000	<0.00000	<0.00000	<0.00000	<0.00000	<0.00000
V51	<0.00000	<0.00000	<0.00000	<0.00000	<0.00000	<0.00000	<0.00000	<0.00000	<0.00000	<0.00000	<0.00000	<0.00000	<0.00000	<0.00000	<0.00000	<0.00000	<0.00000
Cr53	<0.00000	<0.00000	<0.00000	<0.00000	<0.00000	<0.00000	<0.00000	<0.00000	<0.00000	<0.00000	<0.00000	<0.00000	<0.00000	<0.00000	<0.00000	<0.00000	<0.00000
Mn55	<0.00	<0.00	<0.00	<0.00	<0.00	<0.00	<0.00	<0.00	<0.00	<0.00	<0.00	<0.00	<0.00	<0.00	<0.00	<0.00	<0.00
Fe57	<0.00000	<0.00000	<0.00000	<0.00000	<0.00000	<0.00000	<0.00000	<0.00000	<0.00000	<0.00000	<0.00000	<0.00000	<0.00000	<0.00000	<0.00000	<0.00000	<0.00000
Co59	<0.00000	<0.00000	<0.00000	<0.00000	<0.00000	<0.00000	<0.00000	<0.00000	<0.00000	<0.00000	<0.00000	<0.00000	<0.00000	<0.00000	<0.00000	<0.00000	<0.00000
Ni60	0.0443	0.136	0.0488	0.0796	0.0481	0.0258	0.125	0.0817	0.0631	0.0798	0.101	0.095	0.00362	0.00465	0.257	7.6	0.598
Ni62	0.22	0.632	0.195	0.215	0.223	0.131	0.884	0.334	0.359	0.389	0.399	0.36	0.0179	0.0148	1.78	19.23	1.78
Cu65	0.0588	0.155	0.0525	0.817	0.113	0.0495	0.698	0.102	0.0814	2.02	0.13	0.111	0.00479	0.00529	0.365	0.351	0.542
Zn66	<0.00000	<0.00000	<0.00000	<0.00000	<0.00000	<0.00000	<0.00000	<0.00000	<0.00000	<0.00000	<0.00000	<0.00000	<0.00000	<0.00000	<0.00000	<0.00000	<0.00000
Ga71	<0.00	<0.00	<0.00	<0.00	<0.00	<0.00	<0.00	<0.00	<0.00	<0.00	<0.00	<0.00	<0.00	<0.00	<0.00	<0.00	<0.00
As75	1.22	4	1.35	2.47	1.36	0.776	5.1	2.99	2.1	3.08	2.59	2.86	0.127	0.129	10.57	9.6	15.84
Se82	1.41	3.98	1.35	2.51	1.33	0.736	3.85	2.38	1.69	2.44	2.28	2.31	0.108	0.117	8.91	8.24	15.1
Y89	<0.00	<0.00	<0.00	<0.00	<0.00	<0.00	<0.00	<0.00	<0.00	<0.00	<0.00	<0.00	<0.00	<0.00	<0.00	<0.00	<0.00
Zr90	<0.00	<0.00	<0.00	<0.00	<0.00	<0.00	<0.00	<0.00	<0.00	<0.00	<0.00	<0.00	<0.00	<0.00	<0.00	<0.00	<0.00
Nb93	<0.00000	<0.00000	<0.00000	<0.00000	<0.00000	<0.00000	<0.00000	<0.00000	<0.00000	<0.00000	<0.00000	<0.00000	<0.00000	<0.00000	<0.00000	<0.00000	<0.00000
Mo95	<0.00	<0.00	<0.00	<0.00	<0.00	<0.00	<0.00	<0.00	<0.00	<0.00	<0.00	<0.00	<0.00	<0.00	<0.00	<0.00	<0.00
Ru99	0.0258	0.0518	0.0242	0.0539	0.0258	0.0111	0.0714	0.0381	0.0472	0.0289	0.0436	0.044	0.00169	0.00235	0.159	0.26	0.377
Ru101	0.0165	0.064	0.0141	0.0411	0.0199	0.00397	0.0624	0.0272	0.031	0.0252	0.018	0.0141	0.00085	0.0011	0.0983	0.206	0.241
Rh103	0.00969	0.0275	0.00777	0.0196	0.00896	0.00506	0.0272	0.018	0.013	0.0225	0.0135	0.0186	0.00079	0.00082	0.0657	0.088	0.115
Ag107	<0.00000	<0.00000	<0.00000	<0.00000	<0.00000	<0.00000	<0.00000	<0.00000	<0.00000	<0.00000	<0.00000	<0.00000	<0.00000	<0.00000	<0.00000	<0.00000	<0.00000
Pd108	0.0178	0.044	0.0138	0.0255	0.0155	0.00741	0.0388	0.0224	0.0116	0.0286	0.0237	0.0247	0.00106	0.00104	0.0706	0.125	0.14
Cd111	<0.00000	<0.00000	<0.00000	<0.00000	<0.00000	<0.00000	<0.00000	<0.00000	<0.00000	<0.00000	<0.00000	<0.00000	<0.00000	<0.00000	<0.00000	<0.00000	<0.00000
In115	<0.00	<0.00	<0.00	<0.00	<0.00	<0.00	<0.00	<0.00	<0.00	<0.00	<0.00	<0.00	<0.00	<0.00	<0.00	<0.00	<0.00
Sn118	<0.00000	<0.00000	<0.00000	<0.00000	<0.00000	<0.00000	<0.00000	<0.00000	<0.00000	<0.00000	<0.00000	<0.00000	<0.00000	<0.00000	<0.00000	<0.00000	<0.00000
Sb121	<0.00000	<0.00000	<0.00000	<0.00000	<0.00000	<0.00000	<0.00000	<0.00000	<0.00000	<0.00000	<0.00000	<0.00000	<0.00000	<0.00000	<0.00000	<0.00000	<0.00000
Te125	0.0711	0.212	0.111	0.205	0.099	0.0485	0.311	0.192	0.139	0.229	0.19	0.262	0.00996	0.0137	0.632	0.839	0.848
Te128	0.157	0.432	0.154	0.282	0.15	0.0835	0.45	0.264	0.19	0.283	0.25	0.262	0.0124	0.0139	1.05	1	1.62
La139	<0.00	<0.00	<0.00	<0.00	<0.00	<0.00	<0.00	<0.00	<0.00	<0.00	<0.00	<0.00	<0.00	<0.00	<0.00	<0.00	<0.00
Ce140	<0.00	<0.00	<0.00	<0.00	<0.00	<0.00	<0.00	<0.00	<0.00	<0.00	<0.00	<0.00	<0.00	<0.00	<0.00	<0.00	<0.00
Nd146	<0.00000	<0.00000	<0.00000	<0.00000	<0.00000	<0.00000	<0.00000	<0.00000	<0.00000	<0.00000	<0.00000	<0.00000	<0.00000	<0.00000	<0.00000	<0.00000	<0.00000
Hf178	<0.00	<0.00	<0.00	<0.00	<0.00	<0.00	<0.00	<0.00	<0.00	<0.00	<0.00	<0.00	<0.00	<0.00	<0.00	<0.00	<0.00
W182	<0.00	<0.00	<0.00	<0.00	<0.00	<0.00	<0.00	<0.00	<0.00	<0.00	<0.00	<0.00	<0.00	<0.00	<0.00	<0.00	<0.00
Re185	<0.00	<0.00	<0.00	<0.00	<0.00	<0.00	<0.00	<0.00	<0.00	<0.00	<0.00	<0.00	<0.00	<0.00	<0.00	<0.00	<0.00
Re187	<0.00000	<0.00000	<0.00000	<0.00000	<0.00000	<0.00000	<0.00000	<0.00000	<0.00000	<0.00000	<0.00000	<0.00000	<0.00000	<0.00000	<0.00000	<0.00000	<0.00000
Os189	0.028	0.118	0.0338	0.0697	0.0361	0.0174	0.0998	0.0533	0.0448	0.0699	0.0659	0.0275	0.00355	0.00304	0.222	0.279	0.409
Os190	0.0137	0.0561	0.0165	0.0382	0.0198	0.0114	0.0647	0.016	0.011	0.0484	0.0776	0.0495	0.00224	0.00197	0.0667	0.212	0.283
Ir193	0.00506	0.0107	0.00432	0.0115	0.00421	0.00315	0.0128	0.00902	0.00522	0.00632	0.009	0.00704	0.0004	0.00035	0.0426	0.0541	0.0302
Pt195	0.0159	0.0552	0.0149	0.025	0.0112	0.00685	0.0401	0.031	0.0139	0.0416	0.0268	0.0402	0.00104	0.00144	0.109	0.155	0.18
Au197	0.00922	0.0313	0.00788	0.0137	0.00841	0.00629	0.0305	0.0129	0.00789	0.0174	0.0132	0.0168	0.00062	0.00096	0.072	0.128	0.0624
Pb208	<0.00000	<0.00000	<0.00000	<0.00000	<0.00000	<0.00000	<0.00000	<0.00000	<0.00000	<0.00000	<0.00000	<0.00000	<0.00000	<0.00000	<0.00000	<0.00000	<0.00000
Bi209	0.0166	0.0675	0.015	0.0298	0.0145	0.0398	0.0437	0.0244	0.0172	0.0237	0.0243	0.0254	0.00127	0.00163	0.102	0.118	0.15
Th232	<0.00	<0.00	<0.00	<0.00	<0.00	<0.00	<0.00	<0.00	<0.00	<0.00	<0.00	<0.00	<0.00	<0.00	<0.00	<0.00	<0.00
U238	<0.00	<0.00	<0.00	<0.00	<0.00	<0.00	<0.00	<0.00	<0.00	<0.00	<0.00	<0.00	<0.00	<0.00	<0.00	<0.00	<0.00
ThO248	<0.00	<0.00	<0.00	<0.00	<0.00	<0.00	<0.00	<0.00	<0.00	<0.00	<0.00	<0.00	<0.00	<0.00	<0.00	<0.00	<0.00
GLITTER!: Trace element concentrations normalised to chondrite.																	
Element	BG34-PY	BG34-SPH	BG34-CPY	BG34-PY2	BG35-PY	BG35-CPY	BG35-SPH	BG36-PY	BG37-PY	BG37-PY2	BG37-SPH	BG38-SPH	STD610-5	STD610-6	PGEA-5	PGEA-6	BCR2G-2
Al27	<****	<****	<****	<****	<****	<****	<****	<****	<****	<****	<****	<****	<****	<****	<****	<****	<****
Si29	<****	<****	<****	<****	<****	<****	<****	<****	<****	<****	<****	<****	<****	<****	<****	<****	<****
S34	Inf	Inf	Inf	Inf	Inf	Inf	Inf	Inf	Inf	Inf	Inf	Inf	Inf	Inf	Inf	Inf	Inf
Ca43	<****	<****	<****	<****	<****	<****	<****	<****	<****	<****	<****	<****	<****	<****	<****	<****	<****
Sc45	<****	<****	<****	<****	<****	<****	<****	<****	<****	<****	<****	<****	<****	<****	<****	<****	<****
Ti49	0	0	0	0	0	0	0	0	0	0	0	0	0	0	0	0	0
V51	0	0	0	0	0	0	0	0	0	0	0	0	0	0	0	0	0
Cr53	0	0	0	0	0	0	0	0	0	0	0	0	0	0	0	0	0
Mn55	<****	<****	<****	<****	<****	<****	<****	<****	<****	<****	<****	<****	<****	<****	<****	<****	<****

Element	BG34-PY	BG34-SPH	BG34-CPY	BG34-PY2	BG35-PY	BG35-CPY	BG35-SPH	BG36-PY	BG37-PY	BG37-PY2	BG37-SPH	BG38-SPH	STD610-5	STD610-6	PGEA-5	PGEA-6	BCR2G-2
Fe57	0	0	0	0	0	0	0	0	0	0	0	0	0	0	0	0	0
Co59	0	0	0	0	0	0	0	0	0	0	0	0	0	0	0	0	0
Ni60	0.00002	0.00008	0.00006	0.00002	0.00032	0.00001	0.00001	0.00089	0.0443	0.0671	0.00018	0.00001	0.00039	0.00048	43.56	44.27	0.00168
Ni62	0.00004	0	0	0.00005	0.00028	0.00001	0	0.00072	0.00027	0.0644	0.00023	0	0.00038	0.00047	43.7	44.54	0.00139
Cu65	1.367	0.618	1146.04	0	3.6	1080.9	3.21	0.864	1944.07	1.842	9.28	0.1073	0.02121	0.0267	1.482	1.453	0.1454
Zn66	0	0	0	0	0	0	0	0	0	0	0	0	0	0	0	0	0
Ga71	<****	<****	<****	<****	<****	<****	<****	<****	<****	<****	<****	<****	<****	<****	<****	<****	<****
As75	7186.77	3.07	33.72	128.96	1523.05	11676.49	23.95	6.71	0	158.65	12.49	0	1.434	1.727	46.82	48.92	0
Se82	0.51	0.489	0.245	0.49	1.388	0.621	0	3.2	2.25	2.47	0.511	0.126	0.0783	0.0917	9.14	9.3	0
Y89	<****	<****	<****	<****	<****	<****	<****	<****	<****	<****	<****	<****	<****	<****	<****	<****	<****
Zr90	<****	<****	<****	<****	<****	<****	<****	<****	<****	<****	<****	<****	<****	<****	<****	<****	<****
Nb93	0	0	0	0	0	0	0	0	0	0	0	0	0	0	0	0	0
Mo95	<****	<****	<****	<****	<****	<****	<****	<****	<****	<****	<****	<****	<****	<****	<****	<****	<****
Ru99	0	0.081	0.448	0	0.186	0.406	0	0	0.671	0	0	0	0.00262	0	221.41	219.03	0
Ru101	0	0	0.216	0	0	0.187	0	0	0.267	0	0.024	0	0	0.00139	218.74	219.09	0
Rh103	0.221	0.194	107.78	0	0.387	100.71	0.385	0.261	173.89	0.418	0.64	0	0.1216	0.1452	1249.14	1238.5	0
Ag107	0	0	0	0	0	0	0	0	0	0	0	0	0	0	0	0	0
Pd108	0	85.31	2.95	0	0.149	1.214	110.75	0.741	10.17	1.464	122.42	111.39	0.0599	0.0839	320.22	309.87	0
Cd111	0	0	0	0	0	0	0	0	0	0	0	0	0	0	0	0	0
In115	<****	<****	<****	<****	<****	<****	<****	<****	<****	<****	<****	<****	<****	<****	<****	<****	<****
Sn118	0	0	0	0	0	0	0	0	0	0	0	0	0	0	0	0	0
Sb121	0	0	0	0	0	0	0	0	0	0	0	0	0	0	0	0	0
Te125	0.684	0.133	0.094	2	5.85	0.105	0	0.905	0.208	2.16	0.086	0	1.15	1.428	71.74	71.09	0
Te128	0.689	0.232	0.101	1.87	5.64	0.127	0	0.781	0.152	2.3	0	0.11	1.151	1.423	71.49	72.89	0.91
La139	<****	<****	<****	<****	<****	<****	<****	<****	<****	<****	<****	<****	<****	<****	<****	<****	<****
Ce140	<****	<****	<****	<****	<****	<****	<****	<****	<****	<****	<****	<****	<****	<****	<****	<****	<****
Nd146	0	0	0	0	0	0	0	0	0	0	0	0	0	0	0	0	0
Hf178	<****	<****	<****	<****	<****	<****	<****	<****	<****	<****	<****	<****	<****	<****	<****	<****	<****
W182	<****	<****	<****	<****	<****	<****	<****	<****	<****	<****	<****	<****	<****	<****	<****	<****	<****
Re185	<****	<****	<****	<****	<****	<****	<****	<****	<****	<****	<****	<****	<****	<****	<****	<****	<****
Re187	0	0	0	0	0	0	0	0	0	0	0	0	0	0	0	0	0
Os189	0	0	0	0	0	0	0	0	0	0	0	0.059	0	0	195.29	171.19	0
Os190	0	0	0	0	0	0	0	0.034	0.012	0	0	0	0	0	189.4	173.35	0
Ir193	0	0	0	0	0	0	0	0	0	0	0	0	0	0.00073	153.15	149.36	0.119
Pt195	0	0	0	0	0.0083	0.0048	0	0	0.0182	0	0	0	0.0281	0.0348	145.61	143.3	0
Au197	49.77	0	0.381	0.236	13.26	134.76	0	2.12	0.177	1.83	0.21	0.093	1.082	1.414	1078.59	1059.43	0.95
Pb208	0	0	0	0	0	0	0	0	0	0	0	0	0	0	0	0	0
Bi209	126.52	37.64	19.01	659.37	746.76	107.82	1.26	54.83	18.05	79.05	14.04	3.42	29.42	36.74	1406.18	1394.41	4.24
Th232	<****	<****	<****	<****	<****	<****	<****	<****	<****	<****	<****	<****	<****	<****	<****	<****	<****
U238	<****	<****	<****	<****	<****	<****	<****	<****	<****	<****	<****	<****	<****	<****	<****	<****	<****
ThO248	<****	<****	<****	<****	<****	<****	<****	<****	<****	<****	<****	<****	<****	<****	<****	<****	<****

GLITTER4.0: Laser Ablation Analysis Results

G:\KYLIE\MAR14\PGEARUN1 (really Run 6)
Fri Mar 14 19:52:58 2003

All values are reported in ppm

GLITTER!: Trace Element Concentrations MDL filtered.

											Discarded											
	Run6-1	Run6-2	Run6-3	Run6-4	Run6-5	Run6-6	Run6-7	Run6-8	Run6-9	Run6-10	Run6-11	Run6-12	Run6-13	Run6-14	Run6-15	Run6-16	Run6-17	Run6-18	Run6-19	Run6-20	Run6-21	Run6-22
Element	STD610-1	STD610-2	BCRG-1	PGEA-1	PGEA-2	PGEA-3	PGEA-4	WG3-PY	WG3-PY2	WG3-SU1	WG3-PY3	WG3-PY4	WG3-PY5	WG3-PY6	WG3-PY7	WG3-PY8	STD610-3	STD610-4	BCRG-2	PGEA-5	PGEA-6	PGEA-7
Al27	<0.00	<0.00	<0.00	<0.00	<0.00	<0.00	<0.00	<0.00	<0.00	<0.00	<0.00	<0.00	<0.00	<0.00	<0.00	<0.00	<0.00	<0.00	<0.00	<0.00	<0.00	<0.00
Si29	<0.00	<0.00	<0.00	<0.00	<0.00	<0.00	<0.00	<0.00	<0.00	<0.00	<0.00	<0.00	<0.00	<0.00	<0.00	<0.00	<0.00	<0.00	<0.00	<0.00	<0.00	<0.00
S34	277999.97	277999.97	47632.28	277999.97	277999.97	277999.97	277999.97	534495.5	534495.5	332171.75	534495.5	534495.5	534495.5	534495.5	534495.5	534495.5	392.3	277999.97	47632.28	277999.97	277999.97	277999.97
Ca43	<0.00	<0.00	<0.00	<0.00	<0.00	<0.00	<0.00	<0.00	<0.00	<0.00	<0.00	<0.00	<0.00	<0.00	<0.00	<0.00	<0.00	<0.00	<0.00	<0.00	<0.00	<0.00
Sc45	<-NaN	<-NaN	<-NaN	<-NaN	<-NaN	<-NaN	<-NaN	<-NaN	<-NaN	<-NaN	<-NaN	<-NaN	<-NaN	<-NaN	<-NaN	<-NaN	<-NaN	<-NaN	<-NaN	<-NaN	<-NaN	<-NaN
Ti49	<0.00	<0.00	<0.00	<0.00	<0.00	<0.00	<0.00	<0.00	<0.00	<0.00	<0.00	<0.00	<0.00	<0.00	<0.00	<0.00	<0.00	<0.00	<0.00	<0.00	<0.00	<0.00
V51	<0.00	<0.00	<0.00	<0.00	<0.00	<0.00	<0.00	<0.00	<0.00	<0.00	<0.00	<0.00	<0.00	<0.00	<0.00	<0.00	<0.00	<0.00	<0.00	<0.00	<0.00	<0.00
Cr53	<-NaN	<-NaN	<-NaN	<-NaN	<-NaN	<-NaN	<-NaN	<-NaN	<-NaN	<-NaN	<-NaN	<-NaN	<-NaN	<-NaN	<-NaN	<-NaN	<-NaN	<-NaN	<-NaN	<-NaN	<-NaN	<-NaN
Mn55	<-NaN	<-NaN	<-NaN	<-NaN	<-NaN	<-NaN	<-NaN	<-NaN	<-NaN	<-NaN	<-NaN	<-NaN	<-NaN	<-NaN	<-NaN	<-NaN	<-NaN	<-NaN	<-NaN	<-NaN	<-NaN	<-NaN
Fe57	<0.00	<0.00	<0.00	<0.00	<0.00	<0.00	<0.00	<0.00	<0.00	<0.00	<0.00	<0.00	<0.00	<0.00	<0.00	<0.00	<0.00	<0.00	<0.00	<0.00	<0.00	<0.00
Co59	<0.00	<0.00	<0.00	<0.00	<0.00	<0.00	<0.00	<0.00	<0.00	<0.00	<0.00	<0.00	<0.00	<0.00	<0.00	<0.00	<0.00	<0.00	<0.00	<0.00	<0.00	<0.00
Ni60	3755.41	4193.33	42.63	881948.19	721933.25	706358.06	709988.88	1.879	52.78	2.19	96.36	301.27	191.1	115.13	104.8	365.6	4.83	2970.97	59.24	642556.13	728683.81	713996.75
Ni62	3698.15	4218.11	45.56	892909.38	736317.63	711790.5	710558.81	1.94	54.29	1.82	92.25	298.59	189.02	114.68	101.68	364.28	4.86	2944.09	353.79	661368.69	704549.81	726901.75
Cu65	2072.8	2407.21	113.91	275.12	247.14	237.99	244.7	63.3	398.56	145.67	5413.9	931.43	1094.33	191.34	126.74	3057.46	2.687	1606.91	15.57	228.81	240.92	245.13
Zn66	<0.00	<0.00	<0.00	<0.00	<0.00	<0.00	<0.00	<0.00	<0.00	<0.00	<0.00	<0.00	<0.00	<0.00	<0.00	<0.00	<0.00	<0.00	<0.00	<0.00	<0.00	<0.00
Ga71	<-NaN	<-NaN	<-NaN	<-NaN	<-NaN	<-NaN	<-NaN	<-NaN	<-NaN	<-NaN	<-NaN	<-NaN	<-NaN	<-NaN	<-NaN	<-NaN	<-NaN	<-NaN	<-NaN	<-NaN	<-NaN	<-NaN
As75	2634.79	3021.76	<11.74	155.88	136.27	140.55	137.33	1237	14462.91	7	861.64	1348.94	1411.59	10707.17	13311.82	2559.96	3.54	2187.48	<8.53	158.53	129.69	133.96
Se82	1313.04	1675.29	<16.73	254.53	229.1	235.35	249.52	372.02	102.12	12.59	11.13	42.71	8.96	156.81	449.59	2.88	1.78	1053.87	<9.23	215.73	232.6	252.79
Y89	<-NaN	<-NaN	<-NaN	<-NaN	<-NaN	<-NaN	<-NaN	<-NaN	<-NaN	<-NaN	<-NaN	<-NaN	<-NaN	<-NaN	<-NaN	<-NaN	<-NaN	<-NaN	<-NaN	<-NaN	<-NaN	<-NaN
Zr90	<0.00	<0.00	<0.00	<0.00	<0.00	<0.00	<0.00	<0.00	<0.00	<0.00	<0.00	<0.00	<0.00	<0.00	<0.00	<0.00	<0.00	<0.00	<0.00	<0.00	<0.00	<0.00
Nb93	<-NaN	<-NaN	<-NaN	<-NaN	<-NaN	<-NaN	<-NaN	<-NaN	<-NaN	<-NaN	<-NaN	<-NaN	<-NaN	<-NaN	<-NaN	<-NaN	<-NaN	<-NaN	<-NaN	<-NaN	<-NaN	<-NaN
Mo95	<0.00	<0.00	<0.00	<0.00	<0.00	<0.00	<0.00	<0.00	<0.00	<0.00	<0.00	<0.00	<0.00	<0.00	<0.00	<0.00	<0.00	<0.00	<0.00	<0.00	<0.00	<0.00
Ru99	3.89	<1.66	0.158	234.19	187.29	226.59	226.72	<0.027	0.037	<0.055	0.293	0.847	0.79	0.164	0.129	1.398	0.0037	1.42	<0.160	175.83	228.65	232.18
Ru101	<1.11	<1.27	<0.259	229.11	190.35	225.65	225.41	0.0137	0.0114	<0.062	<0.0050	0.0074	<0.0116	<0.0176	<0.0197	0.0067	<0.00110	<0.52	<0.081	175.35	228.16	233.97
Rh103	14.16	30.91	0.33	246.71	201.12	239.85	238.31	0.0185	0.0902	0.0349	0.871	0.1263	0.161	0.0491	0.0234	0.368	0.01728	11.2	<0.043	182.74	245.53	247.1
Ag107	<0.00	<0.00	<0.00	<0.00	<0.00	<0.00	<0.00	<0.00	<0.00	<0.00	<0.00	<0.00	<0.00	<0.00	<0.00	<0.00	<0.00	<0.00	<0.00	<0.00	<0.00	<0.00
Pd108	31.2	35.16	<0.158	288.91	241.05	268.07	241.44	<0.0119	0.446	61.65	0.406	0.0054	0.0117	0.0327	<0.0104	0.2	0.0426	26.68	0.084	211.39	266.3	263.29
Cd111	<0.00	<0.00	<0.00	<0.00	<0.00	<0.00	<0.00	<0.00	<0.00	<0.00	<0.00	<0.00	<0.00	<0.00	<0.00	<0.00	<0.00	<0.00	<0.00	<0.00	<0.00	<0.00
In115	<-NaN	<-NaN	<-NaN	<-NaN	<-NaN	<-NaN	<-NaN	<-NaN	<-NaN	<-NaN	<-NaN	<-NaN	<-NaN	<-NaN	<-NaN	<-NaN	<-NaN	<-NaN	<-NaN	<-NaN	<-NaN	<-NaN
Sn118	<0.00	<0.00	<0.00	<0.00	<0.00	<0.00	<0.00	<0.00	<0.00	<0.00	<0.00	<0.00	<0.00	<0.00	<0.00	<0.00	<0.00	<0.00	<0.00	<0.00	<0.00	<0.00
Sb121	<0.00	<0.00	<0.00	<0.00	<0.00	<0.00	<0.00	<0.00	<0.00	<0.00	<0.00	<0.00	<0.00	<0.00	<0.00	<0.00	<0.00	<0.00	<0.00	<0.00	<0.00	<0.00
Te125	2253.18	2656.91	1.19	231.92	222.4	226.25	238.15	16.33	106.14	<0.39	4.07	3.67	1.5	94.3	79.55	1.077	2.96	1900.24	<0.76	209.75	239.84	252.39
Te128	2280.04	2715.51	<1.89	238.69	233.06	231.06	238.52	16.69	105	<0.57	4.15	3.98	1.366	94.59	82.08	0.928	3.01	1928.23	<1.01	220.67	234.7	253.24
La139	<0.00	<0.00	<0.00	<0.00	<0.00	<0.00	<0.00	<0.00	<0.00	<0.00	<0.00	<0.00	<0.00	<0.00	<0.00	<0.00	<0.00	<0.00	<0.00	<0.00	<0.00	<0.00
Ce140	<0.00	<0.00	<0.00	<0.00	<0.00	<0.00	<0.00	<0.00	<0.00	<0.00	<0.00	<0.00	<0.00	<0.00	<0.00	<0.00	<0.00	<0.00	<0.00	<0.00	<0.00	<0.00
Nd146	<0.00	<0.00	<0.00	<0.00	<0.00	<0.00	<0.00	<0.00	<0.00	<0.00	<0.00	<0.00	<0.00	<0.00	<0.00	<0.00	<0.00	<0.00	<0.00	<0.00	<0.00	<0.00
Hf178	<-NaN	<-NaN	<-NaN	<-NaN	<-NaN	<-NaN	<-NaN	<-NaN	<-NaN	<-NaN	<-NaN	<-NaN	<-NaN	<-NaN	<-NaN	<-NaN	<-NaN	<-NaN	<-NaN	<-NaN	<-NaN	<-NaN
W182	<-NaN	<-NaN	<-NaN	<-NaN	<-NaN	<-NaN	<-NaN	<-NaN	<-NaN	<-NaN	<-NaN	<-NaN	<-NaN	<-NaN	<-NaN	<-NaN	<-NaN	<-NaN	<-NaN	<-NaN	<-NaN	<-NaN
Re185	<-NaN	<-NaN	<-NaN	<-NaN	<-NaN	<-NaN	<-NaN	<-NaN	<-NaN	<-NaN	<-NaN	<-NaN	<-NaN	<-NaN	<-NaN	<-NaN	<-NaN	<-NaN	<-NaN	<-NaN	<-NaN	<-NaN
Re187	<0.00	<0.00	<0.00	<0.00	<0.00	<0.00	<0.00	<0.00	<0.00	<0.00	<0.00	<0.00	<0.00	<0.00	<0.00	<0.00	<0.00	<0.00	<0.00	<0.00	<0.00	<0.00
Os189	<2.54	2.55	<0.42	243.55	162.57	230.1	195.3	<0.032	<0.0250	<0.101	<0.0061	<0.0125	<0.0115	<0.029	<0.032	<0.0108	<0.00178	<1.19	<0.169	181.15	171.51	203.79
Os190	<0.55	<1.06	<0.239	237.22	158.67	233.99	191.56	<0.0272	<0.0107	<0.027	<0.0041	<0.0081	<0.0081	<0.0141	<0.0168	<0.0066	<0.00132	<0.89	<0.092	188.96	171.15	207.07
Ir193	0.53	0.36	0.082	115.67	87.05	111.11	105.54	0.0036	<0.0037	<0.0133	<0.00081	<0.00173	<0.00220	<0.0030	0.0501	<0.00207	0.00029	<0.23	0.036	82.95	103.98	107.94
Pt195	22.95	26.53	0.191	207.96	182.1	210.39	201.05	<0.0252	<0.0141	<0.062	0.0037	<0.0086	<0.0069	<0.0136	<0.0205	<0.0086	0.0347	21.61	<0.079	148.55	202.23	207.13
Au197	150.71	172.33	0.376	295.14	243.48	232.67	225.04	5.26	3.55	0.117	152.74	0.448	0.159	7.88	2.049	0.643	0.1903	115.02	0.421	204.59	237.79	239.42
Pb208	<0.00	<0.00	<0.00	<0.00	<0.00	<0.00	<0.00	<0.00	<0.00	<0.00	<0.00	<0.00	<0.00	<0.00	<0.00	<0.00	<0.00	<0.00	<0.00	<0.00	<0.00	<0.00
Bi209	3094.27	3574.98	4.33	247.42	226.88	234.14	230.26	10.41	59.44	3.09	0.379	0.0461	0.152	173.34	15.97	0.0408	3.89	2434.85	0.395	228.45	225.48	248.95
Th232	<0.00	<0.00	<0.00	<0.00	<0.00	<0.00	<0.00	<0.00	<0.00	<0.00	<0.00	<0.00	<0.00	<0.00	<0.00	<0.00	<0.00	<0.00	<0.00	<0.00	<0.00	<0.00
U238	<-NaN	<-NaN	<-NaN	<-NaN	<-NaN	<-NaN	<-NaN	<-NaN	<-NaN	<-NaN	<-NaN	<-NaN	<-NaN	<-NaN	<-NaN	<-NaN	<-NaN	<-NaN	<-NaN	<-NaN	<-NaN	<-NaN
ThO248	<-NaN	<-NaN	<-NaN	<-NaN	<-NaN	<-NaN	<-NaN	<-NaN	<-NaN	<-NaN	<-NaN	<-NaN	<-NaN	<-NaN	<-NaN	<-NaN	<-NaN	<-NaN	<-NaN	<-NaN	<-NaN	<-NaN

Element	STD610-1	STD610-2	BCRG-1	PGEA-1	PGEA-2	PGEA-3	PGEA-4	WG3-PY	WG3-PY2	WG3-SU1	WG3-PY3	WG3-PY4	WG3-PY5	WG3-PY6	WG3-PY7	WG3-PY8	STD610-3	STD610-4	BCRG-2	PGEA-5	PGEA-6	PGEA-7
GLITTER!: 1 sigma error.																						
Element	STD610-1	STD610-2	BCRG-1	PGEA-1	PGEA-2	PGEA-3	PGEA-4	WG3-PY	WG3-PY2	WG3-SU1	WG3-PY3	WG3-PY4	WG3-PY5	WG3-PY6	WG3-PY7	WG3-PY8	STD610-3	STD610-4	BCRG-2	PGEA-5	PGEA-6	PGEA-7
Al27	<0.00	<0.00	<0.00	<0.00	<0.00	<0.00	<0.00	<0.00	<0.00	<0.00	<0.00	<0.00	<0.00	<0.00	<0.00	<0.00	<0.00	<0.00	<0.00	<0.00	<0.00	<0.00
Si29	<0.00	<0.00	<0.00	<0.00	<0.00	<0.00	<0.00	<0.00	<0.00	<0.00	<0.00	<0.00	<0.00	<0.00	<0.00	<0.00	<0.00	<0.00	<0.00	<0.00	<0.00	<0.00
S34	9262.52	9794.14	1565.65	8804.51	8801.39	8815.06	8808.67	16904.69	16905.38	10513	16902.77	16903.19	16904.08	16904.78	16906	16903.36	13.29	9147.29	1535.4	8797.23	8809.55	8805.61
Ca43	<0.00	<0.00	<0.00	<0.00	<0.00	<0.00	<0.00	<0.00	<0.00	<0.00	<0.00	<0.00	<0.00	<0.00	<0.00	<0.00	<0.00	<0.00	<0.00	<0.00	<0.00	<0.00
Sc45	<0.00	<0.00	<0.00	<0.00	<0.00	<0.00	<0.00	<0.00	<0.00	<0.00	<0.00	<0.00	<0.00	<0.00	<0.00	<0.00	<0.00	<0.00	<0.00	<0.00	<0.00	<0.00
Ti49	<0.00	<0.00	<0.00	<0.00	<0.00	<0.00	<0.00	<0.00	<0.00	<0.00	<0.00	<0.00	<0.00	<0.00	<0.00	<0.00	<0.00	<0.00	<0.00	<0.00	<0.00	<0.00
V51	<0.00	<0.00	<0.00	<0.00	<0.00	<0.00	<0.00	<0.00	<0.00	<0.00	<0.00	<0.00	<0.00	<0.00	<0.00	<0.00	<0.00	<0.00	<0.00	<0.00	<0.00	<0.00
Cr53	<0.00	<0.00	<0.00	<0.00	<0.00	<0.00	<0.00	<0.00	<0.00	<0.00	<0.00	<0.00	<0.00	<0.00	<0.00	<0.00	<0.00	<0.00	<0.00	<0.00	<0.00	<0.00
Mn55	<0.00	<0.00	<0.00	<0.00	<0.00	<0.00	<0.00	<0.00	<0.00	<0.00	<0.00	<0.00	<0.00	<0.00	<0.00	<0.00	<0.00	<0.00	<0.00	<0.00	<0.00	<0.00
Fe57	<0.00	<0.00	<0.00	<0.00	<0.00	<0.00	<0.00	<0.00	<0.00	<0.00	<0.00	<0.00	<0.00	<0.00	<0.00	<0.00	<0.00	<0.00	<0.00	<0.00	<0.00	<0.00
Co59	<0.00	<0.00	<0.00	<0.00	<0.00	<0.00	<0.00	<0.00	<0.00	<0.00	<0.00	<0.00	<0.00	<0.00	<0.00	<0.00	<0.00	<0.00	<0.00	<0.00	<0.00	<0.00
Ni60	125.06	146.06	1.62	28114.54	23009.59	22530.54	22638.18	0.08	1.71	0.13	3.07	9.6	6.1	3.69	3.37	11.66	0.16	97.57	2.03	20474.87	23235.43	22762.05
Ni62	137.94	174.56	2.76	29146.86	24031.27	23248.43	23199.92	0.16	1.94	0.32	3.04	9.79	6.27	3.87	3.52	11.95	0.18	104.54	12.48	21580.18	23004.87	23729.5
Cu65	69.25	84.09	3.85	8.85	7.94	7.71	7.89	2.03	12.74	4.69	172.77	29.73	34.93	6.12	4.06	97.58	0.09	52.92	0.58	7.33	7.78	7.89
Zn66	<0.00	<0.00	<0.00	<0.00	<0.00	<0.00	<0.00	<0.00	<0.00	<0.00	<0.00	<0.00	<0.00	<0.00	<0.00	<0.00	<0.00	<0.00	<0.00	<0.00	<0.00	<0.00
Ga71	<0.00	<0.00	<0.00	<0.00	<0.00	<0.00	<0.00	<0.00	<0.00	<0.00	<0.00	<0.00	<0.00	<0.00	<0.00	<0.00	<0.00	<0.00	<0.00	<0.00	<0.00	<0.00
As75	115.21	138.23	4.5	6.68	5.72	6.62	6.42	50.35	588.39	1.54	35.06	54.88	57.44	435.59	541.57	104.15	0.15	94.69	3.31	6.58	6.33	6.21
Se82	85.65	118.31	6.39	12.97	11.5	12.89	13.28	17.92	5.05	2.14	0.57	2.09	0.6	7.62	21.68	0.32	0.11	62.19	3.65	10.64	12.33	13.01
Y89	<0.00	<0.00	<0.00	<0.00	<0.00	<0.00	<0.00	<0.00	<0.00	<0.00	<0.00	<0.00	<0.00	<0.00	<0.00	<0.00	<0.00	<0.00	<0.00	<0.00	<0.00	<0.00
Zr90	<0.00	<0.00	<0.00	<0.00	<0.00	<0.00	<0.00	<0.00	<0.00	<0.00	<0.00	<0.00	<0.00	<0.00	<0.00	<0.00	<0.00	<0.00	<0.00	<0.00	<0.00	<0.00
Nb93	<0.00	<0.00	<0.00	<0.00	<0.00	<0.00	<0.00	<0.00	<0.00	<0.00	<0.00	<0.00	<0.00	<0.00	<0.00	<0.00	<0.00	<0.00	<0.00	<0.00	<0.00	<0.00
Mo95	<0.00	<0.00	<0.00	<0.00	<0.00	<0.00	<0.00	<0.00	<0.00	<0.00	<0.00	<0.00	<0.00	<0.00	<0.00	<0.00	<0.00	<0.00	<0.00	<0.00	<0.00	<0.00
Ru99	0.96	1.14	0.077	7.6	6.08	7.47	7.4	0.01	0.013	0.022	0.014	0.037	0.042	0.021	0.022	0.056	0.00096	0.64	0.071	5.66	7.47	7.54
Ru101	0.5	0.69	0.094	7.93	6.58	7.88	7.82	0.0059	0.0058	0.023	0.0023	0.0027	0.0039	0.0065	0.0086	0.0032	0.00047	0.25	0.038	6.04	7.92	8.1
Rh103	0.84	1.82	0.04	8.39	6.84	8.18	8.11	0.0035	0.0068	0.0098	0.03	0.0056	0.0079	0.0046	0.0043	0.014	0.00094	0.56	0.018	6.21	8.36	8.41
Ag107	<0.00	<0.00	<0.00	<0.00	<0.00	<0.00	<0.00	<0.00	<0.00	<0.00	<0.00	<0.00	<0.00	<0.00	<0.00	<0.00	<0.00	<0.00	<0.00	<0.00	<0.00	<0.00
Pd108	2.36	3.26	0.072	15.11	12.6	14.05	12.64	0.0044	0.032	3.24	0.023	0.0017	0.0038	0.0066	0.0051	0.014	0.0029	1.76	0.026	11.04	13.94	13.77
Cd111	<0.00	<0.00	<0.00	<0.00	<0.00	<0.00	<0.00	<0.00	<0.00	<0.00	<0.00	<0.00	<0.00	<0.00	<0.00	<0.00	<0.00	<0.00	<0.00	<0.00	<0.00	<0.00
In115	<0.00	<0.00	<0.00	<0.00	<0.00	<0.00	<0.00	<0.00	<0.00	<0.00	<0.00	<0.00	<0.00	<0.00	<0.00	<0.00	<0.00	<0.00	<0.00	<0.00	<0.00	<0.00
Sn118	<0.00	<0.00	<0.00	<0.00	<0.00	<0.00	<0.00	<0.00	<0.00	<0.00	<0.00	<0.00	<0.00	<0.00	<0.00	<0.00	<0.00	<0.00	<0.00	<0.00	<0.00	<0.00
Sb121	<0.00	<0.00	<0.00	<0.00	<0.00	<0.00	<0.00	<0.00	<0.00	<0.00	<0.00	<0.00	<0.00	<0.00	<0.00	<0.00	<0.00	<0.00	<0.00	<0.00	<0.00	<0.00
Te125	115.83	145.32	0.39	11.39	10.87	11.36	11.76	0.84	5.14	0.17	0.21	0.2	0.11	4.55	3.89	0.079	0.15	94.65	0.33	10.15	11.87	12.38
Te128	110.77	135.44	0.74	11.36	11.07	11.06	11.37	0.81	4.98	0.22	0.2	0.2	0.084	4.48	3.9	0.059	0.15	92.69	0.41	10.46	11.19	12.05
La139	<0.00	<0.00	<0.00	<0.00	<0.00	<0.00	<0.00	<0.00	<0.00	<0.00	<0.00	<0.00	<0.00	<0.00	<0.00	<0.00	<0.00	<0.00	<0.00	<0.00	<0.00	<0.00
Ce140	<0.00	<0.00	<0.00	<0.00	<0.00	<0.00	<0.00	<0.00	<0.00	<0.00	<0.00	<0.00	<0.00	<0.00	<0.00	<0.00	<0.00	<0.00	<0.00	<0.00	<0.00	<0.00
Nd146	<0.00	<0.00	<0.00	<0.00	<0.00	<0.00	<0.00	<0.00	<0.00	<0.00	<0.00	<0.00	<0.00	<0.00	<0.00	<0.00	<0.00	<0.00	<0.00	<0.00	<0.00	<0.00
Hf178	<0.00	<0.00	<0.00	<0.00	<0.00	<0.00	<0.00	<0.00	<0.00	<0.00	<0.00	<0.00	<0.00	<0.00	<0.00	<0.00	<0.00	<0.00	<0.00	<0.00	<0.00	<0.00
W182	<0.00	<0.00	<0.00	<0.00	<0.00	<0.00	<0.00	<0.00	<0.00	<0.00	<0.00	<0.00	<0.00	<0.00	<0.00	<0.00	<0.00	<0.00	<0.00	<0.00	<0.00	<0.00
Re185	<0.00	<0.00	<0.00	<0.00	<0.00	<0.00	<0.00	<0.00	<0.00	<0.00	<0.00	<0.00	<0.00	<0.00	<0.00	<0.00	<0.00	<0.00	<0.00	<0.00	<0.00	<0.00
Re187	<0.00	<0.00	<0.00	<0.00	<0.00	<0.00	<0.00	<0.00	<0.00	<0.00	<0.00	<0.00	<0.00	<0.00	<0.00	<0.00	<0.00	<0.00	<0.00	<0.00	<0.00	<0.00
Os189	1.03	1.64	0.15	23.42	15.64	22.17	18.81	0.011	0.0091	0.034	0.0023	0.0046	0.0055	0.01	0.013	0.005	0.00077	0.51	0.08	17.4	16.53	19.61
Os190	0.34	0.72	0.086	24.48	16.38	24.17	19.78	0.0094	0.0037	0.013	0.0015	0.0032	0.0038	0.0054	0.0071	0.0026	0.00057	0.33	0.037	19.49	17.68	21.37
Ir193	0.19	0.2	0.025	4.28	3.22	4.13	3.91	0.0015	0.0014	0.005	0.00038	0.00064	0.00082	0.0013	0.0056	0.0008	0.00015	0.11	0.014	3.06	3.86	4
Pt195	1.91	2.9	0.066	7.21	6.3	7.35	6.99	0.0085	0.0063	0.022	0.0016	0.0029	0.0034	0.0048	0.0076	0.0031	0.0024	1.37	0.036	5.13	7.04	7.18
Au197	6.78	8.55	0.057	11.75	9.69	9.3	8.98	0.22	0.15	0.018	6.06	0.02	0.01	0.32	0.091	0.028	0.0084	4.95	0.044	8.14	9.49	9.54
Pb208	<0.00	<0.00	<0.00	<0.00	<0.00	<0.00	<0.00	<0.00	<0.00	<0.00	<0.00	<0.00	<0.00	<0.00	<0.00	<0.00	<0.00	<0.00	<0.00	<0.00	<0.00	<0.00
Bi209	158.93	186.27	0.26	12.57	11.52	11.91	11.7	0.53	3.02	0.17	0.02	0.0037	0.01	8.79	0.82	0.004	0.2	124.62	0.046	11.59	11.46	12.65
Th232	<0.00	<0.00	<0.00	<0.00	<0.00	<0.00	<0.00	<0.00	<0.00	<0.00	<0.00	<0.00	<0.00	<0.00	<0.00	<0.00	<0.00	<0.00	<0.00	<0.00	<0.00	<0.00
U238	<0.00	<0.00	<0.00	<0.00	<0.00	<0.00	<0.00	<0.00	<0.00	<0.00	<0.00	<0.00	<0.00	<0.00	<0.00	<0.00	<0.00	<0.00	<0.00	<0.00	<0.00	<0.00
ThO248	<0.00	<0.00	<0.00	<0.00	<0.00	<0.00	<0.00	<0.00	<0.00	<0.00	<0.00	<0.00	<0.00	<0.00	<0.00	<0.00	<0.00	<0.00	<0.00	<0.00	<0.00	<0.00
GLITTER!: Minimum detection limits (99% confidence).																						
Element	STD610-1	STD610-2	BCRG-1	PGEA-1	PGEA-2	PGEA-3	PGEA-4	WG3-PY	WG3-PY2	WG3-SU1	WG3-PY3	WG3-PY4	WG3-PY5	WG3-PY6	WG3-PY7	WG3-PY8	STD610-3	STD610-4	BCRG-2	PGEA-5	PGEA-6	PGEA-7
Al27	<0.00000	<0.00000	<0.00000	<0.00000	<0.00000	<0.00000	<0.00000	<0.00000	<0.00000	<0.00000	<0.00000	<0.00000	<0.00000	<0.00000	<0.00000	<0.00000	<0.00000	<0.00000	<0.00000	<0.00000	<0.00000	<0.00000
Si29	<0.00000	<0.00000	<0.00000	<0.00000	<0.00000	<0.00000	<0.00000	<0.00000	<0.00000	<0.00000	<0.00000	<0.00000	<0.00000	<0.00000	<0.00000	<0.00000	<0.00000	<0.00000	<0.00000	<0.00000	<0.00000	<0.00000
S34	3263.63	3657.53	570.32	197.91	112.88	380.04	385.6	63.14	47.33	268.64	17.59	69.97	90.31	137.53	73.73	43	6.99	3748.65	377.2	106.95	366.69	303.05

Element	STD610-1	STD610-2	BCRG-1	PGEA-1	PGEA-2	PGEA-3	PGEA-4	WG3-PY	WG3-PY2	WG3-SU1	WG3-PY3	WG3-PY4	WG3-PY5	WG3-PY6	WG3-PY7	WG3-PY8	STD610-3	STD610-4	BCRG-2	PGEA-5	PGEA-6	PGEA-7
Ca43	<0.00000	<0.00000	<0.00000	<0.00000	<0.00000	<0.00000	<0.00000	<0.00000	<0.00000	<0.00000	<0.00000	<0.00000	<0.00000	<0.00000	<0.00000	<0.00000	<0.00000	<0.00000	<0.00000	<0.00000	<0.00000	<0.00000
Sc45	<0.00	<0.00	<0.00	<0.00	<0.00	<0.00	<0.00	<0.00	<0.00	<0.00	<0.00	<0.00	<0.00	<0.00	<0.00	<0.00	<0.00	<0.00	<0.00	<0.00	<0.00	<0.00
Ti49	<0.00000	<0.00000	<0.00000	<0.00000	<0.00000	<0.00000	<0.00000	<0.00000	<0.00000	<0.00000	<0.00000	<0.00000	<0.00000	<0.00000	<0.00000	<0.00000	<0.00000	<0.00000	<0.00000	<0.00000	<0.00000	<0.00000
V51	<0.00000	<0.00000	<0.00000	<0.00000	<0.00000	<0.00000	<0.00000	<0.00000	<0.00000	<0.00000	<0.00000	<0.00000	<0.00000	<0.00000	<0.00000	<0.00000	<0.00000	<0.00000	<0.00000	<0.00000	<0.00000	<0.00000
Cr53	<0.00	<0.00	<0.00	<0.00	<0.00	<0.00	<0.00	<0.00	<0.00	<0.00	<0.00	<0.00	<0.00	<0.00	<0.00	<0.00	<0.00	<0.00	<0.00	<0.00	<0.00	<0.00
Mn55	<0.00	<0.00	<0.00	<0.00	<0.00	<0.00	<0.00	<0.00	<0.00	<0.00	<0.00	<0.00	<0.00	<0.00	<0.00	<0.00	<0.00	<0.00	<0.00	<0.00	<0.00	<0.00
Fe57	<0.00000	<0.00000	<0.00000	<0.00000	<0.00000	<0.00000	<0.00000	<0.00000	<0.00000	<0.00000	<0.00000	<0.00000	<0.00000	<0.00000	<0.00000	<0.00000	<0.00000	<0.00000	<0.00000	<0.00000	<0.00000	<0.00000
Co59	<0.00000	<0.00000	<0.00000	<0.00000	<0.00000	<0.00000	<0.00000	<0.00000	<0.00000	<0.00000	<0.00000	<0.00000	<0.00000	<0.00000	<0.00000	<0.00000	<0.00000	<0.00000	<0.00000	<0.00000	<0.00000	<0.00000
Ni60	2.15	2.46	0.4	0.122	1.05	0.453	0.277	0.0492	0.0295	0.121	0.00922	0.0067	0.0318	0.0269	0.0453	0.0144	0.00274	1.64	0.229	0.0498	0.257	0.22
Ni62	12.49	13.48	1.86	0.566	2.93	1.31	1.51	0.202	0.16	0.565	0.0378	0.0556	0.111	0.146	0.19	0.0523	0.0399	9.97	1.14	0.338	1.38	0.945
Cu65	2.46	2.32	0.346	0.132	0.0804	0.263	0.244	0.0436	0.0301	0.121	0.00815	0.0332	0.035	0.0338	0.0441	0.0154	0.00287	1.52	0.201	0.0608	0.227	0.176
Zn66	<0.00000	<0.00000	<0.00000	<0.00000	<0.00000	<0.00000	<0.00000	<0.00000	<0.00000	<0.00000	<0.00000	<0.00000	<0.00000	<0.00000	<0.00000	<0.00000	<0.00000	<0.00000	<0.00000	<0.00000	<0.00000	<0.00000
Ga71	<0.00	<0.00	<0.00	<0.00	<0.00	<0.00	<0.00	<0.00	<0.00	<0.00	<0.00	<0.00	<0.00	<0.00	<0.00	<0.00	<0.00	<0.00	<0.00	<0.00	<0.00	<0.00
As75	70.32	71.44	11.74	4.21	2.15	7.54	7.98	1.28	0.858	3.99	0.265	0.435	0.666	1.14	1.47	0.642	0.0998	65.73	8.53	2.46	8.5	7.24
Se82	99.07	96.31	16.73	5.88	3.19	10.44	11.28	1.85	1.23	5.15	0.33	0.528	0.808	1.28	1.67	0.69	0.104	68.69	9.23	2.61	8.9	7.72
Y89	<0.00	<0.00	<0.00	<0.00	<0.00	<0.00	<0.00	<0.00	<0.00	<0.00	<0.00	<0.00	<0.00	<0.00	<0.00	<0.00	<0.00	<0.00	<0.00	<0.00	<0.00	<0.00
Zr90	<0.00000	<0.00000	<0.00000	<0.00000	<0.00000	<0.00000	<0.00000	<0.00000	<0.00000	<0.00000	<0.00000	<0.00000	<0.00000	<0.00000	<0.00000	<0.00000	<0.00000	<0.00000	<0.00000	<0.00000	<0.00000	<0.00000
Nb93	<0.00	<0.00	<0.00	<0.00	<0.00	<0.00	<0.00	<0.00	<0.00	<0.00	<0.00	<0.00	<0.00	<0.00	<0.00	<0.00	<0.00	<0.00	<0.00	<0.00	<0.00	<0.00
Mo95	<0.00000	<0.00000	<0.00000	<0.00000	<0.00000	<0.00000	<0.00000	<0.00000	<0.00000	<0.00000	<0.00000	<0.00000	<0.00000	<0.00000	<0.00000	<0.00000	<0.00000	<0.00000	<0.00000	<0.00000	<0.00000	<0.00000
Ru99	0.779	1.66	0.129	0.108	0.0442	0.142	0.0941	0.0274	0.0198	0.055	0.00472	0.0115	0.0141	0.0267	0.024	0.00765	0.00109	1.36	0.16	0.0421	0.244	0.164
Ru101	1.11	1.27	0.259	0.0546	0.0568	0.117	0.116	0.0113	0.00889	0.0619	0.00504	0.00473	0.0116	0.0176	0.0197	0.00667	0.0011	0.519	0.0807	0.0335	0.117	0.088
Rh103	0.519	0.508	0.0548	0.0244	0.0154	0.0386	0.0463	0.00745	0.00602	0.0214	0.00161	0.00231	0.00337	0.00608	0.00737	0.0036	0.00054	0.302	0.0426	0.013	0.0376	0.0393
Ag107	<0.00000	<0.00000	<0.00000	<0.00000	<0.00000	<0.00000	<0.00000	<0.00000	<0.00000	<0.00000	<0.00000	<0.00000	<0.00000	<0.00000	<0.00000	<0.00000	<0.00000	<0.00000	<0.00000	<0.00000	<0.00000	<0.00000
Pd108	0.586	0.657	0.158	0.0333	0.0304	0.0617	0.0818	0.0119	0.0102	0.0378	0.00205	0.00288	0.00661	0.0098	0.0104	0.00622	0.00075	0.633	0.0402	0.0224	0.0957	0.038
Cd111	<0.00000	<0.00000	<0.00000	<0.00000	<0.00000	<0.00000	<0.00000	<0.00000	<0.00000	<0.00000	<0.00000	<0.00000	<0.00000	<0.00000	<0.00000	<0.00000	<0.00000	<0.00000	<0.00000	<0.00000	<0.00000	<0.00000
In115	<0.00	<0.00	<0.00	<0.00	<0.00	<0.00	<0.00	<0.00	<0.00	<0.00	<0.00	<0.00	<0.00	<0.00	<0.00	<0.00	<0.00	<0.00	<0.00	<0.00	<0.00	<0.00
Sn118	<0.00000	<0.00000	<0.00000	<0.00000	<0.00000	<0.00000	<0.00000	<0.00000	<0.00000	<0.00000	<0.00000	<0.00000	<0.00000	<0.00000	<0.00000	<0.00000	<0.00000	<0.00000	<0.00000	<0.00000	<0.00000	<0.00000
Sb121	<0.00000	<0.00000	<0.00000	<0.00000	<0.00000	<0.00000	<0.00000	<0.00000	<0.00000	<0.00000	<0.00000	<0.00000	<0.00000	<0.00000	<0.00000	<0.00000	<0.00000	<0.00000	<0.00000	<0.00000	<0.00000	<0.00000
Te125	4.73	6.28	0.637	0.466	0.245	0.287	0.467	0.0555	0.0438	0.386	0.0203	0.0521	0.0533	0.0935	0.0842	0.0502	0.00468	5.71	0.761	0.181	0.631	0.307
Te128	12.39	12.14	1.89	0.713	0.358	1.26	1.38	0.214	0.141	0.568	0.0355	0.0617	0.0912	0.154	0.196	0.0829	0.0124	8.06	1.01	0.31	1.03	0.917
La139	<0.00000	<0.00000	<0.00000	<0.00000	<0.00000	<0.00000	<0.00000	<0.00000	<0.00000	<0.00000	<0.00000	<0.00000	<0.00000	<0.00000	<0.00000	<0.00000	<0.00000	<0.00000	<0.00000	<0.00000	<0.00000	<0.00000
Ce140	<0.00000	<0.00000	<0.00000	<0.00000	<0.00000	<0.00000	<0.00000	<0.00000	<0.00000	<0.00000	<0.00000	<0.00000	<0.00000	<0.00000	<0.00000	<0.00000	<0.00000	<0.00000	<0.00000	<0.00000	<0.00000	<0.00000
Nd146	<0.00000	<0.00000	<0.00000	<0.00000	<0.00000	<0.00000	<0.00000	<0.00000	<0.00000	<0.00000	<0.00000	<0.00000	<0.00000	<0.00000	<0.00000	<0.00000	<0.00000	<0.00000	<0.00000	<0.00000	<0.00000	<0.00000
Hf178	<0.00	<0.00	<0.00	<0.00	<0.00	<0.00	<0.00	<0.00	<0.00	<0.00	<0.00	<0.00	<0.00	<0.00	<0.00	<0.00	<0.00	<0.00	<0.00	<0.00	<0.00	<0.00
W182	<0.00	<0.00	<0.00	<0.00	<0.00	<0.00	<0.00	<0.00	<0.00	<0.00	<0.00	<0.00	<0.00	<0.00	<0.00	<0.00	<0.00	<0.00	<0.00	<0.00	<0.00	<0.00
Re185	<0.00	<0.00	<0.00	<0.00	<0.00	<0.00	<0.00	<0.00	<0.00	<0.00	<0.00	<0.00	<0.00	<0.00	<0.00	<0.00	<0.00	<0.00	<0.00	<0.00	<0.00	<0.00
Re187	<0.00000	<0.00000	<0.00000	<0.00000	<0.00000	<0.00000	<0.00000	<0.00000	<0.00000	<0.00000	<0.00000	<0.00000	<0.00000	<0.00000	<0.00000	<0.00000	<0.00000	<0.00000	<0.00000	<0.00000	<0.00000	<0.00000
Os189	2.54	2.07	0.42	0.114	0.0766	0.189	0.266	0.0316	0.025	0.101	0.00609	0.0125	0.0115	0.0285	0.032	0.0108	0.00178	1.19	0.169	0.0644	0.19	0.175
Os190	0.547	1.06	0.239	0.0439	0.0621	0.129	0.175	0.0272	0.0107	0.0273	0.00405	0.00807	0.00807	0.0141	0.0168	0.00657	0.00132	0.885	0.0918	0.0362	0.126	0.0434
Ir193	0.326	0.2	0.0439	0.0151	0.0125	0.0343	0.0394	0.0027	0.0037	0.0133	0.00081	0.00173	0.0022	0.00298	0.00474	0.00207	0.00026	0.233	0.0296	0.00509	0.0308	0.0299
Pt195	0.939	0.815	0.109	0.0377	0.048	0.0698	0.0567	0.0252	0.0141	0.062	0.00318	0.00864	0.00693	0.0136	0.0205	0.00862	0.00131	0.76	0.0788	0.0284	0.0885	0.0912
Au197	0.633	0.275	0.064	0.0127	0.018	0.0408	0.0716	0.00788	0.00508	0.025	0.00136	0.00331	0.00331	0.0082	0.012	0.00381	0.00059	0.392	0.0421	0.00856	0.0366	0.0533
Pb208	<0.00000	<0.00000	<0.00000	<0.00000	<0.00000	<0.00000	<0.00000	<0.00000	<0.00000	<0.00000	<0.00000	<0.00000	<0.00000	<0.00000	<0.00000	<0.00000	<0.00000	<0.00000	<0.00000	<0.00000	<0.00000	<0.00000
Bi209	0.922	1.05	0.157	0.0506	0.0295	0.097	0.104	0.0174	0.0118	0.0423	0.00273	0.00433	0.00607	0.0337	0.0157	0.00626	0.00096	0.637	0.0784	0.0235	0.0706	0.0584
Th232	<0.00000	<0.00000	<0.00000	<0.00000	<0.00000	<0.00000	<0.00000	<0.00000	<0.00000	<0.00000	<0.00000	<0.00000	<0.00000	<0.00000	<0.00000	<0.00000	<0.00000	<0.00000	<0.00000	<0.00000	<0.00000	<0.00000
U238	<0.00	<0.00	<0.00	<0.00	<0.00	<0.00	<0.00	<0.00	<0.00	<0.00	<0.00	<0.00	<0.00	<0.00	<0.00	<0.00	<0.00	<0.00	<0.00	<0.00	<0.00	<0.00
ThO248	<0.00	<0.00	<0.00	<0.00	<0.00	<0.00	<0.00	<0.00	<0.00	<0.00	<0.00	<0.00	<0.00	<0.00	<0.00	<0.00	<0.00	<0.00	<0.00	<0.00	<0.00	<0.00
GLITTER!: Trace element concentrations normalised to chondrite.																						
Element	STD610-1	STD610-2	BCRG-1	PGEA-1	PGEA-2	PGEA-3	PGEA-4	WG3-PY	WG3-PY2	WG3-SU1	WG3-PY3	WG3-PY4	WG3-PY5	WG3-PY6	WG3-PY7	WG3-PY8	STD610-3	STD610-4	BCRG-2	PGEA-5	PGEA-6	PGEA-7
Al27	0	0	0	0	0	0	0	0	0	0	0	0	0	0	0	0	0	0	0	0	0	0
Si29	0	0	0	0	0	0	0	0	0	0	0	0	0	0	0	0	0	0	0	0	0	0
S34	Inf	Inf	Inf	Inf	Inf	Inf	Inf	Inf	Inf	Inf	Inf	Inf	Inf	Inf	Inf	Inf	Inf	Inf	Inf	Inf	Inf	Inf
Ca43	0	0	0	0	0	0	0	0	0	0	0	0	0	0	0	0	0	0	0	0	0	0
Sc45	<****	<****	<****	<****	<****	<****	<****	<****	<****	<****	<****	<****	<****	<****	<****	<****	<****	<****	<****	<****	<****	<****
Ti49	0	0	0	0	0	0	0	0	0	0	0	0	0	0	0	0	0	0	0	0	0	0
V51	0	0	0	0	0	0	0	0	0	0	0	0	0	0	0	0	0	0	0	0	0	0
Cr53	<****	<****	<****	<****	<****	<****	<****	<****	<****	<****	<****	<****	<****	<****	<****	<****	<****	<****	<****	<****	<****	<****
Mn55	<****	<****	<****	<****	<****	<****	<****	<****	<****	<****	<****	<****	<****	<****	<****	<****	<****	<****	<****	<****	<****	<****

PGEARUN6

Element	STD610-1	STD610-2	BCRG-1	PGEA-1	PGEA-2	PGEA-3	PGEA-4	WG3-PY	WG3-PY2	WG3-SU1	WG3-PY3	WG3-PY4	WG3-PY5	WG3-PY6	WG3-PY7	WG3-PY8	STD610-3	STD610-4	BCRG-2	PGEA-5	PGEA-6	PGEA-7
Fe57	0	0	0	0	0	0	0	0	0	0	0	0	0	0	0	0	0	0	0	0	0	0
Co59	0	0	0	0	0	0	0	0	0	0	0	0	0	0	0	0	0	0	0	0	0	0
Ni60	0.2276	0.2541	0.00258	53.45	43.75	42.81	43.03	0.00011	0.0032	0.00013	0.00584	0.01826	0.01158	0.00698	0.00635	0.02216	0.00029	0.1801	0.00359	38.94	44.16	43.27
Ni62	0.2241	0.256	0.00276	54.12	44.63	43.14	43.06	0.00012	0.00329	0.00011	0.00559	0.0181	0.01146	0.00695	0.00616	0.02208	0.00029	0.1784	0.02144	40.08	42.7	44.05
Cu65	12.34	14.33	0.678	1.638	1.471	1.417	1.457	0.377	2.372	0.867	32.23	5.54	6.51	1.139	0.754	18.2	0.01599	9.56	0.0927	1.362	1.434	1.459
Zn66	0	0	0	0	0	0	0	0	0	0	0	0	0	0	0	0	0	0	0	0	0	0
Ga71	<****	<****	<****	<****	<****	<****	<****	<****	<****	<****	<****	<****	<****	<****	<****	<****	<****	<****	<****	<****	<****	<****
As75	918.04	1052.88	0	54.31	47.48	48.97	47.85	431.01	5039.34	2.44	300.22	470.01	491.84	3730.72	4638.27	891.97	1.232	762.19	0	55.24	45.19	46.67
Se82	48.1	61.37	0	9.32	8.39	8.62	9.14	13.63	3.74	0.461	0.408	1.564	0.328	5.74	16.47	0.105	0.0652	38.6	0	7.9	8.52	9.26
Y89	<****	<****	<****	<****	<****	<****	<****	<****	<****	<****	<****	<****	<****	<****	<****	<****	<****	<****	<****	<****	<****	<****
Zr90	0	0	0	0	0	0	0	0	0	0	0	0	0	0	0	0	0	0	0	0	0	0
Nb93	<****	<****	<****	<****	<****	<****	<****	<****	<****	<****	<****	<****	<****	<****	<****	<****	<****	<****	<****	<****	<****	<****
Mo95	0	0	0	0	0	0	0	0	0	0	0	0	0	0	0	0	0	0	0	0	0	0
Ru99	3.64	0	0.148	218.67	174.88	211.56	211.69	0	0.034	0	0.273	0.791	0.738	0.153	0.121	1.306	0.00345	1.33	0	164.18	213.49	216.78
Ru101	0	0	0	213.92	177.73	210.69	210.46	0.0128	0.0107	0	0	0.0069	0	0	0	0.0063	0	0	0	163.73	213.04	218.46
Rh103	70.46	153.79	1.64	1227.43	1000.6	1193.26	1185.64	0.092	0.449	0.174	4.34	0.628	0.801	0.244	0.117	1.829	0.086	55.7	0	909.15	1221.54	1229.35
Ag107	0	0	0	0	0	0	0	0	0	0	0	0	0	0	0	0	0	0	0	0	0	0
Pd108	37.32	42.06	0	345.58	288.34	320.66	288.81	0	0.534	73.74	0.485	0.0065	0.014	0.0391	0	0.239	0.051	31.92	0.1	252.86	318.54	314.94
Cd111	0	0	0	0	0	0	0	0	0	0	0	0	0	0	0	0	0	0	0	0	0	0
In115	<****	<****	<****	<****	<****	<****	<****	<****	<****	<****	<****	<****	<****	<****	<****	<****	<****	<****	<****	<****	<****	<****
Sn118	0	0	0	0	0	0	0	0	0	0	0	0	0	0	0	0	0	0	0	0	0	0
Sb121	0	0	0	0	0	0	0	0	0	0	0	0	0	0	0	0	0	0	0	0	0	0
Te125	658.82	776.87	0.35	67.81	65.03	66.16	69.64	4.77	31.04	0	1.189	1.074	0.44	27.57	23.26	0.315	0.864	555.63	0	61.33	70.13	73.8
Te128	666.68	794.01	0	69.79	68.15	67.56	69.74	4.88	30.7	0	1.212	1.164	0.399	27.66	24	0.271	0.88	563.81	0	64.52	68.63	74.05
La139	0	0	0	0	0	0	0	0	0	0	0	0	0	0	0	0	0	0	0	0	0	0
Ce140	0	0	0	0	0	0	0	0	0	0	0	0	0	0	0	0	0	0	0	0	0	0
Nd146	0	0	0	0	0	0	0	0	0	0	0	0	0	0	0	0	0	0	0	0	0	0
Hf178	<****	<****	<****	<****	<****	<****	<****	<****	<****	<****	<****	<****	<****	<****	<****	<****	<****	<****	<****	<****	<****	<****
W182	<****	<****	<****	<****	<****	<****	<****	<****	<****	<****	<****	<****	<****	<****	<****	<****	<****	<****	<****	<****	<****	<****
Re185	<****	<****	<****	<****	<****	<****	<****	<****	<****	<****	<****	<****	<****	<****	<****	<****	<****	<****	<****	<****	<****	<****
Re187	0	0	0	0	0	0	0	0	0	0	0	0	0	0	0	0	0	0	0	0	0	0
Os189	0	2.43	0	232.17	154.97	219.35	186.18	0	0	0	0	0	0	0	0	0	0	0	0	172.69	163.49	194.27
Os190	0	0	0	226.14	151.26	223.06	182.61	0	0	0	0	0	0	0	0	0	0	0	0	180.13	163.15	197.4
Ir193	0.75	0.51	0.115	162.92	122.6	156.5	148.65	0.0051	0	0	0	0	0	0	0.0705	0	0.00041	0	0.05	116.84	146.44	152.03
Pt195	16.05	18.55	0.133	145.42	127.34	147.13	140.59	0	0	0	0.0026	0	0	0	0	0	0.0243	15.11	0	103.88	141.42	144.85
Au197	691.31	790.48	1.73	1353.87	1116.89	1067.31	1032.28	24.11	16.28	0.537	700.64	2.053	0.731	36.16	9.4	2.95	0.873	527.61	1.93	938.51	1090.8	1098.23
Pb208	0	0	0	0	0	0	0	0	0	0	0	0	0	0	0	0	0	0	0	0	0	0
Bi209	18528.57	21407.04	25.96	1481.56	1358.59	1402.02	1378.82	62.35	355.95	18.51	2.27	0.276	0.908	1037.95	95.65	0.244	23.32	14579.92	2.36	1367.97	1350.15	1490.71
Th232	0	0	0	0	0	0	0	0	0	0	0	0	0	0	0	0	0	0	0	0	0	0
U238	<****	<****	<****	<****	<****	<****	<****	<****	<****	<****	<****	<****	<****	<****	<****	<****	<****	<****	<****	<****	<****	<****
ThO248	<****	<****	<****	<****	<****	<****	<****	<****	<****	<****	<****	<****	<****	<****	<****	<****	<****	<****	<****	<****	<****	<****

Appendix 8
Fluid inclusion results

Appendix 8 - Fluid Inclusion Results (Big Gossan and Wanagon Gold)

Date	sample	area/ grain	position	Description	Mineral		Tfr		Ti		Tm	Salinity	THH(hydrohalite)	Thh (halite)	Th (up)	Th (down)	Phase	heating order	heating comments	Remarks
BIG GOSSAN																				
02/10/03	BG26 (BGU26-4-327.5)	M	3	inclusion with L+V in sph	Sph		-60		-25		-9	13							gone dark - can't see	
02/10/03	BG26 (BGU26-4-327.5)	M	2	inclusion with L+V in sph	Sph	?		~	-20		-5	8			230	213	L+V-->L	1	heat 10/2/03 #1	
02/10/03	BG26 (BGU26-4-327.5)	M	6	inclusion with L+V inc sph. Large striated inc (1x40x)	Sph		-42	?~	-20		-7	10							has gone dark - can't see	
13/02/03	BG26 (BGU26-4-327.5)	I	3	inclusion with L+V in sph	Sph		-58	?			-3	5			239	205	L+V-->L	1	heat 13/2/03 #1	
02/10/03	BG26 (BGU26-4-327.5)	M	7	inclusion with L+V in sph	Sph		-41.2				-7.3	11			256	240	L+V-->L	2	heat 10/2/03 #2	
02/10/03	BG26 (BGU26-4-327.5)	M	5	inclusion with L+V in sph	Sph	?		?			-5	8			250	?	L+V-->L	3	heat 10/2/03 #3	
02/10/03	BG26 (BGU26-4-327.5)	M	1	inclusion with L+V in sph	Sph	?		?			-10	14			250	225	L+V-->L	4	heat 10/2/03 #4	
02/10/03	BG26 (BGU26-4-327.5)	M	4	inclusion with L+V in sph	Sph	?		?			-9	13							gone dark - can't see	
13/02/03	BG26 (BGU26-4-327.5)	I	6	inclusion with L+V in qtz grain in host. Brown ice. Dark inc near 5	Qtz				-40		-25	26			392	370.3	L+V-->L	9	heat 13/2/03 #9	
13/02/03	BG26 (BGU26-4-327.5)	I	12	inclusion with L+V in qtz grain in host. Near 11	Qtz		-53		-34		-16	19			385	355	L+V-->L	4	heat 13/2/03 #4	
13/02/03	BG26 (BGU26-4-327.5)	I	10	inclusion with L+V in qtz grain in host. Top one, near 11	Qtz		-52		-32		-15	19			375	355	L+V-->L	2	heat 13/2/03 #2	
13/02/03	BG26 (BGU26-4-327.5)	I	11	inclusion with L+V in qtz grain in host. bottom one, Near 10	Qtz	?			-33		-18	21			400	385	L+V-->L	3	heat 13/2/03 #3	
13/02/03	BG26 (BGU26-4-327.5)	I	14	inclusion with L+V in qtz grain in host. Right one	Qtz		-56		-30		-14.5	18			395	370	L+V-->L	5	heat 13/2/03 #5	
13/02/03	BG26 (BGU26-4-327.5)	I	13	inclusion with L+V in qtz grain in host. Left one	Qtz		-55		-30		-14.5	18			400		L+V-->L	6	heat 13/2/03 #6	
13/02/03	BG26 (BGU26-4-327.5)	I	5	inclusion with L+V in qtz grain in host. Brown ice.	Qtz	?	-70		-33		-24	25			349	327	L+V-->L	10	heat 13/2/03 #10	
13/02/03	BG26 (BGU26-4-327.5)	M	9	inclusion with L+V in qtz grain in host.	Qtz	~	-30	<	-20		-2.3	4							heat 13/2/03 # can't see	
13/02/03	BG26 (BGU26-4-327.5)	M	10	inclusion with L+V in qtz grain in host.	Qtz	?		?			-3.3	5			305	284	L+V-->L	1	heat 13/2/03 #1	
13/02/03	BG26 (BGU26-4-327.5)	I	15	inclusion with L+V in qtz grain in host.	Qtz	?		?			-8.5	12			345	330	L+V-->L	1	heat 13/2/03 #1	
13/02/03	BG26 (BGU26-4-327.5)	I	9	inclusion with L+V in qtz grain in host. Some brown ice	Qtz		-70				-20	22			358	338	L+V-->L	7	heat 13/2/03 #7	
13/02/03	BG26 (BGU26-4-327.5)	I	8	inclusion with L+V in qtz grain in host.	Qtz	?		?			-4	6			350	326	L+V-->L	8	heat 13/2/03 #8	
13/02/03	BG26 (BGU26-4-327.5)	M	8	inclusion with L+V+?S in qtz grain in host. Image = 1x40X	Qtz	?		?			-2.2	4							heat 13/2/03 # can't see, >380	
13/02/03	BG26 (BGU26-4-327.5)	M	11	inclusion with L+V+?S in qtz grain in host.	Qtz	?		?			-2	3							heat 13/2/03 can't see phase change	
13/02/03	BG26 (BGU26-4-327.5)	I	1	inclusion with L+V in qtz at margins of Su vein. Near 2	Qtz2		-48.6	?			-12	16			366	345	L+V-->L	3	heat 13/2/03 #3	
13/02/03	BG26 (BGU26-4-327.5)	I	2	inclusion with L+V in qtz at margins of Su vein. Near 1	Qtz2		-52		-40		-13	17			359	338	L+V-->L	2	heat 13/2/03 #2	
02/10/03	BG25 (BGU27-5-22)	E	8	small inclusion with L+V in late qtz. Same cluster as #6,7 - adjacent to #6	Qtz		-40				-5	8			190	165	L+V-->L	1	heat 10/2/03 #1	
02/05/03	BG25 (BGU27-5-22)	G	4	inclusion with L+V	Qtz		-35				-3.9	6			270	253	L+V-->L	2	heat 4/2/03 #2	
02/10/03	BG25 (BGU27-5-22)	E	7	inclusion with L+V in late qtz. Same cluster as #6	Qtz		-39.6	?			-5.1	8			170	112	L+V-->L	2	heat 10/2/03 #2 very sure	
02/05/03	BG25 (BGU27-5-22)	G	5	inclusion with L+V	Qtz		-39.5				-5.1	8			265		L+V-->L	1	heat 4/2/03 #1	bubble gone and decrop at 268
02/05/03	BG25 (BGU27-5-22)	G	3	inclusion with L+V	Qtz		-35.6				-6.2	9			260	235	L+V-->L	3	heat 4/2/03 #3	
02/10/03	BG25 (BGU27-5-22)	E	6	inclusion with L+V in late qtz. Good large inc	Qtz		-39	~	-23		-6.4	10			300	284	L+V-->L	3	heat 10/2/03 #3	

Appendix 8 - Fluid Inclusion Results (Big Gossan and Wanagon Gold)

Date	sample	area/ grain	position	Description	Mineral		Tfr		Ti		Tm	Salinity	THH(hydrohalite)	Thh (halite)	Th (up)	Th (down)	Phase	heating order	heating comments	Remarks
02/05/03	BG25 (BGU27-5-22)	G	1	inclusion with L+V	Qtz		-38.7				-5.8	9			260	240	L+V-->L	4	heat 4/2/03 #4	
02/05/03	BG25 (BGU27-5-22)	G	2	inclusion with L+V	Qtz						-1.9	3			270	245	L+V-->L	5	heat 4/2/03 #5	
02/11/03	BG27 (BGU26-3-122.4)	D	1	inclusion with L+V in cte/qtz? (dirty) after py.	?qtz-ccte		-34				-3	5			160	109	L+V-->L	1	heat 11/2/03 #1	
02/11/03	BG27 (BGU26-3-122.4)	A	4	inclusion with L+V in qtz after py. Top	Qtz	?					-6.5	10			185	132	L+V-->L	1	heat 11/2/03 #1	
02/11/03	BG27 (BGU26-3-122.4)	A	6	inclusion with L+V in qtz after py. Second from top	Qtz		-39.8				-6	9			245	208	L+V-->L	2	heat 11/2/03 #2	
02/11/03	BG27 (BGU26-3-122.4)	A	1	inclusion with L+V in qtz after py. Bottom one	Qtz		-39				-6	9			255	222	L+V-->L	3	heat 11/2/03 #3	
02/11/03	BG27 (BGU26-3-122.4)	A	2	inclusion with L+V in qtz after py. Second at left	Qtz		-39				-5	8			260	228	L+V-->L	4	heat 11/2/03 #4	
02/11/03	BG27 (BGU26-3-122.4)	A	7	inclusion with L+V in qtz after py. Right centre.	Qtz	?					-6.5	10			275	246	L+V-->L	5	heat 11/2/03 #5	
02/11/03	BG27 (BGU26-3-122.4)	A	3	inclusion with L+V in qtz after py. Far left	Qtz		-39				-5	8			260	240	L+V-->L	6	heat 11/2/03 #6	
02/11/03	BG27 (BGU26-3-122.4)	A	8	inclusion with L+V in qtz after py Deeper in section.	Qtz		-40			?	-7	10			200	170	L+V-->L	7	heat 11/2/03 #7	
02/11/03	BG27 (BGU26-3-122.4)	A	5	inclusion with L+V in qtz after py. Large one at centre (long clear centre area)	Qtz		-40				-6.9	10							heat 11/2/03 can't see	
02/11/03	BG28 (BGU30-4-137.9)	C	2	inclusion with L+V in qtz after su	Qtz		-30	<	-20		-1.5	3			250	225	L+V-->L	1	heat 11/2/03 #1	
02/11/03	BG28 (BGU30-4-137.9)	C	3	inclusion with L+V in qtz after su	Qtz		?~-30	<	-20		-2	3			245	224	L+V-->L	2	heat 11/2/03 #2	
02/11/03	BG28 (BGU30-4-137.9)	C	1	inclusion with L+V in qtz after su	Qtz	?		?			-0.5	1			270	246	L+V-->L	3	heat 11/2/03 #3	
02/11/03	BG28 (BGU30-4-137.9)	C	5	inclusion with L+V in qtz after su	Qtz		-31	?<	-20		-1.9	3			268	246	L+V-->L	4	heat 11/2/03 #4	
02/11/03	BG28 (BGU30-4-137.9)	C	4	inclusion with L+V in qtz after su	Qtz	?		?			-1.2	2							heat 11/2/03 can't see - too small	
14/02/03	JL10 (BGU30-03-180B)	E	3	L+V inclusion in quartz with/post sulphides	Qtz		-43				-10	14							heat 14/2/03 can't see	
14/02/03	JL10 (BGU30-03-180B)	E	1	L+V inclusion in quartz with/post sulphides	Qtz	?		?			-7	10							heat 14/2/03 can't see	
23/03/03	BG06	a	1	inclusion with L+V in cbt alteration margin	CBT	?		~	-25		-12	16						2	can't see but >300	
23/03/03	BG06	a	2	inclusion with L+V in cbt alteration margin	CBT		-65		-32		-19	22					L+V-->L	3	too dark	
23/03/03	BG06	a	3	inclusion with L+V in cbt alteration margin	CBT		-63.5		-31		-19.5	22			325	296	L+V-->L	5	heat 23/03/03	
23/03/03	BG06	a	4	inclusion with L+V in cbt alteration margin	CBT		-64.7	~	-30		-18	21			321	296	L+V-->L	4	heat 23/03/03	
23/03/03	BG06	a	5	inclusion with L+V in cbt alteration margin	CBT		-61.7		-32		-18.8	22					L+V-->L			
23/03/03	BG06	a	6	inclusion with L+V in cbt alteration margin	CBT		-58.7		-31		-16.5	20			322	292	L+V-->L	6	heat 23/03/03	
23/03/03	BG06	a	7	inclusion with L+V in cbt alteration margin	CBT		-65.4		-33		-18.7	21			283	250	L+V-->L	1	heat 23/03/03	
23/03/03	BG06	a	8	inclusion with L+V in cbt alteration margin	CBT		-63	~	-30		-19	22					L+V-->L			
WANAGON GOLD																				
29/01/03	JL01-D	grain jl1d1-12	12	inc with v bubble, small inclusion adjacent has same charateristics on freezing	sst		-39.4		-16		-3.1	5			275	250?	L+V-->L	7	heat 31/1 #7	grain near edge. Abundant inclusions

Appendix 8 - Fluid Inclusion Results (Big Gossan and Wanagon Gold)

Date	sample	area/ grain	position	Description	Mineral		Tfr		Ti		Tm	Salinity	THH(hydrohalite)	Thh (halite)	Th (up)	Th (down)	Phase	heating order	heating comments	Remarks
02/02/03	JL01-B		4	inclusion with V. long inc in centre	sst		-43	<~	-20		-5	8			345	330	L+V-->L	13	heat 2/2/03 #13	
02/04/03	JL01-B		18a	inclusion with L+V v. close to #18	sst		-44	~<	-20	~	-5	8							too dark	
02/02/03	JL01-B		7	inclusion with V. long inc on secondary inc	sst		-45	<~	-20		-3	5			300		L+V-->L	3	heat 2/2/03 #3 - aprox	
02/02/03	JL01-B		1	inclusion with V	sst	~	-40	<~	-20	~	-3	5			353	273	L+V-->L	14	heat 2/2/03 #14	
02/02/03	JL01-B		10	inclusion with V. same train as 8 and 9 (to the left of location 8 and 9)	sst	?		<~	-20		-2.9	5			272	252	L+V-->L	4	heat 2/2/03 #4	
02/04/03	JL01-B		21	inclusion with L+V	sst	?	-39	~<	-20		-2.8	5			295	276	L+V-->L	11	heat 4/2/03 #11	
02/04/03	JL01-B		18	inclusion with L+V	sst	?		~<	-20		-2.5	4			294	376	L+V-->L	1	heat 4/2/03 #1	
02/04/03	JL01-B		19	inclusion with L+V, photo 1x	sst	?		~<	-20		-2.5	4			342	326	L+V-->L	9	heat 4/2/03 #9	
02/02/03	JL01-B		15a	inclusion with V. Big Inclusion adjacent	sst		-30.8	<	-20		-2.1	4			345	330	L+V-->L	9	heat 2/2/03 #9	
02/02/03	JL01-B		15	inclusion with V. Big Inclusion adjacent to this is the same	sst		-30.8	<	-20		-2.1	4			347	330	L+V-->L	9	heat 2/2/03 #9	
02/02/03	JL01-B		3	inclusion with V	sst	?		<~	-20	~	-2	3						1	heat 2/2/03 #1 Decrepitate	
02/02/03	JL01-B		16	inclusion with V and ?S. irregular shaped near edge. Photo at 1x?	sst		-35		-20		-2	3			332	315	L+V-->L	10	heat 2/2/03 #10	
02/02/03	JL01-B		2	inclusion with V	sst		-42	<~	-20	~	-2	3			380	360	L+V-->L	18	heat 2/2/03 #18	
02/02/03	JL01-B		9a	inclusion with V. above #10	sst	?		<~	-20		-2	3					L+V-->L	19	heat 2/2/03 #19	
02/04/03	JL01-B		22	inclusion with L+V. near 21	sst	?		~<	-20		-2	3			350	320	L+V-->L	12	heat 4/2/03 #12	
02/02/03	JL01-B		5	inclusion with V. near 4, overlapping inc	sst		-41	<~	-20	~	-1.8	3			370	358	L+V-->L	16	heat 2/2/03 #16	
02/04/03	JL01-B		27	small inclusion with L+V	sst			?	-20		-1.7	3			309	290	L+V-->L	7	heat 4/2/03 #7	
02/04/03	JL01-B		20	inclusion with L+V	sst	?		~<	-20		-1.5	3			248	225	L+V-->L	10	heat 4/2/03 #10	
02/04/03	JL01-B		28	inclusion with L+V. large irregular inc. photo 1x	sst		-33.4	?	-20		-1	2			300	281	L+V-->L	8	heat 4/2/03 #8	
29/01/03	JL01-D	grain jl1d1-12	4	type 1 inclusion	sst		-41	<	-20	~	-6.0	9			265	240	L+V-->L	2	heat 31/1 #2	near edge. Abundant inclusions
29/01/03	JL01-D	grain jl1d1-12	5a	smaller inc along same trail as large one, poss xall	sst	~	-40	<	-20		-5.5	9							heat 31/1 #4 can't see	near edge. Abundant inclusions
29/01/03	JL01-D	grain jl1d1-12	5	large type 1 inc	sst		-37.5	<	-20	~	-4.0	6			245	220	L+V-->L	3	heat 31/1 #3	Decrepitated at ~400, near edge. Abundant inclusions
31/01/03	JL01-D	grain jl1d1-12	15	inclusion with V	sst	?		<	-20		-3.2	5			375	360	L+V-->L	11	heat 31/1 #11 BUT after heat to 450 - inclusion stretched?	near edge. Abundant inclusions
29/01/03	JL01-D	grain jl1d1-12	9	inclusion with V	sst		-40	~	-20		-3.0	5			230	210	L+V-->L	5	heat 31/1 #5	near edge. Abundant inclusions
29/01/03	JL01-D	grain jl1d1-12	6	inc with V and large halite cube.	sst	~	-38	<	-20	~			-2	X						Decrepitated at >300, near edge. Abundant inclusions
02/02/03	JL01-B		14	inclusion with V. right one	sst		-44		-22.5		-7.7	11			300	280	L+V-->L	8	heat 2/2/03 #8	

Appendix 8 - Fluid Inclusion Results (Big Gossan and Wanagon Gold)

Date	sample	area/ grain	position	Description	Mineral		Tfr		Ti		Tm	Salinity	THH(hydrohalite)	Thh (halite)	Th (up)	Th (down)	Phase	heating order	heating comments	Remarks
02/02/03	JL01-B		13	inclusion with V. triangle inc. photo at 1.6x possible solids - or way liquid moves while heating?	sst	?			-23		-3.1	5			345	327	L+V-->L	7	heat 2/2/03 #7	
02/02/03	JL01-B		11	inclusion with V	sst		-44	~	-24		-2.5	4			280	260	L+V-->L	5	heat 2/2/03 #5	
02/02/03	JL01-B		8a	inclusion with V. inclusions on trail. Long one on left	sst		-45		-25	~	-8	12			300	270	L+V-->L	2	heat 2/2/03 #2	
29/01/03	JL01-D	grain jl1d1-12	10	inclusion with V bubble. Brown fluid seem to melt first. also contains a solid?	sst		-38.3	~	-25	~	-3.0	5			264	244	L+V-->L	6	heat 31/1 #6	near edge. Abundant inclusions
02/02/03	JL01-B		8	inclusion with V. inclusions on trail - good square one	sst		-39		-28		-3.2	5			300	280	L+V-->L	2	heat 2/2/03 #2	
29/01/03	JL01-D	grain jl1d1-12	11	inclusion with V bubble and possibly crystal. Brown melts first	sst		-52.5	~	-29	~	-15.6	19			265	238	L+V-->L	10	heat 31/1 #10	near edge. Abundant inclusions
02/04/03	JL01-B		26a	inclusion with L+V. middle irregular shaped	sst			~	-40		-23	24			283	259	L+V-->L	16	heat 4/2/03 #16	
02/04/03	JL01-B		26	inclusion with L+V, top - shell shaped inc	sst	?	-75		-45		-23	24			250	230	L+V-->L	14	heat 4/2/03 #14	
02/02/03	JL01-B		6	inclusion with V. rectangular inc	sst		-80		-50	~	-26	26			360	330	L+V-->L	17	heat 2/2/03 #17	
29/01/03	JL01-D	grain jl1d1-12	7	inclusion with V and large xall? Or with 2 bubbles?	sst		-67.5	~	-57		-28.0	27	can't see it		330	310	L+V-->L	9	heat 31/1 #9	near edge. Abundant inclusions
02/04/03	JL01-B		29b	inclusion with L+V. top one	sst						-34	31							? Decrep?	
02/04/03	JL01-B		29a	inclusion with L+V. bottom large	sst						-30	29			350	320	L+V-->L	17	heat 4/2/03 #17	
02/04/03	JL01-B		30a	Clear quartz at edge (new qtz?) inclusion with L+V+S	sst	?	-40			?	-15	19			330	315	L+V-->L	5	heat 4/2/03 #5	NB need to check solid to see if is calcite. This inc may have samll amount of CO2, making lower melting temp.
02/04/03	JL01-B		23	inclusion with L+V. bottom one	sst	?		?			-7	10					L+V-->L		can't see too dark	
02/02/03	JL01-B		9	inclusion with V. inclusions on trail (same as 8). Bottom inc	sst	~	-40	?		~	-5	8			350	337	L+V-->L	12	heat 2/2/03 #12	
02/04/03	JL01-B		32c	inclusion with L+V. smaller right inc	sst		-38.9				-5	8			321	310	L+V-->L	6	heat 4/2/03 #6	
02/02/03	JL01-B		8b	inclusion with V. inclusions on trail. Small round one at right	sst		-39.5	?			-4	6			300	280	L+V-->L	2	heat 2/2/03 #2	
02/02/03	JL01-B		17	inclusion with L+V	sst		-39	?			-4	6			345	328	L+V-->L	11	heat 2/2/03 #11	
02/02/03	JL01-B		14a	inclusion with V. left bottom one	sst	?		?			-3.8	6			300	280	L+V-->L	8	heat 2/2/03 #8	
02/02/03	JL01-B		12	inclusion with V. hard to see inc	sst	?		?			-2.7	4						6	heat 2/2/03 #6. Can't see it	
02/04/03	JL01-B		32a	inclusion with L+V left inc	sst		-38.5				-1.8	3			205	170	L+V-->L	2	heat 4/2/03 #2	
02/04/03	JL01-B		31	inclusion with L+V	sst		-37				-1.7	3			310	291	L+V-->L	22	heat 4/2/03 #22	
02/04/03	JL01-B		25	inclusion with L+V. large one on same trail as 24.	sst		-40				-1.5	3					L+V-->L		heat 4/2/03 too dark	
02/04/03	JL01-B		32b	inclusion with L+V. centre large inc	sst		-38.9				-1	2							>400 v. large v bubble	
02/04/03	JL01-B		33	inclusion with L+V	sst		-28.7				-0.5	1							can't see - dark	
29/01/03	JL01-D	grain jl1d1-12	8	inclusion with V	sst		can't see								285	250	L+V-->L	1	heat 31/1 #1	near edge. Abundant inclusions

Appendix 8 - Fluid Inclusion Results (Big Gossan and Wanagon Gold)

Date	sample	area/ grain	position	Description	Mineral		Tfr		Ti		Tm	Salinity	THH(hydrohalite)	Thh (halite)	Th (up)	Th (down)	Phase	heating order	heating comments	Remarks
29/01/03	JL01-D	grain jl1d1-13	3	type 1 inclusion	sst		-40													near edge. Abundant inclusions
29/01/03	JL01-D	grain jl1d1-14	1	inc with abundant solids? Cannot see any phase changes.	sst															near edge. Abundant inclusions
02/12/03	JL03	A	13	inclusion with L+V in sst. Long clear one	Sst	?			-40	?	-23	24					L+V-->L		heat 12/2/03 can't see	
02/12/03	JL03	A	1	inclusion adjacent to py vein with L+V+S in sst. Hh disapears at +12	Sst		-76	~	-39	~	-20	22	12		319	280	L+V-->L	9	heat 12/2/03 #9	can't see solid?
02/12/03	JL03	A	2	inclusion with L+V in sst. Bottom one	Sst	?			-40	~	-18	21					L+V-->L		heat 12/2/03 # can't see. ?>380?	
02/12/03	JL03	A	5	inclusion with L+V in sst. Not on trail	Sst		-53	~	-30		-12	16					L+V-->L		heat 12/2/03 can't see	
02/12/03	JL03	A	8	inclusion with L+V in sst. Large V bubble at top	Sst		-41.2	~<	-25	~	-7	10			410	392	L+V-->L	5	heat 12/2/03 #5	
02/12/03	JL03	A	9	inclusion with L+V in sst. Right bottom	Sst		-41.8	~<	-20		-5	8			319	292	L+V-->L	4	heat 12/2/03 #4	
02/12/03	JL03	A	14	inclusion with L+V in sst.	Sst		-75.8	?			-20	22					L+V-->L		heat 12/2/03 can't see	
02/12/03	JL03	A	7	inclusion with L+V in sst. Small bubble	Sst		-47	?			-14	18					L+V-->L		heat 12/2/03 can't see	
02/12/03	JL03	A	12	inclusion with L+V in sst. ? Solids?	Sst		-47	?			-10	14			400		L+V-->L	6	heat 12/2/03 #6 >400	
02/12/03	JL03	A	6	inclusion with L+V in sst.	Sst		-44.5	?		~	-9	13			355	335	L+V-->L	3	heat 12/2/03 #3	
02/12/03	JL03	A	15	inclusion with L+V in sst. Best one	Sst		-40	?			-5.7	9			365	348	L+V-->L	7	heat 12/2/03 #7	
02/12/03	JL03	A	10	inclusion with L+V in sst. Long middle one (bubble at top)	Sst		-40	?			-5.5	9			380	355	L+V-->L	5	heat 12/2/03 #5	
02/12/03	JL03	A	16	inclusion with L+V in sst.	Sst	?		?			-5	8			355	306	L+V-->L	8	heat 12/2/03 #8	
02/12/03	JL03	A	11	inclusion with L+V in sst. Bottom at left (clear end)	Sst		-40	?			-5	8					L+V-->L		heat 12/2/03 too dark	
02/12/03	JL03	A	3	inclusion with L+V in sst.	Sst	?		?			-2	3			160	106	L+V-->L	1	heat 12/2/03 #1	
02/12/03	JL03	A	4	inclusion with L+V in sst. Near 3	Sst	?		?			-2	3					L+V-->L	2	heat 12/2/03 #2 >280. Decrep	
14/2/03	JL05 (WAN4-5-50B)	A	2	inclusion with L+V in sst same grain as 1.	Qtz						-2.6	4			375	358	L+V-->L	2	heat 13/2/03 #2	
02/04/03	JL01-B		26b	inclusion with L+V+S, bottom round inc. solid appears at +15degrees (maybe halite is unstable?)	sst	~	-79				-26	26	?		250	230	L+V-->L	15	heat 4/2/03 #15	
02/04/03	JL01-B		30c	inclusion with L+V+S. along same trail further along.	sst	?	-40			?	-5	8			250	237	L+V-->L	3	heat 4/2/03 #3	NB need to check solid to see if is calcite.
02/04/03	JL01-B		30b	inclusion with L+V+S	sst	?	-40			?	-5	8			290	270	L+V-->L	4	heat 4/2/03 #4	NB need to check solid to see if is calcite.
02/04/03	JL01-B		24	inclusion with L+V+HH	sst		-80		-50		-26	26	-6		300	275	L+V-->L	20	heat 4/2/03 #20/23	? Solid also present? And remains until >400. - v. small inc, likely not!

Appendix 8 - Fluid Inclusion Results (Big Gossan and Wanagon Gold)

Date	sample	area/ grain	position	Description	Mineral		Tfr		Ti		Tm	Salinity	THH(hydrohalite)	Thh (halite)	Th (up)	Th (down)	Phase	heating order	heating comments	Remarks
31/01/03	JL01-D	grain jl1d1-12	14	round inclusion with solids (Bin pers comm)	sst		-70		-55		-24.8	25	16		340	322	L+V+S-->L+S	8	heat 31/1 #8	Heated to 450 and no dissolution of ?halite near edge. Abundant inclusions
14/2/03	JL05 (WAN4-5-50B)	A	1	inclusion with L+V+S in sst.	Qtz		?>-70		-40		-25	26			330	302	L+V-->L	1	heat 13/2/03 #1. NB solid does nothing on heating (? Check if calcite)	

Appendix 9

Sulphur isotope sample descriptions and results

Appendix 9 - Sulphur isotopes

Drillhole sample number	Sample annotation (Appendix 2)	Mineral	Paragenesis (Section B)	d34S w.r.t. CDT (permil)	Comments
BGU28-05-268	BG01	Chalcopyrite	1	2.88	LA-ICPMS Technique.
BGU28-05-268	BG01	Pyrite	2	3.88	LA-ICPMS Technique.
BGU24-10-305	BG05	Chalcopyrite	1	0.21	LA-ICPMS Technique. Photo site A.
BGU24-10-305	BG05	Pyrite	1	2.49	LA-ICPMS Technique. Photo site B.
BGU24-10-305	BG05	Galena	2	2.98	LA-ICPMS Technique. Photo site D, adj. Sph.
BGU24-10-305	BG05	Sphalerite	2	1.36	LA-ICPMS Technique. Photo site C.
BGU19-03-184.7	BG13	Chalcopyrite	2	2.18	LA-ICPMS Technique.
BGU19-03-184.7	BG13	Pyrite	2	1.71	LA-ICPMS Technique.
BGU19-03-184.7	BG13	Sphalerite	2	3.75	LA-ICPMS Technique.
BGU28-08-375	BG14	Pyrite	2	0.12	Conventional technique
BGU24-11-343	BG24	Pyrite	2	2.41	LA-ICPMS Technique. Photo site A
BGU24-11-343	BG24	Chalcopyrite	2	2.22	LA-ICPMS Technique. " " B
BGU24-11-343	BG24	Galena	2	-0.46	LA-ICPMS Technique. " " C
BGU24-11-343	BG24	Sphalerite	2	4.35	LA-ICPMS Technique. " " D
BG1-4A-330	BG4a	Chalcopyrite	2	4.11	LA-ICPMS Technique. 3 grains, area B,C and adj.
BG1-4A-330	BG4a	Pyrite	2	1.08	LA-ICPMS Technique. At section rim near site A.
BG1-4A-330	BG4a	Sphalerite	2	2	LA-ICPMS Technique. Second (backup) location.
BG1-4A-330	BG4a	Marcasite	2	0.27	LA-ICPMS Technique.
BGU21-2-13.3B	JL06	Pyrite	2	2.91	LA-ICPMS Technique. Photo extra site, site B
BGU21-2-13.3B	JL06	Pyrite-repeat	2	1.14	LA-ICPMS Technique.
BGU21-2-13.3B	JL06	Aspy-marcasite	2	3.71	LA-ICPMS Technique. Photo site C.
WAN2-2-852	KP09	Galena	1	-0.49	LA-ICPMS Technique. Photo site C.
WAN2-2-852	KP09	Pyrite	1	3.8	LA-ICPMS Technique. Photo site A.
WAN4-6-28	KP10	Pyrite	2	-0.67	Conventional technique
WAN4-3-302.5	KP11	Chalcopyrite	1	0.83	LA-ICPMS Technique. Photo site B,C.
WAN4-3-302.5	KP11	Pyrite	1	5.05	LA-ICPMS Technique. Photo site A.
WAN4-3-302.5	KP11	Sphalerite	1	1.87	LA-ICPMS Technique. Photo site B,C.
Sample Description: Appendix 2a, 10					

Appendix 10

Sample and polished section descriptions and local sample paragenesis

(Big Gossan, Wanagon Gold, EESS, GRS125, West Grasberg)

Big Gossan Polished Section Paragenesis

	Earliest Events						?Second Stage						Late Stage Events					
sample id	Mt	Py (1 OR 2)	Po	Hem Mt	Cpy	Mixed (cpy-dom,dark-sph,po,gn)	py	Sph-dom (mnr gn, cpy)	Pale-sph, gn (mnr cpy)	Bi minerals	Tetrahedrite minerals	Carbonate	Apy	late gn	Marcasite-pyrite	Au	Paragenesis	Minerals
BGU18-03-211.2		X						X?	X? check sph							y	1	inclusion-rich carbonate (2 inc types)
														Or Gn-Au			2	carbonate xalls and py, sph, mnr gn, Au and Au-Fe-S mineral with Au
																	3	late clay/tremolitte?
BGU21-10-12		X															1	pyrite
												Fe-Mn					2	Fe-Mn-Mg carbonate alteration and infill
								dark-pale									2?	Gn, cpy, sph (Probe=dark and light - Fe-bearing and no real chem variation)
													X				3	Apy late
																	5	
BGU21-3-24.3																	1	undulose qtz infill
																	2	cbt xalls
		X															3	cubic py
Same as 21-2-13.3								dark-pale									4	red and pale sph (mnr cpy-gn). Gn usually with pale sph. Dk sph has cpy inc?
													X?		X		5	apy-marc
																	6	qtz
																	7	fg orange cbt
BGU21-2-13.3A							X										1	py-au
								?	X								2	
													X?				3	apy-marc
BGU21-2-13.3B							X											
								?	X									
													X?					
BGU24-13-143.5		X															1	cubic pyrite (mnr po spots)
								X									2	red sph and gn (cpy mnr)
																	2a	- gn veins sph
															X?		3	fg pyrite
																	4	ccte (possibly with py above?)
													X?				5	Apy (white) and? blue mineral (with galena?)?
BGU26-1-151.9		X															1	cubic pyrite - no inclusions
117g/t								X									2	red sphalerite and mnr gn
													X		X		?	mnr Apy +- marcasite
BGU26-1-152.3	X																1	magnetite
117g/t		X															2	Pyrite
								X									2a	red sphalerite-gn-cpy
													X		X		3	arsenopyrite-marcasite
																	4?	coarse grained infill carbonate
																	5	Fe-ox
BGU26-01-151		X														y	1	coarse py and cpy and qtz vein
117g/t						X- ?Au		?					X				2	cpy and apy (mnr) and mnr po and dark sphalerite
															?		2a	fg py at edges
														X-Au?			3	galena with High Ag gold inclusion
BGU27-5-124		X															1	pyrite
								dark-pale									2	red-pale sph (mostly red), gn, mnr cpy
BGU27-5-124.1		X															1	pyrite
						?X											2	cpy and gn, rare sphalerite
BGU28-1-104		X															1	cubic pyrite
								dark-pal	?X								2	red-pale sphalerite and cpy (gn)

Big Gossan Polished Section Paragenesis

	Earliest Events						?Second Stage						Late Stage Events					
sample id	Mt	Py (1 OR 2)	Po	Hem Mt	Cpy	Mixed (cpy-dom,dark-sph,po,gn)	py	Sph-dom (mnr gn, cpy)	Pale-sph, gn (mnr cpy)	Bi minerals	Tetrahedrite minerals	Carbonate	Apy	late gn	Marcasite-pyrite	Au	Paragenesis	Minerals
															X		3	fine py
													X				?	arsenopyrite?
BGU28-7-230		X	X alt		X			dark-pale-check sph				X?					1	po and py
																	2	cpy - marc alteration of po
																	3	Vein of red (mnr pale) sphalerite - mnr gn and cpy
																	4	quartz-cbt pyrite cubes
																	5	coarse carbonate crystalline in vein with sph/gn
															X		6	marcasite? - fibrous mineral
BG1-4-229	X	X						X									1	early colloform py with mt? Inclusions. Very dusty
																	2	dark-Sphalerite dominant (rare po spots). Mnr cpy. Rare gn
																	3	later crystalline pyrite and minor chalcopyrite
															X		4	paler white marcasite?
																	5?	euhedral quartz fragments crosscut by stage4?
BG1-7-167		X						X									1	silica
																	2	cubic pyrite, dominant red sph, gn, (cpy with mnr po)
																	2a	galena after sph
													X				2b	mnr apy
BGU19-03-184.7		X				X			X-Au				X			v	1	(qtz, cbt) crs py
																	2	po, cpy, mnr gn, Apy (mnr dark-Fe-rich Sph)
																	3	qtz, sph (pale), cpy, Au and mnr py?
																	4	late clay altn (hem?) esp alt po and sph
BGU22-1-8	X																1	mt
		X															2	pyrite
								mnr pale sph, cpy									3	mnr sph (pale) and cpy
BGU24-11-343							X-Au									y	1	crs py (Au in py)
																	2	cpy?
									X-Au	Bi-Ag-S	Bi-Sb-As-Ag	X					3	(Pale no-Fe) sph, cpy, Au with Gn, Bi and tet; Mnr Cbt
BGU24-10-305		?X		X	X											v	1	cpy and mt/hem
		X			X												1?	coarse py and cpy and qtz vein
								X	X-Au(gn)		Cu>Fe-As-S-	X					2	sph (pale?##),gn, Au (low fineness) cbt, qtz?vein +py?
																	3	late yellow banded mineral
BGU27-02-204.5							X-?Au									Y	1	py (with Au, gn and cpy spots)
				X	X-?Au	X-?Au		?									2	cpy, mnr po, sph, and hem-mt
														X			3	mnr gn alteration of cpy
BGU27-06-348.5		1															1	crs py
						2		?									2	dk brown sph and cpy
													3				3	late apy after cpy
BGU27-06-349		X														v	1	crs py
						X-Au?		?	Bi-Te-S and Bi-S in py				X				2	cpy, dk sph (Fe-bearing), mnr apy (? Timing)
														X-Au?			3	gn last (Au in gn and in py)
BGU07-06-342		X															1	Crs py, mnr grey (CHECK###) inc
					X												2	cpy and Au?
BGU08-01-225		X															1	crs py
						X											2	cpy+ dk sph and po (v. altered)
BGU08-05-190.1		X															1	Crs py
						X											2	cpy, sph, gn, po (usually in cpy)
BGU18-03-212					X		X						X				1	cpy clasts
																	1a?	coarse py
																	2	cpy, gn, apy
																	?	py altn of hem

Big Gossan Polished Section Paragenesis

	Earliest Events						?Second Stage						Late Stage Events					
sample id	Mt	Py (1 OR 2)	Po	Hem Mt	Cpy	Mixed (cpy-dom,dark-sph,po,gn)	py	Sph-dom (mnr gn, cpy)	Pale-sph, gn (mnr cpy)	Bi minerals	Tetrahedrite minerals	Carbonate	Apy	late gn	Marcasite-pyrite	Au	Paragenesis	Minerals
BGU21-03-224.5	X	X				X											1	crs py, mt (no hem)
																	2	cpy and sph, mnr grey (gn?) and mnr po
BGU21-10-236.7A						X							X				1	cpy with mnr sph, apy, po
														X			2	gn in fx and voids
BGU21-10-236.7B	X	X															1	mt
																	2	pyrite
						X											3	cpy with mnr po, sph, white mins?
BGU21-3-225.1	X																1	magnetite - broken and disaggregated
		X															2	cubic py
						sph+cpy											3	red sphalerite+cpy (Au grain in sph) + pink (bornite?)
																	4	calcite
																	5	
BGU21-3-225.5	X																1	Magnetite
		X															2	Pyrite (minor high relief grey mineral - galena? In pyrite) Mt in py
						sph+cpy											3	red sphalerite, intergrown with cpy
BGU21-3-226.3	X																1	Magnetite
		X															2	pyrite
						sph+cpy											3	red sph + cpy + mnr gn
BGU21-1-20.4		X															1	pyrite
						sph+cpy (po)											2	red sphalerite, cpy (mnr po)
BGU23-3-180	X																1	skarn minerals and magnetite
		X															2	pyrite
						cpy (sph)											3	chalcopyrite and mnr red sph
																	4	late covelite, appears to alter sphalerite
BGU23-8-212.6	X																1	pyrite
						cpy-gn											2	chalcopyrite and galena (or Apy?)
BGU23-6-80		(X)	X		X	X?											1	po and cpy (with mnr py, sph)
													X		X		2	late marc-pyrite and apy
BGU26-10-121.5				X													1	strange prismatic magnetite
		X															2	coarse pyrite
						X											3	interstitial cpy, red sph
																	3a?	galena vein (no timing with cpy and spy)
																	5?	timing? - carbonate
																	6?	timing? - quartz crystal infill
BGU28-08-375							X										1	massive py
								X									2	po, cpy, sph, gn
BGU28-08-375.5							X										2?	crs py
								X					X				2	cpy-sph, gn, apy
BGU29-1-159		X															1	pyrite
						X											2	red sph and gn (mnr cpy
BGU29-2-242		X															1	pyrite
						X											2	red sph, gn mnr cpy
													X				3	apy
																	?	carbonate
BGU30-3-180			X														1	po (clast)
		X															2	pyrite
						X											3	cpy, gn and red sph

Big Gossan Polished Section Paragenesis

	Earliest Events						?Second Stage						Late Stage Events					
sample id	Mt	Py (1 OR 2)	Po	Hem Mt	Cpy	Mixed (cpy-dom,dark-sph,po,gn)	py	Sph-dom (mnr gn, cpy)	Pale-sph, gn (mnr cpy)	Bi minerals	Tetrahedrite minerals	Carbonate	Apy	late gn	Marcasite-pyrite	Au	Paragenesis	Minerals
													X		X		4	marc/apy?
BGU30-3-180B		X	X			X							X		X		1	po (clast)
																	2	pyrite
																	3	cpy, gn and red sph
																	4	marc/apy?
BGU30-6-173		X	X			X?											?	po clast
																	2	pyrite
																	3	cpy, red-sphalerite
BGU30-05-246		X				X-?Au					Cu-Fe-Sb-As-S, Cu-Fe-As-Ag-S					v	1	coarse py
																	2	cpy, sph, gn, ?apy. Au with gn-cpy (high Ag)
																	2	Gold with Tet. On py fx. Not clear if separate stage
BG01-05-238		X				X?							X				1	cg py, mnr po inc
																	2	cpy and apy (mnr gn and sph)
															X		3	late py-marc (also alters apy)
BGU21-5-17.5	X	X															1	mt
			X		X												2	pyrite
																	3	cpy and po
BGU22-1-15.2	X	X															1	mt
			X		X												2	pyrite
																	3	cpy and mnr po
BGU24-13-139		X															1	quartz crystalls
			X		X												2	cubic pyrite (abundant) Mnr grey ?galena in pyrite
																	3	interstitial po and cpy and cubanite. Mnr sph stars in cpy
																	4	(??check timing) calcite with Fl
																	5	Fe-ox alteration
BGU26-1-165.2		X		X												y	1	garnet and magnetite (skarn)
			X														2	py
																	2a	po
					X												3	cpy
																	?	W mineral Scheelite at py grain boundaries. Also Cu-Zn-Fe-S mineral
BGU26-02-207A		X		X													1	Crs py (hem-untimed)
			X		X												2	po and cpy
			alt												?		3	py-marc-apy alteration of po
BGU26-02-207B		X		X													1	Crs py (Au in py) untimed hem-mt
			X		X												2	po and cpy
			alt												?		3	py-marc-apy alteration of po
BGU27-04-174		X															1	crs py
			X-?Au	X	X											Y	2	cpy, large po, hem-mt bladed (observed one Au in po but lost it). Mnr sph
BGU30-6-179		X														v	1	py?
			X														2	po (possibly gold?)
			alt		X?-Au										X?-Au		3	cpy-marcasite/py-Au-
																	?	mnr gn? Spots with cpy? Or within po
BGU21-10-251.4A	X	X															1	Magnetite
																	2	Pyrite (minor high relief grey mineral - galena? In pyrite)
					X												3	chalcopyrite
BGU21-3-234.4	X	X															1	epidote
																	2	pyrite
					X												3	chalcopyrite

Big Gossan Polished Section Paragenesis

	Earliest Events						?Second Stage						Late Stage Events					
sample id	Mt	Py (1 OR 2)	Po	Hem Mt	Cpy	Mixed (cpy-dom,dark-sph,po,gn)	py	Sph-dom (mnr gn, cpy)	Pale-sph, gn (mnr cpy)	Bi minerals	Tetrahedrite minerals	Carbonate	Apy	late gn	Marcasite-pyrite	Au	Paragenesis	Minerals
								X									?4	pale sphalerite focussed in vein within other sulphides
BGU21-10-251.4B	X																1	Magnetite
		X															2	Pyrite (minor high relief grey mineral - galena? In pyrite)
					X												3	chalcopyrite
BGU21-2-14	X	X			X-Au										X	y	1	early = mt, py, cpy, Au and Mo-Sb-Ag and W-Ca (scheelite) mineral
							sph-dom vn					X					2	Other end of sample is sph, py, cpy, (check probe results) and cbt vein
BGU23-8-212		X															1	pyrite
					X					?	?		?				2	chalcopyrite and grey and white minerals
BGU24-08-255.2		X															1	crs py
					X												2	Mnr Cpy
BGU28-05-268					X											y	1	cpy in host
							X											Coarse Py, hem/mt
										X-Au							3?	Au with Grey (gn?) and brown-yellow min (cubanite)
BGU28-05-267							X-Au									y	1	Coarse Py and Au
				X wit	X-Au												2	cpy and hem/mt and Au
BGU30-8-186.5																y	1	
																	2	
BG1-4-330							X										1	cubic pyrite
missing						?sph-cpy		?	?X-check								2	sphalerite and cpy
															X		3	marcasite - elongate, fibrous texture - orthorhombic
BG1-4a-400							X-Au?									y	1	cubic pyrite
																	1?	gold
						?X-check		?	?X-check								2	cpy + sph
BG1-5-256																y	1	carbonate
																	2	carbonate
		X															3	cubic pyrite
						?X-check		?	?X-check								4?	cpy and sp (gn). (Probe= As-Zn includions in sphalerite)
															X		5	marcasite? - fg-fibrous
													X				6	arsenopyrite - zoned
															X		7	colloform pyrite
																	8	fine grained quartz
																	9	dust layer in fg quartz
																	10	quartz xalls
BG1-7-190	X																1	Magnetite
		X															2	pyrite - foram shaped
														?X			3	minor galena

Wanagon Gold Sample Descriptions (this and other studies)

Sample_No	Description	Rock-type	Lith Unit	Hydrothermal system	Infill/Alteration	Petrographic description (paragenesis)	Reference
WAN4-2-234B	sp, py and carbonate	Brecciated carbonate	Tw-bx		Marble	2 types of sphal. Outer one has no cpy disease, easily present in transmitted light. Marcasite present - fibrous in matrix on sphal margins.	Gavin clarke pers comm 2000
WAN4-2-234A	sp, py and carbonate	Brecciated carbonate	Tw-bx		Marble	Qtz seems to infil around py. Strained margins, small cct xalls overprinting boundaries. Cct seems to vein qtz infilland overprint. Py has overgrown qtz xall (changing extinction). cubic py postdated by diseased sphal. Sphal overprints one cct xall. cct changes from crs to v.f.g. (Gav) Timing between carbonate alteration and brecciation not established. Breccia matrix comprised of cpy, sph, ga.	Gavin clarke pers comm 2000
WAN4-3-80.5A	sandstone with vughs, pyrite and clay	Quartzite	Kke	quartz, sulphide, clay	quartz, sulphide, clay	Minor fibrous crustals in holes (PROBE). Minor amount of plagioclase grains. Clarke (2000) interpretation = alteration/leaching of alkali-feldspar and deposition of quartz, clay, sulphide	Gavin clarke pers comm 2000
WAN4-3-80.5B	sandstone with vughs, pyrite and clay	Quartzite	Kke	quartz, sulphide, clay	quartz, sulphide, clay	Clarke (2000) interpretation = alteration/leaching of alkali-feldspar and deposition of quartz, clay, sulphide	Gavin clarke pers comm 2000
WAN4-3-103.6	py and vein	quartzofeldspathic rock	Kke		garnet?	quartz (with sulphide) alteration of garnets, carbonate alteration of alkali-feldspar, patchy chlorite-epidote, clay alteration last	Gavin clarke pers comm 2000
WAN4-3-108.1	py, chlorite, ser, cpy (and Au)	Pyroxene skarn	Kkel	skarn	garnet, pyroxene	skarn overprinted by calcite and feathery silica and sulphides. Later marcsaite and calcite. Last = calcite.	Gavin clarke pers comm 2000
WAN4-3-303.6A	sphalerite, clac, py	Garnet skarn	Tw	skarn, late si, late ccte, sulphides	garnet	Garnet abundant. Sulphides and ?hydrous? mineral alter garnets. Nice garnet zoning. Clay? vein after sulphides. calcite veins late.	Gavin clarke pers comm 2000
WAN4-3-303.6B	sphalerite, clac, py	Garnet skarn	Tw	skarn, late si, late ccte, sulphides	garnet, pyroxene	skarn overprinted by calcite and feathery silica and sulphides. Later marcsaite and calcite. Last = calcite.	Gavin clarke pers comm 2000
WAN4-3-303.4	py, ser, sp	Garnet skarn	Tw	skarn	garnet, pyroxene	Abundant grt zoning. skarn overprinted by calcite and feathery silica and sulphides. Later marcsaite and calcite. Last = calcite vns	Gavin clarke pers comm 2000
WAN4-1-127		Quartzite - fine grained	Kke		K-feldspathised and silicified	silicified. Sericitisation of plagioclase; quartz; orthoclase and with clay as replacement of feldspar. Orthoclase as graphic intergrowths with quartz; clasts; veins; interstitial secondary aggregates. Chlorite alteration of biotite. Mnr py with sphalerite with cpy inclusions, mnr galena	Honea, pers comm 1996b (Jan 22)
WAN4-2-234		Sulphide-dominant	Tw-bx		sulphide-rich marbelised host	Quartz-replacing Tremolite. Sphalerite enclosing coarse-grained pyrite.	Honea, pers comm 1996b (Jan 22)
WAN4-2-243		oolitic limestone	Tw-bx		recrystallised/dolomitised/marbelised calcite.	cross-cut by organic and sulphide bearing stylolites.	Honea, pers comm 1996b (Jan 22)
WAN4-2-264		brecciated oolitic limestone	Tw-bx		Magnetite, pyrite recrystallised calcite matrix. Quartz-replacement of oolites. Dolomite.	Dolomite is with magnetite and epidote and all replace calcite. Calcite has deformation structure	Honea, pers comm 1996b (Jan 22)

Wanagon Gold Sample Descriptions (this and other studies)

Sample_No	Description	Rock-type	Lith Unit	Hydrothermal system	Infill/Alteration	Petrographic description (paragenesis)	Reference
WAN4-2-295		Sandstone replaced by calcite and tremolite (diopside-grossularite)	Tw-bx	skarn	Tremolite-diopside-grossularite hornfels	Calcite with incipient development of tremolite needles. Garnet replaces calcite. Calcite replaces original quartz. Pyrophyllite present. Non-foliated	Honea, pers comm 1996b (Jan 22)
WAN4-2-296.5		Hornfels - very fine grained calcareous, silicified	Tw/Kkeh	potassic	calcareous and K-feldspathised.	Orthoclase replaces v.f. grained calcite. Trace recrystallised calcite associated with magnetite. Epidote in silicified matrix and as veins. Also calcite, sphalerite veins.	Honea, pers comm 1996b (Jan 22)
WAN4-2-345		Hornfels - very fine grained calcareous, silicified	Kkel	skarn	diopside-tremolite	Tremolite corrodes quartz and Acicular crystals part-altered to diopside (? or vise versa?). Diopside-quartz-tremolite-calcite-garnet are associated. Calcite may contain incipient development of tremolite. Trace platey clay. Calcite veins. Non- foliated	Honea, pers comm 1996b (Jan 22)
WAN4-3-54		Sandstone - f-m grained	Kke	pyritic and K-feldspar -bearing	pyritic and K-feldspar -bearing	Orthoclase as clasts and as matrix. Plagioclase (albite twinning) with sericite alteration. Feathery chalcedony interstitial to clastic grains. Interstitial clay (smectite/illite). Veins of quartz, sphene, sulphides.	Honea, pers comm 1996b (Jan 22)
WAN4-3-56.3		Quartzite	Kke	pyritic and K-feldspar -bearing	pyritic and K-feldspar -bearing	Orthoclase interstitial to quartz clasts. Also - chert, siltstone, zircon, sulphides, sericite (illite?)	Honea, pers comm 1996b (Jan 22)
WAN4-3-138.5		Limestone - fine grained	Kkel		orthoclase, epidote, garnet, silica	calcite replaced by fine grained quartz and epidote. V.f.g. orthoclase as matrix. Epidote with crystalline calcite, magnetite and sphene (banded appearance). 2 garnets - One with epidote and pyrite. 2nd = grossularite replaced by late calcite. Tremolite, sulphides.	Honea, pers comm 1996b (Jan 22)
WAN4-3-226		Hornfels - fine grained	Kke	skarn, potassic	garnet, tremolite, orthoclase, calcite, sulphides	Zoned garnet associated with tremolite and calcite. Fibrous tremolite interstitial and included in garnet. K-feldspar - late mineral infill around garnets. Dirty calcite with garnet, magnetite and quartz. Tourmaline in calcite. Sulphides	Honea, pers comm 1996b (Jan 22)
WAN4-3-288.4		Siltstone	Kke	recrystallised calcite, tremolite, epidote, silicified (hornfels!!)	recrystallised calcite, tremolite, epidote, silicified (hornfels!!)	Orthoclase replacing fine grained calcite. Calcite has inclusions. Quartz replaces fine grained calcite. Dolomite present. Calcite veins	Honea, pers comm 1996b (Jan 22)
WAN4-3-324		Marble	Tw		recrystallised calcite.	recrystallised calcite with pressure lamellar twinning. Possible incipient tremolite. f.g. disseminated pyrite. stylolites and superimposed mineralised veinlets	Honea, pers comm 1996b (Jan 22)
WAN-FW-TW						Polished section description	Honea, pers comm 1996a (Jan 3)
WAN4-4-125.5			Kke			Polished section description	Honea, pers comm 1996a (Jan 3)

Wanagon Gold Sample Descriptions (this and other studies)

Sample_No	Description	Rock-type	Lith Unit	Hydrothermal system	Infill/Alteration	Petrographic description (paragenesis)	Reference
WAN4-4-381.5			Kke			Polished section description	Honea, pers comm 1996a (Jan 3)
WAN4-5-189			Kke			Polished section description	Honea, pers comm 1996a (Jan 3)
WAN4-5-278						Polished section description	Honea, pers comm 1996a (Jan 3)
WAN4-6-181						Polished section description	Honea, pers comm 1996a (Jan 3)
WAN4-6-217						Polished section description	Honea, pers comm 1996a (Jan 3)
WAN4-236.5A	sp and py with 50/50 carbonate and stannite						This Study
WAN4-2-245.2A	carbonate host with py, gal, sp		Tw-bx			Mnr py cubes in v.f.g. cct dominated rock. Abundant spotted grt over qtz and ?. can see grt grown on c.g. cct contacts, sphal has overgrown cct gns. Grt in pale sphal?	This Study
WAN1-1-494.4	Black calcareous rock with su (highly oxidised)		Tw				This Study
WAN1-3-181							This Study
WAN1-3-758	green alteration (3 different colours - 3 minerals?) with later mt veinlets		Tw				This Study
WAN1-3-759	mt-rich rock (zone) with areas of medium green. This appears to be altered to pale green and overprinted by py cubes and surrounding cpy. Can see pale green vein cutting mt.		Tw				This Study
WAN1-3-776	green and ? Skarn? Alteration with overprinting mt vn with mnr later su-veins. This is postdated by overprinting 1mm veins of soft opaque-white material (anhydrite/cct?) which offset the su veinlets		Tw				This Study
WAN1-3-781	coarse pyrite?-rich sample with later sulphide vein and qtz with fine disseminated sulphide		Tw				This Study
WAN1-3-789.7	epidote and ? Skarn alteration with crosscutting mt veins postdated by py veins. Mnr pale orange material - garnets?		Tw				This Study
WAN1-3-791.6	py with fibrous-bladed texture and mt and orange weathered carbonate?		Tw				This Study
WAN1-3-818.5	Igneous? Bleached and brown alteration		Tipw				This Study

Wanagon Gold Sample Descriptions (this and other studies)

Sample_No	Description	Rock-type	Lith Unit	Hydrothermal system	Infill/Alteration	Petrographic description (paragenesis)	Reference
WAN1-3-821	Tw? Red altered rock		Tipw				This Study
WAN4-236.5B	sp and py with 50/50 carbonate and stannite			gn+sph, ?Cu		can clearly see gn and sphal veins in py (cubic). Sphal is diseased. Nice eg of py/cpy along cleavage in sphal. Abundant pale gry mineral (Tennanite? Thing) on margins of other su. Cpy with gn and as veins in sphal.	This Study
WAN4-1-22	MS		Tw				This Study
WAN4-1-22.5	3cm massive py		Tw/Kke				This Study
WAN4-1-58A	sphalerite vn, low angle to CA, 1 cm wide		Kke			Variable sphal with lots of inclusions - it is infill around py and gangue. Gangue is euhedral crystals (qtz?) and some twinned laths, mnr fine high bired grains. Fe Ox alteration. Py with coarse gangue. Inclusion trails in qtz. Some undulous qtz (with fspar inc) with py	This Study
WAN4-1-58B1	sphalerite vn, low angle to CA, 1 cm wide		Kke				This Study
WAN4-1-58B2	sphalerite vn, low angle to CA, 1 cm wide		Kke				This Study
WAN4-1-183	si-rock (qtzite) with py vns and yellow? Clay?		Kke				This Study
WAN4-1-362	Qtzite (with red alteration), 3m zone		Kke				This Study
WAN4-2-210	black cbs bx		Tw				This Study
WAN4-2-245.2B	carbonate host with py, gal, sp		Tw				This Study
WAN4-2-300	black veinlets in vfg pale orange "hornfels" rock		Tw/Kkeh				This Study
WAN4-2-307			Tw/Kkeh	skarn, sphal + py, late ccte		matrix = v.f.g. grey mineral with fibrous inclusions. Vn in centre of section with fibrous materail (amphibole) and high biref epidote on vein margins. Also fx filled with chlorite, xcutting epi. Mnr sphal and py. Can see py postdating one stage of cct, can see cct cutting py and sphal. coarse vein Cct replaced by amphibole	This Study
WAN4-2-313	v. pale green alteration (start of 7m zone)		Kkeh/Kkel ?				This Study
WAN4-2-314A	1m bx (cbs lmst?) within pale green zone (313-320)		Kkeh/Kkel ?			Gunge with v.f.g. sulphides	This Study
WAN4-2-314B			Kkeh/Kkel ?				This Study
WAN4-2-357.2	Green skarn rock, looks partly si.		Kkel				This Study
WAN4-3-134.5	Calcrudite, slightly coarser grained than shale		Kkel				This Study
WAN4-3-193.5	1cm py vn in si-qtzite		Kkel				This Study
WAN4-3-234	lmst bx		Kke				This Study
WAN4-3-256	contact between skarn alteration and si-alteration		Kke				This Study
WAN4-3-288	"hornfels" f.g. with black specs and py		Kkeh				This Study
WAN4-3-348	Tw? - marble		Tw				This Study
WAN4-5-21.6	si, vughs, su alteration		Kke				This Study
WAN4-5-39.5	40cm zone of bx in qtzite, fe-ox matrix. Monolithic and rounded mill fragments		Kke				This Study

Wanagon Gold Sample Descriptions (this and other studies)

Sample_No	Description	Rock-type	Lith Unit	Hydrothermal system	Infill/Alteration	Petrographic description (paragenesis)	Reference
WAN4-5-44.2	Si quartzite, vughy with su and clay (original?, slightly yellow)		Kke				This Study
WAN4-5-50B	1cm py vein in si and vughy quartzite, abundant diss py and in vughs		Kke			Creamy rounded qtz grains, xcut by fx with su and f.g. grey interstitial mineral. Mnr py. Mnr py and gy reflective mineral with f.g. interstitial material (isotropic). Can see vughs filled with f.g. sulphide and gunge (clay?)	This Study
WAN4-5-50A	1cm py vein in si and vughy quartzite, abundant diss py and in vughs		Kke			Crs py with fx filled with stuff and fine su at edge of vugh. Mnr pale grey mineral. Py with fine su and gunge and corroded and blue min.	This Study
WAN4-5-90.5	2cm py vn in si, vughy and su qtzite (mnr massive su)		Kke				This Study
WAN4-5-174.5	calcrudite		Kke				This Study
WAN4-5-182	MS		Kke				This Study
WAN4-5-199.5	granular with patchy skarn alteration and diss cpy? (sandy siltstone precursor)		Kkel				This Study
WAN4-5-205	Eg of skarn alteration in calcrudite		Kkel				This Study
WAN4-5-211A	si alteration and massive py (and cubic infill) vns		Kkel				This Study
WAN4-5-211B	si alteration and massive py (and cubic infill) vns		Kkel				This Study

	GRS127 1004-1011						
	Zone of intermittant massive magnetite clearly replaced by su or clay						
	Patchy skarn zones with chlorite alteration. Abundant later white-milky coarse quartz veins have bx skarn assemblages.						
	Sulphides associated with qtz veins - py, cpy, gy-min (hem/gn?) mnr bornite.						
Stage	**Name**	**Name**	**Sample #**	**Alteration/infill**	**Channelway - structur**	**Host**	**Comments**
		Magnetite		Magnetite - alteration and infill?	likely overprinting a fault zone as at Kl		
		Coarse py (+cpy?)		Brassy veins and spots in mt	micro-fx (can see some of the coarse spots are interconnected		
		(timing w.r.t. below?) dull fine py (cpy???)		veins in mt - infill	micro vein and stockwork style - possible postdates coarse py/cpy at 1023.3m - reusing fx		also some more massive diss py assoc with clay - same?
		(timing w.r.t. above?) Clay - talc? (oxidised?)		clay alteration of su-spotty mt rock. Can see shiny soft clay grains - talc-ser? Shiney silver mineral present rimming cpy spots - may be spec-hematite - very fine grained - can't identify.	Narrow shear zones (15cm) with fabric (weak to strong) and pervasive alteration either side. Zones <4m		difficult to establish timing of clay and py - appear very assoc - (obviously using same channelways). In vughs can tell timing by infill order - however doesn't preclude more than one of each event!!!
		Coarse cpy-qtz-bornite		Veins infill - comb texture qtz	vn - brittle fx parallel to CA		Postdates fine diss dull py at 1008m

		GRS127 848-878					
		Grey silica with small vughs or neworks with pale silica(?+ clay? + py?)					
		At 878m is faulted contact with HS (slickensides 45 degrees to CA)					
Stage	**Name**	**Name**	**Sample #**	**Alteration/infill**	**Channelway - structural**	**Host**	**Comments**
		med- gy quartz		silica + ? Alteration of ??	pervasive	Silicified rock	alteration of cbt
		leaching		vughs in med-gy silica	patchy intensity but pervasive	Silicified rock	likely that med-gy silica was pre leaching (or a result of it??!!)
		Clay +- py		clay - py infill in vughs and fx. Also as alteration causing leaching of gy? - or is it the white material - ccte as below	microfracture and pervasive infill of vughs	Silicified rock	py xalls also in vughs with clay
		White material - possible cct - may be assoc with stage above…		veins and alteration	Ccte content inc towards the HS contact - hence dk-gy host inc in whiteness. Some of these are qtz veins as below although some fizz (may be ccte assoc with leaching???).	Carbonate	can also see micro fx of white in gy material with py along them. Unsure if stage above or below?
		White qtz?		veins /alteration of grey material.	microfx and veins		unsure how much is as stages above and how much due to qtz.
		Clay (?same as above)		infill and alteration	inc of clay in fx towards the Hs contact	Carbonate	Same event as above? - likely!
		(timing?) black material		infill of black material	veins and fx - stylolitic in form and predominantly near the Hs contact	Carbonate	Also appear to be in the HS - appear to postdate the clay
		fine py (silver mineral - gn or hem?)		disseminated vein infill	overprint the stylolitic-type black fx/veins	Carbonate	timing dependant on that of clay above - likely to be the same.
		HS py		massive alteration/infill of py	Fault zone as evidenced by the inclination of other stages to increase in concn near contact with HS.		stage dependent on timing of clay and black material - may be the sme as fine py as above - is it distinct to py in vughs with cy
		Sulphur?		alteration of cy filled fx?	reusing fx filled with cy		from 870m cy is yellowish in places - sulphur? - or else different cy (likely the first suggestion

GRS125 747-768

	GRS125 - 747-768m						
Stage	**Name**	**Name**	**Sample #**	**Alteration/infill**	**Channelway - structural**	**Host**	**Comments**
1	Sphalerite	Sphalerite	766.8	Alteration? Of silica-rich? Host. Red-brown clusters up to 4cm.	Fracture and/or replacement of remaining host		Possible blue mineral present
1	Sphalerite		766.9	Alteration? Of silica-rich? Host. Red-brown clusters up to 4cm.	Fracture and/or replacement of remaining host		Possible blue mineral present
1	Sphalerite		760.4	Clast within breccia			possible galena with it
1	Sphalerite		746.7	Red-brown alteration? Cluster of 3cm	replacement of host	Granular silica host	Predates pyrite1?
1	Sphalerite		761.5	Massive alteration, 10cm zone	replacement of host	Carbonate?	Coarse pyrite veins crosscut. Also crosscut by clay filled fractures zone (with py). Cut and broken by later calcite veins.
2	Pyrite1	Pyrite1	746.7	Alteration? Cubic in form, ranging from 0.5 to 2mm	Likely alteration of siliceous host		
2	Pyrite1 or 2	Possibly Heav	747.2	Fragments of cubic Pyrite 1 in break-up breccia zone. With clay gangue.			Possible Fragments?
2	Pyrite1		751	Sub mm to 2mm pyrite cube alteration.	Intergranular channelways?	Granular silica host	
2	Pyrite1		760.4	Fragments of Pyrite 1 with silicous grains in push-up breccia.		Granular silica host	Pale push-up breccia with sulphide clasts (and bornite?), carbonate, quartz, shale, pyrite-replaced fragments and minor clay. Very fine grained version of the breccia sampled at 758m. HCL positive.
2	Pyrite1		766.4	Infill? Of pyrite crystals - submm to 5mm (predominantly 1mm) , replacement also possible	Possible open space infill - quartz veins also crosses core		Banded sulphide rock with unknown minerals.
2	Pyrite1		766.8	Infill/alteration in bands (crystalls predominantly 0.5mm)	Fracture and/or replacement of remaining host		Possibly crosscuts sphalerite (unsure). Dull massive fine pyrite may also be present.
3	Blue/Purple	Blue/Purple	760.4	Possible fragment in Breccia (or may be infill on fracture)			
3	Blue/Purple		766.4	Infill in hairline fracture	Crackle network and banded (scallop shaped) infill		crosscuts coarse pyrite. Unknown silver-brown mineral present - marcasite?
3	Blue/Purple		766.8	Possible infill in hairline fracture	Crackle fracture network		possibly after sphalerite
3	Blue/Purple			Infill in hairline fracture	fraxtures	Massive pyrite	Sample at home
4	black clay +- F	black clay +- F	750.3	infill in breccia matrix	Bx	sulphide	cubic pyrite present - massive sulphide clasts? Or with clay?. Sulphide clasts broken by black cy gangue and diss cubic py
4	black clay +- Pyrite2?		751.3	infill of black clay and very fiine disseminated pyrite in 0.5cm veinlet	fracture parallel to core axis	Massive pyrite (Pyrite1?)	

	GRS125 - 747-768m						
Stage	**Name**	**Name**	**Sample #**	**Alteration/infill**	**Channelway - structural**	**Host**	**Comments**
4	black clay +- Pyrite2?		751.3	Black clay gangue infill in fracture	15cm zone of clay fill	pale push-up breccia	All sulphides within breccia are clasts. Black clay zone is weakly iron-oxide altered with white sulphide spots.
?	Dark bands	Dark bands	763.8	Infill along arcuate stylolite-like fractures. 1-2mm in width, contorted in places.	Possibly defining a foliation	Marble	textureless pale calcite-rich host. May be the same stage as Black clay.
?	grey mineral	grey mineral	766.4	Infill and alteration between pyrite grains			
?	silver mineral	silver mineral	766.4	Infill and alteration between pyrite grains			
?	brown minera	brown minera	766.8	infill?			
?	brown minera	brown minera	766.4	infill?			
?	pyrite?	pyrite1?	766.5	banded blobs			I.e. grown in saturated solution
			Other samples				
			759	black clay and sulphides zone overprints pale pu breccia. Photographed and clay samples			
			767	Rock with very fien blue disseminated and coarser pyrite			
			804.5	HS with gy (mo?) vein			
			779	banded py and black?			
			724.5	Au and clay sample XRD-XRF			
The pale push-up breccia (abundant cbt fragments) contains clasts with disseminated cubic pyrite in a siliceous rock. The breccia is cut by grey-black clay.							
Grey-black clay is the dominant matrix material in all of the breccias in the high gold zones. Is there only one clay? Cubic pyrite is present in the clay in the vicinity of the heavy sulphide zone.							
Is the cubic pyrite gold bearingor related to the heavy sulphide zone. Fine grained disseminated pyrite is present in the grey-black glay.							
Zones of high gold are present at 723m where there is no cubic pyrite (only rubbly breccia with grey-black clay).							
High Au is in the "cy gangue with diss cubic py" zone/bx. These are concentrated on the margin of the heavy sulphide zone.							
Au grade drops off abruptly from 16-32 g/t to 4 g/t across this contact. A coarse grained pyrite stage is recorded from the HS zone.							
2nd scenario is that the "dark-si-py" zones recorded from high grades zones within the HS (see eoh) may be analagous to the cy-py fill on the margins?							
Breccia at 750.4m contains clasts of disseminated cubic py (in si-host-rock). This is cut by black cy.							
Grey-black clay is the predominant material in all the hgh grade Au zones. Need to establish if the clay is the same in each location (and the Au source)							
OR that the cubic pyrite is the Au source. NB there are zones of high grade Au at 723m etc where there is only rubbly cy and NO cubic pyrite.							
It is unclear the relationship between HS coarse pyrite and diss cubic pyrite (in Au-rich zones).							

High grade Au zone GRS125 690-702						
From 698.5 breccia from high grade AU zone, is characterised by grey gangue and py.						
Stage	**Name**	**Sample #**	**Composition Alteration/infill**	**Host**	**Comments**	**Channelway - structural**
Brecciation, infiltration of hot skarn fluids						
1	Skarn	690.4	(690.4) Fine grained alteration of carbonate host	Carbonate	A variety of minerals present. Will be identified at a later stage	Possible vein selvedge alteration (recent calcite vein cutting through centre)
1	Skarn	692.3	(692.3) Infill in carbonate host. 1-5mm veinlets	Carbonate	NB Carbonate host to skarn is recrystallised (as expected adjacent to a fault and infiltrated by skarn fluids) up to 3m outboard (uphole) of 690m	Break-up breccia causing fractures.
	Pyrite1	700.7	Fine grained massive pyrite alteration?	Carbonate?		Alteration of carbonate host
	Chalcopyrite	692.8	Infill in netwprk mm-scale fx	Calcite-rich		Network crackle fractures around calcite crystalls (up to 8cm)
?	Chalcopyrite		Fragments up to 4cm within Breccia	Breccia	Breccia has a calcite matrix and clay gangue with fine grained pyrite	
	Chalcopyrite	700.7	Infill in 1mm veinlets	Pyrite		network crackle fractures in fine grained pyrite host
	Chalcopyrite	700.8	Infill in 1mm veinlets	Pyrite		network crackle fractures in fine grained pyrite host
	Quartz	693.2	Infill in fracture	Chalcopyrite broken by quatrz	Postdates chalcopyrite	Fractures in chalcopyrite host - possibly due to a brecciation event.
	Calcite	692.8	Veins in chalcopyrite rock…			
	Pyrite2	700.7	Infill in 0.5mm veinlets	Pyrite		veins crosscut fine grained pyrite host
?	Serpentine/Sericite?	693.2	5mm zone of infill and alteration along shear fabric	Chalcopyrite broken by quatrz	Associated with pyrite? +- galena?. (Host = Cpy broken by qtz)	Shear fabric providing channelway in host
?	Sphalerite	690.8	Sphalerite and galena (up to 1cm width zones) infill and alteration of carbonate.	Carbonate	Around pyrite crystals. Marble host.	Combination of (possible) weak foliation and fractures acting as channelways.
?	Galena	700.8	Infill in 1mm veinlets		Possible cuts chalcopyrite.	Crackle network fractures
?	Galena	700.7	Infill in 2mm veinlets		Cuts massive pyrite 1 host. May be crosscute by Py2 and cpy?. Need to slab	Crackle network fractures
?	Galena	693.6	Alteration and infill in zones up to 2cm		After chalcopyrite and sphalerite.	? - need to slab
Breccia						
late	Pyrite3 (+- dark material)	692.8	Disseminated pyrite infill in 1mm veinlets with dark material. Rare infill - cubes to 2mm.	Calcite-rich		Network crackle fractures around calcite crystalls (up to 8cm)
	Pyrite3 (+- dark material)	699	alteration/infill of breccia matrix.	Breccia	Intensely broken core. Breccia has galena and sphalerite clasts in other locations (no fragments of other sulphides with the pyrite).	Breccia matrix
	Pyrite3 (+- dark material)	690.4	Alteration in in skarn replaced host	Carbonate with skarn		very fine grained alteration - possibly vein channelway (now broken by calcite). May be alteration of fine grained skarn
	Pyrite3 (+- dark material)	696.4	Breccia matrix infill?	calcite and sulphide fragments (in one very broken location can also see galena fragments - 697.2)		Breaking associated with breccia

	GRS125 605-650				
Leaching has a preferential occurrence in white host in majority of samples.					
In some cases the white are clasts. White appears to be a sst?					
Stage	**Name**	**Sample**	**Alteration/infill**	**Host**	**Channelway - structural**
	Grey si	610	Alteration of carbonate rock	White bleached carbonate	Anastomosing network (5-10mm zones) of channelways
		608.6	Infill? Alteration of grey carbonate	White bleached carbonate	Anastomosing network (5-10mm zones) of channelways. Likely host is pre-brecciated
		608.5	Infill? Alteration of grey carbonate	White bleached carbonate	Anastomosing network (5-10mm zones) of channelways. Likely host is pre-brecciated
	Grey Si2?	632	Alteration of Si-white rocl.	Si-host, brecciated	Possible breccia matric alteration
		620.9	Grey alteration, 1-5mm channelways	Pathways are reused by later py	Anastomosing fx network or possible breccia matrix alteration.
		624.9	Grey alteration, 1-5mm channelways	Pathways are reused by later py	Anastomosing fx network or possible breccia matrix alteration.
	Leaching	631.2	White pin-prick holes		
	Others	631.2	red mineral in vughs		
		669.6	red xalline mineral in vughs		
		610.7	Alteration of carbonate?		
		615	Alteration of carbonate?		
	White si? Alteration of car	612	Grey silica network around?		
Summary Paragenesis					
	grey cbt rock (may have diagenesis)				
	break				
	white cbt? - related to leaching or not?)				
	leaching				
	Break				
	White si?/alteration				
	break				
	Grey si				
	Leaching - clay alteration				
	clay infill?				
	sp and gn				
	py				

	GRS125 590-605				
Carbonate alteration and possibly, the effects of leaching and HS					
Stage	**Name**	**Sample #**	**Alteration/infill**	**Channelway - structural**	**Host**
host	Grey carbonate	602.7??	Grey host rock with variable mottled colour (dark to pale grey). High ccte-content. Mottles very irregular. A previous alteration event or diagenesis?		Grey carbonate
	White ccte	601	Veins and alteration 2-5mm wide	fx	vughs associated. May be ccte alteration associated with leaching
	White ccte	602	White ccte-alteration of host - veinlet infill	Fx and alteration?	Leaching xcuts grey-white
	Grey 1	601.4	Grey crackle network, 1-5mm	crackle fracture network	overprints white alteration
	Grey 1	599	Grey crackle network, 1-5mm	crackle fracture network	overprints white alteration
	Grey 1	602	Grey alteration of carbonate host	fx?	possibly after white?
	Black si	595.6	hailine fx fill and alteration of cbs rock	fx parallel to CA and parallelt o weak foliation	porous gy cbs rock with white alteration ccte-vugh zone and black si with mnr fe-ox.
	White spot	601.4	Possible alteration - white oovoid spots <0.5cm	> (have gy crackle overprinting?)	May be early sedimentary feature?. Can also see another white associated with a different fracture. Vughs?
	White spot	604	lensoid spots with grey defined foliation	?	May be early sedimentary feature?. Can also see another white associated with a different fracture. Vughs?
	py1		disseminated flecks of py alteration in carbonate host	? Seem to be spotted across foliation	
	Leaching (ccte-host)	602	leach vughs up to 1cm in width (5cm long)	fx control, leaching is along fractures	gy-white cbt host, mnr dark si lump present
	Leaching (ccte-host)	601	vugh and fx leaching up to 1cm.	fx control, leaching is along fractures. And mnr rounded vughs along the fractures	White ccte? Present (unclear if related to leaching)
	Leaching (ccte-host)	604	Zone 5x2cm. Possible leaching white spots? (unclear). Boxwork texture present.	fx leaching parallel to foliation	
	Leaching (ccte-host)	600	Zone up to 2x5cm (holes <1cm) irregular vughs, some with infill.	fx leaching parallel to foliation	unclear if white ccte (and mnr gy) vein zones are due to leaching or predate it?
	Leaching (ccte-host)	601.4	zone 4x2cm vughs <1cm. Minor white alteration associated. Irregular shapes	Vughs slightly aligned to fx?	Mnr gy sy and cy infill in vughs in crackle white-gy host. Vughs do not seem related to large white ccte alteration zone.

EESS polished section paragenesis (this study). Polished sections and sample offcuts courtesy of Spera (2001).

									Quantitative Whole Rock XRD					
Sample ID	**host carbonate**	**leaching**	**clear botryoidal +- brown botrioidal**	**inclusion-rich clear carbonate**	**clear infill crystals and veins**	**late stage ?**	**Comments**	**Work**	calcite	ankerite	dolomite	magnetite	siderite	other mineral
DOZ-B1-A	possible fg dirty carbonate clasts	leaching	brown carbonate growth around dirty fg clasts and alteration of other clasts?		Can't see any late stage veins but late clear xalls in voids	late clay-zeolite in voids and minor clay?	phlogopite crystals in voids and in carbonate. Phlogopite may be altered by carbonate? Chalcedony is latest in voids. Mnr mt and su - abundant boxworks. Many other clasts including cpy and bornite altered ones	cut Largest ankerite	23	31	24			22
DOZ-B1-B	Dirty fine grained carbonate				euhedral crystals in voids		sulphide clasts? And chalcedony in voids	no	15				14	71
DOZ-B1-C	dirty fine grained peloidal carbonate with magnetite alteration				clear euhedral crystals in voids associated with late stage veins (post sulphide) Brecciated sulphide into fragments		sulphide clasts? And chalcedony in voids	no	48				36	16
DOZ-B1-D	Dirty brown carbonate is earliest (possible alteration of pre-existing feldspar? Grains - can see grain outlines). Not sure how much is original carbonate host		Post sulphide carbonate is void fill, nicely banded and zoned. Brown bands	inclusion-rich - alteration of original fragments	c.g. clear carbonate infill	infill of yellow late stage clay/zeolite (radial text)	magnetite-rich alteration. Minor mica with sulphides. Nice infill textures	cut - magnesite	22		5	24	5	44
DOZ-B1-E	Brown carbonate - peloid texture. Very fine grained		? Coarse grined rexallisation? Clear and brown growth on Mt grains	equigranular subhedral recrystallised? (coarser-grained) carbonate. Alteration of original?	clear euhedral crystals in voids		clasts are calcite and pyrite altered. Possibly sulphides are embayed?	no	54		1		27	18
DOZ-B1-F	Fe-ox altered v.f.g. brown host. No evidence of peloids	leaching	clear carbonate infill (## check botryoidal?) with growth of dirty colloform carbonate. Unclear how much host alteration due to this or the inclusion-rich carbonate event. dirty colloform carbonate grows on leached host and clear carbonate (on leached host). Timing with later events not clear in this sample	alteration and veins of inclusion-rich clear carbonate	clear carbonate vein crosscuts inclusion-rich carbonate	possible late stage brown event?	lots of fe-ox and late chalcedony. Clear relationship between inclusion-rich alteration and late stage clear cbt vein	photo-probe	72	2			9	17
DOZ-B1-G	Carbonate fine grained and brown. No real texture of host.		previous alteration of host where it is replaced by large grains that are clear with minor inclusions (? This stage or inclusion-rich?).	Abundant inclusion-rich cbt - likely alteration	fine to coarse grained infill? With clear euhedral crystals in voids	large pale yellow crystals - may be same as clear??	magnetite texture suggests replacement of some calcite	CUT - check large crystals	79			1	8	12
DOZ-B2-A	Earlier dirty carbonate with dirty fractures or grain outlines? No peloidal texture		botryoidal ver clear carbonate (minor inclusions) fill on on veins. growth of botryoidal brown crystals (cbt?) on clear crystals.	Inclusion-rich carbonate in vein xcuts host+magnetite and may cause inclusion-rich alteration of host?	clear euhedral carbonate crystals in voids		Can see all STAGES.	cut - good - photo-probe	80	11				9
DOZ-B2-B	Earlier dirty carbonate grains. Peloidal texture	leaching	clear and brown-yellow botryoidal as veins, alteration and vugh fill.	Inclusion-rich veins	late carbonate veins with clear euhedral crystals in voids. Outlining mnr boxwork texture		All stages. magnetite texture suggests replacement of earlier phases		65	16				19
DOZ-B2-C	Dirty brown carbonate - earliest?			inclusion-rich carbonate - timing w.r.t. dirty carbonate not confirmed. Is it altered dirty carbonate or new?	late clear euhedral crystals in voids		sulphide possibly concentrated in fragments, magnetite around and alteration of carbonate-replaced fragments. Not clear which carbonate magnetite is post (dirty-brown or inclusion-rich)		73	2			5	20

EESS polished section paragenesis (this study). Polished sections and sample offcuts courtesy of Spera (2001).

									Quantitative Whole Rock XRD					
Sample ID	**host carbonate**	**leaching**	**clear botryoidal +- brown botrioidal**	**inclusion-rich clear carbonate**	**clear infill crystals and veins**	**late stage ?**	**Comments**	**Work**	calcite	ankerite	dolomite	magnetite	siderite	other mineral
DOZ-B2-D	Dirty brown carbonate - earliest? Also some minor VERY brown carbonate (host variation?). Original peloid textures (Look for cement###) are also present. Magnetite replaces this preferentially	leaching		inclusion-rich carbonate. Grows on dirty boxworks as subhedral crystals. Appears to fill in holes (post mt)	late clear euhedral crystals in voids and on boxworks. Subtle distinction w.r.t. inclusion-rich carbonate (may have some alteration associated with it).		magnetite post early carbonates (unlcear which ones) . Muscovite always near magnetite and host carbonate. Excellent boxworks. Mnr fe-ox	cut?	59	11			10	20
DOZ-B2-E	Dirty brown carbonate. Possible peloidal texture. Where magnetite is carbonate is preserved as dirty. Large yellow cbt xalls in host - may be same as infill xalls		possible very fine grained brown carbonate after leaching? Looks fragmented by later stages	inclusion-rich carbonate - at times appears as alteration of dirty carbonate.	euhedral crystals in voids		magnetite post early carbonates (unlcear which ones) and some mt veins		43	3			10	44
DOZ-B2-F	minor dirty carbonate. F.g. and brown		possible minor brown and clear	mostly equigranular subhedral carbonate infill? With magnetite (or post). Appears euhedral in voids.	abundant late carbonate veins - relationship with subhedral carbonate not clear. Has brecciated earlier dirty and mt. appear slightly banded need to check composition? late carbonate is abundant dolomite-shaped xalls.		strange grey platey mineral. Fe-ox	No	1		34		27	38
DOZ-B2-G	peloidal dirty carbonate. Appears altered as in areas peloids are dirty with rims of clear carbonate. Where magnetite occurs, peloids are unaltered. Magnetite has a rounded texture (from replacing rounded carbonate grains). Minor large grains.	leaching	botrioidal? (peloid-shaped) containing inclusions (check texture/para). Possible original carbonate?	?	clear euhedral crystals in voids and boxwork texture. Minor large grains unclear which stage		late veins cut magnetite etc relict fibrous material (micaceous) with or pre magnetite. Mica appears carbonate altered. Boxwork		56		22			22
DOZ-B2-H	Minor dusty carbonate and altered grains. Pervasive texture retentive aleration (inclusion-rich?).			equigranular clear carbonate alteration with ghosts of original grains (inclusion-rich)	clear carbonate vugh fill and alteration		mica-rich areas may represent rock fragment. Occur in original carbonate areas, mt also		93					7
DOZ-B2-I	Dusty carbonate. Can see single grains are partly altered. Pervasive and variably "clear" altered.		vein with cbt, may be the same as pervasive alteration (vein walls are not sharp). Has small bands of brown cbt and botryoidal texture.	fine-clear inclusion-rich carbonate replaces dusty original carbonate. At one end of slide replacement preserves radial peloidal textures.	late vein of clear crystals with sharp vein walls xcuts earlier clear banded botryoidal clear and brown cbt vein		GOLD present	Cut	76		10		3	11
DOZ-B2-J	Brown carbonate with boxwork ribs. Very leached and porous, mt not in holes. Very minro original - mostly altered to inclusion-rich			minor inclusion-rich clear carbonate in holes.	clear euhedral crystals in voids. Some are very large and not euhedral (separate stage?)	radial growths of clay/zeolite in holes		photo late? Cut?	59		30		4	7
DOZ-B2-K	minor brown early carbonate (not clear). Lots of other fragments			slightly finer-grained inclusion-rich clear alteration/infill.	Clear carbonate veins and infill crystals around sandstone clasts.		no original carbonate?		18					82

West Grasberg Paragenesis and Sample Descriptions (WGZ8 and WGR13)

Name	Infill/Alteration	Structure/Channelway	Host	Details
Early events				
Grey potassic		Breccia matrix	Diatreme	Dominantly intrusive fragments.
Green sericitic	Alteration of feldspars…		Diatreme	Dominantly intrusive fragments.
White potassic		Breccia matrix	Diatreme	Dominantly intrusive fragments.
Epidote			Diatreme	Dominantly intrusive fragments.
Development of channelway for intense white alteration (i.e.85-92m in WGZ8)				
Intense white (Kaolinite?)	(Sample 008 - WGZ8-48m). White alteration front in rock. Infill not observed.	Either fault in rubble-zones in core or re-using breccia matrix as channelway	Diatreme	Dominantly intrusive fragments.
	(WGZ8-35m). Faint white alteration of potassic white alteration.	Re-using breccia matrix as channelway	Diatreme	Dominantly intrusive fragments.
	(WGZ8-90m). Intense and pervasive white alteration. Rock is highly porous and very lightweight. Relict banded texture is highly visible.	Possible fault zone at 85-92m (where intense white alteration is pervasive and there are rubble zones in the core) may be the pathway.	Diatreme	Banded clay fragment. Yellow/white crystals/veins present.
	(WGZ8 70-85m) Intense and pervasive white alteration. Rock is highly porous and very lightweight.	Possible fault zone at 85-92m (where intense white alteration is pervasive and there are rubble zones in the core) may be the pathway.	Diatreme	Grey-white clay (Carbonate?). No banded texture present
Early Sulphides	(WGZ8-76.8m) Sphalerite and pyrite infill in veins and vughs	Fractures in intensely white altered rock and minor vugh fill.	Diatreme	Grey-white clay (Carbonate?)
	(WGZ8-77m) Black tiny spots in white clay - sphalerite and pyrite?		Diatreme	Grey-white clay (Carbonate?).
Crackle fracture pattern developed in gritty push-up breccia, fractures in intrusive-fragment-dominated diatreme, Marble push-up breccia formed				
Massive Sulphide	WGZ8-32m). Vein format, mm scale. Infill of fine-grained pyrite (straight fracture fill). Pyrite alteration of green spots.		Diatreme	Dominantly intrusive fragments. Vein cuts grey-green fragments and feldspathised rock.
	(WGZ8-34m). In a cavity as infill. Crystals are mm scale.		Diatreme	Dominantly intrusive fragments. Pyrite crystals are growing on colourless needle-crystals (quartz?).
	Py alteration of black fragments in …..		Diatreme	Banded clay fragment. Black fragments within rock containing banded clay material. Crosscut and brecciated by white alteration
	(WGZ8-63m). Pyrite infill in white clay rock	A combination of vugh infill and network veins.	Diatreme	Grey-white clay (Carbonate?). Infill in intensely white altered rock, adjacent to alteration/infill of gritty intrusive breccia
	(Sample 014 - WGZ8-64m). Semi-massive pyrite (50% of rock) alteration of gritty intrusive breccia. Minor infill (5% coarser crystals) pyite in channelways	Anastomosing mesh of channelways.	Gritty push-up breccia	Within Diatreme. Contains sphalerite clasts
	(WGZ8-78.8m). Pyrite in ovoid spots as alteration (0.1 - 0.5cm) amalgamate to massive sulphide elongate patches (1.5cm). Alteration of purple anhydrite.	Utilising same structure as purple anhydrite (vein or alteration).	Diatreme	Grey-white clay (Carbonate?) host.
Brecciation: Gritty intrusive breccia formed, Fractures in Intrusive fragment dominated diatreme, Marble push-up breccia formed				
Yellow/white crystals/clay	Vein infill in		Diatreme	Banded clay fragments.
	(Sample 009 - WGZ8-79m). Yellow crystals in 1-2mm vughs. V.f.g (sub mm) white clay associated. Possible mm scale fg white-grey alteration associated.	Crackle fracture network. Veins on mm scale.	Diatreme	Grey-white clay (Carbonate?). In wider zones fragments of previous materials (rock, sulphides). Ovoid sub angular to rounded, general scale 0.5cm (max 1cm).
	(Sample 011 - WGZ8-96). Yellow crystals within veins of white clay.	Vugh and vein fill. Fx network	Diatreme	Grey-white clay (Carbonate?). Yellow crystals become increasingly orange and entire white unit becomes orange crystalline at 98-105m (due to increasing fe-ox?).
	(WGZ8-93m). Yellow crystals with white clay as infill in fractures.	Intense crackle fracture network creating an ovoid broken pattern	Diatreme	Grey-white clay (Carbonate?). Grey textureless host.
	(WGZ8-72.3m). White clay with sporadic yellow crystals occur as infill in veins up to 2cm.	Vugh and vein fill of fracture network that breaks up the gritty push-up breccia.	Gritty push-up breccia	Within Diatreme. Contains sphalerite clasts
	(WGZ8-78.8m). Yellow crystals	Fracture fill that crosscuts purple anydrite and massive sulphide bearing vein.	Diatreme	Grey-white clay (Carbonate?) host.
Shear fabric development in grey-white clay (carbonate?) host or development of fracture system through breccia matrix.				
Grey alteration/infill (same as below?)	(WGZ8-90mInfill in very faint grey bands with rare disseminated pyrite associated	Fracture fill.	Diatreme	Banded clay fragments. Infill in fractures across yellow/white crystals/clay. OR this may be the Pyrite and/or black-carbonaceous stage below
	(Sample 001 - WGZ8-93m) Alteration of white clay with yellow crystals	Pervasive foliation through rock.	Diatreme	Grey-white clay (Carbonate?)
	(WGZ8-72.3m) Infill/alteration in rare hairline parallel fracturesof intense white	Fracture fill.	Diatreme	Grey-white clay (Carbonate?)
	(WGZ8-134m) Pervasive alteration of grey matrix by dark grey material.	Reusing breccia matrix pathway.	Marble push-up breccia	Also intense pyrite spot alteration

West Grasberg Paragenesis and Sample Descriptions (WGZ8 and WGR13)

Name	Infill/Alteration	Structure/Channelway	Host	Details
Late pyrite and/or black-carbonaceous	(WGZ8-119m) Infill of black material and pyrite infill and alteration.	Arcuate fractures rebreaking and overprinting pushup breccia	Diatreme	Predominantly clay fragments. Can see Black cbs and py re-breaking bx. Predominantly clay fragments
	(Sample 002 - WGZ8-92.2). Black infill in stylolitic fractures with v.f.g. disseminated pyrite infill.	cutting across any previous features	Diatreme	Banded clay fragments.
	(Sample 004 - WGZ8-92.4). Black infill in arcuate hairline fractures with v.f.g. disseminated pyrite infill. Minor black alteration may be associated with the fracture in the grey host rock. More intense pyrite development (alteration) is present in this zone.	Slightly parallel to white-yellow vein margins but intrudes part of vein.	Diatreme	Banded clay fragments. Fracture indrudes wide (3cm) white vein/alteration-zone.
	(Sample 007 - WGZ8-101m). Black infill in stylolitic fractures with rare v.f.g. disseminated pyrite infill.	One fracture crosscuts and offsets bands in host. One fracture is seen to crosscut and parallel the host's banding.	Diatreme	Banded clay fragments. Finely (sub mm to 3mm scale) banded grey rock.
Fe-ox	(WGZ8-134m) Intense pyrite spot alteration of previous grey alteration.	Reusing breccia matrix pathway.	Marble push-up breccia	
Untimed Events				
Early Sulphides	Fragments of sphalerite within gritty push-up breccia	unknown	Gritty push-up breccia	Within Diatreme. Coarse sphalerite (up to 1cm)
(NB unsure if same as "Early Sulphide" stage above)	Small fragment of pyrite within breccia	unknown	Marble push-up breccia	
	Small fragment of spahlerite and galena within breccia	unknown	Marble push-up breccia	galena and sphalerite together
Magnetite and quartz	Fragments of magnetite with quartz within intrusive-fragment-dominated diatreme.	unknown	Diatreme	
Black material (carbonaceous?)	Fragments of black material (appear to be clasts of vein infill or bands) 2mm by 5-10mm.	unknown - they may be original black carbonaceous layers in rocks.	Diatreme	Grey-white clay (Carbonate?). Fragments are mineralised by pyrite (massive sulphide?) and broken by yellow/white crystals/clay
Black needles	(WGR13-133m). Blue-black banded crystals as infill in vughs.	Vugh fill.	Diatreme	Postdate the yellow crystals in the vugh.
Anhydrite	(WGZ8-78.8m). Purple anhydrite vein infill (4cm wide by 15cm core section)	Likely to be fracture fill.	Diatreme	Purple anhydrite vein or alteration of Grey-white clay (Carbonate?) host. Crosscut by yellow/white crystals/clay.

Appendix 11

XRF of Wanagon Gold samples

Advanced Analytical Centre
James Cook University
Townsville Qld 4811
Tel. (ISD) 617 47814599 (STD) 07 47814599
Fax. (ISD) 617 47815550 (STD) 07 47815550

Method : ACXRF001 JOB NO. 5445-03

Client K. Prendergast

	Analyte	**SiO2**	**TiO2**	**Al2O3**	**Fe2O3T**	**MnO**	**MgO**	**CaO**	**Na2O**	**K2O**	**P2O5**	**SO3**	**LOI**	**SUM**
	LINE	KA1,2	KA1,2	KA1,2	KA1,2	KA1,2	KA1,2	KA1,2	KA1,2	KA1,2	KA1,2	KA1,2		
	CRYSTAL	InSb	LIF100	PET	LIF100	LIF100	OVO55	LIF100	OVO55	LIF100	GE	GE		
	KV	40	50	40	50	50	40	50	30	50	40	40		
	mA	60	50	60	50	50	60	50	90	50	60	60		
	TIME(SEC)	45	90	65	90	90	40	50	65	25	35	240		
	UNITS	%	%	%	%	%	%	%	%	%	%	%	%	%
SAMPLE	LAB #													
5445-05	5445-05	57.5	0.57	17.34	6.33	0.13	2.35	5.95	3.09	2.43	0.28	0.08	4.4	100.4
5445-06	5445-06	56.6	0.83	24.49	0.97	bd	0.49	0.09	0.35	8.29	0.11	0.02	8.1	100.3

Method : ACXRF002 JOB NO. 5445-03

Client K. Prendergast

	ELEMENT	F
	Maximum	2.6
	LLD	0.0
	UNITS	%
SAMPLE	LAB #	
Igneous	5445-05	0.1
Altered	5445-06	0.0

SAMPLE	**JCU Number**	**Sample_ No**	**Location Hole ID**	**Depth**	**Description**
5445-05	69050	WAN4-5-174	WAN4-5	174.0	intrusive dyke
5445-06	69049	WAN4-5-171	WAN4-5	171.0	clay altered dyke

Advanced Analytical Centre
James Cook University
Townsville Qld 4811
Tel. (ISD) 617 47814599 (STD) 07 47814599
Fax. (ISD) 617 47815550 (STD) 07 47815550

Method : ACXRF002 JOB NO. 5445-03

Client K. Prendergast

	ELEMENT	**Sc**	**Ba**	**Ti**	**V**	**Cr**	**Mn**	**Co**	**Ni**	**Cu**	**Zn**	**Ga**	**As**	**Pb**	**Rb**	**Sr**	**Y**	**Zr**	**Nb**	**Th**	**U**
	Max (ppm)	**55**	**4000**	**22600**	**526**	**4000**	**2500**	**210**	**2360**	**2360**	**290**	**40**	**330**	**133**	**1300**	**700**	**720**	**490**	**268**	**1003**	**650**
	LLD (ppm)	**3**	**10**	**5**	**4**	**3**	**4**	**2**	**3**	**3**	**3**	**3**	**10**	**10**	**2**	**2**	**2**	**3**	**2**	**3**	**3**
	Overlaps																	Sr,Ba	Y,La		
		Ca	Ce,Ti	Ba	Ba,Ti	V,La	Cr	Fe,Sr	Y	Sr,Th			Pb		U		Rb,Pb	Th	U,Th	Bi, Rb	Rb, Sr
	UNITS	**ppm**	**ppm**	**ppm**	**ppm**	**ppm**	**ppm**	**ppm**	**ppm**	**ppm**	**ppm**	**ppm**	**ppm**	**ppm**	**ppm**	**ppm**	**ppm**	**ppm**	**ppm**	**ppm**	**ppm**
SAMPLE	**LAB #**																				
Igneous	5445-05	12	732	3494	108	22	1023	19	8	44	63	19	**6**	22	118	**754**	16	84	3	**bd**	**bd**
Altered	5445-06	13	435	5337	155	**bd**	**bd**	7	**bd**	9	257	25	74	131	476	32	17	155	7	**bd**	**bd**

Method : ACXRF002 JOB NO. 5445-03

Client K. Prendergast

	ELEMENT	**Cl**
	Maximum	**3.1**
	LLD	**0.02**
	UNITS	%
SAMPLE	LAB #	
Igneous	5445-05	0.020
Altered	5445-06	0.004

Valid for SiO_2 28 - 82%, Al_2O_3 0.2 - 38.2%, Fe_2O_3 1.4 - 17.94,CaO 0.4% - 19%, MgO 0.08 - 14.7%,Na_2O 0.02 - 8.94%, P_2O_5 0 - 1.04%, K_2O 0 - 15.35%

Appendix 12
$^{40}Ar/^{39}Ar$ dating reports

$^{40}Ar/^{39}Ar$ Geochronology Results from Muscovite in a Carbonate-Anhydrite Vein

By

Lisa Peters

MAY 6, 2003

Prepared for

Kylie Prendergast
School of Earth Sciences
James Cook University
Townsville, QLD 4811

NEW MEXICO
GEOCHRONOLOGICAL RESEARCH LABORATORY
(NMGRL)

CO-DIRECTORS

DR. MATTHEW T. HEIZLER
DR. WILLIAM C. MCINTOSH

LABORATORY TECHNICIANS

LISA PETERS
RICHARD P. ESSER

Internal Report # : NMGRL-IR-355

Introduction

A muscovite from a carbonate-anhydrite vein was submitted for dating by Kylie Prendergast of James Cook University.

$^{40}Ar/^{39}Ar$ Analytical Methods and Results

The muscovite separate was analyzed by the furnace incremental heating age spectrum method. Additional analytical methods are given in Table 1, and details of the overall operation of the New Mexico Geochronology Research Laboratory are provided in the Appendix. All argon isotopic results are summarized in Table 1 and listed in Table 2.

The majority of the KP 11 muscovite age spectrum is quite well-behaved (Figure 1a). The first 7% of the ^{39}Ar released, however, is very disturbed. The radiogenic yields, K/Ca values and apparent ages are oscillatory. The following three steps (H-J) yield decreasing apparent ages and increasing radiogenic yields and K/Ca values. A weighted mean age of 2.85±0.07 Ma is calculated from steps K-Q (69.1% of the ^{39}Ar released). The final step (0.5% of the ^{39}Ar released) reveals a drop in radiogenic yield and K/Ca value and a rise in apparent age. Inverse isochron analysis of steps F-Q yields a $^{40}Ar/^{36}Ar$ intercept (311.1±8.8) slightly above the atmospheric value of 295.5 and an isochron age (2.82±0.04 Ma) within error of the age spectrum weighted mean age (Figure 1b). Both the weighted mean age and isochron age have high MSWD values that may indicate geological scatter of the data. The scatter maybe caused by incomplete separation of two initial argon trapped components that have variable $^{40}Ar/^{36}Ar$ values.

Discussion

The isochron age assigned to steps F-Q (2.82±0.04 Ma) is the preferred age for the cooling of muscovite KP 11 below its closure temperature (350-400). Increasing radiogenic yields correlated with decreasing apparent ages such as those revealed in steps F-M are suggestive of excess Ar, this is supported by the isochron analysis of steps F-Q. The disturbed nature of the early steps is possibly due to slight contamination of the muscovite with either calcite or anhydrite.

References Cited

Deino, A., and Potts, R., 1990. Single-Crystal $^{40}Ar/^{39}Ar$ dating of the Olorgesailie Formation, Southern Kenya Rift, J. Geophys. Res., 95, 8453-8470.

Samson, S.D., and, Alexander, E.C., Jr., 1987. Calibration of the interlaboratory $^{40}Ar/^{39}Ar$ dating standard, Mmhb-1, Chem. Geol., 66, 27-34.

Steiger, R.H., and Jäger, E., 1977. Subcommission on geochronology: Convention on the use of decay constants in geo- and cosmochronology. Earth and Planet. Sci. Lett., 36, 359-362.

Taylor, J.R., 1982. An Introduction to Error Analysis: The Study of Uncertainties in Physical Measurements,. Univ. Sci. Books, Mill Valley, Calif., 270 p.

York, D., 1969. Least squares fitting of a straight line with correlated errors, Earth and Planet. Sci. Lett., 5, 320-324.

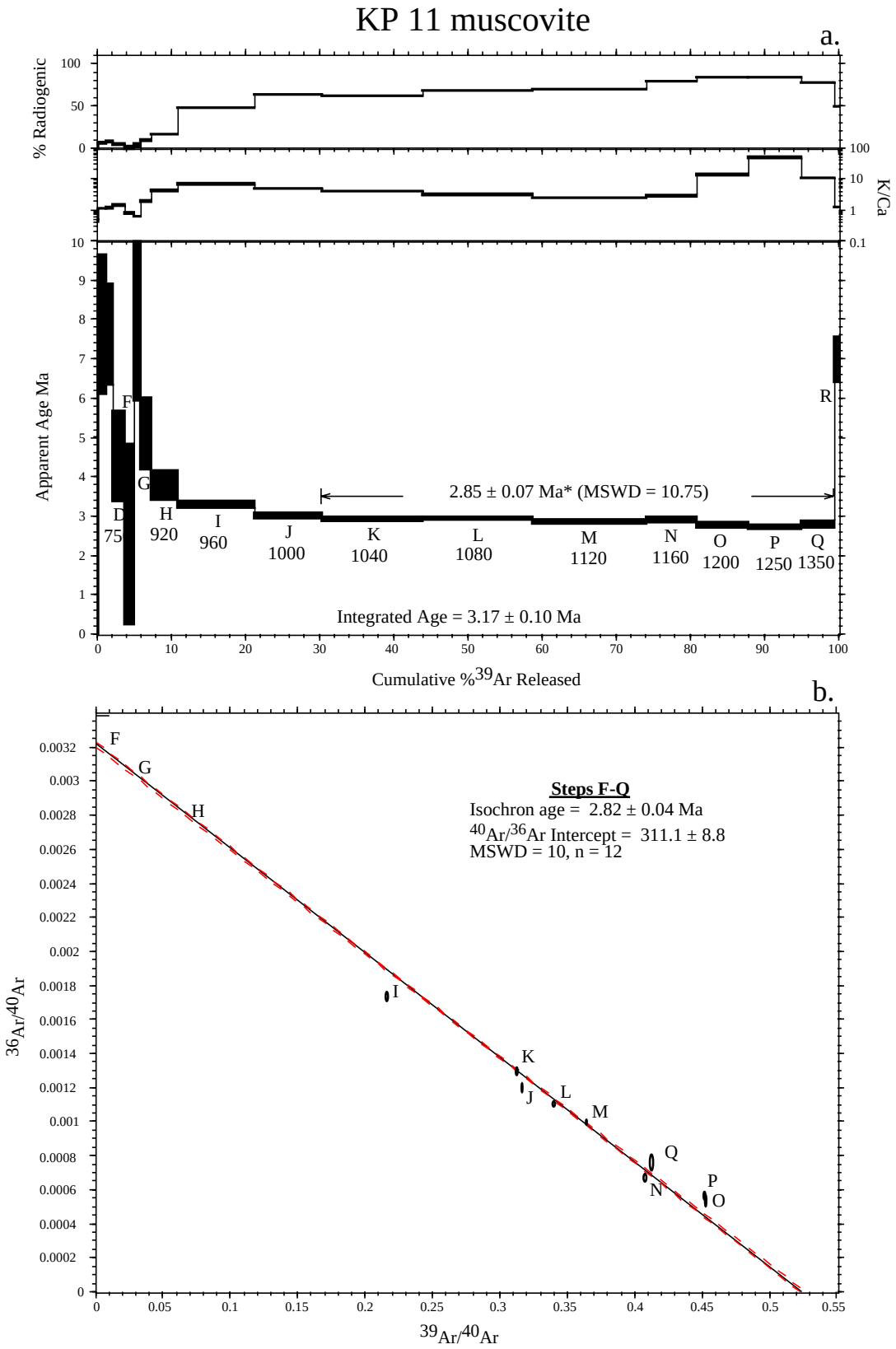

Figure 1. Age spectrum (a) and isochron (b) for sample KP11 muscovite.

Table 1. Summary of $^{40}Ar/^{39}Ar$ data and analytical methods.

Sample	Irradiation	mineral	analysis	# of steps	MSWD	Age	±2σ	Comments
KP 11	NM-162	muscovite	furnace step-heat	12	10.0	2.82	0.04	isochron age

Notes:

Sample preparation and irradiation:

Separate was loaded into a machined Al disc and irradiated for 7 hours in the D-3 position, Nuclear Science Center, College Station, TX.
Neutron flux monitor Fish Canyon Tuff sanidine (FC-1). Assigned age = 27.84 Ma (Deino and Potts, 1990)
relative to Mmhb-1 at 520.4 Ma (Samson and Alexander, 1987).

Instrumentation:

Mass Analyzer Products 215-50 mass spectrometer on line with automated all-metal extraction system.
Separate was step-heated using a Mo double-vacuum resistance furnace. Heating duration in the furnace was 10 minutes
Reactive gases removed during furnace analysis by reaction with 3 SAES GP-50 getters, 2 operated at ~450°C and
1 at 20°C. Gas also exposed to a W filiment operated at ~2000°C.

Analytical parameters:

Electron multiplier sensitivity averaged 2.62 x 10^{-16} moles /pA.
Total system blank and background for the furnace averaged 2020, 27.4, 0.7, 2.8, 5.4 x 10^{-18} moles.
J-factors determined to a precision of ± 0.1% by CO_2 laser-fusion of 4 single crystals from each of 4 radial positions around the irradiation tray.
Correction factors for interfering nuclear reactions were determined using K-glass and CaF_2 and are as follows:
$(^{40}Ar/^{39}Ar)_K$ = 0.0002±0.0003; $(^{36}Ar/^{37}Ar)_{Ca}$ = 0.00028±0.000005; and $(^{39}Ar/^{37}Ar)_{Ca}$ = 0.0007±0.00002

Table 2. $^{40}Ar/^{39}Ar$ analytical data.

ID	Temp (°C)	$^{40}Ar/^{39}Ar$	$^{37}Ar/^{39}Ar$	$^{36}Ar/^{39}Ar$ (x 10^{-3})	$^{39}Ar_K$ (x 10^{-15} mol)	K/Ca	$^{40}Ar^*$ (%)	^{39}Ar (%)	Age (Ma)	±1σ (Ma)
KP11 mu, F6:162, muscovite, 17.86 mg, J=0.0008196±0.09%, D=1.0054±0.001, NM-162, Lab#=53931-01										
A	*600*	*338.7*	*1.187*	*1147.1*	*0.369*	*0.43*	*-0.1*	*0.2*	*-0.27*	*4.56*
B	*650*	*80.39*	*0.4486*	*254.1*	*2.28*	*1.1*	*6.6*	*1.1*	*7.88*	*0.88*
C	*700*	*62.50*	*0.4327*	*194.1*	*2.22*	*1.2*	*8.3*	*2.0*	*7.63*	*0.64*
D	*750*	*56.21*	*0.3605*	*179.9*	*3.98*	*1.4*	*5.5*	*3.6*	*4.54*	*0.57*
E	*800*	*118.5*	*0.6362*	*395.4*	*2.93*	*0.80*	*1.4*	*4.8*	*2.53*	*1.14*
F	*840*	*129.0*	*0.8255*	*418.1*	*2.41*	*0.62*	*4.3*	*5.8*	*8.15*	*1.10*
G	*880*	*36.83*	*0.2682*	*113.1*	*3.25*	*1.9*	*9.4*	*7.2*	*5.09*	*0.45*
H	*920*	*15.11*	*0.1222*	*42.50*	*8.8*	*4.2*	*17.0*	*10.8*	*3.78*	*0.18*
I	*960*	*4.643*	*0.0746*	*8.160*	*25.1*	*6.8*	*48.2*	*21.1*	*3.31*	*0.05*
J	*1000*	*3.180*	*0.1049*	*3.891*	*22.5*	*4.9*	*64.1*	*30.3*	*3.01*	*0.04*
K	1040	3.193	0.1274	4.135	32.9	4.0	62.1	43.8	2.93	0.03
L	1080	2.945	0.1593	3.266	36.0	3.2	67.7	58.6	2.94	0.02
M	1120	2.747	0.2044	2.797	37.4	2.5	70.5	74.0	2.86	0.02
N	1160	2.459	0.1787	1.728	16.6	2.9	79.8	80.8	2.90	0.03
O	1200	2.216	0.0375	1.168	16.9	13.6	84.6	87.8	2.77	0.03
P	1250	2.216	0.0100	1.238	17.4	51.0	83.5	95.0	2.73	0.02
Q	1350	2.431	0.0484	1.836	10.9	10.5	77.9	99.4	2.80	0.04
R	*1700*	*9.557*	*0.4049*	*16.43*	*1.35*	*1.3*	*49.6*	*100.0*	*6.99*	*0.29*
Integrated age ± 2σ			n=18	MSWD=31.82	243.2				3.17	0.10
Plateau ± 2σ		steps K-Q	n=7	MSWD=10.75	168.1	9.6		69.1	2.85	0.07

Notes:

Isotopic ratios corrected for blank, radioactive decay, and mass discrimination, not corrected for interferring reactions.
Ages calculated relative to FC-1 Fish Canyon Tuff sanidine interlaboratory standard at 27.84 Ma.
Errors quoted for individual analyses include analytical error only, without interferring reaction or J uncertainties.
Integrated age calculated by recombining isotopic measurements of all steps.
Integrated age error calculated by recombining errors of isotopic measurements of all steps.
Plateau age is inverse-variance-weighted mean of selected steps.
Plateau age error is inverse-variance-weighted mean error (Taylor, 1982) times square root MSWD where MSWD>1.
Plateau and integrated ages incorporate uncertainties in interferring reaction corrections and J factor.
$^{40}Ar/^{36}Ar_i$ and MSWD values calculated from regression results obtained by the methods of York (1969).
Decay constants and isotopic abundances after Steiger and Jäeger (1977).
Italics denote analyses excluded from plateau age calculations.

Discrimination = 1.0054 ± 0.001

Correction factors:

$(^{39}Ar/^{37}Ar)_{Ca}$ = 0.0007 ± 2e-05
$(^{36}Ar/^{37}Ar)_{Ca}$ = 0.00028 ± 5e-06
$(^{38}Ar/^{39}Ar)_K$ = 0.01077
$(^{40}Ar/^{39}Ar)_K$ = 0.0002 ± 0.0003

$^{40}Ar/^{39}Ar$ Geochronology Results from Adularia in a Mineralized Vein

By

Lisa Peters

AUGUST 21, 2003

Prepared for

Kylie Prendergast
School of Earth Sciences
James Cook University
Townsville, QLD 4811

NEW MEXICO
GEOCHRONOLOGICAL RESEARCH LABORATORY
(NMGRL)

CO-DIRECTORS

DR. MATTHEW T. HEIZLER
DR. WILLIAM C. MCINTOSH

LABORATORY TECHNICIANS

LISA PETERS
RICHARD P. ESSER

Internal Report # : NMGRL-IR-373

Introduction

This report presents $^{40}Ar/^{39}Ar$dating results from an adularia sample supplied by Kylie Prendergast of James Cook University.

$^{40}Ar/^{39}Ar$ Analytical Methods and Results

The supplied adularia was loaded into a machined Al disc and irradiated for 14 hours in the D-3 position, Nuclear Science Center, College Station, TX. The adularia was analyzed by the furnace incremental heating age spectrum method. Additional analytical methods are given in Table 1, and details of the overall operation of the New Mexico Geochronology Research Laboratory are provided in the Appendix. All argon isotopic results are summarized in Table 1 and listed in Table 2.

Prendergast adularia yielded a fairly well-behaved age spectrum (Figure 1a). The radiogenic yields and K/Ca values reveal synchronized oscillatory behavior with older apparent ages correlating with lower K/Ca values and radiogenic yields. A weighted mean of 3.62±0.05 Ma is calculated from 100% of the ^{39}Ar released. Inverse isochron analysis of steps A through J reveals a $^{40}Ar/^{36}Ar$ intercept of 299±13 and an isochron age of 3.61±0.03 Ma (Figure 1b).

Discussion

The weighted mean age (3.62±0.05 Ma) assigned to the age spectrum analysis of Prendergast adularia provides a reliable age of formation for this adularia.

References Cited

Deino, A., and Potts, R., 1990. Single-Crystal $^{40}Ar/^{39}Ar$ dating of the Olorgesailie Formation, Southern Kenya Rift, J. Geophys. Res., 95, 8453-8470.

Samson, S.D., and, Alexander, E.C., Jr., 1987. Calibration of the interlaboratory $^{40}Ar/^{39}Ar$ dating standard, Mmhb-1, Chem. Geol., 66, 27-34.

Steiger, R.H., and Jäger, E., 1977. Subcommission on geochronology: Convention on the use of decay constants in geo- and cosmochronology. Earth and Planet. Sci. Lett., 36, 359-362.

Taylor, J.R., 1982. An Introduction to Error Analysis: The Study of Uncertainties in Physical Measurements,. Univ. Sci. Books, Mill Valley, Calif., 270 p.

York, D., 1969. Least squares fitting of a straight line with correlated errors, Earth and Planet. Sci. Lett., 5, 320-324.

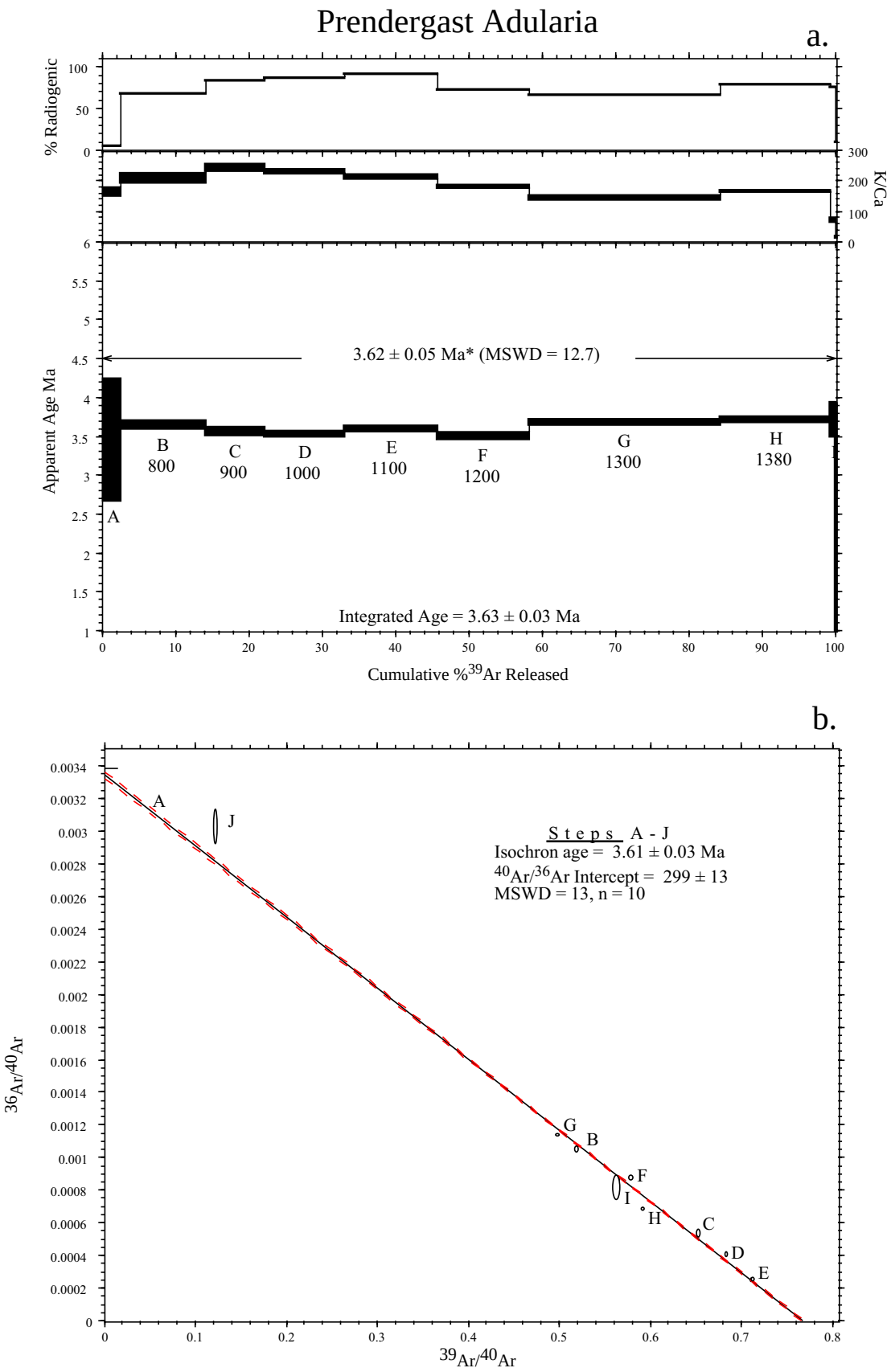

Figure 1. Age spectrum (a) and isochron (b) for sample Prendergast adularia.

Table 1. Summary of $^{40}Ar/^{39}Ar$ data and analytical methods.

Sample	Irradiation	mineral	analysis	# of steps	MSWD	Age	±2σ	Comments
Prendergast adularia	NM-166	adularia	furnace step-heat	10	12.7	3.62	0.05	

Notes:

Sample preparation and irradiation:

Separate was loaded into a machined Al disc and irradiated for 14 hours in the D-3 position, Nuclear Science Center, College Station, TX.
Neutron flux monitor Fish Canyon Tuff sanidine (FC-1). Assigned age = 27.84 Ma (Deino and Potts, 1990)
relative to Mmhb-1 at 520.4 Ma (Samson and Alexander, 1987).

Instrumentation:

Mass Analyzer Products 215-50 mass spectrometer on line with automated all-metal extraction system.
Separate was step-heated using a Mo double-vacuum resistance furnace. Heating duration in the furnace was 10 minutes
Reactive gases removed during furnace analysis by reaction with 3 SAES GP-50 getters, 2 operated at ~450°C and
1 at 20°C. Gas also exposed to a W filiment operated at ~2000°C.

Analytical parameters:

Electron multiplier sensitivity averaged 2.86 x 10^{-16} moles /pA.
Total system blank and background for the furnace averaged 2430, 537, 9.8, 9.3, 6.9x 10^{-18} moles.
J-factors determined to a precision of ± 0.1% by CO_2 laser-fusion of 4 single crystals from each of 4 radial positions
Correction factors for interfering nuclear reactions were determined using K-glass and CaF_2 and are as follows:
$(^{40}Ar/^{39}Ar)_K$ = 0.0002±0.0003; $(^{36}Ar/^{37}Ar)_{Ca}$ = 0.00028±0.000005; and $(^{39}Ar/^{37}Ar)_{Ca}$ = 0.0007±0.00002

Table 2. $^{40}Ar/^{39}Ar$ analytical data.

ID	Power (Watts)	$^{40}Ar/^{39}Ar$	$^{37}Ar/^{39}Ar$	$^{36}Ar/^{39}Ar$ (x 10^{-3})	$^{39}Ar_K$ (x 10^{-15} mol)	K/Ca	$^{40}Ar^*$ (%)	^{39}Ar (%)	Age (Ma)	±1σ (Ma)
Prendergast Adularia, 14.07 mg, J=0.0015352, NM-166, Lab#=54085-02										
A	600	21.72	0.0031	69.25	21.2	164.6	5.8	2.4	3.47	0.39
B	750	1.923	0.0024	2.030	101.8	210.6	68.8	14.0	3.66	0.03
C	850	1.537	0.0021	0.8330	71.6	244.4	84.0	22.1	3.57	0.02
D	950	1.464	0.0022	0.6192	95.8	231.1	87.5	33.0	3.55	0.02
E	1050	1.408	0.0024	0.3526	110.4	213.0	92.6	45.5	3.61	0.02
F	1150	1.729	0.0028	1.543	110.2	182.7	73.6	58.1	3.52	0.02
G	1250	2.018	0.0035	2.315	229.5	147.3	66.1	84.1	3.69	0.02
H	1330	1.689	0.0031	1.152	132.6	167.1	79.9	99.2	3.73	0.02
I	1400	1.779	0.0071	1.464	5.89	71.4	75.7	99.9	3.73	0.11
J	1650	8.351	0.0282	25.42	1.11	18.1	10.1	100.0	2.33	0.80
Integrated age ± 2σ			n=10		880.1		K2O=15.65 %		3.63	0.03
Plateau ± 2σ		steps A-J	n=10	MSWD=12.70	880.1	187.0		100.0	3.62	0.05

Notes:

Isotopic ratios corrected for blank, radioactive decay, and mass discrimination, not corrected for interferring reactions.
Ages calculated ralative to FC-1 Fish Canyon Tuff sanidine interlaboratory standard at 27.84 Ma.
Errors quoted for individual analyses include analytical error only, without interferring reaction or J uncertainties.
Integrated age calculated by recombining isotopic measurements of all steps.
Integrated age error calculated by recombining errors of isotopic measurements of all steps.
Plateau age is inverse-variance-weighted mean of selected steps.
Plateau age error is inverse-variance-weighted mean error (Taylor, 1982) times root MSWD where MSWD>1.
Plateau and integrated ages incorporate uncertainties in interferring reaction corrections and J factors.
Decay constants and isotopic abundances after Steiger and Jaeger (1977).
symbol preceding sample ID denotes analyses excluded from plateau age calculations.

Discrimination = 1.00484 ± 0.00092

Correction factors:

$(^{39}Ar/^{37}Ar)_{Ca}$ = 0.0007 ± 2e-05
$(^{36}Ar/^{37}Ar)_{Ca}$ = 0.00028 ± 5e-06
$(^{38}Ar/^{39}Ar)_K$ = 0.01077
$(^{40}Ar/^{39}Ar)_K$ = 0.0002 ± 0.0003

New Mexico Bureau of Mines and Mineral Resources

Procedures of the New Mexico Geochronology Research Laboratory

For the Period June 1998 – present

Matthew Heizler
William C. McIntosh
Richard Esser
Lisa Peters

$^{40}Ar/^{39}Ar$ and K-Ar dating

Often, large bulk samples (either minerals or whole rocks) are required for K-Ar dating and even small amounts of xenocrystic, authigenic, or other non-ideal behavior can lead to inaccuracy. The K-Ar technique is susceptible to sample inhomogeneity as separate aliquots are required for the potassium and argon determinations. The need to determine absolute quantities (i.e. moles of $^{40}Ar^*$ and ^{40}K) limits the precision of the K-Ar method to approximately 1% and also, the technique provides limited potential to evaluate underlying assumptions. In the $^{40}Ar/^{39}Ar$ variant of the K-Ar technique, a sample is irradiated with fast neutrons thereby converting ^{39}K to ^{39}Ar through a (n,p) reaction. Following irradiation, the sample is either fused or incrementally heated and the gas analyzed in the same manner as in the conventional K-Ar procedure, with one exception, no argon spike need be added.

Some of the advantages of the $^{40}Ar/^{39}Ar$ method over the conventional K-Ar technique are:

1. A single analysis is conducted on one aliquot of sample thereby reducing the sample size and eliminating sample inhomogeneity.
2. Analytical error incurred in determining absolute abundances is reduced by measuring only isotopic ratios. This also eliminates the need to know the exact weight of the sample.
3. The addition of an argon spike is not necessary.
4. The sample does not need to be completely fused, but rather can be incrementally heated. The $^{40}Ar/^{39}Ar$ ratio (age) can be measured for each fraction of argon released and this allows for the generation of an age spectrum.

The age of a sample as determined with the $^{40}Ar/^{39}Ar$ method requires comparison of the measured $^{40}Ar/^{39}Ar$ ratio with that of a standard of known age. Also, several isotopes of other elements (Ca, K, Cl, Ar) produce argon during the irradiation procedure and must be corrected for. Far more in-depth details of the determination of an apparent age via the $^{40}Ar/^{39}Ar$ method are given in Dalrymple et al. (1981) and McDougall and Harrison (1988).

Analytical techniques

Sample Preparation and irradiation details

Mineral separates are obtained in various fashions depending upon the mineral of interest, rock type and grain size. In almost all cases the sample is crushed in a jaw crusher and ground in a disc grinder and then sized. The size fraction used generally corresponds to the largest size possible which will permit obtaining a pure mineral separate. Following sizing, the sample is washed and dried. For plutonic and metamorphic rocks and lavas, crystals are separated using standard heavy liquid, Franz magnetic and hand-picking techniques. For volcanic sanidine and plagioclase, the sized sample is reacted with 15% HF acid to remove glass and/or matrix and then thoroughly washed prior to heavy liquid and magnetic separation. For groundmass concentrates, rock fragments are selected which do not contain any visible phenocrysts.

The NMGRL uses either the Ford reactor at the University of Michigan or the Nuclear Science Center reactor at Texas A&M University. At the Ford reactor, the L67 position is used (unless otherwise noted) and the D-3 position is always used at the Texas A&M reactor. All of the Michigan irradiations are carried out underwater without any shielding for thermal neutrons, whereas the Texas irradiations are in a dry location which is shielded with B and Cd. Depending upon the reactor used, the mineral separates are loaded into either holes drilled into Al discs or into 6 mm I.D. quartz tubes. Various Al discs are used. For Michigan, either six hole or twelve hole, 1 cm diameter discs are used and all holes are of equal size. Samples are placed in the 0, 120 and 240° locations and standards in the 60, 180 and 300° locations for the six hole disc. For the twelve hole disc, samples are located at 30, 60, 120, 150, 210, 240, 300, and 330° and standards at 0, 90, 180 and 270 degrees. If samples are loaded into the quartz tubes, they are wrapped in Cu foil with standards interleaved at ~0.5 cm intervals. For Texas, 2.4 cm diameter discs contain either sixteen or six sample holes with smaller holes used to hold the standards. For the six hole disc, sample locations are 30, 90, 150, 210, 270 and 330° and standards are at 0, 60, 120, 180, 240 and 300°. Samples are located at 18, 36, 54, 72, 108, 126, 144, 162, 198, 216, 234, 252, 288, 306, 324, 342 degrees and standards at 0, 90, 180 and 270 degrees in the sixteen hole disc. Following sample loading into the discs, the discs are stacked, screwed together and sealed

in vacuo in either quartz (Michigan) or Pyrex (Texas) tubes.

Extraction Line and Mass Spectrometer details

The NMGRL argon extraction line has both a double vacuum Mo resistance furnace and a CO_2 laser to heat samples. The Mo furnace crucible is heated with a W heating element and the temperature is monitored with a W-Re thermocouple placed in a hole drilled into the bottom of the crucible. A one inch long Mo liner is placed in the bottom of the crucible to collect the melted samples. The furnace temperature is calibrated by either/or melting Cu foil or with an additional thermocouple inserted in the top of the furnace down to the liner. The CO_2 laser is a Synrad 10W laser equipped with a He-Ne pointing laser. The laser chamber is constructed from a 3 3/8" stainless steel conflat and the window material is ZnS. The extraction line is a two stage design. The first stage is equipped with a SAES GP-50 getter, whereas the second stage houses two SAES GP-50 getters and a tungsten filament. The first stage getter is operated at 450°C as is one of the second stage getters. The other second stage getter is operated at room temperature and the tungsten filament is operated at ~2000°C. Gases evolved from samples heated in the furnace are reacted with the first stage getter during heating. Following heating, the gas is expanded into the second stage for two minutes and then isolated from the first stage. During second stage cleaning, the first stage and furnace are pumped out. After gettering in the second stage, the gas is expanded into the mass spectrometer. Gases evolved from samples heated in the laser are expanded through a cold finger operated at -140°C and directly into the second stage. Following cleanup, the gas in the second stage and laser chamber is expanded into the mass spectrometer for analysis.

The NMGRL employs a MAP-215-50 mass spectrometer which is operated in static mode. The mass spectrometer is operated with a resolution ranging between 450 to 600 at mass 40 and isotopes are detected on a Johnston electron multiplier operated at ~2.1 kV with an overall gain of about 10,000 over the Faraday collector. Final isotopic intensities are determined by linear regression to time zero of the peak height versus time following gas introduction for each mass. Each mass intensity is corrected for mass spectrometer baseline and background and the extraction system blank.

Blanks for the furnace are generally determined at the beginning of a run while the furnace is cold and then between heating steps while the furnace is cooling. Typically, a blank is

run every three to six heating steps. Periodic furnace hot blank analysis reveals that the cold blank is equivalent to the hot blank for temperatures less than about 1300°C. Laser system blanks are generally determined between every four analyses. Mass discrimination is measured using atmospheric argon which has been dried using a Ti-sublimation pump. Typically, 10 to 15 replicate air analyses are measured to determine a mean mass discrimination value. Air pipette analyses are generally conducted 2-3 times per month, but more often when samples sensitive to the mass discrimination value are analyzed. Correction factors for interfering nuclear reactions on K and Ca are determined using K-glass and CaF_2, respectively. Typically, 3-5 individual pieces of the salt or glass are fused with the CO_2 laser and the correction factors are calculated from the weighted mean of the individual determinations.

Data acquisition, presentation and age calculation

Samples are either step-heated or fused in a single increment (total fusion). Bulk samples are often step-heated and the data are generally displayed on an age spectrum or isochron diagram. Single crystals are often analyzed by the total fusion method and the results are typically displayed on probability distribution diagrams or isochron diagrams.

The Age Spectrum Diagram

Age spectra plot apparent age of each incrementally heated gas fraction versus the cumulative % $^{39}Ar_K$ released, with steps increasing in temperature from left to right. Each apparent age is calculated assuming that the trapped argon (argon not produced by *in situ* decay of ^{40}K) has the modern day atmospheric $^{40}Ar/^{36}Ar$ value of 295.5. Additional parameters for each heating step are often plotted versus the cumulative %$^{39}Ar_K$ released. These auxiliary parameters can aid age spectra interpretation and may include radiogenic yield (percent of ^{40}Ar which is not atmospheric), K/Ca (determined from measured Ca-derived ^{37}Ar and K-derived ^{39}Ar) and/or K/Cl (determined from measured Cl-derived ^{38}Ar and K-derived ^{39}Ar). Incremental heating analysis is often effective at revealing complex argon systematics related to excess argon, alteration, contamination, ^{39}Ar recoil, argon loss, etc. Often low-temperature heating steps have low radiogenic yields and apparent ages with relatively high errors due mainly to

loosely held, non-radiogenic argon residing on grain surfaces or along grain boundaries. An entirely or partially flat spectrum, in which apparent ages are the same within analytical error, may indicate that the sample is homogeneous with respect to K and Ar and has had a simple thermal and geological history. A drawback to the age spectrum technique is encountered when hydrous minerals such as micas and amphiboles are analyzed. These minerals are not stable in the ultra-high vacuum extraction system and thus step-heating can homogenize important details of the true ^{40}Ar distribution. In other words, a flat age spectrum may result even if a hydrous sample has a complex argon distribution.

The Isochron Diagram

Argon data can be plotted on isotope correlation diagrams to help assess the isotopic composition of Ar trapped at the time of argon closure, thereby testing the assumption that trapped argon isotopes have the composition of modern atmosphere which is implicit in age spectra. To construct an "inverse isochron" the $^{36}Ar/^{40}Ar$ ratio is plotted versus the $^{39}Ar/^{40}Ar$ ratio. A best fit line can be calculated for the data array which yields the value for the trapped argon (Y-axis intercept) and the $^{40}Ar^{*}/^{39}Ar_{K}$ value (age) from the X-axis intercept. Isochron analysis is most useful for step-heated or total fusion data which have a significant spread in radiogenic yield. For young or low K samples, the calculated apparent age can be very sensitive to the composition of the trapped argon and therefore isochron analysis should be preformed routinely on these samples (cf. Heizler and Harrison, 1988). For very old (>Mesozoic) samples or relatively old sanidines (>mid-Cenozoic) the data are often highly radiogenic and cluster near the X-axis thereby making isochron analysis of little value.

The Probability Distribution Diagram

The probability distribution diagram, which is sometimes referred to as an ideogram, is a plot of apparent age versus the summation of the normal distribution of each individual analysis (Deino and Potts, 1992). This diagram is most effective at displaying single crystal laser fusion data to assess the distribution of the population. The K/Ca, radiogenic yield, and the moles of ^{39}Ar for each analysis are also often displayed for each sample as this allows for visual ease in identifying apparent age correlations between, for instance, plagioclase contamination, signal size and/or radiogenic concentrations. The error (1σ) for each age analysis is generally shown by the horizontal lines in the moles of ^{39}Ar section. Solid symbols represent the analyses used for the weighted mean age calculation and the generation of the solid line on the ideogram, whereas open symbols represent data omitted from the age calculation. If shown, a dashed line represents the probability distribution of all of the displayed data. The diagram is most effective for displaying the form of the age distribution (i.e. gaussian, skewed, etc.) and for identifying xenocrystic or other grains which fall outside of the main population.

Error Calculations

For step-heated samples, a plateau for the age spectrum is defined by the steps indicated. The plateau age is calculated by weighting each step on the plateau by the inverse of the variance and the error is calculated by either the method of Samson and Alexander (1987) or Taylor (1982). A mean sum weighted deviates (MSWD) value is determined by dividing the Chi-squared value by n-1 degrees of freedom for the plateau ages. If the MSWD value is outside the 95% confidence window (cf. Mahon, 1996; Table 1), the plateau or preferred age error is multiplied by the square root of the MSWD.

For single crystal fusion data, a weighted mean is calculated using the inverse of the variance to weight each age determination (Taylor, 1982). Errors are calculated as described for the plateau ages above.

Isochron ages, $^{40}Ar/^{36}Ar_i$ values and MSWD values are calculated from the regression results obtained by the York (1969) method.

References cited

Dalrymple, G.B., Alexander, E.C., Jr., Lanphere, M.A., and Kraker, G.P., 1981. Irradiation of samples for $^{40}Ar/^{39}Ar$ dating using the Geological Survey TRIGA reactor. U.S.G.S., Prof. Paper, 1176.

Deino, A., and Potts, R., 1990. Single-Crystal $^{40}Ar/^{39}Ar$ dating of the Olorgesailie Formation, Southern Kenya Rift, J. Geophys. Res., 95, 8453-8470.

Deino, A., and Potts, R., 1992. Age-probability spectra from examination of single-crystal $^{40}Ar/^{39}Ar$ dating results: Examples from Olorgesailie, Southern Kenya Rift, Quat. International, 13/14, 47-53.

Fleck, R.J., Sutter, J.F., and Elliot, D.H., 1977. Interpretation of discordant $^{40}Ar/^{39}Ar$ age-spectra of Mesozoic tholieiites from Antarctica, Geochim. Cosmochim. Acta, 41, 15-32.

Heizler, M. T., and Harrison, T. M., 1988. Multiple trapped argon components revealed by $^{40}Ar/^{39}Ar$ analysis, Geochim. Cosmochim. Acta, 52, 295-1303.

Mahon, K.I., 1996. The New "York" regression: Application of an improved statistical method to geochemistry, International Geology Review, 38, 293-303.

McDougall, I., and Harrison, T.M., 1988. Geochronology and thermochronology by the ^{40}Ar-^{39}Ar method. Oxford University Press.

Samson, S.D., and, Alexander, E.C., Jr., 1987. Calibration of the interlaboratory $^{40}Ar/^{39}Ar$ dating standard, Mmhb-1, Chem. Geol., 66, 27-34.

Steiger, R.H., and Jäger, E., 1977. Subcommission on geochronology: Convention on the use of decay constants in geo- and cosmochronology. Earth and Planet. Sci. Lett., 36, 359-362.

Taylor, J.R., 1982. An Introduction to Error Analysis: The Study of Uncertainties in Physical Measurements,. Univ. Sci. Books, Mill Valley, Calif., 270 p.

York, D., 1969. Least squares fitting of a straight line with correlated errors, Earth and Planet. Sci. Lett.., 5, 320-324.

Appendix 13
SIMS data processing

Mary Kathlene Calcite Standard

Conventional analyses performed at CSL (Appendix 1)

(cf. Keith Harris, 2003)

Check analyses: IAEA NBS18 carbonatite calcite standard:

Sample I.D.	Wt.(mg.)	$\delta^{13}C_{PDB}$	$\delta^{18}O_{PDB}$	$\delta^{18}O_{SMOW}$	No. of analyses
NBS18	10.8	-5.06(0.01)	-23.11(0.02)	7.04	5
NBS18	5.5	-5.12(0.02)	-22.72(0.04)	7.42	4
Recommended values for this standard are:		**-5.01(0.06)**	**-23.0(0.1)**		

Results from Calcite Standard:

Sample I.D.	Wt.(mg.)	$\delta^{13}C_{PDB}$	$\delta^{18}O_{PDB}$	$\delta^{18}O_{SMOW}$	No. of analyses
Calcite A-1	5.0	-6.37(0.03)	-18.04(0.04)	12.26	4
Calcite A-2	9.6	-6.11(0.01)	-17.81(0.01)	12.50	4
Calcite A-3	21.1	-6.05(0.02)	-17.77(0.02)	12.54	5
Avge.Calcite standard-A:		**-6.18(0.17)**	**-17.87(0.15)**	**12.43**	
Calcite B-1	5.1	-6.27(0.03)	-18.09(0.05)	12.22	4
Calcite B-2	9.7	-6.10(0.01)	-18.15(0.03)	12.15	4
Calcite B-3	20.8	-6.03(0.02)	-18.10(0.03)	12.21	4
Avge.Calcite standard-B:		**-6.13(0.12)**	**-18.11(0.03)**	**12.19**	

(all numbers in brackets are 1 S.D.)

Dolomite Standards
KLS3-1-1855-8 (day 4)
BGU24-11-177 (day1-3)

SIMS values excluded from thesis Section C and final analysis of results

Sample	C	O	Details
KLS3-1-0719-cal	-9.56	12.45	EXCLUDED - values do not reconcile with distribution of all other results in the district. Microprobe reveals mixed composition of dolomite and calcite so SIMs results may represent mixed signature.
KLS3-1-0719-cal	-7.40	12.45	"
KLS3-1-0719-dol	6.83	17.27	"
KLS3-1-0719-dol	7.13	17.27	"
grs125-600 - ALTERATION NEAR FRACTURE	1.99	29.97	Excluded. Sample material is definitely dolomite (checked with probe) Unable to explain extremely high O values (may be due to presence of quartz alteration, so not a pure analysis). Sample is definately alteration (d18O value considered incorrect) and does not compare with conventianal analyses from SAME sample and similar samples which have a good cluster.
grs125-600 - host?	1.72	40.32	"
BGU21-10-13 - infill near su	1.38		Excluded as no O isotope value. C-isotope value from conventional analysis is -4.2 per mil
BGU21-10-12 - Dolomite with siderite veinlets	2.59	14.92	EXCLUDED - values do not reconcile with distribution of all other results in the district. Microprobe reveals mixed composition of dolomite and siderite so SIMS results may represent mixed signature

Carbon Isotope Measurements

PDB = 0.0112372

Standards

Calculating ff-std

Sample	Isotope measured	Composition	Carbon analysis order	SD error SIMS 10^-2	A 13C/12C SIMS 10^-2	B 13C/12C SIMS =A/100	E d13C =((B/PDB)-1)*1000	C 13-12C per mil	Internal Precision per mil	Calculate ff-stand =E/C	Carbon linear cte ff-stand	Carbon linear dof ff-std
Standard	10030302 C	Calcite		0.01452	**1.0420**	**0.0104**	**-72.7227**	**-6.16**	**1.09**	**11.8056**		
Standard	10030303 C	Calcite		0.0105	**1.0320**	**0.0103**	**-81.6218**	**-6.16**	**0.71**	**13.2503**	y=-0.3852x+-13.154	y=-0.3852x+ -27.62439
Standard	10030304 C	Calcite	1	0.01713	**1.0340**	**0.0103**	**-79.8420**	**-6.0257**	**1.15**	**13.2503**	**12.7687**	
KLS3-1-0719-cal	10030305 C	Mixed	2	0.03859	0.9907	0.0099	-118.3747	-9.5590	**2.77**	12.3836	12.3836	-28.3948
KLS3-1-0719-cal	10030306 C	Mixed	3	0.06123	1.0240	0.0102	-88.7410	-7.3961	**4.54**	11.9984	11.9984	-28.7800
KLS3-1-0719-dol	10030307 C	Mixed	4	0.01965	0.9000	0.0090	-199.0887	6.8262	**0.60**	-29.1652	11.6132	-29.1652
KLS3-1-0719-dol	10030308 C	Mixed	5	0.01602	0.8870	0.0089	-210.6575	7.1288	**0.48**	-29.5504	11.2280	-29.5504
	10030309 O		6								10.8428	-29.9356
	10030310 O		7								10.4576	-30.3208
Standard 10/03 3:30pm	10030311 C	Calcite	8	0.03799	**1.0540**	**0.0105**	**-62.0439**	**-6.16**	**3.36**	**10.0721**	**10.0721**	-30.7060
Standard 10/03 3:30pm	10030312 C	Calcite	9	0.02539	**1.054**	**0.0105**	**-62.0439**	**-6.16**	**2.24**	**10.0721**		-31.0912
	10030313 O		10									-31.4764
	10030314 O		11									-31.8616
BGU24-11-177-dol (host)	10030315 C	Dolomite	12	0.01256	**1.044**	**0.0104**	**-70.9429**	**2.2**	**0.35**	**-32.2468**		**-32.2468**
	11030302 O			0.02255							y = 0.0321x + 14.229	y = 0.0321x -33.492
Standard 11/03 am	11030303 C	Calcite	1	0.03794	**1.0250**	**0.0103**	**-87.8511**	**-6.16**	**2.37**	**14.2615**	**14.2615**	
BGU24-11-177-dol (host) 11/03 am	11030304 C	Dolomite	2	0.01542	**1.041**	**0.0104**	**-73.6126**	**2.2**	**0.41**	**-33.4603**	14.2932	**-33.4603**
	11030305 O		3								14.3253	-33.4282
	11030306 O		4								14.3574	-33.3961
BGU24-11-177 - cal alt margin	11030307 C	Calcite	5	0.06087	1.022	0.0102	-90.5208	-6.2908	**3.76**	14.3895	14.3895	-33.3640
BGU24-11-177 - cal infill	11030308 C	Calcite	6	0.03258	1.054	0.0105	-62.0439	-4.3022	**2.01**	14.4216	14.4216	-33.3319
	11030309 O		7								14.4537	-33.2998
	11030310 O		8	0.02514							14.4858	-33.2677
	11030311 C	Nil	9								14.5179	-33.2356
Standard	11030312 C	Calcite	10	0.02032	**1.0230**	**0.0102**	**-89.6309**	**-6.16**	**1.24**	**14.5505**	**14.5505**	-33.2035
	11030310 O										y = -0.0361x + 14.587	y = -0.0361x - 33.167
Standard	11030312 C	Calcite	1	0.02032	**1.0230**	**0.0102**	**-89.6309**	**-6.16**	**1.24**	**14.5505**	**14.5505**	**-33.2035**
BGU21-10-12 - alteration on clast	11030313 C	Dolomite with siderite veinlets	2	0.04223	1.027	0.0103	-86.0713	2.5894	**1.13**	-33.2396	14.5148	-33.2396
	11030314 O		3								14.4787	-33.2757
BGU21-10-12 - infill near su	11030315 C	Dolomite	4	0.06913	1.072	0.0107	-46.0257	1.3817	**1.85**	-33.3118	14.4426	-33.3118
grs125-600 - Alteration near fracture	11030316 C	Dolomite	5	0.01446	1.049	0.0105	-66.4934	1.9939	**0.39**	-33.3479	14.4065	-33.3479
	11030317 O		6								14.3704	-33.3840
	11030318 O		7								14.3343	-33.4201
grs125-600 - host	11030319 C	Dolomite	8	0.01217	1.059	0.0106	-57.5944	1.7215	**0.32**	-33.4562	14.2982	-33.4562
Standard	11030320 C	Calcite	9	0.02109	**1.0250**	**0.0103**	**-87.8511**	**-6.16**	**1.32**	**14.2615**	**14.2615**	-33.4923
	11030321 O			0.04958								
Standard	12030301 C	Calcite	1	0.0186	**1.0770**	**0.0108**	**-41.5762**	**-6.16**	**2.45**	**6.7494**	y = 0.8347x + 5.9147	y = 0.8347x - 41.653 **6.7494**
	12030302 O		2	0.06019							7.5841	-40.8184
	12030303 C	Nil	3								8.4188	-39.9837
	12030304 O		4								9.2535	-39.1490
BGU24-11 - dolomite host	12030305 C	Dolomite	5	0.09393	**1.029**	**0.0103**	**-84.2915**	**2.2000**	**2.18**	**-38.3143**	10.0882	**-38.3143**
DOZ-B2 - clear infill	12030306 C	Calcite	6	0.09812	1.046	0.0105	-69.1631	-6.3319	**7.99**	10.9229	10.9229	-37.4796
	12030307 O		7								11.7576	-36.6449
	12030308 O		8								12.5923	-35.8102
DOZ-B2 - host	12030309 C	Calcite	9	0.03155	1.017	0.0102	-94.9703	-7.0731	**2.09**	13.4270	13.4270	-34.9755
Standard	12030310 C	Calcite	10	0.05892	**1.0250**	**0.0103**	**-87.8511**	**-6.16**	**3.68**	**14.2615**	**14.2615**	-34.1408
	12030311 O		11								y = 0.0525x + 14.209	y = 0.0525x - 34.193
Standard	12030310 C	Calcite	1	0.05892	**1.0250**	**0.0103**	**-87.8511**	**-6.16**	**3.68**	**14.2615**	**14.2615**	**-34.1408**
	12030311 O		2								14.3140	-34.0883
	12030312 O		3								14.3665	-34.0358
KLS1-3-1983 - dol xalls near clear spar FA2	12030313 C	dolomite	4	0.01973	1.06	0.0106	-56.7045	1.6686	**0.52**	-33.9833	14.4190	-33.9833
KLS1-3-1983 - spar (FA=4)	12030314 C	dolomite	5	0.02006	1.099	0.0110	-21.9984	0.6463	**0.53**	-33.9308	14.4715	-33.9308
	12030315 O		6								14.5240	-33.8783
	12030316 O		7								14.5765	-33.8258
KLS1-3-1983 - calcite-peloid? (FA2)	12030317 C	calcite	8	0.09218	1.095	0.0110	-25.5580	-1.7471	**5.61**	14.6290	14.6290	-33.7733
KLS1-3-1983 - flat	12030318 C	dolomite	9	0.01862	1.078	0.0108	-40.6863	1.2066	**0.49**	-33.7208	14.6815	-33.7208
	12030319 O		10								14.7340	-33.6683
	12030320 O		11								14.7865	-33.6158
Standard	12030321 C	Calcite	12	0.03175	**1.0210**	**0.0102**	**-91.4107**	**-6.16**	**1.90**	**14.8394**	**14.8394**	-33.5633
	18030301 O										y = -1.6244x + 25.018	y = -1.6244x + 50.651
Standard	18030302 C	Calcite	1	missing	**0.9618**	**0.0096**	**-144.0928**	**-6.16**		**23.3917**	**23.3917**	
	18030303 C		2	missing							21.7672	49.0265
	18030304 O		3								20.1428	47.4021
DOZB1-D - late infill xalls	18030305 C	Calcite	4	0.03907	1.049	0.0105	-66.4934	-3.5907	**1.88**	18.5184	18.5184	45.7777
	18030306 O		5								16.8940	44.1533
DOZB1-D - nice grain	18030307 C	Dolomite	6	0.0368	1.01	0.0101	-101.1996	-2.3795	**0.77**	42.5289	15.2696	42.5289
KLS3-1-1855-8 - dol	18030308 C	Dolomite	7	0.02225	**1.018**	**0.0102**	**-94.0804**	**-2.3000**	**0.48**	**40.9045**	13.6452	**40.9045**
	18030309 O		8								12.0208	39.2801
	18030310 O		9								10.3964	37.6557
Standard	18030311 C	Calcite	10		**1.063**	**0.0106**	**-54.0348**	**-6.16**		**8.7719**	**8.7719**	36.0313
	18030310 O		1								y = -0.2373x + 9.2466	y = -0.2373x + 36.269
Standard	18030311 C	Calcite	2	0.01059	**1.063**	**0.0106**	**-54.0348**	**-6.16**	**1.07**	**8.7719**	**8.7719**	**36.0313**
KLS1-1-1535-4A	18030312 C	dolomite	3	0.01956	1.102	0.0110	-19.3287	-0.5400	**0.40**	35.7940	8.5347	35.7940
	18030313 O		4								8.2974	35.5567
KLS1-1-1535-4B	18030314 C	dolomite	5	0.01528	1.051	0.0105	-64.7136	-1.8322	**0.38**	35.3194	8.0601	35.3194
	18030315 O		6								7.8228	35.0821
	18030316 O		7								7.5855	34.8448
GRS125-590-7-shells	18030317 C	calcite	8	0.02785	1.093	0.0109	-27.3378	-3.7203	**3.37**	7.3482	7.3482	34.6075
GRS125-590-7-matrix	18030318 C	Calcite	9	0.03054	1.098	0.0110	-22.8863	-3.2188	**3.82**	7.1109	7.1109	34.3702
	18030319 O		10								6.8736	34.1329
	18030320 O		11								6.6363	33.8956
KLS3-1-1582-5-shell	18030321 C	calcite	12	0.02681	1.085	0.0109	-34.4570	-5.3847	**3.73**	6.3990	6.3990	33.6583
KLS3-1-1582-5-matrix	18030322 C	dolomite	13	0.03359	1.079	0.0108	-39.7964	-1.1908	**0.89**	33.4210	6.1617	33.4210
	18030323 O		14								5.9244	33.1837
	18030324 O		15								5.6871	32.9464
Standard	18030325 C	Calcite	16	0.02168	**1.086**	**0.0109**	**-33.5671**	**-6.16**	**3.54**	**5.4492**	**5.4492**	32.7091

Oxygen Isotope Measurements

V-SMOW = 0.002041

Standards

Sample	Composition	date/time	Oxygen analysis order	SD error SIMS 10^-3	A O SIMS 10^-3	B O SIMS =A/100	E d O =((B/PDB)-1)*1000	C 16-18O per mil	Internal Precision per mil	Calculate ff-stand =E/C	Oxygen linear cte ff-stand	Oxygen linear dof ff-std
KLS3-1-0719-dol	Mixed	10/03 pm		0.01308	1.9140	0.0019	-62.2244	17.2692	**1.78**	-3.6032		
Standard		**10/03 3pm**		0.02563	**1.8590**	**0.0019**	-89.1720	**12.3100**	**1.73**	**-7.2439**		
KLS3-1-0719-cal	Mixed	10/03 pm		0.01261	1.8570	0.0019	-90.1519	12.4453	**0.85**	-7.2439		
Dolomite - 24-11 (host)		**10/03 4:45pm**		0.01074	**1.8520**	**0.0019**	-92.6017	**25.7000**	**1.46**	**-3.6032**		
											y = -1.0647x - 5.7414	y = -1.0647x + 0.6395
Standard		**11/03 am**	1	0.02255	**1.8700**	**0.0019**	-83.7825	**12.3100**	**1.62**	**-6.8060**	**-6.8060**	
			2								-7.8708	-0.4252
			3								-8.9355	-1.4899
Dolomite - 24-11 (host)		**11/03am**	4	0.06665	**1.9070**	**0.0019**	-65.6541	**25.7000**	**12.78**	**-2.5546**	-10.0002	**-2.5546**
BGU24-11-177 - cal alt margin	Calcite	11/03 am	5	**0.03104**	1.8540	0.0019	-91.6218	8.2804	**1.37**	-11.0649	-11.0649	-3.6193
			6								-12.1296	-4.6840
			7								-13.1943	-5.7487
BGU24-11-177 - cal infill	Calcite	11/03 am	8	0.01115	1.9890	0.0020	-25.4777	1.7868	**0.38**	-14.2590	-14.2590	-6.8134
Standard		**11/03 mid**	9	0.02514	**1.6560**	**0.0017**	-188.6330	**12.3100**	**0.80**	**-15.3236**	**-15.3236**	-7.8781
Standard		**11/03 mid**	1	0.02514	**1.6560**	**0.0017**	-188.6330	**12.3100**	**0.80**	**-15.3236**	**-15.3236**	**-7.8781**
			2								-14.5032	-7.0582
			3								-13.6833	-6.2383
BGU21-10-12 - alteration on clast	Dol+siderite	11/03 pm	4	0.008301	1.876	0.0019	-80.8427	14.9199	**0.75**	-5.4184	-12.8634	-5.4184
			5								-12.0435	-4.5985
			6								-11.2236	-3.7786
grs125-600 - Alteration near fracture	Dolomite	11/03 pm	7	0.01959	1.86	0.0019	-88.6820	29.9730	**3.24**	-2.9587	-10.4037	-2.9587
grs125-600 - Host	Dolomite	11/03 pm	8	0.0251	1.865	0.0019	-86.2322	40.3174	**5.75**	-2.1388	-9.5838	-2.1388
			9								-8.7639	-1.3189
			10								-7.9440	-0.4990
Standard		**11/03 pm**	11	0.04958	**1.8620**	**0.0019**	-87.7021	**12.3100**	**3.41**	**-7.1245**	**-7.1245**	0.3209
											y = 1x - 6.7662	y = 1x - 2.4021
Standard		**12/03 am**	1	0.06019	**1.8710**	**0.0019**	-83.2925	**12.3100**	**4.36**	**-6.7662**	**-6.7662**	
			2								-6.7662	-2.4021
			3								-6.7662	-2.4021
BGU24-11 - dolomite host	Dolomite	**12/03am**	3	0.02148	**1.915**	**0.0019**	-61.7344	**25.7000**	**4.38**	**-2.4021**	-6.7662	**-2.4021**
			4								-6.7662	-2.4021
			5								-6.7662	-2.4021
DOZ-B2 - clear infill FA=4	Calcite	12/03am	6	0.01923	1.88	0.0019	-78.8829	11.6583	**1.39**	-6.7662	-6.7662	-2.4021
DOZ-B2 - host FA=4	Calcite	12/03am	7	0.07233	1.8	0.0018	-118.0754	17.4512	**5.24**	-6.7662	-6.7662	-2.4021
			8								-6.7662	-2.4021
			9								-6.7662	-2.4021
Standard		**12/03 mid**	10	0.05277	**1.8710**	**0.0019**	-83.2925	**12.3100**	**3.82**	**-6.7662**	**-6.7662**	-2.4021
											y = 0.0133x - 6.7795	y = 0.0133x - 2.4154
Standard		**12/03 mid**	1	0.05277	**1.8710**	**0.0019**	-83.2925	**12.3100**	**3.82**	**-6.7662**	**-6.7662**	**-2.4021**
KLS1-3-1983 - dol xalls (FA=4)	Dolomite	12/03pm	2	0.03466	1.92	0.0019	-59.2847	24.8176	**7.11**	-2.3888	-6.7529	-2.3888
			3								-6.7396	-2.3755
			4								-6.7263	-2.3622
KLS1-3-1983 - spar (FA=3)	Dolomite	12/03pm	5	0.03295	1.897	0.0019	-70.5537	30.0367	**6.87**	-2.3489	-6.7130	-2.3489
KLS1-3-1983 - calcite-peloid? (FA=3)	Calcite	12/03pm	6	0.04353	1.91	0.0019	-64.1842	9.5802	**3.18**	-6.6997	-6.6997	-2.3356
			7								-6.6864	-2.3223
			8								-6.6731	-2.3090
KLS1-3-1983 - flat	dolomite	12/03pm	9	0.04047	1.984	0.0020	-27.9276	12.1650	**9.06**	-2.2957	-6.6598	-2.2957
Standard		**12/03 pm**	10	0.01862	**1.8740**	**0.0019**	-81.8226	**12.3100**	**1.37**	**-6.6468**	**-6.6468**	-2.2824
											y = -0.0708x - 5.2626	y = -0.0708x - 6.093
Standard	calcite	**18/03**	1	0.04162	**1.907**	**0.0019**	-65.6541	**12.3100**	**3.82**	**-5.3334**	**-5.3334**	-6.1638
			2								-5.4042	-6.2346
			3								-5.4750	-6.3054
DOZB1-D - nice grain	dolomite	18/03	4	0.04566	1.889	0.0019	-74.4733	11.6800	**3.51**	-6.3762	-5.5458	-6.3762
			5								-5.6166	-6.4470
DOZB1-D - late infill xalls	calcite	18/03	6	0.08652	1.884	0.0019	-76.9231	13.5252	**7.45**	-5.6874	-5.6874	-6.5178
			7								-5.7582	-6.5886
			8								-5.8290	-6.6594
KLS3-1-1855-8 - dol	Dolomite	**18/03**	9	0.01998	**1.916**	**0.0019**	-61.2445	**9.1000**	**1.45**	**-6.7302**	-5.8998	**-6.7302**
Standard	calcite	**18/03**	10	0.02758	**1.891**	**0.0019**	-73.4934	**12.3100**	**2.26**	**-5.9702**	**-5.9702**	-6.8010
											y = -0.145x - 5.8252	y = -0.145x - 6.656
Standard	calcite	**18/03**	1	0.02758	**1.891**	**0.0019**	-73.4934	**12.3100**	**2.26**	**-5.9702**	**-5.9702**	**-6.8010**
			2								-6.1152	-6.9460
			3								-6.2602	-7.0910
KLS1-1-1535-4A	Dolomite		4	0.04614	1.95	0.0020	-44.5860	6.1617	**3.12**	-7.2360	-6.4052	-7.2360
			5								-6.5502	-7.3810
KLS1-1-1535-4B	Dolomite	18/03	6	0.04261	1.919	0.0019	-59.7746	7.9425	**2.77**	-7.5260	-6.6952	-7.5260
GRS125-590-7-shells	calcite	18/03	7	0.0735	1.951	0.0020	-44.0960	6.4466	**5.26**	-6.8402	-6.8402	-7.6710
			8								-6.9852	-7.8160
			9								-7.1302	-7.9610
GRS125-590-7-matrix	calcite	18/03	10	0.02139	1.939	0.0019	-49.9755	6.8693	**1.44**	-7.2752	-7.2752	-8.1060
KLS3-1-1582-5-shell	calcite	18/03	11	0.04445	1.919	0.0019	-59.7746	8.0557	**2.94**	-7.4202	-7.4202	-8.2510
			12								-7.5652	-8.3960
			13								-7.7102	-8.5410
KLS3-1-1582-5-matrix	Dolomite	18/03	14	0.06137	1.875	0.0019	-81.3327	9.3637	**3.46**	-8.6860	-7.8552	-8.6860
Standard	calcite	**18/03**	15	0.03891	**1.84**	**0.0018**	-98.4811	**12.3100**	**2.38**	**-8.0001**	**-8.0001**	-8.8310